THE EARLY EVOLUTION OF SEA TURTLES

SERJOSCHA W. EVERS

UNIVERSITY COLLEGE

DEPARTMENT OF EARTH SCIENCES

UNIVERSITY OF OXFORD



THESIS SUBMITTED FOR CONSIDERATION FOR THE DEGREE OF

DOCTOR OF PHILOSOPHY

TRINITY, 2018

SUPERVISED BY

PROF ROGER B. J. BENSON & PROF PAUL M. BARRETT

DECLARATION

The contents of this thesis are all my own work, except where otherwise stated; work done in collaboration with others is outlined at the start of each chapter.

_____

Serjoscha Evers, Oxford

ABSTRACT

Turtles are a major group of reptiles with moderate species richness (335 extant species) but high ecological diversity, inhabiting terrestrial, freshwater, and marine habitats. Stem-turtles evolved in the Late Permian or Early Triassic, and the crown-group appeared during the Jurassic. Fossils suggest that even the earliest turtles were ecologically diverse. As an ecologically diverse group with an excellent fossil record, turtles provide information on evolutionary dynamics of ecological transitions in vertebrates. For instance, marine ecologies evolved several times within turtles, although only chelonioid sea turtles survive to the present. Uncertainties regarding the relationships of extinct clades render the precise number of marine transitions uncertain. The unresolved phylogeny further impedes on understanding of trait evolution during early chelonioid evolution.

I address these knowledge gaps by detailed anatomical study of relevant turtle groups. I present new phylogenetic hypotheses of turtles using different inference methods (parsimony, Bayesian). A taxonomically comprehensive dataset (every extant and most extinct clades sampled) of morphological characters was derived from high-resolution computer-tomography data and vetted to reflect homology. Results suggest that protostegids are crown- or stem-group chelonioid sea turtles, implying a single origin of a pelagic lifestyle in turtles. A general flipper bauplan was established early during chelonioid evolution, and modified subsequently in different subgroups.

Time-calibration suggests an Early Cretaceous divergence time for chelonioids. This implies that some main clades of extant cryptodires (Chelonioidea, Chelydroidea, Testudinoidea) diversified earlier that commonly thought, during the Early Cretaceous and simultaneously with pleurodires and trionychians. A range of Jurassic–Cretaceous 'stem-cryptodires' (e.g. sinemydids) are found as stem-turtles. Non-pleurodiran marine turtles from the Jurassic–Paleogene (sandownids, thalassochelydians) form a previously unrecognized clade of stem-turtles, Hyphalochelydia. Marine ecologies evolved five–six times in turtles. All three Late Cretaceous marine turtle clades (hyphalochelydians, chelonioids, bothremydid pleurodires) survived the K/Pg mass extinction despite high levels of extinction in other marine reptiles.

EXTENDED ABSTRACT

Turtles are a major group of reptiles with moderate species richness (335 extant species) but high ecological diversity, inhabiting terrestrial, freshwater, and marine habitats. Stem-turtles evolved in the Late Permian or Early Triassic, and fossil evidence suggests that even the earliest turtles were ecologically diverse. Several clades of stem-turtles (e.g. Meiolaniformes) diversified from the Early Jurassic onwards, and the crown-group of turtles appeared during the Jurassic, although the exact age is uncertain and estimates vary across studies. Crown-group turtles are inferred to have been ancestrally freshwater aquatic. Within the crown-group, different ecologies have repeatedly evolved independently; several extant clades, such as geoemydids, include closely related species with distinct habitats (terrestrial vs. aquatic). As an ecologically diverse extant group with an excellent fossil record, turtles provide information on evolutionary dynamics of ecological transitions in vertebrates.

Of particular interest is the secondary reversion to marine lifestyles. Various reptilian groups have become adapted to marine habitats throughout the Mesozoic, but the early evolution for many of these groups (e.g. sauropterygians, ichthyopterygians) are poorly understood. Whereas most marine reptile groups went extinct during the Mesozoic, turtles survived the Cretaceous/Paleogene mass extinction, and chelonioid sea turtles are still alive today. Therefore, turtles form an excellent study group to integrate different data (e.g. fossil evidence, molecular sequence data and physiological information from extant species) to understand marine adaptation and its evolution. Marine ecologies evolved several times within turtles. However, uncertainties regarding the relationships of extinct clades render the precise number of marine transitions uncertain. Phylogenetic studies support either a highly-inclusive chelonioid total-group including fossil marine clades from the Jurassic and Cretaceous (e.g. protostegids, thalassochelydians, sandownids) or a less inclusive chelonioid total-group excluding those clades. Under this paradigm, these clades belong outside Cryptodira, and represent at least one additional evolutionary transition to marine life in turtles. The unclear phylogenetic position of protostegids, which have been hypothesized to be crown-group chelonioids or stem-group turtles, as well as a range of non-protostegid Cretaceous taxa, also affects the timing of origin of marine adaptation in chelonioids. The unresolved phylogeny further impedes our understanding of trait evolution during early chelonioid evolution. These phylogenetic controversies are in part due to our incomplete knowledge of the anatomy of key fossils, but are also related to poor choices of phylogenetic character definitions.

I address these knowledge gaps by detailed anatomical study of relevant turtle groups. I present new phylogenetic hypotheses of turtles using different inference methods

(parsimony, Bayesian Mk model, Bayesian tip dating combined with a fossilized birth-death model). A taxonomically comprehensive dataset (every extant and most extinct clades sampled) of morphological characters was derived from high-resolution computer tomography (CT) data. My CT data for several fossils are the first of their kind for several turtle clades, allowing a more detailed anatomical investigation than before. Several key taxa (e.g. the protostegid *Rhinochelys*, the putative thalassochelydian *Solnhofia*, the plesiochelyids *Plesiochelys* and *Jurassichelon*, the sandownid *Sandownia*, the cheloniids *Allopleuron*, *Argillochelys*, *Puppigerus* and *Eochelone*, as well as the extant *Lepidochelys* and *Dermochelys*) were fully digitally segmented to document the morphological variation among secondarily marine taxa. Additionally, key taxa of other extinct and extant clades were partially segmented for comparison. One of the segmented fossil species, *Rhinochelys* from the early Late Cretaceous of the United Kingdom, is described in detail within this thesis, and its taxonomy is revised. This example highlights the use of CT data for comparative anatomical research, particularly with fossils. In total, CT data was available for 160 species of extinct and extant turtle species. A subset of this data is published online and publically available to facilitate further work, and more data will be published in the future. I combined previously published character datasets with new characters based on my observations to construct a new matrix that expands previous matrices by 40% in character count. All characters were vetted to reflect primary hypotheses of homology, and discussions of modifications are presented.

Results suggest that protostegids are total-group chelonioid sea turtles, although the exact position of protostegids along the chelonioid stem or within the crown-group differs between analyses using slightly different data and methods. Positions outside of Cryptodira do not have any statistical support and these alternative hypotheses can thus be rejected. Irrespective of their exact position, the chelonioid affinities of protostegids imply a single origin of a pelagic lifestyle in turtles. I investigated the pattern of trait evolution for one of the key marine adaptations of chelonioids, the flipper. A general flipper bauplan was established early during chelonioid evolution, and modified subsequently in different subgroups (e.g. cheloniids, dermochelyids, gigantic protostegids from the Late Cretaceous).

A range of Jurassic–Cretaceous ‘stem-cryptodires’ (e.g. sinemydids, ‘macrobaenids’, xinjiangchelyids) are found as stem-group turtles. I computed pairwise-similarity metrics for taxa included in my dataset, which emphasizes high levels of homoplasy for some of the groups with historically unstable phylogenetic positions, including sinemydids. These patterns can possibly serve as an explanation for the distinct hypotheses of their relations. Non-pleurodiran marine turtles from the Jurassic–Paleogene (sandownids, thalassochelydians) form a previously unrecognized clade of stem-turtles, Hyphalochelydia.

This group is universally found in all analyses within this work, although different analyses result in slightly inconsistent positions of Hyphalochelydia within the turtle tree.

Marine ecologies evolved five or six times in turtles, depending on the number of marine transitions in bothremydid pleurodires: Besides the Triassic marine stem-turtle *Odontochelys*, and the pleurodiran clades Bothremydidae and Stereogyina, all other marine turtles can either be assigned to Hpyhalochelydia or Chelonioidea. All three turtle clades that lived during the Late Cretaceous (hyphalochelydians, chelonioids, bothremydid pleurodires) survived the K/Pg mass extinction, despite high levels of extinction in other marine reptiles. This extensive survival of marine turtles compared to other marine reptiles warrants further investigation.

Time-calibration was achieved using arbitrary minimum-branch length extensions of a basic *a posteriori* calibration method, as well as by a Bayesian tip-dating method. Both methods push the origination of chelonioids deeper into the Cretaceous with regard to the results of previous studies. The Bayesian tip-dating analysis combines a relaxed morphological (Mk) clock model with a fossilized birth-death (FBD) tree model. This analysis suggests an Early Cretaceous (134.5 Ma) divergence time for total-group chelonioids, and an early Late Cretaceous (88.3 Ma) time of origination for the crown-group (with protostegids as stem-group chelonioids). Divergence times for both the crown- and total-groups of Chelonioidea could reasonably even be older than estimated under the currently used model, because the FBD model recovers very old fossils systematically in more stemward positions than a regular Mk model or parsimony analysis, resulting in protostegids being the earliest branching total-group chelonioids. Alternative hypotheses in which *Toxochelys* from the Late Cretaceous of North America is the earliest branching chelonioid, as suggested by Mk model Bayesian analysis or parsimony, would require even older ages for the total-group. Regardless of this, the inferred divergence times imply that some main clades of extant cryptodires (Chelonioidea, Chelydroidea, Testudinoidea) diversified earlier that commonly thought, during the Early Cretaceous and simultaneously with pleurodires and trionychians.

ACKNOWLEDGEMENTS

There are few instances during my life during which I get to thank people for their support, assistance, or simply company in written form. Because I think the completion of a PhD is one of them, I will use this opportunity rather excessively, fully coherent with my personality.

First, I want to thank Roger Benson, my primary supervisor. It is quite obvious that this thesis could not have materialised without his initial and consistently upcoming ideas and input. It is natural to say "thank you" for this support, but I want to elaborate a bit further.

I started this PhD with quite a lot of confidence and also enthusiasm, and I want to thank you, Roger, that I can say these are also feelings involved with which I finish. Regarding the confidence, I have learned that there are a lot of things that I am not capable of, but you consistently help me realizing that those are simply things that I am not capable of yet, and that almost anything can be learned. I really appreciate that you don't necessarily take the time to explain everything in great detail, but that you do take considerable time and effort to point me in the right direction[1], and that you customize your advise to my, and also your other students personal needs. I particularly appreciate the way you influenced my academic writing, a thing I was quite terrible at when I started. Although they sometimes drove me mad, I enjoyed and, more importantly, learned from all the detailed and insightful, and frequently funny[2] comments on my writing. I am very thankful that you also gave me the freedom and in some instances even the active chance to work on projects unrelated to my PhD, as well as the chance to co-supervise students and help with teaching.

[1] Except for when the pointer is "Read more Mike Foote papers".

[2] I guess "funny" is a subjective term. However, to give some evidence that comments on academic writing can objectively be funny, I decided to give a few examples. My suggested writing is given in regular font, Roger's comments are in italics. Example 1: "Some of our characters look superficially like hierarchical compound characters, but are not. These are multistate characters in which one condition of a feature is colloquially called 'absence'. *[It's possible to read this and have no idea what you're trying to say]*". Example 2: "Other observations include protostegids are recovered as crown-chelonioids when more than one protostegid is included in a global analysis *[Sounds like a rule in a really complicated card game]*". Example 3: "The dorsal process has a low ridge that extends (…) *['has' is vague. For example, I 'have' a guinea pig contains no positional information]*". Example 4: "To test the placement of these groups in a global framework, we also included a number of (…) *['a number' is vague because no number is given. For example, 1 is a number, as is zero]*". Example 5: "dorsomedial *[you'd have to be literally insane to write 'mediodorsal']*".

From the very beginning I was not only impressed by your skills as a researcher, but also of your ethical and moral standards as an academic. Many discussions have left deep impressions on me, and it helped that I always thought you paid attention to my opinions as well. It is with some pride that I can say that some of my peers frequently mock me as “little Roger”, which they mean in the sense that I see a lot of things the way you do. It is a correct observation from my peers that some of these viewpoints are directly adopted from yours; but I always thought that changing my own opinions upon being presented new evidence of better alternatives is the only way to intellectually preceed. I certainly advanced intellectually lots over the course of the last four years, and this is what I am most thankful for, because you derserve the highest credit for this achievement.

Finally, I also like you on a personal basis, and even if most of our conversations have been of academic nature, I have very good memories of those moments, for instance in the field, when we left academia besides us for some hours. I hope that we will stay in touch beyond my time as your active student, academically but maybe also more casually.

I also want to thank my co-supervisor Paul Barrett. It is a great honor to have been supervised by someone with this level of experience, while still being taken seriously as a researcher on my own. Your academic as well as administrative help in the NHM were invaluable, and I really enjoyed the retreats and lab meetings you organized.

I would like to thank all the curators and museum staff that facilitated access to specimens under their care, namely: Carl Mehling and Mark Norell (AMNH), Oliver Rauhut (BSPG), Matt Riley (CAMSM), William Simpson and Alan Resatar (FMNH), Jérémy Anquetin (Jurassica), René Lyng Sylvestersen (FUR), Annelise Folie and Cécilia Cousin (IRSNB), Alex Peaker (MIWG), Loïc Costeur (MNB), Anne Schulp (Naturalis and TM), Sandra Chapman and Patrick Campbell (NHMUK), Hilary Ketchum (OUMNH), Torsten Scheyer (PIMUZ), Alexander Kupfer and Rainer Schoch (SMNS), Jason Head (UMZC), Jonah Choiniere and Bruce Rubridge (Wits), Jessica Maisano, Matt Colbert and Tim Rowe (TMM).

I further thank research and technical staff and PIs at the CT scanning facilities I used for this research, namely: Yi Hongyu (AMNH, IVPP); Tom Davies and Ben Moon (University of Bristol), Farah Ahmed (NHMUK), Zhe-Xi Luo and April Isch Neander (University of Chicago), Ulysse Lefévre (IRSNB). I thank Stephanie Wright for help

with segmenting the UMZC specimen of *Dermochelys* for her project work, and Guilherme Hermanson for help segmenting fossil and extant pleurodires. I am also grateful to colleagues who shared CT data, specifically but in no particular order: Paul Barrett, Marc Jones, Gabriela Sobral, Joshua Lively, Don Brinkman, Thorsten Scheyer, Ingmar Werneburg, Walter Joyce, Gabriel Ferreira, Stephan Lautenschlager, Timothy Myers, Nathan Carroll and Jéremy Anquetin. I am very thankful to Walter Joyce and Márton Rabi who shared photographs of turtle specimens from all around the world.

I am very thankful for all the funding bodies and societies that provided financial help for projects related to my thesis work, specifically the Paleontological Society for a Rodney M. Feldmann Award, the Systematics Association and Linnean Society of London for a Systematics Research Fund, the European Union for a SYNTHESYS grant, and University College Oxford for a Research Training Fund and an Old Member's Travel grant. I am also thankful for University College, the Department of Earth Sciences, and the DTP – particularly Victoria Forth – for their support throughout the PhD. I am also very happy for all the administrative support I received in the department, particulary by Jennifer Felsenberg, Asleight Hewson, Jodie Vallance, Cornelius Vermaak, and Martha Brundin.

I also want to thank my collaborateurs that have been or are working on projects related to my PhD (or turtle work more broadly): Walter Joyce, Christian Foth, Gabriel Ferreira, James Neenan, Jonah Choiniere, Nicholas Longrich, Ingmar Werneburg, Stephan Lautenschlager, Guilherme Hermanson, Stephanie Wright, Jérémy Anquetin and Mario Bronzati.

I am very happy to have been among some truly amazing colleagues within the Oxford Palaeontological group, many of which have become close friends. Foremost, I would like to thank my palaeo office mates David Ford, Hermione Beckett, and Gemma Benevento. Thanks Dave for all the palaeo discussions, beers, cigars, and times you hosted me and Judith and your and Jan's place. You have become a good friend, and I am very happy for all the moral support you gace me, especially during the difficult times. I don't think I would have gotten through this PhD without the endless support of Mimi, who helped with coding, keeping on track with official things to take care of, and many other tips and tricks to succeed at this strange place. Thanks Gemma for all the discussions, for the experience we had during ProgPal that you put together so enthusiastically, and also thanks for all the out-of-office fun. Office-thanks are extended to Tom Lamont, who is by now probably the best palaeo

informed non-palaeontologist in this department. A special thanks goes to James Neenan, who has been one of my most supportive friends. Some of the best memories from the last four years are linked to you, and probability of collecting more great memories is basically 1. Thanks also to Donald Davesne. There are few people that I can have more intellectual conservations with, and it is also a fanastic experience to have a greater smart ass around than I myself undoubtedly am. This can also be extended to Andrzej Wolniewicz. Our SVPCA yacht time remains legendary. Thank you Erin (Saupe), for managing to be a supporting professor and a friend to me. When this thing is submitted, we shall raise the glas to the demise of Trump one last[3] time. Thanks also to Sam Giles, for a diverse mixture of help, discussions, arguments, and drinks. I am particularly grateful for all the support from Luke Parry. Without your help and pointers, I could not have finalised the Bayesian chapter of this thesis in time. Thanks to Neil Brocklehurst for the occasional but invaluable help with R. I would like to thank Roger Close for many interesting (and sometimes cryptic) discussions about diversity et al., and I am very happy that we have worked together on a cool project resulting from those discussions. I also thank Marie, as an ever reliable coffee break buddy, dancing partner, and friend. Thanks also to Cesar, Felipe, Gwen, Claire, Armin and John "Fishboi" for discussions and beers. I am grateful to have been given the possibility to co-supervise several amazing students, foremost Guilherme Hermanson and Stephanie Wright. Thanks for putting up with my developing supervisory 'skills', and thanks for pushing my scientific progress further by doing all this hard work.

One of the best things about being a palaeontologist is the wider community. I have provited both academically and personally from a number of people. Some deserve separate mention. First, I would like to thank Oliver Rauhut and Adriana Lopéz-Arbarello. Without your previous supervision and support, I would have never come this far. Then there's Jonah Choiniere. How do you thank a rockstar? You've hosted me at your house, introduced me to the wonderful Kelsey, housed Judith and me like some old friends, given me amazing fieldwork and project opportunities, treated me like your own student, and given me lots of food for thought regarding my work. Thanks also to Kimi, Kathleen, Katherine, Pia, Cory, and Blair – essentially my sisters and brother from another lab. Cheers to Alessandro (Chiarenza) for being one of my best palaeo mates. Many sponateneous night and couch-crashes will be kept in

[3] last refers to 'on your bill'

good memory, let alone the theropod talk and palaeo gossip. Similarly, Emma Dunne, Omar Regalado, Aubrey Roberts, Liz Martin-Silverstone, Lukardis Wencker, Christian Foth, Jelle Wiersma, Mark Loewen, Susie Maidment, and Phil Mannion are thanked for fun nights out and work chat. Thanks also to Walter Joyce, Gabriel Ferreira, Ingmar Werneburg, Jérémy Anquetin, Jim Parham, Juliana Sterli, Stephan Lautenschlager and Márton Rabi for inspiring turtle talk. I would also like to thank Richard Butler, Daniel Field, Matt Carrano, Jakob Vinther, Anjali Goswami and Rob Asher for various discussions that had a lasting imprint on me.

I even have friends outside (!) of palaeo. First, thanks to Shane Chandler. There are few peope that I can do holidays, sports, academic talk, partying and draining sorrows with all together, and I will miss doing these things with you on a regular basis. Thanks also to Guilio Mazzotta and James Silk. Thank you Marisa (Storm) for being such an excellent friend, my go-to fellow German, and smoke companion at all times. Oxford was a lot duller without you. Thanks to Pete Barry, Sean Hopkins, Tim Sweere, Duane Smythe, Jo Katchinoff, and Dave Byrne for some excellent nights much needed to clear my head from work. Thanks to all the good friend who paid me a visit in Oxford, namely Georg, Benni, Mike, Benno, Oli, and Rosa. Thanks to my buddies at home, and particularly to Benno. Your visits to Oxford, pictures and videos of Mika, and telephone support in some of the more difficult times were incredibly important for me. Special thanks go to Leejiah Doward, housmate and landlord *extraordinaire*. Thanks for all the help with whatever I needed help with, thanks for great partys, thanks for the more-than-occasional scotch before bed, thanks for some funny cigarettes, and thanks for never raising the rent.

The people that have given me most support, strength, joy, and affection throughout the PhD but also in previous times leading up to it are my family. Mama und Papa, ich danke euch dafür, dass ihr mich immer in meinem Wunsch, Paläontologe zu werden bedingungslos unterstützt habt. Dominik, danke dass du immer genau der Bruder warst und bist, den ich brauche und den ich mir wünsche. Ihr drei kennt mich besser als alle anderen zusammen und das Gefühl dass ihr mir gebt ist für mich das Wichtigste im Leben. Omi und Opa, danke, dass ihr euch immer interessiert und mich so sehr beinflusst habt, euch immer so sehr um mich und uns alle kümmert und der Mittelpunkt der Familie seid.

Wenn es eine Einzelperson gibt, der ich das Meiste verdanke, dann bist das du Judith. Kein Mensch auf dieser Welt kennt mich so gut wie du. Ich habe mich bei dir

immer zuhause, geborgen und so sehr geliebt gefühlt. Meine tollsten Erinnerungen und die schönsten Gefühle hatte ich mit dir. Das Gefühl, dass du einfach da bist, irgendwo da draußen, selbst wenn wir gerade nicht beieinander sein konnten hat mich immer stark gemacht, und so sehr glücklich. Mit dir war ich nie alleine. Du hast mich so sehr geliebt, und ich habe dich so sehr zurück geliebt. Und dann habe ich dich so sehr geliebt, und du mich so sehr zurück geliebt. Du bist ein riesengroßer Teil von mir. Ohne dich wäre ich nicht derjenige, der ich jetzt bin. Du hast mich immer angefeuert, bestärkt, ermutigt, zurück geholt, aufgemuntert, aufgefangen. Als ich dir von dem Angebot aus Oxford erzählt habe, haben deine Augen mehr gefunkelt als meine eigenen. Du hast viel zurück gesteckt und alles mit gemacht, und ich bin dir unendlich dankbar für deine Hilfe. Du hast dich so sehr und so ernsthaft für mich und was mir wichtig ist interessiert, dass du selbst schon ein Dinospezialist bist. Wir haben zusammen so viel erlebt und wollten noch die ganze Welt erkunden. Eine echte Familie werden. Das war mein Traum, und war unser Traum. Auch wenn ich es kaputt gemacht habe, werde ich unseren Traum und die schönen Gefühle, die ich damit verbinde, nie verlieren. Ich werde dich für immer lieben. Du weißt nicht, wie leid und weh es mir tut, dass ich nicht der Joschi bin, der ich dir eigentlich immer sein wollte.

TABLE OF CONTENTS

DECLARATION ..... **I**
ABSTRACT ..... **III**
EXTENDED ABSTRACT ..... **V**
ACKNOWLEDGEMENTS ..... **IX**
TABLE OF CONTENTS ..... **XV**

1 INTRODUCTION **1**
1.1 Background 1
1.2 Aims of this thesis 8
INSTITUTIONAL ABBREVIATIONS 15

2 A NEW PHYLOGENETIC HYPOTHESIS OF TURTLES WITH IMPLICATIONS FOR THE TIMING AND NUMBER OF EVOLUTIONARY TRANSITIONS TO MARINE LIFESTYLES IN THE GROUP **17**
2.1 INTRODUCTION 18
2.1.1 Independent origins of marine life in turtles 19
2.1.2 Non-pleurodiran marine turtles from the Mesozoic 21
2.1.3 Previous phylogenetic work 23
2.2 MATERIAL AND METHODS 26
2.2.1 Character dataset 26
2.2.2 Coding strategy 27
2.2.3 Taxon sampling 35
2.2.4 CT data and 3D models used in this study 37
2.2.5 Similarity matrix 38
2.2.6 Parsimony Analysis 39
2.2.7 Testing the effect of 'marine' characters and advanced protostegids 42
2.2.8 Testing alternative hypotheses 43
2.3 RESULTS 44
2.3.1 Similarity matrix 44
2.3.2 Phylogenetic Analysis using unordered characters 48
2.3.3 Parsimony Analysis using ordered characters 59
2.3.4 Excluding 'marine' characters and 'least specialised taxa analyses' 60
2.3.5 Templeton's tests 61
2.4 SYSTEMATIC PALAEONTOLOGY 67
2.5 DISCUSSION 72
2.5.1 Independent origins of marine ecologies 72
2.5.2 The phylogenetic position of protostegids 74
2.5.3 Implication on the timing of the origin and biogeographic evolution of Chelonioidea 77
2.6 CONCLUSIONS 83
2.7 DATA ARCHIVING STATEMENT 84

3 CRANIAL OSTEOLOGY, NEUROANATOMY, AND TAXONOMY OF *RHINOCHELYS* (PROTOSTEGIDAE) **87**
3.1 INTRODUCTION 87
3.2 METHODS 89
3.2.1 CT data and 3D models used in this study 89
3.3 SYSTEMATIC PALAEONTOLOGY 93
3.4 DESCRIPTION 95
3.4.1 Cranium 96
3.4.1.1 Nasal 96
3.4.1.2 Prefrontal 100
3.4.1.3 Frontal 109
3.4.1.4 Parietal 114
3.4.1.5 Postorbital 117
3.4.1.6 Jugal 120
3.4.1.7 Quadratojugal 123

3.4.1.8 Squamosal ... 124
3.4.1.9 Premaxilla ... 125
3.4.1.10 Maxilla ... 128
3.4.1.11 Vomer ... 132
3.4.1.12 Palatine ... 134
3.4.1.13 Quadrate ... 136
3.4.1.14 Epipterygoid ... 140
3.4.1.15 Pterygoid ... 141
3.4.1.16 Supraoccipital ... 146
3.4.1.17 Exoccipital ... 147
3.4.1.18 Basioccipital ... 151
3.4.1.19 Prootic ... 153
3.4.1.20 Opisthotic ... 157
3.4.1.21 Parabasisphenoid ... 160
3.4.2 Cavum acustico-jugulare ... 165
3.4.3 Arterial circulation ... 169
3.4.4 Cranial endocast ... 171
3.4.5 Inner ear and associated structures ... 180
3.4.6 Stapes ... 185
3.4.7 Lower Jaw ... 186
3.4.7.1 Dentary ... 186
3.4.7.2 Angular, Prearticular and Splenial ... 190
3.4.7.3 Surangular ... 192
3.4.7.4 Coronoid ... 194
3.4.7.5 Articular ... 194
3.5 PRINCIPAL COMPONENT ANALYSIS ... 195
3.5.1 Skull measurements and PCA procedure ... 195
3.5.2 PCA results ... 197
3.6 DISCUSSION ... 199
3.6.1 Taxonomy of Rhinochelys ... 199
3.6.2 Status of proposed diagnostic characters of Rhinochelys species ... 202
3.6.3 Osteological variation found in this study ... 207
3.6.4 Intraspecific variation in Rhinochelys ... 209
3.6.5 Diversity of turtles from the Cambridge Greensand Member of the West Melbury Marly Chalk Formation ... 211
3.7 CONCLUSIONS ... 218
3.8 DATA ARCHIVING STATEMENT ... 219

4 MARINE ADAPTATION DURING THE EARLY EVOLUTION OF CHELONIOIDS . 221
4.1 INTRODUCTION ... 222
4.2 MATERIAL & METHODS ... 223
4.2.1 Character-taxon matrix ... 224
4.2.2 Cranial character modifications ... 231
4.2.3 Postcranial character modifications ... 231
4.3 RESULTS ... 255
4.3.1 Topological results of phylogenetic analysis ... 255
4.3 DISCUSSION ... 260
4.3.1 Calibrated tree and stratigraphic congruence ... 260
4.3.2 Evolution of flippers ... 262
4.4 CONCLUSIONS ... 267

5 FUTURE RESEARCH: TREE CALIBRATION USING TIP-DATING APPROACHES 270
5.1 Motivation ... 270
5.2 An introduction to time-scaling methods ... 272
5.3 Methods ... 277
5.3.1 Summary of analytical settings ... 277
5.3.2 MrBayes Code ... 281
5.4 Preliminary results ... 284
5.4.1 Topological results ... 284
5.4.2 Divergence times ... 288

5.4.3 Parameters from the FBD and clock models ... 291
5.5 Systematic Palaeontology ... 294
5.6 Discussion ... 295
5.6.1 Comments on phylogenetic nomenclature ... 295
5.6.2 Effects of time data for phylogenetic inference using a Bayesian analysis ... 297
5.7 Planned modifications ... 299
5.7.1 Taxon sampling ... 299
5.7.2 Total-evidence analysis ... 301

CONCLUSIONS ... 303

REFERENCES ... 307

APPENDIX S1 ... 347
S1.1. General notes on my character list ... 347
S1.2. Character list with documentation of modified characters ... 348
S1.3. Extended discussion of characters regarding the carotid arterial system ... 544
S1.4. Deleted phylogenetic characters ... 550
S1.5 Character optimisation: Synapomorphies by node ... 555
S1.6. Analysis of reduced dataset (marine characters omitted) ... 573
S.1.8. Topologies of constraint analyses ... 577
S1.9 Character taxon-matrix ... 597
S1.10 Molecular backbone constraint ... 607
S1.13 R code for similarity matrix ... 607
S1.12 R code for timescaled trees ... 612
S1.13 Code for Templeton's test in PAUP* and R ... 613
S1.14 Supplementary references ... 615

APPENDIX S2 ... 623
S2.1 Additional anatomical illustrations ... 623
S2.2 PCA Supplementary information ... 635
S2.2.1 R code ... 635
S2.2.2 Additional analysis: PCA using measurements of Collins (1970) ... 637
S2.2.3 R Code Analysis Collins (1970) ... 638
S2.2.4 Results ... 639
S2.3 Supplementary References ... 640

APPENDIX S3 ... 642
S3.1 Character optimization ... 642
S3.1.1 Methods ... 642
S3.1.2 Results ... 644
S3.2 Time-calibrated phylogeny ... 672
S3.2.1 R code for timescaled trees ... 674
S3.3 Character list ... 676
S3.3.1. General notes on my character list ... 676
S3.3.2. Character list with documentation of modified characters ... 676
S3.4 Character-taxon matrix ... 765
S3.5 Supplementary References ... 779

APPENDIX S4 ... 781
S4.1 MrBayes code ... 781

1 INTRODUCTION

1.1 Background

Turtles are a major group of reptiles comprising 335 living species (van Dijk *et al.* 2014). They have a high ecological diversity, inhabiting marine, freshwater, and terrestrial environments, and with diets including herbivory, piscivory, omnivory, carnivory, medusivory, and durophagy (Ernst & Barbour 1989). Turtles have a unique body plan among vertebrates, possessing a rigid, akinetic skull without temporal fenestration (Gaffney 2007; Sterli & de la Fuente 2010; Rabi *et al.* 2013), a re-modelled middle ear cavity (e.g. Hensen 1974; Wever 1978; Hetherington 2008), and a splayed rib cage that is modified to form the shell (Kuratani *et al.* 2011; Lyson & Joyce 2012; Lyson *et al.* 2013). This highly modified anatomy of the turtle rib cage implies further anatomical modifications to other body parts, such as the limb girdles (e.g. Lyson *et al.* 2013; Nagashima *et al.* 2014). These derived features are shared among all crown-group turtles, and have complicated assessments of the phylogenetic position of turtles within the vertebrate tree of life. Based on morphological, developmental, and molecular evidence, turtles have been classified in almost every possible position within sauropsids (the reptile total-group) (e.g. Carroll 1988; Lee 1997; Rieppel & deBraga 1996; deBraga & Rieppel 1997; Rieppel 2000, 2001; Lyson *et al.* 2010, 2012; Crawford *et al.* 2012, 2015; Pereira 2017). Molecular and more recently genome-based analyses have transformed our understanding of turtle relationships and indicate that turtles are the extant sister group to archosaurs (e.g. Zardoya & Meyer 1998; Iwabe *et al.* 2004; Chiari *et al.* 2012; Crawford *et al.* 2012, 2015; Wang *et al.* 2013; Field *et al.* 2014). Only recently, morphological evidence has been presented that may corroborate those molecular findings (Bever *et al.* 2015), although this is not consistently found in formal phylogenetic analyses of morphological datasets (e.g. Bever *et al.* 2015; Schoch & Sues 2015; Li *et al.* 2018). Despite the controversy surrounding turtle origins, much is known about the turtle stem-lineage, which is represented by numerous fossils, especially from the Triassic and Jurassic

(e.g. Gaffney 1990; Gaffney & Kitching 1994, 1995; Joyce 2007; Sterli & Joyce 2007; Sterli *et al.* 2007; Sterli 2008, 2010; Li *et al.* 2008, 2018; Anquetin 2010, 2012; Joyce *et al.* 2013*a*; Pérez-García & Codrea 2018; see Joyce 2017 for a recent review). These document the step-wise acquisition of some derived turtle traits (e.g., the middle ear: Gaffney 1990; Gaffney & Kitching 1995), or allow hypotheses about the origins of key traits of turtles (e.g. the akinetic skull: Gaffney 1990; Bever *et al.* 2015; Schoch & Sues 2015). It is also clear that the stem-lineage of turtles is relatively species-rich, comprising several monophyletic clades, some of which extend into the Cenozoic (e.g. Meiolaniformes: Sterli 2015; Paracryptodira: Lipka *et al.* 2006; Cadena & Parham 2015; Evers & Benson 2018*a*), although some of these groups have alternatively been recovered as extinct clades within the crown-group (e.g. Paracryptodira: Joyce 2007).

The turtle crown-group consists of two main extant clades and representatives of their respective stem-lineages (e.g. Anquetin *et al.* 2017*b*; Ferreira *et al.* 2018). These clades are the Cryptodira (hidden-necked turtles) and Pleurodira (side-necked turtles). This dichotomy between extant taxa is supported by molecular data (e.g. Shaffer 1997; Crawford *et al.* 2012; Pereira *et al.* 2017) as well as morphological data (e.g. Gaffney 1975*a*; Dryden 1988; Gaffney & Meylan 1988; Joyce 2007). Whereas most pleurodires are freshwater aquatic animals, cryptodires include fully terrestrial, freshwater aquatic, and marine groups. Ecological disparity can vary greatly even within individual turtle families, such as geoemydids (e.g. Ernst & Barbour 1989; Claude 2004; Foth *et al.* 2017), indicating that ecological transitions happened frequently and convergently among turtle groups. Phylogenetic analyses differ significantly in their inferred content of the pleurodiran and cryptodiran stem-lineages: for example, paracryptodires (Joyce 2007 vs. Lipka *et al.* 2006), xinjiangchelyids (e.g. Zhou *et al.* 2015 vs. Rabi *et al.* 2014), and plesiochelyiids (e.g. Joyce 2007 vs. Sterli 2010), to name three examples alone, have all repeatedly been inferred to be stem-group cryptodires or stem-group turtles. This presents a difficult issue that cannot be resolved by application of molecular data (the relevant taxa are fossils, so only morphological data are available).

The ancestral ecology for crown-turtles is inferred to be aquatic (Joyce & Gauthier 2004) and there is evidence for both terrestrial and aquatic habitats among stem-group turtles (Joyce & Gauthier 2004; Scheyer & Sander 2007; Li *et al.* 2008, 2018; Reisz & Head 2008; Scheyer *et al.* 2014; Cerda *et al.* 2016; Joyce 2017). As an ecologically diverse extant group with an excellent fossil record, turtles provide information on the evolutionary dynamics of ecological transitions in vertebrates. The secondary reversion to marine life is particularly interesting. This transition is not well understood in reptiles, despite its occurrence in at least 18 lineages among many higher groups (mesosaurs, thalattosaurs, ichthyosaurs, sauropterygians, crocodiliforms, rhynchocephalians, squamates, turtles) (Motani 2009; Benson 2013; Bardet *et al.* 2014). In part, this lack of understanding results from the extinction of most marine reptile groups by the end of the Mesozoic, or mid-Cenozoic.

Within turtles alone, multiple lineages independently adapted to marine life from as early as the Triassic (i.e. *Odontochelys*: Li *et al.* 2008; Reisz & Head 2008 Lyson *et al.* 2010), and during the Jurassic (Angolachelonia [*sensu* Evers & Benson 2018*a*]: Meylan *et al.* 2000; Anquetin *et al.* 2015; 2017*a*; Evers & Benson 2018*a*), Cretaceous (bothremydid pleurodires: Gaffney *et al.* 2006; Rabi *et al.* 2012; chelonioid cryptodires: Hirayama 1994, 1998; Evers & Benson 2018*a*), and Cenozoic (Stereogyina, within Pleurodira: Sánchez-Villagra *et al.* 2000; Winkler & Sánchez-Villagra 2006; Gaffney *et al.* 2011; Ferreira *et al.* 2015). Of these, only chelonioids (sea turtles) survive to the present. Extant chelonioids are marine animals with adaptations to a pelagic lifestyle that include modifications in the shell, limbs and skull (e.g. Zangerl 1980; Hirayama 1994). Extant chelonioids are divided into two main clades, the cheloniids (hard-shelled sea turtles) with six living species, and the dermochelyoids with only one living species, the leatherback turtle *Dermochelys coriacea*.

In addition to chelonioids, thalassochelydians (i.e. plesiochelyids, eurysternids, thalassemydids) and sandownids also show evidence (both morphological and contextual, such as sedimentological) for marine adaptation (e.g. Cadena 2015; Anquetin *et al.* 2017*a*). These groups are generally interpreted to have lived in relatively shallow waters, as they lack

key adaptations of pelagic turtles (such as fully developed flippers), and are generally found in depositional environments supporting this interpretation. Secondarily marine groups of turtles discussed in this thesis are reviewed in a later section of this introduction, as well as in chapter 2.

Previous phylogenetic hypotheses imply at least four and as many as eight independent transitions to marine life in turtles, throughout their entire evolutionary history (e.g. Joyce 2007; Li *et al.* 2008; Mateus *et al.* 2009; Rabi *et al.* 2012; Anquetin *et al.* 2015). However, deep uncertainty regarding the phylogenetic affinities of several extinct groups renders the precise number highly uncertain. This lack of consensus on turtle phylogeny also affects our understanding of wider macroevolutionary dynamics, such as the mode and rate of morphological evolution during ecological transitions.

Extant turtles provide genetic (= molecular) data that help to constrain their phylogenetic relationships and allow the estimation of divergence ages for subclades (e.g. Joyce *et al.* 2013*b*). Morphological and molecular phylogenies have resulted in different hypotheses for the interrelationships of extant turtles (for instance regarding the monophyly and content of Chelydroidea: Shaffer *et al.* 1997; Parham *et al.* 2006; Joyce *et al.* 2013*b*; Joyce 2016). Although morphological evidence has subsequently been found to support some of the propositions of molecular studies (e.g. Knauss *et al.* 2011 for the example of Chelydroidea) not all conflicting relationships among crown-turtles have yet been reconciled. At present, it is common for morphological studies of turtle phylogeny to use a backbone constraint informed by the results of molecular studies (Danilov & Parham 2008; Cadena & Parham 2015; Zhou & Rabi 2015). In the second and fourth sections of this thesis, parsimony analysis of morphological data is used in conjunction with constraints informed by molecular studies.

Analysis of morphological data remains important in the 'genomic era' of systematics, because knowledge of the phylogenetic affinities of fossil taxa is required so they can be used as reliable calibration points in molecular clock analyses (Near *et al.* 2005; Parham *et al.* 2012; Joyce *et al.* 2013*b*). Additionally, the consideration of fossils is fundamental to our understanding of the patterns of morphological and ecological evolution during deep

divergences, and in entirely extinct groups. This is well documented by, for example, the evolutionary transition from fish to tetrapods (e.g. Ahlberg & Milner 1994; Ahlberg *et al.* 1996; Carroll 1996; Ahlberg & Johanson 1998; Long & Gordon 2004; Clack 2009) and by the dinosaurian origins of birds (Ostrom 1975; Gauthier 1986).

Several Mesozoic turtle groups exemplify the difficulties associated with robustly estimating the phylogenetic affinities of fossil taxa. These include the marine thalassochelydians (e.g. Joyce 2007; Sterli & De la Fuente 2013; Cadena & Parham 2015; Evers & Benson 2018*a*), sandownids (e.g. Mateus *et al.* 2009; Cadena 2015; Evers & Benson 2018*a*) and protostegids (e.g. Joyce 2007; Anquetin 2012; Cadena & Parham 2015; Evers & Benson 2018*a*), as well as the freshwater xinjiangchelyids, sinemydids and macrobaenids (e.g. Rabi *et al.* 2014; Cadena & Parham 2015; Zhou & Rabi 2015; Evers & Benson 2018*a*). Figure 1.1 shows digital skull renderings of crania of representatives of these groups that are further discussed within this thesis. Most of these groups have been alternatively proposed to be stem-group turtles, stem-group cryptodires, or within the crown-group of cryptodires as stem- or crown-group chelonioids (reviewed below, but see Joyce 2007; Sterli 2010; Anquetin 2012; Cadena & Parham 2015; Evers & Benson 2018*a* for large 'global' turtle phylogenies with grossly different topologies), although this is in part caused by the instability of the position of pleurodires across studies (Sterli 2010). Because the placements of these groups influence reconstructions of morphological changes during deep evolutionary divergences (e.g. Cadena & Parham 2015; Zhou & Rabi 2015), they have implications for the relative phylogenetic placements of other clades.

Particular debate surrounds a marine turtle group called protostegids. Protostegids are a taxonomically and ecologically diverse (e.g. Cope 1871; Wieland 1896; Zangerl 1953*a*; Collins 1970; Hooks 1998; Hirayama 1998; Tong *et al.* 2006; Bardet *et al.* 2013; Cadena & Parham 2015) group of pelagic turtles and achieved a global distribution early in their history (Collins 1970; Hirayama 1998; Kear & Lee 2006; Cadena & Parham 2015).

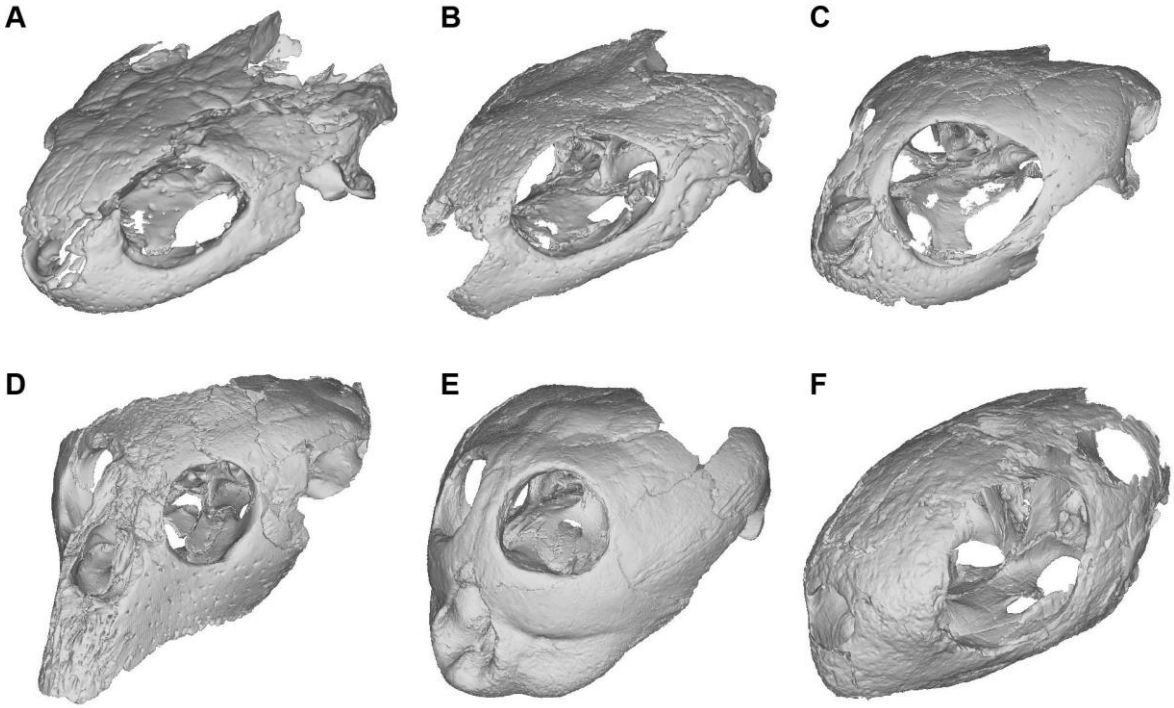


FIG. 1.1. 3D renderings of representatives of non-pleurodiran Mesozoic turtle groups with uncertain phylogenetic positions. **A**, *Annemys* sp. (IVPP V18106), a Jurassic xinjiangchelyid; **B**, *Ordosemys* sp. (IVPP V12092), a Cretaceous sinemydid; **C**, *Jurassichelon oleronensis* (PIMUZ AIII 514), a Jurassic plesiochelyid (mirrored for comparison); **D**, *Solnhofia parsoni* (TM 4023), a Jurassic thalassemydid (mirrored for comparison); **E**, *Sandownia harrisi* (MIWG 3480), a Cretaceous sandownid; **F**, *Rhinochelys pulchriceps* (CAMSM B55783), a Cretaceous protostegid. Note that all skulls are scaled to the same size for illustrative purposes.

Protostegids have frequently been hypothesized to be crown-group chelonioids, on the stem-group of *Dermochelys* (e.g. Hirayama 1994, 1998; Lehman & Tomlinson 2004; Brinkman *et al.* 2006; Kear & Lee 2006; Bardet *et al.* 2013; Cadena 2015; Cadena & Parham 2015; Evers & Benson 2018*a*). This hypothesis has been contested by results from 'global' phylogenetic analyses of testudine interrelationships that were not focussed specifically on marine turtles and that included representatives of most major living and extinct fossil lineages (e.g. Joyce 2007; Sterli 2010; Anquetin 2012). These studies found protostegids in more stemward positions outside of Chelonioidea, on the stem-group of either cryptodires or turtles (see chapter 2 for a summary). However, these analyses included only a single Early Cretaceous species of protostegid, *Santanachelys gaffneyi*, in their taxon samples. Only recently have such global analyses included a wider array of protostegids, as well as other fossil sea turtles (Cadena 2015; Cadena & Parham 2015; Evers & Benson 2018), and these analyses have found

protostegids nested within modern chelonioids on the stem-group of *Dermochelys*, consistent with historical views.

Different phylogenetic hypotheses for protostegids as well as the other groups mentioned above give rise to distinct conclusions regarding: (1) the number of times that marine ecologies have evolved within turtles; (2) the timing of secondarily marine adaptation in the chelonioid total-group; and (3) inferences of character state changes and polarities, which influence hypotheses of morphological evolution on the stem-group of cryptodires, and among turtles more widely. Clearly, resolving the phylogeny of key fossil groups can have substantive implications for our understanding of the evolution of turtles as a whole.

Besides the phylogenetic uncertainty surrounding deep nodes within the turtle tree, and even ignoring the controversy surrounding protostegids as potential crown-group chelonioids, the in-group relationships of chelonioids are not well understood (Hirayama 1995; Parham & Fastovsky 1997; Parham & Pyenson 2010; Evers & Benson 2018*a*). This is a problem because the phylogenetic positions of many Cretaceous non-protostegid chelonioids are instrumental to constraining the age of the crown-group (Joyce *et al.* 2013*b*), and for investigating the evolution of morphological structures related to marine adaptation, such as flippers, secondary palates, and large triturating surfaces indicative of durophagy (Hirayama 1995; Lynch & Parham 2003; Parham & Pyenson 2010).

Numerous fossil taxa have been placed variably on the stem of *Dermochelys*, cheloniids, and chelonioids, but there is little consensus regarding the placement of most taxa. The oldest undisputed stem-group chelonioid is *Toxochelys* spp. from the Coniacian–Campanian of North America (Nicholls 1988; Brinkman *et al.* 2006; Kear & Lee 2006; Joyce *et al.* 2013*b*; Weems & Brown 2017), and several Late Cretaceous taxa (e.g. *Allopleuron hofmanni*) have been proposed to be stem-group cheloniids (Gentry 2016; Evers & Benson 2018*a*; Gentry *et al.* 2018). However, undisputed stem-group taxa for both cheloniids and dermochelyoids are generally much younger and date to the Paleocene–Eocene (e.g. Nielsen 1959; Joyce *et al.* 2013*b*; Weems 2014). This is in part due to the exclusion of representatives of the Dermochelyidae in many studies investigating the phylogenetic positions of Cretaceous

(and also younger) chelonioids, resulting in ambiguity with respect to their position relative to *Dermochelys*, even if they can be shown to fall outside the crown-group of cheloniids (e.g. Parham & Fastovsky 1997; Brinkman *et al.* 2006; Weems & Brown 2017; Myers *et al.* 2018).

1.2 Aims of this thesis

Much of the present thesis is dedicated to elucidating the phylogenetic relationships of secondarily marine turtles, with a specific focus on the early evolution of chelonioids. In the first data chapter of this thesis (section 2), I present a new phylogenetic analysis based on examination of X-ray micro-computed tomographic data of skulls of fossil and extant taxa of nearly all turtle subfamilies that helps to clarify the global phylogeny of turtles.

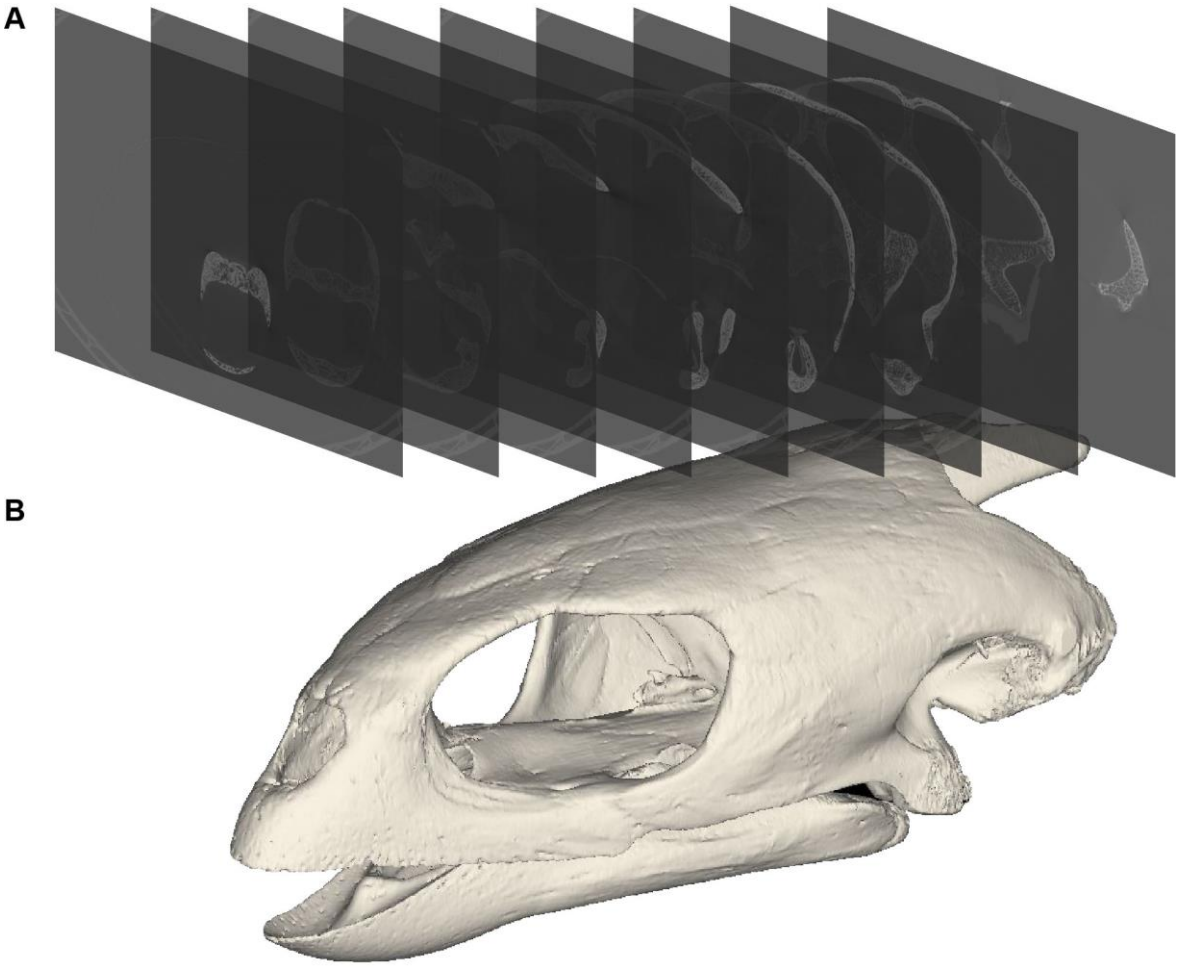


FIG. 1.2. Generating 3D models from CT slice data. **A**, selection of CT slices through a turtle skull (*Eretmochelys imbricata*: FMNH 22242); **B**, 3D model generated with threshold segmentation of CT slices.

Scanning techniques such as X-ray micro-computed tomography have revolutionized the way palaeontologists can examine internal anatomical details of fossils, because the technique allows for a non-destructive, digital preparation of structures (e.g. Conroy & Vannier 1984; Rowe *et al.* 2001; Sutton 2008; Sutton *et al.* 2014). Tomographic data are two-dimensional images (singular: tomogram) that represent parallel sections of a three-dimensional object. Computed tomography (CT in the remainder of this thesis) is a technique in which an object, such as a fossil, is subjected to penetrative radiation (such as X-rays) to produce a tomographic dataset (Sutton 2008; Sutton *et al.* 2014). Radiation is attenuated at a particular frequency range dependent on the material properties of the object, resulting in attenuation contrast between different materials within an object (Rowe *et al.* 2001; Sutton 2008; Cunningham *et al.* 2014; Sutton *et al.* 2014). Objects are rotated between the radiation source and detector to produce digital radiographs (=projections) (Cunningham *et al.* 2014). The attenuation profile from the radiographs is then computationally mapped onto tomograms (Sutton 2008; Cunningham *et al.* 2014). The tomographic dataset can then be used in special software packages to produce volume renderings of regions of interest, whereby tomograph pixels are treated as voxels in a three-dimensional space, and the user identifies corresponding pixels in adjacent tomograms that are assigned to the same region of interest (Sutton 2008; Cunningham *et al.* 2014; Sutton *et al.* 2014). An example of this process in shown in Figure 1.2, in which several tomograms of an extant sea turtle were selected and positioned in their respective positions above a digital volume rendering of the skull. For this thesis, I collected CT data for many fossil taxa representing all major extant and extinct families (see Fig. 1.1 for a small selection of fossils particularly relevant to this thesis). Additionally, I collected CT scans of extant turtles, with every subfamily being sampled (see Fig. 1.3) for a selection. These were collected so that my phylogenetic dataset could be based on a comprehensive sample of turtle diversity.

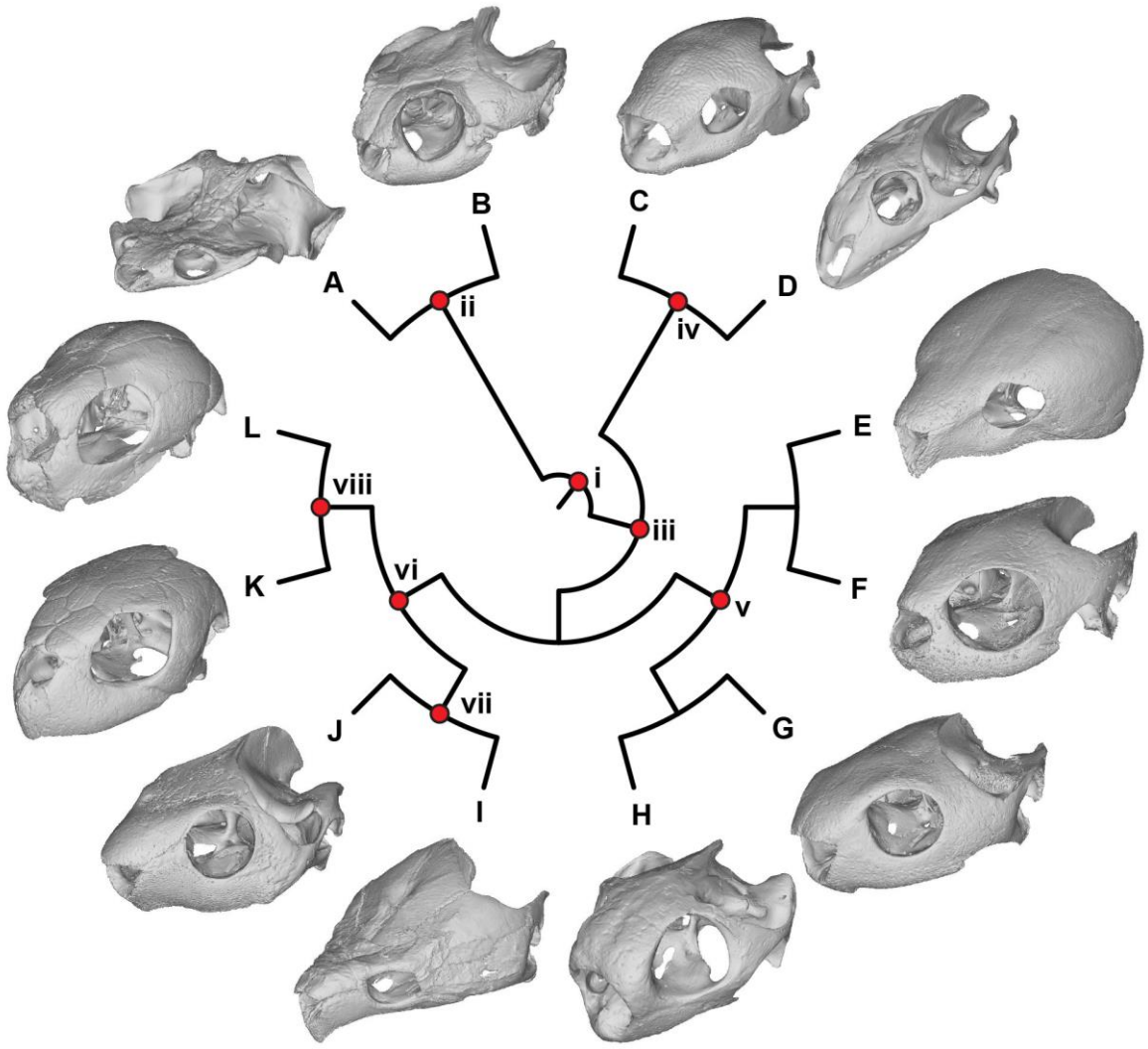


FIG. 1.3. 3D renderings of extant turtle species representing the sampling of higher turtle clades in this study and phylogeny of crown-group turtles (following Pereira *et al.* 2017). **A**, *Chelus fimbriatus* (NHMUK 81.9.72.4), representing Cheliidae; **B**, *Pelomedusa subrufa* (SMF 70540), representing Pelomedusoides; **C**, *Carettochelys insculpta* (NHMUK 1903.7.10.1), representing Carettochelyidae; **D**, *Apalone spinifera emoryi* (FMNH 22178), representing Trionychidae; **E**, *Platysternon megacephalum* (SMF 69684), representing Platysternidae; **F**, *Chrysemys picta*, representing Emydidae (NHMUK 76.1.31.19); **G**, *Geoclemys hamiltoni*, representing Geoemydidae (NHMUK 87.9.30.1); **H**, *Gopherus polyphemus* (FMNH 211815), representing Testudinidae; **I**, *Macrochelys temminckii* (FMNH 22111), representing Chelydridae; **J**, *Sternotherus minor* (FMNH 211696), representing Kinosternidae; **K**, *Lepidochelys olivacea* (SMNS 11070), representing Cheloniidae; **L**, *Dermochelys coriacea* (UMZC R3031), representing Dermochelyidae. Note that Plemodusidae and Podocnemididae are summarized as Pelomedusoides and that Dermatemydidae is not listed separately. Labelled internal nodes represent important clades that are discussed throughout this thesis: *i*, Testudines (crown-group turtles); *ii*, Pleurodira; *iii*, Cryptodira; *iv*, Trionychia; *v*, Testudinoidea; *vi*, Americhelydia; *vii*, Chelydroidea; *viii*, Chelonioidea.

My phylogenetic work includes revisions of previously-used morphological characters, as well as the addition of a large number (>50) of new characters. I paid particular attention to character construction, as numerous studies have shown that the coding strategy

employed by phylogeneticists has large influences on the results of the analysis (e.g. Platnick 1979; Piemental & Riggins 1987; de Pinna 1991; Maddison 1993; Pleijel 1995; Wilkinson 1995; Hawkins *et al.* 1997; Strong & Lipscomb 1999). Because characters should represent primary hypotheses of homology established by the criterion of similarity, and character states represent variation on the level of the character, I used a hierarchical coding strategy with multistate characters and inapplicability scorings (e.g. Hawkins *et al.* 1997). My phylogenetic analysis implies three independent origins of marine ecology among non-pleurodiran turtles, and suggests that two Mesozoic marine turtle groups, the thalassochelydians and sandownids, form a monophyletic clade on the stem-lineage of turtles, for which the name Angolachelonia (Mateus *et al.* 2009) is appropriate. Protostegids are found to be chelonioids, and statistical tests reject the possibility that they represent stem-group cryptodires, or stem-group turtles. Examination of pairwise similarity metrics between taxa used in my phylogeny suggest high levels of convergence between certain turtle groups for different partitions of the underlying data, providing possible explanations for alternative phylogenetic results in previous studies. Furthermore, all marine turtle clades that lived during the end of the Cretaceous survived the Cretaceous–Paleogene mass extinction, which is different to extinction patterns seen in other marine reptiles.

The second data chapter of this thesis (section 3) is the result of my studies of the cranial anatomy of turtles using CT data, which informed many of the character modifications implemented in the first data chapter. I use 3D renderings of CT data to illustrate the cranial and mandibular anatomy of the early Late Cretaceous protostegid *Rhinochelys*. Although some protostegid species are known from numerous specimens, their anatomy is quite poorly known, especially with respect to the skull (Seeley 1869; Lydekker 1889; Moret 1935; Collins 1970; Tong *et al.* 2006; Cadena & Parham 2015). This is because many specimens are either preserved on slabs with crushed skulls (e.g. Hirayama 1998; Tong *et al.* 2006) or in nodules that include completely preserved skulls, but in which most of the internal anatomy is concealed by matrix that is hard to prepare either mechanically or chemically (e.g. Collins 1970; Cadena & Parham 2018). My CT scans provide a unique opportunity to investigate the

cranial osteology and neuroanatomy of protostegids. A thorough understanding of the cranial anatomy of protostegids, especially in early representatives of the group like *Rhinochelys*, is important for several reasons. For example, it has been hypothesized that anatomical adaptations in the postcranial skeleton related to the marine habitat of protostegids could represent convergent acquisitions of these features with chelonioids, and falsely support relationships with those taxa (e.g. Cadena & Parham 2015). Specific focus on cranial anatomy can thus help to find phylogenetic evidence for one hypothesis or another independent of the postcranial characters functionally important for their ecology. Furthermore, cranial features such as the carotid circulation have been important in establishing the phylogenetic relationships of turtles more widely (e.g. Jamniczky 2007; Müller *et al.* 2011; Rabi *et al.* 2013). I CT scanned and segmented six cranial specimens of *Rhinochelys* from the Cambridge Greensand Member of the West Melbury Marly Chalk Formation in the United Kingdom. This sample includes the holotype specimens of all three species considered valid by the latest revision of the material by Collins (1970). My work represents the most detailed account of the cranial and mandibular anatomy of any protostegid, and provides novel data on intraspecific variation and the taxonomy of *Rhinochelys*. I provide a taxonomic revision of *Rhinochelys*, and lay out evidence for the hypothesis that only one taxon from Europe, *R. pulchriceps*, should be considered valid. Nevertheless, other turtle and sea turtle specimens from the Cambridge Greensand Member of the West Melbury Marly Chalk Formation indicate a higher diversity of turtles, specifically sea turtles, in the late Early Cretaceous of England. This previously unrecognized diversity prohibits the assignment of isolated postcranial material to *Rhinochelys* until skull-postcranial associations are found.

In my third data chapter (section four), I extend the phylogenetic work of my first data chapter by analysis of an expanded dataset focussed more specifically on the ingroup relationships of chelonioids, including protostegids. For this work, I considered more postcranial material (including fossil taxa that are only known from postcranial material), for which I did not have CT scans. My observations led to the addition and revision of several postcranial characters and the addition of 16 taxa with regard to the phylogeny presented in

chapter 2. The revision of postcranial characters is specifically aimed at body parts that are related to marine lifestyles, such as the forelimb or shell reduction, because these anatomical structures provide information on the sequence of marine adaptations that appeared throughout chelonioid evolution. The evolution of the chelonioid flipper is discussed in the context of my phylogenetic results. Whereas many important features of flippers were established early during sea turtle evolution, several pulses of character innovation are evident at the base of chelonioid subgroups (i.e. cheloniids, dermochelyids, 'advanced' protostegids). The addition of taxa further firmly establishes the crow-group chelonioid affinities of several Cretaceous taxa, providing further evidence that previous data used to calibrate molecular phylogenies underestimates the divergence times of chelonioids from other americhelydians.

Section 5 of this thesis represents an outlook chapter, but includes preliminary results from a Bayesian tip-dating analysis. I analyse my morphological dataset with a relaxed molecular clock model and a fossilized birth-death (FBD) model as a tree prior, and age data from fossils for the tree calibration. The preliminary analysis is consistent with *a posteriori* time-scaling methods of parsimony trees used in this thesis in estimating an Early Cretaceous age for the total-group of chelonioids, and an early Late Cretaceous age for the crown group. Age estimates are compared with those from a previous study using a node-dating approach (Joyce et al. 2013*b*), which arrived at younger ages for the divergence of chelonioids. Posterior estimates for the parameters of the FBD model, such as speciation and extinction rates, are briefly discussed. The presented analysis serves as a proof of concept and starting point to extend the analysis to a total-evidence model, which additionally uses molecular sequence data to estimate tree topology, branch lengths, and divergence times.

INSTITUTIONAL ABBREVIATIONS

ALMNH, Alabama Museum of Natural History, Tuscaloosa, AL, USA; **AMNH**, American Museum of Natural History, New York City, NY, USA; **AUMP**, Auburn University Museum of Paleontology, Auburn, AL, USA; **BP**, Bernhard Price Institute, Johannesburg, South Africa; **BSPG**, Bayerische Staatsammlung für Paläontologies und Geologie, Munich, Germany; **CAMSM**, Sedgwick Museum of Earth Sciences, Cambridge, UK; **CCNHM**, College of Charleston Natural History Museum, Charleston, SC, USA; **CM**, Carnegie Museum of Natural History, Pittsburgh, PA, USA; **CMM**, Carter County Museum, Ekalaka, MT, USA; **CMNH**, Cleveland Museum of Natural History, Cleveland, OH, USA; **DMNH**, Denver Museum of Nature and Science, Denver, CO, USA; **FCG–CBP**, Fundación Colombiana de Geobiología, Dentro de Investigaciones Paleontológicas, Villa de Leyva, Colombia; **FMNH**, Field Museum of Natural History, Chicago, IL, USA; **FUM**, Fur Museum (Museum Salling), Fur, Denmark; **FWMSH**, Fort Worth Museum of Science and History, Forth Worth, TX, USA; **IVPP**, Institute of Vertebrate Paleontology and Paleoanthropology, Beijing, China; **IRSNB**, Royal Belgian Institute of Natural Sciences, Brussels, Belgium; **IW**, Ingmar Werneburg private collection; **JM**, Jura-Museum, Eichstätt, Germany; **KUVP**, University of Kansas, Lawrence, KS, USA; **MAJ**, Musée d'archéologie du Jura, Lons-le-Saunier, France; **MCZ**, Museum of Comparative Zoology, Harvard University, Cambridge, MA, USA; **MGUAN-PA**, Museo Geológico da Universidade Agistino Neto, Luanda, Angola (Paleo-Angola Project Collection); **MIWG**, Museum of Isle of Wight Geology, Sandown, Isle of Wight; **MJSN**, JURASSICA Museum, Porrentruy, Switzerland; **MNA**, Museum of Northern Arizona, Flagstaff, AZ, USA; **MNB**, Naturhistorisches Museum Basel, Basel, Switzerland; **MPEF**, Museo Paleontológico Egidio Feruglio, Trelew, Argentina; **MRAC**, Musée Royal de l'Afrique Centrale, Tervuren, Belgium; **MSC**, McWane Science Center, Birmingham, AL, USA; **NHMM**, Natuurhistorisch Museum Maastricht, Maastricht, Netherlands; **NHMUK**, Natural History Museum, London, UK; **NMS**, National Museum of Scotland, Edinburgh, UK; **OCPDEK**, Office Chérifien des Phosphates, Khouribga, Morocco; **OUMNH**, Oxford University Museum of Natural History, Oxford, UK; **PIMUZ**,

Paläontologisches Institut und Museum der Universität Zürich, Zurich, Switzerland; **PIN**, Paleontological Insitute, Russian Academy of Sciences, Moscow, Russia; **PMOL**, Paleontological Museum of Liaoning, Shenyang Normal University, China; **QM**, Queensland Museum, Brisbane, Australia; **SMF**, Senckenberg Museum Frankfurt, Frankfurt, Germany; **SMNS**, Staatliches Museum für Naturkunde, Stuttgart, Germany; **SMU**, Shuler Museum of Paleontology, Southern Methodist University, Dallas, TX, USA; **TM**, Teylers Museum, Haarlem, Netherlands; **TMM**, Texas Memorial Museum, Austin, TX, USA; **TMP**, Royal Tyrell Museum, Drumheller, AB, Canada; **UCMP**, University of California Museum of Paleontology, Berkeley, CA, USA; **UJF**, Universite Joseph Fourier, Grenoble, France; **UMZC**, University Museum of Zoology, Cambridge, UK; **USNM**, United States National Museum, Washington, DC, USA; **WGJ**, Waler Joyce private collection; **YPM**, Yale Peabody Museum, New Haven, CT, USA; **ZIN PH**, Zoological Insitute of Russian Academy of Sciences palaeoherpotological collection, St. Petersburg, Russia.

2 A NEW PHYLOGENETIC HYPOTHESIS OF TURTLES WITH IMPLICATIONS FOR THE TIMING AND NUMBER OF EVOLUTIONARY TRANSITIONS TO MARINE LIFESTYLES IN THE GROUP

NOTES

This chapter has been published as a paper as Evers & Benson (2018*a*) in the journal *Palaeontology* (see References for full citation). Roger Benson contributed with CT scannings, analytical advice and text editing. All other data collection, data analysis, and writing have been done by myself.

ABSTRACT

Evolutionary transitions to marine habitats occurred frequently among Mesozoic reptiles. Only one such clade survives to the present: sea turtles (Chelonioidea). Other marine turtles originated during the Mesozoic, but uncertain affinities of key fossils have obscured the number of transitions to marine life, and the timing of the origin of marine adaptation in chelonioids. Phylogenetic studies support either a highly-inclusive chelonioid total-group including fossil marine clades from the Jurassic and Cretaceous (e.g. protostegids, thalassochelydians, sandownids), or a less inclusive chelonioid total-group, excluding those clades. Under this paradigm, these clades belong outside of Cryptodira, and represent at least one additional evolutionary transition to marine life in turtles. We present a new phylogenetic hypothesis informed by high resolution computed tomographic data of living and fossil taxa. Besides a well-supported Chelonioidea, which includes protostegids, we recover a previously unknown clade of stem-group turtles, Angolachelonia, which includes the Late Jurassic thalassochelydians, and the Cretaceous–Palaeogene sandownids. Accounting for the Triassic *Odontochelys*, our results indicate three independent evolutionary transitions

to marine life in non-pleurodiran turtles (plus an additional two–three in pleurodires). Among all independent origins of marine habits, a pelagic ecology only evolved once, among chelonioids. All turtle groups that independently invaded marine habitats in the Jurassic–Cretaceous (chelonioids, angolachelonians, bothremydid pleurodires) survived the Cretaceous–Palaeogene mass extinction event. This highlights extensive survival of marine turtles compared to other marine reptiles. Furthermore, deeply-nested clades such as chelonioids are found by the mid Early Cretaceous, suggesting a rapid diversification of crown-group turtles during the Early Cretaceous.

2.1 INTRODUCTION

Turtles are a major group of reptiles and show high ecological diversity, inhabiting marine, freshwater, and terrestrial environments. As an ecologically diverse extant group with an excellent fossil record, turtles provide information on the evolutionary dynamics of ecological transitions in vertebrates, and in particular the secondary reversion to marine life. Within turtles, multiple lineages independently adapted to marine life from as early as the Triassic (Gaffney *et al.* 2006; Li *et al.* 2008; Mateus *et al.* 2009; Anquetin *et al.* 2015; Ferreira *et al.* 2015). Of these, only chelonioids (sea turtles) survive to the present. Previous phylogenetic hypotheses imply at least four and as many as eight independent transitions to marine life in turtles, throughout their entire evolutionary history (e.g. Joyce 2007; Li *et al.* 2008; Mateus *et al.* 2009; Rabi *et al.* 2012; Anquetin *et al.* 2015). However, deep uncertainty regarding the phylogenetic affinities of several extinct groups renders the precise number highly uncertain. This lack of consensus on turtle phylogeny also affects our understanding of wider macroevolutionary dynamics, such as the mode and rate of morphological evolution during ecological transitions.

Several Mesozoic turtle groups have been recovered in distinctly different phylogenetic positions. These include the marine thalassochelydians, sandownids and protostegids, as well as the freshwater xinjiangchelyids, sinemydids and macrobaenids. Most

of these groups have been alternatively proposed to be stem-group turtles, stem-group cryptodires, or within the crown-group of cryptodires as stem- or crown-group chelonioids. Because the placements of these groups influence reconstructions of morphological changes during deep evolutionary divergences, they have implications for the relative phylogenetic placements of other clades. Furthermore, different phylogenetic hypotheses give rise to distinct conclusions regarding: (1) the number of times that marine ecologies have evolved within turtles; (2) the timing of secondarily marine adaptation in the chelonioid total-group; and (3) inferences of character state changes and polarities, which influence hypotheses of morphological evolution on the stem-group of cryptodires, and among turtles more widely. Resolving the phylogeny of key fossil groups can have substantive implications for our understanding of the evolution of turtles as a whole. In this chapter, I present a new phylogenetic analysis that helps to clarify these issues. Before I outline the methods used for this thesis, I review the diversity of secondarily-marine turtle groups, as well as the phylogenetic hypothesis that have arisen through research history for these groups.

2.1.1 Independent origins of marine life in turtles

Adaptation to marine life evolved independently in stem-group turtles and in both cryptodires and pleurodires. The stem-group turtle *Odontochelys semitestacea* from the middle Late Triassic (220 Ma) is generally interpreted as the oldest marine turtle based on its depositional environment (Li *et al.* 2008; Reisz & Head 2008; Lyson *et al.* 2010). Furthermore, *Odontochelys* has limb proportions characteristic of aquatic turtles, contrasting with other Triassic stem-group turtles (Joyce & Gauthier 2004; Li *et al.* 2008).

Among pleurodires, marine taxa have been identified in two phylogenetically-distinct lineages, documenting at least two independent instances of adaptation to marine life: the Cretaceous–Oligocene (and possibly Miocene) Bothremydidae (Gaffney *et al.* 2006; Rabi *et al.* 2012), and the Eocene–Pleistocene Stereogyina (Sánchez-Villagra *et al.* 2000; Winkler & Sánchez-Villagra 2006; Gaffney *et al.* 2011; Ferreira *et al.* 2015). Bothremydid phylogeny

suggests that there could be two independent origins of marine habits in that group, as the marine Taphrosphyini and the marine Bothremydina do not form a monophyletic group with respect to freshwater bothremydids (Gaffney *et al.* 2006; Rabi *et al.* 2012).

The number of independent lineages of marine turtles within the total group of cryptodires is less well understood. Chelonioidea, which includes all extant sea turtles, represents one unambiguous evolutionary origin of secondarily marine ecologies within the crown of cryptodires. Chelonioids form a clade of highly marine-adapted forms that are characterized by the presence of flippers, salt glands, incipient to well developed secondary palates, and a range of modifications of the shell, all of which represent adaptations to a marine lifestyle, and are observed in at least some fossil chelonioids (Mlynarski 1976; Zangerl 1980; Hirayama 1994). Undisputed marine stem-group chelonioids are also known from that time (*Toxochelys* spp.: Coniacian–Campanian, Nicholls 1988; Joyce *et al.* 2013*b*), but the phylogenetic position of some putative crown-group chelonioids from the Cretaceous (e.g. *Allopleuron hofmanni* from the Late Maastrichtian, Gray 1831) have been uncertain. The only non-marine turtles that have repeatedly been recovered as stem-group chelonioids are various 'macrobaenids' (usually including *Judithemys sukhanovi* from the Campanian of Canada; Parham & Hutchinson 2003) and 'sinemydids' (Brinkman & Wu 1999; Danilov & Parham 2008; Sterli 2010; Pérez-García 2012; Cadena & Parham 2015), but most authors argue against this (e.g. Zhou & Rabi 2015).

Other marine turtles have been recognized, especially from the Late Jurassic and Early Cretaceous. Depending on their phylogenetic position, these groups, the protostegids, thalassochelydians and sandownids, could represent additional, independent origins of marine adaptation (Fig. 2.1). Protostegids are known from the Barremian–Campanian (e.g. Zangerl 1953*a*; Collins 1970; Hirayama 1994, 1998; Hooks 1998; Kear & Lee 2006; Cadena & Parham 2015). Thalassochelydians include 'plesiochelyids', 'eurysternids', 'thalassemydids', *Solnhofia parsoni*, and *Jurassichelon oleronensis* from the Late Jurassic (e.g.; Gaffney 1975*b, c*; Rieppel 1980; Joyce 2000; Anquetin & Joyce 2014; Anquetin *et al.* 2014*a*, *b*, 2015, 2017*a*). Sandownids are known from the Cretaceous and Palaeogene (Aptian–Danian; Meylan *et al.*

2000; Mateus *et al.* 2009; Cadena 2015). Many distinct phylogenetic hypotheses have been proposed, not only for these groups, but also for their members. In the following, I provide summaries on all relevant groups, including evidence for their inferred ecologies and previously proposed phylogenetic relationships.

2.1.2 Non-pleurodiran marine turtles from the Mesozoic

Protostegids are a group of Cretaceous marine turtles with a cosmopolitan distribution (e.g. Zangerl 1953*a*; Collins 1970; Hirayama 1998; Kear & Lee 2006; Cadena & Parham 2015). They include the gigantic forms *Archelon ischryos* (Wieland 1896) and *Protostega gigas* (Cope 1871*a*) from the Campanian of North America, as well as early representatives such as *Santanachelys gaffneyi* from the Late Aptian or Early Albian of Brazil (Hirayama 1998) and *Desmatochelys padillai* form the Late Barremian or Early Aptian of Colombia (Cadena & Parham 2015). These taxa have been found in a monophyletic group in most phylogenetic studies so far (Hirayama 1994, 1998; Hooks 1998; Kear & Lee 2006; Cadena & Parham 2015; but see Gentry *et al.* 2018). They share unambiguous adaptations to a pelagic marine lifestyle with chelonioids, including the modification of hands into flippers and the reduction of the shell, and also an enlarged fenestra interorbitale indicative of salt glands (e.g. Wieland 1896, 1906; Case 1897; Hirayama 1998). Many studies have found protostegids on the stem-lineage of *Dermochelys* (the extant leatherback turtle; Hirayama 1994, Kear & Lee 2006; Bardet *et al.* 2013; Cadena & Parham 2015; Gentry *et al.* 2018), with a few exceptions (Joyce 2007; Anquetin 2012; and studies expanding these matrices; see below).

Thalassochelydians (*sensu* Anquetin *et al.* 2017*a*) are an assemblage of Late Jurassic turtles from central and western Europe (Anquetin & Chapman 2016; Anquetin *et al.* 2017*a*), and possibly Argentina (Fernández and de la Fuente 1988; de la Fuente and Fernández 2011). They are exclusively found in marine depositional environments, with 'plesiochelyids' and 'thalassemydids' found in sediments indicating open-marine carbonate platform

environments, and 'eurysternids' such as *Solnhofia parsoni* coming from more marginal marine settings (Anquetin *et al.* 2017*a*). Plesiochelyids have been found as a monophyletic group by almost all phylogenetic studies (e.g. Sterli 2010; Sterli & de la Fuente 2013; Anquetin *et al.* 2015; Evers & Benson 2018*a*; but see Anquetin 2012), but the monophyly of the more inclusive Thalassochelydia (including *Solnhofia parsoni*, *Jurassichelon oleronensis*, and plesiochelyids) has only recently been demonstrated (Anquetin *et al.* 2015; but see below). The marine habits of these taxa are supported by their oxygen isotope signatures, which indicate brackish environments for 'eurysternids', and fully marine environments for 'plesiochelyids' (Billon-Bruyat *et al.* 2005). Unlike chelonioids and protostegids, thalassochelydian limbs do not take the form of flippers, although their manus is notably elongated, indicating adaptation to aquatic locomotion (Anquetin *et al.* 2017*a*). Furthermore, an expanded fenestra interorbitale indicates the presence of salt glands, and the presence of shell fontanelles provides morphological evidence consistent with a marine lifestyle (Anquetin *et al.* 2017*a*). The shell bone histology is also consistent with an aquatic lifestyle (Scheyer *et al.* 2014).

Sandownids are a secondarily marine group of putative stem-group cryptodires currently known from four taxa ranging in age from the Aptian (*Sandownia harrisi*: Meylan *et al.* 2000) or possibly Late Barremian (*Leyvachelys cipadi*: Cadena 2015) to the Paleocene (*Brachyopsemys tingitana*: Tong & Meylan 2013). These taxa have been recovered as a clade by all phylogenetic studies that included more than one of them (Mateus *et al.* 2009; Tong & Meylan 2013; Cadena 2015). Their fossils come from shallow marine deposits, and distinctive morphological adaptations such as their extensive secondary palate indicative of a durophagous diet have been interpreted as marine adaptations (Mateus *et al.* 2009; Tong & Meylan 2013; Cadena 2015). Informative shell and postcranial material is only known from *Leyvachelys cipadi*. *Leyvachelys* lacks features found in pelagic marine turtles (cheloniids, dermochelyids, and protostegids) as it has an unflattened and unexpanded humerus and metacarpal, a strongly ossified contact between the plastron and carapace, and lacks shell

fontanelles (Cadena 2015). Sandownids are therefore thought to have lived in littoral habitats (Cadena 2015).

2.1.3 Previous phylogenetic work

Extant chelonioids include cheloniids (hard-shelled sea turtles) and the leatherback sea turtle, *Dermochelys olivacea*, the only dermochelyid. Molecular phylogenies find chelonioids within Cryptodira, as the sister group to Chelydroidea (Kinosternoidea + Chelydridae; e.g. Crawford *et al.* 2015; Perreira *et al.* 2017) in a clade called Americhelydia (Joyce *et al.* 2013*b*). The number of independent origins of marine adaptation among eucryptodiran lineages depends on the relationships of fossil marine taxa with respect to chelonioids. A summary of phylogenetic hypotheses recovered in previous studies is presented in Figure 2.1.

Protostegids have frequently been placed on the stem of Dermochelyidae (Hirayama 1994, Kear & Lee 2006; Tong & Meylan 2013; Bardet *et al.* 2013; Cadena & Parham 2015; Evers & Benson 2018*a*; Gentry *et al.* 2018; see Fig. 2.1E, H). However, Joyce (2007) and some subsequent analyses (Danilov & Parham 2006, 2008; Sterli & de la Fuente 2011, 2013; Anquetin 2012) have found protostegids as basal eucryptodires on the cryptodiran stem (Fig. 2.1A–B, F–G), or on the turtle stem (Sterli 2010; Sterli & de la Fuente 2011; Fig. 2.1C). Either position would imply that protostegids evolved marine habits independently of chelonioids, and have typically been found by analysis of the Early Cretaceous *Santanachelys* as the sole representative of protostegids in a global matrix. When recovered outside of Chelonioidea, *Santanachelys* has been found in a clade with *Solnhofia* (Danilov & Parham 2006), or *Solnhofia* and *Jurassichelon* to the exclusion of plesiochelyids (Joyce 2007; Pérez-García *et al.* 2012; Sterli & de la Fuente 2013; Sterli *et al.* 2013), or a clade including *Solnhofia*, *Jurassichelon*, and plesiochelyids (Anquetin 2012).

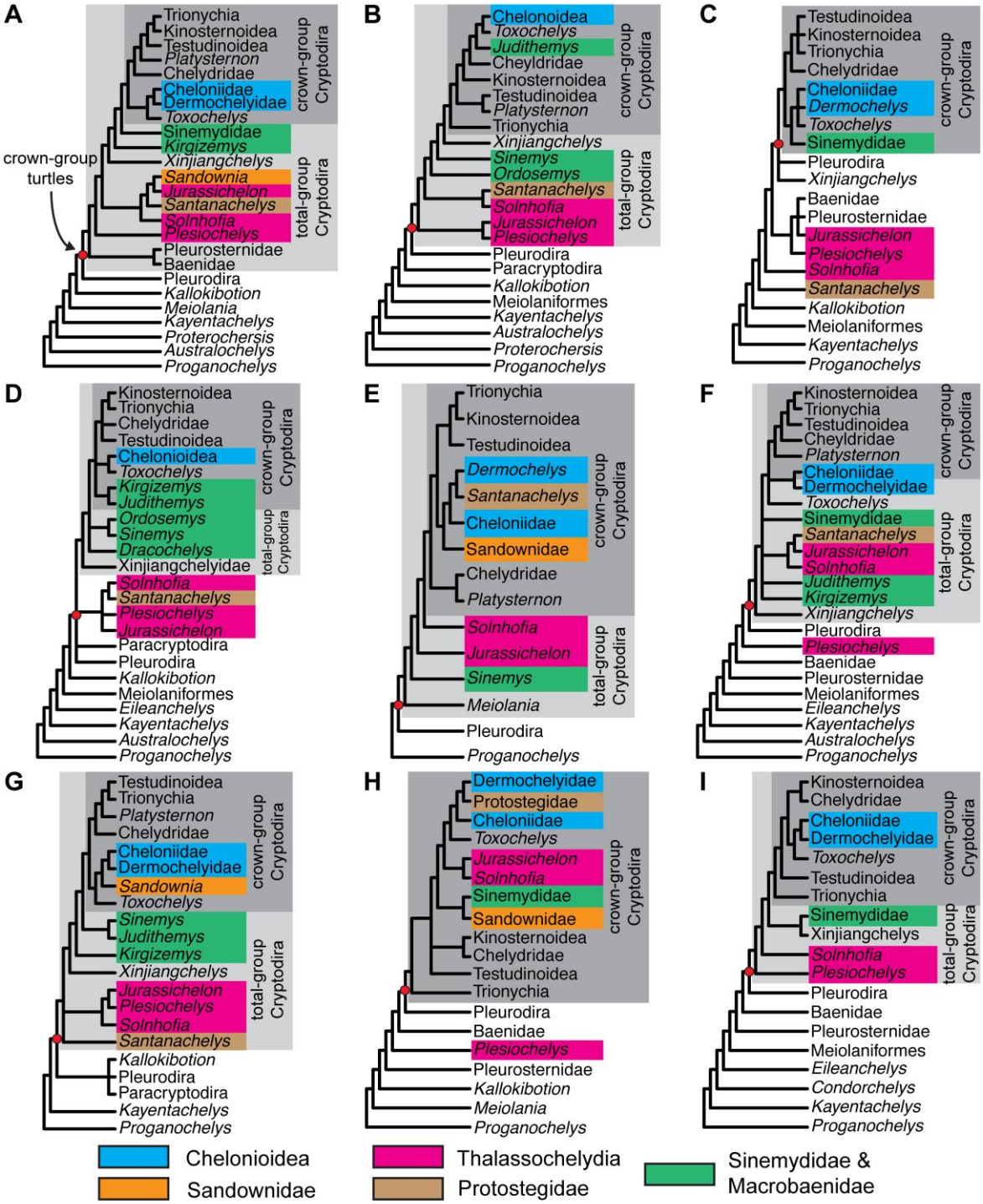


FIG. 2.1. Simplified phylogenetic hypotheses of selected previous studies highlighting different phylogenetic positions that have been proposed for marine, non-pleurodiran turtles. **A**, Joyce (2007); **B**, Danilov & Parham (2008); **C**, Sterli (2010); **D**, Anquetin (2012); **E**, Tong & Meylan (2013); **F**, Sterli & De la Fuente (2013); **G**, Anquetin *et al.* (2015); **H**, Cadena & Parham (2015) and Cadena (2015); **I**, Zhou & Rabi (2015). Note that the colours denote proposed clades, following Anquetin *et al.* (2017) for Thalassochelydia, Tong & Meylan (2013) for Sandownidae; Cadena & Parham (2015) for Protostegidae; Rabi *et al.* (2014) for Sinemydidae/Macrobaenidae. Note that 'Chelonioidea' is used to denote the crown-group herein.

Many previous studies have found the taxa included in Thalassochelydia (*sensu* Anquetin *et al.* 2017*a*) as polyphyletic or paraphyletic (Danilov & Parham 2006, 2008; Joyce 2007; Mateus *et al.* 2009; Anquetin 2012; Pérez-García *et al.* 2012; Sterli & de la Fuente 2013; Sterli *et al.* 2013; Cadena 2015; Cadena & Parham 2015; see Fig. 2.1A–F, I, H). This is in part because of the uncertainty that surrounds the positions of *Jurassichelon* ('*Thalssemys*' *moseri* in studies previous to the revision provided by Pérez-García 2015) and *Solnhofia*, which have been variously grouped with non-thalassochelydian taxa such as the early protostegid *Santanachelys* (Danilov & Parham 2006; Joyce 2007; Pérez-García *et al.* 2012; Sterli & de la Fuente 2013; Sterli *et al.* 2013), but also sandownids (e.g. Mateus *et al.* 2009). Nevertheless, some concept of either one or more clades of Late Jurassic marine turtles has been present in many phylogenetic studies. Three major hypotheses have been presented concerning the positions of these turtles (regardless of their monophyly), as either: (1) stem-group chelonioids, implying an inclusive clade of marine cryptodires that originated in the Late Jurassic; (2) stem-group cryptodires, and therefore representing a distinct, independent origin of marine life from that in chelonioids; (3) stem-group turtles, also representing a distinct origin of marine life. It is clear therefore that thalassochelydians share some traits with chelonioids, and others with stem-group turtles or stem-group cryptodires. Indeed, when constituents of Thalassochelydia have been found as stem-group chelonioids, groups that are otherwise widely regarded as stem-group cryptodires or stem-group turtles (xinjiangchelyids, sinemydids; Zhou & Rabi 2015), have sometimes also been found on the stem-group of chelonioids (Cadena & Parham 2015). However, a sinemydid-chelonioid relationship has also been found in some studies irrespective of the position of thalassochelydians (Brinkman & Wu 1999; Danilov & Parham 2008; Sterli 2010; Pérez-García 2012). Clearly, resolving the phylogenetic affinities of Thalassochelydia is of great importance for our knowledge of turtle evolution.

Little consensus exists about the relative placement of sandownids (Fig. 2.1A, E, G–H). Specifically the relationships of sandownids to 'eurysternids', plesiochelyids and chelonioids are unclear. The first reported sandownid, *Sandownia harrisi*, was originally interpreted as a

basal member of Trionychia (softshell turtles; Meylan *et al.* 2000). However, later studies found little support for this placement (e.g. Joyce 2007), and the patterning of the carapace of *Levyachelys* is also inconsistent with this hypothesis (Cadena 2015). *Sandownia* (commonly the only sandownid taxon included in global phylogenetic studies) was tentatively placed on the stem of Cryptodira as a basal eucryptodire by Joyce (2007). Mateus *et al.* (2009) found sandownids as sister to *Solnhofia* in a group called Angolachelonia, which formed part of a marine grade including *Jurassichelon*, *Portlandemys* and *Plesiochelys* on the stem of Cryptodira. Tong & Meylan (2013) and Anquetin *et al.* (2015) found sandownids as the sister-taxon of chelonioids, and *Solnhofia* and *Jurassichelon* as eucryptodires. Finally, Cadena (2015) recovered sandownids as the sister to xinjianchelyids+sinemydids as stem-group chelonioids, forming a large panchelonioid clade including *Jurassichelon* and *Solnhofia*, but excluding plesiochelyids, which were found as stem-group turtles (Cadena 2015).

2.2 MATERIAL AND METHODS

2.2.1 Character dataset

For my character matrix, I used information from three primary sources: Cadena (2015), Zhou and Rabi (2015), and Anquetin *et al.* (2015). All these matrices are modified versions of previous studies, and can all be traced back to Joyce (2007), which represents the first global phylogenetic analysis of Mesozoic turtles. All three source matrices are global in scope, but have different foci. Cadena's (2015) matrix is a modified version of the work of Cadena and Parham (2015) and includes character information specific to sandownids. The matrix of Cadena and Parham (2015) is a combination of global matrices (Joyce 2007; Anquetin 2012; Sterli 2008; Sterli & de la Fuente 2013) but importantly includes characters from matrices that were designed to specifically test chelonioid relationships (Hirayama 1994; Hirayama 1998; Kear & Lee 2006; Parham & Pyenson 2010). The Zhou and Rabi (2015) matrix is similarly based on several previous studies, which were focussed on the

relationships of stem-group turtles and stem-group cryptodires (Joyce 2007; Sterli 2008; Sterli & de la Fuente 2013; Rabi *et al.* 2013, 2014; Zhou *et al.* 2014). Finally, the analysis of Anquetin *et al.* (2015) was specifically focussed on thalassochelydian relationships. By combining the character lists of these studies, I attempt to capture all morphological variation documented so far among non-pleurodiran turtles. The 257 characters of Cadena (2015) were reconciled with the slightly different character definitions given in the other two studies, and were further modified by my own observations. This resulted in a phylogenetic data matrix of 345 characters and 80 taxa. In total, 70 characters of Cadena & Parham (2015) were modified (see Coding strategy), and modified versions of 13 characters used by Anquetin (2012), Anquetin *et al.* (2015), Cadena (2015), Havlik *et al.* (2014), and Zhou & Rabi (2015) were added. I also added 58 new cranial and mandibular characters. I re-scored all cranial and mandibular characters from both Cadena & Parham (2015) and other sources, for all taxa in my matrix. The scorings are based on first hand examination of specimens (44 taxa), examination of CT scans for 59 taxa, photographs of specimens I did not see first hand (shared by Dr. Walter Joyce), and published descriptions (data sources in Table 2.1). An illustrated character list with discussions of character modifications and additions, and justifications for modified scorings, as well as the matrix itself, are available in Appendix S1.

2.2.2 Coding strategy

Phylogenetic analyses of morphology are used to infer relationships from a set of comparative anatomical observations. The concept of homology is central to the delimitation of these observations as characters and character states. Homology is the hypothesis that similar attributes shared by different species are equivalent to one another due to common ancestry, and therefore reflect their phylogenetic relationships (Platnick 1979; Eldregde & Cracraft 1980; de Pinna 1991; see Patterson 1982 for a disambiguation and extensive discussion of homology). Hypotheses of homology are established based on topographic and ontogenetic correspondence and on compositional similarity of traits (Patterson 1982;

Rieppel 1988; de Pinna 1991; Hawkins *et al.* 1997). These initial ('primary'; de Pinna 1991) hypotheses of homology are embodied by the characters and character states, and are tested against one another by means of congruence in parsimony analysis, which maximizes the number of initial homology propositions that are upheld as true homology rather than the result of convergent evolution (homoplasy; Patterson 1982; de Pinna 1991).

Character construction therefore represents the proposition of initial hypotheses of homology based on observations of similarity. Character states are different forms that a homologous trait (i.e. the character) can take among organisms, and are equivalent transformations of one another on a single hierarchical level (the level of the character) (Platnick 1979; de Pinna 1991; Hawkins 1997). Characters and character states therefore form a hierarchical framework of homology propositions. For example, a specific site in the aligned nucleotide sequences of several organisms is hypothesized to be comparable on the character level, and the (four or five) nucleobases represent possible variation of this character on the character state level (and could therefore not represent separate characters themselves) (Pleijel 1995). Construction of morphological characters is potentially more subjective. Nevertheless, I have taken various steps to ensure that my cladistic characters for turtles, both new, and modified from previous analyses, reflect homology (described below).

Character states should also be independent of each other (e.g. Pimental & Riggins, 1987; Strong & Lipscomb 1999). Non-independence of character states is problematic because it results in a single observation of similarity being coded twice, and therefore the character state is arbitrarily given a greater weight than others (Wilkinson 1995; Strong & Lipscomb 1999). Logical dependence between characters exists when the score of a taxon for one character directly affects the scoring of the same taxon in another character (e.g. coding the absence *and* zero size of a feature; Wilkinson 1995), and this can be readily avoided. Biological dependence is a hypothesis that character states of different characters are non-independent due to functional or developmental linkage (Wilkinson 1995). Information on the underlying biological cause for such a linkage if often not available, which makes is hard to fully avoid biological independence in character construction.

TABLE 2.1. Sources for scorings in my character–taxon matrix.

Taxon	Specimen(s) used for character scoring	References used for character scoring	Personal observation of taxon	CT
Allaeochelys libyca	**BSPG 1991 II 130**	Havlik *et al.* 2014	yes	yes
Allopleuron hoffmanni	**NHMUK R4291;** NHMM 000001	Mulder 2003	yes	yes
Annemys sp.	**IVPP V18106**	Brinkman *et al.* 2013	no	yes
Annemys levensis	PIN 4636-4-2	Shukanov 2000; Rabi *et al.* 2014	no	no
Annemys latiens	PIN 4636-6-1	Rabi *et al.* 2014	no	no
Apalone spinifera emoryi	**FMNH 22178**	no additional references used	yes	yes
Araripemys barretoi	**AMNH 30778**	Meylan 1996; Gaffeny *et al.* 2011	yes	yes
Archelon ischyros	YPM 3000	Wieland 1896, 1900, 1902	yes	no
Argillochelys cuneiceps	**NHMUK R38955; NHMUK R41636**	no additional references used	yes	yes
Arundelemys dardeni	**USNM 497740**	Lipka *et al.* 2006	no	yes
Australochelys africanus	**BP/1/4933**	Gaffney & Kitching 1995	yes	yes
Baptemys wyomingensis	YPM 374, 3758; DMNH 511	Meylan & Gaffney 1989; Knauss 2014	no	no
Bouliachelys suteri	**QMF 31669**	Kear & Lee 2006	no	yes
Brachyopsemys tingitana	AMNH 30001; **AMNH 30612**	Tong & Meylan 2013	yes	yes
Caretta caretta	**NHMUK 1938.1.9.1**	no additional references used	yes	yes
Carettochelys insculpta	**NHMUK 1903.7.10.1**	no additional references used	yes	yes
Chelodina oblonga	**NHMUK 64.12.22**	no additional references used	yes	yes
*Chelodina longicollis**	unknown (specimen # not given in Cadena & Parham 2015)	Cadena & Parham 2015	no	no
Chelonia mydas	**NHMUK 1969.776**	no additional references used	yes	yes
Chelonoidis sp.	**SMF 67582**	no additional references used	no	yes
*Chelonoidis chilensis**	unknown (specimen # not given in Cadena & Parham 2015)	Cadena & Parham 2015	no	no
Chelus fimbriatus	**NHMUK 81.9.27.4**	no additional references used	yes	yes
Chelydra serpentina	**SMF 32846**	no additional references used	no	yes

Taxon	Specimen(s) used for character scoring	References used for character scoring	Personal observation of taxon	CT
Chrysemys picta	**NHMUK 76.1.31.19**	no additional references used	yes	yes
Chubutemys copelloi	MPEF-PV1236	Gaffney et al. 2007; Sterli *et al.* 2015	no	no
Dermatemys mawii	**SMF 59463**	no additional references used	no	yes
Dermochelys coriacea	**FMNH 171756; UMZC R3031**	no additional references used	yes	yes
Desmatochelys lowii	**KUVP 1200**	no additional references used	no	yes
Desmatochelys padillai	FCG-CBP 01, 13, 15, 39, 40; UCMP 38345, 382456	Cadena & Parham 2015	no	no
Dracochelys bicuspis	IVPP V4075; IVPP V12091	Gaffney & Ye 1992; Brinkman 2001	no	no
Eileanchelys waldmanni	**NMS.G.2004.31.15**; NMS.G.2004.31.16a-f	Anquetin 2010	yes	yes
Elseya dentata	**NHMUK 76.5.19.77**	no additional references used	yes	yes
Emarginachelys cretacea	KUVP 23488	Whetstone 1978	no	no
Emys orbicularis	**WGJ1987a**	no additional references used	no	yes
Eochelone brabantica	**NHMUK R37213**	Casier 1968	yes	yes
Eosphargis breineri	FUM-N-1450	Nielsen 1959	yes	no
Eretmochelys imbricata	**FMNH 22242**	no additional references used	yes	yes
Eubaena cephalica	**DMNH 96004**; AMNH 4948, 2602, 2604, 2606; YPM 1785	Gaffney 1972*a*, 1979; Gaffney 1982a, b	no	no
Geoclemys hamiltoni	**NHMUK 87.9.30.1**	no additional references used	yes	yes
Glyptops plicatulus	AMNH 336; YPM 1784, 4717, 5821	Gaffney 1979	no	no
Gopherus polyphemus	**FMNH 211815**	no additional references used	yes	yes
Judithemys sukhanovi	TMP 87.2.1	Parham & Hutchinson 2003	no	no
Jurassichelon oleronensis	**PIMUZ AIII 514**	Rieppel 1980	yes	yes
Kallokibotion bajazidi	NHMUK R4918; **NHMUK R4921**; **NHMUK R4925**	Gaffney & Meylan 1992	yes	yes
Kayentachelys aprix	**TMM 4370-2,** 43653-1; MCZ 8914-8917; MNA V1558, V2664	Sterli & Joyce 2007; Gaffney & Jenkins 2010	no	yes
Kinosternon suburum hippocrepis	**FMNH 211711**	no additional references used	yes	yes

Taxon	Specimen(s) used for character scoring	References used for character scoring	Personal observation of taxon	CT
*Kinosternon flavescens**	unknown (specimen # not given in Cadena & Parham 2015)	Cadena & Parham 2015	no	no
Kirgizemys dmitrievi	ZIN PH7/15	Danilov *et al*. 2006	no	no
Kirgizemys hoburensis	PIN 3334-4; PIN 3334-35; PIN 3334-36	Sukhanov 2000	no	no
Lepidochelys kempii	**M009/08**	Jones *et al*. 2012	no	yes
Lepidochelys olivacea	**SMNS 11070**	no additional references used	yes	yes
Levyachelys cipadi	FCG-CBP-71; SMU 75377, 72852, 74982, 75327; FWMSH 93B-17	Vineyard 2009; Cadena 2015	no	no
Lissemys punctata	SMF 74141	no additional references used	no	yes
Macrochelys temminckii	**FMNH 22111**	no additional references used	yes	yes
Meiolania platyceps	**NHMUK R682**; specimens listed in Gaffney 1983	Gaffney 1983	yes	yes
Natator depressus	**R112123**	Jones *et al*. 2012	no	yes
Notochelone costata	**NHMUK R9590**	no additional references used	yes	yes
Ocepechelon bouyai	OCPDEK/GE516	Bardet *et al*. 2013	no	no
Ordosemys sp.	**IVPP V12092**	Brinkman & Wu 1999	no	yes
Pelodiscus sinensis	**IW576-2**	no additional references used	no	yes
Pelomedusa subrufa	**SMF 70504**	no additional references used	yes	yes
Phrynops geoffranus	**SMF 45470**	no additional references used	no	yes
Platysternon megacephalum	**SMF 69684**	no additional references used	no	yes
Plesiochelys planicpes	**OUMNH J1582**	Gaffney 1975*b*; Gaffney 1976	yes	yes
Plesiochelys etalloni	**MNB 435**	Gaffney 1975*b*; Gaffney1976	yes	yes
Pleurosternon bullockii	**UMZC T1041**	Evans & Kemp 1975	no	yes
Podocnemis unifilis	**FMNH 45657**	no additional references used	yes	yes
*Podocnemis expansa**	unknown (specimen # not given in Cadena & Parham 2015)	Cadena & Parham 2015	no	no
Portlandemys mcdowelli	**NHMUK R2914**	no additional references used	yes	yes

Taxon	Specimen(s) used for character scoring	References used for character scoring	Personal observation of taxon	CT
Proganochelys quenstedti	SMNS 15759, 16980	Gaffney 1990	yes	no
Protostega gigas	AMNH 1502, 1503; CMNH 1421; FMNH PR2, P27385	Case 1897; Hay 1908	yes	no
Puppigerus camperi	**NHMUK R14375**	Moody 1974	yes	yes
Rhinochelys pulchriceps	**CAMSM B55775, B55776, B55783; NHMUK R43980, R2226, R35197**	no additional references used	yes	yes
Sandownia harrisi	**MIWG 3480**	Meylan *et al*. 2000	yes	yes
Sinemys gamera	IVPP V9532-11	Brinkman & Peng 1993	no	no
Sinemys lens	IVPP V9533-1; IVPP V9533-3	Brinkman & Peng 1993	no	no
Solnhofia parsoni	**TM 4023**	Gaffney 1975*c*	yes	yes
Staurotypus salvinii	**NHMUK 1879.1.7.5**	no additional references used	yes	yes
*Staurotypus triporcatus**	unknown (specimen # not given in Cadena & Parham 2015)	Cadena & Parham 2015	no	no
Sternotherus minor	**FMNH 211696**	Bever 2009*a*	yes	yes
*Sternotherus odoratus**	unknown (specimen # not given in Cadena & Parham 2015)	Cadena & Parham 2015	no	no
Testudo marginata	**FMNH 51672**	no additional references used	yes	yes
*Testudo hermanni**	unknown (specimen # not given in Cadena & Parham 2015)	Cadena & Parham 2015	no	no
Toxochelys sp.	AMNH1496, **5118**; FMNH UR3; **FMNH PR219,** PR648	Hay 1896; Nicholls 1988	yes	yes
Xinjiangchelys radiplicatoides	**IVPP V9539-1**	Brinkman et al. 2013	no	yes
Xinjiangchelys wusu	PMOL-SGPA0100-1; PMOL-SGPA0100-3	Rabi *et al.* 2013	no	no

*Species indicated by asterisk were used only for postcranial scores; **Bold** specimen numbers indicate specimens for which CT scans were available.

Many morphological characters used in previous studies of turtle phylogeny combine complex observations across multiple hierarchical levels of similarity, or lump together independently varying character states. I re-coded characters so that independently varying aspects of morphological variation are coded in separate characters. For example, character 10 of Cadena & Parham (2015) was defined as:

> 'Jugals, jugal-squamosal contact: 0 = present; 1 = absent, contact between postorbital and quadratojugal present.'

In this character definition, the absence of a jugal-squamosal character is assumed to be linked to the presence of a postorbital-quadratojugal contact. The character includes the assumption that a postorbital-quadratojugal character must be present when a jugal-squamosal contact is absent. However, these contacts vary independently from one another, as taxa exist (trionychids) in which a postorbital-quadratojugal contact is absent, but a jugal-squamosal contact is also absent. The approach taken here is to break up this character into two separate characters, which each code for one of the contacts (our characters 25 and 42).

I also re-coded characters so that observations across multiple hierarchical levels of similarity are coded in separate characters. For example, I modified character 60 of Cadena & Parham (2015), which was phrased as:

> 'Epipterygoid: 0 = present, rod like; 1 = present, laminar; 2 = absent.'

The comparative anatomical observations underlying this and similar characters include both the absence of a certain feature, and variation in the shape of that feature when present (the 'no tail; red tail; blue tail' problem; Maddison 1993; Smith 1994; Hawkins *et al.* 1997; Brazeau 2011). Coding these observations into a single character, as done in most turtles studies (e.g. Joyce 2007; Cadena & Parham 2015; but see Anquetin 2012) assumes that the condition of having no epipterygoid is on the same hierarchical level as the observed

shape conditions of taxa with epipterygoids. This disregards the homology implied by the presence of an epipterygoid in various taxa, irrespective of its shape (Hawkins *et al.* 1997), resulting in loss of information.

To reflect the hierarchical levels of similarity of these observations of the epipterygoid, and other characters in our analysis, I used a hierarchical coding strategy. For the above example, this reformulation results in two separate characters. One character codes for the presence vs. absence of the feature (e.g. epipterygoid; my character 87), and the second codes for the various shapes that the feature can take (e.g. epipterygoid shape; my character 88) (Hawkins *et al.* 1997; Brazeau 2011; see Anquetin 2012 for a turtle study using the same approach). Logical dependence of the character states of the second character on the first is avoided by scoring the second character as inapplicable ('-') when the first character is scored as 'absent'. Inapplicability does not introduce logical dependency (contra Strong & Limpscomb 1999), because it does not represent a separate character state, and transitions to 'inapplicable' do not count towards the length of a cladogram. However, inapplicable scores can be problematic because inapplicability is treated the same as missing data in software implementations of parsimony analysis (e.g. Platnick *et al.* 1991; Strong & Lipscomb 1999; Brazeau *et al.* 2017). This can introduce illogical character state reconstructions during the optimization process (e.g. Platnick *et al.* 1991; Maddison 1993). This problem relates to computational issues that may be solved in future generations of software (e.g. Brazeau *et al.* 2017), and problems with inapplicable character states are herein taken to be less problematic than the homology issues of compound characters discussed above (Strong & Lipscomb 1999; Hawkins *et al.* 1997).

Some of my characters appear superficially to be hierarchical compound characters (as in Cadena & Parham 2015, character 60; above), because they include an absence state as well as several other non-absence states. However, these characters are measurements such as the size of a structure, for which absence equates to zero. It is therefore appropriate to treat their character states as homologous with each other at the same hierarchical level. For example, my character 7 (character 7of Cadena & Parham (2015)):

> 'Prefrontal, dorsal prefrontal exposure: 0 = present, large; 1 = present, reduced; 2 = absent or near absent.'

My approach also differs from some recent analyses of turtles (e.g. Anquetin 2012) that exclusively used binary characters. Instead, I coded instances for which multiple conditions are observed for a character as multistate characters, reflecting the hypothesis that these alternative conditions represent transformations of a single underlying feature. For example, my character 297 (identical to character 210 of Cadena & Parham (2015)):

> 'Caudals, anterior caudal centra: 0 = amphicoelous; 1 = procoelous or platycoelous; 2 = opisthocoelous.'

The alternative approach of only using binary characters (e.g. Anquetin 2012 for turtles) requires the construction of a series of characters, or ignoring observations to artificially create binary characters, or lumping a set of distinct character states into a single character state (as done for the above example by Anquetin (2012): ch 160, in which the conditions of procoely and opisthocoely are lumped into a single character state). Anquetin (2012) justified the usage of binary characters by stating that this approach minimizes the amount of 'a priori assumptions about homology' (Anquetin 2012: p. 5). However, this avoidance of homology proposition misapplies the similarity criterion used to establish primary hypotheses of homology, which are always *a priori* hypotheses (de Pinna 1991; Hawkins *et al.* 1997). Instead of avoiding assumptions of homology, the approach of Anquetin (2012) generates unexpected hypotheses of homology (e.g. that procoely and opisthocoely are interchangeable, and homologous with each other on a low hierarchical level).

2.2.3 Taxon sampling

Operational taxonomic units (OTUs) were chosen specifically to test the phylogenetic relationships of non-pleurodiran marine turtles, and I preferentially used taxa for which I had CT data. My matrix includes many chelonioids, thalassochelydians, protostegids, and sandownids (Table 2.1). To test the placement of these groups in a global framework, I also included a thorough sample of stem-group turtles, including Triassic and Early Jurassic species, as well as paracryptodires and meiolaniforms. I further included a range of xinjiangchelyids, sinemydids, and macrobaenids, which have been hypothesized to be stem-group cryptodires (e.g. Zhou & Rabi 2015). I sampled extant representatives of modern clades including pleurodires, and all families of turtles. I included early fossil representatives of extant families when CT data was available to us or when sufficiently detailed anatomical descriptions were available in the literature. Of particular importance, two fossil chelydroids, *Emarginachelys cretacea* and *Baptemys wyomingensis,* were included because chelydroids (kinosternoids+chelydrids) are the extant sister-group to chelonioids (Crawford *et al.* 2015), and fossil representatives of this group can thus influence character optimizations for the total group of Americhelydia (chelydroids+chelonioids).

Most of my OTUs represent modern or fossil taxa on the species level, but some OTUs are supraspecific: the extant taxa *Chelodina*, *Chelonoidis*, *Kinosternon*, *Podocnemis*, *Staurotypus*, *Sternotherus*, and *Testudo*. This was done because my CT scans, which were used to re-score the cranial and mandibular characters, belonged to different species from those used by Cadena & Parham (2015) (Table 2.1), and I retained their postcranial characters. I chose to score a supraspecific OTU for *Toxochelys* because this allowed inclusion of data from specimens that have been assigned to different species, and thus score a more complete OTU. Species assignments regarding specimens of *Toxochelys* are currently uncertain (Zangerl 1953*b*; Nicholls 1988; Brinkman *et al.* 2006), particularly because the holotype specimens of valid species are relatively incomplete and lack cranial material. Pending a taxonomic revision of *Toxochelys* material, I consider it best to refer most *Toxochelys* material to *Toxochelys* sp., as done by some other authors (e.g. Brinkman *et al.* 2006).

The protostegid *Rhinochelys pulchriceps* was scored primarily from CT scans of the holotype specimen CAMSM B55775. However, I also used data from CT scans of other specimens, which have been referred to different species of *Rhinochelys* (Collins 1970; see Table 2.1 for specimens used). These added information on the mandible (*R. cantabrigiensis*: CAMSM B55783; *R. elegans*: CAMSM B55776). In my second data chapter, I argue that all British specimens of *Rhinochelys* represent a single species, and I therefore consider all material in Collins (1970) to be *Rhinochelys pulchriceps*.

2.2.4 CT data and 3D models used in this study

I used high-resolution X-ray computed-tomography (CT) data for as many taxa as possible (summarized in Table 2.1). To support my anatomical observations and opinions stated throughout this work, I deposited several CT datasets and 3D models generated through manual segmentation in the software Mimics (versions 16.0–19.0) (http://biomedical.materialise.com/mimics) at MorphoSource (http://www.MorphoSource.org; Evers & Benson 2018*b*; see data archiving statement below). The data provided represent a sample of fossil and extant turtle specimens that have been extensively used in character construction and illustration of characters (see Appendix S1.2). These are: *Apalone spinifera emroyi* (FMNH 222178), *Dermochelys coriacea* (UMZC R3031), *Elseya dentata* (NHMUK 76.5.19.77), *Gopherus polyphemus* (FMNH 211815), *Lepidochelys olivacea* (SMNS 11070), *Phrynops geoffranus* (SMF 45470), *Plesiochelys planiceps* (OUMNH J1582), *Argillochelys cuneiceps* (NHMUK R38955), *Sandownia harrisi* (MIWG 3480), *Solnhofia parsoni* (TM 4023), *Sternotherus minor* (FMNH 211696), and *Rhinochelys pulchriceps* (CAMSM B55783; referred to *Rhinochelys cantabrigiensis* by Collins (1970), but see section on taxon sampling). Because scanning parameters varied between all scans, details are given in the online repository with the data (Evers & Benson 2018*b*), and are not summarized here. Besides these published models, I prepared full skull segmentations (i.e. each bone is individually segmented on at least one side of the skull for all preserved

elements) for a range of fossil and modern turtles, including *Apalone spinifera emroyi*, *Araripemys barretoi*, *Bouliachelys suteri*, *Carettochelys insculpta*, *Chelus fimbriatus*, *Eileanchelys waldmanni*, *Eochelone brabantica*, *Kallokibotion bajazidi*, *Ordosemys* sp., *Podocnemis unifilis*, and *Puppigerus camperi*. Many more species have been partially segmented (for instance only the braincase). These data have not been formally published yet, because I am planning to use them toward other, unpublished manuscripts before making them publically available.

2.2.5 Similarity matrix

To illustrate the structure of my dataset, I produced heatmaps of similarity matrices calculated from my character taxon matrix in R (R Core Team 2016). Polymorphisms and missing data ('?') were treated as inapplicable data. Similarity between two taxa was calculated as the number of identical scoring matches between these taxa divided by the number of comparable scores between them (e.g. Sneath & Sokal 1973; Foote 1994; Wagner 1997; see Benson & Druckenmiller 2014 for a similar code). The resulting values are represented in a symmetric similarity matrix. Similarity matrices were calculated for the total dataset, and partitions of that dataset representing cranial and mandibular characters, shell characters, limb characters, and axial+girdle characters. For the anatomical partitions of the total dataset, taxa with no anatomical information for the respective partition, as well as taxa with 90% or more missing data were excluded. Each similarity matrix was coloured by assigning a spectrum of colours to the similarity values of each matrix using the package gclus (Hurley 2012). The R code for calculating similarity and producing the heatmaps is available in Appendix S1.13.

2.2.6 Parsimony Analysis

Tree searches were performed in TNT 1.5 for Windows (Goloboff *et al.* 2008; Goloboff & Catalano 2016). For all analyses, I used a molecular backbone constraint following the topology of Pereira *et al.* (2017) for extant taxa (see Appendix S1.10 for constraint command used in TNT). All fossil taxa were left unconstrained and were thus allowed to fall anywhere within the constrained topology of extant taxa. *Proganochelys quenstedti* was set as the outgroup. In TNT, new technology algorithms were used with default settings, and tree drifting (Goloboff 1999) and parsimony rachet (Nixon 1999) enabled. The initial level of the driven search was set to 30, and the number of times the minimum tree length should be obtained was set to 30. This procedure does not require specifying a number of replicates to be performed (Goloboff 1999; Giribet 2007). The most parsimonious trees (MPTs) of this analysis were then subjected to a final round of tree bisection and reconnection (TBR). The resulting MPTs were used to construct a strict consensus tree.

Characters were treated as unordered and equally weighted in my initial analysis. I also executed a second run in which several characters were ordered, for comparison (characters 7, 14, 18, 34, 44, 67, 76, 79, 90, 93, 94, 103, 107, 123, 130, 131, 138, 142, 147, 205, 210, 217, 248, 253, 292, 305, 325, 339, 340, 344). Ordering character states represent *a priori* hypotheses that transitions between character states only occur in a specific sequence (e.g. Wilkinson 1992, 1995). However, prior knowledge about the evolutionary sequence of character state transitions is often missing or otherwise not substantiated by evidence. Therefore, I only ordered multistate characters in which one character state was directly intermediate in form, size, or number of two other states (for instance character 340: Size of ulnare vs. intermedium: 0 = ulnare smaller than intermedium; 1 = ulnare nearly as large as intermedium; 2 = ulnare much larger than intermedium). If clear intermediates are not evident, the states were left unordered (for instance character 260: Medial contact of extragulars: 0 = absent; 1 = contacting each other anterior to gulars; 2 = contacting each other posterior to gulars).

Bremer support was calculated in TNT, using the absolute Bremer support setting and TBR branch swapping on existing trees to generate suboptimal trees. Character optimization was performed in PAUP* for Macintosh (Swofford 2002) because TNT only returns unambiguous synapomorphies (i.e. those in which ACCTRAN and DELTRAN agree in determining a character state change), whereas the optimization criterion can be specified in PAUP*. The optimization was computed on a fully resolved tree. This tree was chosen from the MPTs on the basis of high congruence with a 50% majority rule consensus tree. The most important differences of the tree selected for optimization and my consensus topology are that paracryptodires are monophyletic and that the species of *Sinemys* form a clade that is sister group to all remaining sinemydids (see Fig. S1.75). The tree topology chosen for the optimization, as well as unambiguous, ACCTRAN, and DELTRAN optimizations for all characters as well as all nodes are given as Supporting Information (Appendix S1.2 and 1.5).

To illustrate implications of my results for the age of crown-group chelonioids (see Discussion), I produced a time-scaled tree using age-ranges of taxa derived from the literature and the PaleoDB (https://paleobiodb.org), summarized in Table 2.2. Commands from the strap (Bell & Lloyd 2014) and paleotree (Bapst 2012) packages in R were used for time-scaling and visualisation (See Appendix S1.12 for code). I arbitrarily used a minimum branch length argument of 1 myr for zero-branch lengths in the 'timePaleoPhy' command of the paleotree package (Bapst 2012). Because some lineages of turtles have older fossil representatives than the oldest fossils for those groups included in our study, I included minimum constraints for three nodes of our time scaled tree. First, I used the top of the Oxfordian (157.3 Ma) as a minimum constraint for Pleurodira based on *Caribemys oxfordiensis* (De la Fuente & Iturralde-Vinent 2001; Joyce *et al.* 2013*b*). Secondly, I used the base of the Cretaceous (145.0 Ma) as a minimum constraint for Cryptodira based on the total-group trionychian *Sinaspideretes wimani*. Although the type locality of *Sinaspideretes* is not exactly known (Tong *et al.* 2014), it has been argued that the material as well as referred material is from the Shangshaximiao Formation (Danilov & Parham 2006; Tong *et al.* 2014), which is probably of Late Jurassic but possibly even of Middle Jurassic age (Xing *et al.* 2013).

Using the base of the Cretaceous as a minimum age is thus a conservative constraint, following Joyce *et al.* (2013*b*). Lastly, again following Joyce *et al.* (2013*b*), I use the top of the Campanian (72.1 Ma) as a minimum constraint for Chelydroidea based on a peripheral fragment that can be unambiguously identified as belonging to the total-group of Chelydridae, which was described by Brinkman & Rodriguez de la Rosa (2006).

TABLE 2.2. Stratigraphic ranges for taxa used for the time-calibrated tree (Ma).

Taxon	First Appaearance Datum (FAD)	Last Appearance Datum (LAD)	Source
Allopleuron hofmanni	72.1	66.0	Janssen *et al.* 2013
Annemys latiens	163.5	145.5	Rabi *et al.* 2010
Annemys levensis	157.3	145.5	Rabi *et al*. 2010
Annemys sp.	167.7	145.0	PalaeoDB
Araripemys barretoi	112.6	109.0	PalaeoDB
Archelon ischyros	83.6	72.1	Hirayama 1997
Argillochelys cuneiceps	56.0	47.8	Weems & Brown 2017
Arundelemys dardeni	122.46	112.6	PalaeoDB
Australochelys africanus	201.6	189.6	PalaeoDB
Baptemys wyomingensis	55.8	40.4	PalaeoDB
Bouliachelys suteri	105.3	99.7	PalaeoDB
Brachyopsemys tingitana	66.043	61.7	PalaeoDB
Chubutemys copelloi	125.45	112.6	PalaeoDB
Desmatochelys lowii	93.9	89.8	Hirayama 1997
Desmatochelys padillai	125.0	120.0	Cadena & Parham 2015
Dracochelys biscuspis	125.0	100.5	Rabi *et al*. 2010
Eileanchelys waldmanni	168.3	166.1	Joyce *et al.* 2016*b*
Eubaena cephalica	70.6	66.043	PalaeoDB
Emarginachelys cretacea	70.6	66.043	PalaeoDB
Eochelone brabantica	47.8	41.2	Weems & Brown 2017
Eosphargis breineri	56.0	47.8	Nielson 1959
Glyptops plicatulus	150.8	145.5	PalaeoDB
Judithemys sukhanovi	84.9	70.6	PalaeoDB
Jurassichelon oleronensis	152.1	145.0	Rieppel 1980; Anquetin et al. 2017*a*
Kallokibotion bajazidi	72.1	66.0	Joyce *et al.* 2016*b*
Kayentachelys aprix	199.3	182.7	Joyce *et al.* 2016*b*
Kirgizemys dmitrievi	130.0	112.6	PalaeoDB
Kirgizemys hoburensis	125.0	100.5	Rabi *et al.* 2010
Leyvachelys cipadi	130.0	109.0	PalaeoDB
Notochelone costata	109.0	99.7	PalaeoDB
Ocepechelon bouyai	70.6	66.043	PalaeoDB
Ordosemys sp.	129.4	113.0	Rabi *et al*. 2010
Plesiochelys etalloni	157.3	150.0	Anquetin *et al*. 2017*a*

Taxon	First Appaearance Datum (FAD)	Last Appearance Datum (LAD)	Source
Plesiochelys planiceps	152.1	145.0	Anquetin *et al*. 2017*a*
Pleurosternon bullockii	145.2	140.2	PalaeoDB
Portlandemys mcdowelli	152.1	145.0	Anquetin *et al.* 2017*a*
Proganochelys quenstedti	208.5	201.3	Joyce *et al*. 2016*b*
Protostega gigas	85.8	70.6	PalaeoDB
Puppigerus camperi	56.0	41.2	Weems & Brown 2017
Rhinochelys pulchriceps	105.3	102.0	FAD: PalaeoDB; LAD: Collins 1970
Sandownia harrisi	125.45	122.46	PalaeoDB
Santanachelys gaffneyi	112.6	109.0	PalaeoDB
Sinemys gamera	129.4	100.5	Rabi *et al*. 2010
Sinemys lens	163.5	145.0	Rabi *et al*. 2010
Solnhofia parsoni	155.7	145.5	PalaeoDB; Joyce 2000
Toxochelys latiremis	85.8	70.6	PalaeoDB; Weems & Brown 2017
Xinjiangchelys radiplicatoides	168.3	152.1	Rabi *et al.* 2010
Xinjiangchelys wusu	163.5	152.1	PalaeoDB

2.2.7 Testing the effect of 'marine' characters and advanced protostegids

To test if my phylogenetic results were influenced by the inclusion of characters that might be functionally linked to a marine lifestyle, I performed an additional analysis in which characters that were identified to be indicative of a marine lifestyle were deleted. Furthermore, to test if my phylogenetic results (specifically, the recovery of protostegids being crown-group chelonioids, see results) were driven by the inclusion of advanced taxa with a highly specialised body plan with clear adaptations to pelagic life, as suggested by some authors (e.g. Cadena & Parham 2015), I performed a series of analyses in which only certain protostegids with the most plesiomorphic characters were included in the analyses. In the first of these 'least specialised taxa analyses', I only kept *Santanachelys gaffneyi* as the sole representative of protostegids, as done in all studies that previously found protostegids outside of Chelonioidea (e.g. Joyce 2007; Danilov & Parham 2008; Anquetin 2012; Sterli & de la Fuente 2013). In the second analysis ('least specialised taxa analysis 2'), I additionally kept *Rhinochelys pulchriceps*, for which I had the most detailed cranial information (see section 3). In a third analysis ('least specialised taxa analysis 3'), I kept all protostegids but *Archelon*

ischyros and *Protostega gigas*, which are commonly described as 'advanced protostegids' (e.g. Kear & Lee 2006).

2.2.8 Testing alternative hypotheses

To test if my topology was significantly different in tree length compared to alternative hypotheses regarding the placement of key taxa, I used Templeton's nonparametric test (Templeton 1983) in PAUP* for Macintosh (Swofford 2002). Templeton's test uses the differences in counts of character state transitions for each character implied by a pair of trees. Resulting differences are sorted in ascending order and fractional rank scores are assigned to them. Rank scores for characters that have fewer transitions in the suboptimal tree are summed to produce a test statistic, which is subjected to a Wilcoxon's signed rank test. The default for PAUP* is a two-tailed test (Goldman et al. 2000). However, because I use Templeton's test with one tree being known to be optimal (the null hypothesis is that constrained topologies fit the data as well as the optimal, i.e. shortest, tree) a one-tailed test is appropriate (Templeton 1983; Goldman et al. 2000; Hipp et al. 2004). Although p-values of one-tailed tests are less conservative, their use has been advocated because they are generally close to the exact probability values for this test (Felsenstein 1985*a*; Lee 2000), and p-values reported herein were corrected accordingly (see Goldman et al. 2000). Alternative hypotheses were chosen based on phylogenetic results presented in previous studies. My alternative hypotheses test the position of plesiochelyids, thalassochelydians, sandownids, xinjiangchelyids, sinemydids, protostegids as stem-group cryptodires and stem-group chelonioids, respectively, and the position of protostegids as stem-group turtles. The alternative topologies were recovered by running parsimony analyses including one OTU relevant to each hypothesis into the molecular backbone constraint, while all other fossil OTUs were kept as floaters. For hypotheses relating to species-rich groups or groups that have not consistently been found to be monophyletic among previous studies, such as sinemydids or thalassochelydians, several constraints using different OTUs were used.

Because Templeton's test uses character changes across a tree in a pairwise comparison, individual trees had to be selected from the available MPTs of the original and constraint analyses. To do this, I computed symmetric differences (Robinson & Foulds 1981) between all MPTs from each constraint analysis and all MPTs of my original analysis using the command 'treedist' in PAUP* (see Appendix S1.13 for PAUP* and R code), which returns a pairwise symmetric differences matrix. The least and most symmetric tree pairs between original and constraint analyses were selected from the matrix for comparison. If several tree pairs matched the least or most symmetry criterion, I randomly chose a tree pair from the symmetric difference matrix for the Templeton's tests (the procedure, including PAUP* and R code, are provided in Appendix S1.13; the files generated in the process, as well as all MPTs and consensus trees generated for alternative hypotheses are deposited in the Dryad repository (Evers & Benson 2018*c*)).

2.3 RESULTS

2.3.1 Similarity matrix

Similarity heatmaps show high or low similarity of character states. Most clades show relatively low between-group similarity, and relatively high within-group similarity (Fig. 2.2), congruent with my phylogenetic topology. Relatively high between-group similarity of some clades that are not close relatives to one another (according to my phylogenetic results) provide evidence of homoplasy, and possibly indicate convergent evolution.

Some of the highest between-group similarity is seen between protostegids on one hand, and sinemydids, xinjiangchelyids, and angolachelonians (i.e. thalassochelydians+sandownids; details are given below) on the other hand (Fig. 2.2). This pattern has been noted based on qualitative comparisons before (Cadena & Parham 2015), and is according to my matrix driven predominantly by cranial, and, to a lesser extent,

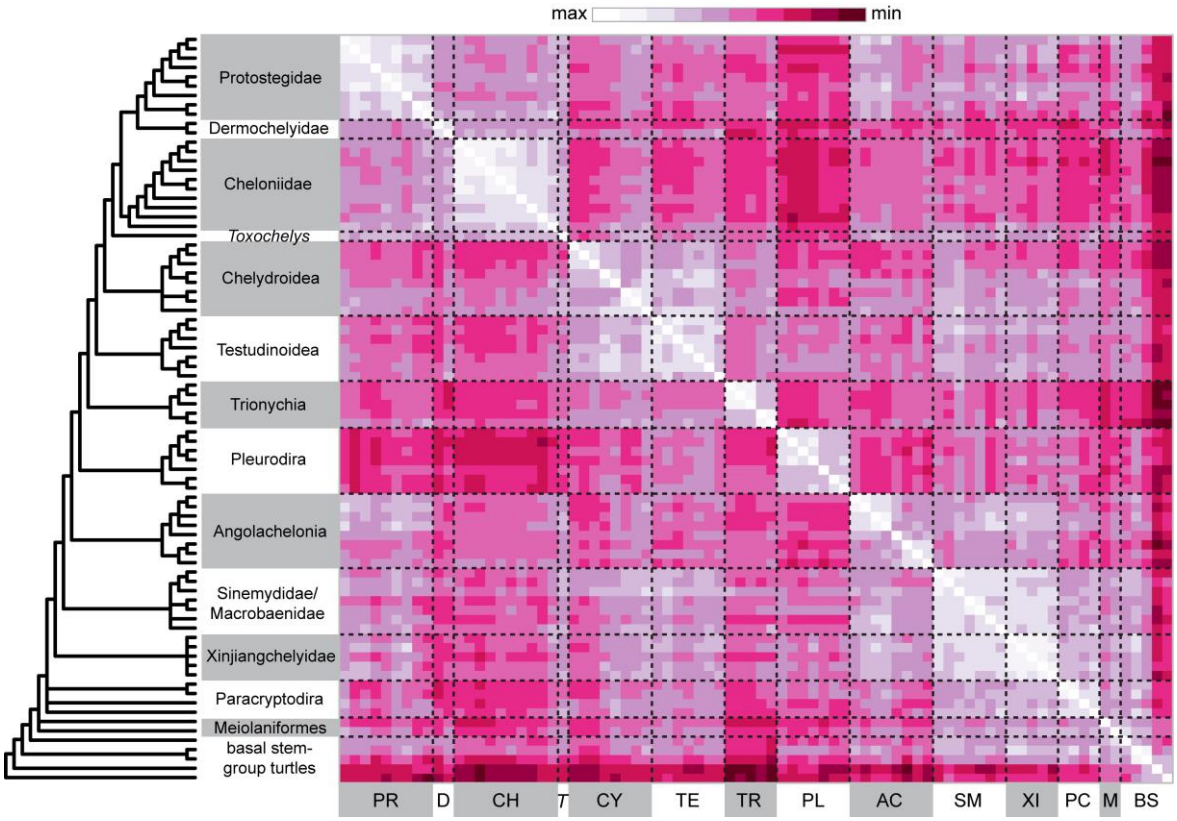


FIG. 2.2. Heatmap of symmetric pairwise-taxon similarity matrix using our full character dataset (n = 345). The phylogenetic tree to the left is identical to our strict consensus tree using unordered character data. Dotted lines delimit turtle subclades for readability. *Abbreviations*: AC, Angolachelonia; BS, basal stem-group turtles; CH, Cheloniidae; CY, Chelydroidea; D, Dermochelyidae; M, Meiolaniformes; PC, Paracryptodira; PL, Pleurodira; PR, Protostegidae; SM; Sinemydidae/Macrobaenidae; T, *Toxochelys* sp.; TE, Testudinoidea; TR, Trionychia, XI, Xinjiangchelyidae.

axial+girdle characters (Fig. 2.3A, C). My phylogenetic results strongly support the hypothesis that protostegids are crown-group chelonioids, deeply nested within Cryptodira. This pattern of similarity therefore indicates a relatively high amount of convergence of the protostegid skull morphology with that of angolachelonians, sinemydids, and xinjiangchelyids. In accordance with my topology, protostegid skull morphology is most similar to the skull morphology of cheloniids. However, unlike in the axial+girdle or shell partitions, cranial similarity between protostegids and cheloniids never exceeds moderate values. Paired with the moderate similarity of cranial morphology of protostegids with non-chelonioid groups, the relatively strong differences of protostegid skulls to cheloniid skulls reveal a high amount of potential character conflict. This might explain the finding of protostegids outside of Chelonioidea in some previous studies (e.g. Joyce 2007; Anquetin 2012). Furthermore, the

character similarity between sinemydids, xinjiangchelyids, and angolachelonians can be used as an explanation for the unstable positions of these groups among previous phylogenetic analyses (e.g. Rabi *et al.* 2013; Cadena & Parham 2015; Zhou & Rabi 2015, see discussion).

Although angolachelonians are particularly similar to protostegids, the similarity of angolachelonians to chelonioids in general is high. This pattern is seen across all data partitions, and is most evident in the cranial data. However, my data partitions also show that whereas angolachelonian skulls share more identical scorings with protostegids than with cheloniids, the shells of angolachelonians are more similar to cheloniids than to those of protostegids. High overall similarity between chelonioids and angolachelonians can possibly be explained by their marine lifestyle. Relatively high cranial similarity between Angolachelonia and Chelonioidea indicates that character convergence is more dominant in the cranium of these marine groups, than in other parts of the body.

Chelonioids (including protostegids) show high within-group similarity for all anatomical partitions, and relatively low similarity to other groups (Fig. 2.3). This is particularly evident for limb morphology (Fig. 2.3D). The same pattern, albeit weaker, is also seen in shell, and axial+girdle morphology. This indicates that chelonioids have a specific set of shell, postcranial, and especially limb characters that differs relatively strongly to the characters of other groups, but that these characters are consistently present among members of Chelonioidea.

For skull characters, low similarity values to non-chelonioid groups are only observed in cheloniids (see discussion of protostegids above). This indicates that within Chelonioidea, the cheloniid skull has a high number of derived character states. Dermochelyoids show a strong dissimilarity to all other groups (but moderate to high similarity to cheloniids) in the shell partition, indicating a strongly derived shell morphology. Although within-group similarity in chelonioids is generally high, cheloniids and dermochelyoids can be distinguished in the cranial and limb partitions, indicating that these parts of the body are less similar than the shell or axial+girdle skeleton.

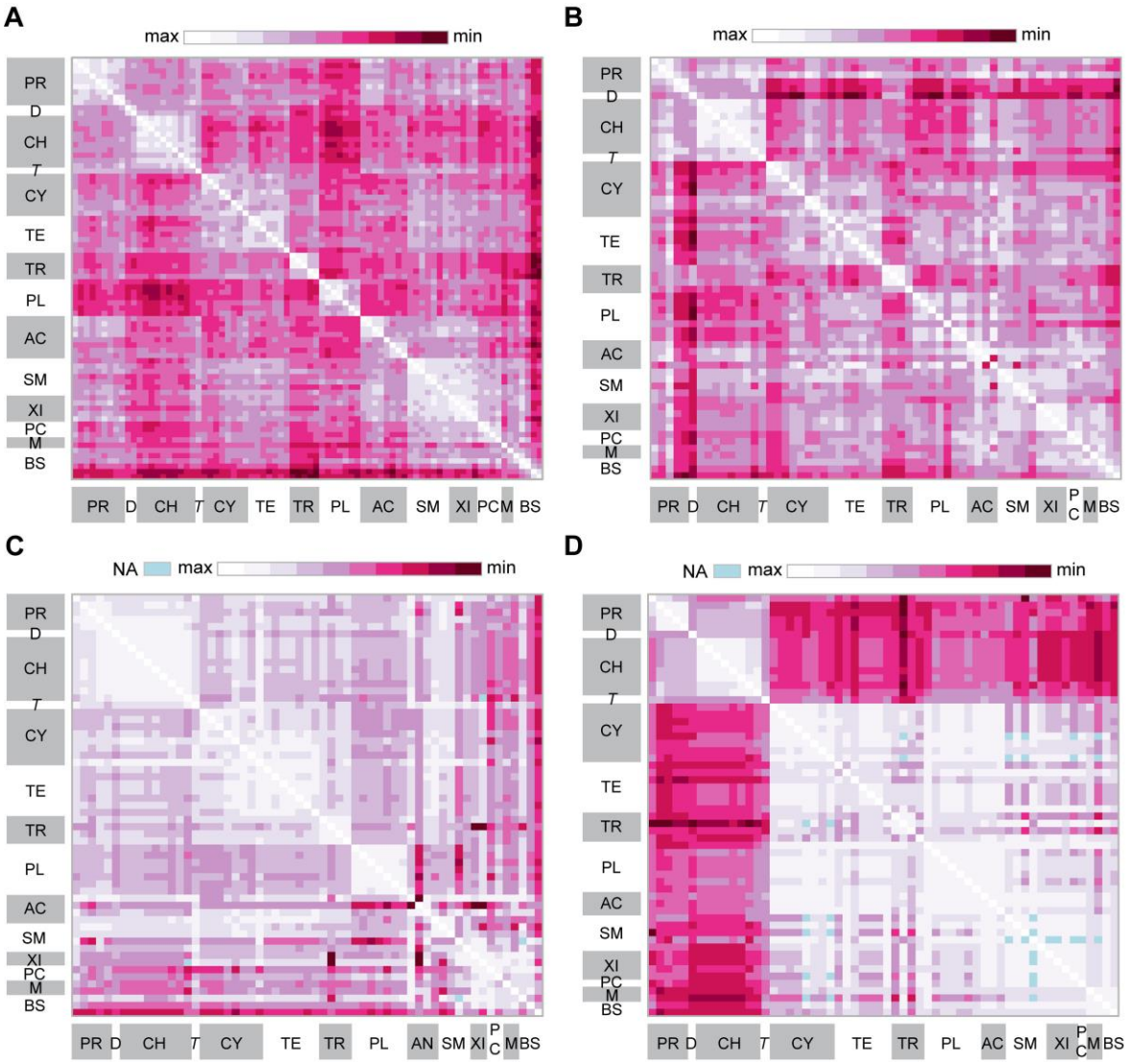


FIG. 2.3. Heatmaps of symmetric pairwise-taxon similarity matrices of subsets of our characters data. **A**, Cranial character data (n = 185); **B**, Shell character data (n = 87); **C**, Axial and girdle character data (n = 50); **D**, Limb character data (n = 23). Note that NA values result from comparisons of taxa with non-overlapping character preservation. *Abbreviations*: AC, Angolachelonia; BS, basal stem-group turtles; CH, Cheloniidae; CY, Chelydroidea; D, Dermochelyidae; M, Meiolaniformes; PC, Paracryptodira; PL, Pleurodira; PR, Protostegidae; SM; Sinemydidae/Macrobaenidae; T, *Toxochelys* sp.; TE, Testudinoidea; TR, Trionychia, XI, Xinjiangchelyidae.

Relatively high between-group similarity is present among xinjiangchelyids, sinemydids and paracryptodires, which is particularly clear in the cranial and shell data, but also seen in the unpartitioned dataset. This is in accordance with my phylogenetic results, which find these groups relatively closely related to one another on the stem-lineage of turtles. Moderate similarity is seen between testudinoids, sinemydids, and xinjiangchelyids,

possibly explaining why the latter groups are sometimes found as stem-group cryptodires (e.g. Péréz-García *et al.* 2012; Sterli *et al.* 2013; Zhou & Rabi 2015).

The similarity of pleurodires to other turtles is lower in the cranial and shell partitions than in the axial+girdle or limb partitions. Therefore, the limbs, girdles and axial elements of pleurodires are similar to those of cryptodires, whereas their skulls and shells are highly different. This might be explained by constraints imposed onto the limbs and postcranium by the presence of the shell in all turtle groups, and apparent absence of these constraints on the shell itself and the cranium.

Indeed, the limbs and axial+girdle partition shows relatively high similarity between almost all groups (Fig. 2.3C). Exceptions to the general pattern include chelonioid limbs, which are modified to flippers and thus dissimilar to those of all other turtles (Fig. 2.3D), and stem-group turtles including meiolaniforms and paracryptodires. These show relatively low similarity (i.e. are dissimilar) to all other groups, especially among early stem-group turtles. This indicates that the axial, girdle and limb morphology underwent substantial transformations on the turtle stem-lineage, but then was relatively conserved within the turtle crown-group. Finally, angolachelonians and sinemydids show higher axial+girdle and cranial similarity to cryptodires than to pleurodires, which could possibly explain their inferred positions as stem-group cryptodires in some studies (e.g. Zhou & Rabi 2015).

2.3.2 Phylogenetic Analysis using unordered characters

Parsimony analysis of the unordered dataset in TNT resulted in 12 most parsimonious trees (MPTs) 1532 steps long. Subsequent TBR branch swapping resulted in recovery of 12 MPTs in total. Zero-branch lengths are collapsed during the construction of a strict consensus tree in TNT. In several cases (Trionychidae, Chelinae), resulting polytomies in our strict consensus tree can actually be resolved on the basis of the molecular backbone constraint, and nodes representing these clades have been added back in to the respective figures (Fig. 2.4).

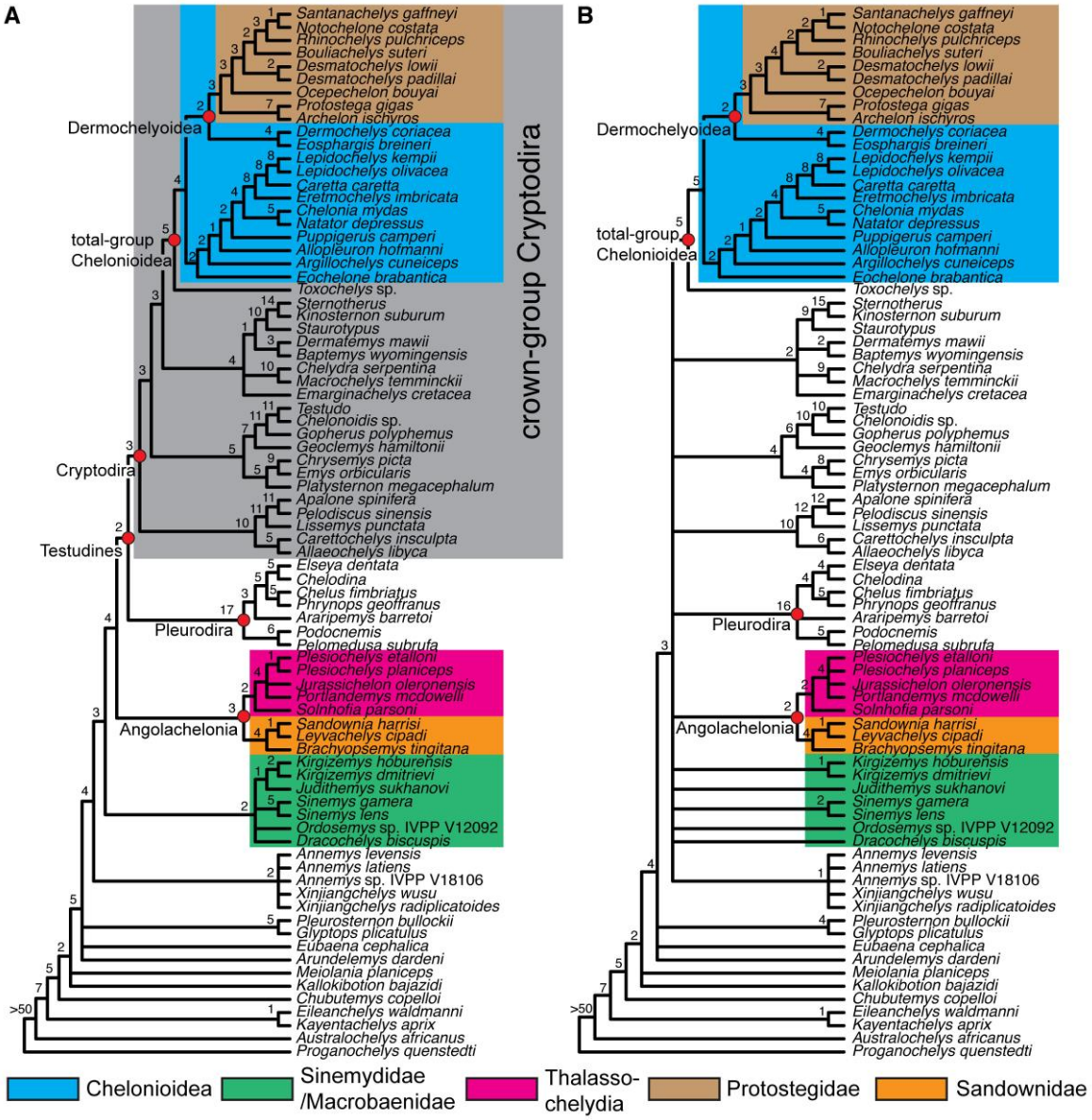


FIG. 2.4. Strict consensus trees of our phylogenetic analysis. **A**, Strict consensus tree of 12 MPTs from analysing our data treating the characters as unordered. **B**, strict consensus tree of 195 MPTs treating characters as ordered. Numbers above nodes are Bremer values.

In the following, results from my unordered analysis are presented. Differences in topology found in the ordered analysis are described in the section below, and shown in Figure 2.4. Key results from our unordered phylogenetic analysis are: (1) the recovery of a previously unknown clade comprised of sandownids + thalassochelydians, Angolachelonia, which is placed as the immediate sister group to crown-group turtles; (2) the recovery of a monophyletic Protostegidae as the sister to Dermochelyidae; (3) the recovery of all sinemydids, macrobaenids, and xinjiangchelyids as stem-group turtles. Our results imply two independent and monophyletic groups of marine turtles outside of Pleurodira,

Angolachelonia and Chelonioidea. This shows that marine ecologies have evolved three times within non-pleurodiran turtles, including *Odontochelys*.

Angolachelonia. Angolachelonia includes two monophyletic groups that have been previously recognized, Sandownidae and Thalassochelydia. The branch support for Angolachelonia is moderate (Bremer support = 3). Angolachelonia is supported by eight unambiguous synapomorphies (all cranial and mandibular; see Figs 2.5–6; Table 2.3), of which none are unique. Within Angolachelonia, sandownids and plesiochelyids have high branch support values (Bremer support = 4), whereas Thalassochelydia (i.e. Plesiochelyidae + *Solnhofia* in the context of my taxon sampling) has moderate support (Bremer support = 2).

TABLE 2.3. Synapomorphies for taxa discussed in the main text.

Taxon	Unambiguous synapomorhies	Sum
Chelonioidea (total-group)	35.1, 39.1, 58.1, 69.0, 94.0, 105.1, 132.2, 139.2, 142.1, 144.1, 163.1, 210.2, 235.0, 242.2, 255.2, 291.1, 295.0, 333.1, 334.1, 338.1, 342.1	21
Chelonioidea (crown-group)	15.0, 93.2, 104.0, 306.1, 307.1, 337.1, 344.1	7
Cheloniidae (total-group)	44.1, 68.1, 109.1, 119.1, 176.1	5
Dermochelyoidea	27.0, 161.1, 237.1, 340.2	4
Dermochelyidae	16.1, 53.1, 96.0, 110.0, 115.0, 149.1	6
Protostegidae	4.0, 62.1, 103.1, 236.1, 291.0, 328.1, 329.1, 335.1	8
Angolachelonia	18.0, 83.1, 84.1, 94.0, 103.1, 181.1, 182.1, 184.1	8
Sandownidae	34.0, 57.1, 68.1, 108.1	4
Thalassochelydia	81.1, 113.1, 142.1, 185.0, 210.2, 211.1, 224.0, 278.0	8
Sinemydidae/Macrobaenidae	113.1, 134.1, 242.2, 243.1	4
Xinjiangchelyidae	38.1, 91.0, 125.1, 203.1, 257.1, 270.1	6

Thalassochelydians share eight unambiguous synapomorphies (four cranial and mandibular, see Fig. 2.7; four postcranial, one of which is unique (ch 278.0); Table 2.3), and sandownids are united by four unambiguous cranial synapomorphies (Fig. 2.8; Table 2.3), one of which is unique (ch 108.1). The sister-group relationship of Angolachelonia and crown-group turtles is well supported (Bremer support = 4).

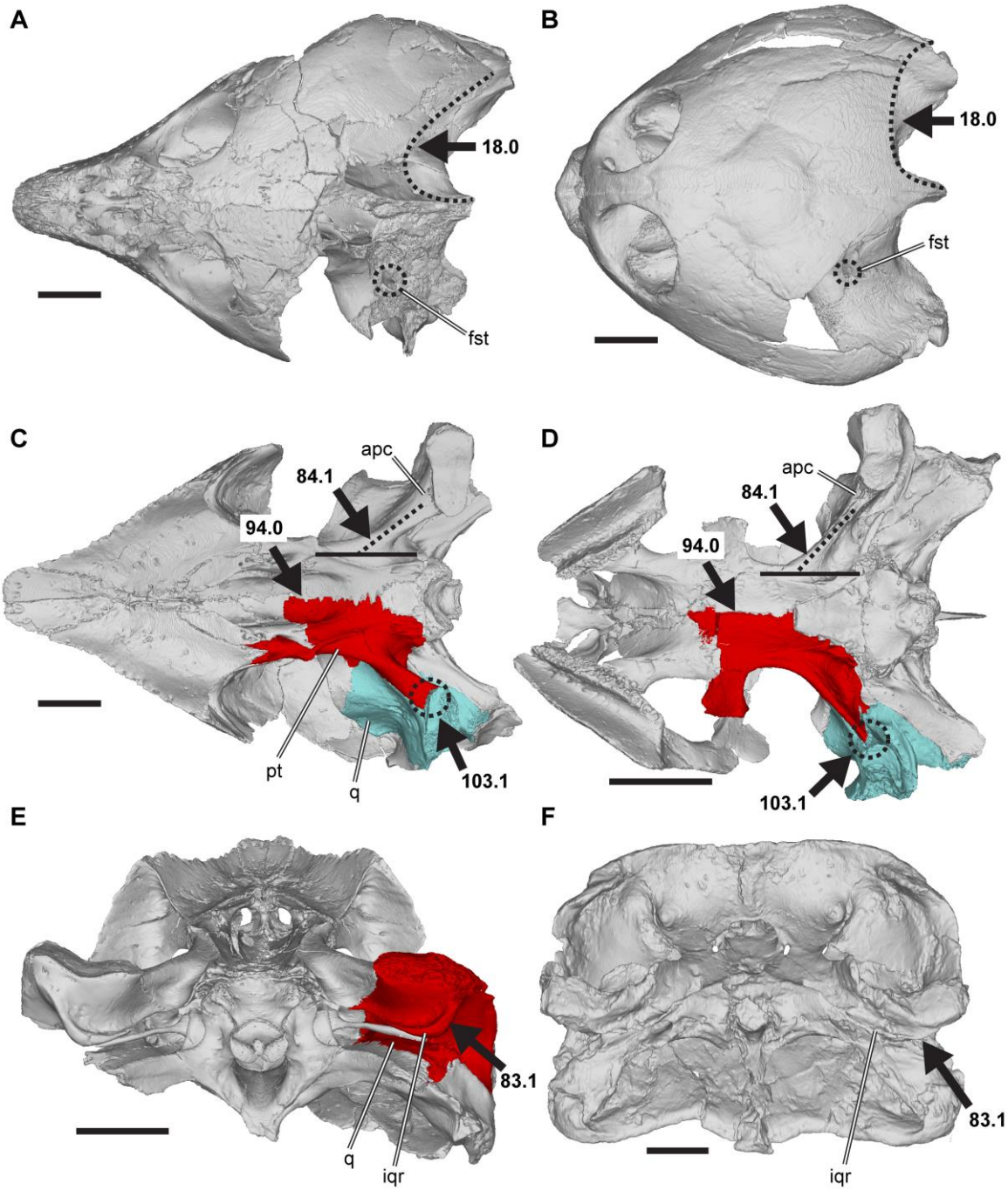


FIG. 2.5. Cranial synapomorphies of Angolachelonia illustrated by renderings of 3D models generated using CT data. **A**, cranium of *Solnhofia parsoni* (TM 4023) in dorsal view showing the extent of the dermal skull roof in the temporal region, obliterating the foramen stapedio-temporale in dorsal view (ch. 18.0); **B**, cranium of *Sandownia harrisi* (MIWG 3480) in dorsal view, showing the same features as in A; **C**, cranium of *Solnhofia parsoni* (TM 4023) in ventral view, showing the posterior direction of the articular process (ch. 84.1), the long interpterygoid contact (ch. 94.0), and the contact of the pterygoid with the mandibular articular surface of the quadrate (ch 103.1); **D**, cranium of *Plesiochelys planiceps* (OUMNH J1582) in ventral view, showing the same features as in C; **E**, cranium of *Solnhofia parsoni* (TM 4023) in posteroventral view, showing the infolding ridge of the quadrate (ch. 83.1); **F**, cranium of *Brachyopsemys tingitana* (AMNH FARB 30612) in posteroventral view, showing the same features as in E. Scale bars in A, B, C, E are 10 mm; scale bars in D, F are 20 mm. Abbreviations: *apc*, articular process of cranium; *fst*, foramen stapedio-temporale; *iqr*, infolding ridge of quadrate; *pt*, pterygoid; *q*, quadrate.

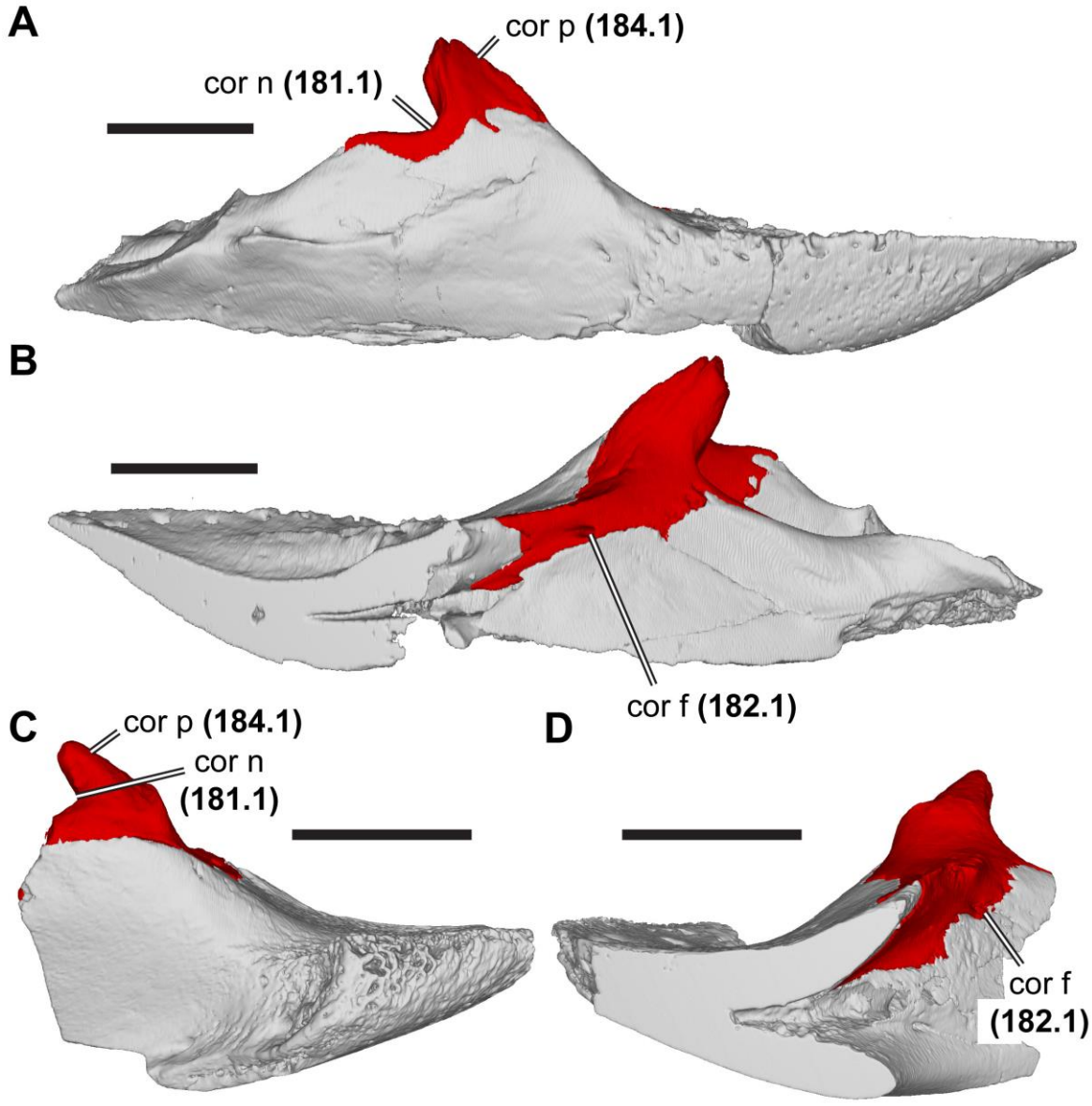


FIG. 2.6. Mandibular synapomorphies of Angolachelonia illustrated by renderings of 3D models generated using CT data. **A**, right mandibular ramus of *Solnhofia parsoni* (TM 4023) in lateral view, showing the coronoid notch (ch. 181.1), and the tall and pointed coronoid process (ch. 184.1); **B**, right mandibular ramus of *Solnhofia parsoni* (TM 4023) in medial view, showing the foramen in the coronoid (ch. 182.1); **C**, right mandibular ramus of *Sandownia harrisi* (MIWG 3480) in lateral view, showing the same features as in A; **D**, right mandibular ramus of *Sandownia harrisi* (MIWG 3480) in medial view, showing the same features as in B. Note that the coronoid has been shaded in all images. Scale bars are 10 mm. Abbreviations*: cor f*, foramen in coronoid; *cor n*, coronoid notch; *cor p*, coronoid process.

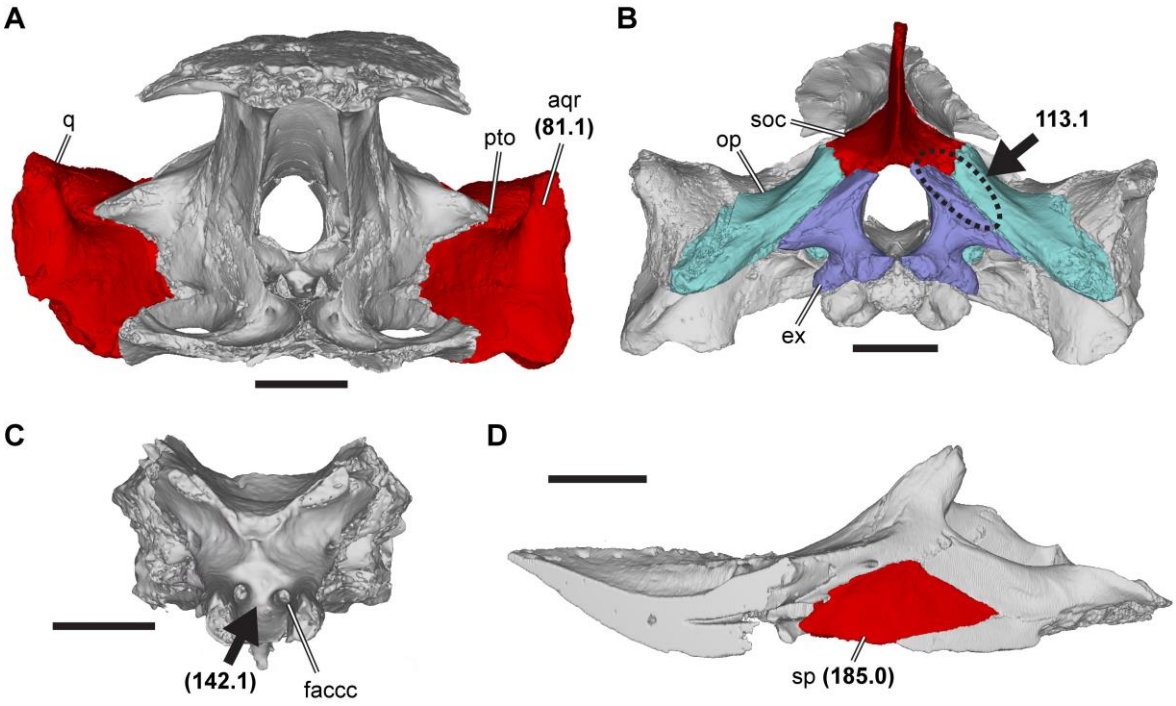


FIG. 2.7. Cranial and mandibular synapomorphies of Thalassochelydia illustrated by renderings of 3D models generated using CT data. **A**, posterior part of the cranium of *Plesiochelys planicpes* (OUMNH J1582) in anterior view, showing the recess on the anterior surface of the quadrate lateral to the processus trochlearis oticum (ch. 81.1); **B**, cranium of *Plesiochelys planicpes* (OUMNH J1582) in posterior view, showing the presence of a fossa on the supraoccipital-opisthotic-exoccipital contact area (ch 113.1); **C**, parabasisphenoid of *Plesiochelys planicpes* (OUMNH J1582) in anterior view, showing the closely-spaced foramina anterius canalis caroticus cerebralis (ch 142.1); **D**, right mandibular ramus of *Solnhofia parsoni* (TM 4023) in medial view, showing the presence of a splenial (ch 185.0). Note that dotted line in B surround fossa. Scale bars in A–B, D are 10 mm, scale bar in B is 5 mm. Abbreviations: *aqr*, anterior quadrate recess; *ex*, exoccipital; *op*, opisthotic; *faccc*, foramen anterius canalis caroticus internus; *pto*, processus trochlearis oticum; *q*, quadrate; soc, supraoccipital; *sp*, splenial.

Chelonioidea. Chelonioidea is a monophyletic group comprised of two major subgroups, Dermochelyoidea and Cheloniidae. *Toxochelys* is found as the only member of the chelonioid stem-group. Within the total-group of Cheloniidae, all extant cheloniids form a clade, and all fossil taxa are found as stem-group cheloniids and form a paraphyletic grade as successive sister-taxa to the crown. *Eochelone* is found as the earliest-diverging cheloniid in our taxon sample across all trees. The total-group of Cheloniidae has a Bremer support of 2, and is supported by five unambiguous synapomorphies (Table 2.3), all of which are cranial, and none of which are unique. Dermochelyoidea includes the extant leatherback turtle *Dermochelys coriacea*, and its stem-group, including *Eosphargis breineri* and protostegids.

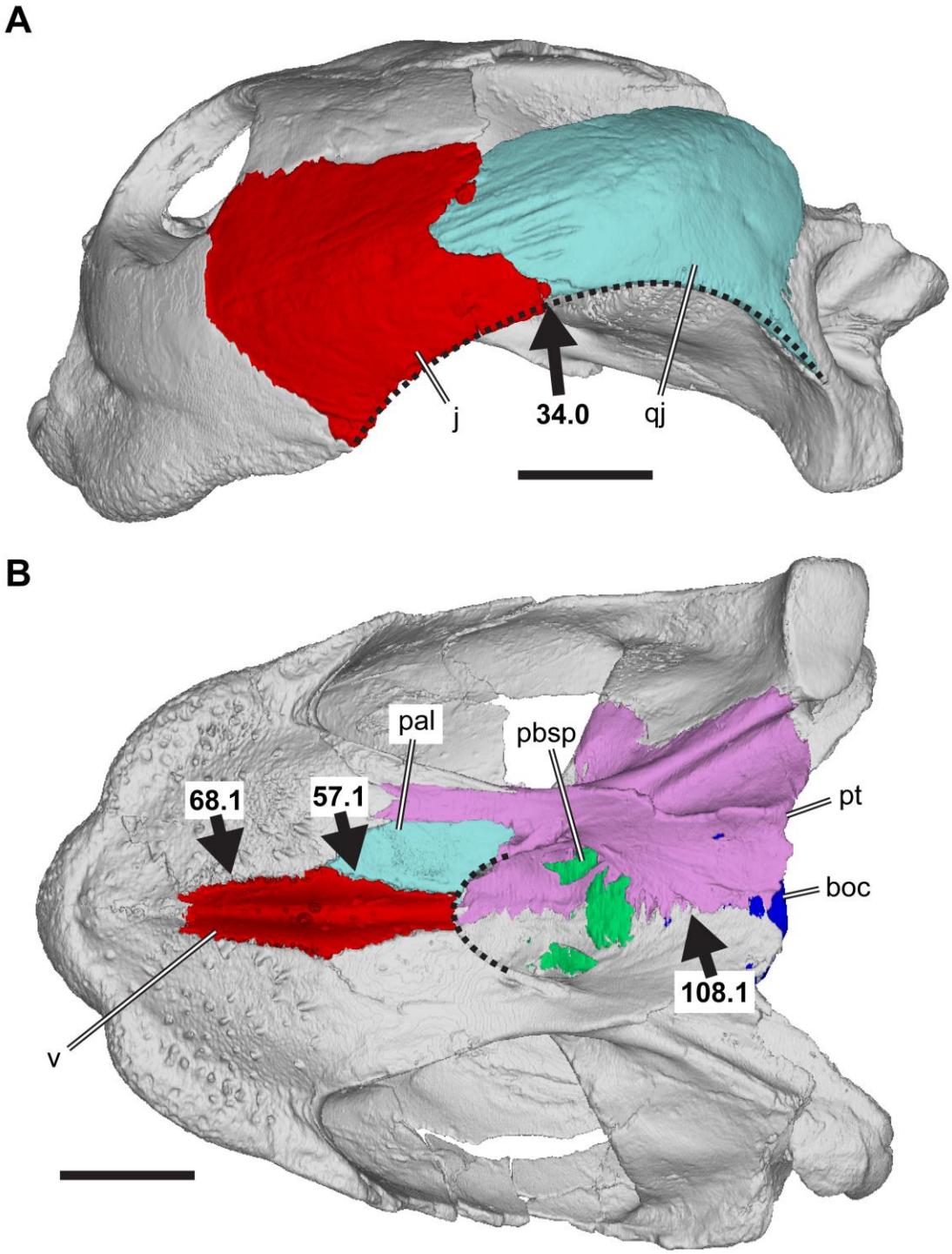


FIG. 2.8. Cranial synapomorphies of Sandownidae illustrated by renderings of 3D models generated using CT data. **A**, cranium of *Sandownia harrisi* (MIWG 3480) in left lateral view, showing the extent of the lower temporal emargination which is exclusively formed by the jugal and quadratojugal (ch 34.0); **B**, cranium of *Sandownia harrisi* (MIWG 3480) in ventral view, showing the vomer-palatine contact anterior to the internal naris (ch. 57.1), the contribution of the vomer to the triturating surface (ch. 68.1), and the posterior process of the pterygoid covering parts of the parabasisphenoid and basioccipital (ch. 108.1). Dotted line in A denotes the ventral margin of the lower temporal emargination, and the dotted line in B denotes the position of the internal naris. Scale bars are 10 mm. Abbreviations: *boc*, basioccipital; *j*, jugal; *pal*; palatine; *pbsp*, parabasisphenoid; *pt*, pterygoid; *q*, quadrate; *qj*, quadratojugal.

Among the stem-group of *Dermochelys*, *Eosphargis* is found as the closest relative of *Dermochelys*. Different authors have used different taxonomic terminology to refer to *Dermochelys* and closely related taxa. The name Dermochelyidae has most frequently been used to describe *Dermochelys* and taxa on its stem-lineage to the exclusion of protostegids (e.g. Hirayama 1994, 1998; Kear & Lee 2006). This has been formalized in a phylogenetic definition by Joyce *et al.* (2004). I use Dermochelyidae in that sense. Dermochelyidae is herein supported by a Bremer support of 4, and by six unambiguous cranial synapomorphies (Table 2.3), none of which are unique. The total-group of *Dermochelys* (i.e. dermochelyids + protostegids) has also received various names (Hirayama 1998; Joyce *et al.* 2004).

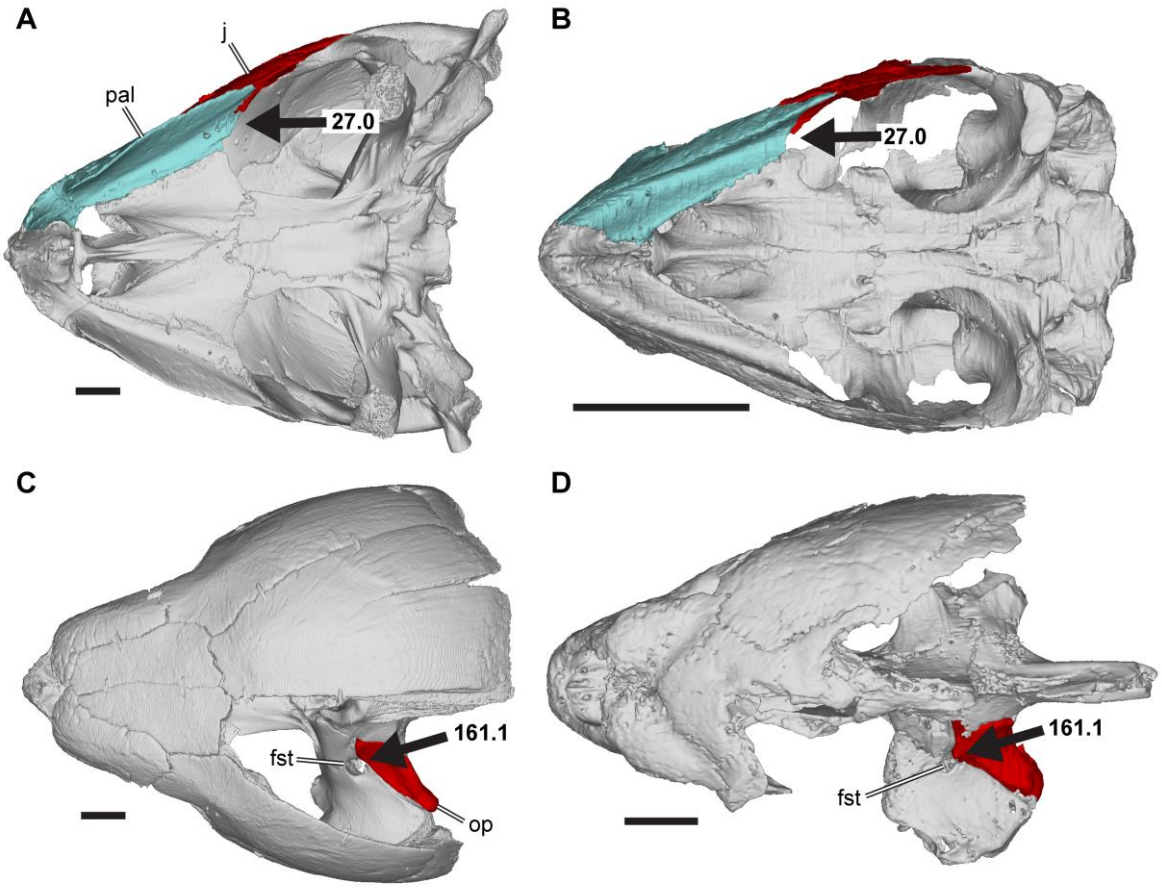


FIG. 2.9. Cranial synapomorphies of Dermochelyoidea illustrated by renderings of 3D models generated using CT data. **A**, cranium of *Dermochelys coriacea* (UMZC R3031) in ventral view, showing absence of medial process of jugal (ch. 27.0); **B**, cranium of *Rhinochelys pulchriceps* (CAMSM B55783) in ventral view, showing the same features as in A; **C**, cranium of *Dermochelys coriacea* (UMZC R3031) in dorsal view with the left postorbital removed, showing the opisthotic contribution to the foramen stapedio-temporale (ch. 161.1); **D**, cranium of *Bouliachelys suteri* (QMF 31669) in dorsal view, showing the same features as in C. Scale bars in A, C, and D are 20 mm; scale bar in B is 1 mm. Abbreviations: *fst*, foramen stapedio-temporale; *j*, jugal; *op*, opisthotic; *pal*, palatine.

Here, I use the name Dermochelyoidea for this group (as in Hirayama 1998; Lehman & Tomlinson 2004). Dermochelyoidea has a low branch support (Bremer support = 2), and has four unambiguous synapomorphies (two cranial; two postcranial, one of which is unique (ch. 237.1); Table 2.3). Cranial synapomorphies of dermochelyoids are shown in Figure 2.9. However, the less inclusive crown-group Chelonioidea (i.e. Dermochelyoidea + Cheloniidae) and total-group Chelonioidea (i.e. *Toxochelys* + Chelonioidea) have a high branch support of a Bremer value of 4 and 5, respectively. This indicates that there is overall strong support for the placement of protostegids within Chelonioidea. The total group of Chelonioidea shares 21 unambiguous synapomorphies (Table 2.3; eleven cranial; ten postcranial, seven of which are unique (ch 255.2; ch 291.1; ch 295.0; ch 333.1; ch 334.1; ch 338.1; ch 342.1)). Crown-group chelonioids (i.e. excluding *Toxochelys*), are united by seven unambiguous synapomorphies (three cranial, one of which is unique (ch. 93.2); four postcranial, two of which are unique (ch. 306.1; ch. 344.1)).

Protostegidae, including *Archelon ischyros*, *Bouliachelys suteri*, *Desmatochelys lowii*, *Desmatochelys padillai*, *Notochelone*, *Ocepechelon bouyai*, *Protostega gigas*, *Santanachelys gaffneyi*, and *Rhinochelys pulchriceps*, is relatively well supported with a Bremer support of 3. Protostegids share eighth unambiguous synapomorphies (Table 2.3; three cranial; five postcranial, four of which are unique (ch 291.0; ch 328.1; ch 329.1; ch 335.1)). Cranial synapomorphies for protostegids are shown in Figure 2.10. The ingroup relationships of Protostegidae differ in my analysis to those of most previous analysis. Commonly, Early Cretaceous protostegids such as *Santanachelys*, *Bouliachelys*, *Notochelone* and *Rhinochelys* are found as a paraphyletic grade leading to a clade of Late Cretaceous taxa, which includes *Desmatochelys lowii*, *Archelon*, and *Protostega* (e.g. Hirayama 1998; Kear & Lee 2006; Bardet *et al.* 2013). Bardet *et al.* (2013) found *Ocepechelon* in a polytomy with *Bouliachelys*, *Santanachelys*, other protostegids and dermochelyids. In my analysis, the gigantic *Archelon* and *Protostega* form a well-supported clade (Bremer support = 7) that is sister group to all other protostegids. Within those, the Early Cretaceous taxa *Santanachelys*, *Bouliachelys*, *Notochelone*, *Desmatochelys padillai* and *Rhinochelys*, and the Late Cretaceous *Desmatochely*

lowii form a well-supported clade (Bremer support = 3) to the exclusion of the Late Cretaceous *Ocepechelon*. The clade including *Ocepechelon* has relatively strong support with a Bremer value of 3. *Desmatochelys lowii* and *Desmatochelys padillai* are sister taxa, as also found in Cadena & Parham (2015). The remaining protostegids from the Early Cretaceous (*Bouliachelys*, *Rhinochelys*, *Notochelone*, *Santanachelys*) are united in a clade that is well nested within the Protostegidae, despite their early branching positions in most other studies.

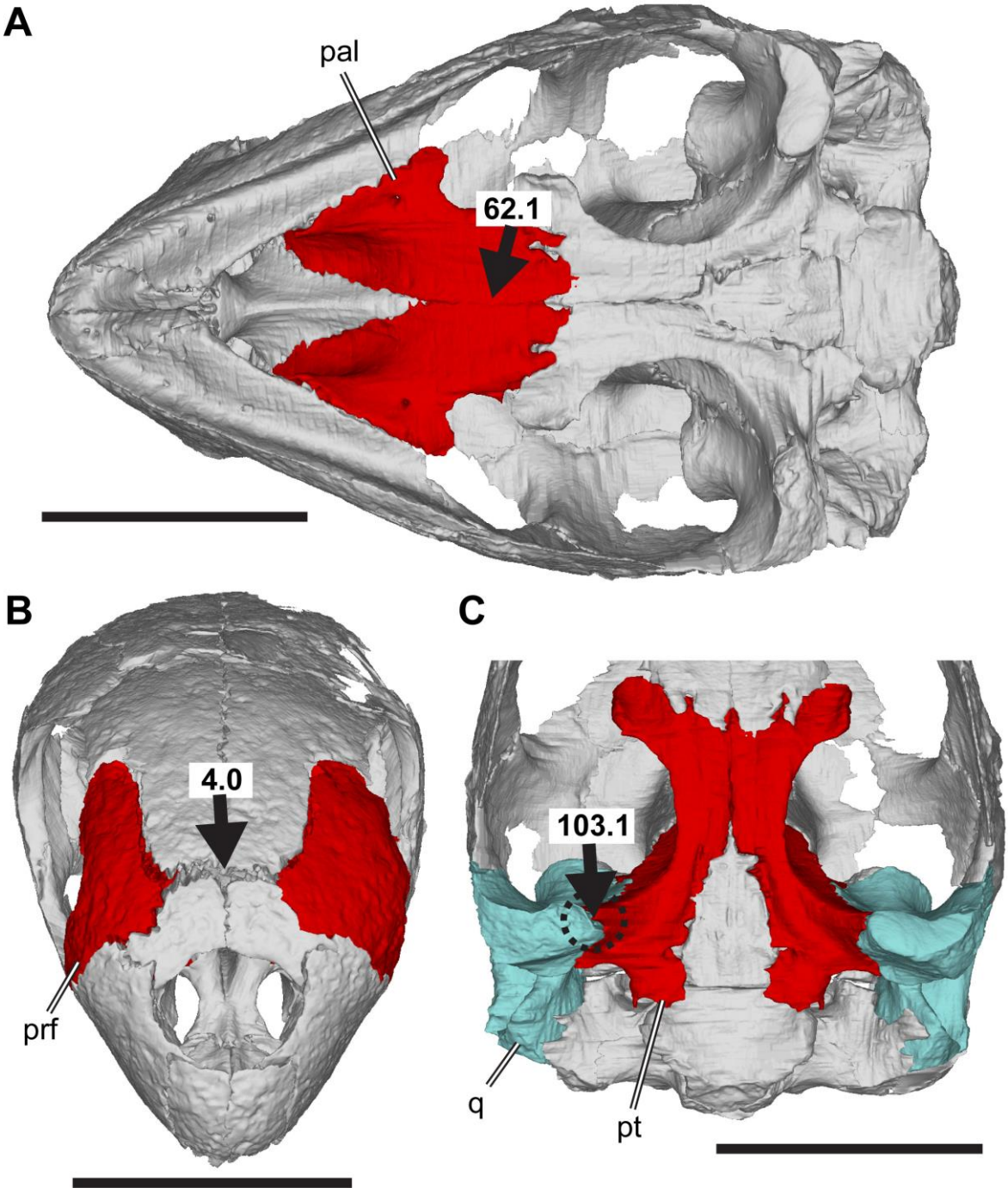


FIG. 2.10. Cranial synapomorphies of Protostegidae illustrated by renderings of 3D models generated using CT data. **A**, cranium of *Rhinochelys pulchriceps* (CAMSM B55783) in ventral view, showing the interpalatine contact (ch. 62.1); **B**, cranium of *Rhinochelys pulchriceps* (CAMSM B55783) in anterodorsal view, showing the lack of a medial contact between the prefrontals (ch. 4.0); **C**, posterior part of cranium of *Rhinochelys pulchriceps* (CAMSM B55783) in ventral view, showing the contact of the pterygoid with the mandibular articular surface of the quadrate (ch 103.1). Scale bars are 1 mm. Abbreviations: *pal*, palatine; *prf*, prefrontal; *pt*, pterygoid; *q*, quadrate. *(continued from previous page)*

Sinemydidae, Macrobaenidae, and Xinjiangchelyidae. Various Asian and North American Mesozoic turtles that have classically been recovered on the stem of Cryptodira (Zhou & Rabi 2015) have been classified as sinemydids, macrobaenids, or xinjiangchelyids (Brinkman & Wu 1999; Sukhanov 2000; Brinkman 2001; Parham & Hutchinson 2003; Danilov *et al.* 2006; Rabi *et al.* 2010, 2014). These groups have been formalized by Rabi *et al.* (2014), who established phylogenetic definitions for the groups. One challenge to the application of these definitions is that they technically cannot be applied, if the 'essential' taxon of such a definition (i.e. the taxon used to defined the clade) is not included in an analysis. In fact, the taxon used to define Macrobaenidae, *Macrobaena mongolica*, has, to my knowledge, never been included in a phylogenetic analysis, so that the taxonomic content of Macrobaenidae is entirely unclear.

I find taxa that have classically been assigned to the three groups defined by Rabi *et al.* (2014) in two monophyletic groups among the stem-group of turtles as successive sister-groups to Angolachelonia + crown-group turtles. The group placed more crownwardly is comprised largely by Cretaceous species, and includes *Sinemys lens* (Late Jurassic, all other species in this list are Cretaceous), *Sinemys gamera*, *Dracochelys biscuspis*, *Ordosemys* sp., *Judithemys sukhanovi*, *Kirgizemys dmitrievi*, and *Kirgizemys hoburensis*. Applying the phylogenetic definitions of Rabi *et al.* (2014), this entire group could be referred to as Sinemydidae. However, within my 'Sinemydidae', *Sinemys lens* and *Sinemys gamera* form a clade that is found in a polytomy with *Dracochelys*, *Ordosemys*, and a clade that includes *Kirgizemys* spp. and *Judithemys*, i.e. species that are commonly referred to as macrobaenids (e.g. Gaffney & Ye 1992; Parham & Hutchinson 2003). Depending on the (unresolved) phylogenetic position of *Macrobaena mongolica*, it is likely that my 'Sinemydidae' in fact

comprises both sinemydids and macrobaenids. Therefore, I refer to the clade including *Sinemys* and *Judithemys* as Sinemydidae/Macrobaenidae throughout this work. My Sinemydidae/Macrobaenidae is moderately supported by a Bremer support of 2, and the placement of sinemydids as the sister to Angolachelonia + crown-group turtles also has a Bremer support of 2. Sinemydids/Macrobaenids share two cranial and two postcranial synapomorphies, none of which are unique (Table 2.3).

The more stemwardly positioned group is comprised of Jurassic Asian turtles, and includes species of *Xinjiangchelys* and *Annemys*. Technically, the phylogenetic definition of Xinjiangchelyidae of Rabi *et al.* (2014) cannot be applied to this group, as I did not include the species of *Xinjiangchelys* used to define the group. However, for ease of communication, I refer to the group as Xinjiangchelyidae within this thesis. Xinjiangchelyidae is moderately supported with a Bremer support of 2, although the ingroup relationships remain unclear in our analysis. Xinjiangchelyids share six unambiguous synapomorphies (three cranial; three postcranial, of which is unique (ch 257.1); Table 2.3). The node support for xinjiangchelyids plus all more crownwardly positioned turtles is high (Bremer support = 4).

2.3.3 Parsimony Analysis using ordered characters

Ordering characters resulted in 116 MPTs initially, and 195 MPTs 1566 steps long after additional TBR branch swapping. The results from the ordered analysis resulted in a large polytomy including all extant clades of turtles, xinjiangchelyids, angolachelonians, and the individual species of sinemydids/macrobaenids (Fig. 2.4B). This is caused by unstable positions of Angolachelonia, 'macrobaenids' (*Judithemys* + the species of *Kirgizemys*), and *Ordosemys* sp. and *Dracochelys biscuspis*. By inspecting the Adams consensus tree, I identified *Ordosemys* sp. as a 'wildcard' taxon that is alternatively found in clades with sinemydids/macrobaenids, only sinemydids, or xinjiangchelyids. When *Ordosemys* is discarded from the set of MPTs, three main topologies are evident, which are summarized in Figure 2.11. The MPT topologies include either (1) Angolachelonians and 'macrobaenids' as

successive sister groups to *Toxochelys* + chelonioids, making them stem-group chelonioids; (2) only Angolachelonians as sister to *Toxochelys* + chelonioids, and sinemydids/macrobaenids forming a clade in the position in which they were also recovered in the unordered analysis; (3) an identical topology to that of the unordered analysis. The topologies in which Angolachelonia is found on the stem-group of chelonioids imply only one origin of marine lifestyles in non-pleurodiran turtles besides *Odontochelys*. However, the ordered analysis agrees with the unordered one in always finding a monophyletic Angolachelonia, and always recovers protostegids as dermochelyoids.

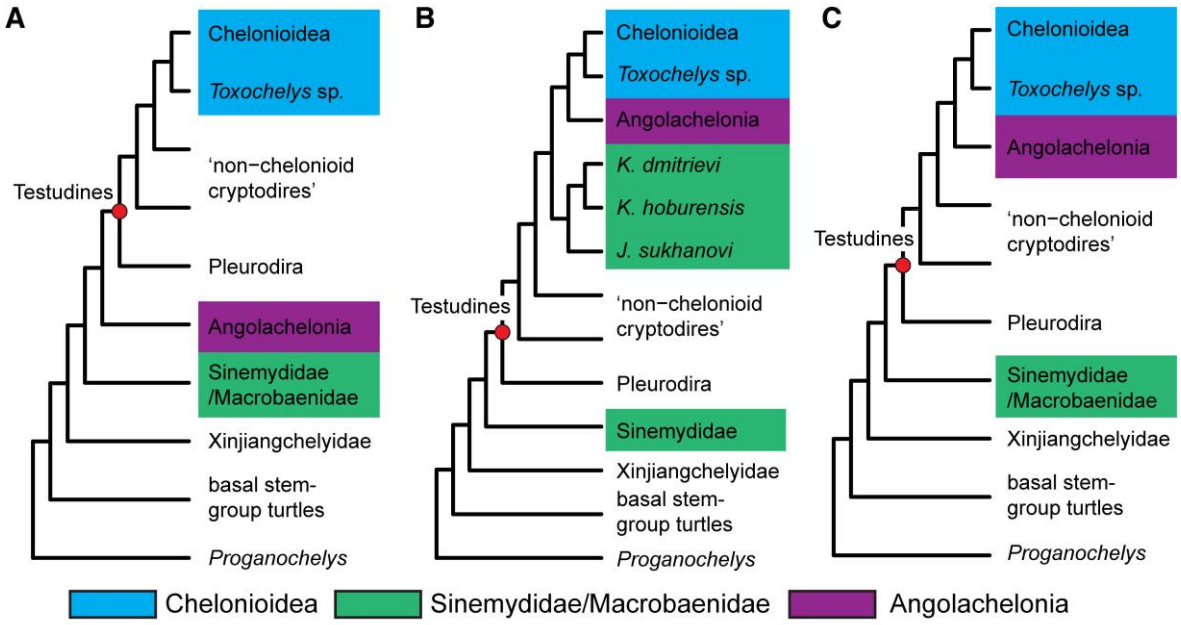


FIG. 2.11. Competing MPT topologies of our ordered analysis resulting in a large polytomy. **A**, topology supported by a subset of MPTs that is identical with results from the unordered analysis; **B**, topology supported by a subset of MPTs in which angolachelonians and macrobaenids are stem-group chelonioids; C, topology supported by a subset of MPTs in which angolachelonians, but not macrobaenids are stem-group chelonioids. Note that *Ordosemys* has been pruned from the MPTs, and that protostegids are included in Chelonioidea.

2.3.4 Excluding 'marine' characters and 'least specialised taxa analyses'

Excluding 'marine' characters resulted in 86 MPTs 1480 steps long initially, and 104 MPTs were recovered in total after a second round of TBR branch swapping. This analysis resulted in a large polytomy that included pleurodires, trionychians, testudinoids, chelydroids, thalassochelydians, sandownids, *Toxochelys*, and chelonioids (Fig. S1.76). This

polytomy resulted from the variable position of sandownids, which in some MPTs were found with thalassochelydians on the stem-group of turtles, and in some MPTs forming a clade with *Toxochelys* on the stem-group of chelonioids. Ingroup relationships of Chelonioidea were poorly resolved, resulting a polytomy of protostegids, crown-group cheloniids, dermochelyids, *Eochelone*, *Allopleuron*, *Argillochelys*, and *Puppigerus*. However, protostegids were found to be chelonioids in all MPTs.

The 'least specialised taxa analysis 1' (only using *Santanachelys*) resulted initially in 91 MPTs 1443 steps long, and 120 MPTs were recovered after a second round of TBR branch swapping. The 'least specialised taxa analysis 2' (*Santanachelys* and *Rhinochelys* included) resulted in 39 MPTs 1453 steps long, and an additional three MPTs recovered during a second round of TBR branch swapping. The 'least specialised taxon analysis 3' (only *Archelon* and *Protostega* excluded) resulted in 12 MPTs 1510 steps long, and a second round of TBR branch swapping did not recover any further MPTs. In the first analysis, *Eochelone* was found in a polytomy with dermochelyids and cheloniids, and *Toxochelys* and *Santanachelys* were found in a polytomy with crown-group chelonioids (Fig. S1.77). In the second analysis, *Sanatanchelys* and *Rhinochelys* formed a monophyletic Protostegidae as the earliest branching stem-group chelonioids (Fig. S1.78). *Toxochelys* was also recovered as a stem-group chelonioid, and as the immediate sister-taxon to crown-group Chelonioidea. *Eochelone* was found as the earliest branching stem-group cheloniid. When only *Archelon* and *Protostega* were excluded, the relationships of all taxa were as in our unordered analysis with the complete taxon sampling, i.e. protostegids were found as dermochelyoids (Fig. S1.79).

2.3.5 Templeton's tests

Of the alternative hypotheses of turtle interrelationships (see Table 2.4) that I tested, only one could be rejected based on significant or near-significant p-values (Table 2.4): the hypothesis that protostegids fall outside of Chelonioidea (discussed below). Alternative hypotheses for xinjiangchelyids, sinemydids, and angolachelonians could not be rejected. A

possible reason for this is illustrated in my similarity results, which show that these groups have relatively high similarity to various cryptodiran groups. Although these similarities in character scores are optimized to be homoplastic in my analysis, alternative interpretations require only a few more steps (see Table 2.4 for differences in step-length) in parsimony analysis and are thus not significantly different to my preferred tree topology.

My procedure of using only one OTU to set up the constraints allowed me to additionally explore the topological effects of these hypotheses. In many cases, alternative placements of individual OTUs resulted in strong topological deviations from the original analysis and affected positions of taxa not relevant to the constraint. Some groups recovered in the analysis are also relatively unstable; for instance, the monophyletic Sinemydidae/Macrobaenidae is broken into paraphyletic or even polyphyletic assemblages in many of the constrained analyses. On the other hand, some groups, such as Angolachelonia or Xinjiangchelyidae, are relatively robustly recovered as monophyletic groups among the constrained analyses, even if their position within the tree structure varied. Consensus trees and MPTs for all constraint analyses in Newick tree format are provided online in the Dryad repository (Evers & Benson 2018*c*), and consensus trees are figured in Appendix S.1 (Figs S1.80–99).

TABLE 2.4. Constraits and hypotheses for Templeton's tests and test results.

Constraint	Hypothesis	Symmetric Distance	Length	Test statistic	N	*p*
All fossil unconstrained	Topology as in Fig. 4A	-	1532	-	-	-
*Plesiochelys etallon*i as a stem-group cryptodire (Constraint 1)	Plesiochelyids are stem-group cryptodires	Maximum	1536	-452.5	44	0.2918
		Minimum		-3,5	6	0.0513×
Jurassichelon oleronensis as a stem-group chelonioid (Constraint 2)	Plesiochelyids are stem-group chelonioids	Maximum	1536	-829.0	59	0.3196
		Minimum		-103.5	22	0.1969
Jurassichelon oleronensis as a stem-group cryptodire (Constraint 3)	Plesiochelyids are stem-group cryptodires	Maximum	1536	-473.5	45	0.2928
		Minimum		-3.5	6	0.0513×
Solnhofia parsoni as a stem-group cryptodire (Constraint 4)	Thalassochelydia are stem-group cryptodires	Maximum	1536	-452.5	44	0.2018
		Minimum		-3.5	6	0.0513×
Solnhofia parsoni as a stem-group chelonioid (Constraint 5)	Thalassochelydia are stem-group chelonioids	Maximum	1536	-829.0	59	0.3196
		Minimum		-103.5	22	0.1969

Constraint	Hypothesis	Symmetric Distance	Length	Test statistic	N	*p*
Sandownia parsoni as a stem-group cryptodire (Constraint 6)	Sandownids are stem-group cryptodires	Maximum	1536	-351.0	39	0.2686
		Minimum		-3.5	6	0.0516×
Sandownia harrisi as a stem-group chelonioid (Constraint 7)	Sandownids are stem-group chelonioids	Maximum	1534	-565.0	48	0.3952
		Minimum		-162.0	26	0.3475
Rhinochelys pulchriceps as a stem-group cryptodire (Constraint 8)	Protostegids are stem-group cryptodires	Maximum	1548	-1538.5	86	0.057(*)
		Minimum		-966.5	70	0.033*
Rhinochelys pulchriceps as a stem-group turtle (Constraint 9)	Protostegids are stem-group turtles	Maximum	1548	-1684.0	89	0.073(*)
		Minimum		-598.5	57	0.02*
Xinjiangchelys wusu as a stem-group cryptodire (Constraint 10)	Xinjiangchelyids are stem-group cryptodires	Maximum	1538	-1088.5	68	0.2857
		Minimum		-646.0	53	0.2535
Sinemys lens as a stem-group cryptodire (Constraint 11)	Sinemydids are stem-group cryptodires	Maximum	1536	-829.0	59	0.3196
		Minimum		-247.5	33	0.2525
Judithemys sukhanovi as a stem-group cryptodire (Constraint 12)	Macrobaenids are stem-group cryptodires	Maximum	1536	-829.0	59	0.3196
		Minimum		-247.5	33	0.2525
Protostega gigas as a stem-group cryptodire (Constraint 13)	Protostegids are stem-group cryptodires	Maximum	1553	-1252.5	81	0.015*
		Minimum		-375.0	50	0.002**
Protostega gigas as a stem-group turtle (Constraint 14)	Protostegids are stem-group turtles	Maximum	1553	-1873.5	96	0.032*
		Minimum		-580.5	59	0.005**
Xinjiangchelys wusu as a stem-group chelonioid (Constraint 15)	Xinjiangchelyids are stem-group chelonioids	Maximum	1542	-855.0	63	0.1192
		Minimum		-638.0	55	0.1074
Sinemys lens as a stem-group Chelonioid (Constraint 16)	Sinemydids are stem-group chelonioids	Maximum	1537	-870.0	61	0.2695
		Minimum		-304.0	37	0.2056
Judithemys sukhanovi as a stem-group chelonioid (Constraint 17)	Macrobaenids are stem-group chelonioids	Maximum	1537	-870.0	61	0.2695
		Minimum		-304.0	37	0.2056
Santanachelys gaffneyi as a stem-group cryptodire (Constraint 18)	Protostegids are stem-group cryptodires	Maximum	1548	-1495.0	85	0.049*
		Minimum		-966.5	70	0.033*
Santanachelys gaffneyi as a stem-group turtle (Constraint 19)	Protostegids are stem-group turtles	Maximum	1547	-594.0	56	0.031*
		Minimum		-128.0	31	0.004*
Santanachelys gaffneyi as a stem-group chelonioid (Constraint 20)	Protostegids are stem-group chelonioids	Maximum	1534	-770.0	56	0.3981
		Minimum		-115.0	22	0.3349

*Significant at $p < 0.05$.
** Significant at $p < 0.01$.
×Low *p*-value due to small N.
(*)Low *p*-values that I refer to as near-significant in the main text.
p-values are the result of a one-tailed test.

Constraining members of Angolachelonia into alternative positions. Angolachelonia was recovered as a monophyletic group regardless of constraints on the positions of individual

thalassochelydians (*Plesiochelys*, *Jurassichelon*, or *Solnhofia;* Figs S1.80–84), and when *Sandownia* is constrained to be a stem-group cryptodire (Fig. S1.85). In other words, specifying an alternative position for one of its members generally resulted in all members of Angolachelonia being found in that position. The one exception to this occurs when *Sandownia* was constrained to be a stem-group chelonioid, in which case only sandownids followed *Sandownia* into this position, and Thalassochelyida was recovered on the stem-group of turtles (Fig. S1.86). None of the constrained analyses in which any member of Angolachelonia was included could be rejected ($p > 0.05$; constraint analyses required between two and four additional steps; see Table 2.4).

Constraining xinjiangchelyids or sinemydids/macrobaenids to be stem-group cryptodires. I could not reject the hypothesis that xinjiangchelyids (i.e. *Xinjianchelys wusu*) or sinemydids/macrobaenids (*Sinemys lens* or *Judithemys sukhanovi*) are stem-group cryptodires ($p > 0.05$; four or six additional steps required; see Table 2.4). Constraining xinjiangchelyids to be stem-group cryptodires resulted in a large polytomy that includes a clade comprising pleurodires and paracryptodires, a monophyletic Xinjiangchelyidae, sinemydids/macrobaenids (not forming a single clade), all cryptodiran clades recovered in our original analyis, and a monophyletic Angolachelonia (Fig. S1.89). Constraining any member of Sinemydidae/Macrobaenidae to be stem-group cryptodires did not change the position of xinjiangchelyids as stem-group turtles, but resulted in the recovery of Angolachelonia as part of the total-group of Chelonioidea, and the recovery of sinemydids/macrobaenids as a clade of stem-group cryptodires (Fig. S1.90–92).

Constraining xinjiangchelyids or sinemydids/macrobaenids to be stem-group chelonioids. Alternative hypotheses in which xinjiangchelyids or sinemydids/macrobaenids were stem-chelonioids could not be rejected (sinemydids/macrobaenids: $p > 0.05$; five additional steps required; see Table 2.4), although p-values for the constraint including *Xinjiangchelys wusu* were relatively low and tree length was relatively high (tree length = 1542 steps, i.e. 10

additional steps; maximum distance tree: p = 0.12; minimum distance tree: p = 0.11). When xinjiangchelydis were constrained to be stem-group chelonioids, xinjiangchelyids and sinemydids formed a monophyletic group, and Angolachelonia was found on the stem-group of turtles (Fig. S1.94). When sinemydids were constrained to be stem-group chelonioids, Angolachelonia was found as the immediate sister to Chelonioidea and *Toxochelys*, and therefore more crownward on the cheloinioid stem than the sinemydids constrained to be stem-group chelonioids, which formed a clade (Fig. S1.95–96). In these analyses, xinjiangchelyids were found to be stem-group turtles.

Constraining members of Protostegidae to be stem-group chelonioids. I conducted an analysis in which *Santanachelys gaffneyi* was constrained to be a stem-group chelonioid. This was done because this topology was found in the 'least specialised taxa analysis 1'. This phylogenetic hypothesis could not be rejected statistically (tree length = 1534, i.e. two additional steps; maximum and minimum distance trees p > 0.5). This constraint resulted in a large polytomy among chelonioids (Fig. S1.99). I additionally explored the Adams consensus tree, in which all fossil cheloniids were found to be members of the chelonioid stem-group: Dermochelyidae (including *Eosphagis*) was sister to a clade comprising extant cheloniids, and taxa recovered as stem-cheloniids in our original analysis formed a paraphyletic grade leading to crown-group chelonioids. A monophyletic Protostegidae formed the next successive sister taxon, and *Toxochelys* was found as the earliest branching stem-group chelonioid. Angolachelonia, Sinemydidae/Macrobaenidae and Xinjiangchelyidae were recovered in positions identical to those in the original analysis.

Constraining members of Protostegidae to be stem-group cryptodires or stem-group turtles. Constraining protostegids into alternative positions onto the stem-group of cryptodires or turtles resulted in statistically significant or near significant p-values, suggesting that alternative hypotheses are unlikely, although not always decisively rejected (see Table 2.4). The topological effects of these constraints resulted in major differences to my trees. When

Rhinochelys or *Santanachelys* were constrained to be stem-group cryptodires (tree length = 1548, i.e. 16 additional steps for either constraint; *Rhinochelys*: maximum distance tree p = 0.054; minimum distance tree p = 0.033; *Santanachelys*: maximum distance tree p = 0.0495; minimum distance tree p = 0.033) or stem-group turtles, protostegids were found to be polyphyletic. The topological effects of these constraints were identical when *Rhinochelys* or *Santanachelys* were constrained to be stem-group cryptodires (Fig. S1.87, S1.97): *Archelon* and *Protostega* formed a clade on the stem of *Dermochelys* as crown-group chelonioids, and the remaining protostegids were found as a monophyletic group that was sister to Thalassochelydia. Sandownids formed a clade one node more stemwardly positioned than the clade that includes *Santanachelys* or *Rhinochelys* and thalassochelydians. When *Santanachelys* was constrained to be a stem-group turtle (tree length = 1547, i.e. 15 additional steps; maximum distance tree p = 0.031; minimum distance tree = 0.004), it was recovered as a plesiochelyid but all remaining protostegids were found as dermochelyoids (Fig. S1.98). Constraining *Rhinochelys* to be a stem-group turtle (tree length = 1548, i.e. 16 additional steps; maximum distance tree p = 0.07; minimum distance tree = 0.02) resulted in the formation of a clade that included all protostegids except *Archelon* and *Protostega* (which remained dermochelyoids), plesiochelyids, and a clade including *Solnhofia* and sandownids (to which the phylogenetic definition of Angolachelonia *sensu* Mateus *et al.* (2009) can be applied, but which differs in taxonomic content of the Angolachelonia in my original analysis) (Fig. S1.88).

When *Protostega* was constrained to be a stem-group cryptodire (tree length = 1553, i.e. 21 additional steps; maximum distance tree p = 0.015; minimum distance tree p = 0.002), a monophyletic Protostegidae was recovered as the sister group to Angolachelonia (Fig. S1.92). This clade was the immediate sister group to cryptodires. Sinemydids/Macrobaenids were found to be paraphyletic, and on the stem-group turtles. Xinjiangchelyids were also found as stem-group turtles. When *Protostega* was constrained to be a stem-group turtle (tree length = 1553, i.e. 21 additional steps; maximum distance tree p = 0.032; minimum distance tree p = 0.005), a monophyletic Protostegidae was recovered as the sister-taxon of

plesiochelyids. This clade was the sister clade to sandownids and *Solnhofia*, which formed a monphyletic group (Fig. S1.93). Sinemydids/macrobaenids and xinjiangchelyids were again recovered as clades on the stem-group turtles. In all constraints including protostegids, sinemydids/macrobaenids and xinjiangchelyids were always found to be stem-group turtles.

2.4 SYSTEMATIC PALAEONTOLOGY

THALASSOCHELYDIA Anquetin *et al.*, 2017*a*

Modified definition. The clade that includes all turtles more closely related to *Eurysternum wagleri* Meyer, 1839, *Plesiochelys etalloni* (Pictet and Humbert, 1857), and *Thalassemys hugii* Rütimeyer, 1873, than to *Pelomedusa subrufa* (Bonnaterre, 1789), *Testudo graeca* Linnaeus, 1758, *Protostega gigas* (Cope, 1871*b*), or *Sandownia harrisi* Meylan et al, 2000.

Diagnosis. Thalassochelydia can be diagnosed on the basis of the following unambiguous synapomorphies: processus trochlearis oticum is limited to the medial part of the otic chamber, and a deep recess is present on the anterior surface of the quadrate medially to the processus trochlearis oticum (ch 81.1); presence of a fossa on the posterodorsal surface of the floor or the supratemporal fossa (ch 113.1); splenial present (ch 185.0); costals lack lateral ossification, allowing the dorsal exposure of the distal end of ribs and the development of fontanelles only at the most anterior and posterior costals (ch 210.2); rib free peripherals are present (ch 211.1); vertebrals 2 to 4 are significantly broader than pleurals (ch 224.0); central articulations of cervical vertebrae are not formed, cervical vertebrae are amphicoelous or platycoelous (ch 278.0).

Remarks. Thalassochelydia was defined by Anquetin *et al.* (2017*a*) to provide a name for the group that includes Eurysternidae, Plesiochelyidae, and Thalassemydidae. To retain the association of the clade name with this taxonomic content, I chose to modify the original

definition of Thalassochelydia to exclude *Sandownia harrisi* (the type species of Sandowniidae).

Phylogenetic definitions have been recently proposed for several commonly recovered clades of Mesozoic turtles (Joyce *et al.* 2004; Mateus *et al.* 2009; Rabi *et al.* 2014; Cadena & Parham 2015; Anquetin *et al.* 2017*a*). These definitions usually include one or several statements of taxa excluded from the definition, and therefore associate a name very specifically to a set of fossil species or higher taxa to the exclusion of others. For example, Anquetin *et al.* (2017*a*: p. 329) provide a phylogenetic definition for their newly coined clade Thalassochelydia, which includes 'all turtles more closely related to *Eurysternon wagleri* Meyer, 1839, *Plesiochelys etalloni* (Pictet and Humbert, 1857), and *Thalassemys hugii* Rütimeyer, 1873, than to *Pelomedusa subrufa* (Bonnaterre, 1789), *Testudo graeca* Linnaeus, 1758, or *Protostega gigas* (Cope, 1871*b*)'. Implicit in the definition of Thalassochelydia is that Anquetin *et al.* (2017*a*) had a specific idea about the content of Thalassochelydia, i.e. the group that *only* includes plesiochelyids, eurysternids, and thalassemydids.

However, there are difficulties with applying definitions like the one above, because some of the specifiers have not been included in any phylogenetic analysis (see also definitions of Rabi *et al.* 2014). For example, no probable thalassemydid has ever been included in a phylogenetic analysis, and the species suitable to define Eurysternidae (i.e *Eurysternon wagleri*) has also not been included in comprehensive analyses (Anquetin *et al.* 2017*a*). Therefore, the application of the name rests on various untested assumptions (such as that *Thalassemys hugii* is more closely related to *Plesiochelys etalloni* than to *Protostega gigas*).

Despite the lack of evidence of the phylogenetic positions of the exact taxa included in the phylogenetic definition of Thalassochelyida as proposed by Anquetin *et al.* (2017*a*), the definition of this taxon seems justifiable on the basis of (i) cladistic evidence that species within the hypodigm of the three traditional families have recently been found to form a clade (plesiochelyids and the putative eurysternid *Solnhofia*; Anquetin *et al.* 2015); and (ii)

informal comparative anatomical evidence suggesting the existence of the group (Anquetin *et al.* 2017*a*).

If the definition for Thalassochelyida is applied to my phylogenetic results, in which I find a clade comprised of *Solnhofia parsoni* (a putative eurysternid), *Plesiochelys etalloni* (a plesiochelyid), and *Sandownia harrisi* (a sandownid) to the exclusion of protostegids, pleurodires, and cryptodires, then sandownids are also included in Thalassochelydia. However, this extended Thalassochelydia would then become an objective junior synonym of Angolachelonia, which is a clade named by Mateus *et al.* (2009) that is phylogenetically defined as the clade containing *Solnhofia* and sandownids. 'Thalassochelydia' as intended by Anquetin *et al.* (2017*a*; i.e. not including sandownids) still exists in my topology, but as a less inclusive clade within the extended Thalassochelydia. I consider it useful to have clade names available for sandownids, thalassochelydians (*sensu* Anquetin *et al.* (2017*a*)) and the clade that includes both of the former. Therefore, it is either necessary to accept the synonymy of Thalassochelydia with Angolachelonia and erect a new name for what Anquetin *et al.* (2017*a*) intended to be Thalassochelydia, or to change the definition of either Angolachelonia or Thalassochelydia. Because Angolachelonia has priority over Thalassochelydia, I modify the definition of Thalassochelyida to specifically exclude sandownids.

ANGOLACHELONIA Mateus *et al.*, 2009

Definition. The clade originating from the most recent common ancestor of *Angolachelys mbaxi* Mateus *et al.*, 2009 and *Solnhofia parson*i Gaffney, 1975*c*.

Diagnosis. Angolachelonia can be diagnosed on the basis of the following unambiguous synapomorphies: the foramen stapedio-temporale is concealed in dorsal view by the temporal skull roof (ch 18.0); the posterior surface of the quadrate bears an infolding ridge ventral to the incisura columella auris (ch 83.1); the articular process of the cranium is strongly posteriorly directed (ch 84.1); the pterygoids are in a very long medial contact with

one another, longer than the basisphenoid total length in midline (ch 94.0); the pterygoid contacts the medial edge of the mandibular condyle when is seem in ventral view (ch 103.1); the posterior margin of the coronoid has a deep notch (ch 181.1); the coronoid bears a foramen at the anterior end, which leads from the fossa meckelii into the space between the mandibular rami (ch 182.1); the coronoid process is relatively high and dorsally or posterodorsally pointed (ch 184.1).

Remarks. Mateus *et al.* (2009) recovered sandownids as more closely related to crown-group cryptodires than to plesiochelyids, and erected the clade Angolachelonia for a group uniting *Solnhofia parsoni* with *Angolachelys mbaxi*, a sandownid not included in my analysis. *Angolachelys* was not included in my analysis, because limited anatomical information is available while new material is in preparation (pers. comm. Octavio Mateus in 2015). However, if *Angolachelys* is in fact a sandownid, as found by previous analyses (Mateus *et al.* 2009; Tong & Meylan 2013; Cadena 2015; see also section 4: since the publication of Evers & Benson (2018*a*), a new paper with additional information on *Angolachelys* has been published (Myers *et al.* 2018), so that *Angolachelys* could be included for analyses in later parts of this thesis), then this name is applicable to the clade that includes thalassochelydians (which include *Solnhofia*) and sandownids (which include *Angolachelys*). Unlike in the analysis of Mateus *et al.* (2009), Angolachelonia includes plesiochelyids as well as *Solnhofia* and sandownids according to my results. Although we find *Solnhofia* as sister to plesiochelyids, branch support for this is only moderate (Bremer support = 2). If future analyses show that *Solnhofia* is indeed more closely related to sandownids than to plesiochelyids or other thalassemydids, *Solnhofia* would be removed from Thalassochelydia, and Angolachelonia would become applicable to the less inclusive clade of sandownids + *Solnhofia*. This is discussed further in section 5 of this thesis, in which I indeed find *Solnhofia* to be closer related to sandownids than to thalassochelydians. The resulting taxonomical issues from this scenario are also discussed in section 5.

SANDOWNIDAE Tong & Meylan, 2013

New definition. The clade that includes *Sandownia harrisi* Meylan *et al.*, 2000, but not *Pelomedusa subrufa* (Bonnaterre, 1789), *Testudo graeca* Linnaeus, 1758, *Solnhofia parsoni* Gaffney, 1975*c, Eurysternum wagleri* Meyer, 1839, *Plesiochelys etalloni* (Pictet and Humbert, 1857), *Thalassemys hugii* Rütimeyer, 1873, or *Protostega gigas* (Cope, 1871*b*).

Diagnosis. Sandownidae can be diagnosed on the basis of the following unambiguous synapomorphies: weak to no lower temporal emargination, the margin of the lower temporal emargination is formed by the quadratojugal or quadratojugal and jugal (ch 34.0); a vomer-palatine contact anterior to the internal naris is present (ch 57.1); the vomer contributes to the upper triturating surface (ch 68.1); the pterygoid forms a posteromedial wing that partially or completely covers the parabasisphenoid, and sometimes the basioccipital in ventral view (ch 108.1); the dorsum sellae is deep, i.e. the dorsal surface of parabasisphenoid between the clinoid processes is a transversely concave floor forming a trough between the posterior part of the dorsal surface of the parabasisphenoid, which is usually cup-like, and the anterior portion of the parabasisphenoid forming the rostrum basisphenoidale and sella turcica (ch 139.0).

Remarks. A monphyletic group including *Sandownia harrisi*, *Brachyopsemys tingitana*, *Angolachelys mbaxi*, and *Leyvachelys cipadi* has been recognized in several studies (Mateus *et al.* 2009; Tong & Meylan 2013; Cadena 2015; see also section 4), and the group has been named as a family following a rank-based definition by Tong & Meylan (2013). Here, I provide a phylogenetic definition of the group that is in accordance with the associated taxon-content of the group implied by previous studies, and phrased coherently in comparison with other phylogenetic definitions for Mesozoic turtles.

2.5 DISCUSSION

2.5.1 Independent origins of marine ecologies

My phylogenetic results using unordered character states support the hypothesis of two independent origins of marine ecologies among non-pleurodiran turtle from the Jurassic onwards: Angolachelonia (thalassochelydians + sandownids) and Chelonioidea (including protostegids). In addition to the Triassic stem-group turtle *Odontochelys*, and 2–3 origins among pleurodires (depending on the phylogenetic relationships of Bothremydidae; Gaffney *et al.* 2006; Rabi *et al.* 2012), this demonstrates a total of 5–6 origins of marine habits through the evolutionary history of turtles. My study represents the first analysis with a large sample of thalassochelydians and sandownids, in which these groups are found to form a clade. The only previous study with a similar sample size for these groups (Cadena 2015), recovered a polyphyletic Thalassochelydia (*Plesiochelys* was recovered as a stem-group turtle, and *Solnhofia* and *Jurassichelon* were found as stem-group chelonioids), and sandownids as stem chelonioids. Compared to previous analyses, I included more observations regarding the cranial anatomy of turtle groups. This was possible thanks to 3D models derived from CT data for species of all major subgroups of turtles included in my taxon sampling, including several sandownids, thalassochelydians, protostegids, and non-protostegid chelonioids. However, alternative hypotheses in which angolachelonians are found to be stem-group chelonioids cannot be rejected at present. Indeed, a parsimony analysis using ordered character states of our data supports this hypothesis in a subset of the resulting MPTs. If anglolachelonians are indeed in the stem-group of Chelonioidea, this would imply only a single origin of marine ecology outside of pleurodires and *Odontochelys*. Angolachelonians are known from Jurassic, Cretaceous and Palaeogene deposits (e.g. Tong & Meylan 2013; Cadena 2015). Furthermore, marine bothremydids and chelonioids are also known both before and after the Cretaceous–Palaeogene boundary. My results therefore indicate that all three major clades of Cretaceous marine turtles survived the K/Pg mass extinction. This

contrasts with other marine reptiles, such as mosasaurs and plesiosaurs (Bardet 1994; Motani 2009; Benson 2013), and explanations of marine turtle survival warrant further investigation.

Differences in the nature of marine adaptation are evident among clades. Members of Angolachelonia are generally interpreted to live in shallow, nearshore marine habitats, because these turtles lack osteological evidence for a pelagic lifestyle, and are found in relatively nearshore deposits (Anquetin *et al.* 2017*a*). Marine pleurodires such as bothremydids also lack evidence for a pelagic ecology, and are usually interpreted to have lived in near-shore marine environments (e.g. Gaffney *et al.* 2006; Ferreira *et al.* 2018). Features interpreted to indicate a pelagic lifestyle, such as rigid inter-phalangeal articulations in the manus, are only present in chelonioids, including protostegids. Because protostegids are found as chelonioids within my analysis, a pelagic lifestyle can be inferred to have evolved only once within turtles. Evolutionary refinement of key adaptations such as flippers cannot be resolved until a better understanding of the ingroup relationships of protostegids is obtained (see Chapter 3).

The Early Cretaceous protostegid *Santanachelys gaffneyi* has flippers in which some moveable articulations are still retained, a condition that is also present in *Toxochelys* (Hirayama 1998). This observation caused Hirayama (1994, 1998) to infer that derived flippers, with rigid manual articulations, evolved independently in dermochelyids, cheloniids, and advanced protostegids. However, *S. gaffneyi* is nested deeply within Protostegidae in my analysis, and *Toxochelys* is found as a stem-group chelonioid rather than a stem-group cheloniid as in Hirayama (1998). Therefore, the presence of less specialized flippers in *Santanachelys* is optimized as a reversal, and the derived condition of flippers in which all manual articulations are rigid is optimized as a synapomorphy for crown-group chelonioids (this was also implied by the matrix of Kear & Lee (2006), although not specifically stated). Unfortunately, the flipper morphology of most Early Cretaceous protostegids (e.g. *Notochelone costata, Rhinochelys pulchriceps*) is not known. However, *Desmatochelys padillai* from the Early Cretaceous of Colombia has been scored to have the advanced flipper

condition (Cadena & Parham 2015), and Late Cretaceous protostegids also lack movable articulations (Hirayama 1994). In-group relationships of Protostegidae require further investigation, because my phylogenetic results differ from those of previous analyses. If protostegids with derived flippers are found to be nested within protostegids showing the primitive condition (as in most previous studies), the flippers of protostegids and other chelonioids could have evolved convergently.

2.5.2 The phylogenetic position of protostegids

Protostegids have been hypothesized to be either (1) on the stem-group of the leatherback turtle *Dermochelys coriacea* within Chelonioidea (i.e. as dermocheyloids; Hirayama 1994, 1998; Brinkman *et al.* 2006; Kear & Lee 2006; Bardet *et al.* 2013; Cadena & Parham 2015; Cadena 2015), (2) to be an independent lineage of pelagic turtles on the stem-group of cryptodires (Danilov & Parham 2006, 2008; Joyce 2007; Sterli & de la Fuente 2011, 2013; Anquetin 2012;), or (3) on the turtle stem (Sterli 2010; Sterli & de la Fuente 2011). The finding of protostegids as stem-group cryptodires, and therefore outside of Chelonioidea by previous analyses, has always been based on the inclusion of the early protostegid *Santanachelys* as the sole representative of that group (Danilov & Parham 2006, 2008; Joyce 2007; Sterli & de la Fuente 2011, 2013; Anquetin 2012). Dermochelyoid affinities for protostegids are usually based on studies focussed on the relationships of marine turtles (e.g. Hirayama 1994; Kear & Lee 2006; Bardet *et al.* 2013; Gentry *et al.* 2018), although some global studies have found protostegids in the same position (e.g. Cadena & Parham 2015; Cadena 2015).

My matrix includes nine protostegids covering their temporal and geographic spread, body size range, and ecological adaptations. Skulls of three Early Cretaceous protostegids, *Rhinochelys pulchriceps*, *Bouliachelys suteri*, and *Notochelone costata,* were CT-scanned and complete skull models have been produced to facilitate character scoring. My 3D models provide the most detailed account of the cranial osteology of protostegids. This allowed me to

score numerous characters, which previously could not be scored, as well as formulate new characters, describing variation in the skull, and particularly the braincase. I find protostegids as dermochelyoids, and the total-group and crown-group of Chelonioidea, as well as Dermochelyoidea (i.e. Dermochelyidae + Protostegidae) are supported by a long list of unambiguous synapomorphies. Furthermore, Bremer support for these groups is robust (see results).

It has been suggested that the finding of protostegids as chelonioids results from the convergent acquisition of a high number of phylogenetically-misleading anatomical character states related to a pelagic lifestyle in both groups (Cadena & Parham 2015). To investigate this, I identified synapomorphies that support the chelonioid relationships of protostegids and could plausibly result from functional constraints on marine adaptation (Table 2.5).

TABLE 2.5. 'Marine' synapomorphies.

Character state	Description	Synapomorphy	Functional relevance
39.1	loose squamosal-quadrate articulation	total-group chelonioids; plesiochelyids	?underwater hearing
58.1	maxillary triturating surface with labial and lingual ridge	total-group chelonioids; plesiochelyids	feeding
68.1	vomer contributing to upper triturating surface	cheloniids; sandownids	secondary palate
210.2	reduction of costal ossification	total-group chelonioids; thalassochelydians	functinal interpretation unclear
231.1	presence of plastral fontanelle	total-group chelonioids	functinal interpretation unclear
333.1	humerus longer than femur	total-group chelonioids	swimming
337.1	rigid articulations in first and second mandual digit	crown-group chelonioids	swimming
338.1	rigid articulations in third through fifth manual digit	total-group chelonioids	swimming
342.1	flattening of carpal and tarsal elements	total-group chelonioids	swimming

These include characters related to the reduction of shell ossification, the modification of limbs to flippers, formation of a secondary palate, and modifications of the triturating surface more generally that could be related to feeding. Several of these characters are also optimized as independently-obtained synapomorphies of angolachelonians or angolachelonian subgroups (Table 2.5). Although I do not support the practice of deleting

characters due to assumed ecological function, protostegids are still recovered as chelonioids by analysis excluding the characters listed in Table 2.5 (see Fig. S1.76). This suggests that protostegids can be found as chelonioids independently of functionally-convergent features related to marine or pelagic life. My 'least specialised taxa analyses' provide further support for the hypothesis that protostegids are chelonioids, although they are found as stem-group chelonioids rather than dermochelyoids when only the taxa from the Early Cretaceous (*Santanachelys*, *Rhinochelys*) are included. Nevertheless, my analysis is the first study in which protostegids are still allied with chelonioids when 'advanced' protostegids are excluded from the analysis.

The heatmaps of similarity indicate that protostegids do show relatively high similarity with various non-chelonioids among stem-group turtles, particularly to sinemydids, xinjiangchelyids, and angolachelonians. Similarities between protostegids and stem-group turtles were also noted by Cadena & Parham (2015). While the high similarity of protostegids to sinemydids and xinjiangchelyids cannot be explained by ecological convergence, it is possible that at least some of the similarity between protostegids (and also chelonioids more generally) and angolachelonians can be explained by their marine lifestyle.

My Templeton's tests provide explicit tests of hypotheses that protostegids are stem-group turtles, or stem-group cryptodires. These hypotheses, although not being strictly rejected in all cases (10 tests result in $p < 0.05$, and two tests result in $0.054 < p < 0.073$; Table 2.4), have poor support, despite the high amount of similarity of protostegid character scorings to those of the non-chelonioid groups. Interestingly, when the Early Cretaceous protostegids *Rhinochelys* or *Santanachelys* are used to constrain protostegids into alternative positions, protostegids are found to be polyphyletic, with Late Cretaceous protostegids still being recovered as the sister to Dermochelyidae. In contrast, when *Protostega* was constrained to alternative positions, protostegids were found to be monophyletic. This provides an explanation for the frequent recovery of protostegids as non-chelonioids, when the early protostegid *Santanchelys* was used as the only protostegid representative in phylogenetic analyses (Danilov & Parham 2006, 2008; Joyce 2007; Sterli & de la Fuente 2011,

2013; Anquetin 2012). Therefore, my matrix provides strong support for the position of protostegids within Chelonioidea. However, the hypothesis that protostegids are stem-group chelonioids, rather than dermochelyoids, cannot be statistically rejected ($p > 0.05$; Table 2.4), and was also found in my 'least specialised taxa analyses' when only Early Cretaceous protostegids were included in the phylogenetic analysis.

2.5.3 Implication on the timing of the origin and biogeographic evolution of Chelonioidea

Molecular phylogenies strongly support a sister-group relationship between Chelydroidea (chelydrids + kinosternids) and Chelonioidea (e.g. Parham *et al.* 2006; Crawford *et al.* 2015; Pereira *et al.* 2017) as a clade called Americhelydia (Joyce *et al.* 2013*b*). Estimates of divergence times place the chelonioid/chelydroid split in the late Early Cretaceous (113 Ma; Joyce *et al.* 2013*b*), and the origin of crown-group chelonioids in the latest Cretaceous (66 Ma; Joyce *et al.* 2013*b*). The fossil calibrations used in these analyses represent the oldest specimens that can be assigned to the respective crown-groups with high certainty (Joyce *et al.* 2013*b*), and these specimens are generally younger than more ambiguous representatives such as protostegids. For example, protostegids, which are recovered confidently as crown-group chelonioids in my analysis, are substantially older (Barremian–Aptian, 120 Ma) than the fossil calibration specimens used by Joyce *et al.* (2013*b*) as the oldest crown-group chelonioids (*Eosphargis breineri* from the Eocene, 55 Ma). Because the oldest protostegids are older than the molecular clock divergence time estimated for Americhelydia, my phylogenetic results have implications for the timings of deep divergences of the turtle crown-group. Furthermore, the inclusion of protostegids into Chelonioidea has implications for the biogeographic evolution of Americhelydia.

The oldest unambiguous (although fragmentary) chelydrid and kinosternoid remains are from the Campanian of Mexico (Brinkman & Rodriguez de la Rosa 2006; Joyce *et al.* 2013*b*; Joyce 2016; Joyce & Bourque 2016) and the United States (Lyson *et al.* 2017), and relatively complete specimens are known from the Maastrichtian of North America

(*Emarginachelys cretacea*; Whetstone 1978; *Hoplochelys clark*; Knauss *et al.* 2011; Joyce & Bourque 2016). Furthermore, the oldest commonly accepted stem-group chelonioid is *Toxochelys* from the Upper Santonian or Lower Campanian Niobrara Formation of North America (Nicholls 1988; Weems & Brown 2017; Gentry *et al.* 2018). Therefore, the earliest undisputed americhelydians suggest a North American origin of the clade (e.g. Crawford *et al.* 2015; Parham *et al.* 2014; Cadena & Parham 2015; Pereira *et al.* 2017), and their ages are consistent with molecular clock estimates dating the origin of Americhelydia into the late Early Cretaceous. A North American origin for Chelonioidea is also supported by a number of pre-Maastrichtian fossils for which phylogenetic positions are currently uncertain, but which have been hypothesized to either be stem-group chelonioids, stem-group cheloniids, or stem-group dermochelyids, such as *Ctenochelys* (e.g. Matzke 2007; Gentry 2016) or *Corsochelys* (Zangerl 1960). Nevertheless, some poorly known fossils of Chelonioidea *incertae sedis* are also found in pre-Maastrichtian deposits outside of North America, such as the putative dermochelyid *Mesodermochelys undulatus* from the Santonian–Maastrichtian of Japan (Sato et al. 2012).

The oldest uncontentious crown-group chelonioids are generally much younger than crown-group chelydroid material, and are not from North America. Although putative dermochelyid specimens are known from the Cretaceous, this mostly fragmentary material has not been included in a phylogenetic analysis (Joyce *et al.* 2013*b*). Therefore, the oldest widely-accepted dermochelyid is the Eocene *Eosphargis breineri* from Denmark (Wood *et al.* 1996; Joyce *et al.* 2013*b*). Similarly, several Eocene taxa from Europe, including *Argillochelys cuneiceps*, *Eochelone brabantica*, and *Puppigerus camperi*, have been consistently found as stem-group cheloniids (e.g. Weems & Brown 2017), and this is supported by my analysis. Putative stem-group cheloniids are also known from the Cretaceous (e.g. Brinkman *et al.* 2006, 2009; Parham *et al.* 2014; Gentry *et al.* 2018), but phylogenetic uncertainty surrounding these taxa has been used as an argument against their use as calibration points (Joyce *et al.* 2013*b*). However, there is a growing body of evidence to suggest that some Cretaceous taxa which have been previously found in alternating phylogenetic positions (like

Ctenochelys from the Coniacian–Campanian of the United States, and *Peritresius* from the Campanian of the United States) can be firmly assigned to the stem-group of cheloniids based on newly discovered or re-analysed material (e.g. Gentry 2016; Gentry *et al.* 2018).

Minimum age constraints for fossil calibrations should be based on strong phylogenetic support indicating the taxon in question is actually a member of the crown-group (Parham *et al.* 2012). Although I reject the possibility that protostegids fall outside of the crown-group of Cryptodira, I cannot reject the possibility that protostegids are stem-group chelonioids. Therefore, protostegids might not be ideal candidates for constraining the crown-group age of Chelonioidea, although they could be used as a calibration for the crown-group of Americhelydia. Nevertheless, I find strong support for the presence of crown-group members of Chelonioidea in the Cretaceous, even ignoring protostegids. For example, *Allopleuron hofmanni* from the Maastrichtian of central Europe is found as a stem-group cheloniid. Irrespective of the affinities of protostegids (i.e. even if protostegids are not crown-group chelonioids), use of *Allopleuron* or even older taxa such as *Ctenochelys* or *Peritresius* (Gentry *et al.* 2018) as a calibration point for the crown-group of Chelonioidea is likely to affect molecular clock estimates for the crown-group age of chelonioids, and should be investigated. Although I do not provide a formal molecular clock analysis, I produced a time-calibrated version of our tree using *a posteriori* calibration methods in R (see Methods), which illustrates the extensions of chelonioid ranges implied by our phylogenetic results (see Fig. 2.12).

The hypothesis of protostegids being crown-group chelonioids complicates biogeographic scenarios for the evolution of Americhelydia (e.g. Joyce *et al.* 2013*b*; Parham *et al.* 2014; Cadena & Parham 2015). This is because the cosmopolitan distribution of the earliest protostegids, lacking any records from the Early Cretaceous of North America, is hard to reconcile with the occurrence of earliest chelydroid and stem-group chelonioid material exclusively in North America. Given the predominantly North American records of all their close relatives, my phylogenetic results nevertheless imply a North American origin of protostegids, and therefore suggest an early, and rapid global dispersal for the group. The

inferred marine ecology for all protostegids, including earliest members of the group (Cadena & Parham 2015) makes this hypothesis plausible. Furthermore, my hypothesised Late Cretaceous age for the chelonioid crown-group also invokes rapid, early dispersal to explain the distribution of stem-cheloniids in the Late Cretaceous: Maastrichtian, stem-group cheloniids have a near-global distribution, indicated by the presence of *Allopleuron* in Europe, and the widespread distribution of *Euclastes* spp. (Parham *et al.* 2014). In the context of my phylogenetic hypothesis, it is also noteworthy that the 'advanced' protostegids *Archelon* and *Protostega*, which are known from the Santonian–Campanian of North America, are, contrary to earlier phylogenetic studies (e.g. Kear & Lee 2006), not deeply nested within the Protostegidae according to my analysis. This topology implies that the last common ancestor of protostegids originated in North America, but so far remains unsampled.

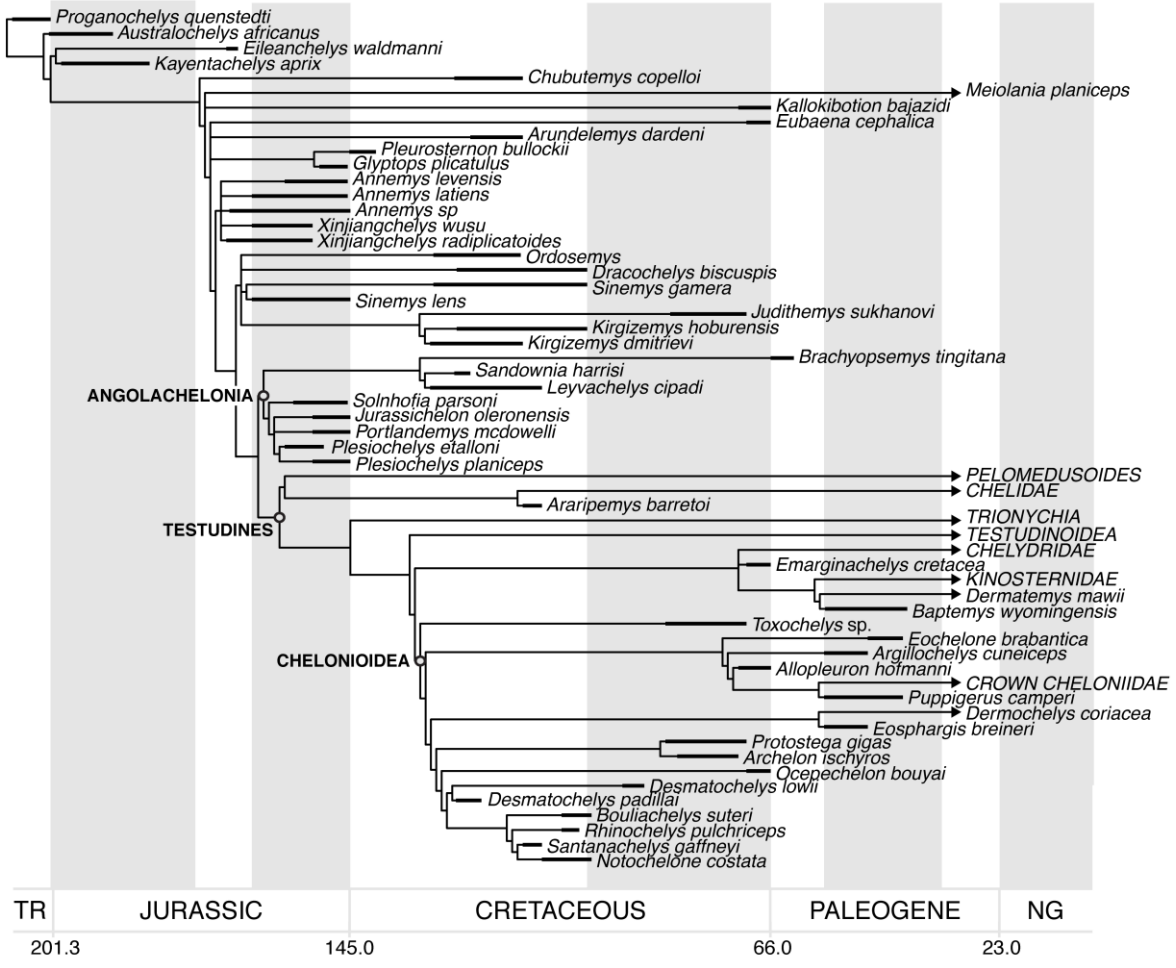


FIG. 2.12. Simplified phylogenetic tree scaled to geologic time using range data for turtles.

If protostegids indeed are crown-group chelonioids, as proposed here, both chelydroids and cheloniids have relatively long ghost lineages of minimally 40 Ma, ranging from the Campanian (the oldest occurrence of chelydroids) or the Maastrichtian (the oldest occurrence of cheloniids) back to the top of the Barremian (the oldest occurrence of protostegids; Cadena & Parham 2015). The cheloniid ghost lineage is significantly shortened, if *Ctenochelys* is accepted as a stem-group cheloniid (Gentry 2016; Gentry *et al.* 2018). The alternative hypothesis, in which protostegids are not chelonioids (e.g. Joyce 2007; Danilov & Parham 2008; Sterli 2010; Anquetin 2012) reduces the ghost-lineages for americhelydian

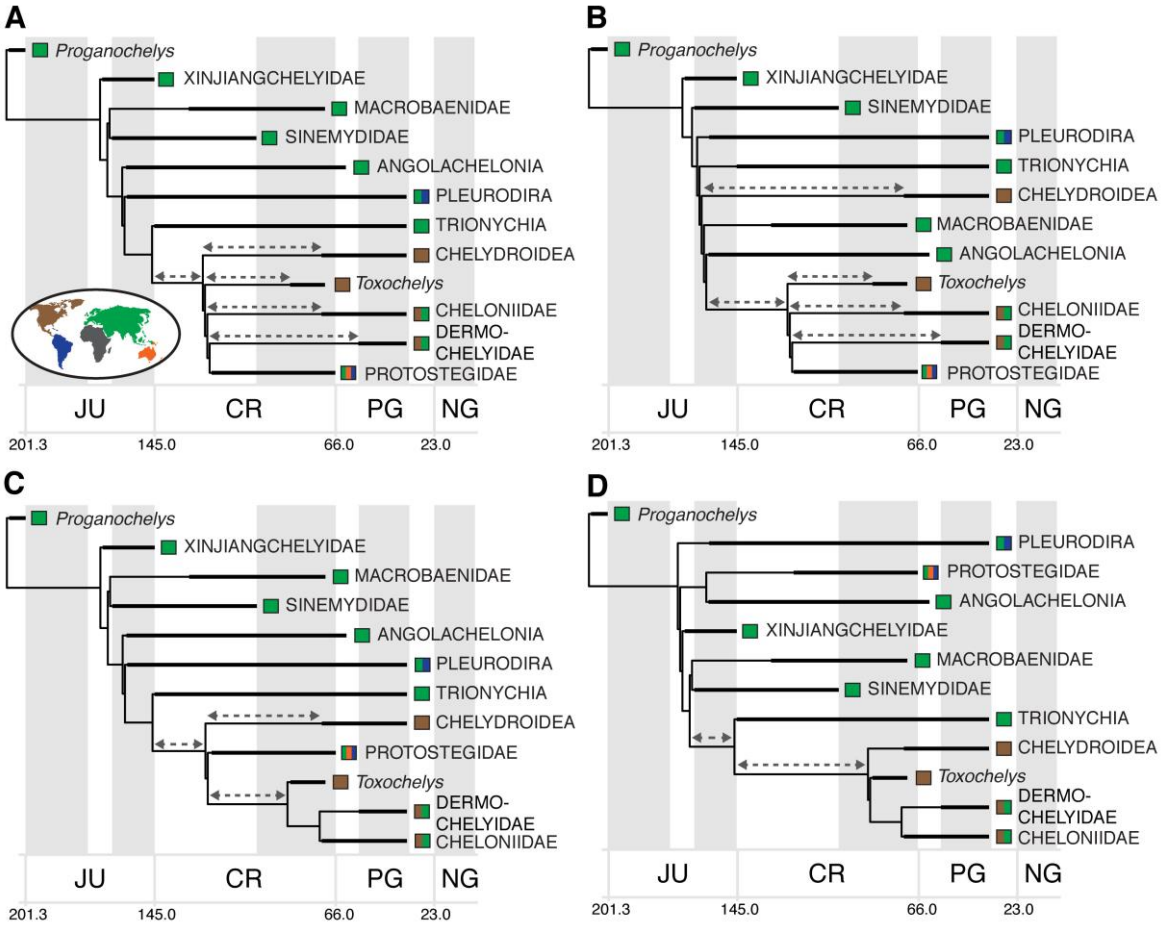


FIG. 2.13. Implications of alternative positions of Protostegidae for americhelydian ghost-lineages and biogeography illustrated by simplified calibrated trees. **A**, preferred hypothesis of this study, supported by unordered phylogenetic analysis; **B**, hypothesis placing Angolachelonia on the stem-group of chelonioids, supported by a subset of MPTs in the ordered analysis; **C**, hypothesis of protostegids being stem-group chelonioids, supported by a subset of our 'least specialised taxa analyses'; **D**, hypothesis following Joyce (2007) and other authors in placing protostegids in close relation to thalassochelydians and sandownids, and having an extended cryptodiran stem-lineage that further includes sinemydids/macrobaenids and xinjiangchelyids. Ghost lineages for americhelydian lineages are indicated by dashed arrows. Coloured squares indicate the distribution of earliest fossils according to continents.

crown-groups, but in doing so implies a long ghost-lineage for the americhelydian stem-group that spans through the entire Early Cretaceous and into the early Late Cretaceous.

Ghost-lineages for various phylogenetic hypotheses are compared in Figure 2.13, and the biogeographic distributions of the earliest members of the different turtle clades considered in this study are indicated to compare biogeographic implications of these hypotheses. The (thus far unsampled) existence of Early Cretaceous americhelydians is not implausible because the sedimentary and fossil record of post-Tithonian to pre-Campanian tetrapods in North America is relatively poor, with only few tetrapod-bearing formations known, and few turtle species of any groups (Ronov *et al.* 1980; Benson *et al.* 2013; Joyce *et al.* 2013*b*; Nicholson 2015). Therefore, the absence of chelydroid, non-protostegid chelonioid, and protostegid fossils in the late Early and early Late Cretaceous of North America could be a taphonomic or discovery artefact.

Finally, an Early Cretaceous age for crown-chelonioids, as implied by my phylogenetic hypothesis of protostegids, is not inconsistent with divergence time estimates for other groups of turtles, or with the oldest crown-group turtle occurrences. The oldest unambiguous total-group pleurodire is *Caribemys oxfordiensis* from the Oxfordian of Cuba (de la Fuente & Iturralde-Vinent 2001; Joyce *et al.* 2013*b*), and stem-group pleurodires are also known from the Late Jurassic of North America, South America, and Europe (Platychelyidae; Lapparent de Broin et al. 2007; López-Conde & Alvarado-Ortega 2017; Sullivan & Joyce 2017), indicating that the cryptodire-pleurodire split occurred by the Late Jurassic. The origin of crown-group Cryptodira has been dated by using representatives of the oldest documented cryptodiran clade, Trionychia (e.g. Joyce *et al.* 2013*b*). The stem-group trionychian *Sinaspideretes wimani* represents the oldest currently known material of Cryptodira, but the ambiguous locality information for specimens of this taxon make it difficult to use *Sinaspideretes* as a calibration point, as the possible age of the fossils range from the Middle Jurassic to the Early Cretaceous (Joyce *et al.* 2013*b*; Tong *et al.* 2014). Therefore, Joyce et al. (2013*b*) used stem-trionychid remains from the Barremian (e.g. Hirayama *et al.* 2013; Joyce *et al.* 2013*b*) as a minimum age constraint for Cryptodira, and dated the origin of Cryptodira to the Early Jurassic, a result

that was partially driven by their soft maximum constraint at the base of the Jurassic. The oldest crown-group trionychians are known from the Aptian and Albian (Tong *et al.* 2009; Joyce 2014; Li *et al.* 2015; Brinkman *et al.* 2017; Vitek *et al.* 2017). Within Trionychia, trionychids have a well-studied fossil record that indicates the group was widely distributed and diverse in the Early Cretaceous (e.g. Hirayama *et al.* 2013; Danilov *et al.* 2014; Vitek & Joyce 2015; Joyce *et al.* 2016; Georgalis & Joyce 2017). Similar patterns of diversification have been observed for Pleurodira: the oldest crown-group pleurodire is *Atolchelys lepida* from the Barremian of Brazil (Romano *et al.* 2014). The pleurodire-cryptodire split and the origin of Trionychia represent early crown-group turtle divergences. In contrast, chelonioids are deeply nested within Cryptodira. Therefore, although not inconsistent with the ages of major groups of crown-group turtles in general, my results imply longer ghost lineages for at least some of the more deeply-nested groups of Cryptodira than have previously been recognised.

The Early Cretaceous diversification of at least some higher clades of the turtle crown-group (pleurodires, trionychids, and chelonioids, as suggested here) is consistent with large increases in subsampled richness estimates for regional turtles assemblages during the Early Cretaceous (Nicholson 2015). My phylogenetic results suggest rapid diversification of crown-groups of turtle subclades during this interval. This hypothesis will continue to be tested by new fossil discoveries, and re-interpretation of existing specimens using methods like CT scanning.

2.6 CONCLUSIONS

My new phylogenetic matrix represents an effort to combine previously observed variation across non-pleurodiran turtles with new observations informed by the study of high-resolution CT scans. The character data has been vetted to directly reflect primary hypotheses of homology. The new phylogenetic hypothesis presented here supports two origins of marine ecology in non-pleurodiran turtles outside of *Odontochelys*. One of these is a newly recognized group, Angolachelonia, which includes thalassochelydians from the Late

Jurassic, and sandownids from the Cretaceous and Palaeogene. Angolachelonians lack features indicative of a pelagic lifestyle, which are only present in chelonioids, supporting a single origin of pelagic ecology in turtles. My results indicate extensive survivorship of marine turtles during the Cretaceous–Palaeogene mass extinction in comparison to other marine tetrapods, because members of all marine clades that were present at the end of the Cretaceous (i.e. bothremydid pleurodires, angolachelonians, and chelonioids) survived into the Cenozoic. Furthermore, my analysis provides strong evidence for the position of protostegids within the crown-group of chelonioids. Alternative positions for protostegids cannot be robustly statistically rejected in all cases, but these alternative hypotheses lack any substantial support from my data, and even the exclusion of 'marine' characters or a reduced taxon sampling only including early and less specialised taxa support my proposed relationships for protostegids. Previously proposed alternative positions for protostegids can be explained by high levels of similarity (i.e. homoplasy) to several turtle clades that are positioned more stemwardly, and have been derived by using only a single early representative of the group, *Santanachelys*. The inclusion of protostegids, as well as some other taxa such as *Allopleuron* from the Maastrichtian, in the crown-group of chelonioids implies an earlier diversification of the group than previously thought, and implies an Early Cretaceous age for the origin of the crown-group of Chelonioidea. Although this needs further exploration, these findings are consistent with the hypothesis of rapid evolution and diversification of subclades of the turtle crown in the Early Cretaceous.

2.7 DATA ARCHIVING STATEMENT

Data for this study (including CT volume files and mesh files for segmented models) are available in the MorphoSource repository (Evers & Benson 2018*b*): http://www.morphosource.org/Detail/ProjectDetail/Show/project_id/462. Additional data (files and instructions for Templeton's tests; files and R code for similarity analysis; appendices including the character-taxon matrix, the character list, and the character

optimisation) are available in the Dryad Digital Repository (Evers & Benson 2018*c*): https://www.datadryad.com/resource/doi:10.5061/dryad.2pb356h

SUPPORTING INFORMATION

Additional Supporting Information can be found in Appendix S1 of this thesis.

3 CRANIAL OSTEOLOGY, NEUROANATOMY, AND TAXONOMY OF *RHINOCHELYS* (PROTOSTEGIDAE)

NOTES

This chapter has been submitted (together with the contents of chapter 3) to the journal *PeerJ* as Evers, Barrett & Benson (201X). Paul Barrett and Roger Benson have assisted with the collection of CT data, and improved drafts of my writing. All other data collection, processing, analysis and synthesis have been done my myself.

ABSTRACT

Knowledge of the early evolution of sea turtles (Chelonioidea) has been limited by conflicting phylogenetic hypotheses resulting in part from a superficial understanding of the morphology of key taxa. One problematic group is the protostegids, Early–Late Cretaceous marine turtles that have been hypothesized to be either stem-turtles, stem-chelonioids, or crown-chelonioids. I present a detailed anatomical study of one of the earliest protostegids, *Rhinochelys pulchriceps* from the early Late Cretaceous of Europe, using high-resolution μCT scanning. Detailed investigation of previously undocumented parts of the cranial anatomy and neuroanatomy are used to inform cladistic characters (implemented in Chapter 1) in order to improve phylogenetic hypotheses for protostegids. I document variation in the genus *Rhinochelys* and synonymize all European species.

3.1 INTRODUCTION

Protostegids are a taxonomically and ecologically diverse clade of Early–Late Cretaceous marine turtles (e.g. Cope 1871*a*; Wieland 1896; Zangerl 1953*a*; Collins 1970; Hooks 1998; Hirayama 1998; Tong *et al.* 2006; Bardet *et al.* 2013; Cadena & Parham 2015)

and achieved a global distribution early in their history (Collins 1970; Hirayama 1998; Kear & Lee 2006; Cadena & Parham 2015). The phylogenetic position of protostegids has been highly debated (e.g. Hirayma 1995; Joyce 2007; Cadena & Parham 2015; Evers & Benson 2018*a*), with the main hypotheses being that protostegids are either stem-group turtles or total-group chelonioids (see Chapter 1). Attempts to resolve the phylogenetic conflict surrounding protostegids must involve detailed study of their fossils. Although some protostegid species are known from numerous specimens, their anatomy is quite poorly known, especially with respect to the skull (Seeley 1869; Lydekker 1889; Moret 1935; Collins 1970; Tong *et al.* 2006; Cadena & Parham 2015). This is because many specimens are either preserved on slabs with crushed skulls (e.g. Hirayama 1998; Tong *et al.* 2006) or in nodules that include completely preserved skulls, but in which most of the internal anatomy is concealed by matrix that is hard to prepare either mechanically or chemically (e.g. Collins 1970; Cadena & Parham 2018). A thorough understanding of the cranial anatomy of protostegids, especially in early representatives of the group, is important for several reasons. For example, it has been hypothesized that anatomical adaptations in the postcranial skeleton related to the marine habitat of protostegids could represent convergent acquisitions of these features with chelonioids, and falsely support relationships with those taxa (e.g. Cadena & Parham 2015). Furthermore, cranial features such as the carotid circulation have been important in establishing the phylogenetic relationships of extant and extinct turtles (e.g. Jamniczky 2007; Müller *et al.* 2011; Rabi *et al.* 2013).

Here, we used X-ray computed-tomography (CT) to illustrate the cranial and mandibular anatomy of the Early Cretaceous protostegid *Rhinochelys*. We present a detailed osteological and neuroanatomical description of this taxon based on digital segmentation of CT scans of six skulls from the Cambridge Greensand Member of the West Melbury Marly Chalk Formation in the United Kingdom. This sample includes the holotype specimens of all three species considered valid by the latest revision of the material by Collins (1970). Our work represents the most detailed account of the cranial and mandibular anatomy of any protostegid. This data was used in a recent phylogenetic paper (Evers & Benson 2018*a*–*c*) to

inform cranial and mandibular phylogenetic character scores and highlights the dermochelyoid affinities of protostegids. We extend that phylogenetic work by analysis of an expanded dataset, including the addition and revision of several postcranial characters and the addition of 16 taxa. Our new phylogenetic analysis recovers protostegids as chelonioids, albeit on their stem-lineage. We provide a taxonomic revision of *Rhinochelys*, and provide evidence for the hypothesis that only one taxon from Europe, *R. pulchriceps*, should be considered valid. Nevertheless, other turtle and sea turtle specimens from the Cambridge Greensand Member of the West Melbury Marly Chalk Formation indicate a higher diversity of turtles, specifically sea turtles, in the late Early Cretaceous of England. This previously unrecognized diversity prohibits the assignment of isolated postcranial material to *Rhinochelys* until skull-postcranial associations are found.

3.2 METHODS

3.2.1 CT data and 3D models used in this study

I used high-resolution X-ray computed-tomography (CT) scanning to generate slice data for six specimens of *Rhinochelys*, including the holotype specimens of *R. pulchriceps*, *R. elegans* and *R. cantabrigiensis*. Because the scanning parameters varied, voxel size information are summarized in Table 3.1 and full details of the scanning parameters are reported with the deposited scans (see data archiving statement below). 3D models were generated through manual segmentation in the software Mimics 16.0–18.0 (http://biomedical.materialise.com/mimics). 3D models were exported as .ply-files, and the software Blender 2.71 (blender.org) was used for visualisation in all figures of digital renderings provided. CT-slice data as well as 3D models are deposited at MorphoSource (see data archiving statement below).

TABLE 3.1 Measurements from different specimens of *Rhinochelys* specimens used in our Principal Component Analyses. PCA 1 is the analysis including only measurements that were used by Collins (1970) for her taxonomic assessment of *Rhinochelys*; PCA 2 includes all measurements taken in this study.

Specimen	Right nasal length–width ratio	Left nasal length–width ratio	Jaw angle (in °)	Width (mm)	Orbital width (mm)	Pre-parietal length (mm)	Height (mm)	PCA 1	PCA 2
CAMSM B55773	?	?	?	40	22	22	20	-	-
CAMSM B55774	1.38	1.10	41	32	15	24	17	included	included
CAMSM B55775	1.33	1.69	49	39	18	26	21	included	included
CAMSM B55776	1.18	1.08	44	30	14	21	18	included	included
CAMSM B55781	1.46	1.81	47	NA	22	NA	13	-	-
CAMSM B55782	1.22	1.13	43	19	9	14	12	included	included
CAMSM B55783	0.89	0.91	47	23	12	17	13	included	included
CAMSM B55784	1.27	1.34	48	30	16	22	18	included	included
CAMSM B55785	1.07	0.94	42	27	14	18	14	included	included
CAMSM B55786	0.73	0.83	43	27	12	17	16	included	included
CAMSM B55787	1.00	1.07	43	24	11	16	16	included	included
CAMSM B55788	1.10	1.10	47	NA	NA	NA	NA	-	-
CAMSM B55791	1.07	0.96	36	20	11	15	10	included	included
CAMSM B55792	1.31	1.31	43	NA	14	25	23	-	-
CAMSM B55793	?	?	40	19	11	14	11	included	-
CAMSM B55794	1.20	1.15	45	21	13	19	16	included	included
CAMSM B55795	0.88	0.85	40	NA	NA	NA	NA	-	-
CAMSM B55796	0.96	NA	47	NA	NA	NA	NA	-	-
CAMSM B55799	?	?	?	15	11	14	11	-	-
CAMSM B56274	NA	NA	39	31	NA	NA	24	-	-
CAMSM B56397	?	?	37	22	11	17	16	included	-

Specimen	Right nasal length–width ratio	Left nasal length–width ratio	Jaw angle (in °)	Width (mm)	Orbital width (mm)	Pre-parietal length (mm)	Height (mm)	PCA 1	PCA 2
CAMSM B56570	1.18	1.29	33	40	17	25	19	included	included
CAMSM B56571	1.38	1.50	41	30	13	17	17	included	included
CAMSM B56572	NA	1.36	43	26	11	16	14	included	-
CAMSM B56573	?	?	43	30	14	20	16	included	-
CAMSM B56574	0.80	0.92	47	22	12	16	13	included	included
CAMSM B56575	1.26	1.40	45	39	18	27	20	included	included
CAMSM B56576	?	?	?	22	11	16	14	-	-
CAMSM B56578	1.17	1.13	41	22	11	NA	15	-	-
CAMSM B56583	0.79	0.87	46	20	10	17	12	included	included
NHMUK PV R11521	1.14	1.04	47	20	11	14	17	included	included
NHMUK PV R1558	1.13	1.13	?	NA	15	NA	20	-	-
NHMUK PV R1806	1.67	1.55	37	27	14	20	NA	-	-
NHMUK PV R2224	0.69	1.09	47	28	19	30	22	included	included
NHMUK PV R2225	0.74	0.74	37	NA	NA	NA	NA	-	-
NHMUK PV R2226	1.11	1.20	48	40	19	30	26	included	included
NHMUK PV R2227	1.50	1.44	47	24	11	18	16	included	included
NHMUK PV R2228	1.72	1.72	45	NA	16	NA	NA	-	-
NHMUK PV R2229	1.48	1.40	NA	NA	NA	NA	NA	-	-
NHMUK PV R2230	1.79	1.67	?	NA	NA	NA	NA	-	-
NHMUK PV R2231	1.62	1.71	38	NA	NA	NA	NA	-	-
NHMUK PV R2233	0.92	1.04	38	13	10	20	16	included	included
NHMUK PV R2234	0.91	1.04	40	23	11	19	18	included	included
NHMUK PV R2235	1.19	1.28	62	NA	NA	NA	NA	-	-
NHMUK PV R2236	1.34	1.28	?	NA	NA	NA	NA	-	-

Specimen	Right nasal length–width ratio	Left nasal length–width ratio	Jaw angle (in °)	Width (mm)	Orbital width (mm)	Pre-parietal length (mm)	Height (mm)	PCA 1	PCA 2
NHMUK PV OR35193	1.85	1.70	47	NA	22	36	NA	-	-
NHMUK PV OR35194	1.77	1.56	48	NA	24	32	NA	-	-
NHMUK PV OR35195	NA	NA	38	NA	NA	NA	NA	-	-
NHMUK PV OR35196	1.28	1.39	47	NA	15	NA	18	-	-
NHMUK PV OR35197	1.04	1.15	43	20	11	15	14	included	included
NHMUK PV OR41796	1.59	1.70	54	NA	21	31	20	-	-
NHMUK PV OR43980	1.00	1.00	56	30	17	22	21	included	included
NHMUK PV OR46371a	0.71	0.73	43	21	11	19	16	included	included
NHMUK PV R8339	1.30	1.30	45	24	12	21	18	included	included
UJF-ID.11167	0.92	0.96	57	43	20	28	29	included	included

3.3 SYSTEMATIC PALAEONTOLOGY

TESTUDINES Linnaeus, 1758

CRYPTODIRA Cope, 1868

CHELONIOIDEA Oppel, 1811

PROTOSTEGIDAE Cope, 1873

RHINOCHELYS Seeley, 1869

Type species: *Rhinochelys pulchriceps* (Owen, 1851)

Diagnosis: A small protostegid sea turtle with a preorbital bulge formed by the maxilla and prefrontal.

Remarks: The genus *Rhinochelys* is known from a series of specimens from Europe (*R. pulchriceps*) and Lebanon (*R. nammourensis*). The type species *R. pulchriceps* is known from cranial specimens, some of which include articulated mandibles, but no postcranial material can be assigned to the genus at present (see Discussion). *R. nammourensis* is known from complete specimens (Tong *et al.* 2006). Because the skulls of *R. nammourensis* are not well known (partially due to the preservation of specimens on slabs of rock), we could not include *R. nammourensis* in this revision, but accept it as a valid species pending a detailed cranial comparison with *R. pulchriceps*. *R. nammourensis* can be referred to *Rhinochelys* due to the presence of a prominent preorbital buldge that is otherwise only known in *R. pulchriceps* (see Tong *et al.* 2006).

Rhinochelys pulchriceps (Owen, 1851)

Chelone pulchriceps Owen, 1851, p. 8, plate 7, Figs 1–3

Rhinochelys mastocephalus Seeley, 1869–Seeley (1869): p. xviii (*nomen nudum*)

Rhinochelys eurycephalus Seeley, 1869–Seeley (1869): p. xviii (*nomen nudum*)

Rhinochelys stenicephalus Seeley, 1869–Seeley (1869): p. xviii (*nomen nudum*)

Rhinochelys cardiocephalus Seeley, 1869–Seeley (1869): p. xviii (*nomen nudum*)

Rhinochelys sphenicephalus Seeley, 1869–Seeley (1869): p. xviii (*nomen nudum*)

Rhinochelys dayi Seeley, 1989–Seeley (1869): p. xviii (*nomen nudum*)

Rhinochelys platyrhinus Seeley, 1869–Seeley (1869): p. xviii (*nomen nudum*)

Rhinochelys rheporhinus Seeley, 1869–Seeley (1869): p. xviii (*nomen nudum*)

Rhinochelys graptocephalus Seeley, 1869–Seeley (1869): p. xviii (*nomen nudum*)

Rhinochelys dacognathus Seeley, 1869–Seeley (1869): p. xviii (*nomen nudum*)

Rhinochelys oolognathus Seeley, 1869–Seeley (1869): p. xviii (*nomen nudum*)

Rhinochelys dimerognathus Seeley, 1869–Seeley (1869): p. xviii (*nomen nudum*)

Rhinochelys grypus Seeley, 1869–Seeley (1869): p. xviii (*nomen nudum*)

Rhinochelys platycephalus Seeley, 1869–Seeley (1869): p. xviii (*nomen nudum*)

Rhinochelys leptognathus Seeley, 1869– Seeley (1869): p. xix (*nomen nudum*)

Rhinochelys pulchriceps (Owen, 1851)–Seeley (1869): p. xviii; Lydekker (1889): p. 230, plate VIII, Fig. 1; Collins (1970) *partim*: p. 358f, Figs 5, 7, plate 67: Figs 1–8, plate 68: Figs 1–2; Hirayama (1994): Figs 1f, 2g, 3g; Hirayama (1997): p. 228, Fig. 7G; Hooks (1998): p. 86f

Rhinochelys macrorhina Lydekker, 1889–Lydekker (1889): p. 230, plate VII Fig. 7; Collins (1970), Fig. 5; plate 68: Fig. 3

Rhinochelys elegans Lydekker, 1889–Lydekker (1889): p. 230, plate VIII Fig. 5; Collins (1970) *partim*: p. 359, Figs 1–2, 5, 8, plate 68: Figs 3–7

Rhinochelys cantabrigiensis Lydekker, 1889–Lydekker (1889): p. 230, plate VIII Fig. 2; Collins (1970) *partim*: p. 359, Fig. 5, plate 68: Figs 8–16

Rhinochelys jessoni Lydekker, 1889–Lydekker (1889): p. 231, plate VIII, Fig. 3; Collins (1970): Fig. 3, plate 68: 11–13

Rhinochelys brachyrhina Lydekker, 1889–Lydekker (1889): p. 231, plate VIII, Fig. 6; Collins (1970), Fig. 4, plate 68: Fig. 4

Rhinochelys ambareti Moret, 1935: p. 606, Figs 1–2; plates XXVII–XXVIII; Collins (1970), Fig. 6; Scavezzoni & Fischer (2018) *partim*: p. 7, Figs 3–6

Holotype: CAMSM B55775, a partially preserved skull.

Type locality and horizon: Cambridge Greensand Member of the West Melbury Marly Chalk Formation (early Cenomanian: Upper Cretaceous), near Barnwell, Cambridgeshire (Owen 1851).

Referred specimens: Cranial specimens: CAMSM B55771–55774, B55776, B55779–55788, B55791–55796, B55798–55800, B55811, B56274, B56397, B56570–56576, B56578, B56580, B56583; IRSNB GS63–65, IRSNB GS67–68, IRSNB GS70; NHMUK R27, R1558, R1806, R2224–2237, R8339, R11521, R35193–35197, R41796, R 43980, R46371, R46371a, R47206; UJF-ID.11167. Mandibles: CAMSM B55809–55810, B55819, B56590, B56593, B59560; NHMUK R2238–2239, R2916, R35183, R35185a, R46373–46374; R49919–49920.

Revised diagnosis: *R. pulchriceps* can be distinguished from other known protostegids by the absence of a median ridge or projection on the dorsum sellae of the parabasisphenoid and by the presence of a splenial in the mandible. However, these features could not be checked for *R. nammourensis* and some other Early Cretaceous protostegids, such as *Santanachelys*.

3.4 DESCRIPTION

The following description is based largely on the specimens that were CT scanned, i.e. CAMSM B55775 (holotype of *R. pulchriceps*; Fig. 3.1; Appendix S2, Fig. S2.1), NHMUK PV OR43980 (holotype of *R. cantabrigiensis*; Fig 3.2; Appendix S2, Fig. S2.2), NHMUK PV R2226 (holotype of *R. elegans*; Fig. 3.3; Appendix S2, Fig. S2.3), CAMSM B55776 (referred to *R. elegans* by Collins 1970; Fig. 3.4; Appendix S2, Fig. S2.4), NHMUK PV OR35197 (referred to *R.*

elegans by Collins 1970; Fig. 3.5; Appendix S1, Fig. S2.5), and CAMSM B55783 (referred to *R. cantabrigiensis* by Collins 1970; Figs 3.6–11; Appendix S2, Fig. S2.6).

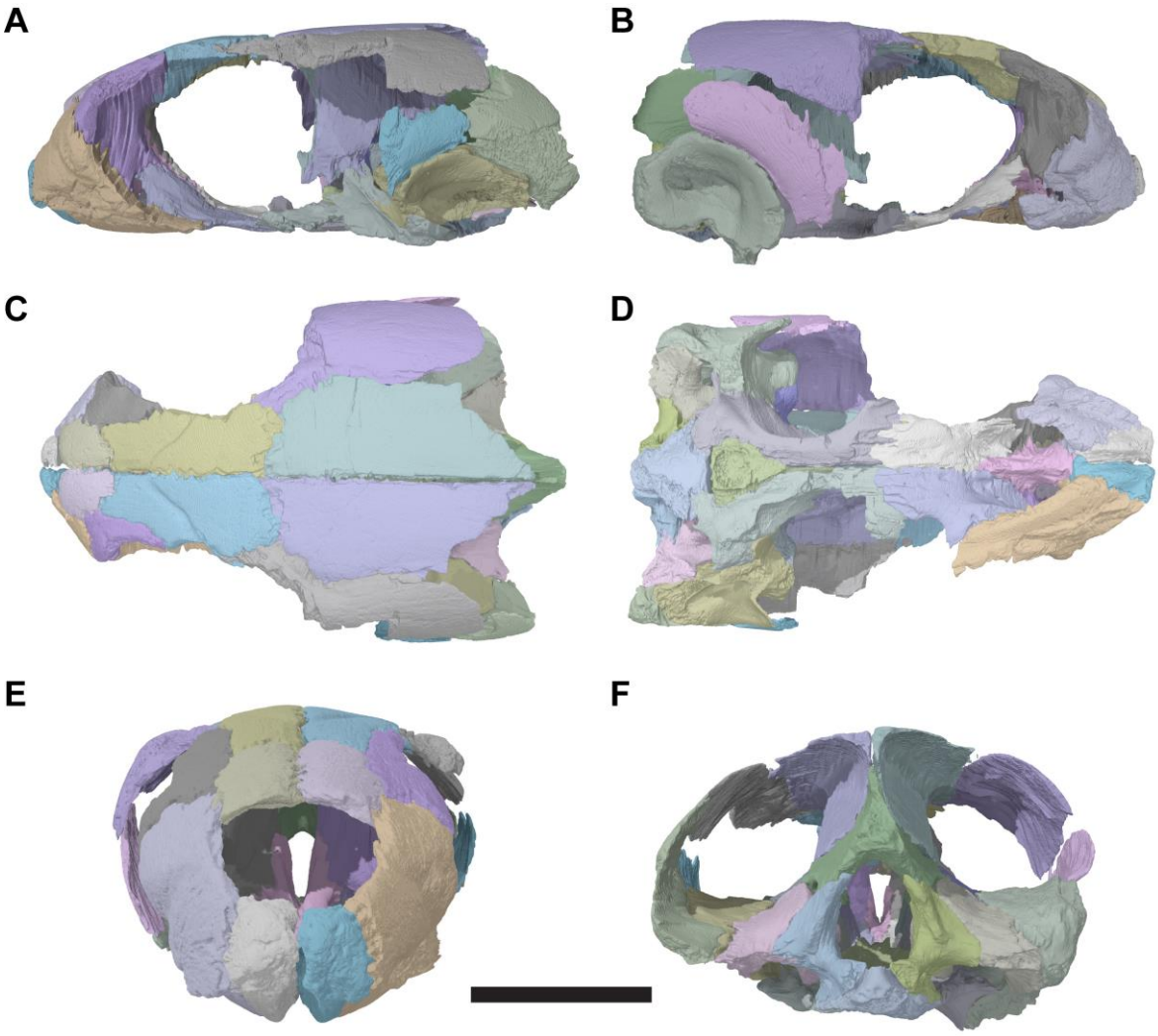


FIG. 3.1. 3D renderings of CAMSM B55775, the holotype of *Rhinochelys pulchriceps*. **A**, left lateral view; **B**, right lateral view; **C**, dorsal view; **D**, ventral view; **E**, anterior view; **F**, posterior view. Scale bar equals 20 mm.

3.4.1 Cranium

3.4.1.1 Nasal

The nasals are the anterior-most bones of the skull roof (Figs 3.1–5, 3.8, 3.11). They are small elements that contact each other on the midline. Their anterior margins border the external

naris dorsally and form the roof of the nasal capsule. Each nasal contacts the maxilla anterolaterally, the prefrontal posterolaterally, and the frontal posteriorly.

The nasal shows considerable variation among specimens referred to *Rhinochelys*. Two gross morphologies can be distinguished, and are described in the following paragraphs, although some features of the nasal are shared by all specimens. In all specimens of *Rhinochelys*, the nasal is a thin plate with a mediolaterally concave anterior margin that

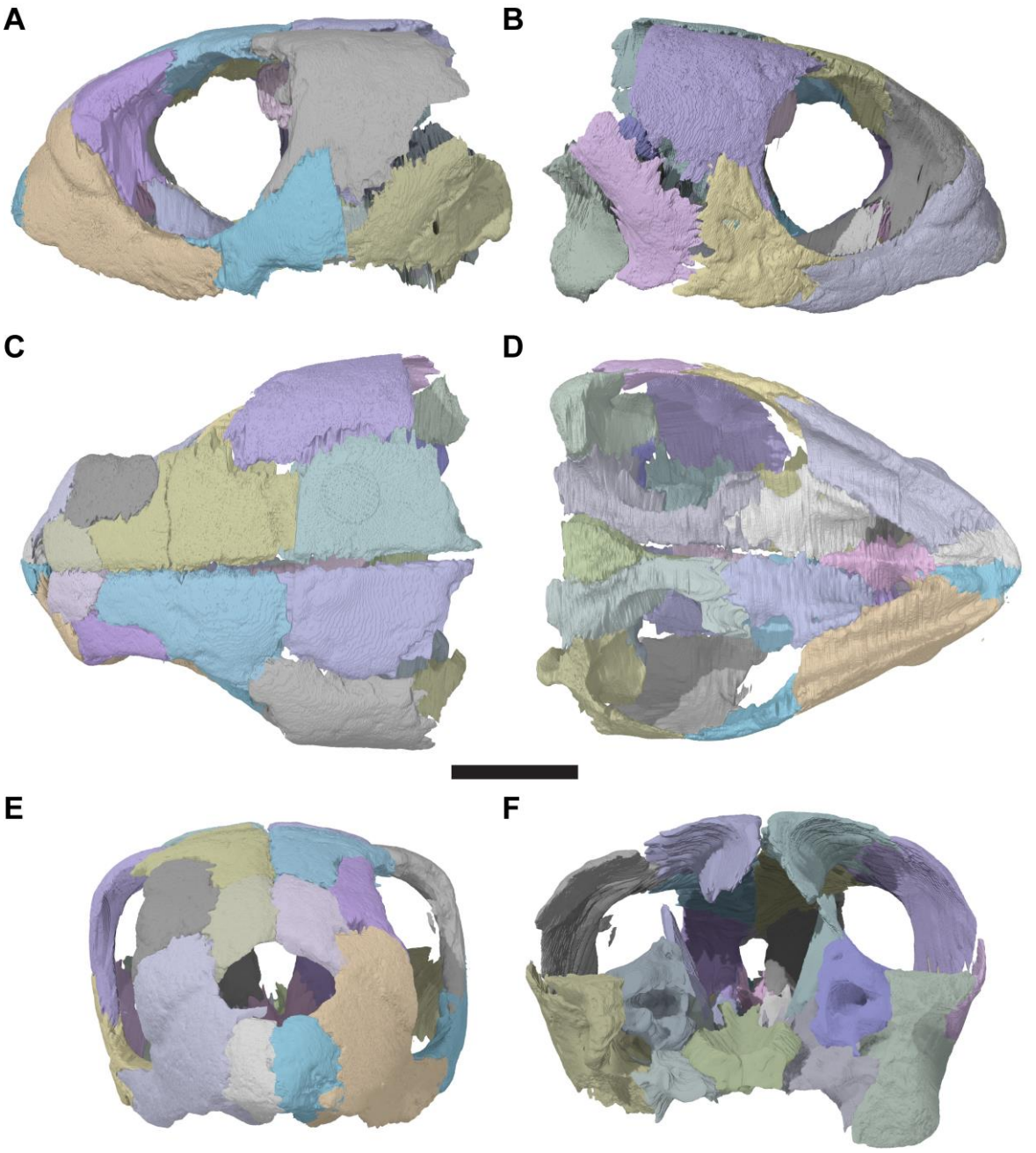


FIG. 3.2. 3D renderings of NHMUK PV OR43980, the holotype of *R. cantabrigiensis*. **A**, left lateral view; **B**, right lateral view; **C**, dorsal view; **D**, ventral view; **E**, anterior view; **F**, posterior view. Scale bar equals 10 mm.

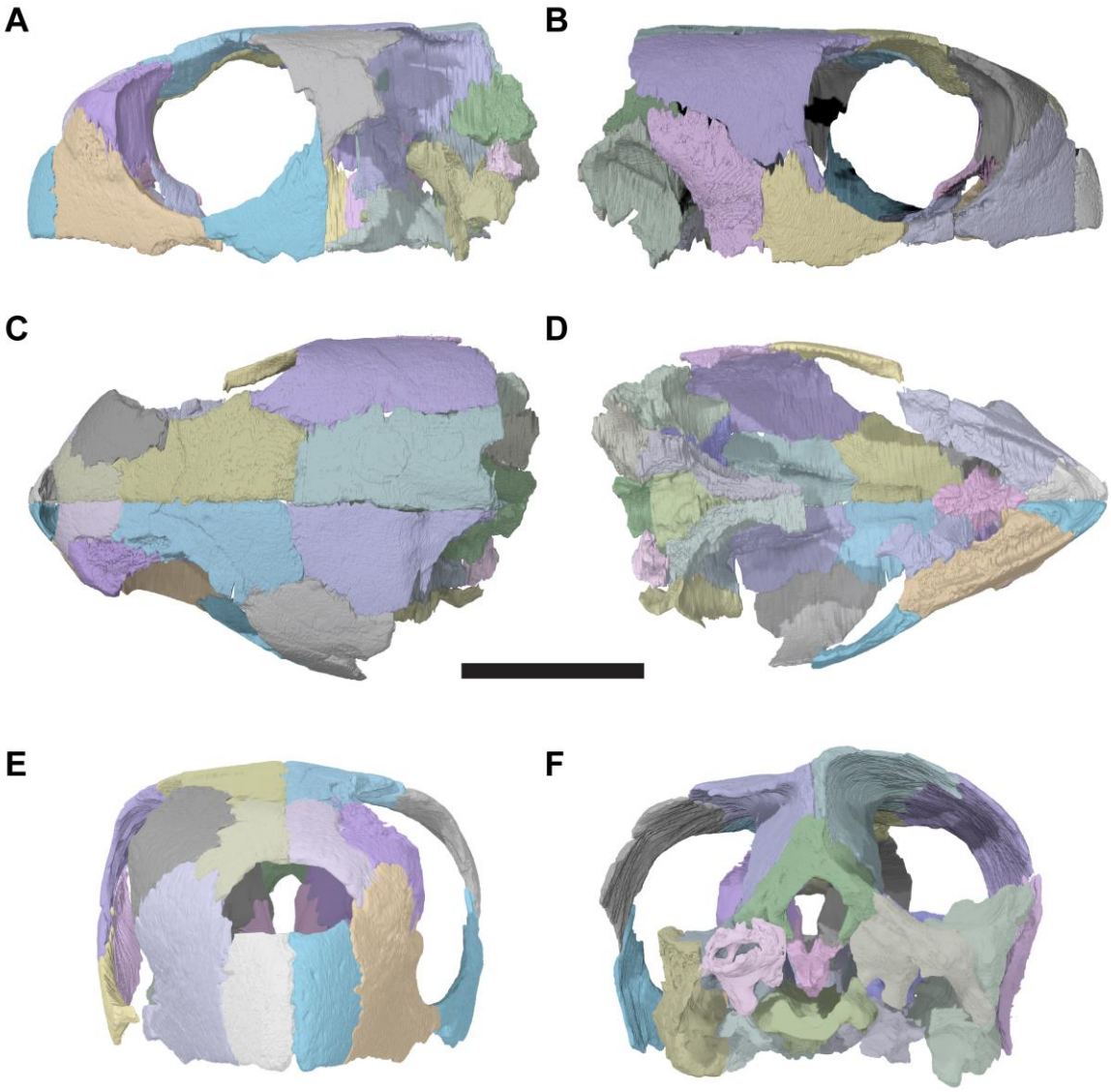


FIG. 3.3. 3D renderings of NHMUK PV R2226, the holotype of *R. elegans*. **A**, left lateral view; **B**, right lateral view; **C**, dorsal view; **D**, ventral view; **E**, anterior view; **F**, posterior view. Scale bar equals 20 mm.

borders the external naris. At its contact with the maxilla, the nasal develops a thin ventrolaterally directed spur that continues for a short distance in the rim of the external naris. In all specimens, the posterior surface of the nasal forms a low transverse crest that slots into a groove in the anterior surface of the frontal. The ventral surface of the nasal is gently excavated and contributes to the fossa forming the dorsal roof of the nasal valve.

One nasal morphotype is shown by CAMSM B55776, CAMSM B55775, and NHMUK PV OR43980, in which the nasal is anteroposteriorly long (c. 35% longer than wide) and has a relatively constant transverse width across its entire length (Fig. 3.1E). The lateral margin of

the nasal is roughly convex in these specimens, and the nasal contacts the frontal posteriorly, the prefrontal posterolaterally, and the ascending process of the maxilla anterolaterally along this margin.

In contrast, the nasals are slightly shorter in CAMSM B55783, NHMUK PV R2226 and NHMUK PV OR35197 (as wide as long at the narial margin; Figs 3.3E, 3.10). In these specimens, the lateral margin is concave posterolaterally adjacent to the prefrontal.

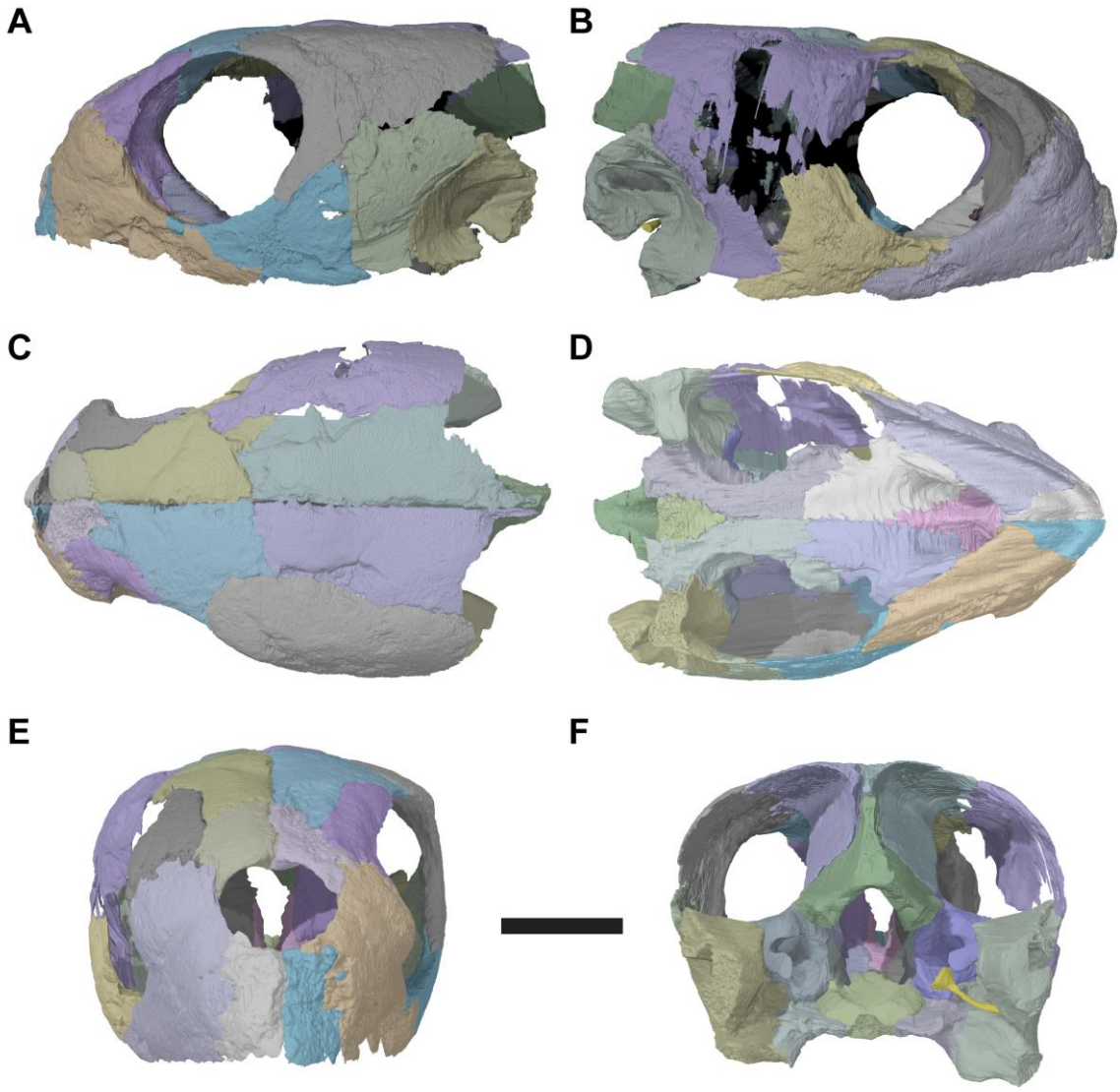


FIG. 3.4. 3D renderings of CAMSM B55776. **A**, left lateral view; **B**, right lateral view; **C**, dorsal view; **D**, ventral view; **E**, anterior view; **F**, posterior view. Scale bar equals 10 mm.

Additionally, the nasal extends laterally between the prefrontal and the ascending process of the maxilla via a short but laterally prominent process. At the level of this process, the nasal

becomes mediolaterally as wide as its anteroposterior length. The length–width ratios of the nasals have been measured for a large number of specimens, and these data are discussed below (see Discussion).

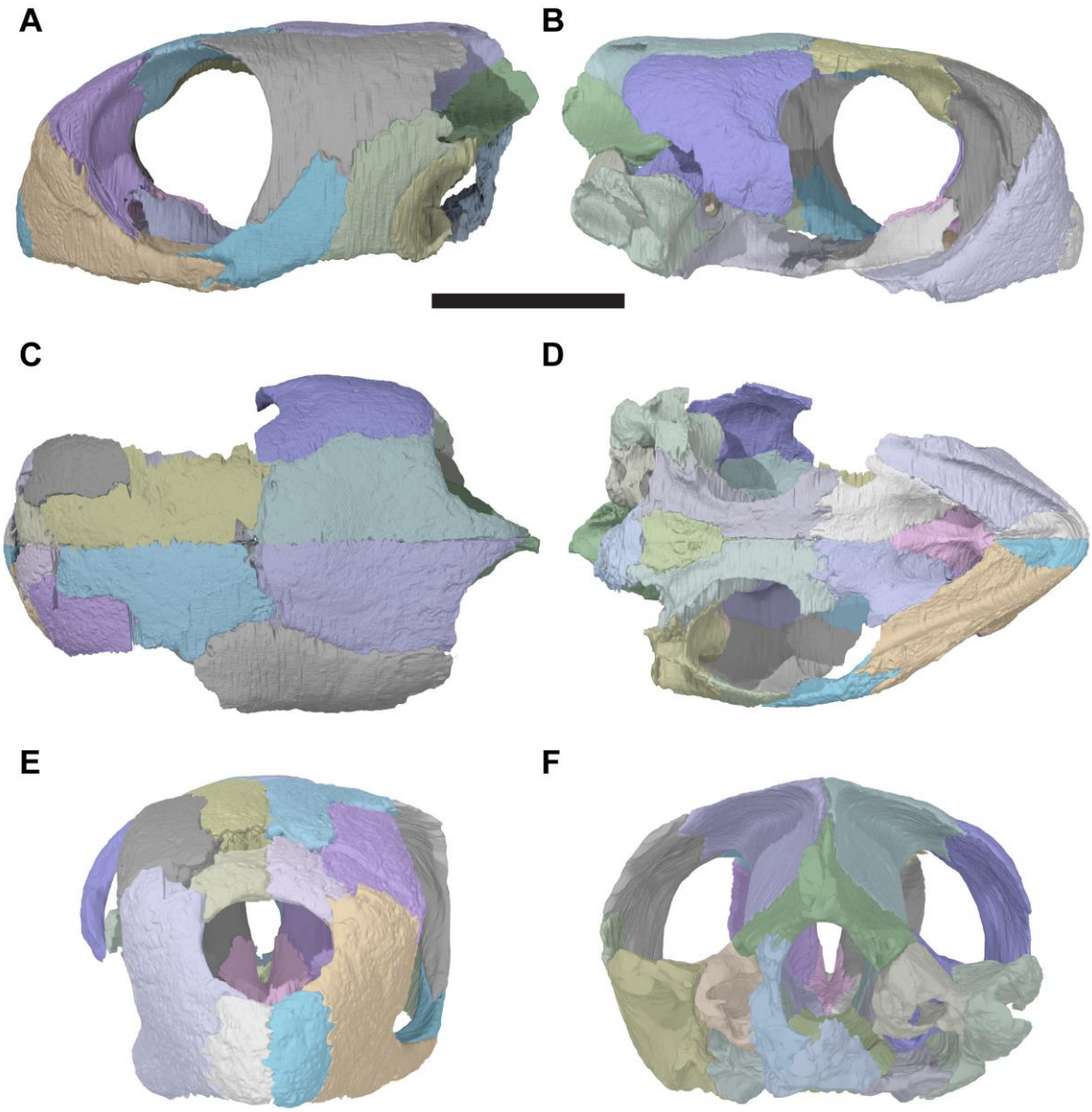


FIG. 3.5. 3D renderings of NHMUK R35197. **A**, left lateral view; **B**, right lateral view; **C**, dorsal view; **D**, ventral view; **E**, anterior view; **F**, posterior view. Scale bar equals 10 mm.

3.4.1.2 Prefrontal

The prefrontals are large bones situated in the anterior part of the skull (Figs 3.1–5, 3.6–2.8, 2.10). Each contributes to the mediolaterally oriented vertical wall that separates the orbital fossa from the nasal cavity. Structurally, the prefrontal is a dorsoventrally tall element that

connects the bony palate with the dorsal skull roof, contacting the vomer, palatine and maxilla ventrally, and the frontal and nasal dorsally. It contributes to the margins of the nasal cavity, orbit, fissura ethmoidalis and foramen orbito-nasale.

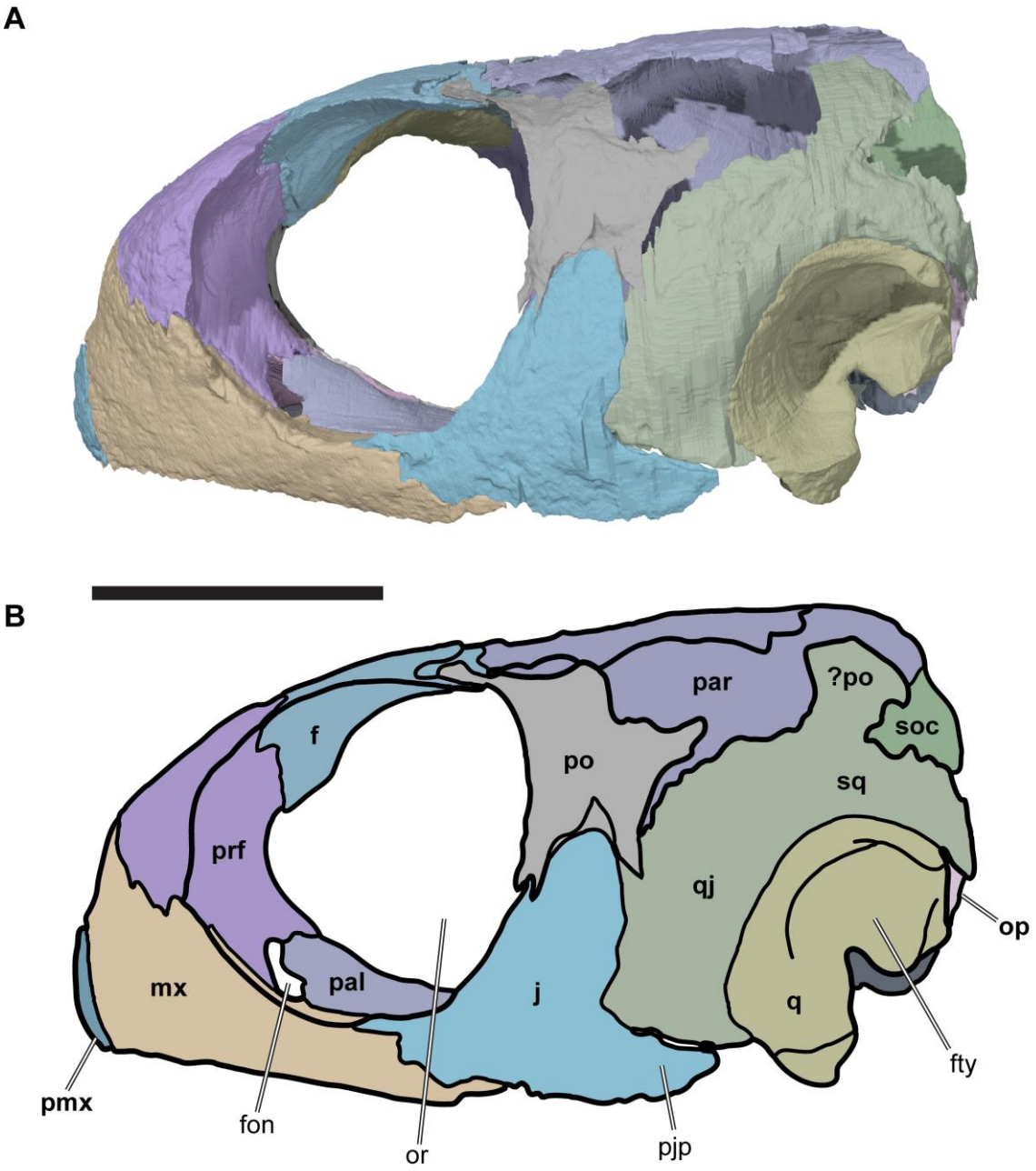


FIG. 3.6. Left lateral view of cranium of CAMSM B55783. **A**, 3D rendering; **B**, interpretative line drawing. Scale bar equals 10 mm. Note that bones are labelled in bold. Abbreviations: *f,* frontal; *fon*, foramen orbito-nasale; *fty*, tympanic fossa; *j*, jugal; *mx*, maxilla; *or*, orbit; *pal*, palatine; *par*, parietal; *pjp*, posterior jugal process; *pmx*, premaxilla; *po*, postorbital; *prf*, prefrontal; *q*, quadrate; *qj*, quadratojugal; *soc*, supraoccipital; *sq*, squamosal.

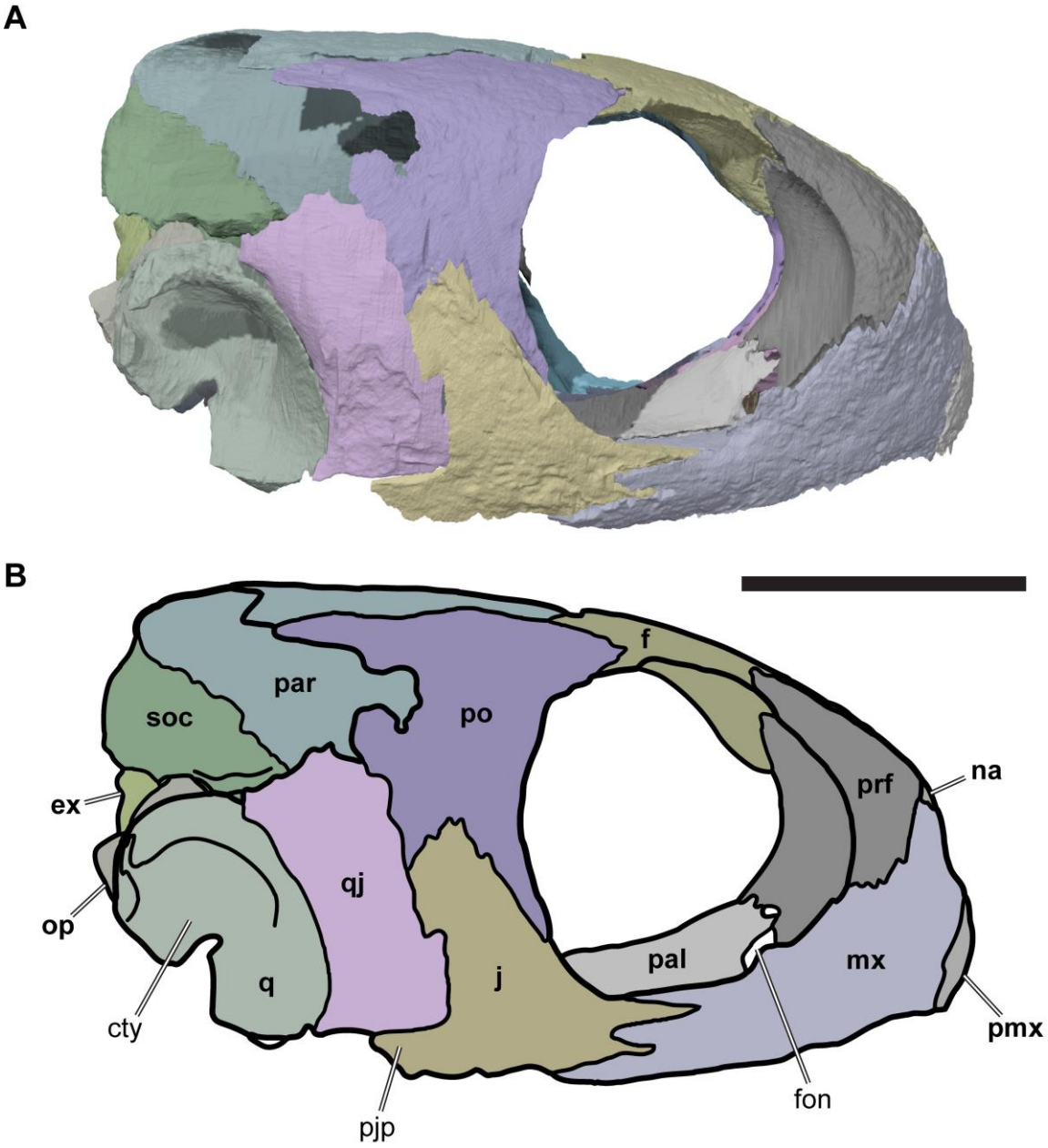


FIG. 3.7. Right lateral view of cranium of CAMSM B55783. **A**, 3D rendering; **B**, interpretative line drawing. Scale bar equals 10 mm. Note that bones are labelled in bold. Abbreviations: *cty*, cavum tympani; *ex*, exoccipital; *f*, frontal; *fon*, foramen orbito-nasale; *j*, jugal; *na*, nasal; *op*, opisthotic; *pal*, palatine; *par*, parietal; *pjp*, posterior jugal process; *pmx*, premaxilla; *prf*, prefrontal; *q*, quadrate; *qj*, quadratojugal; *soc*, supraoccipital.

The prefrontal comprises a long, mediolaterally broad ventral process and a shorter posterodorsal process. The ventral process has a large posterior surface that forms the anterior wall of the orbit, and is excavated deeply by the orbital fossa. The anterior surface of the ventral process forms parts of the posterior wall of the nasal cavity, and is therefore deeply concave (Fig. 3.12). The external orbital margin of the prefrontal is sharp-edged and is

concave when seen in lateral view, contributing to the circular outline of the orbit. This is similar to the condition in the Early Cretaceous prostostegid *Bouliachelys*, in which the pre-

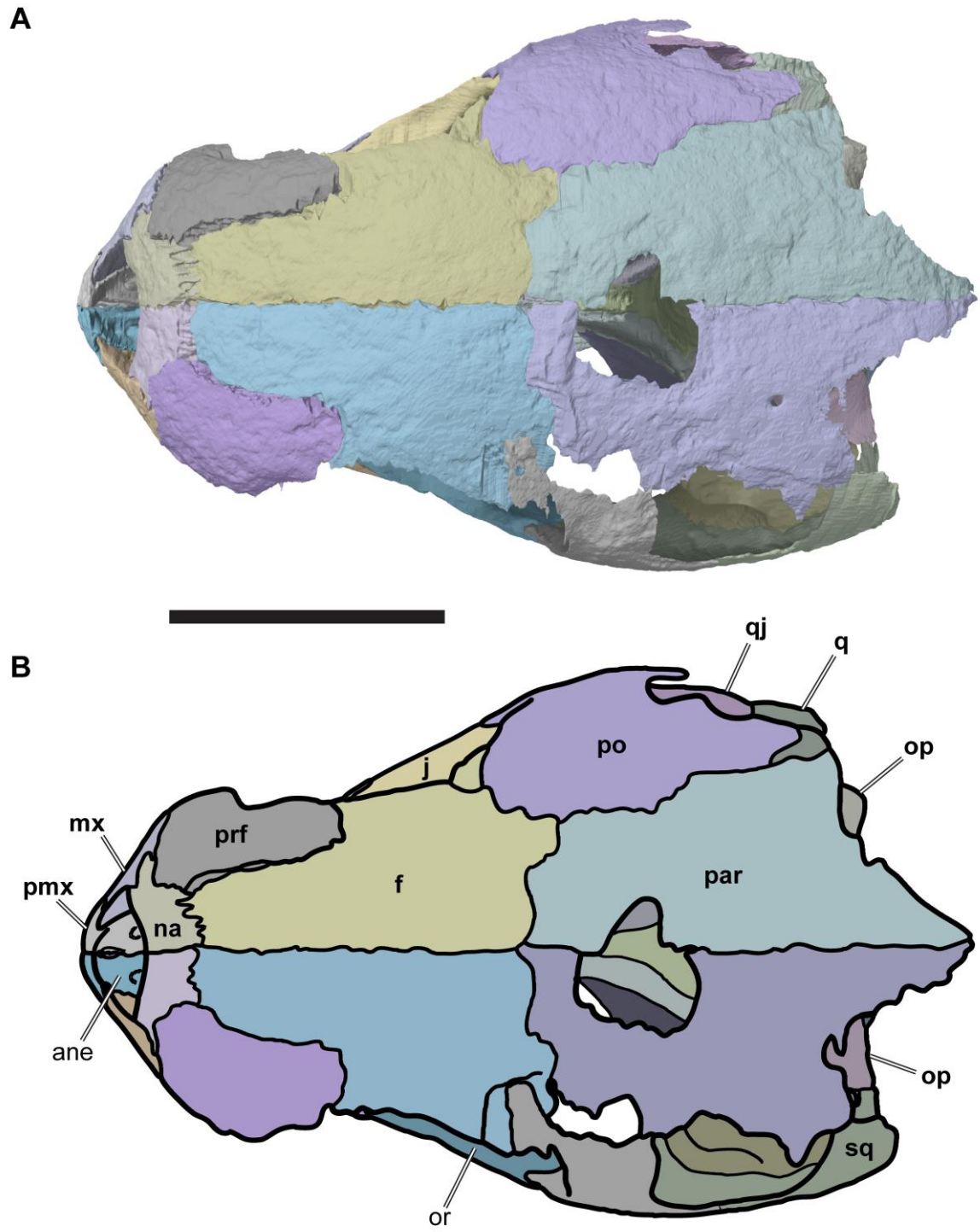


FIG. 3.8. Dorsal view of cranium of CAMSM B55783. **A**, 3D rendering; **B**, interpretative line drawing. Scale bar equals 10 mm. Note that bones are labelled in bold. Abbreviations: *ane*, apertura narium externa; *f*, frontal; *j*, jugal; *mx*, maxilla; *na*, nasal; *op*, opisthotic; *or*, orbit; *par*, parietal; *pmx*, premaxilla; *po*, postorbital; *prf*, prefrontal, *qj*, quadratojugal; *q*, quadrate; *sq*, squamosal.

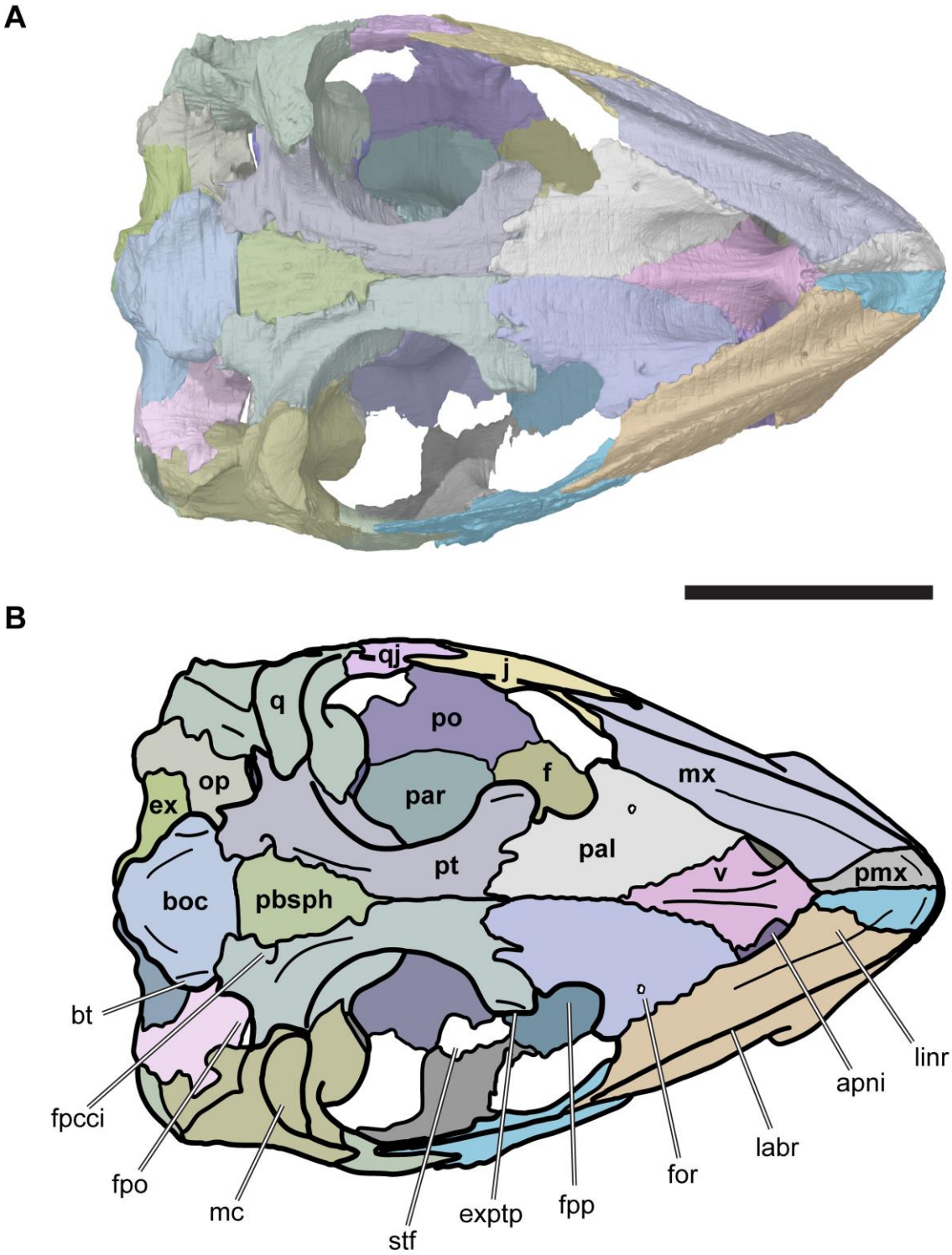


FIG. 3.9. Ventral view of cranium of CAMSM B55783. **A**, 3D rendering; **B**, interpretative line drawing. Scale bar equals 10 mm. Note that bones are labelled in bold. Abbreviations: *apni*, aperture narium intera; *boc*, basioccipital; *bt*, basal tuber; *ex*, exoccipital; *exptp*, external pterygoid process, *f,* frontal; *for*, foramen; *fpcci*, foramen posterius canalis carotici interni; *fpo*, fenestra postotica; *fpp*, foramen posterius palatinum; *j*, jugal; *labr*, labial ridge; *linr*, lingual ridge; *mc*, mandibular condyle; *mx*, maxilla; *op*, opisthotic; *pal*, palatine; *par*, parietal; *pbsph*, parabasisphenoid; *pmx*, premaxilla; *po*, postorbital; *pt*, pterygoid; *q*, quadrate; *qj*, quadratojugal; *stf*, subtemporal fossa; *v*, vomer.

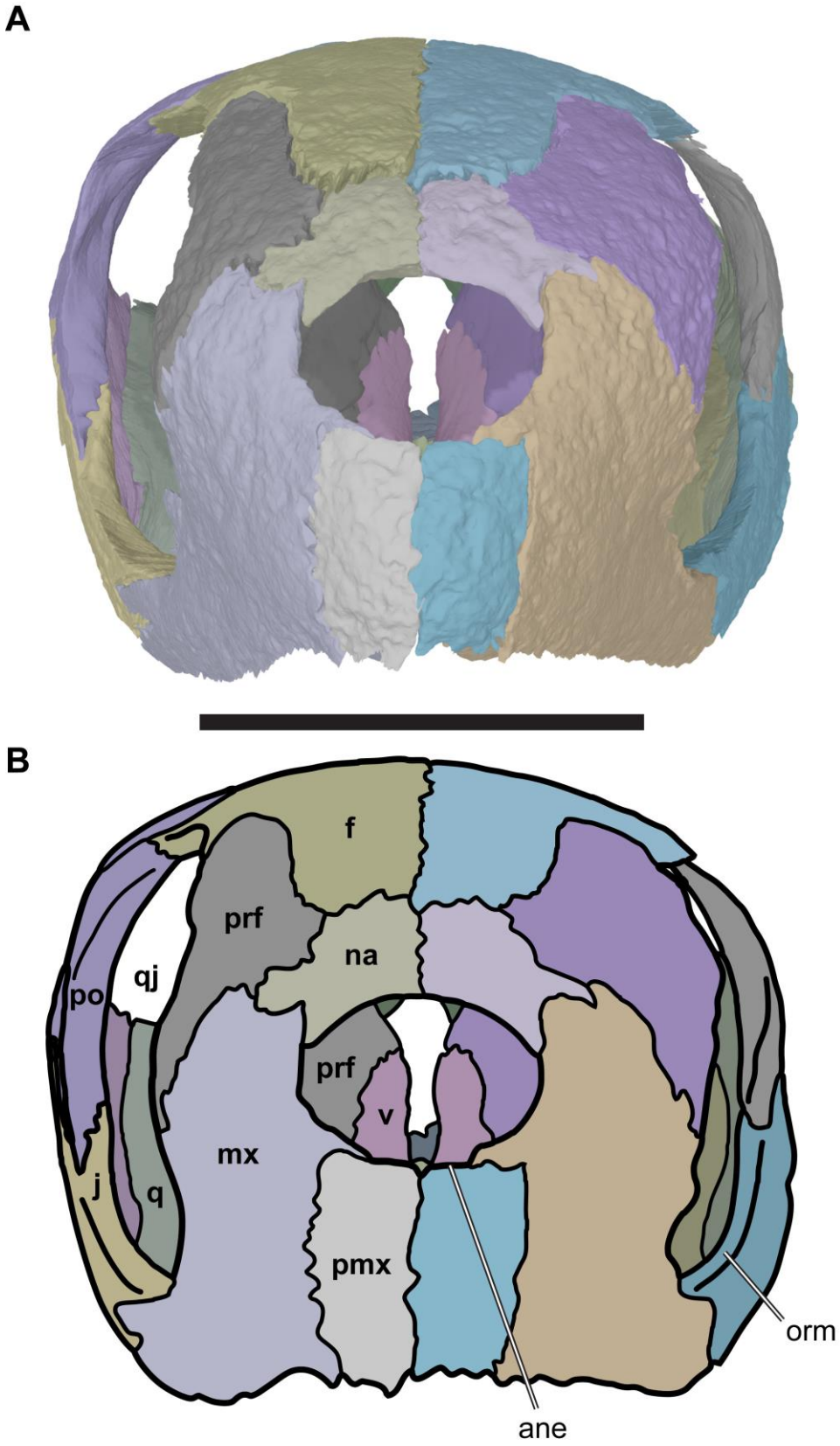


FIG. 3.10. Anterior view of cranium of CAMSM B55783. **A**, 3D rendering; **B**, interpretative line drawing. Scale bar equals 10 mm. Note that bones are labelled in bold. Abbreviations: *ane*, apertura narium externa; *f*, frontal; *j*, jugal; *mx*, maxilla; *na*, nasal; *orm*, orbital margin; *po*, postorbital; *prf*, prefrontal; *q*, quadrate; *qj*, quadratojugal; *v*, vomer.

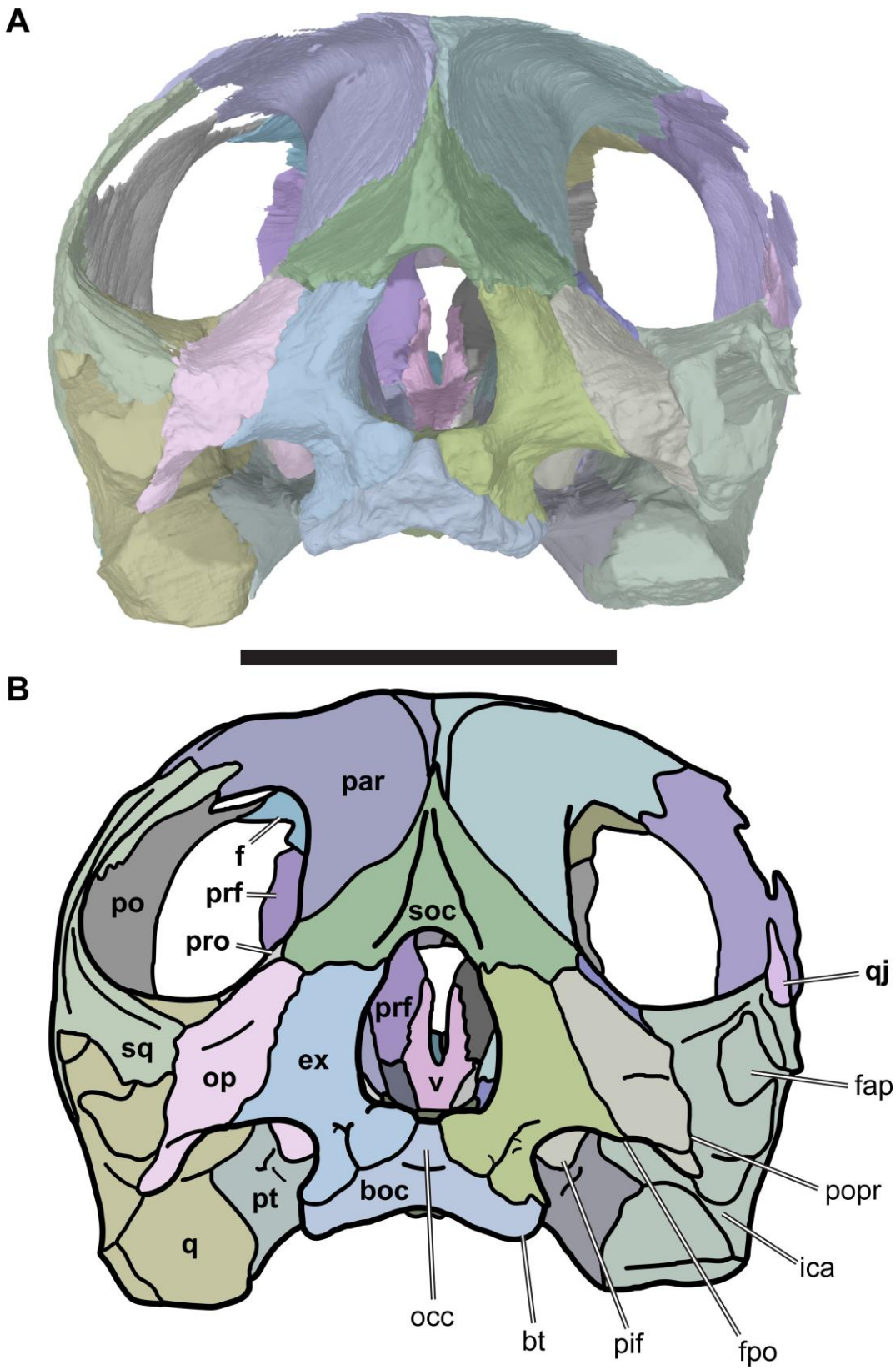


FIG. 3.11. Posterior view of cranium of CAMSM B55783. **A**, 3D rendering; **B**, interpretative line drawing. Scale bar equals 10 mm. Note that bones are labelled in bold. Abbreviations: *boc*, basioccipital; *bt*, basal tuber; *ex*, exoccipital; *f*, frontal; *fap*, foramen antrum postoticum; *fpo*, fenestra postotica; *ica*, incisura columella auris; *occ*, occipital condyle; *op*, opisthotic; *par*, parietal; *pif*, processus interfenestralis; *po*, postorbital; *popr*, paroccipital process; *prf*, prefrontal; *pro*, prootic; *pt*, pterygoid; *q*, quadrate; *qj*, quadratojugal; *sq*, squamosal; *v*, vomer.

frontal also forms a large section of the orbit. In the Late Cretaceous taxon *Desmatochelys lowii* the prefrontal is generally much smaller and contributes less to the orbit (KUVP 1200; Raselli 2018). The anterior orbital wall is very gently inclined in *Rhinochelys*, so that it is oriented posterolaterally, rather than strictly posteriorly, and as a result various internal structures, such as the prefrontal/palate contact and the foramen orbito-nasale, can be seen in lateral view (Figs 3.6–7).

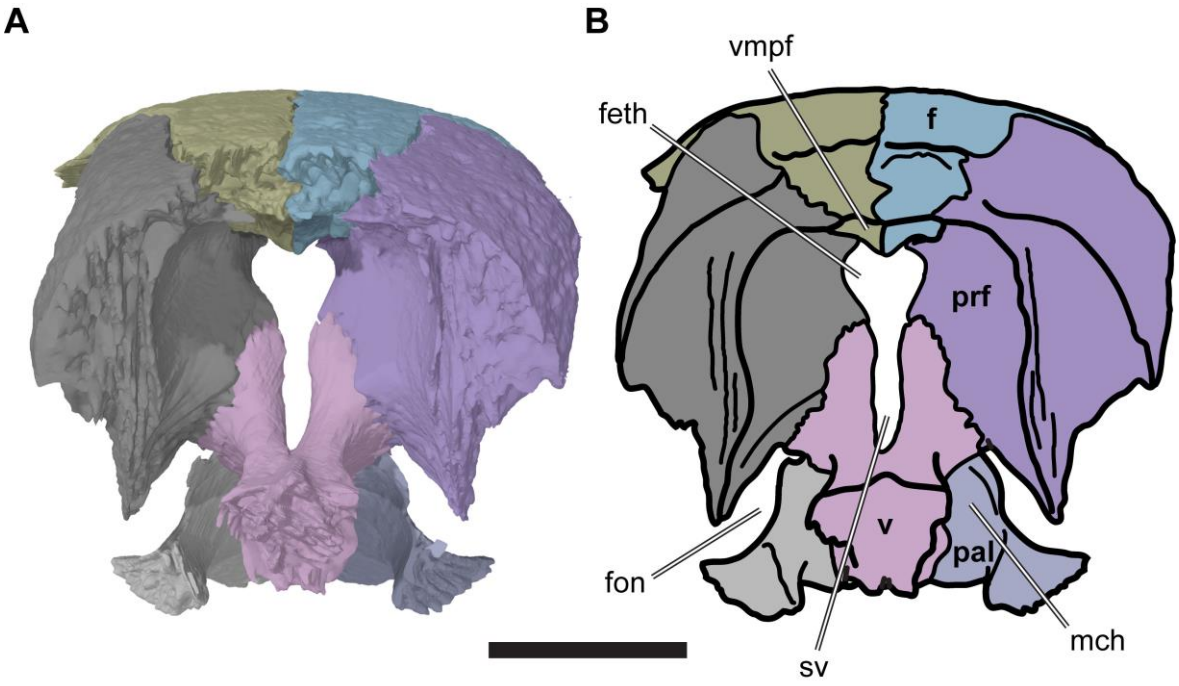


FIG. 3.12. Anterior view of partial anterior part of the cranium of CAMSM B55783 showing parts of the nasal capsule. **A**, 3D rendering; **B**, interpretative line drawing. Scale bar equals 5 mm. Note that bones are labelled in bold. Abbreviations: *f*, frontal; *feth*, fissura ethmoidalis; *fon*, foramen orbito-nasale; *mch*, meatus choane; *prf*, prefrontal; *pal*, palatine; *sv*, sulcus vomeri; *v*, vomer; *vmpf*, ventromedial process of frontal.

The foramen orbito-nasale is enclosed dorsally and anteriorly by the ventral process of the prefrontal, which therefore has a concave posteroventral margin, dividing it into two terminal rami. The lateral ramus tapers towards its end, and contacts the maxilla laterally. The medial ramus is mediolaterally broader, and contacts the vomer medially and palatine posteroventrally (Fig. 3.13).

The medial margins of the prefrontals are separated from the midline by the fissura ethmoidalis dorsally and by the ascending processes of the vomer ventrally. Each of these structures occupies around half of the dorsoventral height of the prefrontal medial margin.

The fissura ethmoidalis is continuous with the more ventrally-located sulcus vomeri, and dorsally enclosed by the olfactory tract formed by the frontals (see Frontal). Together, the fissura ethmoidalis and sulcus vomeri form an opening between the orbital fossa posteriorly and the nasal capsule anteriorly. The fissura ethmoidalis varies slightly in its outline among the *Rhinochelys* specimens that were CT scanned. In some specimens (CAMSM B55775: *R. pulchriceps* holotype; CAMSM B55776 and NHMUK PV OR35197: both *R. elegans sensu* Collins (1970); NHMUK OR43980: *R. cantabrigiensis* holotype), the combined sulcus vomeri and fissura ethmoidalis form a transversely narrow slit that expands slightly in width as it extends dorsally. By contrast, in CAMSM B55783 (*R. cantabrigiensis sensu* Collins 1970) and NHMUK PV R2226 (*R. elegans* holotype) the sulcus vomeri has parallel lateral sides, whereas dorsally the fissura ethmoidalis broadens abruptly due to the concave medial margins of the prefrontals, giving the combined opening a keyhole-like outline (Fig. 3.13).

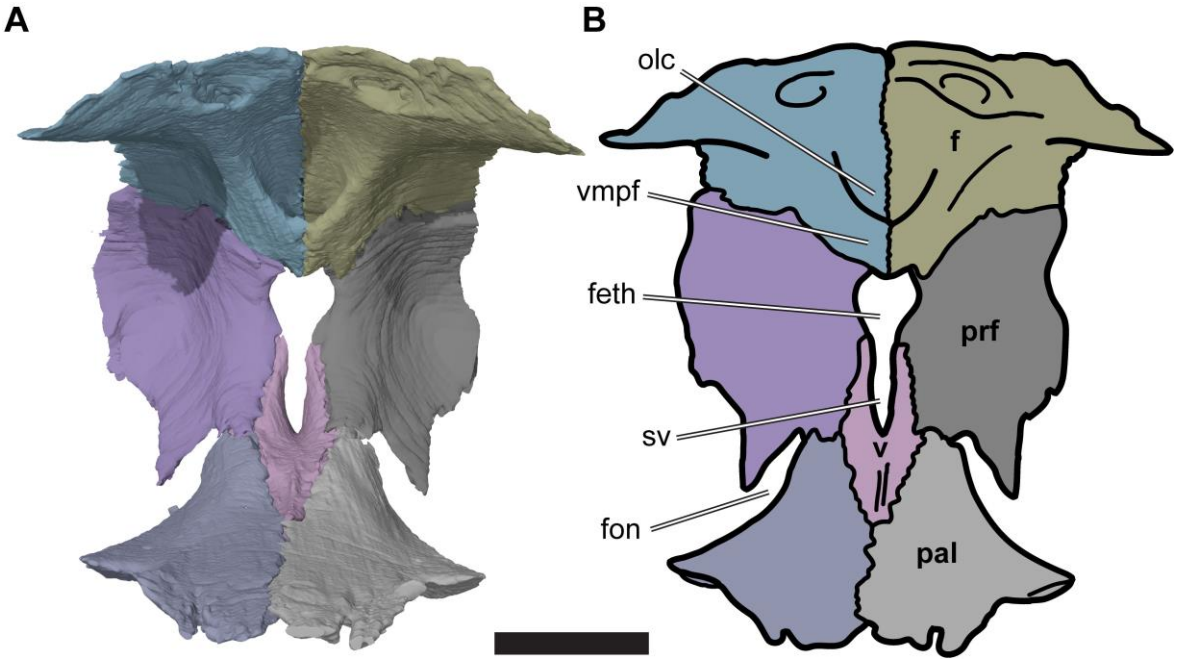


FIG. 3.13. Posterior view of partial anterior part of the cranium of CAMSM B55783 showing the region of the fissura ethmoidalis. **A**, 3D rendering; **B**, interpretative line drawing. Scale bar equals 5 mm. Note that bones are labelled in bold. Abbreviations: *f*, frontal; *feth*, fissura ethmoidalis; *fon*, foramen orbito-nasale; *olc*, olfactory canal; *prf*, prefrontal; *pal*, palatine; *sv*, sulcus vomeri; *v*, vomer; *vmpf*, ventromedial process of frontal.

The posterodorsal process of the prefrontal forms the convex dorsolateral surface of the skull anterodorsal to the orbit. It contacts the maxilla anterolaterally, the nasal

anteromedially, and the frontal posteromedially. It has an approximately triangular outline in dorsolateral view and is widest mediolaterally at its anterior contacts with the nasal and maxilla. The contact between the maxilla and nasal anteriorly excludes the prefrontal from the margin of the external naris.

The external suture of the prefrontal is weakly interdigitating. The suture between the prefrontal and the anterior process of the frontal is parallel to the skull midline. At the posterior end of the posterodorsal process of the prefrontal, the suture becomes mediolaterally oriented, and slightly convex posteriorly. The prefrontal overlaps the frontal here, whereas the medial contact with the anterior process of the frontal is more complex. Medially, the prefrontal is expanded underneath the anterior process of the frontal and forms a broad, dorsomedially facing contact surface for the frontal.

The sutures of the prefrontal with the nasal and maxilla are highly interdigitated. The suture with the nasal extends anteroventrolaterally from the anterior contact with the frontal to the contact with the maxilla. The maxillary-prefrontal contact expands over the entire height of the prefrontal. The prefrontal articular surface for the maxilla faces anteriorly in its dorsal part, and anteroventrally in its ventral part. The surface narrows ventrally.

3.4.1.3 Frontal

The frontals are dorsoventrally thin, anteroposteriorly long bones that form large parts of the skull roof dorsal to the orbits, including the central portions of the dorsal orbital margins (Figs 3.1–5, 3.8). They contact the parietals and postorbitals posteriorly and the nasals and prefrontals anteriorly, and articulate with each other via a weakly interdigitating median suture along their entire anteroposterior length. The length of each frontal exceeds twice its width. The frontals are posteriorly broad but they become mediolaterally narrower anteriorly, terminating in an anterior process that lies anterior to the orbital region. This anterior process has a rectangular outline in dorsal view and is about half the mediolateral width of the posterior portion of the frontal.

The dorsal surface of the frontal is gently curved anteroposteriorly. It is generally smooth, except for a transverse incision that forms the sulcus for a cranial scute. The incision marking the sulcus extends posterolaterally from the skull midline to the orbital margin of the frontal. The part of the frontal posterior to the sulcus is slightly dorsally raised with respect to the surface anterior to it, so that the sulcus appears as a step on the dorsal surface of the frontal. The sulcus is variably developed in the specimens studied. For example, the sulcus is very clearly defined in CAMSM B55775 (*R. pulchriceps* holotype; Figs 3.1C, 3.14), but is discernable only as a faint structure on the well-preserved frontals of CAMSM B55783 (*R. cantabrigiensis sensu* Collins (1970); Figs 3.8, 3.14).

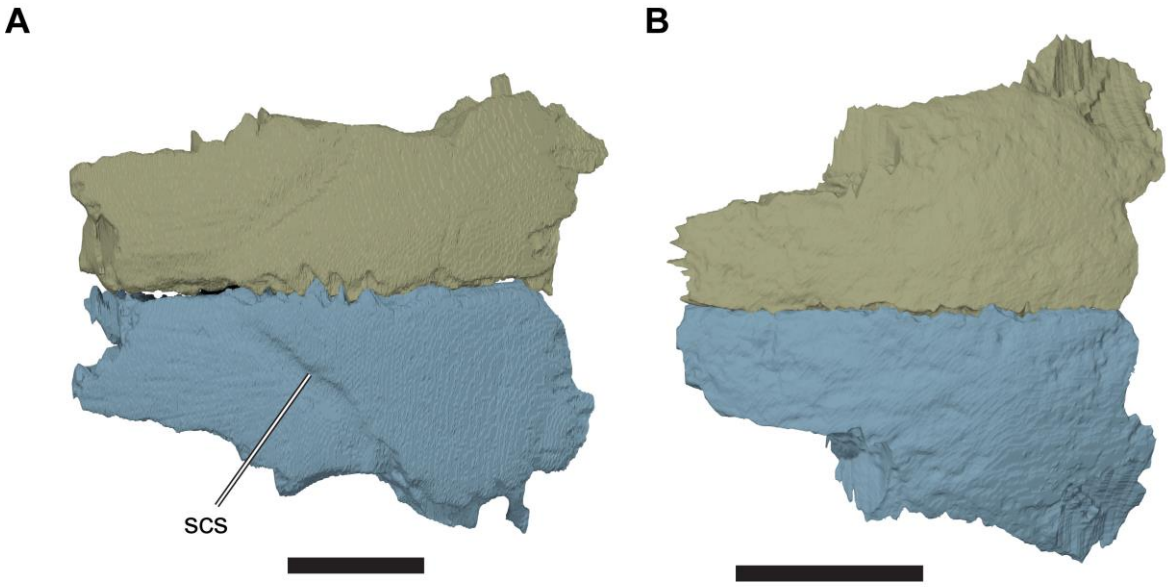


FIG. 3.14. Comparison of frontals in dorsal view. **A**, 3D rendering of CAMSM B55775; **B**, 3D rendering of CAMSM B55783. Scale bars equal 5 mm. Abbreviations: *scs*, scute sulcus.

A small posterolateral spur of the frontal extends between the parietal and postorbital on the external surface of the skull roof. CT scans show that this spur is part of a posterolateral expansion of the frontal that underlays the postorbital. This underlying part is thinner than the externally visible part of the frontal, as it bears a dorsally facing, planar facet for the postorbital that is recessed from the thicker body of the frontal. The externally visible suture of the frontal with the postorbital on the dorsal surface of the skull is gently concave laterally, and extends anterolaterally from the contact with the parietal to the orbital margin.

The suture between the frontal and parietal extends medially from the tip of the spur to the skull midline. The suture is weakly convex anteriorly and the posterior margin of the frontal overlaps the dorsal surface of the parietal. This simple contact is reinforced by a deep, anteriorly recessed socket on the ventral surface of the frontal just anterior to its posterior margin, which receives an anterior peg-like process of the parietal.

The frontal contribution to the orbit margin has a concave lateral margin that contributes to the overall circular outline of the orbit. This margin is constricted medially along its length, so that the ventral floor of the orbital fossa can be seen in dorsal view.

The externally visible suture with the prefrontal extends from the orbital margin medially for about half of the width of the frontal, resulting in the constriction of the anterior process of the frontal relative to its posterior portion. From there, the suture curves anteriorly and continues anteriorly up to its contact with the nasal. The internal contact surfaces for the prefrontal are more complex and generally highly interdigitated (see also Prefrontal, above). Laterally, a thin sheet of the frontal extends anteriorly and underlaps the prefrontal ventrally. Medially, the part of the frontal forming the anterior process laps onto the prefrontal. Additionally, a small prong of the frontal inserts into the posteromedial margin of the prefrontal, immediately dorsolateral to the opening for the fissura ethmoidalis (Fig. 3.15).

The anterior margin of the frontal contacts the nasal. The suture with the nasal is slightly oblique and is oriented anterolaterally/posteromedially rather than strictly mediolaterally. CT images show that the anterior contact surface with the nasal has a transverse groove that receives a transverse ridge from the posterior surface of the nasal. The frontal underlaps the nasal ventrally and thus forms part of the posterodorsal roof of the nasal cavity.

In turtles, and many other tetrapods, the ventral surfaces of the frontals bear paired parasagittal ridges, the cristae cranii, between which the olfactory nerves (CN I) extend anteriorly toward the nasal capsule (Gaffney 1979; Evans 2008; Ali *et al.* 2008). The resulting medially situated, ventrally open trough is called the sulcus olfactorius (Gaffney 1979).

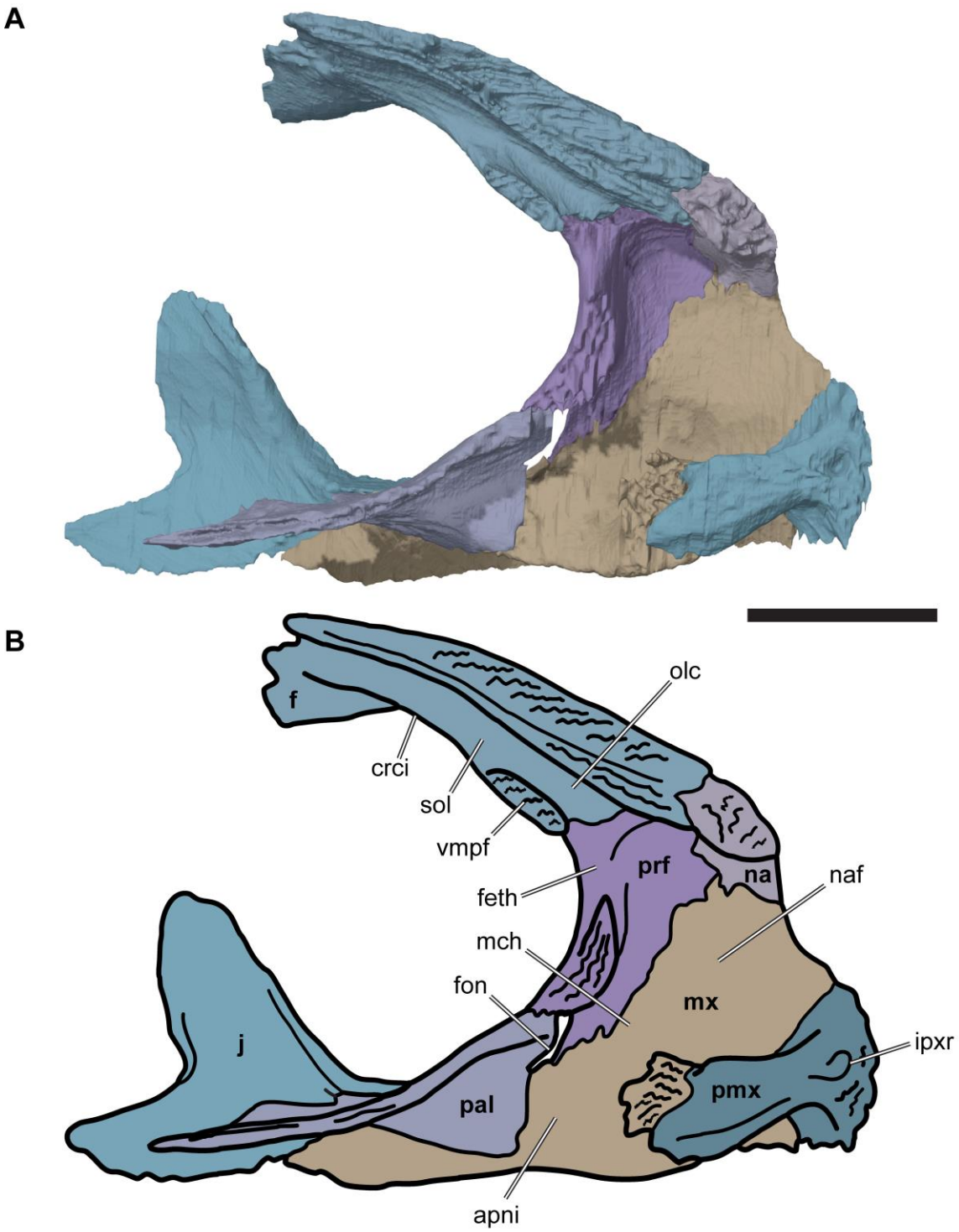


FIG. 3.15. Medial view of the left side of the partial anterior cranium of CAMSM B55783. **A**, 3D rendering; **B**, interpretative line drawing. Scale bar equals 5 mm. Note that bones are labelled in bold. Abbreviations: *apni*, apertura narium interna; *crci*, crista cranii; *feth*, fissura ethmoidalis; *fon*, foramen orbito-nasale; *ipxr*, interpremaxillary recess; *mch*, meatus choane; *mx*, maxilla; *na*, nasal; *naf*, nasal fossa; *olc*, olfactory canal; *pal*, palatine; *prf*, prefrontal; *pmx*, premaxilla; *sol*, sulcus olfactorius; *vmpf*, ventromedial process of frontal.

Although it is formed by the frontals in turtles, it may extend onto the parietals posteriorly and sometimes also onto the nasals anteriorly. The sulcus olfactorius can be a very clearly delimited trough with sharp-edged margins and deep cristae cranii, but can also be developed as a subtler anteroposteriorly directed groove with weakly defined margins, such as that seen in *Dermochelys coriacea* (Evers & Benson 2018*b*).

The sulcus olfactorius of *Rhinochelys* is located entirely on the frontals and its posterior portion is bounded by low cristae cranii. Each crista cranii separates the orbital fossa laterally from the sulcus olfactorius medially. Anteriorly, the cristae cranii expand into prominent, sheet-like ventromedial processes that contact on the midline in an interdigitating suture (Fig. 3.13). These processes therefore enclose the sulcus olfactorius ventrally, forming an anteroposteriorly oriented olfactory canal with a transversely wide, oval transverse cross-section. As the cavum cranii is often filled with matrix in many of the specimens studied, the olfactory canal could only be detected in those specimens that were CT scanned, but it is present in all of those specimens (*R. elegans* NHMUK PV R2226 (holotype), NHMUK PV OR35197, CAMSM B55776; *R. pulchriceps* CAMSM B55775 (holotype), *R. cantabrigiensis* NHMUK PV OR43980 (holotype), CAMSM B55783).

To our knowledge, the presence of a ventrally enclosed olfactory canal has not been reported in any other marine turtle. Nevertheless, we have also observed this structure in our CT scans of another protostegid, *Notochelone costata* (NHMUK PV R9590). However, it is absent in the protostegids *Bouliachelys* (QMF 31669) and *Desmatochelys lowii* (KUVP 1200; Raselli 2018). Furthermore, it is also absent in other modern and fossil chelonioids (e.g. *Argillochelys* NHMUK PV OR49465; *Allopleuron hofmanni* NHMUK PV R4213; *Lepidochelys olivacea* SMNS 11070; Evers & Benson 2018 *b*, *c*). However, a similar condition is present in some taxa outside of the marine cryptodires: the lateral margins of the sulcus olfactorius are hypertrophied in some turtles, including *Macrochelys temminckii* (FMNH 22111) and *Geochelone* (Gaffney 1979), and closely approach the midline, without forming an interdigitated contact (Evers & Benson 2018*c*).

3.4.1.4 Parietal

The paired parietals are the posterior-most and largest bones of the skull roof (Figs 3.1–5, 3.8) and they meet along the midline via a straight suture, which may be slightly interdigitated in its anterior third. The parietal consists of two plates of bone, a horizontal plate and a ventrally directed parasagittal plate that descends ventrally from the horizontal plate as the processus inferior parietalis. The horizontal plate forms the posterior part of the skull roof and contacts the frontal anteriorly and the postorbital laterally. The processus inferior parietalis connects the skull roof with the palatoquadrate and braincase. The processus inferior parietalis reaches its greatest height anteriorly, where it extends ventrally to contact the pterygoid. The height of the processus inferior parietalis decreases posteriorly and it forms parts of the lateral wall of the braincase posterior to the maxillo-mandibular (CN $V_{2–3}$) foramen, contacting the prootic and, more posteriorly, the supraoccipital.

The parietal portion of the skull roof is anteroposteriorly elongate. The anterior suture with the frontal extends from the midline of the skull laterally and slightly posteriorly, until it meets the postorbital. From here, the parietal-postorbital suture is posterolaterally directed for approximately half of its length, so that the parietal becomes progressively broader posteriorly before turning posteriorly. The parietal underlaps the frontal anteriorly and the anterior part of the postorbital anterolaterally. The posterior half of the parietal-postorbital contact does not underlap the postorbital but bears a deep, longitudinal groove for the reception of the postorbital.

The posterior margin of the parietal forms the medial part of the posterior skull emargination. This margin is concave posterolaterally, but the posterior skull emargination is not as deeply developed as in *Desmatochelys lowii* (KUVP 1200; Raselli 2018). The parietal of *Rhinochelys* tapers to a thin posterior process along the skull midline (Fig. 3.8). The skull of *Rhinochelys* is only weakly emarginated compared to many non-marine turtles, so most of the subtemporal fossa is covered by the parietals dorsally. The combined posterior processes of both parietals cover most of the dorsal surface of the supraoccipital (Fig. 3.8).

The processus inferior parietalis forms the lateral surface of the endocranial fossa dorsally. It spans over most of the anteroposterior length of the parietal, extending from the level of the externally visible suture with the frontal to the posterior end of the parietal. The anterior portion of the processus inferior parietalis is oriented ventromedially so that the endocranial cavity is broadest dorsally. The anterior margin of the processus inferior parietalis is weakly concave, with a straight, vertical ventral half and an anterodorsally oriented dorsal part (Fig. 3.16; Appendix S2, Fig. S2.7). This is different to the morphology of *Bouliachelys suteri* (QM F31669), in which the anterior margin of the processus inferior parietalis bears two short anterior projections that divide the margin into a series of three concave sections. However, the morphology seen in *Rhinochelys* matches that of *Desmatochelys lowii* (KUVP 1200; Raselli 2018). As a result of the anteroposteriorly relatively shallow processi inferior parietalis the interorbital fenestrae of *Rhinochelys* are large, as in other protostegids for which this feature can be observed (e.g. *Bouliachelys suteri*, *Notochelone costata*, *Desmatochelys lowii*). This morphology is indicative of salt glands in modern sea turtles (Hirayama 1994) and is compatible with the presence of a well-developed salt gland in *Rhinochelys*. The anterior portion of the processus inferior parietalis is braced against the horizontal plate of the parietal by a low but robust, dorsoventrally oriented ridge on its lateral surface. This ridge is situated at the anterior end of the processus inferior parietalis, and marks the separation of the anteriorly positioned orbital fossa anteriorly from the temporal fossa posteriorly (Appendix S2, Fig. S2.7). The anterior part of the processus inferior parietalis articulates ventrally with the crista pterygoidea, a dorsally ascending process of the pterygoid. Several thin bony prongs extend ventrally from the processus inferior parietalis here to interlock with the crista pterygoidea. A single, large, deep socket is also present on the ventral surface of the processus inferior parietalis for the reception of a posterodorsal projection from the crista pterygoidea, which borders the anterior margin of the maxillo-mandibular (CN V_{2-3}) foramen (Fig. 3.16).

Posterior to its contact with the pterygoid, the ventral margin of the processus inferior parietalis curves posterodorsally and slightly laterally. As a consequence, the

endocranial cavity becomes posteriorly broader and the processus inferior parietalis becomes dorsoventrally shallower. A short portion of the ventral margin of the processus inferior parietalis forms the dorsal margin of the maxillo-mandibular (CN V_{2-3}) foramen (Fig. 3.16; see Pterygoid, below, for more detailed description of the maxillo-mandibular foramen). However, a posteroventral process extending along the posterior margin of the maxillo-mandibular foramen is absent in *Rhinochelys*. Posterior to the position of the maxillo-mandibular foramen the processus inferior parietalis contacts the dorsal surface of the prootic medially, articulating with a shallow groove on the dorsomedial surface of the prootic.

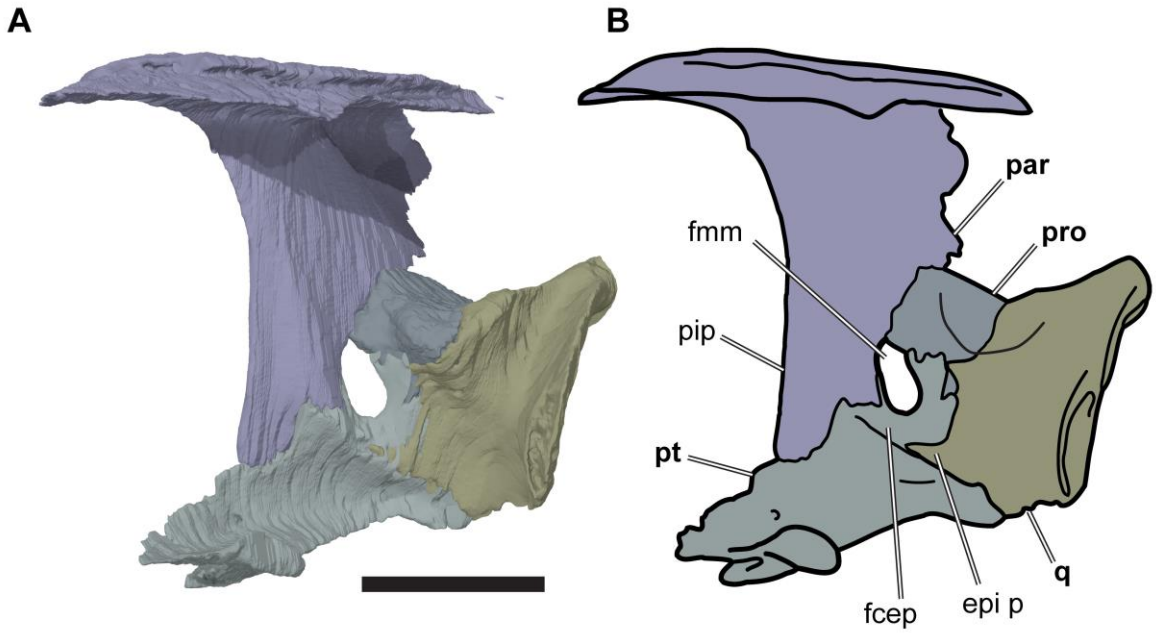


FIG. 3.16. Partial left side of the braincase of NHMUK PV OR35197. **A**, 3D rendering; **B**, interpretative line drawing. Note that bones are labelled in bold . Scale bar equals 5 mm. Abbreviations: *epi p*, epipterygoid process of quadrate; *fcep*, fossa cartilaginis epipterygoidei; *fmm*, maxillo-manidublar foramen; *par*, parietal; *pip*, processus inferior parietalis; *pro*, prootic; *pt*, pterygoid; *q*, quadrate.

Posterior to the prootic the processus inferior parietalis contacts the supraoccipital ventrally, overlapping the anterodorsolateral surface of the supraoccipital. In this region, the endocranial cavity is mediolaterally constricted by the convergence of the processus inferior parietalis posteromedially. This transition is gradual and at the posterior end of the parietal the bases of the right and left processus inferior parietalis contact each other along the

midline. The ventral margins of the right and left processes stay widely separated from the midline, however, so that the lateral surface of each processus inferior parietalis faces dorsolaterally. The transversely thin midline dorsal crest of the supraoccipital is wedged between the left and right parietals. Nevertheless, the parietals retain a midline contact dorsal to the supraoccipital so that the supraoccipital is largely covered by the parietals in dorsal view and is dorsally exposed only at the posterior tip of the crista supraoccipitalis.

3.4.1.5 Postorbital

The postorbital is a large element that forms the posterolateral part of the skull roof, including the posterior and posterodorsal margins of the orbit, and covers large parts of the subtemporal fossa dorsally (Figs 3.1–5, 3.7–8). The postorbital contacts the frontal anteromedially, the parietal medially, the quadratojugal posteroventrolaterally and the jugal anteroventrolaterally. An additional posterolateral contact with the squamosal is not evident from any CT scanned specimens but is visible in CAMSM B55791, which has complete squamosals and postorbitals preserved (Fig. 3.17).

Few specimens of *Rhinochelys* possess a well preserved postorbital. Nevertheless, two of the specimens that were CT scanned do have well preserved postorbitals. In NHMUK PV OR35197 (*R. elegans sensu* Collins (1970) the left postorbital is virtually complete (Fig. 3.5A, C) and CAMSM B55783 (*R. cantabrigiensis sensu* Collins 1970) includes a right postorbital missing only small parts of its posterior margin (Figs 3.7–8).

The postorbital is thin and plate-like. As it connects the skull roof with the lateral skull elements it is strongly flexed with a dorsoventrally convex external surface. The medial skull roof portion of the postorbital faces dorsally whereas the ventrolateral parts contacting the jugal and quadratojugal face laterally.

The suture between the postorbital, frontal and the anterior half of the parietal is medially convex, and the postorbital has its greatest medial extent at the frontal-parietal-postorbital triple junction. Both the frontal and the parietal extend underneath the

postorbital, forming a thin shelf of bone with dorsally recessed articular facets for the postorbital. However, the thin lateral margin of the frontal and parietal at the edge of this shelf, just below the externally visible suture line, is anteroposteriorly grooved, and the medial margin of the postorbital inserts into this groove. The posterior half of the suture between postorbital and parietal is posteriorly directed. In this part of the contact the postorbital does not overlap the parietal, but forms an anteroposteriorly oriented crest along its medial surface, which articulates with a groove on the lateral surface of the parietal.

The jugal process of the postorbital curves along the posteroventral margin of the orbit, so that the anterior margin of the postorbital is concave. The jugal process is slightly expanded into the orbit medially, forming an anteromedially-facing surface that delimits the orbital fossa posteriorly. The jugal process becomes ventrally thinner and tapers distally to a tip that inserts into a facet on the dorsal surface of the jugal. Both the jugal and the postorbital bear articular facets for each other: the jugal process of the postorbital fits into an anterolaterally recessed facet of the jugal, but the posterior margin of the jugal process is deeply recessed to form a wide groove that receives the anterior margin of the jugal. As a result, the jugal process wraps around the anterior margin of the jugal. Additionally, the postorbital has a ventrally directed sheet-like process posterior to the jugal process that braces against the medial side of the dorsal tip of the jugal. Externally, this part of the postorbital is visible as a ventrally narrowing triangular process that inserts between the jugal and quadratojugal.

The suture between the postorbital and quadratojugal is anterodorsally concave and posterodorsally directed so that the postorbital becomes transversely narrower as the quadratojugal becomes higher dorsoventrally. These bones appear to have a simple overlapping contact, whereby the posteroventrolateral margin of the postorbital laterally overlaps the quadratojugal.

The posterior margin of the postorbital is rarely completely preserved. In NHMUK PV OR35197, the specimen with the best preserved postorbital, the posterior margin of the bone forms a short contribution to the posterior skull emargination adjacent to the parietal.

Laterally, this margin develops a posterior notch. It is possible that this notch represents a contact surface for the squamosal, but the latter is not preserved in NHMUK PV OR35197. Alternatively, the notch could be the result of damage.

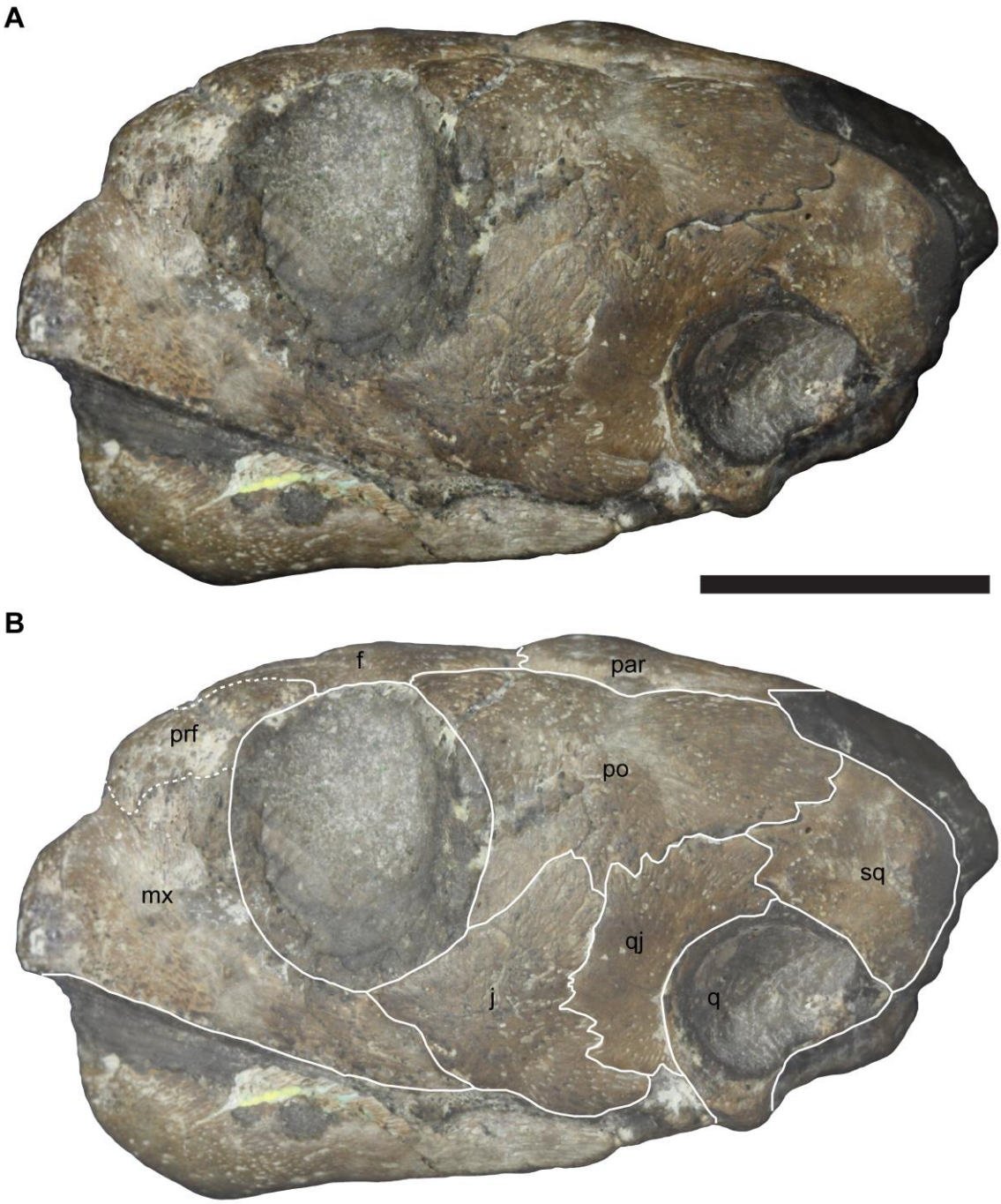


FIG. 3.17. Left lateral side of the cranium of CAMSM B55791, showing the contacts of the squamosal. **A**, Photograph; **B**, Photograph with sutures indicated. Dashed lines represent uncertainity about the exact placement of the suture. Scale bar equals 10 mm. Abbreviations: *f*, frontal; *j*, jugal; *mx*, maxilla; *par*, parietal; *po*, postorbital; *prf*, prefrontal; *q*, quadrate; *qj*, quadratojugal; *sq*, squamosal.

3.4.1.6 Jugal

The morphology of the jugal varies between *Rhinochelys* specimens. Specifically, a posterior jugal process is not present in all specimens. In the following, the jugal is described on the basis of the condition seen in CAMSM B55783 (*R. cantabrigiensis sensu* Collins (1970); Figs 3.6–7), as most other specimens for which we have CT scans also possess this morphology (NHMUK PV OR43980: *R. cantabrigiensis* holotype; NHMUK PV R2226: *R. elegans* holotype; CAMSM B55776: *R. elegans sensu* Collins 1970). The deviating pattern is described based on NHMUK PV OR35197 (*R. elegans sensu* Collins 1970). In CAMSM B55775 the jugals are not preserved.

The jugal is a transversely thin, triradiate bone. It comprises an anterior process that articulates with the maxilla, a posterodorsally oriented ascending process wedged between the postorbital and quadratojugal and a short posterior process that extends ventral to the quadratojugal. As seen in all protostegids from the Early Cretaceous (e.g. Evers & Benson 2018*a*), the jugal lacks a medial process and, as a consequence, it has no contact with either the parietal or pterygoid.

The anterior process of the jugal contacts the maxilla via a deeply interdigitated, bifurcated suture and also forms the posterior part of the suborbital bar. The dorsolateral edge of the anterior process forms a low, sharp crest that bounds the posteroventral portion of the orbital margin. The dorsal surface of the jugal adjacent to this crest extends medially to dorsally overlap the jugal process of the maxilla. This dorsal surface forms the ventral floor of the orbital fossa. It becomes transversely narrower posteriorly and curves posterodorsally, forming the anterior surface of the jugal ascending process.

The lateral surface of the anterior jugal process bears a deep notch for the reception of the laterodorsal ramus of the jugal process of the maxilla. Otherwise, the lateral surface of the jugal is smooth. The lateral surface of the jugal faces slightly ventrolaterally, so that the ascending process of the jugal is positioned slightly more laterally than the ventral portions of the jugal.

The ascending process extends posterodorsally to a point approximately level with orbital midheight. Furthermore, the base of the process is anteroposteriorly broad, occupying about half of the total anteroposterior extent of the jugal. The anterior margin of the ascending process, which forms the posteroventral rim of the orbit, has a concave outline in lateral view, and the anteroposterior width of the ascending process tapers dorsally. The ascending process is inclined posterodorsally at an angle of approximately 70° relative to horizontal. Nevertheless, its posterior edge forms an approximate right angle with the posterior process of the jugal in CAMSM B55783. In NHMUK PV OR35197, which lacks a posterior process, the suture line between the ascending process of the jugal and the anterior surface of the quadratojugal shows a similar inclination. In all *Rhinochelys* specimens, an anteroventral process of the postorbital overlaps the dorsal half of the anterior margin of the ascending process. The lateral surface of the ascending process is recessed to a shallow facet in the area of this contact (see also Postorbital, above). Posterior to this facet, the dorsal end of the ascending process overlaps the postorbital laterally.

The posterior process of the jugal is short and tapers posteriorly to a pointed tip, as its ventral edge curves posterodorsally (e.g. CAMSM B55783). This process ventrally underlaps the plate-like quadratojugal. Because the quadrate extends ventrally beneath the level of the quadratojugal, and the posterior process of the jugal does not extend posteriorly to contact the quadrate, there is a dorsal notch between the jugal and quadrate that forms a very weakly developed lower temporal emargination. The morphology of the articulation between the quadratojugal and jugal is not clear in any of the specimens with a posterior process or in our CT scans. The phosphatic nodules in which *Rhinochelys* skulls are preserved are almost always damaged by erosion in this area, making detailed examination impossible. The CT scans of CAMSM B55783 show that the dorsal surface of the posterior process, which faces the quadratojugal, seems to possess a very shallow, longitudinal groove. Thus, it seems likely that the ventral margin of the quadratojugal would have fitted into this groove. In any case, it appears that these bones did not have a tight sutural contact.

NHMUK PV OR35197, a specimen referred to *Rhinochelys elegans* by Collins (1970), lacks a posterior jugal process (Figs 3.5, 3.18). It seems unlikely that the process is broken, as the ventral margin of the jugal is smooth and seems to be completely preserved. Underneath the ventral margin of the jugal a small amount of matrix preserved, which also indicates that the bone did not extend further ventrally and posteriorly. Additionally, the ventral margin of the jugal aligns with the margin of the quadratojugal. Taken together, both bones form a gently concave ventral margin of the temporal region of the skull, but this area is not markedly emarginated.

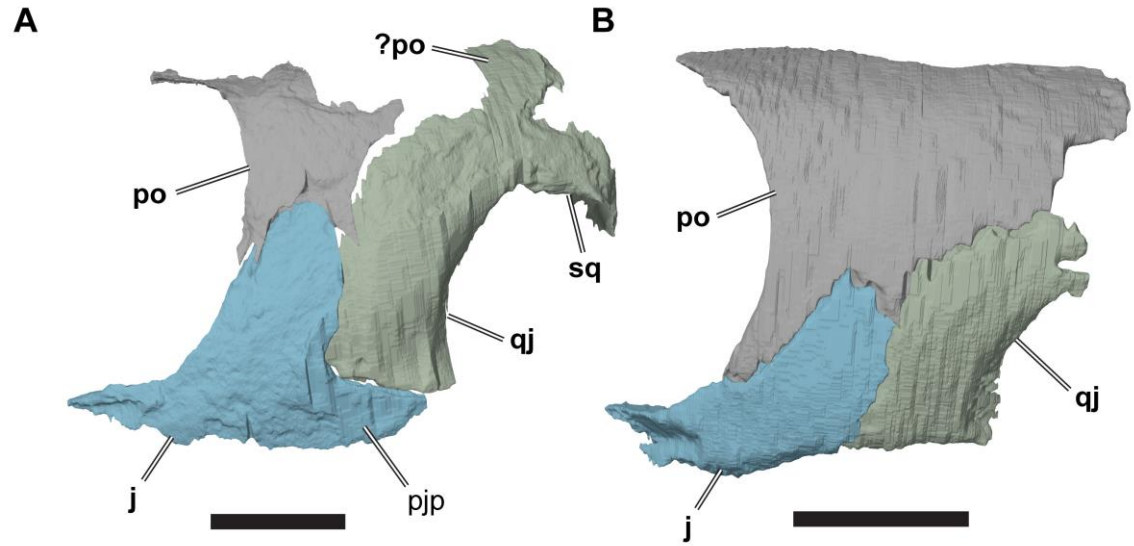


FIG. 3.18. Comparison of left cheek regions showing differences in jugal morphology. **A**, 3D rendering of CAMSM B 55783; **B**, 3D rendering of NHMUK PV OR35197. Scale bars equal 5 mm. Note that bones are labelled in bold. Abbreviations: *j*, jugal; *pjp*, posterior jugal process; *po*, popstorbital; *qj*, quadratojugal; *sq*, squamosal.

In all *Rhinochelys* specimens, the ventral margin of the quadratojugal is situated above the ventral margin of maxilla. In specimens possessing a posterior jugal process, it assumes a position lying approximately between the level of the ventral margins of those bones. In NHMUK PV OR35197, in which the process is absent, the ventral margin of the jugal simply forms a continuously sloping margin between the maxilla and quadratojugal, whereas this transition is more stepped in specimens with a posterior process (Fig. 3.18). Unfortunately, the presence or absence of the posterior jugal process does not occur consistently or

unambiguously among the species holotypes of *Rhinochelys* (*sensu* Collins, 1970), so it is not a taxonomically informative character.

3.4.1.7 Quadratojugal

The quadratojugal is a vertically oriented plate in the lateral temporal region of the skull (Figs 3.1–7, 3.18). It contacts the quadrate posteriorly, the squamosal posterodorsally, the postorbital anterodorsally and the jugal anteriorly. The quadratojugal covers the subtemporal fossa posterolaterally.

The quadratojugal is damaged in many specimens. Furthermore, the sutures of the quadratojugal with the jugal, postorbital and squamosal are hard to distinguish in our CT scans. The sutures are clearest in NHMUK PV OR35197, which preserves a complete left quadratojugal that forms the basis of this description.

The quadratojugal is dorsoventrally much taller than it is anteroposteriorly wide. It curves posterodorsally from its origin at the ventral surface of the temporal region so that its anterior margin is convex and its posterior margin is concave. The posterior margin of the quadratojugal is laterally overlapped by the anterior margin of the cavum tympanum of the quadrate over the entire height of the quadratojugal. The quadratojugal has only a short contact with the squamosal (although the squamosal is not preserved in NHMUK PV OR35197). A squamosal is present on the left side of CAMSM B55783, but the squamosal-quadratojugal suture cannot be located in the CT scan of that specimen so the exact shape of the contact between these bones cannot be determined. In CAMSM B55791, the suture between the quadratojugal and squamosal is externally visible and show widely spaced interdigitations.

The anterodorsal margin of the quadratojugal bears a dorsoventrally oriented groove on its lateral surface for contact with the postorbital. The jugal overlaps the anterior margin of the quadratojugal laterally in a simple, planar contact. In specimens possessing a posterior jugal process, such as CAMSM B55783 (see Jugal, above), the ventral margin of the

quadratojugal articulates with a shallow groove on the ventral margin of the former. In specimens lacking a posterior jugal process (e.g. NHMUK PV OR35197), the quadratojugal forms part of the ventral skull margin. Although its ventral margin is gently concave, it does not form a significant lower temporal skull emargination. In specimens with a posterior jugal process, the quadratojugal contribution to the ventral skull margin is much smaller, but forms a distinct notch between the quadrate and jugal.

3.4.1.8 Squamosal

Of the specimens for which we have CT scans, the squamosal is preserved only in CAMSM B55783 (Fig. 3.6). It is positioned in the posterodorsolateral part of the skull. However, it is incomplete and indistinguishable from the quadratojugal on the basis of CT data, thus limiting our description. Complete squamosals are present in CAMSM B55791 (Fig. 3.17), but we did not CT scan this specimen and the surrounding matrix prohibits medial and posterior views of the squamosal.

The squamosal of *Rhinochelys* contacts the quadratojugal anteroventrally, the postorbital anterodorsally, the quadrate posteroventrally and the opisthotic posteromedially, but a contact with the parietal is absent (CAMSM B55791). The incompletely preserved squamosal of CAMSM B55783 suggests the presence of a dorsomedial process that curves onto the skull roof and covers parts of the subtemporal fossa. The squamosal has a posterior process that covers parts of the quadrate dorsally and posteriorly (CAMSM B55791). The posterior surface of the squamosal is formed as a relatively thin ridge in CAMSM B55791, which curves posteroventrally to form a convex posterior margin in lateral view. Long posterior extensions of the squamosal are absent. The posterior process of the squamosal articulates with a deep groove on the dorsal surface of the quadrate (CAMSM B55783). The tip of the posterior process extends posteroventrally over the posterodorsal surface of the quadrate, thereby covering the open antrum postoticum in CAMSM B55783 and CAMSM B55791. The anterior surface of this part of the squamosal is shallowly excavated to form an

anteriorly open fossa that bounds the antrum postoticum posteriorly, which can be seen in the CT scans of CAMSM B55783. However, the squamosal is excluded from the posterodorsal margin of the cavum tympanum, whereas it forms the margin of the cavum tympanum in *Desmatochelys lowii* (KUVP 1200; Raselli 2018). It is not clear how the squamosal-quadrate contact is formed in specimens with a posteriorly closed quadrate, which implies the absence of a squamosal portion of the antrum postoticum (see Quadrate, below). The posterior process of the squamosal in medially expanded in CAMSM B55783 to form a short, interdigitating contact with the opisthotic at the posterior margin of the subtemporal fossa.

The anterolateroventral extent of the squamosal in *Rhinochelys* is similar to that of most chelonioids (e.g. but also cheloniids such as *Lepidochelys olivacea*: SMNS 11070) in that it is relatively short. However, the squamosal extends much further anteroventrally in *Desmatochelys lowii* (KUVP 1200; Raselli 2018), which is one of the few protostegids for which this region has been described.

3.4.1.9 Premaxilla

The premaxilla is a paired bone at the anterior end of the skull (Figs 3.1–5, 3.9–10). It comprises an anterior portion that contacts the maxilla posterolaterally and the external naris dorsally, and a posterior process that forms the median portion of the triturating surface and parts of the floor of the nasal cavity. This posterior process also contacts the vomer posteriorly.

The left and right premaxillae meet at a midline suture. The suture can be seen in most specimens (e.g. CAMSM B55783, B55791) and is weakly interdigitating, as confirmed by CT scans. The anterior surface of the premaxilla is approximately as high as the external naris dorsoventrally and is weakly convex both transversely and dorsoventrally. The anterior surfaces and labial ridge of the premaxillae curve posterolaterally from the midline until they meet the maxillae, which then extends further posterolaterally at a contant angle (the jaw angle, see below).

The external nares are conjoined to form a single opening that is bordered ventrally by the articulated premaxillae. The narial margin of the joined premaxillae is developed as a transversely oriented, thin crest. The ventral margin of the external naris is mediolaterally concave, contributing to the approximately circular outline of the external naris in anterior view. The dorsal surface of the posterior process of the premaxilla, which forms the floor of the nasal cavity, is concealed by matrix in most specimens. However, it is visible in CT scans and in specimens in which sufficient matrix has been removed (NHMUK PV R1806, NHMUK PV R27).

The ventral floor of the nasal cavity, as formed by the premaxilla, faces posterodorsally. The relevant surfaces of each premaxilla are both anteroposteriorly and transversely concave, so that their mid-parts form shallow depressions either side of a median ridge. This ridge likely anchored an internarial septum that separated the right and left nasal valves. The ridge continues posteriorly on to the dorsal surface of the vomer, terminating just anterior to the sulcus vomeri. The depression on the dorsal surface of each premaxilla extends onto the dorsomedial surface of the maxilla, forming a large fossa that forms the ventral boundary of each nasal valve. The dorsal surface of the premaxilla broadens posteriorly within the nasal cavity. A foramen located anteriorly in the premaxillary depression extends anteroventrally through the premaxilla, exiting as a small foramen on the palatal side of the premaxilla within the triturating surface. It is possible that these foramina are associated with the vomeronasal system. However, this sensory organ is poorly understood even in modern turtles (Schwenk 2008). The topology, symmetry and size of these foramina varies between specimens, although their position is conserved. This foramen does not seem to represent a foramen praepalatinum, as this opening is usually positioned more posteriorly within the premaxilla or in the suture between the premaxillae and vomer, and it is also usually larger (Gaffney 1979). The foramen praepalatinum is also absent in modern cheloniids (Gaffney 1979) and *Dermochelys* (Nick 1912, Wegner, 1959; Albrecht 1976; Evers & Benson 2018*b*).

The median contact of the premaxillae within the nasal cavity is interrupted shortly posteroventral to the external naris, where a slit-like median opening extends anterolaterally into the inter-premaxillary suture. This opening extends anteroventrally into a recess between the premaxillae. The function of this recess is unknown, but no further canals exiting it are visible in our CT data.

The premaxilla articulates laterally with the maxilla over its entire dorsoventral height in a vertical, highly interdigitating suture that is visible externally in all specimens. The ventral surface of the premaxilla forms the anteromedial portion of the triturating surface. The suture between the premaxilla and maxilla extends posteromedially across the palate, crossing the triturating surface. As a consequence, the palatal portions of the premaxillae taper posteriorly. The triturating surface is anterolaterally bounded by the labial margin of the premaxilla, which is elevated to a sharp ridge (the labial ridge). The labial ridge curves posterolaterally from the midline, and continues onto the maxilla, where it retains an almost straight posterolateral course. The angle between the right and left maxillary labial ridges is the 'jaw angle' of Collins (1970: see Maxilla, below). Immediately lingual to the labial ridge, paralleling its course, and also continuous from the premaxilla to the maxilla, is a deep groove (the labial groove). This groove accommodates the sharp-edged margin of the mandible when the jaws are in occlusion. The groove is deepest mesially on the premaxilla and becomes shallower distally on the maxilla. A second more shallowly developed ridge, the lingual ridge, defines the lingual margin of the labial groove. The lingual ridge is located primarily on the maxilla, with only a small portion extending onto the premaxilla.

An anteroposteriorly oriented median groove is present on the palatal surface of the premaxillae and was termed the 'premaxillary groove' by Collins (1970). This groove is also present in some other sea turtles and, because it intersects with the anteriorly convex labial groove, the combined form of the palatal grooves has sometimes been described as being 'anchor-shaped' (Lynch & Parham 2003). The premaxillary groove of *Rhinochelys* terminates abruptly where the premaxillae meet the vomer posteriorly, jointly forming a transversely convex bar between the internal nares.

3.4.1.10 Maxilla

The maxilla forms large parts of the snout (Figs 3.1–7, 3.9). Anteromedially, it contacts the premaxilla, with which it forms the triturating surface and palatal ridges on the ventral side of the snout. Posteromedially, the left and right maxillae contact a columnar ventral process of the vomer just anterior to the internal nares, which prevents midline contact of the maxillae on the triturating surface, although they do approach each other closely. The maxilla has a short, anteriorly positioned ascending process, which is posterodorsally directed and contacts the nasal and prefrontal. The ascending process contributes to the margins of the external naris anteriorly and to the orbit posteriorly. Posteriorly, the maxilla possesses a relatively slender jugal process that extends ventral to the orbit. The jugal process interlocks posteriorly with the jugal and contacts the palatine along its medial margin. Within the orbital fossa, the maxilla contributes to the foramen orbito-nasale. The medial surface of maxilla also forms part of the nasal cavity, the meatus choanae and the internal naris.

The maxillae are directed posterolaterally, diverging from one another at an angle of 33–57°, so that the snout becomes broader posteriorly. The divergence angle between the maxillae was referred to as the 'jaw angle' by Collins (1970: p. 357), who interpreted differences in this angle as one of the features separating the three species of *Rhinochelys* recognised in that paper (see Discussion, below). The maxilla forms most of the triturating surface, which is composed of a sharp labial ridge, a shallower lingual (tomial) ridge and a labial groove separating these ridges (Fig. 3.9). The labial ridge of the maxilla is continuous with the labial ridge of the premaxilla and forms a high but slender cutting edge. The labial ridge becomes more prominent posteriorly and continues to the posterior end of the maxillary jugal process. *Rhinochelys* specimens vary in the curvature of the maxillary labial ridge; while the ridge is completely straight in many specimens (e.g. *R. elegans* holotype, NHMUK PV R2226), others show marked curvature in which the labial ridge is ventrally convex (e.g. *R. cantabrigiensis* holotype, NHMUK PV OR43980). Immediately lingual to the labial ridge is the labial groove, which parallels the course of the labial ridge and is also

continuous between the premaxilla and maxilla. The labial groove gets shallower posteriorly, as it is bordered on the lingual side by the lingual ridge, which also gets lower posteriorly. The lingual ridge is a low plateau that forms most of the grinding or triturating surface and has its deepest and broadest extent at the level of the vomer. This is similar in *Bouliachelys suteri* (QM F31669; Kear & Lee 2006), but different in *Desmatochelys lowii* (KUVP 1200; Raselli 2018) in which the lingual ridge is narrow, robust and deep. The labial and lingual ridges of *Rhinochelys* are not parallel; the medial margin of the lingual ridge diverges from the midline at a higher angle than the labial ridge. Thus, the triturating surface gets progressively narrower posteriorly as the ridges converge posteriorly. The triturating surface is penetrated by many small neurovascular foramina. The anterior half of the medial margin of the lingual ridge forms the lateral margin of the internal naris, which is otherwise bounded by the vomer medially and the palatine posteriorly. The posterior half of the medial margin of the lingual ridge is dorsoventrally slightly expanded and forms the articular surface for the maxillary process of the palatine.

The ascending process of the maxilla extends posterodorsally from the maxillary body. Its anterior margin forms part of the lateral margin of the external naris. This margin is medially concave, contributing to the near circular outline of the external naris. At its anterior end, the ascending process contacts the nasal via a short suture. The latter slots into the ascending process via two bony prongs, the medial of which extends ventrally for several millimetres along the margin of the external naris, while the lateral prong inserts more posteriorly between the maxilla-prefrontal contact. The maxilla achieves its greatest dorsoventral height at the nasal-maxilla-prefrontal suture. Posterior to this contact, the maxilla forms a highly interdigitating, posteroventrally sloping suture with the prefrontal. The ascending process provides only a minor contribution to the orbital margin. CT scans (e.g. CAMSM B55783, NHMUK PV OR35197) show that the maxilla has an anteroposteriorly oriented incision on its contact surface with the prefrontal. This incision runs parallel to the posterodorsomedial margin of the maxilla, into which the prefrontal slots in addition to the

many finger-like extensions on both bones that can be seen externally by tracing the undulating path of the suture.

The lateral surface of the ascending process is separated from the lateral surface of the maxillary body by a moderately deep sulcus. The sulcus runs from the maxillary-nasal suture to the orbital margin a few millimetres below the maxilla-prefrontal suture and is ventrally convex. The ascending process, defined as the maxillary bone above this sulcus, is convexly curved in all directions, so that it appears swollen with a surface that is laterally expanded with respect to the maxillary body. This preorbital bulge is an autapomorphy of *Rhinochelys* (Collins 1970; Tong *et al.* 2006). The surface of the ascending process is confluent with those of the nasal and prefrontal. Therefore, the sulcus distinguishes a slightly lower beak region, formed by most of the lateral surface of the maxilla, the jugal process of the maxilla, and the premaxilla, from a slightly protruding forehead region formed by the ascending process of the maxilla, the nasals, and the prefrontals. The maxillary sulcus is present in all specimens, although its depth, as well as the degree to which the ascending process is bulged, differs between them. This variation does not seem to be ontogenetic, as deep sulci and high degrees of swelling appear in both small and large specimens (see Discussion).

The medial surface of the maxilla is shallowly excavated by a fossa at the base of the ascending process (Fig. 3.15). This fossa is continuous with the fossa on the dorsal surface of the premaxilla: together they form the ventral half of the nasal valve. At its posterior contact with the premaxilla, the maxilla forms a short but stout medial process. This process joins the ventral columnar process of the vomer laterally and articulates with it in a highly interdigitated fashion, as evident from the CT scans.

The jugal process of the maxilla extends from the maxilla-prefrontal suture in the orbital margin posteriorly to the contact with the jugal. Hence, the jugal process extends ventral to the orbit, forming the anterior portion of the suborbital bar. Its dorsal edge forms a slightly raised crest, so that the orbit is well defined anteroventrally and ventrally. This dorsal margin is concavely rounded, contributing to the circular outline of the orbit. The jugal

process becomes shallower posteriorly. Medial to the orbital margin, the jugal process is transversely expanded to form a narrow shelf that frames part of the orbital fossa. Anteromedially, this shelf participates in the formation of the foramen orbito-nasale. The maxillary shelf framing this foramen is also pierced by a tiny circular opening, the foramen alveolare superius (Gaffney 1972*b*, 1979; Albrecht 1976), which leads into a channel within the maxilla, the canalis alveolaris superior. As shown by CT scans, the canalis alveolaris superior extends anteriorly, and branches to form a dense network within the maxilla, and that exits it via the numerous small foramina present on the triturating surface. This canal carries the superior alveolar artery, which supplies the maxilla with blood (Albrecht 1976). As in *Chelonia* (Albrecht 1976), there is no posterior branch (canalis infraorbitals) for the supramaxillary artery off of the canalis alveolaris superior in *Rhinochelys*. The absence of the supramaxillary artery in *Rhinochelys* is also supported by the absence of a foramen supramaxillare, which usually exits the canalis infraorbitalis posteriorly in the floor of the orbital fossa (Gaffney 1979). The condition in *Dermochelys* has not been described (see Albrecht 1976), but CT scans of a *Dermochelys* skull (FMNH 171756) show that a canalis infraorbitalis exists in this taxon and that the posterior exit, the foramen supramaxillare, is located between the jugal and maxilla. The foramen alveolare superius of *Dermochelys* is in the same position as in *Rhinochelys*, but the former has an additional foramen posteriorly adjacent to the foramen alveolare superius, which also connects to the canalis alveolaris superior.

In *Rhinochelys*, at a point halfway along the orbit, the dorsal surface of the maxillary jugal process bears a deep ventral incision for the jugal near its lateral margin, which can be seen in CT scans. The jugal enters this incision via a short anterior process, forming a strongly interlocking contact between the maxilla and jugal. In addition to this interlocking articulation, the posterior end of the maxillary jugal process bifurcates into laterodorsal and medioventral rami. The laterodorsal ramus articulates with a small groove on the lateral surface of the jugal anterior process. The medioventral ramus of the maxillary jugal process,

which bears the posterior end of the labial ridge, extends ventral to the jugal and articulates with a small ventral groove.

3.4.1.11 Vomer

The vomer is an unpaired midline bone situated in the anterior part of the palate (Figs 3.1–5, 3.9, 3.12–13, 3.19; Appendix S2, Fig. S2.8). It contacts the premaxilla anteriorly and the maxilla anterolaterally in the floor of the nasal cavity via an anteroventral process that forms the medial margin of the internal naris. The main portion of the vomer is anteroposteriorly long, transversely narrow and has a concave posterodorsal surface that forms the floor of the orbital fossa. It contacts the palatine posterolaterally, and produces paired dorsal processes that contact the prefrontals laterally. Together with the prefrontals, the vomer forms a vertical bony wall that separates the orbital fossa from the nasal cavity.

The anteroventral process is short and columnar and its anterior end is transversely broadened toward its contacts with the maxilla and premaxilla (Appendix S2, Fig. S2.8). The base of the anteroventral process is constricted between the anterior end of the process and the dorsal processes, forming the medial wall of each meatus choanae. CT scans show that the contact surfaces for the premaxillae and maxillae are highly interdigitated. A low dorsomedian ridge on the anteroventral process of the vomer is continuous with a ridge on the premaxilla and likely served as an anchor for the narial septum. This ridge becomes shallower posteriorly and disappears just anterior to the dorsal processes.

The dorsal processes are gently inclined dorsolaterally and are situated in the anterior one-third of the element (Figs 3.12–13). The right and left dorsal processes are separated from the midline by a deep fissure, the sulcus vomeri. Dorsally, the sulcus vomeri is continuous with the fissure ethmoidalis (see Prefrontal, above). The prefrontal articulates with the posterolateral side of the dorsal process. The contact surface of the vomer with the prefrontal is characterised by many finger-like extensions and deep pockets, indicating rigid interlocking between these elements.

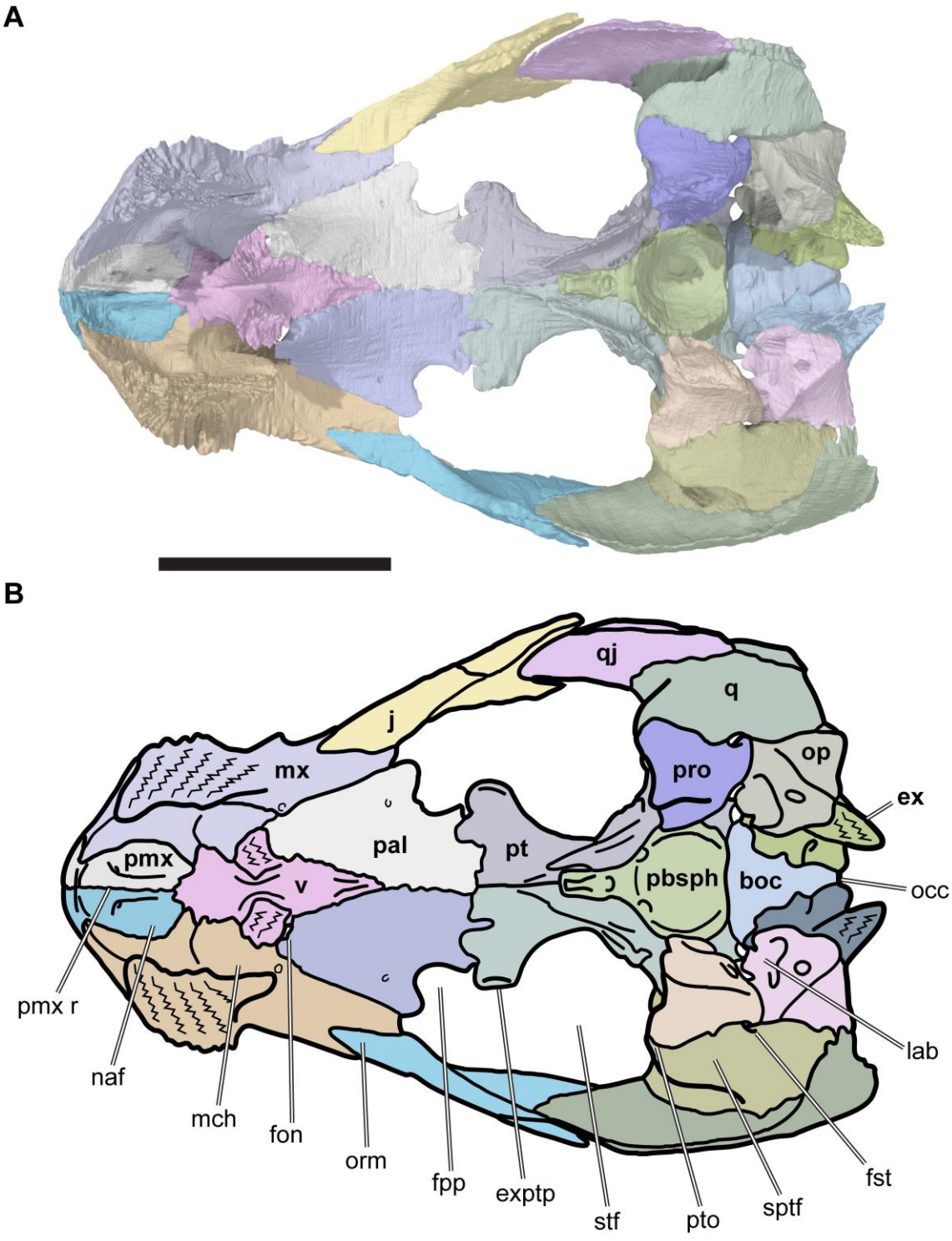


FIG. 3.19. Dorsal view of palate and basicranium of CAMSM B55783. **A**, 3D rendering; **B**, interpretative line drawing. Scale bar equals 10 mm. Note that bones are labelled in bold. Abbreviations: *boc*, basioccipital; *ex*, exoccipital; *exptp*, external pterygoid process; *fon*, foramen orbito-nasale; *fst*, foramen stapedio-temporale; *j*, jugal; *lab*, cavum labyrinthicum; *mch*, meatus choane; *mx*, maxilla; *occ*, occipital condyle; *naf*, nasal fossa; *op*, opisthotic; *orm*, orbital margin; *pal*, palatine; *pbsph*, parabasisphenoid; *pmx*, premaxilla; *pmx r*, premaxilla ridge; *pro*, prootic; *pt*, pterygoid; *pto*, processus trochlearis oticum; *q*, quadrate; *qj*, quadratojugal; *sptf*, supratemporal fossa; *stf*, subtemporal fossa; *v*, vomer.

The posterior process of the vomer forms a narrow triangular contribution to the palate that is wedged between the palatines. This part of the vomer thins dorsoventrally as it extends posteriorly. It also slopes gently posteroventrally toward its posterior margin, contributing to the dorsally concave form of the vomer that is best seen in lateral view. The lateral margins of the vomer that contact the palatines are also slightly curved dorsally, so that the dorsal surface of the vomer forms a shallow dorsally open trough that leads to the sulcus vomeri anteriorly. This trough disappears in the posterior half of the posterior process of the vomer and is replaced by a low, but sharp, median crest that likely served as the anchor for the interorbital septum.

The ventral surface of the vomer is transversely convex. Anteriorly, just before merging with the posterior surface of the anteroventral process, a median, well-rounded keel arises from the ventral surface of the posterior process. The keel separates the left and right internal nares and becomes very shallow posteriorly where the vomer tapers between the palatines.

3.4.1.12 Palatine

The paired palatines are situated in the anterior part of the palate (Figs 3.1–5, 3.9, 3.19). Each palatine contacts the vomer anteromedially, the prefrontal anterolaterally, the pterygoid posteriorly and the maxilla laterally via an anteroposteriorly broad and dorsoventrally deep lateral or maxillary process. The palatine forms the floor of the orbital fossa, the roof of most of the meatus choanae, the posterior and lateral margins of the internal naris and the posteromedial margin of the foramen orbito-nasale. The palatine also forms a clearly developed, albeit posterolaterally open, foramen palatinum posterius.

The palatine is horizontally oriented and plate-like. It is longer anteroposteriorly than it is wide transversely, narrows somewhat anterior to the lateral process and is transversely constricted at the level of the foramen palatinum posterius. Anteromedially, the palatine curves dorsally to contact the vomer and form a domed central part of the palate that roofs

the meatus choane and separates the left and right orbital fossae. The palatines are sutured to each on the midline posterior to their contact with the vomer and form a horizontally flat surface with the posteriorly adjacent pterygoids.

Anteriorly, the palatine develops a narrow, spur-like process that contacts the vomer medially and articulates with the prefrontal anteriorly. The lateral margin of this spur forms the posteromedial border of the foramen orbito-nasale. The palatine contacts the maxilla in the posterolateral margin of this foramen. From here, the suture between the palatine and maxilla extends posterolaterally in a straight line that is visible on the ventral palatal surface and on the floor of the orbital fossa. The lateral margin of the palatine contacting the maxilla is expanded ventrally to form a dorsoventrally thick articular surface. This surface is deeply excavated and wraps around the posterior parts of the maxillary labial ridge. The anteromedial surface of the ventrally expanded articulation surface for the maxilla forms the lateral wall of the meatus choane. The palatine is pierced by a small foramen near the base of the maxillary process. This foramen is dorsoventrally directed, forming a small canal that connects the floor of the orbital fossa with the ventral surface of the palatine.

The posterior end of the palatine maxillary process forms a small tip that extends beyond the distal end of the maxillary labial ridge into the fenestra subtemporalis (Figs 3.9, 3.19). Posterior to the tip of the palatine maxillary process a well-rounded, medial notch is present in the lateral margin of the posterior part of the palatine. The notch is open posterolaterally and represents an open foramen palatinum posterius. This foramen is absent in modern cheloniids, *Dermochelys* (Gaffney 1979) and probably the protostegid *Desmatochelys lowii* (KUVP 1200; see Raselli 2018), but is present in other protostegids from the Early Cretaceous (e.g. Kear & Lee 2006; Cadena & Parham 2015). Posterior to the foramen palatinum posterius the palatine becomes slightly wider transversely, but it does not reach the width of the palatine anterior to the foramen. The palatine articulates with the pterygoid posteriorly. Thin bony sheets arising from the posterior margin of the palatine extend deeply into the anterior surface of the pterygoid, resulting in tight interlocking of these elements.

3.4.1.13 Quadrate

The quadrate is a large bone in the posterolateroventral corner of the skull that forms the mandibular condyle and cavum tympani (Figs 3.1–7, 3.9). It contacts the squamosal dorsolaterally and posteriorly, the quadratojugal anterolaterally, the opisthothic posteromedially and posteriorly, the prootic anterodorsolaterally and the pterygoid anteroventromedially. This description is based on several specimens with well-preserved quadrates, namely the left quadrate of CAMSM B55783 (Fig. 3.6), the right quadrate of CAMSM B55775 (Fig. 3.1B) and the right quadrate of CAMSM B55776 (Fig. 3.4B). Variation between these specimens is noted throughout the text, but they agree in morphology unless stated otherwise.

The quadrate forms a vertical wall of bone that separates the middle ear into a lateral section that includes the cavum tympani and the incisura collumella auris, and a medial part that constitutes the cavum acustico-jugulare. The dorsal portion of the quadrate borders the foramen stapedio-temporale laterally and contributes to the floor of the supratemporal fossa. The anterodorsal portion of the quadrate forms the lateral part of the processus trochlearis oticum (the medial part is formed by the prootic), which forms the posterodorsal border of the subtemporal fossa. Ventrally, the quadrate forms the articular process (=processus articularis of Gaffney 1972*b*), which bears the mandibular condyle for the articulation of the lower jaw. The medial surface of the quadrate borders the canalis stapedio-temporalis at the level of the prootic contact. Its dorsal foramen exits into the supratemporal fossa, while the medial foramen leads into the cavum acustico-jugulare. The medial surface of the quadrate further borders the posterior part of the canalis cavernosus, which extends anteriorly.

The cavum tympani is a large funnel-like cavity on the lateral surface of the quadrate. It is shallowest along the contact with the quadratojugal and squamosal, and deepens centrally. From this deep central portion, a posterodorsally oriented trough extends into a small recess of the squamosal, the antrum postoticum. This trough is bordered dorsally by a prominent, posteroventrally-sloping shelf of the quadrate, and ventrally by a small process

posterodorsal to the incisura columella auris. These structures do not contact each other in most specimens, and so the trough is 'open' laterally. The opening toward the antrum postoticum in the quadrate is referred to herein as the foramen antrum postoticum (Fig. 3.20B). In CAMSM B55775, however, the cavum tympani is closed posterodorsally so that the foramen antrum postoticum is absent. Nevertheless, the cavum tympani extends into a posterodorsally situated pocket-like recess, which excavates the body of the quadrate in a similar way to that seen in other specimens (Fig. 3.20A). Although the squamosal is missing in CAMSM B55775, the quadrate is well preserved and includes its dorsal suture for the squamosal. This indicates that the posterodorsal portion of the cavum tympanum is genuinely formed by the quadrate in this specimen rather than by a partially preserved fragment of the squamosal.

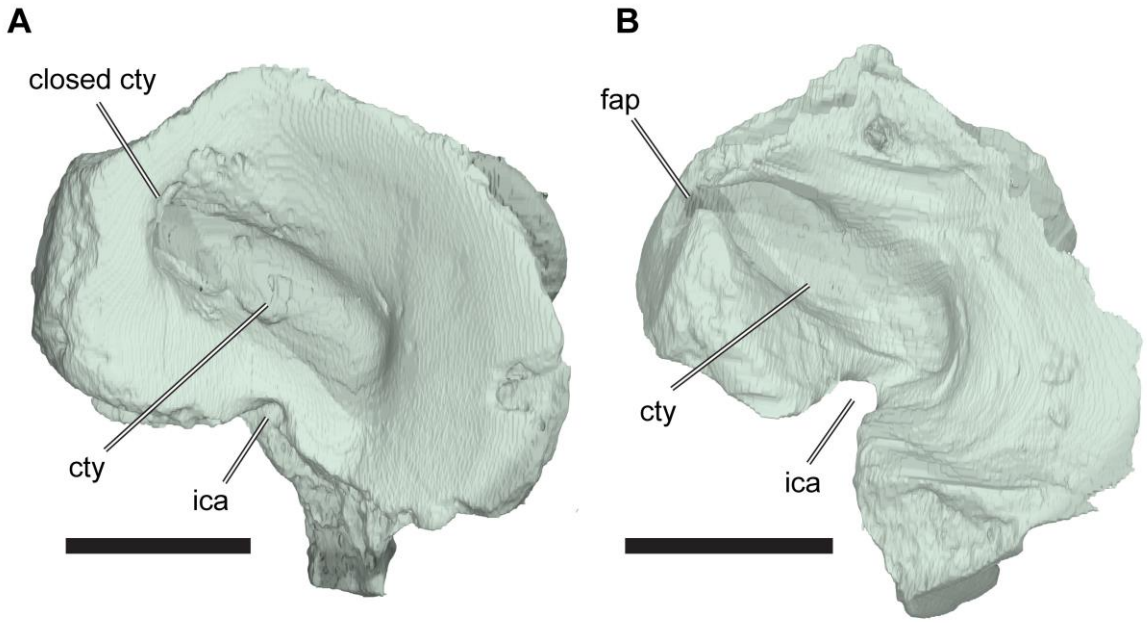


FIG. 3.20. Comparison of quadrates in right lateral view. **A**, 3D rendering of right quadrate of CAMSM B55775; **B**, 3D rendering of right quadrate of CAMSM B55776. Scale bars equal 5 mm. Abbreviations: *cty*, cavum tymani; *fap*, foramen antrum postoticum; *ica*, incisura columella auris.

The posteroventral margin of the cavum tympani is embayed by a posteroventrally open notch, the incisura columella auris, through which the stapes passes (see Stapes, below). The incisura columella auris forms a short, open channel that connects the cavum tympani laterally to the cavum acustico-jugulare medially, just dorsal to the contact with the quadrate

process of the pterygoid, and ventral to the level of the fenestra ovale, which is formed by the opisthotic and prootic.

The quadrate overlaps the lateral surface of the posterolateral surface of the quadratojugal via a simple, planar contact. The contact between these bones has an anteriorly-convex outline in lateral view. The quadrate has a dorsally facing groove along the posterodorsal margin of the cavum tympanum, which is positioned posterior to the quadrate-quadratojugal contact. This groove receives the ventral margin of the squamosal. The groove separates the dorsal surface of the quadrate, which forms the floor of the supratemporal fossa, from the posterolateral margin of the quadrate, which borders the cavum tympanum. The dorsal surface of the quadrate slopes toward the prootic and opisthotic medially, so that it faces dorsomedially. The dorsal surface is anteroposteriorly elongate compared to its transverse width. It is widest centrally, rather than anteriorly or posteriorly, and its combined suture with the prootic and opisthotic is slightly convex medially in dorsal view.

A process bearing the quadrate portion of the processus trochlearis oticum extends anteriorly from the anterodorsal surface of the quadrate. The quadrate part of the processus trochlearis oticum curves medioventrally with respect to its prootic part, so that the process is braced ventrally by the quadrate. The anterior margin of the processus trochlearis oticum is convex and its dorsal surface is transversely concave. The relative contributions of the quadrate and prootic to the processus trochlearis oticum vary among specimens of *Rhinochelys* (Fig. 3.21). In CAMSM B55783 (*R. cantabrigiensis sensu* Collins 1970), CAMSM B55776 (*R. elegans sensu* Collins 1970) and NHMUK PV OR35197 (*R. elegans sensu* Collins 1970), most of the process is formed by the prootic, whereas the quadrate contributes just over half of the width of the process in CAMSM B55775 (*R. pulchriceps*, holotype).

The anterior surface of the quadrate is strongly concave transversely between the quadrate portion of the processus trochlearis oticum and the lateral sheet that articulates with the quadratojugal. Ventral to the processus trochlearis oticum, a thin epipterygoid process (=processus epipterygoidei of Gaffney 1972*b*) of the quadrate extends anteromedially to contact the lateral surface of the pterygoid (Fig. 3.16). The ventral margin

of the epipterygoid process of the quadrate slots into a dorsally open groove on the anterolateral surface of the quadrate process of the pterygoid. The preserved extent of the epipterygoid process toward the maxillo-mandibular (CN V_{2-3}) foramen is variable. Nevertheless, a small area on the lateral surface of the pterygoid ventral to the maxillo-mandibular foramen usually remains uncovered, exposing the fossa cartilaginis epipterygoidei, as is common in cryptodires (Gaffney 1979). Posteromedial to the epipterygoid process, the quadrate and pterygoid are tightly sutured to each other.

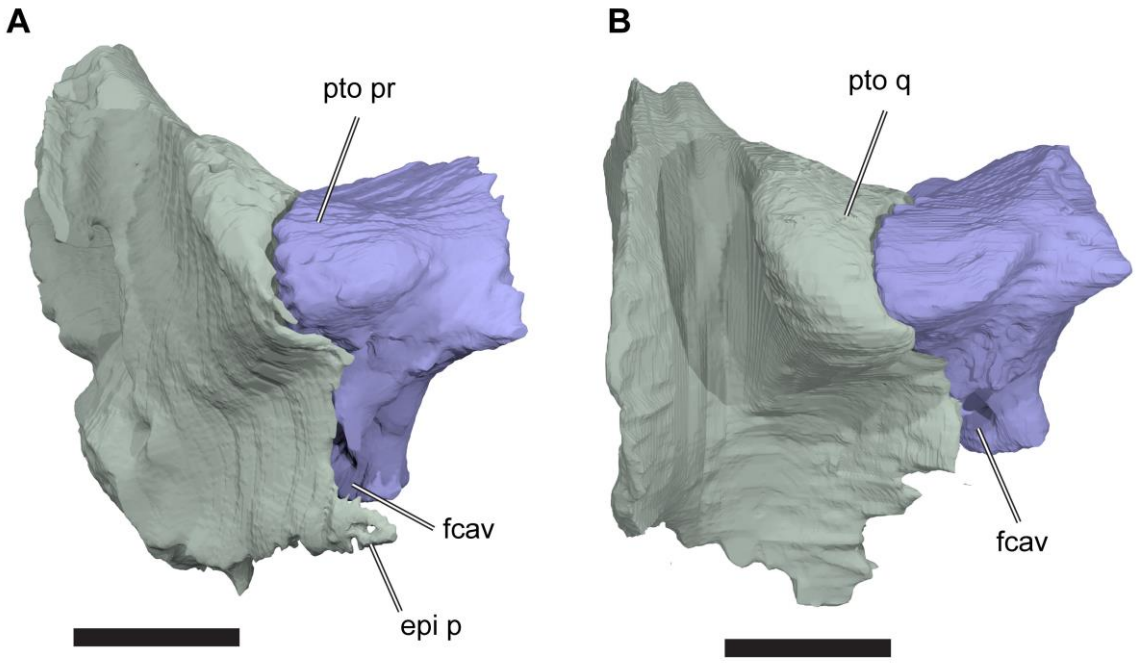


FIG. 3.21. Comparison of trochlear processes in anterior view. **A**, 3D rendering of right quadrate and prootic of NHMUK PV OR35197; **B**, 3D rendering of right quadrate and prootic of CAMSM B55775. Scale bars equal 2 mm in A, and 5 mm in B. Abbreviations: *epi p*, epipterygoid process of quadrate; *fcav*, foramen cavernosum; *pto pr*, prootic portion of processus trochlearis oticum; *pto q*, quadrate portion of processus trochlearis oticum.

The articular process of the quadrate extends ventrolaterally, projecting ventral to the level of the pterygoid. The ventral surface of this process forms the mandibular condyle (=condylus mandibilaris of Gaffney 1972*b*). The mandibular condyle is broad transversely and has a centrally placed, anteroposteriorly-oriented sulcus. The mandibular condyle is constricted anterior and posterior to this sulcus, dividing it into medial and lateral convex facets.

The dorsal part of the medial surface of the quadrate contacts the opisthotic posteriorly and the prootic anteriorly. The opisthotic appears to be loosely connected to the quadrate, as there are no interdigitations between these bones. However, the paroccipital process (=processus paroccipitalis of Gaffney 1972*b*) of the opisthotic wraps ventrally around the posteromedial surface of the quadrate. The canalis stapedio-temporalis extends vertically between the quadrate and prootic near the posterior margin of their contact, connecting the supratemporal fossa dorsally with the cavum acustico-jugulare ventrally through the aditus canalis stapedio-temporalis. The cavum acustico-jugulare is a broad cavity between the quadrate, prootic, opisthotic and pterygoid (see Cavum acustico-jugulare, below).

3.4.1.14 Epipterygoid

Among turtles, the epipterygoid is ossified only in cryptodires and various stem-group turtles. With the exception of *Proganochelys* (Gaffney 1990), the epipterygoid is usually discernable in adults as a small plate of bone situated on the lateral side of the crista pterygoidea of the pterygoid, anterior to the maxillo-mandibular (CN V_{2-3}) foramen. None of the CT scanned specimens of *Rhinochelys* possesses an ossified epipterygoid. Nevertheless, a fossa cartilaginis epipterygoidei, which receives the epipterygoid, is present on the lateral surface of the pterygoid ventral to the maxillo-mandibular foramen, indicating the potential presence of a cartilaginous element. Based on CT scans, we can also confirm the absence of an ossified epipterygoid in *Bouliachelys suteri* (QM F31669) and *Notochelone costata* (NHMUK PV R9590). Raselli (2018) recently described an epipterygoid for *Desmatochelys lowii*. However, the morphology and position of this bone are unusual, in that it is very small, limited to the anterior margin of the secondary lateral wall of the braincase and does not extend further posteriorly. Examination of the same CT scan of KUVP 1200 used by Raselli (2018) could not confirm the presence of an epipterygoid for *Desmatochelys lowii* and the reported 'epipterygoid' is more likely to represent part of the processus inferior paritalis.

3.4.1.15 Pterygoid

The pterygoids form the posterior part of the palate and connect with the braincase and skull roof (Figs 3.1–5, 3.9, 3.19, 3.22; Appendix S2, Fig. S2.9). They are paired, contacting each other anteromedially, and each also contacts the parabasisphenoid posteromedially, the quadrate posterolaterally, the basioccipital posteriorly, the prootic posterodorsally, the parietal dorsally and the palatine anteriorly. As in other Early Cretaceous protostegids (e.g. Hirayama 1998; Kear & Lee 2006; Cadena & Parham 2015) and *Dermochelys*, but unlike in cheloniids (e.g. *Eretmochelys imbricata* FMNH 22242; *Lepidochelys olivacea* SMNS 11070), there is no contact between the pterygoid and the jugal in *Rhinochelys*. The pterygoid floors the canalis cavernosus, sulcus cavernosus and cavum acustico-jugulare, encloses large parts of the maxillo-mandibular (CN V_{2-3}) foramen and parts of the internal carotid arterial system, and forms the ventral border of the fenestra postotica.

The palatal portion of the pterygoid consists of a transversely narrow and anteroposteriorly elongate horizontal plate that is constricted around its midlength so that it has concave lateral margins when seen in ventral view (Fig. 3.22A–B). The anterior halves of the left and right pterygoids contact each other on the midline (Fig. 3.22A–D). The anterior part of the pterygoid forms a dorsoventrally narrow sheet that expands laterally at its anterior end to form the external pterygoid process (=processus pterygoidus externus of Gaffney 1972*b*). The external pterygoid process is slightly thickened anterodorsally at its lateral tip and projects laterally into the subtemporal fenestra. As the foramen palatinum posterius of the palatine is open, and there is no pterygoid contact with the maxilla and/or jugal, the foramen palatinum posterius and the subtemporal fenestra form a large, continuous opening between the palate medially and zygatomal arch laterally, which is roughly reniform (kidney-shaped) in outline (Fig. 3.9). The anterior part of the pterygoid overlaps the palatine for a short distance.

In its posterior third, the palatal portion of the pterygoid forms the posteroventrolaterally directed quadrate process. This process is sutured tightly to the

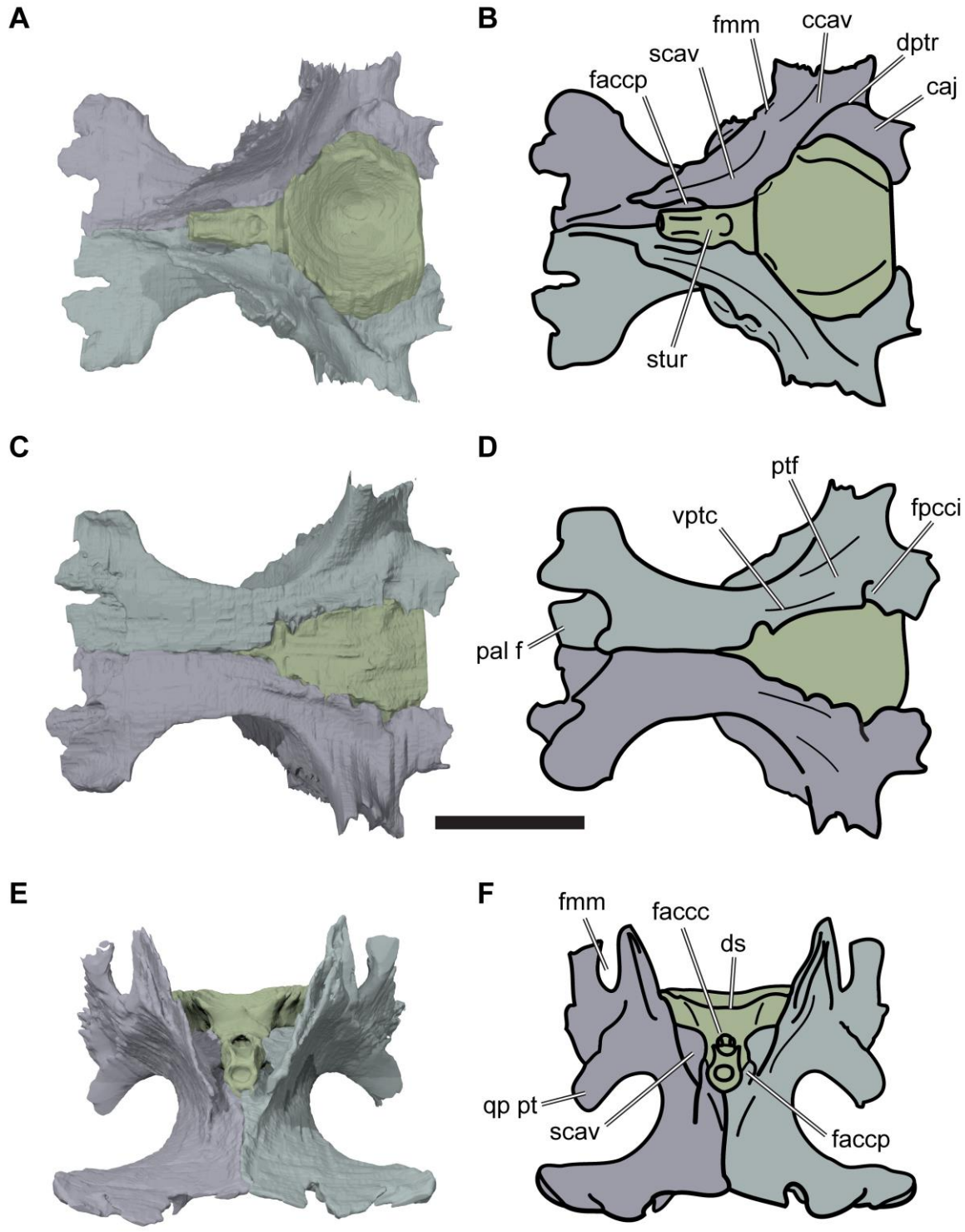


FIG. 3.22. Pterygoids and parabasisphenoid of CAMSM B55783 in articulation. **A**, 3D rendering in dorsal view; **B**, interpretative line drawing of A; **C**, 3D rendering in ventral view; **D**, interpretative line drawing of C; **E**, 3D rendering in anterior view; **F**, interpretative line drawing of E. Scale bar equals 5 mm. Abbreviations: *caj*, cavum acustico-jugulare; *ccav*, canalis cavernosus; *dptr*, dorsal pterygoid ridge; *ds*, dorsum sellae; *faccc*, foramen anterius canalis carotici cerebralis; *faccp*, foramen anterius canalis carotici palatinum; *fmm*, foramen maxillo-mandibularis; *fpcci*, foramen posterius canalis carotici interni; *pal f*, palatine facet; *ptf*, pterygoid fossa; *qp pt*, quadrate process of pterygoid; *scav*, sulcus cavernosus; *stur*, sella turcica; *vptc*, ventral pterygoid ridge.

medial surface of the articular process of the quadrate. The posterior halves of the pterygoids diverge to form a broad triangular opening for the parabasisphenoid (Fig. 3.22 C–D). The ventral surface of the pterygoid lateral to the parabasisphenoid bears the pterygoid fossa, which forms a shallow, anteromedially oriented groove. The medial side of this groove is bounded by a low, anteromedially oriented ridge, immediately adjacent to the parabasisphenoid (see Evers & Benson 2018*a*, *c*). This ridge turns posterolaterally at the level of the foramen posterius canalis carotici interni (fpcci).

The foramen posterius canalis carotici interni (*sensu* Rabi *et al.* 2013) is the entrance for the internal carotid artery and enters the skull between the parabasisphenoid and pterygoid in most specimens. In one specimen (CAMSM B55776: *R. elegans sensu* Collins 1970), the foramen is enclosed completely within the pterygoid, albeit immediately adjacent to its contact with the parabasisphenoid. In all other CT scanned specimens in which this feature can be observed (CAMSM B55783, CAMSM B55775, NHMUK PV OR35197, NHMUK PV OR43980), the parabasisphenoid forms the medial border of the foramen (Fig. 3.22C–D). The canalis caroticus internus extends anteriorly from this foramen and is contained within the internal contact surfaces of pterygoid and parabasisphenoid in all specimens, including CAMSM B55776 (Appendix S2, Fig. S2.9). The course of the internal carotid artery, as well as its bifurcation into the cerebral and palatine arteries, is entirely enclosed by bone (see Carotid circulation, below). This bifurcation occurs at the level of the dorsum sellae of the parabasisphenoid. The canalis caroticus cerebralis for the cerebral artery diverges anteromedially, and is completely contained within the parabasisphenoid (for additional details of the cerebral artery see Parabasisphenoid and Arterial Circulation, below). The canalis caroticus palatinum for the palatine artery is enclosed primarily by the pterygoid, with the parabasisphenoid enclosing only its medial surface. The canalis caroticus palatinum extends anteriorly and slightly dorsally from the bifurcation point of the internal carotid artery. It is positioned ventral to the sulcus cavernosus and is separated from it by a medial, sheet-like extension of the pterygoid. This horizontal sheet of bone contacts the lateral side of the rod-like anterior process of the parabasisphenoid, the rostrum basisphenoidale. The

anterior exit of the canalis caroticus palatinum, the foramen anterius canalis carotici palatinum (faccp), is located approximately halfway along the rostrum basisphenoidale, ventrally below the level of the anterior end of the sulcus cavernosus (Fig. 3.22A–B, E–F). One specimen, NHMUK PV OR35197 (*R. elegans sensu* Collins 1970), has an additional foramen for a short ventromedial branch of the palatine artery. This additional foramen exits on the lateral surface of the pterygoid into the subtemporal fossa.

The posterior process of the pterygoid extends beyond the posterior margin of the parabasisphenoid to contact the basioccipital. The dorsal surface of this posterior process is mediolaterally concave and wraps around the anterior part of the ventrolateral surface of the basal tuber of the basioccipital.

On the dorsal surface of the anterior end of the pterygoids the interpterygoid suture is raised to a low medial ridge. The ridge becomes broader posteriorly and serves as a buttress for the rod-like rostrum basisphenoidale of the parabasisphenoid (Fig. 3.22E–F). Lateral to this median ridge, the dorsal surface of the pterygoid is incised by a narrow, deep, anteroposteriorly oriented trough. This trough marks the course of the palatine artery anterior to the foramen anterius canalis carotici palatinum. The posterior part of the course of the palatine artery is covered dorsally by a medial extension of the crista pterygoidea, which is a vertical sheet of bone that ascends along the lateral margin of the pterygoid.

The medial surface of the crista pterygoidea bears a thin horizontal shelf of bone that projects medially and contacts the rostrum basisphenoidale of the parabasisphenoid. This shelf covers the trough for the palatine artery posterior to the foramen canalis carotici palatinum. The medial shelf of the crista pterygoidea also forms the floor of the sulcus cavernosus. The sulcus cavernosus is a dorsally open trough that carries the vena capitis lateralis (Gaffney 1972*b*). The sulcus cavernosus extends parallel to the rostrum basisphenoidale of the parabasisphenoid anteriorly and curves posterolaterally along the anteromedial margin of the parabasisphenoid more posteriorly. The sulcus cavernous is covered by the prootic dorsally in its posterior third and is termed the canalis cavernous in this region. The opening between the canalis cavernous and sulcus cavernosus is the foramen

cavernosus. In *Rhinochelys*, the foramen cavernosus is positioned at the level of the posterior margin of the maxillo-mandibular foramen. Just anterior to the foramen cavernosus, a short canal extends from the floor of the sulcus cavernosus ventromedially between the pterygoid and parabasisphenoid and connects to the canalis caroticus internus. This canal is the passage for the vidian (or palatine) ramus of the facial (CN VII) nerve (foramen pro ramo nervi vidani of Gaffney 1972*b*) and leads from the sulcus cavernous into the canalis caroticus internus, where it continues anteriorly (Gaffney 1979). This small canal is best preserved in NHMUK PV OR35197. In the posterior part of the pterygoid, the course of the canalis cavernosus is marked by a low ridge on the dorsal surface of the pterygoid (Fig. 3.22A–B). This ridge contacts the lateral margin of the ventromedially directed process of the prootic. The canalis cavernosus opens posteriorly into the cavum acustico-jugulare, but the ridge on the dorsal surface of the pterygoid delimits the course of the vena capitis lateralis posteriorly up to the fenestra postotica.

The crista pterygoidea forms an anteroposteriorly long contact with the processus inferior parietalis of the parietal (see also Parietal, above). Together, these structures form the secondary lateral wall of the braincase (Fig. 3.16). Right and left cristae pterygoideae diverge posterolaterally from the midline. The crista pterygoidea becomes dorsally higher posteriorly. Just anterior to the contact with the quadrate, the crista pterygoidea bifurcates dorsally into two prongs, which form the anterior and posterior margins of the maxillo-mandibular (CN V_{2-3}) foramen. The maxillo-mandibular foramen is a dorsoventrally high, oval opening, with a concave ventral margin that is also formed by the crista pterygoidea. The dorsal margin of the maxillo-mandibular foramen is shared between the prootic posteriorly and the parietal anteriorly.

The lateral surface of the crista pterygoidea of the pterygoid is marked by a small groove, which is posterolateroventrally directed from the ventral margin of the maxillo-mandibular foramen and continues onto the anterior surface of the quadrate process of the pterygoid. This incision receives the epipterygoid process of the quadrate, which is ossified variably. The anterior end of the groove, directly posteroventral to the maxillo-mandibular

foramen, is not usually occupied by the processus epipterygoidei and is termed the fossa cartilaginis epipterygoidei. It possibly indicates the presence of an unossified epipterygoid in *Rhinochelys* (see also Epipterygoid, above).

3.4.1.16 Supraoccipital

The supraoccipital is an unpaired median bone in the posterodorsal corner of the skull (Figs 3.1–5, 3.11). It forms the roof of the posterior part of the endocranial cavity and contacts the parietal anterodorsolaterally, the prootic anteroventrolaterally, the opisthotic lateroventrally and the exoccipital posteroventrolaterally. The supraoccipital forms the dorsal margin of the foramen magnum and houses parts of the endosseous labyrinth.

In transverse cross-section, the posterior part of the supraoccipital has an inverted 'Y'-shaped outline, as it consists of a dorsally placed, vertically oriented plate from which ventrolateral processes diverge to either side. The vertical plate is wedged between the posterior processes of the parietals, but extends posteriorly beyond them and dorsal to the foramen magnum as a short crista supraoccipitalis. The exact posterior extent of the crista supraoccipitalis is unknown, as it is damaged in all *Rhinochelys* skulls. The ventrolateral processes of the supraoccipital are dorsoventrally short at the level of the foramen magnum, but become progressively taller dorsoventrally anteriorly. The vertical sheet of the supraoccipital disappears anteriorly as the ventrolateral processes become dorsoventrally taller. As a consequence, the anterior part of the supraoccipital has a simple arch-shaped transverse cross-section and the endocranial cavity is dorsally expanded anteriorly along the length of the supraoccipital. Anteriorly, the parietal overlaps the dorsolaterally facing surface of the ventrolateral process of the supraoccipital, forming a weakly interdigitating contact.

The prootic and opisthotic facets of the supraoccipital are mediolaterally expanded with respect to the dorsal part of the ventrolateral processes. These facets face almost ventrally, but are inclined slightly anteroventrally (prootic facet) and posteroventrally (opisthotic facet) so that the ventral portion of the supraoccipital appears gently kinked in

lateral view. The contacts between the three bones forming the otic capsule (prootic, opisthotic and supraoccipital) are not tightly closed in any of the specimens that were CT scanned. Instead, the sutures are widely open, suggesting that these specimens might represent ontogenetically immature individuals. However, this region of the skull is the least ossified among turtles more widely (SWE, personal observation), so the implications of this observation for ontogeny are unclear.

The prootic and opisthotic facets of the supraoccipital are penetrated by foramina for the anterior semicircular canal (prootic facet) and the posterior semicircular canal (opisthotic facet). These canals meet within the supraoccipital at the level of the prootic-opisthotic contact, forming the common crus (see Inner ear and associated structures, below). The common crus extends ventrally through the supraoccipital into the space lateral to the hiatus acusticus. In some specimens (CAMSM B55783, NHMUK PV OR35197), the ossification of the ventral surface of the ventrolateral process of the supraoccipital is incomplete, so that the portions of the anterior and posterior semicircular canal that lie within the supraoccipital join via a single, ventrally open and medially convex trough. In one specimen (CAMSM B55775) the foramen aquaducti vestibuli is fully ossified, while it is not ossified or only partially ossified in others (e.g. NHMUK PV OR35197). This foramen is located in the medioventral wall of the supraoccipital, ventral to the common crus, and transmits the endolymphatic duct (Gaffney 1979).

3.4.1.17 Exoccipital

The exoccipitals are paired bones situated in the posterior portion of the braincase (Figs 3.1–5, 3.11). They form the lateral margins of the foramen magnum and contact the supraoccipital dorsally and the basioccipital ventrally. Anterolaterally, each exoccipital is sutured to the opisthotic. A marginal point contact to the pterygoid also seems to be present. The exoccipitals contribute to the formation of the occipital condyle (=condylus occipitalis of Gaffney 1972*b*) just lateral to the basioccipital. The exoccipital also forms the medial margin

of the fenestra postotica, borders the recessus scalae tympani posteriorly, closes the anterior jugular foramen (=foramen jugulare anterius of Gaffney 1972*b*) posteriorly, and houses the foramina and associated canals for the rami of the hypoglossal (CV XII) nerve.

The exoccipital consists of an anterolaterally broad base from which a centrally placed, rod-like dorsal process emerges that forms the lateral wall of the foramen magnum. The base of the exoccipital contacts the basioccipital over its entire anteroposterior length via a ventromedially directed articular surface. Posteriorly, the base of the exoccipital merges into a short, rounded process that forms the dorsolateral portion of the occipital condyle. The processes of the right and left exoccipital approach each other dorsomedially, but they are separated on the midline by the posterior portion of the basioccipital. Anteriorly, the base of the exoccipital broadens dorsoventrally and extends anteroventrolaterally into the floor of the cavum acustico-jugulare and onto the dorsal surface of the basal tuber of the basioccipital. The posterior process of the pterygoid articulates with the basal tuber of the basioccipital. However, this contact is slightly disarticulated in those specimens for which we have CT scans. This makes it difficult to assess if a pterygoid-exoccipital contact was present in *Rhinochelys*, which is the case in *Plesiochelys etalloni* (Anquetin *et al.* 2014*a*) and cheloniids (Gaffney 1979). It also unclear if the exoccipitals and pterygoids are in contact in *Bouliachelys*, but a contact is evident in *Notochelone* (NHMUK PV OR37213). In *Dermochelys coriacea* (UMZC R3031) a pterygoid-exoccipital contact is absent.

The dorsal process of the exoccipital curves dorsomedially around the lateral margin of the foramen magnum, which has a dorsoventrally high, oval outline. The posterior surface of the dorsal process bears a low ridge that extends ventrolaterally from the supraoccipital contact. This ridge merges with the surface of the exoccipital just dorsal to the occipital condyle. The prominence of this ridge varies among specimens: it is strongly developed in CAMSM B55775 (*R. pulchriceps* holotype), but absent in CAMSM B55783 (*R. cantabrigiensis sensu* Collins 1970) (Fig. 3.23). It is likely that this ridge is an attachment site for axial musculature, and differences in its development might represent intraspecific variation (see Discussion, below).

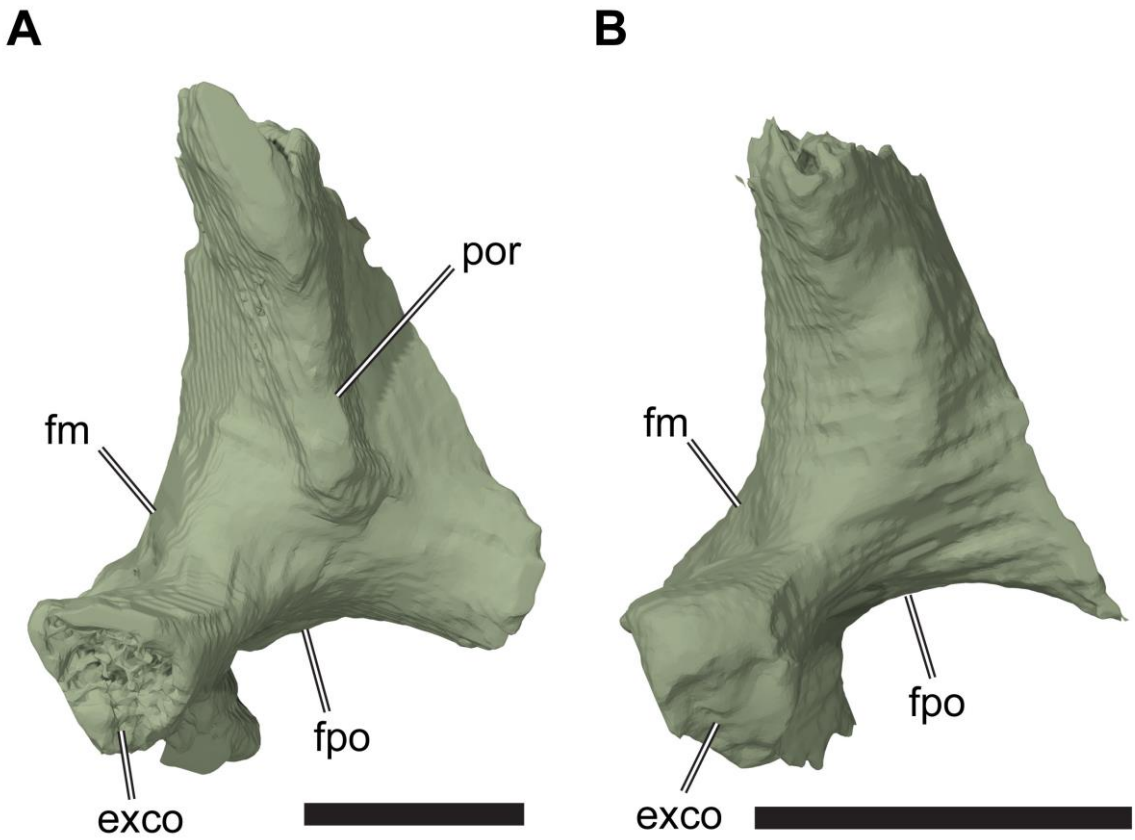


FIG. 3.23. Comparison of right exoccipitals. **A**, 3D rendering of CAMSM B55775; **B**, 3D rendering of CAMSM B55783. Scale bars equal 3 mm. Abbreviations: *exco*, exoccipital part of the condylus occipitalis; *fm*, foramen magnum; *fpo*, fenestra postotica; *por*, posterior ridge of exoccipital.

The lateral portion of the exoccipital has complicated geometry with several surfaces of different orientation. The exoccipital underlaps the opisthotic forming a transversely broad, concave contact surface that buttresses the posteroventromedial surface of the opisthotic. A concave ridge on the ventrolateral surface of the process contacting the opisthotic forms the dorsomedial margin of the fenestra postotica. This ridge separates the ventrolateral surface of the exoccipital into a posterior portion and an anterior portion. The fenestra postotica is transversely wide in *Rhinochelys* and incorporates the passage of the vena cerebralis posterior, contrasting with the condition present in many cryptodires, including some sea turtles such as *Allopleuron hofmanni* (NHMUK PV R4213), in which this vein is housed in a separate posterior jugular foramen (=foramen jugulare posterius of Gaffney 1972*b*) (Gaffney 1979). The absence of an ossified boundary between the fenestra

postotica and posterior jugular foramen is, however, common in turtles and occurs in most chelonioids (e.g. Gaffney 1979; Evers & Benson 2018*a*–*c*).

The portion of the ventrolateral surface of the exoccipital posterior to the margin of the fenestra postotica extends from the medial margin of the fenestra postotica to the exoccipital part of the occipital condyle posteriorly, and the posterior surface of the process that contacts the basal tuber of the basioccipital. This surface is roughly triangular, faces posteroventrolaterally, and is excavated to form a shallow fossa. The fossa is penetrated by two circular foramina for the hypoglossal (XII) nerve (the foramina nervi hypoglossi). The posterior foramen is oval in outline and approximately three times the diameter of the anterior foramen, which has a circular outline. In turtles, the hypoglossal nerve frequently exits the skull through three openings (Gaffney 1979), so that it seems likely that the posterior foramen nervi hypoglossi transmits two rami of the hypoglossal nerve. The nerve canals are anterodorsomedially directed and connected to the endocranial cavity by two internal foramina near the base of the exoccipital.

The portion of the ventrolateral surface anterior to the margin of the fenestra postotica lies within the cavum acustico-jugulare. The recessus scalae tympani is a medial extension of the cavum acustico-jugulare (see Cavum acustico-jugulare, below). The anterior surface of the dorsal process of the exoccipital forms the posterior wall of the recessus scalae tympani, which is anteriorly bordered by the opisthotic. The recessus scalae tympani connects the cavum acustico-jugulare with the endocranial cavity via the anterior jugular foramen (Fig. 3.24). This foramen is formed by the exoccipital posteriorly and forms the passage for the vagus (CN X) and accessory (CN XI) nerves and the vena cerebralis posterior (Gaffney 1972*b*). The anterior surface of the exoccipital does not quite contact the processus interfenestralis of the opisthotic, which forms the anterior margin of the anterior jugular foramen and the anterior wall of the recessus scalae tympani (see Opisthotic, below). The resulting gap between these bones was presumably covered by cartilage. The fenestra perilymphatica, an opening between the cavum labyrinthicum and the recessus scalae

tympani, is bordered ventrally by the exoccipital but lies mostly within the processus interfenstralis of the opisthotic (see Opisthotic, below).

3.4.1.18 Basioccipital

The basioccipital is an unpaired, median bone in the posteroventral region of the braincase (Figs 3.1–5, 3.9, 3.24). It contacts the parabasisphenoid anteriorly, the pterygoid anterolaterally and the exoccipital dorsolaterally. The basioccipital forms the posterior floor of the endocranial cavity, the ventral margin of the foramen magnum, the posteroventral portion of the occipital condyle and the basal tubera.

The basioccipital is horizontally aligned with the parabasisphenoid and broadens anteriorly so that is has a triangular outline in ventral view (Fig. 3.9). The anterior surface of the basioccipital is flat and faces the parabasisphenoid. In all CT scanned specimens of *Rhinochelys* with preserved basioccipitals, there is a small vertical space between these bones. The posterior part of the basioccipital is mediolaterally broad ventrally and mediolaterally constricted dorsally between the posterior portions of the exoccipitals. The basioccipital and exoccipitals jointly form the occipital condyle.

The dorsal surface of the basioccipital forms the floor of the endocranial cavity and slopes gently anteroventrally from the foramen magnum towards the parabasisphenoid. This surface has a narrow triangular outline that tapers posteriorly towards the basioccipital portion of the occipital condyle. The lateral margins of this surface are elevated to form shallow, sharp-edged ridges, so that the dorsal surface is gently transversely concave. In NHMUK PV OR35197, a low parasagittal, median crest is present on the dorsal surface of the basioccipital. This is the crista dorsalis basioccipitalis, which separates the dorsal surface of the basioccipital into two transversely concave regions either side of the midline. The crista dorsalis basioccipitalis is not present in CAMSM B55783 or CAMSM B55775. Another median structure on the dorsal surface of the basioccipital is the basis tuberculi basalis. This is a low, mound-like tubercle at the anterior end of the crista dorsalis basioccipitalis (Fig. 3.24). In all

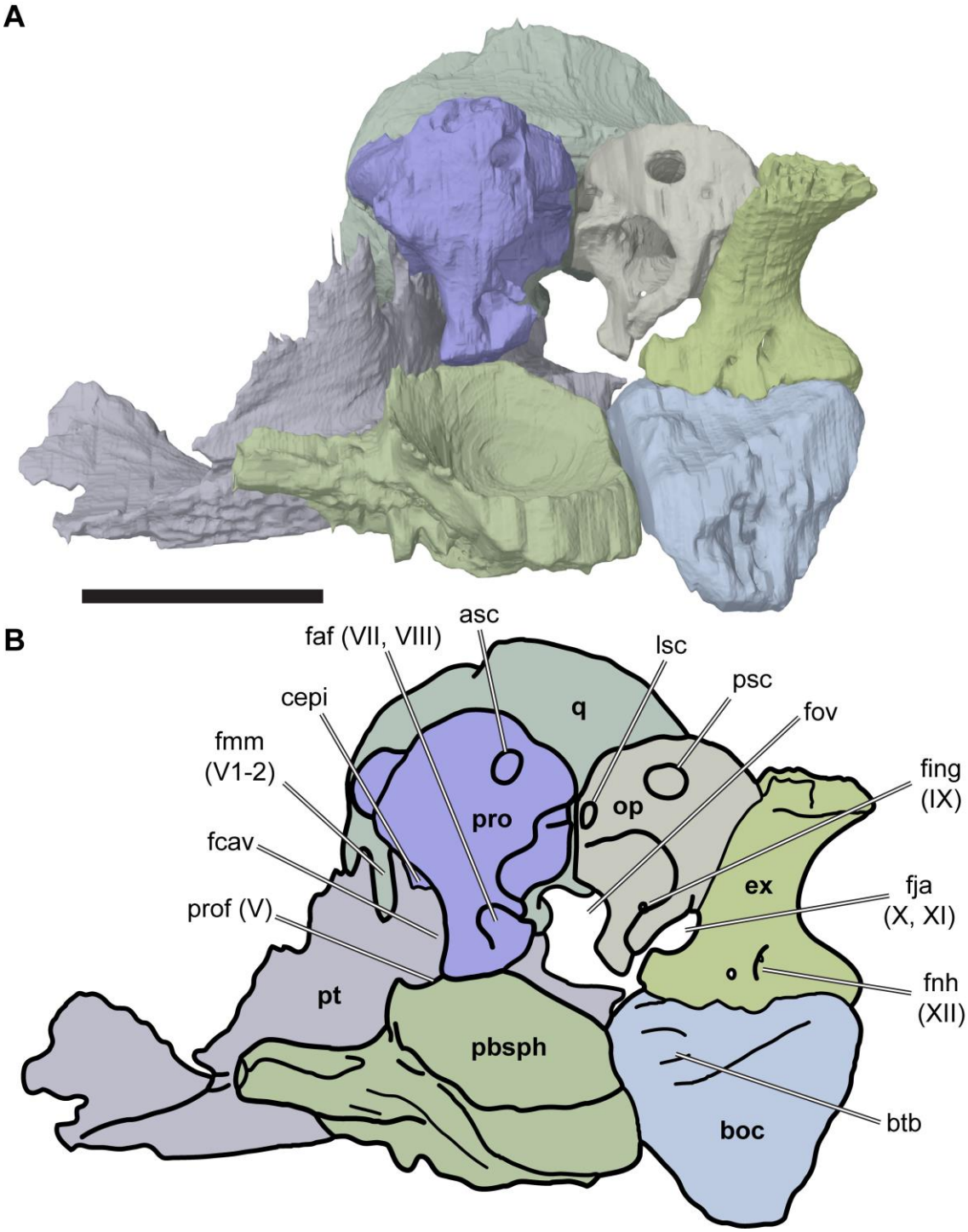


FIG. 3.24. Medial view of the right otic capsule and partial basicranium of CAMSM B55783. **A**, 3D rendering; **B**, interpretative line drawing. Scale bar equals 5 mm. Note that bones are labelled in bold. Abbreviations: *asc*, anterior semicircular canal; *boc*, basicoccipital; *btb*, basis tuberculi basalis; *cepi*; cavum epitericum; *ex*, exoccipital; *faf (VII; VIII)*, fossa acustico-facialis; *fcav*, foramen cavernosum; *fing (IX)*, foramen internum nervi glossopharyngei; *fja (X, XI)*, foramen jugulare anterius; *fmm (V_{1-2})*, foramen maxillomandibularis; *fnh (XII)*, foramina nervi hypoglossi *fov*, fenestra ovalis; *lsc*, lateral semicircular canal; *op*, opisthotic; *pbsph*, parabasisphenoid; *pro*, prootic; *prof (V)*, prootic foramen; *psc*, posterior semicircular canal; *pt*, pterygoid; *q*, quadrate.

specimens preserving a basioccipital, the basis tuberculi basalis is positioned at the anterodorsal margin of the basioccipital and projects slightly anteriorly into the otherwise vertically flat anterior surface of the basioccipital. The posterodorsal edge of the parabasisphenoid has a small notch for this tubercle, which is most clearly developed in NHMUK PV OR35197, but is present in all specimens examined.

The posterolateral surfaces of the basioccipital are sutured to the exoccipitals, which become slightly broader anteriorly than posteriorly. The basal tubera emerge ventrolaterally from the basioccipital and are positioned slightly anterior its midlength. The basal tubera are anteroposteriorly longer than they are dorsoventrally deep and have rounded posteroventral surfaces. The anterior surfaces of the basal tubera contact the posterior processes of the pterygoids. The anteroventrolateral bases of the tubera are also covered ventrally by short extensions from the posterior processes of the pterygoids. The ventral surface of the basioccipital between the basal tubera is gently concave transversely and smooth.

3.4.1.19 Prootic

The prootic forms the anterior part of the otic capsule (Figs 3.24–25; Appendix S2, Fig. S2.10). It contacts the parietal anteromediodorsally, the pterygoid anteroventrally, the quadrate laterally, the opisthotic posteriorly, the supraoccipital posterodorsomedially and the parabasisphenoid ventromedially. The prootic forms the anterior part of the cavum labyrinthicum and fenestra ovale and contributes to the cavum acustico-jugulare, the canalis stapedio-temporale, the canalis cavernosus and foramen cavernosum, the maxillo-mandibular (CN V_{2-3}) foramen and the processus trochlearis oticum. It further forms the foramina nervi facialis (CN VII) and the foramina nervi acustici (CN VIII).

The prootic has its most extensive contact with the quadrate, which it abuts along its entire lateral surface. The prootic and quadrate are sutured to each other and the externally visible suture line in the floor of the supratemporal fossa is laterally concave. The dorsomedial margin of the prootic, which contacts the parietal anteriorly and the opisthotic

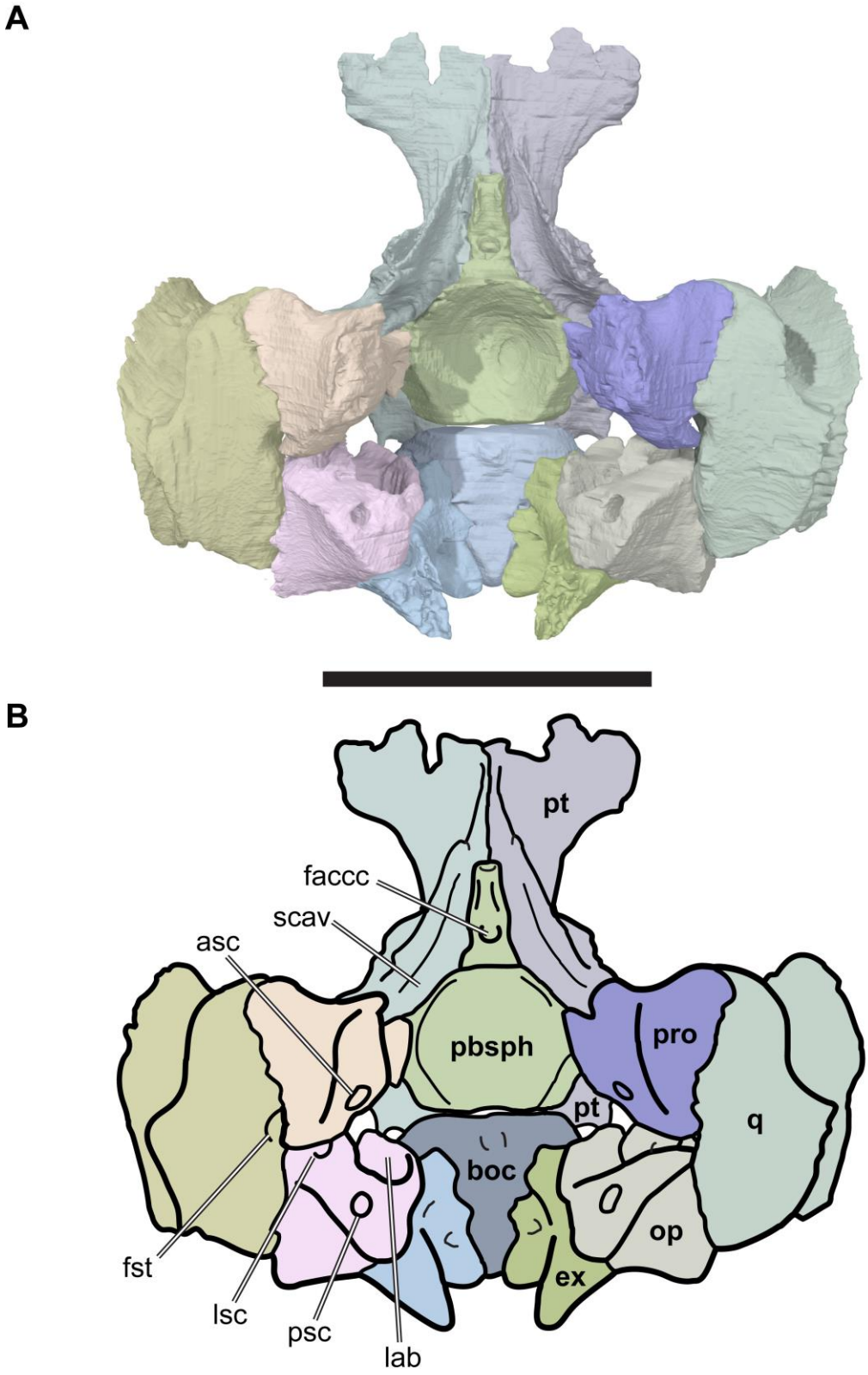


FIG. 3.25. Dorsal view of basicranium of CAMSM B55783. **A**, 3D rendering; **B**, interpretative line drawing. Scale bar equals 10 mm. Note that bones are labelled in bold. Abbreviations: *asc*, anterior semicircular canal; *boc*, basioccipital; *ex*, exoccipital; *faccc*, foramen anterius canalis carotici cerebralis; *fst*, foramen stepadio-temporale; *lab*, cavum labyrinthicum; *lsc*, lateral semicircular canal; *op*, opisthotic; *pbsph*, parabasisphenoid; *pro*, prootic; *psc*, posterior semicircular canal; *pt*, pterygoid; *q*, quadrate; *scav*, sulcus cavernosus.

posteriorly, is roughly convex in dorsal view. As a result, the prootic has a roughly semilunate shape in dorsal view.

Together, the prootic and quadrate form the vertically directed canalis stapedio-temporale, which exits dorsally into the supratemporal fossa via the foramen stapedio-temporale and exits ventrally into the cavum acustico-jugulare via the aditus canalis stapedio-temporalis. The foramen stapedio-temporale is large in *Rhinochelys* and exceeds the diameter of the foramina associated with the carotid circulation. Anteromedially, the quadrate and prootic form the processus trochlearis oticum (see Quadrate, above, with respect to the variation seen in this feature). The prootic part of the processus trochlearis oticum protrudes anterolaterally and is separated from the anteromedial corner of the prootic by a concave notch. The anteromedial corner of the prootic forms a short, anteriorly projecting, pointed process. This process forms the posterodorsal border of the maxillo-mandibular (CN V_{2-3}) foramen. The anterior surface of the prootic is covered largely by the epipterygoid process of the quadrate and, more medially, the posterior ramus of the crista pterygoidea of the pterygoid. The latter excludes the prootic from the posterior margin of the maxillo-mandibular foramen. The anteromediodorsal margin of the prootic contacts the ventral surface of the processus inferior parietalis and has a weakly developed, parasagitally oriented incision for its articulation.

The prootic has a prominent ventromedial process (Fig. 3.24). The process is broad and has a subtriangular cross-section. It terminates dorsally above the floor of the pterygoid, and nearly contacts the laterodorsal surface of the parabasisphenoid. In all CT scans, the ventral surface of the ventromedial process of the prootic approaches the parabasisphenoid very closely, but they are never sutured to one another. The small gap between the prootic and parabasisphenoid was likely closed by cartilage during life. The ventromedial process of the prootic forms a bony bridge over the trough in the pterygoid for the course of the lateral head vein, thereby forming the roof of the canalis cavernosus. The resulting foramen between the ventromedial process of the prootic medially, and the pterygoid laterally, is the foramen

cavernosum. The foramen cavernosum is located directly posterior to the level of the maxillo-mandibular (CN V_{2-3}) foramen (Fig. 3.24).

The medial surface of the ventromedial process of the prootic is penetrated by a deep fossa acustico-facialis (Fig. 3.24). Several canals extend laterally from the fossa acustico-facialis. The facial nerve (CV VII) has a short, anterolaterally directed canal that connects the endocranial cavity with the canalis cavernosus. The medial foramen nervi facialis is a small oval opening located in the anterior corner of the fossa acustico-facialis (Appendix S2, Fig. S2.1H, K). The lateral foramen that exits into the canalis cavernosus is of similar size and shape. This is indicative of a facial nerve innervation like that of crytodires, in which the facial nerve forms the geniculate ganglion in the canalis cavernosus, which gives off an anteriorly directed Vidian (or palatine) branch, and a posteriorly directed hyomandibular branch (Soliman 1964; Gaffney 1979). The fossa acustico-facialis is penetrated by two further foramina for the acoustic nerve (CN VIII). These foramina are located in the posterodorsal corner of the fossa acustico-facialis and connect the endocranial cavity with the prootic recess for the cavum labyrinthicum. Two distinct foramina nervi acustici can be distinguished in CAMSM B55775 (Appendix S2, Fig. S2.1C, F) and CAMSM B55776. In those specimens, the more anteriorly positioned foramen is about three times larger than the other foramen. In the other specimens that were CT scanned, the thin bony bar separating these foramina is not preserved, so that both foramina nervi acustici share a single, large opening toward the cavum labyrinthicum.

The posteromedial margin of the prootic has a deep, posteriorly concave notch positioned just dorsal to the ventromedial process. This notch forms the anterior margin of the hiatus acusticus, which is a large opening between the endocranial cavity medially and the cavum labyrinthicum laterally, and between the prootic anteriorly and the opisthotic posteriorly.

The prootic is invaded by a large cavity that makes up the prootic part of the cavum labyrinthicum (recessus labyrinthicus prooticus of Gaffney 1979). The cavum labyrinthicum is anteroventrally bordered by the ventromedial process of the prootic and extends

anteriorly deep into the body of the prootic. Laterally, the cavum labyrinthicum is closed by an extensive wall of bone, which laterally abuts the quadrate. The anterior semicircular canal projects through the dorsal part of the body of the prootic and connects to the large chamber of the cavum labyrinthicum in its anterodorsal corner. The canal then curves posterodorsomedially and opens in the posterodorsomedial surface of the prootic. This surface faces the supraoccipital. In all *Rhinochelys* specimens there is a gap between this surface and the supraoccipital, suggesting that the contact of these bones was covered by cartilage. An imprint of the lateral semicircular canal can be seen on the medial surface of the lateral wall of the cavum labyrinthicum. The lateral canal is bordered medially by bone only on the opisthotic side, whereas the prootic part is medially confluent with the large cavity for the cavum labyrinthicum (Fig. 3.24). The prootic and opisthotic contact each other on via the posterolateral surface of the prootic, and both surround the lateral semicircular canal dorsally, ventrally and laterally. The contact surfaces between the prootic and opisthotic are planar, with only a minor gap between them in comparison with to the widely open contact to the supraoccipital.

The ventral side of the lateral wall of the cavum labyrinthicum connects with the posteromedioventral side of the medioventral process of the prootic, forming a concave margin between both structures. This concave margin forms the anterodorsal border of the fenestra ovale, which is the lateral opening of the cavum labyrinthicum toward the cavum acustico-jugulare. The fenestra ovale serves as the attachment for the stapedial footplate of the stapes. The fenestra ovale is completed posteriorly by the opisthotic, but ventrally it has no bony border and opens above the level of the floor of the cavum acustico-jugulare, which is formed by the pterygoid.

3.4.1.20 Opisthotic

The opisthotic forms the posterior half of the otic capsule (Figs 3.1–5, 3.11, 3.24–25; Appendix S2, Fig. S2.11). It contacts the prootic anteriorly, the supraoccipital dorsomedially,

the exoccipital posterodorsomedially, the quadrate laterally and the squamosal posterodorsolaterally. The opisthotic forms the posterior floor of the supratemporal fossa, the posterior part of the roof of the cavum acustico-jugulare, the posterior margin of the fenestra ovale, the posterior part of the cavum labyrinthicum, the anterior wall of the recessus scalae tympani, contributes to the anterior jugular foramen (=foramen jugulare anterius of Gaffney 1972*b*) and forms the fenestra perilymphatica, as well as the canal for the glossopharyngeal nerve (CN IX). Two important processes emerge from the body of the opisthotic, namely the processus interfenestralis anteroventrally, and the paroccipital process (=processus paroccipitalis of Gaffney 1972*b*) lateroventrally.

The lateral surface of the opisthotic is buttressed against the quadrate and is also confluent with the dorsolateral surface of the paroccipital process. The latter forms a relatively thin posteroventrolaterally directed extension of the opisthotic. The paroccipital process wraps around the posteroventromedial surface of the quadrate ventrally and terminates just before reaching the incisura columella auris of the quadrate. The large contact surface between the opisthotic and quadrate is smooth: these bones are not sutured but merely abut each other.

The dorsal surface of the body of the opisthotic forms the floor of the supratemporal fossa. This surface is roughly triangular and narrows anteriorly toward the prootic contact. The squamosal has a very small contact with the posterodorsolateral corner of the opisthotic, which is preserved only in CAMSM B55783. The facet for this contact is preserved in other specimens also, such as CAMSM B55775 (Appendix S2, Fig. S2.11C, F). On the posteromedial side, the opisthotic has an extensive contact surface for the exoccipital and these bones are sutured to each other.

The anterior margin of the opisthotic toward the prootic and the dorsomedial margin that faces the supraoccipital are angled at approximately 120° to each other, resulting in a roughly ‘Y’-shaped suture between the prootic, opisthotic and supraoccipital. As mentioned previously (see Supraoccipital and Prootic, above), all of the bones in the otic capsule are widely spaced, with cartilage presumably filling in the voids between them.

The anterior surface of the opisthotic that contacts the prootic is penetrated by the canal for the lateral semicircular canal. By contrast with the prootic, the opithostic completely encloses the lateral semicircular canal on all sides, so that it is a true canal rather than a medially open trough. The lateral semicircular canal extends posteromedially into the body of the opisthotic and opens internally into a large cavity that forms the opisthotic portion of the cavum labyrinthicum (recessus labyrinthicus opisthoticus of Gaffney 1979). The cavum labyrinthicum extends deep into the body of the opisthotic posterolaterally and is connected to another canal in its dorsolateral corner. The latter is the posterior semicircular canal, which extends dorsomedially in a slightly arched trajectory above the opisthotic portion of the cavum labyrinticum and exits the opisthotic via its articular surface for the supraoccipital. The posterior semicircular canal continues into the supraoccipital, where its meets the anterior semicircular canal in the common crus (see Supraoccipital, above and Inner ear and associated structures, below).

The main body of the opisthotic bears a ventrally and slightly anteromedially directed process termed the processus interfenestralis (Fig. 3.24; Appendix S2, Fig. S2.11). The processus interfenestralis projects into the otherwise continuous, unossified space between the ventral part of the cavum labyrinthicum and the cavum acustico-jugulare, and thus forms a landmark separating these two cavities. The processus does not contact the ventral floor of the skull, so a gap remains between the ventral margin of the processus interfenestralis and the area around the pterygoid-basioccipital contact. The processus interfenestralis also separates the fenestra ovale and fenestra perilymphatica. The former is situated anterolaterally with respect to the latter and the margins of the processus interfenestralis are oriented accordingly; the margin toward the fenestra ovale faces anterolaterally, and is markedly concave, and the margin toward the fenestra perilymphatica faces posterolaterally and slightly ventrally. The fenestra perilymphatica is not covered by bone posteroventromedially, so that the fenestra forms a deep, but open, semicircular notch in the posteromedial margin of the processus interfenestralis. The fenestra perilymphatica opens posteroventrally from the cavum labyrinthicum into the recessus scalae tympani. The

recessus scalae tympani is a transversely oriented cavity between the opisthotic and exoccipital and is the medial portion of the cavum acustico-jugulare (see Cavum acustico-jugulare, below). It is laterally open toward, and thus continuous with, the more anteroposteriorly oriented cranioquadrate space portion of the cavum acustico-jugulare (see Gaffney 1979).

A short, posteroventrally directed canal for the glossopharyngeal nerve (CN IX) pierces the floor of the cavum labyrinthicum, near the base of the processus interfenestralis, and exits into the recessus scalae tympani. The respective foramen on the internal surface of the opisthotic facing the cavum labyrinthicum is called the foramen internum nervi glossopharyngei (Fig. 3.24), whereas the foramen in the surface facing the recessus scalae tympani is the foramen externum nervi glossopharyngei. An additional foramen (foramen medialis nervi glossopharyngei of Gaffney 1979) for the exit of the glossopharyngeal nerve from the endocranial cavity remains usually unossified in the hiatus acusticus, although it is evident in CT scans of CAMSM B55775 (Appendix S2, Fig. S2.11A, D, H, K>). In this specimen, the foramen medialis nervi glossopharyngei is located at the posteromedial margin of the processus interfenestralis and opens anterolaterally into the cavum labyrinthicum.

The posteroventral side of the opisthotic is a relatively thin wall of bone between the cavum labyrinthicum and recessus scalae tympani. The posterior wall of the recessus scalae tympani is formed by the exoccipital, ventral to its sutural contact with the opisthotic. The medial margin of the opisthotic and the anteromediodorsal margin of the exoccipital form an elongate anterior jugular foramen, which forms the medial opening of the recessus scalae tympani toward the endocranial cavity. The medial connection between the recessus scalae tympani and the cranioquadrate space portion of the cavum acustico-jugulare is positioned in the posterior-most third of the latter, posterior to the position of the processus interfenestralis and just anterior to the fenestra postotica.

3.4.1.21 Parabasisphenoid

The parabasisphenoid is an unpaired median bone in the centre of the basicranium (Figs 3.1–5, 3.9, 3.22, 3.25; Appendix S2, Fig. S2.12–13). It forms the anterior floor of the endocranial cavity and contacts the pterygoid laterally, the prootic posterolaterally and the basioccipital posteriorly. Several important nervous and vascular structures traverse the parabasisphenoid, including the canals for the abducens (CN VI) nerve, the canalis caroticus cerebralis, as well as parts of the canalis caroticus internus and canalis caroticus palatinum. Other important structures formed by the parabasisphenoid include the clinoid process (=processus clinoideus of Gaffney 1972*b*), the dorsum sellae and the rostrum basisphenoidale.

The parabasisphenoid consists of a cup-shaped portion posteriorly and extends anteriorly into a thin, rod-like process, the rostrum basisphenoidale (Figs 3.22, 3.25). The posterior cup-shaped portion of the parabasisphenoid is anteroposteriorly approximately as long as it is transversely wide. Its dorsal surface is transversely and anteroposteriorly concave, producing a deeply excavated area that forms the floor of the central part of the endocranial cavity.

The dorsal surface of the parabasisphenoid cup is pierced by paired foramina for the abducens nerve (CN VI). The foramina are located at a level just anterior to the prootic contact of the parabasisphenoid. Each respective canalis nervi aducentis projects anteriorly and slightly medially through the dorsolateral wall of the parabasisphenoid, exiting into the sulcus cavernosus. Unfortunately, the thin canals and small foramina cannot be unambiguously identified in all specimens, but the position of the anteriorly exiting foramen seems to vary slightly. In CAMSM B55783 (*R. cantabrigiensis sensu* Collins 1970), the anterior foramen nervi abducentis is located directly ventral to the clinoid process, but it is more posterolaterally placed in NHMUK PV OR35197 (*R. elegans sensu* Collins (1970); Appendix S2, Fig. S2.12–13).

The dorsal margin circumscribing the parabasisphenoid cup forms various structures. Posteriorly, the margin is very low and often bears a small posterior notch for the basis tuberculi basalis of the basioccipital, which is especially well developed in CAMSM B55776

and NHMUK PV OR35197. Posterolaterally and laterally, the margin becomes taller, forming a broad surface that faces posterodorsolaterally, which changes orientation slightly in its anterior part to face dorsolaterally. The posterodorsolaterally oriented portion of this margin faces the cavum acustico-jugulare and forms the ventral border of the hiatus acusticus ventral to the inner ear. The dorsolaterally oriented portion of the dorsal parabasisphenoid margin faces the ventromedial process of the prootic. A gap remains between both structures, but the space between them was likely bridged by cartilage. The parabasisphenoid margin anterior to the contact with the prootic is thin and sharp-edged. The margin also becomes taller in this portion of the parabasisphenoid. The anterolateral part of the margin forms the medial wall of the sulcus cavernosus. The clinoid processes arise on either side from the anterolateral margin at the level of the anterior margin of the maxillo-mandibular foramen, and project dorsally beyond the rest of the parabasisphenoid. The clinoid process is thin, and variably preserved in the specimens that were CT scanned, but seems to be complete in NHMUK PV OR35197. Medially, the clinoid processes are connected through the anterior margin of the parabasisphenoid cup, the dorsum sellae.

The raised dorsum sellae of turtles usually forms the posterior wall of the sella turcica, a distinct, relatively broad and often 'U'-shaped depression or pit for the pituitary on the dorsal surface of the rostrum basisphenoidale (Gaffney 1972*b*). In turtles, the cerebral artery usually exits through paired foramina anterius canalis carotici cerebralis (unless stated otherwise, all carotid foramina and canals follow the nomenclature of Rabi *et al.* 2013), which are located in the posterolateral corners of the sella turcica, over which the dorsum sellae may anteriorly project to hide the foramina in dorsal view (Gaffney 1979). *Rhinochelys* varies somewhat from this generalised condition. Instead of paired foramina for the cerebral artery, there is a single orifice at the contact of dorsum sellae and rostrum basisphenoidale (Fig. 3.25C; Appendix S2, Fig. S2.13). This foramen anterius canalis carotici cerebralis (faccc) is usually large and circular (although it is square in CAMSM B55775) and ramifies posteroventrally into a canal that bifurcates into right and left branches deep within the parabasisphenoid. We refer to these internal foramina as internal faccc (ifaccc). The canals

for the right and left cerebral canals diverge posteroventrolaterally and merge with the canalis caroticus palatinum to continue posteriorly as the canalis caroticus internus (see Pterygoid, above, for descriptions of the latter two canals). If the parabasisphenoid is seen in isolation (Appendix S2, Fig. S2.12C–F), the point of bifurcation between the cerebral and palatine arteries can be located from the position of a medially directed foramen in the lateral surface of the parabasisphenoid (for the cerebral artery). According to the nomenclature of Rabi *et al.* (2013), this is not a true foramen posterius canalis carotici cerebralis (fpccc), as this foramen is said to only be developed in turtles in which the split between both arteries remains uncovered by bone. Here, we refer to the foramen as the internal fpccc (ifpccc) to avoid confusion with respect to Rabi *et al.*'s (2013) nomenclature.

The sella turcica of *Rhinochelys* is an elongate trough with dorsally raised lateral margins that excavates the dorsal surface of the rostrum basisphenoidale anterior to the foramen anterius canalis carotici cerebralis. The morphology of the sella turcica and the presence of a single canal for the anterior-most course of the cerebral arteries is also present in *Notochelone* (NHMUK PV R9590) and *Bouliachelys* (QM F31669) (visible in CT scans). However, the parabasisphenoids of *Notochelone* and *Bouliachelys* vary slightly from that of *Rhinochelys* in having a median vertical ridge on the anterior surface of the dorsum sellae, situated dorsal to the foramen anterius canalis carotici cerebralis. The condition in *Rhinochelys*, *Notochelone* and *Bouliachelys* is similar to that present in modern cheloniids: *Chelonia mydas* (NHMUK 1969.776) has a narrow, trough-like sella turcica, in which the paired foramina anterius canalis carotici cerebralis lie close together and that extends anteriorly onto the dorsal surface of the rostrum basisphenoidale, and is laterally bordered by dorsally raised crests. *Eretmochelys imbricata* (FMNH 22242) has the same morphology, except that the lateral margins of the sella turcica terminate in anterodorsolateral processes that project from the rostrum basisphenoidale, the trabeculae. These trabeculae are very long in *Caretta caretta* (NHMUK 1940.3.15.1). In *Lepidochelys kempii* (M009/08; see Jones *et al.* 2012) the sella turcica is limited to a deep pit at the dorsal base of the rostrum basisphenoidale. However, the foramina anterius canalis carotici cerebralis seems to remain

separate openings in all modern cheloniids, as well as in fossil chelonioids for which either the condition is described or noted during this study (*Ocepechelon*: Bardet *et al.* 2013; *Nichollsemys*: Brinkman *et al.* 2006; *Ctenochelys*: Matzke 2007, FMNH PR 444; *Toxochelys*: FMNH PR 219; *Allopleuron*: NHMUK PV R4213; *Puppigerus*: NHMUK PV R14375). Although *Toxochelys* has closely spaced, separate foramina anterius canalis carotici cerebralis as in modern cheloniids, the sella turcica differs from that in *Rhinochelys* and the aforementioned chelonioids, and is more like that in most other cryptodires in having a broad, 'U'-shaped fossa on the dorsal surface of a flat rostrum basisphenoidale that is well sutured to the pterygoids (FMNH PR 219).

In *Rhinochelys*, the rostrum basisphenoidale is rod-like and emerges ventral to the dorsum sellae, projecting anteriorly and slightly dorsally. The rostrum basisphenoidale forms the medial wall of the anterior course of the canalis caroticus palatinum, which is otherwise largely contained within the pterygoid (see Pterygoid, above). At its anterolateral margin, the rostrum basisphenoidale of *Rhinochelys* has two weakly dorsally projecting flanges, which are interpreted as trabeculae.

The pterygoid contacts the parabasisphenoid along its entire lateral side, covering its ventral half. In the posterior part, where the margin of the parabasisphenoid cup is thickened, the contact surface of the parabasisphenoid for the pterygoid is broad and faces strongly ventrolaterally, so that the parabasisphenoid effectively overlaps the pterygoid. Anteriorly, parallel to the course of the sulcus cavernosus, the contact surface faces anterolaterally, but not ventrally. Further anteriorly, from the base of the rostrum basisphenoidale, the pterygoids form a midline contact and extend ventrally to the rostrum. The rostrum basisphenoidale is partially embedded in the dorsal part of the interpterygoid suture. Only the anterior end of the rostrum loses contact with the pterygoids, as also occurs in modern cheloniids and some fossil taxa (e.g. *Nichollsemys*: Brinkman *et al.* 2006, TMP 97.99.1).

The ventral surface of the parabasisphenoid of *Rhinochelys* is exposed as a triangular wedge between the pterygoids. Its surface texture is roughened by short, irregular

longitudinal ridges, which are also present in modern cheloniids where they serve as muscle attachments (Gaffney 1979).

3.4.2 Cavum acustico-jugulare

The cavum acustico-jugulare is a broad cavity in the posteroventrolateral region of the skull (Fig. 3.26). It is bordered by the quadrate laterally, the opisthotic and prootic dorsally, the prootic anterolaterally, the pterygoid ventrally, the exoccipital posteromedially and the basioccipital posteroventromedially. The cavum acustico-jugulare represents a ventrally closed cranioquadrate space, which is unique to turtles amongst reptiles due to their fused basipterygoid articulation, which sutures the palatoquadrate to the neurocranium (Gaffney 1979). The cavum acustico-jugulare can be separated into two sub-chambers, which Gaffney (1979) refers to as the cranioquadrate space portion and the recessus scalae tympani.

The cranioquadrate space portion is larger than the recessus scalae tympani and is positioned centrally between the canalis cavernosus anteriorly and the fenestra postotica posteriorly, and centrally between the cavum labyrinthicum medially and the cavum tympanum laterally. The cranioquadrate space portion of the cavum acustico-jugulare includes the medial part of the middle ear and is connected to its lateral part, the cavum tympanum, by the incisura columella auris of the quadrate. The stapes passes from the cavum tympanum through the incisura columella auris and then traverses the cranioquadrate space portion of the cavum acustico-jugulare (Fig. 3.27). The stapedial footplate enters the fenestra ovale medially. The latter is formed by the prootic anteriorly and the processus interfenestralis of the opisthotic posteriorly. Ventrally, the margin of the fenestra ovale remains unossified in *Rhinochelys*. Therefore, the cranioquadrate space portion of the cavum acustico-jugulare and the cavum labyrinthicum are confluent with the fenestra ovale ventrally. However, a parasagittal ridge on the dorsal surface of the pterygoid, which borders the course of the vena capitis lateralis medially, is aligned approximately with the border

between the cavum acustico-jugulare and the cavum labyrinthicum (Fig. 3.22; Appendix S2, Fig. S2.9).

The recessus scalae tympani is a medial extension of the cavum acustico-jugulare in its posterior portion. It is formed by the opisthotic anteriorly and the exoccipital posteriorly. Medially, the recessus scalae tympani opens into the endocranial cavity via the anterior jugular foramen, which is bound by the opisthotic and exoccipital. The vena cerebralis posterior, as well as the vagus (CN X) and accessory (CN XI) nerves, enters the recessus scalae tympani through this opening (Gaffney 1979). The fenestra perilymphatica is a ventrally open notch in the posterior surface of the opisthotic. It defines the posteromedial margin of the processus interfenestralis and connects the cavum labyrinthicum anteriorly with the recessus scalae tympani posteriorly. The fenestra perilymphatica is important for the dissipation of sound energy in the turtle ear. In turtles, a round window is absent (Henson 1974; Wever 1978; Hetherington 2008) and has a re-entrant fluid flow instead, in which endolymph passes through the fenestra perilymphatica into a perilymphatic recess. This perilymphatic recess passes through the recessus scalae tympani and into the cranioquadrate space portion of the cavum acustico-jugulare, where it connects to the fenestra ovale to close the flow circuit.

The floor of the cavum acustico-jugulare is formed by the pterygoid. However, the pterygoid only extends posteriorly to the level of the incisura columella auris of the quadrate laterally and to the lateral process of the basioccipital medially. Hence, large parts of the posterior portion of the cavum acustico-jugulare are not closed ventrally, so that the ventral surface of the opisthotic is visible in ventral view. The posterior margin of the cavum acustico-jugulare is also unossified and the large, posteroventrally directed opening that results is termed the fenestra postotica. Several blood vessels enter the skull through the fenestra postotica, most notably the vena capitis lateralis, which continues anteriorly on the floor of the cavum acustico-jugulare into the canalis cavernosus, and the stapedial artery (Albrecht 1967; Gaffney 1979). In *Rhinochelys*, a separate posterior jugular foramen is not present, but is incorporated in the medial margin of the fenestra postotica instead (Fig. 3.26).

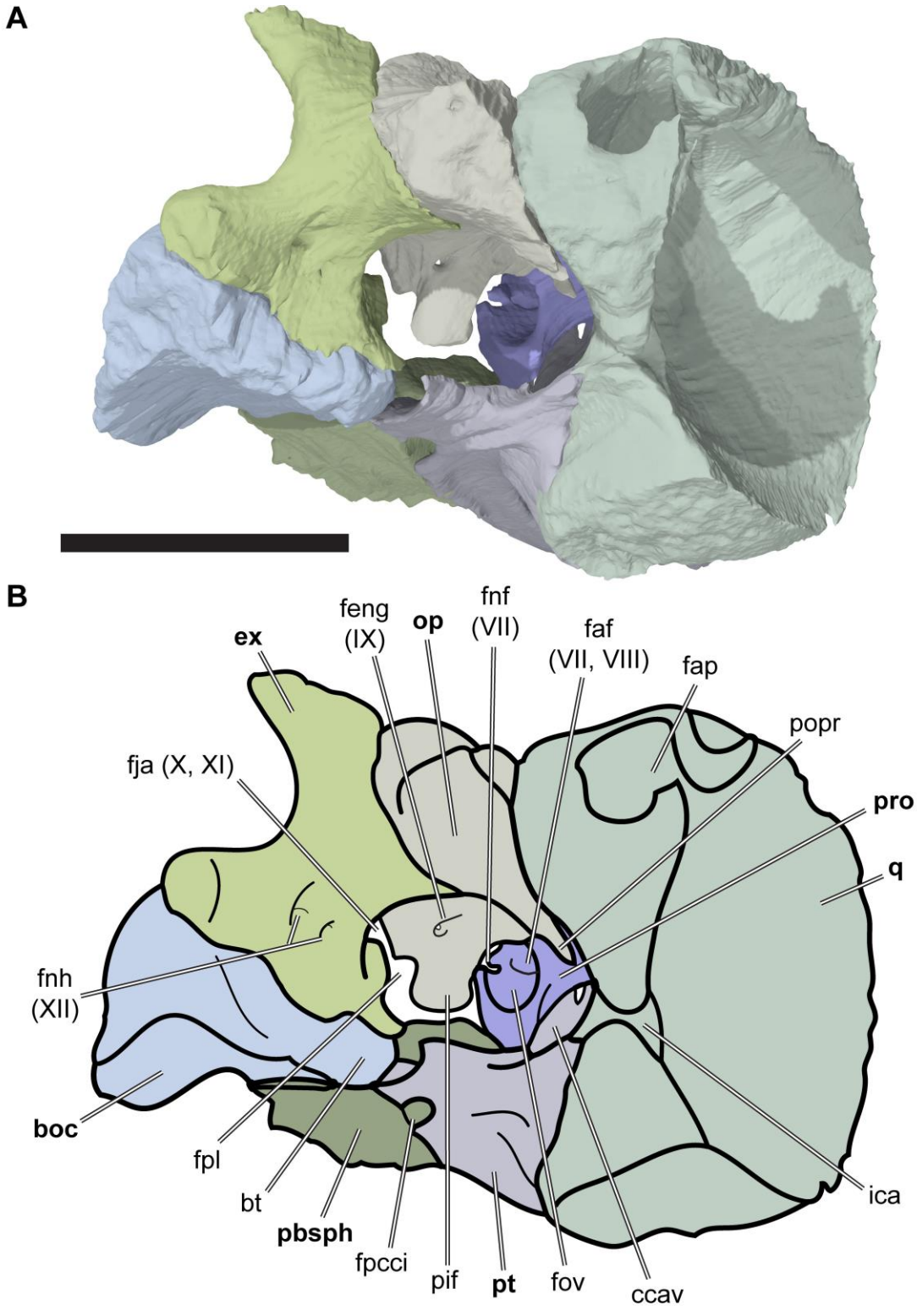


FIG. 3.26. Cavum acustico-jugulare of CAMSM B55783 in posteroventrolateral view. **A**, 3D rendering; **B**, interpretative line drawing. Scale bar equals 5 mm. Note that bones are labelled in bold. Abbreviations: *boc*, basioccipital; *bt*, basal tuber; *ccav*, canalis cavernosus; *ex*, exoccipital; *faf* (VI**I** VIII), fossa acustico-facialis; *fap*, foramen antrum postoticum; *feng* (IX), foramen externum nervi glossopharyngei; *fnf* (VII), foramen nervi facialis; *fnh* (XII), foramina nervi hypglossi; *fja* (X, XI), foramen jugulare anterius; *fpcci*, foramen posterius canalis carotici interni; *fpl*, fenestra perilymphatica; *fov*, foramen ovalis; *ica*, incisura columalla auris; *op*, opisthotic; *pbsph*, parabasisphenoid; *pif*, processus interfenestralis; *popr*, paroccipital process; *pro*, prootic; *pt*, pterygoid; *q*, quadrate.

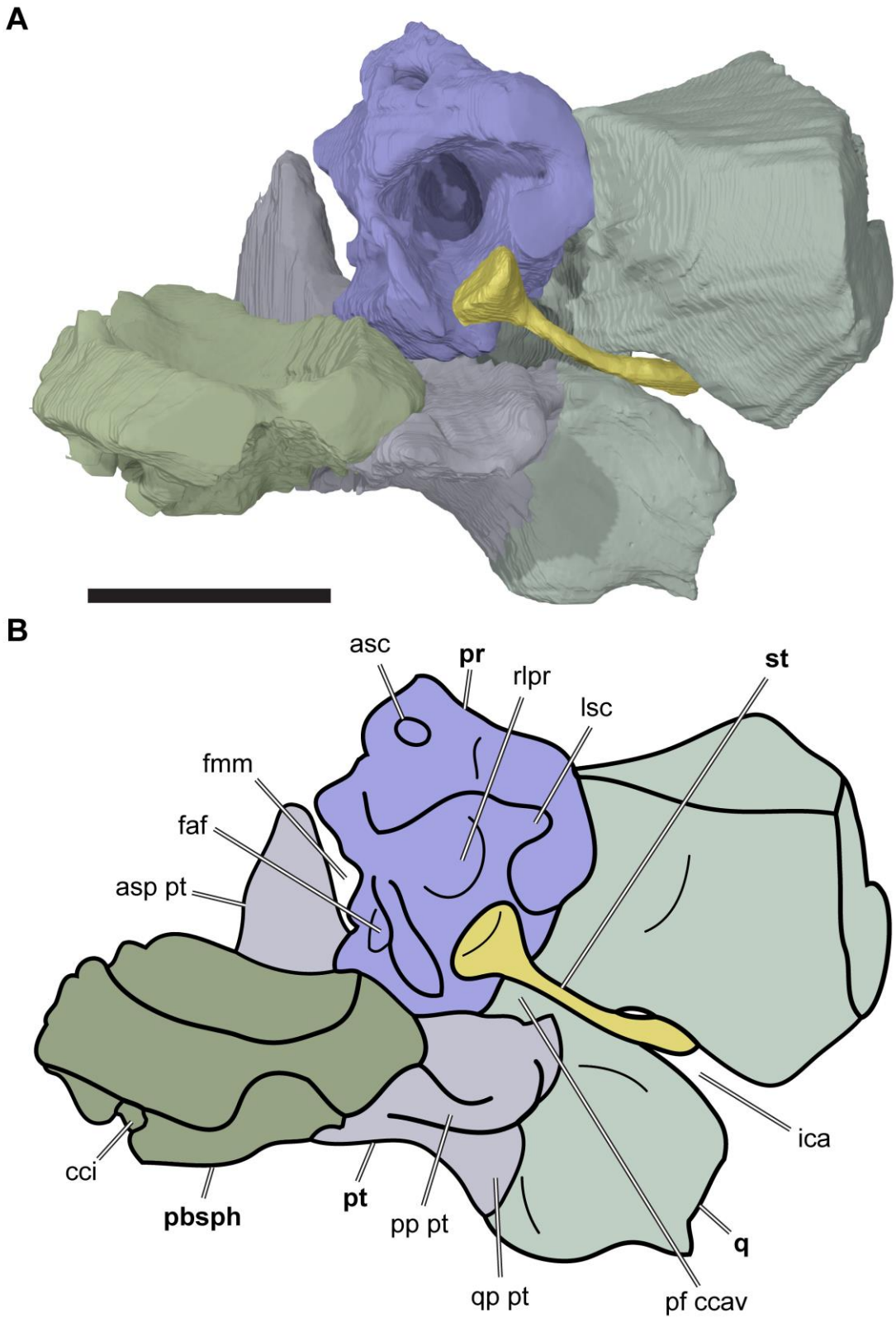


FIG. 3.27. Posteromedial view of partial otic capsule and cavum acustico-jugulare of CAMSM B55776 with stapes *in situ*. **A**, 3D rendering; **B**, interpretative line drawing. Scale bar equals 5 mm. Note that bones are labelled in bold. Abbreviations: *asc*, anterior semicircular canal; *asp pt*, ascending process of pterygoid; *cci*, canalis caroticus internus; *faf*, fossa acustico-facialis; *fmm*, maxillo-mandibular foramen; *ica*, incisura columella auris; *lsc*, lateral semicircular canal; *pbsph*, parabasisphenoid; *pf ccav*, posterior foramen for the canalis cavernosus; *pp pt*, posterior process of pterygoid; *pr*, prootic; *pt*, pterygoid; *q*, quadrate; *qp pt*, quadrate process of pterygoid; *rlpr*, recessus labyrinthicus prooticus; *st*, stapes.

Consequentially, the path of the vena cerebralis posterior is contained within the cavum acustico-jugulare but limited to the recessus scalae-tympani portion.

The roof of the cavum acustico-jugulare is pierced by a foramen shared between the quadrate and prootic, the aditus canalis stapedio-temporale. This foramen leads into a vertical tunnel dorsally, the canalis stapedio-temporale, which opens into the supratemporal fossa via the foramen stapedio-temporale. The stapedial artery exits the cavum acustico-jugulare through the canalis stapedio-temporale (Albrecht 1967; Gaffney 1979). Anteriorly, the cavum acustico-jugulare becomes constricted transversely and dorsoventrally and leads into the canalis cavernous, which extends anteroventrally from the cavum acustico-jugulare and between the quadrate, prootic and pterygoid. The anterior part of the cavum acustico-jugulare serves as a passage for the hyomandibular branch of the facial nerve (CN VII), which extends posteriorly from the prootic contribution to the medial wall of the canalis cavernosus. The mandibular artery, an anterior branch of the stapedial artery, usually passes through the anterior portion of the cavum acustico-jugulare in cryptodires also and continues through the canalis cavernosus before it exits into the subtemporal fossa via the maxillo-mandibular foramen (Gaffney 1979). However, this cannot be confirmed for *Rhinochelys*, as the mandibular artery leaves no osteological correlate.

3.4.3 Arterial circulation

The course of the carotid arteries is described above (see Pterygoid and Parabasisphenoid). However, because the carotid circulation is systematically important in turtles, it is summarised here briefly. In turtles, the common carotid artery branches extracranially into the internal carotid artery and the stapedial artery. In *Rhinochelys*, the internal carotid artery enters the skull through the foramen posterius canalis carotici interni (all foramina and canal terminology follows Rabi *et al.* 2013; Fig. 3.28), which is located on the sutural contact between the parabasisphenoid and pterygoid, just anterior to the posterior process of the latter. The canalis carotici interni continues anteriorly between these bones and diverges into

lateral and medial branches inside the cranium just posterior to the level of the base of the rostrum basisphenoidale. The lateral branch is the palatine artery, which is contained within the canalis caroticus palatinum. This canal continues anteriorly and is bound medially by the rostrum basisphenoidale of the parabasisphenoid, but is otherwise enclosed by the pterygoid. Anteriorly, the palatine artery exits its canal through the foramen anterius canalis carotici palatinum, which is positioned ventral to the level of the sulcus olfactorius and about halfway along the length of the rostrum basisphenoidale. The second, medial branch of the internal carotid artery is the cerebral artery. It projects anterodorsomedially into the parabasisphenoid. Left and right cerebral arteries have separate posterior courses, but join to run through a single, median canalis caroticus cerebralis within the parabasisphenoid more anteriorly. The canalis caroticus cerebralis opens anteriorly within the sella turcica on the dorsal surface of the rostrum basisphenoidale via a single, large foramen anterius canalis carotici cerebralis. The shared anterior canal for the right and left cerebral arteries is an unusual feature with respect to other turtles, which until recently had been reported only for several protostegids, including *Calcarichelys gemma* and *Protostega gigas* (both Hooks 1998) and *Notochelone costata* (Evers & Benson 2018*c*). However, this condition is also present in some cheloniids, such as *Lepidochelys olivacea* (Evers & Benson 2018*b*, *c*). More commonly, the left and right cerebral arteries exit the parabasisphenoid through separate openings, which can vary from closely spaced (as in most chelonioids; e.g. Hirayama 1998; Myers *et al.* 2018) to widely separated (as in most other turtles; Hirayama 1998; Cadena & Parham 2015; Evers & Benson 2018*a*, *c*).

The course of the stapedial artery can be traced in *Rhinochelys* vertically through the canalis stapedio-temporale between the quadrate and prootic. Its exact course through the cavum acustico-jugulare cannot be reconstructed, but it is usually parallel and dorsal to the vena capitis lateralis, the course of which can be followed on the floor of the cavum acustico-jugulare and canalis cavernosus. Assuming a cryptodiran arterial circulation, the mandibular artery in *Rhinochelys* would have branched off of the stapedial artery within the cavum

acustico-jugulare, exiting into the fossa subtemporalis through the maxillo-mandibular foramen.

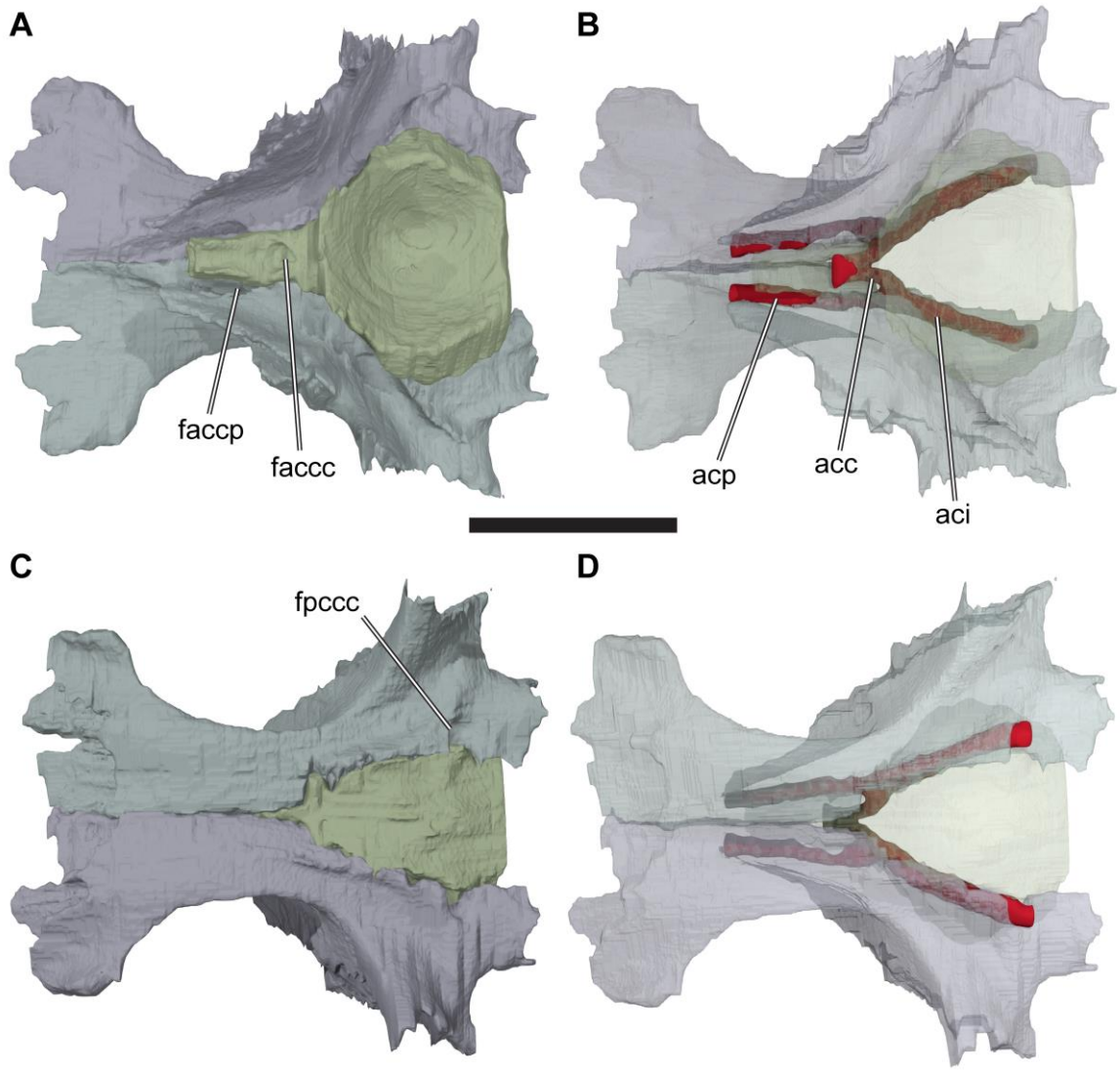


FIG. 3.28. 3D renderings of the partial basicranium of CAMSM B55783. **A**, dorsal opaque view; **B**, dorsal translucent view, including carotid arteries; **C**, ventral opaque view; **D**, ventral translucent view, including carotid arteries. Scale bar equals 5 mm. Abbreviations: *acc*, cerebral artery; *aci*, internal carotid artery; *acp*, palatine artery; *faccc*, foramen anterius canalis caroticus cerebralis; *faccp*, foramen anterius canalis caroticus palatinum.

3.4.4 Cranial endocast

A digital endocast has been segmented for CAMSM B55775 (Fig. 3.29). This specimen was selected as its the braincase is completely preserved, including the posterior elements, and the nasal capsule is also preserved. Following the description of *Plesiochelys etalloni* provided by Carabajal *et al.* (2013), the nasal capsule has been included in the endocast of *Rhinochelys*.

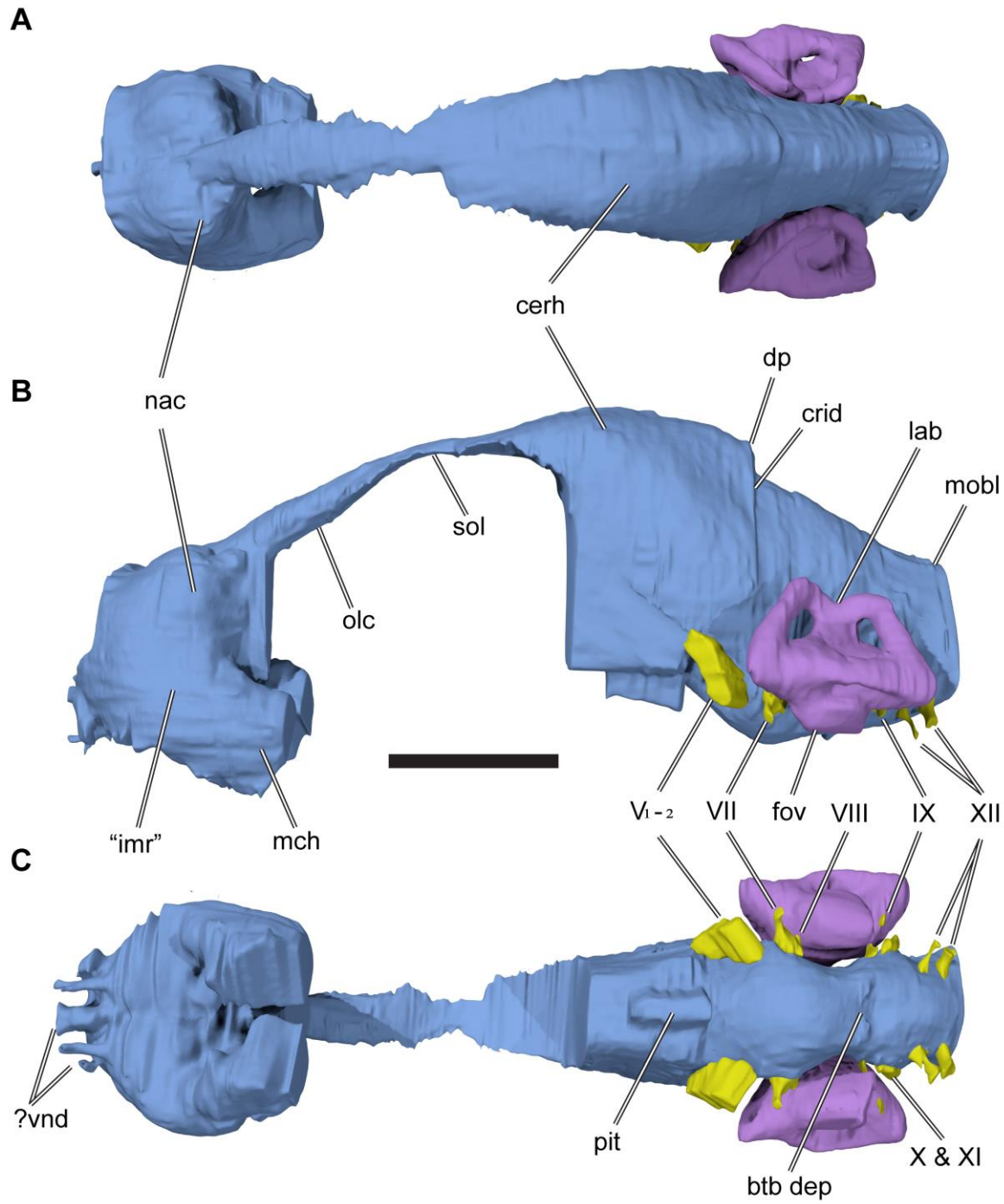


FIG. 3.29. 3D renderings of digital endocast of the braincase, nasal capsule, bony labyrinth of CAMSM B55775. **A**, dorsal view; **B**, left lateral view; **C** ventral view. Scale bar equals 10 mm. Abbreviations: *btb dep*, basis tuberculi basalis depression; *cerh*, cerebral hemisphere; '*crid*'; cartilaginous 'rider'; *IX*, glossopharyngeal nerve (CN IX); '*imr*', 'intermediate region'; *lab*, labyrinth; *mch*, meatus choane; *mobl*, medulla oblongata; *nac*, nasal capsule; *olc*, olfactory canal; *pit*, pituitary fossa; *sol*, sulcus olfactorius; V_{1-2}, maxillomandibular division of the trigeminal nerve (CN V); *VII* facial nerve (CN VII); *VIII* acustic nerve (CN VIII); *vnd*, vomeronasal diverticulae; *X*, vagus nerve; *XI* accessory nerve; *XII* hypoglossal nerves.

Turtle endocasts represent only the gross morphology of the brain, for several reasons. Brains of modern non-avian reptiles are much smaller than their respective

endocranial cavities (Hopson 1979) and the resulting shape difference between endocranial cavity and brain has been reported to be particularly large in turtles (Edinger 1929; Zangerl 1960). A dural envelope surrounds the brain, and subdural and epidural spaces exist in extant sea turtles (Wyneken 2001), which further minimize the correspondence between brain and endocranial cavity shape. In addition, the turtle braincase is peculiar in possessing a secondary lateral braincase wall anterior to the prootic, which is formed by the processus inferior parietalis of the parietal. A primary lateral braincase wall anterior to the prootic, which is commonly formed by the laterosphenoid in other reptiles (e.g. Holliday & Witmer 2007), is absent in turtles (although present in early developmental stages of the chondrocranium: Rieppel 1993). Consequentially, the primary endocranial cavity is laterally expanded beyond the parabasisphenoid cup and extends dorsally over the sulcus cavernosus to include the cavum epiptericum. The cavum epitericum houses the trigeminal ganglion (Soliman 1964; Starck 1979; Holliday & Witmer 2007) and is generally an extracranial space that becomes enclosed within the laterally expanded endocranial cavity in turtles (Starck 1979). However, a membranous wall separates the cavum epiptericum form the endocranial cavity *sensu stricto* in turtles (Starck 1979). Carabajal *et al.* (2013) included both the sulcus cavernosus and the cavum epiptericum in their digital endocast of *Plesiochelys*. For *Rhinochelys*, however, we excluded both structures. As a consequence, the pituitary is visible in our endocast as a protuberance on the ventral surface of the endocast (Fig. 3.29C), as also shown in Lautenschlager *et al.* (2018) (rather than as a depression between the sulci cavernosi). This is a more accurate representation of the pituitary than that provided in Carabajal *et al.* (2013), because our model fills the sella turcica to the exclusion of the ventrally underlying rostrum basisphenoidale, whereas the depression between the sulci cavernosi includes both the depth of the pituitary and the rostrum basisphenoidale. Our rendering of the trigeminal nerve includes most of the space within the cavum epiptericum (i.e. the trigeminal ganglion is segmented as part of the nerve masks, rather than part of the endocast).

In spite of the above-mentioned difficulties regarding the reliability of turtle endocranial cavities as indicators of brain shape, several general statements can be made, which include the passages of those cranial nerves that are contained by bone, as well as brain flexures (e.g. Lautenschlager *et al.* 2018). The canals for the cranial nerves have been described above in the respective sections describing the bones they traverse, but this information is repeated here briefly to provide an inclusive description of the endocast and its associated neural structures.

Although the endocast of *Rhinochelys* is principally tubular (Fig. 3.29A–B), it is more strongly flexed than in *Plesiochelys etalloni* (Carabajal *et al.* 2013) or *Proganochelys quenstedti* (Lautenschlager *et al.* 2018), but not as strongly as in *Meiolania planiceps* (Carabajal *et al.* 2017). The cephalic flexure between the forebrain and hindbrain is much more strongly developed than in *Plesiochelys etalloni* and mirrors the form of modern cheloniids (compare with the images provided in Zangerl 1960), but not *Dermochelys* (Nick 1912; Wyneken 2001). The cerebral area and olfactory lobe area form a continuously curved, convex shape. The olfactory lobes, however, are not discernable in *Rhinochelys*, while they have been identified in *Plesiochelys etalloni* as small, weakly convex structures lying anteromedial to the cerebral hemispheres (Carabajal *et al.* 2013).

The forebrain of *Rhinochelys* extends anteroventrally from the cephalic flexure as a cast of the sulcus olfactorius ventral to the frontals. The anterior extent of the olfactory bulbs cannot be distinguished from the course of the olfactory nerves, which are anteroventrally directed from them. The anterior part of the olfactory nerve path is well defined by the olfactory canal (see Frontal, above), and enters the nasal cavity above the fissura ethmoidalis. The fissura etmoidalis is visible as a narrow, 'V'-shaped median structure on the posterior surface of the nasal cavity.

The nasal cavity itself is dorsolaterally expanded, to form a strongly convex hemisphere on either side of the skull midline. It is in this dorsal part that the olfactory epithelium of the olfactory sacs lies (Wyneken 2001; Schwenk 2008). In the dorsal part of the nasal cavity, left and right nasal valves, which would be separated in life by the median,

vertically oriented internarial septum, can be distinguished by a shallow median sulcus. Ventrally, this division is also discernable from a median groove in the endocast of the nasal cavity (Fig. 3.29C), which is the imprint of the median ridge shared between premaxillae anteriorly and vomer posteriorly. Although the nasal capsule is a large chamber, it is not as large as in the stem-group turtles *Proganochelys* (Lautenschlager *et al.* 2018) or *Meiolania* (Carabajal *et al.* 2017).

Anterodorsally, the nasal cavity opens via the single external naris. Ventral to the external naris, the nasal capsule extends anteriorly to form a short, bulbous hemisphere, termed the 'intermediate region' (Parsons 1970; Schwenk 2008), which houses vomeronasal epithelium in sea turtles (Parsons 1970; Wyneken 2001; Schwenk 2008). The intermediate region extends anteriorly into the interpremaxillary suture, a feature that is visible in the endocast as an anteromedian, vertically oriented ridge with a centrally placed, anteriorly directed, short tubular protuberance. It is possible that this anterior cavity positioned between the premaxillae is associated with the vomeronasal organ. Anteroventrally, but lateral with respect to the aforementioned extension, short canals extend through the premaxilla and reach the triturating surface of the palate (Fig. 3.29C). The nature of these canals is unclear; it is possible that they represent vascular canals, but they might also be related to the vomeronasal organ. The vomeronasal epithelium in sea turtles is sequestered into dorsal and ventral diverticulae from the intermediate region (Parsons 1970; Schwenk 2008), and the ventral extensions seen in *Rhinochelys* are in accordance with this morphology.

The midbrain posterior to the cephalic flexure is posteroventrally directed. The cerebral hemispheres of the midbrain are visible in *Rhinochelys* as shallow convexities on the dorsolateral surface of the endocast to either side of its midline (Fig. 3.29A). The anterior surface of the midbrain in *Rhinochelys* is segmented until the anterior end of the processi inferior parietalis, resulting in a flat surface ventral to the anteriorly extending olfactory tract. The vertical anterior end of the endocranial cavity results in a large interorbital fenestra, which has been interpreted as being indicative of well-developed salt glands (Hirayama

1998). The anterior surface of the midbrain between the parietal margins is unossified in turtles (with the possible exception of *Proganochelys quenstedti*: Bhullar & Bever 2009; but see Lautenchlager *et al.* 2018), so that the foramina for the cranial nerves II–IV are not encased in bone and cannot be represented in the digital endocast of *Rhinochelys*, as is also the case in *Plesiochelys* (Carabajal *et al.* 2013).

The ventral part of the midbrain in *Rhinochelys* is marked by a narrow, longitudinal protrusion, which represents the digital infill of the sella turcica. This protrusion includes the pituitary, but almost certainly overestimates its size, as the sella turcica is not usually completely filled by neural tissue (Hopson 1979). The cast of the pituitary is posteriorly confluent with the foramen anterius canalis carotici cerebralis, through which the cerebral artery exits the parabasisphenoid. Posterolateral to the pituitary, the abducens nerve (CN VI) exits the cranial cavity through small, paired foramina near the base of the clinoid processes. In CAMSM B55775, these nerves have not been segmented as their respective canals are not visible in the CT scans.

The most distinctive feature of the mid- to hindbrain region in *Rhinochelys* is a transversely oriented step between the surface of the posterior portion of the midbrain and the metencephalon of the hindbrain. This step is dorsally hypertrophied by a centrally placed eminence, the dural peak, but is also visible laterally as a vertical step dorsal to the posterior level of the trigeminal nerve (Fig. 3.29B). This transverse ridge is the margin of the 'cartilaginous rider' of Zangerl (1960), who described this feature first in an endocast of the chelonioid *Corsochelys*, and who also found this structure in modern cheloniid endocasts. The cartilaginous rider is a triangular, slightly dorsally elevated area on the dorsal surface of the midbrain region of endocasts in these turtles (Zangerl 1960). It narrows anteriorly between the cerebral hemispheres. Except for its posterior border, the cartilaginous rider is not discernable in *Rhinochelys*. Zangerl (1960) interpreted the cartilaginous rider as a cartilaginous anterior extension of the supraoccipital, a view that was adopted by Hopson (1979). In addition to its presence in *Corsochelys* and modern cheloniids, it has also been identified in *Plesiochelys etalloni* (Carabajal *et al.* 2013), various fossil bothremydid

pleurodires (Gaffney & Zangerl 1968) and stem-turtles (e.g. Carabajal *et al.* 2017; Lautenschlager *et al.* 2018). However, in bothremydids the rider forms a narrow, vaguely tubular dorsal protrusion of the endocast, rather than a low triangular area with well delimited posterior and posterolateral borders. Carabajal *et al.* (2013) explain the presence of the lateral, ridge-like demarcations of the rider and its alignment with the ventrally adjacent maxillo-mandibular (CN V_{2-3}) foramen in *Plesiochelys* as indicators for the course of the dorsal head vein and rostral cerebral vein. However, the posterior border of the rider in *Rhinochelys* is clearly an artifact of the anterior margin of the supraoccipital: the supraoccipital ends anteriorly at the level of the position of the trigeminal nerve and, anterior to this point, the roof of the endocranial cavity is formed by the parietals, which overlie the dorsal surface of the supraoccipital. Unless the anterior end of the supraoccipital coincides with the course of the dorsal head vein and the rostral cerebral vein, the cartilaginous rider appears to be unrelated to either the central nervous system or associated vascular structures, supporting the original proposal of Zangerl (1960). However, the dorsally hypertrophied dural peak in the posterodorsal border of the cartilaginous rider seems to represent a genuine feature: If the endocast of *Rhinochelys* is posteriorly segmented to include the anterior parts of the supraoccipital, the lateral ridges of the rider vanish, whereas a small dorsal convexity remains. This is consistent with other studies in which the dural peak is present, whereas lateral demarcations of the cartilaginous rider are absent (e.g. Lautenschlager *et al.* 2018). Wyneken (2001) has shown that the pineal gland of chelonioids extends dorsally from the brain into the region of the dural peak, and that the pineal gland connects to the skull roof in *Dermochelys*. The presence of a well-developed pineal organ has also been proposed for the protostegid *Desmatochelys lowii* (Raselli 2018). *Desmatochelys lowii* and *Desmatochelys padillai* show evidence for the presence of a pineal foramen, although the pineal foramen of *Desmatochelys lowii* has recently been reinterpreted as breakage (Raselli 2018). Nevertheless, a pineal foramen is present in several specimens of *Desmatochelys padillai* (Cadena & Parham 2015). In several well-preserved *Rhinochelys* specimens (e.g. CAMSM B55783; Fig. 3.8), the anterior part of the parietals is damaged,

indicating that this area of the skull roof was possibly thinner than other parts. It would be ambiguous to declare the dural peak of *Rhinochelys* as evidence of a pocket for the pineal gland similar to that of *Dermochelys*, but this possibility should be considered.

The metencephalon part of the hindbrain (anterior to the pontine flexure) continues to be posteroventrally directed posterior to the cartilaginous rider. Its lateroventral side is marked by the origins of cranial nerves V and VII–VIII. The nerve stem for the trigeminal nerve (CN V) exits the primary cranial cavity dorsal to the anterolateral margin of the basisphenoid cup, posterior to the clinoid process and anterior to the prootic. It extends into the cavum epiptericum and forms a single ganglion (Starck 1979). The ophthalmic (V_1) ramus of the trigeminal nerve diverges anteriorly from this ganglion, and medial to the secondary lateral wall of the braincase formed by the processus inferior parietalis, but leaves no osteological trace. Only the maxillo-mandibular rami (V_{2-3}) exit into the subtemporal fossa through the foramen between the parietal, pterygoid and prootic. Turtle workers commonly refer to this foramen as the trigeminal foramen (e.g. Gaffney 1979). However, the term 'trigeminal foramen' is potentially misleading due to the evolution of the braincase secondary lateral wall in turtles: in *Proganochelys*, a medial foramen in the prootic and possibly laterosphenoid (Gaffney 1990; Bhullar & Bever 2009; but see Lautenschlager *et al.* 2018) is formed in the primary lateral wall of the braincase, and the neomorphic 'trigeminal foramen' of anatomically modern turtles (i.e. formed largely by the parietal and pterygoid) is absent. In some turtles, both a medial and neomorphic lateral foramen coexist (e.g. *Plesiochelys*: Anquetin *et al.* 2015; but see Evers & Benson 2018*c* for a wider distribution among turtles). Several alternative terms have been proposed to highlight the position of the 'trigeminal foramen' in a secondary lateral wall of the braincase (e.g. foramen otico-parietale: Starck 1979). Given that only the maxillo-mandibular rami of the trigeminal nerve pass through the foramen, the name maxillo-mandibular foramen is advocated here, whereas the medial foramen could be called a prootic foramen (as in Gaffney 1990) or the trigeminal foramen, as it is homologous with the foramen for the CN V nerve stem in other reptiles.

Shortly posterior to the maxillo-mandibular foramen, the facial (CN VII) and acoustic (CN VIII) nerve foramina exit the cranial cavity. Their base is combined in the endocast, due to their shared position within the fossa acustico-facialis. The canals of three rami can be discerned, however: a single canal for the facial nerve exits into the canalis cavernosus anteroventrolaterally, and two short, anteroposteriorly aligned canals for the acustic nerve rami are directed dorsolaterally into the cavum labyrinthicum. The passage of the facial nerve (CN VII) of *Rhinochelys* is consistent with the patterns observed in cryptodires, but is distinct from the pleurodiran condition and that seen in some extinct marine turtles, such as plesiochelyids (see Evers & Benson 2018*c*).

The endocast is mediolaterally constricted at the metencephalon, posterior to the position of the fossa acustico-facialis. The inner ear is positioned at the level of this constriction. The inner ear and endocast are confluent via the hiatus acusticus, an unossified space between the medial margins of the prootic and opisthotic. Because of this, the separation between the cavum labyrinticum of the inner ear and endocranial cavity cannot be determined exactly, and the surface of the endocast facing the inner ear model is somewhat arbitrary (see Inner ear and associated structures, below, for details of how the inner ear has been segmented along the hiatus acusticus). In its dorsal part, the endocast space for the inner ear has a short, dorsolaterally directed protuberance, which represents the endolymphatic duct that passes through the supraoccipital dorsolaterally to the common crus.

The ventral surface of the metencephalon is a convex hemisphere that fills the parabasisphenoid cup. At its posterior border, there are two small ventral protuberances to either side of the endocast midline, which are formed by the centrally positioned basis tuberculi basalis on the anterior margin of the basioccipital.

The metencephalon and myencephalon of the hindbrain form the pontine flexure. In *Rhinochelys*, the pontine flexure is less marked than the cephalic flexure. The myencephalon is horizontally oriented posterior to the pontine flexure but continues as a short tubular process posterior to the level of the inner ear. The medulla oblongata is narrower and lower

than the metencephalon region of the hindbrain and does not expand toward the foramen magnum. Ventrally, the surface of the myencephalon is smooth, as a crista dorsalis basioccipitalis is absent in CAMSM B55775.

The glossopharyngeal nerve (CN IX) is associated with three foramina in *Rhinochelys*: the medial foramen for the exit of the nerve from the brain, the internal foramen on the dorsal surface of the cavum layrinthicum at the base of the processus interfenestralis, and the external foramen entering the recessus scalae tympani. The course of the nerve between the medial foramen and the short canal spanning the internal and external foramina has been segmented continuously on the floor of the cavum labyrinthicum. Consequentially, CN IX is visible as a long, thin structure diverging laterally from the endocast and extending through parts of the inner ear model (see Fig. 3.29C). Directly posterior to the internal glossopharyngeal (CN IX) foramen is the anterior jugular foramen, through which several structures pass, including the vagus (CN X) and accessory (CN IX) nerves. This entire foramen has been segmented as a single structure, so that it is shown as a narrow, dorsoventrally high opening. Just anterior to the foramen magnum, the hypoglossal nerve (CN XII) rami diverge ventrolaterally from the endocast, exiting through two anteroposteriorly aligned foramina.

3.4.5 Inner ear and associated structures

Morphological information on the inner ear of turtles has been limited to a few studies based on anatomical dissections, naturally preserved fossil endocasts, or digital renderings of CT data (Zangerl 1960; Gaffney & Zangerl 1968; Gaffney 1977, 1982*a*; Baird 1974; Thewissen & Nummela 2008; Georgi 2008; Walsh *et al.* 2009; Carabajal *et al.* 2013, 2017; Neenan *et al.* 2017; Ferreira *et al.* 2018; Lautenschlager *et al.* 2018).

The inner ear of vertebrates is organised roughly into a superior division (endosseous labyrinth) and inferior division (saccule and cochlea) (Wever 1978). The inner ear includes eight sensory endorgans, only one of which, housed in the cochlea, is known to be auditory in function (Wever 1978). The vestibular system governing balance and orientation consists of

three semicircular canals (detecting angular movements), which are orthogonally arranged to one another and housed in bony canals, and the vestibule, which is the chamber housing the otolithic organs, namely the saccule (detecting vertical movements) and utricle (detecting horizontal movements).

The bony semicircular canals are contained within the prootic, opisthotic and supraoccipital, and can be segmented from CT scans, enabling reliable reconstructions of the bony labyrinth, although it is unclear how reliably the size and shape of the bony canals reflects those of the membranous canals. In turtles, the auditory part of the inner ear and the vestibule is not completely enclosed by bone, making segmentation difficult. Medially, the inner ear cavity is confluent with the endocranial cavity via a large space called the hiatus acusticus. Ventrally, the inner ear cavity is floored by the pterygoid and parabasisphenoid, but it is not clear how far ventrally the structures of the inner ear actually extend. Additionally, the inner ear cavity is connected posteroventrally with the recessus scalae tympani via the fenestra perilymphatica, a ventrally open aperture in the processus interfenestralis of the opisthotic (see Opisthotic, above). Laterally, the inner ear opens toward the cavum acustico-jugulare portion of the middle ear via the fenestra ovale, an opening between the prootic and opisthotic that remains open ventrally in *Rhinochelys*. The inner ear models presented herein (Figs 3.29–30) are extended ventrally to the ventral-most level of the prootic and opisthotic, which corresponds with the ventral margin of the fenestra ovale. Medially, the model is bounded by the medial-most extents of the prootic and opisthotic.

In the bony labyrinth of *Rhinochelys*, the three semicircular canals can be clearly distinguished (Fig. 3.30). Anterior and posterior semicircular canals meet within the supraoccipital, forming the common crus. From the common crus, the anterior semicircular canal extends anterodorsolaterally within the supraoccipital, and then turns anterolateroventrally to pass through the prootic. The part of the anterior semicircular canal housed within the prootic is very weakly arched, and the greatest curvature is accommodated between the dorsal end of the prootic and the common crus. Anterolateroventrally, the

anterior semicircular canal ends in the anterior ampulla. The anterior ampulla of *Rhinochelys* is confluent with the lateral ampulla, which is situated at the anterior end of the lateral semicircular canal. In *Rhinochelys*, the combined anterior and lateral ampullae form a slightly dorsally convex and roughly oval surface between the anterior and lateral semicircular canals and the ventral base of the common crus. The utricle, which connects the common crus with the ampullae, is not discernable as a distinct canal, but is merged with the dorsal part of the central inner ear cavity.

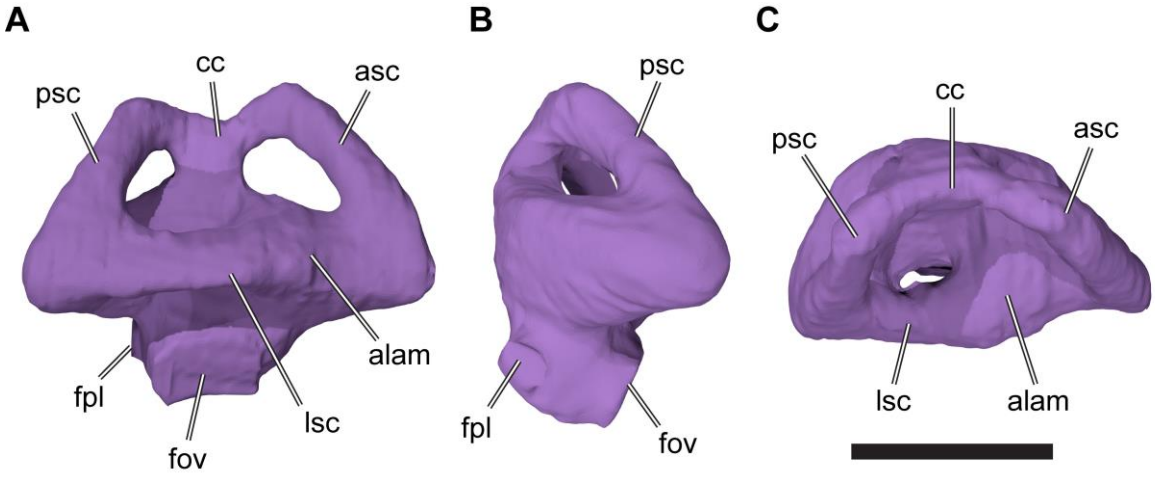


FIG. 3.30. 3D renderings of the right labyrinth of CAMSM B55775. A, lateral view; B, posterior view; C, dorsal view. Scale bar equals 5 mm. Abbreviations: *alam*, anterior and lateral ampullae; *asc*, anterior semicircular canal; *cc*, common crus; *fov*, fenestra ovalis; *fpl*, fenestra perilympahtica; *lsc*, lateral semicircular canal; *psc*, posterior semicircular canal.

The posterior semicircular canal is roughly symmetrical to the anterior semicircular canal (Fig. 3.30A). Analogously to the anterior semicircular canal, the posterior semicircular canal extends posterodorsolaterally from the common crus into the posterodorsal part the supraoccipital, and then turns posterolateroventrally through the opisthotic. The opisthotic part of the posterior semicircular canal is also almost straight, with the greatest curvature of the canal again being between the dorsal end of the opisthotic and the common crus. According to Weaver (1979), the posterior semicircular canal of reptiles continues ventrally to the posterior extent of the lateral semicircular canal and turns anteroventromedially to join the common crus ventrally. This ventral path of the posterior semicircular canal cannot be distinguished from the posteromedial course of the lateral semicircular canal in

Rhinochelys (or most other turtles; SWE, pers. obs.), as these structures traverse a joint cavity within the ventromedial part of the opisthotic part of the inner ear cavity, which is further confluent anteriorly with the saccule. Therefore, the ventrolateral part of the posterior semicircular canal and the posterior part of the lateral semicircular canal merged into a large cavity that represents the posterolateral-most corner of the inner ear model presented here.

The common crus is strongly concave between the highest extent of the anterior and posterior semicircular canals, a feature that is observed in many, but not all, turtles (SWE, per. obs.). The functionality, as well as the distribution of this feature, among turtles is not understood currently and will be explored further elsewhere. The common crus is short and has a diameter about twice as wide as that of the anterior and posterior semicircular canals, which assume a subequal diameter and approximately circular cross-section. Measuring the divergence angle between the anterior and posterior semicircular canals was difficult, because the canals are not perfectly straight. Here, we projected a vertical plane through the centre of the straight parts of the anterior and posterior semicircular canals (i.e. the parts from the ampullae to the dorsal-most points of the respective canals) and measured the angle between these planes. The receptive divergence angle was 79° and can be approximated from Figure 2.30C. Although almost symmetrical, there are some minor differences between the anterior and posterior semicircular canals. The anterior canal is slightly longer than its posterior counterpart and the posterior canal is slightly more strongly laterally directed than the anterior semicircular canal: if a coronal plane is laid through the midpoint of the common crus, the anterior semicircular canal accounts for the greater portion of the total divergence angle between both canals. The dorsal-most point of the anterior semicircular canal is also extends slightly more dorsally than the corresponding point on the posterior semicircular canal.

The lateral semicircular canal appears to be the shortest in the digital models, because its posteromedial path, medial to the posterior semicircular canal, is obscured by being housed in a single space with the ventromedial path of the posterior semicircular canal (see above). Therefore, the course of the lateral semicircular canal can be traced only from

the lateral ampulla to the posterior-most corner of the labyrinth. Between these points, the lateral semicircular canal is laterally arched, so that it has a convex lateral outline in dorsal view. The curvature of the lateral semicircular canal is stronger than that of the other semicircular canals. The cross-section of the lateral semicircular canal is elliptical, as it is dorsoventrally thin and mediolaterally broad. The medial margin of the lateral semicircular canal is separated from the saccule by a bar formed by the opisthotic. In the model, this feature shows as a vertically directed opening between the lateral semicircular canal and the central area of the inner ear cavity. The lateral canal is not parallel to the skull roof (as formed by the parietals) or the palate (as formed by the pterygoids), which form two parallel horizontal planes. Instead, the lateral canal intersects an axial plane parallel to the parietals/pterygoid at approximately 15°, whereby the anterior portion of the canal is dorsally inclined in relation to the horizontal plane defined by the skull roof and palate.

Turtle ears show several specialisations that are not found in other reptiles. The turtle ear lacks the round window (fenestra rotunda) that serves as a pressure relief structure in other reptilian inner ears, but instead has a continuous, reentrant fluid flow system around the stapedial footplate in a space named the pericapsular recess (Henson 1974; Wever 1978; Hetherington 2008). The pericapsular recess is not formed by bone, and thus cannot be reconstructed for *Rhinochelys*. However, the pericapsular sac is situated in the recessus scalae tympani and communicates with the inner ear cavity through the fenestra perilymphatica, a ventrally open aperture on the medial margin of the processus interfenestralis. The fenestra perilymphatica in *Rhinochelys* is posteroventrally directed and subcircular in outline (Fig. 3.30B). The pericapsular recess in *Rhinochelys* would have extended from the recessus scalae tympani into the anteromedial section of the cranioquadrate space portion of the cavum acustico-jugulare, lateral to the fenestra ovale, which is covered by the pericapsular recess.

Another feature of turtle ears is a medially closed middle ear with a tubular recess or stapedial foramen that funnels the stapes medially (Henson 1974). The latter configuration has been interpreted as an aquatic adaptation in turtles in general, as the closed middle ear region consists of cancellous bone that might acoustically isolate the inner ear to prevent

bone conduction of sound waves under water, making the tympanic middle ear with the ossicular chain the only relevant structure for sound reception in turtles and permitting directional hearing when submerged (Hetherington 2008). However, CT scans of *Rhinochelys* show that bones that do not contribute to the otic capsule, such as the parabasisphenoid, are cancellous to the same extent as the former. Also, large parts of the inner ear are surrounded by open spaces, including the widely open sutural contacts between prootic, opisthotic and supraoccipital, so that acoustic isolation by cancellous bone does not seem likely, at least for *Rhinochelys*.

3.4.6 Stapes

One specimen (CAMSM B55776) preserves a stapes in its original position, with the stapedial footplate articulated with the prootic part of the fenestra ovale (the opisthotic is not preserved in this specimen) (Figs 3.27, 3.31). It consists of a disk-shaped stapedial footplate, which is continuous with an elongate, lateral rod-like shaft.

The stapedial shaft is gently curved, with the convex part facing ventrally. This contrasts with the straight stapes of *Plesiochelys etalloni* (Carabajal *et al.* 2013). The stapedial shaft of *Rhinochelys* has a circular cross-section. The stapedial shaft traverses the incisura columella auris of the quadrate. The part of the stapedial shaft that projects laterally into the cavum tympanum is slightly expanded in relation to the mid-part of the shaft. It extends only a few millimetres into the cavum tympanum and does not reach the lateral extent of the cavum, where the tympanic membrane would presumably close the cavum tympanum laterally. The space between the tympanic membrane and lateral tip of the stapes was most likely bridged by a cartilaginous extrastapes.

Medially, the stapedial shaft expands to form a circular stapedial footplate. The medial surface of the stapedial footplate is gently depressed to form a shallow fossa. The anterior margin of the stapedial footplate articulates closely with the prootic margin of the fenestra ovale, leaving no space between them.

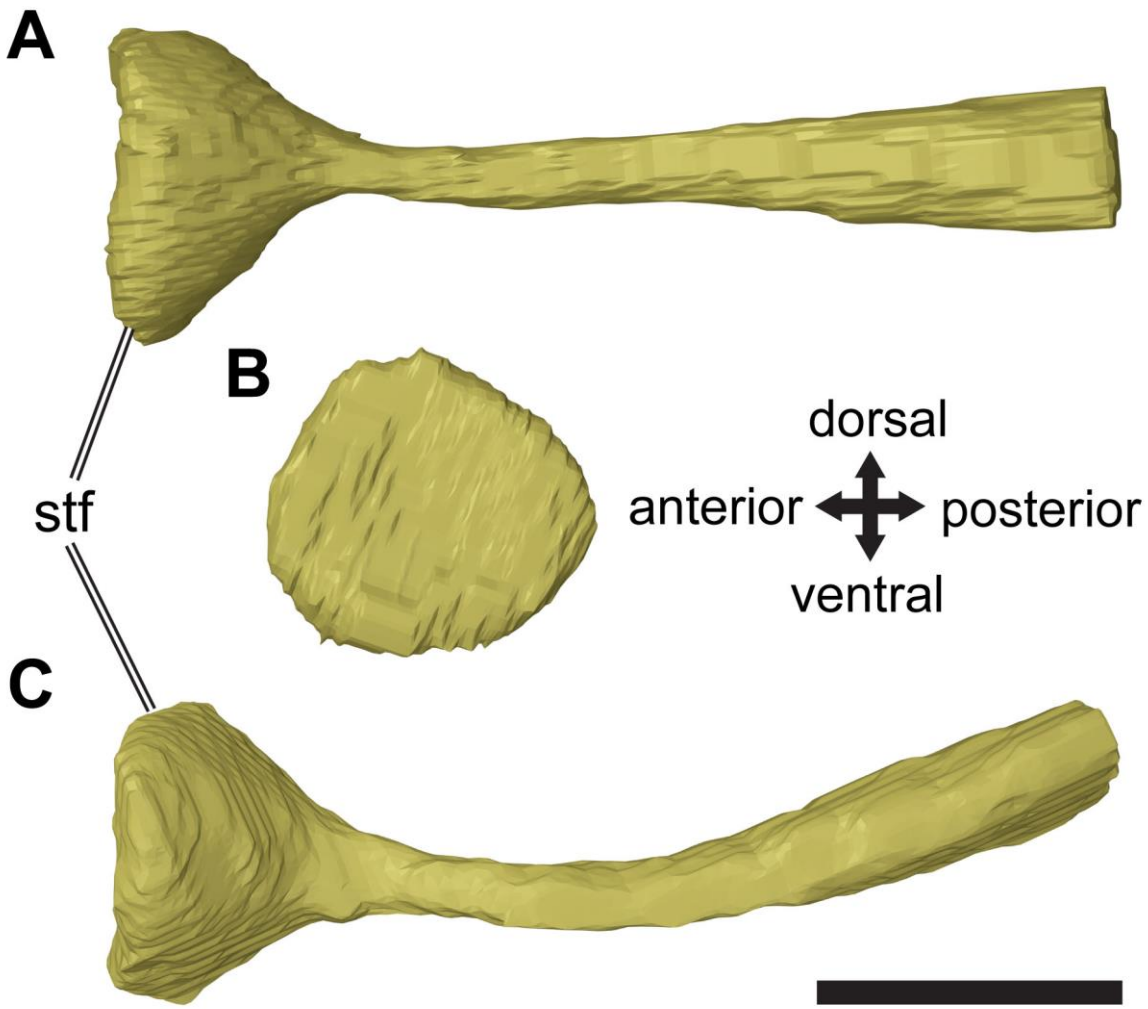


FIG. 3.31. 3D renderings of stapes of CAMSM B55776. **A**, dorsal view; **B**, medial view; **C**, posterior view. Scale bar equals 2 mm. Abbreviations: *stfp*, stapedial footplate.

3.4.7 Lower Jaw

3.4.7.1 Dentary

The dentary is preserved in articulation with the cranium in two of the *Rhinochelys* specimens that were CT scanned: CAMSM B55776 (*R. elegans sensu* Collins (1970); Fig. 3.32) and CAMSM B55783 (*R. cantabrigiensis sensu* (Collins 1970); Fig. 3.33). Both specimens have consistent dentary morphology, but CAMSM B55776 also includes the rest of the lower jaw elements on the right side, whereas CAMSM B55783 preserves only the left surangular. The

dentary contacts the coronoid posteromediodorsally, the surangular posteriorly, and the prearticular and angular medially.

The dentary of *Rhinochelys* consists of fused right and left rami, which meet in an anteroposteriorly extended symphysis that forms a triangular triturating surface dorsally. The symphyseal region is longer than in *Dermochelys coriacea* (UMZC R3031), but shorter than in cheloniids with extensive secondary palates, such as *Lepidochelys olivacea* (SMNS 11070). The rami of the dentary in *Rhinochelys* are mediolaterally narrow and straight processes that diverge at an angle of 55° from the symphysis in dorsal view. In lateral view, the depth of the rami increases slightly posteriorly toward the coronoid process (=processus coronoideus of Gaffney, 1979). Anteriorly, the dentary is gently curved dorsally to form a shallow, pointed beak. The labial ridge of the dentary is sharp-edged around the triturating surface and continues as a blunt ridge on the diverging dentary rami. The triturating surface also bears a median ridge, which extends over its entire anteroposterior length (Fig. 3.33). The edge of the ridge is sharp in both specimens, but the posterior end of the ridge is slightly expanded transversely in CAMSM B55776 (Fig. 3.32C), but it is not in CAMSM B55783. The triturating surface extends posteriorly onto the rami of the dentary, where it forms a narrow surface that slopes lingually.

A lingual ridge is absent in *Rhinochelys*. The lingual margin of the triturating surface forms the dorsal margin of the sulcus cartilaginis meckelii. This sulcus forms a shallow, longitudinal groove that extends from the medial surface of the dentary rami to the posterior surface of the symphyseal region. Here, it forms a deep anterior pocket that extends into the dentary ventrally to the level of the triturating surface. The sulcus cartilaginis meckelii becomes dorsoventrally deeper posteriorly on the dentary rami, and merges into the fossa meckelii. The subalveolar foramen (=foramen alveolare inferius of Gaffney 1979) opens from the posterodorsal margin of the sulcus cartilaginis meckelii into the dentary ramus. It extends anteromedially as the subalveolar canal (=canalis alveolaris inferior of Gaffney 1979). CT scans of CAMSM B55783 show that this canal extends to the anterior tip of the dentary and emits numerous smaller canals. Most of these canals branch from the dorsal side of the sub-

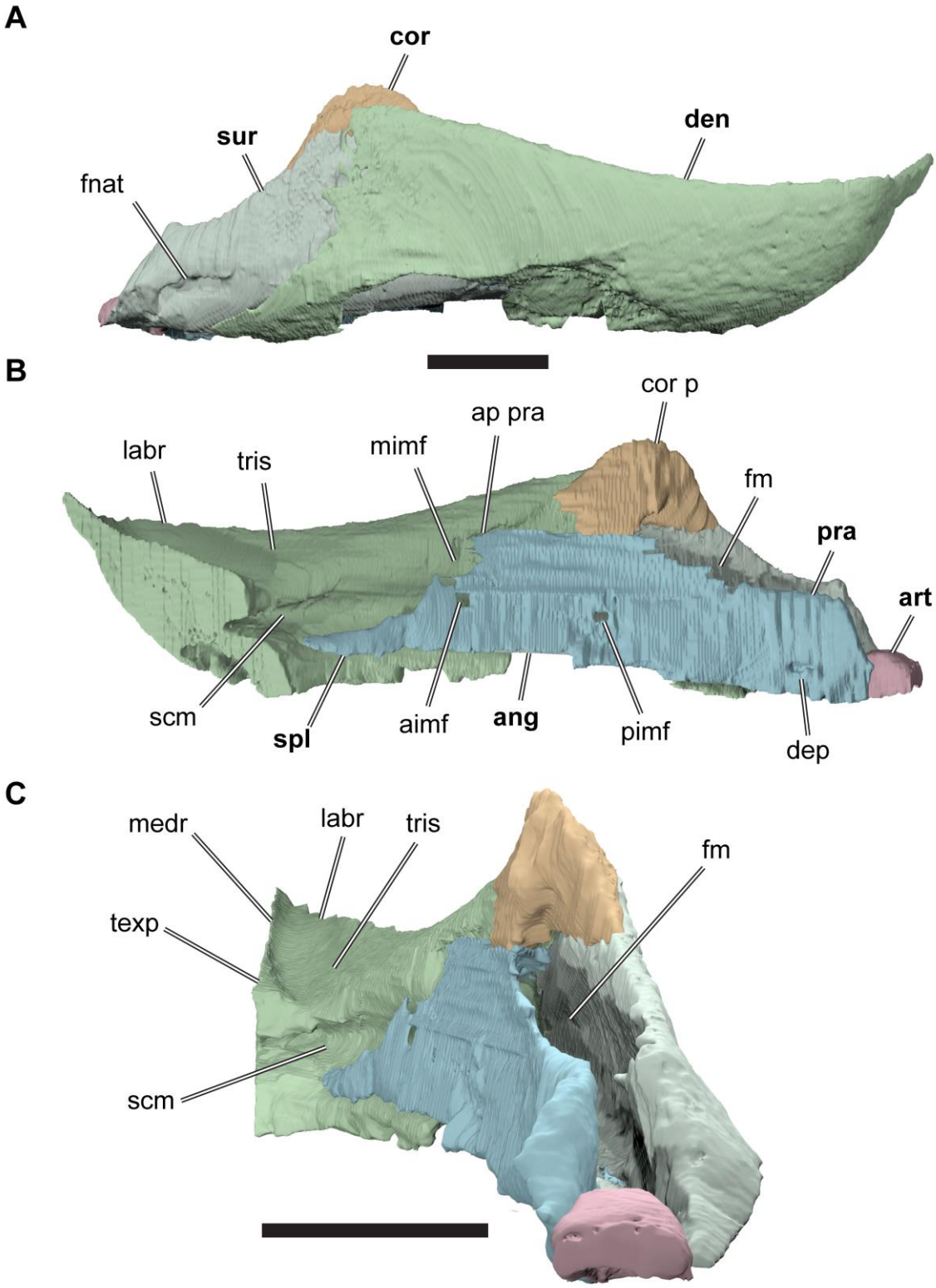


FIG. 3.32. 3D renderings of the right mandibular ramus of CAMSM B55776. **A**, lateral view; **B**, medial view; **C**, posterior view. Scale bars equal 5 mm. Note that bones are labelled in bold. Abbreviations: *aimf*, anterior intermandibular foramen; *ang*, angular; *ap pra*, anterior process of prearticular; *art*, articular; *cor*, coronoid; *cor p*, coronoid process; *den*, dentary; *dep*, depression; *fm*, fossa meckelii; *fnat*, foramen nervi auricolotemporalis *labr*; labial ridge; *medr*; median dentary ridge; *mimf*, medial intermanibular foramen; *pimf*, posterior intermandibular foramen; *pra*, prearticular; *scm*, sulcus meckelii; *spl*, splenial; *sur*, surangular; *texp*, triangular expansion; *tris*, triturating surface.

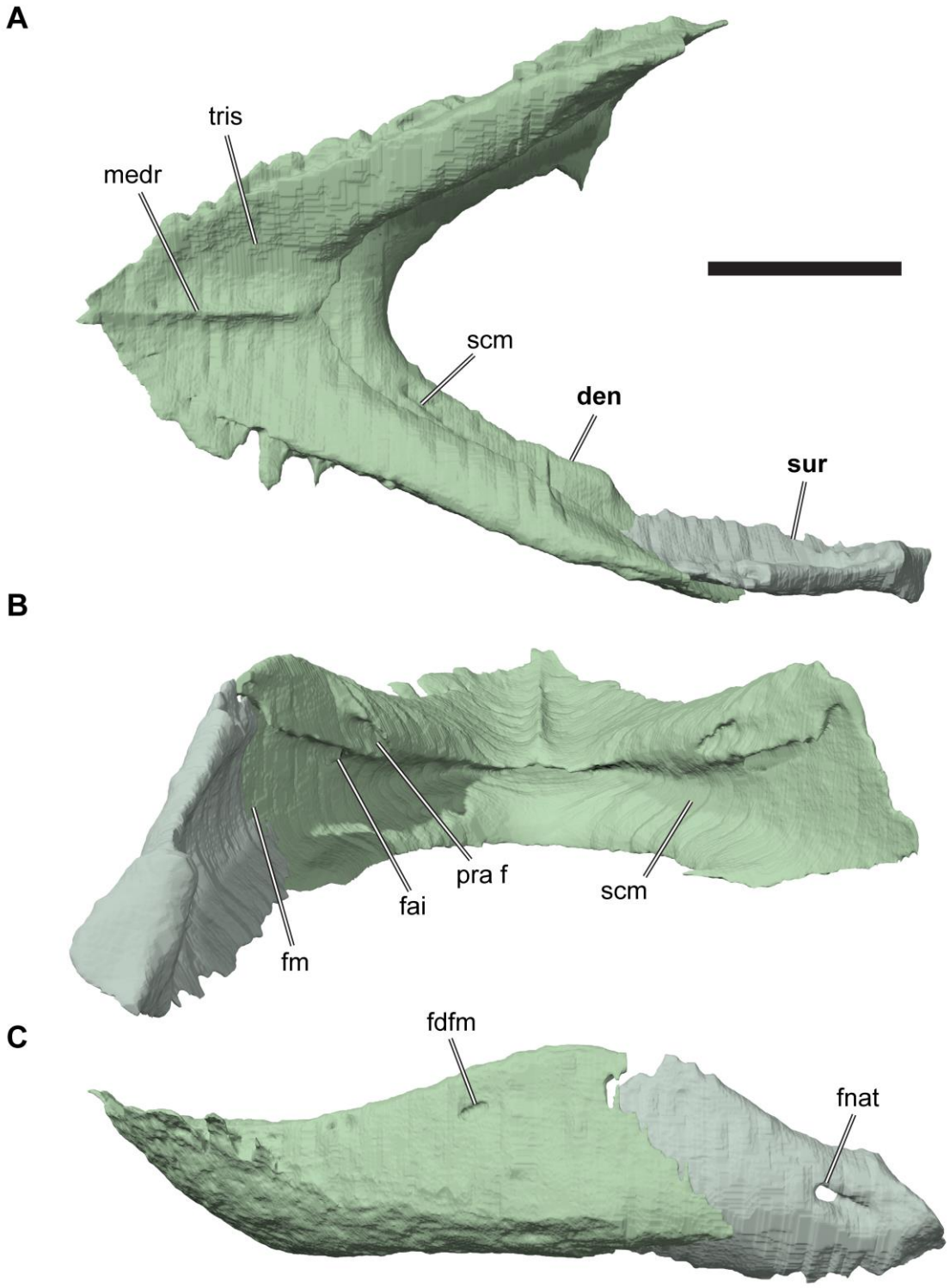


FIG. 3.33. 3D renderings of the mandible of CAMSM B55783. **A**, dorsal view; **B**, posterior view; **C**, left lateral view. Scale bar equals 5 mm. Note that bones are labelled in bold. Abbreviations: *den*, dentary; *fai*, foramen alveolare inferius; *fm*, fossa meckelii; *fnat*, foramen nervi auricolotemporalis; *for*, foramen; *medr*, median dentary ridge; *pra f*, prearticular facet; *scm*, sulcus meckelii; *sur*, surangular; *tris*, triturating surface.

alveolar canal, are posterodorsally directed, and exit the dentary on its lateral surface just ventral to the lingual ridge. The subalveolar foramen is covered medially by the prearticular

and angular and is not level with the medial intermandibular foramen (=foramen intermandibularis medius of Gaffney 1979; see Angular, Prearticular and Splenial, below), but positioned ventral to it.

The medial surface of the dentary has a small, anteriorly directed pocket on the posterior end of the triturating surface, dorsal to the level of the subalveolar foramen and the fossa meckelii. This pocket receives an anterior process of the prearticular. The ventral surface of the dentary is lingually expanded and ventrally convex, so that is covers the surangular ventrally. The lateral surfaces of the dentary rami are flat, and no distinct depression for the external mandibular adductor musculature is evident. Anterior to the coronoid process, the lateral surface bears a small foramen dentofaciale majus, which is anteromedially directed. The associated canal merges internally with the subalveolar canal.

3.4.7.2 Angular, Prearticular and Splenial

The bones on the medial surface of the mandible are preserved in CAMSM B55776, but the sutures between them cannot be completely traced in CT scans of the specimen. Consequently, these bones have been segmented as a single structure and are described together here (Fig. 3.32B–C). The topological positions of the preserved bones are consistent with their identification as a prearticular, which seems to be completely preserved, and a partially preserved angular. The angular usually covers most of the ventral margin of the mandible, but also extends onto its medial surface where it has its deepest extent at the level of the coronoid process. In CAMSM B55776, the ventral margin of the mandible is incompletely preserved, so large parts of the angular seem to be missing. As the sutural contacts between the elements of the medial mandibular surface are not clear in the available CT scans, and because our model of these elements extends far anteriorly, it is likely that a splenial is incorporated into the segmented model, which would be located in the anterior portion of the prearticular (Gaffney 1979).

The angular and prearticular form a thin vertical sheet that provides the medial wall of the fossa meckelii. The angular is anteroventrally positioned with respect to the prearticular (Gaffney 1979). Anteriorly, a thin, rod-like process extends into the floor of the sulcus cartilaginis meckelii, which we interpret to be the splenial. This anterior rod gets dorsoventrally deeper posteriorly, at which point it clearly represents part of the angular. The position of the angular-splenial contact is unclear. The medial mandibular elements cover the sulcus cartilaginis meckelii completely posterior to the position of the medial intermandibular foramen (foramen intermandibulare medius of Gaffney 1979). Posterior to this foramen, the sulcus cartilaginis meckelii is confluent with the fossa meckelii. In most turtles, the medial intermandibular foramen is located slightly posterior to the level of the subalveolar foramen (Gaffney 1979), but in *Rhinochelys* the angular and prearticular extend anteriorly to cover the subalveolar foramen medially.

Some indication of the angular-prearticular contact can be seen anteriorly, between the anterior and posterior intermandibular foramina (foramen intermandibulare oralis and foramen intermandibulare caudalis of Gaffney 1979, respectively). The former is located just ventral to the medial intermandibular foramen and seems to be contained mainly in the angular. The posterior intermandibular foramen is positioned posteroventral to the former, at the level of the anterior end of the coronoid process and seems to be formed largely by the prearticular. Posterior to this foramen the suture cannot be traced.

The prearticular articulates with a pocket of the dentary posterodorsal to the medial intermandibular foramen. The combined angular and prearticular have their deepest extent posterior to this articulation. The prearticular contacts the coronoid medially to the dorsal margin of the fossa meckelii.

Posterior to the contact with the coronoid, the prearticular gets dorsoventrally shallower, so that the surangular is exposed in medial view above the dorsal margin of the prearticular. At its posterior end, the prearticular becomes transversely slightly broader and contributes to the medial portion of the mandibular articulation facet (= area articularis mandibularis of Gaffney 1979). The posteroventral margin of the prearticular (and possibly

of the angular) contacts the articular. Just anterior to this expanded posterior end, there is a small but deep circular depression on the medial surface of the prearticular. The CT scans do not reveal if this depression leads to an interior canal and its identity is unclear.

The ventral margin of the angular forms a sharp edge that lies medially against the dentary with this contact continuing along the surangular more posteriorly. Along the surangular contact, the angular, and possibly more posteriorly the prearticular, are laterally expanded to form a short shelf that forms parts of the medial floor of the fossa meckelii.

3.4.7.3 Surangular

Surangulars are preserved on the right side of CAMSM B55776 (Fig. 3.32) and the left side of CAMSM B55783 (Fig. 3.33). The surangular of *Rhinochelys* is plate-like and situtated in the posterolateral portion of the mandible. It contacts the dentary anterolaterally, the coronoid anterodorsally, the prearticular/angular ventrally, the articular posteromedially and covers the fossa meckelii laterally. The ventral surface of the surangular is slightly expanded medially and meets the prearticular in the floor of the fossa meckelii.

The surangular reaches its greatest depth at the level of the coronoid, which it contacts along its dorsomedial surface. Both specimens have a semicircular, recessed facet on the medial surface of the dorsal tip of the surangular for articulation with the coronoid. The dorsal margin of the surangular is convex anteriorly around the coronoid contact. Posteriorly, the dorsal surangular margin is concave and slopes posteroventrally to the mandibular glenoid fossa. The surangular has an anteroventral process, which is preserved only in CAMSM B55776. The anteroventral process has a narrow, splint-like shape and extends along the angular in the floor of the fossa meckelii. More than half of the length of the surangular is covered laterally by the dentary.

The fossa meckelii is expressed as a broad depression on the medial surface of the surangular. The dorsal opening of the fossa meckelii is formed by the concave posterodorsal margin of the surangular laterally, the prearticular medially and the coronoid anterodorsally.

Posteriorly, the surangular expands mediolaterally to form a relatively broad articular process. The ventral margin of the posterior process is horizontally aligned with the anteroventral margin of the element in CAMSM B55776, so that the ventral margin of the surangular appears relatively straight. In contrast, the ventral margin is strongly curved convexly in CAMSM B55783 (Fig. 3.34). The posterior surface of the articular process is roughly triangular in outline in both specimens and forms a posterodorsally exposed facet for the mandibular glenoid. A short canal pierces the surangular just anterior to its articular process. The lateral opening of this canal is the foramen nervi auricolotemporalis, which is oval in shape. The short canal leads anteromedially through the surangular and exits into the posterior corner of the fossa meckelii. In CAMSM B55776, this medial opening is posteroventrally overlapped by a small lamina that is absent in CAMSM B55783 (Fig. 3.34).

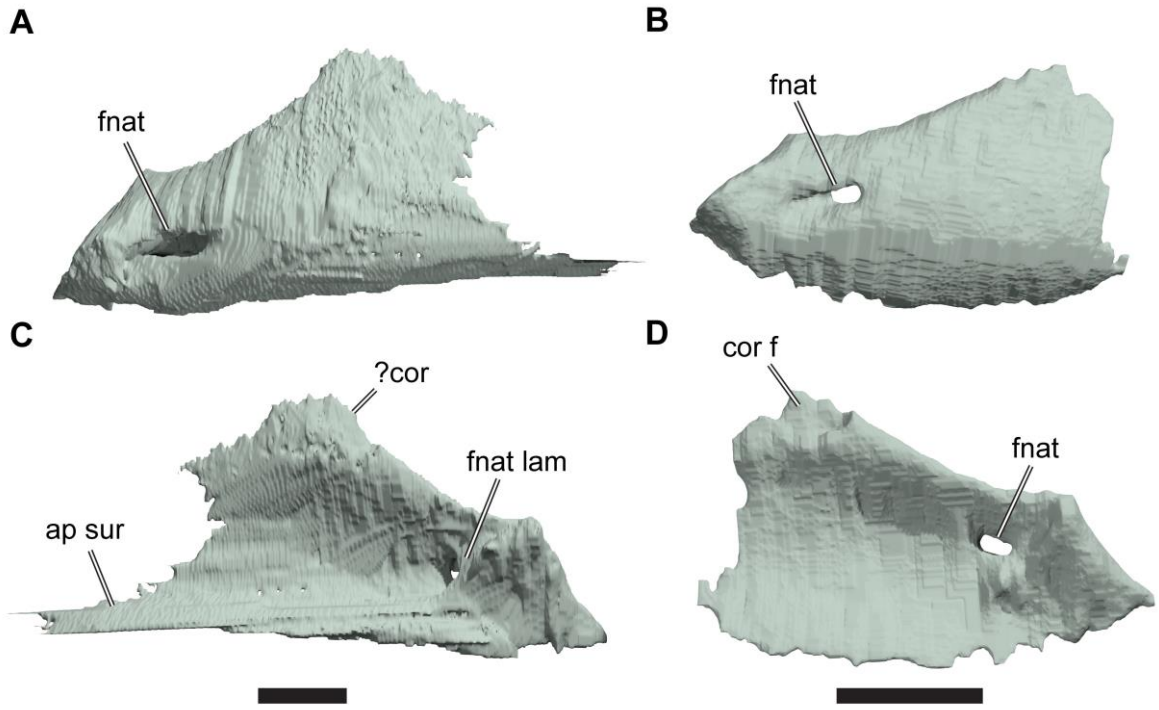


FIG. 3.34. Comparison of surangulars. **A**, 3D rendering of right surangular of CAMSM B55776 in lateral view; **B**, 3D rendering of left surangular of CAMSM B55783 in lateral view, reflected for comparison; **C**, 3D rendering of right surangular of CAMSM B55776 in medial view; **D**, 3D rendering of left surangular of CAMSM B55783 in medial view, reflected for comparison. Scale bars equal 3 mm. Abbreviations: *ap sur*, anterior process of surangular; *cor f*, coronoid facet; *fnat*, foramen nervi auricolotemporalis, *fnat lam*, foramen nervi auricolotemporalis lamina.

3.4.7.4 Coronoid

CAMSM B55776 is the only CT scanned specimen that includes a (right) coronoid. It is a small bone on the dorsal margin of the mandibular ramus (Fig. 3.32) and is positioned in its posterior third, so that the mandibular rami have much longer pre-coronoid than post-coronoid portions. The coronoid contacts the dentary anterolaterally, the surangular posterolaterally and the prearticular anteromedially.

The coronoid has a semilunate outline with a convex dorsal margin and an approximately straight ventral margin. Ventrally, it is slightly broader transversely than at its dorsal margin. The convex dorsal margin forms the coronoid process, which is relatively low in *Rhinochelys*. With its ventral surface, the coronoid forms a bridge over the fossa meckelii, forming parts of its roof and its anterodorsal border. The coronoid is overlapped laterally by the dentary in its anterior part and by the surangular in its posterior part, so that most of its lateral surface is obscured in lateral view.

3.4.7.5 Articular

The articular is preserved on the right side of CAMSM B55776. It is a small, block-like element situated at the posterior end of the jaw (Fig. 3.32B–C). In *Rhinochelys*, it is triangular, anteriorly narrow and posteriorly broad. It is wedged between the posterolateral end of the prearticular and the posteromedial corner of the articular process of the surangular. In many turtles, the articular forms the posterior wall of the fossa meckelii, but in *Rhinochelys* the element is dorsoventrally low and posteriorly displaced, so that the fossa meckelii seems to be completely closed posteriorly by the surangular and prearticular. The dorsal surface of the articular is a convex hemisphere as in pleurodires and lacks the longitudinal ridge that commonly separates it into medial and lateral articular facets as commonly observed in cryptodires (Gaffney 1979). The mandibular glenoid fossa is shared between the prearticular, surangular and articular, with the latter two bones contributing most of its surface. A

foramen posterius chorda tympani is absent, which is also the case in modern cheloniids (Gaffney 1979). A convexity for the insertion of the M. depressor mandibulae is also absent in *Rhinochelys*.

3.5 PRINCIPAL COMPONENT ANALYSIS

3.5.1 Skull measurements and PCA procedure

I recorded a set of measurements for all specimens of *Rhinochelys* that I investigated first-hand. Proportional differences based on these measurements have been used as autapomorphies for various species of *Rhinochelys* (Collins 1970; Scavezzoni & Fischer 2018; see Discussion). Because some authors have raised doubts regarding the taxonomic utility of these measurements and ratios (Smith 1989; Hooks 1998), I reproduced the measurements of Collins (1970) and added some new measurements: (1) pre-parietal skull length (measurement 'z' of Collins 1970); (2) skull width (measurement 'x' of Collins 1970); (3) skull height (measurement 'y' of Collins 1970). I modified measurement 'y' of Collins (1970), which was illustrated as the skull height from the labial ridge of the skull to the frontal sulcus, and instead measured the skull height from the lateroventral skull margin to the skull roof formed by the parietals, because this was easier to measure; (4) interorbital skull width (new measurement); (5) nasal length–width ratio (new measurement). Because we found the nasal bones to show extreme shape variation (see Description and Discussion), I measured the anteroposterior length of the left and right nasals along their median contact on the skull roof, the straight-line mediolateral width of the nasals at the narial margin, and calculated the length–width ratio for nasals from these measurements; (6) the 'jaw angle' of Collins (1970), which was described as the 'angle between the two maxillae' (Collins 1970: p. 357), was measured by drawing straight lines through the labial ridges of the maxillae in ventral view of photographs and taking the angle between the resulting lines. All length measurements were taken with digital calipers and the 'jaw angle' was measured in the software ImageJ. I

did not take individual measurements when a specimen was extremely distorted, which was specifically the case for several skull height and width measurements. Data for *R. ambareti* were measured from the figures provided in Scavezzoni & Fischer (2018). All measurements are shown in Table 3.2.

TABLE 3.2. PCA results for our analysis using all measurements (n=27).

	PC1	PC2	PC3	PC4	PC5	PC6	PC7
Eigenvalues	3.962	1.712	0.751	0.243	0.164	0.128	0.041
Proportion of total variance explained	0.566	0.245	0.107	0.035	0.023	0.018	0.006
Proportion of shape variance explained	-	0.563	0.247	0.08	0.054	0.042	0.014
Eigenvector coefficients							
Right nasal length–width ratio	-0.143	-0.686	-0.235	0.261	-0.422	0.453	0.050
Left nasal length–width ratio	-0.255	-0.606	-0.129	-0.446	0.438	-0.400	-0.011
Jaw angle	-0.245	0.318	-0.881	0.043	0.164	0.093	-0.160
Width	-0.460	-0.034	0.190	0.664	0.055	-0.386	-0.398
Orbital width	-0.477	0.117	0.145	0.180	0.355	0.250	0.719
Pre-parietal length	-0.455	0.118	0.307	-0.392	0.059	0.528	-0.498
Heigth	-0.456	0.178	-0.032	-0.322	-0.686	-0.368	0.222

To determine whether these measurements support the taxonomy of Collins (1970) and Scavezzoni & Fischer (2018), I used Principal Component Analysis (PCA) to investigate if specimens assigned to different species form separate clusters in morphospace. I only included the skull width, the skull height, the pre-parietal skull length and the 'jaw angle' in a first analysis, as these were the measurements considered originally by Collins (1970). All my measurements were included in a second analysis. The PCA was conducted on those specimens, for which all respective measurements could be taken (n= 31 for first analysis; n = 27 for second analysis; see Table 3.2) and was computed in R (R Core Team 2016) using the *prcomp* command and the 'scale = TRUE' argument. This argument transforms the data to have unit variance, which is important for my data because it includes measurements of different units and equivalent to using a correlation matrix (Jolliffe & Cadima 2016). Because the first Principal Component (PC1) described size and allometric shape changes (see PCA results), I excluded it for constructing bivarite morphospace plots and re-scaled the absolute variance explained by the remaining PCs to represent the proportion of non-size (i.e. shape)

variation. I assigned colours to individual specimens according to the taxonomic identification of Collins (1970) and assigned a different point symbol to the holotype specimens of all four species. R code for the PCAs used in this study are printed in Appendix S2.

3.5.2 PCA results

The principal component analyses show similar patterns across our data partitions. For brevity, only results from the second PCA (including all measurements) are presented in detail but results for the first PCA are presented in Appendix S2 (Table S2.1, Fig. S2.14).

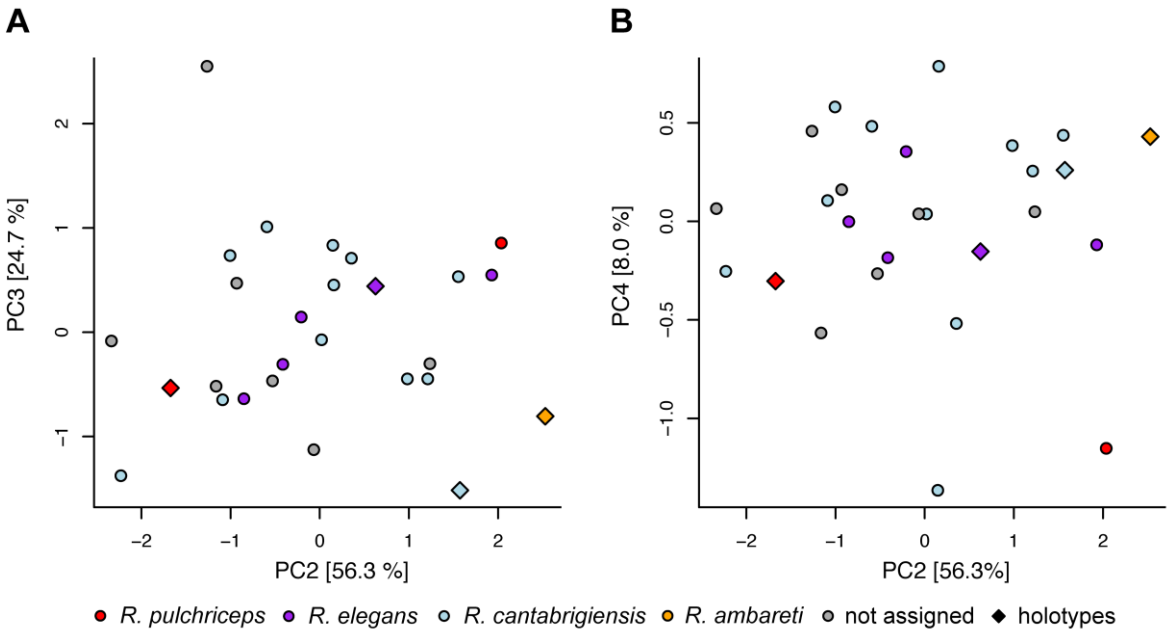


FIG. 3.35. Distribution of specimens of *Rhinochelys* (n = 27) in cranial geometry morphospaces recovered by Principal Component Analysis of seven cranial measurements. **A**, PC1 vs. PC2; **B**, PC1 vs. PC3.

More than 90% of the variance can be explained by the first three principal components (PC1–3) (see Table 3.3; Fig. 3.35). PC1 explains 56.6% of the variance in the data and describes relative increases in skull size, 'jaw angle' and nasal length–width ratio, as the eigenvector coefficients all have the same sign (Table 3.3). PC1 therefore represents size and allometric shape changes. For the bivariate morphospace plots in Figure 3.35, PC1 was

excluded to only visualise non-size variation among the data. PC2 explains 56.3% of the shape variance (24.5% of total variance including PC1) and largely describes relative increases in the nasal length–width ratio with decreases in skull size. PC3 explains 24.7% of the shape variance (10.7% of the total variance) and is predominantly determined by relative increases in nasal length–width ratio and 'jaw angle' with decreases in length measurements. PC4 explains 8% of the shape variance (5.4% of the total variance), and describes asymmetry between the right and left nasals, as well as a trend of decreasing skull height and length with increasing width.

Figure 3.35A–B shows that specimens do not form clusters but are seemingly randomly distributed in morphospace. The colouration of specimens according to the identification published by Collins (1970) indicates that specimens that were said to belong to different species are not separated from specimens of other species. Instead, the distribution of points on PC2–4 indicates a continuum of variation among Collins' (1970) diagnostic characters and my new measurements. Furthermore, the holotype specimens are relatively close to one another in morphospace, and do not fall in extreme opposites of the morphospace as would be expected if strong and systematic morphological variation was present between them.

TABLE 3.3. PCA results for our analysis using all measurements (n=27).

	PC1	PC2	PC3	PC4	PC5	PC6	PC7
Eigenvalues	3.962	1.712	0.751	0.243	0.164	0.128	0.041
Proportion of total variance explained	0.566	0.245	0.107	0.035	0.023	0.018	0.006
Proportion of shape variance explained	-	0.563	0.247	0.08	0.054	0.042	0.014
Eigenvector coefficients							
Right nasal length–width ratio	-0.143	-0.686	-0.235	0.261	-0.422	0.453	0.050
Left nasal length–width ratio	-0.255	-0.606	-0.129	-0.446	0.438	-0.400	-0.011
Jaw angle	-0.245	0.318	-0.881	0.043	0.164	0.093	-0.160
Width	-0.460	-0.034	0.190	0.664	0.055	-0.386	-0.398
Orbital width	-0.477	0.117	0.145	0.180	0.355	0.250	0.719
Pre-parietal length	-0.455	0.118	0.307	-0.392	0.059	0.528	-0.498
Heigth	-0.456	0.178	-0.032	-0.322	-0.686	-0.368	0.222

3.6 DISCUSSION

3.6.1 Taxonomy of Rhinochelys

The type species of *Rhinochelys* was described by Owen (1851) as *Chelone pulchriceps* based on a skull in a phosphatic nodule from the Cambridge Greensand Member of the West Melbury Marly Chalk Formation (early Cenomanian, 100.5–93.9 Ma; Hopson 2005), near Barnwell, Cambridgeshire (Owen 1851). Seeley (1869) made *C. pulchriceps* the type species of a new genus, *Rhinochelys*, without giving specific reasons. However, he provided a diagnosis for the genus (Seeley 1869: p. 25). Seeley (1869) also named 15 other species of *Rhinochelys* but did not provide descriptions for any of these species, so that they were soon considered to be invalid by Lydekker (1889: p. 229) and were later considered to be *nomina nuda* (e.g. Collins 1970). Lydekker (1889) named five new species of *Rhinochelys* (*R. cantabrigiensis*, *R. macrorhina*, *R. elegans*, *R. brachyrhina*, *R. jessoni*), and provided specimen numbers, figures, and differential diagnoses for all of them. Half a century later, Moret (1935) coined another species, *Rhinochelys ambareti*, based on a skull from the late Aptian–Cenomanian Marnes Bleues Formation near Villard-de-Lans in France, which is roughly contemporaneous with the Cambridge Greensand Member (the locality for the specimen is dated to be late Albian [113–100.5 Ma]; Moret 1935; Scavezzoni & Fischer 2018).

Collins (1970) revised the British material of *Rhinochelys* based on specimens in the CAMSM and NHMUK. She recognized three morphotypes and accordingly only considered three previously named British species of *Rhinochelys* valid: *R. pulchriceps*, *R. elegans* and *R. cantabrigiensis* (Collins 1970). These species were distinguished from one another based on seven features, four of which were angles or ratios of skull measurements, and the rest were based on osteological features related to the snout and cranial scale sulci. Collins (1970) considered *R. ambareti* distinct from the British material based on slightly different skull ratios and a wider angle with which the maxillae diverge posterolaterally from the midline of the skull ('jaw angle' of Collins 1970). Collins' (1970) work represents a thorough description

of the *Rhinochelys* material, but the preservation of most specimens in phosphatic nodules prevented detailed description of the internal anatomy. Collins' (1970) braincase description was based on a specimen (CAMSM B94606) that is larger than all of the other specimens of *Rhinochelys* (Hooks 1998). Other authors (Smith 1989; Hooks 1998) noticed this size discrepancy and Hooks (1998) provided some anatomical arguments (such as the large contributions of the vomer and palatine to the palate) to exclude this specimen from *Rhinochelys*. Collins (1970) referred *Rhinochelys* to Protostegidae based on comparative anatomical arguments such as the presence of nasal bones, the absence of a secondary palate and the contribution of frontals to the orbit. Since then most authors have agreed with this referral and later phylogenetic work provided further evidence for the protostegid affinities of *Rhinochelys* (Hirayama 1994; Hooks 1998; Cadena & Parham 2015; Evers & Benson 2018*a*).

Collins (1970) tentatively assigned postcranial material of the species *Cimochelys benstedti*, which was also found in the Cambridge Greensand Member of the West Melbury Marly Chalk Formation, to *Rhinochelys* because of the protostegid affinities of the former, despite a lack of overlapping skeletal elements. Later authors largely followed this referral (Hirayama 1997; Hooks 1998; Tong *et al.* 2006). Hooks (1998) provided a systematic review of the Protostegidae. For his phylogenetic work, he used all *Rhinochelys* material (i.e. all four species considered valid by Collins 1970) to score a monotypic *Rhinochelys* because the different species did not vary from one another in the characters he used. However, Hooks (1998) did not provide a formal synonymization and stated that "it is clear that more work needs to be done on the systematics of *Rhinochelys*" (Hooks 1998: p. 87). Similarly, Hooks (1998) listed *Cimochelys benstedti* as a valid species in the systematic palaeontology section of his work, but none the less combined the hypodigms of *Cimochelys* and *Rhinochelys* in the production of his phylogeny.

Tong *et al.* (2006) described another species, *Rhinochelys nammourensis*, from the middle Cenomanian of Lebanon. The new material presented by Tong *et al.* (2006) includes completely preserved specimens with skull–postcranium associations on slabs, and even soft

tissue is preserved around the flippers. Several individuals were described, including hatchling, juvenile and adult specimens. The material was referred to *Rhinochelys* based on the presence of large nasal bones and an anteriorly bulged maxilla-prefrontal region (Tong *et al.* 2006). The shell of *Rhinochelys nammourensis* shows clear protostegid synapomorphies, such as 'star-shaped' plastral elements with strongly serrated margins. The shell of *Rhinochelys nammourensis* differs from the *Cimochelys* material from England in the number of suprapygals and the successive posterior increase in width of the vertebral scutes (Tong *et al.* 2006). Tong *et al.* (2006) accepted the synonymy of *Cimochelys* with *Rhinochelys*, but presented only gross morphological observations, such as the carapacial outline and the size of fontanelles as evidence for this hypothesis.

Recently, Scavezzoni & Fischer (2018) reassessed the holotype material of *R. amabareti* and argued for the validity of this species based on a number of proposed autapomorphies related to the narial region (e.g. shape of the nasal bone and the external naris outline), the preorbital bulge and skull measurement ratios. However, many of their comparisons are based on accepting the taxonomy of Collins (1970) for British species of *Rhinochelys*. Scavezzoni & Fischer (2018) referred several previously unreported skulls from the Cambridge Greensand Member to 'morphotypes' that follow the taxonomy of Collins (1970). These specimens were then used, together with published information, to code the OTUs for phylogenetic analysis including the different *Rhinochelys* species. Characters relevant to the diagnoses of the proposed *Rhinochelys* species were included to achieve resolution within the dataset (Scavezzoni & Fischer 2018). Scavezzoni & Fischer (2018) found *Rhinochelys* to be polyphyletic, whereby *R. ambareti*, *R.nammourensis* and *R. pulchriceps* formed a clade that was the sister group to a clade including Late Cretaceous protostegids such as *Archelon ischyros* and *Protostega gigas*, whereas the *R. cantabrigiensis* and *R. elegans* morphotypes were found in a clade with Early Cretaceous taxa such as *Santanachelys gaffneyi*, *Bouliachelys suteri* and *Desmatochelys padillai*. Scavezzoni & Fischer (2018) suggested that some specimens in their sample showed differences to all other morphotypes, and may thus represent an additional, unnamed species of *Rhinochelys*.

My CT scans, and the resulting 3D models of individual skull bones, allow me to systematically assess variation among specimens that have been assigned to the species *Rhinochelys pulchriceps*, *Rhinochelys cantabrigiensis* and *Rhinochelys elegans*, including the holotypes. Although variation is present among the sample of specimens used for my work, I demonstrate that the apparent variation does not reflect the species delimitation proposed by Collins (1970). Furthermore, I do not find evidence for distinct morphotypes (i.e. clusters) in either morphometric or osteological features. The continuum of variation observed here suggests instead the presence of intraspecific variation of a single species. The holotype specimens of *R. elegans* and *R. cantabrigiensis* do not show unique autapomorphies or unique character combinations and are therefore considered subjective junior synonyms of *R. pulchriceps*. *R. ambareti* is also synonymised with *R. pulchriceps*, as the holotype of the former also lacks distinctive features (see Discussion below for details). Therefore, I only consider the type species, *R. pulchriceps*, to be valid from among the proposed European species.

Nevertheless, the presence of morphologically distinguishable cranial, mandibular and postcranial material in the collections of the CAMSM indicates a formerly cryptic diversity of sea turtles, and possibly protostegids, in the Cambridge Greensand Member of the West Melbury Marly Chalk Formation. Although I agree with previous authors that the holotype postcranium of *Cimochelys benstedti* has protostegid affinities, the lack of anatomical overlap with the holotype skull of *R. pulchriceps* prevents synonymisation of *C. benstedti* with *R. pulchriceps*, which I therefore reject provisionally. Future discoveries could resolve whether the holotype of *C. benstedti* is conspecific with *R. pulchriceps*, or with one of the other (unnamed) turtles of the Cambridge Greensand Member.

I provisionally accept *Rhinochelys nammourensis* as a valid species pending a detailed comparison of its cranial material with *Rhinochelys pulchriceps*.

3.6.2 Status of proposed diagnostic characters of Rhinochelys *species*

Rhinochelys is known from an exceptional number of skulls, many of which are largely complete and relatively well-preserved (at least 30 essentially complete skulls). Regardless of their taxonomic conclusions, all papers on the anatomy *Rhinochelys* have found a large amount of variation among specimens (Collins 1970; Scavezzoni & Fischer 2018; this study). This variation has been used to support the validity of four species (*R. pulchriceps*, *R. cantabrigiensis*, *R. elegans*, *R. ambareti*) from Europe alone (Collins 1970; Scavezzoni & Fischer 2018). Scavezzoni & Fischer (2018) even tentatively suggested the existence of a new, albeit unnamed, species. However, several authors questioned this high species diversity (e.g. Smith 1989; Hirayama 1997; Hooks 1998) and have argued that the variation documented by Collins (1970) is insufficient to support her proposed taxonomy. Both Collins (1970) and Scavezzoni & Fischer (2018) used cranial measurements and proportions, as well as osteologically variable features, to support their taxonomic opinions. Here, I discuss and reinterpret previously proposed autapomorphies for the various European species of *Rhinochelys*.

Measurements of the holotype specimens. My CT scans and derived 3D models allowed me to more accurately measure aspects of the morphology of *Rhinochelys*, because I could use digitally enlarged versions of the skulls and make our measurements explicitly in three-dimensions. The digital removal of matrix also allowed me to take some taphonomic artefacts into account. For the holotype specimens that I CT scanned, I find less variance than reported by Collins (1970). For example, the 'jaw angle' of Collins (1970) was a central part of her proposed taxonomy. However, my measurements for the 'jaw angle' differ considerably from those of Collins (1970), with values ranging from 49–57° for the holotype specimens of the European *Rhinochelys* species (Table 3.4), whereas the values measured by Collins (1970) range from 50–105°.

I found similar discrepancies regarding the dorsoventral height of the skull relative to the anteroposterior length, and the mediolateral width relative to the anteroposterior length, ratios that were used by Collins (1970) to group specimens into categories of narrow or wide and deep or high skulls. Moreover, some measurements of Collins (1970) do not reflect the

actual dimensions of the skulls when preservation is taken into account. For example, *R. cantabrigiensis* was said to have the relatively broadest skull of the three British species (Collins 1970). However, my digital model of the *R. cantabrigiensis* holotype (NHMUK PV OR43980) shows that the specimen is partially disarticulated across the skull midline, artificially increasing the apparent width of the specimen (Fig. 3.2C). Additionally, the postorbitals on both sides are not tightly articulated with the parietals and frontals and seem to have slipped laterally, further increasing the width. These gaps between the bones account for c. 12% of the uncorrected postorbital width of the specimen. If this artificial widening is removed (as in the measurement reported in Table 3.4), the holotype specimen of *R. cantabrigiensis* has similar proportions to other specimens of *Rhinochelys*.

TABLE 3.3. Comparison of measurements taken by Collins (1970) and this study for holotype specimens of different *Rhinochelys* specimens. 'X' denotes Collins' (1970) measurement of the skull width; 'Y' denotes Collins' (1970) measurements of the skull height; 'Z' denotes Collins' (1970) measurement of pre-parietal skull length. Note that measurements of 'Y' used for this table were measured as originally done by Collins (1970), whereas this measurement was modified for the data used as input for the PCA.

		Jaw angle [in °]		X/Z*100		Y/Z*100	
Specimen number	**Holotype**	**Collins (1970)**	**This study**	**Collins (1970)**	**This study**	**Collins (1970)**	**This study**
CAMSM B55775	*R. pulchriceps*	72	49	107	150	51	88
NHMUK PV OR43980	*R. cantabrigiensis*	50	57	107	136	62	96
NHMUK PV R2226	*R. elegans*	57	48	96	133	57	118
UJF-ID.11167	*R. ambareti*	?105	57	135	154	65	122

Similar arguments can be made for the holotype and only specimen of *R. ambareti* (UJF-ID.11167): Scavezzoni & Fischer (2018) suggested that a 'dorsoventrally compressed' skull was an autapomorphic feature of *R. ambareti*. However, this specimen lacks most of the braincase, palate and the descending processes of the parietal. Therefore, the central architecture for structural support of the skull is absent, resulting in little resistance to taphonomic dorsoventral compression. Indeed, the posterior view of the specimen (Scavezzoni & Fischer 2018: Fig. 3.3C) shows clearly that the skull is distorted, with the right quadrate and parietal/postorbital being quite strongly dorsoventrally compressed.

Therefore, the low depth of *R. ambareti* can be explained by taphonomic compression and should not be regarded as supporting evidence for the validity of this taxon. This taphonomic compression also undermines two of the other autapomorphies proposed by Scavezzoni & Fischer (2018), namely the parallel outlines of the skull roof and the ventral margin of the maxilla and the mediolaterally broad external naris, which are both unlikely to reflect the original morphology. Furthermore, my PCA results (using only the measurements of Collins 1970, as well as an extended measurement dataset) show no clusters that would support proportional differences between the specimens assigned to previously recognized species (see Results).

Osteological variation. Although proportional differences among proposed species of *Rhinochelys* are not supported by our study, Collins (1970), Scavezzoni & Fischer (2018) and I noted variation in some osteological features that might support species-level distinctions. Collins (1970) only found unique osteological traits for *R. cantabrigiensis*, while *R. elegans* and *R. pulchriceps* were distinguished based solely on proportional differences. Proposed autapomorphies of *R. cantabrigiensis* were the presence of a ridge of the maxillary sulcus, a convex profile to the premaxillae and a hooked tip to the upper jaw (Collins 1970). My CT scans of the *R. cantabrigiensis* holotype (NHMUK PV OR43980) show that the anterior parts of the labial margins of both skull sides are broken in this specimen (see Fig. 3.2D). This results in a strongly convex labial margin of the maxillae when seen in lateral view (Fig. 3.2A–B), and also in a somewhat acute tip to the premaxillary labial margin. The strongly curved labial margins and the hooked tip of the upper jaw are the result of this breakage. I also investigated if referred specimens of *R. cantabrigiensis* preserve a hooked beak but found them to be absent in all specimens in which this part of the skull is well-preserved (e.g. CAMSM B55783; Fig. 3.10).

When considering only adequately preserved specimens, I agree with Collins (1970) that the outline shape of the ventral margin of the maxilla is somewhat variable. This margin is relatively straight in lateral view in several *Rhinochelys* specimens (e.g. NHMUK PV OR35197), but moderately ventrally convex in others (e.g. CAMSM B55783). Despite this

variation, breakage in the holotype specimens of *R. pulchriceps* and *R. cantabrigiensis* make a consistent association between the shape of the ventral margin of the maxilla and the species proposed by Collins (1970) impossible. Additionally, several authors have reported large amounts of intraspecific variation in the shape of the snout and triturating surface margin for several turtle species, including sea turtles (e.g. Dalrymple 1977; Smith 1989), which indicates that slight variation in the shape of the labial ridges are not well suited for species distinction. I agree with Collins (1970) that the maxillary sulcus of NHMUK PV OR43980 is particularly deep, which gives the impression of a 'ridge' dorsal to the sulcus (Fig. 3.2A–B). However, the sulci are very variably developed among all specimens of *Rhinochelys* (see below), and virtually absent in some of the specimens that Collins (1970) considered to belong to *R. cantabrigiensis* (CAMSM B55783; see Fig. 3.10), so that I do not think that this feature is diagnostic for *R. cantabrigiensis*.

Most of the autapomorphies listed by Scavezzoni & Fischer (2018) for *R. ambareti* are dubious, because they can be explained by dorsoventral compression of the holotype specimen, or because they are not unique to *R. ambareti*. For example, the antorbital bulge of the maxilla and prefrontal is said to be more prominent in *R. ambareti* than in other species of *Rhinochelys*, and its visibility in ventral view is listed as a proxy for this (Scavezzoni & Fischer 2018). However, the antorbital bulge is visible in ventral view in almost all specimens of *Rhinochelys* (e.g. Figs 3.1D, 3.2D, 3.3D, 3.4D, 3.5D, 3.9), and its presence is generally considered apomorphic for the genus (e.g. Collins 1970; Tong *et al.* 2006). Another proposed autapomorphy of *R. ambareti*, a mediolaterally broad external naris (with a horizontal long axis), is also present in other specimens, notably in the holotype of *R. pulchriceps* (CAMSM B55775; see Fig. 3.1E), and thus cannot be an autapomorphy for *R. ambareti*. I agree with Scavezzoni & Fischer (2018) that the nasal of *R. ambareti* is extremely short anteroposteriorly and broad mediolaterally. However, my nasal length-width ratio measurements show that there is great variation in the nasal shape of *Rhinochelys*, and the PCA including nasal shape does not distinguish *R. ambareti* significantly from other *Rhinochelys* specimens. The mediolaterally short contact between the nasals and the frontals

of *R. ambareti* is indeed shorter than in most other specimens of *Rhinochelys*. However, UK specimens of *Rhinochelys* also show high levels of variation in this aspect of nasal morphology, so this feature does not provide a reliable diagnosis of *R. ambareti*. In summary, I do not consider the osteological evidence presented by either Collins (1970) or Scavezzoni & Fischer (2018) to unambiguously support the existence of multiple European species of *Rhinochelys*.

3.6.3 Osteological variation found in this study

Osteological features that varied across the *Rhinochelys* specimens that I CT scanned are mentioned above (see Description), but to facilitate taxonomic discussion they are listed here and shown in Table 3.5. The most distinct variation that I observed in my sample of *Rhinochelys* occurs in the dermatocranium. Besides the nasal shape, which has already been discussed, variation in the dermatocranium is found in the configuration of the jugal, the shape of the fissura ethmoidalis, in the presence vs. absence of a foramen antrum postoticum (indicating the internal presence of an antrum postoticum) and in the otic trochlear process. Variation is also evident in the braincase elements, namely the exoccipitals (presence vs. absence of a posterior ridge), the basioccipital (presence vs. absence of a crista dorsalis basioccipitalis) and the position of the foramen posterius canalis carotici interni (fpcci) either between the pterygoid and parabasisphenoid, or only within the pterygoid. The epidermal sulci of *Rhinochelys* are also variably developed. In most specimens, a distinct maxillary sulcus is present between the body of the maxilla and the ascending process. This sulcus pronounces the antorbital bulge of the maxilla and prefrontal that is characteristic of all *Rhinochelys* specimens, but is only faintly developed or absent in some specimens. Similarly, the sulcus present on the frontals is variably developed.

TABLE 3.4. Osteological variation found across specimens of *Rhinochelys* that were examined using CT data. Note that 'fpcci' means foramen posterius canalis carotici interni; 'ptery.' means pterygoid; and 'pbsph' means parabasisphenoid.

	Osteological features									
Specimen number	**Taxonomy (*sensu* Collins [1970])**	**Foramen antrum post-oticum**	**Trochlear process bulk formation**	**Fissura ethmoi-dalis**	**Posterior jugal process**	**Exoccipital ridge**	**Fpcci formation**	**Crista dorsalis basi-occipitalis**	**Maxillary sulcus**	**Frontal sulcus**
CAMSM B55775	*R. pulchriceps* (holotype)	absent	quadrate	V-shaped	NA	present	ptery. + pbsph	absent	deep	deep
NHMUK PV R2226	*R. elegans* (holotype)	absent	prootic	con-stricted	present	NA	NA	NA	moderate	faint
NHMUK PV OR43980	*R. cantabrigiensis* (holotype)	absent	prootic	V-shaped	present	NA	ptery. + pbsph	absent	deep	absent
CAMSM B55783	*R. cantabrigiensis*	present	prootic	con-stricted	present	absent	ptey. + pbsph	NA	absent	absent
CAMSM B55776	*R. elegans*	present	prootic	V-shaped	present	NA	ptery	NA	moderate	moderate
NHMUK PV OR35197	*R. elegans*	present	prootic	V-shaped	absent	NA	ptery. + pbsph	present	faint	absent

Taxonomic interpretation. In most cases, the osteological variation documented herein does not correspond with the possible species proposed for *Rhinochelys* (see Table 5). Most of these features are either present in several of the holotype specimens for *R. pulchricpes*, *R. cantabrigiensis* and *R. elegans*, or present in a holotype specimen but not in any of the other specimens that were referred to that species by Collins (1970). Also, there is no obvious pattern of covariation between the variable traits, so that this variation does not support an alternative taxonomic division of *Rhinochelys*. The only possible exceptions are two features that are present exclusively in the *R. pulchriceps* holotype (CAMSM B55775), namely the presence of an exoccipital ridge (see Fig. 3.23) and the enlarged quadrate contribution to the processus trochlearis oticum (see Fig. 3.20). Both of these features are best interpreted as related to soft tissue attachments. The position of the exoccipital ridge along the occipital surface of the skull makes it likely that it served as an attachment site for soft tissue structures, such as axial musculature (Werneburg 2011). Similarly, the otic trochlear process of turtles is related to musculature, as it guides the jaw adductor muscles from their origins on the supratemporal surfaces to their insertions on the lower jaw. Ossification occurs at places with increased loading of respective bone surfaces (e.g. Goodship *et al.* 1979; Lanyon *et al.* 1982) and hypertrophied musculature-related osteological features have been reported for turtles before (Dalrymple 1977). Therefore, rather than interpreting these features as autapomorphic for *R. pulchriceps*, I hypothesize that they represent individual variation. Due to the absence of any systematic distribution for this osteological variation, I argue for the presence of a single European species with relatively high instraspecific variation, *Rhinochelys pulchriceps*. This is supported by an assessment of intraspecific variation reported for other turtles, as explained below.

3.6.4 Intraspecific variation in Rhinochelys

I argue that the observed variation among *Rhinochelys* specimens does not support the hypothesis of multiple European species, but that this trait variability can be explained by

intraspecific variation. Intraspecific variation can be the result of geographic variation across different populations, sexual dimorphism, ontogenetic changes or 'true' intraspecific variation (i.e. polymorphic traits that cannot be explained by the former categories). Since all UK *Rhinochelys* specimens come from the same region, the existing variation patterns cannot be explained by biogeography. Sexually dimorphic traits are known among modern turtles, including chelonioids specifically, and usually include size variation between females and males (male sea turtles being smaller; Godley *et al.* 2002), and the presence of longer tails and larger claws in the front flippers of males (Wibbels *et al.* 1991; Wibbels 1999; Wyneken 2001; Casale *et al.* 2005). Cranial osteological features are not known to be sexually dimorphic in sea turtles, however, and as a result I do not interpret any of the observed osteological variation of *Rhinochelys* as sexual dimorphism (although I note that my sample of CT scanned specimens is too small to test for sexual dimorphism statistically).

Most specimens of *Rhinochelys* are small (< 35 mm total skull length) and of similar size, but the largest skulls are approximately twice as large as the smallest, so I can investigate if some of the externally visible variable features (i.e. those that can be found without CT scanning specimens) could be explained by ontogeny. My initial hypothesis for the variability of skull sulci was that the depth of the sulci increases ontogenetically. However, the depth of the skull sulci is variable on both large and small skulls, so that I do not consider this feature to be under ontogenetic control. Consequentially, all variable features observed are interpreted to be 'true' intraspecific variation. I surveyed the literature to see if the variation of *Rhinochelys* is comparable with the amount of intraspecific variation documented for other turtles. Only a few studies have focussed on 'true' intraspecific osteological variation while considering or controlling for geographic variation, ontogenetic changes or sexual dimorphism in turtles (e.g. Dalrymple 1977; Bever 2009*b*). These studies provide important proxies for the extent of intraspecific variation that cannot be explained by sexual dimorphism or ontogenetic changes. The most notable results of Dalrymple's (1977) study of variation of cranial features in the soft-shelled turtle *Trionyx ferox* were that the majority of skull shape variation was related to the feeding mechanism, including variation in

the size and shape of the triturating surface, the size and shape of the supraoccipital crest, the size of the supratemporal passages for the jaw adductor musculature, and the size of the otic trochlear process that redirects this musculature. Furthermore, the variable traits identified by Dalrymple (1977) did not covary, so that the presence of one feature did not necessitate the presence of another. These results are consistent with the hypothesis that much of the variation in *Rhinochelys* (e.g. variation in the curvature of labial margins) can be the result of individual variation. Bever (2009*b*) found that of the 200 discrete characters used in his study on the variation of a single population of the emydid turtle *Pseudemys texana*, which were collected from a lake over the duration of four years, over 50% exhibited some level of variation. Intraspecific variation that could not be explained by ontogeny or sex included changes in the shape of bones, changes in ratios of skull measurements, the participation of certain bones to structures in the cranium such as skull openings, and the shape of sutures between bones. The studies of Dalrymple (1977) and Bever (2009*b*) demonstrate that, given a large enough sample and control for ontogeny, sexual dimorphism and geography, turtles exhibit a range of cranial variations that are comparable to the variation observed for *Rhinochelys*, which itself represents a fossil taxon for which an unusual number of well preserved specimens is available. This supports my hypothesis that only one European species, *Rhinochelys pulchriceps*, can be considered valid.

3.6.5 Diversity of turtles from the Cambridge Greensand Member of the West Melbury Marly Chalk Formation

Turtle specimens from the Cambridge Greensand Member of the West Melbury Marly Chalk Formation indicate the presence of several distinct morphotypes among cranial remains that are distinct from *Rhinochelys* and additional diversity among mandibular and postcranial materials. These include three cranial specimens (Fig. 3.36) and three distinct mandible morphotypes that are documented by a number of specimens (Fig. 3.37) in addition to those referred to *Rhinochelys*. At least three humerus morphotypes are present (Fig. 3.38).

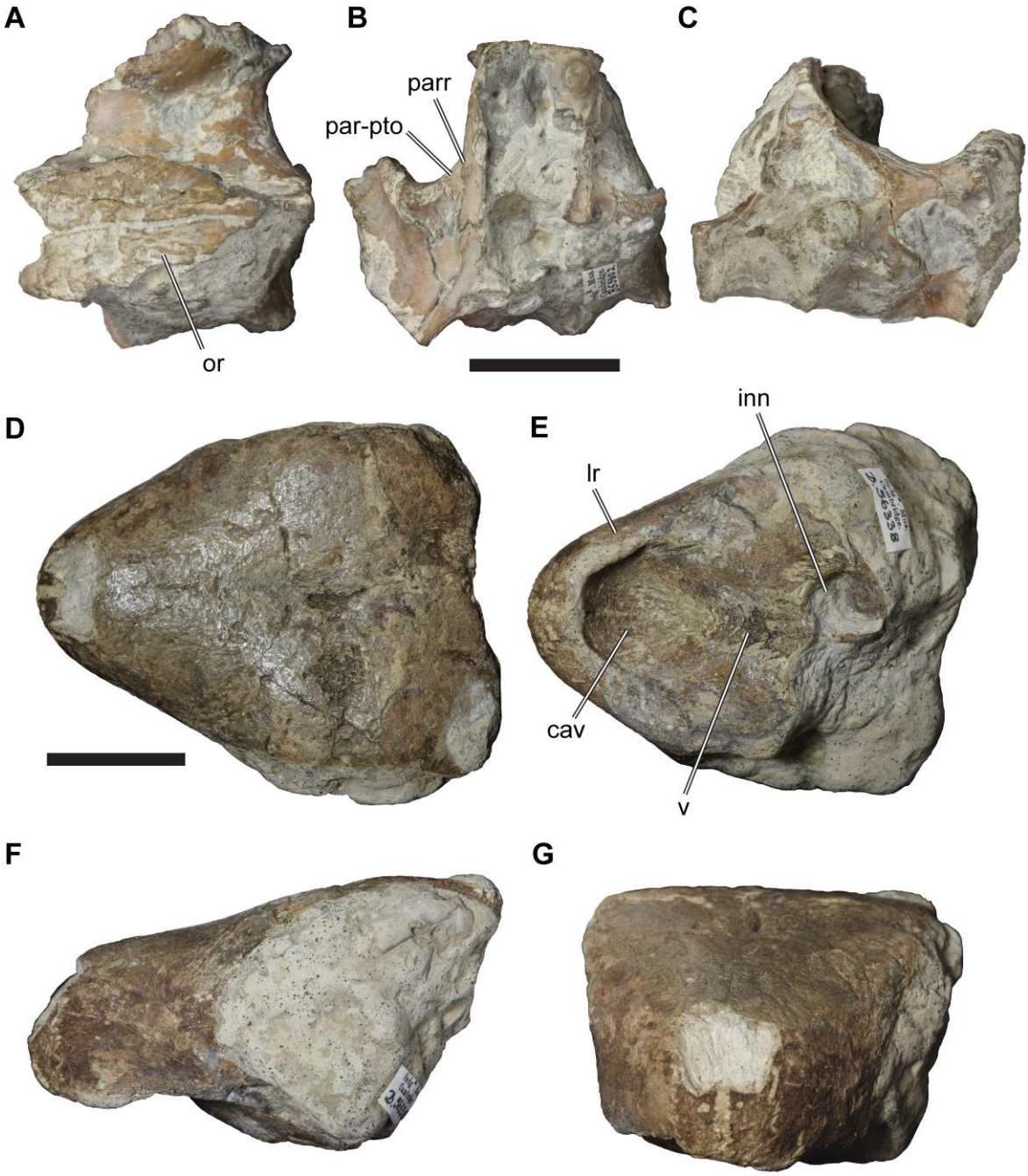


FIG. 36. Cranial specimens from the Cambridge Greensand Member of the West Melbury Marly Chalk Formation that cannot be referred to *Rhinochelys*. **A**, CAMSM B55802 in dorsal view; **B**, CAMSM B55802 in anteroventral view; **C**, CAMSM B55802 in posterior view; **D**, CAMSM B56338 in dorsal view; **E**, CAMSM B56338 in ventral view; **F**, CAMSM B56338 in left lateral view; **G**, CAMSM B56338 in anterior view. Scale bars equal 20 mm. Abbreviations: *cav*, cavity on the anterior surface of the triturating surface; *inn*, internal naris; *lr*, labial ridge; *par-pto*, parietal contribution to the processus trochlearis oticum; *parr*, parietal ridge; *v*, vomer.

Although the systematic identity of most of these specimens is unclear, and I do not provide a detailed taxonomic treatment, some can be assigned to Chelonioidea. The presence of chelonioid material distinct from *Rhinochelys* is important, as it prevents any firm assignment

of carapaces and plastra currently referred to as *Cimochelys benstedti* (e.g. NHMUK PV OR39112, OR47210).

Distinct braincase morphotype. CAMSM B55802 is a partial braincase (Fig. 3.36A–C). The specimen is relatively large (estimated 55 mm skull width), and therefore larger than specimens of *Rhinochelys*. CAMSM B55802 shows some osteological differences from all other specimens referred to *Rhinochelys*. These are: (1) a clearly sculptured parietal dorsal surface; (2) a short lateral expansion of the parietal that contributes to the processus trochlearis oticum; (3) a strongly dorsally concave processus trochlearis oticum; and (4) a strongly developed ridge on the lateral surface of the descending process of the parietal, which is posteroventrally continuous with a ridge on the pterygoid, and which forms an anteroventrally facing trough on the anterior margin of the descending process of the parietal. The skull roof ornamentation of CAMSM B55802 is absent in all known chelonioids. The ornamentation of CAMSM B55802 consists of low, sinuous ridges, which differs from the tubercular ornamentation of solemydid turtles like *Helochelydra nopcsai*, which is known from the Early Cretaceous of the UK (Joyce *et al.* 2011). The ornamentation of CAMSM B55802 is more similar to that of *Pleurosternon bullockii* (UMCZ T1041; Evans & Kemp 1975), which is also known from the Early Cretaceous of the UK, but also to carettochelyids such as *Allaeochelys libyca* (BSPG 191 II 130; Havlik *et al.* 2014) and *Carettochelys insculpta* (NHMUK 1903.7.10.1). All of these taxa have low ridges of various lengths on their parietals.

Additionally, following the anatomical considerations of Hooks (1998), I do not consider the braincase specimen CAMSM B94606 that was used for the braincase description presented by Collins (1970) to belong to *Rhinochelys*. Unfortunately, I could not examine this specimen first-hand, because it is on long-term loan (M. Riley pers. comm., 2018).

Distinct rostral morphotype. CAMSM B56338 is a partially preserved skull (Fig. 3.36D–G) referred to '*Trachydermochelys*' on the specimen label. This skull shows numerous differences from *Rhinochelys*, the most important being: (1) the presence of a secondary palate with a long vomerine contribution to the triturating surface; (2) the presence of massive, rounded labial ridges of the maxillae; (3) the presence of a deep medial cavity on the

triturating surface, possibly indicating the presence of a mandibular hook; (4) the presence of medial processes of the jugal which contacts palatal elements; and (5) the presence of a posteriorly extended skull roof with no temporal emarginations. These features suggest that CAMSM B56338 is a chelonioid, because this combination of features is unknown outside Chelonioidea. However, CAMSM B56338 is probably not a protostegid due to the presence of a secondary palate and a medial jugal process, which is absent in all protostegids.

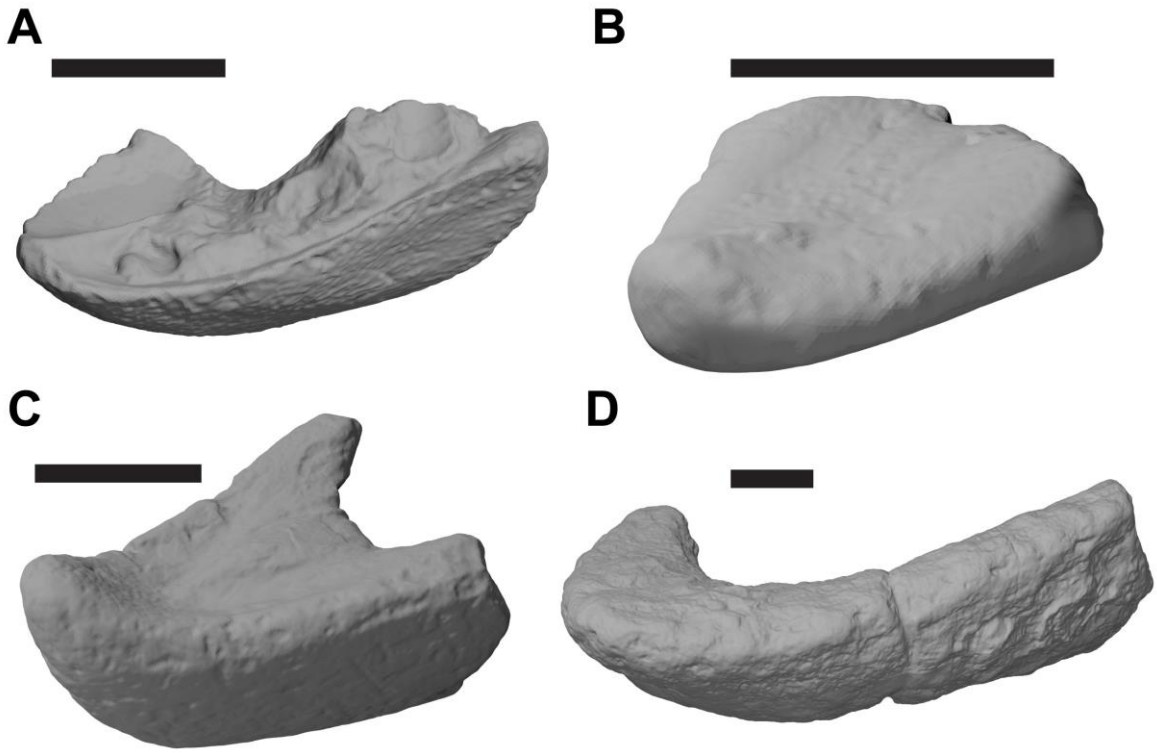


FIG. 3.37. Comparisons of mandibular morphotypes from the Cambridge Greensand Member of the West Melbury Marly Chalk Formation. **A**, morphotype 1, 3D rendering of partial mandible of CAMSM B59560 in right anterodorsolateral view, reflected for comparison; **B**, morphotype 2, 3D rendering of partial mandible of CAMSM B55848 in left anterodorsolateral view; **C**, morphotype 3, 3D rendering of partial mandible of CAMSM B55860 in left anterodorsolateral view; **D**, morphotype 4, 3D rendering of partial mandible of CAMSM B56586 in left anterodorsolateral view. Scale bars equal 20 mm.

Mandibular morphotypes. The Cambridge Greensand Member assemblage includes many isolated mandibles that can be categorized into several morphotypes (mandibular morphotypes 1–3 herein), in addition to those with the morphology of *R. pulchriceps* described above (e.g. isolated mandibles CAMSM B55809, B55810, B55819, B56590, B56593;

Fig. 3.37A). Isolated mandibles of *R. pulchriceps* occupy the same range of sizes as those of crania, with a maximum preserved dentary length <35 mm.

Mandibles of morphotype 1 (e.g. CAMSM B55836, B55847; Fig. 3.37B) are characterised by a relatively acute 'mandibular angle' of 45–50°, have an elongate and flat triturating surface, extremely low and broadly rounded labial margins, a low depth of the dentary, and a rounded anterior margin with a very low symphyseal hook. They differ from *R. pulchriceps* in showing no evidence of a symphyseal ridge and in the absence of well-defined labial ridges.

Mandibles of morphotype 2 (e.g. CAMSM B55860, B55854, B56587, B56589, B76722; Fig. 3.37C) are characterised by a strongly acute 'jaw angle' of ~35°, have an elongate triturating surface with a low but broad ridge that is limited to the posterior two–thirds of the triturating surface, the absence of labial ridges, a deep lateral surface of the dentary, and an upturned anterior end of the symphysis that forms a well developed hook. Mandibles of this morphotype are generally large (e.g. 80 mm long in CAMSM B55860). This morphotype is similar to large protostegids such as *Archelon* (Wieland 1900) and *Protostega* (FMNH PR 2; FMNH P 27385) although the mandibular hook is much weaker in those taxa. Scavezzoni & Fischer (2018) described an isolated partial mandible that they assigned to *R. ambareti* (using the holotype specimen number, UJF-ID.11167, although this mandible was collected several years later than the cranium). This mandible is referable to my morphotype 2, as it has a small symphyseal hook and a weakly developed median ridge on the posterior end of the triturating surface (Scavezzoni & Fischer 2018).

Mandibles of morphotype 3 (e.g. CAMSM B56301, B56586, B56592; Fig. 3.37D) have a relatively wide 'jaw angle' >60°, an anteroposteriorly short triturating surface, a low labial ridge, and moderately deep rami of the dentary, which become mediolaterally narrower at their posterior end. Mandibles of morphotype 3 are much larger than the mandible of *Rhinochelys*: despite their comparatively short triturating surface, the length of this surface exceeds the absolute size of *Rhinochelys* mandibles.

Humerus morphotypes. A high diversity of chelonioid humeri from the Cambridge Greensand Member has been noted before (e.g. Hirayama 1994). I recognize at least three distinct morphotypes. All humeri that I found in the collections of the CAMSM and NHMUK belong to chelonioids, as the lateral process is positioned relatively far distally on the humeral shaft (a synapomorphy of Chelonioidea; Zangerl 1953*b*; Gaffney & Meylan 1988; Hirayama 1994). In humerus morphotype 1 (e.g. CAMSM B56167, CAMSM B56168; Fig. 3.38A), the humerus shaft is moderately flattened, and the distal end of the humerus is broadened. The caput humeri is rounded and positioned on the proximal surface of the humerus, being separated from the medial process by a shallow notch. A short preaxial shoulder on the anterior side of the proximal surface leads from the caput humeri to the lateral process, which is in a proximal positioned on the humeral shaft. An ectepicondylar foramen is not evident. Morphotype 1 is similar to the humeri of some cheloniids (e.g. *Eochelone brabantica*: Hirayama 1994), but also some protostegids (e.g. *Chelospahrgis advena*: Hirayama 1994).

In humerus morphotype 2 (e.g. CAMSM B55987; Fig. 3.38B), the humeral shaft is more flattened than in morphotype 1 and the medial process is broader and extends further medially than in morphotype 1. A preaxial shoulder is absent, and the lateral process is a robust, knob-like structure that is further distally placed on the humeral shaft than in morphotype 1, but still in the proximal half of the humerus. A shallow ectepicondylar groove is apparent in some specimens. This humerus morphotype is similar in most shape aspects to AMNH FARB 1975, which has been referred to *Chelosphargis advena* (e.g. Hirayama 1994, who referred to CAMSM B55987 as an 'aberrant chelonioid'). However, in AMNH FARB 1975 the lateral process is pointed and roughly triangular, while the process is more massive in humerus morphotype 2.

Humerus morphotype 3 (e.g. CAMSM B55988; Fig. 3.38D) is distinctly different from morphotypes 1 and 2. Hirayama (1994) classified humeri from the Cambridge Greensand Member into comparative categories and referred CAMSM B55988 to '*Protostega' anglica*.

The specimens belonging to morphotype 3 are larger in absolute size than humeri of the other morphotypes and the humerus is strongly flattened along the shaft and the distal end.



FIG. 3.38. Comparisons of humeri morphotypes from the Cambridge Greensand Member of the West Melbury Marly Chalk Formation. **A**, morphotype 1, left humerus of CAMSM B56168; **B**, morphotype 2, left humerus of CAMSM B55987; **C**, morphotype 3, left humerus of CAMSM B55988. Top row in ventral view, bottom in dorsal view. Scale bars equal 20 mm. Abbreviations: *ch*, caput humeri; *eecg*, ectepicondylar groove; *hlp*, lateral process of humerus; *hmp*, medial process of humerus; *pas*, preaxial shoulder.

The medial process of the humerus is separated from the caput humeri by a deep notch and projects further proximally in regard to the caput humeri than in morphotypes 1–2. This is different in most specimens of large protostegids, such as *Protostega* (FMNH P27482; FMNH

UR 80; but similar to AMNH FARB 180) or *Archelon* (Wieland 1896), that possess only a shallow notch between the caput and medial process. The lateral process is positioned on the mid-point of the anterior surface of the humerus shaft and is, therefore, in a more distal position than the lateral process of *Archelon* and *Protostega*. This is similar to dermochelyids, in which the lateral process is associated with a prominent crest that extends onto the dorsal surface of the humerus shaft, which is absent in CAMSM B55988. The distal margin of the lateral process is damaged by breakage in CAMSM B55988, so that it is unclear if the process forms a tapered and distally directed tip as in dermochelyids.

In summary, the Cambridge Greensand Member of the West Melbury Marly Chalk Formation provides evidence for a minimum of four taxa in the assemblage (*Rhinochelys* and at least three others based on mandibles). Associations between mandibles, humeri and skulls are unknown, but it is possible that some of the reported material pertaining to different body parts belong to the same taxa. The assemblage is largely composed of chelonioids, although the partial braincase CAMSM B55802 could not be identified taxonomically and might represent a non-chelonioid taxon. In any case, the assemblage indicates a higher chelonioid diversity that previously recognized, which prevents referring postcranial material to *Rhinochelys* until associated material is found.

3.7 CONCLUSIONS

My study represents the most detailed anatomical treatment of the cranial morphology of any protostegid to date. Besides providing digital models for six specimens of *Rhinochelys*, including the holotypes of the three British species considered valid by Collins (1970), I also evaluated other specimens to revise the taxonomy of the genus. Although anatomical variation was observed among specimens, qualitative assessment of the variable traits, as well as multivariate statistical analysis of skull measurements of a broad sample of specimens does not support the occurrence of clusters that could form the basis for objective species delimitation. Therefore, previously named species of *Rhinochelys* are synonymized, and only

the type species, *Rhinochelys pulchriceps*, is considered valid among the European species. Nevertheless, my assessment of non-cranial remains from the West Melbury Marly Chalk Formation indicates that several species of chelonioids are present in addition to *R. puchriceps*. This prevents referral of protostegid postcranial bones from the assemblage to *Rhinochelys* with any certainty.

3.8 DATA ARCHIVING STATEMENT

Data for this study (including CT volume and mesh files for segmented models) will soon be available in MorphoSource; they have been uploaded, but I am waiting to formerly publish them with the respective paper.

SUPPORTING INFORMATION

Additional Supporting Information can be found in Appendix S2 of this thesis.

4 MARINE ADAPTATION DURING THE EARLY EVOLUTION OF CHELONIOIDS

NOTES

This chapter has been submitted (together with the contents of chapter 2) to the journal *PeerJ* as Evers, Barrett & Benson (201X). Paul Barrett and Roger Benson have assisted with the collection of CT data, and improved drafts of my writing. All other data collection, procession, analysis and synthesis have been done my myself.

ABSTRACT

Conflicting phylogenetic hypotheses of chelonioids limit our understanding of evolutionary adaptation to marine life in turtles, and in amniotes more broadly. Phylogenetic conflict results from sparse and non-overlapping taxon sampling in previous studies, as well as from a superficial understanding of the morphology of key taxa. Work presented in previous chapters of this thesis was carried out to improve our phylogenetic understanding of secondarily marine turtle groups more widely, and to document the cranial anatomy of sea turtles, and specifically protostegids. Although protostegids were found to be members of Chelonioidea in Chapter 1, the dataset using cranial character modifications was insufficient to conclusively elucidate total-group chelonioid ingroup relationships, and different treatments of the data (e.g. ordered, unordered characters, omission of taxa or characters related to marine lifestyles) resulted in different topologies, especially with regard to the position of protostegids. Different phylogenetic hypotheses for protostegids suggest different answers to key questions, including (1) the age of the chelonioid crown-group, and (2) patterns of skeletal evolution during marine adaptation. A phylogeny of turtles with increased chelonioid taxon sampling and revised postcranial characters is provided in this chapter, recovering protostegids as stem-chelonioids. These results imply a mid Early Cretaceous origin of total-group chelonioids and an early Late Cretaceous age for crown-chelonioids, which may inform molecular clock analyses in future. Specialisations of the

chelonioid flipper evolved in a stepwise-fashion, with innovations clustered into pulses at the origin of total-group chelonioids, and subsequently among dermochelyids, crown-cheloniids, and gigantic protostegids from the Late Cretaceous.

4.1 INTRODUCTION

Extant chelonioids are marine animals with adaptations to a pelagic lifestyle that include modifications in the shell, limbs and skull (e.g. Zangerl 1980; Hirayama 1994). Modifications in the forelimbs, and specifically the manus, are of interest for the study of form-function relationships. In terrestrial and freshwater aquatic turtles, the manus generally consists of five digits with relatively short, moveable phalanges, but in chelonioids the manus takes the form of flippers in which elongated phalanges have transformed to rigid rod-like structures joined by immovable butt-joints. Flippers evolved convergently in many secondarily-marine tetrapods, but early representatives with transitional manus morphology are unknown for many reptilian groups, such as sauropterygians or ichthyopterygians. Early sea turtle fossils can thus help to investigate the evolution of one of the main locomotor adaptations observed across secondarily marine-reptiles (i.e. the flippers). To study flipper evolution in turtles, the phylogenetic positions of early fossil chelonioids preserving mani need to be established.

Numerous fossil taxa have been placed variably on the stem of chelonioids, as well as on the two main clades of chelonioids, i.e. the cheloniids (hard-shelled sea turtles; six living species) and the dermochelyoids (with only one living species, the leatherback turtle *Dermochelys coriacea*). However, there is little consensus regarding the placement of most taxa. The oldest undisputed stem-group chelonioid is *Toxochelys* spp. from the Coniacian–Campanian of North America (Nicholls 1988; Brinkman *et al.* 2006; Kear & Lee 2006; Joyce *et al.* 2013; Weems & Brown 2017; Evers & Benson 2018*a*), and several Late Cretaceous taxa (e.g. *Allopleuron hofmanni*; Evers & Benson 2018*a*) have been proposed to be stem-group cheloniids. However, undisputed stem-group taxa for both cheloniids and dermochelyoids

are generally much younger and date to the Paleocene–Eocene (e.g. Nielsen 1959; Joyce *et al.* 2013*b*; Weems 2014).

A diverse assemblage of Early–Late Cretaceous marine turtles, the protostegids, has frequently been hypothesized to be on the stem-group of *Dermochelys* (e.g. Hirayama 1994, 1998; Lehman & Tomlinson 2004; Brinkman *et al.* 2006; Kear & Lee 2006; Bardet *et al.* 2013; Cadena 2015; Cadena & Parham 2015; Evers & Benson 2018*a*). This hypothesis has been contested by results from 'global' phylogenetic analyses of testudine interrelationships, which were not focussed specifically on marine turtles and that included representatives of most major living and extinct fossil lineages (e.g. Joyce 2007; Sterli 2010; Anquetin 2012). These studies found protostegids in more stemward positions outside of Chelonioidea, on the stem-group of either cryptodires or turtles (see Evers & Benson 2018*a* for a recent summary). However, these analyses included only a single Early Cretaceous species of protostegid, *Santanachelys gaffneyi*, in their taxon samples. Only recently have such global analyses included a wider array of protostegids, as well as other fossil sea turtles (Cadena 2015; Cadena & Parham 2015; Evers & Benson 2018*a*), and found protostegids nested within modern chelonioids on the stem-group of *Dermochelys*, consistent with historical views.

I extend the phylogenetic work presented in Chapter 1, which was largely concerned with revising and extending the cladistic dataset assembled with regard to cranial data, by analysis of an expanded dataset. This dataset includes the addition and revision of several postcranial characters, most of which are aimed to capture observed variation in skeletal anatomy that is modified specifically in chelonioids and could therefore be interpreted to be linked to functional adaptation to marine ecology. Furthermore 16 taxa were added, some of which are only known from postcranial remains. The new phylogenetic analysis recovers protostegids as chelonioids, albeit on their stem-lineage. The implications of this finding for the evolution of flippers, as well as the timing of origination of chelonioids is discussed.

4.2 MATERIAL & METHODS

4.2.1 Character-taxon matrix

I used a modified version of the data matrix from Chapter 1 (i.e Evers & Benson 2018*a*) that included 16 additional taxa (*Adocus beatus*, *Angolachelys mbaxi*, *Cabindachelys landanensis*, *Calcarichelys gemma*, *Chelosphargis advena*, *Corsochelys halinches*, *Erquelinnesia gosseleti*, *Nichollsemys baieri*, *Ctenochelys* sp., *Galianemys whitei*, *Oligochelone rupelensis*, *Peritresius martini*, *Petrochelys kyrgyzensis*, *Plesiochelys bigleri*, *Procolphochelys charlestonensis*, and *Rhinochelys nammourensis*). *Adocus* and *Petrochelys* were added because they are presumed stem-group trionychians (*Adocus*) or early members of the trionychian crown-group (*Petrochelys*) and can therefore influence character optimisation and polarisation at the base of Cryptodira. For both these taxa, I used CT scans of their crania to complement published sources to inform our character scorings (data for *Petrochelys* were downloaded from MorphoSource project M9547-13212; Vitek *et al.* 2018). *Galianemys* was added as a bothremydid pleurodire using information from CT scans for the cranium, personal observations and the literature, because bothremydids were not represented in the original matrix of Evers & Benson (2018*a*). *Plesiochelys bigleri* was included as an additional plesiochelyid, as a CT scan of the cranium was available, and because it represents a thalassochelydian for which cranial as well as postcranial material is known (Pünterer *et al.* 2017). *Angolachelys* was added to include all currently known sandownids included in the matrix. *Cabindachelys*, *Oligochelone* and *Procolpochelys* were incorporated as presumed stem-group cheloniids from the Cenozoic. *Ctenochelys* and *Peritresius* were added because these have been recently interpreted as Cretaceous stem-group cheloniids (Gentry 2016; Gentry *et al.* 2018). *Corsochelys* and *Nichollsemys* were included as they represent Cretaceous taxa with contentious phylogenetic positions within the total-group of chelonioids (Zangerl 1960; Brinkman *et al.* 2006). *Erquelinnesia* was added to represent osteopygid chelonioids, which were not included in the original matrix of Evers & Benson (2018*a*). Finally, *Calcarichelys*, *Chelosphargis* and *Rhinochelys nammourensis* were added to the matrix as they all represent protostegid taxa for which cranial and postcranial material is available. The information

sources for each taxon are detailed in Table 4.1, and the matrix is available in nexus-format in Appendix S3.

In the second section of this thesis, I focussed largely on a revision of cranial characters and modified postcranial characters only by vetting their implied homology statements according to the hierarchical coding strategy (e.g. Hawkins *et al.* 1997), retaining postcranial character scores directly from Cadena & Parham (2015). Here, I provide a more thorough revision of postcranial characters (see below) in an attempt to code variation among chelonioids for parts of the skeleton that have been interpreted to be important for their marine lifestyle, such as carapacial and plastral ossification and limb morphology. I further added and/or revised postcranial scorings for several species based on first-hand observations of holotype and referred specimens (e.g. *Puppigerus camperi*, *Eochelone brabantica*, *Eosphargis breineri*; see Table 4.1 for details). Two new cranial characters have also been added, based on observations made during my investigations of *Rhinochelys* (see Chapter 2). A full character list is available in Appendix S3. The modifications resulted in a data matrix containing 96 taxa and 355 characters.

TABLE 4.1. Sources for scorings in my character–taxon matrix.

Taxon	Specimen(s) used for character scoring	References used for character scoring	Personal observation of taxon	CT
Adocus beatus	**CCM 60-15**	Meylan & Gaffney 1989; Cadena & Parham 2015	no	yes
Allaeochelys libyca	**BSPG 1991 II 130**	Havlik *et al.* 2014	yes	yes
Allopleuron hoffmanni	IRSNB R 0008, 3668; **NHMUK PV OR42913**	Mulder 2003	yes	yes
Angolachelys mbaxi	MGUAN-PA 002, 296	Mateus *et al.* 2009; Myers *et al.* 2018	no	no
Annemys sp.	**IVPP V18106**	Brinkman *et al.* 2013	no	yes
Annemys levensis	PIN 4636-4-2	Shukanov 2000; Rabi *et al.* 2014	no	no
Annemys latiens	PIN 4636-6-1	Rabi *et al.* 2014	no	no
Apalone spinifera emoryi	**FMNH 22178**	no additional references used	yes	yes
Araripemys barretoi	**AMNH FARB 30778**	Meylan 1996; Gaffeny *et al.* 2011	yes	yes
Archelon ischyros	YPM 3000	Wieland 1896, 1900, 1902	yes	no
Argillochelys cuneiceps	**NHMUK PV OR41636**	no additional references used	yes	yes
Arundelemys dardeni	**USNM 497740**	Lipka *et al.* 2006	no	yes
Australochelys africanus	**BP/1/4933**	Gaffney & Kitching 1995	yes	yes
Baptemys wyomingensis	YPM 374, 3758; DMNH 511	Meylan & Gaffney 1989; Knauss 2014	no	no
Bouliachelys suteri	**QMF 31669**	Kear & Lee 2006	no	yes
Brachyopsemys tingitana	AMNH FARB 30001; **AMNH FARB 30612**	Tong & Meylan 2013	yes	yes
Cabindachelys landanensis	**MGUAN-PA 298;** MRAC 4796	Myers *et al*. 2018	no	yes
Calcarichelys gemma	RMM 3216	Zangerl 1953; Hooks 1998; Cadena & Parham 2015	no	no
Caretta caretta	**NHMUK 1938.1.9.1**	no additional references used	yes	yes
Carettochelys insculpta	**NHMUK 1903.7.10.1**	no additional references used	yes	yes
Chelodina oblonga	**NHMUK 64.12.22**	no additional references used	yes	yes
*Chelodina longicollis**	unknown (specimen number not given in Cadena & Parham 2015)	Cadena & Parham 2015	no	no
Chelonia mydas	**NHMUK 1969.776**	no additional references used	yes	yes

Taxon	Specimen(s) used for character scoring	References used for character scoring	Personal observation of taxon	CT
Chelonoidis sp.	**SMF 67582**	no additional references used	no	yes
*Chelonoidis chilensis**	unknown (specimen number not given in Cadena & Parham 2015)	Cadena & Parham 2015	no	no
Chelosphargis advena	KUVP 1209	Zangerl 1953; Cadena & Parham 2015	no	no
Chelus fimbriatus	**NHMUK 81.9.27.4**	no additional references used	yes	yes
Chelydra serpentina	**SMF 32846**	no additional references used	no	yes
Chrysemys picta	**NHMUK 76.1.31.19**	no additional references used	yes	yes
Chubutemys copelloi	MPEF-PV1236	Gaffney et al. 2007; Sterli *et al.* 2015	no	no
Corsochelys halinches	**FMNH PR 249**	Zangerl 1960	yes	yes
Ctenochelys sp.	**AMNH FARB 6137**, 234**; FMNH PR444, PR 1047**, PR97, P27352, P27337, P27366; MSC 35085; USNM 357166	Matzke 2007; Gentry 2016	yes	yes
Dermatemys mawii	**SMF 59463**	no additional references used	no	yes
Dermochelys coriacea	**FMNH 171756; UMZC R3031**	no additional references used	yes	yes
Desmatochelys lowii	**KUVP 1200**	no additional references used	no	yes
Desmatochelys padillai	FCG-CBP 01, 13, 15, 39, 40; UCMP 38345, 382456	Cadena & Parham 2015	no	no
Dracochelys bicuspis	IVPP V4075; IVPP V12091	Gaffney & Ye 1992; Brinkman 2001	no	no
Eileanchelys waldmanni	**NMS.G.2004.31.15**; NMS.G.2004.31.16a-f	Anquetin 2010	yes	yes
Elseya dentata	**NHMUK 76.5.19.77**	no additional references used	yes	yes
Emarginachelys cretacea	KUVP 23488	Whetstone 1978	no	no
Emys orbicularis	**WGJ1987a**	no additional references used	no	yes
Eochelone brabantica	**IRSNB R0001, 0061, 0062;** IRSNB NIG 8475, 18733**; NHMUK PV OR37213**	Casier 1968	yes	yes
Eosphargis breineri	FUM-N-1450	Nielsen 1959, 1963	yes	no
Eretmochelys imbricata	**FMNH 22242**	no additional references used	yes	yes
Eubaena cephalica	**DMNH 96004**; AMNH FARB 4948, 2602, 2604, 2606; YPM 1785	Gaffney 1972*a ,b*, 1979; Gaffney 1982*a, b*; Rollot *et al.* 2018	no	no
Erquelinnesia gosseleti	IRSNB R1563, 0067–68, 0070–71, 1642–43, 1650	Zangerl 1971	yes	no

Taxon	Specimen(s) used for character scoring	References used for character scoring	Personal observation of taxon	CT
Galianemys whitei	**AMNH FARB 29987**	Gaffney *et al.* 2002, 2006	yes	yes
Geoclemys hamiltoni	**NHMUK 87.9.30.1**	no additional references used	yes	yes
Glyptops plicatulus	AMNH FARB 336; YPM 1784, 4717, 5821	Gaffney 1979	no	no
Gopherus polyphemus	**FMNH 211815**	no additional references used	yes	yes
Judithemys sukhanovi	TMP 87.2.1	Parham & Hutchinson 2003	no	no
Jurassichelon oleronensis	**PIMUZ AIII 514**	Rieppel 1980	yes	yes
Kallokibotion bajazidi	NHMUK PV R4918; **NHMUK PV R4921**; **NHMUK PV R4925**	Gaffney & Meylan 1992	yes	yes
Kayentachelys aprix	**TMM 4370-2,** 43653-1; MCZ 8914-8917; MNA V1558, V2664	Sterli & Joyce 2007; Gaffney & Jenkins 2010	no	yes
Kinosternon suburum	**FMNH 211711**	no additional references used	yes	yes
*Kinosternon flavescens**	unknown (specimen number not given in Cadena & Parham 2015)	Cadena & Parham 2015	no	no
Kirgizemys dmitrievi	ZIN PH7/15	Danilov *et al*. 2006	no	no
Kirgizemys hoburensis	PIN 3334-4; PIN 3334-35; PIN 3334-36	Sukhanov 2000	no	no
Lepidochelys kempii	**M009/08**	Jones *et al*. 2012	no	yes
Lepidochelys olivacea	**SMNS 11070**	no additional references used	yes	yes
Levyachelys cipadi	FCG-CBP-71; SMU 75377, 72852, 74982, 75327; FWMSH 93B-17	Vineyard 2009; Cadena 2015	no	no
Lissemys punctata	SMF 74141	no additional references used	no	yes
Macrochelys temminckii	**FMNH 22111**	no additional references used	yes	yes
Meiolania platyceps	**NHMUK PV R682**; specimens listed in Gaffney 1983	Gaffney 1983	yes	yes
Natator depressus	**R112123**	Jones *et al*. 2012	no	yes
Nichollsemys baieri	**TMP 97.99.1**	Brinkman *et al.* 2006; Cadena & Parham 2015	no	yes
Notochelone costata	**NHMUK PV R9590**	no additional references used	yes	yes
Ocepechelon bouyai	OCPDEK/GE516	Bardet *et al*. 2013	no	no
Oligochelone rupelensis	IRSNB VERT 18733-03906	no additional references used	yes	no
Ordosemys sp.	**IVPP V12092**	Brinkman & Wu 1999	no	yes

Taxon	Specimen(s) used for character scoring	References used for character scoring	Personal observation of taxon	CT
Pelodiscus sinensis	**IW576-2**	no additional references used	no	yes
Pelomedusa subrufa	**SMF 70504**	no additional references used	yes	yes
Peritresius martini	ALMNH 6191	Gentry *et al.* 2018	no	no
Petrochelys kyrgyzensis	**ZIN-PHT-F67-218**	Vitek *et al.* 2018	no	yes
Phrynops geoffranus	**SMF 45470**	no additional references used	no	yes
Platysternon megacephalum	**SMF 69684**	no additional references used	no	yes
Plesiochelys bigleri	**MJSN TCH007-252**; specimens listed in Pünterer *et al*. 2017	Pünterer *et al.* 2017	yes	yes
Plesiochelys planicpes	**OUMNH J1582**	Gaffney 1975*b*; Gaffney 1976	yes	yes
Plesiochelys etalloni	**MNB 435**; MAJ 2005-11-1	Gaffney 1975*b*, 1976; Anquetin *et al.* 2014*a*	yes	yes
Pleurosternon bullockii	**UMZC T1041**	Evans & Kemp 1975	no	yes
Podocnemis unifilis	**FMNH 45657**	no additional references used	yes	yes
*Podocnemis expansa**	unknown (specimen number not given in Cadena & Parham 2015)	Cadena & Parham 2015	no	no
Portlandemys mcdowelli	**NHMUK PV R2914**	no additional references used	yes	yes
Procolpochelys charlestonensis	CCNHM 893, 300.1	Weems & Sanders 2014; Weems & Brown 2017	no	no
Proganochelys quenstedti	SMNS 15759, 16980	Gaffney 1990	yes	no
Protostega gigas	AMNH FARB 1502, 1503; AUMP 412; CMNH 1421; FMNH PR2, P27385;	Case 1897; Williston 1902; Wieland 1906; Hay 1908; Hooks 1998	yes	no
Puppigerus camperi	**IRSNB R0074–76;** IRSNB R0072–73, 0077, 0081**; NHMUK PV OR38955, R14375**	Moody 1974	yes	yes
Rhinochelys nammourensis	MSNM V3933; specimens listed in Tong *et al.* 2006	Tong *et al.* 2006; Cadena & Parham 2015	no	no
Rhinochelys pulchriceps	**CAMSM B55775, B55783, B55776; NHMUK PV OR43980, R2226, OR35197**	no additional references used	yes	yes
Sandownia harrisi	**MIWG 3480**	Meylan *et al*. 2000	yes	yes
Sinemys gamera	IVPP V9532-11	Brinkman & Peng 1993	no	no

Taxon	Specimen(s) used for character scoring	References used for character scoring	Personal observation of taxon	CT
Sinemys lens	IVPP V9533-1; IVPP V9533-3	Brinkman & Peng 1993	no	no
Solnhofia parsoni	**TM 4023;** JM SCHA 70	Gaffney 1975*c*; Joyce 2000	yes	yes
Staurotypus salvinii	**NHMUK 1879.1.7.5**	no additional references used	yes	yes
*Staurotypus triporcatus**	unknown (specimen number not given in Cadena & Parham 2015)	Cadena & Parham 2015	no	no
Sternotherus minor	**FMNH 211696**	Bever 2009*a*	yes	yes
*Sternotherus odoratus**	unknown (specimen number not given in Cadena & Parham 2015)	Cadena & Parham 2015	no	no
Testudo marginata	**FMNH 51672**	no additional references used	yes	yes
*Testudo hermanni**	unknown	Cadena & Parham 2015	no	no
Toxochelys sp.	AMNH FARB 1496, **5118**; FMNH UR3; **FMNH PR219,** PR648	Hay 1896; Nicholls 1988	yes	yes
Xinjiangchelys radiplicatoides	**IVPP V9539-1**	Brinkman et al. 2013	no	yes
Xinjiangchelys wusu	PMOL-SGPA0100-1; PMOL-SGPA0100-3	Rabi *et al.* 2013	no	no

*Species indicated by asterisk were used only for postcranial scores.
Bold specimen numbers indicate specimens for which CT scans were available.

4.2.2 Cranial character modifications

My observations for *Rhinochelys pulchriceps* that were described in section 3 of this thesis show that this taxon has a peculiar articulation between the pterygoid and the basisphenoid (e.g. Fig. 3.26). The pterygoid of *Rhinochelys* has a posterodorsally facing, concave socket that receives an anterolateral knob-like process of the basioccipital. Hooks (1998) described this feature for *Calcarichelys gemma* and *Protostega gigas* and found it to be a synapomorphy of Protostegidae (excluding *Rhinochelys*). To my knowledge, the respective character (Hooks 1998: character 10) has not been used in other matrices, but I include it here:

> **Character 93**: Basioccipital, anterolateral edge of basioccipital with knob-like processes fitting into sockets on the posterior processes of the pterygoids: 0 = absent; 1 = present.

I also code another new cranial character, based on the observations of Collins (1970), Tong *et al.* (2006), Scavezzoni & Fischer (2018) and my work, regarding the peculiar antorbital bulge found in *Rhinochelys pulchriceps* and *Rhinochelys nammourensis*, but no other protostegid (e.g. Figs 3.1–7).

> **Character 10 (new)**: Prefrontal, preorbital bulge formed between the prefrontal and premaxilla: 0 = absent; 1 = present.

4.2.3 Postcranial character modifications

Costal characters. Previously, variation regarding the costo-peripheral fontanelles was coded in a single multistate character encoding both the presence vs. absence of fontanelles, plus various aspects of their morphology if present (Evers & Benson 2018*a*: character 210;

Cadena & Parham 2015: character 132). Here, I have modified the coding to consider differences in the arrangement of costo-peripheral fontanelles and their presence/absence separately. Adopting this coding strategy results in three different characters (character 212–214). The first character considers the presence vs. absence of fontanelles, which I regard as a single observation on one level of homology, following the coding strategy of Hawkins *et al.* (1997). Contrary to the postcranial scorings in Evers & Benson (2018*a*), which were adopted from Cadena & Parham (2015), I scored chelydrids, as well as some trionychids and *Araripemys*, as having fontanelles. The presence of fontanelles in chelydrids is unambiguous (see also Joyce 2016). For trionychids, costo-peripheral fontanelles are harder to define because this group lacks peripherals (Meylan 1987; except for *Lissemys punctata*). However, many trionychid taxa have distal rib ends that extend laterally beyond the margin of the costals, therefore creating 'fontanelles' that are laterally open. In this study, I scored trionychid taxa as possessing fontanelles when the distal rib end is visible beyond the costal margin in dorsal or ventral view. My second costal character captures variation regarding the position of the costo-peripheral fontanelles: in many chelonioid taxa (e.g. *Toxochelys*, *Allopleuron*, *Caretta*; Fig. 4.1B, D–E), costo-peripheral fontanelles are present along all peripherals, whereas fontanelles are present only in certain parts of the carapace (usually the central parts) in many other taxa, such as the thalassemydid *Palaeomedusa* (Fig. 4.1C), the chelydrids *Macrochelys* and *Chelydra*, and some trionychids. I also add a caveat concerning the ontogenetic stage of the fossils considered for scoring: in some taxa, such as *Plesiochelys etalloni* and *Puppigerus camperi*, fonatenelles are present along the lateral margin of the costals in juvenile and subadult specimens but are entirely absent in large specimens (Fig. 4.1B). This differs from how these taxa were scored in many previous studies (e.g. Cadena & Parham 2015). My third character captures variation in the shape of the fontanelle between the first costal, nuchal and the first few peripherals. This fontanelle is usually only present in those taxa that have fontanelles along the entire costo-peripheral series. However, in *Toxochelys, Corsochelys* and *Erquelinnesia* this fontanelle is reduced in size (Fig. 4.1B), with the first costal nearly contacting the posterior margin of the first peripherals.

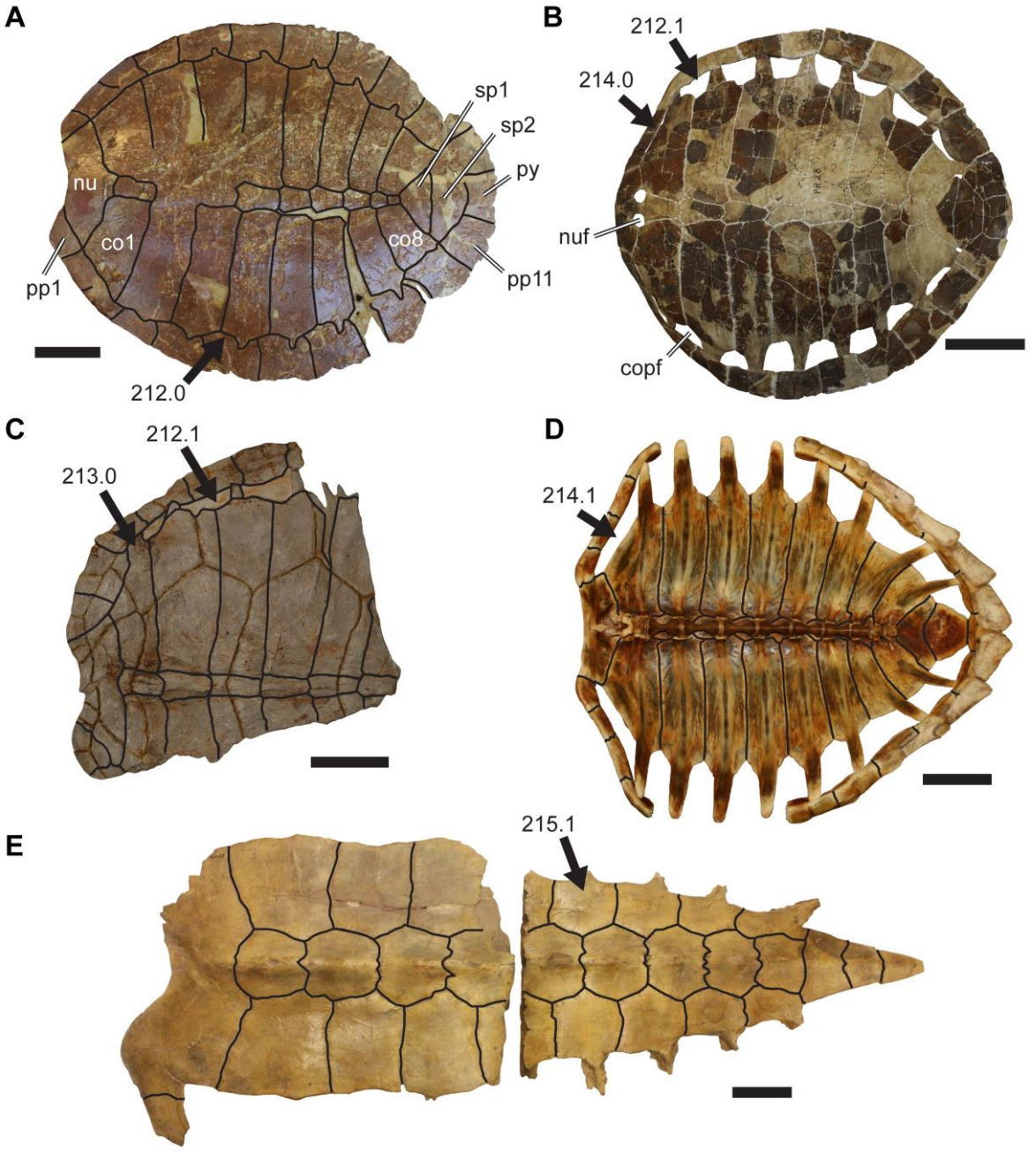


FIG. 4.1. Carapaces of selected turtles illustrating the variability of carapacial fontanelles. **A**, dorsal view of carapace of *Puppigerus camperi* (IRSNB R 0072); **B**, dorsal view of carapace of *Toxochelys* sp. (FMNH PR 28); **C**, dorsal view of partial carapace of *Palaeomedusa testa* (BSPG AS I 818); **D**, ventral view of carapace of *Caretta caretta* (AMNH 129869); **E**, dorsal view of partial carapace of *Allopleuron hofmanni* (IRSNB R 0008). Scale bars in A & C equal 5 cm, all other scale bars equal 10 cm. Numbers represent characters and character states. Abbreviations: *co*, costal; *copf*, costo-peripheral fonatnelle; *nu*, nuchal; *nuf*, nuchal fonatanelle; *pp*, peripheral; *py*, pygal; *sp*, suprapygal.

Character 212: Costals, lateral ossification: 0 = all costals fully ossified laterally with strong sutural contact with peripherals, lack of dorsal exposure of distal end of costal

ribs and absence of costo-peripheral fontanelles; 1 = lateral sutural contact contact between costals and peripherals absent in at least parts of the costo-peripherial series, resulting in the presence of costo-peripheral fontanelles and/or the exposure of the distal rib ends.

Character 213: Costals, position of costo-peripheral fontanelles and exposure of dorsal rib ends: 0 = limited to parts of the carapace; 1 = fontanelles and exposed rib ends present and retained in adults between all costals and along the anterior margin of the first costal. Scored as inapplicable for taxa that lack costo-peripheral fontanelles (character 212.0).

Previous character definition: Character 210 (Evers & Benson 2018*a*); character 132 (Cadena & Parham 2015). Costals, distal rib end and lateral ossification of the costal: 0 = costals fully ossified laterally with strong sutural contact with peripherals, lack of dorsal exposure of distal end of costal ribs; 1 = costals fully ossified laterally with strong sutural contact with peripherals, distal end of costal ribs exposed on dorsal surface and surrounded by the peripheral; 2 = costals lack lateral ossification, allowing the dorsal exposure of the distal end of ribs and the development of fontanelles only at the most anterior and posterior costals; 3 = costals with extreme lost of lateral ossification, allowing the dorsal exposure of the distal end of ribs, in almost all series of costals.

Character 214 (new): Costal, fontanelle along anterior margin of costal 1: 0 = anterior margin of first costal positioned very close to nuchal and/or anterior-most peripherals, reducing the fontanelle to an anteroposteriorly narrow, slot-like opening; 1 = extensive fontanelle between first costal and anterior margin of carapace. Scored inapplicable for taxa without costo-peripheral fontanelles (character 212.0) or when costo-peripheral fontanelles are absent along the first costal.

I also observed further variation in the shape of the costal bones. The costal bones are mediolaterally relatively wide and anteroposteriorly narrow, forming rectangular plate-like structures in most turtles, including most chelonioids. However, in some taxa with a heavily reduced carapace, such as *Eosphargis breineri* or *Allopleuron hofmanni*, the costals are significantly reduced in mediolateral width, and the posterior costals are approximately as wide as they are long (Fig. 4.1E). I included this observation as a separate character:

> **Character 215 (new)**: Posterior costals, shape: 0 = rectangular, much wider mediolaterally than long anteroposteriorly; 1 = square or hexagonal, as wide as long.

Entoplastron and epiplastron characters. In previous analyses, the definitions for several characters describing entoplastron shape repeated information from other characters or differed from my observations. Previously, Evers & Benson (2018*a*: character 240) adopted a character (character 156 of Cadena & Parham 2015; character 79 of Joyce 2007) that was originally defined to capture a peculiar feature appearing in the entoplastron of several stem-turtles, including Late Triassic taxa such as *Proganochelys quenstedti* and *Proterochersis robusta*. These taxa have a long posteriorly directed process that overlaps the hypoplastra on the dorsal surface of the plastron and sometimes reaches the mesoplastra (Fig. 4.2B). I deleted this character from my modified matrix, because the presence of a posteriorly elongate ('dagger-shaped') entoplastral process is also described in state 0 of character 242 of Evers & Benson (2018*a*; originally from Cadena & Parham 2015: character 158). As a solution to coding the morphological information of the entoplastron, I modified the previous definition of the entoplastron shape character (Evers & Benson 2018*a*: character 242) to include more anatomical descriptive statements, whereas the shapes were previously defined solely as geometric shapes (e.g. 'diamond', 'T-shaped', *etc*.).

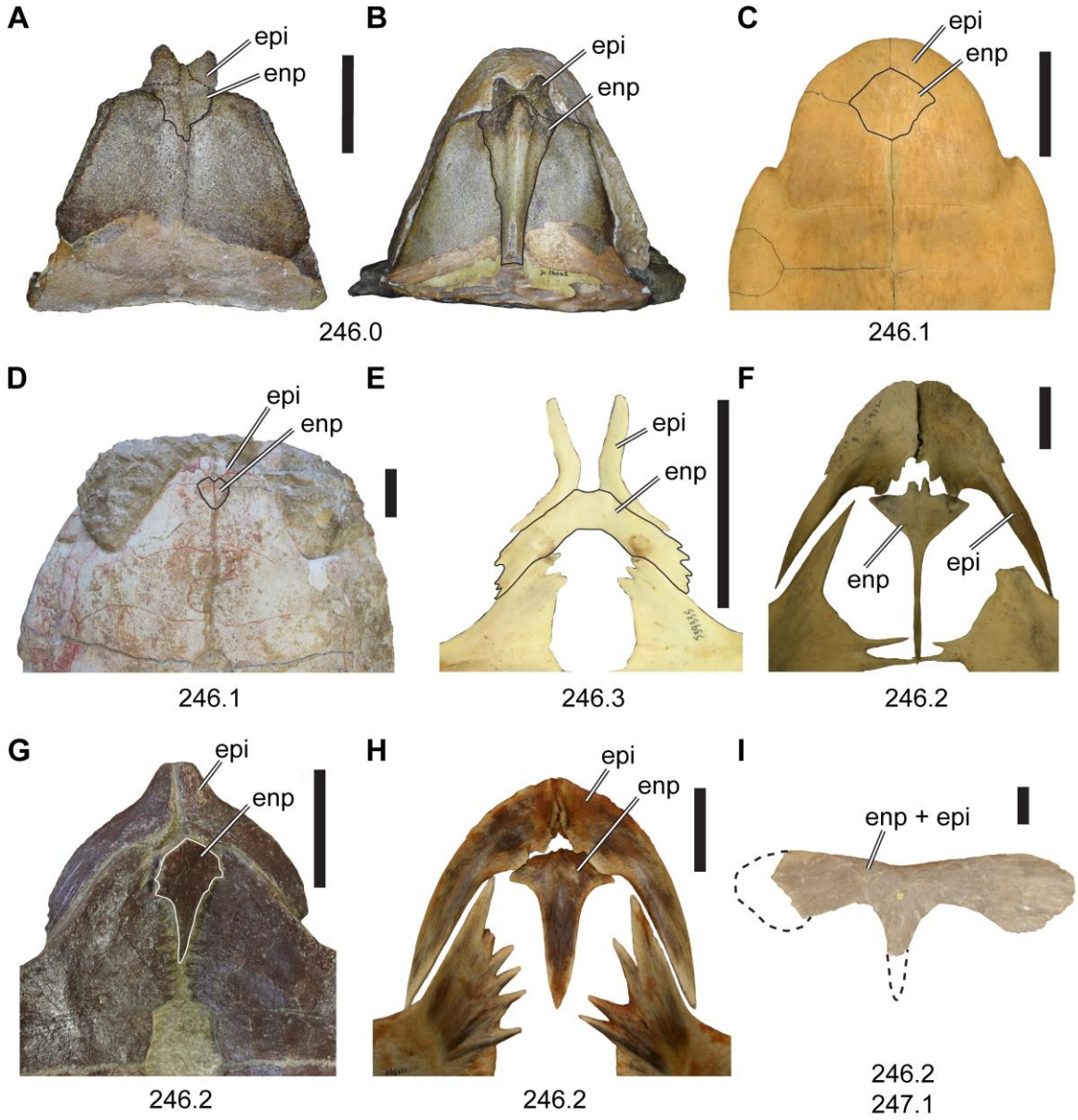


FIG. 4.2. Entoplastra of selected turtles. **A**, ventral view of *Proterochersis robusta* (SMNS 16442); **B**, dorsal view of *Proterochersis robusta* (SMNS 16442); **C**, ventral view of *Podocnemis sextuberculata* (NHMUK 16075); **D**, ventral view of *Plesiochelys etalloni* (MAJ-2005-11-1); **E**, ventral view of *Pelodiscus sinensis* (USNM 539335); **F**, ventral view of *Chelonia mydas* (AMNH 5912); **G**, ventral view of *Puppigerus camperi* (IRSNB R 0073); **H**, ventral view of *Caretta caretta* (AMNH 129869); **I**, ventral view of *Protostega* sp. (NHMUK R 5433). All scale bars equal 5 cm. Numbers represent characters and character states. Abbreviations: *enp*, entoplastron; *epi*, epiplastron.

Character 246: Entoplastron, shape of the entoplastron: 0 = 'dagger-shaped', with dorsoventrally thick anterior end and long posterior process that extends along the dorsal surface of the plastron and sometimes reaches the mesoplastra; 1 = plate-like and diamond-shaped or hexagonal in ventral view, with all margins of subequal

length; 2 = 'T'-shaped or triangular, i.e. entoplastron has a mediolaterally expanded anterior end and a progressively narrowing posterior process; 3 = strap-like and 'V'-shaped, with posterolateral processes diverging from the midline of the plastron.

Previous character definitions:

(1) Character 240 (Evers & Benson 2018*a*); character 156 (Cadena & Parham 2015). Entoplastron, size of the posterior entoplastral process: 0 = posterior process long, reaching as far posteriorly as the mesoplastra; 1 = posterior process reduced in length.

(2) Character 242 (Evers & Benson 2018*a*); character 158 (Cadena & Parham 2015). Entoplastron, shape of the entoplastron in ventral view: 0 = dagger-shaped; 1 = massive diamond-shaped; 2 = T- shaped, longer than wide; 3 = T-shaped, wider than long, forming broad lateral wings; 4 = strap like and V-shaped.

In addition to the above revisions, I only included one state for a 'T-shaped' entoplastron in our character 246. The two distinct states (states 2 and 3) for a 'T-shaped' entoplastron from the previous definition were combined to a single state (new state 2) to better reflect the homology proposition of having a 'T-shaped' entoplastron versus other possible shapes of this element. The previous state 3 was scored only for *Protostega* and *Archelon* in the matrix of Evers & Benson (2018*a*), following Cadena & Parham (2015). These taxa were said to have extensive lateral wings of the entoplastron (Fig. 4.2I) that are different from the moderate wings of *Chelonia* (Fig. 4.2F) or the small wings of *Puppigerus* or *Caretta* (Fig. 4.2F–G). Furthermore, the same morphology is present in *Calcarichelys gemma* (Hooks 1998). However, it seems that these lateral wings result from fusion of the entoplastron with the epiplastra (e.g. Hirayama 1994; Tong *et al.* 2006). Evidence for this hypothesis comes from several taxa, in which the entoplastron and epiplastra are preserved and present as separate

elements, but in which these elements in combination form a shape that is identical to that present in *Archelon*, *Protostega* and *Calcarichelys*. Examples for this include *Chelosphargis advena* (Zangerl 1953*a*) and *Rhinochelys nammourensis* (Tong *et al.* 2006). The epiplastra of these taxa are expanded into wing-like processes at their lateral ends, but the entoplastron itself is very similar to some cheloniids (such as *Chelonia mydas*), in which the lateral entoplastron processes are moderately expanded and a long posterior process is present. Therefore, we scored *Chelosphargis advena* and *Rhinochelys nammourensis* as having state 2 for character 246. In *Archelon*, *Protostega* and *Calcarichelys*, in which the entoplastron and epiplastra are fused to an entepiplastron, the exact shape of the entoplastron part of the entepiplastron is not discernable due to the absence of sutures. However, the posterior parts of the entepiplastra of *Archelon*, *Protostega* and *Calcarichelys* are indistinct from the entoplastra of other chelonioids, including *Caretta, Chelonia, Rhinochelys* and *Chelosphargis*. Thus, I think it is justified to merge the previously distinct states for 'T-shaped' entoplastra into a single state. However, I added a new character that considers the fusion of the entoplastron with the epiplastra so that the morphological similarity of *Calcarichelys*, *Protostega* and *Archelon* is still considered in our matrix:

> **Character 247 (new):** Entepiplastron: 0 = absent, entoplastron and epiplastra are separate elements; 1 = present, entoplastron is fused with epiplastra, resulting in a laterally extremely expanded entepiplastron wings.

Furthermore, the laterally expanded epiplastra, which are present in a number of protostegids irrespective of whether they are fused to the entoplastron or not, such as *Rhinochelys nammourensis*, *Chelosparhis advena* or *Protostega gigas*, need to be considered as a separate character, because the similarity between the epiplastra of the these taxa is not encoded in previous studies. Therefore, I modified the scorings and definition of character 244 of Evers & Benson (2018*a*) (character 249 of this study; character 160 of Cadena & Parham 2015). This character had a state (state 2) that described the shape of the epiplastra

for *Archelon* and *Protostega*, which were the only taxa contained within in the matrices of Cadena & Parham (2015) and Evers & Benson (2018*a*) scored with this state. According to my observations, *Archelon ischryos*, *Protostega gigas*, *Rhinochelys nammourensis*, *Chelospargis advena*, *Calcarichelys gemma* and *Santanachelys gaffneyi* have the same epilastron shape.

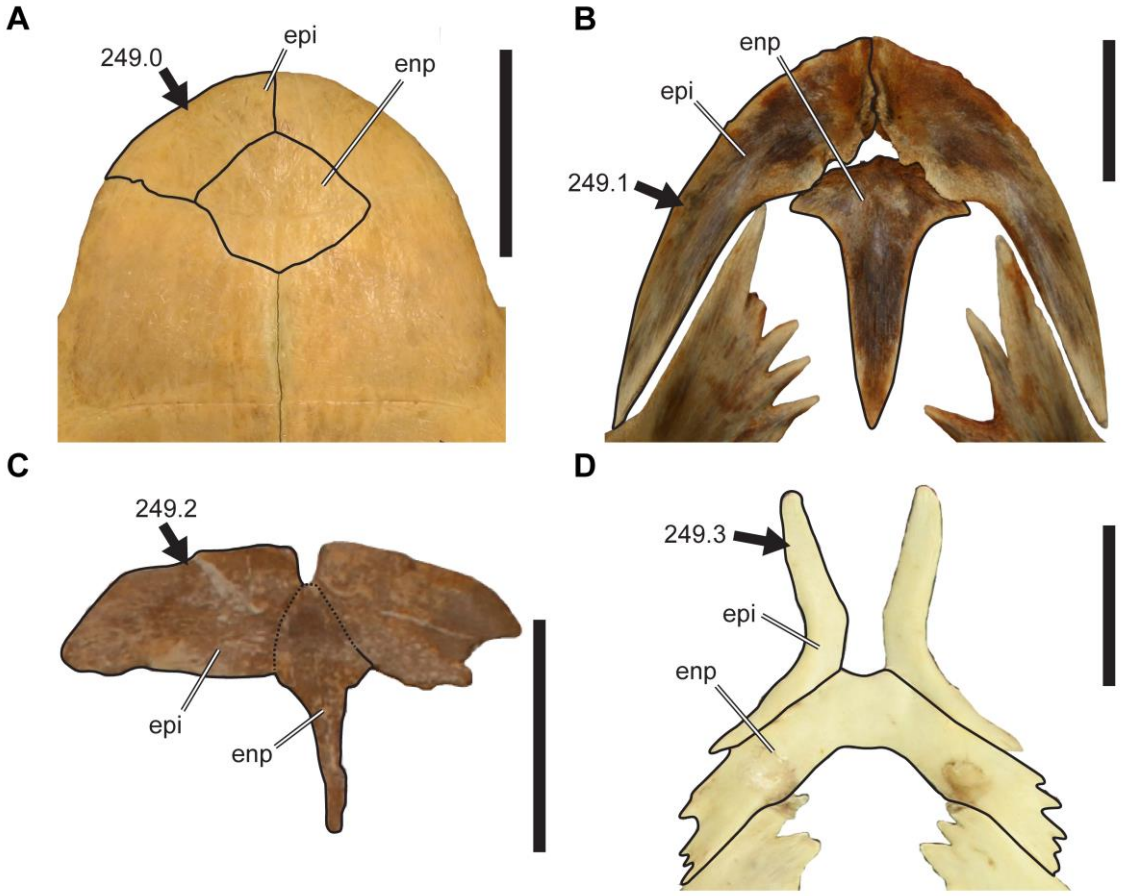


Fig. 4.3. Epiplastra of selected turtles. **A**, ventral view of *Podocnemis sextuberculata* (NHMUK 16075); **B**, ventral view of *Caretta caretta* (AMNH 129869); **C**, ventral view of *Chelosphargis advena* (KUVP 1219); **D**, ventral view of *Pelodiscus sinensis* (USNM 539335). Scale bars in A–B equal 5 cm, scale bar in D equals 2 cm. Scale bar in C equals approximately 3 cm, as the specimen dimensions were estimated from Zangerl (1953*a*). Numbers represent characters and character states. Abbreviations: *enp*, entoplastron; *epi*, epiplastron.

The condition is unclear in *Desmatochelys lowii*, as the lateral margins of the epiplastra are broken (Zangerl & Sloan 1960). I further modified the definition of this character to encode variation in epiplastron shape only. Previously, this character included observations on the contact of the epiplastra with one another, which is already encoded in a different character (character 239 of Evers & Benson 2018*a*; character 155 of Cadena & Parham 2018; character

244 of this study). Besides the changes described above, I added an additional state that distinguishes 'elongate' epiplastron morphologies. In previous matrices (e.g. Cadena & Parham 2015; Evers & Benson 2018*a*), the vast majority of taxa was scored as having 'elongate' epilastra, despite considerate variation between, for example, the 'elongate' epiplastra of cheloniids and chelydrids on one hand, and trionychids on the other (Fig. 4.3B, D).

> **Character 249**: Epiplastra, shape: 0 = epiplastra squarish in shape and forming parts of the anterior plastral lobe; 1 = epiplastra elongate, become narrower posteriorly along the anterolateral margin of the hyoplastron, and with gently convex lateral margin; 2 = epiplastra are laterally strongy expanded to a wing-like shape; 3 = epiplastra rod-like and anteriorly as narrow as posteriorly, with concave lateral margin.
>
> *Previous character definition*: Character 244 (Evers & Benson 2018*a*); character 160 (Cadena & Parham 2015). Epiplastra, shape and contact of epiplastra: 0 = epiplastra squarish in shape, lack a contact between each other due to the narrow participation of the antoplastron in the anterior plastral lobe edge; 1 = epiplastra elongate in shape, with medial contact located anterior to the entoplastron; 2 = epiplastra squarish in shape, lack of medial contact due to the extensive anterior projections of the entoplastron.

Xiphiplastron characters. In extant chelonioids, as well as some fossil taxa (e.g. *Allopleuron, Eopshargis*), the xiphiplastra are anteroposteriorly elongate rods that are separated from each other by a posterior fontanelle and have no midline contact (Fig. 4.4D). This state has commonly been coded for all chelonioids (e.g. *Puppigerus*: see Cadena & Parham 2015). However, examination of fossil chelonioids shows that the xiphiplastra in many fossil sea turtles vary substantially from the condition observed in modern forms.

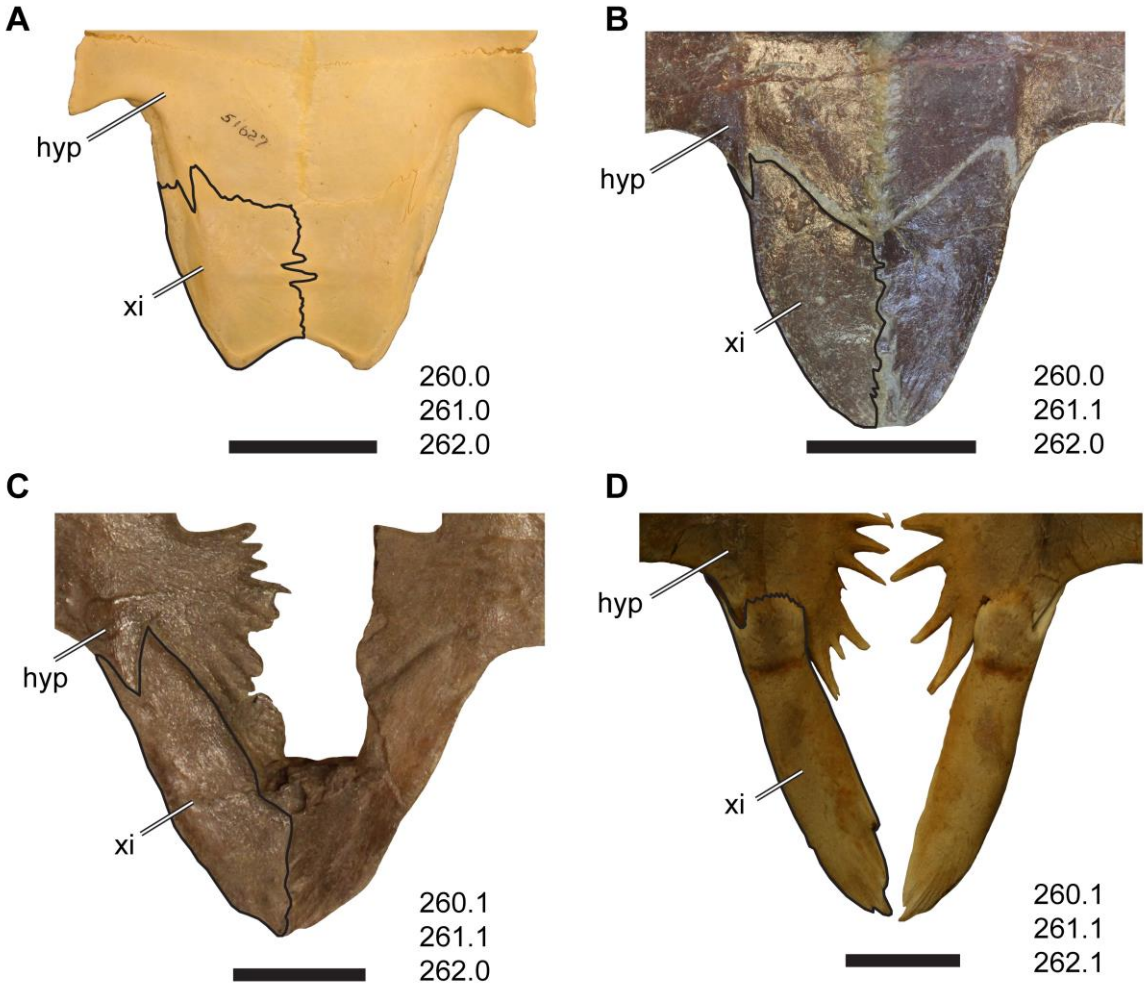


FIG. 4.4. Ventral view of posterior part of plastron of selected turtles. **A**, *Platysternon megacephalum* (FMNH 51627); **B**, *Puppigerus camperi* (IRSNB R 0073); **C**, *Eochelone brabantica* (IRSNB R 0061); **D**, *Caretta caretta* (AMNH 129869). Scale bar in A equals 3 cm, all other scale bars equal 5 cm. Black outlines denote the shape of the right xiphiplastron. Numbers represent characters and character states. Abbreviations: *hyp*, hypoplastron; *xi*, xiphiplastron.

For example, in *Puppigerus* (Fig. 4.4B), *Toxochelys* and Early Cretaceous protostegids such as *Santanachelys*, the xiphiplastra are plate-like structures that articulate with one another over their entire anteroposterior length and form a posterior plastral lobe. In other species, such as *Eochelone* (Fig. 4.4C), the plastral lobe is still present, but the xiphiplastra are separated from one another anteriorly and are more elongate and thus more similar to those of modern chelonioids, despite being not quite as narrow as in *Caretta* (Fig. 4.4D). However, all chelonioids share an oblique suture of the xiphilastron with the hypoplastron, whereby the xiphiplastron has an anterolateral process that extends along the posterolateral margin of the

hypoplastron. Some taxa, such as Late Cretaceous protostegids (*Desmatochelys*, *Archelon*, *Protostega*), have rod-like xiphiplastra similar to those of extant chelonioids, but they are sutured to each other posteriorly along the midline. To capture this variability, I coded three characters that describe distinct homologous features: the general shape of the xiphiplastron (character 260, plate like vs. rod-like); the nature of the suture with the hypoplastron (character 261, horizontal vs. oblique); and the inter-xiphiplastron contact resulting in a posterior plastral lobe (character 262, present vs. absent). I deleted the previous xiphiplastron shape character (character 255 of Evers & Benson 2018*a*; character 169 of Cadena & Parham 2015).

Character 260: Xiphiplastra, shape of xiphiplastra: 0 = triangular, trapezoidal, or rectangular plate-like element; 1 = anteroposterior elongate rods.

Character 261: Xiphiplastra, articulation with hypoplastron: 0 = the xiphiplastra articulate with the hypoplastra along an anteriorly facing margin, forming a mediolaterally broad suture; 1 = the xiphiplastra have an elongate anterolateral process articulating along the posterolateral margin of the hypoplastron, resulting in an oblique suture, and the hypoplastra extend posteriorly along the anteromedial margin of the xiphiplastra.

Character 262: Xiphiplastra, posteriorly in contact with one another, often sutured along the midline and forming a plastral lobe: 0 = present; 1 = absent.

Previous character definition: Character 255 (Evers & Benson 2018*a*); character 169 (Cadena & Parham 2015): character 169). Xiphiplastra, shape of xiphiplastra: 0 = almost triangular to trapezoidal, with lateral straight to convex margin; 1 = rectangular elongated in shape, coupled forming together with the hypoplastron a

very narrow posterior plastral lobe; 2 = narrow struts, separacted by the posterior fontanelle.

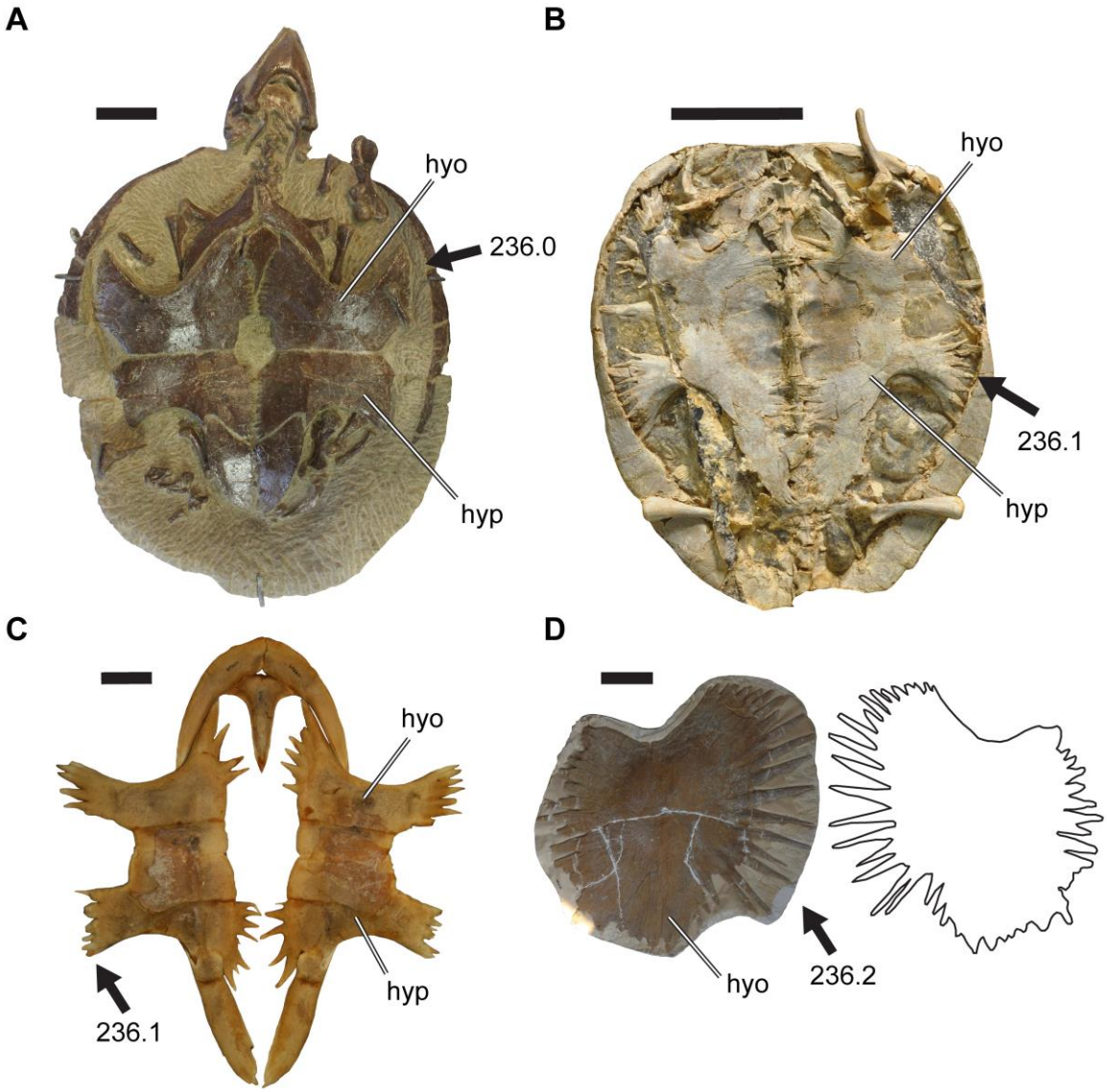


FIG. 4.5. A, ventral view of plastron of *Puppigerus camperi* (IRSN B 0073); **B**, ventral view of plastron of *Eurysternum wagleri* (CM 3409); **C**, ventral view of plastron of *Caretta caretta* (AMNH 129869); **D**, ventral view of right hyoplastron of *Protostega gigas* (FMNH PR 680). Note that outline of left hyoplastron in D is mirrored from the right element and added to give a better overview of the partial plastral arrangement. Numbers represent characters and character states. Scale bar in D is 10 cm, all other scale bars equal 5 cm. Abbreviations: *hyo*, hyoplastron; *hyp*, hypoplastron.

Plastral serrations. Evers & Benson (2018*a*) simplified a complex multistate character regarding the configuration of plastral fontanelles, the hyo-hypolastron contact and the axillar and inguinal notches that had been proposed by Cadena & Parham (2015: character 153) into a series of separate characters (characters 235–237 of Evers & Benson 2018*a*).

However, during my review of the scorings for chelonioids, I observed additional variation concerning the hyo- and hypoplastron serrations, which warrant a further modification to character 236 of Evers & Benson (2018*a*). Serrated margins to the hyo- and hypoplastra are variably developed among turtles and are present in multiple groups, including trionychians, some thalassochelydians and chelonioids. To better capture the degree of variation in serrations, I added an additional state to character 241 (= character 236 of Evers & Benson 2018*a*) that captures the hyo- and hypoplastron shape of most chelonioids (Fig. 4.5C) and most thalassochelydians with serrations (Fig. 4.5B). These taxa have strong serrations, which are limited to the anterolateral, anteromedial, posterolateral and posteromedial corners of the hyo- and hypoplastra. 'Star-shaped' hyo- and hypopastra with extreme serration along their almost entire bone margins are present in some protostegids such as *Archelon* and *Protostega* (Fig. 4.5D). I scored *Allopleuron hofmanni* as state 1, because despite its extremely long hyo- and hypoplastral serrations these are limited to those margins facing the opposite hyo- and hypoplastra, the entoplastron, xiphiplastra and the peripherals (e.g. Mulder 2003). The chelonioids *Puppigerus* (Fig. 4.5A) and *Eochelone* are scored as having state 0, because their serrations are only very weakly developed.

> **Character 241**: Plastron, hyo-hypoplastra serrations: 0 = serrations on the lateral and medial margins absent or weakly developed; 1 = strong serrations present along the surfaces that face other bones, but serrations are absent along the margin of the central fontanelle and the lateral contact area of hyo- and hypoplastro; 2 = strong serrations along all margins but the anterolateral margin of the hyoplastra and the posterlateral margin of the hypoplastra present, giving these elements a 'star-shaped' appearance.
>
> *Previous character definition***:** Character 236 (Evers & Benson 2018*a*), which was modified from character 153 of Cadena & Parham (2015). Plastron, hyo-hypoplastra

serrations: 0 = serrations on the lateral and medial margins absent or weakly developed; 1 = strong serrations along medial and lateral margins present.

Humerus characters. The matrix of Evers & Benson (2018*a*) adopted six characters (characters 325–330) from Cadena & Parham (2015: characters 237–242) that captured variation in the lateral processes of the humerus. However, as noted by previous authors (e.g. Bardet *et al.* 2013), some widely-used characters regarding humerus morphology have not been completely explained (e.g. Hirayama 1998; Parham & Pyenson 2010; Bardet *et al.* 2013). Most originated with the observations of Hirayama (1994), who coded a series of characters to capture what he called the 'cheloniid', 'dermochelyid' and 'protostegid' humeri. A conspicuous feature of chelonioid humeri is the position and shape of the lateral process, which in turtles is usually a rounded, knob-like process on the anterior surface of the proximal humerus (Fig. 4.6A, C) that is separated from the humeral head by a small notch or a bony ridge termed the preaxial 'shoulder' (Gaffney 1990). However, in chelonioids the lateral process is positioned more distally along the humeral shaft (Fig. 4.6D–G) and is therefore separated from the proximal end of the humerus, and the preaxial shoulder is either absent, or relatively low. The shift in position of the lateral process is apparent in the stem-group chelonioid *Toxochelys*, in which the lateral process is only moderately distally removed from the humeral head, but which retains a preaxial shoulder (e.g. Hirayama 1992; pers. obs. of FMNH P27403; Fig. 4.6D).

In cheloniids, including Cretaceous taxa such as *Allopleuron hofmanni* (e.g. Mulder 2003) and most protostegids (e.g. ?*Chelosphargis advena*: AMNH FARB 1975; *Desmatochelys padillai*: Cadena & Parham 2015), the lateral process is positioned further distally on the shaft of the humerus and the preaxial shoulder is absent. In *Dermochelys coriacea* (e.g. Völker 1913; Nielsen 1963; Hirayama 1992; Wyneken 2001), *Eosphargis breineri* (Nielsen 1963; pers. obs. SWE of FUR N 1450) and the gigantic Late Cretaceous protostegids from North America (e.g. *Archelon ischryos*: Wieland 1896; *Protostega gigas*: AMNH FARB 1503; Case

1897), the lateral process is positioned near mid-shaft (Fig. 4.6F–G). The lateral process is generally rounded (e.g. *Protostega*; Fig. 4.6F) and can be almost hemispherical.

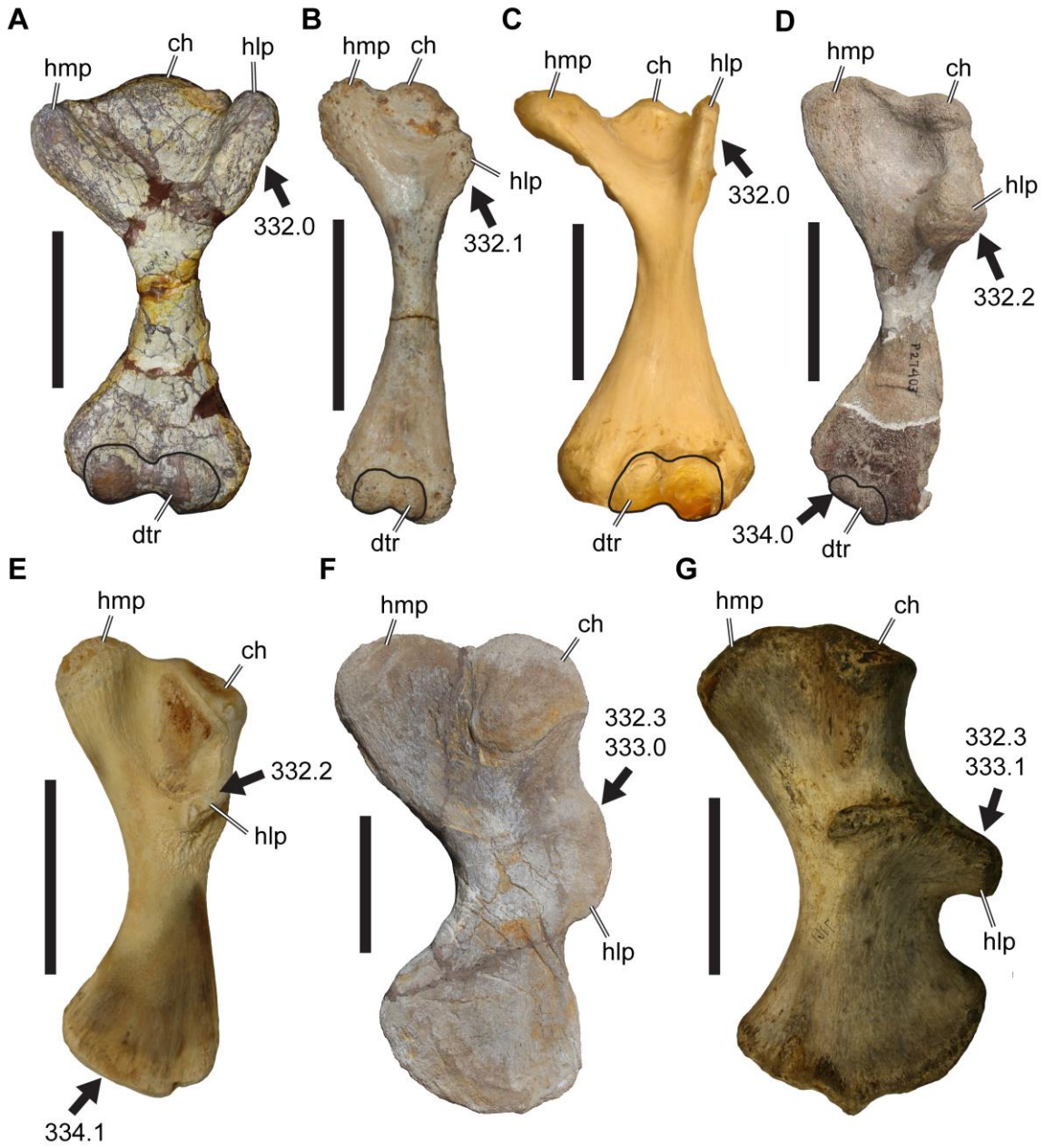


FIG. 4.6. **A**, right humerus of *Proganochelys quenstedti* (SMNS 16980) in ventral view, reflected for comparison; **B**, left humerus of *Sinemys gamera* (IVPP unnumbered) in ventral view; **C**, right humerus of *Chelydra serpentina* (FMNH 22056) in ventral view, reflected for comparison; **D**, left humerus of *Toxochelys* sp. (FMNH P27403) in ventral view; **E**, right humerus of *Caretta caretta* (AMNH 129869) in ventral view, reflected for comparison; **F**, left humerus of *Protostega gigas* (FMNH UR80) in ventral view; **G**, right humerus of *Dermochelys coriacea* (AMNH 7161) in ventral view, reflected for comparison. Scale bars in A, D, E–F equal 5 cm, scale bar in B equals 2 cm, scale bar in C equals 3 cm, scale bar in G equals 10 cm. Note that distal trochleae are outlined in A–D. Numbers represent characters and character states. Abbreviations: *ch*, humeral head; *dtr*, distal trochlea; *hlp*, lateral process of humerus; *hmp*, medial process of humerus.

This is different in *Dermochelys* and *Eosphargis*, in which the lateral process tapers to form a distally recurved tip, a feature that is only observed in these two taxa among my taxon sampling (Fig. 4.6G). Whereas the above-mentioned morphological variation is encoded in characters 331 (preaxial shoulder; character 324 of Evers & Benson 2018*a*), 332 (position of lateral process; character 325 of Evers & Benson 2018*a*) and 333 (tip-like expansion of lateral process; character 330 of Evers & Benson 2018*a*), a number of additional characters (326–329 in Evers & Benson 2018*a*, originally taken from Cadena & Parham 2015) have been used previously to express shape variation of the lateral process. However, I could not understand the characters or reproduce the scorings of previous authors based on our literature research and personal examination of specimens. Also, I think that variation in humerus morphology is adequately captured in the remaining characters. Therefore, I deleted characters 326–329 of Evers & Benson (2018*a*) from my matrix. The only characters pertaining to the lateral process of the humerus used in this study are:

> **Character 332**: Humerus, lateral process of humerus: 0 = abuts caput humeri; 1 = slightly separated from caput humeri; 2 = located distal to caput humeri but along proximal end of shaft; 3 = located at middle of humeral shaft.

> **Character 333**: Humerus, prominent anterior projection of lateral process: 0 = absent; 1 = present.

I coded an additional humeral character that has, to my knowledge, not been discussed previously: in crown-group chelonioids, as well as a range of fossil chelonioids, the distal surface of the humerus lacks a distinct trochlea for articulation with the antebranchium (Fig. 4.6E–G), whereas non-chelonioid turtles (Fig. 4.6A–C), as well as some chelonioids (e.g. *Toxochelys*: Fig. 4.6D; *Erquelinnesia*: IRSNB R 0067), have a distinct trochlea (Fig. 4.6A–B).

Character 334 (new): Humerus, distal articulation: 0 = articular surface forms distinct trochlea; 1 = rounded epiphyseal surface without clearly defined articulation facets.

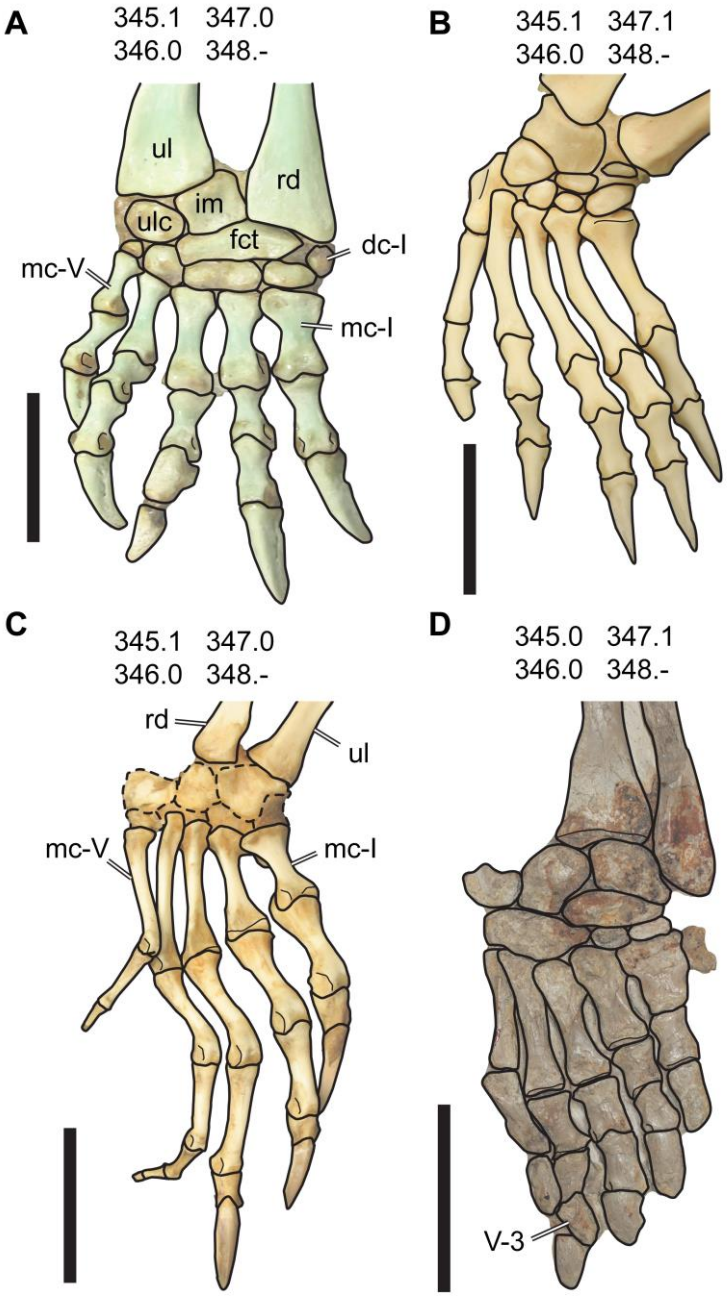


FIG. 4.7. Hands of selected non-americhelydian turtles. **A**, right manus of *Emys blandingii* (USNM 220869); **B**, right manus of *Chelus fimbriatus* (USNM 64154); **C**, right manus of *Apalone ferox* (USNM 71069); **D**, right manus of *Palaeomedusa testa* (BSPG AS I 818). Scale bar in A equals 10 mm, scale bars in B–D equal 30 mm. Note that Roman letters denote digits and Arabic numbers denote phalangeal position. Numbers represent characters and character states. Abbreviations: *dc*, distal carpal; *fct*, fused centralia; *im*, intermedium; *mc*, metacarpal; *pi*, pisiform; *rd*, radius; *ul*, ulna; *ulc*, ulnare.

Manus characters. Tong *et al.* (2006) discussed variation in the structure of the manus among chelonioids, but most of this variation has never been coded as phylogenetic characters. I add new characters to encode this variation here. To illustrate the manus morphology of chelonioids, as well as non-chelonioid turtles, I provide summary illustrations in Figures 4.7 and 4.8.

Tong *et al.* (2006) noticed that the ulnare of protostegids is much larger than the intermedium, whereas both these proximal carpals are subequally sized in dermochyids and cheloniids. This character was already included in previous studies and is retained herein as character 344 (character 340 of Evers & Benson 2018*a*; character 251 of Cadena & Parham 2015). I also include a new character that compares the sizes of the proximal carpals to the distal carpals, as that these bones are subequal in size in the stem-chelonioid *Toxochelys* (Fig. 4.8B), whereas the proximal carpals are generally larger than the distal ones in other chelonioids, including protostegids (Fig. 4.8C–F).

> **Character 345 (new)**: Size of proximal carpals vs. distal carpals: 0 = proximal carpals are of similar size with respect to distal carpals; 1 = proximal carpals are much larger than distal carpals.

Tong *et al.* (2006) noticed various differences in the digits of the chelonioid subgroups, (i.e. the dermochelyids, protostegids and cheloniids). For example, the second phalanx of the 3rd and 4th digits is long compared to the 1st phalanx in cheloniids (Fig. 4.8D–E), but not in protostegids (Fig. 4.8C), dermochelyids (Fig. 4.8F) or non-chelonioid americhelydians (Fig. 4.8A). Furthermore, protostegids have a third manual phalanx on their fifth digit (Fig. 4.8C), resulting in a manus phalangeal formula of 2-3-3-3-3 (Tong *et al.* 2006). The V-3 is absent in dermochelyids (Fig. 4.8F) or cheloniids (Fig. 4.8D–E), but present in *Toxochelys* and extant and extinct chelydroids (e.g. Fig. 4.8A). Another observation is that the 4th digit is the longest in protostegids and *Toxochelys* (Fig. 4.8B–C), whereas it is the 3rd in dermochelyids (Fig. 4.8F) and cheloniids (Fig. 4.8D–E). I included these observations as three characters:

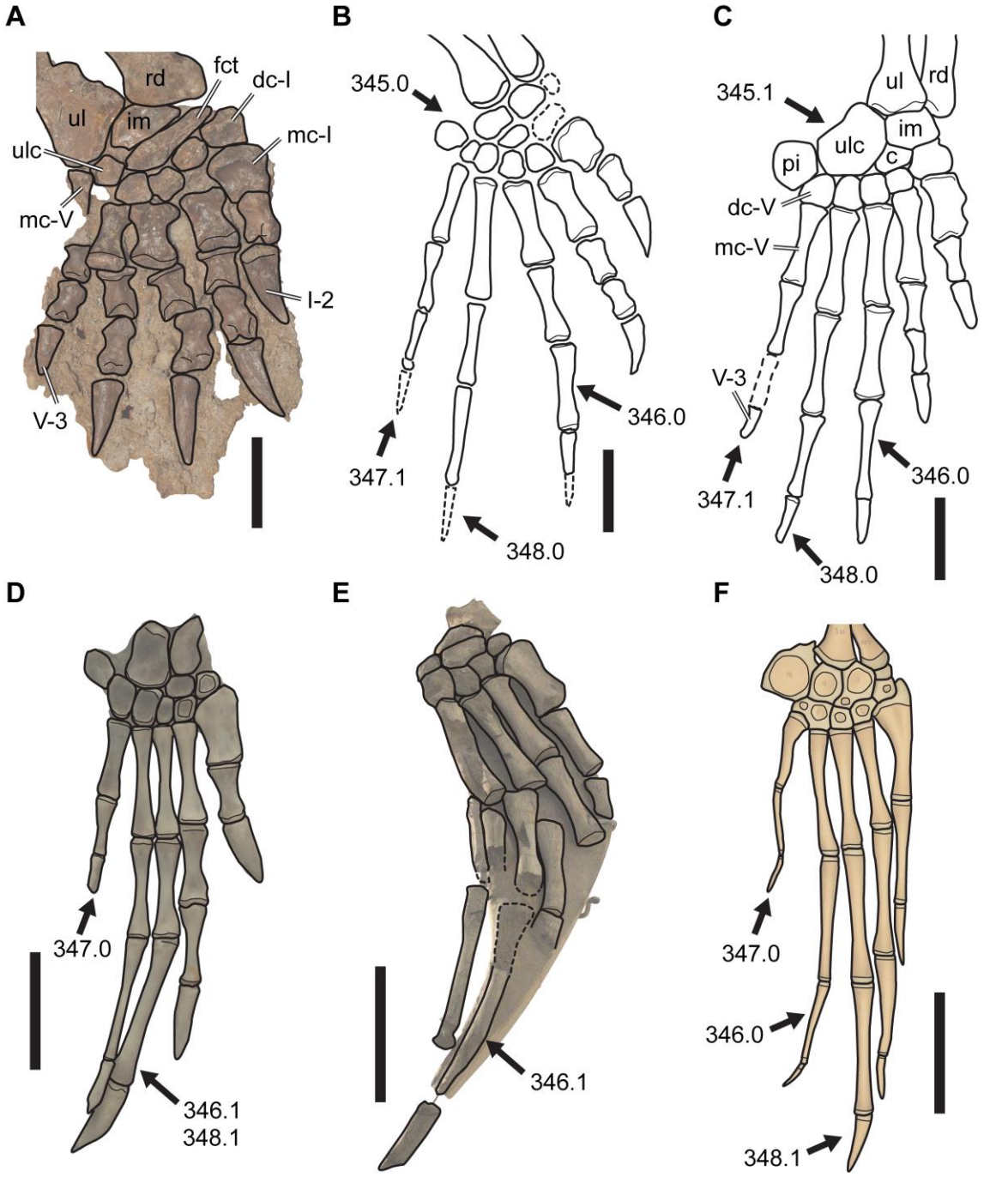


FIG. 4.8. Hands of selected americhelydian turtles. **A**, left manus of *Emarginchelys cretacea* (KUVP 23488), reflected for comparison; **B**, left manus of *Toxochelys latiremis* (YPM 2491), reflected for comparison and re-drawn from Wieland (1902); **C**, right manus *Protostega gigas* (CMNH 1421), re-drawn from Wieland (1906); **D**, left manus of *Eretmochelys imbricata* (MNHN Pal 1934-563), reflected for comparison; **E**, right manus of *Allopleuron hofmanni* (IRSNB R 3668); **F**, left manus of *Dermochelys coriacea* (unnumbered), reflected for comparison and re-drawn from Völker (1913). Scale bar in A approximates 3 cm (estimated from Whetstone 1978); scale bar in B approximates 5 cm (estimated from Wieland 1902); scale bar in C approximates 10 cm (estimated from Wieland 1906); scale bar in D equals 3 cm, scale bar in E equals 10 cm; scale bar in F approximates 20 cm (estimated from Völker 1913). Note that Roman letters denote digits and Arabic numbers denote phalangeal position.

Numbers represent characters and character states. Abbreviations: *c*, centrale; *dc*, distal carpal; *fct*, fused centralia; *im*, intermedium; *mc*, metacarpal; *pi*, pisiform; *rd*, radius; *ul*, ulna; *ulc*, ulnare. *(continued from previous page)*

Character 346 (new): Relative lengths of manual phalanges on the 3rd and 4th digit: 0 = the 1st phalanx is longer than or equally long as the 2nd phalanx; 1 = the 2nd phalanx is longer than the 1st phalanx. This character is scored as inapplicable when the manus digits only have two phalanges (i.e. the second phalanx is an ungual).

Character 347 (new): 3rd phalanx on 5th manual digit: 0 = absent; 1 = present.

Character 348 (new): Longest digit in the manus: 0 = 4th digit; 1 = 3rd digit. This character is scored as inapplicable when the 3rd and 4th digits are equally long.

Femur characters. The only femoral character in the matrix of Evers & Benson (2018*a*: character 344; taken from Cadena & Parham 2015: character 255) was originally taken from Hirayama's (1998; character 79) chelonioid phylogeny. The character reflects the webbing between the femoral trochanters in chelonioids, which is generally absent in non-chelonioid turtles, in which the trochanters are distinct processes that are not interconnected. However, in the previous character, variation in the depth of the intertrochanteric ridge was considered in the same character as the absence of the ridge. Here, I separate these observations into individual characters:

Character 352: Femur, femoral trochanters: 0 = distinct, and separated from one another; 1 = connected by a ridge.

Character 353: Femur, intertrochanteric ridge: 0 = ridge is low and concave, creating a notch between the major and minor trochanter; 1 = ridge is high and obliterates intertrochanteric notch, and the proximal surface of the trochanters and their

connecting ridge forms a continuous surface. This character is scored as inapplicable when an intertrochanteric ridge is absent (character 352.0)

Previous character definition: Character 344 (Evers & Benson 2018*a*); character 255 (Cadena & Parham 2015). Femur, femoral trochanters: 0 = distinct, and separated from one another; 1 = fossa obliterated, space between trochanters not concave, but notch present; 2 = fossa obliterated, trochanters connected by bony ridge without a notch.

In addition, I observed that the major trochanter and the femoral head form a continuous surface primitively in turtles like *Proganochelys quenstedti* (Fig. 4.9A, D) and also in crown group sea turtles (Fig. 4.9I, L) and some fossil chelonioids (Fig. 4.9H, K), but not in the stem-group chelonioid *Toxochelys* (Fig. 4.9G, J) or non-chelonioid crown-group turtles (Fig. 4.9B, E). I coded these observations in a separate character:

Character 354 (new): Femur, connection between femoral head surface and the major trochanter: 0 = the femoral head and major trochanter have distinct proximal surfaces separated by a deep notch; 1 = the femoral head surface slopes toward the major trochanter and forms a continuous proximal surface with it.

3.2.4 Parsimony analysis

The dataset was analysed using TNT 1.5 for Windows (Goloboff *et al.* 2008; Goloboff & Catalano 2016). I used a molecular backbone constraint following the topology of Pereira *et al.* (2017) for extant taxa, whereas all fossil taxa were left unconstrained. *Proganochelys quenstedti* was used as the outgroup. All characters were treated as equally weighted and unordered. I employed the new technology search algorithm in TNT with default settings and enabled tree drifting (Goloboff 1999) and parsimony rachet (Nixon 1999). The initial level of

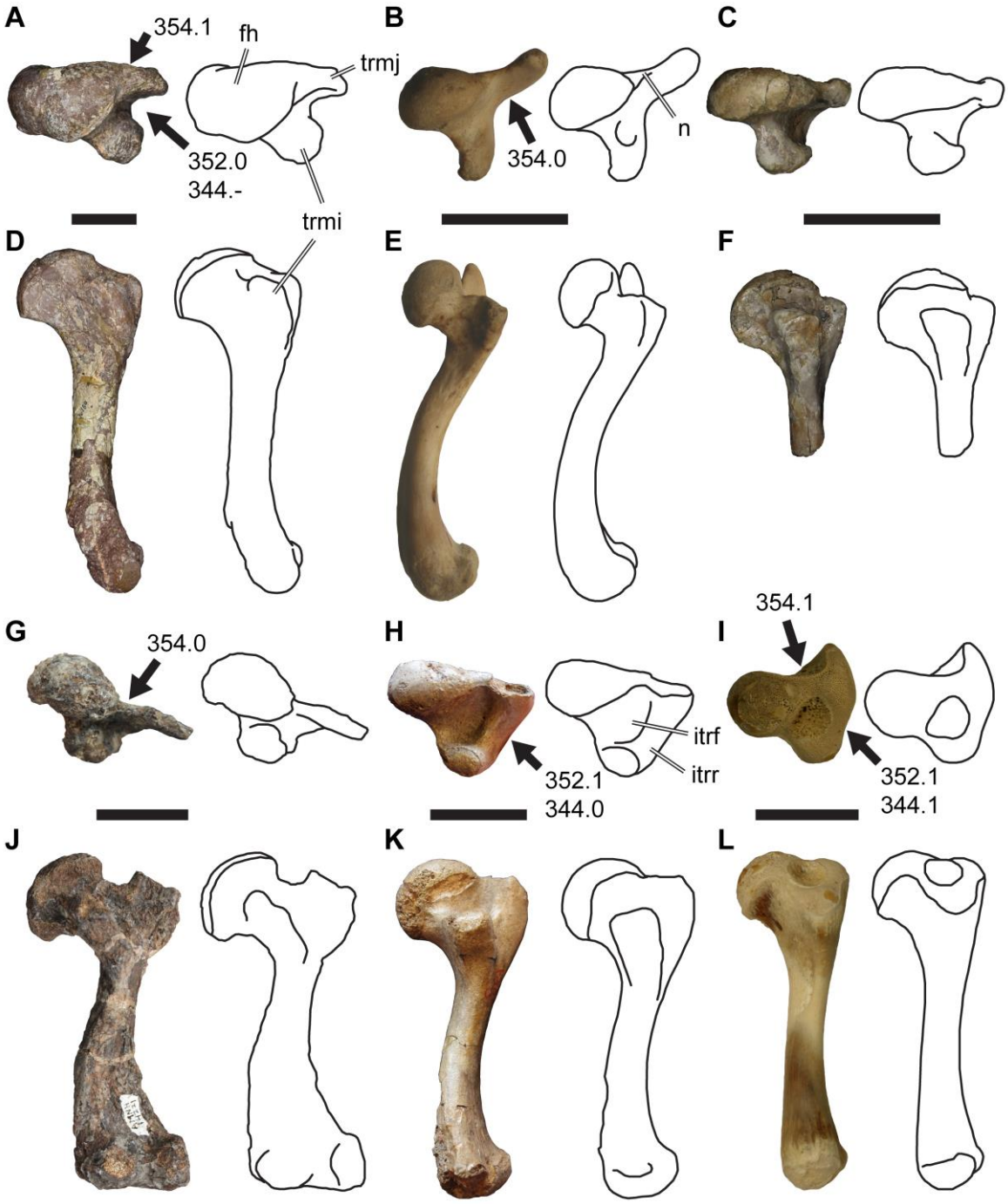


FIG. 4.9. Photographs and interpretative line drawings of femora in proximal (top row and third row) and anterior (second and bottom row). **A & D**, right femur of *Proganochelys quenstedti* (SMNS 16980); **B & E**, right femur of *Apalone spinifera* (YPM R190893); **C & F**, partial left femur of *Jurassichelon oleronensis* (PIMUZ AIII 514), reflected for comparisons; **G & J**, right femur of *Toxochelys browni* (AMNH FARB 14221); **H & K**, left femur of *Eochelone brabantica* (IRSNB R 0001), reflected for comparisons; **I & L**, right femur of *Caretta caretta* (AMNH 129869). All scale bars equal 3 cm. Abbreviations: *fh*, femoral head; *itrf*, intertrochanteric fossa; *itrr*, intertrochanteric ridge; *n*, notch between femoral head and major trochanter; *trmi*, minor trochanter; *trmj*, mahor trochanter.

driven search was set to 30, and the number of times the minimum tree length should be obtained was set to 30. I subjected the most parsimonious trees (MPTs) of this initial analysis to further tree bisection and reconnection (TBR). The resulting MPTs were used to construct a strict consensus tree, shown in Figure 4.10A. TNT was used to calculate absolute Bremer decay indices as a measure of branch support. Because the strict consensus tree topology was unresolved in part (see Results of phylogenetic analysis below), I used the following approaches to identify 'wildcard' taxa that occupied multiple distinct phylogenetic positions among the set of MPTs: (1) inspection of an Adams consensus tree in PAUP* for Macintosh (Swofford 2002) and (2) executing an iterative PCR (Pol & Escapa 2009) in TNT. Both methods identified the *Sinemys* clade (*Sinemys lens* + *Sinemys gamera*), *Erquelinnesia gosseleti* and *Oligochelone rupelensis* as the most unstable taxa which, if pruned from the consensus tree, result in an increase in resolution. Among the MPTs, the *Sinemys* clade was variously grouped with other sinemydids/macrobaenids or was found as the sister group to xinjiangchelyids. *Erquelinnesia* was found in various positions along the stem-group of cheloniids with *Allopleuron*, *Procolpochelys*, the group that included *Eochelone* or the group that included *Ctenochelys*. *Oligochelone* was found in the same positions, except it was never found to form a clade with *Allopleuron*. These 'wildcard' taxa were pruned accordingly to produce a reduced strict consensus tree (Fig. 4.10B). For visualisation, this tree was scaled to geological time using an *a posteriori* scaling method that uses first and last appearance dates for fossil taxa and an arbitrary minimum branch length parameter (Laurin 2004), by using commands from the *strap* (Bell & Lloyd 2014) and *palaeotree* packages (Bapst 2012). Ages and calibration settings, including minimum constraints for the ages of Cryptodira and Pleurodira, were used as in Evers & Benson (2018*a*), and these data and the additional age ranges for taxa added to our study are provided in Appendix S3. I chose this simple time calibration method to illustrate gross effects of our topological results on the timing of origination for the chelonioid subgroups investigated. A probabilistic approach to time-calibration that models divergence times simultaneously with topology is beyond the scope of this chapter and is provided in preliminary form in section 5 of this thesis. The calibrated

tree resulting from the minimum branch length scaling was further summarized to focus on chelonioids (see Calibrated tree and stratigraphic congruence below).

Character optimization was performed in PAUP*, because TNT only returns unambiguous synapomorphies, whereas the optimality criterion (i.e. ACCTRAN or DELTRAN) can be manually set in PAUP*. For the optimisation, a single MPT was selected from all MPTs. To select an MPT for optimisation, I computed a 50% majority rule consensus tree from the MPTs gained from the original analysis. The topology of this majority rule consensus tree was used as a constraint in PAUP* to find all MPTs compatible with the majority consensus rule topology. One of these MPTs was chosen at random for the optimisation. The topologies for the majority rule consensus tree (Appendix S3, Fig. S3.1), the MPT selected for optimisation (Appendix S3, Fig. S3.2), and the optimisation for all nodes, as well as for all characters are given in the Appendix 3.

4.3 RESULTS

4.3.1 Topological results of phylogenetic analysis

Parsimony analyses resulted in 138 MPTs that are 1724 steps in length. Additional TBR branch-swapping on these MPTs resulted in >10,000 MPTs. The most important gross topological findings of the analysis are (1) the recovery of xinjiangchelyids as stem-group turtles (as in Evers & Benson 2018*a*); (2) low resolution for sinemydids and macrobaenids, which form a polytomy with xinjiangchelyids and crown-group turtles (sinemydids-macrobaenids formed a clade in Evers & Benson 2018*a*); (3) the recovery of a monoplyletic Angolachelonia as the sister-group to pleurodires (Angolachelonia was the sister taxon to crown-group turtles in Evers & Benson 2018*a*); (4) protostegids form a monophyletic group on the stem-lineage of chelonioids, in a position one node more crownward than *Toxochelys* (protostegids were recovered as dermochelyoids in Evers & Benson 2018*a*) (Fig. 4.10).

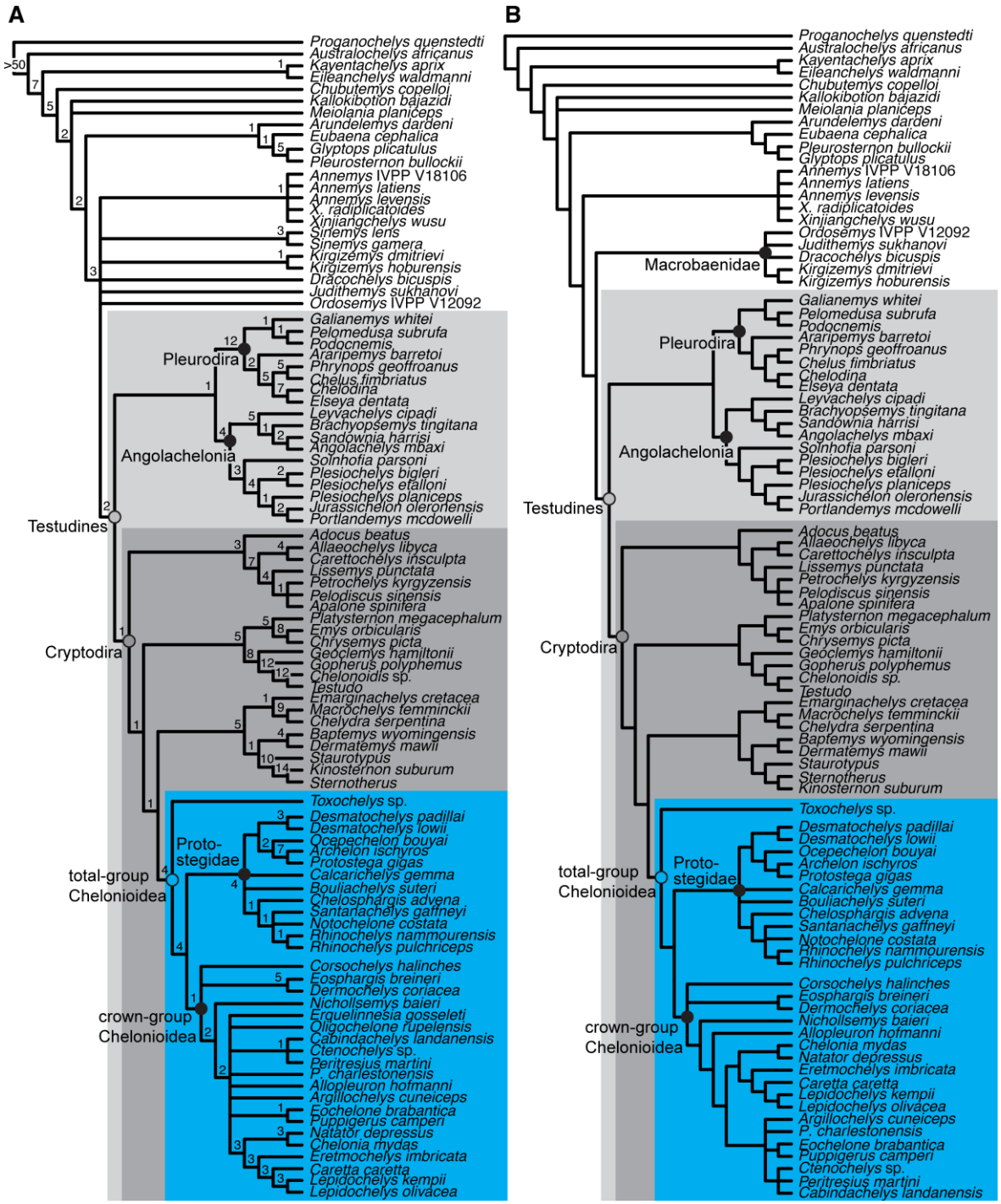


FIG. 4.10. Consensus trees of our phylogenetic analysis. **A**, strict consensus tree of >10,000 MPTs. **B**, reduced strict consensus tree obtained by pruning the *Sinemys* clade (*Sinemys lens* + *Sinemys gamera*), *Erquelinnesia gosseleti* and *Oligochelone rupelensis*.

The finding of angolachelonians as the sister-group to pleurodires was unexpected. Evers & Benson (2018*a*) found Angolachelonia (i.e. thalassochelydians + sandownids) as the most crownwardly positioned group of stem turtles. The topological change from this

inferred position to being stem-group pleurodires is relatively little in terms of parsimony cost, and the sister-group relationship of pleurodires and angolachelonians found in this study is poorly supported (Bremer support value = 1). Because I am primarily concerned with the ingroup relationships of the total-group of chelonioids in this study, I do not further explore the angolachelonian-pleurodire relationship herein. Examination of a more complete sample of early stem- and crown-group pleurodires will be important for character polarisations at the base of Pleurodira and resolving the membership of their total-group.

Evers & Benson (2018*a*) found protostegids to be dermochelyoids, as the sister group to *Dermochelys* + *Eosphargis* (i.e. dermochelyids). The position of protostegids within Chelonioidea was relatively strongly supported. However, in a series of Templeton's tests, Evers & Benson (2018*a*) could not reject the hypothesis that protostegids are stem-group chelonioids, and this relationship was found by Evers & Benson (2018*a*) in an analysis in which they only included a subset of Early Cretaceous protostegids (*Rhinochelys*, *Santanachelys*). Recently, Raselli (2018) also found protostegids as stem-group chelonioids by addition of five characters to the dataset of Cadena & Parham (2015), which had previously recovered protostegids as dermochelyoids. My results are mainly due to the modifications of postcranial characters and scores relative to Evers & Benson (2018*a*). More crownward positioned chelonioids (with regard to protostegids), as well as crown-group chelonioids, share several postcranial features that are absent in both protostegids and *Toxochelys*. These include, for instance, the presence of rib-free peripherals (character 216.1), the absence of a posterior contact of the xiphiplastra (character 262.0; independently absent in some cheloniids such as *Puppigerus*), the absence of a 3rd phalanx on the 5th manual digit (character 347.0), or the 3rd manual digit being the longest within the hand (character 348.1).

Most phylogenetic studies that have included protostegids have found the Late Cretaceous taxa *Archelon* and *Protostega* to be nested within a paraphyletic grade of protostegids from the Early Cretaceous, and *Santanachelys* was often found as the earliest branching protostegid. The analysis of Evers & Benson (2018*a*) instead found *Archelon* + *Protostega* in a clade that was the sister group to all other protostegids. Here, I find two

principal clades of protostegids: one includes the Late Cretaceous *Protostega*, *Archelon*, *Ocepechelon*, *Desmatochelys lowii* and the Early Cretaceous *Desmatochelys padillai* (Fig. 4.10). The species of *Desmatochelys* are found as sister taxa, as in Cadena & Parham (2015) and Evers & Benson (2018*a*). The second clade of protostegids is composed mainly of Early Cretaceous and early Late Cretaceous taxa and includes *Rhinochelys pulchriceps*, *Rhinochelys nammourensis*, *Santanchelys*, *Notochelone*, and *Chelosphargis*. The species of *Rhinochelys* are found as sister taxa, supporting the generic assignment of *R. nammourensis* by Tong *et al.* (2006). *Bouliachelys suteri* and *Calcarichelys gemma* are found in a polytomy with both protostegid subclades.

Corsochelys halinches is recovered in a polytomy with dermochelyids and cheloniids: therefore, it is currently unclear if *Corsochelys* is a stem-group chelonioid or a crown-group chelonioid on the stem of either *Dermochelys* or extant cheloniids. Consistent with previous suggestions (Nielsen 1959; Wood *et al.* 1996; Joyce *et al.* 2013*b*) and the findings of Evers & Benson (2018*a*), *Eosphargis* is found on the stem-group of *Dermochelys*.

The ingroup relationships of cheloniids show poorer resolution in this study than in Evers & Benson (2018*a*), but this is because I included more taxa and taxa with relatively fragmentary remains, such as *Peritresius martini*. I find *Nichollsemys baieri* from the late Campanian of North America as the earliest stem-group cheloniid, rather than as a toxochelyid stem-group chelonioid as in study first describing *Nichollsemys* (Brinkman *et al.* 2006). One node more crownward, I find a large polytomy that includes extant cheloniids (as a clade), (*Eochelone* + *Puppigerus*), (*Cabindachelys* + *Ctenochelys* + *Peritresius*), *Erquelinnesia*, *Oligochelone*, *Procolpochelys*, *Allopleuron* and *Argillochelys*. My results support the hypothesis of several recent studies that proposed cheloniid affinities for *Ctenochelys* (Gentry 2016; Gentry *et al.* 2018). Alternatively, *Ctenochelys* had been hypothesized to be a stem-group chelonioid, often in a clade with *Toxochelys* (e.g. Brinkman *et al.* 2006). Gentry *et al.* (2018) found a clade that includes *Ctenochelys* and *Peritresius*, which is supported by my study, but I additionally find *Cabindachelys* within this clade. *Cabindachelys* was instead found in a clade with *Erquelinnesia* in Myers *et al.* (2018).

My finding of a *Puppigerus* + *Eochelone* clade is in accordance with previous studies of these taxa (e.g. Moody 1974). *Eochelone* was found as the earliest branching stem-group cheloniid in Evers & Benson (2018*a*), but that was most likely the result of poor character sampling: in Evers & Benson (2018*a*), *Eochelone* was scored primarily on the basis of an incomplete, CT-scanned skull and no postcranial material. Since this earlier paper, I studied the holotype and referred specimens of *Eochelone brabantica*, so that I could now expand the cranial scorings and add postcranial scorings for this taxon.

Puppigerus (and by extension the clade of *Puppigerus* + *Eochelone*) is most often found to be the immediate sister taxon of crown-group cheloniids (e.g. Hirayama 1994; Cadena & Parham 2015; Gentry 2016; Gentry *et al.* 2018), although this could sometimes be an artifact of small sample sizes of fossil cheloniids (e.g. Weems & Brown 2017 find some rarely included Oligocene and Miocene taxa more closely related to crown-group cheloniids than is *Puppigerus*). The cheloniid in-group relationships in this study are too poorly resolved to thoroughly examine whether *Puppigerus* + *Eochelone* represent a more recently or less recently diverging clade of stem-group cheloniids with respect to the youngest (Oligocene and Miocene) taxa I included, because *Oligochelone* and *Procolpochelys* are found in a polytomy that includes crown-group cheloniids as well as *Puppigerus* + *Eochelone*.

Many studies have also found *Argillochelys* to be closely related to *Eochelone* and *Puppigerus* (e.g. Hirayama 1994) and Moody (1968; 1974) referred these three taxa to his subfamily Eochelyinae. The phylogenetic position of *Argillochelys* is unresolved with regard to other stem-group cheloniids in my analysis. This likely results from the fact that I did not include postcranial scorings for *Argillochelys* as most of the material that I studied (in the NHMUK) have incorrect or contradictory specimen labels, and many specimens are labelled as various combinations of '*Argillochelys*', '*Lytoloma*', '*Eochelys*' and '*Puppigerus*'. Therefore, in the absence of cranial-postcranial associations of *Argillochelys*, it is not entirely clear to me, which postcranial specimens pertain to *Argillochelys*. Specimens of *Puppigerus* are easier to identify, because several near-complete specimens have been found in association (NHMUK PV R14375) or articulation (IRSNB R 0072, 0073) with *Puppigerus* skulls. In my reduced

strict consensus tree, *Argillochelys* is found in a polytomy with (*Eochelone* + *Puppigerus*) and (*Ctenochelys* + *Cabindachelys* + *Peritresius*), indicating that there is some support for a relatively close relationship with *Puppigerus*.

Pruning *Erquelinnesia* and *Oligochelone* from the strict consensus tree results in an additional node, placing *Allopleuron* as a stem-group cheloniid that is positioned one node more crownward than *Nichollsemys*. Excluding *Sinemys lens* and *Sinemys gamera* also improves the resolution, and results in a clade that contains macrobaenids and sinemydids, which are found as the sister group to crown-group turtles and thus one node crownward of xinjiangchelyids. This result is compatible with the topology found in Evers & Benson (2018*a*).

4.3 DISCUSSION

4.3.1 Calibrated tree and stratigraphic congruence

The recovery of protostegids as stem-group chelonioids positioned one node more crownward than *Toxochelys* reduces ghost-lineages for total-group cheloniids and dermochelyids in comparison to those implied by the alternative hypothesis of protostegids being the sister group to dermochelyids (see Cadena & Parham 2015; Evers & Benson 2018*a*). However, despite this apparent increase in stratigraphic congruence, the new placement for protostegids found in this study still implies long ghost lineages for crown-group chelonioids (c. 35 Ma), *Toxochelys* (c. 45 Ma) and chelydroids (c. 60 Ma; Fig. 4.11; see also Evers & Benson 2018*a*). Raselli (2018) recently argued that placing protostegids on the stem-lineage of chelonioids increases the congruence between the stratigraphic occurences of crown-group chelonioids and molecular divergence time estimates. However, this is not the case: molecular clock estimates are informed by fossil calibration points representing the oldest members of crown-groups. Origination times for the chelonioid crown-group around the Cretaceous/Palaeocene boundary recovered by previous studies (e.g. Joyce *et al.* 2013*b*)

were the result of using Eocene calibration points that are likely too young (Evers & Benson 2018*a*). A number of studies have demonstrated recently that some mid-Late and Late Cretaceous fossils can be placed confidently within the chelonioid crown-group (e.g. *Ctenochelys*: Gentry 2016; *Peritresius*: Gentry *et al.* 2018; *Allopleuron*: Evers & Benson 2018*a*). Considering these fossils as minimum age constraints for the chelonioid crown-group (and ignoring protostegids as members of the stem-group) pushes the origin of crown-group chelonioids back to at least the Turonian (c. 90 Ma; Fig. 4.11). Furthermore, the Early Cretaceous age of protostegids requires ghost-lineages within Americhelydia irrespective of their exact position within this clade.

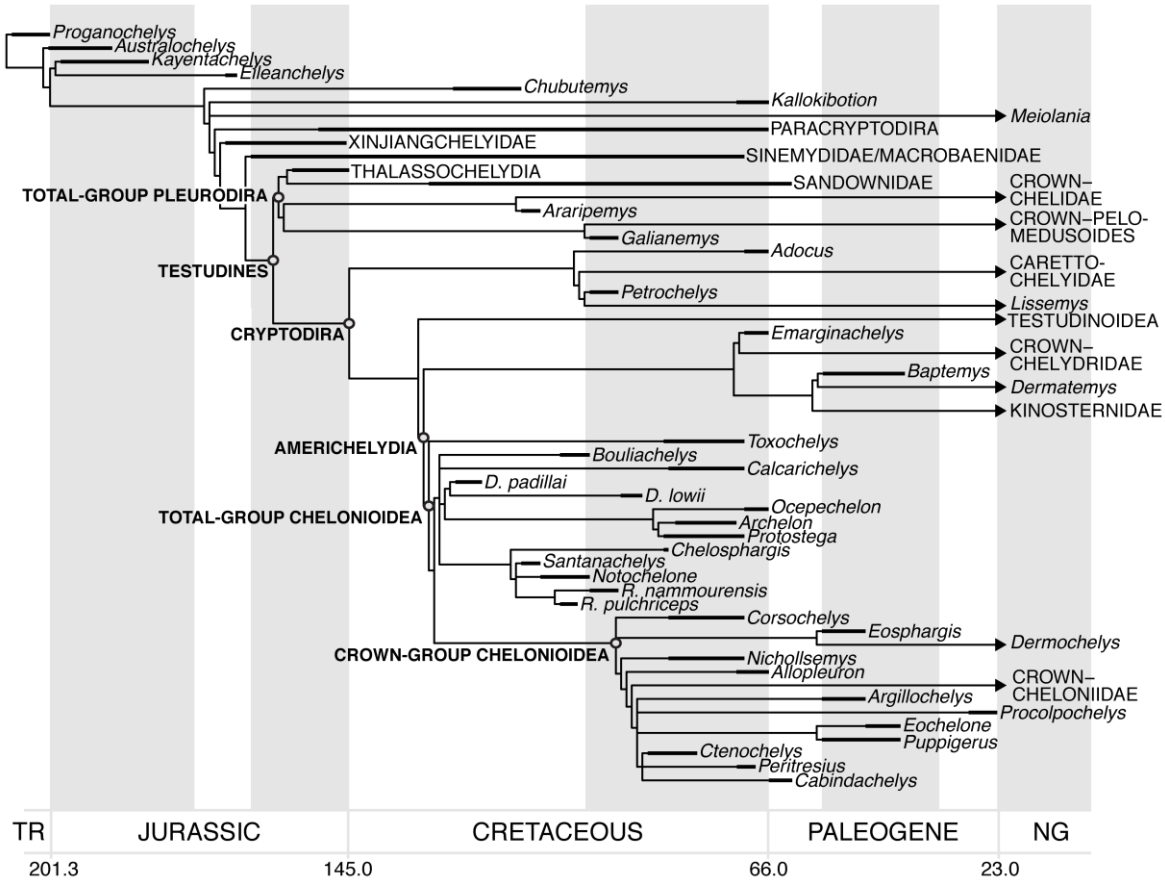


FIG. 4.11. Simplified reduced strict consensus tree scaled to geologic time using range data for turtles.

Although the earliest fossil evidence for chelydroids, crown-group chelonioids (e.g. *Ctenochelys*) and the earliest branching stem-group chelonioid (*Toxochelys*) all come from North America, it is conspicuous that North American americhelydian fossils, including

protostegids such as *Calcarichelys*, *Desmatochelys lowii*, *Archelon* and *Protostega*, only appear from the Coniacian (Late Cretaceous) onwards. Americhelydians most likely have a North American origin (e.g. Joyce *et al.* 2013*b*; Crawford *et al.* 2014; Parham *et al.* 2014; Cadena & Parham 2015; Gentry 2016; Perreira *et al.* 2017; Evers & Benson 2018*a*), but the oldest americhelydian fossils are protostegids from South America (*Desmatochelys padillai*: Cadena & Parham 2015; *Santanachelys*: Hirayama 1998), Europe (*Rhinochelys*: Collins 1970) and Australia (*Bouliachelys*: Kear & Lee 2006). The absence of Early Cretaceous americhelydians from North America can likely be explained by the limited exposure of terrestrial rocks from that time in this region (Evers & Benson 2018*a*). Therefore, the stratigraphic incongruence implied by chelonioid affinities for protostegids is possibly a discovery artefact.

4.3.2 Evolution of flippers

The evolution of chelonioid flippers has been discussed in several studies (e.g. Hirayama 1998; Kear & Lee 2006; Joyce 2007), with different authors arriving at different conclusions regarding the homology vs. convergence of the flipper features observed in protostegids, dermochelyids and cheloniids. My expanded chelonioid taxon sampling and revision of characters specifically related to the marine ecology of chelonioids allowed me to re-interpret chelonioid flipper evolution in the context of my tree topology. I identified characters related to the pectoral girdle and forelimb that are related to the modification of chelonioid arms and hands into flippers. These characters encode structural modifications of the scapula (character 313), muscle attachment sites (characters 332, 336), relative lengths of bones (characters 314, 337, 334–336, 348), flattening of bones (character 350), flipper reinforcement by means of articular surface modification from ginglymoid joints to butt joints (characters 334, 341–342) and the phalangeal formula (character 347). These features are summarized in Table 4.2 and were mapped onto the tree topology that was used during the optimization process (Fig. 4.12).

TABLE 4.2. Character evolution of traits relevant to the formation of flippers across the total-group of Chelonioidea. Note that 'Taxon+++' denotes a clade including that taxon and all more crownward positioned taxa, and that 'Taxon A ++ Taxon B' denotes the most inclusive clade including taxa A and B.

Character	Plesio-morphic state	Apo-morphic state	Transition at node	Optimisation
313; internal angle of scapula	0	1	Protostegidae+++	Unambiguous
314; relative coracoid–humerus length	0	1	Protostegidae+++	Unambiguous
332; position of lateral humerus process	0	2	total-group Chelonioidea	Unambiguous
	2	1	*Corsochelys halinches*	Unambiguous
	2	3	Dermochelyidae	Unambiguous
	2	3	*Ocepechelon* ++ *Protostega*	ACCTRAN
			Archelon + *Protostega*	DELTRAN
	2	0	*Peritresius* ++ *Ctenochelys*	ACCTRAN
			Ctenochelys	DELTRAN
333; anterior projection of lateral humeral process	0	1	Dermochelyidae	Unambiguous
334; distal humerus trochlea	0	1	Protostegidae+++	Unambiguous
	1	0	*Erquelinnesia*	Unambiguous
336; M. latissimus dorsi muscle scar	0	1	crown-group Cheloniidae	Unambiguous
	0	1	*Ocepechelon* ++ *Protostega*	ACCTRAN
			Archelon + *Protostega*	DELTRAN
337; relative humerus–femur length	0	1	total-group Chelonioidea	Unambiguous
341; rigid 1st–2nd digit articulations	0	1	Protostegidae+++	Unambiguous
	1	0	*Santanachelys* + *Notochelone*	ACCTRAN
			Santanachelys	DELTRAN
342; rigid 3rd–5th digit articulations	0	1	total-group Chelonioidea	Unambiguous
344; relative ulnare–intermedium size	1	2	total-group Chelonioidea	ACCTRAN
			Protostegidae+++	DELTRAN
	2	1	total-group Cheloniidae	ACCTRAN
			Allopleuron+++	DELTRAN
345; relative proximal–distal carpal size	0	1	Protostegidae+++	Unambiguous
346; relative lengths of manual phalanges	0	1	total-group Cheloniidae	ACCTRAN
			Allopleuron+++	DELTRAN
347; presence of 3rd phalanx on 5th digit	1	0	crown-group Chelonioidea	ACCTRAN
			total-group Cheloniidae	DELTRAN
348; longest manual digit	0	1	crown-group Chelonioidea	ACCTRAN
			total-group Cheloniidae	DELTRAN

Character	Plesio-morphic state	Apo-morphic state	Transition at node	Optimisation
350; flattening of carpals	0	1	total-group Chelonioidea	Unambiguous

The tree topology and character optimization imply step-wise acquisition of the traits that characterise flippers. Many flipper character states are unambiguously optimized to appear at the base of the chelonioid tree (Fig. 4.12) and are either shared among all total group chelonioids, or are shared between protostegids and crown-group chelonioids, but are absent in *Toxochelys*, the earliest branching stem-group chelonioid. The traits that evolved earliest are: a shift in the position of the lateral process of humerus so that it is removed from the humeral head (332.2); a humerus that is elongated with respect to the femur (337.1); reduction of ginglymoid interphalangeal joints in the 3rd–5th manual digits (342.1); and a flattening of tarsal and carpal elements (350.1). One node more crownward, and thus shared by all total-group chelonioids but *Toxochelys*, the optimization implies: the evolution of a wide internal angle of the scapula (313.1); relative elongation of the coracoid (314.1); reduction of the trochlea on the distal end of the humerus for the antebranchium (334.1); reduction of ginglymoid interphalangeal joints in the 1st and 2nd manual digits (341.1); and relative enlargement of proximal carpals with regard to distal carpals (345.1). Furthermore, the relatively large ulnare (344.2) evolves either at the base of total-group Chelonioidea (ACCTRAN) or in Protostegidae + more-crownwardly positioned chelonioids (DELTRAN). This pattern of character evolution suggests that some fundamental biomechanical features typical for flippers in general (e.g. flattening of elements, lengthening of the humerus and reduction of mobility between individual flipper elements) as well a traits likely important for moving the flippers effectively (e.g. lateral humeral process position and internal scapula angle) evolved first.

It has been hypothesized that many of these features evolved convergently in at least protostegids and dermochelyids + cheloniids, but possibly in all three groups (e.g. Hirayama 1998; Kear & Lee 2006). However, hypotheses about these character state transitions are

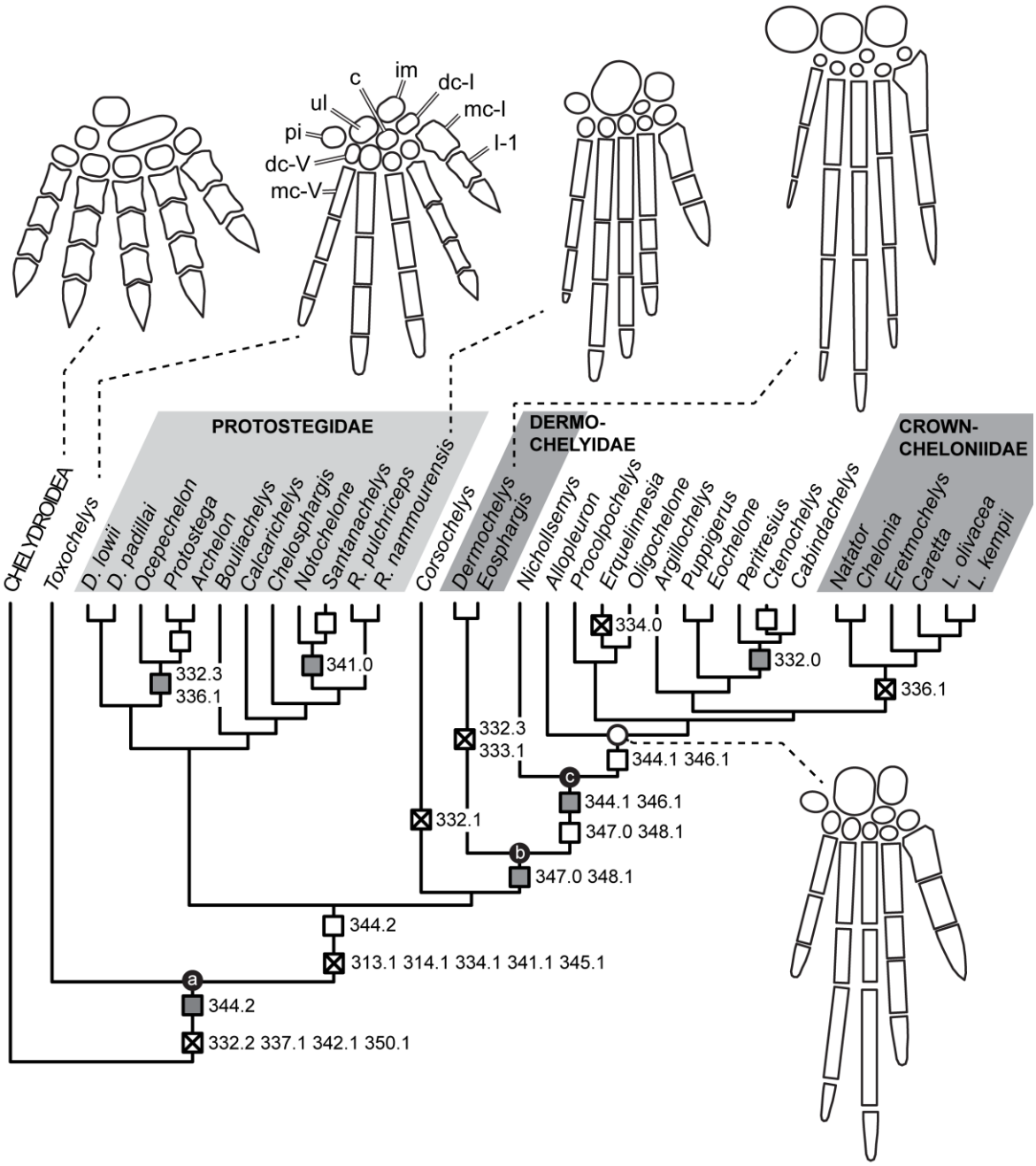


FIG. **4.12**. Simplified topology of chelonioids with character state transitions mapped onto the tree. The topology is the one used for character optimization and represents one MPT from the original analysis that is consistent with the topology of a 50% majority rule consensus tree. Boxes with crosses represent unambiguous character transitions, open boxes represent DELTRAN, and shaded boxes represent ACCTRAN. Numbers above boxes represent character numbers, numbers below boxes show the apomorphic state. For plesiomorphic states, please refer to Table 7. Line drawings represent schematic flipper morphology for specific OTUs (top row), and the generalised flipper morphology of early cheloniids (bottom right). Note that Roman letters denote digits and Arabic numbers denote phalangeal position. Abbreviations: *c*, centrale; *dc*, distal carpal; *im*, intermedium; *mc*, metacarpal; *pi*, pisiform; *ulc*, ulnare.

sensitive to the phylogenetic positions of individual taxa. For example, the recovery of *Toxochelys,* which lacks many of the derived flipper traits of other chelonioids (e.g. rigid interphalangeal articulations between the 1st and 2nd manual digits), as a stem-group cheloniid in Hirayama (1994, 1998) resulted in the optimization of absence of these traits as plesiomorphic within cheloniids. The recovery of the Early Cretaceous protostegid *Santanachelys* on the stem-group of *Dermochelys* in the same analysis implied independent evolutionary tranistions to a fully rigid flipper in cheloniids and dermochelyids (as *Santanachelys* has the same 1st and 2nd digit articulation pattern observed for *Toxochelys*; Hirayama 1998). *Toxochelys* has been unambiguously accepted as a stem-group chelonioid in later studies and I find *Santanachelys* well-nested within Protostegidae (see also Evers & Benson 2018*a*). My results therefore imply a single origin of fully rigid flippers but require a reversal within protostegids to accommodate *Santanachelys*. It is noteworthy that *Santanachelys* has only been described in a relatively short paper, which does not illustrate the flipper morphology in detail (Hirayama 1998). To further elucidate some aspects of flipper evolution, the flippers of *Sanatachelys* should be re-investigated, but this was beyond the scope of this study.

The optimization also suggests that the fundamental flipper bauplan outlined by the character state changes above was later modified in different ways by different groups of chelonioids (Fig. 4.12). For instance, the position of the lateral process of the humerus was independently shifted further distally (332.3) in dermochelyids and some protostegids (DELTRAN: *Archelon* + *Protostega*; ACCTRAN: *Ocepechelon* ++ *Archelon*). Similarly, the muscle scar for the *M. latissimus dorsi* shifted distally on the humerus shaft (336.1) in crown-group cheloniids and convergently in *Archelon* + *Protostega* (DELTRAN; ACCTRAN: *Ocepechelon* ++ *Archelon*).

A number of flipper traits appear first early in the evolution of cheloniids (Fig. 4.12). For example, the absence of a 3rd phalanx on the 5th manual digit (347.0) and the relative elongation of the 3rd digit with regard to the 4th (348.1) are optimised at the node of total-group cheloniids under DELTRAN, but could have evolved in crown-group chelonioids

(ACCTRAN). Within total-group cheloniids, the second phalanges become elongated relative to the first phalanges (346.1) sometime during the early evolution of the group (ACCTRAN: *Nichollsemys*+++; DELTRAN: *Allopleuron*+++). Similar to the pattern observed for cheloniids, flipper modifications specific to dermochelyids appear in the early evolution of the group: the only fossil dermochelyid included in my study, *Eosphargis breineri* from the Ypresian of Denmark, already shows the mid-shaft position of the lateral humeral process (332.3) and the anterior projections of said lateral process (333.1), which is otherwise only seen in the extant leatherback *Dermochelys* (Fig. 4.12).

In summary, forelimb modifications related to the formation of flippers are concentrated at deep nodes and can thus be inferred to have happened early in the evolution of total-group chelonioids. Further modifications specific to cheloniids and dermochelyids are also observed early in the respective records of stem taxa. Protostegids generally retain the flipper morphology that evolved early among chelonioids more generally, as no flipper character state changes are observed along the lineage leading to the deeply nested *Rhinochelys nammourensis*, which preserves complete flippers (Tong *et al.* 2006). However, some modifications that are optimised as being convergent with cheloniids (336.1; see above) or dermochelyids (332.3; see above) are observed in the gigantic taxa from the Late Cretaceous (*Archelon* and *Protostega*). The lack of detailed knowledge of flipper morphology outside of these well-known protostegids currently precludes a more detailed investigation of the protostegid flipper.

4.4 CONCLUSIONS

I modified the recently published character-taxon matrix of Evers & Benson (2018*a*) to specifically include more chelonioid taxa. Additionally, I revised the postcranial characters used in Evers & Benson (2018*a*), based on new observations regarding body parts that are particularly modified in chelonioids, such as the forelimbs and the shell. The characters were also vetted to ensure that they adequately reflect primary hypotheses of homology. Analysis

of this dataset removes protostegids from the chelonioid crown-group and places them onto the stem of chelonioids. This results from the absence of several synapomorphies of more crownwardly positioned chelonioids in protostegids.

The position of protostegids as stem-group chelonioids implies shorter ghost lineages for crown-group chelonioids, but still requires long ghost lineages for deeper divergences of americhelydians. The ingroup relationships of protostegids are different to those reported in most previous studies: Rather than finding Early Cretaceous taxa as a paraphyletic grade leading to gigantic forms from the Late Cretaceous, I find two clades of protostegids, which largely correspond to Early and Late Cretaceous taxa. Although protostegids are removed from the crown-group of chelonioids, I find other evidence for the presence of crown-group chelonioids in the Late Cretaceous. For example, *Ctenochelys*, *Nichollsemys*, *Allopleuron*, *Peritresius*, and possibly others are found as stem-group cheloniids.

My tree topology implies that most traits fundamental to modern chelonioid flippers evolved only once, early on the chelonioid stem-lineage. However, secondary modifications to the general flipper bauplan are observed at the base of crown-cheloniids and dermochelyids, as well as in the clade delimiting the gigantic protostegids *Archelon* and *Protostega*. Although instances of convergent evolution between the chelonioid subgroups are apparent for individual characters, the flipper morphology of extant sea turtles is the result of a stepwise acquisition of derived characters that are concentrated at deep nodes in their phylogeny.

SUPPORTING INFORMATION

Additional Supporting Information can be found in Appendix S2 of this thesis.

5 FUTURE RESEARCH: TREE CALIBRATION USING TIP-DATING APPROACHES

NOTES

This chapter has been prepared using advise about model parameter choices by Luke Parry.

5.1 Motivation

Phylogenies are hypotheses of relatedness among organisms. Phylogenetic hypotheses can be derived in various ways, but the most commonly used approach in palaeontological sciences is a cladistic analysis (Hennig 1966; Felsenstein 1983). In a cladistic analysis, relationships of organisms are inferred from comparative character data by minimizing evolutionary change following the parsimony criterion (e.g. Camin & Sokal 1965; Estabrook 1968; Felsenstein 1882, 1983; de Pinna 1991; Kitching *et al.* 1998; see section 2.2.2). The outcome of a cladistic analysis is a cladogram (Camin & Sokal 1965), in which organisms for which the character data were observed (operational taxonomic units, OTUs) are tips in a tree-like branching diagram and are connected internally by nodes representing the most recent common ancestor of two OTUs or a sets of OTUs (e.g. Camin & Sokal 1965; Kitching *et al.* 1998). Therefore, OTUs and their internal nodes form hierarchically nested sets (clades) that represent a sequence of relationships (e.g. Kitching *et al.* 1998). Cladograms allow characterization of some evolutionary patterns. For instance, the acquisition sequence of morphological traits related to an ecological function can be mapped onto a cladogram, as done in section 4.3.2 of this thesis for traits related to the evolution of flippers. However, besides including topological information on the relative relatedness of organisms, the lengths for branches connecting nodes or nodes and tips of a topology can be inferred for a phylogeny. The branches of a phylogeny represent evolutionary distances between speciation events, and their lengths are thus proportional to the evolutionary rate of character change

along the branch multiplied by the time elapsed to accumulate these changes on the branch (e.g. Thorne *et al.* 1998). The length of a branch can either be measured in inferred amounts of character change (either mapping character changes implied by a most parsimonious tree from a cladistic analysis, or inferring expected changes per character from an explicit evolutionary model, such as a nucleotide substitution model), or in 'duration' of time for which a branch existed (e.g. Mooers & Heard 1997; O'Meara 2012). Phylogenies with branch lengths are desirable for analysing macroevolutionary processes (e.g. Revell 2012; Pennel & Harmon 2013), because these can be used to estimate rates of evolution, and the time information contained in branch lengths can be converted into absolute time using clock approaches that model the evolutionary process of the input data (e.g. Zuckerkandl & Pauling 1965; Lewis 2001). Many (palaeo-)biologists are interested in the absolute timing of evolutionary divergences, because dated phylogenies allow analysis of tempo and mode of macroevolutionary processes by explicitly testing hypotheses of diversity dynamics (e.g. Nee *et al.* 1992; Mooers & Heard 1997; Quental & Marshall 2010) or trait evolution (e.g., Felsenstein 1985*b*; Pagel 1994; Harmon *et al.* 2010; Slater *et al.* 2012; Close *et al.* 2015; Lloyd 2016), for instance by modelling evolutionary processes over the branches of a phylogeny using phylogenetic comparative methods (e.g. Pennel & Harmon 2013; Harmon 2018).

In previous chapters of this thesis, I used stratigraphic range data from fossils to time-calibrate nodes of a cladogram derived from parsimony phylogenetic analysis. The age of the oldest observed fossil of a clade was used as the age of that respective node, and zero-length branches resulting from 'old' clades being nested within 'younger' ones were extended by arbitrary minimum branch length arguments (Laurin 2004; 'mbl' time-scaling method in Bapst 2013). This *a posteriori* method of deriving divergence times is quick and computationally easy. However, the choice of minimum branch length is essentially an arbitrary one (Bapst *et al.* 2016; Lloyd *et al.* 2016). Other, explicitly process-based methods exist, such as probabilistic *a posteriori* dating using birth-death-sampling models (e.g. the 'cal3' method; Bapst 2013), node-dating (e.g. Parham *et al.* 2012), or tip-dating approaches (e.g. Ronquist *et al.* 2012*a*; Heath *et al.* 2014). Advantages of these methods (although the

listed advantages do not universally apply to all methods) are that they (i) allow for uncertainty in divergence times estimates (e.g. Bapst 2013; Parham *et al.* 2012; Ronquist *et al.* 2012*a*; Heath *et al.* 2014) (ii) allow for uncertainty in tree topology (e.g. Bapst 2013; Heath *et al.* 2014; Stadler *et al.* 2018); and (iii) can include age information provided by fossils during the inference of topology (e.g. Ronquist *et al.* 2012*a*; Heath *et al.* 2014).

In this outlook chapter, I present some preliminary work alongside ideas for future work that aims to develop a time-scaled phylogeny of turtles in a Bayesian framework. I present a preliminary analysis using morphological data only and the fossilized birth-death model (Heath *et al.* 2014) as a tree prior for divergence estimation, and outline present limitations of my data that I need to address before finalizing my dating analysis. My morphological character-taxon matrix used in previous sections of this thesis and for the preliminary Bayesian analysis includes 31 extant taxa, for which molecular sequence data are available (e.g. Pereira *et al.* 2017). Therefore, I can combine my data with available molecular sequence data in the future to produce a dataset suited for total-evidence dating analyses in which morphological and molecular data are combined with a tree prior to produce a time-scaled phylogeny (e.g. Ronquist *et al.* 2012*a*). Such a time-scaled turtle tree is important to further scrutinize hypotheses formulated within this thesis about the divergence times of chelonioids, but it can also test divergence times of other clades as previously inferred from node-based dating methods (e.g. Joyce *et al.* 2013*b*). The dated tree will then be used in further comparative phylogenetic research, for instance to test if ecological preferences can be used to explain shape variation in the osseous labyrinth (vestibular organ) of turtles.

5.2 An introduction to time-scaling methods

Both morphological and molecular data used to infer tree topologies contain information about the relative timing of evolutionary events in the form of amounts of character change (for molecular data, the number of expected substitutions per site; e.g. Zuckerkandl & Pauling 1965; Lewis 2001; Heath *et al.* 2014). Unlike parsimony analysis,

model-based methods of phylogenetic inference make use of this information to estimate branch lengths, describing inferred amounts of change along evolutionary lineages. The processes that generate change are far better understood for molecular sequence data than for morphological data, and many probabilistic substitution models for molecular evolution have been defined to account for various parameters such as the base frequency distributions (Felsenstein 1981; Hasegawa *et al.* 1985; Tamura 1992), differential likelihoods for the various possible nucleotide substitutions (e.g. transition/transversion rate; Kimura 1980; Hasegawa *et al.* 1985), or rate heterogeneity over alignment sites and differences in evolutionary rate at different codon positions (Yang 1993, 1994, 1996; Goldman & Yang 1994; Yang *et al.* 2000).

Models of morphological evolution are harder to formulate for phylogenetic reconstruction and have received less research effort, but some are available (e.g. Lewis 2001; Alekseyenko *et al.* 2008). The relative timescale implicit in phylogenetic trees can be converted into absolute time by using information on the timing of at least one divergence event to infer the 'clock' rate with which changes occur over the tree (measured in units of evolutionary change over time) from the branch lengths (Zuckerkandl & Pauling 1965; Thorne & Kishino 2002; Marshall 2008; Heath *et al.* 2014). Early implementations of molecular clocks applied a 'strict' (single, constant rate) clock (e.g. Zuckerkandl & Pauling 1965; Kumar & Hedges 1998; Pisani *et al.* 2004). However, evolutionary rates vary among lineages (e.g. Britten 1986; Peterson *et al.* 2004). Much subsequent research has therefore been focussed on how to account for heterogeneity with which molecular sequences change over a given tree topology, thereby relaxing the assumptions of a 'strict' molecular clock (i.e. relaxed clock models; Sanderson 1997; Thorne *et al.* 1998; Huelsenbeck *et al.* 2000; Yoder & Yang 2000; Kishino *et al.* 2001; Thorne & Kishino 2002; Drummond *et al.* 2006; Lepage *et al.* 2007; Rannala & Yang 2007; Heath *et al.* 2012). Calibration of the 'clock' (irrespective of the 'clock' model) is required because molecular data alone cannot be used to estimate absolute ages, because genetic divergences (i.e. branch lengths) are the product of the substitution rate and elapsed time, and these two components cannot be separated (e.g. Thorne *et al.*

1998; Ho & Phillips 2009; dos Reis & Yang 2013; Heath *et al.* 2014; Donoghue & Yang 2016). The most common sources of information about estimated divergence times of branching events in the tree topology used to calibrate the 'clock' are fossils (Zuckerkandl & Pauling 1965; Benton & Donoghue 2007; Marshall 2008; Parham *et al.* 2012). A fossil taxon provides a minimum age constraint for the age of the node that specifies the most recent common ancestor (MRCA) of the fossil and a set of extant taxa (e.g. Benton & Donoghue 2007).

The most widely-employed methods for inferring divergence times from sequence data and calibration information are now Bayesian frameworks using Markov chain Monte Carlo (MCMC) algorithms (Yang & Rannala 1997), in which observed data (e.g. a sequence alignment) and *a priori* knowledge about divergence times determine probability distributions known as posteriors (e.g. Thorne *et al.* 1998). However, there are major challenges about how to specifically incorporate age information from fossils into the divergence time estimates of a phylogeny in a Bayesian framework. One commonly used approach is node-dating: the position of an extinct taxon within a phylogeny of extant taxa for which sequence data exists is determined prior to the analysis (ideally, this is done by phylogenetic inference using the available morphological data of the fossil and the sampled extant taxa, e.g. Near *et al.* 2005; Pyron 2011; Parham *et al.* 2012). The age data from the fossil(s) are then used to construct calibration densities that are included as age priors in a Bayesian framework (e.g. Parham *et al.* 2012). An age prior is modelled as a probability distribution that is set around the minimum age imposed by the fossil (Ronquist *et al.* 2012*a*; Heath *et al.* 2014). Lastly, the molecular sequence data are used to estimate the dated phylogeny using MCMC. The calibration densities are parametric probability distributions that account for the uncertainty associated with the fossil ages (Kishino *et al.* 2001; Ho & Phillips 2009; Heath *et al.* 2014). However, two drawbacks with this approach have been discussed (e.g. Ronquist *et al.* 2012*a*; Heath *et al.* 2014; Gavryushkina *et al.* 2017). First, the parameterization of the probability distributions (e.g. uniform, exponential, etc.) used as calibration priors are rarely informed by biological processes or knowledge of the fossil record (Ronquist *et al.* 2012*a*; Heath *et al.* 2014; Gavryushkina *et al.* 2017, Donoghue & Yang

2016). Ideally, these should be informed by the preservation history of the group (Heath *et al.* 2014). This is particularly important because the precision of age estimates derived from node dating is directly controlled by the precision of prior distributions on calibrated nodes (Warnock *et al.* 2012; Heath *et al.* 2014). Second, the sequential treatment of different types of input data (i.e. phylogenetic positions of fossils, age information for fossils, sequence data) implies that the processes that generate the data are independent (Heath *et al.* 2014; Gavryushkina *et al.* 2017), when in fact they are actually the result of a single macroevolutionary process.

Tip-dating provides a potential solution to the problems that arise when using fossils as *post hoc* calibrations for internal nodes of a phylogeny during node-dating. Tip-dating methods analyse sequence data (morphological, e.g. Lee *et al.* 2014; morphological and molecular, e.g. Ronquist *et al.* 2012*a*; or only molecular if such data are present for recently extinct lineages, e.g. Krause *et al.* 2008) for both fossils and extant species. A substitution model has to be specified for the molecular data partition, and a morphological clock model is included for the morphological data partition (e.g. Lewis 2001). The phylogenetic positions of fossil taxa are then directly inferred during the analysis, and need not be specified *a priori* (Pyron 2011; Ronquist *et al.* 2012*a*). The phylogenetic positions of fossil taxa are determined analytically by the morphological data partition, and simultaneously the divergence times for taxon pairs are inferred based on estimates of the molecular and morphological clock, using the phylogenetic positions and stratigraphic age of the fossil taxa (Pyron 2011; Ronquist *et al.* 2012*a*). Such tip-dating analyses can also be applied to fossil only data (e.g. Lee *et al.* 2014; Slater 2015; Bapst *et al.* 2016; Matzke & Wright 2016; King *et al.* 2017; Zhang & Wang 2018).

Tip-dating approaches use all fossil data available in a dataset (rather than just the oldest member of a clade) for calibration (Ronquist *et al.* 2012*a*; Heath *et al.* 2014). Calibration is achieved by specifying a tree prior in a Bayesian framework, which describes the distribution of divergence times (Bapst *et al.* 2016). Heath *et al.* (2014) proposed a tree prior for incorporating the age information contained by fossils by modelling the data from extant and extinct species as a unified macroevolutionary process, the fossilized birth-death

process (FBD), originally developed by Stadler (2010). The FBD model estimates a speciation rate (λ) and extinction rate (μ), which produce extant and extinct tips in the tree topology (Stadler 2010; Heath *et al.* 2014; Stadler *et al.* 2018). An additional free model parameter is the fossil sampling rate (ψ), which defines the probability of fossil observations (the combination of fossilization, i.e. the rate with which lineages produce fossils, and the probability with which these are observed, following a Poisson process) (Stadler 2010; Heath *et al.* 2014; Stadler *et al.* 2018). The FBD probability is conditioned on the proportion of extant species sampled, by assigning a fixed parameter to an extant sampling probability prior (ρ) (Stadler 2010; Heath *et al.* 2014; Stadler *et al.* 2018). The FBD prior for the branching process of the tree is thus based on diversity dynamics (Heath *et al.* 2014), and does not assume a uniform prior probability (as done in the original tip-dating method; Ronquist *et al.* 2012*a*). Pruning all lineages with unsampled descendants from the 'complete tree' modelled by the FBD process results in a 'sampled tree', which represents a time-calibrated phylogenetic hypothesis inferred from empirical data (Heath *et al.* 2014; Stadler *et al.* 2018).

A dating analysis using an FBD model therefore combines a relaxed-clock model (for both molecular and morphological evolution) with a unified tree model of lineage diversification (constant birth-death model; Stadler 2010) and fossil sampling (modelling fossil preservation and recovery) (Stadler 2010; Heath *et al.* 2014; Gavryushkina *et al.* 2017; Zhang *et al.* 2016; Stadler *et al.* 2018). Importantly, the FBD approach is suited for datasets with large uncertainty regarding the phylogenetic positions of fossils (which is problematic in approaches using other parameterizations of the tree prior, as the position of fossil taxa has large influence on the age estimates; Pyron 2011; Heath *et al.* 2014), because it allows the exact placements of fossils to be unspecified while the branching time information is still used to infer node ages (Heath *et al.* 2014). The probability of a tree topology including fossils with uncertain positions is then calculated as the sum of probabilities of all possible trees resolving that fossil as being member of a lineage that was alive during its time of sampling (Heath *et al.* 2014). This approach can even allow for the possibility that some fossils

represent direct ancestors of other taxa in the dataset by inferring an attachment age of a fossil that is identical to its observed age (Heath *et al.* 2014; see also Gavryushkina *et al.* 2017; Stadler *et al.* 2018), accounting for the relatively high probability that at least some fossils represent direct ancestors of other fossil or extant taxa (Foote 1996).

Since the initial description of the FBD model, several extensions of the model have also been published, mostly addressing unrealistic elements of the original model such as assuming consistent fossil sampling rates or diversity dynamics (e.g. Hunt & Slater 2016). For instance, Gavryushkina *et al.* (2014) modified the model so it can accommodate changes in the rate of speciation, extinction, and sampling. Zhang *et al.* (2016) incorporated diversified sampling (i.e. sampling that is not complete or uniform, but assumes that the taxon sample has been chosen to maximize diversity) into the FBD model. Stadler *et al.* (2018) expanded the FBD model to allow multiple observations of a species over time (i.e. stratigraphic ranges of a species) by modelling different modes of speciation, such as (sympatric) budding, bifurcation, and anagenetic (i.e. direct ancestor-descendant relationships).

My morphological dataset of turtles is suited to be combined with molecular sequence data into a total-evidence dataset. This can then be analysed in a Bayesian framework treating fossils as tips of the tree (Ronquist *et al.* 2012*a*), accounting for sampling and fossilization (Heath *et al.* 2014; Zhou *et al.* 2016), and treating age data for calibration as stratigraphic ranges (Stadler *et al.* 2018). In the remainder of this chapter, I report on the preliminary development of such a protocol, using only a morphological data partition for the time being.

5.3 Methods

5.3.1 Summary of analytical settings

I have run a preliminary Bayesian tip-dating analysis in MrBayes 3.2.6 (Ronquist *et al.* 2012*b*). I used morphological data of extant and extinct species, set to evolve under the Mk

model of morphological evolution of Lewis (2001) with equal state frequencies, rate variation across characters drawn from a gamma distribution, and a correction for the ascertainment bias of morphological matrices, which systematically omits constant characters during matrix construction (Lewis 2001). This correction is implemented by the variable characters option, and implies that only variable characters had the possibility of being sampled (excluding any constant characters scored in the matrix automatically). If such a correction is not applied, rates of evolution are overestimated (Lewis 2001). However, the variable option does not mean that all characters need to be parsimony informative (i.e. autapomorphic characters are allowed, because they contribute to character change in a particular lineage). Although I did not include a partition for molecular sequence data, I used a molecular backbone constraint following the topology of Pereira *et al.* (2017), and *Proganochelys* was set as the outgoup.

The clock model was set to a relaxed-clock that allows rates to vary over time. Specifically, I am using the independent gamma rate (IGR; Lepage *et al.* 2007) model in which each branch has an independent rate drawn from a gamma distribution. The variance of the gamma distribution is parameterized with an exp(10) distribution, following Zhang (2016). A prior probability following a normal distribution with mean of 0.001 and variance of 0.1 was assigned to the clock rate to accommodate uncertainty. The standard deviation for the clock rate prior was set to be larger than the mean, because the posterior is proportional to the likelihood multiplied to the prior, so that values with a high prior probability (i.e. small standard deviation of the normal distribution) could bias the analysis towards the setting of prior on the clockrate. In other words, the used settings establish a relatively wide distribution for the prior, allowing the analysis to sample from highly-variable clock rates (pers. comm. Luke Parry, 2018).

Priors for the tree model were specified using an FBD process (Stadler 2010; Heath *et al.* 2014). The speciation rate (λ), extinction rate (μ), and fossilization rate (φ) of the FBD model are parameterized in MrBayes as the net diversification prior $d = \lambda - \mu$, turnover prior $e = \mu/\lambda$, and fossil sampling probability prior $s = \varphi/(\mu+\varphi)$, so that turnover and fossil sampling probability range from 0 to 1 (Zhang 2016). For the parameters of these priors, default values

(*d* = exponential(10); *e* = beta(1,1); *s* = beta(1,1)) as implemented in MrBayes were used. The sampling strategy and a fixed prior for the proportion of extant taxa sampled determine the extant sampling probability. A diversified sampling strategy was employed (Zhou *et al.* 2016), because extant taxa in the dataset were sampled to maximize diversity — every turtle family is represented by at least one species in my dataset, and not in proportion to actual species per family. The extant sampling proportion was fixed to the number of extant turtle species sampled (31 species) divided by the number of existing turtle species (335 species; van Dijk *et al.* 2014), resulting in a value of 0.09254.

Age priors were assigned to all tips of the tree. Fixed ages of 0 were used as priors for extant taxa. Uniform probability distributions with minimum and maximum values corresponding to last and first appearance dates (LADs, FADs) were used as priors for fossil taxa. This setting was chosen because for many fossils, only vague age data is provided, so that minimum and maximum ages for many taxa used in this study represent the lower and upper bounds of the geologic stage in which the fossils were found. The uniform prior specifies that the respective fossil is as old as sometime between the set minimum and maximum values. The root of the tree was given an offset exponential prior because this distribution assumes that the likelihood of the root age being older than the specified minimum age decreases exponentially, while the shape of the exponential decay is determined by a specified mean value (Zhang 2016). For this, I used the FAD of the outgroup and oldest taxon in the dataset, *Proganochelys*, as the minimum age (208.5 Ma), and a mean age of 220 Ma as parameters for the offset exponential distribution. The mean age was chosen because it roughly corresponds to the LAD of *Odontochelys*, which is the next oldest and more basally branching turtle (but which was not included in my dataset) (Li *et al.* 2008). The mean age is close in absolute time to the minimum age, resulting in a relatively restrictive prior, but the impact of more and less restrictive priors on divergence time estimates have previously been reported to be low (Zhang *et al.* 2016).

To estimate the posterior distribution, I used Markov chain Monte Carlo (MCMC) algorithms with Metropolis Coupling (MCMCMC, or MC^3) of chains to allow effective

exploration of parameter space. Markov chains move through the parameter space in a step-wise fashion, whereby the parameter value at a current position and the parameter value for a proposed next step determine the direction in which the chain moves forward (Ronquist *et al.* 2009). Parameter values with higher posterior probabilities than the current values are always accepted, and steps implying lower values are sometimes accepted (Ronquist *et al.* 2009). Markov chains converge toward equilibrium of highest posterior probabilities. Because Markov chains can be stuck in local optima of the parameter space, Metropolis Coupling of chains is useful (Ronquist *et al.* 2009). With this approach, the posterior probability surface is flattened for several Markov chains (heated chains), but not for one chain (cold chain) (Ronquist *et al.* 2009). The heated chains can move more easily through valleys in parameter space to reach distant peaks due to the flattened landscape (Ronquist *et al.* 2009). The heated chains, at regular intervals, offer to swap states with the cold chain. If such a swap is accepted, the cold chain can make large jumps from one tree island to another (Ronquist *et al.* 2009). At the end of the run, samples from the heated chains are discarded.

For my initial analysis, two independent runs of four Markov chains (three heated chains, one cold chain) were run for 10 million generations, and the default heating coefficient of 0.1 was used. For all MCMC runs across analyses, samples from the posteriors were recorded every 500th generation with 25% of trees discarded as burn-in. The average deviation of split frequencies (0.187) of the first analysis suggested incomplete convergence, and appending another 10 million generations did not improve convergence by a large margin (0.167). Therefore, I changed the MCMC settings to use six chains for 15 million runs, and I modified the heat parameter of the heated chains to 0.05 to allow for better exchange between the chains, which resulted in better convergence diagnostics: The average deviation of split frequencies, which should converge to 0 when sampled trees are very similar between runs (Ronquist *et al.* 2009), was 0.010652. The Potential Scale Reduction Factors, which should approach 1.0, indicating similar between- and within-run variances of posterior samples (Gelman & Rubin 1992; Ronquist *et al.* 2009), was 1 for the posterior distributions of all parameters. Visual inspection of the trace plot of the number of generations vs. the log

probability of the data given by the `sump` command of MrBayes 3.2.6. indicated convergence on stationary posteriors as well. Lastly, estimated sample sizes (ESS) for all parameters were > 200, which is an arbitrary cut-off taken to indicate convergence (Rambaut *et al.* 2018).

In the following section, I provide the commands used in MrBayes with short justifications and comments. These commands are appended to a nexus file that contains the character-taxon matrix (see Appendix S4).

5.3.2 MrBayes Code

For the morphological data, I have to specify a morphological model of evolution. The parameters of the likelihood model are set with the `lset` command. The following code specifies a gamma-distributed rate variation under the Mk model (Lewis 2001), and includes an ascertainment bias correction.

```
lset rates=gamma coding=variable;
```

The relaxed-clock model is set to an independent gamma rate (IGR; Lepage *et al.* 2007) model in which each branch has an independent rate drawn from a gamma distribution. The variance of the gamma distribution is parameterized with the `prset igrvarpr` command. The prior probability distribution of the clock rate is specified with the `prset clockratepr` command.

```
prset clockvarpr=igr;
prset igrvarpr=exp(10);
prset clockratepr = normal(0.001,0.01);
```

I am using *Proganochelys* as the outgroup, and use a root constraint (following Zhou 2016), which is necessary for clock-constrained trees.

```
outgroup Proganochelys_quenstedti;
constraint root = 1-. ;
```

Because I am currently only using morphological data, I specified additional constraints as a molecular backbone, following the topology of Pereira *et al.* (2017). The full constraints are listed in Appendix S4, and here only two are given as an example. The first example constrains the two species of *Lepidochelys* to be monophyletic with respect to all other taxa in the constraint. The second constraint shown defines the crown-group of turtles to be monophyletic with respect to the outgroup *Proganochelys*. This constraint was originally not included, but the constraints only seem to work when it is included. The constraints are partial constraints, so that taxa not listed in the constraint (i.e. fossils except for the outgroup) are allowed to fall anywhere within the tree topology.

```
constraint lepidochelys partial = Lepidochelys_olivacea
Lepidochelys_kempii : Pelomedusa_subrufa Podocnemis
Chelus_fimbriatus Phrynops_geoffroanus Chelodina
Elseya_dentata Carettochelys_insculpta Lissemys_punctata
Pelodiscus_sinensis  Apalone_spinifera
Platysternon_megacephalum Emys_orbicularis Chrysemys_picta
Geoclemys_hamiltonii Gopherus_polyphemus Testudo
Chelonoidis_sp. Macrochelys_temminckii Chelydra_serpentina
Dermatemys_mawii Staurotypus Kinosternon_suburum_hippocrepis
Sternotherus Dermochelys_coriacea Chelonia_mydas
Natator_depressus Eretmochelys_imbricata Caretta_caretta
Proganochelys_quenstedti;

[…]

constraint testudines partial = Pelomedusa_subrufa Podocnemis
Chelus_fimbriatus Phrynops_geoffroanus Chelodina
Elseya_dentata Carettochelys_insculpta Lissemys_punctata
Pelodiscus_sinensis  Apalone_spinifera
Platysternon_megacephalum Emys_orbicularis Chrysemys_picta
Geoclemys_hamiltonii Gopherus_polyphemus Testudo
Chelonoidis_sp. Macrochelys_temminckii Chelydra_serpentina
Dermatemys_mawii Staurotypus Kinosternon_suburum_hippocrepis
Sternotherus Dermochelys_coriacea Chelonia_mydas
Natator_depressus Eretmochelys_imbricata Caretta_caretta
Lepidochelys_olivacea Lepidochelys_kempii :
Proganochelys_quenstedti;
```

The constraints are then enforced using the following command.

```
prset topologypr = constraints (lepidochelys, […],
testudines);
```

Next, the OTUs of the analysis are assigned age-priors. The full list of calibrations is available in Appendix S4. The calibrations are then enforced.

```
CALIBRATE  Apalone_spinifera     = fixed (0);
CALIBRATE  Adocus_beatus    = uniform (66.043,70.6);

PRSET nodeagepr = calibrated;
```

To generate the tree, the fossilized birth death model has to be parameterized. The FBD prior is defined as a prior probability distribution on branch lengths, and the FBD option is set with `clock:fossilization`. I use the default distributions and parameter values of MrBayes for the priors for speciation, extinction and fossilization.

```
PRSET brlenspr = clock:fossilization;
PRSET sampleprob = 0.09254;
PRSET samplestrat = diversity;
PRSET speciationpr = exponential(10)
PRSET extinctionpr = beta(1,1);
PRSET fossilizationpr = beta(1,1)
```

For a FBD model, the prior probability distribution on the tree age needs to be specified, because the FBD prior is conditioned on the root of the tree (Zhang 2016).

```
PRSET treeagepr = offsetexponential(208.5, 220);
```

Finally, the settings for the MCMC are specified, whereby I use two independent runs of four chains for 10 million generations, sampling every 500th generation and specifying a 25% relative burnin of trees. Diagnostics are printed every 5000 generations, and branch lengths are saved.

```
mcmcp nrun = 2 nchain = 4 ngen=1000000 samplefreq=500
   printfreq=500 diagnfr = 5000  savebrlens=yes
   relburnin=yes burninfrac=0.25;
mcmc;
```

5.4 Preliminary results

5.4.1 Topological results

The main topological results from the Bayesian analysis (Fig. 5.1) are: (1), the recovery of an extended stem of Chelonioidea, including several taxa that under parsimony analysis were found to be stem-group cheloniids; (2) the recovery of a monophyletic Protostegidae as the earliest-branching stem-group of chelonioids; (3) the recovery of monophyletic 'Macrobaenidae', Sinemydidae, and Xinijanchelyidae as successively more stem-ward positioned stem-group turtles; (4) the recovery of a monophyletic clade comprised of sandownids and thalassemydids on the stem-group of turtles, but that differs from parsimony results in the relative placement of *Solnhofia* and for which the name Angolachelonia cannot be used; (5) the recovery of a monophyletic Paracryptodira on the stem-group of turtles; (6) the recovery of a monophyletic Meiolaniformes on the stem-group of turtles. Despite using the same character-taxon matrix, the topology from the Bayesian analysis differs from parsimony results reported in section 4.3 of this thesis in several key aspects, but some similar patterns are also recovered. The most important differences and similarities are outlined below in individual sections for the clades of interest.

Cheloniidae. Crown-group relationships of cheloniids were constrained in the analysis to be identical to that recovered by analysis of molecular sequence data (following Pereira *et al.* 2017). The stem-group of cheloniids is formed exclusively by Cenozoic taxa: The Oligocene and Miocene taxa *Oligochelone* and *Procolpochelys* form a clade that is the immediate sister taxon to the crown-group. *Erquelinnesia gosseleti* forms the next sister-taxon. One node more stemwardly, the Eocene taxa *Puppigerus*, *Eochelone*, and *Argillochelys* form a clade, with *Eochelone* being more closely related to *Puppigerus* that to *Argillochelys*. All taxa mentioned in this section were also found to be stem-group cheloniids using parsimony analysis, although

the specific relationships (except for *Puppigerus*+*Eochelone*) were not resolved among the MPTs (see section 4.3).

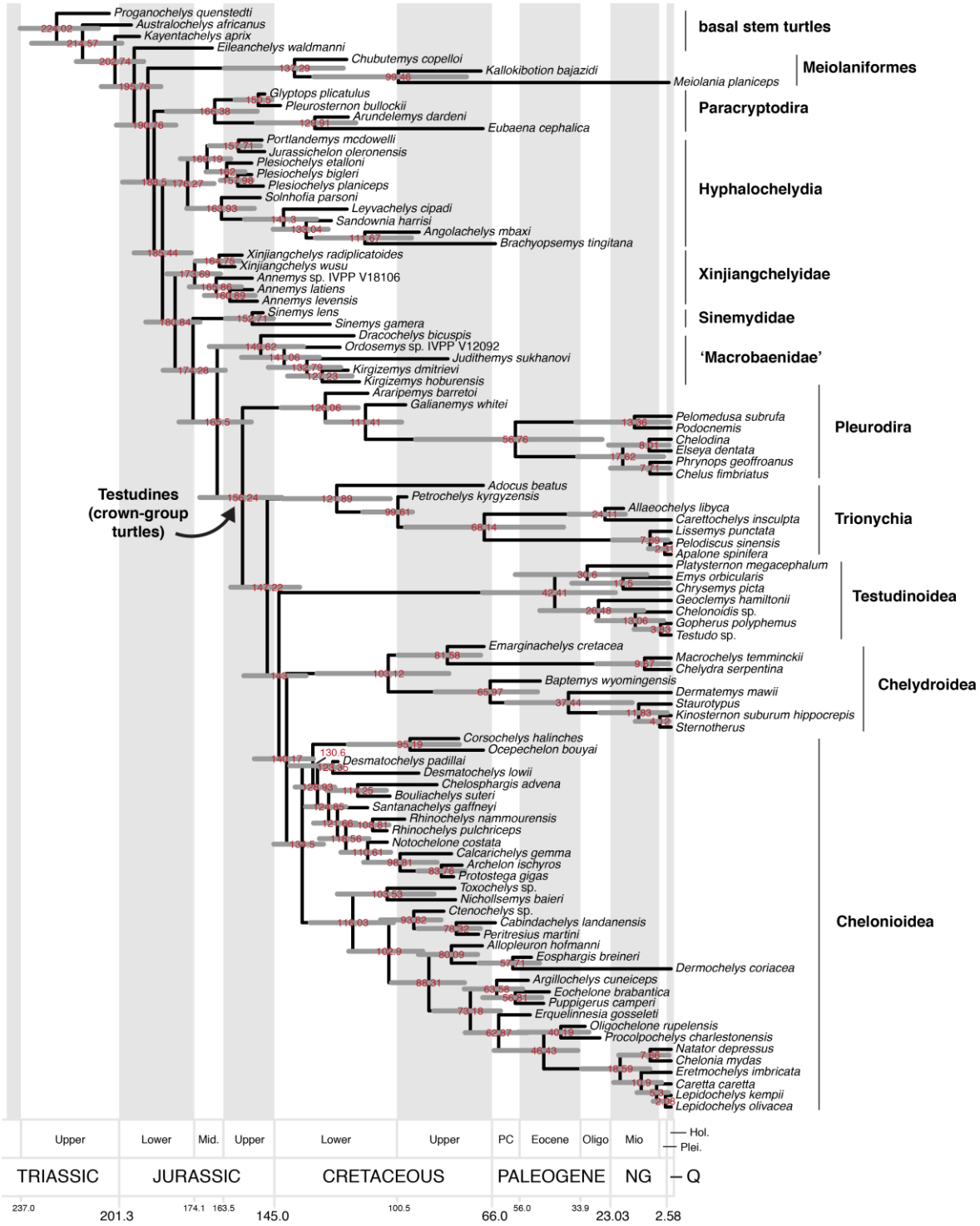


FIG. 5.1. Time-calibrated phylogenetic FBD tree of turtles. Red numbers on internal nodes are median ages from the posterior distribution, and grey boxes are 95% HPD intervals. *Abbrevialtions*: Hol., Holocene; Plei., Pleistocene; Q, Quarternary.

Dermochelyidae. As with parsimony, Bayesian inference recovers *Eosphargis* as the closest extinct relative of *Dermochelys*. However, the Bayesian analysis additionally recovers the

Maastrichtian *Allopleuron* as a dermochelyid, whereas all parsimony analyses performed throughout this thesis found *Allopleuron* to be a stem-group cheloniid.

Non-protostegid stem-group chelonioids. In the Bayesian analysis, all Cretaceous taxa that were recovered as stem-group cheloniids under parsimony were instead found in more stemward positions (with the exception of *Allopleuron*, which was found as a dermochelyid). *Peritresius*, *Cabindachelys*, and *Ctenochelys* were found in a clade (as in parsimony), but instead of stem-group cheloniids they form the immediate sister group to the crown of Chelonioidea under Bayesian inference. *Toxochelys*, which in all parsimony analyses performed throughout this thesis was recovered as the earliest-branching member of the chelonioid stem, is found one node more crownwardly positioned than protostegids. Furthermore, *Toxochelys* is found in a clade with *Nichollsemys*.

Protostegidae. As in the parsimony analyses, protostegids are found to be monophyletic. However, the ingroup relationships of the Bayesian analysis differ from parsimony. *Archelon*+*Protostega* are well-nested within protostegids. Successive sister-taxa to these 'derived protostegids' are *Calcarichelys*, *Notochelone*, the *Rhinochelys*-clade, *Santanachelys*, (*Bouliachelys*+*Chelosphargis*), the *Desmatochelys*-clade, and (*Corsochelys*+*Ocepechelon*). *Corsochelys* is the only taxon recovered as a protostegid that was previously (i.e. under parsimony) excluded from this group (it was found in a polytomy with dermochelyids and cheloniids in section 4.3 of this thesis).

'Macrobaenidae', Sinemydidae, and Xinjiangchelyidae. Consistent with parsimony analysis of the same dataset, all 'macrobaenid', sinemydid, and xinijangchelyid taxa are found to be stem-group turtles. As in all parsimony analysis performed throughout this thesis, xinjiangchelyids are monophyletic, include the genera *Annemys* and *Xinjiangchelys*, and are the most stemwardly positioned group of the turtles discussed in this section. Unlike in the parsimony analyses, in which the ingroup relationships of xinjiangchelyids were unresolved, the

Bayesian analysis finds the genera *Annemys* and *Xinjiangchelys* to be monophyletic. Sinemydidae in this analysis consists exclusively of species belonging to the genus *Sinemys*. Sinemydids are positioned one node more crownwardly than xinjiangchelyids. The remaining taxa, which are all from the Cretaceous, form a monophyletic group that is the immediate sister group to crown-group turtles. This clade is herein referred to as 'Macrobaenidae', with inverted commas indicating that this name cannot properly be applied as the defining taxon, *Macrobaena*, has not been included in my dataset (or any phylogenetic analysis to date). The North American taxon *Judithemys* is nested within 'Macrobaenidae', and is found as the sister taxon to the *Kirgizemys*-clade.

Thalassochelydia+Sandownidae. As in the parsimony analyses performed in this thesis, Bayesian inference suggests a close relationship of sandownids with thalassochelydians. In the parsimony analyses, this Thalassochelydia (*sensu* Anquetin *et al.* (2017*a*)) included *Solnhofia* and was found as the sister group of Sandownidae. The name Angolachelonia was justified for this clade (see section 2.4 of this thesis), because Mateus *et al.* (2009) defined Angolachelonia as the clade including *Solnhofia* and sandownids. The Bayesian analysis, however, recovers *Solnhofia* as the sister taxon to sandownids, so that the name Angolachelonia becomes applicable to this less inclusive clade. Because *Solnhofia* was not included in the phylogenetic definition of Thalassochelydia (see Anquetin *et al.* 2017*a*; and Evers & Benson 2018*a* for a revision), Thalassochelydia as a name remains stable within the context of my Bayesian analysis. However, the clade comprising Angolachelonia (i.e. *Solnhofia* + sandownids) and Thalassochelydia is now without a name. I propose the name Hyphalochelydia new clade for the group that includes both taxa. Hyphalochelydia is recovered in an earlier-branching position in the Bayesian analysis than Angolachelonia was in the parsimony analyses performed. In the parsimony analysis using the same dataset as the Bayesian analysis, Angolachelonia was found as the sister-group to Pleurodires, and it was found as the immediate sister to crown-group turtles in the earlier dataset used in section 2 (i.e. Evers & Benson 2018*a*).

Paracryptodira. As in the parsimony analysis from section 4.3, paracryptodires are found as a monophyletic group on the stem of turtles. Unlike in the parsimony analysis, the distinction of Baenidae and Pleurostenidae is supported in the Bayesian analysis.

Meiolaniformes. The Bayesian analysis recovers a clade that includes *Meiolania*, *Kallokibotion*, and *Chubutemys*, to which the name Meiolaniformes in applicable, and which is consistent with latest parsimony analyses of the group (e.g. Sterli *et al.* 2015).

Early stem-group turtles. The relative relationships of early stem-group turtles differs slightly from parsimony results. Whereas parsimony analysis consistently recovered *Eileanchelys* and *Kayentachelys* to form a clade, these now form successive branching events more stemwardly than Meiolaniformes.

5.4.2 Divergence times

Divergence times inferred from the Bayesian analysis are only briefly discussed, because they are interpreted to be preliminary given that some of the oldest fossils for several clades (e.g. Pleurodira) are currently not included in the analysis, and given that no molecular data was used so far. Divergence times for major clades are given in table 5.1, and also shown in Figure 5.1 for all nodes.

The analysis implies a Late Jurassic origin of crown-group turtles (156.2 Ma). This is significantly younger than the late Norian (212.33 Ma) age derived for crown-group turtles by Joyce *et al.* (2013*b*). For their node-calibrations, Joyce *et al.* (2013*b*) used a late Oxfordian (155.7 Ma) minimum age constraint for Testudines, based on the oldest known

TABLE 5.1. Divergence times estimates for selected nodes inferred in this study and comparison with results from Joyce et al. (2013*b*). All values are in millions of years before present (Ma), except for values in last column are myr, with '+' indicating older ages were inferred in this study, and '-' indicating older ages were inferred in the study by Joyce et al. (2013*b*).

Node	This study				Joyce *et al.* (2013*b*)	Difference in mean
	Mean age	Median age	Lower 95% HPD	Upper 95% HPD		
root	224.84	224.02	208.79	241.20	-	-
Meiolaniformes	138.76	137.29	119.51	162.96	-	-
Paracryptodira	166.93	166.38	150.89	183.90	-	-
Hyphalochelydia	176.56	176.27	166.64	187.14	-	-
Thalassochelydia	169.62	169.19	160.56	178.91	-	-
Angolachelonia	164.09	163.93	151.95	176.59	-	-
Sandownidae	141.86	141.30	129.25	155.51	-	-
Xinjiangchelyidae	173.91	173.69	164.28	183.80	-	-
Sinemydidae	153.42	152.71	145.00	162.44	-	-
Macroabenidae	150.05	149.62	134.01	168.38	-	-
Testudines	156.69	156.24	141.91	171.82	212.33	-55.64
Pleurodira	127.13	126.06	114.04	142.19	164.09	-36.96
Cryptodira	147.53	147.22	135.40	160.54	190.42	-42.89
Trionychia	122.25	121.89	102.39	141.61	162.83	-40.58
Durocryptodira	143.60	143.00	133.05	155.75	118.57	+25.03
Testudinoidea	43.51	42.41	20.30	68.76	85.83	-42.32
Americhelydia	140.71	140.17	130.41	151.93	113.14	+27.57
Chelydroidea	104.18	103.12	81.03	129.11	110.41	-6.23
Chelydridae	82.83	81.58	69.46	99.48	-	-
Kinosternoidea	66.90	65.97	48.70	85.97	91.05	-24.15
Total-group Chelonioidea	135.01	134.50	126.72	144.83	-	-
Protostegidae	131.01	130.60	123.32	139.02	-	-
Crown-group Chelonioidea	88.72	88.31	75.32	101.97	66.18	+22.54
Dermochelyidae	80.67	80.09	70.55	92.15	-	-
Total-group Cheloniidae	73.65	73.18	62.20	86.54	-	-
Crown-group Cheloniidae	19.37	18.59	7.76	32.64	-	-

total-group pleurodire *Caribemys oxfordiensis* (de la Fuente & Iturralde-Vinent 2001). Inclusion of *Caribemys* would likely also push back my date for the crown of turtles, because the fossil age is less than ten million years younger than my inferred age. For Pleurodira, my analysis infers a Barremian (126.1 Ma) age, again significantly younger than the late Middle Jurassic (164.09 Ma) age found by Joyce *et al.* (2013*b*). The divergence of Cryptodira is inferred to have happened in the latest Jurassic (142.99 Ma) in my analysis. Joyce *et al.* (2013*b*) arrived at a Sinemurian (190.42 Ma) age for this node. The deep divergences for

cryptodires and pleurodires in the analysis of Joyce *et al.* (2013*b*) can be explained by their construction of age constraints: their soft maxima are conservatively broad, considering even weak evidence for the potential presence of a group at a certain time. Combined with the use uniform distributions on age priors, this could lead to particularly old divergence time estimates. It is interesting that the ages given by the analysis of Joyce *et al.* (2013*b*) for pleurodires and cryptodires are both far older than the oldest certain fossils of those groups used to establish the minimum age priors, and instead are near their respective maximum prior age constraints (base of Late Jurassic: 165.2 Ma for Pleurodira; base of Jurassic: 199.6 Ma for Cryptodira).

The divergence time for crown-group chelonioid is inferred to be Coniacian (88.30 Ma) in my analysis. In contrast with deeper nodes in the phylogeny, this node age is much older than the one inferred in Joyce *et al.* (2013*b*), which is Maastrichtian (66.18 Ma). The discrepancy of these ages is a direct result of estimating the topology and divergence estimates simultaneously: in my analysis, the Maastrichtian taxon *Allopleuron* is recovered as a crown-group chelonioid, pushing back the origin of chelonioids. However, it is noteworthy that my analysis even implies an older total-group age for cheloniids (Campanian, 73.17 Ma) than Joyce *et al.* (2013*b*) did for the entire crown-group of chelonioids. However, their minimum for Chelonioidea was based on the Eocene taxon *Eosphargis*, which is arguably a very young calibration taxon (albeit it was the only taxon fulfilling the rigorously applied approach of using only taxa for which no phylogenetic uncertainty exists). The inclusion of protostegids in the total-group of chelonioids also has impacts on the divergence time of Americhelydia, i.e. Chelonioidea + their sister group Chelydroidea. Whereas divergence time estimates for Chelydroidea are similar between my analysis (Albian, 103.1 Ma) and that of Joyce *et al.* (2013*b*) (Albian, 110.4 Ma), my inferred age of the total group of Chelonioidea (Valanginian, 134.5 Ma) pushes back the origin of Americhelydia to the Berresian (140.2 Ma) and increases ghost-lineages for Chelydroidea. Joyce *et al.* (2013*b*) inferred an Aptian age of 113.1 Ma for this group.

Although further differences could be explored, the last pattern I want to highlight is that specifically the older ages for Chelonioidea and Americhelydia inferred by my analysis change ideas about the diversification of crown turtle subclades. While Joyce *et al.* (2013*b*) recognized a relatively deep divergence of Trionychia some time in the Middle–Late Jurassic, their shallow (Aptian) ages for Durocryptodira (i.e. all non-trionychian cryptodires) resulted in a long-ghost lineage for the stem of Durocryptodira, despite the absence of potential stem durocryptodiran fossils. My analysis implies a deeper origin of Durocryptodira, sometime in the earliest Cretaceous. This fits better with direct observation from the fossil record, because potential stem-group representatives of all major durocryptodiran groups (testudinoids, chelydroids, chelonioids) have been identified (e.g. Whetstone 1979; Danilov & Parham 2005; Cadena *et al.* 2013; Brinkman *et al.* 2006).

5.4.3 Parameters from the FBD and clock models

The posteriors for parameters that were estimated in the analysis are shown in Table 5.2. The mean clockrate inferred by the analysis is 0.0027 character–state changes per character per myr. The rate heterogeneity among sites inferred from the model is strong, because the α parameter that determines the shape of the gamma distribution is <1 (α = 0.9811; Table 5.2). The gamma distribution describes the clockrates for individual branches (which are the product of the mean clockrate and the relative rate for each branch, whereby the branch rate is gamma distributed and its variance term is scaled over the geologic time duration of a branch; Zhang & Wang 2018). Gamma distributions with α > 1 are bell-shaped and model weak rate heterogeneity (Strimmer & Haeseler 2009). Gamma distributions with a shape parameter of α = 1 describe an exponential distribution. The probability density functions for gamma distributions with α parameter values <1 also result in L-shaped graphs, which indicate that most values are concentrated around low rate values but the distribution has a long tail indicating that some rates are high (Strimmer & Haeseler 2009).. The value of α = 0.9811 is close to 1, indicating that the difference between extreme rate values is high, but

rate heterogeneity among sites is weak in the sense that most rates are similar to one another and low. Only some characters are inferred to have high rates of character-state changes. Similarly, the shape parameter for the gamma distribution that models rate heterogeneity across branches is <1 (igrvar = 0.036), indicating that rates vary across the tree. However, because the shape parameter is much smaller than 1, rate heterogeneity across branches is strong, and the gamma distribution is more light tailed (compared to a distribution with alpha closer to or equal to 1).

Although analysing diversity metrics is not the main focus of this chapter, I briefly report and discuss the inferences that can be made from the posterior estimates of the FBD process. The 'net speciation' rate (i.e. diversification rate, d) is inferred to be 0.0057 lineages per myr, and the 'relative extinction' rate (i.e. turnover, e) is 0.9993. The low net diversification rate indicates that long-term speciation rates only slightly exceed extinction rates. Speciation and extinction rates with near-identical values are also commonly found in other empirical studies using birth-death models (e.g. Alfaro et al. 2009; Friedman & Sallan 2012; Near et al. 2013).

The speciation rate (λ) and extinction rate (μ) can be calculated from diversification and turnover, whereby $\lambda = d/(1-e)$, and $\mu = (e*d)/(1-e)$. Therefore, speciation is inferred to be λ = 8.142857 lineages per myr, and extinction is μ = 8.137157 lineages per myr. These inferred rates are high compared to those inferred from studies of palaeontological time series (e.g. λ*(non-tetrapod fishes)* = 0.77, μ*(non-tetrapod fishes)* = 0.67: Friedman & Sallan 2012; λ*(Perciformes)* = 0.589, μ*(Perciformes)* = 0.508, λ*(Eutelestei)* = 0.338, μ*(Euteleostei)* = 0.312: Near et al. 2013; λ*(Cetacea)* = 0.17, μ*(Cetacea)* = 0.11: Quental & Marshall 2010, Etienne et al. 2011; see also Pyron & Burbrink 2013). Nevertheless, they are consistent with speciation and extinction rates inferred from a birth-death process to model a time tree of gnathostomes (Alfaro et al. 2009: λ = 5.05 lineages per myr; e = 5.04 lineages per myr). Moreover, Alfaro et al. (2009) found particularly low net speciation rates and high relative extinction for crocodylians (d = 0.00006 lineages per myr; μ = 0.99) (in comparison to, for instance, neoavian birds: d = 0.089 lineages per myr; μ could not be estimated due to

unresolved tree topology), which are possibly comparable to turtles by their phylogenetic proximity and similarity in relative small extant species richness among tetrapods.

Speciation and extinction rates were inferred under a homogeneous birth-death model (the FBD model used herein is a modification of a simple birth-death model that accounts for sampling (Stadler 2010; Heath et al. 2014)). In homogeneous birth-death models, the probabilities of branching and extinction remain constant over time, and predict exponential growth of speciation exceeds extinction (Raup 1985):

$$m_t = a^* e^{(\lambda-\mu)t}; \qquad \text{(Eq. 1)}$$

whereby a is the initial number of species, m_t is the number of species after some time t, and λ and μ are speciation and extinction rates, respectively. From this exponential function, a species doubling time can be derived, whereby $T_{x2} = \ln(2)/(\lambda - \mu)$ (Raup 1985). Because extinction is nearly as large as speciation in my analysis, the doubling time for speciation and extinction rates inferred herein is large (121.6 myr).

Although equation 1 assumes that speciation and extinction are independent, similar values for both rates as inferred here have been interpreted as potential evidence for non-independence of these rates (e.g. diversity-dependence) (Raup 1985). My doubling time is further consistent with results from other studies using fossils to estimate diversity dynamics: for instance, my inferred doubling time is on the same order of magnitude as values recovered for Mesozoic tetrapods, which double species diversity over a duration of 213.5 myr (Benson et al. 2016). Another property that can be calculated from the extinction rate is the median lineage duration or species half-life: $T_{(1/2)} = -\ln(0.5)/\mu$ (Raup 1985, 1978), which equals 0.085 myr for my data. The expected mean duration of a species is $T_d = 1/\mu$ (Raup 1985, 1978), and is 0.123 myr. Both values are low and are consistent with the high turnover rate inferred from the data. The estimates for relative fossilization (i.e. probability of observing a fossil prior to extinction of its lineage, s) was estimated to be low with s = 0.000012. The fossil recovery rate (φ) can be caluculated by $\varphi = (s/(1\text{-}s))^*((e^*d)/(1\text{-}e))$, and

is 0.0002279. The low values for the sampling rate indicates that there is much unobserved diversity, and can also explain high values of speciation and extinction rates. However, it is extremely low compared to empirical estimates of the fossil record sample rate, such as preservation rates inferred for Late Cretaceous and Cenozoic mammals (Foote & Raup 1996; Foote 1997; lowest rates were inferred for Late Cretaceous mammals, and approximate 0.25 lineages per million year: Foote, et al. 1999). It should be noted that Foote et al. (1999) considered all known Late Cretaceous mammal fossils, and my low rates could potentially be explained by my fossil sample, which represents only a fraction of known fossil turtle species.

TABLE 5.2. Summaries of model parameters from 45002 post burn-in posterior samples of two MCMC runs. alpha is the gamma shape parameter of the character rate variation; igrvar is the gamma shape parameter for rate variation across branches in the relaxed clock model.

Parameter	Mean	Variance	Lower 95% HPD	Upper 95% HPD	Median
Tree Height	0.6095	0.0046	0.4859	0.7483	0.6055
Tree Length	8.6919	0.6433	7.1732	10.3137	8.6600
Proportion of ancestral fossils	0.0252	0.0003	0.0000	0.0606	0.0303
alpha	0.9811	0.0189	0.7162	1.2533	0.9779
Net speciation	0.0057	0.00001	0.0003	0.0114	0.0054
Relative extinction	0.9993	0.0000	0.9986	0.9999	0.9993
Relative fossilization	0.000012	0.0000	0.00001	0.00002	0.00001
igrvar	0.036	0.00004	0.0241	0.0483	0.0355
clockrate	0.0027	0.0000	0.0021	0.0033	0.0027

5.5 Systematic Palaeontology

HYPHALOCHELYDIA new clade

Definition. The clade that includes *Plesiochelys etalloni* (Pictet and Humbert, 1857), *Solnhofia parsoni* Gaffney, 1975*b*, *Sandownia harrisi* Meylan *et al.*, 2000, but not *Pelomedusa subrufa* (Bonnaterre, 1789), *Testudo graeca* Linnaeus, 1758, or *Protostega gigas* (Cope, 1871*b*).

Derivation of name. Modified from the ancient greek words *hyphalos* (υφαλος), meaning under the sea or submerged, and *chelys* (Χελυς), meaning turtle.

Remarks. Hyphalochelydia refers to a group that contains thalassochelydians (*sensu* Anquetin *et al.* 2017*a*) and angolachelonians (*sensu* Mateus *et al.* 2009). The uncertain or unknown relationships of most species within its constituent group Thalassochelydia do not affect the clade itself, unless one of the species used in the definition for Thalassochelydia that have not been included in a comprehensive phylogenetic analysis so far (i.e. *Thalassemys hugii* or *Eurysternum wagleri*) are found to be more closely related to *Sandownia harrisi* than to *Plesiochelys etalloni*.

5.6 Discussion

5.6.1 Comments on phylogenetic nomenclature

Phylogenetic definitions for clades have become common within the turtle research community (e.g. Joyce *et al.* 2004; Mateus *et al.* 2009; Rabi *et al.* 2014; Cadena & Parham 2015; Anquetin *et al.* 2017*a*; Evers & Benson 2018*a*). As discussed in section 2.4 of this thesis, the application of such definitions for higher clades becomes problematic under certain circumstances, one of which is when the relative positions of some taxa used in the definition are highly unstable across studies. The unstable relationship of *Solnhofia parsoni* across phylogenetic analyses (even within this thesis) highlights the pitfalls of phylogenetic nomenclature. Specifically, the position of *Solnhofia*, which is one of the defining taxa in the phylogenetic definition of Angolachelonia (Mateus *et al.* 2009), affects whether this name is applicable to a highly inclusive group (including all currently known non-chelonioid, non-pleurodiran marine turtles from the Jurassic onwards), or a less inclusive group (*Solnhofia* + sandownids).

All phylogenetic analyses performed in this thesis imply the existence of a clade that includes *Sandownia*, *Solnhofia*, and *Plesiochelys*. *Sandownia* is the defining part of a group of turtles called sandownids (for which a rank based definition was provided first by Tong &

Meylan 2013; and a phylogenetic definition was given by Evers & Benson 2018*a*). *Plesiochelys* is a defining part of a group called Thalassochelydia (Anquetin *et al.* 2017*a*, modified by Evers & Benson 2018*a* [section 2.4 of this thesis]). Under the hypodigm of *Solnhofia* being a thalassochelydian, the name Angolachelonia is applicable (and has priority over alternatives) for the clade that includes *Sandownia* (i.e. sandownids), *Plesiochelys* (i.e. thalassochelydians), and *Solnhofia* (see Evers & Benson 2018*a*). Under the alternative hypodigm of *Solnhofia* being more closely related to *Sandownia* (i.e. sandownids) than to *Plesiochelys* (i.e. thalassochelydians), as found by my Bayesian analysis, the name Angolachelonia has to be restricted to a less inclusive group, i.e. the group that includes *Sandownia* (i.e. sandownids) and *Solnhofia*. Angolachelonia in this sense mirrors the phylogenetic hypothesis from Mateus *et al.* (2009) for which the name was originally coined: A group that includes *Solnhofia* and sandownids, but excludes *Plesiochelys*. The more inclusive group that includes *Sandownia* (i.e. sandownids), *Plesiochelys* (i.e. thalassochelydians) and *Solnhofia*, still exists in the topology inferred by the Bayesian analysis, but no previously existing phylogenetic definition applies to it, leaving it nameless. As a Jurassic–Paleocene group of secondarily marine turtles, the clade is of significant interest and it is useful to have a name for it. For this reason, I herein propose the name Hyphalochelydia for Thalassocheydia+Sandownidae. Problematic with the definition of Hyphalochelyida is, however, that it is also applicable in the scenario in which *Solnhofia* is closer related to *Plesiochelys* than to *Sandownia* (i.e. as in section 2.4). Following that phylogenetic hypothesis, Hyphalochelydia is an objective junior synonym of Angolachelonia. When names of higher taxa rise and fall with the change of phylogenetic placement of single taxa like is the case here, it could be argued that the naming system as such is flawed.

Hyphalochelydia in the context of the Bayesian analysis, and Angolachelonia in the context of earlier parsimony analyses of this thesis have the exact same taxon content, albeit with different ingroup relationships. This exemplifies the true nature of phylogenetic clade definitions: They represent phylogenetic hypotheses conditioned on a few key taxa, rather than a collective and stable term for a large set of taxa or relationships between taxa.

Angolachelonia is the hypothesis that *Solnhofia* is closer related to *Sandownia* than to *Plesiochelys*, and Hyphalochelydia is the hypothesis that *Solnhofia*, *Sandownia*, and *Plesiochelys* are all closer related to one another than to cryptodires, pleurodires, or protostegids. A possible solution to the taxonomic confusion that inevitably arises from the current phylogenetic definitions would be to more specifically acknowledge that these definitions, in absence of stable a phylogenetic consensus, remain hypotheses themselves. For instance, if the phylogenetic definition of Angolachelonia had been more reflective of the phylogenetic hypothesis it was based on (Mateus *et al.* 2009), it could have included a statement that specifically excludes plesiochelyids from the hypodigm of Angolachelonia. Because the definition lacks such a statement, the name Angolachelonia tracks the phylogenetic uncertainty of *Solnhofia*, and thus becomes applicable to quite different sets of taxa and even phylogenetic hypotheses, as long as each such hypothesis is consistent with the vague phylogenetic definition of Angolachelonia. Another possible solution is to base phylogenetic definitions only on taxa that have much more stable phylogenetic positions than *Solnhofia*. However, this is far from the current reality, in which many name definitions are based on taxa that have not even been included in any phylogenetic analyses (see section 2.4). Furthermore, the second solution might be too simplistic, as even historically long-standing phylogenetic hypotheses (e.g. protostegids are chelonioids) can change over time given new discoveries or methods of inferring phylogeny.

5.6.2 Effects of time data for phylogenetic inference using a Bayesian analysis

Some general comments can be made as to how the Bayesian analysis using an FBD tree prior differs systematically from the results of parsimony analysis of the same character dataset. Most notably, the inclusion of age data during the analysis affects the inferred topology: Older fossils are repeatedly inferred to be in more stemward positions in the FBD tree in comparison with the parsimony tree, potentially indicating an unrealistically strong influence of the age priors on the topology. For instance, all fossil taxa from the Cretaceous

that were inferred to be stem-group cheloniids during parsimony analysis (analyses within this thesis, but also see Gentry 2016; Gentry *et al.* 2018) are found on the stem-group of chelonioids under Bayesian inference (with the exception of *Allopleuron*, which is now recovered as a dermochelyid). Similarly, *Baptemys* is found a stem-group kinosternoid rather than a crown-group kinosternoid (i.e. Dermatemydidae; e.g. Knauss 2014; Bourque *et al.* 2015; Joyce & Bourque 2016), *Petrochelys* is moved to a position on the stem of Trionychia, rather than being a crown-group trionychid (e.g. Vitek *et al.* 2017), and the fossil pleurodires included (i.e. the bothremydid *Galianemys* and the stem-pelomedusoid *Araripemys*; e.g. Ferreira *et al.* 2018) are recovered as stem-group pleurodires. Additionally, protostegids are recovered as earlier-branching stem-group chelonioids than *Toxochelys*, although this has never been suggested in any parsimony analysis that found protostegids as stem-group turtles (Evers & Benson 2018*a*; Raselli 2018; this thesis). For all these examples, phylogenetic positions inferred by the Bayesian analysis increase stratigraphic consistency, because ghost lineages are reduced within chelonioids, kinosternoids, trionychians, and pleurodires by these new placements with respect to results from parsimony. This implies that the stratigraphic order with which fossil taxa appear have a relatively strong effect on inferring topology in the framework of the Bayesian analysis. However, it is also clear that this is not universally the case: For instance, *Emarginachelys* is still recovered as a stem-group chelydrid in the Bayesian analysis, although support for this node was relatively weak in the parsimony framework and an alternative position more stemwardly (on the stem of Chelydroidea) would reduce ghost lineages within the chelydroid crown-group.

To test if the stemward-bias observed in the Bayesian analysis using an FBD tree prior was primarily driven by the settings of the FBD model, I ran a second Bayesian analysis in which only an Mk model of morphological evolution (Lewis 2001) was specified. No age data was included in the analysis. Two independent runs of four MCMCs for 10 million generations were used to sample trees every 500th generation from the posterior distribution, and 25% of sampled trees were discarded as burn-in for the construction of a maximum clade credibility tree. The average standard deviation of split frequencies after 10

million generation of 0.08758, the plot of the number of generations vs. the log probability of the data, and estimated sample sizes of >200 were taken as evidence for convergence. The topology of the Mk-model tree (Fig. 5.2) indicates that the stemward-bias observed in the combined Mk + FBD model analysis is indeed partly driven by the inclusion of age data for fossils: *Nichollsemys* and *Toxochelys* are recovered as more stemwardly positioned stem-chelonioids than protostegids, *Baptemys* is recovered as a stem-kinosternid, *Petrochelys* is nested within the crown-group of Trionychidae, *Galianemys* is found as a pelomedusoid, and *Araripemys* is recovered as a stem-group cheliid within the crown-group of Pleurodira. These placements are consistent with results from parsimony analysis. However, the Cretaceous 'stem-cheloniids' *Cabindachelys*, *Ctenochelys*, and *Peritresius* are still found as stem-group chelonioids, and *Allopleuron* is found to be a dermochelyid, as in the FBD analysis. Hyphalochelydia is found in a more crownward position than sinemydids, 'macrobaenids', and xinjiangchelyids, which is similar to the results of the parsimony analysis and differs from the FBD tree. Other notable differences to the FBD tree include that *Ordosemys* and *Dracochelys* are recovered as sinemydids rather than 'macrobaenids'.

Including molecular data for extant taxa can possibly further test the stemward bias discussed above. In the current Bayesian analysis using an FBD tree prior, rates of evolution are solely inferred from the data using a morphological model of evolution. Branch lengths inferred from a molecular data partition could be longer than suggested by morphology alone, which could increase posterior probabilities for accepting a 'more crownward' placement of the fossil taxa discussed above.

5.7 Planned modifications

5.7.1 Taxon sampling

I am planning several additions to the taxon sampling for future analyses. The sampling parameters of the FBD model assume random sampling for fossil taxa. This is clearly not the case in my analysis, in which extinct taxa have been chosen so to maximise

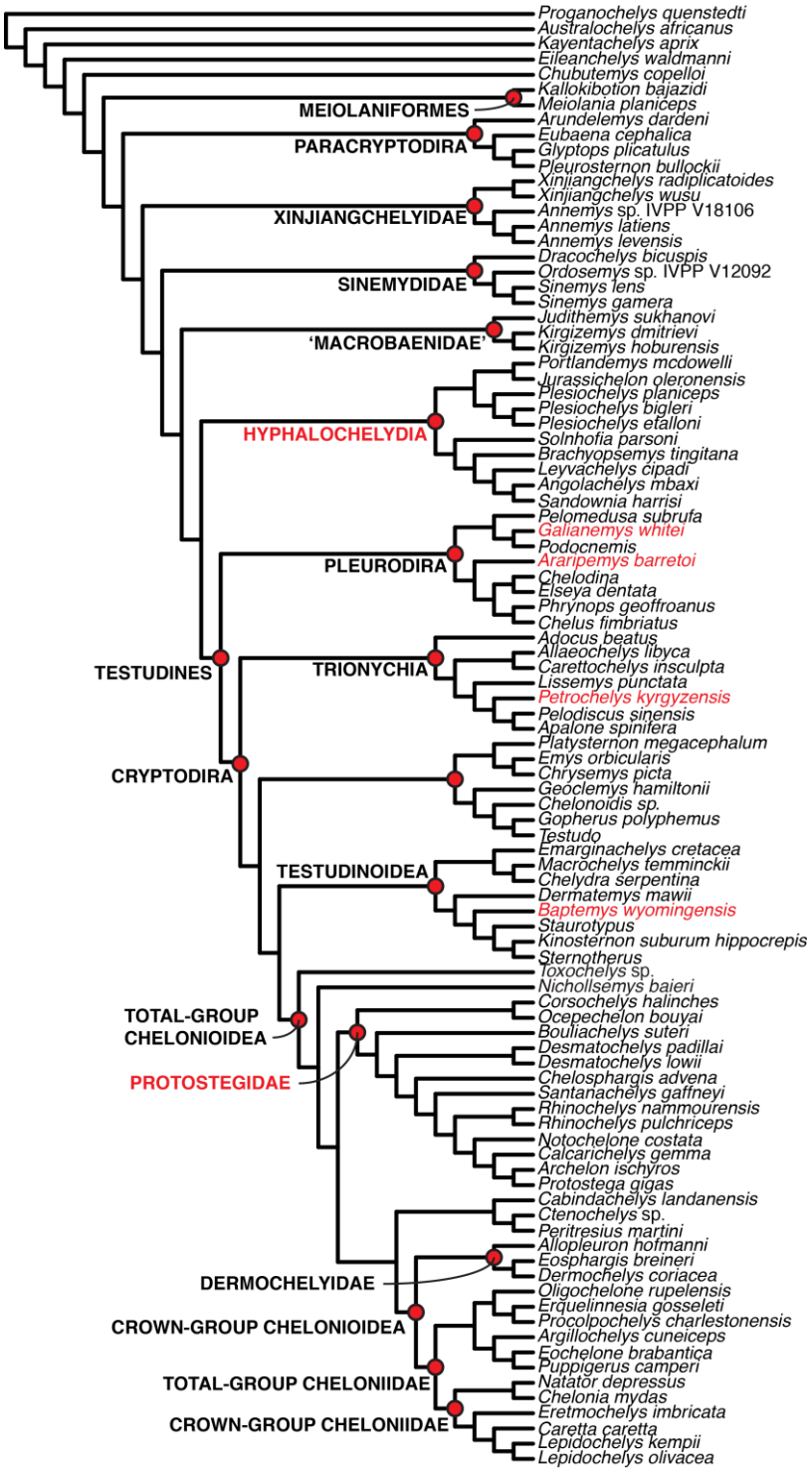


FIG. 5.2. Cladogram showing the topology inferred from an Mk model of morphological evolution. Lables of selected fossil taxa and two fossil clades (Hyphalochelydia, Protostegidae) recovered in more crown-ward positions in the Mk tree than in the FBD tree are coloured in red.

diversity for chelonioids (including protostegids), and marine taxa more widely (e.g. hyphalochelydians). Additionally, well-preserved early representatives have been added for several groups (specifically trionychians as the earliest-branching cryptodires, and

chelydroids as the sister group to chelonioids), because they can affect character polarization and patterns of trait evolution that I was interested in. However, for other groups, such as pleurodires and testudinoids, I included no stem-taxa.

I can potentially scrutinize the stemward-bias observed for several extinct taxa in the Bayesian analysis (discussed in section 4.6) by including further fossil representatives of affected groups. Specifically, I plan to sample a few taxa that under parsimony have consistently been recovered as being members of crown groups of subfamilies included in this study, and that do not represent the earliest diverging members of their respective groups (e.g. *Xenochelys* as a kinosternid; Hutchinson 2001; Joyce & Bourque 2016; *Hadrianus* as a testudinoid; Joyce *et al.* 2013*a*). If nearly all fossil taxa included are recovered as stem-group representatives of their respective lineages, despite morphological evidence for their position as members of the crown, it could be inferred that the age data included in the Bayesian framework has a much stronger effect on phylogenetic reconstruction than morphological data alone. Additionally, I plan to sample stem-group representatives of all groups, including pleurodires (e.g. platychelyids; Cadena & Joyce 2015; López-Conde *et al.* 2016; Ferreira *et al.* 2018) and testudinoids (e.g. lindholmemydids such as *Mongolemys*; Danilov & Parham 2005; Cadena *et al.* 2013). Inclusion of stem-group pleurodires possibly has an effect on the positions of *Galianemys* and *Araripemys*, which in my Bayesian analysis were found to be stem-group pleurodires but which are usually inferred to be crown-group pleurodires under parsimony analysis (e.g. Ferreira *et al.* 2018).

5.7.2 Total-evidence analysis

Pereira *et al.* (2017) recently published a dataset of mitochondrial and nuclear genes from 294 turtles, including all extant species included in my morphological dataset. As mentioned in earlier section, the next step I plan to do is to use this data and integrate it with my morphological data to a total-evidence dataset.

CONCLUSIONS

In this thesis, I provide new data that advances our understanding of the evolution of early sea turtles. My observations are based largely on personal examination of specimens and are further informed by high-resolution CT scans. I collected a large dataset of CT scans, which includes scans of the crania of 160 turtle species, whereby every subfamily of extant turtles and representatives of most fossil clades of turtles are included. This dataset was primarily used to inform morphological character construction and scoring for phylogenetic analysis. However, I also completely segmented a selection of fossil and extant taxa in great detail in order to produce anatomical descriptive work. Key conclusions regarding different aspects of my work are summarized below.

Anatomy. Despite the preservation of many fossils, the cranial anatomy of chelonioids is relatively poorly understood, which impedes our possibilities of constructing phylogenetic characters that comprehensively include most aspects of systematic variation. For example, no detailed cranial anatomy of any protostegid has been provided to date, despite a wealth of fossils, their early fossil discovery in the 1880's, and their unclear phylogenetic position. Herein, I prepared the most detailed anatomical treatment of the cranial morphology of any protostegid to date. Besides providing digital models for six specimens of *Rhinochelys*, including the holotypes of the three British species considered valid by Collins (1970), I also evaluated other specimens to revise the taxonomy of the genus. Although anatomical variation was observed among specimens, qualitative assessment of the variable traits, as well as multivariate statistical analysis of skull measurements of a broad sample of specimens does not support the occurrence of clusters that could form the basis for objective species delimitation. Therefore, previously named species of *Rhinochelys* are synonymized, and only the type species, *Rhinochelys pulchriceps*, is considered valid among the European species. Nevertheless, my assessment of non-cranial remains from the West Melbury Marly Chalk

Formation indicates that several species of chelonioids are present in addition to *R. pulchriceps*. This prevents referral of protostegid postcranial bones from the assemblage to *Rhinochelys* with any certainty.

Phylogeny of turtles. I constructed a new phylogenetic matrix that represents an effort to combine previously published variation across non-pleurodiran turtles with new observations. Particular emphasis in taxon sampling was put on the diversity of secondarily marine turtles, including chelonioid and non-chelonioid species. Based on digital examination and segmentation of CT scans and direct specimen observations, I revised and added > 80 morphological characters, and also >25 postcranial characters. The character data has been vetted to directly reflect primary hypotheses of homology. Characters were scored for 96 extant and extinct turtle species.

The resulting character-taxon matrix, and versions thereof that reflect research progress at particular points throughout my PhD, were analysed with both parsimony and model-based methods for phylogenetic reconstruction. Although the topological results of different analyses from this thesis vary, several common patterns emerge. First, protostegids are never found to be stem-group turtles or stem-group cryptodires, as suggested by most comprehensive hypotheses of turtle relationships. Instead, protostegids are always recovered as total-group chelonioids (Bayesian FBD and Mk trees, parsimony), and sometimes as crown-group chelonioids on the stem of *Dermochelys* (parsimony). Alternatively, more stemward positions for protostegids could statistically be robustly rejected using Templeton's tests. Second, all phylogenetic inference methods recover a clade of Late Jurassic–Paleogene secondarily marine turtles, which includes thalassochelydians, sandownids, and *Solnhofia*. Depending on the relative phylogenetic position of *Solnhofia*, this clade can be named Angolachelonia, or Hyphalochelydia. Phylogenetic nomenclature of turtles is complicated by poor choices of definitions and problems inherent to a taxonomy based on phylogenetic hypotheses. This is discussed in relevant sections of this thesis and exemplified by the Angolachelonia/Hyphalochelydia clade. Although the phylogenetic

position of Hyphalochelydia is unstable across different analyses within my thesis (it is either found as the sister group of pleurodires, the sister group of crown-group turtles, or in earlier branching positions on the stem-group of turtles), all analyses agree that hyphalochelydians lie outside of Cryptodira. Third, xinjiangchelyids, sinemydids, and 'macrobaenids' are not recovered as stem-group cryptodires, but instead as stem-group turtles, with somewhat varying positions, species-content, and ingroup relationships, depending on the analysis.

Divergence times of chelonioids. All phylogenetic analyses carried out throughout this thesis find support for the presence of Late Cretaceous crown-group chelonioids. For instance, *Allopleuron* from the Maastrichtian is found as a stem-group cheloniid (parsimony) or a dermochelyid (Bayesian inference). Inclusion of Cretaceous chelonioids in my analyses has implications for the divergence times of chelonioids, but also deeper nodes in the turtle tree, such as americhelydians (chelydroids + chelonioids). I used different methods to calibrate the inferred phylogenies to geologic time. Specifically, I used *a posteriori* minimum-branch length methods to time-scale cladograms based on my parsimony analyses, and I used a Bayesian tip-dating approach with a morphological relaxed clock model and a fossilized birth-death (FBD) tree model to estimate the topology and divergence times simultaneously. The latter approach will be further developed in future work. Estimated divergence times for chelonioids depend on the relative phylogenetic position of protostegids: When protostegids are considered to be crown-group chelonioids, divergence times for the crown-group are inferred to be Early Cretaceous (Barremian, c. 125 Ma). When protostegids are considered to be stem-group chelonioids instead (as in the Bayesian tip-dating analysis), the crown age is inferred to be Late Cretaceous (Coniacian, c. 88 Ma). Regardless of the exact position of protostegids within the total-group of Chelonioidea, my results push back the origin of Americhelydia by 27.5 Ma (with regard to Joyce *et al.* 2013*a*) to the Barresian (c. 140 Ma), significantly extending the ghost lineage for chelydroids. However, the inferred biogeographic origin of Americhelydia in North America, and a poor post-Tithonian and pre-

Campanian North American fossil record make it possible that Early Cretaceous americhelydians have simply not been sampled so far.

Transitions to secondarily marine lifestyles. Because phylogenetic hypotheses generated throughout this theses agree in finding chelonioid affinities of protostegids, as well as a clade consisting of thalassochelydians+sandownids, and accounting for the Triassic marine turtle *Odontochelys*, three non-pleurodiran transitions to marine life are supported by my results. Marine turtles show extensive survivorship during the Cretaceous–Paleogene mass extinction in comparison to other marine tetrapods, because members of all marine clades that were present at the end of the Cretaceous (i.e. bothremydid pleurodires, hyphalochelydians, chelonioids) survived into the Cenozoic.

Marine adaptation in chelonioids – flipper evolution. Because hyphalochelydians are universally inferred to have been shallow-marine animals, Chelonioidea is the only turtle group in which a pelagic ecology evolved. Extant chelonioids are well adapted to marine life and particularly pelagic locomotion, by modification of their limbs to flippers. However, the evolution of traits related to a marine ecology can be analysed by consideration of fossils. After reviewing and modifying characters related to flipper morphology, I mapped forelimb trait evolution onto one of the cladograms derived from a parsimony analysis that supports a stem-group chelonioid position for protostegids (in agreement with the Bayesian analyses). My tree topology implies that most traits fundamental to modern chelonioid flippers evolved only once, early on the chelonioid stem-lineage. However, secondary modifications to the general flipper bauplan are observed at the base of crown-cheloniids and dermochelyids, as well as in the clade delimiting the gigantic protostegids *Archelon* and *Protostega*. Although instances of convergent evolution between the chelonioid subgroups are apparent for individual characters, the flipper morphology of extant sea turtles is the result of a stepwise acquisition of derived characters that are concentrated at deep nodes in their phylogeny.

REFERENCES

AHLBERG, P. E. and MILNER, A. R. 1994. The origin and early diversification of tetrapods. *Nature*, **368**, 507–514.

——— and JOHANSON, Z. 1998. Osteolepiforms and the ancestry of tetrapods. *Nature*, **395**, 792–794.

———, CLACK, J. A. and LUKŠEVIČS, E. 1996. Rapid braincase evolution between Panderichthys and the earliest tetrapods. *Nature*, **381**, 61–64.

ALBRECHT, P. W. 1976. The cranial arteries of turtles and their evolutionary significance. *Journal of Morphology*, **149**, 159–182.

ALEKSEYENKO, A. V., LEE, C. J. and SUCHARD, M. A. 2008. Wagner and Dollo: A stochastic duet by composing two parsimonious solos. *Systematic Biology*, **57** (5), 772–784.

ALFARO, M. E., SANTINI, F., BROCK, C., ALAMILLO, H., RABOSKY, D. L., CARNEVALE, G. and HARMON, L. 2009. Nine exceptional radiations plus high turnover explain species diversity in jawed vertebrates. *Proceedings of the National Academy of Sciences*, **106** (32), 13410–13414.

ALI, F., ZELENITZKY, D. K., THERRIEN, R. and WEISHAMPEL, D. 2008. Homology of the "ethmoid complex" of tyrannosaurids and its implications for the reconstruction of the olfactory apparatus of non-avian theropods. *Journal of Vertebrate Palaeontology*, **28** (1), 123–133.

ANQUETIN, J. 2010. The anatomy of the basal turtle *Eileanchelys waldmani* from the Middle Jurassic of the Isle of Skye, Scotland. *Earth and Environmental Science Transactions of the Royal Society of Edinburgh*, **101**, 67–96.

——— 2012. Reassessment of the phylogenetic interrelationships of basal turtles (Testudinata). *Journal of Systematic Palaeontology*, **10**, 3–45.

——— and CHAPMAN, S. D. 2016. First report of *Plesiochelys etalloni* and *Tropidemys langii* from the Late Jurassic of the UK and the palaeobiogeography of plesiochelyid turtles. *Royal Society Open Science*, **3**, 150470.

——— and JOYCE, W. G. 2014. A reassessment of the Late Jurassic turtle Eurysternum wagleri (Eucryptodira, Eurysternidae). *Journal of Vertebrate Paleontology*, **34**, 1317–1328.

———, DE LA FUENTE, M. S. and ROUGIER, G. W. 2007. Anatomy and relationships of *Palaeochersis talampayensis*, a Late Triassic turtle from Argentina. *Palaeographica Abteilung A*, **281**, 1–61.

———, DESCHAMPS, S. and CLAUDE, J. 2014*a*. The rediscovery and redescription of the holotype of the Late Jurassic turtle *Plesiochelys etalloni*. *PeerJ*, **2**, e258.

———, PÜNTENER, C. and BILLON-BRUYAT, J.-P. 2014*b*. A taxonomic review of the Late Jurassic eucryptodiran turtles from the Jura Mountains (Switzerland and France). *PeerJ*, **2**, e369.

———, PÜNTENER, C. and BILLON-BRUYAT, J.-P. 2015. *Portlandemys gracilis* n. sp., a New Coastal Marine Turtle from the Late Jurassic of Porrentruy (Switzerland) and a Reconsideration of Plesiochelyid Cranial Anatomy. *PLOS ONE*, **10**, e0129193.

———, PÜNTENER, C. and JOYCE, W. G. 2017*a*. A Review of the Fossil Record of Turtles of the Clade Thalassochelydia. *Bulletin of the Peabody Museum of Natural History*, **58**, 317–369.

———, TONG, H. and CLAUDE J. 2017*b*. A Jurassic stem pleurodire sheds light on the functional origin of neck retraction in turtles. *Scientific Reports*, **7**, 1–10.

BAIRD, I. L. 1974. Anatomical features of the inner ear in submammalian vertebrates. 159–212. *In* KEIDEL, W. D. and NEFF, W. D. (eds.). *Handbook of Sensory Physiology, Volume V/1: Auditory System: Anatomy Physiology (Ear)*. Springer-Verlag, Berlin, 736 pp.

BAPST, D. W. 2012. paleotree: an R package for paleontological and phylogenetic analyses of evolution. *Methods in Ecology and Evolution*, **3** (5), 803-807.

——— 2013. A stochastic rate-calibrated method for time-scaling phylogenies of fossil taxa. *Methods in Ecology and Evolution*, **4**, 724–733.

———, WRIGHT, A. M., MATZKE, N. J. and LLOYD, G. T. 2016. Topology, divergence dates, and macroevolutionary inferences vary between different tip-dating approaches applied to fossil theropods (Dinosauria). *Biology Letters*, **12**, 201602237.

BARDET, N. 1994. Extinction events among Mesozoic marine reptiles. *Historical Biology*, **7** (4), 313–324.

———, JALIL, N. E., DE LAPPARENT DE BROIN, F., GERMAIN, D., LAMBERT, O. and AMAGHZAZ, M. 2013. A giant chelonioid turtle from the Late Cretaceous of Morocco with a suction feeding apparatus unique among tetrapods. *PLoS ONE*, **8**, 1–10.

———, FALCONNET, J., FISCHER, V., HOUSSAYE, A., JOUVE, S., PEREDA SUBERBIOLA, X., PÉREZ-GARCÍA, A., RAGE, J.-C. and VINCENT, P. 2014. Mesozoic marine reptile palaeobiogeography in response to drifting plates. *Gondwana Research*, **26**, 869–887.

BELL, M. a. and LLOYD, G. T. 2014. strap: an R package for plotting phylogenies against stratigraphy and assessing their stratigraphic congruence. *Palaeontology*, **58** (2), 379–389.

BENSON, R. B. J. 2013. Marine Reptiles. *In* MACLEOD, N., ARCHIBALD, J. D. and LEVIN, P. S. (eds.) *Grzimek's Animal Life Encyclopedia, Extinction*, Gale Cengage Learning, Farminton Hills, Michigan, 267–279 pp.

——— and DRUCKENMILLER, P. S. 2014. Faunal turnover of marine tetrapods during the Jurassic-Cretaceous transition. *Biological Reviews*, **89**, 1–23.

———, MANNION, P. D., BUTLER, R. J., UPCHURCH, P., GOSWAMI, A. and EVANS, S. E. 2013. Cretaceous tetrapod fossil record sampling and faunal turnover: Implications for biogeography and the rise of modern clades. *Palaeogeography, Palaeoclimatology, Palaeoecology*, **372**, 88–107.

———, BUTLER, R. J., ALROY, J., MANNION, P. D., CARRANO, M. T. and LLOYD, G. 2016. Near-stasis in long-term diversification of Mesozoic tetrapods. *PLoS Biology*, **14** (1): e1002359.

BENTON, M. J. and DONOGHUE, P. C. 2007. Paleontological evidence to date the tree of life. *Molecular Biology and Evolution*, **24** (1), 26–53.

BEVER, G. S. 2009 *a*. Postnatal ontogeny of the skull in the extant North American turtle *Sternotherus odoratus* (Cryptodira, Kinosternidae). *Bulletin of the American Museum of Natural History*, **330**, 1–97.

——— 2009*b*. The postnatal skull of the extant North American Turtle Pseudemys texana (Cryptodira: Emydidae), with comments on the study of discrete intraspecific variation. *Journal of Morphology*, **270**, 97–128.

———, LYSON, T. R., FIELD, D. and BHULLAR, B.-A. S. 2015. Evolutionary origin of the turtle skull. *Nature*, **525**, 1–4.

BHULLAR, B.-A. S. and BEVER, G. S. 2009. An archosaur-like laterosphenoid in early turtles (Reptilia: Pantestudines). *Breviora*, **518**, 1–11.

BILLON-BRUYAT, J.-P., LÉCUYER, C., MARTINEAU, F. and MAZIN, J.-M. 2005. Oxygen isotope compositions of Late Jurassic vertebrate remains from lithographic limestones of western Europe: implications for the ecology of fish, turtles, and crocodilians. *Palaeogeography, Palaeoclimatology, Palaeoecology*, **216**, 359–375.

BONNATERRE, P.-J. 1789. *Tableau Encyclopédique et Méthodique Des Trois Règnes De La Nature. Erpétologie*. Paris.

BOURQUE, J. R., HUTCHINSON, J. H., HOLROYD, P. A. and BLOCH, J. I. 2015. A new dermatemydid (Testudines, Kinosternoidea) from the Paleocene–Eocene Thermal Maximum, Willwood Formation, southeastern Bighorn Basin, Wyoming. *Journal of Vertebrate Palaeontology*, **35** (2), e905481.

BRAZEAU, M. D. 2011. Problematic character coding methods in morphology and their effects. *Biological Journal of the Linnean Society*, **104**, 489–498.

———, GUILLERME, T. and SMITH, M. R. 2017. Morphological phylogenetic analysis with inapplicable data. *BioRxiv*, published online 26 October, 2017. doi: https://doi.org/10.1101/209775

BRINKMAN, D. B. 2001. New material of *Dracochelys* (Eucryptodira: Sinemydidae) from the Junggar Basin, Xinjiang, People's Republic of China. *Canadian Journal of Earth Sciences*, **38**, 1645–1651.

——— and PENG, J.-H. 1993. New material of *Sinemys* (Testudines, Sinemydidae) from the Early Cretaceous of China. *Canadian Journal of Earth Sciences*, **30**, 2139–2152.

——— and RODRIGUEZ-DE LA ROSA, R. 2006. Nonmarine turtles from the Cerro Delpueblo

Formation (Campanian), Coahuila State, Mexico. *Late Cretaceous Vertebrates from the Western Interior: Bulletin*, **35**, 229.

——— and WU, X.-C. 1999. The skull of *Ordosemys*, an early Cretaceous turtle from Inner Mongolia, People's Republic of China, and the interrelationships of Eucryptodira (Chelonia, Cryptodira). *Paludicola*, **2**, 134–147.

———, HART, M., JAMNICZKY, H. and COLBERT, M. 2006. *Nichollsemys baieri* gen. et sp. nov., a primitive chelonioid turtle from the Late Campanian of North America. *Paludicola*, **5**, 111–124.

———, AQUILLON-MARTINEZ, M. C., DE LEON DÁVILA, C. A., JAMNICZKY, H., EBERTH, D. A. and COLBERT, M. 2009. *Euclastes coahuilaensis* sp. nov., a basal cheloniid turtle from the late Campanian Cerro del Pueblo Formation of Coahuila State, Mexico. *PaleoBios*, **28**, 76–88.

———, EBERTH, D. A., XU, X., CLARK, J. M. and WU, X.-C. 2013. Turtles from the Jurassic Shishugou Formation of the Junggar Basin, People's Republic of China, with comments on the basicranial region of basal eucryptodires. *In* BRINKMAN, D. B., HOLROYD, P. A. and GARDNER, J. D. (eds.) *Morphology and Evolution of Turtles*, Springer, Dordrecht, 147–172 pp.

———, RABI, M. and ZHAO, L. 2017. Lower Cretaceous fossils from China shed light on the ancestral body plan of crown softshell turtles (Trionychidae, Cryptodira). *Scientific Reports*, **7**, 6719.

BRITTEN, R. J. 1986. Rates of DNA sequence evolution differ between taxonomic groups. *Science*, **231** (4744), 1393–1398.

CADENA, E. 2015. The first South American sandownid turtle from the Lower Cretaceous of Colombia. *PeerJ*, **3**, e1431.

——— and JOYCE, W. G. 2015. A review of the fossil record of turtles of the clades Platycheyidae and Dortokidae. *Bulletin of the Peabody Museum of Natural History*, **56** (1), 3–20.

——— and PARHAM, J. F. 2015. Oldest known marine turtle? A new protostegid from the

Lower Cretaceous of Colombia. *PaleoBios*, **32**, 1–421.

———, KSEPKA, D. T. and NORELL, M. A. 2013. New material of *Mongolemys elegans* Khosatzky and Mlynarski, 1971 (Testudines: Lindholmemydidae), from the Late Cretaceous of Mongolia with comments on bone histology and phylogeny. *American Museum Novitates*, **3766**, 1–28.

CAMIN, J. H. and SOKAL, R. R. 1965. A method for deducing branching sequences in phylogeny. *Evolution*, **19**, 311–326.

CARABAJAL, A. P., STERLI, J., MÜLLER, J. and HILGER, A. 2013. Neuroanatomy of the marine Jurassic turtle *Plesiochelys etalloni* (Testudinata, Plesiochelyidae). *PLoS ONE*, **8** (7), e69264.

——— ——— ,GEORGI, J., POROPAR, S. F. and KEAR, B. P. 2017. Comparative neuroanatomy of extinct horned turtles (Meiolaniidae) and extant terrestrial turtles (Testudinidae), with comments on the palaeobiological implications of selected endocranial features. *Zoological Journal of the Linnean Socitey*, **180** (4), 930–950.

CAROLL, R. L. 1988. Vertebrate paleontology and evolution. Freeman, New York.

——— 1996. Revealing the patterns of macroevolution. *Nature*, **381**, 19–20.

CASALE, P., FREGGI, D., BASSO, R. and ARGANO, R. 2005. Size at male maturity, sexing methods and adult sex ratio in loggerhead turtles (*Caretta caretta*) from Italian waters investigated through tail measurements. *Herpetological Journal*, **15**, 145–148.

CASE, E. C. 1897. On the osteology and relationships of protostega. *Journal of Morphology*, **14**, 21–60.

CASIER, E. 1968. Le squelette cephalique de *Eochelone brabantica* L. Dollo, du Bruxellien (Lutetien inférieour) de Belgique, et sa comparaison avec celui *Chelone mydas* Linné. *Bulletin de l'Institut Royal des Sciences Naturelles de Belgique, Sciences de la Terre*, **44**, 1–22.

CERDA, I. A., STERLI, J. and SCHEYER, T. M. 2016. Bone shell microstructure of *Condorchelys antiqua* Sterli, 2008, a stem turtle from the Jurassic of Patagonia. *Comptes Rendus Palevol*, **15**, 128–141.

CHIARI, Y., CAHAIS, V., GALTIER, N. and DELSUC F. 2012. Phylogenomic analyses support the position of turtles as the sister group of birds and crocodiles (Archosauria). *BMC Biology*, **10** (65), 1–14.

CLACK, J. A. 2009. The Fish–Tetrapod Transition: New Fossils and Interpretations. *Evolution: Education and Outreach*, **2**, 213–223.

CLAUDE, J., PRITCHARD, P., TONG, H., PARADIS, E. and AUFFRAY, J.-C. 2004. Ecological correlates and evolutionary divergence in the skull of turtles: A geometric morphometric assessment. *Systematic Biology*, **53** (6), 933–948.

CLOSE, R. A., FRIEDMAN, M., LLOYD, G. T. and BENSON, R. B. J. 2015. Evidence for a Mid-Jurassic adaptive radiation in mammals. *Current Biology*, **25** (16), 2137–2142.

COLLINS, J. I. 1970. The chelonian *Rhinochelys* Seeley from the Upper Cretaceous of England and France. *Palaeontology*, **13**, 355–378.

CONROY, G. C. and VANNIER, M. W. 1984. Non-invasive three-dimensional computer imaging of matrix-filled fossil skulls by high-resolution computed tomography. *Science*, **226** (4673), 456–458.

COPE, E. D. 1868. On the origin of genera. *Proceedings of the Academy of Natural Sciences of Philadelphia*, **20**, 242–300.

——— 1871*a*. A description of the genus *Protostega*, a Form of Extinct Testudinata. *Proceedings of the American Philosophical Society*, **12**, 422–433.

——— 1871*b*. Letter to Professor Lesley giving an account of a journey in the valley of the Smoky Hill River in Kansas. *Proceedings of the American Philosophical Society*, **12**, 174–176.

——— 1872. *On the geology and paleontology of the Cretaceous strata of Kansas*. U.S. Geological Survey, Fifth Annual Report, 323–335.

CRAWFORD, N. G., FAIRCLOTH, B. C., McCORMACK, J. E., BRUMFIELD, R. T., WINKER, K. and GLENN, T. C. 2012. More than 1000 ultraconserved elements provide evidence that turtles are the sister group of archosaurs. *Biology Letters*, **8**, 783–786.

———, PARHAM, J. F., SELLAS, A. B., FAIRCLOTH, B. C., GLENN, T. C., PAPENFUSS, T. J.,

HENDERSON, J. B., HANSEN, M. H. and SIMISON, W. B. 2015. A phylogenomic analysis of turtles. *Molecular Phylogenetics and Evolution*, **83**, 250–257.

CUNNINGHAM, J. A., RAHMAN, I. A., LAUTENSCHLAGER, S., RAYFIELD, E. J. and DONOGHUE, C. J. 2014. A virtual world of paleontology. *Trends in Ecology & Evolution*, **29** (6), 347–357.

DALRYMPLE, G. H. 1977. Intraspecific variation in the cranial feeding mechanism of turtles of the genus *Trionyx* (Reptilia, Testudines, Trionychidae). *Journal of Herpetology*, **11** (3), 255–285.

DANILOV, I. G. and PARHAM, J. F. 2005. A reassessment of the referral of an isolated skull from the Late Cretaceous of Uzbekistan to the stem-testudinoid turtle genus *Lindholmemys*. *Journal of Vertebrate Palaeontology*, **25** (4), 784–791.

——— ——— 2006. A redescription of '*Plesiochelys*' *tatsuensis* from the Late Jurassic of China, with comments on the antiquity of the crown clade Cryptodira. *Journal of Vertebrate Paleontology*, **26**, 573–580.

——— ——— 2008. A reassessment of some poorly known turtles from the Middle Jurassic of China, with comments on the antiquity of extant turtles. *Journal of Vertebrate Paleontology*, **28**, 306–318.

———, AVERIANOV, A. O., SKUTCHAS, P. P. and REZVYI, A. S. 2006. *Kirgizemys* (Testudines, 'Macrobaenidae'): New material from the Lower Cretaceous of Buryatia (Russia) and taxonomic revision. *In* DANILOV, I. G. and PARHAM, J. F. (eds.) *Fossil Turtle Research. Proceedings of the Symposium on Turtle Origins, Evolution and Systematics*, St. Petersburg.

———, HIRAYAMA, R., SUKHANOV, V. B., SUZUKI, S., WATABE, M. and VITEK, N. S. 2014. Cretaceous soft-shelled turtles (Trionychidae) of Mongolia: new diversity, records and a revision. *Journal of Systematic Palaeontology*, 37–41.

DEBRAGA, M. and RIEPPEL, O. 1997. Reptile phylogeny and the interrelationships of turtles. *Zoological Journal of the Linnean Society*, **120**, 281–354

DIJK, P. P. VAN; IVERSON, J. B.; RHODIN, A. G. J., SHAFFER, H. B. and BOUR, R. 2014. Turtle Taxonomy Working Group, Turtles of the World, 7th Edition: Annotated checklist of

taxonomy, synonymy, distribution with maps, and conservation status. *In* RHODIN, A. G. J., PRITCHARD, P. C. H., VAN DIJK, P. P., SAUMURE, R. A., BUHLMANN, K. A., IVERSON, J. B. and MITTERMEIER, R. A. (eds.). *Conservation Biology of Freshwater Turtles and Tortoises: A Compilation Project of the IUCN/SSC Tortoise and Freshwater Turtle Specialist Group*, **5**, 329–479.

DONOGHUE, P. C. J. and YANG, Z. 2016. The evolution of methods for establishing evolutionary timescales. *Philosophical Transactions of the Royal Society B*, **371**, 20160020.

DRUMMOND, A. J., HO, S. Y. W., PHILIPPS, M. J. and RAMBAUT A. 2006. Relaxed phylogenetics and dating with confidence. *PLoS Biology*, **4** (5), e88.DRYDEN, L. S. 1988. *Paraphyly of the Cryptodira and phylogenetic systematics of turtles. M. Sc. thesis*. University of Kansas, Kansas, 142 pp.

EDINGER, T. 1929. Die fossilen Gehirne. *Ergebnisse der Anatomie und Entwicklungsgeschichte*, **28**, 249 pp.

ELDREDGE, N. and CRACRAFT, J. 1980. *Phylogenetic patterns and the evolutionary process. Method and theory in comparative biology*. Columbia University Press, New York, 329 pp.

ERNST, C. H. and BARBOUR, R. W. 1989. Turtles of the World. Smithsonian Institution Press, Washington, DC.

ESTABROOK, G. F. 1968. A general solution in partial orders for the CAmin-Sokal model in phylogeny. *Journal of Theoretical Biology*, **21**, 421–438.

ETIENNE, R. S., HAEGEMAN, B., STADLER, T., AZE, T., PEARSON, P. N., PURVIS, A. and PHILLIMORE, A. B. 2011. Diversity-dependence brings molecular phylogeneies closer in agreement with the fossil record. *Proceedings of the Royal Society B*, 1–10.

EVANS, J. and KEMP, T. S. 1975. The cranial morphology of a new Lower Cretaceous turtle from southern England. *Palaeontology*, **18**, 25.

EVANS, S. E. 2008. The skull of lizards and tuatara. 1–347. *In* GANS, C., GAUNT, A. S. and ADLER, K. (eds.). *Biology of the Reptilia, Volume 20, Morphology H, The skull of Lepidosauria*. Academic Press, London, 758 pp.

EVERS, S. W. and BENSON, R. B. J. 2018*a*. A new phylogenetic hypothesis of turtles with implications for the number of evolutionary transitions to marine lifestyles supports an Early Cretaceous origin and rapid diversification of Chelonioidea. *Palaeontology*, 1–42.

——— ———. 2018*b*. Project: Evers & Benson 2018, Turtle CT data and 3D models. *MorphoSource*. http://www.morphosource.org/Detail/ProjectDetail/Show/project_id/462

——— ———. 2018*c*. Data from: A new phylogenetic hypothesis of turtles with implications for the number of evolutionary transitions to marine lifestyles supports an Early Cretaceous origin and rapid diversification of Chelonioidea. *Dryad Digital Repository*. http://datadryad.org/review?doi=doi:10.5061/dryad.2pb356h

FELSENSTEIN, J. 1981. Evolutionary trees from DNA sequences: a maximum likelihood approach. *Journal of Molecular Evolution*, **17**, 368–376.

——— 1982. Numerical methods for inferring evolutionary trees. *The Quarterly Review of Biology*, **57** (4), 379–404.

——— 1983. Parsimony in systematics: Biological and statistical issues. *Annual Reviews of Evology and Systematics*, **14**, 313–333.

——— 1985*a*. Confidence limits on phylogenies with a molecular clock. *Systematic Biology*, **34**, 152–161.

——— 1985*b*. Phylogenies and the comparative method. *The American Naturalis*, **125** (1), 1–15.

FERNÁNDEZ, M. S. and DE LA FUENTE, M. S. 1988. Nueva tortuga (Cryptodira: Thalassemydidae) de la Formación Vaca Muerta (Jurásico, Tithoniano) de la provincia de Neuquén, Argentina. *Ameghiniana,* **25** (2), 129–138.

FERREIRA, G. S., RINCÓN, A. D., SOLÓRZANO, A. and LANGER, M. C. 2015. The last marine pelomedusoids (Testudines: Pleurodira): a new species of *Bairdemys* and the paleoecology of Stereogenyina. *PeerJ*, **3**, e1063.

———, BRONZATI, M., LANGER, M. C., and STERLI, J. 2018. Phylogeny, biogeography and diversification patterns of side-necked turtles (Testudines: Pleurodira). *Royal Society*

Open Science, **5**, 171773, 1–17.

FIELD, D. J., GAUTHIER, J. A., KING, B. L., PISANI, D., LYSON, T. L. and PETERSON, K. J. 2014. Toward consilience in reptile phylogeny: miRNAs support an archosaur, not lepidosaur, affinity for turtles. *Evolution & Development*, **16** (4), 189–196.

FOOTE, M. 1994. Morphological disparity in Ordovician-Devonian crinoids and the early saturation of morphological space. *Paleobiology*, **20**, 320–344.

——— 1996. On the probability of ancestors in the fossil record. *Paleobiology*, **22** (2), 141–151.

——— 1997. Estimating taxonomic durations and preservation probability. *Paleobiology*, **23** (3), 278–300.

——— and RAUP, D. M. 1996. Fossil preservation and the stratigraphic ranges of taxa. *Paleobiology*, **22** (2), 121–140.

———, HUNTER, J. P., JANIS, C. M. and SEPKOSKI Jr., J. J. 1999.Evolutionary and preservational constraints on origins of biologic g.roups: divergence times of eutherian mammals. *Science*, **283** (5406), 1310–1314.

FRIEDMAN, M. and SALLAN, L. C. 2012. Five hundred million years of extinction and recovery: A Phanerozoic survey of large-scale diversity patterns in fishes. *Palaeontology*, **55** (4), 707–742.

FOTH, C., RABI, M. and JOYCE, W. 2017*a*. Skull shape variation in extant and extinct Testudinata and its relation to habitat and feeding ecology. *Acta Zoologica*, **98**, 310–325.

GAFFNEY, E. S. 1972*a*. The systematics of the North American family Baenidae (Reptilia, Cryptodira). *Bulletin of the American Museum of Natural History*, **147**, 243–319.

——— 1972*b*. An illustrated glossary of turtle skull nomenclature. *American Museum Novitates*, **2486**, 1–33.

——— 1975*a*. A phylogeny and classification of the higher categories of turtles. *Bulletin of the American Museum of Natural History*, **55** (5), 387–436.

——— 1975*b*. A taxonomic revision of the Jurassic turtles *Portlandemys* and *Plesiochelys*. *American Museum Novitates*, **2574**, 1–19 .

——— 1975*c*. *Solnhofia parsonsi*, a new cryptodiran turtle from the late Jurassic of Europe. *American Museum Novitates*, **2576**, 1–25.

——— 1976. Cranial morphology of the European Jurassic turtles *Portlandemys* and *Plesiochelys*. *Bulletin of the American Museum of Natural History*, **157**, 487–544.

——— 1977. An endocranial cast of the side-necked turtle, *Bothremys*, with a new reconstruction of the palate. *American Museum Novitates*, **2639**, 1–12.

——— 1979. Comparative cranial morphology of recent and fossil turtles. *Bulletin of the American Museum of Natural History*, **164**, 65–376.

——— 1982*a*. Cranial morphology of the baenid turtles. *American Museum Novitates*, **2737**, 1–22.

——— 1982*b*. The lower jaws of baenid turtles. *American Museum Novitates*, **2749**, 1–10.

——— 1983. The cranial morphology of the extinct horned turtle, *Meiolania platyceps*, from the Pleistocene of Lord Howe Island, Australia. *Bulletin of the American Museum of Natural History*, **175**, 361–480.

——— 1990. The comparative osteology of the Triassic turtle *Proganochelys*. *Bulletin of the American Museum of Natural History*, **194**, 1–176.

——— and JENKINS JR, F. A. 2010. The cranial morphology of *Kayentachelys* , an Early Jurassic cryptodire, and the early history of turtles. *Acta Zoologica*, **91**, 335–368.

——— and KITCHING, J. W. 1995. The morphology and relationships of *Australochelys*, an early Jurassic turtle from South Africa. *American Museum Novitates*, **3130**, 1–29.

——— and MEYLAN, P. A. 1988. A phylogeny of turtles. 157–219. *In* BENTON, M. J. (eds.). *The phylogeny and classification of the tetrapods, Volume 1: Amphibians, Reptiles, Birds. Systematics Association Special Volume No. 35A*. Clarendon Press, Oxford, 377 pp.

——— and MEYLAN, P. A. 1992. The Transylvanian turtle, *Kallokibotion*, a primitive cryptodire of Cretaceous Age. *American Museum Novitates*, 3040, 1–37.

——— and YE, X. 1992. *Dracochelys*: a new cryptodiran turtle from the early Cretaceous of China. *American Museum Novitates,* **3048**, pages.

——— and ZANGERL, R. 1968. A revision of the chelonian genus Bothremys (Pleurodira:

Pelomedusidae). *Fieldiana. Geology Memoirs*, **16** (7), 193–239.

———, TONG, H. and MEYLAN, P. A. 2002. *Galianemys*, a new side-necked turtle (Pelomedusoides: Bothremydidae) from the Late Cretaceous of Morocco. *American Museum Novitates*, **3379**, 1–20.

———, ——— and ———. 2006. Evolution of the side-necked turtles: the families Bothremydidae, Euraxemydidae, and Araripemydidae. *Bulletin of the American Museum of Natural History*, **300**, 1–698.

———, RICH, T. H., VICKERS-RICH, P., CONSTANTINE, A., VACCA, R. and KOOL, L. 2007. *Chubutemys*, a new eucryptodiran turtle from the Early Cretaceous of Argentina, and the relationships of the Meiolaniidae. *American Museum Novitates*, **3599**, 1–35.

———, MEYLAN, P. A., WOOD, R. C., SIMONS, E. and DE ALMEIDA CAMPOS, D. 2011. Evolution of the side-necked turtles: the family Podocnemididae. *Bulletin of the American Museum of Natural History*, **350**, 1–237.

GAUTHIER, J. 1986. Saurischian monophyly and the origin of birds. *Memoirs of the California Academy of Sciences,* **8**, 1–55.

GAVRYUSHKINA, A., WELCH, D., STADLER, T. and DRUMMOND, A. J. 2014. Bayesian inference of sampled ancestor trees fro epidemiology and fossil calibration. *PLoS Computational Biology*, **10** (12), e1003919.

———, HEATH, T.A., KSEPKA, D. T., STADLER, T., WELCH, D. and DRUMMOND, A. J. 2017. Bayesian total-evidence dating reveals the recent crown radiation of penguins. *Systematic Biology*, **66** (1), 57–73.

GELMAN, A. and RUBIN, D. B. 1992. Inference from iterative simulation using multiple sequences. *Statistical Science*, **4**, 457–511.

GENTRY, A. D. 2016. New material of the Late Cretaceous marine turtle *Ctenochelys acris* Zangerl, 1953 and a phylogenetic reassessment of the 'toxochelyid'-grade taxa. *Journal of Systematic Palaeontology*, **15** (8), 675–696.

———, PARHAM, J. F., EHRET, D. J., and EVERSOLE J. A. 2018. A new species of *Peritresius* Leidy, 1856 (Testudines: Pan-Cheloniidae) from the Late Cretaceous (Campanian) of

Alabama, USA, and the occurrence of the genus within the Mississippi Embayment of North America. *PLoS ONE*, **13** (4), e0195651.

GEORGALIS, G. L. and JOYCE, W. G. 2017. A review of the fossil record of old world turtles of the clade *Pan-Trionychidae*. *Bulletin of the Peabody Museum of Natural History*, **58**, 115–208.

GEORGI, J. A. 2008. Semicircular canal morphology as evidence of locomotot environment in amniotes. Unpublished PhD thesis, Stony Brook University, Stony Brook, New York, 223 pp.

GIRIBET, G. 2007. Efficient tree searches with available algorithms. *Evolutionary Bioinformatics*, **3**, 341–356.

GODLEY, B. J., BRODERICK, A. C., FRAUENSTEIN, R., GLEN, F. and HAYS, G. C. 2002. Reproductive seasonality and sexual dimorphism in green turtles. *Marine Ecology Progress Series*, **226**, 125–133.

GOLDMAN, N. and YANG, Z. 1994. A codon-based model of nucleotide substitution fro protein-coding DNA sequences. *Molecular Biology and Evolution*, **11** (5), 725–736.

———, ANDERSON, J. P., RODRIGO, A. G. and OLMSTEAD, R. 2000. Likelihood-based tests of topologies in phylogenetics. *Systematic Biology*, **49**, 652–670.

GOLOBOFF, P. A. 1999. Analyzing large data sets in reasonable times: solutions for composite optima. *Cladistics*, **15**, 415–428.

——— and CATALANO, S. A. 2016. TNT version 1.5, including a full implementation of phylogenetic morphometrics. *Cladistics*, **32**, 221–238.

———, FARRIS, J. S. and NIXON, K. C. 2008. TNT, a free program for phylogenetic analysis. *Cladistics*, **24**, 774–786.

GOODSHIP, A. E., LANYON, L. E. and MCFIE, H. 1979. Functional adaptation of bone increased stress. An experimental study. *The Journal of bone and joint surgery. American volume*, **61** (4), 539–546.

GRAY, J. E. 1831. *Synopsis reptilium: or short descriptions of the species of reptiles. PartI., Cataphracta. Tortoises, crocodiles, and enaliosaurians.* G.B. Sowerby: London, 84 pp.

HARMON, L. J. 2018. *Phylogenetic Comparative Methods, Learning from Trees.* pp. 230

———, LOSOS, J. B., DAVIES, T. J., GILLESPIE, R. G., GITTLEMAN, J. L., JENNINGS, W. B., KOZAK, K. H. MCPEEK, M. A., MORENO-ROARK, F., NEAR, T. J., PURVIS, A., RICKLEFS, R. E., SCHLUTER, D., SCHULTE II, J. A., SEEHAUSEN, O., SIDLAUSKAS, B. L., TORRES-CARVAJAL, O., WEIR, J. and MOOERS, A. O. 2010. Early bursts of body size and shape evolution are rare in comparative data. *Evolution*, **64** (8), 2385–2396.

HASEGAWA, M., KISHINO, H. and YANO, T. 1985. Dating the human-ape splitting by a molecular clock of motochondrial DNA. *Journal of Molecular Evolution*, **22**, 160–174.

HAVLIK, P. E., JOYCE, W. G. and BÖHME, M. 2014. *Allaeochelys libyca* , a new carettochelyine turtle from the Middle Miocene (Langhian) of Libya. *Bulletin of the Peabody Museum of Natural History*, **55**, 201–214.

HAWKINS, J., HUGHES, C. and SCOTLAND, R. 1997. Primary homology assessment, characters and character states. *Cladistics*, **283**, 275–283.

HAY, O. P. 1896. On the skeleton of *Toxochelys latiremis*. *Field Columbian Museum Publications, Zoological Series*, **1**.

———. 1908. *The fossil turtles of North America*. Carnegie Institution of Washington.

HEATH, T. A., HOLDER, M. T. and HUELSENBECK, J. P. 2012. A Dirichlet process prior for estimating lineage-specific substitution rates. *Molecular Biology and Evolution*, **29** (3), 939–955.

———, HUELSENBECK, J. P. and STADLER, T. 2014. The fossilized birth-death process for coherent calibration of divergence-time estimates. *Proceedings of the National Academy of Sciences*, **111** (2), E2957–E2966.

HENNIG, W. 1966. *Phylogenetic systematics*. Translated by D. D. DAVIES and R. ZANGERL. University of Illinois Press, Chicago, 263 p.

HENSON, O. W. 1974. Comparative anatomy of the middle ear. 40–110. *In* KEIDEL, W. D. and NEFF, W. D. (eds.). *Handbook of Sensory Physiology, Volume V/1: Auditory System: Anatomy Physiology (Ear)*. Springer-Verlag, Berlin, 736 pp.

HETHERINGTON, T. 2008. Comparative anatomy and function of hearing in aquatic

amphibians, reptiles, and birds. 183–2009. *In* THEWISSEN, J. H. M. and NUMMELA, S. (eds.). *Sensory evolution on the threshold, Adaptations in secondarily aquatic vertebrates*. University of California Press, Berkeley, 351 pp.

HIPP, A. L., HALL, J. C., SYTSMA, K. J. and LUTZONI, F. 2004. Congruence versus phylogenetic accuracy: revisiting the incongruence length difference test. *Systematic Biology*, **53**, 81–89.

HIRAYAMA, R. 1992. Humeral morphology of chelonioid sea-turtles; its functional analysis and phylogenetic implications. *Bulletin of the Hobetsu Museum*, **8**, 17–57.

——— 1994. Phylogenetic systematics of chelonioid sea turtles. *Island Arc*, **3**, 270–284.

——— 1997. Distribution and Diversity of Cretaceous Chelonioids. *In Ancient Marine Reptiles*, Elsevier, 225–241 pp.

——— 1998. Oldest known sea turtle. *Nature*, **392**, 705–708.

———, ISAJI, S. and HIBINO, T. 2013. *Kappachelys okurai* gen. et sp. nov., a new stem soft-shelled turtle from the Early Cretaceous of Japan. 179–185. *In* BRINKMAN, D. B., HOLROYD, P. A. and GARDNER, J. D. (eds.). *Morphology and Evolution of Turtles*. Springer, Dordrecht, 577 pp.

HO, S. Y. W. and PHILLIPS, M. J. 2009. Accounting for calibration uncertainty in the phylogenetic estimation of evolutionary divergence times. *Systematic Biology*, **58** (3), 367–380.

HOLLIDAY, C. M. and WITMER, L. M. 2007. Archosaur adductor chamber evolution: Integration of muscoskeletal and topological criteria in jaw muscle homology. *Journal of Morphology*, **268**, 457–484.

HOOKS, G. E. 1998. Systematic revision of the Protostegidae, with a redescription of *Calcarichelys gemma* Zangerl, 1953. *Journal of Vertebrate Paleontology*, **18**, 85–98.

HOPSON, J. A. 1979. Paleoneurology. 39–146. *In* GANS, C., NORTHCUTT, R. G. and ULINSKI, P. (eds.). *Biology of the Reptilia, Volume 9, Neurology A*. Academic Press, London, 462 pp.

HUELSENBECK, J. P., LARGET, B. and SWOFFORD, D. 2000. A compound Poisson process for relaxing the molecular clock. *Genetics*, **154**, 1879–1892.

HUNT, G. and SLATER, G. 2016. Integrating paleontological and phylogenetic approaches to macroevolution. *Annual Review of Ecology, Evolution, and Systematics*, **47**, 189–213.

HURLEY, C. 2012. gclus: Clustering Graphics. R package version 1.3.1. https://cran.r-project.org/package=gclus

HUTCHINSON, J. H. 2001. Early Kinosterninae (Reptilia: Testudines) and their phylogenetic significance. *Journal of Vertebrate Palaeontology*, **11** (2), 145–167.

IWABE, N., HARA, Y., KUMAZAWA, Y., SHIBAMOTO, K., SAITO, Y. MIYATA, T. and KATOH, K. Sister Group Relationship of Turtles to the Bird-Crocodilian Clade Revealed by Nuclear DNA–Coded Proteins. *Molecular Biology and Evolution*, **22** (4), 810–813.

JAMNICZKY, H. A. 2008. Turtle carotid circulation: a character analysis case study. *Biological Journal of the Linnean Society*, **93**, 239–256.

JANSSEN, R., VAN BAAL, R. R. and SCHULP, A. S. 2011. On the taphonomy of the late Maastrichtian (Late Cretaceous) marine turtle *Allopleuron hofmanni*. *Geologie en Mijnbouw/Netherlands Journal of Geosciences*, **90**, 187–196.

JOLLIFFE, I. T. and CADIMA J. 2016. Principal component analysis: a review and recent developments. *Philosophical Transactions A*, **374**, 20150202.

JONES, M. E. H., WERNEBURG, I., CURTIS, N., PENROSE, R., O'HIGGINS, P., FAGAN, M. J. and EVANS, S. E. 2012. The head and neck anatomy of sea turtles (Cryptodira: Chelonioidea) and skull shape in testudines. *PLoS ONE*, **7**, e47852.

JOYCE, W. G. 2000. The first complete skeleton of *Solnhofia parsonsi* (Cryptodira, Eurysternidae) from the Upper Jurassic of Germany and its taxonomic implications. *Journal of Paleontology*, **74**, 684–700.

——— 2007. Phylogenetic relationships of Mesozoic turtles. *Bulletin of the Peabody Museum of Natural History*, **48**, 3–102.

——— 2014. A review of the fossil record of turtles of the clade Pan-*Carettochelys*. *Bulletin of the Peabody Museum of Natural History*, **55**, 3–33.

——— 2016. A review of the fossil record of turtles of the clade Pan-Chelydridae. *Bulletin of the Peabody Museum of Natural History*, **57**, 21–56.

——— 2017. A review of the fossil record of basal Mesozoic turtles. *Bulletin of the Peabody Museum of Natural History*, **58**, 65–113.

——— and BOURQUE, J. R. 2016. A review of the fossil record of turtles of the clade Pan-Kinosternoidea. *Bulletin of the Peabody Museum of Natural History*, **57**, 57–95.

——— and GAUTHIER, J. A. 2004. Palaeoecology of Triassic stem turtles sheds new light on turtle origins. *Proceedings of the Royal Society B*, **271**, 1–5.

——— PARHAM, J. F. and GAUTHIER, J. A. 2004. Developing a protocol for the conversion of rank-based taxon names to phylogenetically defined clade names, as exemplified by turtles. *Journal of Paleontology*, **78**, 989–1013.

———, CHAPMAN, S. D., MOODY, R. T. J. and WALKER C. A. 2011. The skull of the solemydid turtle *Helochelydra nopcsai* from the early Cretaceous of the Isle if Wight (UK) and a review of Solemydidae. *Special Papers in Palaeontology*, **86**, 75–97.

———, SCHOCH, R. R. and LYSON, T. R. 2013*a*. The girdles of the oldest fossil turtle, *Proterochersis robusta*, and the age of the turtle crown. *BMC Evolutionary Biology*, **13**, 266.

———, PARHAM, J. F., LYSON, T. R., WARNOCK, R. C. M. and DONOGHUE, P. C. J. 2013*b*. A divergence dating analysis of turtles using fossil calibrations: an example of best practices. *Journal of Paleontology*, **87**, 612–634.

——— LYSON, T. R. and WILLIAMS, S. 2016*a*. New cranial material of *Gilmoremys lancensis* (Testudines, Trionychidae) from the Hell Creek Formation of southeastern Montana, U.S.A. *Journal of Vertebrate Paleontology*, **36**, e1225748.

———, RABI, M., CLARK, J. M. and XU, X. 2016*b*. A toothed turtle from the Late Jurassic of China and the global biogeographic history of turtles. *BMC Evolutionary Biology*, **16**, 236.

KEAR, B. P. and LEE, M. S. Y. 2006. A primitive protostegid from Australia and early sea turtle evolution. *Biology letters*, **2**, 116–119.

KIMURA M. 1980. A simple method for estimating evolutionary rates of base substitutions through comparative studies of nucleotide sequences. *Journal of Molecular Evolution*, **16**, 111–120.

KING, B., QIAO, T., LEE, M. S. Y., ZHU, M. and LONG, J. A. 2017. Bayesian morphological clock methods resurrect placoderm monophyly and reveal rapid early evolution in jawed vertebrates. *Systematic Biology*, **66** (4), 499–516.

KISHINO, H., THORNE, J. L. and BRUNO W. J. 2001. Performance of a divergence time estimation method under a probabilistic model of rate evolution. *Molecular Biology and Evolution*, **18** (3), 352–361.

KNAUSS, G. E. 2014. A morphological description of *Baptemys wyomingensis* and an analysis of its phylogenetic relationship within Kinosternoidea. Unpublished M.Sc. thesis, University of Iowa, Iowa City, 181 pp.

———, JOYCE, W. G., LYSON, T. R. and PEARSON, D. 2011. A new kinosternoid from the Late Cretaceous Hell Creek Formation of North Dakota and Montana and the origin of the *Dermatemys mawii* lineage. *Paläontologische Zeitschrift*, **85**, 125–142.

KRAUSE, J., UNGER, T., NOCON, A., MALASPINAS, A.-S., KOLOKOTRONIS, S.-O., STILLER, M., SOIBELZON, L., SPRIGGS, H., DEAR, P. H., BRIGGS, A. W., BRAY, S. C. E., O'BRIEN, S. J., RABEDER, G., MATHEUS, P., COOPER, A., SLATKIN, M. PÄÄBO, S. and HOFREITE, M. 2008. Mitochondiral genomes reveal an explosive radiation of extinct and extant bears near the Miocene–Pliocene boundary. *BMC Evolutionary Biology*, **8** (220), 1–12.

KUMAR, S. and HEDGES, S. B. A molecular timescale for vertebrate evolution. 1998. *Nature*, **392**, 917–920.

KURATANI, S., KURAKU, S. and NAGASHIMA, H. 2011. Evolutionary developmental perspective for the origin of turtles: the folding theory for the shell based on the developmental nature of the carapacial ridge. *Evolution & Development*, **13** (1), 1–14.

DE LA FUENTE, M. S. and FERNÁNDEZ, M. S. 2011. An unusual pattern of limb morphology in the Tithonian marine turtle *Neusticemys neuquina* from the Vaca Muerta Formation, Neuquén Basin, Argentina. *Lethaia*, **44**, 15–25.

——— and ITURRALDE-VINENT, M. 2001. A new pleurodiran turtle from the Jagua Formation (Oxfordian) of western Cuba. *Journal of Paleontology*, **75**, 860–869.

LANYON, L. E., GOODSHIP, A. E., PYE, C. J. and MACFIE, J. H. 1982. Mechanically adaptive bone

remodelling. *Journal of Biomechanics*, **15** (3), 141–154.

DE LAPPARENT DE BROIN, F., DE LA FUENTE, M. S., and FERNANDEZ, M. S. 2007. *Notoemys laticentralis* (Chelonii, Pleurodira), Late Jurassic of Argentina: new examination of the anatomical structures and comparisons. *Revue de Paléobiologie*, **26** (1), 99–136.

LAURIN, M. 2004. The evolution of body size, Cope's Rule and the origin of amniotes. *Systematic Biology*, **53** (4), 594–622.

LAUTENSCHLAGER, S., FERREIRA, G. S. and WERNEBURG I. 2018. Sensory evolution and ecology of early turtles revealed by digital endocranial reconstructions. *Frontiers in Ecology and Evolution*, **6** (7), 1–16.

LEE, M. S. Y. 1997. Pareiasaur phylogeny and the origin of turtles. *Zoological Journal of the Linnean Society*, **120**, 197–280.

——— 2000. Tree robustness and clade significance. *Systematic Biology*, **49**, 829–836.

———, CAU, A., NAISH, D. and DYKE, G. 2014. Morphological clocks in palaeontology, and a mid-Cretaceous origin of crown Aves. *Systematic Biology*, **63** (3), 442–449.

LEHMAN, T. M. and TOMLINSON, S. L. 2004. *Terlinguachelys fischbecki*, a new genus and species of sea turtle (Chelonioidea: Protostegidae) from the Upper Cretaceous of Texas. *Journal of Paleontology*, **78**, 1163–1178.

LEPAGE, T., BRYANT, D., PHILIPPE, H. and LARTILLOT, N. 2007. A general comparison of relaxed molecular clock models. *Molecular Biology and Evolution*, **24** (12), 2669–2680.

LEWIS, P. O. 2001. A likelihood approach to estimating phylogeny from discrete morphological character data. *Systematic Biology*, **50** (6), 913–925.

LI, C., WU, X.-C., RIEPPEL, O., WANG, L.-T. and ZHAO, L.-J. 2008. An ancestral turtle from the Late Triassic of southwestern China. *Nature*, **456**, 497–501.

———, FRASER, N. C., RIEPPEL, O. and WU, X.-C. 2018. A Triassic stem turtle with an edentulous beak. *Nature*, **476**, 476–479.

LI, L., JOYCE, W. G. and LIU, J. 2015. The first soft-shelled turtle from the Jehol Biota of China. *Journal of Vertebrate Paleontology*, **35**, e909450.

LINNAEUS, C. 1758. *Systema Naturae*. Stockholm: Laurentius Salvius.

LIPKA, T. R., THERRIEN, F., WEISHAMPEL, D. B., JAMNICZKY, H. a., JOYCE, W. G., COLBERT, M. W. and BRINKMAN, D. B. 2006. A new turtle from the Arundel Clay facies (Potomac Formation, Early Cretaceous) of Maryland, U.S.A. *Journal of Vertebrate Paleontology*, **26**, 300–307.

LLOYD, G. T. 2016. Estimating morphological diversity and tempo with discrete character-taxon matrices: implementation, challenges, progress, and future directions. *Biological Journal of the Linnean Society*, **118**, 131–151.

———, BAPST, D. W., FRIEDMAN, M and DAVIES, K. E. 2016. Probabilistic divergence time estimation without branch lengths: dating the origins of dinosaurs, avian flight and crown birds. *Biology Letters*, **12**, 20160609.

LONG, J. A. and GORDON, M. S. 2004. The greatest step on vertebrate history: a paleobiological review of the fish-tetrapod transition. *Physiological and Biochemical Zoology*, **77**, 700–719.

LÓPEZ-CONDE, O. A. and ALVARADO-ORTEGA, J. 2017. Revisión morfólogica de las trotugas del género *Notoemys*. *Paleontología Mexicana*, **6** (2), 79–89.

———, STERLI, J., ALVARADO-ORTEGA, J. and CHAVARRÍA-ARELLANO, M. L. 2016. A new platychelyid turtle (Pan-Pleurodira) from the Late Jurassic (Kimmeridgian) of Oaxaca, Mexico. *Papers in Palaeontology*, **3** (2), 161–174.

LYDEKKER, R. 1889. On remains of Eocene and Mesozoic Chelonia and a tooth of (?) *Ornithopsis*. *Quarterly Journal of the Geological Society*, **45**, 227–246.

LYNCH, S. C. and PARHAM, J. F. 2003. The first report of hard-shelled sea turtles (Cheloniidae *sensu lato*) from the Miocene of California, including a new species (*Euclastes hutchisoni*) with unusually plesiomorphic characters. *PaleoBios*, **23** (3), 21–35.

LYSON, T. R. and JOYCE, W. G. 2012. Evolution of the turtle bauplan: the topological relationship of the scapula relative to the ribcage. *Biology Letters,* **8** (6), 1028–1031.

———, BEVER, G. S., BHULLAR, B.-A. S., JOYCE, W. G. and GAUTHIER, J. A. 2010. Transitional fossils and the origin of turtles. *Biology letters*, **6**, 830–833.

———, SPERLING, E. A., HEIMBERG, A. M., GAUTHIER, J. A, KING, B. L. and PETERSON, K. J.

2012. MicroRNAs support a turtle + lizard clade. *Biology Letters,* **8**, 104–107.

———, BHULLAR, B.-A. S., BEVER, G., JOYCE, W. G., DE QUEIROZ, K., ABZHANOV, A and GAUTHIER, J. A. 2013. Homology of the enigmatic nuchal bone reveals novel reorganization of the shoulder girdle in the evolution of the turtle shell. *Evolution & Development,* **15** (5), 317–325.

———, JOYCE, W. G. and SERTICH, J. J. W. 2017. A new chelydroid turtle, *Lutemys warreni*, gen. et sp. nov., from the Upper Cretaceous (Campanian) Kaiparowits Formation of southern Utah. *Journal of Vertebrate Paleontology*, **37** (6), e1390672-10.

MADDISON, W. P. 1993. Missing data versus missing characters in phylogenetic analysis. *Systematic Biology*, **42**, 576–581.

MARSHALL, C. R. 2008. A simple method for bracketing absolute divergence times on molecular phylogenies using multiple fossil calibration points. *The American Naturalist*, **171** (6), 726–742.

MATEUS, O., JACOBS, L., POLCYN, M., SCHULP, A. S., VINEYARD, D., BUTA NETO, A. and TELLES ANTUNES, M. 2009. The oldest African eucryptodiran turtle from the Cretaceous of Angola. *Acta Palaeontologica Polonica*, **54**, 581–588.

MATZKE, A. T. 2007. An almost complete juvenile specimen of the cheloniid turtle *Ctenochelys stenoporus* (Hay, 1905) from the Upper Cretaceous Niobrara Formation of Kansas, USA. *Palaeontology*, 50 (3), 669–691.

MATZKE, N. J. and WRIGHT, A. 2016. Inferring node dates from tip dates in fossil Canidae: the importance of tree priors. *Biology Letters*, **12**, 20160328.

VON MEYER, H. 1839. *Eurysternum wagleri*, Münster. Eine Schildkröte aus dem Kalkschiefer von Solnhofen. *Beiträge zur Petrefacten-Kunde*, **1**, 75–82.

MEYLAN, P. A. 1987. The phylogenetic relationships of soft-shelled turtles (family Trionychidae). *Bulletin of the American Museum of Natural History*, **186**, 1–101.

——— 1996. Skeletal morphology and relationships of the early Cretaceous side-necked turtle, *Araripemys barretoi* (Testudines: Pelomedusoides: Araripemydidae), from the Santana Formation of Brazil. *Journal of Vertebrate Paleontology*, **16**, 20–33.

——— and GAFFNEY, E. S. 1989. The skeletal morphology of the Cretaceous cryptodiran turtle, *Adocus*, and the relationships of the Trionychoidea. *American Museum Novitates*, **2941**, 1–60.

———, MOODY, R. T. J., WALKER, C. a and CHAPMAN, S. D. 2000. *Sandownia harrisi*, a highly derived trionychoid turtle (Testudines : Cryptodira) from the Early Cretaceous of the Isle of Wight, England. *Journal of Vertebrate Paleontology,* **20**, 522–532.

MLYNARSKI, M. 1976. Teil 6. Testudines. *In* KUHN, O (eds). *Handbuch der Paläoherpetologie = Encyclopedia of paleoherpetology.* Verlag Dr. Friedrich Pfeil, Stuttgart: 130pp.

MOERS, A. O. and HEARD, S. B. 1997. Inferring evolutionary process from phylogenetic tree shape. *The Quarterly Review of Biology*, **72** (1), 31–54.

MOODY, R. T. J. 1968. A turtle, *Eochelys crassicostata* (Owen), from the London Clay of the Isle of Sheppey. *Proceedings of the Geologists' Association*, **79** (2), 129–140.

——— 1974. The taxonomy and morphology of *Puppigerus camperi* (Gray), an Eocene sea-turtle from Northern Europe. *Bulletin of the British Museum (Natural History), Geology*, **25**, 153–186.

MORET L. 1935. *Rhinochelys amaberti*, nouvelle espèce de tortue marine du Vraconien de la Fauge près du Villard-de-Lans (Isère). *Bulletin de la Societe Geologique de France*, **5**, 605–619.

MOTANI, R. 2009. The evolution of marine reptiles. *Evolution: Education and Outreach*, **2**, 224–235.

MÜLLER, J., STERLI, S. and ANQUETIN, J. 2011. Carotid circulation in amniotes and its implications for turtle relationships. *Neues Jahrbuch für Geologie und Paläontologie-Abhandlungen*, **261** (3), 289–297.

MULDER, E. W. A. 2003. Comparative osteology, palaeoecology and systematics of the Late Cretaceous turtle *Allopleuron hofmanni* (Gray 1831) from the Maastrichtian type area. *Pubicaties van het Natuurhistorisch Genootschap in Limburg*, 23–92.

MYERS, T. S., POLCYN, M. J., MATEUS, O., VINEYARD, D. P., GONÇALVES, A. O. and JACOBS, L. L. 2018. A nre durophagous stem cheloniid turtle from the Lower Paleocene of Cabinda,

Angola. *Papers in Palaeontology*, **4** (2), 161–176.

NAGASHIMA, H., SUGAHARA, F., TAKECHI, M., SATO, N. and KURATANI, S. 2014. On the homology of the shoulder girdle in turtles. *Journal of Experimental Zoology (Molecular and Developmental Evolution)*, **324**, 244–254.

NEAR, T. J., MEYLAN, P. A. and SHAFFER, H. B. 2005. Assessing concordance of fossil calibration points in molecular clock studies: an example using turtles. *The American naturalist*, **165** (2), 137–46.

——— and DORNBURG, A., EYTAN, R. I., KECK, B. P., SMITH, W. L., KUHN, K. L., MOORE, J. A., PRICE, S. A:, BURBRINK, F. T., FRIEDMAN, M. and WAINWRIGHT, P. C. 2013. Phylogeny and tempo of diversification in the superradiation of spiny-rayed fishes. *Proceedings of the National Academy of Sciences*, **110** (31), 12738–12743.

NEE, S., MOOERS, A. O. and HARVEY, P. H. 1992. Tempo and mode of evolution revealed from molecular phylogenies. *Proceedings of the National Academy of Sciences*, **89**, 8322–8326.

NEENAN, J. M., REICH, T., EVERS, S. W., DRUCKENMILLER, P. S., VOETEN, D. F. A. E., CHOINIERE, J. N., BARRETT, P. M., PIERCE, S. E. and BENSON, R. B. J. 2017. Evolution of the sauropterygian labyrinth with increasingly pelagic lifestyles. *Current Biology*, **27** (24), 3852–3858.

NICHOLLS, E. L. 1988. New material of *Toxochelys latiremis* Cope, and a revision of the genus *Toxochelys* (Testudines, Chelonioidea). *Journal of Vertebrate Paleontology*, **8**, 181–187.

NICHOLSON, D. B., HOLROYD, P. A., BENSON, R. B. J. and BARRETT, P. M. 2015. Climate-mediated diversification of turtles in the Cretaceous. *Nature Communications*, **6**, 7848.

NICK, L. 1912. Das Kopfskelet von *Dermochelys coriacea* L. *Zoologische Jahrbücher, Abteilung für Anatomie und Ontogenie der Tiere*, **33** (1), 431–552.

NIELSEN, E. 1959. Eocene turtles from Denmark. *Dansk Geologisk Forening*, **14**, 96–114.

——— 1963. On the post-cranial skeleton of Eosphargis breineri Nielsen. *Bulletin of the Geological Society of Denmark*, **15**, 281–328.

NIXON, K. C. 1999. The parsimony ratchet, a new method for rapid parsimony analysis. *Cladistics*, **15**, 407–414.

O'MEARA, B. C. 2012. Evolutionary inferences from ohylogenies: A review of methods. *Annual Reviews in Ecology, Evolution and Systematics*, **43**, 267–285.

OPPEL, M. 1881. *Die Ordnungen, Familien, und Gattungen der Reptilien als Prodrom einer Naturgeschichte derselben*. Joseph Lindauer, München, 86 pp.

OSTROM, J. H. 1975. The origin of birds. *Annual review of earth and Planetary Sciences*, **3**, 55–77.

OWEN, R. 1851. *Monograph on the fossil Reptilia of the Cretaceous Formations. Part I. Chelonia*. The Palaeographical Society, London, 118 pp.

PAGEL, M. 1994. Detecting correlated evolution on phylogenies: a general method for the comparative analysis of discrete characters. *Proceedings of the Royal Society B*, **255**, 37–45.

PARHAM, J. F. and FASTOVSKY, D. E. 1997. The phylogeny of cheloniid sea turtles revisited. *Chelonian Conservation and Biology*, **2** (4), 548–554.

——— and HUTCHISON, J. H. 2003. A new eucryptodiran turtle from the Late Cretaceous of North America (Dinosaur Provincial Park, Alberta, Canada). *Journal of Vertebrate Paleontology*, **23**, 783–798.

——— and PYENSON, N. D. 2010. New sea turtle from the Miocene of Peru and the iterative evolution of feeding ecomorphologies since the Cretaceous. *Journal of Paleontology*, **84**, 231–247.

———, FELDMAN, C. and BOORE, J. 2006. The complete mitochondrial genome of the enigmatic bigheaded turtle (*Platysternon*): description of unusual genomic features and the reconciliation of phylogenetic hypotheses based on mitochondrial and nuclear DNA. *BMC Evolutionary Biology*, **6**, 11.

———, DONOGHUE, P. C. J., BELL, C. J., CALWAY, T. D., HEAD, J. J., HOLROYD, P. A., INOUE, J. G., IRMIS, R. B., JOYCE, W. G., KSEPKA, D. T., PATANE, J. S. L., SMITH, N. D., TARVER, J. E., VAN TUINEN, M., YANG, Z., ANGIELCZYK, K. D., GREENWOOD, J. M., HIPSLEY, C. A., JACOBS, L., MAKOVICKY, P. J., MULLER, J., SMITH, K. T., THEODOR, J. M., WARNOCK, R. C. M. and BENTON, M. J. 2012. Best practices for justifying fossil calibrations. *Systematic*

Biology, **61**, 346–359.

———, OTERO, R. A. and SUÁREZ, M. E. 2014. A sea turtle skull from the Cretaceous of Chile with comments on the taxonomy and biogeography of *Euclastes* (formerly Osteopygis). *Cretaceous Research*, **49**, 181–189.

PARSONS, T. S. 1970. The nose and Jacobson's organ. 99–191. *In* CARL, G. and PARSONS, T. S. (eds.). *Biology of the Reptilia, Volume 2, Morphology B*. Academic Press, London, 373 pp.

PATTERSON, C. 1982. Morphological characters and homology. *In* JOYSEY, K. A. and FRIDAY, A. E. (eds.) *Problems of Phylogenetic Reconstruction*, Academic Press, London, 21–74 pp.

PENNEL, M. W. and HARMON, L. J. 2013. An integrative view of phylogenetic comparative methods: connections to population genetics, community ecology, and paleobiology. *Annals of the New York Academy of Sciences*, **1289**, 90–105.

PEREIRA, A. G., STERLI, J., MOREIRA, F. R. R. and SCHRAGO, C. G. 2017. Multilocus phylogeny and statistical biogeography clarify the evolutionary history of major lineages of turtles. *Molecular Phylogenetics and Evolution*, **113**, 59–66.

PÉREZ-GARCÍA, A. 2012. The European early Cretaceous cryptodiran turtle *Chitracephalus dumonii* and the diversity of a poorly known lineage of turtles. *Acta Palaeontologica Polonica*, **57**, 575–588.

——— 2015. New data on the poorly-known Late Jurassic European turtles *Thalassemys* and *Enaliochelys* and description of a new basal eucryptodiran taxon. *Journal of Iberian Geology*, **41**, 21–30.

——— and CODREA, V. 2018. New insights on the anatomy and systematics of *Kallokibotion* Nopcsa, 1923, the enigmatic uppermost Cretaceous basal turtle (stem Testudines) from Transylvania. *Zoological Journal of the Linnean Society*, **182** (2), 419–443.

———, FUENTE, M. S. de la and ORTEGA, F. 2012. A new freshwater basal eucryptodiran turtle from the Early Cretaceous of Spain. *Acta Palaeontologica Polonica*, **57**, 285–298.

PETERSON, K. J., Lyons, J. B., NOWAK, K. S., TAKACS, C. M:, WARGO, M. J. and MCPEEK, M. A. 2004. Estimating metazoan divergence times with a molecular clock. *Proceedings of the National Academy of Sciences*, **101** (17), 6536–6541.

PICTET, F.-J. and HUMBERT, A. 1857. Description d'une emyde nouvelle (*Emys etalloni*) du terrain jurassique supérieur des environs de Saint-Claude. *Matériaux pour la Paléontologie Suisse*, **1**, 1–10.

PIMENTAL, R. A. and RIGGINS, R. 1987. The nature of cladistic data. *Cladistics*, **3**, 201–209.

PINNA DE, M. G. G. 1991. Concepts and tests of homology in the cladistic paradigm. *Cladistics*, **7**, 367–394.

PISANI, D., POLING, L. L., LYONS-WEILER, M. and HEDGES, S. B. 2004. The colonization of land by animals: molecular phylogeny and divergence times among arthropods. *BMC Biology*, **2** (1), 1–10.

PLATNICK, N. I. 1979. Philosophy and the transformation of cladistics. *Systematic Biology*, **28**, 537–546.

———, GRISWOLD, C. E. and CODDINGTON, J. A. 1991. On missing entries in cladistic analysis. *Cladistics*, **7**, 337–343.

PLEIJEL, F. 1995. On character coding for phylogeny reconstruction. *Cladistics*, **11**, 309–315.

POL, D. and ESCAPA, I. H. 2009. Unstable taxa in cladistic analysis: identification and the assessment of relevant characters. *Cladistics*, **25**, 515–527.

PÜNTERER, C., ANQUETIN, J. and BILLOT-BRUYAT, J.-P. 2017. The comparative osteology of *Plesiochelys bigleri* n. sp., a new coastal marine turtle from the Late Jurassic of Porrentruy (Switzerland). *PeerJ*, **5**, e3482.

PYRON, R. A. 2011. Divergence time estimation using fossils as terminal taxa and the origins of Lissamphibia. *Systematic Biology*, **60** (4), 466–481.

——— and BURBRINK, F. T. 2013. Phylogenetic estimates of speciation and extinction rates for testing ecological and evolutionary hypotheses. *Trends in Ecology and Evolution*, **28** (12), 729–736.

QUENTAL, T. B. and MARSHALL, C. R. 2010. Diversity dynamics: molecular phylogenies need the fossil record. *Trends in Ecology and Evolution*, **25**, 434–441.

R CORE TEAM. 2016. *R: a language and environment for statistical computing*. Version 3.3.1. R Foundation for Statistical Computing. http://www.R-project.org

RABI, M., JOYCE, W. G. and WINGS, O. 2010. A review of the Mesozoic turtles of the Junggar Basin (Xinjiang, Northwest China) and the paleobiogeography of Jurassic to Early Cretaceous Asian testudinates. *Palaeobiodiversity and Palaeoenvironments*, **90**, 259–273.

———, TONG, H. and BOTFALVAI, G. 2012. A new species of the side-necked turtle *Foxemys* (Pelomedusoides: Bothremydidae) from the Late Cretaceous of Hungary and the historical biogeography of the Bothremydini. *Geological Magazine*, **149**, 662–674.

———, ZHOU, C.-F., WINGS, O., GE, S. and JOYCE, W. G. 2013. A new xinjiangchelyid turtle from the Middle Jurassic of Xinjiang, China and the evolution of the basipterygoid process in Mesozoic turtles. *BMC Evolutionary Biology*, **13**, 203.

———, SUKHANOV, V. B., EGOROVA, V. N., DANILOV, I. G. and JOYCE, W. G. 2014. Osteology, relationships, and ecology of *Annemys* (Testudines, Eucryptodira) from the Late Jurassic of Shar Teg, Mongolia, and phylogenetic definitions for Xinjiangchelyidae, Sinemydidae, and Macrobaenidae. *Journal of Vertebrate Paleontology*, **34**, 327–352.

RAMBAUT, A., DRUMMOND, A. J., XIE, D., BAELE, G. and SUCHARD, M. A. 2018. Posterior summarization in Bayesian phylogenetics using Tracer 1.7. *Systematic Biology*, **67** (5), 901–904.

RANNALA, B. and YANG, Z. 2007. Inferring speciation times under an episodic molecular clock. *Systematic Biology*, **56** (3), 453–466.

RASELLI, I. 2018. Comparative cranial morphology of the Late Cretaceous protostegid sea turtle *Desmatochelys lowii*. *PeerJ Preprints*, **6**, e26863v1.

RAUP, D. M. 1985. Mathematical models of cladogenesis. *Paleobiolog*, **11** (1), 42–52.

——— 1978. Cohort analysis of generic survivorship. *Paleobiology*, **4** (1), 1–15.

DOS REIS, M. and YANG, Z. 2013. The unbearable uncertainty of Bayesian divergence time estimation. *Journal of Systematics and Evolution*, **51** (1), 30–43.

REISZ, R. R. and HEAD, J. J. 2008. Palaeontology: Turtle origins out to sea. *Nature*, **456**, 450–451.

REVELL, L. J. 2012. phytools: an R package for phylogenetic comparative biology (and other things). *Methods in Ecology and Evolution*, **3**, 217–223.

RIEPPEL, O. 1980. The skull of the Upper Jurassic cryptodire turtle *Thalassemys*, with a reconsideration of the chelonian braincase. *Palaeontographica Abteilung A*, 105–140.

——— 1988. *Fundamentals of comparative biology*. Birkhauser Verlag.

——— 1993. Patterns of Diversity in the reptilian skull. 344–390. *In* HANKEN, J. and HALL, B. K. (eds). *The skull, Volume 2, Patterns of structural and systematic diversity*. The University of Chicago Press, Chicago, 566 pp.

——— 2000. Turtles as diapsid reptiles. *Zoologica Scripta*, **29** (3), 199–212.

——— 2001. Turtles as hopeful monsters. *BioEssays* **23**, 987–991.

——— and DEBRAGA, M. 1996. Turtles as diapsid reptiles. *Nature*, **384**, 453–455.

ROBINSON, D. F. and FOULDS, L. R. 1981. Comparison of phylogenetic trees. *Mathematical Biosciences*, **53**, 131–147.

ROLLOT, Y., LYSON, T. R. and JOYCE, W. G. 2018. A description of the skull of *Eubaena cephalica* (Hay, 1904) and new insights into the cranial circulation and innervation of baenid turtles. *Journal of Vertebrate Paleontology*, **38** (3), e1474886

ROMANO, P. S. R., GALLO, V., RAMOS, R. R. C. and ANTONIOLI, L. 2014. *Atolchelys lepida*, a new side-necked turtle from the Early Cretaceous of Brazil and the age of crown Pleurodira. *Biology letters*, **10**, 20140290.

RONOV, A. B., KHAIN, V. E., BALUKHOVSKY, A. N. and SESLAVINSKY, K. B. 1980. Quantitative analysis of Phanerozoic sedimentation. *Sedimentary Geology*, **25**, 311–325.

RONQUIST, F., VAN DER MARK, P. and HUELSENBECK, J. P. 2009. Bayesian phylogenetic analysis using Mr Bayes. 210–266. *In* LEMEY, P., SALEMI, M. and VANDAMME, A.-M. (eds.). *The Phylogenetic Handbook, Second Edition*. Cambridge University Press, Cambridge, 723 pp.

———, KLOPFSTEIN, S., VILHELMSEN, L., SCHULMEISTER, S., MURRAY, D. L. and RASNITSYN, A. P. 2012*a*. A total-evidence approach to dating with fossils, applied to the early radiation of Hymenoptera. *Systematic Biology*, **61** (6), 973–999.

———, TESLENKO, M., VAN DER MARK, P., AYRES, D. L., DARLING, A., HÖHNA, S., LARGET, B., LIU, L., SUCHARD, M. A. and HUELSENBECK, J. P. 2012*b*. MrBayes 3.2: Efficient Bayesian

phylogenetic inference and model choice across a large model space. *Systematic Biology*, **61** (3), 539–542.

ROWE, T. B., COLBERT, M., KETCHAM, R. A., MAISANO, J. and OWEN, P. 2001. High-resolution X-ray computed tomography in vertebrate morphology. *Journal of Morphology*, **248** (3), 277–278.

RÜTIMEYER, L. 1973. Die fossilen Schildkröten von Solothurn und der übrigen Juraformation. *Neue Denkschriften der allgemeinen Schweizerischen Gesellschaft für die gesamten Naturwissenschaften*, **25**, 1–185.

SÁNCHEZ-VILLAGRA, M. R., BURNHAM, R. J., CAMPBELL, D. C., FELDMANN, R. M., GAFFNEY, E. S., KAY, R. F., LOZSÁN, R., PURDY, R. and THEWISSEN, J. G. M. 2000. A new near-shore marine fauna and flora from the Early Neogene of northwestern Venezuela. *Journal of Paleontology*, **74**, 957–968.

SANDERSON, M. J. 1997. A nonparametric approach to estimating divergence times in the absence of rate constancy. *Molecular Biology and Evolution*, **14** (12), 1218–1231.

SATO, T., KONISHI, T., HIRAYAMA, R., and CALDWELL, M. W. 2012. A review of the Upper Cretaceous marine reptiles from Japan. *Cretaceous Research*, **37**, 319–340.

SCAVEZZONI, I. and FISCHER, V. 2018. *Rhinochelys ambareti* Moret (1935), a protostegid from the Early Cretaceous of France. *PeerJ*, **6**, e4594.

SCHEYER, T. M. and SANDER, P. M. 2007. Shell bone histology indicates terrestrial palaeoecology of basal turtles. *Proceedings. Biological sciences*, **274**, 1885–93.

———, DANILOV, I. G., SUKHANOV, V. B. and SYROMYATNIKOVA, E. V. 2014. The shell bone histology of fossil and extant marine turtles revisited. *Biological Journal of the Linnean Society*, **112**, 701–718.

SCHOCH, R. R. and SUES, H.-D. 2015. A Middle Triassic stem-turtle and the evolution of the turtle body plan. *Nature*, **523**, 584–587.

SCHWENK, K. 2008. 65–81. Comparative anatomy and physiology of chemical senses in nonavian aquatic reptiles. *In* THEWISSEN, J. H. M. and NUMMELA, S. 2008. *Sensory evolution on the threshold, Adaptations in secondarily aquatic vertebrates*. University of

California Press, Berkeley, 351 pp.

SEELEY, H. G. 1869. *Index to the fossil remains of Aves, Ornithosauria, and Reptilia from the secondary system of starta arranged in the Woodwardian Museum of the University of Cambridge*. Cambridge University Press, Cambridge, 143 pp.

SHAFFER, H. B., MEYLAN, P., MCKNIGHT, M. L. and LARSON, A. 1997. Tests of turtle phylogeny: molecular, morphological, and paleontological approaches. *Systematic Biology*, **46**, 235–268.

SLATER, G. J. 2015. Iterative adaptive radiations of fossil canids show no evidence for diversity-dependent trait evolution. *Proceedings of the National Academy of Sciences*, 201403666.

———, HARMON, L. J. and ALFARO, M. E. 2012. Integrating fossils with molecular phylogenies improves inference of trait evolution. *Evolution*, **66** (12), 3931–3944.

SMITH, A. B. 1994. *Systematics and the fossil record: Documenting evolutionary patterns*. Blackwell Scientific, Oxford, 223 pp.

SMITH, D. T. J. 1989. The cranial morphology of fossil and living sea turtles (Cheloniidae, Dermochelyidae and Desmatochelyidae). Unpublished PhD thesis, Kingston Poltechnic, London, 334 pp.

SNEATH, P. H. A., SOKAL, R. R. and OTHERS. 1973. *Numerical taxonomy. The principles and practice of numerical classification.* W. H. Friedman and Company, San Francisco, 573 pp.

SOLIMAN, M. A. 1964. Die Kopfnerven der Schildkröten. *Zeitschrift für Wissenschaftliche Zoologie,* **169***,* 216–312.

STADLER, T. 2010. Sampling-through-time in birth-death trees. *Journal of Theoretical Biology*, **267**, 396–404.

———, GAVRYUSHKINA, A., WARNOCK, R. C. M., DRUMMOND, A. J. and HEATH, T. A. 2018. The fossilized birth-death model for the analysis of stratigraphic range data under different speciation modes. *Journal of Theoretical Biology*, **447**, 41–55.

STARCK, D. 1979. Cranio-cerebral relations in recent reptiles. 1–38. *In* GANS, C., NORTHCUTT, R. G. and ULINSKI, P. (eds.). *Biology of the Reptilia, Volume 9, Neurology A*. Academic

Press, London, 462 pp.

STERLI, J. 2008. A new, nearly complete stem turtle from the Jurassic of South America with implications for turtle evolution. *Biology Letters*, **4**, 286–289.

——— 2010. Phylogenetic relationships among extinct and extant turtles: The position of pleurodira and the effects of the fossils on rooting crown-group turtles. *Contributions to Zoology*, **79**, 93–106.

——— 2015. A review of the fossil record of Gondwanan turtles of the clade Meiolaniformes. *Bulletin of the Peabody Museum of Natural History*, **56** (1), 21–45.

——— and DE LA FUENTE, M. S. 2010. Anatomy of *Condorchelys antiqua* Sterli, 2008, and the origin of the modern jaw closure mechanism in turtles. *Journal of Vertebrate Paleontology*, **30** (2), 351–366.

——— ——— 2011. A new turtle from the La Colonia Formation (Campanian-Maastrichtian), Patagonia, Argentina, with remarks on the evolution of the vertebral column in turtles. *Palaeontology,* **54**, 63–78.

——— and DE LA FUENTE, M. S. 2013. New evidence from the Palaeocene of Patagonia (Argentina) on the evolution and palaeo-biogeography of Meiolaniformes (Testudinata, new taxon name). *Journal of Systematic Palaeontology*, **11**, 835–852.

——— and JOYCE, W. G. 2007. The cranial anatomy of the Early Jurassic turtle *Kayentachelys aprix*. *Acta Palaeontologica Polonica*, **52**, 675–694.

———, POL, D. and LAURIN, M. 2013. Incorporating phylogenetic uncertainty on phylogeny-based palaeontological dating and the timing of turtle diversification. *Cladistics*, **29**, 233–246.

———, DE LA FUENTE, M. S. and UMAZANO, A. M. 2015. New remains and new insights on the Gondwanan meiolaniform turtle *Chubutemys copelloi* from the Lower Cretaceous of Patagonia, Argentina. *Gondwana Research*, **27**, 978–994.

STRIMMER, K. and VON HAESELER, A. 2009. 181–209. Phylogenetic inference using maximum likelihood methods. *In* LEMEY, P., SALEMI, M. and VANDAMME, A.-M. (eds.). *The Phylogenetic Handbook, Second Edition*. Cambridge University Press, Cambridge, 723

pp.

STRONG, E. E. and LIPSCOMB, D. 1999. Character coding and inapplicable data. *Cladistics*, **15**, 363–371.

SUKHANOV, V. B. 2000. Mesozoic turtles of middle and central Asia. *The age of dinosaurs in Russia and Mongolia*, **17**, 309–367.

SULLIVAN, P. M. and JOYCE W. G. 2017. The shell and pelvic anatomy of the Late Jurassic turtle *Platychelys oberndorferi* based on material from Solothurn, Switzerland. *Swiss Journal of Palaeontology*, 136 (2), 323–343.

SUTTON, M. D. 2008. Tomographic techniques for the study of exceptionally preserved fossils. *Proceedings of the Royal Society B*, **275** (1643), 1587–1593.

———, RAHMAN, I. A. and GARWOOD, R. J. 2014. *Techniques for Virtual Palaeontology*. Wiley-Blackwell, Oxford, 208 p.

SWOFFORD, D. L. 2002. PAUP*. Phylogenetic Analysis Using Parsimony (*and other methods). Version. 4.0. Sinauer Associates, Sunderland, MA.

TAMURA, K. 1992. Estimation of the number of nucleotide substitutions when there are strong transition-transversion and G+C-content biases. *Molecular Biology and Evolution*, **9** (4), 678–687.

TEMPLETON, A. R. 1983. Phylogenetic inference from restriction endonuclease cleavage site maps with particular reference to the evolution of humans and the apes. *Evolution,* 37 (2), 221–244.

THEWISSEN, J. H. M. and NUMMELA, S. 2008. *Sensory evolution on the threshold, Adaptations in secondarily aquatic vertebrates*. University of California Press, Berkeley, 351 pp.

THORNE, J. L. and KISHINO, H. 2002. Divergence time and evolutionary rates estimation with multilocus data. *Systematic Biology*, **51** (5), 689–702.

——— ———. and PAINTER, I. S. 1998. Estimating the rate of evolution of the rate of molecular evolution. *Molecular Biology and Evolution*, **15** (12), 1647–1657.

TONG, H. and MEYLAN, P. 2013. Morphology and Relationships of *Brachyopsemys tingitana* gen. et sp. nov. from the Early Paleocene of Morocco and Recognition of the New

Eucryptodiran Turtle Family: Sandownidae. 187–212. *In* BRINKMAN, D. B., HOLROYD, P. A. and GARDNER, J. D. (eds.). *Morphology and Evolution of Turtles*. Springer, Dordrecht, 577 pp.

———, HIRAYAMA, R., MAKHOUL, E. and ESCUILLIÈ, F. 2006. *Rhinochelys* (Chelonioidea: Protoszegidae) from the Late Cretaceous (Cenomanian) of Nammoura, Lebanon. *Atti della Società italiana di scienze naturali e del museo civico di storia naturale di Milano*, **147** (1), 113–138.

———, CLAUDE, J., SUTEETHORN, V., NAKSRI, W. and BUFFETAUT, E. 2009. Turtle assemblages of the Khorat Group (Late Jurassic-Early Cretaceous) of NE Thailand and their palaeobiogeographical significance. *Geological Society, London, Special Publications*, **315**, 141–152.

VINEYARD, D. 2009. A new eucryptodiran turtle from the Lower Cretaceous Glen Rose Formation of Texas. Unpublished M.Sc. thesis, Southern Methodist University, Dallas, 123pp.

VITEK, N. S. and JOYCE, W. G. 2015. A review of the fossil record of new world turtles of the clade Pan-Trionychidae. *Bulletin of the Peabody Museum of Natural History*, **56**, 185–244.

———, DANILOV, I. G., NAKAJIMA, Y. and HIRAYAMA, R. 2018. Redescription of the skull of '*Trionyx*' *kyrgyzensis* and improved phylogenetic taxon sampling of Cretaceous and Palaeogene soft-shelled turtles (Trionychidae) of Asia, including the oldest crown trionychids. *Journal of Systematic Palaeontology*, **16**, 199–211.

VÖLKER, H. 1913. Über das Stamm-, Gliedmaßen- und Hauptskelet von *Dermochelys coriacea* L. *Zoologische Jahrbücher, Abteilung für Anatomie und Ontogenie der Tiere*, **33** (3), 431–552.

WAGNER, P. J. 1997. Patterns of morphologic diversification among the Rostroconchia. *Paleobiology*, **23**, 115–150.

WALSH, S. A., BARRETT, P. M., MILNER, A. C., MANLEY, G. and WITMER, L. M. 2009. Inner ear anatomy is a proxy for deducing auditory capability and behaviour in reptiles and birds. *Proccedings of the Royal Society B*, **276**, 1355–1360.

WANG, Z., PASCUAL-ANAYA, J., ZADISSA, A., LI, W., NIIMURA, Y., HUANG, Z., LI, C., WHITE, S., XONG, Z., FANG, D., WANG, B., MING, Y., CHEN, Y., ZHENG, Y., KURAKU, S., PIGNATELLI, M., HERRERO, J., BEAL, K., NOZAWA, M., LI, Q., WANG, J., ZHANG, H., YU, L., SHIGENOBU, S., WANG, J., Liu, J., FLIVEK, P., SEARLE, S., WANG, J., KURATANI, S., YIN, Y., AKEN, B., ZHANG, G. and IRIE, N. 2013. The draft genomes of soft-shell turtle and green sea turtle yield insights into the development and evolution of the turtle-specific body plan. *Nature Genetics*, **45** (6), 701–706.

WARNOCK, R. C. M., YANG, Z. and DONOGHUE, P. C. J. 2012. Exploring uncertainty in the calibration of the molecular clock. *Biology Letters*, **8**, 156–159.

WEEMS, R. E. 2014. Paleogene chelonians from Maryland and Virginia. *PaleoBios*, **31** (1), 1–32.

——— and BROWN, K. M. 2017. More-complete remains of *Procolpochelys charlestonensis* (Oligocene, South Carolina), an occurrence of *Euclastes* (upper Eocene, South Carolina), and their bearing on Cenozoic pancheloniid sea turtle distribution and phylogeny. *Journal of Paleontology*, **91**, 1228–1243.

——— and SANDERS. 2014. Oligochene pancheloniid sea turtle from the vicinity of Charleston, South Carolina, U.S.A. *Journal of Vertebrate Paleontology*, **34** (1), 80–99.

WEGNER, R. N. 1959. Der Schädelbau der Lederschildkröte *Dermochelys coriacea* Linné (1766). *Abhandlungen der Deutschen Akademie der Wissenschaften zu Berlin, Klasse für Chemie, Geologie und Biologie*, **4**, 1–80.

WERNEBURG, I. 2011. The cranial musculature of turtles. *Palaeontologia Electronica*, **14** (2), 1–99.

WEVER, E. G. 1978. *The reptile ear*. Princeton University Press, Princeton, 1024 pp.

WHETSTONE, K. N. 1978. A new genus of cryptodiran turtles (Testudinoidea, Chelydridae) from the Upper Cretaceous Hell Creek Formation of Montana. *The University of Kansas Sciene Bulletin*, v. 51, 539–563.

WIBBELS, T. 1999. Diagnosing the sex of sea turtles in foraging habitats. 139–143. *In* ECKERT, K. L., BJORNDAL, K. A., ABREU-GROBOIS, F. A., and DONNELLY, M. (eds.). *Research and*

Management Techniques for the conservation of sea turtles. IUCN/SSC Marine Turtle Specialist Group Publication No. 4, Consolidates Graphic Communications, Blanchard, Pennsylvania, 232 pp.

——— , OWENS, D. W. M., and ROSTAL, D. 1991. Soft plastra of adult male sea turtles: An apparent secondary sexual characteristic. *Herpetological Review*, **22** (2), 47–49.

WIELAND, G. R. 1896. *Archelon ischyros*: A new gigantic Cryptodire Testudinate from the Fort Pierre Cretaceous of South Dakota. *American Journal of Science (1880-1910)*, **2**, 399.

——— 1900. The skull, pelvis, and probable relationships of the huge turtles of the genus *Archelon*. *American Journal of Science*, **9** (52), 1–237.

——— 1902. Notes on the Cretaceous turtles, *Toxochelys* and *Archelon*, with a classification of the marine Testudinata. *The American Journal of Science*, **14**, 95–108.

———. 1906. The osteology of *Protostega*. *Memoirs of the Carnegie Museum*, **II**, 279–305.

WILKINSON, M. 1992. Ordered versus unordered characters. *Cladistics*, **8**, 375–385.

——— 1995. A comparison of two methods of character construction. *Cladistics*, **11**, 297–308.

WILLISTON, S. W. 1902. On the hindlimb of *Protostega*. *American Journal of Science*, **13** (76), 276–276.

WINKLER, J. D. and SANCHEZ-VILLAGRA, M. R. 2006. A nesting site and egg morphology of a Miocene turtle from Urumaco, Venezuela: evidence of marine adaptations in Pelomedusoides. *Palaeontology*, **49**, 641–646.

WOOD, R. C., JOHNSON-GOVE, J., GAFFNEY, E. S. and MALEY, K. F. 1996. Evolution and phylogeny of the leatherback turtles (Dermochelyidae), with descriptions of new fossil taxa. *Chelonian Conservation and Biology*, **2**, 266–286.

WYNEKEN, J. 2001. The anatomy of sea turtles. *U.S. Department of Commerce NOAA Technical Memorandum NMFS-SEFC-470*, 1–172.

YANG, Z. 1993. Maximum-likelihood estimation of phylogeny from DNA sequences when substitution rates differ over sites. *Molecular Biology and Evolution*, **10** (6), 1396–1401.

——— 1994. Estimating the pattern of nucleotide substitution. *Journal of Molecular*

Evolution, **39**, 105–111.

———1996. Among-site rate variation and its impact on phylogenetic analyses. *TREE*, **11** (9), 367–372.

——— and RANNALA, B. 1997. Bayesian phylogenetic inference using DNA sequences: a Markov chain Monte Carlo method. *Molecular Biology and Evolution*, **14** (7), 717–724.

———, NIELSEN, R., GOLDMAN, N. and KRABBE PEDERSEN, A.-M. 2000. Codon-substitution models for heterogeneous selection pressure at amino acid sites. *Genetics*, **155**, 431–449.

YODER, A. D. and YANG, Z. 2000. Estimation of primate speciation using local molecular clocks. *Molecular Biology and Evolution*, **17** (7), 1081–1090.

ZANGERL, R. 1953*a*. The vertebrate fauna of the Selma Formation of Alabama. Part III. The turtles of the family Protostegidae. *Fieldiana. Geology Memoirs*, **3** (3), 63–133.

——— 1953*b*. The vertebrate fauna of the Selma Formation of Alabama. Part IV. The turtles of the family Toxochelyidae. *Fieldiana. Geology Memoirs*, **3** (4), 1–176.

——— 1960. The vertebrate fauna of the Selma Formation of Alabama. Part V. An advance cheloniid sea turtle. *Fieldiana. Geology Memoirs*, **3** (5), 281–312.

——— 1971. Two toxochelyid sea turtle from the Landenian sands of Erquelinnes (Hainaut), of Belgium. *Institute Royal des Sciences Naturelles de Belgique Mémoires*, **169**, 3–32.

——— 1980. Patterns of phylogenetic differentiation in the toxochelyid and cheloniid sea turtles. *Integrative and Comparative Biology*, **20**, 585–596.

——— and SLOAN, R. E. 1960. A new specimen of *Desmatochelys lowi* Williston, A primitive cheloniid sea turtle from the Cretaceous of South Dakota. *Fieldiana. Geology Memoirs*, **14** (2), 7–39.

ZARDOYA, R. and MEYER, A. 1998. Complete mitochondrial genome suggests diapsid affinities of turtles. *Proceedings of the National Academy of Sciences*, **95**, 14226–14231.

ZHANG, C. 2016. Molecular clock dating using MrBayes. *arXiv*, 1603.05707v2

——— and WANG, M. 2018. Bayesian tip dating reveals heterogeneous morphological clocks in Mesozoic birds. *bioRxiv*, doi: 10.1101/350496

———, STADLER, T., KLOPFSTEIN, S., HEATH, T. A. and RONQUIST, F. 2016. Total-evidence dating under the fossilized birth-death process. *Systematic Biology*, **65** (2), 228–249.

ZHOU, C.-F. and RABI, M. 2015. A sinemydid turtle from the Jehol Biota provides insights into the basal divergence of crown turtles. *Scientific Reports*, **5**, 16299.

———, and RABI, M.and JOYCE, W. G. 2014. A new specimen of *Manchurochelys manchoukuoensis* from the Early Cretaceous Jehol Biota of Chifeng, Inner Mongolia, China and the phylogeny of Cretaceous basal eucryptodiran turtles. *BMC Evolutionary Biology*, **14**, 77.

ZUCKERKANDL, E. and PAULING, L. Molecules as documents of evolutionary history. *Journal of Theoretical Biology*, **8**, 357–366.

APPENDICES

TO THE D.PHIL THESIS

THE EARLY EVOLUTION OF SEA TURTLES

BY

SERJOSCHA W. EVERS

APPENDIX S1

S1.1. General notes on my character list

My character list aims to capture all variation documented so far for non-pleurodiran turtles. This includes 43 characters that, with respect to my taxon sampling, are parsimony uninformative because they are only scored for one taxon differently from all other taxa or invariant. I keep these characters in the list, because other people might chose to test the phylogenetic positions of additional taxa using my matrix in future.

Three previous studies are the main sources for my characters: Cadena (2015), Zhou & Rabi (2015), and Anquetin *et al.* (2015). All three are modified from Joyce (2007) by the addition and modification of different characters. The character list of Cadena (2015) is essentially identical to that of Cadena & Parham (2015), with only one character addition (although some additional scores were also modified). I used the character list of Cadena & Parham (2015) as a baseline, as this list was published in full with reference to the history of individual characters and included discussions of modifications from previous work. In contrast, Zhou & Rabi (2015) listed their characters in a nexus file, without detailed reference to previous studies, and Anquetin *et al.* (2015) followed the idiosyncratic numbering system of TNT, starting at '0'. Therefore, all sections labelled as "Cadena & Parham (2015): character X" refer to descriptions used by Cadena & Parham (2015). "Modified from study X" refers to my modified versions of the characters presented by others; "Adopted from study X" indicates characters from other studies added to the matrix without changing their definition; and "new character" describes characters based on my own observations.

All character modifications and additions are discussed, and new and modified cranial and mandibular characters are illustrated. Additionally, some characters that were not modified from Cadena & Parham (2015) are discussed in respective sections. These are characters for which I made many modifications to the previous scorings, possibly indicating some level of ambiguity in the characters.

Each character is followed by a section called "character optimization", which lists the characters state changes of that character for each node in my phylogeny. "Unambiguous" synapomorphies are those found under both ACCTRAN and DELTRAN optimization. Because some nodes of the phylogeny represent unnamed clades, I use a code to denote the content of these clades. Hereby, the notation "Taxon+++" indicates the clade comprising the named taxon and all more crownwardly positioned taxa. The notation "(Taxon A ++ Taxon B)" indicates the most inclusive clade including Taxon A and Taxon B.

As explained in the main text of the thesis, I refer all Bristish material of *Rhinochelys* to the type species, *Rhinochelys pulchriceps*. Whenever observations mentioned in the remarks section of the character list were based on specific specimens of *Rhinochelys*, the specimen numbers are given. Please refer to Collins (1970) for previous taxonomic assignments to various species of *Rhinochelys*.

S1.2. Character list with documentation of modified characters

CRANIUM

Character 1 (Cadena & Parham (2015): character 1). Nasals: 0 = present; 1 = absent.

Character optimisation: Testudines (0->1), (*Ocepechelon* ++ *Santanachelys*) (1->0), *Toxochelys latiremis* (1->0); DELTRAN: *Phrynops geoffranus* (1->0), Chelodininae (1->0); ACCTRAN: crown-group Chelidae (1->0), *Chelus fimbriatus* (0->1).

Character 2 (Cadena & Parham (2015): character 2). Nasal, medial contact of nasals: 0 = nasals contact one another medially along their entire length; 1 = medial contact of nasals partially or fully hindered by long an- terior frontal process.

Character optimisation: Unambiguous: *Sinemys gamera* (0->1), (*Annemys* sp. ++ *Xinjiangchelys*) (0->1); DELTRAN: crown-group Chelidae (0->1), *Sandownia harrisi* (0->1), *Brachyopsemys tingitana* (0->1), Pleurosternidae (0->1), *Arundelemys dardeni* (0->1);

ACCTRAN: Pleurodira (0->1), Sandownidae (0->1), *Leyvachelys cipadi* (1->0), Paracryptodira (0->1), *Eubaena cephalica* (1->0).

Character 3 (Cadena & Parham (2015): character 3). Nasal, size of nasals: 0 = dorsal exposure of nasals large; 1 = dorsal exposure of nasals greatly reduced relative to that of the frontals.

Character optimisation: Unambiguous: Xinjiangchelyidae+++ (0->1), *Ocepechelon bouyai* (1->0), *Leyvachelys cipadi* (1->0), Pleurosternidae (0->1).

Character 4 (Cadena & Parham (2015): character 4). Prefrontals, medial contact of prefrontals on the dorsal skull surface: 0 = absent; 1 = present, absence of contact between the nasal or apertura narium externa and the frontal.

Character optimisation: Unambiguous: Protostegidae (1->0), *Bouliachelys suteri* (0->1), crown-group Chelidae (1->0), (*Portlandemys* ++ *Plesiochelys*) (1->0), *Plesiochelys etalloni* (0->1), *Chubutemys copelloi* (0->1); DELTRAN: Angolachelonia+++ (0->1), *Dracochelys bicuspis* (0->1), (*Judithemys* ++ *Kirgizemys*) (0->1), *Annemys levensis* (0->1); ACCTRAN: Xinjiangchelyidae+++ (0->1), *Ordosemys* sp. IVPP V12092 (1->0), (*Sinemys lens* + *Sinemys gamera*) (1->0), (*Annemys latiens* ++ *Xinjiangchelys*) (1->0).

Character 5 (Cadena & Parham (2015): character 5). Prefrontal, prefrontal-vomer contact: 0 = present; 1 = absent.

Character optimisation: Unambiguous: (*Eileanchelys* + *Kayentachelys*)+++ (1->0), Pleurodira (0->1).

Character 6 (Cadena & Parham (2015): character 6). Prefrontal, prefrontal-palatine contact: 0 = present; 1 = absent.

Character optimisation: Unambiguous: *Puppigerus*+++ (0->1), *Chelus fimbriatus* (1->0); DELTRAN: *Dermochelys coriacea* (0->1), Trionychia (0->1), Pleurodira (0->1); ACCTRAN: Testudines (0->1), Durocryptodira (1->0), Dermochelyidae (0->1).

Character 7 (Cadena & Parham (2015): character 7). Prefrontal, dorsal prefrontal exposure: 0 = present, large; 1 = reduced; 2 = absent or near absent.

Character optimisation: Unambiguous: total-group Chelidae (0->1), (*Sandownia* + *Leyvachelys*) (0->1), (*Sinemys lens* + *Sinemys gamera*) (0->1), (*Annemys latiens* ++ *Xinjiangchelys*) (0->1), Paracryptodira (0->1), *Eubaena cephalica* (1->2), (*Eileanchelys* + *Kayentachelys*) (0->1); DELTRAN: (*Desmatochelys lowii* + *Desmatochelys padillai*) (0->1), *Ocepechelon bouyai* (0->1), *Jurassichelon oleronensis* (0->1), *Portlandemys mcdowelli* (0->1); ACCTRAN: (*Ocepechelon* ++ *Santanachelys*) (0->1), (*Bouliachelys* ++ *Santanachelys*) (1->0), (*Portlandemys* ++ *Plesiochelys*) (0->1), (*Plesiochelys etalloni* + *Plesiochelys planiceps*) (1->0).

Character 8 (Cadena & Parham (2015): character 8). Prefrontal, cranial scutes on the prefrontal: 0 = one pair; 1= two pairs or more.

Character optimisation: Unambiguous: (*Eretmochelys* ++ *Lepidochelys*) (0->1).

Character 9 (adopted from Zhou & Rabi (2015)). Prefrontal, sculpturing: 0 = heavily sculptured; 1 = sculpturing absent.

Remarks: This character is taken from Zhou & Rabi (2015): Character 8 (Prefrontal E), and was also used in Sterli and De la Fuente (2013: Prefrontal E).

Besides *Proganochelys quenstedti*, I also scored *Bouliachelys suteri* and *Chelydra serpentina* as having a sculptured prefrontal.

Character optimisation: Unambiguous: (*Eileanchelys* + *Kayentachelys*)+++ (0->1), *Bouliachelys suteri* (1->0), *Chelydra serpentina* (1->0).

Character 10 (Cadena & Parham (2015): character 9). Lacrimal: 0 = present; 1 = absent. JY1 & Sterli & de la Fuente (2013: ch 9, Lacrimal A).

Character optimisation: Unambiguous: (*Eileanchelys* + *Kayentachelys*)+++ (0->1).

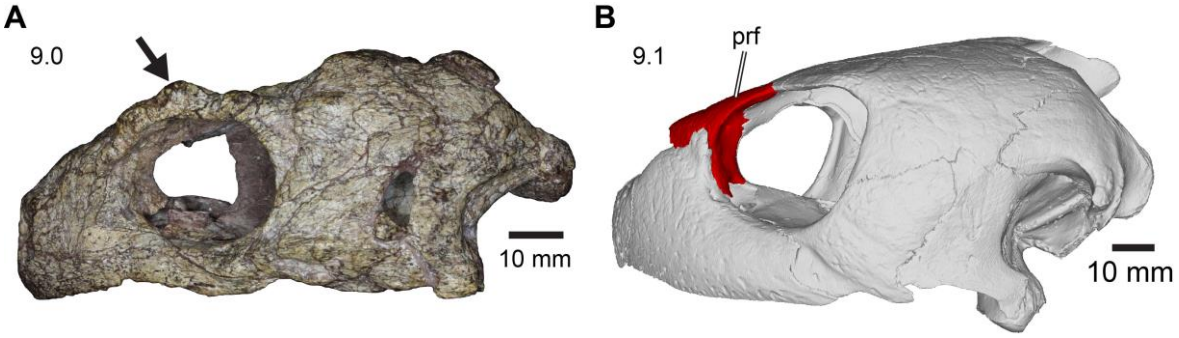


FIG. S1.1. Illustration of character 9. **A**, state 0 (*Proganochelys quenstedti*, SMNS 16980, lateral view of right side of the cranium, reflected for comparison); **B**, state 1 (*Lepidochelys olivacea*, SMNS 11070, left lateral view of cranium). Arrow points to sculptured prefrontal. Abbreviations: *prf*, prefrontal.

Character 11 (Cadena & Parham (2015): character 10). Frontal, frontal contribution to orbit: 0 = absent, contact between prefrontal and postorbital; 1 = present.

Character optimisation: Unambiguous: *Bouliachelys suteri* (1->0), crown-group Chelydridae (1->0), Kinosternidae (1->0), *Eubaena cephalica* (1->0); DELTRAN: Paracryptodira+++ (0->1), (*Protostega* + *Archelon*) (1->0), Dermochelyidae (1->0), *Lepidochelys olivacea* (1->0), *Caretta caretta* (1->0), *Emys orbicularis* (1->0), *Platysternon megacephalum* (1->0), *Geoclemys hamiltonii* (1->0), *Kallokibotion bajazidi* (0->1), (*Eileanchelys* + *Kayentachelys*) (0->1); ACCTRAN: *Australochelys*+++ (0->1), Dermochelyoidea (1->0), (*Ocepechelon* ++ *Santanachelys*) (0->1), (*Caretta* ++ *Lepidochelys*) (1->0), *Lepidochelys kempii* (0->1), Testudinoidea (1->0), *Chrysemys picta* (0->1), Testudinidae (0->1), *Meiolania planiceps* (1->0), *Chubutemys copelloi* (1->0).

Character 12 (Cadena & Parham (2015): character 11). Frontals, both frontals medially fused: 0 = absent; 1 = present.

Character optimisation: Unambiguous: *Chelodina* (0->1).

Character 13 (Cadena & Parham (2015): character 12). Frontal, direction of the orbits in dorsal view of the skull: 0 = laterally facing, with a very narrow to almost complete absent dorsal exposure of the maxilla and jugal; 1 = dorsolateral facing, with portions of the maxilla and jugal dorsally exposed.

Character optimisation: Unambiguous: Xinjiangchelyidae+++ (0->1), *Ocepechelon bouyai* (0->1), *Toxochelys latiremis* (0->1), *Chelonoidis* sp. (0->1), *Kirgizemys dmitrievi* (1->0); DELTRAN: Durocryptodira (1->0), *Carettochelys insculpta* (1->0); ACCTRAN: Cryptodira (1->0), Trionychidae (0->1).

Character 14 (new character). Frontals, development of crista cranii: 0 = crista cranii on ventral surface of frontals very shallow, sulcus olfactorius developed is a low trough; 1 = crista cranii developed as moderately deep parasagittal ridges on the ventral surface of each frontal, forming a ventrally open, median trough (the sulcus olfactorius) that extends from the anterior margin of the cavum cranii posteriorly to the fissura ethmoidalis anteriorly; 2 = crista cranii very deep anteriorly, forming extended processes that meet along the midline of the cranium and are sutured to one another, forming an ossified olfactory canal.

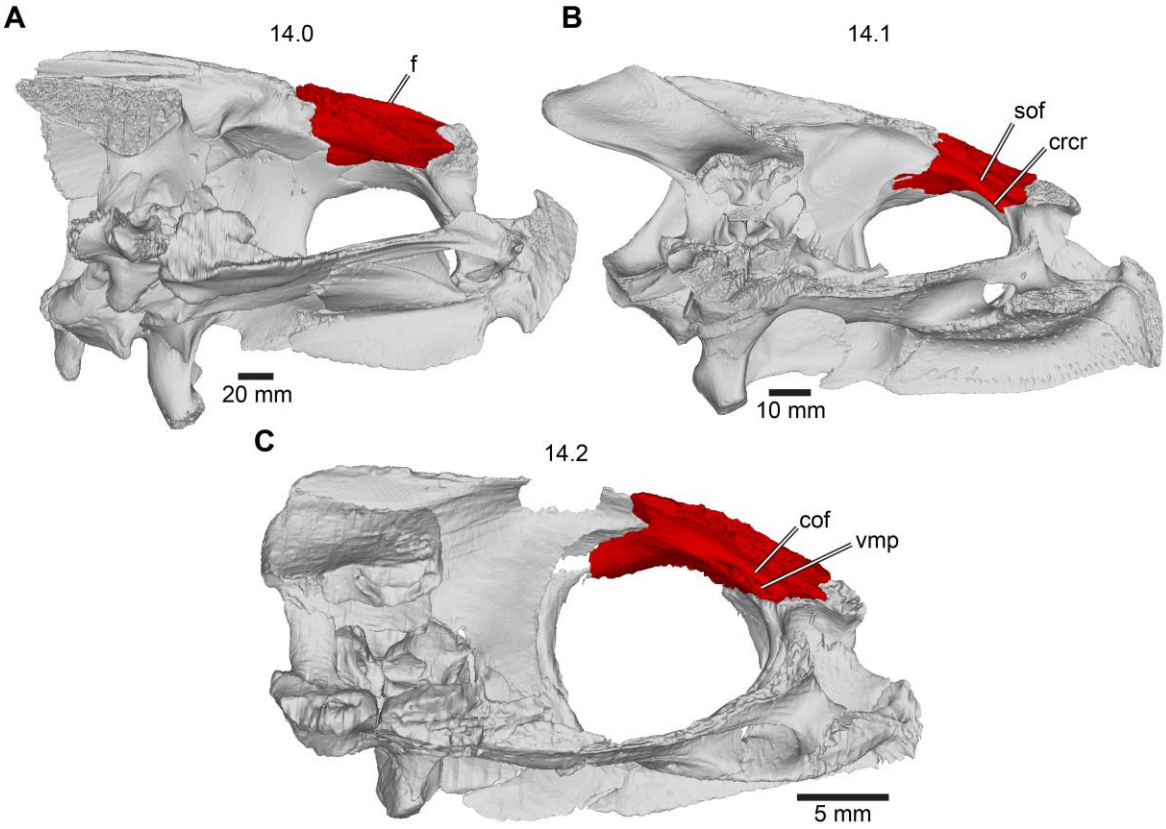


FIG. S1.2. Illustration of character 14. **A**, state 0 (*Dermochelys coriacea*, UMCZ R 3031, medioventral view of left side of the cranium); **B**, state 1 (*Lepidochelys olivacea*, SMNS 11070); **C**, state 2 (*Rhinochelys cantabrigiensis*, CAMSM B55783). Abbreviations: *cof*, canalis olfactorius; *crcr*, crista cranii; *f*, frontal; *sof*, sulcus olfactorius; *vmp*, ventromedial process of prefrontal.

Remarks: The crista cranii are parasagittal ridges to either side of the skull midline on the ventral surface of the frontals. They frame the median sulcus olfactorius. These ridges are usually relatively low, and do not contact one another medially. However, in *Rhinochelys* (e.g. CAMSM B55783) and *Notochelone* (NHMUK R9590), the ridges are ventromedially expanded at their anterior end, and form a short canal.

Character optimisation: Unambiguous: (*Rhinochelys* ++ *Santanachelys*) (1->2); DELTRAN: *Dermochelys coriacea* (1->0); ACCTRAN: Dermochelyidae (1->0).

Character 15 (Cadena & Parham (2015): character 13). Parietal, parietal-squamosal contact: 0 = present, upper temporal emargination absent or poorly developed; 1 = absent, upper temporal emargination well developed.

Character optimisation: Unambiguous: Testudines (0->1), crown-group Chelonioidea (1->0), (*Desmatochelys* ++ *Santanachelys*) (0->1), (*Sinemys lens* + *Sinemys gamera*) (0->1), *Eubaena cephalica* (0->1); DELTRAN: Chelinae (1->0), *Elseya dentata* (1->0); ACCTRAN: crown-group Chelidae (1->0), *Chelodina* (0->1).

Character 16 (Cadena & Parham (2015): character 15). Parietal, posterodorsal margin of the temporal fossa roofed by an overhanging process of the skull roof: 0 = absent; 1 = present.

Character optimisation: Unambiguous: Paracryptodira+++ (1->0), Dermochelyidae (0->1), *Argillochelys*+++ (0->1), *Puppigerus camperi* (1->0), *Platysternon megacephalum* (0->1), *Elseya dentata* (0->1); DELTRAN: *Leyvachelys cipadi* (0->1), *Brachyopsemys tingitana* (0->1); ACCTRAN: Sandownidae (0->1), *Sandownia harrisi* (1->0).

Character 17 (Cadena & Parham (2015): character 16). Parietal, contribution to the processus trochlearis oticum: 0 = absent; 1 = present.

Character optimisation: Unambiguous: Kinosternidae (0->1), Trionychia (0->1), *Solnhofia parsoni* (0->1); DELTRAN: *Geoclemys hamiltonii* (0->1), (*Testudo* + *Chelonoidis*) (0->1),

Pleurosternon bullockii (0->1); ACCTRAN: Testuguria (0->1), *Gopherus polyphemus* (1->0), Pleurosternidae (0->1).

Character 18 (Cadena & Parham (2015): character 17). Parietals, foramen stapedio-temporalis: 0 = absent or weak, foramen stapedio- temporale concealed in dorsal view; 1 = moderate foramen stapedio-temporale, partial exposition of the processes trochlearis in dorsal view; 2 = strong, entire exposition of the processus trochlearis in dorsal view.

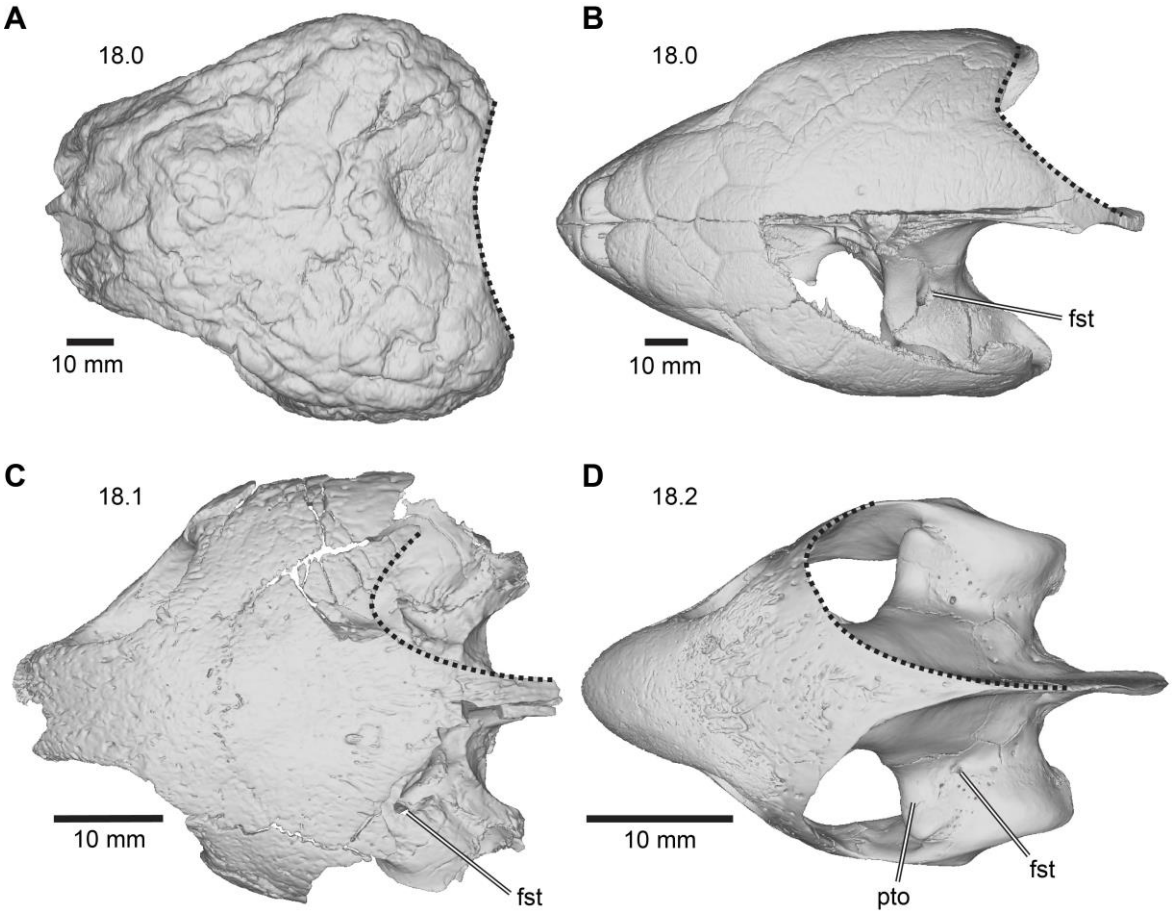


FIG. S1.3. Illustration of character 18. **A**, state 0 (*Australochelys africanus*, BP/1/4903, dorsal view of the cranium); **B**, state 0 (*Lepidochelys olivacea*, SMNS 11070); **C**, state 1 (*Ordosemys* sp., IVPP V12092); **D**, state 2 (*Sternotherus minor*, FMNH 211696). Note that the parietal has been removed in B to expose the foramen stapedio-temnporale, which is used as a landmark in the character state definitions. Dotted lines indicate the margin of the upper temporal emargination. Abbreviations: *fst*, foramen stapedio-temporal; *pto*, processus trochlearis oticum.

Remarks: Cadena & Parham (2015: ch 17) only scored state 1 of this character as present in *Australochelys* and *Palaeochersis*. However, this state has a more widespread distribution, as taxa having extremely weakly developed upper temporal emarginations, such as *Leyvachelys*

(Cadena 2015) or *Brachyopsemys* (AMNH 30612; AMNH 30001: Tong & Meylan 2013; but not *Sandownia*), as well as most chelonioids (e.g. *Dermochelys coriacea*; *Argillochelys cuneiceps*; all extant cheloniids) have the posterodorsal margin of the temporal fossa completely covered by a posterior extension of the skull roof. I modified the scorings of all taxa accordingly.

Character optimisation: Unambiguous: Paracryptodira+++ (0->2), *Desmatochelys padillai* (0->1), *Platysternon megacephalum* (2->0), *Elseya dentata* (2->0), *Podocnemis* (2->0), Angolachelonia (2->0), (*Ordosemys* ++ *Kirgizemys*) (2->1), Pleurosternidae (2->0); DELTRAN: crown-group Chelonioidea (2->0), *Toxochelys latiremis* (2->1), *Jurassichelon oleronensis* (0->1); ACCTRAN: total-group Chelonioidea (2->0), *Toxochelys latiremis* (0->1), (*Jurassichelon* ++ *Plesiochelys*) (0->1).

Character 19 (Cadena & Parham (2015): character 18). Parietal, pineal foramen located medially between parietals: 0 = absent; 1 = present.

Character optimisation: Unambiguous: (*Destmatochelys padillai* + *Desmatochelys lowii*) (0->1).

Character 20 (modified from Zhou & Rabi (2015)). Parietal, processus inferior parietalis: 0 = weak or absent, parietal does not contact the pterygoid, epipterygoid, and/or palatine; 1 = present and well developed, the parietal contacts the pterygoid, epipterygoid, and/or palatine.

Remarks: This character is slightly modified from Zhou & Rabi (2015): Character 13 (Parietal B), and has previously been used by others (e.g. Joyce 2007: character 12, Parietal B; Sterli and De la Fuente 2013: Parietal B; Anquetin *et al.* 2015: character 11, Parietal B). *Kayentachelys* is scored as 0, in spite of the parietal possibly contacting the epipterygoid (Gaffney & Jenkins 2010): The epipterygoid of *Kayentachelys* has a dorsally projected process that reaches the parietal, but a ventral process of the parietal itself is absent (see Gaffney & Jenkins 2010, fig. 12B,C).

Character optimisation: DELTRAN: *Chubutemys*+++ (0->1), *Eileanchelys waldmanni* (0->1); ACCTRAN: (*Eileanchelys* + *Kayentachelys*)+++ (0->1), *Kayentachelys aprix* (1->0).

Character 21 (Cadena & Parham (2015): character 14). Parietal, closure of foramen nervi trigemini and the length of the anterior extension of the lateral braincase wall: 0 = foramen nervi trigemini anteriorly open, anterior extension of lateral braincase wall absent; 1 = foramen nervi trigemini anteriorly closed, processus inferior parietalis only produces a narrow strut anterior to the foramen nervi trigemini, usually absence of contact with palatine; 2 = foramen nerivi trigemini anteriorly closed, processus inferior parietalis produces an ex- tended process anterior to the foramen nervi trigemini, contact with palatine commonly present.

Character optimisation: Unambiguous: *Chubutemys*+++ (0->1), Kinosternoidea (1->2), *Gopherus polyphemus* (1->2), Trionychia (1->2), Pelomedusoides (1->2), (*Sandownia* + *Leyvachelys*) (1->2); DELTRAN: *Dermochelys coriacea* (1->0); ACCTRAN: Dermochelyidae (1->0).

Character 22 (modified from Zhou & Rabi (2015)). Parietal, posterior ramus of processus inferior parietalis forming the posterior margin of the trigeminal foramen: 0 = absent; 1 = present.

Remarks: This character is adopted from previous matrices (Anquetin et al 2015: character 13, Parietal D; Zhou & Rabi (2015): character 16, Parietal E), and was first used by Sterli & De la Fuente (2011: Parietal E). Anquetin *et al.* (2015) discussed this character, and noted the presence of a posterior ramus in thalassochelydians and *Ordosemys*. However, Anquetin *et al.* (2015) employ a slightly different character definition, specifying that the posterior ramus excludes the prootic from the margin of the trigeminal foramen. Here, I use the character without this qualifier (as in Zhou & Rabi (2015)), but code this observation of Anquetin *et al.* (2015) in a separate character (see ch 23). I also notice that this character is more

widespread across turtles: besides in thalassochelydians and *Ordosemys*, I also observed the posterior parietal process in chelydrids, several testudinoids, all xinjiangchelyids, sinemydids, and macrobaenids for which the character could be scored, and in most pleurodires.

Character optimisation: Unambiguous: *Chrysemys picta* (1->0), *Gopherus polyphemus* (1->0), *Chelus fimbriatus* (1->0), *Pelomedusa subrufa* (1->0); DELTRAN: Xinjiangchelyidae+++ (0->1), crown-group Chelonioidea (1->0), *Desmatochelys lowii* (0->1), Kinosternoidea (1->0), Trionychia (1->0), *Pleurosternon bullockii* (0->1); ACCTRAN: Paracryptodira+++ (0->1), Cryptodira (1->0), (*Desmatochelys lowii* + *Desmatochelys padillai*) (0->1), total-group Chelydridae (0->1), Testudinoidea (0->1), *Arundelemys dardeni* (1->0).

Character 23 (modified from Anquetin *et al.* 2015). Posterior ramus of processus inferior parietalis of the parietal: 0 = short; 1 = long, excludes the prootic from the trigeminal foramen. This character is scored inapplicable for taxa that lack the process altogether.

Remarks: See remarks for character 22 for a general discussion of the posterior ramus of the processus inferior parietalis of the parietal.

When present, the posterior ramus of the processus inferior parietalis can be relatively short, so that the prootic still forms the posterior margin of the trigeminal foramen (state 0), as in chelydrids, *Platysternon*, and xinjiangchelyids. Alternatively, the posterior ramus of the processus inferior parietalis is long and often relatively robust, and directly contacts the quadrate, epipterygoid or pterygoid in the posterior margin of the trigeminal foramen, so that the prootic is exluded from contributing to the foramen (state 1). This is seen in thalassochelydians (as discussed by Anquetin *et al.* 2015), but also in several testudinoids and pleurodires.

I scored *Pleurosternon bullockii* (UMZC T1041) and *Ordosemys* sp. (IVPP V12092) as "?", because the region around the trigeminal foramen is partially broken in Pleurosternon, and my CT data of *Ordosemys* do not allow to see if the prootic has a small contribution to the trigeminal foramen or not.

Character optimisation: Unambiguous: *Platysternon megacephalum* (1->0), total-group Chelidae (1->0), *Elseya dentata* (0->1); DELTRAN: Sinemydidae/Macrobaenidae+++ (0->1), crown-group Chelydridae (1->0); ACCTRAN: Sinemydidae/Macrobaenidae+++ (0->1), Americhelydia (1->0).

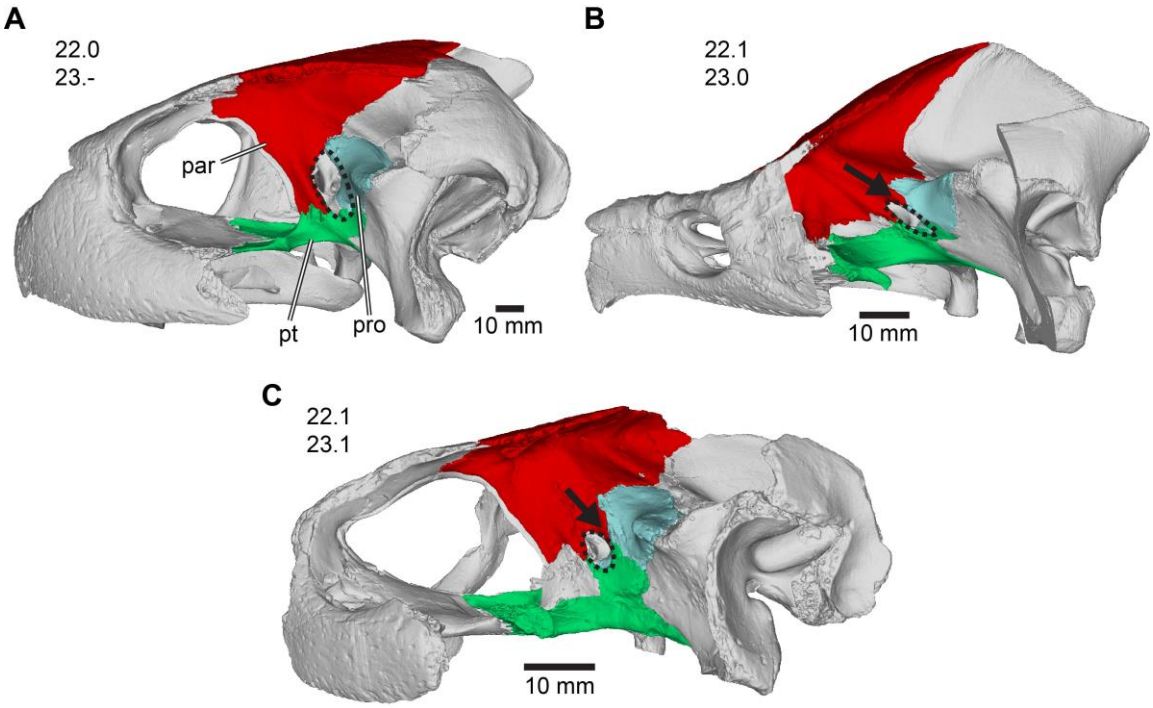


FIG. S1.4. Illustration of characters 22 and 23. **A**, *Lepidochelys olivacea* (SMNS 11070, left lateral view of cranium); **B**, *Macrochelys temminckii* (FMNH 22111); **C**, *Plesiochelys planiceps* (OUMNH J1582). Elements of the temporal region have been removed in A-C. Arrows in B and C indicate ventral process of parietal posterior to the trigeminal foramen. Dotted lines circumscribe the trigeminal foramen. Note pterygoid-parietal contact posterior to the trigeminal foramen in C. Abbreviations: *par*, parietal; *pt*, pterygoid; *pro*, prootic.

Character 24 (new character). Parietal, ridge on lateral surface of processus inferior parietalis: 0 = absent; 1 = present, a ridge between the ventral surface of the parietal and the lateral surface of the descending process marks the border between the temporal and orbital fossae.

Remarks: I noticed a low ridge on the ventral surface of the parietal in various stem-turtles (including *Kayentachelys aprix*: TMM 4370-2), plus trionychids and some kinosternids. The ridge extends medially to the descending process of the parietal and approximately marks the border of the temporal fossa with the orbital fossa.

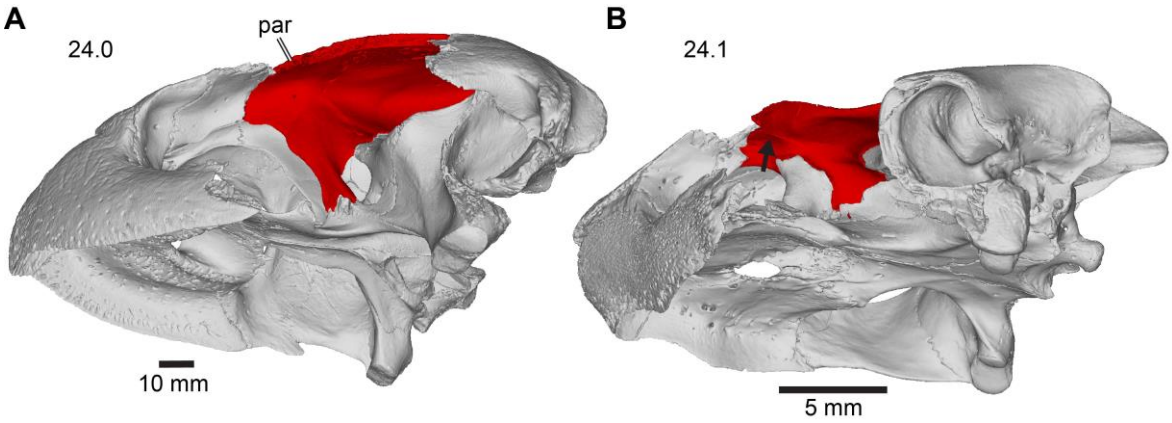


FIG. S1.5. Illustration of character 24. **A**, state 0 (*Lepidochelys olivacea*, SMNS 11070, posteroventrolateral view of left side of cranium); **B**, state 1 (*Sternotherus minor*, FMNH 211696). Note that the postorbital, jugal, and quadratojugal have been removed in A and B. Arrow in B indicates ridge on parietal. Abbreviations: *par*, parietal.

Character optimisation: Unambiguous: *Chelydra serpentina* (0->1), Kinosterninae (0->1), Trionychia (0->1), *Phrynops geoffranus* (0->1), *Elseya dentata* (0->1), *Podocnemis* (0->1); DELTRAN: *Sinemys gamera* (0->1), Paracryptodira (0->1), *Kayentachelys aprix* (0->1), *Australochelys africanus* (0->1); ACCTRAN: *Australochelys*+++ (0->1), *Chubutemys*+++ (1->0), (*Sinemys lens* + *Sinemys gamera*) (0->1), Paracryptodira (0->1).

Character 25 (modified from Cadena & Parham (2015)). Jugal, jugal-squamosal contact: 0 = present; 1 = absent.

Previous definition (Cadena & Parham (2015), ch. 19): Jugals, jugal-squamosal contact: 0 = present; 1 = absent, contact between postorbital and quadratojugal present. Joyce (2007: ch 14) & Sterli & De la Fuente (2013: ch 20) (Jugal A); Hiryama (1994: ch 8).

Remarks: In the character definition used by Cadena & Parham (2015), the absence of a jugal-squamosal contact is linked to the presence of a contact between the postorbital and quadratojugal. However, these contacts vary independently of one another. In trionychids (e.g. *Apalone spinifera emoryi*: FMNH 22178), the postorbital is reduced to a small element in the posterodorsal margin of the orbit. Because of this, the thin temporal bar is formed by the jugal, which contacts a relatively small quadratojugal posteriorly. Therefore, the

quadratojugal and postorbital do not contact each other, but neither do the squamosal and jugal (see Fig. S1.12*b*).

I changed the definition of state 1 to a simple "absent". A new character (character 42 of this study) is defined for the presence vs. absence of a postorbital-quadratojugal contact.

Character optimisation: Unambiguous: *Dermochelys coriacea* (1->0), *Allopleuron hofmanni* (1->0), *Meiolania planiceps* (1->0); DELTRAN: (*Eileanchelys* + *Kayentachelys*)+++ (0->1); ACCTRAN: *Australochelys*+++ (0->1).

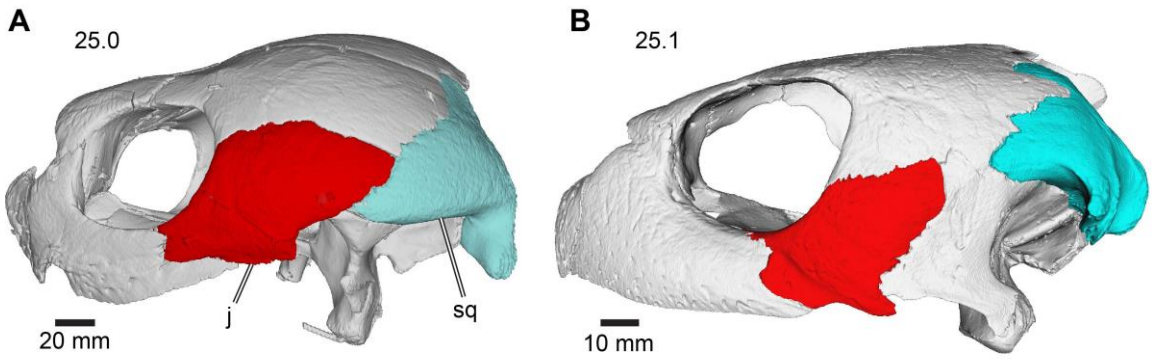


FIG. S1.6. Illustration of character 25. **A**, state 0 (*Dermochelys coriacea*, UMCZ R 3031, left lateral view of cranium); **B**, state 1 (*Lepidochelys olivacea*, SMNS 11070). Abbreviations: *j*, jugal; *sq*, squamosal.

Character 26 (Cadena & Parham (2015): character 20). Jugal, jugal participation in the margin of the upper temporal emargination: 0 = absent; 1 = present, upper temporal emargination extensive.

Character optimisation: Unambiguous: Kinosternidae (0->1), *Geoclemys hamiltonii* (0->1), Trionychidae (0->1).

Character 27 (previously character 22.) (modified from Cadena & Parham (2015)). Jugal, medial process of jugal ventral to orbit: 0 = weakly developed or absent, jugal contacts only the maxilla; 1 = present and well developed, jugal contacts the maxilla as well as the palatine and/or pterygoid.

Previous definition (Cadena & Parham (2015): character 22): Jugals, medial process of jugal beneath orbit, seen in ventral view to slightly ventroposterior view: 0 = weakly developed or absent, jugal only contacts the maxilla; 1 = weak to moderately developed, presence of a contact between the jugal and pteygoid due to the lateral extension of this last; 2 = strongly developed, jugal contacts the pterygoid, the palatine, and the maxilla. Combined and modified from Hirayama (1998), Kear & Lee (2006) & Bardet *et al.* (2013: ch 10 and ch 11).

Remarks: I divided character 22 of Cadena & Parham (2015) into three different characters (characters 27, 28, 29 of this study). The original character of Cadena & Parham (2015) describes the presence vs. absence of a medial process of the jugal ventral to the orbit, and the contacts of this expansion together in a single multistate character. This means that the set of taxa possessing a medial process of the jugal were scored as possessing various distinct character states. I argue that the shared presence of a medial process of the jugal is an observation of similarity, irrespective of the exact configuration of its contacts, which can vary independently (see Fig. S1.7 for examples). In addition to its clarity with respect to homology and similarity, the new character definition is also able to accommodate taxa in which the jugal contacts only the maxilla and palatine (i.e. excluding the pterygoid), as seen in some cheloniids (*Lepidochelys olivacea:* SMNS11070, *Caretta:* NHMUK1938.1.9.1, *Eretmochelys:* FMNH22242). I also do not specify in which view the possible contacts of the jugal can be seen, because this is somewhat dependent on the architecture of the palatal region (see figure Fig. S1.7).

The medial process of the jugal is found in most turtles, with the exception of protostegids, dermochelyids, thalassochelydians, and testudinids.

Character optimisation: Unambiguous: Dermochelyoidea (1->0), Testudinidae (1->0), (*Portlandemys* ++ *Plesiochelys*) (1->0), *Leyvachelys cipadi* (1->0), *Chubutemys copelloi* (1->0).

Character 28 (new character). Jugal, contact with the palatine: 0 = absent; 1 = present. This character is scored as inapplicable when the jugal lacks a medial process (ch 27.0).

Remarks: In most turtles, the jugal is medially expanded ventrally to the orbit (see character 27). This expansion leads to a contact between the jugal and elements of the palate, sometimes including the palatine. See remarks for character 27 for further discussion.

Character optimisation: Unambiguous: Testudines (0->1), *Toxochelys latiremis* (1->0), *Chelydra serpentina* (1->0), *Emys orbicularis* (1->0), (*Eileanchelys* + *Kayentachelys*) (0->1); DELTRAN: (*Eubaena* ++ *Pleurosternon*) (0->1); ACCTRAN: Paracryptodira (0->1).

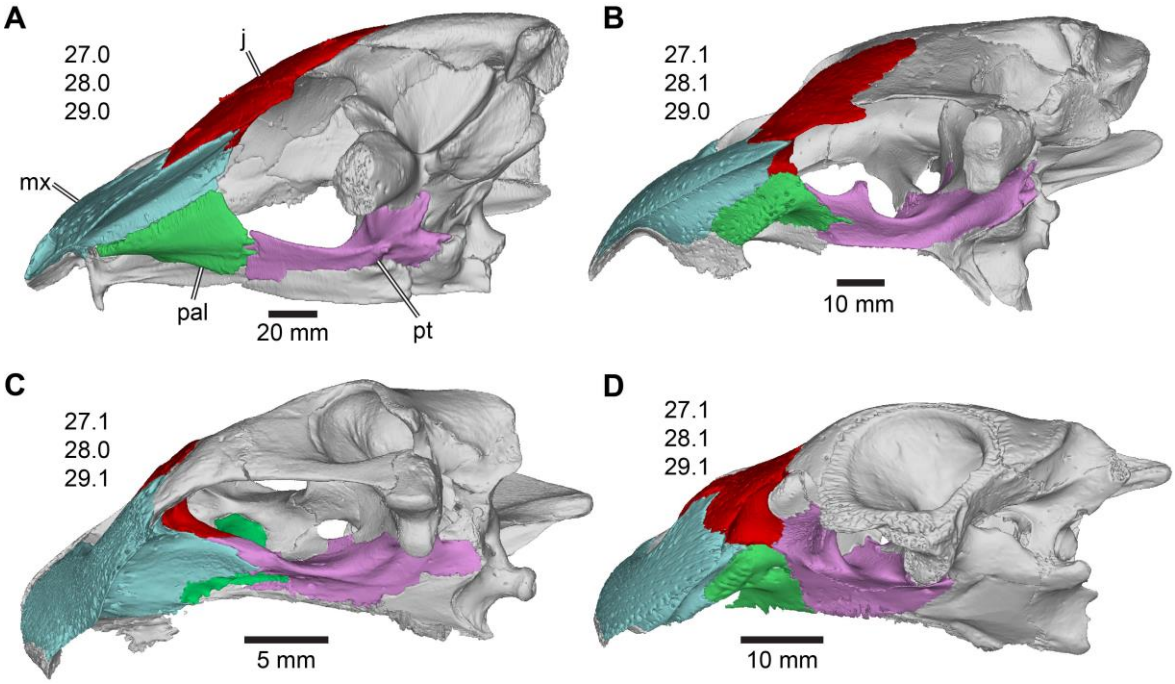


FIG. S1.7. Illustration of characters 27, 28, and 29. **A**, absence of medial process of jugal and resulting contacts (*Dermochelys coriacea*, UMCZ R 3031, ventrolateral view of left side of cranium); **B**, presence of medial process of jugal, and contact with palatine present (*Lepidochelys olivacea*, SMNS 11070); **C**, presence of medial process of jugal, and contact with pterygoid present (*Sternotherus minor*, FMNH 211696); **D**, presence of medial process of jugal, and contact with palatine and pterygoid present (*Podocnemis unifilis*, FMNH 45657). Abbreviations: *j*, jugal; *mx*, maxilla; *pal*, palatine; *pt*, pterygoid.

Character 29 (new character). Jugal, contact with the pterygoid: 0 = absent; 1 = present.

This character is scored as inapplicable when the jugal lacks a medial process (ch 27.0).

Remarks: In most turtles, the jugal is medially expanded ventrally to the orbit (see character 27). This expansion leads to a contact between the jugal and elements of the palate, sometimes including the pterygoid. See remarks for character 27 for further discussion.

Character optimisation: Unambiguous: (*Eretmochelys* ++ *Lepidochelys*) (1->0), *Lepidochelys kempii* (0->1), *Emarginachelys cretacea* (1->0), *Lissemys punctata* (1->0), *Chubutemys copelloi* (1->0).

Character 30 (new character). Jugal, jugal-parietal contact: 0 = absent; 1 = present.

Remarks: Some trionychids (e.g. *Apalone spinifera emoryi*: FMNH 22178; *Pelodiscus sinensis*: IW576-2; *Lissemys punctata*: SMF74141) have a jugal-parietal contact.

Character optimisation: Unambiguous: Trionychidae (0->1), *Podocnemis* (0->1).

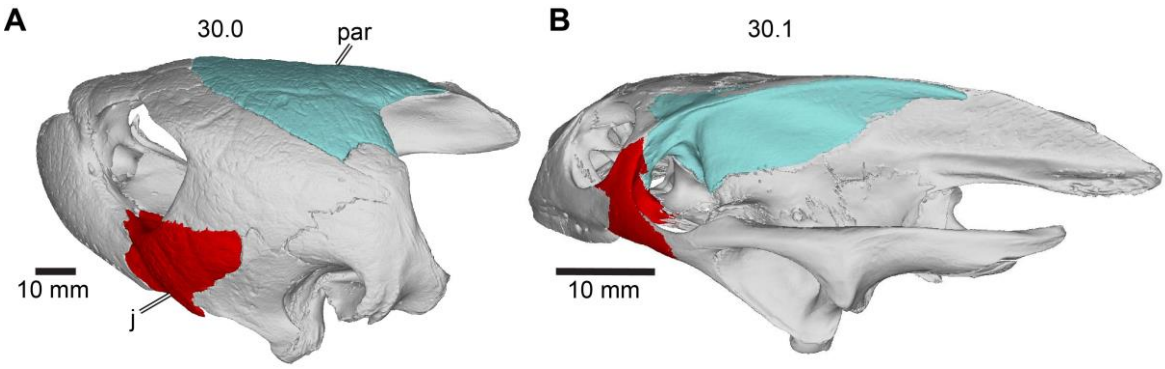


FIG. S1.8. Illustration of character 30. **A**, state 0 (*Lepidochelys olivacea*, SMNS 11070, posterodorsolateral view of left side of cranium); **B**, state 1 (*Apalone spinifera emoryi*, FMNH 22178). Abbreviations: *j*, jugal; *par*, parietal.

Character 31 (modified form Cadena & Parham (2015)). Quadratojugal: 0 = present; 1 = absent.

Previous definition (Cadena & Parham (2015): character 23): Quadratojugals, deep lower temporal emargination extending above the upper limit of the cavum tympani and the resulting loss of the quadratojugal: 0 = absent; 1 = present. Reworded from Joyce (2007: ch

16), Sterli & De la Fuente (2013: ch 22) (Quadratojugal A) and Anquetin (2012: ch 22); Hirayama (1994), Kear & Lee (2006) & Bardet *et al.* (2013) (ch 12).

Remarks: I changed the wording of the character definition with respect to Cadena & Parham (2015: ch 23), who use this character as a way to code for variation observed in the extent of the lower temporal emargination. However, this character is essentially a presence vs. absence character for the quadratojugal, and no further character for the extent of the lower temporal emagination was used in the study of Cadena & Parham (2015). Because I think that the extent of the lower temporal emargination can be qualified more finely, I coded a new character (ch 34) for variation of this feature among turtles.

Character optimisation: Unambiguous: crown-group Chelidae (0->1).

Character 32 (Cadena & Parham (2015): character 24). Quadratojugal, quadratojugal-maxilla contact: 0 = absent; 1 = present, jugal does not contribute to lower temporal emargination.

Character optimisation: Unambiguous: Kinosternidae (0->1), *Platysternon megacephalum* (0->1); DELTRAN: *Carettochelys insculpta* (0->1); ACCTRAN: total-group Carettochelyidae (0->1).

Character 33 (Cadena & Parham (2015): character 25). Quadratojugal, quadratojugal-squamosal contact below the cavum tympani: 0 = absent; 1 = present.

Character optimisation: Unambiguous: *Meiolania planiceps* (0->1).

Character 34 (new character). Quadratojugal, lower temporal emargination: 0 = weak to no emargination, the margin of the lower temporal emargination is formed by the quadratojugal or quadratojugal and jugal; 1 = moderate emargination, the margin of the lower temporal emargination is principally formed by the quadratojugal and jugal, but the maxilla is included

in the anterior section of the margin and/or the quadrate is included in the posterior section of the margin; 2 = large emargination, the postorbital and/or squamosal and parietal are included in the margin of the lower temporal emargination.

Remarks: I added this character to add observations of variation regarding the lower temporal emargination.

To discretise the degree of temporal emargination seen among turtles, I use the elements that form the margin of the temporal emargination. In turtles with a weak emargination or in turtles in which no emargination is present, the ventral margin of the temporal region of the skull is formed by the jugal and quadratojugal, or only the quadratojugal in taxa in which the jugal does not contribute to the cranial margin (e.g. kinosternids). This condition is scored as state 0 in my character, and seen in basal stem-turtles such as *Proganochelys quenstedti*, *Kayentachelys aprix*, or *Chubutemys copelloi*, meiolaniformes, chelonioids, trionychians, chelydrids, kinosternids, *Playsternon*, and sandownids.

Turtles with state 1 have a moderately deep lower temporal emargination. The jugal and quadratojugal form most of the margin of the emargination, but these elements are more dorsally positioned due to the presence of the emargination. Consequentially, the anterior and posterior adjacent elements to the jugal and quadratojugal, the maxilla and quadrate, respectively, are oncluded in the margin of the temporal emargination. This is seen in most testudinoids, *Araripmeys*, pelomedusoids, paracryptodires, some thalassochelydians (e.g. *Solnhofia parsoni*: TM 4023; *Plesiochelys etalloni:* MNB 435; *Jurassichelon oleronensis:* PIMUZ AIII 514), and many macrobaenids and sinemydids (e.g. *Judithemys sukhanovi:* Gaffney *et al.* 2007, fig. 13C; *Ordosemys* sp.: IVPP V12092, Brinkman & Wu 1999; *Dracochelys biscuspis:* Gaffney & Ye 1992), and xinjiangchelyids (e.g. *Xinjiangchelys wusu:* Rabi *et al.* 2013).

State 2 describes turtles with a large lower temporal emargination. Turtles with a large emargination are characterised by the inclusion of the postorbital, and/or the squamosl and parietal in the margin of the emargination. This is the case in chelids, chelydrids, some

xinjiangchelyids (e.g. *Annemys* spp.: Sukhanov 2000; Brinkman *et al.* 2012; Rabi *et al.* 2014), some macrobaenids and sinemydids (e.g. *Kirgizemys* spp.: Sukhanov 2000, Danilov *et al.* 2006; *Sinemys* spp.: Brinkman & Peng 1993*a*), and *Plesiochelys planiceps* (OUMNH J1582).

Character optimisation: Unambiguous: Paracryptodira+++ (0->1), Cryptodira (1->0), total-group Dermatemydidae (0->1), Emydidae (0->1), Testudinidae (0->1), crown-group Chelidae (1->2), *Plesiochelys planiceps* (1->2), Sandownidae (1->0), (*Kirgizemys hoburensis* + *Kirgizemys dmitrievi*) (1->2), (*Sinemys lens* + *Sinemys gamera*) (1->2); DELTRAN: *Annemys levensis* (1->2), *Annemys* sp. IVPP V18106 (1->2); ACCTRAN: Xinjiangchelyidae (1->2), (*Xinjiangchelys wusu* + *Xinjiangchelys radiplactoides*) (2->1).

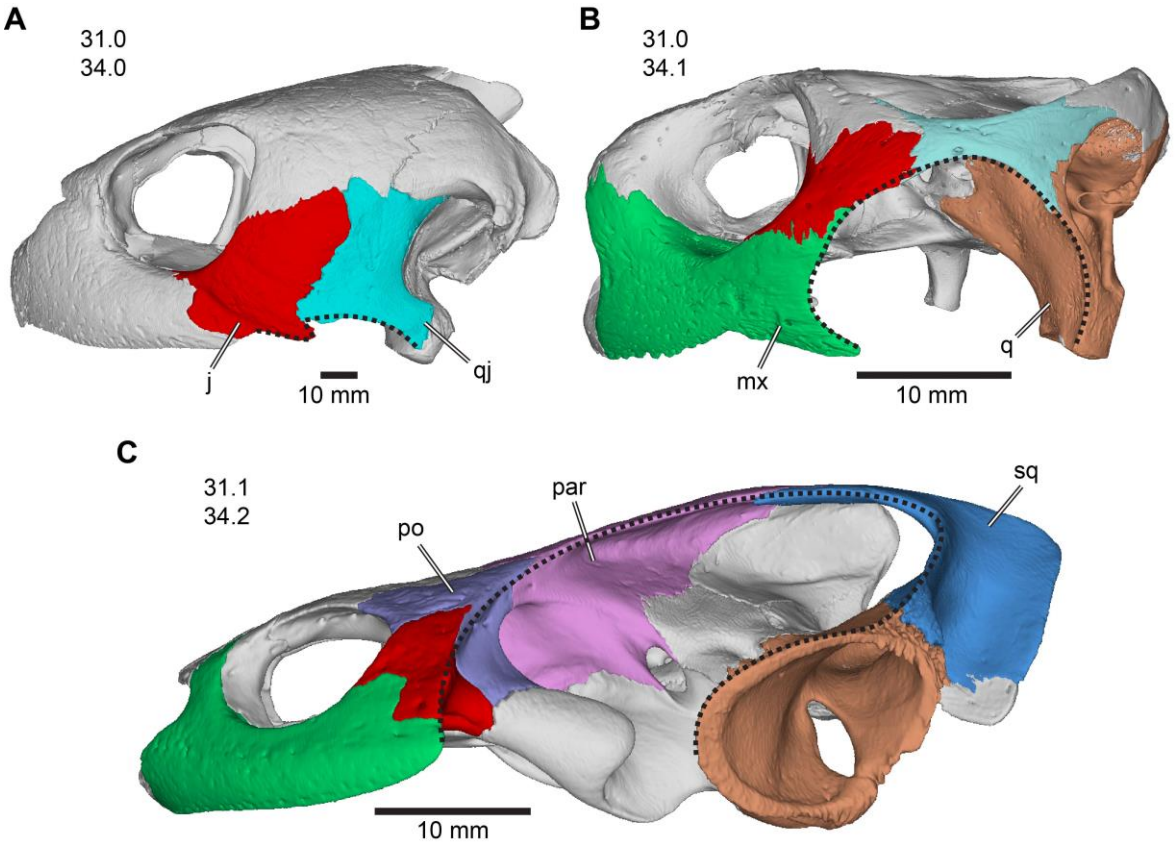


FIG. S1.9. Illustration of character 31 and 34. **A**, *Lepidochelys olivacea* (SMNS 11070, left lateral view of cranium); **B**, state 1 *Gopherus polyphemus* (FMNH 211815); **C**, state 1 (*Phrynops geoffroanus*, SMF 45470). Dotted lines indicate the ventral margin of the temporal region, which forms the lower temporal emargination. Note the absence of the quadratojugal in C. Abbreviations: *j*, jugal; *mx*, maxilla; *par*, parietal; *po*, postorbital; *q*, quadrate; *qj*, quadratojugal; *sq*, squamosal.

Character 35 (modified from Cadena & Parham (2015)). Squamosal, squamosal-postorbital contact: 0 = present; 1 = absent.

Previous definition (Cadena & Parham (2015): character 26): Squamosal, squamosal-postorbital contact: 0 = present; 1 = absent, temporal roofing well developed, but postorbital short; 2 = absent, due to lower temporal emargination; 3 = absent, due to upper temporal emargination. Joyce (2007: ch 18) & Sterli & De la Fuente (2013: ch 25) (Squamosal A).

Remarks: I simplified character 26 of Cadena & Parham (2015) to only encode the presence vs. absence of a squamosal-postorbital contact. This follows Zhou & Rabi (2015: character 25, Squamosal A), who in turn followed Sterli and De la Fuente (2013: Character 25, Squamosal A) in simplifying the more complex version of this character used by Joyce (2007: Character 18, Squamosal A).

I think that the character states 1 through 3 of Cadena & Parham (2015: character 26) should be merged to a single state qualifying the absence of a squamosal-postorbital character. These states explicitly suggest why a contact between the squamosal and postorbital is absent. However, the version of the character used here considers the shared similarity of the absence of such a contact independently of these observations. Furthermore, hypotheses about the reason for the absence of this contact cannot be tested with certainty and are subjective. This becomes clear when the scorings of Cadena & Parham (2015) are revised: In testudinoids, the upper temporal emargination is quite extensive, while the postorbital is relatively large, suggesting that state 3 of Cadena & Parham (2015) should be scored. However, these authors score state 1 for those testudinoids that lack a squamosal-postorbital contact. In some trionychids (e.g. *Apalone spinifera emoryi:* FMNH22178, *Pelodiscus sinensis*: IW576-2, *Lissemys punctata:* SMF74141), the postorbital is a small element (the postorbital does not reach the margin of the upper temporal emargination, and the jugal contacts the parietal), but the upper temporal emargination is also extensive, so that scoring states 1 and 3 would be warranted. In chelids without merged upper and lower temporal emarginations (e.g. *Chelus fimbriatus:* NHMUK81.9.27.4, *Phrynops geoffroanus:* SMF45470, *Elseya dentata:* NHMUK76.5.19.77), the lower temporal emargination is extensive

and the postorbital is large, so that state 2 should be scored. However, Cadena & Parham (2015) score state 1, implying an absence of the contact due to a small postorbital. In taxa with a merged upper and lower temporal emargination (e.g. *Chelodina oblonga:* NHMUK64.12.22), states 2 and 3 could be scored, whereas Cadena & Parham (2015) again score state 1.

Character optimisation: Testudines (0->1), total-group Chelonioidea (1->0), crown-group Chelydridae (1->0), *Platysternon megacephalum* (1->0), *Pleurosternon bullockii* (0->1); DELTRAN: *Sinemys gamera* (0->1); ACCTRAN: (*Sinemys lens* + *Sinemys gamera*) (0->1).

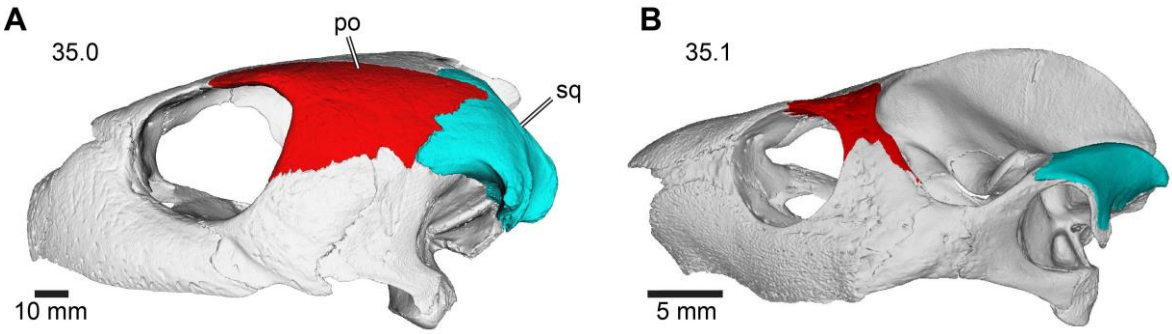


FIG. S1.10. Illustration of character 35. **A**, state 0 (*Lepidochelys olivacea*, SMNS 11070, left lateral view of cranium); **B**, state 1 (*Sternotherus minor*, FMNH 211696). Abbreviations: *po*, postorbital; *sq*, squamosal.

Character 36 (Cadena & Parham (2015): character 27). Squamosal, squamosal-supraoccipital contact: 0 = absent; 1 = present.

Character optimisation: Unambiguous: *Meiolania planiceps* (0->1).

Character 37 (Cadena & Parham (2015): character 28). Squamosal, posterolateral protuberances developing horns: 0 = absent; 1 = present.

Character optimisation: Unambiguous: *Meiolania planiceps* (0->1).

Character 38 (Cadena & Parham (2015): character 29). Squamosal, very long posterior process, formed exclusively by the squamosal and protruding beyond condyles occipitalis: 0 = absent; 1 = present.

Character optimisation: Unambiguous: *Ocepechelon bouyai* (0->1), *Toxochelys latiremis* (0->1), *Staurotypus* (0->1), *Chrysemys picta* (0->1), Trionychia (0->1), *Araripemys barretoi* (0->1), *Pelomedusa subrufa* (0->1), (*Ordosemys* ++ *Kirgizemys*) (0->1), Xinjiangchelyidae (0->1).

Character 39 (Cadena & Parham (2015): character 30). Squamosal, squamosal-quadrate contact: 0 = tightly sutured; 1 = wide open.

Character optimisation: Unambiguous: total-group Chelonioidea (0->1), (*Portlandemys* ++ *Plesiochelys*) (0->1)

Character 40 (modified from Cadena & Parham (2015)). Squamosal, posterodorsal margin of cavum tympanum: 0 = the squamosal forms the posterodorsal margin of the cavum tympanum; 1 = the squamosal is excluded from the posterodorsal margin of the cavum tympanum.

Previous definition (Cadena & Parham (2015): character 55): Quadrate, antrum postoticum: 0 = absent; 1 = present, quadrate does not fully enclose the anterior perimeter of the antrum; 2 = present, quadrate fully encloses the anterior perimeter of the antrum. Joyce (2007: ch 35, Quadrate E), Sterli & De la Fuente (2013: ch 53, Antrum postoticum A).

Remarks: This character includes variation that was partially encoded in character 55 of Cadena & Parham (2015), based on Joyce (2007: character 35). These previous characters combine two different sources of morphological variation and has thus been split into two characters: The absence/presence of the antrum postoticum, and the identity of bones (squamosal or quadrate) forming the posterodorsal margin of the cavum tmypanum. Please refer to the remarks of character 76 of this study for a detailed discussion.

My version of character 40 essentially includes the variation encoded by states 1 and 2 of the character defined by Joyce (2007: character 35). Anquetin (2012) omitted this character, primarily on the basis of not being able to score many taxa. I agree with Joyce

(2007) that the contribution of the squamosal to the rim of the cavum tympanum might have phylogenetic value, especially as I code a similar character for the quadratojugal (character 80). However, as discussed in the remarks section of character 73, I argue that this observation represents a feature of the squamosal and cavum tympanum, and not the antrum postoticum. Therefore, my modified character definition lacks an absence state in relation to the antrum postoticum, and is a simple binary character. Even if my character state definitions are different to those of Joyce (2007: character 35) and Cadena & Parham (2015: character 55), my state 0 corresponds to state 1 of those studies, and my state 1 corresponds to state 2 of those studies.

Character optimisation: Unambiguous: (*Ocepechelon* ++ *Santanachelys*) (0->1), *Desmatochelys lowii* (1->0), *Kirgizemys hoburensis* (0->1); DELTRAN: *Chelydra serpentina* (0->1), Kinosterninae (0->1), *Dermatemys mawii* (0->1), Emydidae (0->1), *Geoclemys hamiltonii* (0->1), *Testudo* (0->1), total-group Carettochelyidae (0->1), Pleurodira (0->1), *Leyvachelys cipadi* (0->1), *Annemys* sp. IVPP V18106 (0->1); ACCTRAN: Xinjiangchelyidae+++ (0->1), Americhelydia (1->0), *Chelydra serpentina* (0->1), Kinosternoidea (0->1), *Baptemys wyomingensis* (1->0), *Platysternon megacephalum* (1->0), *Chelonoidis* sp. (1->0), Trionychidae (1->0), Thalassochelydia (1->0), Sinemydidae/Macrobaenidae (1->0).

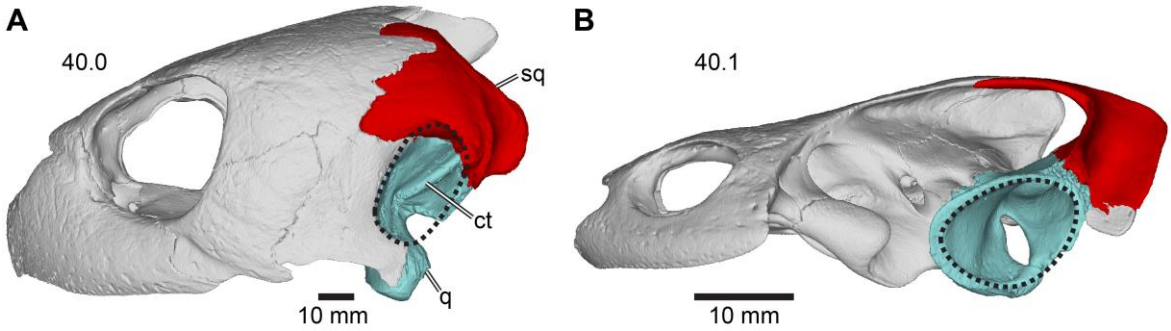


FIG. S1.11. Illustration of character 40. **A**, state 0 (*Lepidochelys olivacea*, SMNS 11070, left lateral view of cranium); **B**, state 1 (*Phrynops geoffroanus*, SMF 45470). Dotted line circumscribes the margin of the cavum tympanum. Abbreviations: *ct*, cavum tympanum; *q*, quadrate; *sq*, squamosal.

Character 41 (Cadena & Parham (2015): character 31). Postorbital, postorbital-palatine contact: 0 = absent; 1 = present, foramen palatinum posterius situated posterior to the orbital wall.

Character optimisation: Unambiguous: Pleurodira (0->1).

Character 42 (new character). Postorbital, contact with the quadratojugal: 0 = present; 1 = absent.

Remarks: A contact between the postorbital and quadratojugal was considered by Cadena & Parham (2015, ch. 19; see remarks for my character 25 above). However, Cadena & Parham (2015) linked the presence of this contact with the absence of a jugal-squamosal contact. I consider these two contacts in separate presence vs. absence characters. This is necessary, because some taxa (trionychids: *Apalone spinifera amoryi:* FMNH 22178, *Pelodiscus sinensis:* IW576-2) lack a contact between the postorbital and quadratojugal, and also lack a jugal-squamosal contact. This combination of features was impossible to score within the original character definition used by Cadena & Parham (2015). These observations show that the contacts in question vary independently from one another, which justifies coding this variation in different characters.

Character optimisation: Unambiguous: *Dermochelys coriacea* (0->1), *Allopleuron hofmanni* (0->1), *Geoclemys hamiltonii* (0->1), *Testudo* (0->1), Trionychidae (0->1), *Podocnemis* (0->1); DELTRAN: *Kinosternon suburum hippocrepis* (0->1), *Staurotypus* (0->1), *Proganochelys quenstedti* (0->1); ACCTRAN: Kinosternidae (0->1), *Sternotherus* (1->0), *Proganochelys quenstedti* (0->1).

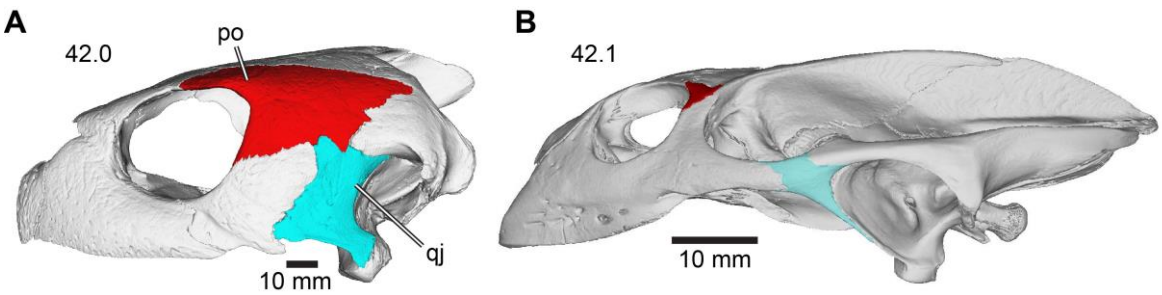


FIG. S1.12. Illustration of character 42. **A**, state 0 (*Lepidochelys olivacea*, SMNS 11070, left lateral view of cranium); **B**, state 1 (*Apalone spinifera emoryi*, FMNH 22178). Abbreviations: *po*, postorbital; *qj*, quadratojugal.

Character 43 (adopted from Anquetin 2012). Postorbital, postorbital-maxilla contact preventing the jugal from entering the orbital margin: 0 = absent; 1 = present.

Remarks: This character is taken from Anquetin (2012: ch 28). Contra Anquetin (2012), I score *Emys orbicularis* as having state 0; Anquetin (2012) cites Gaffney (1979) for evidence that the postorbital and maxilla of *Emys* contact each other. While Gaffney (1976) indeed shows a line-drawing in which *Emys* is reconstructed in this way, the specimen I examined using CT scanning (IW 1987a) lacks this contact, and the jugal instead contributes to the orbital margin.

Character optimisation: Unambiguous: *Platysternon megacephalum* (0->1), Paracryptodira (0->1).

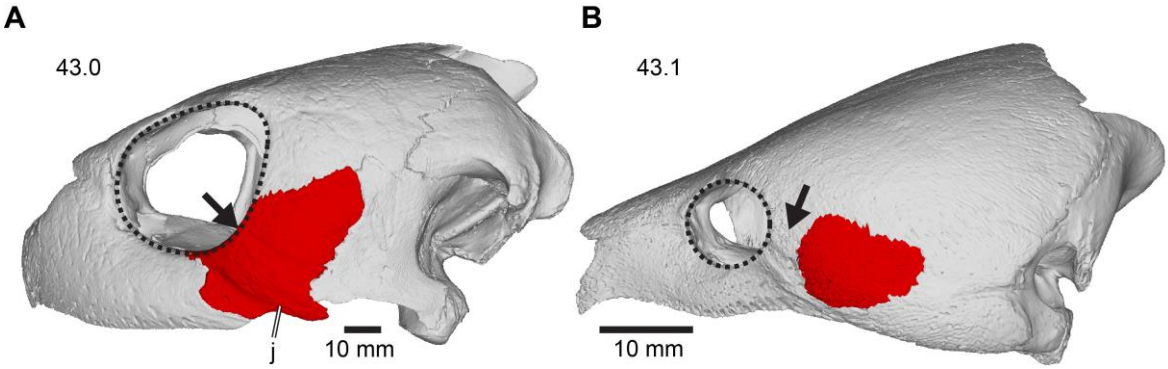


FIG. S1.13. Illustration of character 43. **A**, state 0 (*Lepidochelys olivacea*, SMNS 11070, left lateral view of cranium); **B**, state 1 (*Platysternon megacephalum*, SMF 69684). Dotted lines circumscribe the orbit. Arrow indicates jugal contribution to orbit in A, and postorbital-maxilla contact anterior to jugal in B. Abbreviations: *j*, jugal.

Character 44 (new character). Postorbital, dorsal margin of orbit: 0 = continuously and concavely curved margin between frontals and jugal; 1 = frontal margin relatively narrow, with lateral bulge of postorbital.

Remarks: In cheloniids (e.g. *Allopleuron hofmanni*: NHMUK R 42931; *Argillochely cuneiceps*: NHMUK 38955; *Lepidochelys olivacea*: SMNS 11070), the dorsal margin of the orbit has a

marked lateral bulging at the level of the postorbital. In most other turtles, the orbital margin is gently concave.

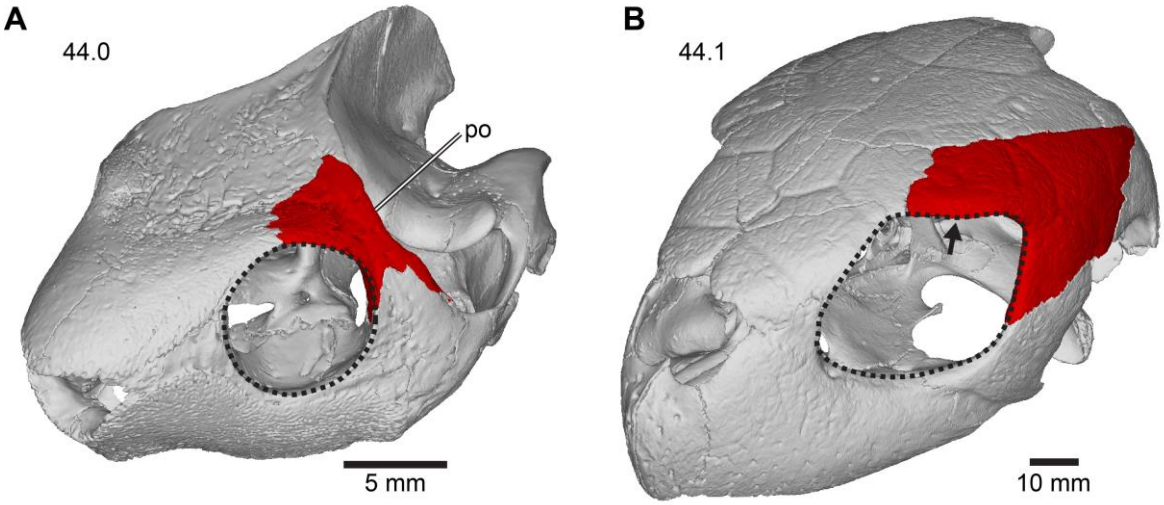


FIG. S1.14. Illustration of character 44. **A**, state 0 (*Sternotherus minor*, FMNH 211696, left anterodorsolateral view of cranium); **B**, state 1 (*Lepidochelys olivacea*, SMNS 11070). Dotted line circumscribes the orbit. Arrow in B indicates lateral bulge of postorbital. Abbreviations: *po*, postorbital.

Character optimisation: Unambiguous: *Archelon ischyros* (0->1), total-group Cheloniidae (0->1), *Allopleuron hofmanni* (1->0); DELTRAN: *Plesiochelys etalloni* (0->1); ACCTRAN: (*Plesiochelys etalloni* + *Plesiochelys planiceps*) (0->1).

Character 45 (Cadena & Parham (2015): character 32). Supratemporal: 0 = present; 1 = absent.

Character optimisation: DELTRAN: *Chubutemys*+++ (0->1); ACCTRAN: *Australochelys*+++ (0->1).

Character 46 (adopted from Zhou & Rabi (2015)). Teeth in premaxilla, maxilla, and dentary: 0 = present; 1 = absent.

Remarks: This character is taken from Zhou & Rabi (2015: Character 117, Teeth A), and was first used by Sterli (2008: Character 68: Teeth A). Currently, no taxa in my matrix are present that have teeth in the premaxilla, maxilla, and dentary. However, I keep this character from Zhou & Rabi (2015) for future reference.

Character optimisation: -.

Character 47 (Cadena & Parham (2015): character 33). Premaxilla, subdivision of the apertura narium externa by an internarial process of the premaxilla: 0 = present; 1 = absent.

Character optimisation: Unambiguous: Paracryptodira+++ (0->1), (*Eileanchelys* + *Kayentachelys*) (0->1).

Character 48 (Cadena & Parham (2015): character 34). Premaxilla, fusion of premaxillae: 0 = absent; 1 = present.

Character optimisation: Unambiguous: *Ocepechelon bouyai* (0->1), Trionychia (0->1), *Chelus fimbriatus* (0->1), *Brachyopsemys tingitana* (0->1).

Character 49 (modified form Cadena & Parham (2015)). Premaxilla, foramen praepalatinum: 0 = absent; 1 = present.

Previous description (Cadena & Parham (2015): character 35): Premaxilla, foramen praepalatinum: 0 = present; 1 = absent; 2 = absent, foramen intermaxillaris present. Joyce (2007: ch 24) and Sterli & De la Fuente (2013: ch 34) (Premaxilla C); Hirayama (1994), Kear & Lee (2006) & Bardet *et al.* (2013) (ch 14).

Remarks: I split character 35 of Cadena & Parham (2015) into two binary characters that code for the presence of the foramen praepalatinum and foramen intermaxillaris separately. As stated in Anquetin (2012), there is currently no evidence that the foramen intermaxillaris observed in trinychids is homologous to the foramen praepalatinum observed in most turtles.

Character optimisation: Unambiguous: *Allopleuron hofmanni* (0->1), *Staurotypus* (1->0), Trionychia (1->0); DELTRAN: (*Eileanchelys* + *Kayentachelys*)+++ (0->1), (*Bouliachelys* ++ *Santanachelys*) (1->0), *Ocepechelon bouyai* (1->0), total-group Cheloniidae (1->0), *Solnhofia*

parsoni (1->0), *Sandownia harrisi* (1->0), *Brachyopsemys tingitana* (1->0); ACCTRAN: *Australochelys*+++ (0->1), crown-group Chelonioidea (1->0), (*Desmatochelys lowii* + *Desmatochelys padillai*) (0->1), Dermochelyidae (0->1), Angolachelonia (1->0), (*Portlandemys* ++ *Plesiochelys*) (0->1), *Leyvachelys cipadi* (0->1).

Character 50 (modified form Cadena & Parham (2015)). Premaxilla, foramen intermaxillaris: 0 = absent; 1 = present.

Previous description (Cadena & Parham (2015): character 35): Premaxilla, foramen praepalatinum: 0 = present; 1 = absent; 2 = absent, foramen intermaxillaris present. . Joyce (2007: ch 24) and Sterli & De la Fuente (2013: ch 34) (Premaxilla C); Hirayama (1994), Kear & Lee (2006) & Bardet *et al.* (2013) (ch 14).

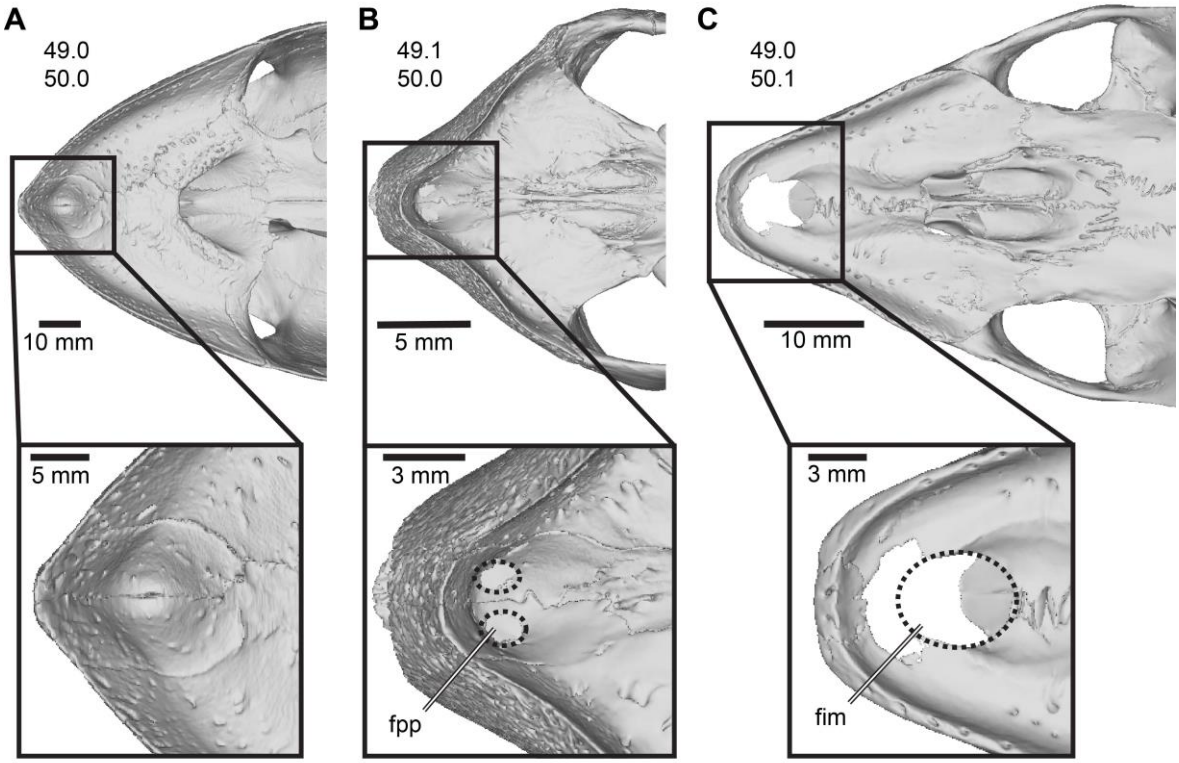


FIG. S1.15. Illustration of character 49 and 50. **A**, *Lepidochelys olivacea* (SMNS 11070, ventral view of anterior half of cranium with boxed close-up); **B**, *Sternotherus minor* (FMNH 211696); **C**, *Apalone spinifera emoryi* (FMNH 22178). Abbreviations: *fim*, foramen intermaxillaris; fpp, foramen praepalatinum.

Remarks: See remarks for character 49.

Character optimisation: Unambiguous: Trionychidae (0->1).

Character 51 (Cadena & Parham (2015): character 36). Premaxilla, exclusion of the premaxillae from the apertura narium externa: 0 = absent; 1 = present.

Character optimisation: Unambiguous: Trionychidae (0->1).

Character 52 (Cadena & Parham (2015): character 37). Premaxilla, distinct, median premaxillary hook along the labial margin of the premaxillae: 0 = absent; 1 = present.

Character optimisation: Unambiguous: (*Protostega* + *Archelon*) (0->1), *Lepidochelys kempii* (0->1), crown-group Chelydridae (0->1), *Kinosternon suburum hippocrepis* (0->1), *Platysternon megacephalum* (0->1).

Character 53 (new character) Premaxilla, cusps developed on the labial ridge in conjunction with maxilla: 0 = absent; 1 = present.

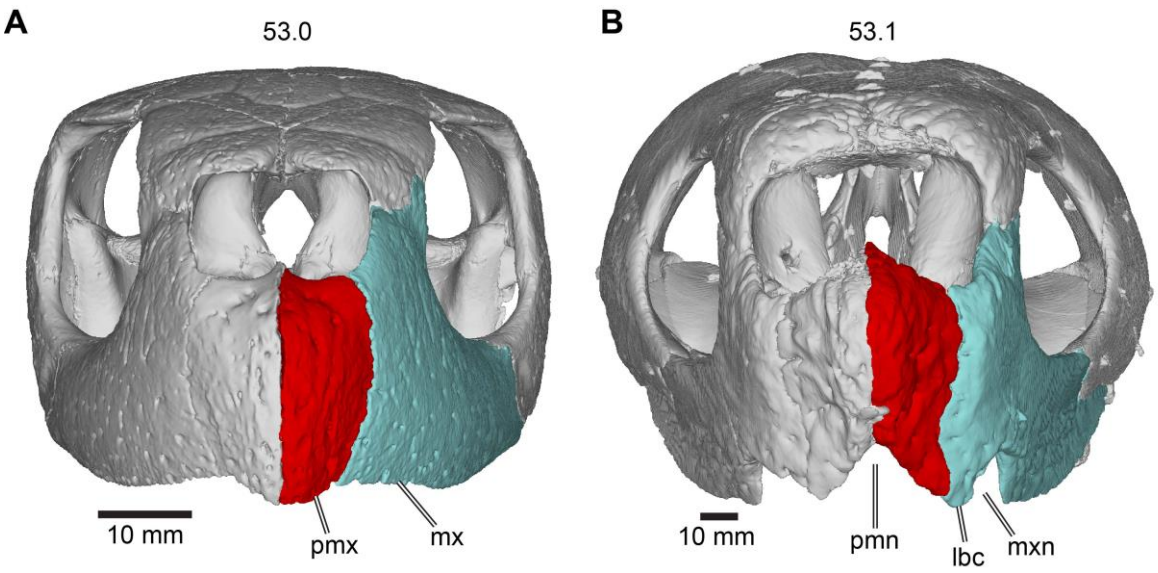


FIG. S1.16. Illustration of character 53. **A**, state 0 (*Lepidochelys olivacea*, SMNS 11070, anterior view of cranium); **B**, state 1 (*Dermochelys coriacea*, UMCZ R 3031). Abbreviations: *lbc*, labial cusp; *mx*, maxilla; *mxn*, maxillary notch; *pmn*, premaxillary notch; *pmx*, premaxilla.

Remarks: The labial ridge of *Dermochelys coriacea* bears a ventrally directed cusp at the premaxilla-maxilla suture on each side. Besides in *Dermochelys coriacea* (UMZC R3031), I also observed these structures in the dermochelyid *Eosphargis breineri* (FUM-N-1450). I also scored *Dracochelys* (IVPP V4075) as having cusps, which likely represent a convergent appearance of this feature.

Character optimisation: Unambiguous: Dermochelyidae (0->1), *Dracochelys bicuspis* (0->1).

Character 54 (Cadena & Parham (2015): character 38). Palatine, contribution to the anterior extension of the lateral braincase wall: 0 = absent; 1 = present.

Character optimisation: Unambiguous: Kinosternoidea (0->1), *Gopherus polyphemus* (0->1), Trionychia (0->1), Pelomedusoides (0->1), *Sandownia harrisi* (0->1).

Character 55 (Cadena & Parham (2015): character 39). Palatine, contribution to the upper triturating surface: 0 = absent or less than 30% of the total width of the triturating surface; 1 = present, at least 30% or more of the total width of the triturating surface.

Character optimisation: Unambiguous: *Argillochelys*+++ (0->1), *Podocnemis* (0->1), *Sandownia harrisi* (0->1).

Character 56 (Cadena & Parham (2015): character 40). Palatine, secondary palate: 0 = absent; 1 = present, complete separation of the narial cavity from the oral cavity.

Character optimisation: Unambiguous: *Argillochelys*+++ (0->1); DELTRAN: *Solnhofia parsoni* (0->1), Sandownidae (0->1); ACCTRAN: Angolachelonia (0->1), (*Portlandemys* ++ *Plesiochelys*) (1->0).

Character 57 (Cadena & Parham (2015): character 41). Palatine, vomer-palatine contact anterior to internal naris (apertura narium interna): 0 = absent; 1 = present.

Character optimisation: Unambiguous: Sandownidae (0->1); DELTRAN: Dermochelyidae (0->1), *Argillochelys*+++ (0->1), *Toxochelys latiremis* (0->1); ACCTRAN: total-group Chelonioidea (0->1), Protostegidae (1->0), *Eochelone* (1->0).

Character 58 (Cadena & Parham (2015): character 42). Maxilla, triturating surface definition: 0 = triturating surface with labial ridge only; 1 = triturating surface with labial and lingual ridge; 2 = triturating surface with labial, lingual, and accessory ridge(s).

Character optimisation: Unambiguous: total-group Chelonioidea (0->1), *Ocepechelon bouyai* (1->0), *Dermochelys coriacea* (1->0), *Allopleuron*+++ (1->0), *Chelydra serpentina* (0->1), *Emarginachelys cretacea* (0->2), total-group Dermatemydidae (0->2), *Chrysemys picta* (0->2), *Platysternon megacephalum* (0->1), Testudinidae (0->2), *Apalone spinifera* (0->1), *Elseya dentata* (0->2), Pelomedusoides (0->2), (*Portlandemys* ++ *Plesiochelys*) (0->1), *Dracochelys bicuspis* (0->1), *Kirgizemys dmitrievi* (0->1), *Pleurosternon bullockii* (1->0), *Meiolania planiceps* (0->2); DELTRAN: Xinjiangchelyidae+++ (1->0), *Lepidochelys kempii* (0->2), *Eretmochelys imbricata* (0->2), (*Chelonia* + *Natator*) (0->2), *Carettochelys insculpta* (0->1), *Chubutemys copelloi* (1->0); ACCTRAN: *Chubutemys*+++ (1->0), crown-group Cheloniidae (0->2), (*Caretta* ++ *Lepidochelys*) (2->0), *Lepidochelys kempii* (0->2), total-group Carettochelyidae (0->1), Paracryptodira (0->1).

Character 59 (Cadena & Parham (2015): character 43). Maxilla, accessory ridge(s): 0 = accessory ridge(s) on maxilla present along the triturating surface; 1 = accessory ridge(s) only in some sectors of the triturating surface. Thic character is scored as inapplicable when no accessory ridges are present (ch 58.0 or ch 58.1).

Character optimisation: DELTRAN: *Emarginachelys cretacea* (0->1), *Baptemys wyomingensis* (0->1); ACCTRAN: Chelydroidea (0->1), *Dermatemys mawii* (1->0).

Character 60 (adopted from Zhou & Rabi (2015)). Maxilla, median contact between right and left maxilla on the palate: 0 = absent; 1 = present.

Remarks: Trionychids (e.g. *Apalone spinifera emoryi*: FMNH 22178), as well as some members of various other groups (e.g. *Solnhofia parsoni*, TM 4023), have an intermaxillary contact on

the palate. This feature was considered as variation resulting from the absence of a vomer-premaxilla contact by Cadena & Parham (2015: character 47 state 2). Here, I dedicate a separate character to this feature, following Sterli and De la Fuente (2013: Character 37, Maxilla A), and others including Zhou & Rabi (2015). See remarks on character 64 for further details of the justification for this character.

Character optimisation: Unambiguous: *Caretta caretta* (0->1), Trionychidae (0->1), *Elseya dentata* (0->1), *Solnhofia parsoni* (0->1), *Kallokibotion bajazidi* (0->1).

Character 61 (Cadena & Parham (2015): character 44). Vomer, number of vomer(s): 0 = paired; 1 = single, but large; 2 = single and greatly reduced or absent.

Character optimisation: Unambiguous: Pelomedusoides (1->2), *Kirgizemys dmitrievi* (1->0); DELTRAN: (*Eileanchelys* + *Kayentachelys*)+++ (0->1); ACCTRAN: *Australochelys*+++ (0->1).

Character 62 (Cadena & Parham (2015): character 45). Vomer, vomer-pterygoid contact in palatal view: 0 = present; 1 = absent, medial contact of palatines present.

Character optimisation: Unambiguous: Protostegidae (0->1), *Chubutemys copelloi* (0->1); DELTRAN: Trionychia (0->1), *Araripemys barretoi* (0->1), Pelomedusoides (0->1), *Solnhofia parsoni* (0->1), *Jurassichelon oleronensis* (0->1), *Plesiochelys planiceps* (0->1), *Leyvachelys cipadi* (0->1), *Xinjiangchelys radiplicatoides* (0->1); ACCTRAN: Angolachelonia+++ (0->1), Durocryptodira (1->0), crown-group Chelidae (1->0), *Plesiochelys etalloni* (1->0), *Portlandemys mcdowelli* (1->0), Sandownidae (1->0), *Leyvachelys cipadi* (0->1), (*Xinjiangchelys wusu* + *Xinjiangchelys radiplactoides*) (0->1).

Character 63 (Cadena & Parham (2015): character 46). Vomer, vomerine and palatine teeth: 0 = present; 1 = absent.

Character optimisation: DELTRAN: *Australochelys*+++ (0->1); ACCTRAN: *Australochelys*+++ (0->1).

Character 64 (modified from Cadena & Parham (2015)). Vomer, vomer-premaxilla contact in ventral view: 0 = present; 1 = absent.

Previous definition (Cadena & Parham (2015): character 47): Vomer, vomer-premaxilla contact in ventral view: 0 = broad, anterior margin of the vomer straight; 1 = very reduced, anterior margin of vomer forming an acute tip; 2 = absent, both maxilla meeting medially. Sterli (2008: ch 31); Parham & Pyenson (2010: ch 4 and ch 9); Sterli & De la Fuente (2013: ch 45, Vomer D).

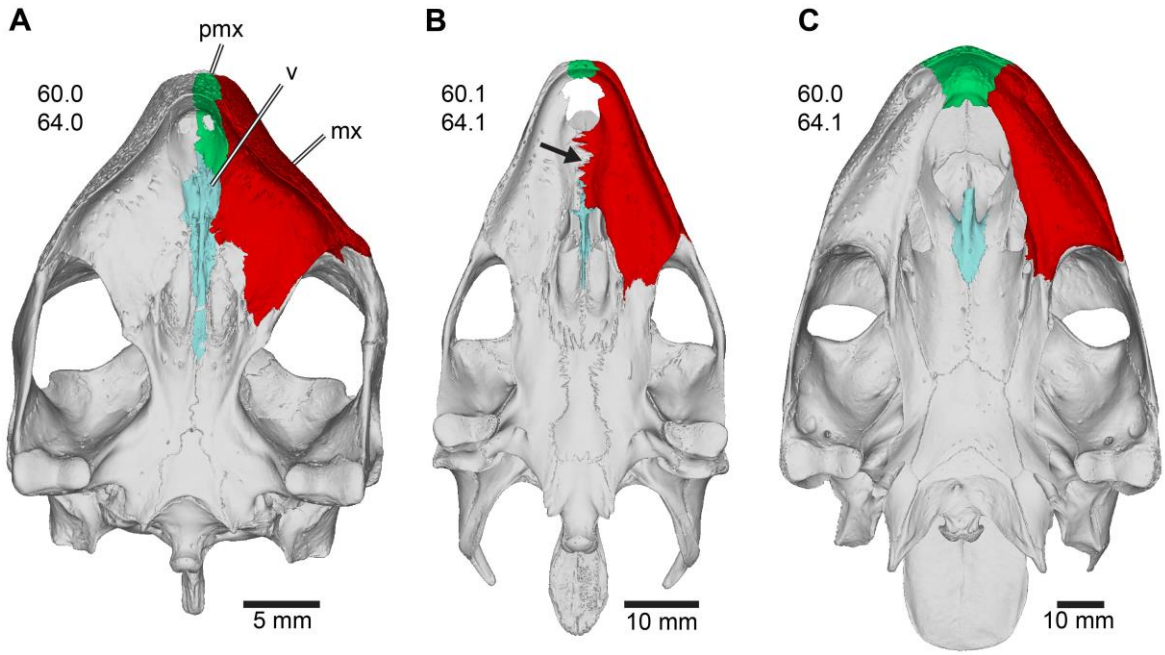


FIG. S1.17. Illustration of characters 60 and 64. **A**, vomer-premaxilla contact present (*Sternotherus minor*, FMNH 211696, ventral view of cranium); **B**, vomer-premaxilla contacts absent, and intermaxillary contact present (*Apalone spinifera emoryi*, FMNH 22178); **C**, vomer-premaxilla contact absent, and intermaxillary contact absent (*Carettochelys insculpta*, NHMUK1903.7.10.1). Abbreviations: *mx*, maxilla; *pmx*, premaxilla; *v*, vomer.

Remarks: I split the original character used by Cadena & Parham (2015: character 47) into two separate characters (characters 60 and 64 of this study), following some previous studies (Sterli & De la Fuente 2013: characters 37, Maxilla A; and 45, Vomer D; Zhou & Rabi (2015): characters 37, Maxilla A ; and 45, Vomer D).

In the character definition used by Cadena & Parham (2015), the absence of a vomer-premaxilla contact is linked with the presence of an intermaxillary contact. However, because

some turtles, such as *Sandownia* (MIWG3480) or *Carettochelys* (NHMUK1903.7.10.1), have maxillae that do not meet on the ventral skull midline, but none-the-less lack a vomer-premaxilla contact, I limit this character to variation regarding the presence or absence of a vomer-premaxilla contact, as also done by Sterli (2008: character 31, Vomer D). The median intermaxillary contact is herein considered in a new character (character 60).

Character optimisation: Unambiguous: *Caretta caretta* (0->1), *Dermatemys mawii* (0->1), Trionychia (0->1), *Solnhofia parsoni* (0->1), *Brachyopsemys tingitana* (0->1).

Character 65 (modified from Cadena & Parham (2015)). Vomer, ventral median crest: 0 = absent, ventral surface of vomer is smooth; 1 = present, shallow ridge extends along the ventral surface posterior to ventral process of the vomer, ridge becomes shallower posteriorly; 2 = narrow and tall ventral crest present all along the vomer.

Previous definition (Cadena & Parham (2015): character 48): Vomer, ventral crest: 0 = absent; 1 = narrow and tall ventral crest present all along the vomer. Reworded from Sterli & De la Fuente (2013: ch 46, Vomer E).

Remarks: An additional character state (state 1 of this study) has been added to the original character definition of Cadena & Parham (2015: character 48). State 2 (state 1 in Cadena & Parham (2015)) describes the morphology seen in meiolaniids and testudinids (see Sterli & De la Fuente 2011), and also some trionychids (e.g. *Apalone spinifera emoryi*: FMNH 21178) and sinemydids (e.g. *Ordosemys* sp.: IVPP V12092), in which an elongate and tall crest extends over the entire ventral surface of the vomer, which often becomes more prominent posteriorly.

I have noted that some chelonioids (e.g. *Argillochelys cuneiceps*: NHMUK 38955, NHMUK R14375) and protostegids (e.g. *Rhinochelys:* CAMSM B55783, NHMUK R43980, CAMSM B55776, NHMUK R2226, NHMUK R35197, CAMSM B55775; *Bouliachelys suteri:* QMF

31669) also have a ventrally placed, keel-like structure on the vomer, for which I added the new state. Unlike in testudinids such as *Chelonoidis* sp. (SMF67582), this structure forms a relatively low and robust ridge, which extends posteriorly from the posterior surface of the ventral process of the vomer. The ridge becomes shallower posteriorly and eventually merges with this the posteroventral surface of the vomer.

Character optimisation: Unambiguous: *Chubutemys*+++ (0->2), Angolachelonia+++ (2->0), *Puppigerus camperi* (0->1), Chelydroidea (0->1), *Macrochelys temminckii* (1->0), *Platysternon megacephalum* (2->1), Trionychidae (0->2), *Dracochelys bicuspis* (2->0), *Kirgizemys dmitrievi* (2->1); DELTRAN: (*Ocepechelon* ++ *Santanachelys*) (0->1), Dermochelyidae (0->1), *Chrysemys picta* (0->2), Testuguria (0->2), Pleurosternidae (2->0), *Arundelemys dardeni* (2->0); ACCTRAN: Dermochelyoidea (0->1), (*Protostega* + *Archelon*) (1->0), Testudinoidea (0->2), *Emys orbicularis* (2->0), Paracryptodira (2->0), *Eubaena cephalica* (0->2).

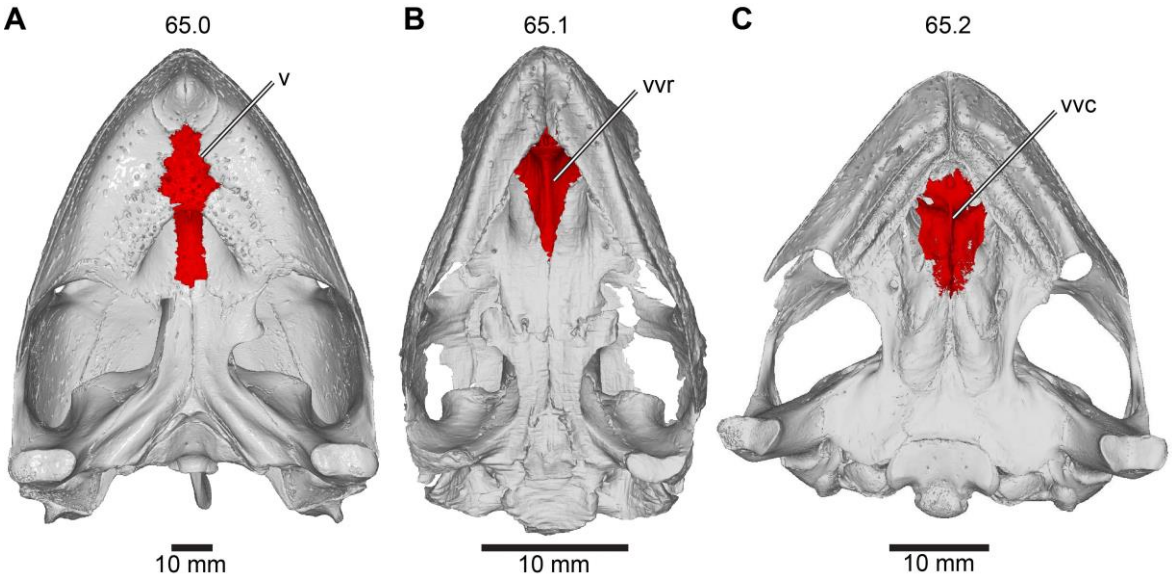


FIG. S1.18. Illustration of character 65. **A**, state 0 (*Lepidochelys olivacea*, SMNS 11070, ventral view of cranium); **B**, state 1 (*Rhinochelys cantabrigiensis*, CAMSM B55783); **C**, state 2 (*Gopherus polyphemus*, FMNH 211815). Abbreviations: *v*, vomer; *vvc*, ventral vomerine crest; *vvr*, ventral vomerine ridge.

Character 66 (Cadena & Parham (2015): character 49). Vomer, shape of the palate roof: 0 = flat; 1 = domed.

Character optimisation: Unambiguous: (*Eileanchelys* + *Kayentachelys*)+++ (1->0), Testuguria (0->1), *Testudo* (1->0), *Meiolania planiceps* (0->1); DELTRAN: *Carettochelys insculpta* (0->1); ACCTRAN: total-group Carettochelyidae (0->1).

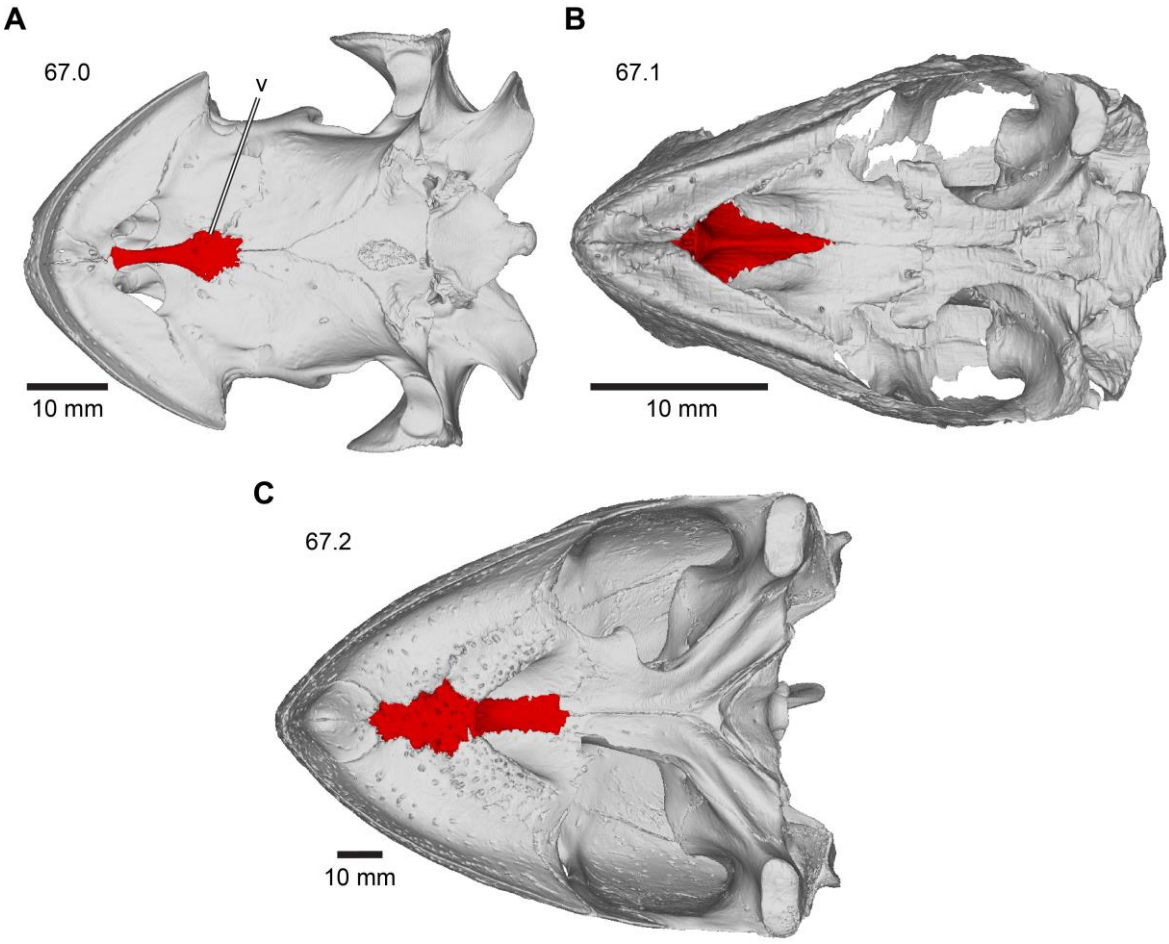


FIG. S1.19. Illustration of character 67. **A**, state 0 (*Phrynops geoffroanus*, SMF 45470, ventral view of cranium); **B**, state 1 (*Rhinochelys cantabrigiensis*, CAMSM B55783); **C**, state 2 (*Lepidochelys olivacea*, SMNS 11070). Abbreviations: *v*, vomer.

Character 67 (modified form Cadena & Parham (2015)). Vomer, shape of anterior end contacting the maxillae and praemaxillae: 0 = flat, near horizontal contact with maxillae; 1 = the anterior end of the vomer is anteroventrally directed and laterally expanded; 2 = the anterior end of the vomer is ventrally expanded to form a horizontal footplate with a flat ventral surface.

Previous definition (Cadena & Parham (2015): character 50): Vomer, vomerine pillar visible in ventral view: 0 = vomerine pillar absent; 1 = present; 2 = present but obscured in ventral view by the posterior extension of the triturating surface of the vomer. Modified from Parham & Pyenson (2010: ch 2); Hirayama (1998), Kear & Lee (2006), & Bardet *et al.* (2013) (ch 17).

Remarks: I modified the wording of the character states of Cadena & Parham (2015: ch 50), but otherwise the character remains the same. In turtles, the vomer contacts maxilla and premaxillae with its anterior end, but this contact can have various forms: In most turtles, the vomer forms a relatively flat, horizontal sheet anteriorly. However, in some turtles, the vomer is less flat and dorsally convex, so that the anterior part of the vomer forms an anteroventrally projecting "pillar", which contacts the maxillae and premaxillae. In taxa with such a structure of the anterior end of the vomer, the lateral sides are usually expanded to contact the maxillae. In cheloniids with an extensive secondary palate, the ventral end of the vomerine pillar is expanded to form a sheet-like footplate, which is integrated into the palate and conceals the pillar in ventral view. I think that although the anterior end of the vomer takes different forms, it is confusing to encode this variation in terms of presence, absence, or expansion of a "pillar", and thus use the character definitions given above.

Character optimisation: Unambiguous: Americhelydia (0->1), *Notochelone* (1->0), *Argillochelys*+++ (1->2), crown-group Chelydridae (1->0), *Geoclemys hamiltonii* (0->1); DELTRAN: *Ocepechelon bouyai* (1->0), (*Protostega* + *Archelon*) (1->0), *Dermochelys coriacea* (1->0), *Sternotherus* (1->2), *Staurotypus* (1->2), *Solnhofia parsoni* (0->2), Sandownidae (0->2); ACCTRAN: Dermochelyoidea (1->0), (*Desmatochelys* ++ *Santanachelys*) (0->1), *Eosphargis breineri* (0->1), Kinosternidae (1->2), *Kinosternon suburum hippocrepis* (2->1), Angolachelonia (0->2), (*Portlandemys* ++ *Plesiochelys*) (2->0).

Character 68 (Cadena & Parham (2015): character 51). Vomer, contribution to the upper triturating surface: 0 = absent, triturating surface narrow to absent; 1 = present.

Character optimisation: Unambiguous: total-group Cheloniidae (0->1), *Chrysemys picta* (0->1), *Geoclemys hamiltonii* (0->1), Sandownidae (0->1); DELTRAN: *Sternotherus* (0->1), *Staurotypus* (0->1); ACCTRAN: Kinosternidae (0->1), *Kinosternon suburum hippocrepis* (1->0).

Character 69 (new character). Vomer, median trough on dorsal surface posterior to sulcus vomeri: 0 = absent, dorsal surface of vomer flat or transversely convex; 1 = present, dorsal surface bears a median trough that extends posteriorly from the sulcus vomeri.

Remarks: In some turtles (kinosternoids, testudinoids, *Carettochelys*, some cheloniids), the dorsal surface of the vomer is deeply incised by a median trough that extends from the sulcus vomeri anteriorly to the contact with the pterygoid posteriorly. The trough shows some variation: it is narrow and deep in kinosternoids (e.g. *Sternotherus minor*: FMNH 211696, *Staurotypus salvinii*: NHMUK 1879.1.7.*5, Dermatemys mawii*: SMF 59463) and testudinoids (e.g. *Gopherus polyphemus*: FMNH 211815), but is shallow in the chelydrid *Macrochelys temminckii* (FMNH 22111), in which the vomer nevertheless has a concave transverse cross-section posterior to the sulcus vomeri.

Character optimisation: Unambiguous: Cryptodira (0->1), total-group Chelonioidea (1->0), *Lissemys punctata* (1->0); DELTRAN: *Notochelone* (0->1), (*Lepidochelys olivacea* + *Lepidochelys kempii*) (0->1), *Eretmochelys imbricata* (0->1), *Natator depressus* (0->1), *Eubaena cephalica* (0->1), *Proganochelys quenstedti* (0->1); ACCTRAN: (*Santanachelys* + *Notochelone*) (0->1), crown-group Cheloniidae (0->1), *Caretta caretta* (1->0), Chelonia mydas (1->0), (*Eubaena* ++ *Pleurosternon*) (0->1), *Proganochelys quenstedti* (0->1).

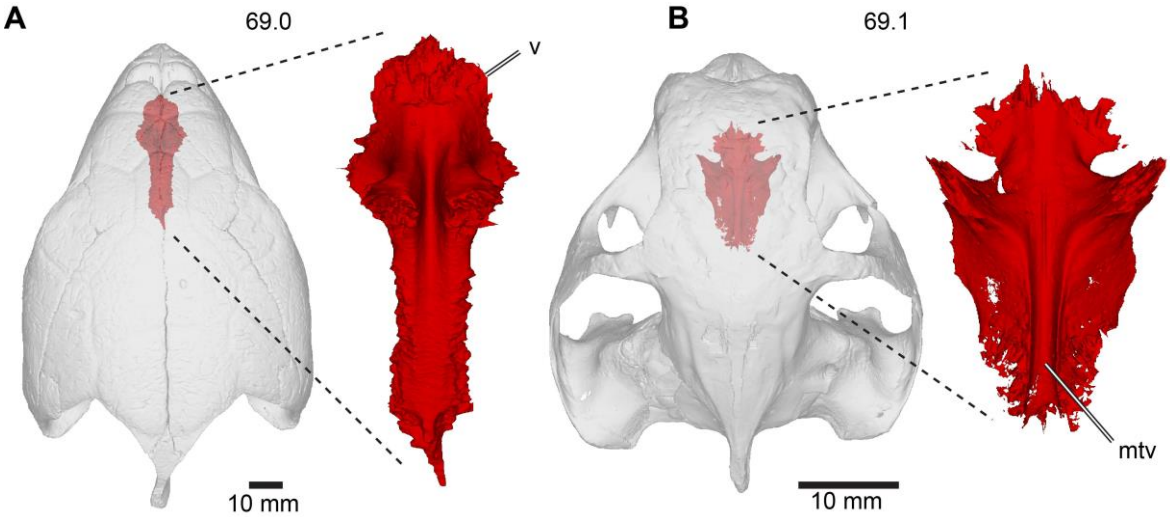


FIG. S1.20. Illustration of character 69. **A**, state 0 (*Lepidochelys olivacea*, SMNS 11070, dorsal view of cranium and vomer); **B**, state 1 (*Gopherus polyphemus*, FMNH 211815). Crania in A and B are rendered transparent to show original position of vomer. Abbreviations: *mtv*, median trough of vomer; *v*, vomer.

Character 70 (new character). Foramen orbito-nasale: 0 = formed as true foramen that is surrounded by bone from all sides; 1 = foramen orbito-nasale is not completely surrounded by bone and coalescent with the passage between the fossa orbitalis and the fossa nasalis.

Remarks: The foramen orbito-nasale is a passage for the posterior orbital artery, connecting the orbital and nasal fossae (Albrecht 1967; Gaffney 1972). In *Proganochelys* and cryptodires, the foramen is completely surrounded, but in pleurodires the foramen is open medially and coalescent with the fissure ethmoidalis and sulcus vomeri.

Character optimisation: Unambiguous: Pleurodira (0->1).

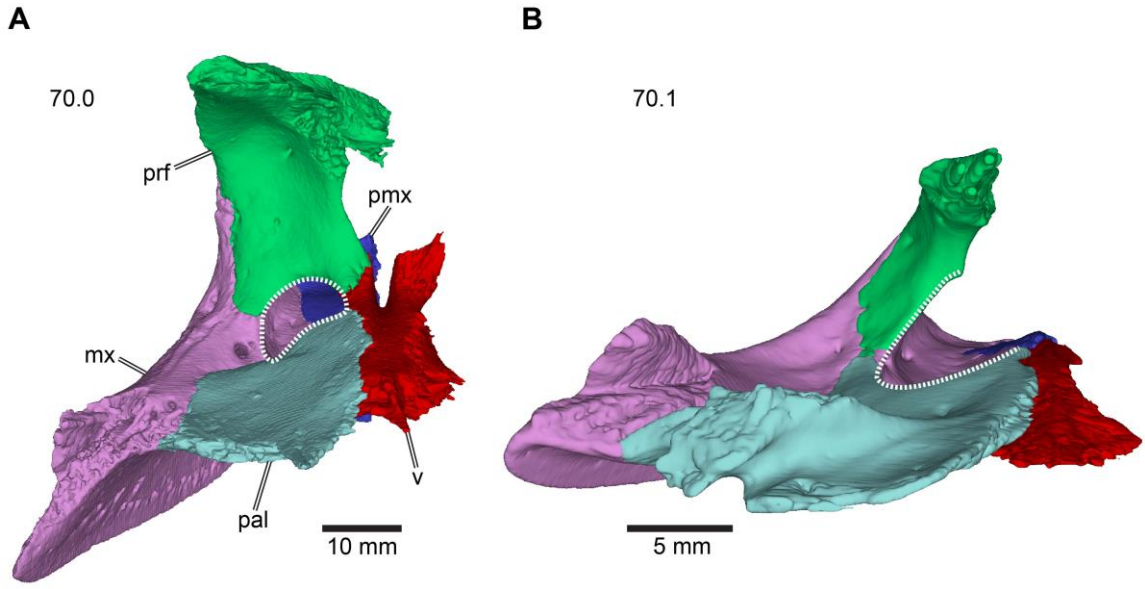


FIG. S1.21. Illustration of character 70. **A**, state 0 (*Lepidochelys olivacea*, SMNS 11070, posterior view of partial left snout); **B**, state 1 (*Phrynops geoffroanus*, SMF 45470). Dotted line indicates outline of the foramen orbito-nasale. Abbreviations: *mx*, maxilla; *pal*, palatine; *pmx*, premaxilla; *prf*, prefrontal; *v*, vomer.

Character 71 (new character). Foramen orbito-nasale, contribution of vomer: 0 = absent; 1 = present.

Remarks: The foramen orbito-nasale is formed minimally by the prefrontal and the palatine in all turtles. However, variation exists in the contribution of additional elements to the margin of the foramen. In *Proganochelys*, the lacrimal contributes to the foramen, whereas in

most crown-group cryptodires, the maxilla forms part of the margin (with many exceptions within testudinoids: e.g. *Geoclemys hamiltonii*: NHMUK 87.9.30.1). Additionally, the vomer is sometimes included in the margin (e.g. many chelonioids, e.g. *Lepidochelys olivacea*: SMNS 11070; all members crown-Trionychia scored in this study).

Here, I code two characters concerning the formation of the foramen orbito-nasale: One about the presence vs. absence of the vomer to the margin of the foramen (this character), and one about the presence vs. absence of the maxilla to the margin of the foramen (character 72). A character for the contribution of the lacrimal is not coded, because this character list includes a character about the presence of the lacrimal. The scorings for the presence of a lacrimal and its contribution to the foramen orbito-nasale would be identical, suggesting that these features are linked.

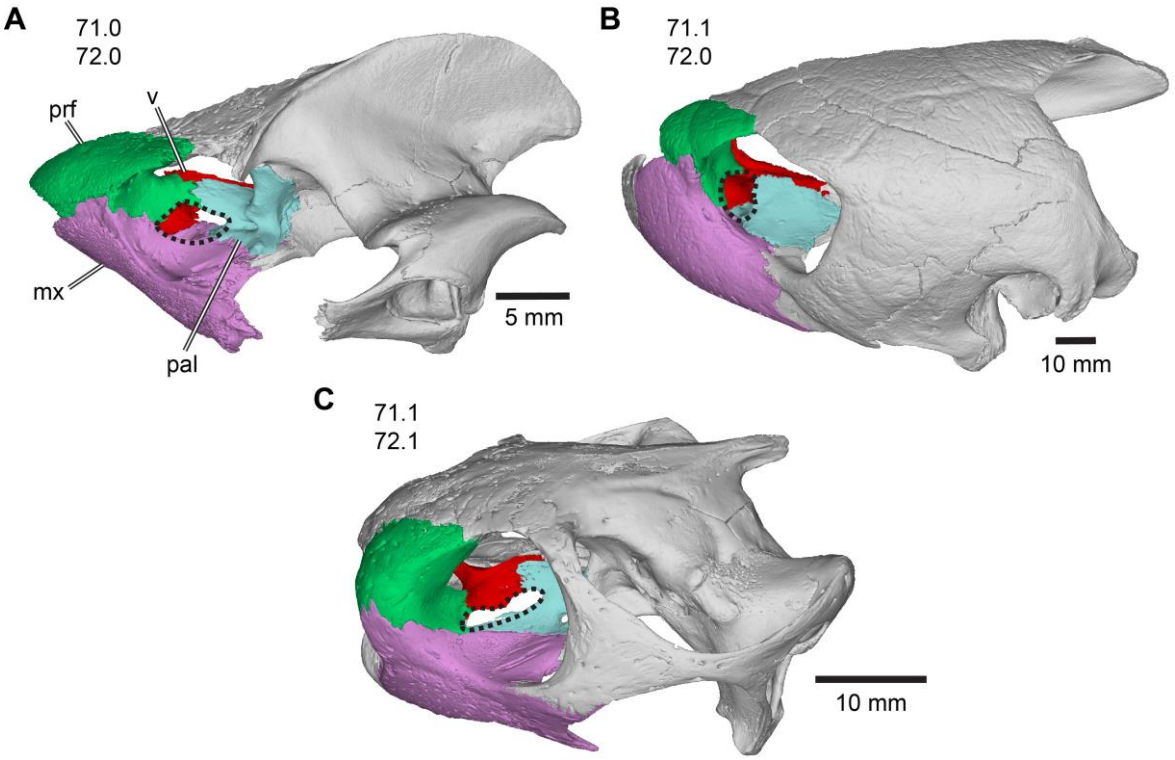


FIG. S1.22. Illustration of characters 71 and 72. **A**, foramen orbito-nasale formed without contribution of vomer, and with contribution of maxilla (*Sternotherus minor*, FMNH 211696, dorsolateral view of left side of cranium); **B**, foramen orbito-nasale formed with contribution of vomer, and with contribution of maxilla (*Lepidochelys olivacea*, SMNS 11070); **C**, foramen orbito-nasale formed with contribution of vomer, and without contribution of maxilla (*Gopherus polyphemus*, FMNH 211815). Dotted line indicates outline of the foramen orbito-nasale. Note that the jugal and postorbital have been removed in A to enable view of foramen orbito-nasale. Abbreviations: *mx*, maxilla; *pal*, palatine; *pmx*, premaxilla; *prf*, prefrontal; *v*, vomer.

Character optimisation: Unambiguous: *Puppigerus*+++ (0->1), *Chelonia mydas* (1->0), *Gopherus polyphemus* (0->1), Trionychia (0->1), *Brachyopsemys tingitana* (0->1); DELTRAN: *Dermochelys coriacea* (0->1); ACCTRAN: Dermochelyidae (0->1).

Character 72 (new character). Foramen orbito-nasale, contribution of the maxilla: 0 = absent; 1 = present.

Remarks: See remarks for character 71.

Character optimisation: Unambiguous: *Emys orbicularis* (1->0), Testuguria (1->0), total-group Chelidae (1->0); DELTRAN: Xinjiangchelyidae+++ (0->1), *Meiolania planiceps* (0->1); ACCTRAN: *Australochelys*+++ (0->1), Paracryptodira (1->0).

Character 73 (Cadena & Parham (2015): character 54). Quadrate, precolumellar fossa: 0 = absent; 1 = present.

Character optimisation: DELTRAN: *Araripemys barretoi* (0->1), Pelomedusoides (0->1), *Sinemys gamera* (0->1); ACCTRAN: Pleurodira (0->1), crown-group Chelidae (1->0), (*Sinemys lens* + *Sinemys gamera*) (0->1).

Character 74 (Cadena & Parham (2015): character 53). Quadrate, development of the cavum tympani: 0 = shallow, but not developed anteroposteriorly; 1 = shallow, but anteroposteriorly developed; 2 = deep and anteroposteriorly developed.

Character optimisation: DELTRAN: (*Eileanchelys* + *Kayentachelys*)+++ (0->2), *Australochelys africanus* (0->1); ACCTRAN: *Australochelys*+++ (0->1), (*Eileanchelys* + *Kayentachelys*)+++ (1->2).

Character 75 (new character). Quadrate, anterior margin of the cavum tympanum: 0 = formed entirely by the quadrate; 1 = formed by the quadratojugal, which overlaps the lateral surface of the quadrate, reaching the anterior margin of the cavum tympanum.

Remarks: The cavum tympanum is present in turtles placed more crownwardly than *Proganochelys*. The cavum tympanum is a funnel shaped, laterally open cavity of the middle ear that in life is covered by a tympanic membrane. In turtles, the cavum typamum is located on the lateral surface of the quadrate, and the margin of the cavum is often formed by that bone. In sinemydids, chelydrids (e.g. *Macrochelys*: FMNH 22111), kinosternoids (e.g. *Sternotherus minor*: FMNH 211696), crown-Trionychia (but not *Adocus beatus*: CM 60-15), most chelonioids (but *Natator*: R112123; *Desmatochelys lowii*: KUVP 1200; protostegids), the quadratojugal extends posteriorly far along the quadrate, and overlaps the quadrate laterally. In these taxa, the anterior margin, but often also parts of the ventral and dorsal margin of the cavum tympanum, are formed by the quadratojugal.

Character optimisation: Unambiguous: Cryptodira (0->1), (*Ocepechelon* ++ *Santanachelys*) (1->0), *Natator depressus* (1->0), *Platysternon megacephalum* (1->0), (*Testudo* + *Chelonoidis*) (1->0), *Jurassichelon oleronensis* (0->1), *Judithemys sukhanovi* (0->1), (*Xinjiangchelys wusu* + *Xinjiangchelys radiplactoides*) (0->1), *Eubaena cephalica* (0->1), *Meiolania planiceps* (0->1); DELTRAN: *Santanachelys gaffneyi* (0->1); ACCTRAN: (*Santanachelys* + *Notochelone*) (0->1).

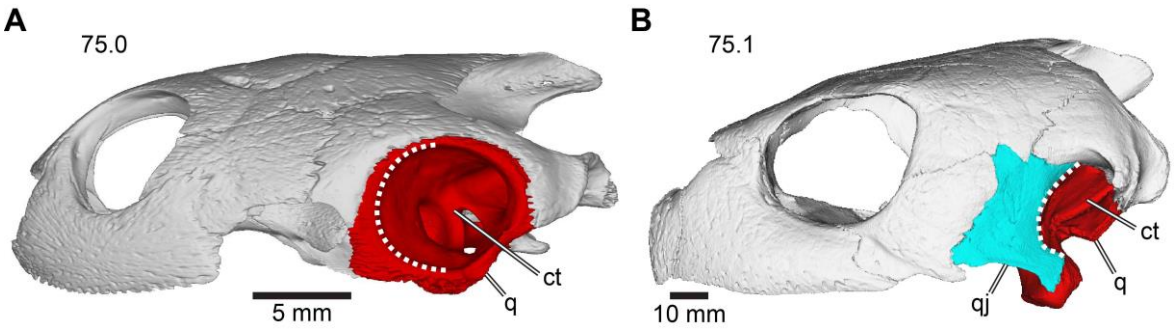


FIG. S1.23. Illustration of character 75. **A**, state 0 (*Podocnemis unifilis*, FMNH 45657, left lateral view of cranium); **B**, state 1 (*Lepidochelys olivacea*, SMNS 11070). Dotted line indicates anterior margin of the cavum tympanum. Abbreviations: *ct*, cavum tympanum; *q*, quadrate; *qj*, quadratojugal.

Character 76 (modified from Zhou & Rabi (2015)). Quadrate, antrum postoticum: 0 = absent; 1 = incipient, the antrum postoticum is completely formed within quadrate (irrespective of the elements involved in forming the margin of the cavum tympanum); 2 = antrum postoticum fully developed, and extending posterodorsally into the squamosal (i.e.

there is a large posterodorsal fenestra in the quadrate that leads to a pocket within the squamosal). This character is scored as inapplicable for turtles without a cavum tympanum.

Previous definition (Cadena & Parham (2015): character 55): Quadrate, antrum postoticum: 0 = absent; 1 = present, quadrate does not fully enclose the anterior perimeter of the antrum; 2 = present, quadrate fully encloses the anterior perimeter of the antrum. Joyce (2007: ch 35, Quadrate E), Sterli & De la Fuente (2013: ch 53, Antrum postoticum A).

Remarks: My new character definition captures variation in the depth of the antrum postoticum, a posterodorsal extension of the cavum tympanum observed in many turtles.

In some taxa, the antrum postoticum is not developed at all (state 0). This is the case in some primitive turtles with a cavum tympanum, such as *Australochelys africanus* (BP/1/4933), but also in the crown-group turtle *Carettochelys insculpta* (see Fig. S1.24*a*). In other taxa, the antrum postoticum is a small posterodorsal concavity that is entirely contained within the quadrate (state 1; e.g. *Chelonoidis* sp.: SMF 67582). In yet other taxa, the antrum postoticum is a deeper pocket that extends through the quadrate and into the squamosal, irrespective of whether the squamosal forms the posterolateral margin of the cavum tympanum or not (state 2). To illustrate state 2, I show *Sternotherus minor* (FMNH 211696) with the squamosal removed in Fig. S1.24*d*, exposing a posterodorsal opening in the quadrate through which the antrum postoticum extends into the squamosal.

A similar character was previously used by Sterli (2008: ch 36), Anquetin (2012: ch 51), and Zhou & Rabi (2015: ch 52). Here, I employ a modified character state definition broadly following the definition of Zhou & Rabi (2015). I modify Zhou & Rabi's (2015: ch 52) definition by qualifying the terms 'incipient' and 'fully developed' and use the participation of the squamosal as an indication of a 'fully developed' antrum postoticum. All previous versions of this character refer to character 35 of Joyce (2007) for the history of this character (see also Cadena & Parham (2015): ch 55). However, the character defined by Joyce (2007) primarily refers to the identity of the element forming the posterodorsal margin of

the cavum tympanum: either the squamosal or quadrate. To clearly separate the two independent morphological issues of the relative depth of the antrum postoticum (absent, shallow, deep), and variation in which element forms the posterodorsal margin of the cavum tympanum (squamosum or quadrate), I scored two seprate characters for these observations. My character 40 captures the variation regarding to the identity of the element forming the posterodorsal margin of the cavum tympanum observed by Joyce (2007), whereas this character refers to the relative depth of the antrum postoticum itself.

Character optimisation: Unambiguous: *Bouliachelys suteri* (1->0), *Allopleuron hofmanni* (2->1), Testudinidae (2->1), (*Xinjiangchelys wusu* + *Xinjiangchelys radiplactoides*) (2->1), Pleurosternidae (2->1), *Meiolania planiceps* (2->0); DELTRAN: *Chubutemys*+++ (0->2), (*Desmatochelys lowii* + *Desmatochelys padillai*) (2->1), *Carettochelys insculpta* (2->0), *Allaeochelys libyca* (2->1), *Kayentachelys aprix* (0->1); ACCTRAN: (*Eileanchelys* + *Kayentachelys*)+++ (0->1), *Chubutemys*+++ (1->2), (*Desmatochelys* ++ *Santanachelys*) (2->1), total-group Carettochelyidae (2->0), *Allaeochelys libyca* (0->1).

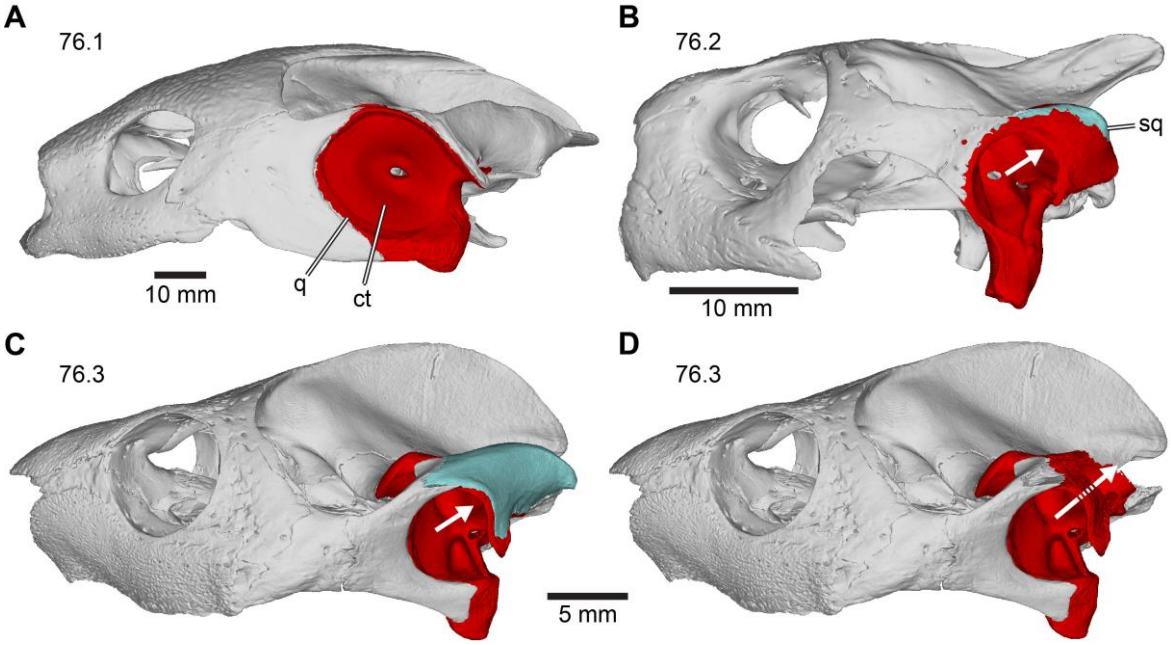


FIG. S1.24. Illustration of character 76. **A**, state 0 (*Carettochelys insculpta*, NHMUK1903.7.10.1, left lateral view of cranium); **B**, state 1 (*Chelonoidis* sp., SMF 67582); **C**, state 2 (*Sternotherus minor*, FMNH 211696); **D**, as C but with squamosal removed. Arrows indicate antrum postoticum. Abbreviations: *ct*, cavum tympanum; *q*, quadrate; *sq*, squamosal.

Character 77 (modified from Cadena & Parham (2015)). Quadrate, incisura columellae auris: 0 = absent, stapes extends posteroventrall to quadrate body; 1 = present, but open posteroventrally; 2 = present and closed, but only enclosing the stapes; 3 = present and closed, enclosing stapes and the Eustachian tube.

Previous character definition (Cadena & Parham (2015): character 56): Quadrates, arrangement between the quadrate, opisthotic, stapes and Eustachian tube: 0 = the quadrate and the opisthotic form an angle of 90 degrees in lateral view; 1 = present, but the quadrate and the opisthotic form an angle less than 90 degrees in lateral view; 2 = the quadrate is well developed posteroventrally enclosing only the stapes; 3 = the quadrate is well developed posteroventrally enclosing the stapes and the Eustachian tube; 4 = the quadrate enclosing stapes and the Eustachian tube helped by the posteroventral projection of the squamosal and posterior of the quadratojugal. Modified from Joyce *et al.* (2011: ch 36) & Sterli & De la Fuente (2013: ch 53) (Quadrate F).

Remarks: This character has been modified to only reflect variation in the incisura columella auris. The previous character definition combined several aspects of the morphology of the posterolateral region of the skull in a single character complex. For example, the arrangement between quadrate and opisthotic is referred to in two character states of the original character definition (Cadena & Parham (2015): character 56 states 0 and 1), but none of the others. Additionally, these character states were described in lateral view, although the opisthotic is not visible in lateral views of turtle skulls.

Cadena & Parham (2015) cite Joyce (2007: ch 36) for the history of this character. My modified character definition above is close to the original definition by Joyce (2007). However, the first character state has been simplified to “absent, stapes extends posteroventrally to quadrate body”, compared to “absent, stapes articulates along the medial side of the quadrate” in Joyce (2007: ch 36, p. 21). This was done because some stem turtles such as *Australochelys africanus* (BP/1/4933) lack an incisura columella auris, but also lack

an articulation facet for the stapes on the quadrate (Gaffney & Kitching 1994, 1995). An additional character has been added (character 86) for the articulation of the stapes with the quadrate or a tympanic membrane, which captures the variation between *Australochelys* (BP/1/4933) and more basal stem-turtles, such as *Proganochelys*. Another character has been added (character 78) that captures the variation observed in regard to elements involved in the formation of the incisura columella auris (i.e. quadrate-only, or other elements involved). The latter character captures some of the variation included in character states 3 and 4 of the original character definition of character 56 of Cadena & Parham (2015), so that this observed variation is not entirely deleted from this matrix, but simply considered in a separate character.

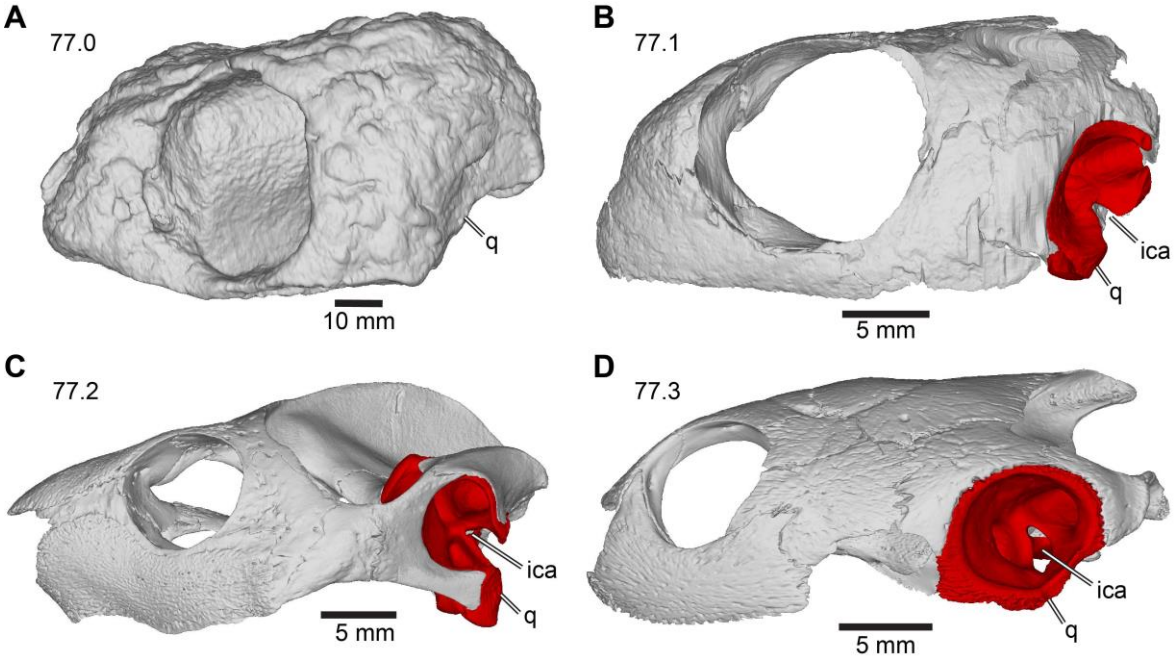


FIG. S1.25. Illustration of character 77. **A**, state 0 (*Australochelys africanus*, BP/1/4933, left lateral view of cranium); **B**, state 1 (*Rhinochelys cantabrigiensis*, CAMSM B55783); **C**, state 2 (*Sternotherus minor*, FMNH 211696); **D**, state 3 (*Podocnemis unifilis*, FMNH 45657). Abbreviations: *ica*, incisura columella auris; *q*, quadrate.

Character optimisation: Unambiguous: (*Eileanchelys* + *Kayentachelys*)+++ (0->1), crown-group Chelydridae (1->2), *Platysternon megacephalum* (1->2), Testudinidae (1->2), Trionychia (1->2), (*Sandownia* + *Leyvachelys*) (1->2), (*Sinemys lens* + *Sinemys gamera*) (1->2), *Meiolania planiceps* (1->3); DELTRAN: *Sternotherus* (1->2), *Staurotypus* (1->2), crown-group Chelidae (1->3), Pelomedusoides (1->3); ACCTRAN: Kinosternidae (1->2), *Kinosternon suburum hippocrepis* (2->1), Pleurodira (1->3), *Araripemys barretoi* (3->1).

Character 78 (new character). Quadrate, formation of incisura columella auris: 0 = formed exclusively by quadrate; 1 = formed by quadrate and squamosal and/or quadratojugal.

Remarks: This character has been split from the character 56 of Cadena & Parham (2015), and reflects variation in the formation of the incisura columella auris that was previously captured by character states 3 and 4 of the original character definition. See remarks for character 77 for further discussion.

In my matix, *Meiolania planiceps* is currently the only taxon scored for the derived condition, but I keep this character as its distribution might be more widespread among taxa currently not considered in my matrix.

Character optimisation: Unambiguous: *Meiolania planiceps* (0->1).

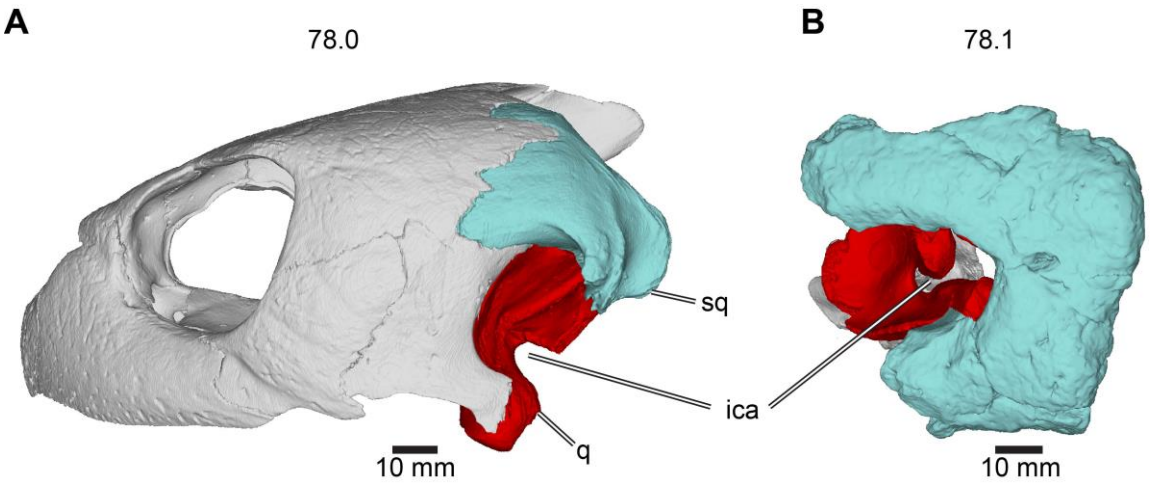


FIG. S1.26. Illustration of character 78. **A**, state 0 (*Lepidochelys olivacea*, SMNS 11070, left lateral view of cranium); **B**, state 1 (*Meiolania planiceps*, NHMUK R 682, left lateral view of otic capsule). Abbreviations: *ica*, incisura columella auris; *q*, quadrate; *sq*, squamosal.

Character 79 (Cadena & Parham (2015): character 57). Quadrate, processus trochlearis oticum: 0 = absent; 1 = present, very reduced; 2 = present, large forming a well defined musculatory facet.

Character optimisation: Unambiguous: *Chubutemys*+++ (0->1), Angolachelonia+++ (1->2), (*Chelonia* + *Natator*) (2->1), *Allopleuron hofmanni* (2->1), *Eochelone* (2->1), total-group

Dermatemydidae (2->1), Pleurodira (2->0), *Kirgizemys dmitrievi* (1->2), *Kallokibotion bajazidi* (1->2); DELTRAN: *Dermochelys coriacea* (2->1), *Emys orbicularis* (2->1), *Platysternon megacephalum* (2->1), Testudinidae (2->1); ACCTRAN: Dermochelyidae (2->1), Testudinoidea (2->1), *Chrysemys picta* (1->2), *Geoclemys hamiltonii* (1->2).

Character 80 (Cadena & Parham (2015): character 58). Quadrate, contribution to the musculatory facet of the processus trochlearis oticum: 0 = extensive contribution; 1 = small contribution, facet formed principally by the protic and/or parietal. This character is scored as inapplicable when a processus trochlearis oticum is absent (ch 79.0).

Character optimisation: Unambiguous: Trionychidae (0->1), *Ordosemys* sp. IVPP V12092 (0->1); DELTRAN: *Protostega gigas* (0->1), *Puppigerus camperi* (0->1), *Allopleuron hofmanni* (0->1), *Pleurosternon bullockii* (0->1); ACCTRAN: (*Protostega* + *Archelon*) (0->1), *Allopleuron*+++ (0->1), crown-group Cheloniidae (1->0), Pleurosternidae (0->1).

Character 81 (new character). Quadrate, width of processus trochlearis oticum: 0 = the otic process spans all the mediolateral space between the braincase wall and the lateral surface of the skull; 1 = the otic process is limited to the medial part of the otic chamber, and there is a deep recess laterally. This character is scored as inapplicable when a processus trochlearis oticum is absent (ch 79.0).

Remarks: There is considerable variation associated with the trochlear process on the otic capsule. I have noticed that the otic process occupies the entire transverse width of the otic capsule in some taxa, therefore extending from the lateral wall of the braincase to the medial surface of the lateral elements of the skull, which form the temporal region. For example, this is the case in all testudinoids considered in my matrix, sandownids, chelydrids, as well as paracryptodires and stem-turtles that have an otic trochlear mechanism (e.g. *Eileanchelys waldmanni*: NMS.G.2004.31.15; *Kallokibotion bajazidi*: NHMUK R 4921). Other taxa (e.g. *Plesiochelys planiceps*: OUMNH J1582) have a prominent otic trochlear process that is

restricted to the medial part of the otic chamber, producing a deep recess that separates the process from the temporal skull wall. However, the systematic distribution of this character is homoplastic, as various kinosternoids, chelonioids, sinemydids, xinjiangchelyids, macrobaenids, and plesiochelyids show either condition.

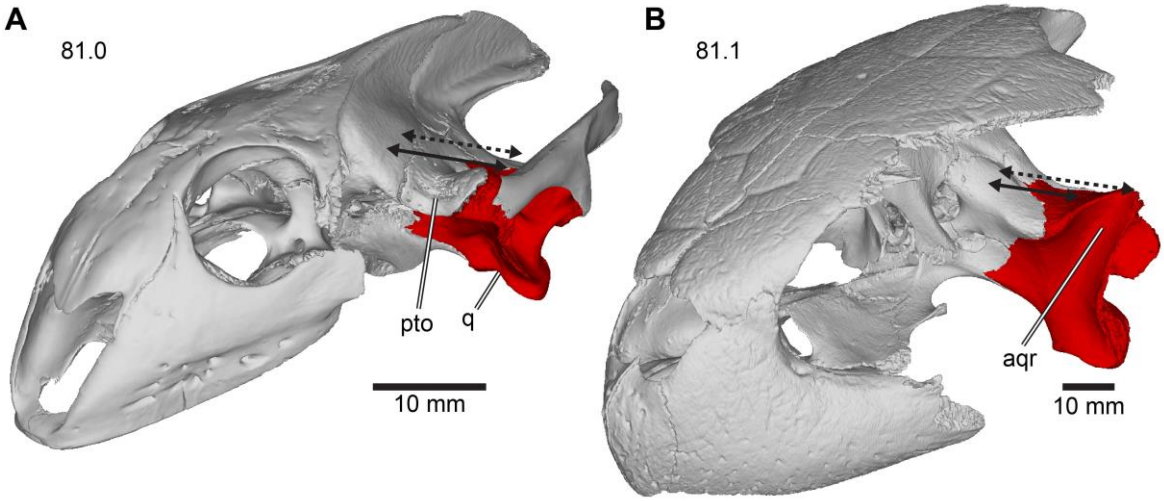


FIG. S1.27. Illustration of character 81. **A**, state 0 (*Apalone spinifera emoryi*, FMNH 22178, left anterodorsolateral view of cranium); **B**, state 1 (*Lepidochelys olivacea*, SMNS 11070). Solid arrows indicate mediolateral width of processus trochlearis oticum; dashed arrow indicates mediolateral width of supratemporal fossa. Note that the jugal, postorbital and quadratojugal have been removed in A and B, and additionally the squamosal in B. Abbreviations: *aqr*, anterior quadrate recess; *pto*, processus trochlearis oticum; *q*, quadrate.

Character optimisation: Unambiguous: *Argillochelys*+++ (0->1), total-group Chelydridae (0->1), *Staurotypus* (0->1), Thalassochelydia (0->1), *Jurassichelon oleronensis* (1->0), (*Ordosemys* + *Dracochelys*) (0->1), *Annemys* sp. IVPP V18106 (0->1); DELTRAN: (*Desmatochelys* ++ *Santanachelys*) (0->1), *Notochelone* (1->0); ACCTRAN: Protostegidae (0->1), (*Santanachelys* + *Notochelone*) (1->0).

Character 82 (Cadena & Parham (2015): character 59). Quadrate, quadrate-basisphenoid contact: 0 = absent; 1 = present.

Character optimisation: Unambiguous: *Chelodina* (0->1), Pelomedusoides (0->1).

Character 83 (modified from Anquetin *et al.* 2015). Quadrate, infolding ridge on the posterior surface of the quadrate ventral to the incisura columella auris: 0 = absent; 1 = present.

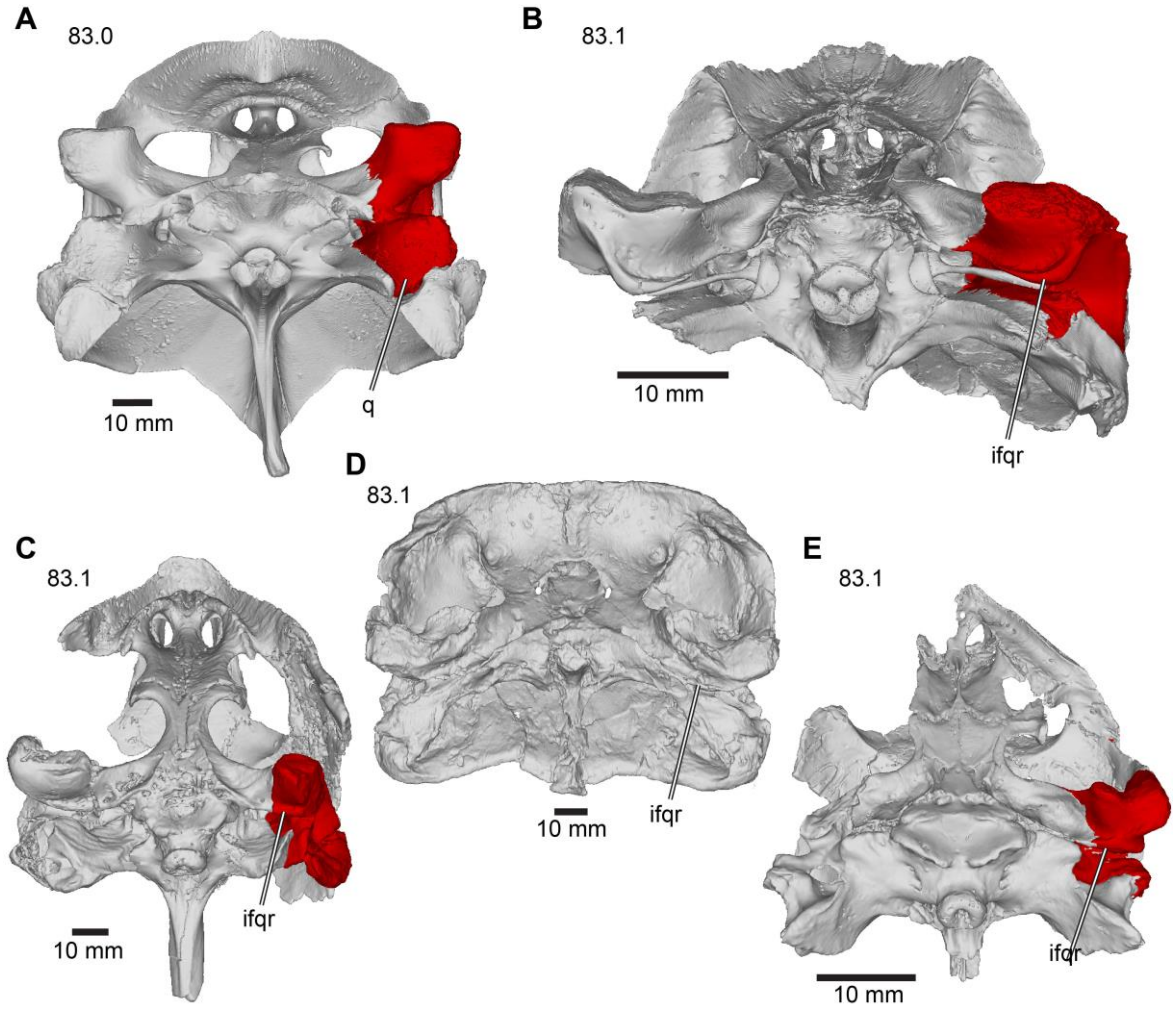


FIG. S1.28. Illustration of character 83. **A**, state 0 (*Lepidochelys olivacea*, SMNS 11070, posteroventral view of cranium); **B**, state 1 (*Solnhofia parsoni*, TM 4023, cranium horizontally reflected); **C**, state 1 (*Brachyopsemys tingitana*, AMNH 30612); **D**, state 1 (*Bouliachelys suteri*, QMF 31669); **E**, state 1 (*Ordosemys* sp., IVPP V12092, cranium horizontally reflected). Abbreviations: *ifqr*, infolding ridge of quadrate; *q*, quadrate.

Remarks: This character is taken from Anquetin *et al.* (2015: character 37, Quadrate G). These authors first noted that in some turtles (thalassochelydians), the quadrate produces a shelf of bone that projects posteriorly from the articular process. The shelf forms the ventral portion of the incisura columella auris with its lateral part. Medially, it curves around the posterior surface of the articular process of the quadrate, and into the cavum acustico-jugulare. Here, it meets the posterolateral process of the pterygoid. The posterior margin of the shelf is ventrally curved, leading Anquetin *et al.* (2015) to name this feature the "infolding ridge", which is adopted here.

However, while Anquetin *et al.* (2015) regard the infolding ridge of the quadrate as a feature unique to thalassochelydians (confirmed here for *Solnhofia:* TM 4023, *Plesiochelys* spp.*:* OUMNH J1582; MNB 435; *Jurassichelon oleronensis*: PIMUZ A III 514) I also find it in sandownids (*Sandownia*: MIWG 3480, *Brachyopsemys:* AMNH 30612; *Leyvachelys cipadi*: e.g. SMU 74983; Vineyard 2009). Additionally, I also found an infolding ridge in *Ordosemys* sp. (IVPP V12092), and *Bouliachelys suteri* (QMF 31669). However, the ridge does not seem to be present in other sinemydids or protostegids.

I observed some variation in the development of the infolding ridge of the quadrate. The ridge is a very large, laminar process in thalassochelydians such as *Solnhofia parsoni* (TM 4023), whereas it is a less conspicuous structure in most of the taxa I additionally score as having such a ridge (e.g. *Sandownia harrisi*: MIWG 3480), but also in *Portlandemys mcdowelli* (NHMUK R 2914).

Character optimisation: Unambiguous: *Bouliachelys suteri* (0->1), Angolachelonia (0->1), *Ordosemys* sp. IVPP V12092 (0->1).

Character 84 (new character). Quadrate, direction of cranial articular process: 0 = ventrolaterally directed; 1 = with strong posterior inclination.

Remarks: In thalassochelydians (e.g. *Solnhofia:* TM 4023, *Plesiochelys* spp.*:* OUMNH J1582; MNB 435; *Jurassichelon oleronensis*: PIMUZ A III 514) and sandownids (e.g. *Sandownia*: MIWG 3480, *Brachyopsemys:* AMNH 30612), the articular processes of the quadrate are strongly posterolaterally direceted from the skull midline, whereas in most other turtles, the articular processes are laterally directed.

Character optimisation: Unambiguous: *Allopleuron hofmanni* (0->1), *Macrochelys temminckii* (0->1), Angolachelonia (0->1), *Kayentachelys aprix* (0->1).

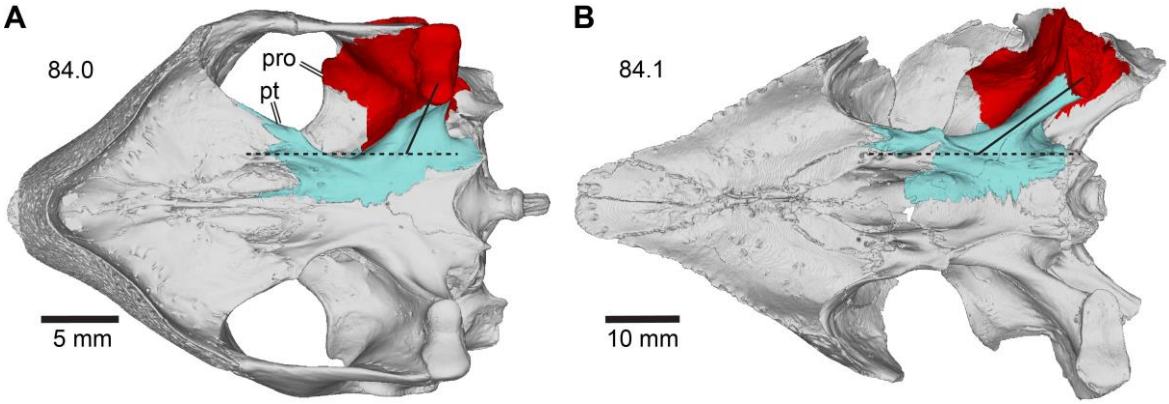


FIG. S1.29. Illustration of character 84. **A**, state 0 (*Sternotherus minor*, FMNH 211696, ventral view of cranium); **B**, state 1 (*Solnhofia parsoni*, TM 4023). Dotted lines indicate a parasagittal plane and solid lines indicate angle with which the articular process diverges from this plane. Abbreviations: *pro*, prootic; *pt*, pterygoid.

Character 85 (modified from Havlik *et al.* 2014). Posterior quadrate fossa: 0 = absent; 1 = present.

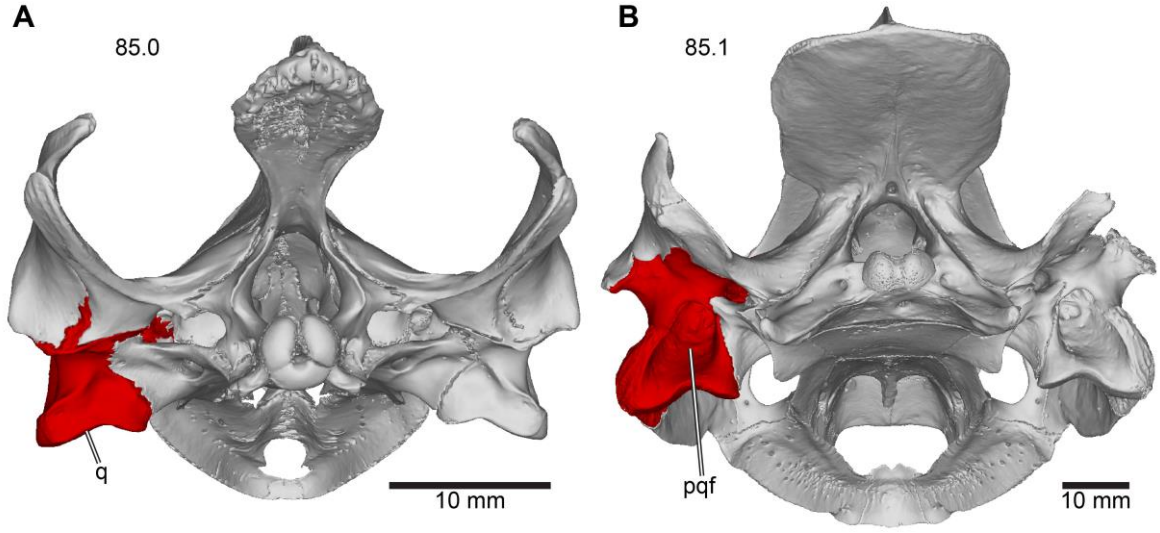


FIG. S1.30. Illustration of character 85. **A**, state 0 (*Apalone spinifera emoryi*, FMNH 22178, posteroventral view of cranium); **B**, state 1 (*Carettochelys insculpta*, NHMUK1903.7.10.1). Abbreviations: *pqf*, posterior quadrate fossa; *q*, quadrate.

Remarks: Pancarettochelyids (e.g. *Allaeochelys libyca*: BSPG 1991 II 130; *Carettochelys insculpta*: NHMUK 1903.7.10.1) have a shallow or deep fossa on the posterior surface of the articular surface of the quadrate. The character used herein is a modified version of character 137 of Havlik *et al.* (2014). I modified the original character of Havlik *et al.* (2014) to a simple presence-absence character. This is for two reasons: First, I believe that the shared presence of the posterior quadrate fossa is information that should be coded in a separate character

that does not include further gradational states of the depth of the fossa. Secondly, I refrain from using such a second character here, because I use few pancharettochelyids in this study and the ingroup relationships of this clade is not of further interest here.

Character optimisation: Unambiguous: total-group Carettochelyidae (0->1).

Character 86 (new character). Stapes, lateral articulation: 0 = stapes articulates with medial surface of the quadrate, quadrate has stapedial pit; 1 = stapes articulates with tympanic membrane, pit on medial surface of quadrate is absent.

Remarks: This character is included in order to capture additional variation in the arrangement of the stapes. Character 77 describes the absence vs. presence of an incisura columella auris. However, in some taxa lacking an incisura columella auris, such as *Australochelys*, the stapes does not articulate with the quadrate but with a tympanic membrane (Gaffney & Kitching 1994, 1995), whereas the quadrate in *Proganochelys* has a pit for the articulation of the stapes (Gaffney 1990).

Character optimisation: DELTRAN: *Australochelys*+++ (0->1); ACCTRAN: *Australochelys*+++ (0->1).

Character 87 (modified form Cadena & Parham (2015)). Epipterygoid: 0 = present; 1 = absent.

Previous definition (Cadena & Parham (2015): character 60): Epipterygoids: 0 = present, rod like; 1 = present, laminar; 2 = absent. Joyce *et al.* (2001: ch 37) & Sterli & De la Fuente (2013: ch 57) (Epipterygoid A).

Remarks: I score the presence and absence of an epipterygoid, and the shape of an epipterygoid if present as separate characters, as done in the study of Anquetin (2012). I chose this coding pattern, because the shared presence of an epipterygoid is parsimony informative.

Character optimisation: Unambiguous: (*Desmatochelys* ++ *Santanachelys*) (0->1), *Puppigerus*+++ (0->1), Pleurodira (0->1), *Eubaena cephalica* (0->1); DELTRAN: *Dermochelys coriacea* (0->1); ACCTRAN: Dermochelyidae (0->1).

Character 88 (modified form Cadena & Parham (2015)). Epipterygoid, shape: 0 = rod-like element; 1 = laminar element. This character is scored as inapplicable if an epipterygoid is absent (ch 87.1).

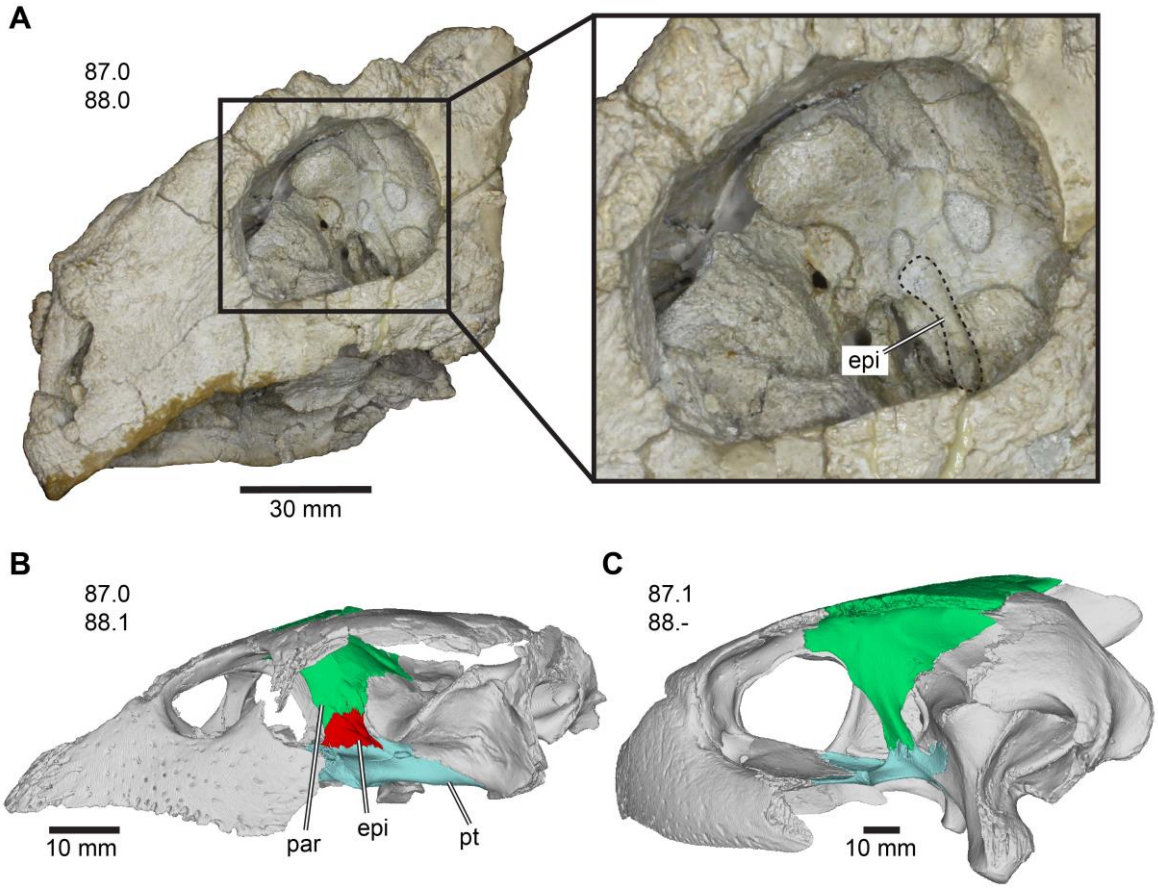


FIG. S1.31. Illustration of characters 87 and 88. **A**, *Proganochelys quenstedti* (SMNS 15759, left lateral view of cranium with boxed close-up); **B**, *Solnhofia parsoni* (TM 4023); **C**, *Lepidochelys olivacea* (SMNS 11070, posteroventral view of cranium). Dotted line in close-up of A shows outline of the epipterygoid. Abbreviations: *epi*, epipterygoid; *par*, parietal; *pt*, pterygoid.

Previous definition (Cadena & Parham (2015): character 60): Epipterygoids: 0 = present, rod like; 1 = present, laminar; 2 = absent. Joyce *et al.* (2001: ch 37) & Sterli & De la Fuente (2013: ch 57) (Epipterygoid A).

Remarks: See remarks of character 87.

Character optimisation: Unambiguous: *Annemys latiens* (1->0); DELTRAN: *Meiolania*+++ (0->1); ACCTRAN: *Chubutemys*+++ (0->1).

Character 89 (Cadena & Parham (2015): character 61). Pterygoid, pterygoid teeth: 0 = present; 1 = absent.

Character optimisation: DELTRAN: *Chubutemys*+++ (0->1), *Australochelys africanus* (0->1); ACCTRAN: *Australochelys*+++ (0->1), (*Kayentachelys* + *Eileanchelys*) (1->0).

Character 90 (Cadena & Parham (2015): character 62). Pterygoid, basipterygoid process and basipterygoid articulation: 0 = basipterygoid process present with a movable basiptergoid articulation; 1 = basipterygoid process present with a sutured basipterygoid articulation; 2 = basipterygoid process absent and sutured basipterygoid articulation.

Remarks: Rabi *et al.* (2013) gave a comprehensive overview and discussion of the distribution of the basipterygoid process in turtles. While I largely agree with the assessment given by these authors, I disagree with their recommendation to score *Sandownia harrisi* as not having a basipterygoid process. Rabi *et al.* (2013) argued that the basipterygoid process in *Sandownia* is reduced in size and only visible through the fenestra caroticus. However, even if the basipterygoid process in *Sandownia* is not as clearly ventrally exposed as in some other turtles, it is clearly present as a small laterally projecting boss on the parabasisphenoid (Fig. S1.32*c*). Models derived from my CT scans of MIWG 3480, the holotype and only specimen of *Sandownia harrisi*, show that the process itself and the corresponding pocket in the pterygoid

is morphologically not different from taxa for which Rabi *et al.* (2013) agree the structure is present, such as *Pleurosternon bullockii* (UMZC T1041). Accordingly, I score *Sandownia* as having state 1, *contra* Rabi *et al.* (2013), and *contra* the scoring of Cadena & Parham (2015).

Cadena & Parham (2015) include *Trinitichelys hiatti* as the basalmost baenid in their analysis, and score it as having state 2. *Trinitichelys* is not included in my analysis, but instead I include the more basal *Arundelemys dardeni* (based on CT scan of the specimen USNM 497740). The CT scans and derived models for this specimen show a similar morphology to *Sandownia*: A small lateral process of the parabasisphenoid projects into the pterygoid, but this process is not entirely visible in a ventral view of the cranium as it is surrounded by bone of the pterygoid. Therefore, I also score *Arundelemys* as having state 1. However, CT scans of more derived baenids (e.g. *Eubaena cephalica*: DMNH 96004) show that the basipterygoid process is absent in these taxa. My results are only partially consistent with those of Rabi *et al.* (2013), who report that all baenids have lost this structure, whereas I find the structure to be present at least in the basalmost member considered in this study.

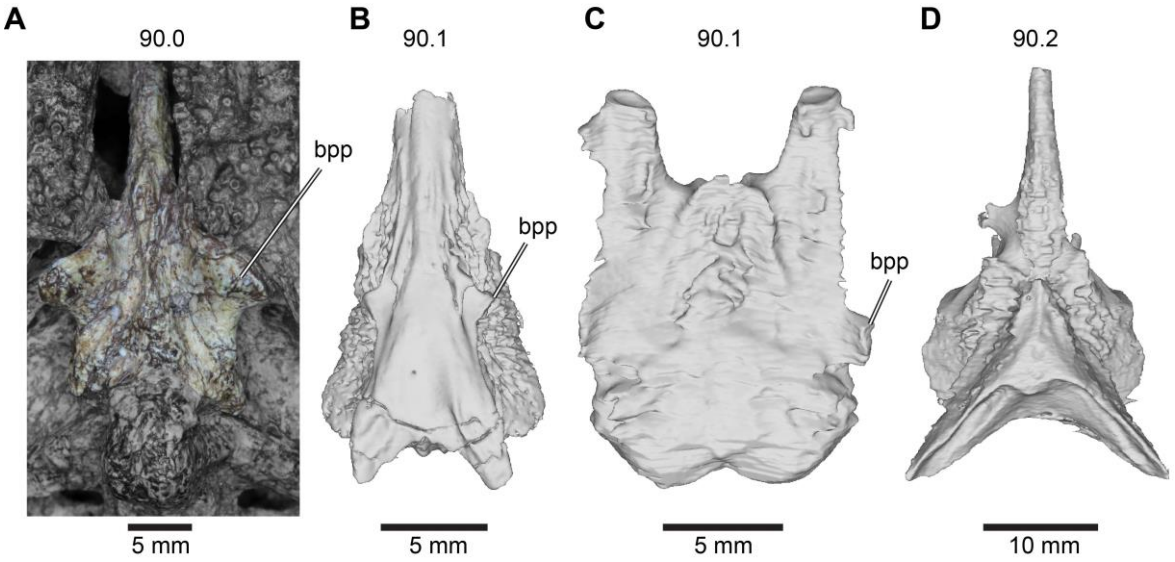


FIG. S1.32. Illustration of character 90. **A**, state 0 (*Proganochelys quenstedti*, SMNS 16980, ventral view of parabasisphenoid area); **B**, state 1 (*Pleurosternon bullockii,* UMZC T1041, parabasisphenoid in ventral view); **C**, state 1 (*Sandownia harrisi*, MIWG 3480); **D**, state 2 (*Lepidochelys olivacea*, SMNS 11070). Note that the parabasisohenoid in A is shown in colour, and surrounding bones are shown in grey. Abbreviations: *bpp*, basipterygoid process.

Character optimisation: Unambiguous: Testudines (1->2), *Solnhofia parsoni* (1->2), (*Plesiochelys etalloni* + *Plesiochelys planiceps*) (1->2), *Judithemys sukhanovi* (1->2), *Eubaena*

cephalica (1->2), *Meiolania planiceps* (1->2); DELTRAN: *Australochelys*+++ (0->1); ACCTRAN: *Australochelys*+++ (0->1).

Character 91 (Cadena & Parham (2015): character 64). Pterygoid, pterygoid-basioccipital contact: 0 = absent; 1 = present.

Character optimisation: Unambiguous: *Kallokibotion*+++ (0->1), *Eosphargis breineri* (1->0), *Emys orbicularis* (1->0), Pleurodira (1->0), (*Sinemys lens* + *Sinemys gamera*) (1->0), Xinjiangchelyidae (1->0), *Xinjiangchelys radiplicatoides* (0->1).

Character 92 (Cadena & Parham (2015): character 65). Pterygoid, processus trochelaris pterygoideus: 0 = absent; 1 = present.

Character optimisation: Unambiguous: Pleurodira (0->1).

Character 93 (Cadena & Parham (2015): character 66). Pterygoid, foramen palatinum posterius: 0 = present; 1 = present, but open laterally; 2 = absent.

Character optimisation: Unambiguous: crown-group Chelonioidea (0->2), (*Desmatochelys* ++ *Santanachelys*) (2->1), *Desmatochelys lowii* (1->0), *Allopleuron hofmanni* (2->0), (*Jurassichelon* ++ *Plesiochelys*) (0->1).

Character 94 (Cadena & Parham (2015): character 67). Pterygoid, medial contact of pterygoid: 0 = present, pterygoids in a very long medial contact with one another, longer than the basisphenoid total length in midline; 1 = present, pterygoids in medial contact with one another, contact length equal or shorter than the basisphenoid total length in midline; 2 = absent, contact of the basisphenoid with the vomer and/or palatines present.

Character optimisation: Unambiguous: total-group Chelonioidea (1->0), *Rhinochelys pulchriceps* (0->1), *Dermochelys coriacea* (0->1), crown-group Chelydridae (1->0), *Platysternon megacephalum* (1->0), Trionychia (1->2), *Araripemys barretoi* (1->2), Angolachelonia (1->0), *Jurassichelon oleronensis* (0->1), *Xinjiangchelys radiplicatoides* (1->2), Pleurosternidae (1->2).

Character 95 (Cadena & Parham (2015): character 68). Pterygoid, pterygoid contribution to foramen palatinum posterius: 0 = present; 1 = absent. This character is scored inapplicable when the foramen palatinum posterius is absent (ch. 66.0).

Character optimisation: Unambiguous: (*Rhinochelys* ++ *Santanachelys*) (1->0), *Desmatochelys padillai* (1->0), *Toxochelys latiremis* (1->0), *Apalone spinifera* (1->0), *Solnhofia parsoni* (0->1), *Sandownia harrisi* (0->1), *Chubutemys copelloi* (0->1); DELTRAN: Cryptodira (0->1), *Chelonoidis* sp. (1->0), *Gopherus polyphemus* (1->0), *Araripemys barretoi* (0->1), *Podocnemis* (0->1); ACCTRAN: Testudines (0->1), Testudinidae (1->0), *Testudo* (0->1), crown-group Chelidae (1->0), *Pelomedusa subrufa* (1->0).

Character 96 (Cadena & Parham (2015): character 70). Pterygoid, contact with the exoccipital: 0 = absent; 1 = present.

Character optimisation: Unambiguous: *Meiolania*+++ (0->1), (*Santanachelys* + *Notochelone*) (1->0), Dermochelyidae (1->0), *Sternotherus* (1->0), total-group Dermatemydidae (1->0), Testudinoidea (1->0), Pleurodira (1->0), *Solnhofia parsoni* (1->0), (*Plesiochelys etalloni* + *Plesiochelys planiceps*) (1->0), (*Sinemys lens* + *Sinemys gamera*) (1->0), *Annemys* sp. IVPP V18106 (1->0); DELTRAN: *Kirgizemys dmitrievi* (1->0); ACCTRAN: (*Kirgizemys hoburensis* + *Kirgizemys dmitrievi*) (1->0).

Character 97 (Cadena & Parham (2015): character 71). Pterygoid, fossa podocnemidoidea or cavum pterygoidei: 0 = absent; 1 = present.

Character optimisation: Unambiguous: *Podocnemis* (0->1).

Character 98 (modified from Cadena & Parham (2015)). Pterygoid, lateral margin: 0 = a processus pterygoideus externus is developed as a process that projects into the subtemporal fenestra; 1 = the lateral margin of the pterygoid is gently expanded laterally and/or expanded dorsoventrally; 2 = absent, i.e. the lateral margin of the pterygoid forms a straight or concave outline that forms the medial margin of the subtemporal fenestra. Scored inapplicable for pleurodires.

Previous definition (Cadena & Parham (2015): character 72): Pterygoids, processus pterygoideus externus: 0 = large, forming an extensive lateral wing; 1 = reduced, forming an acute tip; 2 = extremely reduced due to the posterolateral projection of the pterygoid; 3 = absent. Modified from Parham & Pyenson (2010: ch 11); Hirayama (1998), KL, & Bardet *et al.* (2013: ch 22); Sterli & De la Fuente (2013: ch 70, Pterygoid L). Ordered.

Remarks: I scored variation regarding the processus pterygoideus externus in two separate characters (ch 98 and ch 99), because I think that the variation described by character 72 of Cadena & Parham (2015) combines variation that concerns the absence versus presence of an external pterygoid process that projects laterally off the margin of the subtemporal fenestra, and variation among turtles that have such a process.

This first character distinguishes between three possible states regarding the morphology of the lateral margin of the pterygoid, which forms the medial margin of the subtemporal fenestra. In some turtles (see Fig. S1.33), the lateral margin of the pterygoid is strongly expanded to a form a process, the processus pterygoideus externus, that projects into the subtemporal fenestra (state 0). Variation among turtles with this condition is considered in character 99. In other turtles, such as sandownids, *Solnhofia parsoni* (TM4023) and trionychians, a laterally projecting processus pterygoideus externus is absent, but the lateral margin of the pterygoid is gently expanded in the topological position where the process would be expected (state 1). The third state describes the condition seen in Late Cretaceous protostegids, dermochelyids, as well as *Chelonia mydas* (NHMUK 1969.776), in which a processus pterygoideus externus or any thickening in its usual position along the pterygoid margin is entirely absent, and the margin of ther pterygoid is straight or concave.

I disagree with some scorings of Cadena & Parham (2015). For example, *Caretta caretta* was scored as state 1 in Cadena & Parham (2015: ch 72; equivalent to the character combination 98.0 and 99.2). However, in *Caretta* (NHMUK 1938.1.9.1), the lateral margin of the pterygoid is gently expanded laterally in addition to having to dorsoventral expansion

forming a shallow vertical sheet along the pterygoid margin. According to my character scheme, this is scored as the combination 98.1 and 99.- (inapplicable).

Character optimisation: Unambiguous: *Caretta caretta* (0->1), *Chelonia mydas* (0->2), *Sternotherus* (0->1); DELTRAN: (*Protostega* + *Archelon*) (0->2), Dermochelyidae (0->2), Trionychia (0->1), *Solnhofia parsoni* (0->1), Sandownidae (0->1); ACCTRAN: Angolachelonia+++ (0->1), Durocryptodira (1->0), Dermochelyoidea (0->2), (*Ocepechelon* ++ *Santanachelys*) (2->0), (*Portlandemys* ++ *Plesiochelys*) (1->0).

Character 99 (modified from Cadena & Parham (2015)). Pterygoid, processus pterygoideus externus: 0 = forming an extensive process that contacts the maxilla anterolaterally at the posteromedial end of the triturating surface, is anteriorly sutured to the anterior palate, and has a posterior projection into the subtemporal fenestra; 1 = forming a large lateral wing that projects as a free process into the subtemporal fenestra; 2 = forming a pointed triangular process that projects laterally into the subtemporal fenestra. Scored inapplicable for taxa that lack a processus pterygoideus externus (i.e. ch 98.1 or 98.2)

Previous definition (Cadena & Parham (2015): character 72): Pterygoids, processus pterygoideus externus: 0 = large, forming an extensive lateral wing; 1 = reduced, forming an acute tip; 2 = extremely reduced due to the posterolateral projection of the pterygoid; 3 = absent. Modified from Parham & Pyenson (2010: ch 11); Hirayama (1998), KL, & Bardet *et al.* (2013: ch 22); Sterli & De la Fuente (2013: ch 70, Pterygoid L). Ordered.

Remarks: This character captures the variation associated with the external pterygoid process (see also character 98). In my modification of the character definition, I tried to summarise different configurations of this process based on shared similarity. Specifically, I looked at the contacts the external pterygoid process has with other skull elements to differentiate between states that concern “large” processes that project into the subtemporal fenestra. I think that this is more helpful in terms of formulating primary hypotheses of

homology than the previous approach that was used by Cadena & Parham (2015), which is a more qualitative assessment of relative sizes of the process.

My states 0 and 1 effectively represent a distinction between two different types of external pterygoid process that were both previously contained within state 0 of Cadena & Parham (2015: character 72). Turtles scored for either my state 0 or state 1 share that the pterygoid is laterally expanded to a "wing-like" process at its anterior end. However, in turtles scored as having state 0, the anterolateral margin of the pterygoid process contacts the maxilla. Additionally, the pterygoid has a broad transversely oriented suture with the palatine medial to the foramen palatinum posterius, which is posteriorly enclosed by the pterygoid. Therefore, the anterior margin of the external pterygoid process forms the posterior margin of the foramen palatinum posterius, as in most xinjiangchelyids, sinemydids, macrobaenids, as well as some chelonioids (*Allopleuron*: NHMUK R42913; *Toxochelys latiremis*: AMNH 5118), and additionally in *Platysternon megacephalum* (SMF 69684) and *Emys orbicularis* (IW 1154). In these taxa, the external pterygoid process additionally forms a distinct hooked tip that projects posteriorly from the region of contact with the maxilla into the subtemporal fenestra. This projecting tip may be relatively small as in *Platysternon megacephalum* (SMF 69684), or extremely long as in *Dracochelys bicuspis* (IVPP V4075; Gaffney & Ye 1992; Brinkman 2001), and may be expanded dorsoventrally to have a vertical plate (as in *Dracochelys*). Other taxa with state 0 lack this expansion (e.g. *Platysternon*), but the variation associated with the vertical plate is encoded in a separate character (character 100 of this study). The tip-like process of taxa scored as state 0 is superficially similar to the acute tip described in state 2 of the new character description. However, taxa scored for state 2 have this tip on the lateral margin of the pterygoid, rather than on the posterolateral part of an expanded transverse process. This is topologically different and thus scored in a separate state. In my definition of state 0, basal turtles like *Proganochelys* (e.g. SMNS 16980) or *Kayentachelys* (e.g. TMM 43670-2) are also scored as having state 0: In these taxa, the pterygoid is anterolaterally expanded and contacts the

maxilla at the posteromedial end of the triturating surface (Gaffney 1990; Sterli & Joyce 2007; *contra* Gaffney & Jenkins 2010).

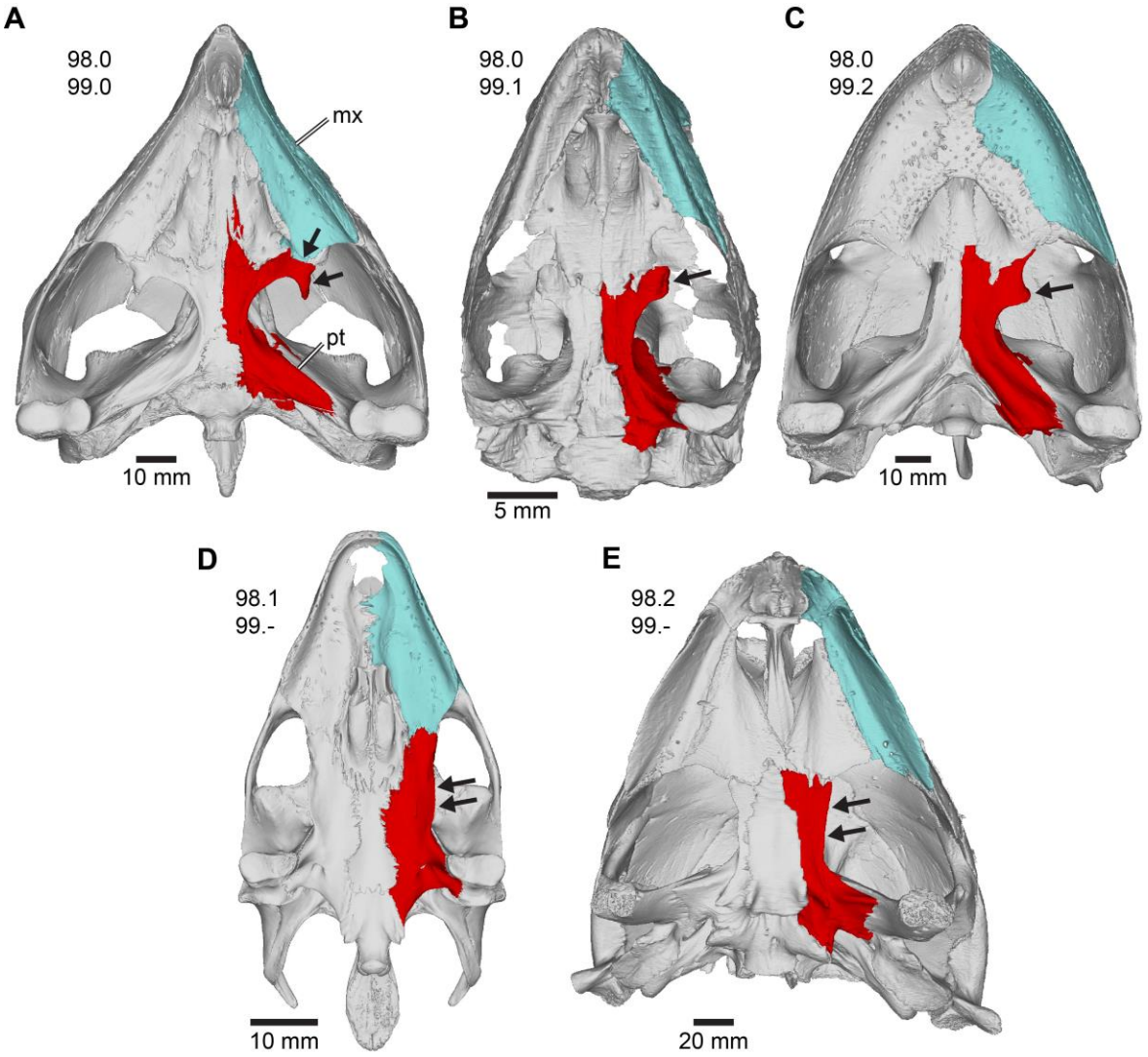


FIG. S1.33. Illustration of characters 98 and 99. **A**, *Macrochelys temminckii* (FMNH 22111, ventral view of cranium); **B**, *Rhinochelys cantabrigiensis* (CAMSM B55783); **C**, *Lepidochelys olivacea* (SMNS 11070); **D**, *Apalone spinifera emoryi* (FMNH 22178); **E**, *Dermochelys coriacea* (UMCZ R 3031). Arrows denote relevant structures of the lateral margin of the pterygoid discussed in the character descriptions and character remarks. Abbreviations: *mx*, maxilla; *pt*, pterygoid.

The morphology described above for taxa scored as state 0 differs from the taxa I scored as state 1. Taxa scored as having state 1 have a pterygoid process that is developed as a free process that projects laterally from the margin of the pterygoid and into the subtemporal fossa. It is thus not integrated into the anterior parts of the palate with its anterior margin, but still forms a relatively large, and "wing-like" process. This character state

is observed in early protostegids (e.g. *Rhinochelys*: CAMSM B55783; but not *Archelon ischryos* or *Protostega gigas*), some thalassochelydians (*Plesiochelys* spp.: OUMNH J 1582, MNB 435; *Jurassichelon oleronensis*: PIMUZ III A 514; but not *Solnhofia parsoni*: TM 4023 or *Portlandemys mcdowelli*: NHMUK R 2914).

State 2 describes taxa in which there is a comparatively small, triangular process projecting from the lateral margin of the pterygoid into the subtemporal fossa. This is not to be confused with the posteriorly directed, tip like process that projects off the transverse process of taxa scored as having state 0 (see above). State 2 is present in many but not all cheloniids, most kinosternids (but *Sternotherus*), and all testudinoids.

Character optimisation: Unambiguous: *Desmatochelys padillai* (1->2), *Toxochelys latiremis* (2->0), crown-group Chelydridae (2->0), (*Jurassichelon* ++ *Plesiochelys*) (0->1), *Ordosemys* sp. IVPP V12092 (0->2); DELTRAN: Durocryptodira (0->2), (*Ocepechelon* ++ *Santanachelys*) (2->1); ACCTRAN: Testudines (0->2), Dermochelyoidea (2->1).

Character 100 (modified from Cadena & Parham (2015)). Pterygoid, vertical flange on anterolateral margin of the pterygoid: 0 = absent; 1 = present. Zhou *et al.* (2014) & Joyce (2007: ch 67) (Pterygoid I).

Previous definition (Cadena & Parham (2015): character 69): Pterygoid, vertical flange on processus pterygoideus externus: 0 = absent; 1 = present. Zhou *et al.* (2014) & Joyce (2007: ch 67) (Pterygoid I).

Remarks: I modified the wording of this character from "processus pterygoideus externus" to "anterolateral margin of the pterygoid" because I also modified the characters related to the processus pterygoideus externus (see character 98). In my coding scheme, I differentiate between a 'true' processus pterygoideus externus, i.e. a lateral projection on the lateral margin of the pterygoid, and other morphologies of this lateral margin (see character 98). However, even taxa in which a 'true' lateral process is absent, a lateral flange on the pterygoid

margin may occur (e.g. some trionychids, such as *Apalone spinifera emoryi*: FMNH 22178), necessitating the changes adopted here for this character.

Character optimisation: Unambiguous: Paracryptodira+++ (0->1), *Lepidochelys olivacea* (1->0), *Chelonia mydas* (1->0), *Platysternon megacephalum* (1->0), *Testudo* (1->0), *Lissemys punctata* (1->0), *Solnhofia parsoni* (1->0); DELTRAN: *Kinosternon suburum hippocrepis* (1->0), *Staurotypus* (1->0); ACCTRAN: Kinosternidae (1->0), *Sternotherus* (0->1).

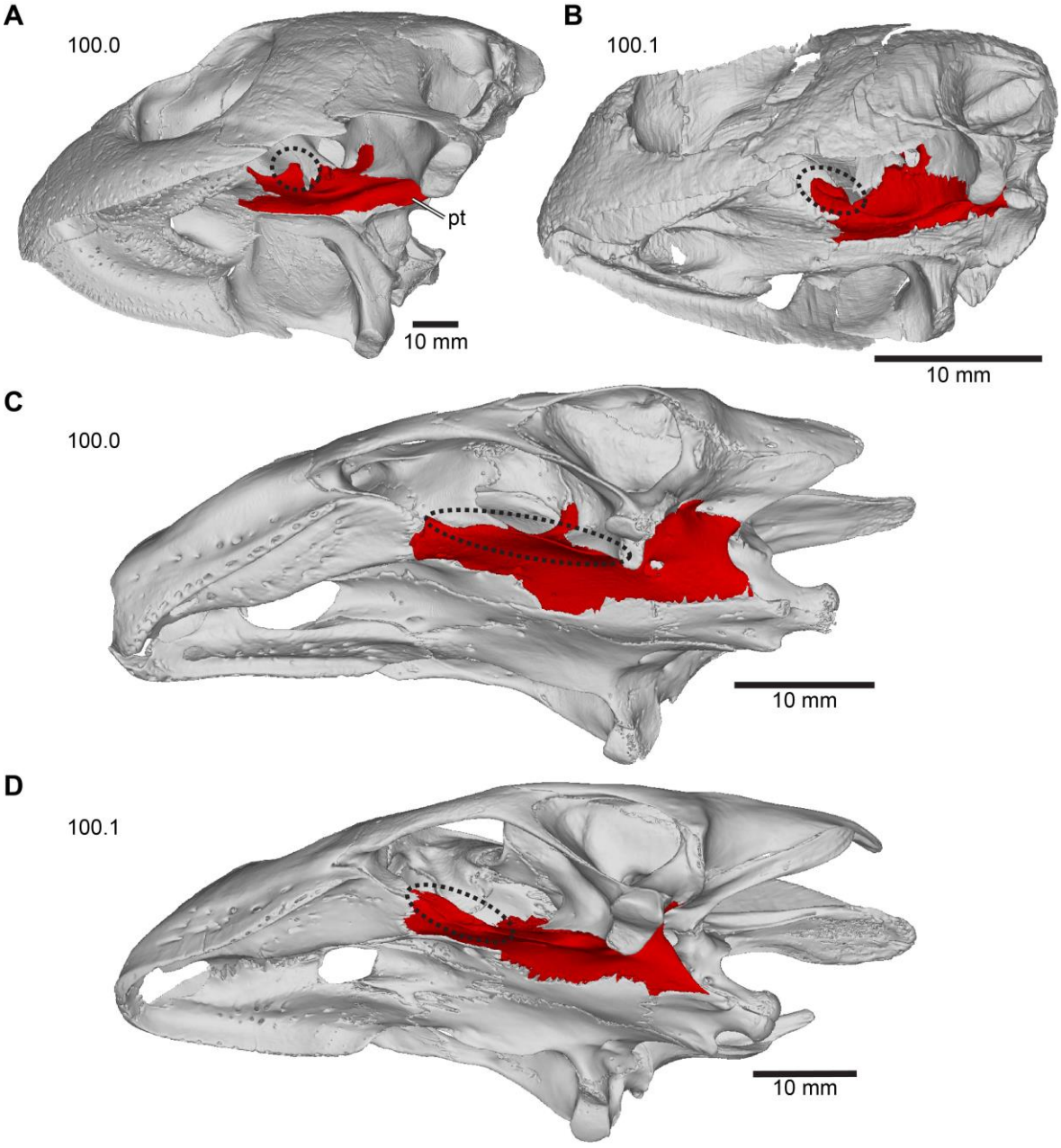


FIG. S1.34. Illustration of character 100. **A**, state 0 (*Lepidochelys olivacea,* SMNS 11070, left lateroventral view of cranium); **B**, state 1 (*Rhinochelys cantabrigiensis*, CAMSM B55783); **C**, state 0 (*Lissemy punctatas*, SMF 74141); **D**, state 1 (*Apalone spinifera emoryi*, FMNH 22178). Dotted lines circumscribe the lateral margin of the pterygoid, which can be vertically expanded (state 1). Not that A-B and C-D represent comparisons between close relatives with different character states. Abbreviations: *pt*, pterygoid.

Character 101 (Cadena & Parham (2015): character 73). Pterygoid, level of the position of the pterygoid respect to basisphenoid: 0 = both bones are at the same level on ventral surface; 1 = two different levels, creating a step between the two bones.

Character optimisation: Unambiguous: *Eosphargis breineri* (0->1), *Argillochelys*+++ (0->1), *Chelonia mydas* (1->0), *Platysternon megacephalum* (0->1).

Character 102 (previously character 74.) (modified from Cadena & Parham (2015)). Pterygoid, ventral median ridge: 0 = incipient to absent; 1 = present, ridge spans nearly the full length of the pterygoids, sometimes reaching the most posterior portion of the vomer. This character is scored as inapplicable for taxa in which the pterygoids lack a midline contact.

Previous definition (Cadena & Parham (2015): character 74): Pterygoid, medial ridge: 0 = incipient to absent; 1 = present, ridge spans nearly the full length of the pterygoids, sometimes reaching the most posterior portion of the vomer. The medial ridge is produced by the extremely concave posterolateral portions of both pterygoids. Reworded from Parham & Pyenson (2010: ch 14); Hirayama (1998), KL, & Bardet *et al.* (2013: ch 23).

Remarks: The definition of this character has been modified only slightly. The word "medial" has been exchanged with "median" in order to precisely refer to the midline ridge that is formed along the interpterygoid suture of some taxa. This is necessary, as some taxa (e.g. *Toxochelys:* AMNH 1496; *Bouliachelys suteri:* QMF31669; *Rhinochelys:* CAMSM B55783; *Plesiochelys* spp.*:* OUMNH J1582*,* MNB 435; *Solnhofia parsoni:* TM 4023; *Sandownia harrisi:* MIWG 3480) have non-median parasagittal ridges on the ventral surface of the pterygoid (see character 104) that could be confused if the original character definition of Cadena & Parham (2015) was kept.

I also modified the scorings of some taxa. Some turtles that have non-median ridges, such as *Toxochelys*, *Bouliachelys*, and *Rhinochelys* were scored with state 1 by Cadena &

Parham (2015), while other taxa with non-median ridges, such as *Plesiochelys*, *Sandownia* and *Solnhofia* were scored as 0, This illustrates that some confusion of ventral pterygoid ridges exists. Taxa with a true median ridge are cheloniids such as *L. olivacea*, which are scored as state 1 in Cadena & Parham (2015).

Character optimisation: Unambiguous: (*Protostega* + *Archelon*) (0->1), *Argillochelys*+++ (0->1), *Lepidochelys kempii* (1->0), *Chelonia mydas* (1->0), *Gopherus polyphemus* (0->1).

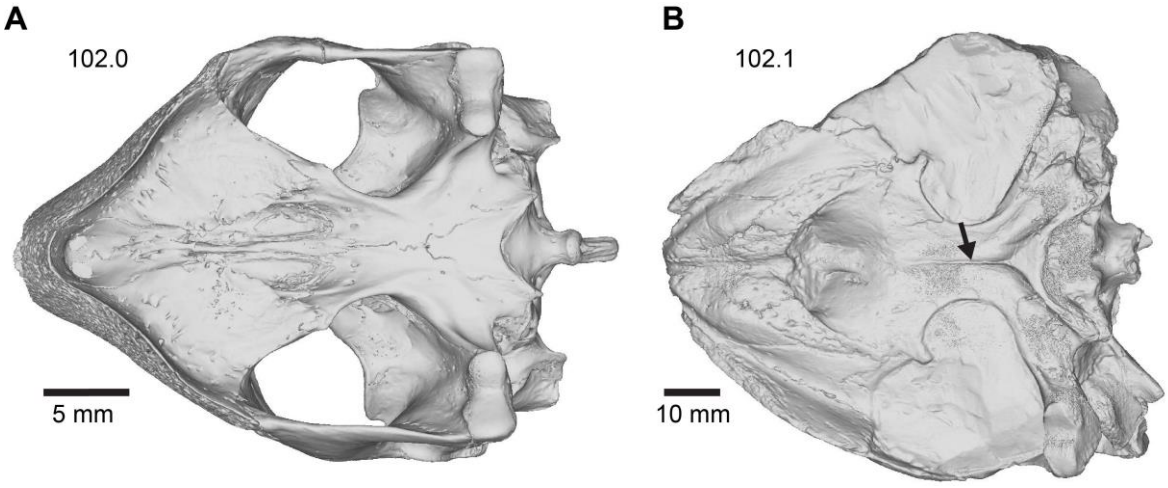


FIG. S1.35. Illustration of character 102. **A**, state 0 (*Sternotherus minor*, FMNH 211696, ventral view of cranium); **B**, state 1 (*Argillochelys cuneiceps*, NHMUK R41636). Arrow indicates median pterygoid ridge in B.

Character 103 (Cadena & Parham (2015): character 75). Pterygoid, extending laterally almost reaching the mandibular condyle facet: 0 = absent; 1 = present, the pterygoid contacts the medial edge of the mandibular condyle when is seem in ventral view; 2 = present, the pterygoids extends not only laterally to reach the outline of the mandibular condyle facet, but also posteriorly far from the level of the condyles.

Character optimisation: Unambiguous: Protostegidae (0->1), Trionychia (0->1), *Lissemys punctata* (1->2), *Phrynops geoffranus* (0->1), *Chelodina* (0->1), *Pelomedusa subrufa* (0->1), Angolachelonia (0->1).

Character 104 (new character). Pterygoid, ventral ridge on the palatal surface lateral to skull midline. 0 = absent; 1 = present, each pterygoid has a parasagittal ridge on its ventral surface.

Remarks: I noticed that some taxa have a ridge on the ventral surface of each pterygoid. This ridge is different from the median ridge seen in cheloniids: The median ridge (ch. 102.1, above) is positioned on the interpterygoid suture, whereas the double ridges referred to in the present character are more laterally positioned (i.e. non-median). In taxa with particularly well developed double ridges (e.g. *Solnhofia parsoni:* TM 4023; see Fig. S1.36*c*), these ridges extend from the posterior margin of the processus pterygoideus externus, and extend along the ventral surface of the pterygoid onto the posterolateral process of the pterygoid, where they approximately parallel the pterygoid-parabasisphenoid sutures. I observed the ventral pterygoid ridges in several taxa, including: most early protostegids (e.g. *Rhinochelys:* CAMSM 55775, 55776, 55783; NHMUK R35197, R43980; but not *Ocepechelon bouyai*), *Toxochelys* (e.g. *T. moorevillensis* FMNH PR 219), most thalassochelyidans (*Solnhofia:* TM 4024; *Plesiochelys* spp.: OUMNH J1582; MB 435), sandownids (e.g. *Sandownia:* MIWG 3480), chelydrids (*Macrochelys temminckii*: FMNH 22111), carettochelyids (*Carettochelys inscuplta*: NHMUK 1903.7.10.1), sinemydids (*Sinemys lens*: IVPP V9533-1; Brinkman & Peng 1993*a*), macrobaenids (*Judithemys sukhanovi*: TMP 87.2.1; Parham & Hutchinson 2003), xinjiangchelyids (*Xinjiangchelys radiplicatoides*: IVPP V9539-1), and paracryptodires (*Pleurosternon bullockii*: UMZC T1041). The ridges are absent in pleurodires, most testudinoids, trionychids, and early stem turtles such as *Kayentachelys aprix* (TMM 4370-2).

The double ridges can very prominent, as in *Solnhofia parsoni*, or relatively subtle, as in *Judithemys sukhanovi*. Additional variation in the relative anteroposterior length of these ridges is considered in character 105.

Character optimisation: Unambiguous: *Chubutemys*+++ (0->1), crown-group Chelonioidea (1->0), (*Desmatochelys* ++ *Santanachelys*) (0->1), *Dermatemys mawii* (1->0), Emydidae (1->0),

Trionychidae (1->0), Pleurodira (1->0), *Plesiochelys etalloni* (1->0), *Meiolania planiceps* (1->0); DELTRAN: *Testudo* (1->0), *Gopherus polyphemus* (1->0); ACCTRAN: Testudinidae (1->0), *Chelonoidis* sp. (0->1).

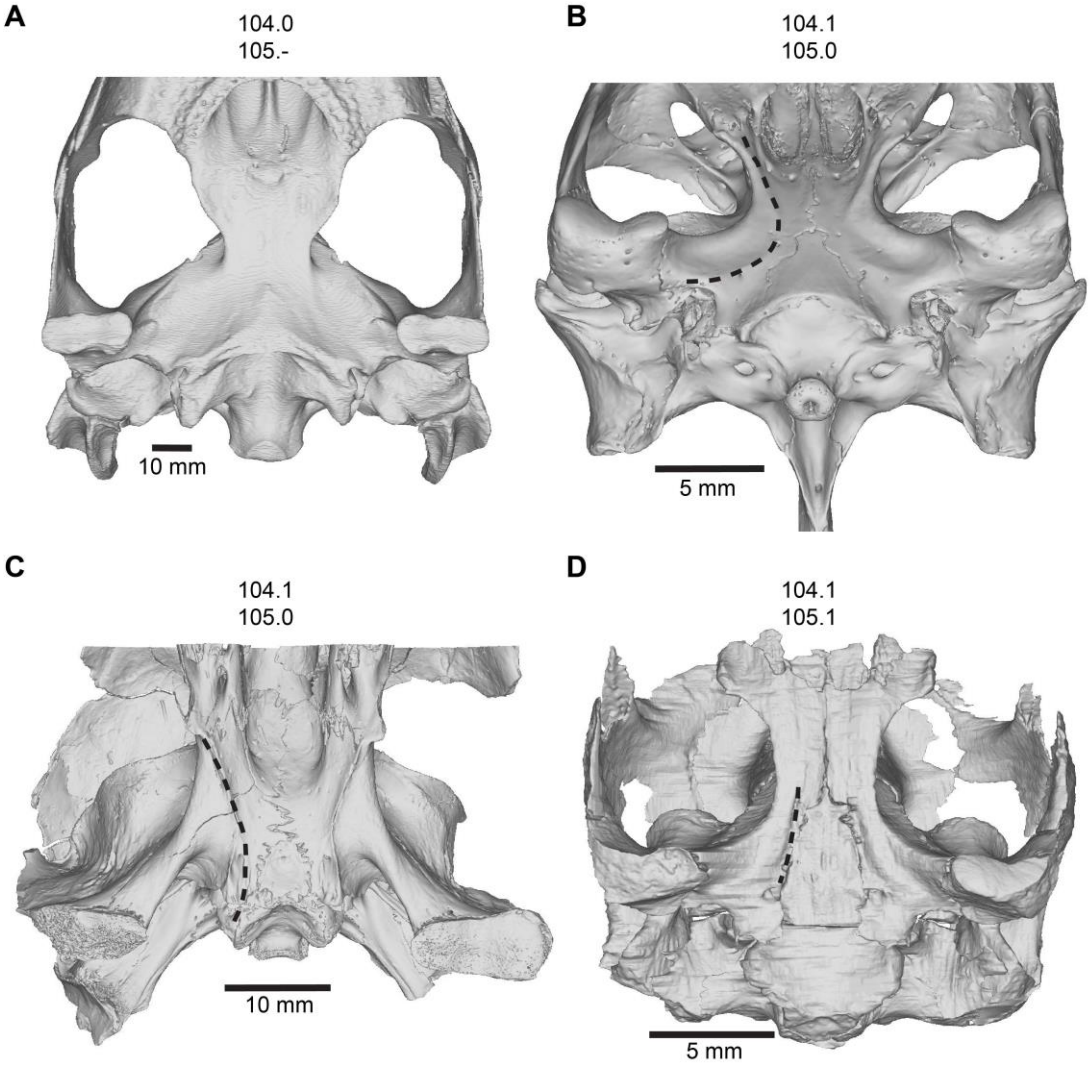


FIG. S1.36. Illustration of characters 104 and 105. **A**, ventral pterygoid ridge is absent (*Chelonia mydas*, NHMUK 1969.776, ventral view of partial cranium); **B**, ventral pterygoid ridge is present and extends over the entire length of the pterygoid (*Sternotherus minor*, FMNH 211696); **C**, same as B, but the ridge is strongly developed (*Solnhofia parsoni*, TM 4023); **D**, ventral pterygoid ridge is present and extends only over the posterior part of the pterygoid (*Rhinochelys cantabrigiensis*, CAMSM B55783). Dashed lines indicate the course of the ventral pterygoid ridge.

Character 105 (new character). Pterygoid, extent of ventral ridge on the palatal surface lateral to skull midline: 0 = each ridge extends along most of the ventral surface of the pterygoid, from the anteromedial margin of the pterygoid fossa to the processus pterygoideus externus; 1 = each ridge extends only along the posterior part of the pterygoid,

along the level of the parabasisphenoid. This character is scored inapplicable in turtles in which ventral pterygoid ridges are absent (ch 104.0).

Remarks: See discussion for new character 104 for more information on the ventral pterygoid ridges. In some taxa, like *Sandownia harrisi* (MIWG 3480), *Plesiochelys planiceps* (e.g. OUMNH J1582) and *Solnhofia parsoni* (TM 4023), the ventral pterygoid ridges extend from the posterior margin of the processus pterygoideus externus onto the ventral surface of the pterygoid, and then posteriorly along the parabasisphenoid contact to the posterior margin of the pterygoid. However, in some taxa, such as *Toxochelys* (e.g. *T. moorevillensis* FMNH PR 219), *Rhinochelys* (e.g. CAMSM B55783), and *Bouliachelys suteri* (QMF 31669), the ridges are restricted to the posterior part of the pterygoid, where they approximately parallel the contact with the parabasisphenoid.

Character optimisation: Unambiguous: total-group Chelonioidea (0->1), *Santanachelys gaffneyi* (1->0), *Staurotypus* (0->1), *Arundelemys dardeni* (0->1); DELTRAN: *Chelonoidis* sp. (0->1), *Leyvachelys cipadi* (0->1), *Brachyopsemys tingitana* (0->1); ACCTRAN: Testudinidae (0->1), Sandownidae (0->1), *Sandownia harrisi* (1->0).

Character 106 (modified from Cadena & Parham (2015)). Pterygoid/Quadrate, flooring of cavum acustico-jugulare and recessus scalae typmani: 0 = absent; 1 = present, formed primarily by the posterior part of the pterygoid; 2 = present, produced by the ventral process of the quadrate or prootic or a posterolateral expansion of the parabasisphenoid.

Previous definition (Cadena & Parham (2015): character 52): Quadrates, flooring of cavum acustico-jugulare and recessus scalae tympani: 0 = absent; 1 = fully or partially present, produced by the posterior process of the pterygoid, but the pterygoid does not cover the prootic; 2 = produced by the posterior process of the pterygoid, and the pterygoid covers the prootic; 3 = fully or partially present, *produced* by the ventral process of the quadrate or the prootic, or both. Joyce (2007: ch 31) & Sterli & De la Fuente (2013: ch 49) (Quadrate A).

Remarks: This character has been modified to match the definition used in Joyce (2007: character 31, Quadrate A). Cadena & Parham (2015: character 52) included a state that effectively splits state 1 of the current definition to include information on whether the prootic is covered by the posterior process of the pterygoid or not. However, I think that additional variation regarding the extent of the pterygoid should be coded in a separate character (character 107 of this study).

Here, I employ a character definition that only distinguishes between taxa in which the cavum acustico-jugulare is entirely exposed (state 0), covered primarily by the pterygoid (state 1), or covered by the quadrate, prootic, and/or parabasisphenoid. I do not split this character further into a presence/absence character about the covering of the cavum acustico-jugulare, because the two conditions described by state 1, which is generally seen in non-pleurodiran turtles with a partially or fully closed cavum acustico-jugulare, and state 2, which is seen in pleurodires, could have evolved convergently.

I include the word "primarily" in the description of character state 1, because in some cryptodires (e.g. *Gopherus*: FMNH211815, *Chelonoidis*: SMF67582) the opisthotic is also included in the flooring of the cavum acustico-jugulare (this is considered in character 131).

To justify my scorings for this character, it is necessary to comment on the definition of the "absence" of any flooring to the cavum acustico-jugulare. The cavum acustico-jugulare is the medial part of the middle ear, and generally consists of a space between the incisura columella auris and the fenestra ovalis, through which the stapes traverses. A good indication for an unfloored cavum aucstico-jugulare is when the entire stapes and region of the fenestra ovalis is visible in ventral view. I herein only score *Proganochelys quenstedti*, *Australochelys africanus*, *Kayentachelys aprix*, *Eileanchelys waldmanni*, and *Chubutemys copelloi* as having state 0. All these taxa are similar in the regards that the middle ear region is not ventrally enclosed, and the stapes is fully exposed in ventral view.

In some taxa, such as *Plesiochelys planiceps* (OUMNH J1582), *Solnhofia* (TM4023), *Annemys* (*Annemys* sp.: IVPP V18106; *Annemys levensis*: PIN 4636-4-2), the cavum acustico-

jugulare is largely exposed, so that much of the stapes (when preserved) can be seen in ventral view. However, all of these taxa have a pterygoid that is posteriorly more expanded than the taxa scored as 0. Therefore, these taxa are herein scored as having state 1 (as in cryptodires). The variation seen between the taxa mentioned above and other cryptodires with a more extensive ventral flooring of the cavum acustico-jugulare is considered in character 103.

Character optimisation: Unambiguous: *Meiolania*+++ (0->1), Pleurodira (1->2).

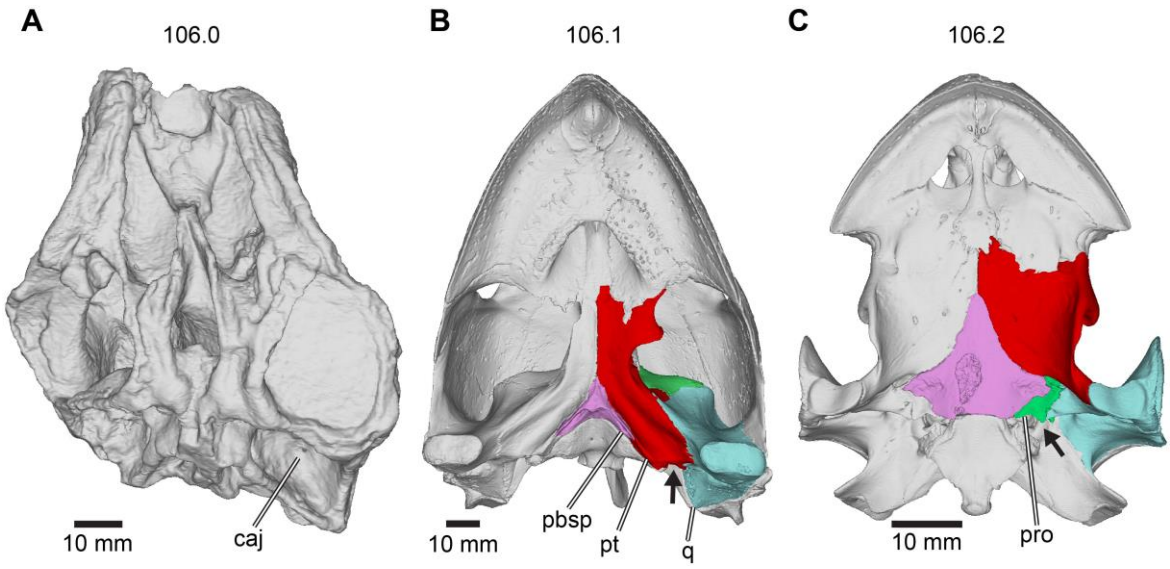


FIG. S1.37. Illustration of character 106. **A**, state 0 (*Australochelys africanus*, BP/1/4933, ventral view of cranium); **B**, state 1 (*Lepidochelys olivacea*, SMNS 11070); **C**, state 2 (*Phrynops geoffroanus*, SMF 45470). Arrows in B and C point to fenestra postotica, the entrance to the cavum acustico-jugulare. Abbreviations: *caj*, cavum acustico-jugulare; *pbsp*, parabasisphenoid; *pro*, prootic; *pt*, pterygoid; *q*, quadrate.

Character 107 (new character). Pterygoid, posterior process: 0 = posterior process of pterygoid is absent, the cranioquadrate space or posterior foramen for the canalis cavernosus is not covered by the pterygoid; 1 = posterior process of pterygoid present but very short, process extends posteriorly to cover the posterior foramen for the canalis cavernosus (i.e. the modified cranioquadrate space), but the cavum-acustico jugulare remains largely exposed ventrally; 2 = posterior process of the pterygoid present and developed as an extensive sheet that projects posteriorly and covers large parts of the cavum acustico-jugulare.

Remarks: This character is intended to capture some of the additional variation in the ventral covering of the cavum acustico-jugulare in addition to character 106. Character 106 qualifies whether the cavum acustico-jugulare is unfloored, floored by the pterygoid, or floored by the quadrate, prootic, or parabasisphenoid. For details of the definition of the flooring, please see discussion of character 106.

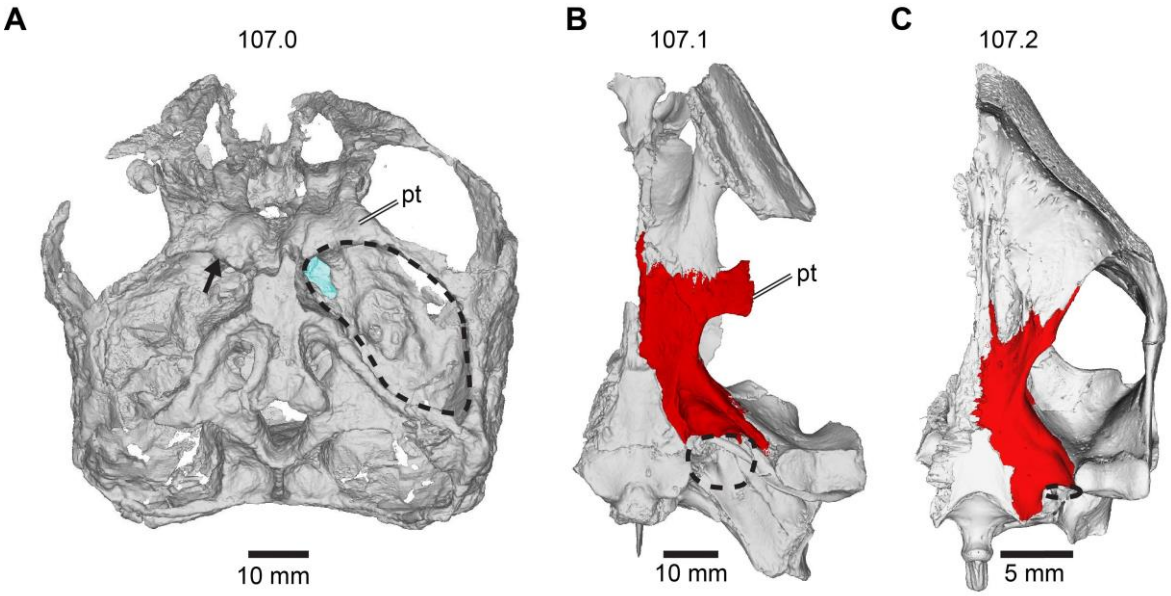


FIG. S1.38. Illustration of character 107. **A**, state 0 (*Australochelys africanus*, BP/1/4933, posteroventral view of cranium); **B**, state 1 (*Plesiochelys planiceps*, OUMNH J1582, ventral view of left side of cranium); **C**, state 2 (*Sternotherus minor*, FMNH 211696, ventral view of left side of cranium). Dashed lines indicate uncovered parts of the cavum acustico-jugulare. Blue in A indicates cranio-quadrate space of *Australochelys*. Abbreviations: *pt*, pterygoid.

State 0 describes the absence of a posterolateral process of the pterygoid, which is seen in early stem turtles such as *Proganochelys quenstedti* (SMNS 16980), but also in pleurodires. The pterygoid flooring of the cavum acustico-jugulare is present in cryptodires, but is also seen in some stem-turtles (e.g. *Kallokibotion bajazidi*: NHMUK R4921; *Meiolania planiceps*: NHMUK RR682), paracryptodires, and some sinemydids, macrobaenids, and xinjiangchelyids. However, variation in the relative length of the pterygoid process exists among these taxa. State 1 of this character describes turtles in which large parts of the cavum acustico-jugulare remain exposed ventrally, due to the relative shortness of the posterolateral process of the pterygoid. For instance, in *Plesiochelys planiceps* (OUMNH J 1582), the process covers the posterior foramen for the canalis cavernosus, which is the

modified cranioquadrate space, but more posterior portions of the cavum acustico-jugulare are unfloored. In most crown-cryptodires, the posterolateral process is relatively expanded in comparison that that condition, and the entire cavum acustico-jugulare is floored. This is represented in state 2.

Character optimisation: Unambiguous: (*Eileanchelys* + *Kayentachelys*)+++ (0->1), *Kallokibotion*+++ (1->2), *Emarginachelys cretacea* (2->1), Pleurodira (2->0), *Solnhofia parsoni* (2->1), *Plesiochelys planiceps* (2->1), *Sinemys lens* (2->1), Pleurosternidae (2->1); DELTRAN: *Kirgizemys hoburensis* (2->1), *Annemys levensis* (2->1), *Annemys* sp. IVPP V18106 (2->1); ACCTRAN: (*Kirgizemys hoburensis* + *Kirgizemys dmitrievi*) (2->1), Xinjiangchelyidae (2->1), (*Xinjiangchelys wusu* + *Xinjiangchelys radiplactoides*) (1->2).

Character 108 (adopted from Cadena 2015). Pterygoid, development of a posteromedial wing covering partially to completely the basisphenoid and sometime the basioccipital too, seen in ventral view of the skull: 0 = absent; 1 = present.

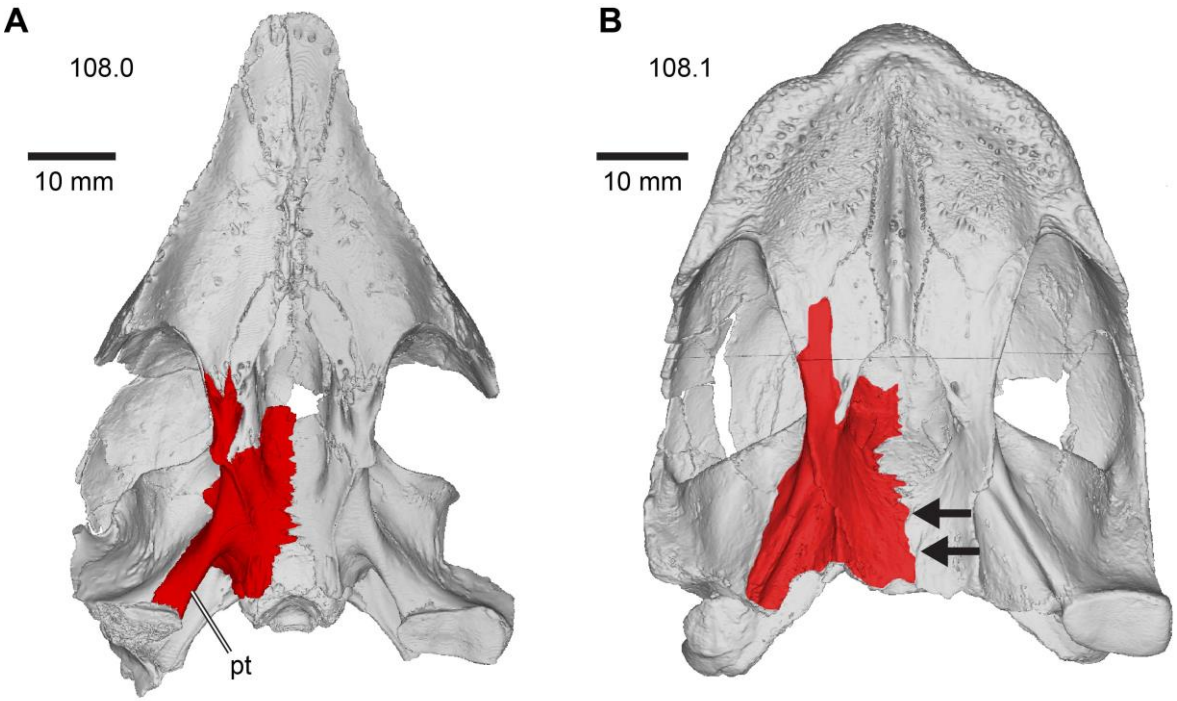


FIG. S1.39. Illustration of character 108. **A**, state 0 (*Solnhofia parsoni*, TM 4023, ventral view of cranium); **B**, state 1 (*Sandownia harrisi*, MIWG 3480). Arrows in B indicate inter-pterygoid contact posterior to the parabasisphenoid. Abbreviations: *pt*, pterygoid.

Remarks: This character was added by Cadena (2015: ch 257) to the matrix of Cadena & Parham (2015) to code for additional variation of the pterygoid observed specifically in sandownids. I confirm the observations of Cadena (2015) and also included this character.

Character optimisation: Unambiguous: Sandownidae (0->1).

Character 109 (new character). Pterygoid, pterygoid fossa: 0 = weakly developed; 1 = developed as a deep concavity between the articular process of the quadrate and the basicranium.

Remarks: This character documents the relative depth of the pterygoid fossa, located posteriorly on the ventral surface of the pterygoid. Cheloniids have a deep pterygoid fossa, but this is also present in various taxa pertaining to other groups. Notably, deep pterygoid fossae are also present in many thalassochelydians, and sandownids.

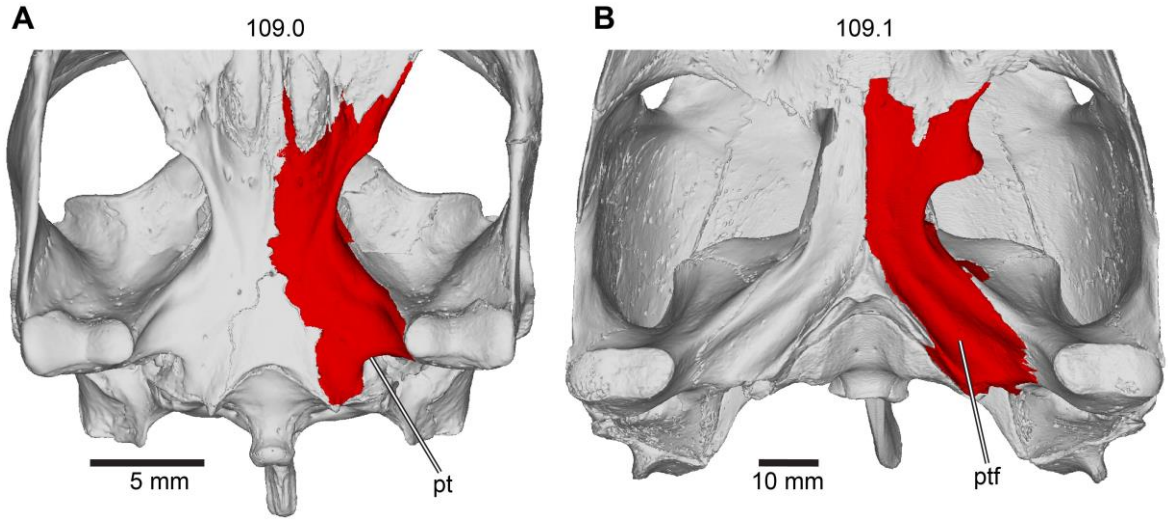


FIG. S1.40. Illustration of character 109. **A**, state 0 (*Sternotherus minor*, FMNH 211696, ventral view of partial cranium); **B**, state 1 (*Lepidochelys olivacea*, SMNS 11070). Abbreviations: *pt*, pterygoid; *ptf*, pterygoid fossa.

Character optimisation: Unambiguous: Paracryptodira+++ (0->1), total-group Cheloniidae (0->1), *Emarginachelys cretacea* (0->1), *Platysternon megacephalum* (0->1), *Allaeochelys libyca* (0->1), *Solnhofia parsoni* (1->0), *Plesiochelys etalloni* (1->0), (*Judithemys* ++ *Kirgizemys*) (1->0), *Xinjiangchelys radiplicatoides* (1->0), (*Eileanchelys* + *Kayentachelys*) (0->1); DELTRAN: Cryptodira (1->0); ACCTRAN: Testudines (1->0).

Character 110 (Cadena & Parham (2015): character 76). Supraoccipital, crista supraoccipitalis: 0 = poorly developed; 1 = protruding significantly posterior to the foramen magnum.

Character optimisation: Unambiguous: *Chubutemys*+++ (0->1), *Ocepechelon bouyai* (1->0), Dermochelyidae (1->0), *Kinosternon suburum hippocrepis* (1->0), *Jurassichelon oleronensis* (1->0*), Sandownia harrisi* (1->0); DELTRAN: Chelinae (1->0), Chelodina (1->0); ACCTRAN: total-group Chelidae (1->0), *Elseya dentata* (0->1).

Character 111 (Cadena & Parham (2015): character 77). Supraoccipital, large supraoccipital exposure on dorsal skull roof: 0 = absent; 1 = present.

Character optimisation: Unambiguous: *Caretta caretta* (0->1), *Meiolania planiceps* (0->1).

Character 112 (Cadena & Parham (2015): character 78). Supraoccipital, horizontal crest in the crista supraoccipitalis: 0 = absent or poorly developed anteriorly; 1 = present, along the entire crista supraoccipitalis.

Character optimisation: Unambiguous: Trionychia (0->1).

Character 113 (new character). Supraoccipital, fossa on the posterodorsal surface of the floor of the supratemporal fossa: 0 = absent; 1 = present, fossa is formed on the lateral surface of the suparoccipital, dorsal to the contact area between exoccipital, opisthotic, and supraoccipital.

Remarks: The supratemporal fossa of turtles is the "space above and behind the otic chamber and below the temporal roof (if present)" (Gaffney 1972, p. 26). The posterior part of the floor of the supratemporal fossa is usually formed by the exoccipital, the opisthotic, the supraoccipital, the quadrate, and the squamosal. Exoccipital, opisthotic, and supraoccipital constitute a triple junction in the floor of the supratemporal fossa.

In turtles, the surface around this contact may be a smooth and flat surface (e.g. protostegids such as *Rhinochelys:* CAMSM B55783, some chelonioids such as *Eretmochelys imbricata:* FMNH 22242, sandownids such as *Sandownia harrisi:* MIWG 3480, kinosternoids, and most testudinoids). In other taxa, such as some trionychians (*Lissemys punctata:* SMF 74141, *Carettochelys insculpta:* NHMUK 1903.7.10.1), some testudinoids (*Testudo:* FMNH 51672, *Chrysemys picta:* NHMUK 76.1.31.19), chelydrids (*Macrochelys temminckii:* FMNH 2211), and various chelonioids (e.g. *Argillochelys cuneiceps:* NHMUK R41636, *Allopleuron hoffmanni:* NHMUK R42913*, Chelonia mydas:* NHMUK 1969*.776*), as well as *Solnhofia parsoni* (TM 4023*)* and *Plesiochelys planiceps* (OUMNH J1582), there is a distinct, shallow fossa on the surface between the contact of the above mentioned skull elements.

Character optimisation: Unambiguous: (*Eileanchelys* + *Kayentachelys*)+++ (1->0), *Argillochelys*+++ (0->1), (*Eretmochelys* ++ *Lepidochelys*) (1->0), crown-group Chelydridae (0->1), *Chrysemys picta* (0->1), *Testudo* (0->1), Trionychia (0->1), Thalassochelydia (0->1), Sinemydidae/Macrobaenidae (0->1); DELTRAN: *Notochelone* (0->1); ACCTRAN: (*Santanachelys* + *Notochelone*) (0->1).

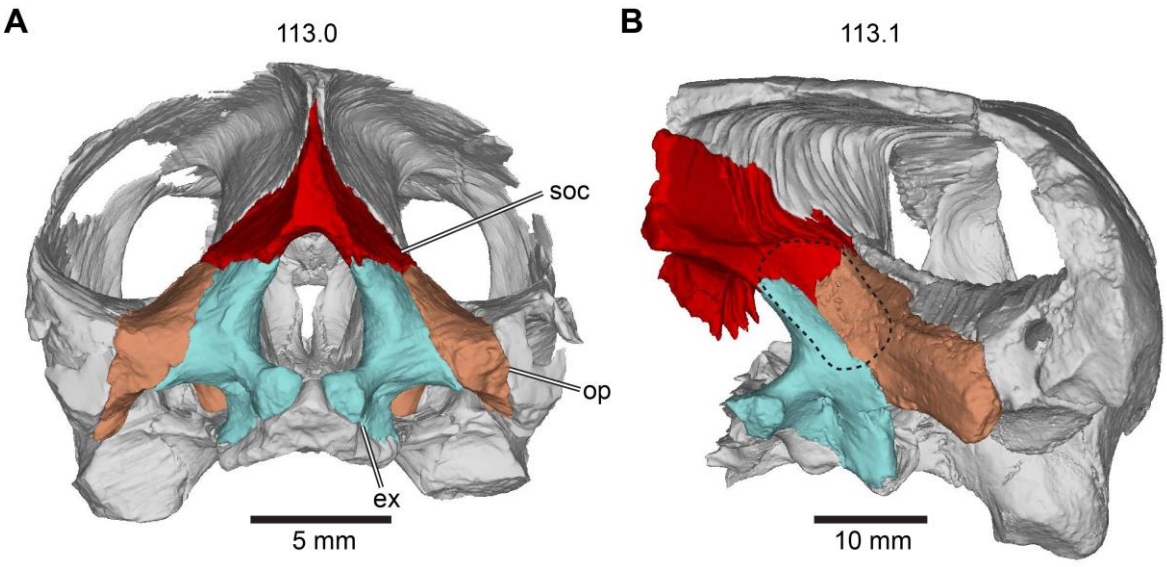


FIG. S1.41. Illustration of character 113. **A**, state 0 (*Rhinochelys cantabrigiensis*, CAMSM B55783, posterior view of cranium); **B**, state 1 (*Argillochelys cuneiceps*, NHMUK R41636, posterolateral view of right side of cranium). Dashed line circumscribes fossa. Abbreviations: *ex*, exoccipital; *oc*, occipital condyle; *op*, opisthotic; *soc*, supraoccipital.

Character 114 (Cadena & Parham (2015): character 79). Exoccipital, medial contact of exoccipitals dorsal to foramen magnum: 0 = absent; 1 = present.

Character optimisation: Unambiguous: *Kinosternon suburum hippocrepis* (0->1); DELTRAN: Chelinae (0->1), *Chelodina* (0->1); ACCTRAN: crown-group Chelidae (0->1), *Elseya dentata* (1->0).

Character 115 (new character). Exoccipital, median contact of exoccipitals in the floor of the foramen magnum, excluding the basioccipital from the latter: 0 = absent; 1 = present.

Remarks: I observed variation in the formation of the floor of the foramen magnum. In many turtles, the basioccipital is part of the floor of this foramen (e.g. *Rhinochelys cantabrigiensis*: CAMSM B55783), whereas in other turtles the exoccipitals meet ventromedially and exclude the basioccipital from the foramen (e.g. *Apalone spinifera emoryi*: FMNH 22178).

Character optimisation: Unambiguous: Xinjiangchelyidae+++ (0->1), (*Bouliachelys* ++ *Santanachelys*) (1->0), Dermochelyidae (1->0), *Allopleuron*+++ (1->0), *Chelonia mydas* (0->1), *Toxochelys latiremis* (1->0), *Sternotherus* (1->0), *Dermatemys mawii* (1->0), *Araripemys barretoi* (1->0), *Podocnemis* (1->0), *Solnhofia parsoni* (1->0), (*Sandownia* + *Leyvachelys*) (1->0); DELTRAN: *Chrysemys picta* (1->0), *Platysternon megacephalum* (1->0), *Geoclemys hamiltonii* (1->0), *Ordosemys* sp. IVPP V12092 (1->0); ACCTRAN: Testudinoidea (1->0), *Emys orbicularis* (0->1), Testudinidae (0->1), (*Ordosemys* + *Dracochelys*) (1->0).

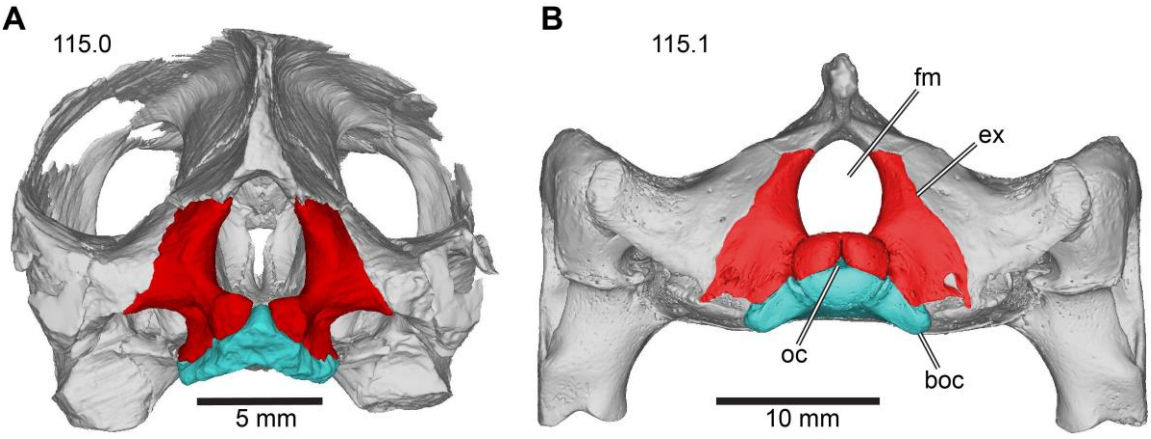


FIG. S1.42. Illustration of character 115. **A**, state 0 (*Rhinochelys cantabrigiensis*, CAMSM B55783, posterior view of cranium); **B**, state 1 (*Gopherus polyphemus*, FMNH 211815). Abbreviations: *boc*, basioccipital; *ex*, exoccipital; *fm*, foramen magnum.

Character 116 (modified from Cadena & Parham (2015)). Foramen nervi hypoglossi (XII), ventral covering: 0 = exposed in ventral view; 1 = covered in ventral view by an extension of the pterygoid and the basioccipital; 2 = covered in ventral view an extension of the basioccipital; 3 = covered in ventral view by an expansion of the exoccipital and basioccipital.

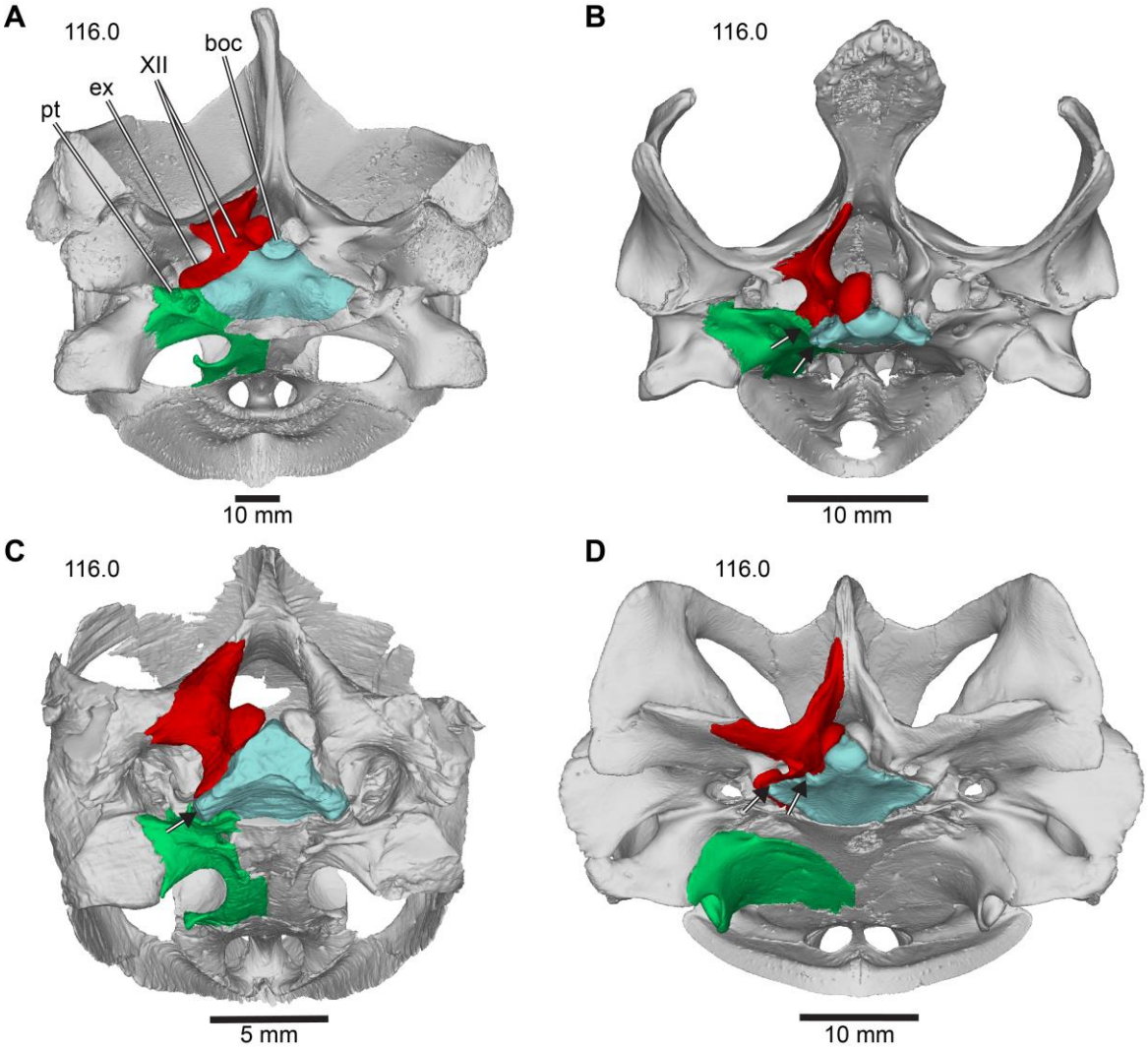


FIG. S1.43. Illustration of character 116. **A**, state 0 (*Lepidochelys olivacea*, SMNS 11070, posteroventral view of cranium); **B**, state 1 (*Apalone spinifera emoryi*, FMNH 22178); **C**, state 2 (*Rhinochelys cantabrigiensis*, CAMSM B55783); **D**, state 3 (*Phrynops geoffroanus*, SMF 45470). Arrows indicate ventral covering structures of foramina nervi hypoglossi. Abbreviations: *XII*, foramina nervi hypoglossi (CN XII); *boc*, basioccipital; *ex*, exoccipital; *pt*, pterygoid.

Previous definition (Cadena & Parham (2015): character 98): Foramen nervi hypoglossi (XII), ventral covering: 0 = exposed in ventral view; 1 = covered in ventral view by an extension of

the pterygoid and the basioccipital; 2 = covered in ventral view an extension of the basioccipital. Sterli & De la Fuente (2013: ch 95, Foramen nervi hypoglossi A).

Remarks: A fourth state (state 3) has been added for taxa in which the foramina nervi hypoglossi are covered in ventral view by the exoccipital and basioccipital, such as *Chelus fimbriatus* (NHMUK 81.9.27.4) or *Phyrynops geoffroanus* (SMF 45470).

Character optimisation: Unambiguous: (*Ocepechelon* ++ *Santanachelys*) (0->2), *Eretmochelys imbricata* (0->1), *Sternotherus* (2->0), *Solnhofia parsoni* (0->2), (*Ordosemys* + *Dracochelys*) (0->2), (*Eubaena* ++ *Pleurosternon*) (0->2); DELTRAN: *Macrochelys temminckii* (0->1), Kinosternoidea (0->2), Emysternia (0->2), *Geoclemys hamiltonii* (0->2), Trionychidae (0->1), total-group Carettochelyidae (0->2), Chelinae (0->3), Chelodininae (0->2), *Podocnemis* (0->2), *Plesiochelys planiceps* (0->2), *Sandownia harrisi* (0->1), (*Annemys* sp. ++ *Xinjiangchelys*) (0->2); ACCTRAN: Testudines (0->2), Americhelydia (2->0), *Macrochelys temminckii* (0->1), Kinosternoidea (0->2), Testudinidae (2->0), Trionychidae (2->1), Chelinae (2->3), *Araripemys barretoi* (2->0), *Pelomedusa subrufa* (2->0), (*Plesiochelys etalloni* + *Plesiochelys planiceps*) (0->2), (*Sandownia* + *Leyvachelys*) (0->1), (*Annemys latiens* ++ *Xinjiangchelys*) (0->2).

Character 117 (new character). Exoccipital, foramina nervi hypoglossi: 0 = the foramina nervi hypoglossi exit the exoccipital on the occipital surface posteriorly to the margin of the fenestra postotica; 1 = at least one foramen nervi hypoglossi opens within the recessus scalae tympani anterior to margin of the fenestra postotica, and the others exit the exoccipital on the occipital surface; 2 = all foramina nervi hypoglossi open within the recessus scalae tympani anterior to the margin of the fenestra postotica.

Remarks: In most turtles, the external foramina for the hypoglossal nerves are located on the posterior surface of the exoccipital, and are visible in posterior view (state 0). Consequentially, they are positioned medially in respect to the fenestra postotica. However, in *Kallokibotion*, these foramina are positioned more anterolaterally on the exoccipital, and open within the inner margin of the fenestra postotica (state 2). *Eileanchelys waldmanni*

(NHS.G.2004.31.15) and *Meiolania platyceps* (NHMUK RR682) show an intermediate state (state 1), because the anterior more positioned foramen is located within the margin of the fenestra postotica, but the posterior foramen is exposed on the posterior, occipital surface of the exoccipital.

Character optimisation: Unambiguous: *Kallokibotion bajazidi* (0->1); DELTRAN: Chelinae (0->2), *Chelodina* (0->2); ACCTRAN: crown-group Chelidae (0->2), *Elseya dentata* (2->0).

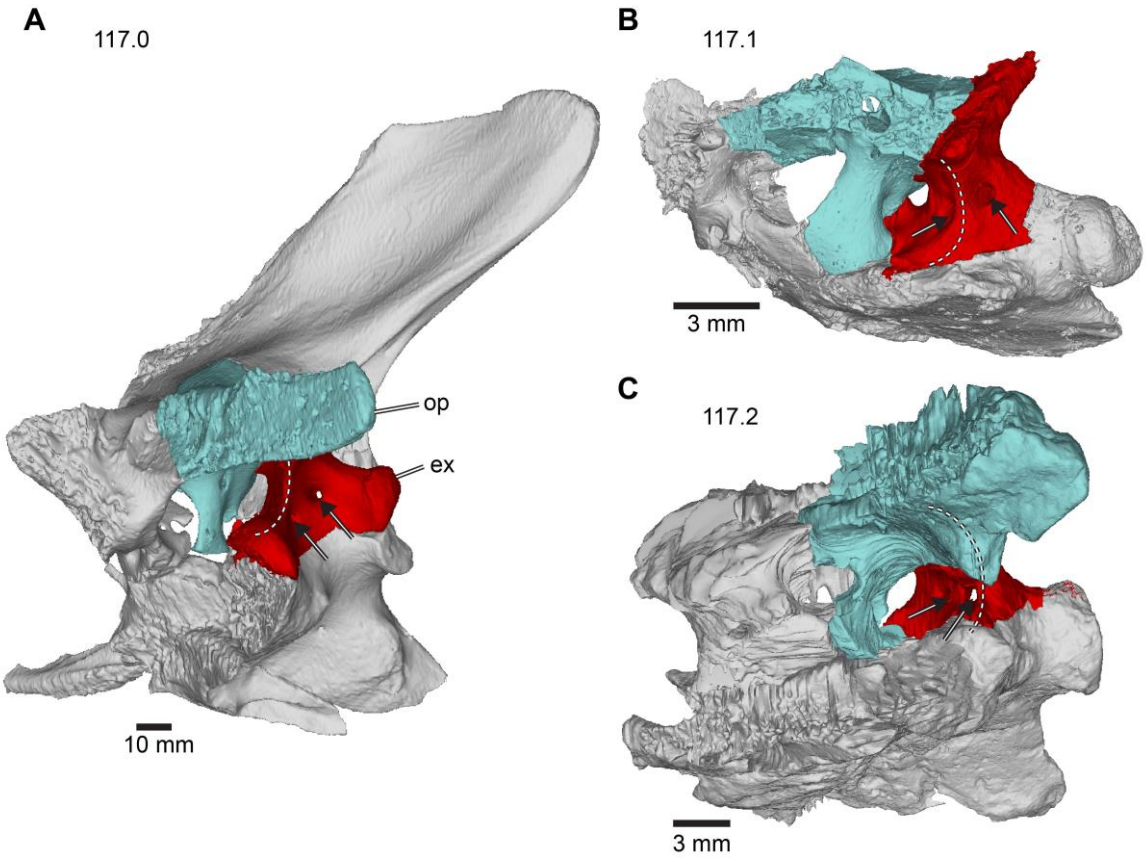


FIG. S1.44. Illustration of character 117. **A**, state 0 (*Lepidochelys olivacea*, SMNS 11070, left posteroventrolateral view of partial basicranium); **B**, state 1 (*Eileanchelys waldmanni*, NMS.G.2004.21.15; right posteroventral view of partial basicranium, reflected for comparison); **C**, state 2 (*Kallokibotion bajazidi*, NHMUK R4925, left posteroventrolateral view of partial basicranium). Arrows indicate positions of foramina nervi hypoglossi. Dashed lines indicates the medial margin of the fenestra postotica. Abbreviations: *ex*, exoccipital; *op*, opisthotic.

Character 118 (Cadena & Parham (2015): character 80). Basioccipital, morphology of the anteriormost part of the basioccipital: 0 = with two or one ventral tubercle; 1 = tubercle absent.

Remarks: Cadena & Parham (2015) cited Sterli (2008: character 52) and Sterli and de la Fuente (2013: character 76) for the history of this character. In Sterli (2008), who refer to Sterli *et al.* (2007) for the character history, this character is a multistate character that distinguishes between a singular ventral tubercle on the anteriormost part of the basioccipital (Sterli 2008: character 52 state 0); a groove limited by two lateral ridges that are finished in horns (state 1); and the absence of any tubercle (state 2). In Sterli and de la Fuente (2013), this character is modified to a binary character that defines states qualifying the presence of one or two tubercles (Sterli & de la Fuente 2013: character 76 state 0), or the absence of these structures (state 1). The character definition used by Cadena & Parham (2015: character 80) adopts the definition used by Sterli and de la Fuente (2013).

Sterli *et al.* (2007: p. 21) provided the most comprehensive discussion of this character. The character is based on a feature described for *Proganochelys quenstedti* by Gaffney (1990), who observed a centrally placed tubercle on the ventral surface of the basioccipital. A similar observation has been made for *Australochelys* (Gaffney & Kitching 1995), but the exact morphology of the tubercle in this taxon could not be determined as its ventral surface is broken off. Sterli *et al.* (2007) then observed a potentially homologous structure in *Palaeochersis* that they describe as two strong ridges to either side of a central pit, which posteriorly finish as "basioccipital horns". As in *Proganochelys* and *Australochelys*, these structures are placed relatively far anteriorly on the ventral surface of the basiccopital, and are in this regard unlike the basioccipital tubera, which ususally project off the basioccipital around the posterior margin of the bone. Sterli *et al.* (2007) further argue that the preserved part of the basioccipital of *Australochelys* suggest a greater similarity to the condition on *Palaeochersis* than in *Proganochelys*.

In both Sterli (2008) and Sterli and de la Fuente (2013), *Australochelys* is scored as "?", although Sterli *et al.* (2007) argued that *Australochelys* resembles *Palaeochersis*, and although all authors that have commented on *Australochelys* specifically (Gaffney & Kitching 1995; Sterli *et al.* 2007) seem to agree that *Australochelys* has some sort of median tubercle, even if the exact morphology is unknown.

Examination of the scorings of Sterli (2008) and Sterli and de la Fuente (2013) also reveals that the basioccipital tubercle character has been scored inconsistently. Sterli (2008) and Sterli and de la Fuente (2013) agree in their scorings of a number of taxa (*Proganochelys*, *Palaeochersis*, *Kayentachelys*, *Condorchelys*, *Mongolemys*, *Kallokibotion*, *Glyptops*, *Ordosemys leios*, *Mongolemys*), which all are scored to have some sort of ventral tubercle. However, Sterli (2008) additionally scored all members of Trionychia (*Adocus*, *Apalone*, *Lissemys*, *Anosteira*, *Carettochelys*, *Sandownia*) to have a basioccipital tubercle, but all of these taxa (except for *Sandownia*, which is not scored in Sterli and de la Fuente (2013) are scored as not having a tubercle in Sterli and de la Fuente (2013). Conversely, Sterli and de la Fuente (2013) score *Peligrochelys*, *Dorsetochelys*, *Judithemys*, and *Sinemys lens* as having a tubercle, while these taxa are scored as "absent" for the tubercle character in Sterli (2008). Furthermore, meiolaniforms are scored as having a tubercle in Sterli and de la Fuente (2013).

In summary, a range stem-group turtles, including members or potential members of the Pleurosternidae and the Meiolaniformes, as well as a mix of cryptodires, including trionychians and a range of sinemydids, have previously been scored to have some sort of median basioccipital tubercle.

In my re-examination of taxa, both based on personal observations and literature research, I have paid specific attention to those taxa that have been reported to have a basioccipital tubercle comparable to the structure seen in *Proganochelys*. With the exception of *Australochelys*, I disagree that any other turtle than *Proganochelys* has a centrally placed turbercle on the basioccipital. *Proganochelys* (and, possibly *Australochelys*) are different from all other turtles in that the ventral surface of the basioccipital is not formed as a relatively broad and flat structure. *Kayentachelys* (MCZ 8917), for instance, has a ventral surface of the basioccipital that lacks any distinct midline structures. The midline portion of the ventral surface is gently concave between two roughly parasagitally oriented ridges, which are similar to the paired basioccipital tubera seen in most turtles. The ridges become shallower anteriorly and become slightly less spaced from the midline, but there is no distinct similarity

to the central tubercle of *Proganochelys*. Therefore, I have scored all taxa but *Proganochelys* and *Australochelys* as having state 1.

Character optimisation: Unambiguous: (*Kayentachelys*+*Eileanchelys*)+++ (0->1).

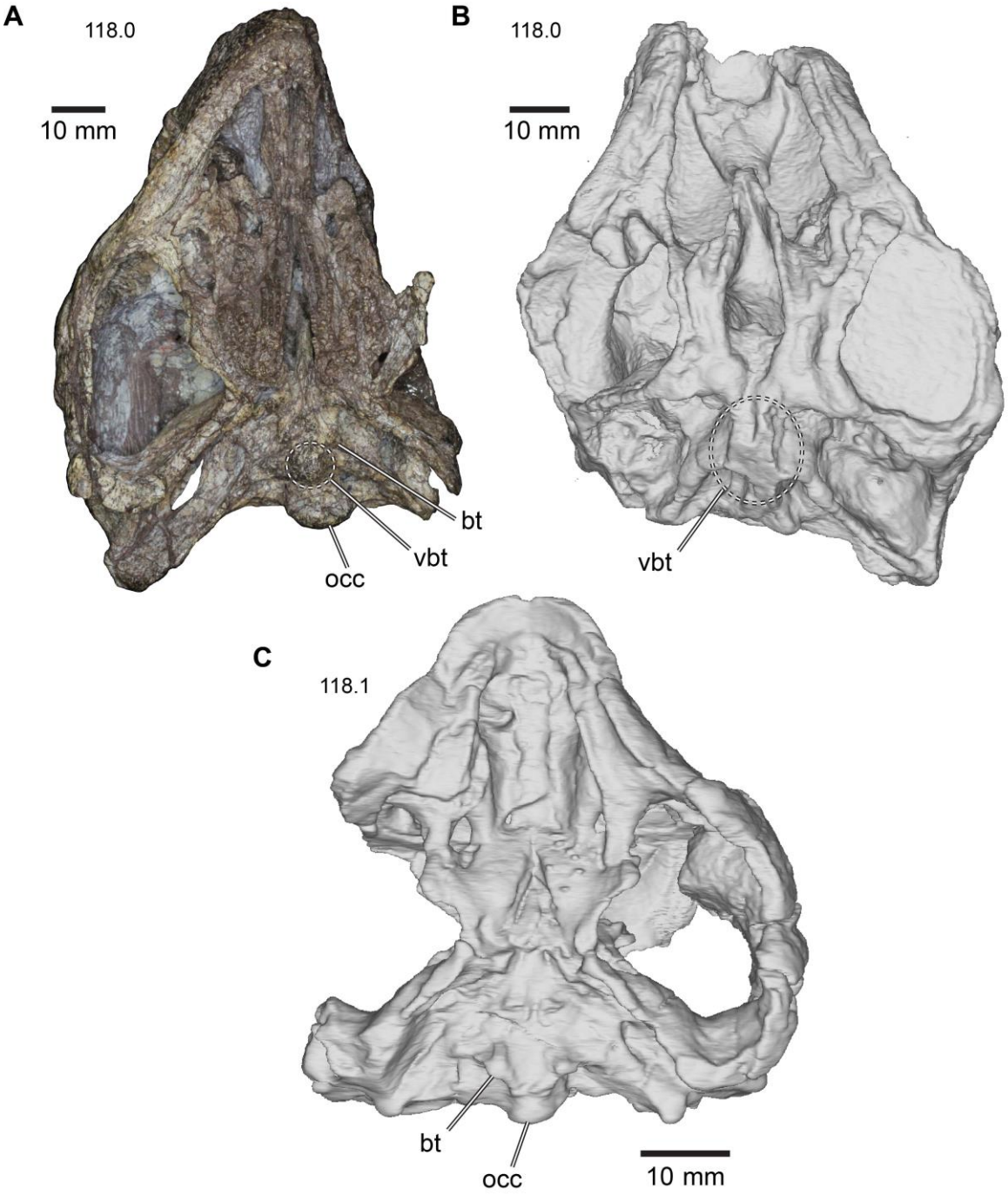


FIG. S1.45. Illustration of character 118. **A**, state 0 (*Proganochelys quenstedti*, SMNS 16980, ventral view of cranium); **B**, state 0 (*Australochelys africanus*, BP/1/4933); **C**, state 1 (*Kayentachelys aprix*, TMM 4370-2). Dashed circles indicate positions of the ventral basioccipital tubercle. Abbreviations: *bt*, basi tuber; *occ*, occipital condyle; *vbt*, ventral basioccipital tubercle.

Character 119 (Cadena & Parham (2015): character 81). Basioccipital, deep C-shaped concavity between basioccipital tubera: 0 = absent; 1 = present.

Character optimisation: Unambiguous: *Chubutemys*+++ (0->1), Paracryptodira+++ (1->0), *Eosphargis breineri* (0->1), total-group Cheloniidae (0->1), *Baptemys wyomingensis* (0->1), total-group Carettochelyidae (0->1), *Solnhofia parsoni* (0->1).

Character 120 (previously xxxxxii) (new character). Basioccipital, basal tubera: 0 = the basal tubera are completely formed by the basioccipital; 1 = the exoccipitals and the basioccipital form the basal tubera; 2 = the pterygoids and the basioccipital form the basal tubera; 3 = the basal tubera are formed by the exoccipitals, basioccipital and pterygoids.

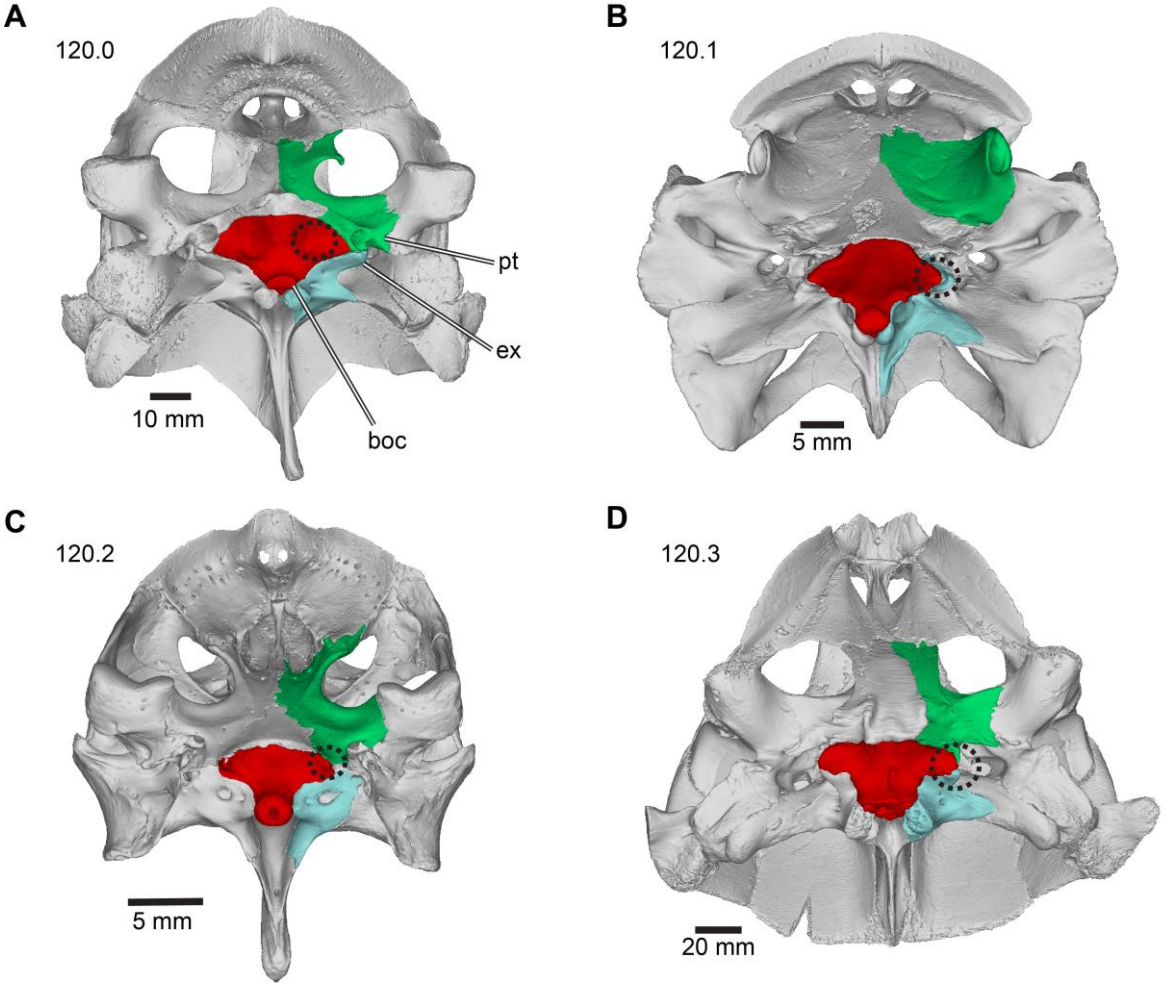


FIG. S1.46. Illustration of character 120. **A**, state 0 (*Lepidochelys olivacea*, SMNS 11070, posteroventral view of cranium); **B**, state 1 (*Phrynops geoffroanus*, SMF 45470); **C**, state 2 (*Sternotherus minor*, FMNH 211696); **D**, state 3 (*Dermochelys coriacea*, UMCZ R 3031). Dashed circles indicate positions of the basi tuber. Abbreviations: *boc*, basioccipital; *ex*, exoccipital; *pt*, pterygoid.

Remarks: The paired basal tubera are shallow processes on the ventral surface of the basicranium. This character captures variation associated with the formation of these processes. The basioccipital is always involved in the formation of the basal tubera, but other cranial elements can be incolved as well.

Character optimisation: Unambiguous: *Kallokibotion*+++ (0->2), Xinjiangchelyidae+++ (2->0), *Eretmochelys imbricata* (0->1), *Chelonia mydas* (0->1), *Eochelone* (0->2), *Chrysemys picta* (0->1), *Geoclemys hamiltonii* (0->3), total-group Carettochelyidae (0->3); DELTRAN: *Dermochelys coriacea* (0->3*), Eosphargis breineri* (0->1), *Sternotherus* (0->2), *Staurotypus* (0->2), *Baptemys wyomingensis* (0->2), Chelinae (0->1), *Araripemys barretoi* (0->1), *Solnhofia parsoni* (0->1), *Leyvachelys cipadi* (0->1), *Glyptops plicatulus* (2->0); ACCTRAN: Dermochelyidae (0->1), *Dermochelys coriacea* (1->3), Kinosternoidea (0->2), *Kinosternon suburum hippocrepis* (2->0), *Dermatemys mawii* (2->0), total-group Chelidae (0->1), Chelodininae (1->0), Angolachelonia (0->1), (*Portlandemys* ++ *Plesiochelys*) (1->0), Pleurosternidae (2->0).

Character 121 (Cadena & Parham (2015): character 82). Prootic, dorsal exposure: 0 = large; 1 = very reduced or absent.

Character optimisation: Unambiguous: Emydidae (0->1), *Geoclemys hamiltonii* (0->1), *Testudo* (0->1), *Annemys latiens* (0->1); DELTRAN: *Meiolania planiceps* (0->1), *Kallokibotion bajazidi* (0->1); ACCTRAN: *Chubutemys*+++ (0->1), Paracryptodira+++ (1->0).

Character 122 (new character). Prootic, lateral semicircular canal enclosure by bone: 0 = canal only formed by bone of the opisthotic, the prootic portion of the canal is not ossified and is instead medially confluent with the recessus labyrinthicus prooticus; 1 = prootic and opisthotic both contribute to the formation of the lateral semicircular canal.

Remarks: In turtles, the lateral semicircular canal traverses the prootic and opisthotic. However, the lateral semicircular canal is generally weakly ossified. Only some portions of the membranous canal are surrounded by bone on the medial side of the canal. I observed that this portion of the endosseous lateral semicircular canal is often formed exclusively by

the opisthotic (e.g. *Caretta caretta:* NHMUK1938.1.9.1), but sometimes the prootic also contributes to the bony canal (all pleurodires examined for this study, but also taxa pertaining to other groups, e.g. *Sternotherus minor:* FMNH 211696).

With the increased availability of CT scanning, it will be possible to score this character for larger numbers of taxa, and this character aims to capture observed variation to test if this variation could be parsimony-informative. *Dermochelys* is scored as inapplicable, because its lateral semicircular canal lacks a medially ossified wall altogether.

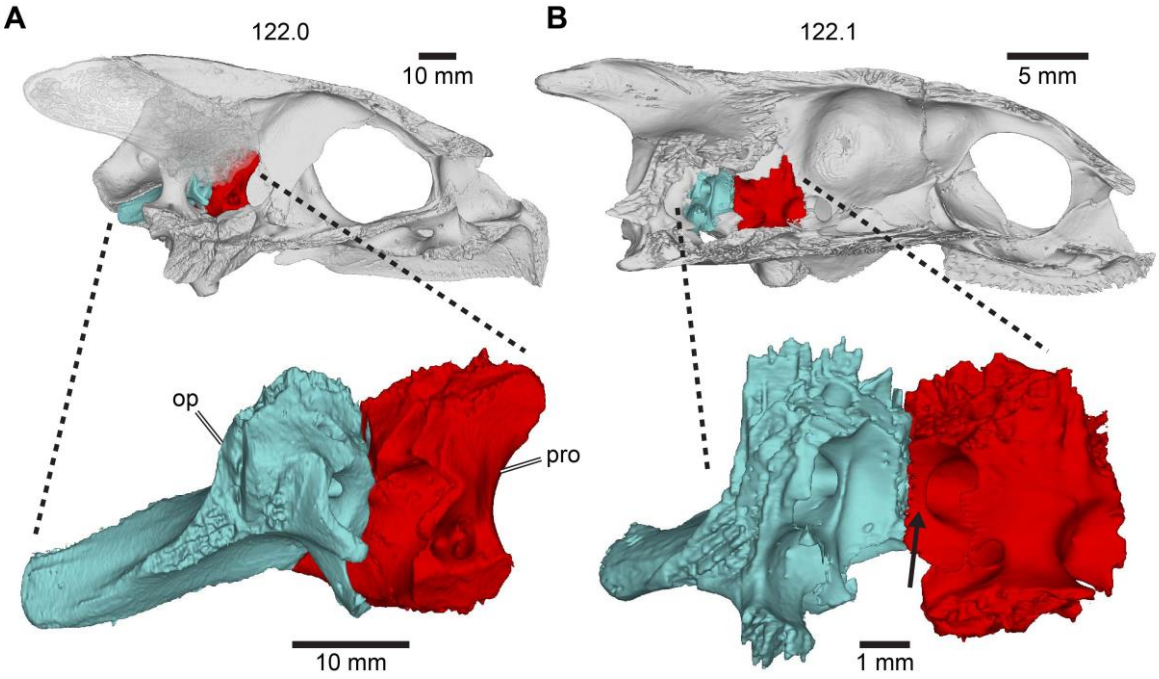


FIG. S1.47. Illustration of character 122. **A**, state 0 (*Lepidochelys olivacea*, SMNS 11070, medial view of left side of cranium, with close-up of prootic and opisthotic); **B**, state 1 (*Sternotherus minor*, FMNH 211696). Note that the supraoccipital is rendered transparent in A, and removed in B. Abbreviations: *op*, opisthotic; *pro*, prootic.

Character optimisation: Unambiguous: Cryptodira (1->0), *Bouliachelys suteri* (0->1), *Chrysemys picta* (0->1), *Pelodiscus sinensis* (0->1), (*Plesiochelys etalloni* + *Plesiochelys planiceps*) (1->0), *Arundelemys dardeni* (1->0); DELTRAN: *Kallokibotion*+++ (0->1), *Staurotypus* (0->1), *Dermatemys mawii* (0->1), *Kirgizemys hoburensis* (1->0); ACCTRAN: *Chubutemys*+++ (0->1), Kinosternoidea (0->1), Kinosterninae (1->0), Sinemydidae/Macrobaenidae (1->0).

Character 123 (new character). Prootic, ventral process: 0 = ventral process is short and without extensive posterior contact with the pterygoid; 1 = ventral process is large, with a broad contact with the pterygoid along a posteriorly expanded footplate, forming parts of the

floor of the inner ear cavity; 2 = ventral process is extensive, and forms parts of the floor of the basicranium so that it is visible on the ventral surface of the skull. This character is scored as inapplicable for taxa that lack an anatomically modern middle ear chamber.

Remarks: The ventral process of the prootic houses the fossa acustico-facialis and forms the medial wall to the canalis cavernosus. The morphology of this process varies amongst turtles.

In chelonioids (including protostegids such as *Rhinochelys*), trionychids (e.g. *Apalone spinifera emoryi*: FMNH22178), chelydrids (e.g. *Macrochelys temminckii*: FMNH22111), *Emarginachelys cretacea* (KUVP 23488), thalassochelydians (e.g. *Plesiochelys planiceps*: OUMNH J1582), and sandownids (e.g. *Sandownia harrisi*: MIWG 3480), the ventral process of the prootic is relatively short, extending ventrally almost to the floor of the cavum acustico-jugulare laterally and the floor of the inner ear cavity posteromedially. However, an extensive contact with the pterygoid is absent, so that the pterygoid floors most of the cavum acustico-jugulare and parts of the inner ear cavity. This morphology is accounted for in character state 0.

State 1 describes the morphology observed in crown-kinosternoids, such as *Sternotherus minor* (FMNH 211696), and testudinoids, such as *Gopherus polyphemus* (FMNH211815). The ventral process of the prootic is long in these taxa, and reaches the floor of the braincase, onto which it extends posteriorly via a footplate. The footplate is posteriorly and laterally expanded at its ventral end, and floors the anterior part of the inner ear cavity and by dorsally overlying the pterygoid, to which it is sutured, but usually does not extend laterally to the fenestra ovalis to floor parts of the cavum acustico-jugulare.

In most pleurodires (but not *Podocnemis unifilis*: FMNH 45657), the ventral process of the prootic is extensive, and is integrated into the ventral surface of the basicranium. The ventral part of the prootic is usually laterally strongly expanded to floor parts of the cavum acustico-jugulare lateral to the fenestra postotica. This condition is coded in state 2.

This character is scored as inapplicable for stem-taxa that lack an anatomically modern middle ear chamber (e.g. *Proganochelys* or *Kayentachelys*). The prootic is ventrally exposed in these forms, but the prootic does not form a ventral process.

Character optimisation: Unambiguous: Angolachelonia+++ (1->0), *Chelydra serpentina* (0->1), Kinosternoidea (0->1), Testudinoidea (0->1); DELTRAN: total-group Chelidae (0->2), *Pelomedusa subrufa* (0->2), *Xinjiangchelys radiplicatoides* (1->0); ACCTRAN: Pleurodira (0->2), *Podocnemis* (2->0), (*Xinjiangchelys wusu* + *Xinjiangchelys radiplactoides*) (1->0).

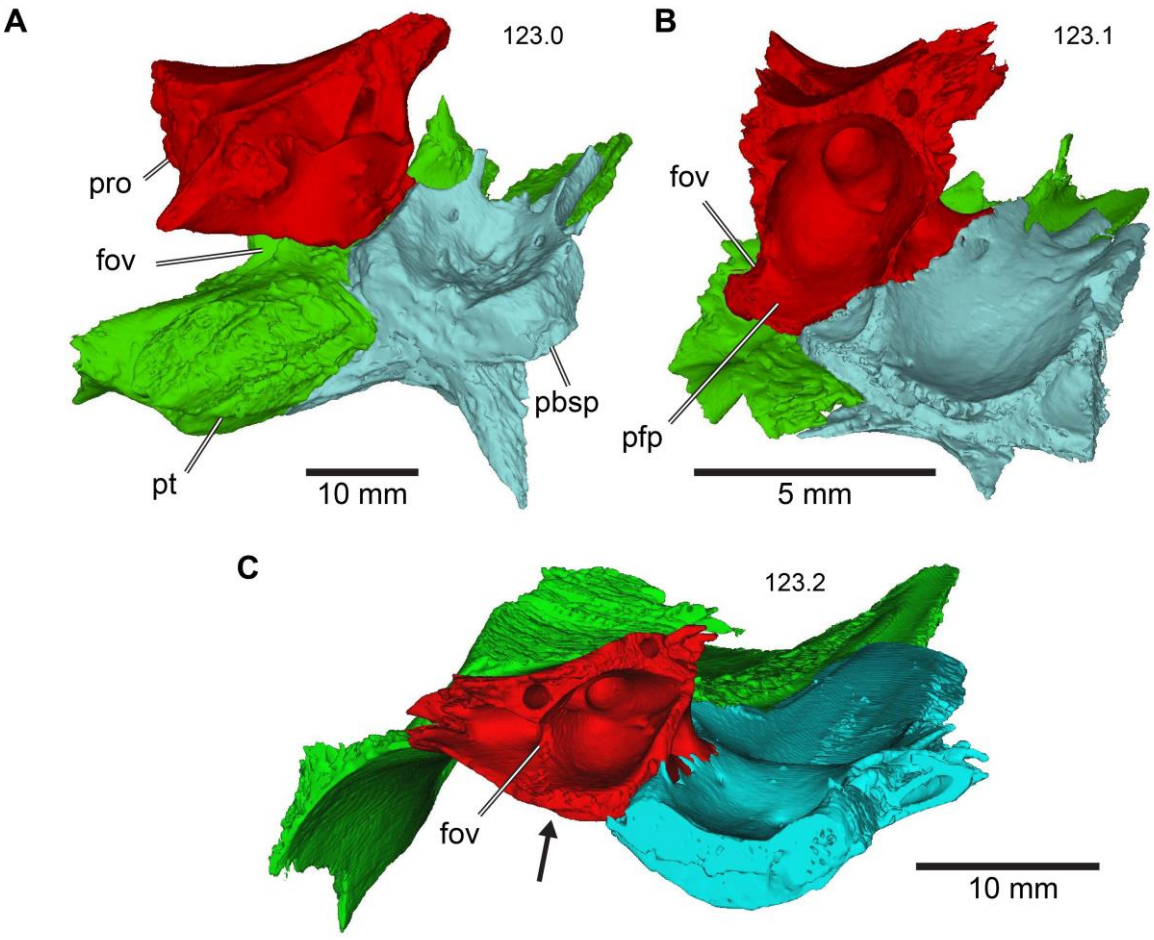


FIG. S1.48. Illustration of character 123. **A**, state 0 (*Lepidochelys olivacea*, SMNS 11070, posterodorsomedial view of partial left basicranium); **B**, state 1 (*Sternotherus minor*, FMNH 211696); **C**, state 2 (*Chelus fimbriatus*, NHMUK 81.9.27.4). Arrow in C indicates exposure of prootic on the ventral surface of the basicranium. Abbreviations: *fov*, fenestra ovalis; *pbsp*, parabasisphenoid; *pfp*, prootic footplate; *pro*, prootic; *pt*, pterygoid.

Character 124 (new character). Prootic, unnamed foramen exiting into the subtemporal fossa from the canalis cavernosus: 0 = absent; 1 = present.

Remarks: In most turtles, the canalis cavernosus or equivalent cranio-quadrate space is a canal or throughlet that connects the middle-ear region/cavum acustico-jugulare with the cavum cranii. The canalis cavernosus is usually formed by the prootic dorsally and the pterygoid ventrally, and the anterior foramen of the canalis cavernosus opens into the sulcus cavernosus just posteriorly and ventrally to the position of the trigeminal foramen. In most turtles, the canalis stapedio-temporale branches off the dorsal surface of the canalis cavernous, and opens via the foramen stapedio-temporale on the dorsal or anterodorsal surface of the otic capsule. However, there is an additional foramen branching off the canalis cavernosus in some turtles, for which I construct this characrer. This foramen is usually formed minimally by the prootic and quadrate, and is positioned between the trigeminal foramen anteriorly and the foramen stapedio-temporale posteriorly on the anteroventral surface of the otic capsule.

I do not designate a new name to the foramen, as its function is, to my knowledge, unknown. I speculate that the foramen could be an exit foramen for the mandibular artery (in which case the term “mandibular foramen” might be appropiate). Gaffney (1976) discussed the course of the mandibular artery, and summarised two principal patterns seen in turtles: In pleurodires, the mandibular artery branches off the stapedial artery after the latter exits the foramen stapedio-temporale (Gaffney 1979). In cryptodires, the mandibular artery branches off the stapedial artery within the cranium, traverses the canalis cavernsus, and exits through the trigeminal foramen (Gaffney 1979). It is conveivable that the mandibular artery, instead of being transmitted through the trigeminal foramen, exists the canalis cavernosus posteriorly to the trigeminal foramen through the extra formen observed here.

I found the foramen in carrettochelyids (e.g. *Carettochelys inscuplta*: NHMUK 1903.7.10.1; *Allaeochelys libyca*: BSPG 1991 II 130), some testudinoids (e.g. *Gopherus polyphemus*: FMNH 211815), *Chelonia mydas* (NHMUK 1969.776), and *Dermochelys coriacea* (UMCZ R 3031). It should be noted that I also found the additional foramen in one pleurodire, *Pelomedusa subrufa* (SMF 70504). This indicates that either the summary of Gaffney (1976) that all pleurodires have a mandibular artery that branches off the stapedial artery after the

latter exits the skull through the foramen stapedio-temporale is incorrect, or that the foramen indeed serves another function than transmitting the mandibular artery.

Character optimisation: Unambiguous: *Chelonia mydas* (0->1), *Platysternon megacephalum* (0->1), *Gopherus polyphemus* (0->1), total-group Carettochelyidae (0->1), *Pelomedusa subrufa* (0->1); DELTRAN: *Dermochelys coriacea* (0->1); ACCTRAN: Dermochelyidae (0->1).

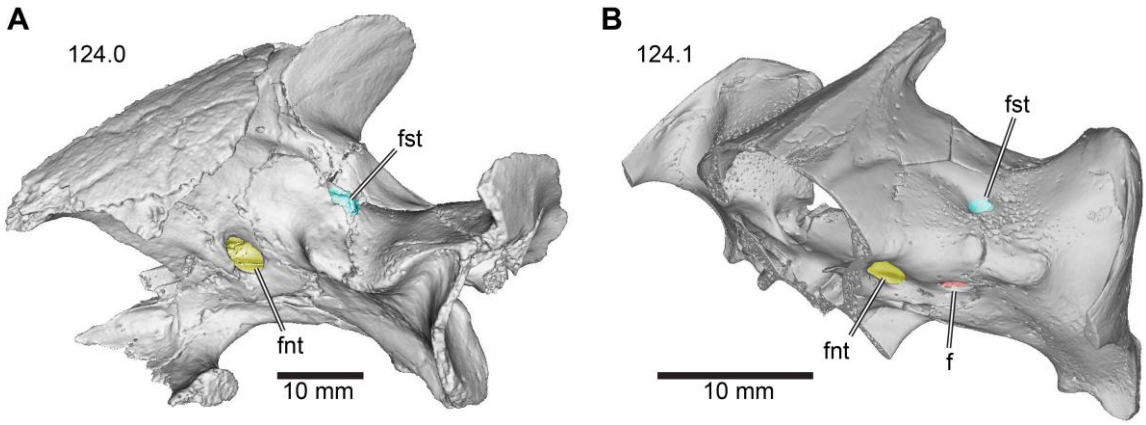


FIG. S1.49. Illustration of character 124. **A**, state 0 (*Plesiochelys planiceps*, OUMNH J1582, reflected anterodorsolateral view of right braincase); **B**, state 1 (*Gopherus polyphemus*, FMNH 211815, anterodorsolateral view of left braincase region). Abbreviations: *f*, additional foramen; *fnt*, foramen nervi trigemini; *fst*, foramen stapedio-temporale.

Character 125 (new character). Prootic/pterygoid, posteroventral elongation of the trigeminal foramen: 0 = absent, the trigeminal foramen is approximately circular or oval, but the ventral margin of the foramen is positioned above the level of the canalis/sulcus cavernosus; 1 = the trigeminal foramen is oval, anterodorsally-posteroventrally elongate and anteroventrally-posterodorsaly narrow, and the ventral margin is level with the canalis/sulcus cavernosus. This character is scored inapplicable for turtles without a trigeminal foramen (i.e. without a neomorphic secondary lateral wall of the braincase formed by the parietal and pterygoid).

Remarks: Some taxa (cheloniids but *Chelonia mydas*; chelydrids, some kinosternids, trionychids, xinjiangchelyids) have a posteroventrally elongated trigeminal foramen (state 1),

whereas the trigeminal foramen is less elongated and more circular in all other turtles (state 0).

The posteroventral portion of the elongated trigeminal foramen is positioned at the level of the floor of the sulcus cavernosus, just anterior to the position of the foramen cavernosum, and ventral to the level of the cavum epipteryocum, which houses the trigeminal ganglion. It is likely, that the maxillary and mandibular rami of the trigeminal formen therefore exit through the dorsal part of the elongated trigeminal foramen (i.e. at the level of the trigeminal ganglion), and that the posteroventral part of the foramen transmits other vessels. The posteroventral margin of the trigeminal foramen in turtles scored as having state 1 is topologically near the position of the additional foramen regarded in character 124. I think it is possible that the posteroventral elongation is an intermediate state between having a small trigeminal foramen and no additional foramen, and having a small trigeminal foramen and an additional foramen. The posteroventral elongation could thus be an aperture for the exit of the mandibular artery. This condition could essentially represent a conjoined foramen for the mandibular artery and the trigeminal foramen. However, this remains speculative until the course mandibular artery and trigeminal nerves have been investigated for a range of taxa. Therefore I have coded two separate characters for the observations of a second foramen (ch 124) and for an elongated trigeminal foramen (this character).

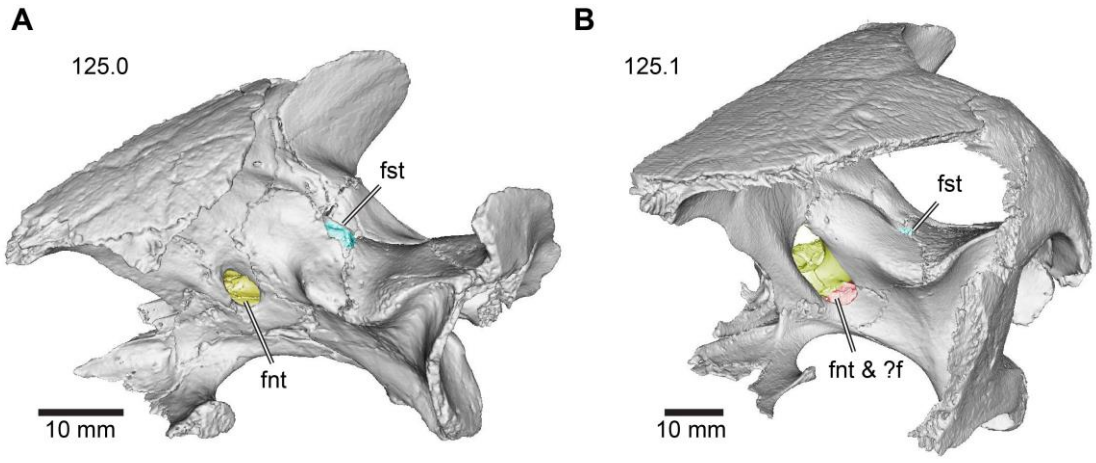


FIG. S1.50. Illustration of character 125. **A**, state 0 (*Plesiochelys planiceps*, OUMNH J1582, reflected anterodorsolateral view of right braincase); **B**, state 1 (*Lepidochelys olivacea*, SMNS 11070, anterodorsolateral view of left braincase region). Abbreviations: *f*, additional foramen; *fnt*, foramen nervi trigemini; *fst*, foramen stapedio-temporale.

Character optimisation: Unambiguous: *Notochelone* (0->1), *Puppigerus camperi* (1->0), *Kinosternon suburum hippocrepis* (0->1), *Platysternon megacephalum* (0->1), Trionychia (0->1), Xinjiangchelyidae (0->1), *Arundelemys dardeni* (0->1); DELTRAN: *Desmatochelys lowii* (0->1), total-group Cheloniidae (0->1), crown-group Chelydridae (0->1); ACCTRAN: crown-group Chelonioidea (0->1), (*Bouliachelys* ++ *Santanachelys*) (1->0), total-group Chelydridae (0->1).

Character 126 (new character). Prootic, recess on posterior surface of the element anterodorsolaterally to the fenestra ovalis: 0 = absent; 1 = present.

Remarks: In turtles, the fenestra ovalis is anteriorly formed by the prootic. The fenestra ovalis laterally opens into a large space called the cavum acustico-jugulare, which houses several anatomical structures. One such structure is the pericapsular recess, which extends through the recessus scalae tympani, and anterolaterally to the fenestra ovalis to form a continuous and re-entrant circuit of fluids moved by oscillations of the stapes (Wever 1978). The pericapsular recess surrounds the fenestra ovalis, and in some taxa the prootic shows a posteriorly facing concavity that is positioned anterodorsally and laterally to the fenestra ovalis. While the function of this recess is not clear, it could be related to an anterior extension of the pericapsular recess (see also Gaffney 1983: p. 446 for a similar argument). The margins of the prootic recess are usually sharp, low ridges, which could indicate that the membranous lining of the pericapsular recess (paracapsular sac drawn in Gaffney 179: fig. 46A) attached to these ridges.

In this character, I score the absence or presence of the described fossa. The fossa is for example present in plesiochelyids, chelydrids, trionychians (but not *Allaeochelys libyca*: BSPG 1991 II 130), pleurodires, paracryptodirans, and most kinosternids (but not *Dermatemys mawii*: SMF 59563). Testudinoids and chelonioids vary in the presence of states 0 and 1, but none of the protostegids for which this character could be scored show a posterior prootic fossa (i.e. all protostegids have state 0).

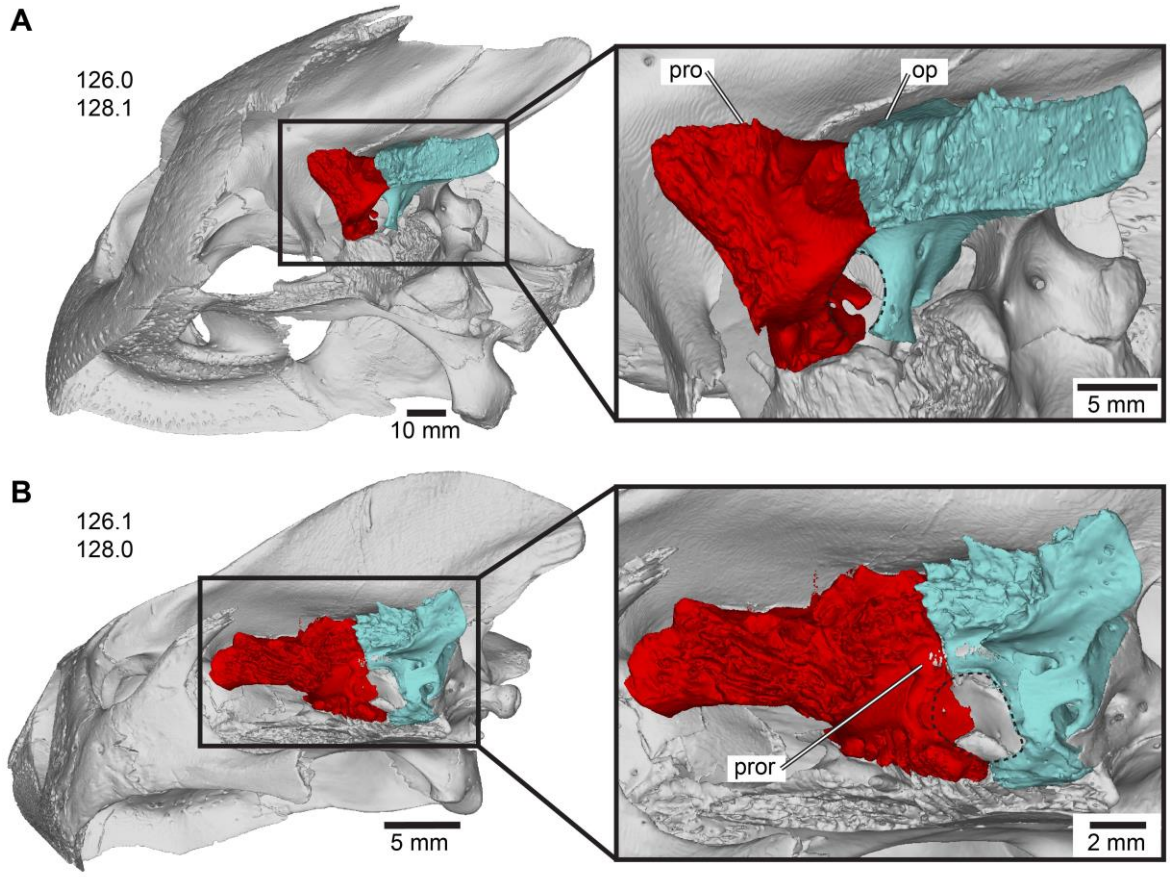


FIG. S1.51. Illustration of characters 126 and 128. **A**, state 0 (*Lepidochelys olivacea*, SMNS 11070, posteroventrolateral view of otic region, with close-up of the lateral side of the otic capsule); **B**, state 1 (*Sternotherus minor*, FMNH 211696). Note that the quadratojugal, quadrate, pterygoid, and squamosal have been removed in A and B. Abbreviations: *op*, opisthotic; *pro*, prootic; *pror*, prootic recess.

Character optimisation: Unambiguous: *Meiolania*+++ (0->1), *Chrysemys picta* (1->0), *Gopherus polyphemus* (1->0), *Allaeochelys libyca* (1->0), *Solnhofia parsoni* (1->0); DELTRAN: Dermochelyoidea (1->0), *Lepidochelys olivacea* (1->0), *Eretmochelys imbricata* (1->0), *Natator depressus* (1->0), *Allopleuron hofmanni* (1->0), *Argillochelys cuneiceps* (1->0), *Dermatemys mawii* (1->0); ACCTRAN: total-group Chelonioidea (1->0), *Puppigerus*+++ (0->1), *Lepidochelys olivacea* (1->0), *Eretmochelys imbricata* (1->0), *Natator depressus* (1->0), *Eochelone* (0->1), total-group Dermatemydidae (1->0).

Character 127 (modified from Cadena & Parham (2015)). Prootic, position of the geniculate ganglion and the split of the facial nerve into the hyomandibular and palatine branches: 0 = the geniculate ganglion is positioned with the canalis cavernosus; 1 = the geniculate ganglion is positioned within the facial nerve canal; 2 = the geniculate ganglion is positioned in the canalis carotici interni.

Previous definition (Cadena & Parham (2015): character 93): Hyomandibular, path of hyomandibular branch of the facial nerve: 0 = hyomandibular nerve passes through cranioquadrate space parallel to vena capitis lateralis; 1 = hyomandibular nerve runs independent from vena capitis lateralis. Joyce (2007: ch 52) & Sterli & De la Fuente (2013: ch 95) (Hyomandibular Nerve A).

Remarks: Gaffney (1979) discussed two main patterns for the course of facial nerve, based on observation by Siebenrock (1897) and Soliman (1964). These patterns were based on dissections or skull section of a few species of cryptodires and pleurodires, and Gaffney extrapolated these observations as generalised patterns for both of these groups. The summary provided by Gaffney (1976) lead to the construction of a character for the passage of the hyomandibular branch of the facial nerve (e.g. Joyce 2007: character 52, Hyomandibular Nerve A). Most following authors, including Cadena & Parham (2015: character 93), left this character unchanged.

Although I have not done any dissections for this work, the facial nerve runs through a series of bony canals that can be traced in my CT data. My observations largely confirm differences between pleurodires (state 2) and cryptodires (state 0), but I also observed additional variation, most importantly a previously unrecognized pattern for the subdivisions of the facial nerve (state 1).

In all turtles, the facial nerve enters the braincase via the fossa acustico-facialis on the medial surface of the prootic. From this fossa, the facial nerve canal transmits the undivided facial nerve laterally. The facial nerve splits into two subordinate branches, the hyomandibular (=posterior) and palatine (=anterior) branch at the geniculate ganglion. For the character descriptions above I have chosen to use the point of division of the facial nerve into its posterior and anterior branches, i.e. the position of the geniculate ganglion, as landmarks distinguishing the character states. However, longer descriptions of the canal patterns observed in my CT data are provided here.

In turtles scored as having state 0 (cryptodires; *Sandownia harrisi*: MIWG 3480), the facial nerve canal traverses the prootic laterally, and enters the canalis cavernosus. The geniculate ganglion is positioned here. A short canal, termed the foramen pro ramo nervi vidani (Gaffney 1972, 1976), transmits the palatine branch from the floor of the canalis cavernosus into the slightly more ventrally positioned canalis carotici interni. The palatine branch of the facial nerve passes anteriorly within the canalis carotici interni. The hyomandibular branch of the facial nerve passes posteriorly through the canalis cavernosus, paralleling the course of the vena capitis lateralis. In testudinids (*Gopherus polyphemus*: FMNH 211815; *Chelonoidis* sp.: SMF 67582; *Testudo marginata*: FMNH 51672), the hyomandibular branch of the facial nerve has its own canal that parallels the posterior course of the canalis cavernosus. The canal is positioned just ventral to the canalis cavernosus, and housed within the prootic, but some parts are partially walled by the pterygoid. In the traditional use of this character, the condition of testudinids sounds superficially similar to that of pleurodires. However, the branching pattern of the palatine and hyomandibular nerves of testudinids and other cryptodires are identical, and only the separate ossification of a pathway for the hyomandibular branch are different. To accommodate these differences, I have coded an additional character (character 155, see below).

In turtles scored as having state 1 (*Meiolania planiceps*: NHMUK R 682; *Eileanchelys waldmanni*: NMS G2004-31-15; *Plesiochelys planicpes*: OUMNH J1582; *Plesiochelys etalloni*: MNB 435; *Jurassichelon oleronensis*: PIMUZ AIII 514; *Kallokibotion bajazidi*: NHMUK R 4925; *Arundelemys dardeni*: USNM 497740; *Pleurosternon bullockii*: UMZC T1041; *Eubaena cephalica*: DMNH 96004; *Solnhofia parsoni*: TM 4023; *Annemys* sp.: IVPP V1806; *Ordosemys* sp.: IVPP V12092), the geniculate ganglion is inferred to be positioned within the facial nerve canal that emerges laterally from the fossa acustico-facilis. In these turtles, the main differences observed in relation to the pattern described above can be summarised as: First, the facial nerve canal is strongly posterolaterally curved, so that is does not merge with the canalis cavernus along the mid-course of the latter but in a more posterior section. Second, the canal that transmits the palatine branch of the facial nerve to the canalis carticus internus

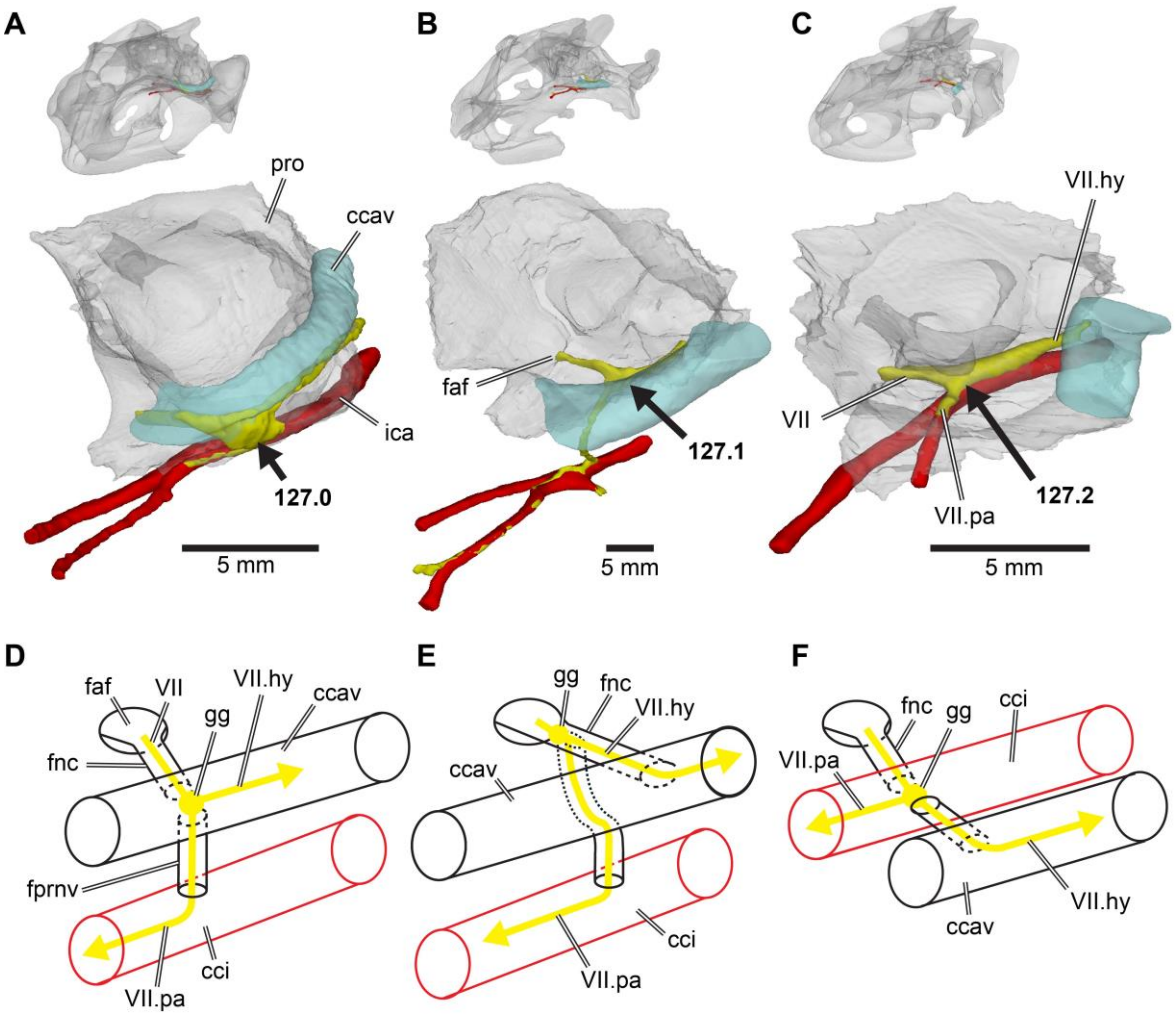


FIG. S1.52. Illustration of character 127. **A**, state 0 (*Gopherus polyphemus*, FMNH 211815, left anterodorsolateral view of cranium, with close-up of the prootic and internal structures); **B**, state 1 (*Plesiochelys planiceps*, OUMNH J1582); **C**, state 2 (*Phrynops geoffroanus*, SMF 45470); **D-F**, schematic representations of facial nerve branching pattern for A-C, respectively. Note that the cranium, prootic, and canalis cavernosus are rendered transparent in A-C. *Abbreviations*: *VII*, facial nerve; *VII.hy*, hyomandibular branch of the facial nerve; *VII.pa*, palatine branch of the facial nerve; *ccav*, canalis cavernosus; *cci*, canalis caroticus internus; *faf*, fossa acustico-facialis; *fnc*, facial nerve canal, *fprnv*, foramen pro ramo nervi vidani; *gg*, geniculate ganglion; *ica*, internal carotid artery, *pro*, prootic.

branches directly off the facial nerve canal, and not from the canalis cavernosus (albeit close to the point where the facial canal merges with the canalis cavernosus). Third, the canal transmitting the palatine branch of the facial nerve is also notably longer than the short foramen pro ramo nervi vidani of turtles with state 0. In many taxa scored as having state 1, the short extension of the facial canal that transmits the hyomandibular branch of the facial nerve canal exits into the canalis cavernosus near the posterior foramen of the canalis cavernosus to the cavum acustico-jugulare (e.g., plesiochelyids). In *Meiolania*, this foramen is

even positioned medially to the posterior foramen for the canalis cavernosus, so that the hyomandibular branch of the facial nerve does not pass through any section of the canalis cavernosus. Carabajal *et al.* (2017: fig. 4) show a similar position for a foramen associated with the facial nerve for the meiolanid *Gaffneylania*, so that the morphology described for *Meiolania* might be widespread within the group. I currently do not score this additional variation as a separate character.

In turtle scored as having state 2, the facial nerve canal is laterally directed, and directly connected to the canalis caroticus internus. The geniculate ganglion is positioned within an enlarged fossa that forms at the point where both canals meet. From here, the palatine branch of the facial nerve travels anteriorly with the internal carotid artery. The hyomandibular branch is transmitted posterolaterally within its own canal that connects the canalis carotici interni with the canalis cavernosus. The foramen through which the hyomandibular nerve exits is positioned in the posterior section of the canalis cavernosus, near its posterior foramen with the cavum acustico-jugulare.

Character optimisation: DELTRAN: Cryptodira (1->0), Pleurodira (1->2), *Sandownia harrisi* (1->0); ACCTRAN: Angolachelonia+++ (1->0), *Pleurodira* (0->2), Thalassochelydia (0->1).

Character 128 (new character). Prootic/opisthotic, enclosure of fenestra ovalis: 0 = the fenestra ovalis is ventrally enclosed by the prootic and opisthotic; 1 = the prootic and opisthotic do not have a contact ventrally to the fenestra ovalis.

Remarks: The fenestra ovalis is completely surrounded by bone in early turtles, including Triassic (e.g. *Proganochelys quenstedti*: SMNS 16980) and Jurassic stem-group turtles (e.g. *Eileanchelys waldmanni*: NMS.G.2004.31.15), as well as those sinemydids/macrobaenids for which this character could be assessed (e.g. *Ordosemys* sp.: IVPP V12092), and some thalassochelydians (e.g. *Jurassichelon oleronensis*: PIMUZ III A 514; nut not *Plesiochelys planiceps*: OUMNH J1582). However, it is ventrally open in most crown-turtles.

Character optimisation: Unambiguous: Angolachelonia+++ (0->1), *Allopleuron hofmanni* (1->0), *Sternotherus* (1->0), *Chelus fimbriatus* (1->0), *Chelodina* (1->0); DELTRAN: *Desmatochelys lowii* (1->0), *Ocepechelon bouyai* (1->0), *Jurassichelon oleronensis* (1->0), *Portlandemys mcdowelli* (1->0), *Pleurosternon bullockii* (0->1); ACCTRAN: Protostegidae (1->0), (*Bouliachelys* ++ *Santanachelys*) (0->1), (*Portlandemys* ++ *Plesiochelys*) (1->0), (*Plesiochelys etalloni* + *Plesiochelys planiceps*) (0->1), (*Eubaena* ++ *Pleurosternon*) (0->1).

Character 129 (Cadena & Parham (2015): character 83). Opisthotic, wide transverse occipital plane with depression for the nuchal musculature: 0 = absent; 1 = present.

Character optimisation: Unambiguous: *Eubaena cephalica* (0->1), *Kallokibotion bajazidi* (0->1), *Australochelys africanus* (0->1).

Character 130 (modified from Cadena & Parham (2015)). Opisthotic, processus interfenestralis: 0 = developed as a robust ridge that does not form a ventrally projecting process and does not reach closely to the floor of the basicranium; 1 = incipient, developed as a ventrally low and mediolaterally broad, robust structure that separates the cavum labyrinthicum anteriorly from an incipient recessus scalae tympani posteriorly; 2 = present, developed as a ventrally directed process that separates the cavum labyrinthicum anteriorly from the recessus scalae tympani posteriorly.

Previous character definitions:

(1) Cadena & Parham (2015: character 85): Opisthotics, processus interfenestralis: 0 = present, but not reaching the floor of cavum acustico-jugulare; 1 = present, reaching the floor of the cavum acustico- jugulare but small; 2 = present, reaching the floor of the cavum acustico-jugulare but robust. Sterli (2008: ch 56); Sterli & De la Fuente (2013: ch 82, Opisthotic D).

(2) Cadena & Parham (2015: character 84): Opisthotics, ventral ridge on opisthotic: 0 = absent; 1 = present, with an incipient enclosed middle ear region; 2 = present, but modified

with an enclosed middle ear region. Sterli (2008: ch 55); Sterli & De la Fuente (2013: ch 81, Opisthotic C).

Remarks: My character 130 is essentially a combination of characters 84 and 85 of Cadena & Parham (2015). The morphological variation encoded in this character concerns the morphology of the processus interfenestralis of the opisthotic, and I believe that aspects of the variation encoded in both previous characters are repetitive. I deleted character 84 of Cadena & Parham (2015; see discussion in section of deleted characters), and modified character 85 of Cadena & Parham (2015).

This character was first used by Sterli (2008: character 56), who refer to Sterli and Joyce (2007) for the rationale of this character. Cadena & Parham (2015: character 85) swapped character states 1 and 2 in comparison to the original definition of Sterli (2008). While Sterli (2008) originally treated her characters as unordered, this character was ordered in later studies that kept the original definition of Sterli (2008), such as Sterli and De la Fuente (2013: character 82). By changing the sequence of states 1 and 2, Cadena & Parham (2015), who also ordered this character, changed the meaning of this character in respect to the definition of the original authors.

There are further issues with this character as used previously: The character definition, and scorings used by Cadena & Parham (2015: character 85) for several taxa are inconsistent with the definition of the processus interfenestralis (*sensu* Gaffney 1979), as well as with the observations and descriptions of fossil taxa for which they are scored. I therefore provide some information on the definition of the processus interfenestralis before giving a detailed justification for my modified character state definitions.

The general morphology of crown-turtles is that the processus interfenestralis forms a process that extends ventrally from the opisthotic into the cavum acustico-jugulare (Gaffney 1979). It separates the cavum labyrinthicum anteriorly from the recessus scalae tympani posteriorly, which is a medial extension of the cavum acustico-jugulare. The processus interfenstralis is usually pierced by a short canal for the glossopharyngeal nerve

(CN IX) near its dorsal base (Gaffney 1979). The evolution of the processus interfenestralis is difficult to trace because in some basal stem-turtles, including *Proganochelys* and *Australochelys*, the middle ear region has not yet been modified to have a clearly defined cavum acustico-jugulare, or recessus scalae tympani (Gaffney 1990). In *Proganochelys* and *Australochelys*, the opisthotic bears a robust ventral ridge posteromedial to the fenestra ovalis (Gaffney 1990; Gaffney & Kitching 1995). This ridge is ventrally not nearly as deep as the processus interfenestralis *sensu stricto* as developed in crown-turtles, but extends posterolaterally further than the process of crown-turtles. The ridge of *Proganochelys* is laterally pierced by a foramen for the CN IX, and has thus been interpreted to be homologous with the processus interfenestralis of crown turtles (Gaffney 1990). My definition of state 0 accommodates the morphology of the processus interfenestralis as a low ridge, as described for *Proganochelys* and *Australochelys*. This is consistent with the scoring of Sterli (2008), who originally defined this character state.

The character definition of Cadena & Parham (2015: character 85) includes a character state 2 (= character state 1 of character 56 in Sterli 2008), which states that the processus interfenestralis is a robust structure reaching the floor of the cavum acustico-jugulare. This character state is only scored as present in *Kayentachelys* and *Condorchelys* in the matrix of Cadena & Parham (2015), as is also the case in Sterli (2008). However, both of these taxa have a robust processus interfenestralis that does not reach the floor of the basicranium (Sterli & Joyce 2007; Sterli & De la Fuente 2010). Indeed the morphology of both taxa is explicitly described as being similar to that of taxa more basal than *Heckerochelys*, which include forms like *Proganochelys* and *Australochelys* (Sterli & Joyce 2007; Sterli & De la Fuente 2010). Additonally, the cavum acustico-jugulare remains unfloored in *Kayentachelys*, which disagrees with the definition of state 2 *sensu* Cadena & Parham (2015), and also with the definition of state 1 *sensu* Sterli (2008).

I investigated the morphology of *Kayentachelys* based on CT scans of TMM 43670-2. Based on my observations, I agree with the description of Sterli and Joyce (2007), which states that *Kayentachelys* has certain similarities to *Australochelys* and *Proganochelys*.

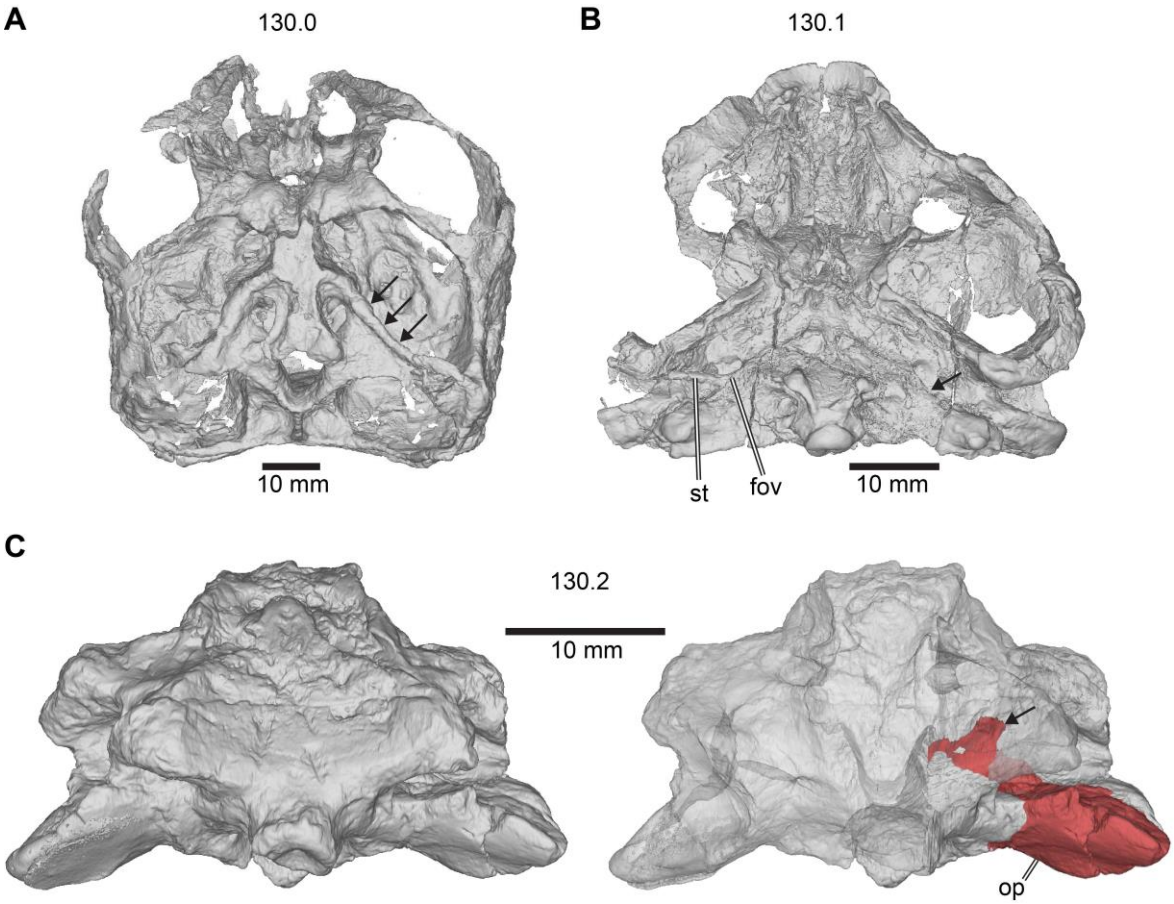


FIG. S1.53. Illustration of character 130. **A**, state 0 (*Australochelys africanus*, BP/1/4933, posteroventral view of cranium); **B**, state 1 (*Kayentachelys aprix*, TMM 4370-2); **C**, state 2 (*Kallokibotion bajazidi*, NHMUK R4925, posteroventral view of basicranium, rendered solid on the left and transparent on the right with opisthotic coloured.). Arrow in C indicates anatomically modern processus interfenestralis. Abbreviations: *fov*, fenestra ovalis; *op*, opisthotic; *st*, stapes.

However, I also note important differences: Other than in *Proganochelys* and *Australochelys*, a fenestra perilymphatica and an incipient recessus scalae tympani are clearly present, and the ventral surface of the opisthotic between the jugular area and the fenestra ovalis does not develop a ventrally deep ridge as seen in *Proganochelys* or *Australochelys*. The medial portion of the opisthotic between the jugular region and the fenestra ovalis is ventrally deeply developed, forming a process that is ventrally sutured to the exoccipital-basioccipital region just dorsally to the basal tubera. This latter feature was probably meant by Sterli (2008) (and by extension Cadena & Parham (2015)) when describing the processus interfenestralis of *Kayentachelys* as "reaching the floor of the cavum acustico-jugulare". In this regard, *Kayentachelys* could be described as having a true processus interfenestralis (*sensu* Gaffney 1979). However, the process is mediolaterally much wider than in anatomically modern taxa,

and near the fenestra ovalis, the process is not at all ventrally expanded. In anatomically modern turtles, the region around the fenestra ovalis is usually most expanded ventrally. I therefore coded a new character state (state 1) specifically for the morphology seen in *Kayentachelys* (and *Condorchelys*).

My state 2 describes the anatomically modern condition (i.e., processus interfenestralis *sensu* Gaffney 1979), in which the processus interfenestralis is transversely relatively short but ventrally deep. However, I also acknowledge that there is additional variation to the morphology of the processus interfestralis *sensu* Gaffney (1979), which is not currently accounted for in my modified version of character 28. For that reason, I coded an additional character (character 128, see below).

Character optimisation: Unambiguous: (*Kayentachelys*+*Eileanchelys*)+++ (0->2), *Kayentachelys aprix* (2->1).

Character 131 (new character). Opisthotic, development of the processus interfenestralis: 0 = developed as a ventrally directed process that separates the cavum labyrinthicum anteriorly from the recessus scalae tympani posteriorly, the process is not expanded at its ventral end, and almost or just about reaches the floor of the basicranium, but a small gap (hiatus postlagenum) usually remains; 1 = developed as a ventrally directed process that separates the cavum labyrinthicum anteriorly from the recessus scalae tympani posteriorly, but the process has a horizontally expanded footplate at its ventral end that is sutured to elements of the basicranium; 2 = developed as a ventrally directed process that separates the cavum labyrinthicum anteriorly from the recessus scalae tympani posteriorly, and the ventral surface of the process is integrated into the basicranium to form parts of the ventral surface of the cranium. This character is scored as inapplicable if an anatomically modern processus interfenestralis is absent (i.e. ch 131.0 or 131.1).

Remarks: This new character addresses variation observed within the processus interfenestralis *sensu stricto*, i.e a ventrally directed process in a fully developed cavum acustico-jugulare is assumed, and taxa lacking this feature are scored as inapplicable. For a discussion of the processus interfenestralis, see the remarks for my character 130.

Character state 0 includes a statement on the relative dorsoventral length of the processus interfenstralis in relation to the floor of the cavum acustico-jugulare. Character state 0 accounts for those turtles, in which the processus interfenestralis comes close to, or just about contacts the floor of the cavum acustico-jugulare. However, in all turtles scored as having state 0, the processus interfenestralis is not sutured to elements of the basicranium via an expanded footplate, or even expressed on the ventral surface of the basicranium. State 0 is observed in the earliest turtles that have a true processus interfenestralis (e.g. *Chubutemys copelloi*: MPEF-PV1236, Gaffney *et al.* 2007; Sterli *et al.* 2015; *Eileanchelys waldmanni*: NMS.G.2004.31.15; *Kallokibotion bajazidi*: NHMUK R4921), the early baenid *Arundelemys dardeni* (USNM 497740), xinjiangchelyids (except *Annemys* sp: IVPP V18106), thalassochelydians (e.g. *Solnhofia parsoni*: TM 4023), sandownids (e.g. *Sandownia harrisi*: MIWG 3480), all pleurodires, and most cryptodires.

My definition of character state 1 is superficially similar to state 2 of character 85 of Cadena & Parham (2015), but the scorings across taxa varies drastically, as outlined in the remarks for character 130 (modified from Cadena & Parham (2015) character 85). Based on my comparative CT dataset, I noticed that in some taxa, the ventral tip of the processus interfenestralis is expanded to a horizontal plate that is sutured to the dorsal surface of the basicranium. Examples are kinosternids (*Sternotherus*: FMNH211696; *Staurotypus*: NHMUK1879.1.7.5; *Kinosternon* spp.: FMNH211711, FMNH211705, SMF71893), in which the process is sutured to elements forming the floor of the cavum acustico-jugulare, hereby often forming parts of the floor of the inner ear cavity.

My state 2 is scored for taxa in which the processus interfenestralis is integrated into the basicranium, leading to its exposure on the ventral surface of the cranium. This means the ventral surface of the processus interfenestralis is visible in a ventral view of the cranium,

and the margins of the ventral surface are in contact with other basicranial elements (rather than sitting on their dorsal surface as in state 2). This state is observed in some testudinids (*Gopherus polyphemus*: FMNH211815; *Chelonoidis*: SMF67582), as well as some sinemydids (*Sinemys lens* and *Sinemys gamera*; Brinkman & Peng 1993*a*). Consequentially, in these taxa, the cavum acustico-jugulare is not only floored by the pterygoid, but additionally by the opisthotic.

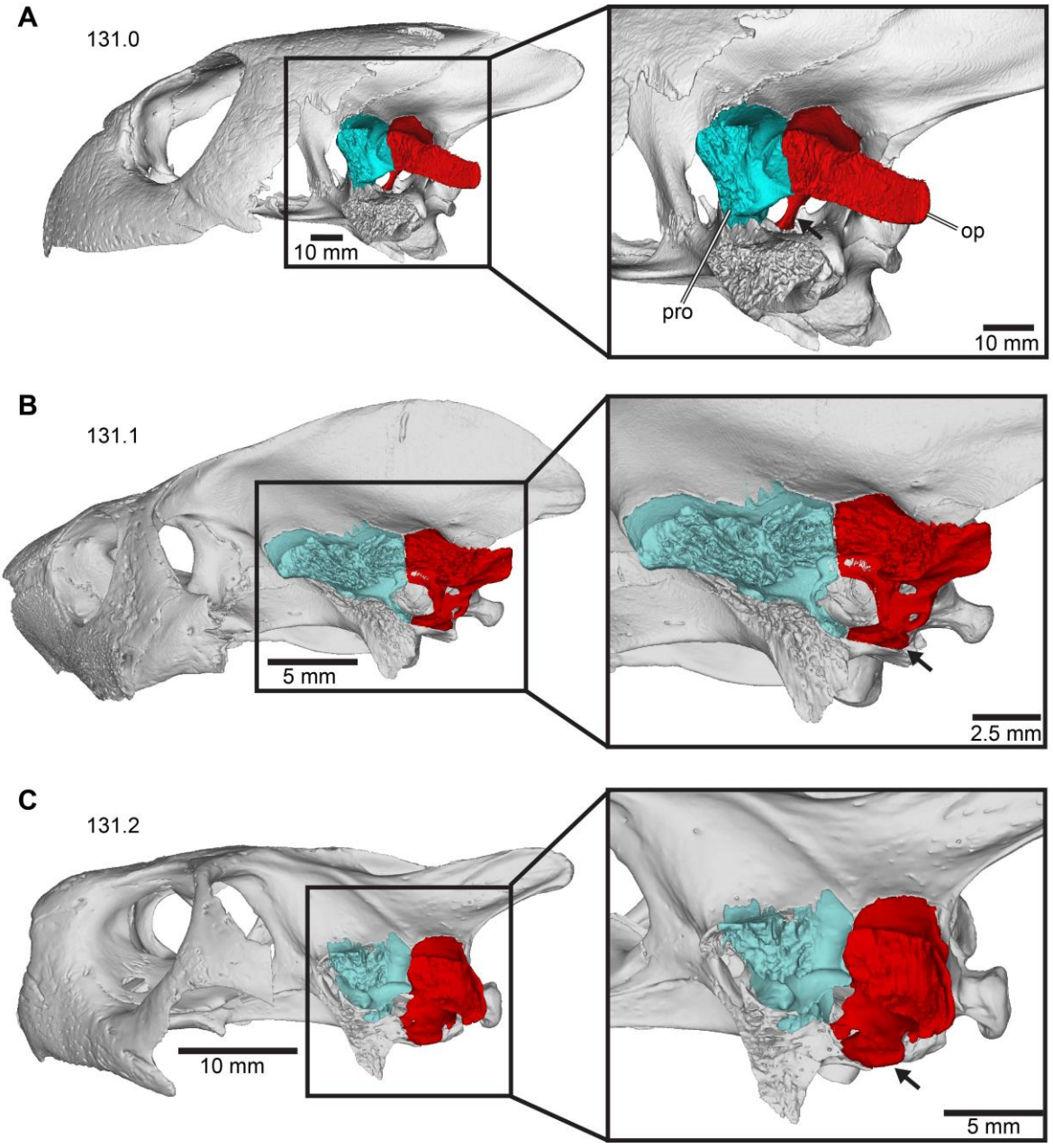


FIG. S1.54. Illustration of character 131. **A**, state 0 (*Lepidochelys olivacea*, SMNS 11070, posteroventrolateral view of left otic region, with close-up of prootic and opisthotic); **B**, state 1 (*Sternotherus minor*, FMNH 211696); **C**, state 2 (*Chelonoidis* sp., SMF 67582). Arrows show processus interfenestralis. Note that the quadratojugal, quadrate, pterygoid, and squamosal have been removed in A-C. Abbreviations: *op*, opisthotic; *pro*, prootic.

Character optimisation: Unambiguous: *Allopleuron hofmanni* (0->1), Kinosternidae (0->1), *Annemys* sp. IVPP V18106 (0->1), (*Eubaena* ++ *Pleurosternon*) (0->1), *Pleurosternon bullockii* (1->2); DELTRAN: *Desmatochelys lowii* (0->1), *Chelonoidis* sp. (0->2), *Gopherus polyphemus* (0->2), *Jurassichelon oleronensis* (0->1), *Portlandemys mcdowelli* (0->1), (*Sinemys lens* + *Sinemys gamera*) (0->2); ACCTRAN: (*Desmatochelys lowii* + *Desmatochelys padillai*) (0->1), Testudinidae (0->2), *Testudo* (2->0), (*Portlandemys* ++ *Plesiochelys*) (0->1), (*Plesiochelys etalloni* + *Plesiochelys planiceps*) (1->0), Sinemydidae/Macrobaenidae (0->2).

Character 132 (new character). Opisthotic, posterior surface of paroccipital process: 0 = the occipital side of the paroccipital process is developed as a posteriorly exposed, broad, planar or gently concave surface; 1 = the occipital side of the paroccipital process is dorsoventrally flattened and forms a posterior ridge that traverses the paroccipital process mediolaterally; 2 = the paroccipital process has a dorsoventrally convex surface.

Remarks: In some turtles (e.g. Sternotherus minor: FMNH 211696), the posterior surface of the opisthotic forms a broad and flat surface (state 0). In trionychians, sandownids, and pleurodires, the opisthotic is posteriorly narrowed to a sharp-edged ridge, which extends from the contact area with the exoccipital medially to the posterolateral contact with the squamosal on the paroccipital process (state 1). In plesiochelyids and various other turtles, the posterior surface of the opisthotic is convexely thickened to a robust but low ridge that extends to the tip of the paroccipital process.

Character optimisation: Unambiguous: total-group Chelonioidea (0->2), *Lepidochelys olivacea* (2->1), *Eretmochelys imbricata* (2->0), *Chelonia mydas* (2->0), *Eochelone* (2->0), Pleurosternidae (0->1); DELTRAN: *Notochelone* (2->0), Trionychia (0->1), Pleurodira (0->1), (*Portlandemys* ++ *Plesiochelys*) (0->2), Sandownidae (0->1), (*Eileanchelys* + *Kayentachelys*) (0->1), *Australochelys africanus* (0->1); ACCTRAN: *Australochelys*+++ (0->1), *Chubutemys*+++ (1->0), Angolachelonia+++ (0->1), Durocryptodira (1->0), (*Santanachelys* + *Notochelone*) (2->0), Thalassochelydia (1->0), (*Portlandemys* ++ *Plesiochelys*) (0->2).

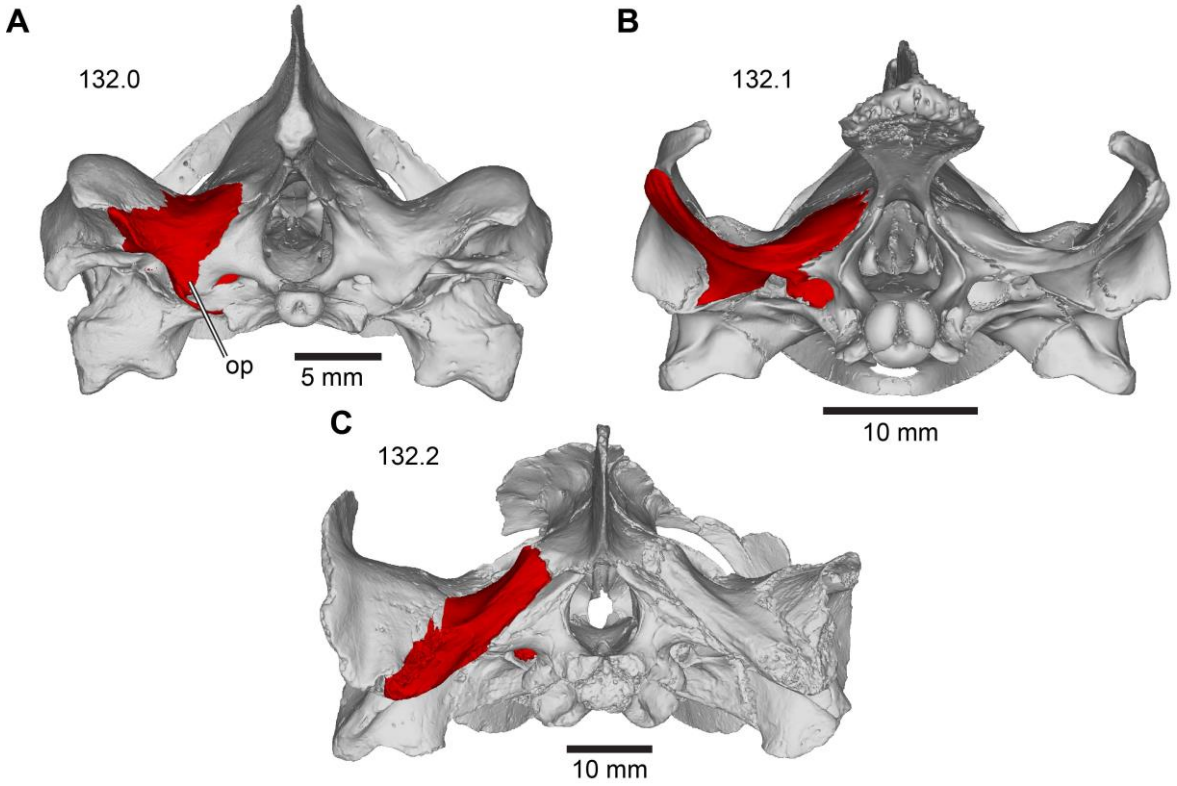


FIG. S1.55. Illustration of character 132. **A**, state 0 (*Sternotherus minor*, FMNH 211696, posterior view of cranium); **B**, state 1 (*Apalone spinifera emoryi*, FMNH 22178); **C**, state 2 (*Plesiochelys planiceps*, OUMNH J1582). Abbreviations: *op*, opisthotic.

Character 133 (Cadena & Parham (2015): character 102). Fenestra perilymphatica: 0 = large; 1 = reduced in size to that of a small foramen.

Character optimisation: Unambiguous: *Bouliachelys suteri* (0->1); DELTRAN: *Pleurosternon bullockii* (0->1); ACCTRAN: (*Eubaena* ++ *Pleurosternon*) (0->1).

Character 134 (Cadena & Parham (2015): character 87). Parabasisphenoid, paired pits on ventral surface of basisphenoid: 0 = absent; 1 = present.

Character optimisation: Unambiguous: Sinemydidae/Macrobaenidae (0->1), *Dracochelys bicuspis* (1->0); DELTRAN: *Kayentachelys aprix* (0->1); ACCTRAN: (*Eileanchelys* + *Kayentachelys*) (0->1).

Character 135 (Cadena & Parham (2015): character 88). Parabasiphenoid, ventral surface: 0= flat to slightly convex, with posterior margin straight or slightly concave; 1= V-

shaped crest, with posterior margin forming the basipterygoid process projected posterolaterally.

Character optimisation: DELTRAN: *Eosphargis breineri* (0->1), total-group Cheloniidae (0->1), *Toxochelys latiremis* (0->1); ACCTRAN: total-group Chelonioidea (0->1), Dermochelyoidea (1->0), *Eosphargis breineri* (0->1).

Character 136 (Cadena & Parham (2015): character 89). Parabasiphenoid, rough surface between basisphenoid and basioccipital: 0 = absent; 1 = present.

Character optimisation: Unambiguous: *Eosphargis breineri* (0->1), *Annemys levensis* (0->1).

Character 137 (previously xxxxxix) (new character). Parabasisphenoid, posterolateral processes lapping onto the ventral surface of the basioccipital: 0 = absent; 1 = present.

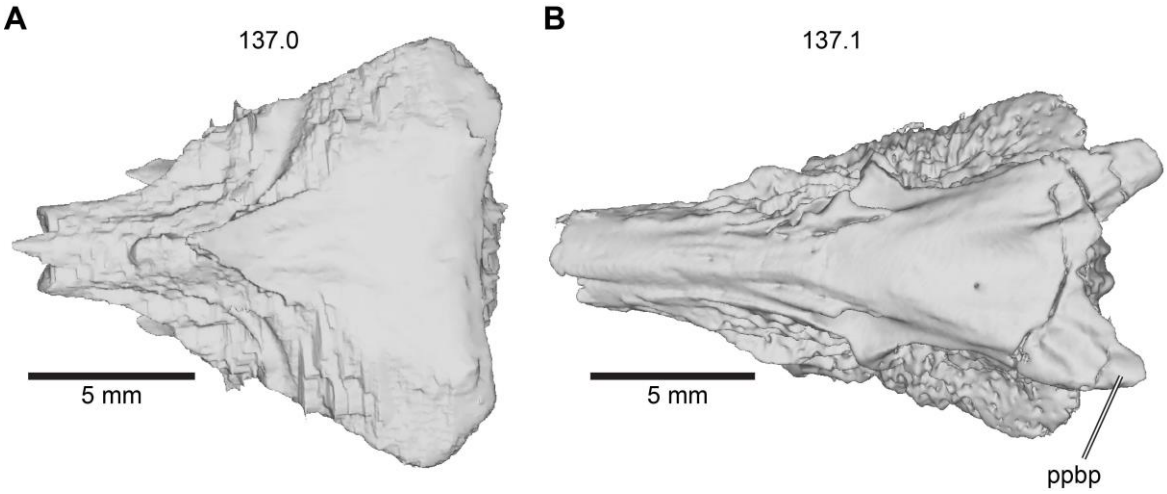


FIG. S1.56. Illustration of character 137. **A**, state 0 (*Gopherus polyphemus*, FMNH 211815, ventral view of parabasisphenoid); **B**, state 1 (*Pleurosternon bullockii*, UMZC T1041). Abbreviations: ppbp, posterior process of parabasisphenoid.

Remarks: This character was constructed to account for the presence of posterolateral processes that lap onto the ventral surface of the basioccipital in some paracryptodires, such as *Glyptops plicatus* (AMNH 336; Gaffney 1979b). I also confirmed the presence of these processes in *Pleurosternon bullockii* (UMZC T1041) and *Eubaena cephalica*, although they are absent in *Arundelemys dardeni* (USNM 497740). I further found such processes in carettochelyids, and *Sternotherus minor* (FMNH 211696).

Character optimisation: Unambiguous: *Sternotherus* (0->1), total-group Carettochelyidae (0->1), (*Eubaena* ++ *Pleurosternon*) (0->1).

Character 138 (modified from Cadena & Parham (2015)). Parabasisphenoid, rostrum basisphenoidale: 0 = flat; 1 = flat base, but with trabeculae contact one another medially forming a short rod at the anterior end of the parabasisphenoid; 2 = singular median, rod-like, thick and rounded process.

Previous character definition: Basisphenoid, rostrum basisphenoidale: 0 = flat; 1 = rod-like, thick and rounded. Joyce *et al.* (2011: ch 56) & Sterli & De la Fuente (2013: ch83) (Basisphenoid A); Parham & Pyenson (2010: ch 15); Hirayama (1998), KL, & Bardet *et al.* (2013: ch 34).

Remarks: The history of this character in the form used by Cadena & Parham (2015) can be traced to the analysis of Joyce (2007: character 50, Basisphenoid A). Joyce (2007) finds a rod-like rostrum basisphenoidale as an unambiguous synapomorphy of chelonioids. I included a range of stem-cheloniids and the stem-chelonioid *Toxochelys* into my analysis, and investigated the respective basicrania with my CT data. Hereby, I noticed that some stem-cheloniids (*Eochelone brabantica*: NHMUK R37213; *Puppigerus camperi*: NHMUK 39855) do not have the derived chelonioid condition. Instead, they have an intermediate structure, as the trabeculae are posteriorly well separated, but join anteriorly. I added an additional state (state 1) to account for this observation.

Character optimisation: Unambiguous: *Puppigerus camperi* (2->1), *Platysternon megacephalum* (0->2); DELTRAN: (*Ocepechelon* ++ *Santanachelys*) (0->2), *Argillochelys*+++ (0->2), *Eochelone* (0->1); ACCTRAN: crown-group Chelonioidea (0->2), Dermochelyidae (2->0), *Eochelone* (2->1).

Character 139 (modified from Cadena & Parham (2015)). Parabasisphenoid, dorsum sellae: 0 = deep, i.e. the dorsal surface of parabasisphenoid between the clinoid processes is a transversely concave floor forming a trough between the posterior part of the dorsal surface of the parabasisphenoid, which is usually cup-like, and the anterior portion of the parabasisphenoid forming the rostrum basisphenoidale and sella turcica; 1 = low, i.e. the dorsum sellae is formed as a transverse ridge between the clinoid processes that projects anteriorly at a low angle from posterodorsal surface of the parabasisphenoid; 2 = high, i.e. a transverse ridge or wall of bone between the clinoid processes is present that projects dorsally at a high angle from the posteriorly positioned cup, separating the cup very clearly from of the anteriorly positioned rostrum basisphenoidale and sella turcica.

Previous character definition (Cadena & Parham (2015): character 90): Basisphenoid, dorsum sellae: 0 = low; 1 = high. Parham & Pyenson (2010: ch 16); Hirayama (1998), Kl, & Bardet *et al.* (2013: ch 33).

Remarks: Hirayama (1995: character 26) and subsequent authors (e.g. Hirayama 1998: character 33; Parham & Pyenson 2010: character 16; Kear & Lee 2006: character 33; Bardet *et al.* 2013: character 33; Cadena & Parham (2015): character 90) used this character as a binary character with short character state descriptions (low vs. high).

Hirayama (1995) noted that the high dorsum sellae seen in chelonioids does not conceal the posterior portion of the sella turcia. Subsequently, Hirayama (1998) explained that a high dorsum sellae means that this structure is separated from the sella turcica. Bardet *et al.* (2013: supplements p. 38) noted that "when the *dorsum sellae* is high, there is a sagittal crest in a relatively long and elevated space separating the *sella* from the highest posterior border of the *dorsum sellae"*, but these authors retain the short character state definitions used by previous authors. Here, I chose to extend the definitions of the character states to more explicitly refer to the transverse wall between the clinoid processes described by Bardet *et al.* (2013).

Besides extending the character state descriptions, I add a new state (state 0) for additional variation observed by us that was not considered in previous binary versions of this character.

My state 0 describes the morphology seen in *Chelonia mydas* (NHMUK1969.776), *Sandownia harrisi* (MIWG3480), *Macrochelys temminckii* (FMNH22111), *Staurotypus salvinii* (NHMUK1879.1.7.5), *Dermatemys mawii* (SMF59463), *Gopherus polyphemus* (FMNH211815), *Platysternon megacephalum* (SMF69684). In these taxa, a ridge between the clinoid processes is absent and the dorsum sellae consequentially is a flat or transversely concave surface between the more posteriorly positioned cup-like portion of the parabasisphenoid and the anteriorly positioned sella turcica and rostrum basisphenoidale. The condition in these taxa is different from those taxa for which I score having a "low" dorsum sellae (state 1). To stick with the traditional nomenclature of "low" and "high", I refer to this state as "deep", acknowledging the deep trough between the clinoid processes.

According to my definition, a "low" dorsum sellae (character state 1) comprises a ridge between the clinoid processes. However, the clinoid processes project anteriorly at a low angle in taxa scored as having state 1, so that the ridge between the processes does not rise very high dorsally off the level of the parabasisphenoid cup. The ridge commonly extends with its anterodorsal margin anteriorly to the posterior margin of the sella turcica, hereby concealing the posterior portion of the sella turcica in which the foramina for the exit of the cerebral artery are positioned. Taxa with a low dorsum sellae include all pleurodires, all trionychians, most testudinoids (but *Gopherus polyphemus* and *Platysternon megacephalum*), *Dermochelys coriacea* (FMNH 171756; UMZC R3031), and several kinosternoids (including *Emarginachelys creatacea:* KUVP 23488; *Baptemys wyomingensis:* Meylan & Gaffney 1989, Knauss 2014).

A third variation of the dorsum sellae is described as "high" in state 2. Taxa with a high dorsum sellae have a ridge between the clinoid processes, but the clinoid processes are anterodorsally directed (i.e. form a high angle to the surface of the parabasisphenoid cup). Consequentially, the ridge between the clinoid processes forms a near vertical wall between

the parabasisphenoid cup and the rostrum basisphenoidale and sella turcica. This is consistent with the observations of Hirayama (1995) cited above, as the vertical dorsum sellae does indeed not conceal the posterior portion of the sella turcica as is the case for taxa scored as "1". Taxa scored with state 2 in this study are chelonioids (including protostegids; but not *Chelonia mydas*, *Dermochelys coriacea*), plesiochelyids, and *Brachyopsemys tingitana* (AMNH FARB 30612).

Anquetin *et al.* (2015) provide a discussion of the dorsum sellae in thalassochelydians. They defined a new character that is similar to my states 1 and 2, in which the overhang of the dorsum sellae in respect to the sella turcica is defined. While I agree with most scorings of Anquetin *et al.* (2015) (e.g. chelonioids, *Toxochelys*, plesiochelyids have a "high" dorsum sellae that does not overhang sella turcica), I disagree with the scorings of *Jurassichelon oleronensis* ("'*Thalassemys' moseri*" in Anquetin *et al.* 2015) and *Sandownia harrisi*. CT scans of *Jurassichelon* show that it has the same morphology as other plesiochelyids, and CT scans of *Sandownia* show that is has state 0, which is a form of variation not considered in the character concept of Anquetin *et al.* (2015). However, I agree with their scoring for *Solnhofia parsoni* as my CT scans confirm that the dorsum sellae forms a low ridge that overhangs the sella turcica.

Character optimisation: Unambiguous: (*Eileanchelys* + *Kayentachelys*)+++ (2->1), total-group Chelonioidea (1->2), *Chelonia mydas* (2->0), *Macrochelys temminckii* (1->0), *Staurotypus* (1->0), *Dermatemys mawii* (1->0), *Platysternon megacephalum* (1->0), *Gopherus polyphemus* (1->0), *Meiolania planiceps* (1->0); DELTRAN: (*Portlandemys* ++ *Plesiochelys*) (1->2), (*Sandownia* + *Leyvachelys*) (1->0), *Brachyopsemys tingitana* (1->2), *Xinjiangchelys radiplicatoides* (1->2); ACCTRAN: Angolachelonia (1->2), *Solnhofia parsoni* (2->1), (*Sandownia* + *Leyvachelys*) (2->0), (*Xinjiangchelys wusu* + *Xinjiangchelys radiplactoides*) (1->2).

Character 140 (new character). Parabasisphenoid, anterior surface of dorsum sellae: 0 = anterior surface of the dorsum sellae is flat and smooth; 1 = vertical median ridge on anterior surface of dorsum sellae between the clinoid processes is present, ridge may have a small anterodorsal projection.

Remarks: The dorsum sellae is a wall of bone between the clinoid processes of the parabasisphenoid (see character 139 for a detailed discussion of the dorsum sellae). Its

anterior surface slopes ventrally to the sella turcica, and is smooth in many taxa, including *Proganochelys quenstedti* (SMNS 16980). However, in some taxa, including most protostegids, most cheloniids (e.g. *Allopleuron hoffmanni*: NHMUK R42913; *Argillochelys cuneiceps*: NHMUK R41636; *Lepidochelys olivacea*: SMNS 11070; but not some of the early diverging taxa such as *Eochelone brabantica*: NHMUK R37213; or *Puppigerus camperi*: NHMUK R38955), and *Plesiochelys* spp. (OUMNH J1582, MNB 435), the anterior surface has a median ridge that runs vertically across the dorsum sellae. This character is inapplicable for those taxa (e.g. *Chelonia mydas* or *Sandownia*) in which the dorsum sellae is not developed as a transverse ridge between the clinoid processes (see remarks for character 139).

Character optimisation: Unambiguous: *Rhinochelys pulchriceps* (1->0), *Puppigerus camperi* (1->0), (*Plesiochelys etalloni* + *Plesiochelys planiceps*) (0->1), *Kirgizemys dmitrievi* (0->1); DELTRAN: Dermochelyoidea (0->1), *Argillochelys*+++ (0->1), *Kayentachelys aprix* (0->1), *Australochelys africanus* (0->1); ACCTRAN: *Australochelys*+++ (0->1), *Chubutemys*+++ (1->0), crown-group Chelonioidea (0->1), *Eochelone* (1->0).

Character 141 (new character). Parabasisphenoid, retractor bulbi pits on anterolateral surface: 0 = absent; 1 = present.

Remarks: Retractor bulbi pits are moderately deep concavities on the anterolateral surface of the parabasisphenoid, usually situated slightly dorsally to the level of the sella turcica.

The reduction or absence of retractor pits is a feature that has been associated with the reduction or less of the retractor bulbi muscles in other reptiles (e.g. Evans 2008). Retractor bulbi pits are absent in most turtles (including *Proganochelys quenstedti*: SMNS 16980), but are present in most other early stem turtles (e.g. *Kayentachelys aprix*: TMM 4370-2; *Eileanchelys waldmanni*: NMS.G.2004.31.15; *Kallokibotion bajazidi*: NHMUK R4925), all paracryptodires for which this character could be scored, and in all sinemydids, macrobaenids, and xinjiangchelyids for which this character could be scored. The retractor bulbi pits may be well developed, as for instance in *Ordosemys leios* (IVPP V9534-1; Brinkman

& Peng 1993*b*). Within crown-group turtles, retractor bulbi pits are present in a taxonomically broad set of turtles.

Character optimisation: Unambiguous: Angolachelonia+++ (1->0), *Chelydra serpentina* (0->1), *Kinosternon suburum hippocrepis* (0->1), *Emys orbicularis* (0->1), Testudinidae (0->1), *Phrynops geoffranus* (0->1), *Pelomedusa subrufa* (0->1), *Leyvachelys cipadi* (0->1); DELTRAN: *Australochelys*+++ (0->1); ACCTRAN: *Australochelys*+++ (0->1).

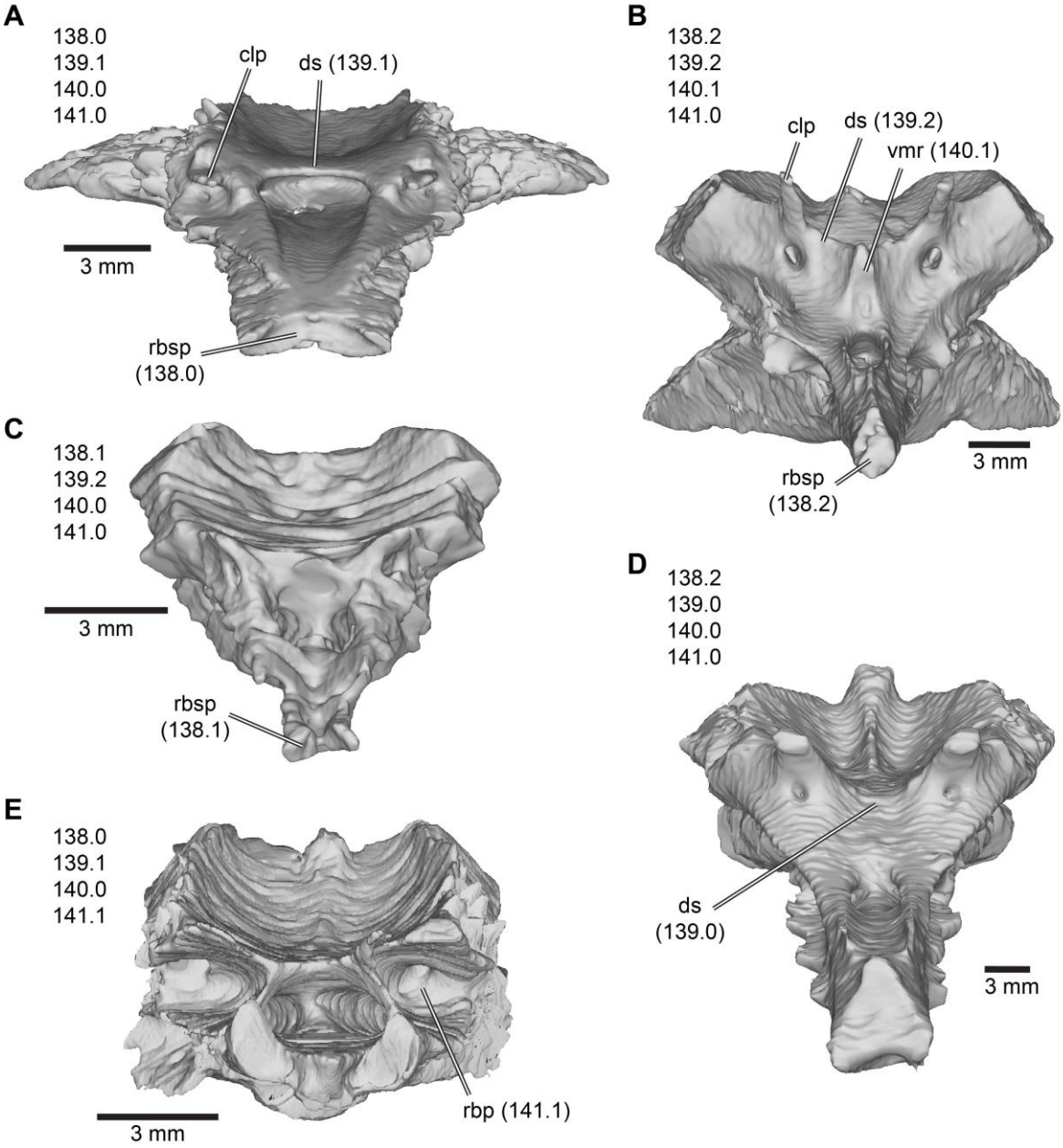


FIG. S1.57. Illustration of characters 138-141. **A**, *Phrynops geoffroanus* (SMF 45470, anterodorsal view of parabasisphenoid); **B**, *Lepidochelys olivacea* (SMNS 11070); **C**, *Argillochelys cuneiceps* (NHMNUK R 38955); **D**, *Chelonia mydas* (NHMUK 1969.776); **E**, *Kallokibotion bajazidi* (NHMUK R4925). Abbreviations: *clp*, clinoid process; *ds*, dorsum sellae; *rbp*, retractor bulbi pit; *rbsp*, rostrum basisphenoidale, *vmr*, vertical medial ridge on dorsum sellae.

Character 142 (modified from Cadena & Parham (2015)). Parabasisphenoid, foramina anterius canalis carotici cerebralis: 0 = widely separated; 1 = close together; 2 = right and left cerebral arteries converge within the parabasisphenoid and run within a short joint canal, and exit anteriorly into the cavum cranii via a single foramen within the sella turcica.

Previous character definition (Cadena & Parham (2015): character 92): Basiphenoid, foramen anterius canalis carotici interni visible in dorsalanterior view of basisphenoid: 0 = widely separated; 1 = close together. Hirayama (1998), Kear & Lee (2006), & Bardet *et al.* (2013: ch 29).

Remarks: The name of the foramen (previously 'foramen anterius canalis carotici interni' in Cadena & Parham (2015): character 92) was corrected to foramina anterius canalis carotici cerebralis, following Rabi *et al.* (2013).

A third state (state 2) has been added to accommodate the condition observed in some taxa such as *Lepidochelys olivacea* (SMNS 11070) or *Rhinochelys* sp. (CAMSM 55775, 55776, 55783; NHMUK R35197, R43980), in which the cerebral arteries have a short joint canal within the parabasisphenoid before exiting into the sella turcica anteriorly.

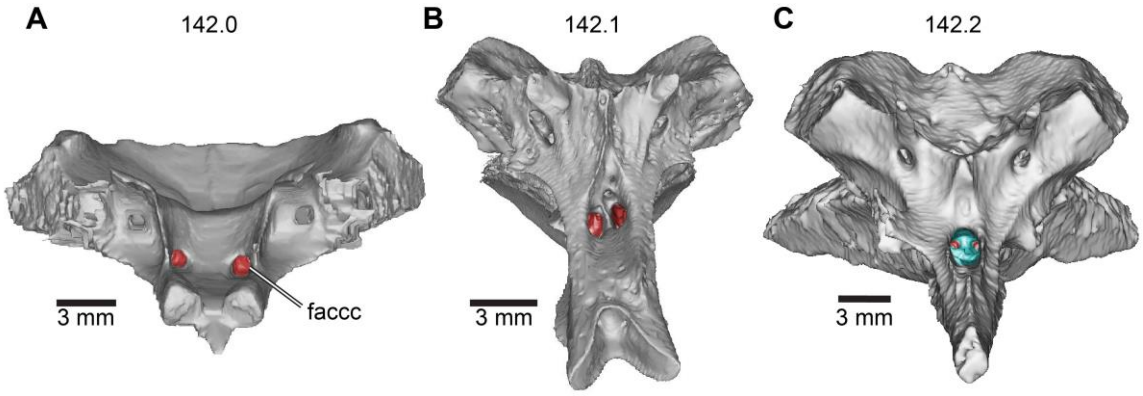


FIG. S1.58. Illustration of character 142. **A**, state 0 (*Gopherus polyphemus*, FMNH211815, anterodorsal view of parabasisphenoid); **B**, state 1 (*Eretmochelys imbricata*, specimen number unknown); **C**, state 2 (*Lepidochelys olivacea*, SMNS 11070). Red indicates position of foramina anterius canalis carotici cerebralis, blue indicates singular orifice for the exit of the cerebral artery in C. Abbreviations: *facc*, foramen anterius canalis carotici cerebralis.

Character optimisation: Unambiguous: Sinemydidae/Macrobaenidae+++ (1->0), total-group Chelonioidea (0->1), (*Desmatochelys* ++ *Santanachelys*) (1->2), *Natator depressus* (1->2),

Eochelone (1->0), *Macrochelys temminckii* (0->1), *Baptemys wyomingensis* (0->1), *Platysternon megacephalum* (0->1), Thalassochelydia (0->1), *Leyvachelys cipadi* (0->1), *Meiolania planiceps* (1->0); DELTRAN: *Lepidochelys olivacea* (1->2), *Caretta caretta* (1->2); ACCTRAN: (*Caretta* ++ *Lepidochelys*) (1->2), *Lepidochelys kempii* (2->1).

Character 143 (modified from Anquetin *et al.* 2015). Parabasisphenoid, prootic foramen in primary lateral wall of the braincase: 0 = present, the clinoid process of the parabasisphenoid and parts of the prootic, an ossified pila antotica, the laterosphenoid, and/or parts of the parietal form a foramen medially to the cavum epiptericum; 1 = the prootic foramen is reduced, and the clinoid processes are free structures.

Remarks: This character is equivalent to character 55 (Basisphenoid D) of Anquetin *et al.* (2015), but my state definitions are slightly different.

The trigeminal foramen is a term generally used to refer to the orifice through which the fifth cranial nerve (trigeminal nerve, CN V) exits the braincase into the adductor chamber. The trigeminal foramen is a large opening in the lateral wall of the braincase anterior and ventral to the level of the otic capsule in reptiles (Holliday & Witmer 2007). In turtles, the term "trigeminal foramen" has been applied to the opening in the neomorphic secondarily lateral wall of the braincase that is formed by ventral expansions of the parietal and dorsal expansions of the pterygoid (e.g. Joyce 2007; but see Gaffney 1990). Other cranial elements such as the epipterygoid and prootic may be involved in the formation of this foramen. Medially to the trigeminal foramen, the prootic usually forms a broad anterior surface dorsally to the position of the foramen cavernosum. This area is known as the cavum epiptericum, and houses the trigeminal ganglion. From the ganglion, the three main divisions of the trigeminal nerve, the ophthalmic, maxillary, and mandibular rami diverge. Off those, only the maxillary and mandibular rami exit the braincase laterally through the "trigeminal foramen", which might thus be more appropriately called the maxillomandibular foramen. The ophthalmic branch of the trigeminal nerve passes medially to the secondary lateral wall of the braincase (as formed by the ventral process of the parietal) anteriorly, and has thus no

associated foramen or canal. However, a second foramen associated with the trigeminal nerve system exists in some turtles (*Proganochelys*: SMNS 16980, Gaffney 1990; *Plesiochelys etalloni*: MNB 435; Anquetin *et al.* 2015). Following Gaffney (1990), who first identified such a foramen in *Proganochelys*, I refer to this as the prootic foramen. I also found this foramen in *Pelomedusa subrufa* (SMF 70704). This foramen is located between the parabasisphenoid and the prootic (and possibly a partially ossified laterosphenoid, Bhullar and Bever (2009)). Specifically, the space between the tip of the clinoid processes and the prootic is dorsally bridged by bone, which is referred to as an ossified pila antotica in Anquetin *et al.* (2015). Here, I extend the definition of "an ossified pila antotica" and name the prootic, laterosphenoid, and parietal as possibly contributing to the pila prootica, because these bones have been interpreted to form part of this structure in *Proganochelys* (Gaffney 1990; Bhullar & Bever 2009), and developmental studies that identify the origin of this bony structure are currently lacking.

In *Proganochelys*, the prootic foramen is the only true foramen associated with the trigeminal nerve system that is formed, as the neomorphic trigeminal foramen is not yet established. In *Plesiochelys etalloni* and *Pelomedusa rubrufa*, which have ventrally extended parietals forming a secondary wall of the braincase, both foramina coexists. Rieppel (1993) reports that the prootic foramen is present in early embryonical stages of extant turtles, but not expressed in adults due to the absence of laterosphenoid ossification. In turtles without a fully ossified foramen, the prootic foramen exists only as a dorsally open aperture between the clinoid processes anteriorly, and the prootic posteriorly. Because the prootic foramen is positioned medially to the position of the cavum epiptericum, the foramen likely transmits the stem for the trigeminal nerve to the ganglion, where the nerve then diverges into its branches.

I include this character, because it is likely that the condition is *Proganochelys* is the plesiomorphic condition of turtles and might be informative in relation to non-testudinate outgroups (see also Anquetin *et al.* 2015).

Character optimisation: Unambiguous: *Pelomedusa subrufa* (1->0), *Plesiochelys etalloni* (1->0), *Annemys* sp. IVPP V18106 (1->0); DELTRAN: *Australochelys*+++ (0->1); ACCTRAN: *Australochelys*+++ (0->1).

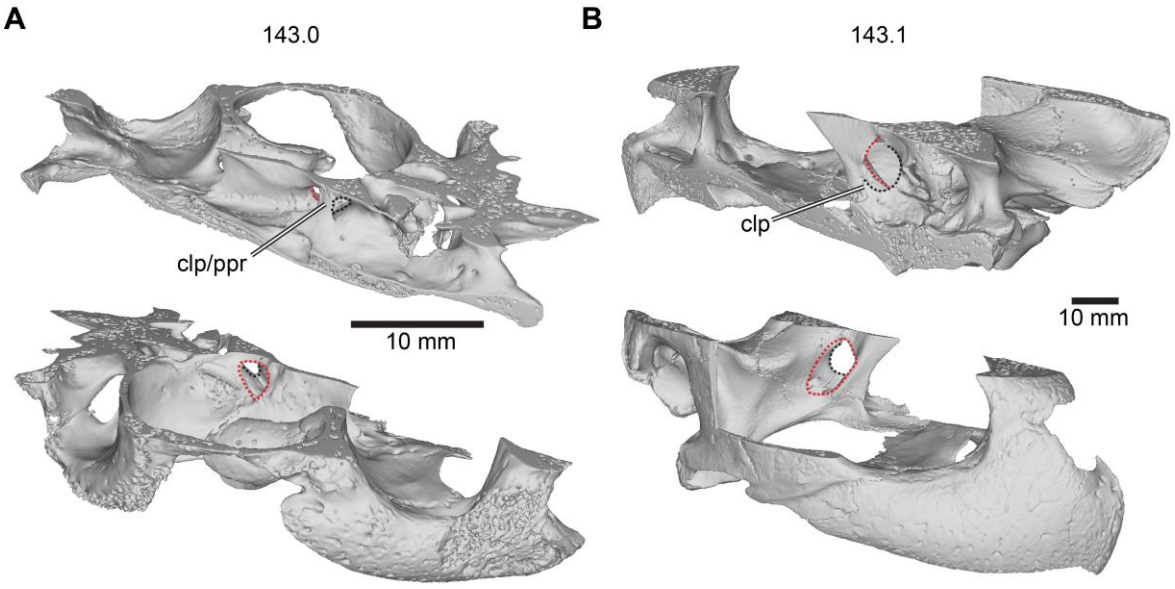


FIG. S1.59. Illustration of character 143. **A**, state 0 (*Pelomedua subrufa*, SMF 70504, posterodorsomedial [top] and anterodorsomedial [bottom] view of axially sectioned cranium); **B**, state 1 (*Lepidochelys olivacea*, SMNS 11070). Black dashed line indicates prootic foramen; red dashed line indicates trigeminal (maxillomandibular) foramen. Abbreviations: *clp*, clinoid process; *ppr*, pila prootica.

Character 144 (new character). Parabasisphenoid, crista tuberculi basalis developed on posterior part of dorsal surface: 0 = absent, parabasisphenoid dorsal surface is relatively flat or gently concavely excavated; 1 = present as median, dorsally high projecting tubercle or ridge.

Remarks: The crista tuberculi basalis is a median, dorsally projecting ridge or tubercle seen in some turtles at the contact between the basioccipital and parabasisphenoid (Gaffney 1979). When developed, the basis tuberculi basalis is usually more prominent on the basioccipital, and often restricted to this element. This character is defined to capture the morphology of those turtles that have the basis tuberculi basalis developed on the parabasisphenoid. This condition is widespread among cheloniids, but not universally present in this group.

Character optimisation: Unambiguous: total-group Chelonioidea (0->1), (*Lepidochelys olivacea* + *Lepidochelys kempii*) (1->0), *Puppigerus camperi* (1->0), *Emys orbicularis* (0->1), *Kallokibotion bajazidi* (0->1); DELTRAN: (*Bouliachelys* ++ *Santanachelys*) (1->0); ACCTRAN: Protostegidae (1->0).

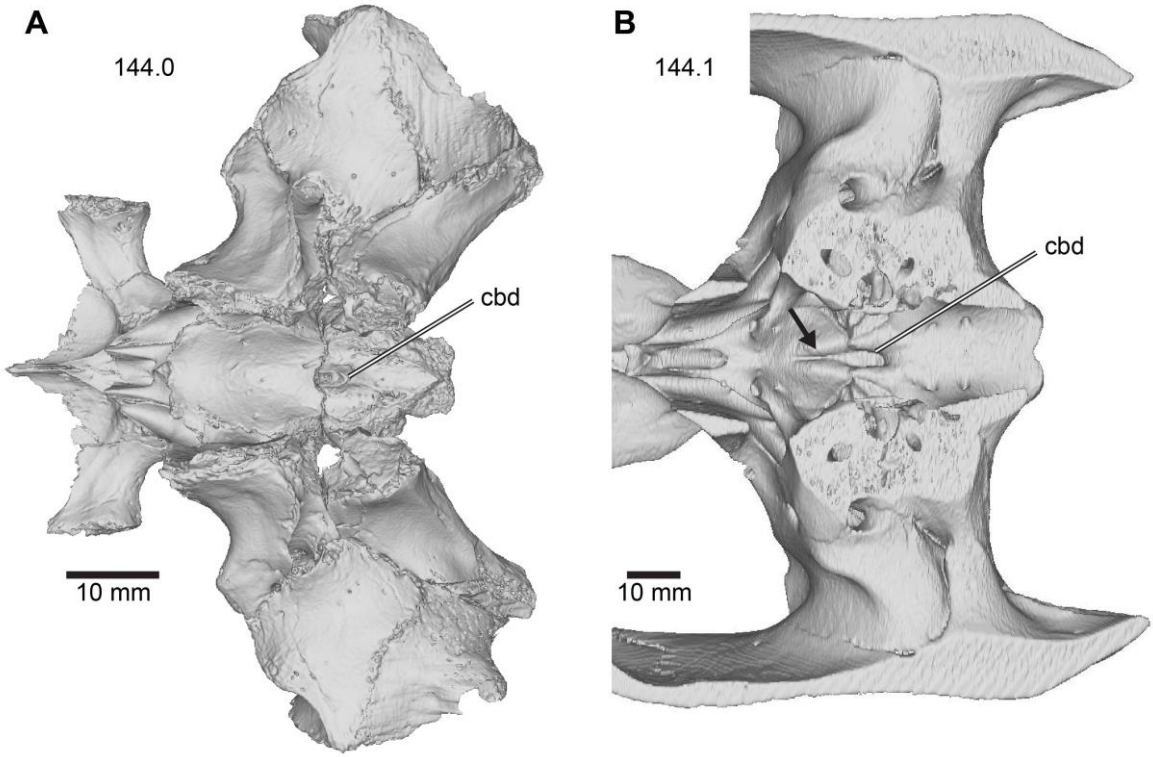


FIG. S1.60. Illustration of character 144. **A**, state 0 (*Plesiochelys planiceps*, OUMNH J1582, dorsal view of basicranium); **B**, state 1 (*Chelonia mydas*, NHMUK 1969.776). Arrow in B indicated extension of crista basis tuberculi basalis onto the parabasisphenoid. Abbreviations: *cbd*, crista basis tuberculi basalis.

Character 145 (modified from Cadena & Parham (2015)). Carotid artery/Pterygoid, interpterygoid vacuity: 0 = large opening, triangular in shape; 1 = reduced to an interpterygoid slit; 2 = entirely closed, no foramina posterius canalis carotici palatinum present. Scored inapplicable for taxa with a bony canal for the palatine artery (ch 146.1)

Previous definition (Cadena & Parham (2015): character 63): Pterygoids, interpterygoid vacuity: 0 = triangular in shape; 1 = reduced to an interpterygoid slit; 2 = reduced to a paired foramen caroticum laterale. Joyce (2007: ch 40) & Sterli & De la Fuente (2013: ch 60) (Pterygoid C).

Remarks: I deleted the state 2 used by Cadena & Parham (2015: ch 62) for this character, because it is not independent from the scorings of my character 146: All turtles in which the palatine artery is enclosed in a bony canal (ch146.1) also have their interpterygoid opening reduced to paired foramina posterius canalis carotici palatinum. These foramina are only visible when a fenestra caroticus is present, but in turtles with a ventrally embedded internal carotid split, these foramina are simply covered by a more extensively ossified basicranium. Therefore, this character is scored inapplicable for turtles with a bony canal for the palatine artery.

Additionally to these modifications, I added a state (my state 2) to account for the morphology of paracryptodires, in which no interpterygoid vacuity is present, but foramina or canals for the palatine artery are also absent (Rollot *et al.* in press; personal observation S.W.E.). See the section on carotid circulation characters below for an extended discussion.

Character optimisation: Unambiguous: *Chubutemys*+++ (0->1), (*Annemys latiens* ++ *Xinjiangchelys*) (1->0), Paracryptodira (1->2).

Character 146 (modified from Cadena & Parham (2015)). Embedding of the palatine division of carotid artery: 0 = the palatine artery is not encased in a bony canal (artery enters the skull through the interpterygoid cavuity, interpterygoid slit, or possibly other skull openings); 1 = the palatine artery is encased in a bony canal (irrespective of the exposure or embedding of the internal carotid artery split).

Previous character definition: Palatine Artery, entering in the skull: 0 = through the interpterygoid vacuity or intrapterygoid slit; 1 = through the foramen posterius carotici palatinum between basisphenoid and pterygoid. Reworded from Sterli & De la Fuente (2013: ch 99, Canalis Caroticum F).

Remarks: This character is a modified version of character 101 of Cadena & Parham (2015), which addresses which structure of the entry of the palatine artery. The palatine artery is a

vessel that enters the ventral surface of the cranium. As the ventral surface of the cranium ossifies more strongly during turtle evolution the artery becomes trapped.

According to the scorings of Cadena & Parham (2015), their character 101 should be a multistate character with three states. However, only two states are given in their character description: State 0, which specifies that the palatine artery enters through the interpterygoid vacuity or slit; and state 1, which specifies that the artery enters through the foramen posterius canalis carotici interni (implying a ventrally open fenestra caroticus through which the carotid split is exposed). However, as the character presented by Cadena & Parham (2015) was a modified version of character 99 (Canalis caroticum F) of Sterli & De la Fuente (2013), I infer the third state of Cadena & Parham (2015) to likely specify that an external opening for the palatine artery is absent (implying a closed fenestra caroticus).

I think that this previous character definition combines two independent morphological features: the presence vs. absence of an interpterygoid vacuity or slit and related embedding of the palatine artery, and the presence vs. absence of a fenestra caroticus. State 0 of Cadena & Parham (2015: character 101) implies the presence of an interpterygoid opening, whereas states 1 and 2 imply its absence. However, state 1 implies the presence of a fenestra caroticus, whereas state 2 implies its absence and the complete encasing of the internal carotid and palatine artery in bone. A possible solution to this interdependence problem is the approach of Zhou & Rabi (2015: character 98), which I follow here. Zhou & Rabi (2015) code the variation regarding the encasing of the palatine artery in a binary character, recognizing that the palatine artery can either enter through an interpterygoid opening (irrespective of whether this opening is a large vacuity or a small slit), or through paired foramina (irrespective of whether these are ventrally exposed or covered by bone). Variation associated with the interpterygoid vacuity is coded in a different character (character 145 of this study). Variation regarding the presence or absence of a fenestra caroticus is, in my opinion, yet a separate source of morphological variation that is furthermore related to the internal carotid artery itself, and coded in this study in another

separate character (character 147). For a wider discussion and rationale for my carotid artery characters, also see the respective discussion chapter below.

Paracryptodires lack foramina for the palatine artery, but an interpterygoid opening is also absent (Rollot *et al.* in press; personal observation S.W.E). Assuming the palatine artery is not completely lost in paracryptodires, the artery will have likely been embedded in the soft tissue and possibly entered the cranium through another opening. In this study, paracryptodires are scored with state 0 for that reason (as for instance *Proganochelys*). The differences between paracryptodires and early stem-turtles such as *Proganochelys* is a difference in the fusion of the basicranial elements, and this difference is accounted for in character 145 of the present study (see also discussion of carotid characters below).

Character optimisation: Unambiguous: Xinjiangchelyidae+++ (0->1), *Dracochelys bicuspis* (1->0), *Kallokibotion bajazidi* (0->1).

Character 147 (modified from Cadena & Parham (2015)). Embedding of internal carotid artery and its bifurcation: 0 = Internal carotid arterial system is not embedded by bone, a foramen posterius canalis carotici is absent, and the split into palatine and cerebral artery occurs extracranially; 1 = internal carotid arterial system is partially embedded, a foramen posterius canalis carotici interni is present, and the split into palatine and cerebral artery happens at the fenestra caroticus and is thus ventrally exposed; 2 = internal carotid arterial system is ventrally fully embedded by bone, a foramen posterius canalis carotici interni is present and the split into palatine and cerebral artery is ventrally covered by bone.

Original character definition (Cadena & Parham (2015): character 99): Internal Carotid Artery, splitting of the internal carotid artery and the cerebral and palatine arteries: 0 = not embedded in braincase bone elements, the cerebral artery enters at the foramen posterius canalis carotici cerebralis (known previously as the foramen caroticum basisphenoidale) in the basisphenoid; 1 = partially embedded, the internal carotid artery enters in the braincase elements through the foramen posterius canalis carotici interni, running along the pterygoid

canal, and then splitting into the cerebral and palatine arteries at the fenestra caroticus; 2 = fully embedded, the internal carotid artery enters in the braincase elements through the foramen posterius canalis carotici interni, and split inside the braincase, lack of a ventral exposed fenestra caroticus. Combined character from Hirayama (1998), Kear & Lee (2006), & Bardet *et al.* (2013: ch 30 and 36). Ordered.

Remarks: This character is equivalent to character 99 of Cadena & Parham (2015). This character deals with the embedding of the internal carotid arterial system in the ventral surface of the skull. Please refer to Rabi *et al.* (2013) for discussion of these patterns, and see the discussion of my carotid characters below for a detailed rationale of the construction of my characters regarding the carotid arterial system.

Character state 0 is observed in basal stem-turtles (e.g. Proganochelys quenstedti, Australochelys africanus, Kayentachelys apriy, Kallokibotion bajazidi, Eileanchelys waldmanni, Chubutemys copelloi). Character state 1 is mainly observed in macrobaenids, sinemydids, and xinjiangchelyids, and the fenestra caroticus and carotid artery split for these taxa is discussed in Rabi *et al.* (2013). *Sandownia harrisi* and *Jurassichelon oleronesis* are also scored as 1, because they also show a clear fenestra caroticus. *Leyvachelys* is scored as 1&2, because in some specimens at least parts of the course of the internal carotid artery are exposed in a ventrally open groove (SMU 75327; Vineyard 2009), but this does not seem to be the case in all specimens (see Vineyard 2009).

Paracryptodires have a foramen on the ventral surface of the basicranium that is positioned halfway along the parabasisphenoid-pterygoid contact. This foramen has been interpreted to be the foramen posterius canalis carotici interni (Lipka *et al.* 2006; Rabi *et al.* 2013; but see Joyce & Lyson 2015), warranting state 2 in the above description of character states. However, I interpret the foramen to be the foramen posterius canalis carotici cerebralis, and score paracryptodires as having state 0. CT scans of paracryptodires show that the foramen is the entrance to a canal that is relatively short and directly leads to the sella turcica (personal observation S.W.E.: *Arundelemys dardeni*: USNM 497740,

Pleurosternon bullockii: UMZC T1041), which is consistent with the interpretation that it housed the cerebral artery. Furthermore, the location of the foramen in question is topologically identical to the location of the foramen posterius canalis carotici cerebralis in turtles that have such a foramen exposed at the fenestra caroticus (Rabi *et al.* 2013), while the position would be unusual for a foramen posterius canalis carotici interni. In support of this interpretation, my CT scans show that paracryptodires lack foramina or canals for the palatine artery (*Arundelemys dardeni*: USNM 497740, Lipka *et al.* 2006; *Pleurosternon bullockii*: UMZC T1041; *Eubaena cephalica*: DMNH 96004, Rollot *et al.* in press; Gaffney 1982). It is worth noting that in baenids (*Arundelemys*; *Eubaena*), the foramen posterius canalis carotici cerebralis is also found in a small ventral recess that is morphologically similar, and topologically corresponds to, to the fenestra caroticus of some other turtles, such as sinemydids. In sinemydids, the carotid split happens at the fenestra caroticus, as evident from the presence of foramina for the cerebral and palatine arteries in the anterior margins of the fenestra (Rabi *et al.* 2013). Possibly, the carotid split in baenids was located in the recess just posterior to the foramen for the cerebral artery, the difference to sinemydids being that the palatine artery lacks a canal and the posterior course of the internal carotid was not covered in bone.

Assuming that the palatine artery is not entirely lost in paracryptodires (in which case the cerebral and internal carotid arteries could not be distinguished, and the interpretation of the paracryptodiran foramen as a foramen posterius canalis carotici interni could be justified), the interpretation of the paracryptodire condition that is most consistent with the patterns seen in other turtles is the following: The internal carotid artery is posteriorly not embedded in bone, and splits into cerebral and palatine before the former enters the cranim through the foramen posterius canalis carotici cerebralis. The palatine artery, rather than entering the skull through a nearby foramen, is embedded in the soft tissue and takes an unknown anterior course. Consequentially, paracryptodires are scored as early stem-turtles like *Proganochelys* in my matrix for this character. Differences to taxa like *Proganochelys* are considered in different characters, such as character 145.

Character optimisation: Unambiguous: Angolachelonia+++ (1->2), *Jurassichelon oleronensis* (2->1), *Sandownia harrisi* (2->1); DELTRAN: Xinjiangchelyidae+++ (0->1), *Meiolania planiceps* (0->1); ACCTRAN: Meiolania+++ (0->1), Paracryptodira (1->0).

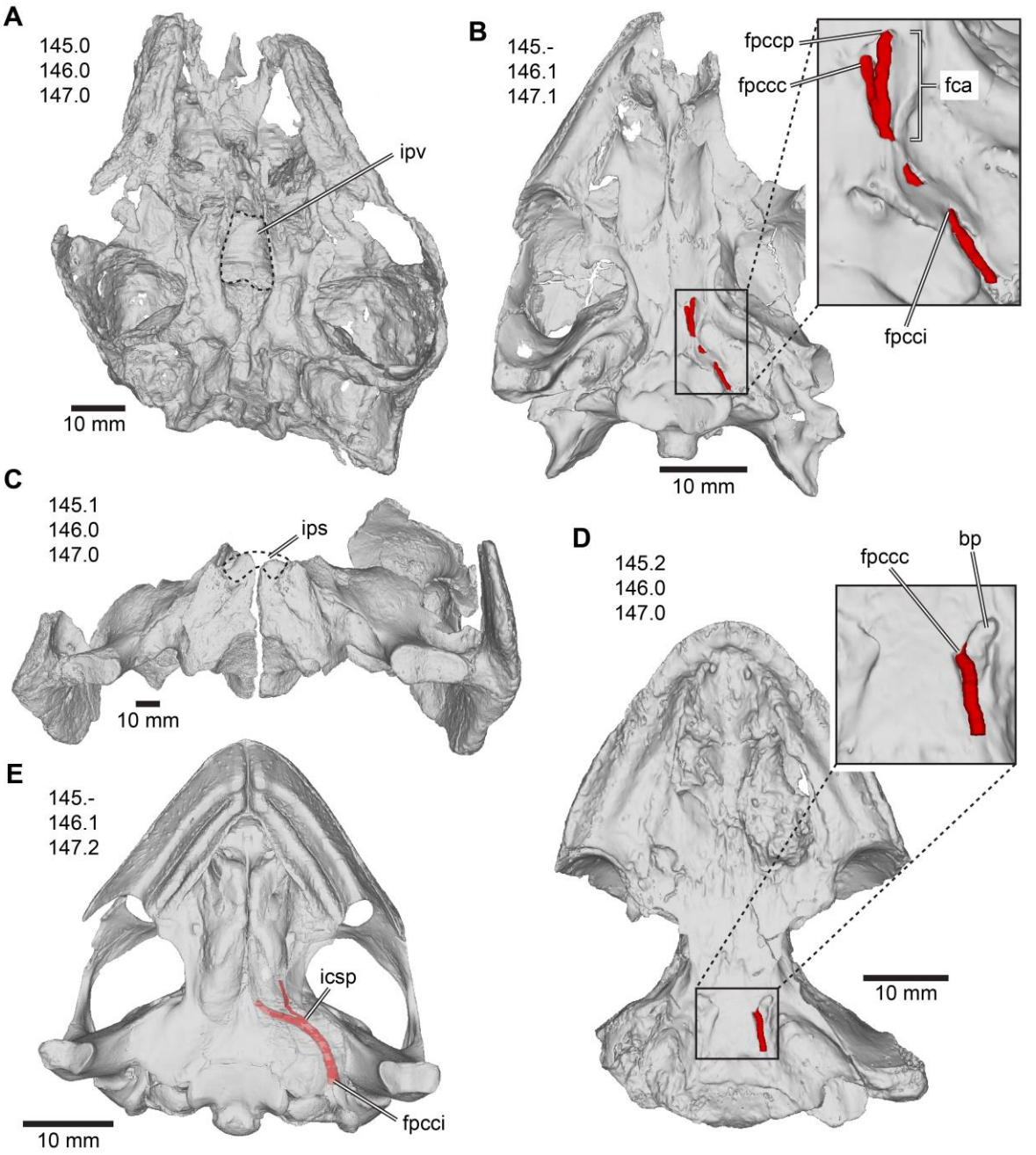


FIG. S1.61. Illustration of characters 145-147. **A**, *Australochelys africanus* (BP/1/4933, ventral view of cranium); **B**, *Ordosemys* sp. (IVPP V12092); **C**, *Meiolania planiceps* (NHMUK R 682, ventral view of basicranium); **D**, *Arundelemys dardeni* (USNM 497740); **E**, *Gopherus polyphemus* (FMNH 211815). Dashed lines in A and C show interpterygoid openings. Boxes in B and D show close-ups of the carotid circulation. Red shows interpretative models of the carotid arteries. Note that the left pterygoid is rendered transparently in E to show internal structures of the carotid arterial system. Abbreviations: *bp*, blind pocket without foramen; *fca*, fenestra caroticus; *fpccc*, foramen posterius canalis carotici cerebralis; *fpcci*, foramen posterius canalis carotici interni; *fpccp*, foramen posterius canalis carotici palatinum; *icsp*, internal carotid splitting point; *ips*, interpterygoid slit; *ipv*, interpterygoid vacuity.

Character 148 (adopted from Zhou & Rabi (2015)). Position of the foramen posterius canalis carotici interni (fpcci): 0 = the fpcci is located at the ventral surface of the skull in a position far anterior to the margin of the fenestra postotica; 1 = the fpcci is located at the posterior end of the skull, either on the ventral surface of the skull close to the margin of the fenestra postotica, or on the posterior surface of the skull at the ventral margin of the fenestra postotica. This character is scored inapplicable for taxa that lack a foramen posterius canalis carotici interni.

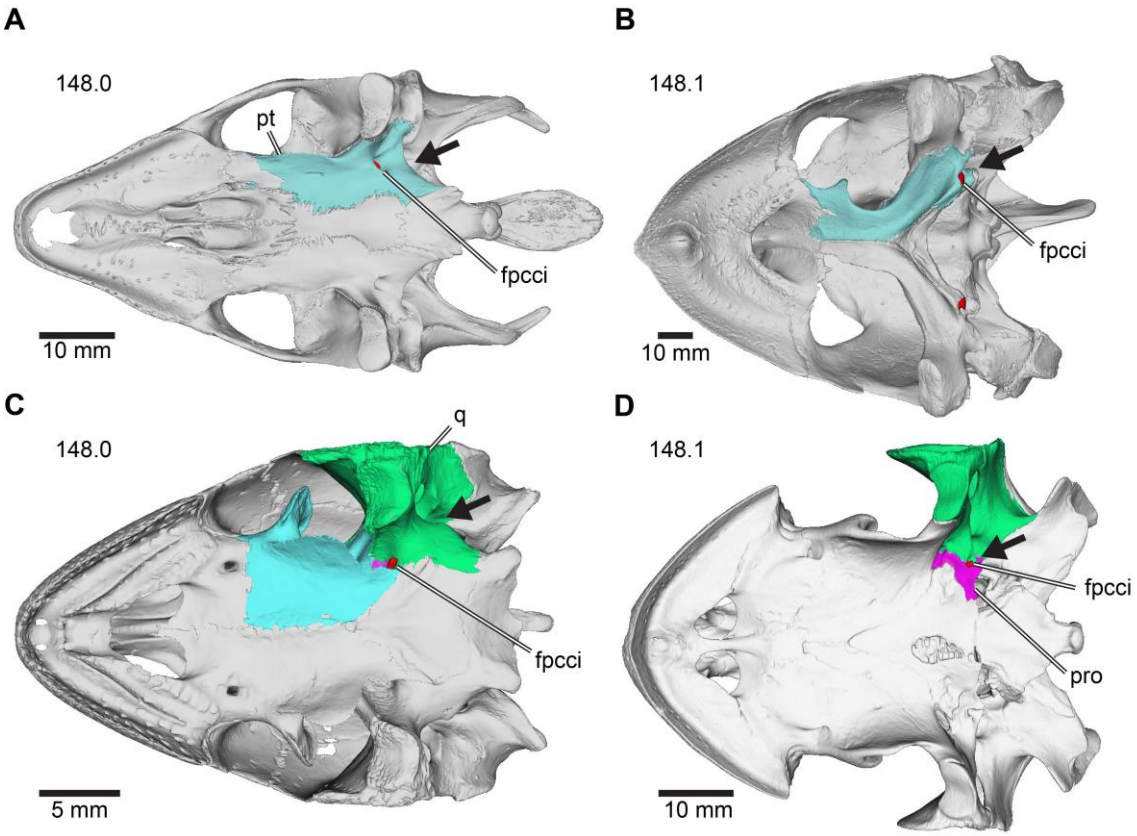


FIG. S1.62. Illustration of character 148. **A**, state 0 (*Apalone spinifera emoryi*, FMNH 22178, ventral view of cranium); **B**, state 1(*Lepidochelys olivacea*, SMNS 11070); **D**, state 0 (*Podocnemis unifilis*, FMNH 45657); **E**, state 1(*Phrynops geoffroanus*, SMF 45470). Arrows indicate the position of the fenestra postotica as a landmark denoting the posteroventral margin of the cranium. Note that A-B and C-D represent comparisons between cryptodires and pleurodires, respectives, in which character states differ. Red indicates carotid arteries. Abbreviations: *fpcci*, foramen posterius canalis carotici interni; *pt*, pterygoid; *pro*, prootic; *q*, quadrate.

Remarks: This character is adopted from Zhou & Rabi (2015: character 253). Zhou & Rabi (2015: supplements p. 12) noted morphological similarities between taxa assumed to be stem-group cryptodires (sinemydids, macrobaenids, xinjiangchelyids) and crown-group

cryptodires, which, according to Zhou & Rabi (2015) share a position of the foramen posterius canalis carotici interni at the posterior end of the skull. Pan-pleurodires on the other hand are reported to have the foramen posterius canalis carotici interni more anteriorly positioned. I include this character because the relative anteroposterior position of the foramen indeed varies between turtle species. However, my examination of specimens does not show the clear cryptodire-pleurodire separation reported by Zhou & Rabi (2015), and my scorings reflect these different observations.

Trionychians (commonly found to be the sister group to all remaining cryptodires in molecular studies: e.g. Crawford *et al.* 2015) have their foramen posterius canalis carotici interni positioned within the ventral surface of the pterygoid, relatively far anteriorly from the posterior end of the skull (e.g. *Apalone spinifera emoryi*: FMNH 22178; see Fig. S1.62*a*). The same is true for some taxa that are recovered as cryptodires in my analysis, such as protostegids (Fig. S1.62*c*). Conversely, many pleurodires (e.g. *Phrynops geoffroanus*: SMF 45470; Fig. S1.62*e*), have their foramen posterius canalis carotici positioned at the far posterior end of their skull: it is positioned just anteriorly to the ventral margin of the fenestra postotica.

This character is scored inapplicable for taxa that lack a foramen posterius canalis carotici interni.

Character optimisation: Unambiguous: *Santanachelys gaffneyi* (1->0), Trionychidae (1->0), *Chelus fimbriatus* (1->0), *Podocnemis* (1->0); DELTRAN: *Protostega gigas* (1->0); ACCTRAN: (*Protostega* + *Archelon*) (1->0).

Character 149 (new character). Entry of the internal carotid artery into skull relative to cavum acustico-jugulare: 0 = internal carotid enters the skull ventrally to the level of the cavum acustico-jugulare; 1 = internal carotid artery enters the skull within the cavum acustico-jugulare, artery lies in dorsally open trough on dorsal surface of pterygoid and only becomes dorsally covered within the cavum acustico-jugulare.

Remarks: This character encodes variation seen in the relative vertical positioning of the entry point of the internal carotid artery into the cranium. Two patterns are observed: the internal carotid artery either enters the cranium on the ventral surface of the cranium, or enters posteriorly on the occipital surfaces. In the latter case, the entry for the internal carotid artery (i.e. the foramen posterius canalis carotici interni) is positioned within the cavum acustico-jugulare, which opens posteriorly via the fenestra postotica.

State 1 was observed for all testudinoids examined, as well as all kinosternoids but *Baptemys* (Meylan & Gaffney1989; Knauss 2014) and *Macrochelys* (FMNH 22111). State 1 was further observed in some stem-cheloniids (*Argillochelys*: NHMUK R41636, NHMUK 38955, *Puppigerus*: NHMUK R14375).

This character is scored inapplicable for those taxa in which only more terminal branches of the internal carotid artery are embedded in bone, but not the internal carotid artery artery itself.

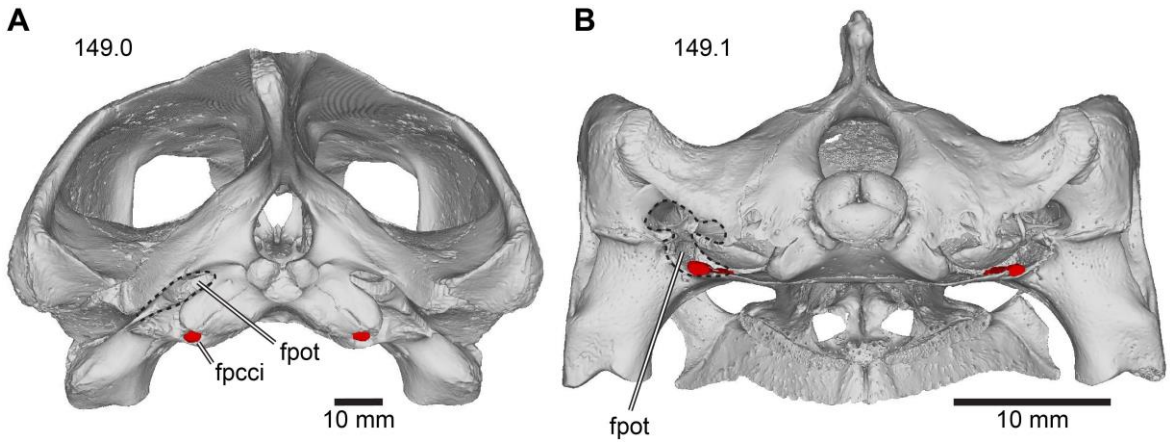


FIG. S1.63. Illustration of character 149. **A**, state 0 (*Lepidochelys olivacea*, SMNS 11070, posterior view of cranium); **B**, state 1 (*Gopherus polyphemus*, FMNH211815, posteroventral view of cranium). Red indicates internal carotid artery. Note that foramen posterius canalis carotici interni in B lies within the cavum acustico-jugulare, and is thus not visible in this view. Dashed line circumscribes the margin of the fenestra postotica. Abbreviations: *fpcci*, foramen posterius canalis carotici interni; fpot, fenestra postotica.

Character optimisation: Unambiguous: Dermochelyidae (0->1), *Puppigerus camperi* (0->1), *Argillochelys cuneiceps* (0->1), *Macrochelys temminckii* (1->0), *Baptemys wyomingensis* (1->0), (*Kirgizemys hoburensis* + *Kirgizemys dmitrievi*) (0->1); DELTRAN: Chelydroidea (0->1), Testudinoidea (0->1), *Meiolania planiceps* (0->1); ACCTRAN: Durocryptodira (0->1), total-group Chelonioidea (1->0), *Meiolania planiceps* (0->1).

Character 150 (new character). Dorsal exposure of the palatine artery and/or anterior parts of the internal carotid artery: 0 = absent, the split of the internal carotid artery is dorsally covered by bone, and the palatine artery exits the basicranium into the cavum cranii via the foramen anterius canalis carotici palatinum; 1 = the internal carotid artery exits the braincase anterodorsally into the sulcus cavernosus where it continues on the floor of the sulcus cavernosus (= sulcus caroticus of Gaffney 1979), and the split into cerebral and palatine arteries occurs within the sulcus cavernosus. The cerebral artery enters the parabasisphenoid medially, whereas the palatine artery continues in the sulcus cavernosus anteriorly without ever being embedded in a canal. This character is scored as inapplicable when the carotid split is ventrally exposed (i.e. ch 148.0 or 148.1).

Remarks: In most turtles in which the splitting point of the internal carotid artery is embedded within the basicranium, the split into palatine and cerebral branches is dorsally covered by bone, and the cerebral and palatine arteries are embedded in bony canals. This is encoded in state 0.

However, some taxa diverge from this pattern: in crown-group chelonioids (but not *Argillochelys*: NHMUK R41636, NHMUK 38955; *Puppigerus*: NHMUK R14375; *Allopleuron*: NHMUK R42913; or protostegids; also not in the stem-group chelonioid *Toxochelys*: Zangerl 1953, AMNH FR 1042;), the internal carotid artery exits the basicranium anteriorly into the sulcus cavernosus, before it splits into its more peripheral branches. The split into cerebral and palatine arteries happens within the sulcus cavernosus, and is dorsally not roofed by the pterygoid or parabasisphenoid (e.g *Chelonia*: Zangerl, 1953; NHMUK 1969.776). A foramen anterius canalis carotici palatinum (sensu Rabi *et al.* 2013; = foramen caroticum laterale sensu Gaffney 1979) is therefore not present in crown cheloniids (see discussion for character 91 of Cadena & Parham (2015), which was deleted in my matrix). While the cerebral artery enters the parabasisphenoid medially through a short canal that openis into the sella turcica, the palatine artery remains without a bony canal in crown-chelonioids.

The condition coded in state 1 can only occur in taxa, in which the split of the carotid artery is embedded within the basicranium. Therefore, this character is scored as inapplicable for all taxa in which the carotid split happens on the ventral surface of the skull, including taxa with a fenestra caroticus.

Character optimisation: Unambiguous: crown-group Cheloniidae (0->1).

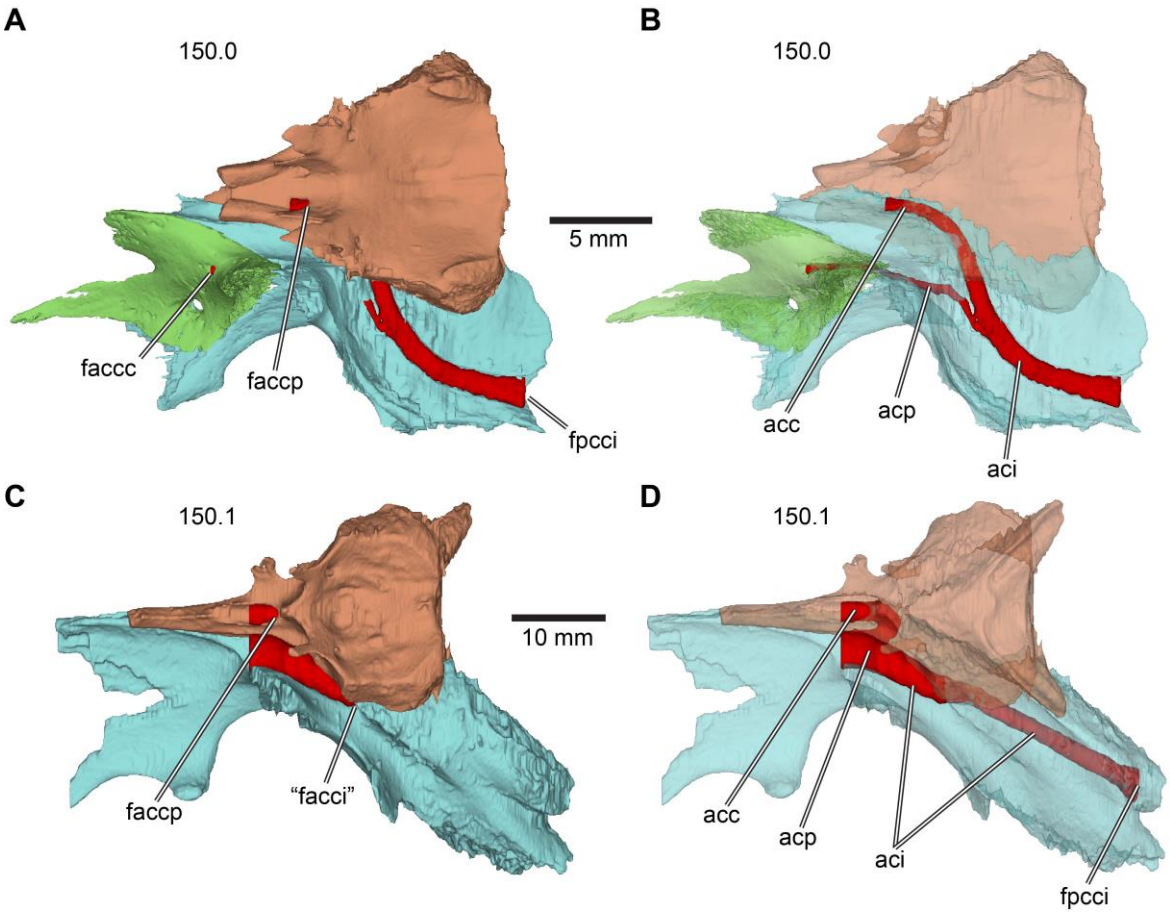


FIG. S1.64. Illustration of character 150. **A**, state 0 (*Gopherus polyphemus*, FMNH211815, dorsal view of parabasisphenoid, left pterygoid, and left palatine); **B**, as A but bones rendered transparent; **C**, state 1 (*Lepidochelys olivacea*, SMNS 11070, dorsal view of parabasisphenoid and left pteryygoid); **D**, as C but bones rendered transparent. Red indicates internal carotid artery and its branches. Abbreviations: *acc*, cerebral artery; *aci*, internal carotid artery; *acp*, palatine artery; *faccc*, foramen anterius canalis carotici cerebralis; *faccp*, foramen anterius canalis carotici palatinum; "*facci*", foramen anterius canalis carotici interni; *fpcci*, foramen posterius canalis carotici interni.

Character 151 (modified from Cadena & Parham (2015)). Formation of the foramen posterius canalis carotici interni, pterygoid involvement: 0 = present; 1 = absent.

Previous character definition: Internal Carotid Artery, foramen posterius canalis carotici interni: 0 = absent; 1 = formed by pterygoid; 2 = formed by pterygoid and basisphenoid halfway along the basisphenoid-pterygoid suture; 3 = formed by prootic, prootic and basisphenoid, or prootic and pterygoid; 4 = formed by basisphenoid only. Rewoded fromJoyce (2007: ch 56, Canalis Caroticum A); Sterli & De la Fuente (2013: ch 100, Canalis Caroticum G).

Remarks: Previous authors have captured variation associated with the formation of the formen posterius canalis carotici interni in a multi-state character in which the states define a range of elements included in the formation of the foramen (Joyce 2007: character 56; Sterli & De la Fuente 2013: character 100; Cadena & Parham (2015): character 100; Zhou & Rabi (2015): character 99)). I chose to split the observations underlying this character into several binary characters that code for the involvement of cranial elements in the formation of the foramen posterius canalis carotici interni (fpcci).

The formation of the fpcci in turtles is highly variable across taxa: the foramen may be formed by the pterygoid alone (e.g. cheloniid sea turtles, trionychians), formed by the pterygoid and parabasisphenoid (e.g. *Plesiochelys planiceps*: OUMNH J1582, *Dermochelys coriacea*: FMNH171756, UMZCR3031; most protostegids), formed as an open trough on the dorsal surface of the pterygoid, and the true foramen lies between the pterygoid and prootic within the cavum acustico-jugulare (e.g. all extant Kinosternoidea examined, but not *Emarginachelys cretacea* or *Baptemys wyomingensis;* but also in many testudinoids such as *Gopherus polyphemus*: FMNH 211815), formed by the prootic only (*Chelus fimbriatus*: NHMUK 81.9.27.4, *Elseya dentata*: NHMUK 76.5.19.77), formed primarily by the prootic with the parabasisphenoid touching on the margin of the foramen (*Pelomedusa subrufa:* SMF 70504), or the parabasipshenoid and the quadrate touching on the margin (*Emydura subglobosa*: IW91c; *Hydromedusa tectifera*: SMF 70500), formed between the prootic and quadrate suture (*Araripemys barretoi*: AMNH FR 24454; *Chelodina oblonga*: NHMUK 64.12.22; *Phrynops geoffroanus*: SMF 45470; *Phrynops hilarii*: NHMUK 91.3.16.1), formed by the prootic and

pterygoid (without the dorsally open trough; seen in *Emarginachelys cretacea*), or formed by the pterygoid and quadrate (*Podocnemis unifilis*: FMNH45657; *Peltocephalus dumerilianus*: NHMUK 60.4.16.9, SMF 55470).

Use of a complex multi-state character to account for all of the above variation, as done in previous studies (e.g. Joyce 2007; Sterli & De la Fuente 2013; Cadena & Parham (2015); Zhou & Rabi (2015)), might confound some phylogenetic signal. For example, the shared contribution of the pterygoid (generally observed in cryptodires) or prootic (generally observed in pleurodires) to the foramen might be phylogenetically informative, irrespective of additional contribution of other cranial elements. Furthermore, previous versions of this character (Joyce 2007; Sterli & De la Fuente 2013; Cadena & Parham (2015); Zhou & Rabi (2015)) used character states that are very precise about the location of the foramen when the pterygoid is involved (as is generally the case in non-pleurodiran turtles). However, all variation seen among pleurodires, in which the prootic is usually involved, were scored in just a single state, which defines the location as "in prootic, prootic & basisphenoid, or prootic and pterygoid" (e.g. Cadena & Parham (2015): character 100 state 3).

As a last modification to previous ways of encoding the variation seen in regard to the foramen posterius canalis carotici interni, I chose to not include a separate state for the absence of the foramen, because the presence vs. absence of this foramen is implied in another character (character 147 state 0) as it is related more to the embedding of the carotid artery. Instead, taxa that lack a foramen posterius canalis carotici interni are scored as inapplicable.

Character optimisation: DELTRAN: total-group Chelidae (0->1), *Pelomedusa subrufa* (0->1); ACCTRAN: Pleurodira (0->1), *Podocnemis* (1->0).

Character 152 (new character). Formation of the foramen posterius canalis carotici interni, parabasisphenoid involvement: 0 = present; 1 = absent.

Remarks: See remarks for character 151.

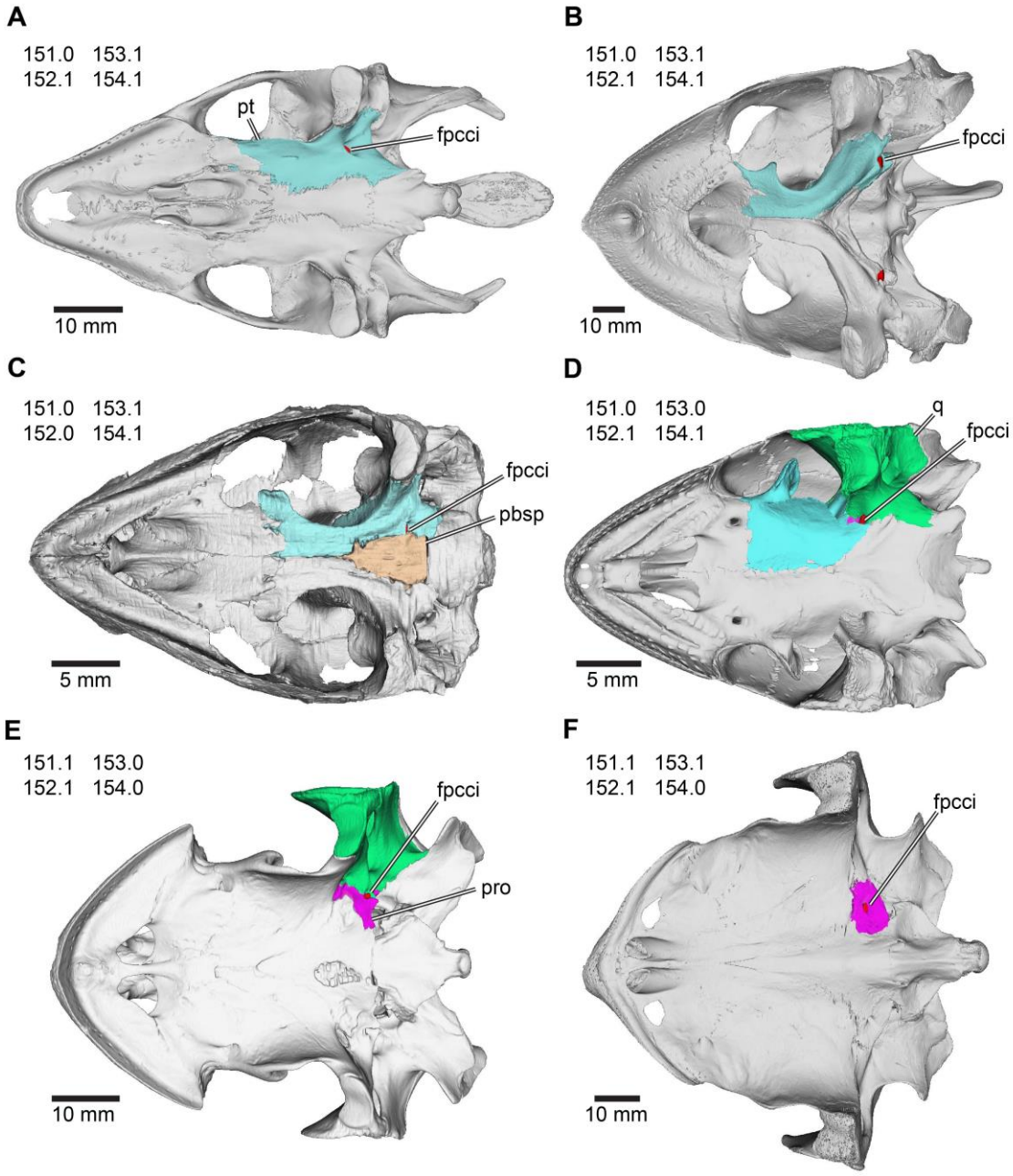


FIG. S1.65. Illustration of characters 151-154. **A**, foramen posterius canalis carotici interni formed by the pterygoid only (*Apalone spinifera emoryi*, FMNH 22178, ventral view of cranium); **B**, foramen posterius canalis carotici interni formed by the pterygoid only (*Lepidochelys olivacea*, SMNS 11070); **C**, foramen posterius canalis carotici interni formed by the pterygoid and parabasisphenoid (*Rhinochelys cantabrigiensis*, CAMSM B55783); **D**, foramen posterius canalis carotici interni formed by pterygoid and quadrate (*Podocnemis unifilis*, FMNH 45657); **E**, foramen posterius canalis carotici interni formed by prootic and quadrate (*Phrynops geoffroanus*, SMF 45470); **F**, foramen posterius canalis carotici interni formed by prootic only (*Chelus fimbriatus*, NHMUK 81.9.27.4). Note that only bones contributing to the foramen are colour coded. Red indicates carotid arteries. Abbreviations: *fpcci*, foramen posterius canalis carotici interni; *pt*, pterygoid; *pro*, prootic; *q*, quadrate.

Character optimisation: Unambiguous: (*Rhinochelys* ++ *Santanachelys*) (1->0), *Desmatochelys padillai* (1->0), (*Portlandemys* ++ *Plesiochelys*) (1->0); DELTRAN: *Protostega gigas* (1->0), *Ordosemys* sp. IVPP V12092 (1->0), *Annemys* sp. IVPP V18106 (1->0), *Xinjiangchelys*

radiplicatoides (1->0); ACCTRAN: (*Protostega* + *Archelon*) (1->0), (*Ordosemys* + *Dracochelys*) (1->0), Xinjiangchelyidae (1->0), *Xinjiangchelys wusu* (0->1).

Character 153 (new character). Formation of the foramen posterius canalis carotici interni, quadrate involvement: 0 = present; 1 = absent.

Remarks: See remarks for character 151.

Character optimisation: DELTRAN: *Phrynops geoffranus* (1->0), Chelodina (1->0), *Araripemys barretoi* (1->0), *Podocnemis* (1->0); ACCTRAN: Pleurodira (1->0), *Chelus fimbriatus* (0->1), *Elseya dentata* (0->1), *Pelomedusa subrufa* (0->1).

Character 154 (new character). Formation of the foramen posterius canalis carotici interni, prootic involvement: 0 = present; 1 = absent.

Remarks: See remarks for character 151.

Character optimisation: Unambiguous: *Argillochelys cuneiceps* (1->0), Chelydroidea (1->0), *Macrochelys temminckii* (0->1), *Baptemys wyomingensis* (0->1), Emydidae (1->0), Testudinidae (1->0); DELTRAN: total-group Chelidae (1->0), *Pelomedusa subrufa* (1->0), *Kirgizemys hoburensis* (1->0); ACCTRAN: Pleurodira (1->0), *Podocnemis* (0->1), (*Kirgizemys hoburensis* + *Kirgizemys dmitrievi*) (1->0).

Character 155 (new character). Hyomandibular branch of the facial nerve: 0 = contained within the canalis cavernosus; 1 = contained in a sulcus or separate canal paralleling the canalis cavernosus.

Remarks: The general patterns of the facial nerve divisions are discussed in the remarks section for character 127.

This character captures some additional variation about the path of the hyomandibular branch of the facial nerve posterior to its entry into the canalis cavernosus.

While the hyomandibular branch of the facial nerve passes posteriorly through the canalis cavernosus in most turtles (state 0), testudinids have a separate canal that parallels the course of the canalis cavernosus. (state 1) In a range of other taxa (e.g. *Plesiochelys planiceps*: OUMNH J1582), the hyomandibular branch is positioned in a sulcus in the medial wall of the canalis canvernosus. This sulcus extends posteriorly from the medial foramen of the facial nerve canal, but is laterally not walled by bone, therefore not forming a true canal is in testudinids. I also score these taxa as having state 1.

Character optimisation: Unambiguous: Testuguria (0->1), (*Jurassichelon* ++ *Plesiochelys*) (0->1), *Annemys* sp. IVPP V18106 (0->1); DELTRAN: *Meiolania planiceps* (0->1), *Eileanchelys waldmanni* (0->1); ACCTRAN*: Meiolania planiceps* (0->1), (*Eileanchelys* + *Kayentachelys*) (0->1).

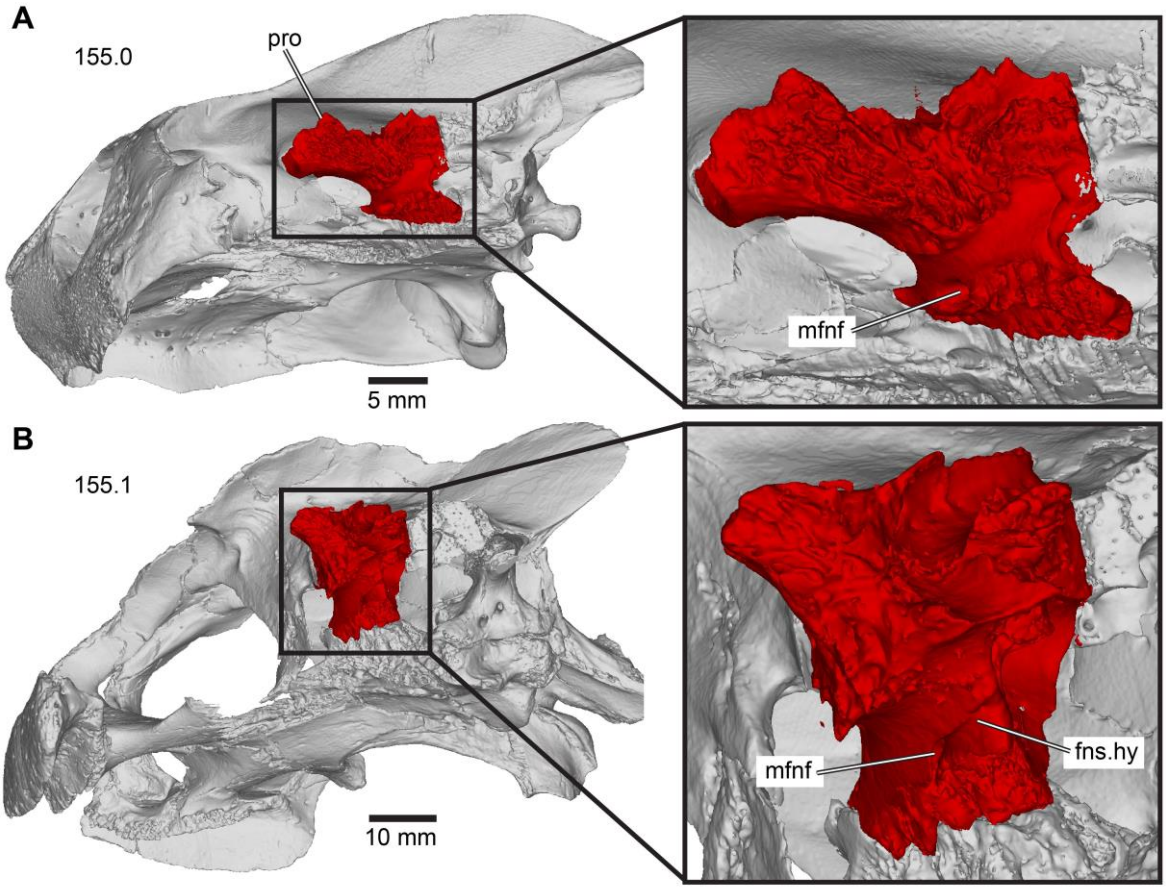


FIG. S1.66. Illustration of character 155. **A**, state 0 (*Sternotherus minor*, FMNH 211696, posteroventrolateral view of otic region, with close-up of the prootic); **B**, state 1 (*Plesiochelys planiceps*, OUMNH J1582). Note that the quadratojugal, quadrate, pterygoid, and squamosal have been removed in A and B. Abbreviations: *mfnf*, medial foramen nervi facialis; *fns.hy*, facial nerve sulcus for the hyomandibular nerve; *pro*, prootic.

Character 156 (modified from Cadena & Parham (2015)). Stapedial artery, foramen stapedio-temporale: 0 = present; 1 = absent.

Previous definition (Cadena & Parham (2015): character 94): Stapedial artery, size of foramen stapedio-temporale: 0 = relatively large (the size of a large blood foramina, ≥5 mm diameter); 1 = significantly reduced in size (the size of a nerve foramina, ≤3 mm diameter); 2 = absent. Joyce (2007: ch 54) & Sterli & de la Fuente (2013: ch 90) (Stapedial Artery B).

Remarks: As done in Anquetin (2012), I split the character used originally by Joyce (2007: ch 54) into a presence vs. absence character, and a character that regards the relative size of the foramen stapedio-temporale.

Character optimisation: Unambiguous: total-group Dermatemydidae (0->1).

Character 157 (modified from Cadena & Parham (2015)). Stapedial artery, size of foramen stapedio-temporale: 0 = relatively large (the size of a large blood foramina, ≥5 mm diameter); 1 = significantly reduced in size (the size of a nerve foramina, ≤3 mm diameter. This character is scored as inapplicable for taxa without a foramen stepedio-temporale (i.e. ch 156.1).

Previous definition (Cadena & Parham (2015): character 94): Stapedial artery, size of foramen stapedio-temporale: 0 = relatively large (the size of a large blood foramina, ≥5 mm diameter); 1 = significantly reduced in size (the size of a nerve foramina, ≤3 mm diameter); 2 = absent. Joyce (2007: ch 54) & Sterli & de la Fuente (2013: ch 90) (Stapedial Artery B).

Remarks: See remarks for chatacter 156.

Character optimisation: DELTRAN: Kinosternidae (0->1); ACCTRAN: Kinosternoidea (0->1).

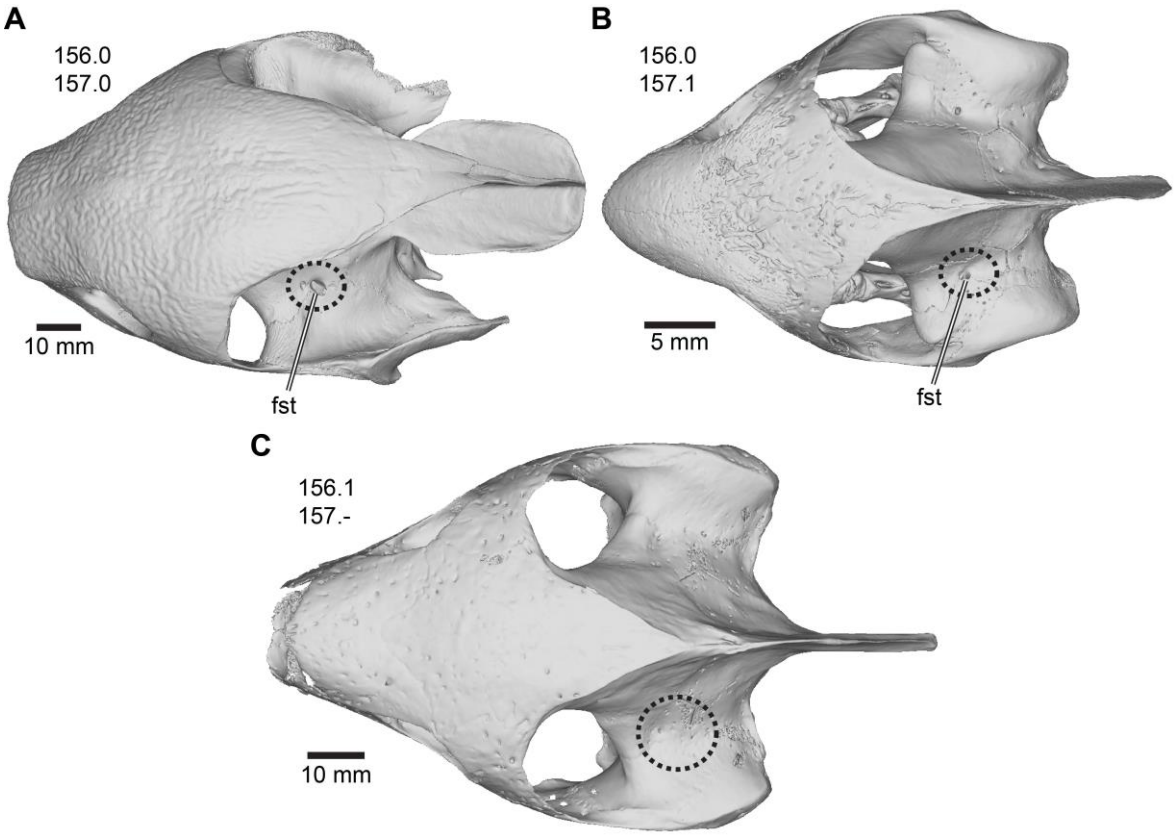


FIG. S1.67. Illustration of character 156 and 157. **A**, *Carettochelys insculpta* (NHMUK 1903.7.10.1, dorsal view of cranium); **B**, *Sternotherus minor* (FMNH 211696); **C**, *Dermatemys mawii* (SMF 59463). Dashed circles surround area where foramen stapedio-temporal is expected. Note the small size of the foramen in B, and the absence of the foramen in C. Abbreviations: *fst*, foramen stapedio-temporal.

Character 158 (Cadena & Parham (2015): character 95). Stapedial artery, foramen stapedio-temporale location in the otic chamber: 0 = on dorsal part and pointing dorsally; 1 = on the anterior wall of the otic region, pointing anteriorly. This character is scored as inapplicable for taxa without a foramen stepedio-temporale (i.e. ch 156.1).

Character optimisation: DELTRAN: total-group Chelidae (0->1), *Pelomedusa subrufa* (0->1); ACCTRAN: Pleurodira (0->1), *Podocnemis* (1->0).

Character 159 (new character). Stapedial artery, formation of the foramen stapedio-temporale, contribution of the quadrate: 0 = absent; 1 = present. Scored inapplicable for taxa without a foramen stapedio-temporale. This character is scored as inapplicable for taxa without a foramen stepedio-temporale (i.e. ch 156.1).

Remarks: In most turtles, the foramen stapedio-temporale is formed between the prootic and quadrate. However, variation exists, as some turtles have an additional contribution from the opisthotic (e.g. *Bouliachelys suteri*: QMF31669, *Chelonoidis* sp.: SMF67582), others have the foramen completely formed by the prootic (e.g. *Platysternon megacephalum*: SMF69684, *Chelus fimbriatus*: NHMUK81.9.27.4), and yet others have the foramen positioned between the quadrate and the opisthotic (e.g. *Proganochelys quenstedti*: SMNS 16980). I coded these observations into several binary characters that code for the involvement of cranial elements in the formation of the foramen stapedio-temporale.

Character optimisation: Unambiguous: *Kinosternon suburum hippocrepis* (1->0), *Platysternon megacephalum* (1->0), *Chelus fimbriatus* (1->0), *Meiolania planiceps* (1->0).

Character 160 (new character). Stapedial artery, formation of the foramen stapedio-temporale, contribution of the prootic: 0 = absent; 1 = present. Scored inapplicable for taxa without a foramen stapedio-temporale. This character is scored as inapplicable for taxa without a foramen stepedio-temporale (i.e. ch 156.1).

Remarks: See remarks for character 159.

Character optimisation: DELTRAN: (*Eileanchelys* + *Kayentachelys*)+++ (0->1); ACCTRAN: *Australochelys*+++ (0->1).

Character 161 (new character). Stapedial artery, formation of the foramen stapedio-temporale, contribution of the opisthotic: 0 = absent; 1 = present. Scored inapplicable for taxa without a foramen stapedio-temporale. This character is scored as inapplicable for taxa without a foramen stepedio-temporale (i.e. ch 156.1).

Remarks: See remarks for character 159.

Character optimisation: Unambiguous: Dermochelyoidea (0->1), (*Rhinochelys* ++ *Santanachelys*) (1->0), *Caretta caretta* (0->1), *Chelonoidis* sp. (0->1), *Brachyopsemys tingitana* (0->1), *Kirgizemys dmitrievi* (0->1), *Meiolania planiceps* (0->1); DELTRAN: *Proganochelys quenstedti* (0->1); ACCTRAN: *Proganochelys quenstedti* (0->1).

Character 162 (new character). Stapedial artery, formation of the foramen stapedio-temporale, contribution of the supraoccipital: 0 = absent; 1 = present. Scored inapplicable for taxa without a foramen stapedio-temporale. This character is scored as inapplicable for taxa without a foramen stepedio-temporale (i.e. ch 156.1).

Remarks: See remarks for character 159.

Character optimisation: Unambiguous: *Eubaena cephalica* (0->1).

Character 163 (Cadena & Parham (2015): character 97). Foramen jugulare posterius, relationship with the fenestra postotica: 0 = separate from fenestra postotica; 1 = coalescent with fenestra postotica.

Character optimisation: Unambiguous: total-group Chelonioidea (0->1), *Allopleuron hofmanni* (1->0), *Platysternon megacephalum* (0->1), *Brachyopsemys tingitana* (1->0), *Kirgizemys hoburensis* (1->0); DELTRAN: Cryptodira (1->0), *Apalone spinifera* (0->1), Chelinae (1->0), Pelomedusoides (1->0); ACCTRAN: Testudines (1->0), Trionychinae (0->1), total-group Chelidae (0->1), Chelinae (1->0).

Character 164 (modified from Zhou & Rabi (2015)). Foramen jugulare posterius, formation of lateral bar separating foramen from fenestra postotica: 0 = formed by pterygoid; 1 = formed by opisthotic and/or exoccipital. The character is scored inapplicable for taxa in which the foramen jugulare posterius is coalescent with the fenestra postotica (ch. 163.1).

Remarks: This character is taken, and slightly modified from Zhou & Rabi (2015): Character 93 (Foramen jugulare posterius B). The character first appeared in similar form in Sterli

(2008: character 62, Jugular Foramina A), who stated this character to be a modified version of a character used by Joyce (2007: character 55, Jugular Foramina A). However, while the character of Joyce (2007) was concerned about the general ossification patterns of the area of the skull through which the jugular vein enters the skull, the character of Sterli (2008) and following authors (such as Zhou & Rabi (2015)) is concerned with the details of ossification of the posterior jugular foramen specifically.

Character optimisation: Unambiguous: *Eochelone* (1->0), *Lissemys punctata* (1->0).

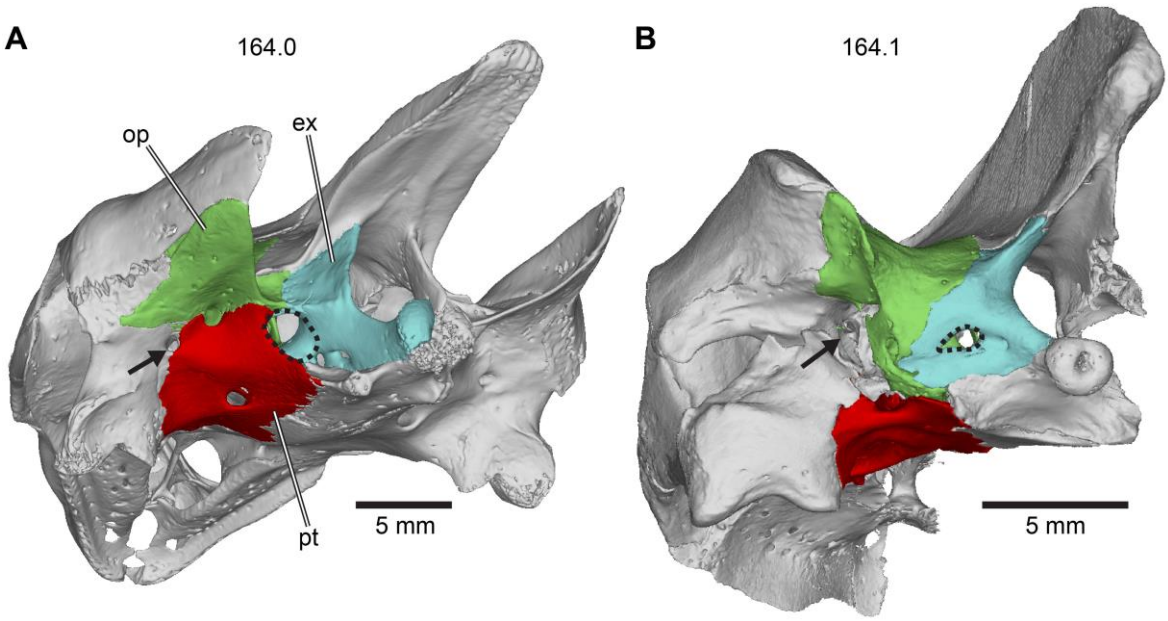


FIG. S1.68. Illustration of character 164. **A**, state 0 (*Lissemys punctata*, SMF 74141, left posteroventrolateral view of cranium); **B**, state 1 (*Sternotherus minor*, FMNH 211696). Dashed line indicates foramen jugulare posterius, arrow indicates fenestra postotica. Abbreviations: *ex*, exoccipital; *op*, opisthotic; *pt*; pterygoid.

Character 165 (Cadena & Parham (2015): character 96). Recessus scalae tympani: 0 = almost nonexistent, not surrounded by bone; 1 = well developed.

Character optimisation: DELTRAN: *Chubutemys*+++ (0->1), *Eileanchelys waldmanni* (0->1); ACCTRAN: (*Eileanchelys* + *Kayentachelys*)+++ (0->1), *Kayentachelys aprix* (1->0).

Character 166 (Cadena & Parham (2015): character 103). Cranial scutes, scute D meeting in midline: 0 = absent; 1 = present.

Character optimisation: DELTRAN: *Meiolania planiceps* (0->1); ACCTRAN: *Meiolania planiceps* (0->1).

Character 167 (Cadena & Parham (2015): character 104). Cranial scutes, scute X much smaller than scute D: 0 = absent; 1 = present.

Character optimisation: -.

Character 168 (Cadena & Parham (2015): character 105). Cranial scutes, scute X partially separates scutes G: 0 = absent; 1 = present.

Character optimisation: -.

Character 169 (Cadena & Parham (2015): character 106). Cranial scutes, scutes A, B, and C forming a continuous posterolateral shelf: 0 = absent; 1 = present.

Character optimisation: -.

Character 170 (Cadena & Parham (2015): character 107). Cranial scutes, scute F: 0 = formed by several scutes; 1 = formed by a single scute.

Character optimisation: DELTRAN: *Meiolania planiceps* (0->1); ACCTRAN: *Meiolania planiceps* (0->1).

Character 171 (Cadena & Parham (2015): character 108). Cranial scutes, scute J: 0 = formed by several scutes; 1 = formed by a single scute.

Character optimisation: -.

Character 172 (Cadena & Parham (2015): character 109). Dentary, medial contact of dentaries: 0 = fused; 1 = open suture.

Character optimisation: Unambiguous: *Toxochelys latiremis* (0->1), *Baptemys wyomingensis* (0->1), total-group Chelidae (0->1), *Elseya dentata* (1->0), (*Eileanchelys* + *Kayentachelys*) (0->1).

Character 173 (Cadena & Parham (2015): character 110). Dentary, width triturating surface vs. jaw length: 0 = narrow triturating surface, symphysis less than 1/3 of jaw length; 1 = broad triturating surface, symphysis ≥1/3 jaw length.

Character optimisation: Unambiguous: *Lepidochelys olivacea* (0->1), *Puppigerus camperi* (0->1); DELTRAN: *Solnhofia parsoni* (0->1), Sandownidae (0->1); ACCTRAN: Angolachelonia (0->1), (*Portlandemys* ++ *Plesiochelys*) (1->0).

Character 174 (modified from Cadena & Parham (2015)). Dentary, symphyseal ridge: 0 = absent; 1 = present.

Previous definition (Cadena & Parham (2015): character 111): Dentary, symphyseal ridge: 0 = absent, at triturating surface; 1 = present, but not visible in lateral view, flat to slightly convex triturating surface; 2 = present and greatly developed, visible in lateral view, ridge along entire length of symphysis. Reworded from Hirayama 1998 (ch 41 & 42); Parham & Pyenson (2010: ch 6), & Kear & Lee (2006: ch 41).

Remarks: I modified this character to a binary presence vs. absence state. Some variation exists in the relative height of the sympheseal ridge, if present, but the previous state definitions did not take the relative height of the labial ridge of the dentary into account.

Character optimisation: Unambiguous: (*Bouliachelys* ++ *Santanachelys*) (0->1), *Elseya dentata* (0->1), *Solnhofia parsoni* (0->1); DELTRAN: (*Lepidochelys olivacea* + *Lepidochelys kempii*) (0->1), (*Chelonia* + *Natator*) (0->1), *Puppigerus camperi* (0->1), *Argillochelys cuneiceps* (0->1), crown-group Chelydridae (0->1); ACCTRAN: *Argillochelys*+++ (0->1), (*Eretmochelys* ++ *Lepidochelys*) (1->0), (*Lepidochelys olivacea* + *Lepidochelys kempii*) (0->1), *Allopleuron hofmanni* (1->0), total-group Chelydridae (0->1).

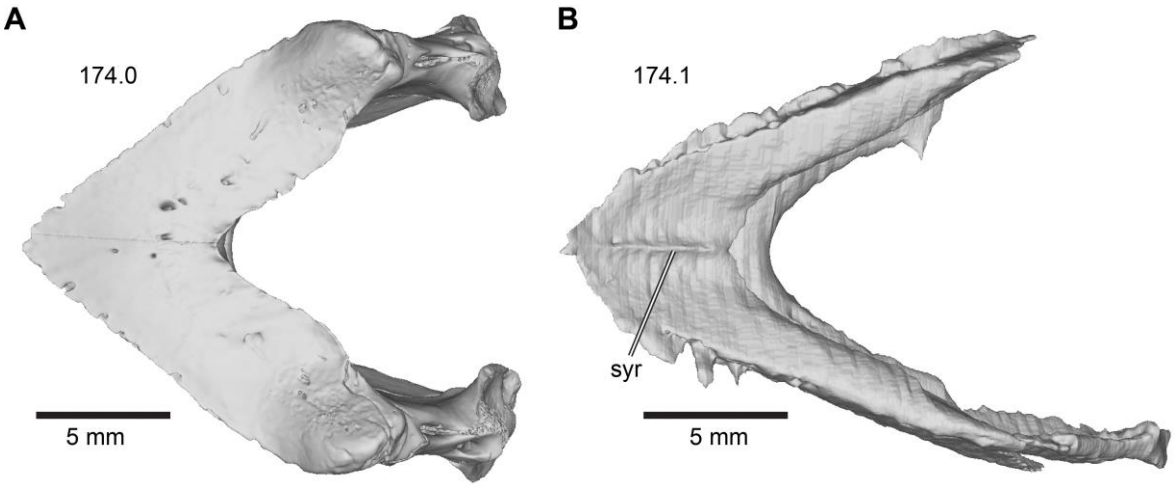


FIG. S1.69. Illustration of character 174 **A**, state 0 (*Sternotherus minor*, FMNH 211696, dorsal view of mandible); **B**, state 1 (*Rhinochelys cantabrigiensis*, CAMSM B55783). Abbreviations: *syr*, symphyseal ridge.

Character 175 (Cadena & Parham (2015): character 112). Dentary, lingual (tomial) ridge: 0 = prominent; 1 = weak or absent.

Character optimisation: Unambiguous: *Eretmochelys imbricata* (1->0), *Natator depressus* (1->0), *Allopleuron hofmanni* (1->0), *Sternotherus* (1->0), total-group Dermatemydidae (1->0), Testudinoidea (1->0), *Elseya dentata* (1->0), Pelomedusoides (1->0), (*Portlandemys* ++ *Plesiochelys*) (1->0), *Kallokibotion bajazidi* (0->1); DELTRAN: Sinemydidae/Macrobaenidae+++ (0->1), *Carettochelys insculpta* (1->0), *Xinjiangchelys radiplicatoides* (0->1); ACCTRAN: Xinjiangchelyidae+++ (0->1), total-group Carettochelyidae (1->0), *Annemys levensis* (1->0).

Character 176 (new character). Dentary, size of foramen dentofaciale majus: 0 = small, size of a small vessel; 1 = enlarged, foramen is several mm in diameter.

Remarks: The foramen dentofaciale majus is a foramen on the lateral surface of the dentary, positioned posterior to the posterior limit of the ramphotheca (Gaffney 1979). The foramen is relatively small in most groups, but it is notably enlarged in cheloniids (e.g. *Lepidochelys olivacea*: SMNS 11070), and in various cryptodires (e.g. *Gopherus polyphemus*: FMNH 211815; *Dermatemys mawii*: SMF 59463; *Carettochelys insculpta*: NHMUK 1903.7.10.1). *Toxochelys* is

scored as polymorphic, because the foramen is small in some specimens (e.g. AMNH 5118), but enlarged in others (e.g. AMNH 14221).

Character optimisation: Unambiguous: total-group Cheloniidae (0->1), total-group Dermatemydidae (0->1); DELTRAN: *Chrysemys picta* (0->1), *Geoclemys hamiltonii* (0->1), *Gopherus polyphemus* (0->1), *Carettochelys insculpta* (0->1); ACCTRAN: Testudinoidea (0->1), *Platysternon megacephalum* (1->0), (*Testudo* + *Chelonoidis*) (1->0), total-group Carettochelyidae (0->1).

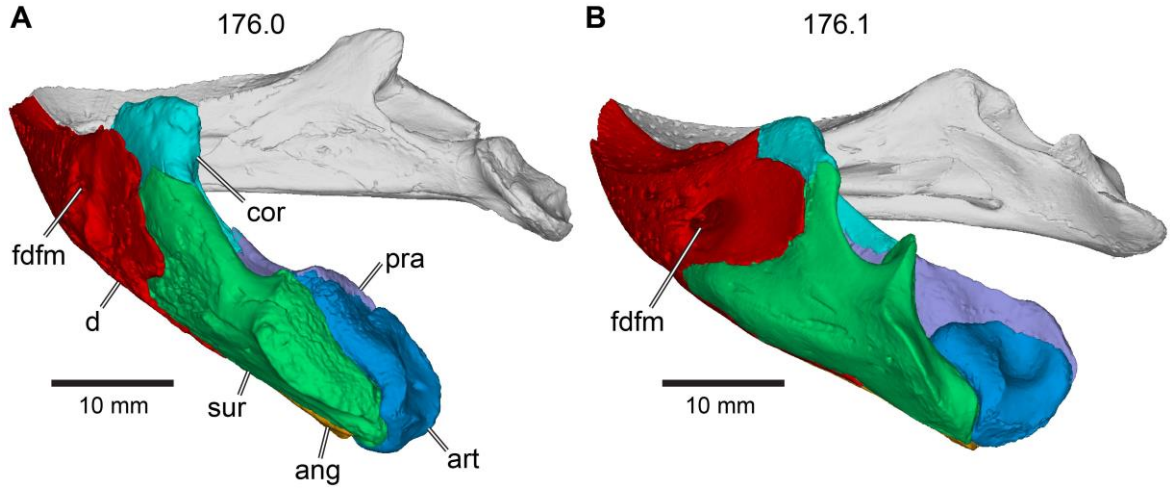


FIG. S1.70. Illustration of character 176. **A**, state 0 (*Plesiochelys planiceps*, OUMNH J1582, left posterodorsolateral view of mandible); **B**, state 1 (*Lepidochelys olivacea*, SMNS 11070). Abbreviations: *ang*, angular; *art*, articular; *cor*, coronoid; *d*, dentary; *fdfm*, foramen dentofaciale majus; *pra*, prearticular; *sur*, surangular.

Character 177 (Cadena & Parham (2015): character 113). Dentary-Surangular arrangement: 0 = lack of a posterior expansion of dentary and anterior projection of surangular; 1 = posterior expansion of dentary present almost reaching the articular surface, covering the dorsal half of the surangular in lateral view, surangular with anterior projection.

Character optimisation: Unambiguous: *Bouliachelys suteri* (0->1), crown-group Cheloniidae (0->1), *Lepidochelys kempii* (1->0), *Toxochelys latiremis* (0->1); DELTRAN: *Dermochelys coriacea* (0->1), crown-group Chelydridae (0->1); ACCTRAN: Dermochelyidae (0->1), total-group Chelydridae (0->1).

Character 178 (new character). Surangular, with anteromedial process forming a vertical lamina that projects anteriorly into the fossa meckelii: 0 = absent; 1 = present.

Remarks: The surangular forms the lateral wall of the fossa meckelii, and is a sheet-like element in turtles (Gaffney 1979). In various cryptodires, a process at the posterior end of the surangular projects anteromedially into the fossa meckelii. The presence of this process is homoplastic among most subclades of cryptodires, but I found it to be absent in all testudinids (*Gopherus polyphemus*: FMNH 211815; *Chelonoidis* sp.: SMF 67582; *Testudo marginata*: FMNH 51672), trionychids (*Apalone spinifera emoryi*: FMNH 22178; *Pelodiscus sinensis*: IW576-2; *Lissemys punctata*: SMF 74141), pleurodires, as well as stem-group turtles for which I have data (including *Proganochelys quenstedti*: SMSM 16980). It is variably present in chelonioids and thalassochelydians, as well as some kinosternoids (e.g. *Macrochelys temminckii*: FMNH 22111), testudinoids (e.g. *Chrysemys picta*: NHMUK 76.1.31.19) and *Carettochelys insculpta*: NHMUK 1903.7.10.1).

Character optimisation: Unambiguous: (*Chelonia* + *Natator*) (1->0); DELTRAN: Americhelydia (0->1), Emysternia (0->1), *Carettochelys insculpta* (0->1), *Solnhofia parsoni* (0->1), *Plesiochelys planiceps* (0->1); ACCTRAN: Xinjiangchelyidae+++ (0->1), Testuguria (1->0), Trionychidae (1->0), Pleurodira (1->0), *Plesiochelys etalloni* (1->0).

Character 179 (new character). Coronoid, anteromedial process: 0 = absent; 1 = present.

Remarks: The coronoid is a roughly triangular bone positioned approximately centrally on the dorsal surface of each mandibular ramus. In some taxa (thalassocheyldians, sandownids, cheloniids, *Toxochelys*, xinjiangchelyids, trionychians, pelomedusoids) the coronoid has an expanded anteromedial process, whereas this process is absent in early stem-group turtles such as *Proganochelys quenstedti*, kinosternoids, testudinids, protostegids, macrobaenids, and sinemydids.

Character optimisation: Unambiguous: Chelydroidea (1->0), Testuguria (1->0), *Chelodina* (1->0), *Araripemys barretoi* (1->0); DELTRAN: Angolachelonia+++ (0->1), Xinjiangchelyidae (0->1); ACCTRAN: Paracryptodira+++ (0->1), Sinemydidae/Macrobaenidae (1->0).

Character 180 (new character). Coronoid, contribution to triturating surface: 0 = absent; 1 = present.

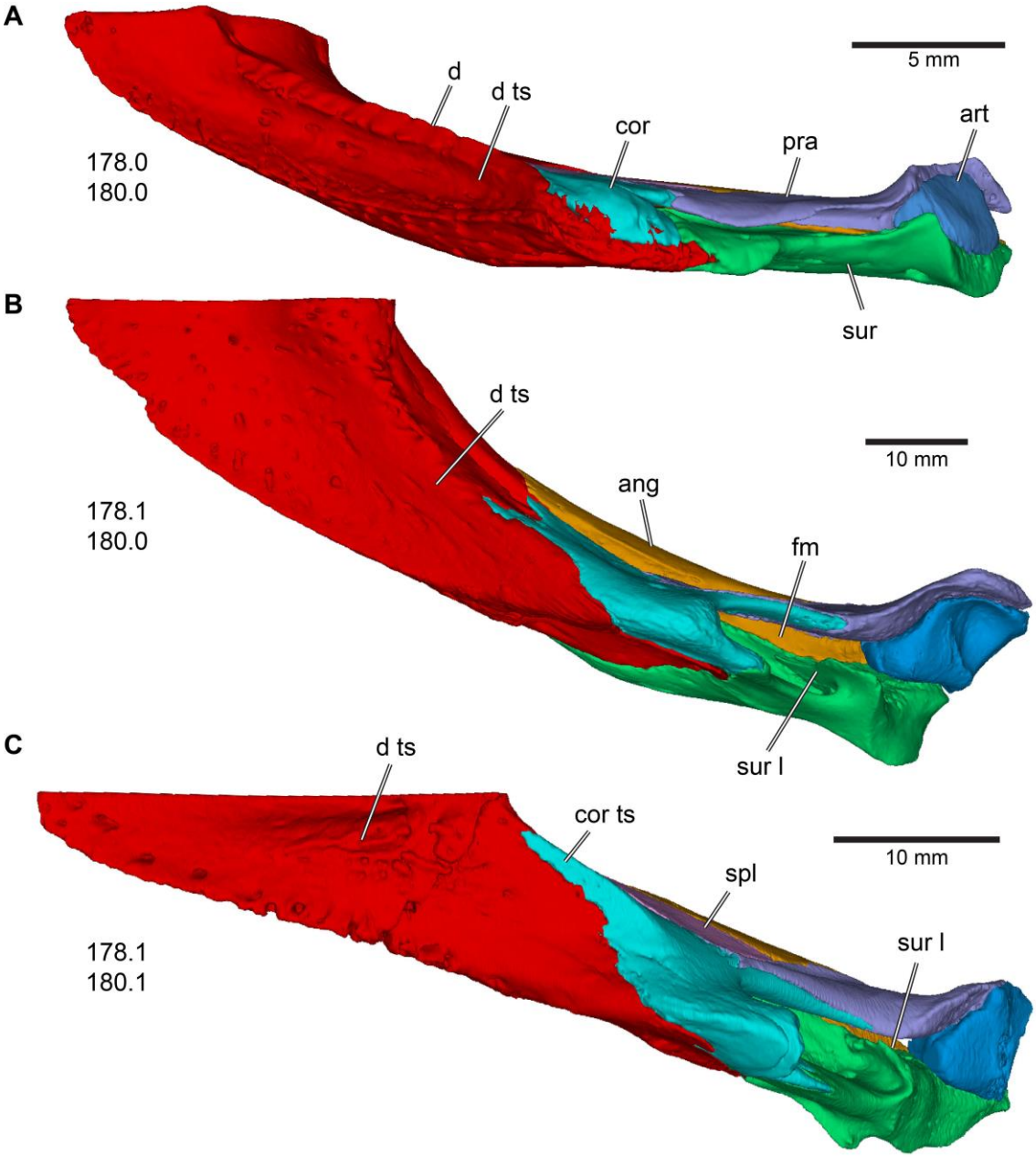


FIG. S1.71. Illustration of characters 178 and 180. **A**, surangular without lamina, and triturating surface confined to dentary (*Elseya dentata*, NHMUK 76.5.19.77, dorsal view of left mandibular ramus); **B**, surangular with lamina, and triturating surface confined to dentary (*Lepidochelys olivacea*, SMNS 11070); C, surangular with lamina, and coronoid contributes to triturating surface (*Solnhofia parsoni*, TM 4023, right mandibular ramus deflected). Abbreviations: *ang*, angular; *art*, articular; *cor*, coronoid; *cor ts*, coronoid triturating surface; *d*, dentary; *d ts*, dentary triturating surface; *fm*, fossa meckelii; *pra*, prearticular; *sp*, splenial; *sur*, surangular; *sur l*, surangular lamina.

Remarks: In most turtles, the coronoid is a relatively small bone that is limited to the central and anteroventromedial part of the mandible. However, in some taxa in which the coronoid is

anteriorly expanded (see character 179), this expansion continues onto the anterior half of the dorsal surface of the mandible, and contributes to the triturating surface (trionychians, pelomedusoids, sandownids, *Solnhofia*).

Character optimisation: Unambiguous: Angolachelonia+++ (0->1), *Platysternon megacephalum* (1->0), (*Testudo* + *Chelonoidis*) (1->0), total-group Chelidae (1->0), (*Portlandemys* ++ *Plesiochelys*) (1->0); DELTRAN: total-group Chelonioidea (1->0), crown-group Chelydridae (1->0), *Kinosternon suburum hippocrepis* (1->0), *Baptemys wyomingensis* (1->0); ACCTRAN: Americhelydia (1->0), Kinosternoidea (0->1), *Kinosternon suburum hippocrepis* (1->0), *Baptemys wyomingensis* (1->0).

Character 181 (new character). Coronoid, notch on posterior margin of coronoid: 0 = absent; 1 = present.

Remarks: In most turtles, the apex of the cornoid projects dorsally, and the posterior margin of the coronoid is convexly rounded or approximately straight. However, in thalassochelydians (e.g. *Solnhofia parsoni*: TM 4023) and sandownids (e.g. *Sandownia harrisi*: MIWG 3480), the posterior margin of the coronoid is gently concave, creating a notch, and the apex of the coronoid is slightly posteriorly directed. This is also seen in a few cryptodires (e.g. *Carettochelys insculpta*: NHMUK 1903.7.10.1).

Character optimisation: Unambiguous: *Kinosternon suburum hippocrepis* (0->1), *Platysternon megacephalum* (0->1), Angolachelonia (0->1), *Portlandemys mcdowelli* (1->0); DELTRAN: Trionychinae (0->1), *Carettochelys insculpta* (0->1); ACCTRAN: Trionychia (0->1), *Lissemys punctata* (1->0).

Character 182 (new character). Coronoid, foramen at anterior end, leading from fossa meckelii into space between mandibular rami: 0 = absent; 1 = present.

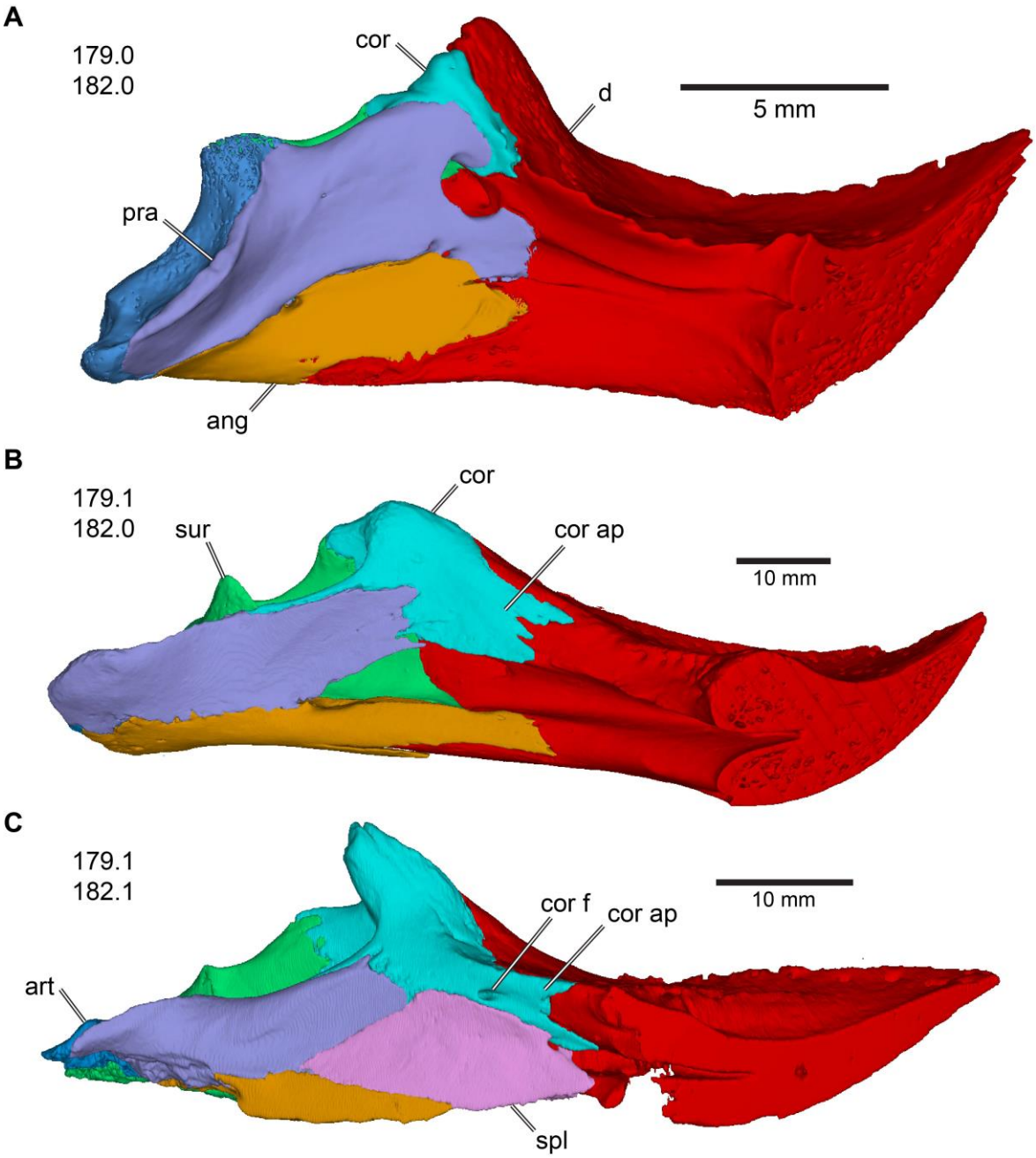


FIG. S1.72. Illustration of characters 179 and 182. **A**, coronoid without anteromedial process, and without foramen (*Sternotherus minor*, FMNH 211696, medial view of left mandibular ramus); **B**, coronoid with anteromedial process, and without foramen (*Lepidochelys olivacea*, SMNS 11070); **C**, coronoid with anteromedial process, and with foramen (*Solnhofia parsoni*, TM 4023, right mandibular ramus deflected). Abbreviations: *ang*, angular; *art*, articular; *cor*, coronoid; *cor ap*, coronoid anteromedial process; *cor f*, coronoid foramen; *d*, dentary; *pra*, prearticular; *spl*, splenial; *sur*, surangular; *sur l*, surangular lamina.

Remarks: Sandownids (e.g. *Sandownia harrisi*: MIWG 3480), thalassochelydians (e.g. *Solnhofia parsoni*: TM 4023), some cheloniids (e.g. *Lepidochelys olivacea*: SMNS 11070), and *Meiolania planicpes* (AM F:57984; Gaffney 1983) have a foramen within the coronoid that has not yet

been named (see Gaffney 1979; see Fig. S1.72*c*). With this character, I document the variation associated with the absence vs. presence of this foramen.

Character optimisation: Unambiguous: *Natator depressus* (0->1), *Toxochelys latiremis* (0->1), Angolachelonia (0->1), *Meiolania planiceps* (0->1); DELTRAN: *Lepidochelys olivacea* (0->1), *Caretta caretta* (0->1), *Phrynops geoffranus* (0->1), *Elseya dentata* (0->1); ACCTRAN: (*Caretta* ++ *Lepidochelys*) (0->1), *Lepidochelys kempii* (1->0), crown-group Chelidae (0->1), *Chelodina* (1->0).

Character 183 (new character). Coronoid process, principally formed by: 0 = coronoid; 1 = dentary; 2 = surangular.

Remarks: The coronoid process is the dorsal apex of the mandibular ramus and serves as the attachment of the adductor musculature (Gaffney 1979). In most turtles, this area is formed by the coronoid. However, in kinosternids (e.g. *Sternotherus minor*: NHMUK 211696), as well as *Testudo marginata* (FMNH 51672) and *Elseya dentata* (NHMUK 76.5.19.77), the process is primarily formed by the dentary. In *Dermochelys coriacea*, in which the coronoid is absent (Gaffney 1979), the surangular forms the coronoid process of the mandible. Although *Dermochelys* is the only taxon for which state 2 is scored within my matrix, I leave this state in because mandibles of dermochelyids such as *Eosphargis breineri* are currently unknown.

Character optimisation: Unambiguous: *Testudo* (0->1), *Elseya dentata* (0->1); DELTRAN: *Dermochelys coriacea* (0->2), Kinosternidae (0->1), *Dermatemys mawii* (0->1); ACCTRAN: Dermochelyidae (0->2), Kinosternoidea (0->1), *Baptemys wyomingensis* (1->0).

Character 184 (new character). Coronoid process: 0 = relatively low, dorsally well rounded; 1 = relatively high, process is dorsally or posterodorsally pointed.

Remarks: The coronoid process of the coronoid is a relatively low and well-rounded process in most turtles (e.g. *Proganochelys*, chelonioids, pleurodires). However, in some turtles, such as thalassochelydians, sandownids, trionychians (other than *Lissemys punctata*: SMF 74141),

the coronoid process is dorsally elongated, and developed as a more pointed process. In some turtle groups, such as testudinoids or kinosternoids, this character is variable among the species I examined.

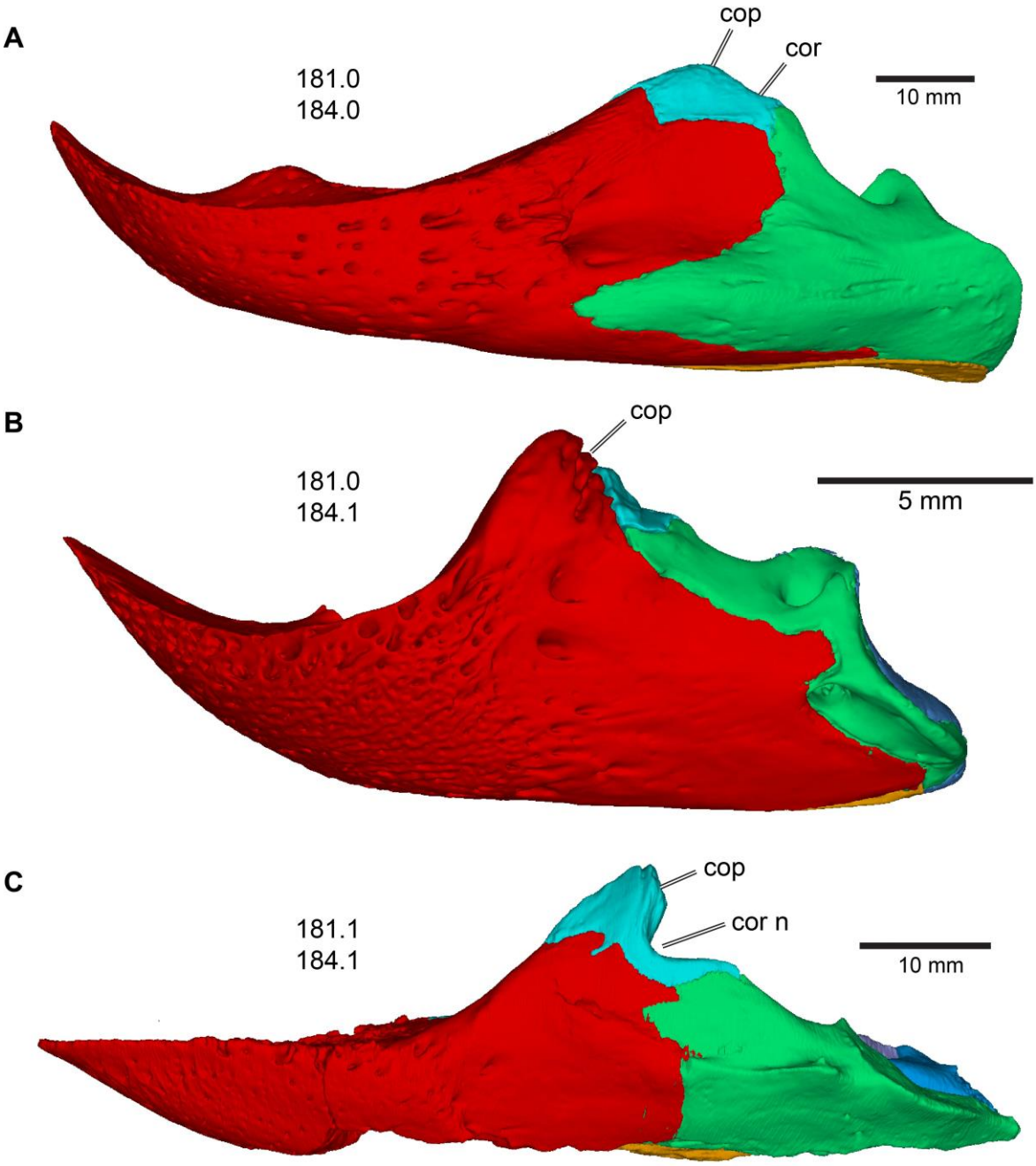


FIG. S1.73. Illustration of character 183. **A**, state 0 (*Lepidochelys olivacea*, SMNS 11070, lateral view of left mandibular ramus); **B**, state 1 (*Sternotherus minor*, FMNH 211696); **C**, state 2 (*Dermochelys coriacea*, UMCZ R 3031). Abbreviations: *cop*, coronoid process; *cor*, coronoid; *d*, dentary; *sur*, surangular.

Character optimisation: Unambiguous: Kinosterninae (0->1), *Baptemys wyomingensis* (0->1), *Platysternon megacephalum* (0->1), Angolachelonia (0->1); DELTRAN: Trionychinae (0->1), *Carettochelys insculpta* (0->1); ACCTRAN: Trionychia (0->1), *Lissemys punctata* (1->0).

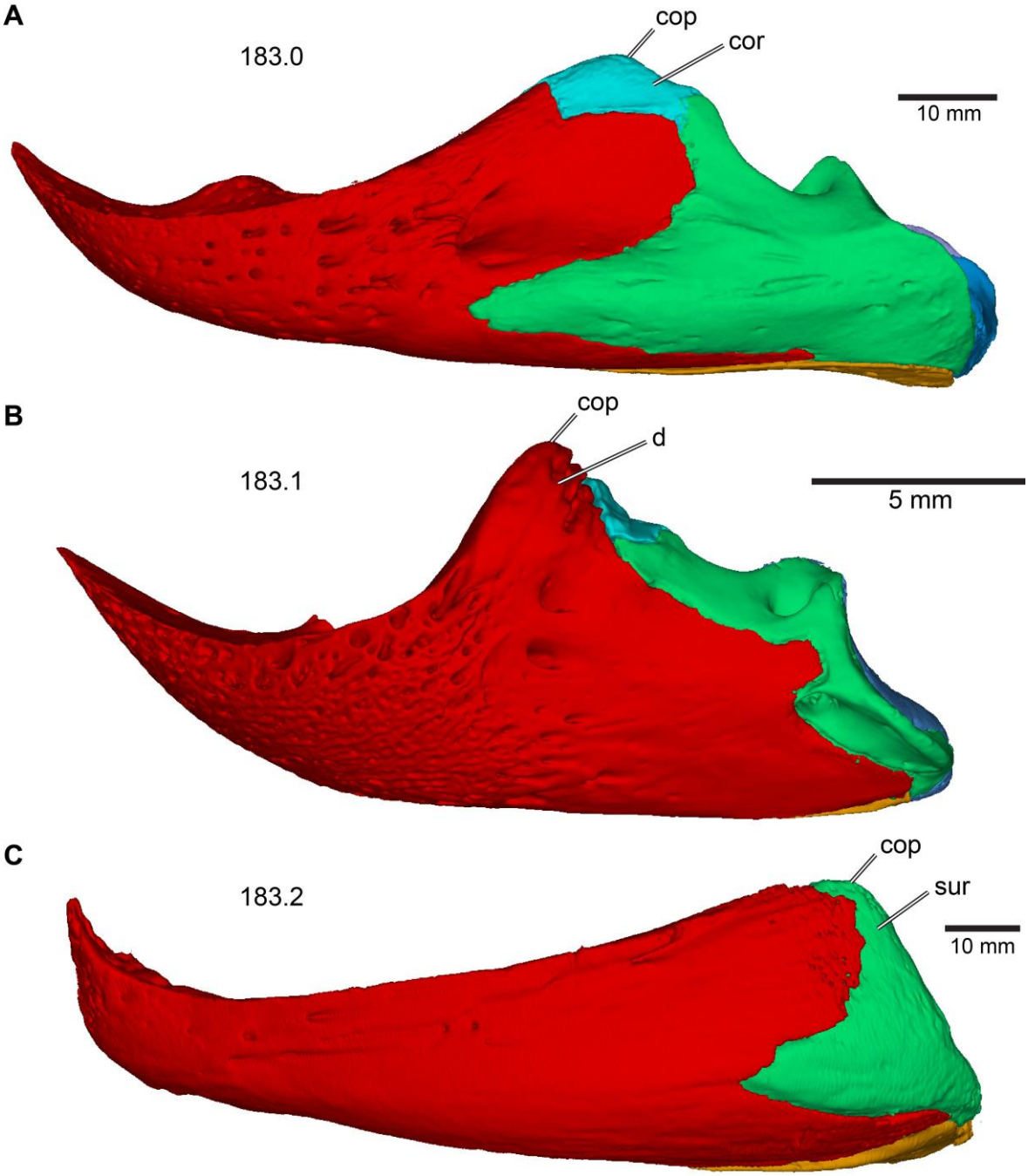


FIG. S1.74. Illustration of characters 181 and 184. **A**, coronoid without posterior notch, and coronoid process low (*Lepidochelys olivacea*, SMNS 11070, lateral view of left mandibular ramus); **B**, coronoid without posterior notch, and coronoid process high (*Sternotherus minor*, FMNH 211696); **C**, coronoid with posterior notch, and coronoid process high (*Solnhofia parsoni*, TM 4023, right mandibular ramus reflected). Abbreviations: *cop*, coronoid process; *cor*, coronoid; *cor n*, coronoid notch.

Character 185 (Cadena & Parham (2015): character 114). Splenial: 0 = present; 1 = absent.

Character optimisation: Unambiguous: Sinemydidae/Macrobaenidae+++ (0->1), *Protostega gigas* (1->0), *Allopleuron hofmanni* (1->0), crown-group Chelidae (1->0), Thalassochelydia (1->0), *Xinjiangchelys radiplicatoides* (0->1); DELTRAN: *Rhinochelys pulchriceps* (1->0); ACCTRAN: (*Rhinochelys* ++ *Santanachelys*) (1->0).

POSTCRANIUM

Character 186 (modified from Cadena & Parham (2015)). Carapace, carapacial scutes: 0 = present; 1 = absent.

Previous definition (Cadena & Parham (2015): character 115): Carapace, carapacial scutes: 0 = present; 1 = reduced not fully covering the carapace; 2 = absent. Reworded from Joyce (2007: ch 60) & Sterli & de la Fuente (2013: ch 121) (Carapace A) and Hirayama (1998), Kear & Lee (2006), and Bardet *et al.* (2013) (ch 80).

Remarks: This character has been modified into two character to acknowledge the phylogenetic information of the shared presence of carapacial scutes.

Character optimisation: Unambiguous: Trionychidae (0->1); DELTRAN: (*Protostega* + *Archelon*) (0->1), *Dermochelys coriacea* (0->1), *Allopleuron hofmanni* (0->1); ACCTRAN: crown-group Chelonioidea (0->1), (*Ocepechelon* ++ *Santanachelys*) (1->0), *Puppigerus*+++ (1->0).

Character 187 (modified from Cadena & Parham (2015)). Carapace, carapacial scutes: 0 = present, fully covering the carapace; 1 = reduced not fully covering the carapace.

Previous definition (Cadena & Parham (2015): character 115): Carapace, carapacial scutes: 0 = present; 1 = reduced not fully covering the carapace; 2 = absent. Reworded from Joyce (2007: ch 60) & Sterli & de la Fuente (2013: ch 121) (Carapace A) and Hirayama (1998), Kear & Lee (2006), and Bardet *et al.* (2013) (ch 80).

Remarks: See character 186.

Character optimisation: DELTRAN: *Carettochelys insculpta* (0->1); ACCTRAN: Trionychia (0->1).

Character 188 (modified from Cadena & Parham (2015)). Carapace, continuous keel on costals: 0 = absent; 1 = present.

Previous definition (Cadena & Parham (2015): character 116): Carapace, three parallel lines of keels: 0 = absent; 1 = present, but only poorly developed; 2 = present and pronounced; 3 = present, but only with a medial line of keels on neurals, absence of keels on costals. Joyce (2007: ch 61) & Sterli & de la Fuente (2013: ch 122) (Carapace B) and Hirayama (1998), Kear & Lee (2006), and Bardet *et al.* (2013) (ch 84).

Remarks: In the previous definition of this character, the keels that are present across the costals of some turtles were coded in character that also includes variation regarding the presence of a median keel acorss the neurals. As some turtles exist in which the median keel is present, but the costal keels are not, these features can be seen as independent variation that should be scored in separate characters.

Character optimisation: Unambiguous: *Geoclemys hamiltonii* (0->1), *Chelus fimbriatus* (0->1), *Araripemys barretoi* (0->1); DELTRAN: *Emarginachelys cretacea* (0->1), Kinosternidae (0->1), *Baptemys wyomingensis* (0->1); ACCTRAN: Chelydroidea (0->1), crown-group Chelydridae (1->0), *Dermatemys mawii* (1->0).

Character 189 (modified from Cadena & Parham (2015)). Carapace, continuous keel on neurals: 0 = absent; 1 = present.

Previous definition (Cadena & Parham (2015): character 116): Carapace, three parallel lines of keels: 0 = absent; 1 = present, but only poorly developed; 2 = present and pronounced; 3 = present, but only with a medial line of keels on neurals, absence of keels on costals. Joyce (2007: ch 61) & Sterli & de la Fuente (2013: ch 122) (Carapace B) and Hirayama (1998), Kear & Lee (2006), and Bardet *et al.* (2013) (ch 84).

Remarks: See character 188.

Character optimisation: Unambiguous: (*Protostega* + *Archelon*) (0->1), *Chelonia mydas* (0->1), *Allopleuron hofmanni* (0->1), *Geoclemys hamiltonii* (0->1), *Chelus fimbriatus* (0->1), *Araripemys barretoi* (0->1); DELTRAN: *Lepidochelys olivacea* (0->1), *Caretta caretta* (0->1), *Emarginachelys cretacea* (0->1), Kinosternidae (0->1), *Baptemys wyomingensis* (0->1); ACCTRAN: (*Caretta* ++ *Lepidochelys*) (0->1), *Lepidochelys kempii* (1->0), Chelydroidea (0->1), crown-group Chelydridae (1->0), *Dermatemys mawii* (1->0).

Character 190 (Cadena & Parham (2015): character 117). Shell, sculpturing of dorsal surface (carapace) and ventral surface (plastron): 0 = absent, smooth to slightly rugose; 1 = present, development of striations, vermiculations, striations, or pitting.

Character optimisation: Unambiguous: Trionychia (0->1), total-group Chelidae (0->1), *Phrynops geoffranus* (1->0); DELTRAN: *Sinemys gamera* (0->1), Pleurosternidae (0->1); ACCTRAN: (*Sinemys lens* + *Sinemys gamera*) (0->1), Paracryptodira (0->1).

Character 191 (Cadena & Parham (2015): character 118). Shell, pattern of sculpturing of the dorsal surface (carapace) and ventral surface (plastron): 0 = parallel to radial striations; 1 = vermiculation; 2 = highly dense pattern of pitting combined with striations; 3 = dichotomic striations; 4 = spread pitting without marked striation pattern; 5 = granules (positive relief).

Character optimisation: Unambiguous: *Araripemys barretoi* (3->4), *Pleurosternon bullockii* (0->3); DELTRAN: Kinosternidae (0->1), Trionychia (0->2), Pleurodira (0->3); ACCTRAN: Testudines (0->1), Trionychia (1->2), Pleurodira (1->3).

Character 192 (Cadena & Parham (2015): character 119). Carapacial Sutures: 0 = carapacial elements finely sutured or the contact is smooth; 1 = carapacial sutures strongly serrated in adult stage.

Character optimisation: DELTRAN: *Dracochelys bicuspis* (0->1); ACCTRAN: (*Ordosemys* + *Dracochelys*) (0->1).

Character 193 (modified from Cadena & Parham (2015)). Nuchal, articulation of nuchal with neural spine of eighth cervical vertebra: 0 = articulation via a blunt facet is present; 1 = articulation along a blunt facet absent.

Previous definition (Cadena & Parham (2015): character 120): Nuchal, articulation of nuchal with neural spine of eighth cervical vertebra: 0 = cervical articulates with nuchal along a blunt facet; 1 = articulation absent; 2 = cervical articulates with nuchal along a raised pedestal. Joyce (2007: ch 62) & Sterli & de la Fuente (2013: ch 126) (Nuchal A).

Remarks: I break the previous character into two (as done by Anquetin 2012), because the raised pedestal seen in chelonioids is interpreted as an independent structure not homologous to the facet on the nuchal seen in some early stem turtles.

Character optimisation: Unambiguous: *Meiolania*+++ (0->1); DELTRAN: *Carettochelys insculpta* (1->0); ACCTRAN: total-group Carettochelyidae (1->0).

Character 194 (Cadena & Parham (2015): character 120). Raised pedestal on the visceral surface of the nuchal for the articulation with the neural spine of the eighth cervical vertebra: 0 = absent; 1 = present.

Previous definition (Cadena & Parham (2015): character 120): Nuchal, articulation of nuchal with neural spine of eighth cervical vertebra: 0 = cervical articulates with nuchal along a

blunt facet; 1 = articulation absent; 2 = cervical articulates with nuchal along a raised pedestal. Joyce (2007: ch 62) & Sterli & de la Fuente (2013: ch 126) (Nuchal A).

Remarks: See character 193.

Character optimisation: Unambiguous: crown-group Cheloniidae (0->1), *Toxochelys latiremis* (0->1); DELTRAN: *Dermochelys coriacea* (0->1); ACCTRAN: Dermochelyidae (0->1).

Character 195 (modified from Cadena & Parham (2015)). Nuchal, elongate costiform process: 0 = absent; 1 = present.

Previous definition (Cadena & Parham (2015): character 121): Nuchal, elongate costiform process: 0 = absent; 1 = present, crosses peripheral 1; 2 = present, well developed reaches peripherals 2 or 3. Modified from Joyce (2007: ch 63) & Sterli & de la Fuente (2013: ch 127) (Nuchal B).

Remarks: I split the previous character in two characters, thereby acknowledging the phylogenetic information of the shared presence of a costiform process on the nuchal.

Character optimisation: Unambiguous: Chelydroidea (0->1).

Character 196 (modified from Cadena & Parham (2015)). Nuchal, length of costiform process: 0 = crosses peripheral 1; 1 = reaches peripherals 2 or 3. This character is scored inapplicable for taxa without a costiform process on the nuchal (ch. 195.0).

Previous definition (Cadena & Parham (2015): character 121): Nuchal, elongate costiform process: 0 = absent; 1 = present, crosses peripheral 1; 2 = present, well developed reaches peripherals 2 or 3. Modified from Joyce (2007: ch 63) & Sterli & de la Fuente (2013: ch 127) (Nuchal B).

Remarks: See character 195.

Character optimisation: Unambiguous: *Chelydra serpentina* (1->2).

Character 197 (Cadena & Parham (2015): character 122). Nuchal, length versus width: 0 = wider than long; 1 = longer than wide or as long as wide.

Character optimisation: Unambiguous: *Chelonoidis* sp. (1->0), Pleurodira (0->1); DELTRAN: Emydidae (0->1), Testuguria (0->1); ACCTRAN: Testudinoidea (0->1), *Platysternon megacephalum* (1->0).

Character 198 (Cadena & Parham (2015): character 123). Nuchal, posteriomedial fontanelles: 0 = absent; 1 = present.

Character optimisation: Unambiguous: *Desmatochelys lowii* (0->1), *Toxochelys latiremis* (0->1).

Character 199 (Cadena & Parham (2015): character 124). Neurals, neural formula 6>4<6<6<6<6: 0 = absent; 1 = present.

Character optimisation: -.

Character 200 (Cadena & Parham (2015): character 125). Neurals, shape of neurals: 0 = very irregular in shape, wider than long or squared; 1 = regular, often perfectly hexagonal or pentagonal, longer than wide.

Character optimisation: Unambiguous: *Platysternon megacephalum* (1->0), Testudinidae (1->0), *Chelus fimbriatus* (1->0); DELTRAN: *Kallokibotion*+++ (0->1), crown-group Chelydridae (1->0); ACCTRAN: *Chubutemys*+++ (0->1), total-group Chelydridae (1->0).

Character 201 (modified from Cadena & Parham (2015)). Neurals: 0 = present; 1 = absent.

Previous definition (Cadena & Parham (2015): character 126): Neurals, number of neurals: 0 = ten or more; 1 = nine or less; 2 = all neurals lost even in ventral view. Modified character from Hirayama (1998), Kear & Lee (2006), and Bardet *et al.* (2013) (ch 85 & ch 87) and Parham & Pyenson (2010: ch 33).

Remarks: The previous character was split into two, because the shared presence of neurals was previously not considered as independent phylogenetic information.

Character optimisation: Unambiguous: *Archelon ischyros* (0->1), Chelodininae (0->1); DELTRAN: *Dermochelys coriacea* (0->1), (*Lepidochelys olivacea* + *Lepidochelys kempii*) (0->1), *Eretmochelys imbricata* (0->1), *Chelonia mydas* (0->1); ACCTRAN: Dermochelyidae (0->1), crown-group Cheloniidae (0->1), *Caretta caretta* (1->0), *Natator depressus* (1->0).

Character 202 (modified from Cadena & Parham (2015)). Neurals, number of neurals: 0 = ten or more; 1 = nine or less.

Previous definition (Cadena & Parham (2015): character 126): Neurals, number of neurals: 0 = ten or more; 1 = nine or less; 2 = all neurals lost even in ventral view. Modified character from Hirayama (1998), Kear & Lee (2006), and Bardet *et al.* (2013) (ch 85 & ch 87) and Parham & Pyenson (2010: ch 33).

Remarks: See chatacter 201.

Character optimisation: DELTRAN: *Kallokibotion*+++ (0->1), *Eileanchelys waldmanni* (0->1); ACCTRAN: *Australochelys*+++ (0->1), *Kayentachelys aprix* (1->0).

Character 203 (Cadena & Parham (2015): character 127). Peripheral Gutter: 0 = peripheral gutter absent of only anteriorly developed; 1 = peripheral gutter extensively developed along anterior and bridge peripherals.

Character optimisation: Unambiguous: *Phrynops geoffranus* (0->1), Xinjiangchelyidae (0->1), *Eileanchelys waldmanni* (0->1); DELTRAN: *Kirgizemys hoburensis* (0->1); ACCTRAN: (*Kirgizemys hoburensis* + *Kirgizemys dmitrievi*) (0->1).

Character 204 (modified from Cadena & Parham (2015)). Peripherals,: 0 = present; 1 = absent.

Previous definition (Cadena & Parham (2015): character 128): Peripherals, number of peripherals: 0 = more than 11 pairs of peripherals present; 1 = 11 pairs of peripherals present; 2 = 10 pairs of peripherals present; 3 = less than 10 pairs of peripherals present. Joyce (2007: ch 65) & Sterli & de la Fuente (2013: ch 131) (Peripheral A).

Remarks: I split the previous character into two characters, as already done in Anquetin (2012). The first character codes for the presence vs. absence of peripherals, because I believe that the shared presence of peripherals, irrespective of their number, can be phylogenetically informative. The second character codes for the number of peripherals. I retain the second character as a multistate character (unlike in Anquetin 2012) using the character state definitions of Cadena & Parham (2015). However, the third state of Cadena & Parham (2015: "less than 10 pairs of peripherals present") is dropped, because it is equivalent to the absence of peripherals.

Character optimisation: Unambiguous: Trionychidae (0->1); DELTRAN: *Dermochelys coriacea* (0->1); ACCTRAN: Dermochelyidae (0->1).

Character 205 (modified from Cadena & Parham (2015)). Peripherals, number of peripherals: 0 = more than 11 pairs of peripherals present; 1 = 11 pairs of peripherals present; 2 = 10 pairs of peripherals present. This character is scored as inapplicable when peripherals are absent (ch. 204.1).

Previous definition (Cadena & Parham (2015): character 128): Peripherals, number of peripherals: 0 = more than 11 pairs of peripherals present; 1 = 11 pairs of peripherals present; 2 = 10 pairs of peripherals present; 3 = less than 10 pairs of peripherals present. Joyce (2007: ch 65) & Sterli & de la Fuente (2013: ch 131) (Peripheral A).

Remarks: See character 2014.

Character optimisation: Unambiguous: Kinosternidae (1->2); DELTRAN: (*Eileanchelys* + *Kayentachelys*)+++ (0->1), *Caretta caretta* (1->0), *Carettochelys insculpta* (1->0); ACCTRAN: *Australochelys*+++ (0->1), (*Caretta* ++ *Lepidochelys*) (1->0), Trionychia (1->0).

Character 206 (Cadena & Parham (2015): character 129). Peripherals, anterior peripherals incised by musk ducts: 0 = absent; 1 = present.

Character optimisation: Unambiguous: Cryptodira (1->0), Kinosternoidea (0->1), *Kinosternon suburum hippocrepis* (1->0), *Platysternon megacephalum* (0->1), *Geoclemys hamiltonii* (0->1), *Chelonoidis* sp. (0->1), *Araripemys barretoi* (1->0); DELTRAN: Xinjiangchelyidae+++ (0->1), *Kayentachelys aprix* (0->1); ACCTRAN: Paracryptodira+++ (0->1), (*Eileanchelys* + *Kayentachelys*) (0->1).

Character 207 (Cadena & Parham (2015): character 130). Costals, medial contact of the first pair of costals: 0 = absent; 1 = present.

Character optimisation: Unambiguous: Kinosterninae (0->1), Chelodininae (0->1).

Character 208 (modified from Cadena & Parham (2015)). Costals, medial contact of posterior costals: 0 = absent; 1 = present.

Previous definition (Cadena & Parham (2015): character 131): Costals, medial contact of posterior costals: 0 = absent; 1 = medial contact of up to three posterior costals present; 2 =

medial contact of all costals present. Modified from Joyce (2007: ch 68) & Sterli & de la Fuente (2013: ch 134) (Costal B).

Remarks: I split the previous character into two characters, because the shared presence of a medial contact of the posterior costals is viewed as a separate character providing independent phylogenetic information.

Character optimisation: Unambiguous: Angolachelonia+++ (0->1), Durocryptodira (1->0), *Chelus fimbriatus* (1->0), *Annemys levensis* (0->1); DELTRAN: *Desmatochelys lowii* (0->1), Kinosterninae (0->1), *Dermatemys mawii* (0->1), *Proganochelys quenstedti* (0->1); ACCTRAN: (*Desmatochelys lowii* + *Desmatochelys padillai*) (0->1), Kinosternoidea (0->1), *Baptemys wyomingensis* (1->0), *Proganochelys quenstedti* (0->1).

Character 209 (modified from Cadena & Parham (2015)). Costals, number of costals involved in medial contact: 0 = medial contact of up to three posterior costals; 1 = medial contact of all costals. This character is scored as inapplicable for turtles without a medial contact of posterior costals.

Previous definition (Cadena & Parham (2015): character 131): Costals, medial contact of posterior costals: 0 = absent; 1 = medial contact of up to three posterior costals present; 2 = medial contact of all costals present. Modified from Joyce (2007: ch 68) & Sterli & de la Fuente (2013: ch 134) (Costal B).

Remarks: See character 208.

Character optimisation: Unambiguous: *Sternotherus* (0->1), Chelodininae (0->1); DELTRAN: *Desmatochelys lowii* (0->1), Thalassochelydia (0->1); ACCTRAN: total-group Chelonioidea (0->1), Angolachelonia (0->1).

Character 210 (Cadena & Parham (2015): character 132). Costals, distal rib end and lateral ossification of the costal: 0 = costals fully ossified laterally with strong sutural contact

with peripherals, lack of dorsal exposure of distal end of costal ribs; 1 = costals fully ossified laterally with strong sutural contact with peripherals, distal end of costal ribs exposed on dorsal surface and surrounded by the peripheral; 2 = costals lack lateral ossification, allowing the dorsal exposure of the distal end of ribs and the development of fontanelles only at the most anterior and posterior costals; 3 = costals with extreme lost of lateral ossification, allowing the dorsal exposure of the distal end of ribs, in almost all series of costals.

Character optimisation: Unambiguous: total-group Chelonioidea (0->2), *Caretta caretta* (2->3), *Chelonia mydas* (2->3), *Chelydra serpentina* (0->2), *Araripemys barretoi* (0->2), Thalassochelydia (0->2), (*Sinemys lens* + *Sinemys gamera*) (0->2); DELTRAN: *Dracochelys bicuspis* (0->1); ACCTRAN: (*Ordosemys* + *Dracochelys*) (0->1).

Character 211 (modified from Cadena & Parham (2015)). Rib free peripherals: 0 = absent; 1 = present.

Previous definition (Cadena & Parham (2015): character 133): Rib free peripherals: 0 = absent; 1 = present, only anterior and posterior to ribs; 2 = present, between sixth and seventh ribs; 3 = present, between seventh and eighth ribs. Reworded from Parham & Pyenson (2010: ch 29).

Remarks: I coded the presence vs. absence of rib free peripherals as a separate character from variation regarding their position to capture phylogenetic information contained in the shared presence of rib free peripherals.

Character optimisation: Unambiguous: *Puppigerus*+++ (0->1), Thalassochelydia (0->1).

Character 212 (modified from Cadena & Parham (2015)). Position of rib free peripherals: 0 = only present anterior and posterior to ribs; 1 = present between sixth and seventh ribs. This character is scored as inapplicable for taxa that lack rib free peripherals (ch. 211.0).

Previous definition (Cadena & Parham (2015): character 133): Rib free peripherals: 0 = absent; 1 = present, only anterior and posterior to ribs; 2 = present, between sixth and seventh ribs; 3 = present, between seventh and eighth ribs. Reworded from Parham & Pyenson (2010: ch 29).

Remarks: See character 2011. The state "present between seventh and eighth ribs" was deleted, because no taxon was scored for this condition in the matrix of Cadena & Parham (2015).

Character optimisation: DELTRAN: (*Eretmochelys* ++ *Lepidochelys*) (0->1), *Natator depressus* (0->1); ACCTRAN: crown-group Cheloniidae (0->1), *Chelonia mydas* (1->0).

Character 213 (Cadena & Parham (2015): character 134). Costals, alternative short and long ends in the lateral part of costals: 0 = absent; 1 = present.

Character optimisation: DELTRAN: *Testudo* (0->1), *Gopherus polyphemus* (0->1); ACCTRAN: Testudinidae (0->1), *Chelonoidis* sp. (1->0).

Character 214 (Cadena & Parham (2015): character 135). Costals, costal 9: 0 = present; 1 = absent.

Character optimisation: Unambiguous: (*Protostega* + *Archelon*) (1->0), *Kayentachelys aprix* (1->0).

Character 215 (Cadena & Parham (2015): character 136). Costals, shape of Costal 3: 0 = tapering towards the lateral side of the shell or with parallel anterior and posterior borders; 1 = broadens towards the lateral side of the shell.

Character optimisation: Ch215: DELTRAN: *Dracochelys bicuspis* (0->1); ACCTRAN: (*Ordosemys* + *Dracochelys*) (0->1).

Character 216 (modified from Cadena & Parham (2015)). Suprapygals: 0 = present; 1 = absent.

Previous definition (Cadena & Parham (2015): character 137): Suprapygals, number of suprapygals: 0 = one; 1 = two; 2 = more than two; 3 = absent. Hirayama *et al.* (2000) and Sterli & de la Fuente (2013: ch 137) (Suprapygal A). Ordered.

Remarks: I coded the presence vs. absence of suprapygals as a separate character from variation regarding their number to capture phylogenetic information contained in the shared presence suprapygals.

Character optimisation: Unambiguous: Trionychidae (0->1).

Character 217 (modified from Cadena & Parham (2015)). Suprapygals, number of suprapygals: 0 = one; 1 = two; 2 = more than two.

Previous definition (Cadena & Parham (2015): character 137): Suprapygals, number of suprapygals: 0 = one; 1 = two; 2 = more than two; 3 = absent. Hirayama *et al.* (2000) and Sterli & de la Fuente (2013: ch 137) (Suprapygal A). Ordered.

Remarks: See character 2016.

Character optimisation: Unambiguous: *Chelydra serpentina* (0->2), *Solnhofia parsoni* (1->2), *Pleurosternon bullockii* (1->0), *Kayentachelys aprix* (1->0); DELTRAN: (*Protostega* + *Archelon*) (1->0), Chelydroidea (1->0), Emydidae (1->0), *Carettochelys insculpta* (1->0), Pleurodira (1->0); ACCTRAN: Testudines (1->0), Durocryptodira (0->1), Dermochelyoidea (1->0), Chelydroidea (1->0), Emydidae (1->0).

Character 218 (Cadena & Parham (2015): character 138). Suprapygals, size between suprapygal 1 and 2: 0 = suprapygal 1 smaller than suprapygal 2; 1 = suprapygal 1 larger.

Reworded from KL (ch 88). Turtles with only one suprapygal or suprapygals absent are coding as inapplicable.

Character optimisation: Unambiguous: *Caretta caretta* (1->0), *Kallokibotion bajazidi* (0->1); DELTRAN: total-group Chelonioidea (0->1); ACCTRAN: Americhelydia (0->1).

Character 219 (modified from Cadena & Parham (2015)). Cervical scutes: 0 = present; 1 = cervical scutes absent.

Previous definition (Cadena & Parham (2015): character 139): Cervical scute: 0 = more than one cervical scute present; 1 = one cervical scute present; 2 = cervical scutes absent, carapacial scutes otherwise present. Joyce (2007: ch 70) & Sterli & de la Fuente (2013: ch 138) (Cervical A).

Remarks: I consider the number of cervicals and the presence vs. absence of cervicals as separate characters because they convey independent phylogenetic information. Additionally, I do not agree with Joyce (2007) who constructed this character with a conditional phrase on other carpacial scutes (Joyce 2007: ch 70 state 1: "cervicals absent, carapacial scutes otherwise present"), because there is no evidence for the biological dependence between the presence of carapacial and cervical scutes.

Character optimisation: Unambiguous: *Pleurosternon bullockii* (0->1); DELTRAN: (*Protostega* + *Archelon*) (0->1), *Dermochelys coriacea* (0->1), *Allopleuron hofmanni* (0->1), Trionychia (0->1), *Elseya dentata* (0->1), *Araripemys barretoi* (0->1), Pelomedusoides (0->1), *Dracochelys bicuspis* (0->1), *Sinemys lens* (0->1); ACCTRAN: Sinemydidae/Macrobaenidae+++ (0->1), Durocryptodira (1->0), crown-group Chelonioidea (0->1), (*Ocepechelon* ++ *Santanachelys*) (1->0), *Puppigerus*+++ (1->0), crown-group Chelidae (1->0), *Elseya dentata* (0->1), Angolachelonia (1->0), (*Judithemys* ++ *Kirgizemys*) (1->0).

Character 220 (modified from Cadena & Parham (2015)). Number of cervical scutes: 0 = more than one cervical scute present; 1 = one cervical scute present. This character is scored as inapplicable when cervical scutes are absent (ch. 219.1)

Previous definition (Cadena & Parham (2015): character 139): Cervical scute: 0 = more than one cervical scute present; 1 = one cervical scute present; 2 = cervical scutes absent, carapacial scutes otherwise present. Joyce (2007: ch 70) & Sterli & de la Fuente (2013: ch 138) (Cervical A).

Remarks: See character 219.

Character optimisation: DELTRAN: *Plesiochelys etalloni* (1->0); ACCTRAN: (*Portlandemys* ++ *Plesiochelys*) (1->0).

Character 221 (Cadena & Parham (2015): character 140). Pygal, posterior notch: 0 = present; 1 = absent.

Character optimisation: Unambiguous: *Eretmochelys imbricata* (1->0*), Natator depressus* (1->0), *Allopleuron hofmanni* (1->0), Emysternia (1->0), *Chelonoidis* sp. (1->0), *Chelus fimbriatus* (1->0), *Meiolania planiceps* (1->0); DELTRAN: (*Eileanchelys* + *Kayentachelys*)+++ (0->1), *Santanachelys gaffneyi* (1->0), crown-group Chelydridae (1->0), *Plesiochelys etalloni* (1->0), *Dracochelys bicuspis* (1->0); ACCTRAN: *Australochelys*+++ (0->1), (*Ocepechelon* ++ *Santanachelys*) (1->0), total-group Chelydridae (1->0), Thalassochelydia (1->0), (*Ordosemys* + *Dracochelys*) (1->0).

Character 222 (modified from Cadena & Parham (2015)). Supramarginals: 0 = present; 1 = absent.

Previous definition (Cadena & Parham (2015): character 141): Supramarginals: 0 = complete row present, fully separating marginals from pleurals; 1 = partial row present, incompletely

separating marginals from pleurals; 2 = absent. Joyce (2007: ch 71) & Sterli & de la Fuente (2013: ch 139) (Supramarginal A).

Remarks: I code the presence vs. absence of supramarginals as a separate character from additional variation observed for supramarginals, because the shared presence can contain phylogenetic information.

Character optimisation: Unambiguous: *Macrochelys temminckii* (1->0); DELTRAN: (*Eileanchelys* + *Kayentachelys*)+++ (0->1); ACCTRAN: *Australochelys*+++ (0->1).

Character 223 (modified from Cadena & Parham (2015)). Supramarginals, separating marginal and pleurals: 0 = complete row present, fully separating marginals from pleurals; 1 = partial row present, incompletely separating marginals from pleurals. This character is scored as inapplicable for turtles in which supramarginals are absent.

Previous definition (Cadena & Parham (2015): character 141): Supramarginals: 0 = complete row present, fully separating marginals from pleurals; 1 = partial row present, incompletely separating marginals from pleurals; 2 = absent. Joyce (2007: ch 71) & Sterli & de la Fuente (2013: ch 139) (Supramarginal A).

Remarks: See character 222.

Character optimisation: -.

Character 224 (Cadena & Parham (2015): character 142). Vertebrals, shape of the verterbrals: 0 = vertebrals 2 to 4 signicantly broader than pleurals; 1 = vertebrals 2 to 4 as narrow as, or narrower than, pleurals.

Character optimisation: Unambiguous: Xinjiangchelyidae+++ (0->1), Thalassochelydia (1->0); DELTRAN: *Santanachelys gaffneyi* (1->0); ACCTRAN: Dermochelyoidea (1->0).

Character 225 (Cadena & Parham (2015): character 143). Vertebrals, position of vertebral 3-4 sulcus in taxa with five vertebrals: 0 = sulcus positioned on neural 6; 1 = sulcus positioned on neural 5.

Character optimisation: Unambiguous: *Annemys levensis* (1->0); DELTRAN: Paracryptodira+++ (0->1), *Santanachelys gaffneyi* (1->0); ACCTRAN: *Meiolania*+++ (0->1), (*Bouliachelys* ++ *Santanachelys*) (1->0).

Character 226 (Cadena & Parham (2015): character 144). Vertebrals, vertebral 3-4 sulcus with a wide posteriorly oriented medial embayment: 0 = absent; 1 = present.

Character optimisation: DELTRAN: *Annemys levensis* (0->1), *Annemys latiens* (0->1); ACCTRAN: Xinjiangchelyidae (0->1), (*Annemys* sp. ++ *Xinjiangchelys*) (1->0).

Character 227 (Cadena & Parham (2015): character 145). Vertebrals, verebral 1: 0 = vertebral 1 does not enter anterior margin of carapace; 1 = enters anterior margin.

Character optimisation: Unambiguous: *Araripemys barretoi* (0->1); DELTRAN: *Dracochelys bicuspis* (0->1), *Sinemys lens* (0->1); ACCTRAN: Sinemydidae/Macrobaenidae (0->1), (*Judithemys* ++ *Kirgizemys*) (1->0).

Character 228 (Cadena & Parham (2015): character 146). Marginals, marginal scutes overlap onto costals: 0 = absent, marginals restricted to peripherals; 1 = present.

Character optimisation: Unambiguous: *Meiolania*+++ (0->1), Sinemydidae/Macrobaenidae+++ (1->0).

Character 229 (Cadena & Parham (2015): character 147). Pleurals, at least one pair of additional pleural scutes located laterally of vertebral scute 1, with anterior contact with cervical scute: 0 = absent; 1 = present.

Character optimisation: Unambiguous: (*Caretta* ++ *Lepidochelys*) (0->1).

Character 230 (Cadena & Parham (2015): character 148). Plastron, connection between carapace and plastron: 0 = osseous; 1 = ligamentous.

Character optimisation: Unambiguous: Kinosternoidea (1->0), *Chrysemys picta* (1->0), Testuguria (1->0), *Chelonoidis* sp. (0->1); DELTRAN: (*Eileanchelys* + *Kayentachelys*)+++ (0->1), crown-group Chelidae (1->0), Pelomedusoides (1->0), *Plesiochelys etalloni* (1->0), *Leyvachelys cipadi* (1->0), Pleurosternidae (1->0); ACCTRAN: *Australochelys*+++ (0->1), Angolachelonia+++ (1->0), Cryptodira (0->1), *Araripemys barretoi* (0->1), *Solnhofia parsoni* (0->1), Paracryptodira (1->0).

Character 231 (Cadena & Parham (2015): character 149). Plastron, central plastral fontanelle: 0 = absent; 1 = present.

Character optimisation: Unambiguous: total-group Chelonioidea (0->1), crown-group Chelydridae (0->1), Trionychidae (0->1), *Araripemys barretoi* (0->1), *Meiolania planiceps* (0->1); DELTRAN: Thalassochelydia (0->1), *Dracochelys bicuspis* (0->1); ACCTRAN: Angolachelonia (0->1), (*Ordosemys* + *Dracochelys*) (0->1).

Character 232 (Cadena & Parham (2015): character 150). Plastron, posterior plastral fontanelle, posterior plastral fontanelle between the xiphiplastra and/or the hypoplastra: 0 = absent in adult stage; 1 = retained in adult stage.

Character optimisation: Unambiguous: Trionychidae (0->1), *Araripemys barretoi* (0->1); DELTRAN: crown-group Chelonioidea (0->1), *Santanachelys gaffneyi* (1->0); ACCTRAN: total-group Chelonioidea (0->1), (*Bouliachelys* ++ *Santanachelys*) (1->0).

Character 233 (Cadena & Parham (2015): character 151). Plastron, plastral kinesis: 0 = absent, scutes sulci and bony sutures do not overlap; 1 = present, scutes sulci coincide with epiplastral-hyoplastral contact.

Character optimisation: Unambiguous: Kinosternidae (0->1), *Emys orbicularis* (0->1).

Character 234 (Cadena & Parham (2015): character 152). Plastron, plastral kinesis: 0 = between hyoplastron and hypoplastron; 1 = between hyoplastron and epiplastron-entoplastron.

Character optimisation: DELTRAN: Kinosternidae (0->1); ACCTRAN: Americhelydia (0->1).

Character 235 (modified from Cadena & Parham (2015)). Plastron, hyo-hypoplastra contact: 0 = contact between hyo-hyoplastra absent or reduced; 1 = extensive contact between hyo-hyoplastra (even for those taxa with plastral kinesis).

Previous definition (Cadena & Parham (2015): character 153): Plastron, hyo-hypoplastra contact and shape: 0 = deep U or V-shaped axillar and inguinal notches, contact between hyo-hyoplastra absent or reduced due to the presence of mesoplastra or a central fontanelle; 1 = deep axillar and inguinal notches, reduced contact between both elements due to the existence of central and lateral fontanelles; 2 = deep axillar and inguinal notches, extensive contact between hyo-hyoplastra (even for those taxa with plastral kinesis); 3 = a very narrow to absent contact between each other, star-shaped with extremely serrate medial edges, very shallow axillar and inguinal notches, and long lateral edges; 4 = extreme loss of ossification of hyo-hypoplastra, lack of contact between each other. Combined from Hirayama (1998), Kear & Lee (2006), and Bardet *et al.* (2013) (ch 96) and Parham & Pyenson (2010: ch 28).

Remarks: Character 153 of Cadena & Parham (2015) was broken into several characters because indipendent variation regarding different parts oft he plastron was coded into a single compound character. In this character, I distinguish between the contact between hyo- and hpoplastra: In the previous character definition, a reduced or absent contact was considered in four different states, so that the shared observation of a reduced contact is not captured as phylogenetic information. I did not code the absence of a contact separately from a reduced contact, because the contact between both elements represents a qunatitative

continuum, and absence is equivalent to a contact length of zero. My second character (character 236) codes shape variation regarding the margins of the hyo- and hypoplastra. In a third character (character 237), I code the depth oft he axillar and inguinal notches. Deep notches were coded in three different states oft he previous character definition. The observations coded in my separate characters is independent, because taxa with a reduced hypoplastron-hyoplastron contact can have deep or shallow axillar and inguinal nothces.

Character optimisation: Unambiguous: total-group Chelonioidea (1->0); DELTRAN: Cryptodira (0->1), crown-group Chelidae (0->1), Sinemydidae/Macrobaenidae (0->1), Xinjiangchelyidae (0->1); ACCTRAN: Xinjiangchelyidae+++ (0->1), Angolachelonia+++ (1->0), Cryptodira (0->1), crown-group Chelidae (0->1).

Character 236 (modified from Cadena & Parham (2015)). Plastron, hyo-hypoplastra serrations: 0 = serrations on the lateral and medial margins absent or weakly developed; 1 = strong serrations along medial and lateral margins present.

Previous definition (Cadena & Parham (2015): character 153): Plastron, hyo-hypoplastra contact and shape: 0 = deep U or V-shaped axillar and inguinal notches, contact between hyo-hyoplastra absent or reduced due to the presence of mesoplastra or a central fontanelle; 1 = deep axillar and inguinal notches, reduced contact between both elements due to the existence of central and lateral fontanelles; 2 = deep axillar and inguinal notches, extensive contact between hyo-hyoplastra (even for those taxa with plastral kinesis); 3 = a very narrow to absent contact between each other, star-shaped with extremely serrate medial edges, very shallow axillar and inguinal notches, and long lateral edges; 4 = extreme loss of ossification of hyo-hypoplastra, lack of contact between each other. Combined from Hirayama (1998), Kear & Lee (2006), and Bardet *et al.* (2013) (ch 96) and Parham & Pyenson (2010: ch 28).

Remarks: See character 235. I scored *Allopleuron* as 1 (see for instance Hiryama 1995).

Character optimisation: Unambiguous: Protostegidae (0->1), *Allopleuron hofmanni* (0->1).

Character 237 (modified from Cadena & Parham (2015)). Axillar and inguinal notches: 0 = deep U or V-shaped axillar and inguinal notches; 1 = very shallow axillar and inguinal notches, and long lateral edges.

Previous definition (Cadena & Parham (2015): character 153): Plastron, hyo-hypoplastra contact and shape: 0 = deep U or V-shaped axillar and inguinal notches, contact between hyo-hyoplastra absent or reduced due to the presence of mesoplastra or a central fontanelle; 1 = deep axillar and inguinal notches, reduced contact between both elements due to the existence of central and lateral fontanelles; 2 = deep axillar and inguinal notches, extensive contact between hyo-hyoplastra (even for those taxa with plastral kinesis); 3 = a very narrow to absent contact between each other, star-shaped with extremely serrate medial edges, very shallow axillar and inguinal notches, and long lateral edges; 4 = extreme loss of ossification of hyo-hypoplastra, lack of contact between each other. Combined from Hirayama (1998), Kear & Lee (2006), and Bardet *et al.* (2013) (ch 96) and Parham & Pyenson (2010: ch 28).

Remarks: See. character 235.

Character optimisation: Unambiguous: Dermochelyoidea (0->1).

Character 238 (Cadena & Parham (2015): character 154). Entoplastron: 0 = present; 1 = absent.

Character optimisation: Unambiguous: Kinosterninae (0->1); DELTRAN: *Dermochelys coriacea* (0->1); ACCTRAN: Dermochelyidae (0->1).

Character 239 (Cadena & Parham (2015): character 155). Entoplastron, anterior entoplastral process: 0= present, medial contact of epiplastra absent; 1 = absent, medial contact of epiplastra present.

Character optimisation: DELTRAN: *Kallokibotion*+++ (0->1), *Eileanchelys waldmanni* (0->1); ACCTRAN: *Australochelys*+++ (0->1), *Kayentachelys aprix* (1->0).

Character 240 (Cadena & Parham (2015): character 156). Entoplastron, size of the posterior entoplastral process: 0 = posterior process long, reaching as far posteriorly as the mesoplastra; 1 = posterior process reduced in length.

Character optimisation: Unambiguous: Paracryptodira+++ (0->1), *Emys orbicularis* (1->0).

Character 241 (Cadena & Parham (2015): character 157). Entoplastron, distinct posterolateral process: 0 = present; 1 = absent.

Character optimisation: DELTRAN: (*Eileanchelys* + *Kayentachelys*)+++ (0->1); ACCTRAN: *Australochelys*+++ (0->1).

Character 242 (Cadena & Parham (2015): character 158). Entoplastron, shape of the entoplastron in ventral view: 0 = dagger-shaped; 1 = massive diamond-shaped; 2 = T-shaped, longer than wide; 3 = T-shaped, wider than long, forming broad lateral wings; 4 = strap like and V-shaped.

Character optimisation: Unambiguous: total-group Chelonioidea (1->2), (*Protostega* + *Archelon*) (2->3), crown-group Chelydridae (1->2), Trionychidae (1->4), Sinemydidae/Macrobaenidae (1->2); DELTRAN: Paracryptodira+++ (0->1), *Kallokibotion bajazidi* (0->1); ACCTRAN: *Chubutemys*+++ (0->1), *Meiolania planiceps* (1->0).

Character 243 (Cadena & Parham (2015): character 159). Entoplastron, suture with hyoplastra: 0 = tightly sutured; 1 = lightly sutured to almost absent contact between both.

Character optimisation: Unambiguous: Americhelydia (0->1), total-group Dermatemydidae (1->0), Trionychidae (0->1), *Araripemys barretoi* (0->1), *Solnhofia parsoni* (0->1), Sinemydidae/Macrobaenidae (0->1)

Character 244 (Cadena & Parham (2015): character 160). Epiplastra, shape and contact of epiplastra: 0 = epiplastra squarish in shape, lack a contact between each other due to the narrow participation of the entoplastron in the anterior plastral lobe edge; 1 = epiplastra elongate in shape, with medial contact located anterior to the entoplastron; 2 = epiplastra squarish in shape lack of medial contact due to the extensive anterior and lateral projections of the entoplastron.

Character optimisation: Unambiguous: (*Protostega* + *Archelon*) (1->2), (*Sinemys lens* + *Sinemys gamera*) (1->0); DELTRAN: *Kallokibotion*+++ (0->1); ACCTRAN: *Chubutemys*+++ (0->1).

Character 245 (Cadena & Parham (2015): character 161). Epiplastra, very thick anterior lip in dorsal view: 0 = present; 1 = absent.

Character optimisation: Unambiguous: Testuguria (1->0), *Chelonoidis* sp. (0->1).

Character 246 (Cadena & Parham (2015): character 162). Hyoplastra, contacts of axillary buttresses: 0 = absent to slightly contacting peripherals only; 1 = peripherals and costal 1.

Character optimisation: Unambiguous: total-group Dermatemydidae (0->1), *Chrysemys picta* (0->1), Testuguria (0->1), *Chelonoidis* sp. (1->0), Pleurodira (0->1); DELTRAN: (*Jurassichelon* ++ *Plesiochelys*) (0->1), *Glyptops plicatulus* (0->1); ACCTRAN: (*Portlandemys* ++ *Plesiochelys*) (0->1), Paracryptodira (0->1).

Character 247 (modified from Cadena & Parham (2015)). Hyoplastra, axillary buttresses: 0 = present; 1 = ossified axillary buttresses absent.

Previous definition (Cadena & Parham (2015): character 163): Hyoplastra, termination of axillary buttresses: 0 = terminates on peripheral 1 or 2; 1 = terminates on peripheral 3; 2 = terminates on peripheral 4 or 5 level; 3 = ossified axillary buttresses absent. Reworded from Hutchinson (1991) and Sterli & de la Fuente (2013: ch 159) (Hyoplastron B).

Remarks: I herein code the presence vs. absence of axillary buttresses as a separate character to separate phylogenetical information about the shared presence of thus structure from variation regarding the extend of the process.

Character optimisation: Unambiguous: *Platysternon megacephalum* (0->1), *Chelonoidis* sp. (0->1), Trionychidae (0->1); DELTRAN: total-group Chelonioidea (0->1), *Santanachelys gaffneyi* (1->0), crown-group Chelydridae (0->1); ACCTRAN: Americhelydia (0->1), (*Bouliachelys* ++ *Santanachelys*) (1->0), Kinosternoidea (1->0).

Character 248 (modified from Cadena & Parham (2015)). Hyoplastra, termination of axillary buttresses: 0 = terminates on peripheral 1 or 2; 1 = terminates on peripheral 3; 2 = terminates on peripheral 4 or 5 level. This character is scored as inapplicable for turtles without axillary buttresses (ch. 247.1).

Previous definition (Cadena & Parham (2015): character 163): Hyoplastra, termination of axillary buttresses: 0 = terminates on peripheral 1 or 2; 1 = terminates on peripheral 3; 2 = terminates on peripheral 4 or 5 level; 3 = ossified axillary buttresses absent. Reworded from Hutchinson (1991) and Sterli & de la Fuente (2013: ch 159) (Hyoplastron B).

Remarks: See character 247.

Character optimisation: Unambiguous: Testudines (0->1), Kinosternidae (1->2), Testudinidae (1->0), *Elseya dentata* (1->0); DELTRAN: *Carettochelys insculpta* (1->2), Pleurosternidae (0->1), *Meiolania planiceps* (0->1); ACCTRAN: *Meiolania*+++ (0->1), Xinjiangchelyidae+++ (1->0), Trionychia (1->2).

Character 249 (modified from Cadena & Parham (2015)). Mesoplastron: 0 = present; 1 = absent.

Previous definition (Cadena & Parham (2015): character 164): Mesoplastron: 0 = two present; 1 = one present; 2 = absent. Modified from Joyce (2007: ch 85) & Sterli & de la Fuente (2013: ch 160) (Mesoplastron A) and Anquetin (2012: ch 120 and ch 121).

Remarks: I code the presence vs. absence of mesoplastra in a separate character to include phylogenetic information regarding the shared presence of mesoplastra, irrespective from their number.

Character optimisation: Unambiguous: Pelomedusoides (1->0); DELTRAN: Xinjiangchelyidae+++ (0->1), *Meiolania planiceps* (0->1); ACCTRAN: *Meiolania*+++ (0->1), Paracryptodira (1->0).

Character 250 (modified from Cadena & Parham (2015)). Number of mesoplastra: 0 = two; 1 = one. This character is scored as inapplicable when mesoplastra are absent (ch. 249.1).

Previous definition (Cadena & Parham (2015): character 164): Mesoplastron: 0 = two present; 1 = one present; 2 = absent. Modified from Joyce (2007: ch 85) & Sterli & de la Fuente (2013: ch 160) (Mesoplastron A) and Anquetin (2012: ch 120 and ch 121).

Remarks: See character 249.

Character optimisation: -.

Character 251 (Cadena & Parham (2015): character 165). Mesoplastron, medial contact of mesoplastra: 0=present, or virtually present when a central plastral fonta- nelle is present, absence of contact between hyoplastron and hypoplastron; 1 = absent, partial contact between hyoplastron and hypoplastron present.

Character optimisation: DELTRAN: Pelomedusoides (0->1), *Kallokibotion bajazidi* (0->1); ACCTRAN: *Chubutemys*+++ (0->1), Paracryptodira (1->0).

Character 252 (Cadena & Parham (2015): character 166). Hypoplastra, contacts of inguinal buttresses: 0 = absent to slightly contacting peripherals; 1 = peripheral and costal 5; 2 = peripheral, costals 5 and 6; 3 = peripherals and costal 4.

Character optimisation: Unambiguous: *Baptemys wyomingensis* (0->1), *Chrysemys picta* (0->1); DELTRAN: *Geoclemys hamiltonii* (0->1), *Gopherus polyphemus* (0->1), *Chelus fimbriatus* (0->3), *Phrynops geoffranus* (0->1), *Elseya dentata* (0->1), Pelomedusoides (0->1), *Plesiochelys etalloni* (0->1), *Leyvachelys cipadi* (0->1), Pleurosternidae (0->1); ACCTRAN: Angolachelonia+++ (0->1), Cryptodira (1->0), Testuguria (0->1), (*Testudo* + *Chelonoidis*) (1->0), *Chelus fimbriatus* (1->3), *Chelodina* (1->0), *Araripemys barretoi* (1->0), *Solnhofia parsoni* (1->0), Paracryptodira (0->1).

Character 253 (Cadena & Parham (2015): character 167). Hypoplastra, termination of inguinal buttresses: 0 = peripheral 8; 1 = peripheral 7; 2 = peripheral 6.

Character optimisation: Unambiguous: *Chrysemys picta* (1->0), *Platysternon megacephalum* (1->2), Testudinidae (1->0), *Chelonoidis* sp. (0->2), *Kallokibotion bajazidi* (0->2); DELTRAN: Cryptodira (0->1), *Dermatemys mawii* (1->0), *Chelus fimbriatus* (0->1), *Chelodina* (0->1), *Araripemys barretoi* (0->1); ACCTRAN: Testudines (0->1), total-group Dermatemydidae (1->0), *Phrynops geoffranus* (1->0), *Elseya dentata* (1->0), Pelomedusoides (1->0).

Character 254 (Cadena & Parham (2015): character 168). Xiphiplastra, distinct anal notch: 0 = absent; 1 = present.

Character optimisation: Unambiguous: *Dermatemys mawii* (0->1), Testudinoidea (0->1), *Emys orbicularis* (1->0), Pleurodira (0->1).

Character 255 (Cadena & Parham (2015): character 169). Xiphiplastra, shape of xiphiplastra: 0 = almost triangular to trapezoidal, with lateral straight to convex margin; 1 =

rectangular elongated in shape, coupled forming together with the hypoplastron a very narrow posterior plastral lobe; 2 = narrow struts, separated by the posterior fontanelle.

Character optimisation: Unambiguous: total-group Chelonioidea (0->2), *Chelydra serpentina* (0->1), *Staurotypus* (0->1); DELTRAN: (*Desmatochelys* ++ *Santanachelys*) (2->0), *Sinemys lens* (0->1); ACCTRAN: (*Ocepechelon* ++ *Santanachelys*) (2->0), (*Sinemys lens* + *Sinemys gamera*) (0->1).

Character 256 (Cadena & Parham (2015): character 170). Plastral scutes: 0 = present; 1 = absent.

Character optimisation: Unambiguous: Trionychia (0->1); DELTRAN: (*Protostega* + *Archelon*) (0->1), *Dermochelys coriacea* (0->1), *Allopleuron hofmanni* (0->1); ACCTRAN: crown-group Chelonioidea (0->1), (*Ocepechelon* ++ *Santanachelys*) (1->0), *Puppigerus*+++ (1->0).

Character 257 (Cadena & Parham (2015): character 171). Plastral scutes, midline sulcus: 0 = straight; 1 = distinctly sinuous, at least for part of its length.

Character optimisation: Unambiguous: Xinjiangchelyidae (0->1*), Xinjiangchelys wusu* (1->0).

Character 258 (Cadena & Parham (2015): character 172). Gular, number of gulars: 0 = one pair of scutes; 1 = only one scute.

Character optimisation: Unambiguous: Pleurodira (0->1), *Pleurosternon bullockii* (0->1).

Character 259 (Cadena & Parham (2015): character 173). Extragulars: 0 = present; 1 = absent.

Character optimisation: Unambiguous: *Araripemys barretoi* (0->1); DELTRAN: Durocryptodira (0->1), (*Judithemys* ++ *Kirgizemys*) (0->1); ACCTRAN: Cryptodira (0->1), Sinemydidae/Macrobaenidae (0->1).

Character 260 (Cadena & Parham (2015): character 174). Extagulars, medial contact: 0 = absent; 1 = present, contacting one another anterior to gular(s); 2 = present, contacting one another posterior to gular(s).

Character optimisation: Unambiguous: *Chelus fimbriatus* (0->2), *Chelodina* (0->1).

Character 261 (Cadena & Parham (2015): character 175). Extragulars, anterior plastral tuberosities: 0 = present; 1 = absent.

Character optimisation: DELTRAN: (*Eileanchelys* + *Kayentachelys*)+++ (0->1); ACCTRAN: *Australochelys*+++ (0->1).

Character 262 (Cadena & Parham (2015): character 176). Extragulars, restricted to epiplastra: 0 = present; 1 = absent, extragulars reach the entoplastron.

Character optimisation: Unambiguous: *Chelus fimbriatus* (0->1); DELTRAN: *Proganochelys quenstedti* (0->1); ACCTRAN: *Proganochelys quenstedti* (0->1).

Character 263 (Cadena & Parham (2015): character 177). Intergulars: 0 = absent; 1 = present.

Character optimisation: Unambiguous: Kinosterninae (0->1), *Dermatemys mawii* (0->1); DELTRAN: *Eretmochelys imbricata* (0->1), (*Chelonia* + *Natator*) (0->1); ACCTRAN: total-group Chelonioidea (0->1), (*Caretta* ++ *Lepidochelys*) (1->0).

Character 264 (Cadena & Parham (2015): character 178). Humerals, number of pairs: 0 = one pair present; 1 = two pairs present, subdivided by a plastral hinge.

Character optimisation: Unambiguous: Kinosterninae (0->1).

Character 265 (Cadena & Parham (2015): character 179). Humerals, humero-pectoral sulcus: 0 = restricted to hyoplastra; 1 = crossing the posterior portion of ento- plastron.

Character optimisation: Unambiguous: *Emys orbicularis* (0->1), *Geoclemys hamiltonii* (0->1), *Chelus fimbriatus* (0->1), *Podocnemis* (0->1); DELTRAN: *Chelydra serpentina* (0->1), *Baptemys wyomingensis* (0->1); ACCTRAN: Americhelydia (0->1), *Dermatemys mawii* (1->0).

Character 266 (Cadena & Parham (2015): character 180). Pectorals: 0 = present; 1 = absent.

Character optimisation: Unambiguous: Kinosternoidea (0->1).

Character 267 (Cadena & Parham (2015): character 181). Pectorals, antero-posteriorly developed: 0 = present; 1 = absent, very short antero-posterior development.

Character optimisation: Unambiguous: *Chrysemys picta* (0->1), Testuguria (0->1), *Chelonoidis* sp. (1->0).

Character 268 (modified from Cadena & Parham (2015)). Abdominals: 0 = present; 1 = absent.

Previous definition (Cadena & Parham (2015): character 182): Abdominals: 0 = present, in medial contact with one another; 1 = present, medial contact absent; 2 = absent. Joyce (2007: ch 98) & Sterli & de la Fuente (2013: ch 177) (Abdominal A).

Remarks: I code the presence vs. absence of abdominals in a separate character, because the shared presence of abdominals can be phylogenetically informative.

Character optimisation: Unambiguous: *Toxochelys latiremis* (0->1), Kinosternidae (0->1); DELTRAN: *Plesiochelys etalloni* (0->1); ACCTRAN: (*Plesiochelys etalloni* + *Plesiochelys planiceps*) (0->1).

Character 269 (modified from Cadena & Parham (2015)). Abdominals, medial contact to one another: 0 = present; 1 = absent. This character is scored as inapplicable for turtles that lack abdominals.

Previous definition (Cadena & Parham (2015): character 182): Abdominals: 0 = present, in medial contact with one another; 1 = present, medial contact absent; 2 = absent. Joyce (2007: ch 98) & Sterli & de la Fuente (2013: ch 177) (Abdominal A).

Remarks: See character 268.

Character optimisation: Unambiguous: total-group Chelydridae (0->1), *Araripemys barretoi* (0->1).

Character 270 (Cadena & Parham (2015): character 183). Anals: 0 = only cover parts of the xiphiplastra; 1 = overlap anteromedially onto the hypoplastra.

Character optimisation: Unambiguous: *Toxochelys latiremis* (0->1), crown-group Chelydridae (0->1), Xinjiangchelyidae (0->1).

Character 271 (modified from Cadena & Parham (2015)). Inframarginals: 0 = present; 1 = absent.

Previous definition (Cadena & Parham (2015): character 184): Inframarginals: 0 = more than two pair present, plastral scales do not contact marginals; 1 = two pair present (axillaries and inguinals), limited contact between plastral scales and marginals present; 2 = absent, unrestricted contact between plastral scales and marginals present. Reworded from Hutchison (1991) and Sterli & de la Fuente (2013: ch 159) (Hyoplastron B).

Remarks: I code the presence vs. absence of inframarginals in a separate character to include phylogenetic information regarding the shared presence of inframarginals, regardless of their number.

Character optimisation: Unambiguous: Sinemydidae/Macrobaenidae+++ (0->1), *Toxochelys latiremis* (0->1*), Judithemys sukhanovi* (1->0); DELTRAN: Durocryptodira (1->0); ACCTRAN: Cryptodira (1->0).

Character 272 (modified from Cadena & Parham (2015)). Number of inframarginals: 0 = more than two pair present, plastral scales do not contact marginals; 1 = two pair present (axillaries and inguinals), limited contact between plastral scales and marginals present. This character is scored as inapplicable when inframarginals are absent (ch. 271.1).

Previous definition (Cadena & Parham (2015): character 184): Inframarginals: 0 = more than two pair present, plastral scales do not contact marginals; 1 = two pair present (axillaries and inguinals), limited contact between plastral scales and marginals present; 2 = absent, unrestricted contact between plastral scales and marginals present. Reworded from Hutchison (1991) and Sterli & de la Fuente (2013: ch 159) (Hyoplastron B).

Remarks: See character 271.

Character optimisation: Unambiguous: Kinosternidae (0->1), *Chelonoidis* sp. (1->0); DELTRAN: *Chrysemys picta* (0->1), Testuguria (0->1); ACCTRAN: Testudinoidea (0->1), *Platysternon megacephalum* (1->0).

Character 273 (Cadena & Parham (2015): character 185). Cervical ribs: 0 = large cervical ribs present; 1 = cervical ribs reduced or absent.

Character optimisation: Unambiguous: Angolachelonia+++ (0->1).

Character 274 (Cadena & Parham (2015): character 186). Cervicals, position of the transverse processes: 0 = middle of the centrum; 1 = anterior end of the centrum.

Character optimisation: Unambiguous: (*Desmatochelys lowii* + *Desmatochelys padillai*) (1->0), *Archelon ischyros* (1->0), Pleurodira (1->0); DELTRAN: Sinemydidae/Macrobaenidae+++ (0->1), *Meiolania planiceps* (0->1), *Proganochelys quenstedti* (0->1); ACCTRAN: Sinemydidae/Macrobaenidae+++ (0->1), *Meiolania planiceps* (0->1), *Proganochelys quenstedti* (0->1).

Character 275 (Cadena & Parham (2015): character 187). Cervicals, posterior cervicals with strongly developed ventral keels: 0 = absent or slightly developed in all vertebrae; 1 = present, more developed on posterior vertebrae.

Character optimisation: Unambiguous: Durocryptodira (0->1), *Platysternon megacephalum* (1->0), *Chelonoidis* sp. (1->0), *Chelus fimbriatus* (0->1); DELTRAN: *Leyvachelys cipadi* (0->1), (*Ordosemys* ++ *Kirgizemys*) (0->1); ACCTRAN: Sandownidae (0->1), Sinemydidae/Macrobaenidae (0->1).

Character 276 (Cadena & Parham (2015): character 188). Cervicals, cervical 8 centrum significantly shorter than cervical 7: 0 = absent; 1 = present.

Character optimisation: Unambiguous: Cryptodira (0->1), *Chelus fimbriatus* (0->1), (*Ordosemys* ++ *Kirgizemys*) (0->1).

Character 277 (Cadena & Parham (2015): character 189). Cervicals, triangular diapophyses: 0 = absent; 1 = present.

Character optimisation: Unambiguous: Pleurodira (0->1), Chubutemys copelloi (0->1); DELTRAN: *Glyptops plicatulus* (0->1); ACCTRAN: Paracryptodira (0->1).

Character 278 (Cadena & Parham (2015): character 190). Cervicals, central articulations of cervical vertebrae: 0 = articulations not formed, cervical vertebrae am- phicoelous or platycoelous; 1 = articulations formed, cervical vertebrae procoelous or opisthocoelous.

Character optimisation: Unambiguous: Sinemydidae/Macrobaenidae+++ (0->1), Thalassochelydia (1->0), *Meiolania planiceps* (0->1).

Character 279 (Cadena & Parham (2015): character 191). Cervicals, articulation between cervical 8 and dorsal vertebrae 1: 0 = 8 (dorsal 1; 1 = 8) dorsal 1; 2 = vertebrae articulate along zygapophyses only.

Character optimisation: Unambiguous: Trionychidae (1->2).

Character 280 (Cadena & Parham (2015): character 192). Cervicals, biconvex cervical vertebrae in the middle of the neck: 0 = absent; 1 = present.

Character optimisation: Unambiguous: *Dermatemys mawii* (1->0), Trionychia (1->0); DELTRAN: *Dracochelys bicuspis* (1->0); ACCTRAN: (*Ordosemys* + *Dracochelys*) (1->0).

Character 281 (Cadena & Parham (2015): character 193). Cervicals, biconvex cervical vertebra in the middle of the neck: 0 = cervical 2; 1 = cervical 3; 2 = cervical 4; 3 = cervical 5.

Character optimisation: Unambiguous: Pleurodira (2->0), crown-group Chelidae (0->3); DELTRAN: Kinosternidae (2->1); ACCTRAN: Kinosternoidea (2->1).

Character 282 (Cadena & Parham (2015): character 194). Cervicals, biconcave cervical vertebrae: 0 = absent; 1 = present.

Character optimisation: Unambiguous: Testudinoidea (0->1), crown-group Chelidae (0->1).

Character 283 (Cadena & Parham (2015): character 195). Cervicals, double articulation between cervical 5 and 6: 0 = absent; 1 = present.

Character optimisation: Unambiguous: *Chrysemys picta* (0->1).

Character 284 (Cadena & Parham (2015): character 196). Cervicals, double articulation between cervical 6 and 7: 0 = absent; 1 = present.

Character optimisation: Unambiguous: Cryptodira (0->1); DELTRAN: crown-group Chelonioidea (1->0); ACCTRAN: total-group Chelonioidea (1->0).

Character 285 (Cadena & Parham (2015): character 197). Cervicals, central articulation between cervical 6 and 7: 0 = cervical 6 concave (cervical 7 convex; 1 = platycoelous, cervical 6 II cervical 7.

Character optimisation: DELTRAN: *Dermochelys coriacea* (0->1), *Argillochelys*+++ (0->1); ACCTRAN: total-group Chelonioidea (0->1), Protostegidae (1->0).

Character 286 (Cadena & Parham (2015): character 198). Cervicals, double articulation between cervical 7 and 8: 0 = absent; 1 = present.

Character optimisation: Unambiguous: Cryptodira (0->1), *Toxochelys latiremis* (1->0); DELTRAN: (*Desmatochelys* ++ *Santanachelys*) (1->0); ACCTRAN: Protostegidae (1->0).

Character 287 (Cadena & Parham (2015): character 199). Cervicals, height versus length of centra and neural arch: 0 = total height of centra and neural arch longer than the anteroposterior length of the cervical centra; 1 = total height of centra and neural arch much shorter than the anteroposterior length of the cervical centra.

Character optimisation: DELTRAN: Xinjiangchelyidae+++ (0->1), *Dermochelys coriacea* (1->0), *Jurassichelon oleronensis* (1->0); ACCTRAN: Paracryptodira+++ (0->1), Dermochelyidae (1->0), Thalassochelydia (1->0).

Character 288 (Cadena & Parham (2015): character 200). Cervicals, modification of neural arch on cervical 8: 0 = neural arch without modificiation of postzygapophyses; 1 = neural arch with postzygapophyses pointing anteroventrally.

Character optimisation: Unambiguous: Cryptodira (0->1); DELTRAN: crown-group Chelonioidea (1->0), *Kirgizemys hoburensis* (0->1); ACCTRAN: total-group Chelonioidea (1->0), (*Judithemys* ++ *Kirgizemys*) (0->1).

Character 289 (Cadena & Parham (2015): character 201). Cervicals, postzygapophyses united in midline: 0 = absent; 1 = present.

Character optimisation: Unambiguous: total-group Chelidae (0->1), *Phrynops geoffranus* (1->0).

Character 290 (Cadena & Parham (2015): character 202). Cervicals, ventral process on cervical 8: 0 = absent; 1 = present, well developed (as tall or taller than the height of the centrum).

Character optimisation: Unambiguous: *Chelonoidis* sp. (1->0); DELTRAN: Chelydroidea (0->1), Emydidae (0->1), Testuguria (0->1), *Judithemys sukhanovi* (0->1); ACCTRAN: Durocryptodira (0->1), total-group Chelonioidea (1->0), *Platysternon megacephalum* (1->0), (*Judithemys* ++ *Kirgizemys*) (0->1).

Character 291 (Cadena & Parham (2015): character 203). Cervicals, shape of central articulation of cervicals 7 and 8: 0 = as high as wide; 1 = much wider than high.

Character optimisation: Unambiguous: total-group Chelonioidea (0->1), Protostegidae (1->0).

Character 292 (Cadena & Parham (2015): character 204). Ribs, length of first dorsal rib: 0 = long, extends full length of first costal and may even contact peripherals distally; 1 = intermediate, in contact with well-developed anterior bridge buttresses; 2 = intermediate to short, extends less than halfway across first costal.

Character optimisation: Unambiguous: (*Judithemys* ++ *Kirgizemys*) (0->2); DELTRAN: Testudines (0->2), *Santanachelys gaffneyi* (2->0), *Jurassichelon oleronensis* (0->1), *Leyvachelys cipadi* (0->2); ACCTRAN: *Angolachelonia*+++ (0->2), (*Bouliachelys* ++ *Santanachelys*) (2->0), Thalassochelydia (2->0), *Jurassichelon oleronensis* (0->1).

Character 293 (Cadena & Parham (2015): character 205). Ribs, contact of dorsal ribs 9 and 10 with costals: 0 = present; 1 = absent.

Character optimisation: Unambiguous: Kinosternidae (0->1).

Character 294 (Cadena & Parham (2015): character 206). Dorsal rib 10: 0 = long, spanning full length of costals and contacting peripherals distally; 1 = short, not span- ning father distally than pelvis.

Character optimisation: DELTRAN: Sinemydidae/Macrobaenidae+++ (0->1), *Glyptops plicatulus* (0->1); ACCTRAN: *Chubutemys*+++ (0->1), Xinjiangchelyidae (1->0).

Character 295 (Cadena & Parham (2015): character 207). Dorsals, anterior articulation of the first dorsal centrum: 0 = faces at most slightly anteroventrally; 1 = faces strongly anteroventrally.

Character optimisation: Unambiguous: Cryptodira (0->1), total-group Chelonioidea (1->0); DELTRAN: crown-group Cheloniidae (0->1); ACCTRAN: *Puppigerus*+++ (0->1).

Character 296 (Cadena & Parham (2015): character 208). Caudals, tail club: 0 = present; 1 = absent.

Character optimisation: DELTRAN: Paracryptodira+++ (0->1), *Kayentachelys aprix* (0->1); ACCTRAN: *Australochelys*+++ (0->1), *Meiolania planiceps* (1->0).

Character 297 (Cadena & Parham (2015): character 210). Caudals, anterior caudal centra: 0 = amphicoelous; 1 = procoelous or platycoelous; 2 = opisthocoelous.

Character optimisation: Unambiguous: *Macrochelys temminckii* (1->2); DELTRAN: Sinemydidae/Macrobaenidae+++ (0->1), *Meiolania planiceps* (0->2); ACCTRAN: *Chubutemys*+++ (0->1), *Meiolania planiceps* (1->2).

Character 298 (Cadena & Parham (2015): character 211). Caudals, posterior caudal centra: 0 = amphicoelous; 1 = procoelous or platycoelous: 2 = opisthocoelous.

Character optimisation: Unambiguous: *Platysternon megacephalum* (1->2), *Chelonoidis* sp. (1->2); DELTRAN: *Meiolania*+++ (0->2), Testudines (2->1), crown-group Chelydridae (1->2); ACCTRAN: *Chubutemys*+++ (0->2), Angolachelonia+++ (2->1), total-group Chelydridae (1->2).

Character 299 (Cadena & Parham (2015): character 212). Caudals, chevrons: 0 = present on nearly all caudal vertebrae: 1 = absent, or only poorly developed, along the posterior caudal vertebrae.

Character optimisation: Unambiguous: *Toxochelys latiremis* (1->0), *Platysternon megacephalum* (1->0), *Chelonoidis* sp. (1->0); DELTRAN: Sinemydidae/Macrobaenidae+++ (0->1), crown-group Chelydridae (1->0); ACCTRAN: Paracryptodira+++ (0->1), total-group Chelydridae (1->0).

Character 300 (Cadena & Parham (2015): character 213). Caudals, tail ring: 0 = absent; 1 = present.

Character optimisation: Unambiguous: *Meiolania planiceps* (0->1).

Character 301 (Cadena & Parham (2015): character 214). Scapula, anterodorsal ridge of acromion: 0 = present; 1 = absent.

Character optimisation: DELTRAN: (*Eileanchelys* + *Kayentachelys*)+++ (0->1); ACCTRAN: *Australochelys*+++ (0->1).

Character 302 (Cadena & Parham (2015): character 215). Scapula, ventral ridge of acromion: 0 = present; 1 = absent developed proximally near glenoid.

Character optimisation: Unambiguous: *Chubutemys*+++ (0->1).

Character 303 (Cadena & Parham (2015): character 216). Scapula, horizontal ridge of acromion: 0 = well-developed, coracoid foramen present; 1 = reduced, only developed along distal portion of acromion.

Character optimisation: DELTRAN: (*Eileanchelys* + *Kayentachelys*)+++ (0->1); ACCTRAN: *Australochelys*+++ (0->1).

Character 304 (Cadena & Parham (2015): character 217). Scapula, glenoid neck on scapula: 0 = absent; 1 = present.

Character optimisation: DELTRAN: crown-group Chelidae (0->1), *Podocnemis* (0->1), *Glyptops plicatulus* (0->1); ACCTRAN: Pleurodira (0->1), *Pelomedusa subrufa* (1->0), Paracryptodira (0->1).

Character 305 (Cadena & Parham (2015): character 218). Scapula, lamina between the dorsal process of the scapula and the acromion: 0 = well developed; 1 = reduced; 2 = absent.

Character optimisation: Unambiguous: Paracryptodira+++ (0->2), *Kallokibotion bajazidi* (0->1).

Character 306 (Cadena & Parham (2015): character 219). Scapula, internal angle between acromion process and scapular process ≥110°: 0 = absent; 1 = present.

Character optimisation: Unambiguous: crown-group Chelonioidea (0->1), (*Caretta* ++ *Lepidochelys*) (1->0).

Character 307 (Cadena & Parham (2015): character 220). Coracoid, coracoid vs humerus length: 0 = shorter than humerus; 1 = at least as long as humerus.

Character optimisation: Unambiguous: crown-group Chelonioidea (0->1).

Character 308 (Cadena & Parham (2015): character 221). Coracoid, foramen: 0 = present; 1 = absent.

Character optimisation: DELTRAN: (*Eileanchelys* + *Kayentachelys*)+++ (0->1); ACCTRAN: *Australochelys*+++ (0->1).

Character 309 (modified from Cadena & Parham (2015)). Cleithrum: 0 = present; 1 = absent.

Previous definition (Cadena & Parham (2015): character 222): Cleithrum: 0 = present and in contact with the carapace; 1 = present, osseous contact with carapace absent; 2 = absent. Joyce (2007: ch 120) & Sterli & de la Fuente (2013: ch 214) (Cleithrum A). Ordered.

Remarks: I code the presence vs. absence of the cleithrum in a separate character from variation regarding its contacts, because the phylogenetic information of the shared presence of a cleithrum is otherwise not considered.

Character optimisation: Unambiguous: Sinemydidae/Macrobaenidae+++ (0->1).

Character 310 (modified from Cadena & Parham (2015)). Cleithrum, contact with carapace: 0 = present; 1 = osseous contact with carapace absent.

Previous definition (Cadena & Parham (2015): character 222): Cleithrum: 0 = present and in contact with the carapace; 1 = present, osseous contact with carapace absent; 2 = absent. Joyce (2007: ch 120) & Sterli & de la Fuente (2013: ch 214) (Cleithrum A). Ordered.

Remarks: See character 309.

Character optimisation: DELTRAN: (*Eileanchelys* + *Kayentachelys*)+++ (0->1); ACCTRAN: *Australochelys*+++ (0->1).

Character 311 (Cadena & Parham (2015): character 223). Pelvis, pelvis-shell attachment: 0 = pelvis-shell attachment by ligaments; 1 = pelvis attached by strong sutural contact of the ischium and pubis with the plastron, and illium with the carapace.

Character optimisation: Unambiguous: Pleurodira (0->1).

Character 312 (Cadena & Parham (2015): character 224). Pelvis, thyroid fenestra: 0 = coalescent; 1 = two separated fenestra completely or partially separated.

Character optimisation: Unambiguous: *Chelonoidis* sp. (1->0); DELTRAN: Testudines (1->0), *Dermochelys coriacea* (0->1), Kinosterninae (0->1), total-group Dermatemydidae (0->1), Emydidae (0->1), Testuguria (0->1); ACCTRAN: Paracryptodira+++ (1->0), Dermochelyidae (0->1), Kinosternoidea (0->1), *Staurotypus* (1->0), Testudinoidea (0->1), *Platysternon megacephalum* (1->0).

Character 313 (Cadena & Parham (2015): character 225). Ilium, elongated iliac neck: 0 = absent; 1 = present.

Character optimisation: DELTRAN: (*Eileanchelys* + *Kayentachelys*)+++ (0->1); ACCTRAN: *Australochelys*+++ (0->1).

Character 314 (Cadena & Parham (2015): character 226). Ilium, iliac scar: 0 = extends from costals onto the peripherals and pygal; 1 = positioned on costals only.

Character optimisation: -.

Character 315 (Cadena & Parham (2015): character 227). Ilium, shape of the ilium articular site on the visceral surface of the carapace: 0 = narrow and pointed poste- riorly; 1 = oval.

Character optimisation: -.

Character 316 (Cadena & Parham (2015): character 228). Ilium, posterior notch in acetabulum: 0 = absent; 1 = present.

Character optimisation: DELTRAN: Kinosternidae (0->1), *Baptemys wyomingensis* (0->1); ACCTRAN: Kinosternoidea (0->1), *Dermatemys mawii* (1->0).

Character 317 (Cadena & Parham (2015): character 229). Ilium, thelial process: 0 = absent; 1 = present.

Character optimisation: Unambiguous: *Emarginachelys cretacea* (0->1), Kinosternidae (0->1); DELTRAN: *Lissemys punctata* (0->1), *Carettochelys insculpta* (0->1); ACCTRAN: Trionychia (0->1), Trionychinae (1->0).

Character 318 (Cadena & Parham (2015): character 230). Pubis, lateral process: 0 = small, poorly developed, columnar; 1 = well developed and flat.

Character optimisation: DELTRAN: crown-group Chelonioidea (0->1), Kinosternoidea (0->1), Trionychia (0->1); ACCTRAN: Cryptodira (0->1), total-group Chelydridae (1->0), Testudinoidea (1->0).

Character 319 (Cadena & Parham (2015): character 231). Pubis, epipubis process: 0 = osseus or calcified; 1 = cartilaginous or absent.

Character optimisation: Unambiguous: *Kinosternon suburum hippocrepis* (0->1); DELTRAN: Testudines (0->1), *Macrochelys temminckii* (1->0), Kinosternoidea (1->0); ACCTRAN: Paracryptodira+++ (0->1), Chelydroidea (1->0), *Chelydra serpentina* (0->1).

Character 320 (Cadena & Parham (2015): character 232). Ischium, ischial contacts with plastron: 0 = contact via a large central tubercle; 1 = contact via two separate ischial processes.

Character optimisation: DELTRAN: (*Eileanchelys* + *Kayentachelys*)+++ (0->1); ACCTRAN: *Australochelys*+++ (0->1).

Character 321 (Cadena & Parham (2015): character 233). Ischium, lateral process of ischium or metischial process: 0 = absent; 1 = present.

Character optimisation: DELTRAN: *Toxochelys latiremis* (0->1), *Macrochelys temminckii* (0->1), Testudinoidea (0->1); ACCTRAN: Durocryptodira (0->1), crown-group Chelonioidea (1->0), Kinosternoidea (1->0).

Character 322 (Cadena & Parham (2015): character 234). Hypoischium: 0 = present; 1 = absent.

Character optimisation: DELTRAN: (*Eileanchelys* + *Kayentachelys*)+++ (0->1); ACCTRAN: *Australochelys*+++ (0->1).

Character 323 (Cadena & Parham (2015): character 235). Humerus, ectepicondylar foramen: 0 = in a channel; 1 = only a groove.

Character optimisation: Unambiguous: Angolachelonia+++ (0->1), *Platysternon megacephalum* (1->0); DELTRAN: *Chelonoidis* sp. (1->0), *Gopherus polyphemus* (1->0), *Carettochelys insculpta* (1->0); ACCTRAN: Testudinidae (1->0), *Testudo* (0->1), total-group Carettochelyidae (1->0).

Character 324 (Cadena & Parham (2015): character 236). Humerus, proximal articular surface of humerus: 0 = with shoulder on preaxial side, upturned; 1 = without shoulder, not upturned.

Character optimisation: Unambiguous: Trionychidae (0->1), *Podocnemis* (0->1); DELTRAN: crown-group Chelonioidea (0->1), *Chelodina* (0->1); ACCTRAN: total-group Chelonioidea (0->1), Chelodininae (0->1).

Character 325 (Cadena & Parham (2015): character 237). Humerus, lateral process of humerus: 0 = abuts caput humeri; 1 = slightly separated from caput humeri; 2 = located distal to caput humeri but along proximal end of shaft; 3 = located at middle of humeral shaft.

Character optimisation: DELTRAN: crown-group Chelonioidea (0->2), *Dermochelys coriacea* (2->3), *Toxochelys latiremis* (0->1); ACCTRAN: total-group Chelonioidea (0->1), crown-group Chelonioidea (1->2), Dermochelyidae (2->3).

Character 326 (Cadena & Parham (2015): character 238). Humerus, lateral process of humerus: 0 = visible in dorsal view: 1 = not visible in dorsal view.

Character optimisation: Unambiguous: Kinosternoidea (0->1), *Chelonoidis* sp. (1->0), Trionychidae (0->1); DELTRAN: Emydidae (0->1), Testuguria (0->1); ACCTRAN: Testudinoidea (0->1), *Platysternon megacephalum* (1->0).

Character 327 (Cadena & Parham (2015): character 239). Humerus, lateral process shape: 0 = rounded to slightly squared; 1 = V-shaped or triangular.

Character optimisation: Unambiguous: crown-group Cheloniidae (0->1); DELTRAN: *Dermochelys coriacea* (0->1); ACCTRAN: Dermochelyidae (0->1).

Character 328 (Cadena & Parham (2015): character 240). Humerus, expansion of lateral process: 0 = limited toanterior surface of shaft; 1 = expands onto ventral surface.

Character optimisation: Unambiguous: Protostegidae (0->1).

Character 329 (Cadena & Parham (2015): character 241). Humerus, medial concavity of lateral process: 0 = absent; 1 = present.

Character optimisation: Unambiguous: Protostegidae (0->1).

Character 330 (Cadena & Parham (2015): character 242). Humerus, prominent anterior projection of lateral process: 0 = absent; 1 = present.

Character optimisation: DELTRAN: *Dermochelys coriacea* (0->1); ACCTRAN: Dermochelyidae (0->1).

Character 331 (Cadena & Parham (2015): character 243). Humerus, length of the humerus versus the width of the proximal end: 0 = two times or less the width of the proximal end: 1 = more than two times the width of the proximal end.

Character optimisation: Unambiguous: Paracryptodira+++ (0->1).

Character 332 (Cadena & Parham (2015): character 244). Humerus, scar for Muscle latissimus dorsi and Muscle teres major: 0 = located anterior to humeral shaft; 1 = located at middle of shaft.

Character optimisation: Unambiguous: (*Protostega* + *Archelon*) (0->1), crown-group Cheloniidae (0->1).

Character 333 (Cadena & Parham (2015): character 245). Humerus, humerus length vs femur length: 0 = shorter than femur; 1 = longer than femur.

Character optimisation: Unambiguous: total-group Chelonioidea (0->1).

Character 334 (Cadena & Parham (2015): character 246). Ulna, contact with radius through rugosity and ridge: 0 = absent; 1 = present.

Character optimisation: Unambiguous: total-group Chelonioidea (0->1); DELTRAN: *Santanachelys gaffneyi* (1->0), *Dermochelys coriacea* (1->0); ACCTRAN: (*Bouliachelys* ++ *Santanachelys*) (1->0), Dermochelyidae (1->0).

Character 335 (Cadena & Parham (2015): character 247). Radius, curves towards anterior: 0 = absent; 1 = present.

Character optimisation: Unambiguous: Protostegidae (0->1).

Character 336 (Cadena & Parham (2015): character 248). Manus, phalangeal formula of the manus: 0 = most digits with two shortenened phalanges: 1 = most digits with three elongated phalanges.

Character optimisation: DELTRAN: Xinjiangchelyidae+++ (0->1), *Testudo* (1->0), *Gopherus polyphemus* (1->0); ACCTRAN: Paracryptodira+++ (0->1), Testudinidae (1->0), *Chelonoidis* sp. (0->1).

Character 337 (modified from Cadena & Parham (2015)). Manus, rigid articulations in 1st and 2nd digit: 0 = absent; 1 = present.

Previous definition (Cadena & Parham (2015): character 249): Manus, paddles: 0 = absent, moveable articulations of all digits; 1 = 'half-paddle' digits 3 and 5 modified into paddle with rigid articulations. But digits 1 and 2 immoveable; 2 = elongate paddles present, digits 1 and 2 modified into paddle with rigid articulations, and very flat carpal and tarsal elements. Combined from Joyce (2007: ch 133, Manus B) and Hirayama (1998), Kear & Lee (2006), and Bardet *et al.* (2013) (chs 76, 77 and 78).

Remarks: I herein follow the approach of various previous authors, such as Hirayama (1998), and code two characters for the formation of paddles.

Character optimisation: Unambiguous: crown-group Chelonioidea (0->1); DELTRAN: *Santanachelys gaffneyi* (1->0); ACCTRAN: (*Bouliachelys* ++ *Santanachelys*) (1->0).

Character 338 (modified from Cadena & Parham (2015)). Manus, rigid articulations in 3rd to 5th digit: 0 = absent; 1 = present.

Previous definition (Cadena & Parham (2015): character 249): Manus, paddles: 0 = absent, moveable articulations of all digits; 1 = 'half-paddle' digits 3 and 5 modified into paddle with rigid articulations. But digits 1 and 2 immoveable; 2 = elongate paddles present, digits 1 and

2 modified into paddle with rigid articulations, and very flat carpal and tarsal elements. Combined from Joyce (2007: ch 133, Manus B) and Hirayama (1998), Kear & Lee (2006), and Bardet *et al.* (2013) (chs 76, 77 and 78).

Remarks: See character 337.

Character optimisation: Unambiguous: total-group Chelonioidea (0->1).

Character 339 (Cadena & Parham (2015): character 250). Manus, flippers: 0 = absent; 1 = short flippers present; 2 = elongate flippers present. Joyce (2007: ch 134, Manus C).

Character optimisation: DELTRAN: Trionychidae (0->1), *Carettochelys insculpta* (0->2); ACCTRAN: Trionychia (0->1), total-group Carettochelyidae (1->2).

Character 340 (Cadena & Parham (2015): character 251). Ulnare, size of the ulnare vs the intermedium: 0 = smaller than intermedium: 1 = nearly as large as intermedium; 2 = much larger than intermedium.

Character optimisation: Unambiguous: Dermochelyoidea (1->2); DELTRAN: Testudines (0->1), *Carettochelys insculpta* (1->2), *Meiolania planiceps* (0->1); ACCTRAN: *Australochelys*+++ (0->1), total-group Carettochelyidae (1->2), Xinjiangchelyidae (1->0).

Character 341 (Cadena & Parham (2015): character 252). Pes, number of digits: 0 = five; 1 = four.

Character optimisation: DELTRAN: *Macrochelys temminckii* (0->1), *Testudo* (0->1), *Gopherus polyphemus* (0->1); ACCTRAN: total-group Chelydridae (0->1), Testudinidae (0->1), *Chelonoidis* sp. (1->0).

Character 342 (Cadena & Parham (2015): character 253). Manus and Pes, flattening of carpals and tarsal elements: 0 = absent; 1 = present.

Character optimisation: Unambiguous: total-group Chelonioidea (0->1).

Character 343 (Cadena & Parham (2015): character 254). Manus and Pes, hyperphalangy manus digits 4 and 5, pes digit 4: 0 = absent; 1 = present.

Character optimisation: Unambiguous: Trionychidae (0->1).

Character 344 (Cadena & Parham (2015): character 255). Femur, femoral trochanters: 0 = distinct, and separated from one another; 1 = fossa obliterated, space between trochanters not concave, but notch present; 2 = fossa obliterated, trochanters connected by bony ridge without a notch.

Character optimisation: Unambiguous: crown-group Chelonioidea (0->1), (*Eretmochelys* ++ *Lepidochelys*) (1->2).

Character 345 (Cadena & Parham (2015): character 256). Tibia, tibial pit for pubotibialis and flexor tibialis internus muscles: 0 = absent; 1 = present.

Character optimisation: Unambiguous: *Natator depressus* (0->1), *Puppigerus camperi* (0->1).

S1.3. Extended discussion of characters regarding the carotid arterial system

The carotid arterial system has been a very prominent character complex in the history of turtle phylogenetics. However, the respective characters used by most previous studies tend to be complex multistate characters, which combine several potentially independent sources of morphological variation. I have investigated the carotid arterial system of all turtle groups considered in this study on the basis of 3D models generated from high resolution CT data. Additionally, I have reviewed characters used in previous studies to classify the variation observed. I have identified the following questions that these previous characters have generally tried to address, and separated them into distinct observations:

(1) Is the palatine division of the carotid artery encased in a bony canal located ventrally in the basicranium, or does it enter the skull through large skull openings on the ventral surface of the skull (i.e. interpterygoid vacuity or slit) (e.g. Cadena & Parham (2015): ch 63 & 101; Zhou & Rabi (2015): ch 60 & ch 98)? This is represented by my characters 145 and 146.

(2) Is the carotid artery itself and its splitting point into its more anterior divisions (the palatine artery and cerebral artery) embedded in bone or exposed ventrally (e.g. Cadena & Parham (2015: ch 99))? This is represented by my character 147.

(3) Where is the entry foramen for the internal carotid artery (foramen posterius canalis carotici interni, fpcci) topologically located on the skull (e.g. Zhou & Rabi (2015): ch 255)? This is represented by my characters 148 and 149.

(4) Which cranial elements form this foramen (fpcci) (e.g. Cadena & Parham (2015): ch 100; Zhou & Rabi (2015): ch 99). This is represented by my characters 151–154.

(5) How closely are the exit foramina for cerebral artery (foramina anterius canalis carotici cerebralis) spaced in the sella turcica (e.g. Cadena & Parham (2015): ch 92)? This is coded by my character 142.

In amniotes in general, the internal carotid artery splits into two major divisions, the cerebral artery and the palatine artery (Müller *et al.* 2011). The cerebral artery always enters the parabasisphenoid or basisphenoid (depending on whether these bones are co-ossified or not, see Sterli *et al.* 2010; Müller *et al.* 2011) from the ventral surface of the skull, and exits into the hypophyseal fossa (=sella turcica) within the cavum cranii. The palatine artery continues anteriorly in a more lateral position than the cerebral artery, and can be variously encased by bone or not. In turtles, the variation associated with the embedding of the branches of the carotid circulation concern the palatine artery. In contrast, the path of the cerebral artery is realtively invariant: it enters the parabasisphenoid to run through a bony canal into the sella turcica in all turtles known, including the early stem-turtle *Proganochelys quenstedti* (SMNS 16980; Gaffney 1990). In the earliest stem-group turtles, including *Proganochelys quenstedti*, *Australochelys africanus* and *Kayentachelys aprix*, the palatine

artery leaves no osteological trace, and is inferred to have entered the cranium through the interpterygoid vacuity, a large opening between the pterygoid present in these taxa. In some turtles (e.g. *Meiolania*, *Annemys levensis*, *Dracochelys*), this vacuity is reduced to a slit like opening, but the palatine artery still enters through this opening without being enclosed in a canal. However, younger turtles (with the possible exception of baenids, see below) are characterised by more complete ossification of the basicranium, and as a result the palatine artery becomes enclosed in bone, such that both the cerebral and palatine arteries are encased in bony canals. I chose to score the above variation in two distinct characters: Character 146 differentiates between turtles in which the palatine artery has no bony canal, and turtles in which this artery is enclosed in a canal. This character is essentially identical with character 98 (Canalis Caroticum F) of Zhou & Rabi (2015), but differs from character 101 of Cadena & Parham (2015) in which variation associated with the encasing of the palatine artery is combined with variation regarding the closure of the interpterygoid opening and the exposure of the carotid split.

Variation concerning the interpterygoid openings is considered in another character of this study: my character 145 differentiates between the more subtle variation observed in the closure of the interpterygoid opening. My character 145 has three states, accounting for the presence of an interpterygoid vacuity, the reduction of this vacuity to a slit-like opening, or the closure of the opening without forming foramina for the palatine artery (as in paracryptodires). The condition of my third state has, to my knowledge, not been considered in previous characters. However, previous characters (e.g. Cadena & Parham (2015): ch 63) usually included the reduction of an interpterygoid opening to foramina and canals for the palatine artery as a separate state. I deleted the state 2 used by Cadena & Parham (2015: ch 62) for this character, because it is not independent from the scorings of my character 146: All turtles in which the palatine artery is enclosed in a bony canal (ch146.1) also have their interpterygoid opening reduced to paired foramina posterius canalis carotici palatinum. These foramina are only visible when a fenestra caroticus is present, but in turtles with a ventrally embedded internal carotid split, these foramina are simply covered by a more

extensively ossified basicranium. Therefore, this character is scored inapplicable for turtles with a bony canal for the palatine artery.

Several combinations of characters 145 and 146 are observed among turtles, justifying their independence. The earliest turtles (e.g. *Proganochelys, Australochelys, Kayentachelys*) have an interpterygoid vacuity, and lack bony canals for the palatine artery (resulting in Ch145:0 and Ch146:0). Some turtles (*Meiolania*, *Chubutemys*, *Dracochelys*) have an interpterygoid slit and lack bony canals for the palatine artery (resulting in Ch145:1 and Ch146:0). Anatomically modern turtles (e.g. thalassochelydians, sinemydids, macrobaenids, crown cryptodires, crown-pleurodires) lack any interpterygoid opening, and have bony canals for the palatine artery (resulting in Ch145:- and Ch146:1). A more unusual pattern is observed in paracryptodires: These turtles lack an interpterygoid opening, but also lack a bony canal for the palatine artery (resulting in Ch145:3 and Ch143:0). Because paracryptodires are entirely extinct, it is not known if the absence of a bony correlate for the palatine artery is indicative of the total absence of this artery, or if the artery branches off extracranially and enters the skull in a position more anteriorly than is usual for turtles.

The embedding of the palatine artery is independent of the embedding of the internal carotid artery posterior to its split into palatine and cerebral arteries. In anatomically modern turtles, the internal carotid artery is encased in a bony canal from some point onwards (this is indicated by the presence of an entry foramen, the foramen posterius canalis carotici interni, fpcci), and remains enclosed in the basicranium around the area in which it splits into the palatine and cerebral arteries. Thus, the split is ventrally covered by bone. In the earliest turtles known (including *Proganochelys*), there is no canal for the internal carotid artery (implying the absence of an fpcci), and the split of the artery into its divisions must therefore occur extracranially. This same pattern is observed in paracryptodires, in which only an entry foramen for the cerebral artery (i.e. foramen posterius canalis carotici cerebralis) is present. Rabi *et al.* (2013) summarized a morphological condition that seems intermediate between the conditions seen in early stem-turtles and crown-group turtles: In some Mesozoic turtles (xinjiangchelyids, sinemydids, macrobaenids, *Jurassichelon*,

Sandownia), the internal carotid artery is partially embedded along its posterior course (implying the presence of an fpcci), but its division into the cerebral and palatine arteries is ventrally exposed in an opening called the fenestra caroticus. This observed variation is considered in my character 147, which is equivalent to character 99 of Cadena & Parham (2015). My character 147 is similar to character 255 of Zhou & Rabi (2015) in that the previous characters "Canalis Caroticus D" and "E" (as used for instance in Sterli & De la Fuente (2013)) are merged into a single character. However, Zhou & Rabi (2015) further split the state that describes a fully enclosed arterial system (my state 2) to take the relative position of the foramen posterius canalis carotici interni into account. I consider this variation separately (see below).

Zhou & Rabi (2015: supplements, ch 255) discussed further variation associated with the embedding of the internal carotid artery. These authors noted that the internal carotid, when at least partially covered by bone, may enter the skull at different positions along the ventral surface of the skull. Specifically, these authors state that pan-pleurodires have a carotid artery that is "not floored from the back of the skull" (Zhou & Rabi (2015): supplements p.12), whereas many "stem cryptodires (…) have their carotid extending in the pterygoid from the posterior edge of the skull as in all crown-cryptodires" (Zhou & Rabi (2015): supplements p.12). I disagree at least partially with Zhou & Rabi (2015). My observations show that many cryptodires, most notably trionychians (e.g. *Apalone spinifera emoryi:* FMNH 22178), and also taxa that are inferred to be cryptodires based on my topology (protostegids, e.g. *Rhinochelys*: CAMSM B55783) have their foramina posterius canalis carotici interni not at the posterior end of the ventral skull surface, but in positions at the same level as the articular process of the quadrate. Conversely, some pleurodires, such as *Phrynops geoffroanus* (SMF 45470), have their foramen posterius canalis carotici interni at the posterior end of their skull, immediately anterior to the ventral margin of the fenestra postotica. I include the information of character states 2 and 3 of character 255 of Zhou & Rabi (2015) as a separate character (character 148), because it is a true observation that in some turtles the foramen is positioned at the posterior end of the skull, while it is further

anteriorly positioned in others. However, I change the scorings for taxa for which I observed different patterns than those reported by Zhou & Rabi (2015).

I include another character that captures variation associated with the position of the foramen posterius canalis carotici interni: My character 149 specifies whether the foramen for the internal carotid is positioned on the ventral surface of the skull, or on the posterior surface of the skull. In turtles that have the second condition, the foramen posterius canails caroticus internus lies within the cavum acustico-jugulare.

Many studies (e.g. Joyce 2007: character 56; Cadena & Parham (2015): character 100, Zhou & Rabi (2015): character 99) have used a character that specifies which cranial elements form the foramen posterius canalis carotici interni. However, the respective variation is usually coded in a multi-state character in which the states define a range of elements included in the formation of the foramen, in addition to a state that specifies the absence of the foramen altogether. Having a complex multi-state character might be confounding some phylogenetic signal. For example, the shared contribution of the pterygoid to the foramen might be phylogentically informative, irrespective of additional contribution of another cranial element, such as the parabasisphenoid. Additionally, in previous versions of this character, the character states used are relatively precise about the various possibilities of the location of the foramen for cases in which the pterygoid is involved (generally the case in non-pleurodiran turtles). However, the pleurodiran possibilities of foramen position, in which the prootic is usually involved, are all scored in a single state, which defines usually the location as in the prootic, prootic and basisphenoid, or prootic and palatine. Therefore, I chose to split the observations underlying this character into several binary characters (characters 151-154) that describe the involvement of cranial elements in the formation of the foramen posterius canalis carotici interni (fpcci). The absence of the foramen is not specifically coded in my model, because the absence of the foramen posterius canalis carotici interni is implied in another character (character 147 state 0). Instead, taxa that lack a foramen posterius canalis carotici interni are scored as inapplicable.

Another observation that is commonly coded into a character is the spacing of the foramina anterius canalis caroticus cerebralis, which transmit the cerebral artery into the sella turcica. This character has been changed little in respect to definitions used in early studies (e.g. Hirayama 1998), and is uncontroversial. However, my new observations of a singular cerebral canal in some chelonioids warrant a new state, as described in more detail in the discussion of character 142 (see above).

I also observed additional variation regarding the path of the palatine artery in cheloniids, coded in my character 150. In crown-group cheloniids, the palatine artery splits from the internal carotid artery within the sulcus cavernosus, and continues anteriorly without ever being embedded in a canal. See remarks for character 150 for further details

S1.4. Deleted phylogenetic characters

Character 21 (Cadena & Parham (2015)) 26 (previously ch 26 my matrix).

Character definition (Cadena & Parham (2015): character 21): Jugals, jugal-quadrate contact: 0= absent; 1= present, quadratojugal does not contribute to lower temporal margin. Hirayama (1998), Kear & Lee (2006) & Bardet *et al.* (2013: ch 9).

Remarks: Cadena & Parham (2015) scored various protostegids, as well as *Dermochelys,* and *Erymnochelys* as having a jugal-quadrate contact. However, my first hand observations of *Dermochelys* (FMNH 171756; UMZC R3031) and *Rhinochelys* (e.g. CAMSMB55783), as well as my CT scans of *Desmatochelys lowi* (KUVP 1200) show that all of these taxa lack such a contact. Therefore, to my knowledge, no turtle has a jugal that directly contacts the quadrate, making state 1 of Cadena & Parham (2015)) obsolete. Therefore, this character would be invariant and was deleted from my matrix.

Character 84 (Cadena & Parham (2015) (previously ch 126 my matrix)

Character definition: Opisthotics, ventral ridge on opisthotic: 0 = absent; 1 = present, with an incipient enclosed middle ear region; 2 = present, but modified with an enclosed middle ear region.

*Remarks***:** This character was used by Sterli (2008: character 55), who refers to Sterli (2007) and Gaffney and Kitching (1995: character 17) for the history of this character. Sterli (2007: pp-22-23) describe the ventral ridge of the opisthotic for *Palaeochersis* as a "bar of bone between the fenestra ovalis and the foramen jugulare anterius, which is not developed neither in neither *Captorhinus*, pareiasaurs, or Testudines. However, this structure is similar to that described by Gaffney (1990) for *Proganochelys* and by Gaffney & Kitching (1995) for *Australochelys* (…). Gaffney (1990) and Gaffney & Kitching (1995) proposed this structure is homologous to the processus interfenestralis of the opisthotic found in Testudines." However, Gaffney & Kitching (1995: p. 24) reported the ridge of *Australochelys* to be a common character (i.e. synapomorphy) of *Australochelys* and casichelydians (i.e. turtles placed more crownwardly than *Australochelys*, in which the ridge is strongly modified to a proper processus interfenestralis), and say this feature is absent in *Proganochelys*. I agree with Sterli (2007) that *Proganochelys* indeed has the same ridge seen in *Australochelys* and *Palaeochersis*: The ridge was clearly illustrated and described by Gaffney (1990), and is well visible in the specimen SMNS 16980 (pers. obs. SWE). I also agree with previous authors that the ridge is homologous to the processus interfenestralis of later turtles.

Despite acknowledging the presence of the ridge in *Proganochelys*, *Australochelys*, and *Palaeochersis* (Sterli 2007), Sterli (2008) scored *Proganochelys* as not having the ridge (charater 55, state 0 of that study), but scored *Australochelys*, *Palaeochersis*, *Kayentachelys*, *Condorchelys*, *Heckerochelys*, *Mongolochelys*, and *Kallokibotion* as having the ridge (character 55, state 1 in Sterli 2008). The same scoring scheme was used by Cadena & Parham (2015).

I re-examined all taxa in this study, and find the ridge described by Gaffney (1990), Gaffney and Kitching (1995), and Sterli (2007) to only be present in *Proganochelys*,

Australochelys, and *Palaeochersis*. The early stem-group turtle *Kayentachelys aprix* (TMM 4370-2) lacks the ridge and instead has a modified ventral surface of the opisthotic that is possible intermediate between the condition seen in *Australochelys* and anatomically modern turtles with a fully developed processus interfenestralis, recessus scalae tympani, and fully enclosed middle ear region. Other stem-turtles examined in this study, such as *Kallokibotion* (NHMUK R4925), have an anatomically modern middle ear structure. I therefore initially changed the scorings for this character to reflect these observations. However, the scoring pattern for this character is then identical to the scorings of character 127 of this study, which describes the processus interfenestralis. Since the ventral opisthotic ridge is interpreted to be homologous with the processus interfenestralis of the opisthotic, separation of this character from character 127 would lead to the repeated consideration of this feature. Therefore, I deleted character 84 of Cadena & Parham (2015) from my matrix.

Character 91 (Cadena & Parham (2015))

Original character: Basisphenoid, foramen caroticum laterale larger than foramen anterius canalis carotici interni: 0 = absent; 1 = present. Parham & Pyenson (2010: ch 5); Hirayama (1998), Kear & Lee (2006), & Bardet *et al.* (2013: ch 37).

Remarks: Previous authors have not explicitly discussed the morphological observations on which this character was originally based (Cadena & Parham (2015): character 91). Cadena & Parham (2015) scored a number of chelonioids *sensu lato* as exhibiting state 1 (e.g. *Allopleuron hoffmanni*, *Caretta caretta*, *Chelonia mydas*, *Ctenochelys stenoporus*, *Eochelone brabantica*, *Eretmochelys imbricata*, *Lepidochelys kempii*, *Lepidochelys olivacea*, *Natator depressus*, and *Puppigerus camperi*), and non-chelonioids as states 1 or ? (missing data).

It is likely that the original character definition is based on a comment by Gaffney (1979), who cites Albrecht (1976) and other sources, saying the palatine artery in extant chelonioids (i.e. extant cheloniids and *Dermochelys*) is larger or equal in diameter to that of

the internal carotid artery. This statement was based on direct observation of actual arterial sizes in dissected extant animals (see Albrecht 1976). Cadena & Parham (2015), and others (e.g. Hirayama 1998; Kear & Lee 2006; Parham & Pyenson 2010; Bardet *et al.* 2013) refer to the size of the anterior foramen for the palatine artery, an osteological feature, in their character description (i.e. foramen caroticum laterale in the definition of Cadena & Parham (2015)). This was clarified as being the foramen anterius canalis carotici palatinum by Rabi *et al.* (2013).

Reference to the osteological foramen is reasonable in the context of a morphological character-taxon matrix that is largely based on osteological characters that can also be scored for fossils. However, the foramen anterius canalis carotici palatinum is absent in crown-cheloniids (but not the Eocene cheloniid *Puppigerus*: NHMUKR14375): in crown-cheloniids, the internal carotid artery exits the braincase anteriorly, and the split into palatine and cerebral arteries occurs within the cavum cranii, in the floor of the sulcus cavernosus (see character 146 of this study). After this split, the palatine artery remains without a canal. Evidence for this was already presented by Gaffney (1976), who stated that "one of the most characteristic specialisations of the cheloniid skull is the absence of a bony roof for the anterior portion of the canalis caroticus internus and for the entire canalis caroticus lateralis (remark: = canalis caroticus palatinum following Rabi *et al.* 2013)" (Gaffney 1979: p.102). This observation is supported in this study based on the examination of CT-scans of crown-cheloniids (*Caretta caretta*: NHMUK 1938.1.9.1; *Chelonia mydas*: NHMUK 1969.776; *Eretmochelys imbricata*: FMNH 22242; *Lepidochelys kempii*: M009/08; *Lepidochelys olivacea*: SMNS 11070; *Natator depressus*: R112123). Gaffney (1976) further stated that strictly speaking, because of the absence of a bony canal for the palatine artery, a foramen anterius canalis caroticus palatinum (previously foramen caroticum laterale) as an anterior exiting foramen of the palatine artery is also absent. Following this argumentation, the exiting foramen for the internal carotid artery into the sulcus cavernosus of most cheloniids should be called foramen anterius canalis carotici interni. However, calling the anterior exit of the internal carotid artery into the sulcus cavernosus 'foramen anterius canalis carotici interni' is

at odds with the definition of this foramen given by Rabi *et al.* (2013), who state that this foramen is only present in turtles with a fenestra caroticus (which is absent in cheloniids). However, Rabi *et al.* (2013) did not specifically consider the condition described for crown-cheloniids, so that I herein refrain from adding an additional name for the foramen in question, and keep the use 'foramen anterius canalis carotici interni' as a descriptively correct term for the foramen (see "facci" in Fig. S1.64*c*).

Albrecht (1976) hypothesized that the foramen anterius canalis caroticus palatinum of cheloniids has simply migrated posteriorly, and that the anterior foramen exiting into the sulcus cavernosus could thus be called a foramen caroticum laterale, or foramen anterius canalis carotici palatinum *sensu* Rabi *et al.* (2013). However, this alternative hypothesis is demonstrably incorrect: the position of the split of the internal carotid is indicated by the position of the canal for the cerebral artery, which in cheloniids enters the parabasisphenoid medially from the sulcus cavernosus. This shows that the splitting of cerebral and palatine arteries of cheloniids occurs within the sulcus cavernosus, and is not dorsally covered by bone.

Because the palatine artery has no ossified canal in crown-cheloniids, its size cannot be, directly or indirectly, estimated on osteological specimens of cheloniid crania, including all fossils pertaining to the crown group. Therefore, character 91 of Cadena & Parham (2015) is inapplicable for crown-group cheloniids unless used to refer only to the soft, arterial anatomy (in which case it should be scored as ? for all extinct taxa). Despite this, Cadena & Parham (2015) scored character state 1 for various extant and extinct cheloniids as well as some non-cheloniid pan-chelonioids (e.g. *Allopleuron*, *Eochelone*, *Ctenochelys*), possibly following Albrecht's (1976) incorrect identification of the foramen anterius canalis caroticus palatinum. Other taxa were either scored as state "0" or "?", although Gaffney (1979: p. 101) specifically mentioned large diameters of the canal for the palatine artery in trionychids, kinosternids, and dermatemydids. In its current form and way it is coded and scored, character 91 of Cadena & Parham (2015) thus serves as grouping chelonioids, maybe at least partially based on incomplete taxon sampling for this character.

To incorporate Gaffney's (1976) and Albrecht's (1976) observations of larger chelonioid palatine artery diameters, the character definition would have to be modified to represent the actual soft tissues. This is impractical for a matrix seeking to score fossil material, in spite of the arterial diameters possibly being parsimony-informative. Therefore, I chose to delete character 91. The absence of a bony canal for the palatine artery in itself, however, is an observable and potentially phylogenetically informative observation, and is considered in character 146 of this study.

Character 209 (Cadena & Parham (2015)).

Original character: Caudals, caudal centra: 0 = all centra amphicoelous; 1 = all centra more or less pronounced procoelous; 2 = all centra more or less pronounced opisthocoelous; 3 = anterior few centra procoelous, posterior centra predominantly opisthocoelous.

Remarks: Character 209 of Cadena & Parham (2015) has been deleted from my matrix, because the character is redundant with the information encoded in characters 210 and 211 of Cadena & Parham (2015) (my characters 297 and 298).

S1.5 Character optimisation: Synapomorphies by node

'Unambiguous' synapomorphies are those found under both ACCTRAN and DELTRAN optimization. Because some nodes of the phylogeny represent unnamed clades, I use a code to denote the content of these clades. Hereby, the notation 'Taxon+++' indicates the clade comprising the named taxon and all more crownwardly positioned taxa. The notation '(Taxon A ++ Taxon B)' indicates the most inclusive clade including Taxon A and Taxon B.

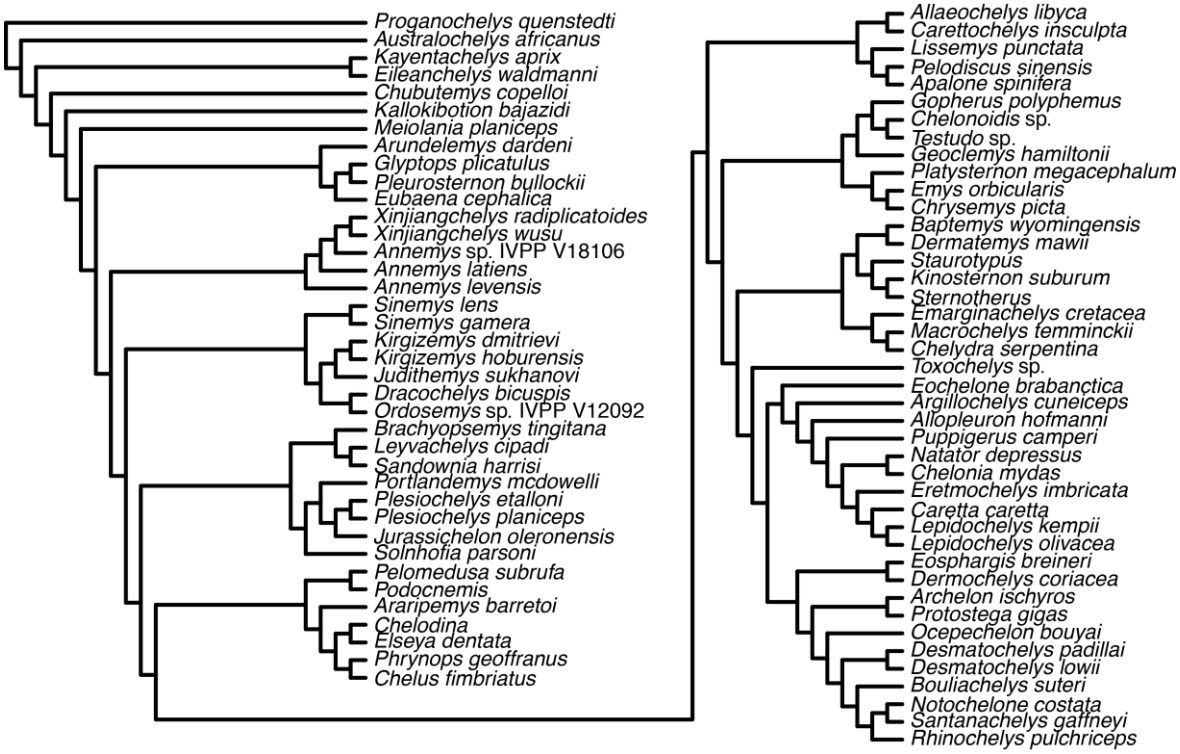


FIG S1.75. Tree topology for character optimisation. Note that this tree is a fully resolved MPT from the analysis using unordered characters.

Optimization by node with node numbers:

Australochelys+++:
DELTRAN: CH63: 0->1, CH86: 0->1, CH90: 0->1, CH141: 0->1, CH143: 0->1;
ACCTRAN: CH11: 0->1, CH24: 0->1, CH25: 0->1, CH45: 0->1, CH49: 0->1, CH61: 0->1, CH63: 0->1, CH72: 0->1, CH74: 0->1, CH86: 0->1, CH89: 0->1, CH90: 0->1, CH132: 0->1, CH140: 0->1, CH141: 0->1, CH143: 0->1, CH160: 0->1, CH202: 0->1, CH205: 0->1, CH221: 0->1, CH222: 0->1, CH230: 0->1, CH239: 0->1, CH241: 0->1, CH261: 0->1, CH296: 0->1, CH301: 0->1, CH303: 0->1, CH308: 0->1, CH310: 0->1, CH313: 0->1, CH320: 0->1, CH322: 0->1, CH340: 0->1.

(*Eileanchelys* + *Kayentachelys*)+++:
Unambiguous: CH5: 1->0, CH9: 0->1, CH10: 0->1, CH66: 1->0, CH77: 0->1, CH107: 0->1, CH113: 1->0, CH118: 0->1, CH130: 0->2, CH139: 2->1;
DELTRAN: CH25: 0->1, CH49: 0->1, CH61: 0->1, CH74: 0->2, CH160: 0->1, CH205: 0->1, CH221: 0->1, CH222: 0->1, CH230: 0->1, CH241: 0->1, CH261: 0->1, CH301: 0->1, CH303: 0->1, CH308: 0->1, CH310: 0->1, CH313: 0->1, CH320: 0->1, CH322: 0->1;
ACCTRAN: CH20: 0->1, CH74: 1->2, CH76: 0->1, CH165: 0->1.

Chubutemys+++:
Unambiguous: CH21: 0->1, CH65: 0->2, CH79: 0->1, CH104: 0->1, CH110: 0->1, CH119: 0->1, CH145: 0->1, CH302: 0->1;
DELTRAN: CH20: 0->1, CH45: 0->1, CH76: 0->2, CH89: 0->1, CH165: 0->1;
ACCTRAN: CH24: 1->0, CH58: 1->0, CH76: 1->2, CH88: 0->1, CH121: 0->1, CH122: 0->1, CH132: 1->0, CH140: 1->0, CH200: 0->1, CH242: 0->1, CH244: 0->1, CH251: 0->1, CH294: 0->1, CH297: 0->1, CH298: 0->2.

Kallokibotion+++:
Unambiguous: CH91: 0->1, CH106: 0->1, CH107: 1->2, CH120: 0->2;
DELTRAN: CH88: 0->1, CH122: 0->1, CH200: 0->1, CH202: 0->1, CH239: 0->1, CH244: 0->1.

Meiolania+++:
Unambiguous: CH96: 0->1, CH126: 0->1, CH193: 0->1, CH228: 0->1;
DELTRAN: CH298: 0->2;
ACCTRAN: CH147: 0->1, CH225: 0->1, CH248: 0->1, CH249: 0->1.

Paracryptodira+++:
Unambiguous: CH16: 1->0, CH18: 0->2, CH34: 0->1, CH47: 0->1, CH100: 0->1, CH109: 0->1, CH119: 1->0, CH240: 0->1, CH305: 0->2, CH331: 0->1;
DELTRAN: CH11: 0->1, CH225: 0->1, CH242: 0->1, CH296: 0->1;
ACCTRAN: CH22: 0->1, CH121: 1->0, CH179: 0->1, CH206: 0->1, CH287: 0->1, CH299: 0->1, CH312: 1->0, CH319: 0->1, CH336: 0->1.

Xinjiangchelyidae+++:
Unambiguous: CH3: 0->1, CH13: 0->1, CH115: 0->1, CH120: 2->0, CH146: 0->1, CH224: 0->1;
DELTRAN: CH22: 0->1, CH58: 1->0, CH72: 0->1, CH147: 0->1, CH206: 0->1, CH249: 0->1, CH287: 0->1, CH336: 0->1;
ACCTRAN: CH4: 0->1, CH40: 0->1, CH175: 0->1, CH178: 0->1, CH235: 0->1, CH248: 1->0.

Sinemydidae/Macrobaenidae+++:
Unambiguous: CH142: 1->0, CH185: 0->1, CH228: 1->0, CH271: 0->1, CH278: 0->1, CH309: 0->1;
DELTRAN: CH23: 0->1, CH175: 0->1, CH274: 0->1, CH294: 0->1, CH297: 0->1, CH299: 0->1;
ACCTRAN: CH23: 0->1, CH219: 0->1, CH274: 0->1.

Angolachelonia+++:
Unambiguous: CH65: 2->0, CH79: 1->2, CH123: 1->0, CH128: 0->1, CH141: 1->0, CH147: 1->2, CH180: 0->1, CH208: 0->1, CH273: 0->1, CH323: 0->1;
DELTRAN: CH4: 0->1, CH179: 0->1;
ACCTRAN: CH62: 0->1, CH98: 0->1, CH127: 1->0, CH132: 0->1, CH230: 1->0, CH235: 1->0, CH252: 0->1, CH292: 0->2, CH298: 2->1.

Testudines:
Unambiguous: CH1: 0->1, CH15: 0->1, CH28: 0->1, CH35: 0->1, CH90: 1->2, CH248: 0->1;
DELTRAN: CH292: 0->2, CH298: 2->1, CH312: 1->0, CH319: 0->1, CH340: 0->1;
ACCTRAN: CH6: 0->1, CH95: 0->1, CH99: 0->2, CH109: 1->0, CH116: 0->2, CH163: 1->0, CH191: 0->1, CH217: 1->0, CH253: 0->1.

Cryptodira:
Unambiguous: CH34: 1->0, CH69: 0->1, CH75: 0->1, CH122: 1->0, CH206: 1->0, CH276: 0->1, CH284: 0->1, CH286: 0->1, CH288: 0->1, CH295: 0->1;
DELTRAN: CH95: 0->1, CH109: 1->0, CH127: 1->0, CH163: 1->0, CH235: 0->1, CH253: 0->1;
ACCTRAN: CH13: 1->0, CH22: 1->0, CH230: 0->1, CH235: 0->1, CH252: 1->0, CH259: 0->1, CH271: 1->0, CH318: 0->1.

Durocryptodira:
Unambiguous: CH208: 1->0, CH275: 0->1;
DELTRAN: CH13: 1->0, CH99: 0->2, CH259: 0->1, CH271: 1->0;
ACCTRAN: CH6: 1->0, CH62: 1->0, CH98: 1->0, CH132: 1->0, CH149: 0->1, CH217: 0->1, CH219: 1->0, CH290: 0->1, CH321: 0->1.

Americhelydia:
Unambiguous: CH67: 0->1, CH243: 0->1;
DELTRAN: CH178: 0->1;
ACCTRAN: CH23: 1->0, CH40: 1->0, CH116: 2->0, CH180: 1->0, CH218: 0->1, CH234: 0->1, CH247: 0->1, CH265: 0->1.

total-group Chelonioidea:
Unambiguous: CH35: 1->0, CH39: 0->1, CH58: 0->1, CH69: 1->0, CH94: 1->0, CH105: 0->1, CH132: 0->2, CH139: 1->2, CH142: 0->1, CH144: 0->1, CH163: 0->1, CH210: 0->2, CH231: 0->1, CH235: 1->0, CH242: 1->2, CH255: 0->2, CH291: 0->1, CH295: 1->0, CH333: 0->1, CH334: 0->1, CH338: 0->1, CH342: 0->1;
DELTRAN: CH180: 1->0, CH218: 0->1, CH247: 0->1;
ACCTRAN: CH18: 2->0, CH57: 0->1, CH126: 1->0, CH135: 0->1, CH149: 1->0, CH209: 0->1, CH232: 0->1, CH263: 0->1, CH284: 1->0, CH285: 0->1, CH288: 1->0, CH290: 1->0, CH324: 0->1, CH325: 0->1.

crown-group Chelonioidea:
Unambiguous: CH15: 1->0, CH93: 0->2, CH104: 1->0, CH306: 0->1, CH307: 0->1, CH337: 0->1, CH344: 0->1;
DELTRAN: CH18: 2->0, CH22: 1->0, CH232: 0->1, CH284: 1->0, CH288: 1->0, CH318: 0->1, CH324: 0->1, CH325: 0->2;
ACCTRAN: CH49: 1->0, CH125: 0->1, CH138: 0->2, CH140: 0->1, CH186: 0->1, CH219: 0->1, CH256: 0->1, CH321: 1->0, CH325: 1->2.

Dermochelyoidea:
Unambiguous: CH27: 1->0, CH161: 0->1, CH237: 0->1, CH340: 1->2;
DELTRAN: CH126: 1->0, CH140: 0->1;
ACCTRAN: CH11: 1->0, CH65: 0->1, CH67: 1->0, CH98: 0->2, CH99: 2->1, CH135: 1->0, CH217: 1->0, CH224: 1->0.

Protostegidae:
Unambiguous: CH4: 1->0, CH62: 0->1, CH103: 0->1, CH236: 0->1, CH291: 1->0, CH328: 0->1, CH329: 0->1, CH335: 0->1;
ACCTRAN: CH57: 1->0, CH81: 0->1, CH128: 1->0, CH144: 1->0, CH285: 1->0, CH286: 1->0.

(*Ocepechelon* ++ *Santanachelys*):
Unambiguous: CH1: 1->0, CH40: 0->1, CH75: 1->0, CH116: 0->2;
DELTRAN: CH65: 0->1, CH99: 2->1, CH138: 0->2;
ACCTRAN: CH7: 0->1, CH11: 0->1, CH98: 2->0, CH186: 1->0, CH219: 1->0, CH221: 1->0, CH255: 2->0, CH256: 1->0.

(*Desmatochelys* ++ *Santanachelys*):
Unambiguous: CH15: 0->1, CH87: 0->1, CH93: 2->1, CH104: 0->1, CH142: 1->2;
DELTRAN: CH81: 0->1, CH255: 2->0, CH286: 1->0;
ACCTRAN: CH67: 0->1, CH76: 2->1.

(*Bouliachelys* ++ *Santanachelys*):
Unambiguous: CH115: 1->0, CH174: 0->1;
DELTRAN: CH49: 1->0, CH144: 1->0;
ACCTRAN: CH7: 1->0, CH125: 1->0, CH128: 0->1, CH225: 1->0, CH232: 1->0, CH247: 1->0, CH292: 2->0, CH334: 1->0, CH337: 1->0.

(*Rhinochelys* ++ *Santanachelys*):
Unambiguous: CH14: 1->2, CH95: 1->0, CH152: 1->0, CH161: 1->0;
ACCTRAN: CH185: 1->0.

Rhinochelys pulchriceps:
Unambiguous: CH94: 0->1, CH140: 1->0;
DELTRAN: CH185: 1->0.

(*Santanachelys* + *Notochelone*):
Unambiguous: CH96: 1->0;
ACCTRAN: CH69: 0->1, CH75: 0->1, CH81: 1->0, CH113: 0->1, CH132: 2->0.

Santanachelys gaffneyi:
Unambiguous: CH105: 1->0, CH148: 1->0;
DELTRAN: CH75: 0->1, CH221: 1->0, CH224: 1->0, CH225: 1->0, CH232: 1->0, CH247: 1->0, CH292: 2->0, CH334: 1->0, CH337: 1->0.

Notochelone:
Unambiguous: CH67: 1->0, CH125: 0->1;
DELTRAN: CH69: 0->1, CH81: 1->0, CH113: 0->1, CH132: 2->0.

Bouliachelys suteri:
Unambiguous: CH4: 0->1, CH9: 1->0, CH11: 1->0, CH76: 1->0, CH83: 0->1, CH122: 0->1, CH133: 0->1, CH177: 0->1.

(*Desmatochelys lowii* + *Desmatochelys padillai*):
Unambiguous: CH19: 0->1, CH274: 1->0;
DELTRAN: CH7: 0->1, CH76: 2->1;
ACCTRAN: CH22: 0->1, CH49: 0->1, CH131: 0->1, CH208: 0->1.

Desmatochelys lowii:
Unambiguous: CH40: 1->0, CH93: 1->0, CH198: 0->1;
DELTRAN: CH22: 0->1, CH125: 0->1, CH128: 1->0, CH131: 0->1, CH208: 0->1, CH209: 0->1.

Desmatochelys padillai:
Unambiguous: CH18: 0->1, CH95: 1->0, CH99: 1->2, CH152: 1->0.

Ocepechelon bouyai:
Unambiguous: CH3: 1->0, CH13: 0->1, CH38: 0->1, CH48: 0->1, CH58: 1->0, CH110: 1->0;
DELTRAN: CH7: 0->1, CH49: 1->0, CH67: 1->0, CH128: 1->0.

(*Protostega* + *Archelon*):
Unambiguous: CH52: 0->1, CH102: 0->1, CH189: 0->1, CH214: 1->0, CH242: 2->3, CH244: 1->2, CH332: 0->1;
DELTRAN: CH11: 1->0, CH67: 1->0, CH98: 0->2, CH186: 0->1, CH217: 1->0, CH219: 0->1, CH256: 0->1;
ACCTRAN: CH65: 1->0, CH80: 0->1, CH148: 1->0, CH152: 1->0.

Protostega gigas:
Unambiguous: CH185: 1->0;
DELTRAN: CH80: 0->1, CH148: 1->0, CH152: 1->0.

Archelon ischyros:
Unambiguous: CH44: 0->1, CH201: 0->1, CH274: 1->0.

Dermochelyidae:
Unambiguous: CH16: 0->1, CH53: 0->1, CH96: 1->0, CH110: 1->0, CH115: 1->0, CH149: 0->1;
DELTRAN: CH11: 1->0, CH57: 0->1, CH65: 0->1, CH98: 0->2;

ACCTRAN: CH6: 0->1, CH14: 1->0, CH21: 1->0, CH49: 0->1, CH71: 0->1, CH79: 2->1, CH87: 0->1, CH120: 0->1, CH124: 0->1, CH138: 2->0, CH177: 0->1, CH183: 0->2, CH194: 0->1, CH201: 0->1, CH204: 0->1, CH238: 0->1, CH287: 1->0, CH312: 0->1, CH325: 2->3, CH327: 0->1, CH330: 0->1, CH334: 1->0.

Dermochelys coriacea:
Unambiguous: CH25: 1->0, CH42: 0->1, CH58: 1->0, CH94: 0->1;
DELTRAN: CH6: 0->1, CH14: 1->0, CH21: 1->0, CH67: 1->0, CH71: 0->1, CH79: 2->1, CH87: 0->1, CH120: 0->3, CH124: 0->1, CH177: 0->1, CH183: 0->2, CH186: 0->1, CH194: 0->1, CH201: 0->1, CH204: 0->1, CH219: 0->1, CH238: 0->1, CH256: 0->1, CH285: 0->1, CH287: 1->0, CH312: 0->1, CH325: 2->3, CH327: 0->1, CH330: 0->1, CH334: 1->0;
ACCTRAN: CH120: 1->3.

Eosphargis breineri:
Unambiguous: CH91: 1->0, CH101: 0->1, CH119: 0->1, CH136: 0->1;
DELTRAN: CH120: 0->1, CH135: 0->1;
ACCTRAN: CH67: 0->1, CH135: 0->1.

total-group Cheloniidae:
Unambiguous: CH44: 0->1, CH68: 0->1, CH109: 0->1, CH119: 0->1, CH176: 0->1;
DELTRAN: CH49: 1->0, CH125: 0->1, CH135: 0->1.

Argillochelys+++:
Unambiguous: CH16: 0->1, CH55: 0->1, CH56: 0->1, CH67: 1->2, CH81: 0->1, CH101: 0->1, CH102: 0->1, CH113: 0->1;
DELTRAN: CH57: 0->1, CH138: 0->2, CH140: 0->1, CH285: 0->1;
ACCTRAN: CH174: 0->1.

Allopleuron+++:
Unambiguous: CH58: 1->0, CH115: 1->0;
ACCTRAN: CH80: 0->1.

Puppigerus+++:
Unambiguous: CH6: 0->1, CH71: 0->1, CH87: 0->1, CH211: 0->1;
ACCTRAN: CH126: 0->1, CH186: 1->0, CH219: 1->0, CH256: 1->0, CH295: 0->1.

crown-group Cheloniidae:
Unambiguous: CH150: 0->1, CH177: 0->1, CH194: 0->1, CH327: 0->1, CH332: 0->1;
DELTRAN: CH295: 0->1;
ACCTRAN: CH58: 0->2, CH69: 0->1, CH80: 1->0, CH201: 0->1, CH212: 0->1.

(*Eretmochelys* ++ *Lepidochelys*):
Unambiguous: CH8: 0->1, CH29: 1->0, CH113: 1->0, CH344: 1->2;
DELTRAN: CH212: 0->1;
ACCTRAN: CH174: 1->0.

(*Caretta* ++ *Lepidochelys*):
Unambiguous: CH229: 0->1, CH306: 1->0;
ACCTRAN: CH11: 1->0, CH58: 2->0, CH142: 1->2, CH182: 0->1, CH189: 0->1, CH205: 1->0, CH263: 1->0.

(*Lepidochelys olivacea* + *Lepidochelys kempii*):
Unambiguous: CH144: 1->0;
DELTRAN: CH69: 0->1, CH174: 0->1, CH201: 0->1;
ACCTRAN: CH174: 0->1.

Lepidochelys olivacea:
Unambiguous: CH100: 1->0, CH132: 2->1, CH173: 0->1;
DELTRAN: CH11: 1->0, CH126: 1->0, CH142: 1->2, CH182: 0->1, CH189: 0->1;
ACCTRAN: CH126: 1->0.

Lepidochelys kempii:
Unambiguous: CH29: 0->1, CH52: 0->1, CH102: 1->0, CH177: 1->0;
DELTRAN: CH58: 0->2;
ACCTRAN: CH11: 0->1, CH58: 0->2, CH142: 2->1, CH182: 1->0, CH189: 1->0.

Caretta caretta:
Unambiguous: CH60: 0->1, CH64: 0->1, CH98: 0->1, CH111: 0->1, CH161: 0->1, CH210: 2->3, CH218: 1->0;
DELTRAN: CH11: 1->0, CH142: 1->2, CH182: 0->1, CH189: 0->1, CH205: 1->0;
ACCTRAN: CH69: 1->0, CH201: 1->0.

Eretmochelys imbricata:
Unambiguous: CH116: 0->1, CH120: 0->1, CH132: 2->0, CH175: 1->0, CH221: 1->0;
DELTRAN: CH58: 0->2, CH69: 0->1, CH126: 1->0, CH201: 0->1, CH263: 0->1;
ACCTRAN: CH126: 1->0.

(*Chelonia* + *Natator*):
Unambiguous: CH79: 2->1, CH178: 1->0;
DELTRAN: CH58: 0->2, CH174: 0->1, CH263: 0->1.

Chelonia mydas:
Unambiguous: CH71: 1->0, CH98: 0->2, CH100: 1->0, CH101: 1->0, CH102: 1->0, CH115: 0->1, CH120: 0->1, CH124: 0->1, CH132: 2->0, CH139: 2->0, CH189: 0->1, CH210: 2->3;
DELTRAN: CH201: 0->1;
ACCTRAN: CH69: 1->0, CH212: 1->0.

Natator depressus:
Unambiguous: CH75: 1->0, CH142: 1->2, CH175: 1->0, CH182: 0->1, CH221: 1->0, CH345: 0->1;
DELTRAN: CH69: 0->1, CH126: 1->0, CH212: 0->1;
ACCTRAN: CH126: 1->0, CH201: 1->0.

Puppigerus camperi:
Unambiguous: CH16: 1->0, CH65: 0->1, CH125: 1->0, CH138: 2->1, CH140: 1->0, CH144: 1->0, CH149: 0->1, CH173: 0->1, CH345: 0->1;
DELTRAN: CH80: 0->1, CH174: 0->1.

Allopleuron hofmanni:
Unambiguous: CH25: 1->0, CH42: 0->1, CH44: 1->0, CH49: 0->1, CH76: 2->1, CH79: 2->1, CH84: 0->1, CH93: 2->0, CH128: 1->0, CH131: 0->1, CH163: 1->0, CH175: 1->0, CH185: 1->0, CH189: 0->1, CH221: 1->0, CH236: 0->1;
DELTRAN: CH80: 0->1, CH126: 1->0, CH186: 0->1, CH219: 0->1, CH256: 0->1;
ACCTRAN: CH174: 1->0.

Argillochelys cuneiceps:
Unambiguous: CH149: 0->1, CH154: 1->0;
DELTRAN: CH126: 1->0, CH174: 0->1.

Eochelone:

Unambiguous: CH79: 2->1, CH120: 0->2, CH132: 2->0, CH142: 1->0, CH164: 1->0;
DELTRAN: CH138: 0->1;
ACCTRAN: CH57: 1->0, CH126: 0->1, CH138: 2->1, CH140: 1->0.

Toxochelys latiremis:
Unambiguous: CH1: 1->0, CH13: 0->1, CH28: 1->0, CH38: 0->1, CH95: 1->0, CH99: 2->0, CH115: 1->0, CH172: 0->1, CH177: 0->1, CH182: 0->1, CH194: 0->1, CH198: 0->1, CH268: 0->1, CH270: 0->1, CH271: 0->1, CH286: 1->0, CH299: 1->0;
DELTRAN: CH18: 2->1, CH57: 0->1, CH135: 0->1, CH321: 0->1, CH325: 0->1;
ACCTRAN: CH18: 0->1.

Chelydroidea:
Unambiguous: CH65: 0->1, CH154: 1->0, CH179: 1->0, CH195: 0->1;
DELTRAN: CH149: 0->1, CH217: 1->0, CH290: 0->1;
ACCTRAN: CH59: 0->1, CH188: 0->1, CH189: 0->1, CH217: 1->0, CH319: 1->0.

total-group Chelydridae:
Unambiguous: CH81: 0->1, CH269: 0->1;
ACCTRAN: CH22: 0->1, CH125: 0->1, CH174: 0->1, CH177: 0->1, CH200: 1->0, CH221: 1->0, CH298: 1->2, CH299: 1->0, CH318: 1->0, CH341: 0->1.

crown-group Chelydridae:
Unambiguous: CH11: 1->0, CH35: 1->0, CH52: 0->1, CH67: 1->0, CH77: 1->2, CH94: 1->0, CH99: 2->0, CH113: 0->1, CH231: 0->1, CH242: 1->2, CH270: 0->1;
DELTRAN: CH23: 1->0, CH125: 0->1, CH174: 0->1, CH177: 0->1, CH180: 1->0, CH200: 1->0, CH221: 1->0, CH247: 0->1, CH298: 1->2, CH299: 1->0;
ACCTRAN: CH188: 1->0, CH189: 1->0.

Chelydra serpentina:
Unambiguous: CH9: 1->0, CH24: 0->1, CH28: 1->0, CH58: 0->1, CH123: 0->1, CH141: 0->1, CH196: 1->2, CH210: 0->2, CH217: 0->2, CH255: 0->1;
DELTRAN: CH40: 0->1, CH265: 0->1;
ACCTRAN: CH40: 0->1, CH319: 0->1.

Macrochelys temminckii:
Unambiguous: CH65: 1->0, CH84: 0->1, CH139: 1->0, CH142: 0->1, CH149: 1->0, CH154: 0->1, CH222: 1->0, CH297: 1->2;
DELTRAN: CH116: 0->1, CH319: 1->0, CH321: 0->1, CH341: 0->1;
ACCTRAN: CH116: 0->1.

Emarginachelys cretacea:
Unambiguous: CH29: 1->0, CH58: 0->2, CH107: 2->1, CH109: 0->1, CH317: 0->1;
DELTRAN: CH59: 0->1, CH188: 0->1, CH189: 0->1.

Kinosternoidea:
Unambiguous: CH21: 1->2, CH54: 0->1, CH123: 0->1, CH206: 0->1, CH230: 1->0, CH266: 0->1, CH326: 0->1;
DELTRAN: CH22: 1->0, CH116: 0->2, CH318: 0->1, CH319: 1->0;
ACCTRAN: CH40: 0->1, CH116: 0->2, CH120: 0->2, CH122: 0->1, CH157: 0->1, CH180: 0->1, CH183: 0->1, CH208: 0->1, CH247: 1->0, CH281: 2->1, CH312: 0->1, CH316: 0->1, CH321: 1->0.

Kinosternidae:
Unambiguous: CH11: 1->0, CH17: 0->1, CH26: 0->1, CH32: 0->1, CH131: 0->1, CH205: 1->2, CH233: 0->1, CH248: 1->2, CH268: 0->1, CH272: 0->1, CH293: 0->1, CH317: 0->1;

DELTRAN: CH157: 0->1, CH183: 0->1, CH188: 0->1, CH189: 0->1, CH191: 0->1, CH234: 0->1, CH281: 2->1, CH316: 0->1;
ACCTRAN: CH42: 0->1, CH67: 1->2, CH68: 0->1, CH77: 1->2, CH100: 1->0.

Kinosterninae:
Unambiguous: CH24: 0->1, CH184: 0->1, CH207: 0->1, CH238: 0->1, CH263: 0->1, CH264: 0->1;
DELTRAN: CH40: 0->1, CH208: 0->1, CH312: 0->1;
ACCTRAN: CH122: 1->0.

Sternotherus:
Unambiguous: CH96: 1->0, CH98: 0->1, CH115: 1->0, CH116: 2->0, CH128: 1->0, CH137: 0->1, CH175: 1->0, CH209: 0->1;
DELTRAN: CH67: 1->2, CH68: 0->1, CH77: 1->2, CH120: 0->2;
ACCTRAN: CH42: 1->0, CH100: 0->1.

Kinosternon suburum hippocrepis:
Unambiguous: CH52: 0->1, CH110: 1->0, CH114: 0->1, CH125: 0->1, CH141: 0->1, CH159: 1->0, CH181: 0->1, CH206: 1->0, CH319: 0->1;
DELTRAN: CH42: 0->1, CH100: 1->0, CH180: 1->0;
ACCTRAN: CH67: 2->1, CH68: 1->0, CH77: 2->1, CH120: 2->0, CH180: 1->0.

Staurotypus:
Unambiguous: CH38: 0->1, CH49: 1->0, CH81: 0->1, CH105: 0->1, CH139: 1->0, CH255: 0->1;
DELTRAN: CH42: 0->1, CH67: 1->2, CH68: 0->1, CH77: 1->2, CH100: 1->0, CH120: 0->2, CH122: 0->1;
ACCTRAN: CH312: 1->0.

total-group Dermatemydidae:
Unambiguous: CH34: 0->1, CH58: 0->2, CH79: 2->1, CH96: 1->0, CH156: 0->1, CH175: 1->0, CH176: 0->1, CH243: 1->0, CH246: 0->1;
DELTRAN: CH312: 0->1;
ACCTRAN: CH126: 1->0, CH253: 1->0.

Dermatemys mawii:
Unambiguous: CH64: 0->1, CH104: 1->0, CH115: 1->0, CH139: 1->0, CH254: 0->1, CH263: 0->1, CH280: 1->0;
DELTRAN: CH40: 0->1, CH122: 0->1, CH126: 1->0, CH183: 0->1, CH208: 0->1, CH253: 1->0;
ACCTRAN: CH59: 1->0, CH120: 2->0, CH188: 1->0, CH189: 1->0, CH265: 1->0, CH316: 1->0.

Baptemys wyomingensis:
Unambiguous: CH119: 0->1, CH142: 0->1, CH149: 1->0, CH154: 0->1, CH172: 0->1, CH184: 0->1, CH252: 0->1;
DELTRAN: CH59: 0->1, CH120: 0->2, CH180: 1->0, CH188: 0->1, CH189: 0->1, CH265: 0->1, CH316: 0->1;
ACCTRAN: CH40: 1->0, CH180: 1->0, CH183: 1->0, CH208: 1->0.

Testudinoidea:
Unambiguous: CH96: 1->0, CH123: 0->1, CH175: 1->0, CH254: 0->1, CH282: 0->1;
DELTRAN: CH149: 0->1, CH321: 0->1;
ACCTRAN: CH11: 1->0, CH22: 0->1, CH65: 0->2, CH79: 2->1, CH115: 1->0, CH176: 0->1, CH197: 0->1, CH272: 0->1, CH312: 0->1, CH318: 1->0, CH326: 0->1.

Emysternia:
Unambiguous: CH221: 1->0;

DELTRAN: CH116: 0->2, CH178: 0->1.

Emydidae:
Unambiguous: CH34: 0->1, CH104: 1->0, CH121: 0->1, CH154: 1->0;
DELTRAN: CH40: 0->1, CH197: 0->1, CH217: 1->0, CH290: 0->1, CH312: 0->1, CH326: 0->1;
ACCTRAN: CH217: 1->0.

Chrysemys picta:
Unambiguous: CH22: 1->0, CH38: 0->1, CH58: 0->2, CH68: 0->1, CH113: 0->1, CH120: 0->1, CH122: 0->1, CH126: 1->0, CH230: 1->0, CH246: 0->1, CH252: 0->1, CH253: 1->0, CH267: 0->1, CH283: 0->1;
DELTRAN: CH65: 0->2, CH115: 1->0, CH176: 0->1, CH272: 0->1;
ACCTRAN: CH11: 0->1, CH79: 1->2.

Emys orbicularis:
Unambiguous: CH28: 1->0, CH72: 1->0, CH91: 1->0, CH141: 0->1, CH144: 0->1, CH233: 0->1, CH240: 1->0, CH254: 1->0, CH265: 0->1;
DELTRAN: CH11: 1->0, CH79: 2->1;
ACCTRAN: CH65: 2->0, CH115: 0->1.

Platysternon megacephalum:
Unambiguous: CH16: 0->1, CH18: 2->0, CH23: 1->0, CH32: 0->1, CH35: 1->0, CH43: 0->1, CH52: 0->1, CH58: 0->1, CH65: 2->1, CH75: 1->0, CH77: 1->2, CH94: 1->0, CH100: 1->0, CH101: 0->1, CH109: 0->1, CH124: 0->1, CH125: 0->1, CH138: 0->2, CH139: 1->0, CH142: 0->1, CH159: 1->0, CH163: 0->1, CH180: 1->0, CH181: 0->1, CH184: 0->1, CH200: 1->0, CH206: 0->1, CH247: 0->1, CH253: 1->2, CH275: 1->0, CH298: 1->2, CH299: 1->0, CH323: 1->0;
DELTRAN: CH11: 1->0, CH79: 2->1, CH115: 1->0;
ACCTRAN: CH40: 1->0, CH176: 1->0, CH197: 1->0, CH272: 1->0, CH290: 1->0, CH312: 1->0, CH326: 1->0.

Testuguria:
Unambiguous: CH66: 0->1, CH72: 1->0, CH155: 0->1, CH179: 1->0, CH230: 1->0, CH245: 1->0, CH246: 0->1, CH267: 0->1;
DELTRAN: CH65: 0->2, CH197: 0->1, CH272: 0->1, CH290: 0->1, CH312: 0->1, CH326: 0->1;
ACCTRAN: CH17: 0->1, CH178: 1->0, CH252: 0->1.

Geoclemys hamiltonii:
Unambiguous: CH26: 0->1, CH42: 0->1, CH67: 0->1, CH68: 0->1, CH120: 0->3, CH121: 0->1, CH188: 0->1, CH189: 0->1, CH206: 0->1, CH265: 0->1;
DELTRAN: CH11: 1->0, CH17: 0->1, CH40: 0->1, CH115: 1->0, CH116: 0->2, CH176: 0->1, CH252: 0->1;
ACCTRAN: CH79: 1->2.

Testudinidae:
Unambiguous: CH27: 1->0, CH34: 0->1, CH58: 0->2, CH76: 2->1, CH77: 1->2, CH141: 0->1, CH154: 1->0, CH200: 1->0, CH248: 1->0, CH253: 1->0;
DELTRAN: CH79: 2->1;
ACCTRAN: CH11: 0->1, CH95: 1->0, CH104: 1->0, CH105: 0->1, CH115: 0->1, CH116: 2->0, CH131: 0->2, CH213: 0->1, CH323: 1->0, CH336: 1->0, CH341: 0->1.

(*Testudo* + *Chelonoidis*):
Unambiguous: CH75: 1->0, CH180: 1->0;
DELTRAN: CH17: 0->1;
ACCTRAN: CH176: 1->0, CH252: 1->0.

Testudo:
Unambiguous: CH42: 0->1, CH66: 1->0, CH100: 1->0, CH113: 0->1, CH121: 0->1, CH183: 0->1;
DELTRAN: CH40: 0->1, CH104: 1->0, CH213: 0->1, CH336: 1->0, CH341: 0->1;
ACCTRAN: CH95: 0->1, CH131: 2->0, CH323: 0->1.

Chelonoidis sp.:
Unambiguous: CH13: 0->1, CH161: 0->1, CH197: 1->0, CH206: 0->1, CH221: 1->0, CH230: 0->1, CH245: 0->1, CH246: 1->0, CH247: 0->1, CH253: 0->2, CH267: 1->0, CH272: 1->0, CH275: 1->0, CH290: 1->0, CH298: 1->2, CH299: 1->0, CH312: 1->0, CH326: 1->0;
DELTRAN: CH95: 1->0, CH105: 0->1, CH131: 0->2, CH323: 1->0;
ACCTRAN: CH40: 1->0, CH104: 0->1, CH213: 1->0, CH336: 0->1, CH341: 1->0.

Gopherus polyphemus:
Unambiguous: CH21: 1->2, CH22: 1->0, CH54: 0->1, CH71: 0->1, CH102: 0->1, CH124: 0->1, CH126: 1->0, CH139: 1->0;
DELTRAN: CH95: 1->0, CH104: 1->0, CH131: 0->2, CH176: 0->1, CH213: 0->1, CH252: 0->1, CH323: 1->0, CH336: 1->0, CH341: 0->1;
ACCTRAN: CH17: 1->0.

Trionychia:
Unambiguous: CH17: 0->1, CH21: 1->2, CH24: 0->1, CH38: 0->1, CH48: 0->1, CH49: 1->0, CH54: 0->1, CH64: 0->1, CH71: 0->1, CH77: 1->2, CH94: 1->2, CH103: 0->1, CH112: 0->1, CH113: 0->1, CH125: 0->1, CH190: 0->1, CH256: 0->1, CH280: 1->0;
DELTRAN: CH6: 0->1, CH22: 1->0, CH62: 0->1, CH98: 0->1, CH132: 0->1, CH191: 0->2, CH219: 0->1, CH318: 0->1;
ACCTRAN: CH181: 0->1, CH184: 0->1, CH187: 0->1, CH191: 1->2, CH205: 1->0, CH248: 1->2, CH317: 0->1, CH339: 0->1.

Trionychidae:
Unambiguous: CH26: 0->1, CH30: 0->1, CH42: 0->1, CH50: 0->1, CH51: 0->1, CH60: 0->1, CH65: 0->2, CH80: 0->1, CH104: 1->0, CH148: 1->0, CH186: 0->1, CH204: 0->1, CH216: 0->1, CH231: 0->1, CH232: 0->1, CH242: 1->4, CH243: 0->1, CH247: 0->1, CH279: 1->2, CH324: 0->1, CH326: 0->1, CH343: 0->1;
DELTRAN: CH116: 0->1, CH339: 0->1;
ACCTRAN: CH13: 0->1, CH40: 1->0, CH116: 2->1, CH178: 1->0.

Trionychinae:
DELTRAN: CH181: 0->1, CH184: 0->1;
ACCTRAN: CH163: 0->1, CH317: 1->0.

Apalone spinifera:
Unambiguous: CH58: 0->1, CH95: 1->0;
DELTRAN: CH163: 0->1.

Pelodiscus sinensis:
Unambiguous: CH122: 0->1.

Lissemys punctata:
Unambiguous: CH29: 1->0, CH69: 1->0, CH100: 1->0, CH103: 1->2, CH164: 1->0;
DELTRAN: CH317: 0->1;
ACCTRAN: CH181: 1->0, CH184: 1->0.

total-group Carettochelyidae:
Unambiguous: CH85: 0->1, CH119: 0->1, CH120: 0->3, CH124: 0->1, CH137: 0->1;

DELTRAN: CH40: 0->1, CH116: 0->2;
ACCTRAN: CH32: 0->1, CH58: 0->1, CH66: 0->1, CH76: 2->0, CH175: 1->0, CH176: 0->1, CH193: 1->0, CH323: 1->0, CH339: 1->2, CH340: 1->2.

Carettochelys insculpta:
DELTRAN: CH13: 1->0, CH32: 0->1, CH58: 0->1, CH66: 0->1, CH76: 2->0, CH175: 1->0, CH176: 0->1, CH178: 0->1, CH181: 0->1, CH184: 0->1, CH187: 0->1, CH193: 1->0, CH205: 1->0, CH217: 1->0, CH248: 1->2, CH317: 0->1, CH323: 1->0, CH339: 0->2, CH340: 1->2.

Allaeochelys libyca:
Unambiguous: CH109: 0->1, CH126: 1->0;
DELTRAN: CH76: 2->1;
ACCTRAN: CH76: 0->1.

Pleurodira:
Unambiguous: CH5: 0->1, CH41: 0->1, CH70: 0->1, CH79: 2->0, CH87: 0->1, CH91: 1->0, CH92: 0->1, CH96: 1->0, CH104: 1->0, CH106: 1->2, CH107: 2->0, CH197: 0->1, CH246: 0->1, CH254: 0->1, CH258: 0->1, CH274: 1->0, CH277: 0->1, CH281: 2->0, CH311: 0->1;
DELTRAN: CH6: 0->1, CH40: 0->1, CH127: 1->2, CH132: 0->1, CH191: 0->3, CH217: 1->0;
ACCTRAN: CH2: 0->1, CH73: 0->1, CH77: 1->3, CH123: 0->2, CH127: 0->2, CH151: 0->1, CH153: 1->0, CH154: 1->0, CH158: 0->1, CH178: 1->0, CH191: 1->3, CH304: 0->1.

total-group Chelidae:
Unambiguous: CH7: 0->1, CH23: 1->0, CH72: 1->0, CH172: 0->1, CH180: 1->0, CH190: 0->1, CH289: 0->1;
DELTRAN: CH123: 0->2, CH151: 0->1, CH154: 1->0, CH158: 0->1;
ACCTRAN: CH110: 1->0, CH120: 0->1, CH163: 0->1.

crown-group Chelidae:
Unambiguous: CH4: 1->0, CH31: 0->1, CH34: 1->2, CH185: 1->0, CH281: 0->3, CH282: 0->1;
DELTRAN: CH2: 0->1, CH77: 1->3, CH230: 1->0, CH235: 0->1, CH304: 0->1;
ACCTRAN: CH1: 1->0, CH15: 1->0, CH62: 1->0, CH73: 1->0, CH95: 1->0, CH114: 0->1, CH117: 0->2, CH182: 0->1, CH219: 1->0, CH235: 0->1.

Chelinae:
DELTRAN: CH15: 1->0, CH110: 1->0, CH114: 0->1, CH116: 0->3, CH117: 0->2, CH120: 0->1, CH163: 1->0;
ACCTRAN: CH116: 2->3, CH163: 1->0.

Chelus fimbriatus:
Unambiguous: CH6: 1->0, CH22: 1->0, CH48: 0->1, CH128: 1->0, CH148: 1->0, CH159: 1->0, CH188: 0->1, CH189: 0->1, CH200: 1->0, CH208: 1->0, CH221: 1->0, CH260: 0->2, CH262: 0->1, CH265: 0->1, CH275: 0->1, CH276: 0->1;
DELTRAN: CH252: 0->3, CH253: 0->1;
ACCTRAN: CH1: 0->1, CH153: 0->1, CH252: 1->3.

Phrynops geoffranus:
Unambiguous: CH24: 0->1, CH103: 0->1, CH141: 0->1, CH190: 1->0, CH203: 0->1, CH289: 1->0;
DELTRAN: CH1: 1->0, CH153: 1->0, CH182: 0->1, CH252: 0->1;
ACCTRAN: CH253: 1->0.

Chelodininae:
Unambiguous: CH201: 0->1, CH207: 0->1, CH209: 0->1;
DELTRAN: CH1: 1->0, CH116: 0->2;

ACCTRAN: CH120: 1->0, CH324: 0->1.

Elseya dentata:
Unambiguous: CH16: 0->1, CH18: 2->0, CH23: 0->1, CH24: 0->1, CH58: 0->2, CH60: 0->1, CH172: 1->0, CH174: 0->1, CH175: 1->0, CH183: 0->1, CH248: 1->0;
DELTRAN: CH15: 1->0, CH182: 0->1, CH219: 0->1, CH252: 0->1;
ACCTRAN: CH110: 0->1, CH114: 1->0, CH117: 2->0, CH153: 0->1, CH219: 0->1, CH253: 1->0.

Chelodina:
Unambiguous: CH12: 0->1, CH82: 0->1, CH103: 0->1, CH128: 1->0, CH179: 1->0, CH260: 0->1;
DELTRAN: CH110: 1->0, CH114: 0->1, CH117: 0->2, CH153: 1->0, CH253: 0->1, CH324: 0->1;
ACCTRAN: CH15: 0->1, CH182: 1->0, CH252: 1->0.

Araripemys barretoi:
Unambiguous: CH38: 0->1, CH94: 1->2, CH115: 1->0, CH179: 1->0, CH188: 0->1, CH189: 0->1, CH191: 3->4, CH206: 1->0, CH210: 0->2, CH227: 0->1, CH231: 0->1, CH232: 0->1, CH243: 0->1, CH259: 0->1, CH269: 0->1;
DELTRAN: CH62: 0->1, CH73: 0->1, CH95: 0->1, CH120: 0->1, CH153: 1->0, CH219: 0->1, CH253: 0->1;
ACCTRAN: CH77: 3->1, CH116: 2->0, CH230: 0->1, CH252: 1->0.

Pelomedusoides:
Unambiguous: CH21: 1->2, CH54: 0->1, CH58: 0->2, CH61: 1->2, CH82: 0->1, CH175: 1->0, CH249: 1->0;
DELTRAN: CH62: 0->1, CH73: 0->1, CH77: 1->3, CH163: 1->0, CH219: 0->1, CH230: 1->0, CH251: 0->1, CH252: 0->1;
ACCTRAN: CH253: 1->0.

Podocnemis:
Unambiguous: CH18: 2->0, CH24: 0->1, CH30: 0->1, CH42: 0->1, CH55: 0->1, CH97: 0->1, CH115: 1->0, CH148: 1->0, CH265: 0->1, CH324: 0->1;
DELTRAN: CH95: 0->1, CH116: 0->2, CH153: 1->0, CH304: 0->1;
ACCTRAN: CH123: 2->0, CH151: 1->0, CH154: 0->1, CH158: 1->0.

Pelomedusa subrufa:
Unambiguous: CH22: 1->0, CH38: 0->1, CH103: 0->1, CH124: 0->1, CH141: 0->1, CH143: 1->0;
DELTRAN: CH123: 0->2, CH151: 0->1, CH154: 1->0, CH158: 0->1;
ACCTRAN: CH95: 1->0, CH116: 2->0, CH153: 0->1, CH304: 1->0.

Angolachelonia:
Unambiguous: CH18: 2->0, CH83: 0->1, CH84: 0->1, CH94: 1->0, CH103: 0->1, CH181: 0->1, CH182: 0->1, CH184: 0->1;
ACCTRAN: CH49: 1->0, CH56: 0->1, CH67: 0->2, CH120: 0->1, CH139: 1->2, CH173: 0->1, CH209: 0->1, CH219: 1->0, CH231: 0->1.

Thalassochelydia:
Unambiguous: CH81: 0->1, CH113: 0->1, CH142: 0->1, CH185: 1->0, CH210: 0->2, CH211: 0->1, CH224: 1->0, CH278: 1->0;
DELTRAN: CH209: 0->1, CH231: 0->1;
ACCTRAN: CH40: 1->0, CH127: 0->1, CH132: 1->0, CH221: 1->0, CH287: 1->0, CH292: 2->0.

Solnhofia parsoni:

Unambiguous: CH17: 0->1, CH60: 0->1, CH64: 0->1, CH90: 1->2, CH95: 0->1, CH96: 1->0, CH100: 1->0, CH107: 2->1, CH109: 1->0, CH115: 1->0, CH116: 0->2, CH119: 0->1, CH126: 1->0, CH174: 0->1, CH217: 1->2, CH243: 0->1;
DELTRAN: CH49: 1->0, CH56: 0->1, CH62: 0->1, CH67: 0->2, CH98: 0->1, CH120: 0->1, CH173: 0->1, CH178: 0->1;
ACCTRAN: CH139: 2->1, CH230: 0->1, CH252: 1->0.

(*Portlandemys* ++ *Plesiochelys*):
Unambiguous: CH4: 1->0, CH27: 1->0, CH39: 0->1, CH58: 0->1, CH152: 1->0, CH175: 1->0, CH180: 1->0;
DELTRAN: CH132: 0->2, CH139: 1->2;
ACCTRAN: CH7: 0->1, CH49: 0->1, CH56: 1->0, CH67: 2->0, CH98: 1->0, CH120: 1->0, CH128: 1->0, CH131: 0->1, CH132: 0->2, CH173: 1->0, CH220: 1->0, CH246: 0->1.

(*Jurassichelon* ++ *Plesiochelys*):
Unambiguous: CH93: 0->1, CH99: 0->1, CH155: 0->1;
DELTRAN: CH246: 0->1;
ACCTRAN: CH18: 0->1.

Jurassichelon oleronensis:
Unambiguous: CH75: 0->1, CH81: 1->0, CH94: 0->1, CH110: 1->0, CH147: 2->1;
DELTRAN: CH7: 0->1, CH18: 0->1, CH62: 0->1, CH128: 1->0, CH131: 0->1, CH287: 1->0, CH292: 0->1;
ACCTRAN: CH292: 0->1.

(*Plesiochelys etalloni* + *Plesiochelys planiceps*):
Unambiguous: CH90: 1->2, CH96: 1->0, CH122: 1->0, CH140: 0->1;
ACCTRAN: CH7: 1->0, CH44: 0->1, CH116: 0->2, CH128: 0->1, CH131: 1->0, CH268: 0->1.

Plesiochelys planiceps:
Unambiguous: CH34: 1->2, CH107: 2->1;
DELTRAN: CH62: 0->1, CH116: 0->2, CH178: 0->1.

Plesiochelys etalloni:
Unambiguous: CH4: 0->1, CH104: 1->0, CH109: 1->0, CH143: 1->0;
DELTRAN: CH44: 0->1, CH220: 1->0, CH221: 1->0, CH230: 1->0, CH252: 0->1, CH268: 0->1;
ACCTRAN: CH62: 1->0, CH178: 1->0.

Portlandemys mcdowelli:
Unambiguous: CH181: 1->0;
DELTRAN: CH7: 0->1, CH128: 1->0, CH131: 0->1;
ACCTRAN: CH62: 1->0.

Sandownidae:
Unambiguous: CH34: 1->0, CH57: 0->1, CH68: 0->1, CH108: 0->1;
DELTRAN: CH56: 0->1, CH67: 0->2, CH98: 0->1, CH132: 0->1, CH173: 0->1;
ACCTRAN: CH2: 0->1, CH16: 0->1, CH62: 1->0, CH105: 0->1, CH275: 0->1.

(*Sandownia* + *Leyvachelys*):
Unambiguous: CH7: 0->1, CH21: 1->2, CH77: 1->2, CH115: 1->0;
DELTRAN: CH139: 1->0;
ACCTRAN: CH116: 0->1, CH139: 2->0.

Sandownia harrisi:
Unambiguous: CH54: 0->1, CH55: 0->1, CH95: 0->1, CH110: 1->0, CH147: 2->1;

DELTRAN: CH2: 0->1, CH49: 1->0, CH116: 0->1, CH127: 1->0;
ACCTRAN: CH16: 1->0, CH105: 1->0.

Leyvachelys cipadi:
Unambiguous: CH3: 1->0, CH27: 1->0, CH141: 0->1, CH142: 0->1;
DELTRAN: CH16: 0->1, CH40: 0->1, CH62: 0->1, CH105: 0->1, CH120: 0->1, CH230: 1->0, CH252: 0->1, CH275: 0->1, CH292: 0->2;
ACCTRAN: CH2: 1->0, CH49: 0->1, CH62: 0->1.

Brachyopsemys tingitana:
Unambiguous: CH48: 0->1, CH64: 0->1, CH71: 0->1, CH161: 0->1, CH163: 1->0;
DELTRAN: CH2: 0->1, CH16: 0->1, CH49: 1->0, CH105: 0->1, CH139: 1->2.

Sinemydidae/Macrobaenidae:
Unambiguous: CH113: 0->1, CH134: 0->1, CH242: 1->2, CH243: 0->1;
DELTRAN: CH235: 0->1;
ACCTRAN: CH40: 1->0, CH122: 1->0, CH131: 0->2, CH179: 1->0, CH227: 0->1, CH259: 0->1, CH275: 0->1.

(*Ordosemys* ++ *Kirgizemys*):
Unambiguous: CH18: 2->1, CH38: 0->1, CH276: 0->1;
DELTRAN: CH275: 0->1.

(*Ordosemys* + *Dracochelys*):
Unambiguous: CH81: 0->1, CH116: 0->2;
ACCTRAN: CH115: 1->0, CH152: 1->0, CH192: 0->1, CH210: 0->1, CH215: 0->1, CH221: 1->0, CH231: 0->1, CH280: 1->0.

Ordosemys sp. IVPP V12092:
Unambiguous: CH80: 0->1, CH83: 0->1, CH99: 0->2;
DELTRAN: CH115: 1->0, CH152: 1->0;
ACCTRAN: CH4: 1->0.

Dracochelys bicuspis:
Unambiguous: CH53: 0->1, CH58: 0->1, CH65: 2->0, CH134: 1->0, CH146: 1->0;
DELTRAN: CH4: 0->1, CH192: 0->1, CH210: 0->1, CH215: 0->1, CH219: 0->1, CH221: 1->0, CH227: 0->1, CH231: 0->1, CH280: 1->0.

(*Judithemys* ++ *Kirgizemys*):
Unambiguous: CH109: 1->0, CH292: 0->2;
DELTRAN: CH4: 0->1, CH259: 0->1;
ACCTRAN: CH219: 1->0, CH227: 1->0, CH288: 0->1, CH290: 0->1.

Judithemys sukhanovi:
Unambiguous: CH75: 0->1, CH90: 1->2, CH271: 1->0;
DELTRAN: CH290: 0->1.

(*Kirgizemys hoburensis* + *Kirgizemys dmitrievi*):
Unambiguous: CH34: 1->2, CH149: 0->1;
ACCTRAN: CH96: 1->0, CH107: 2->1, CH154: 1->0, CH203: 0->1.

Kirgizemys hoburensis:
Unambiguous: CH40: 0->1, CH163: 1->0;
DELTRAN: CH107: 2->1, CH122: 1->0, CH154: 1->0, CH203: 0->1, CH288: 0->1.

Kirgizemys dmitrievi:
Unambiguous: CH13: 1->0, CH58: 0->1, CH61: 1->0, CH65: 2->1, CH79: 1->2, CH140: 0->1, CH161: 0->1;
DELTRAN: CH96: 1->0.

(*Sinemys lens* + *Sinemys gamera*):
Unambiguous: CH7: 0->1, CH15: 0->1, CH34: 1->2, CH77: 1->2, CH91: 1->0, CH96: 1->0, CH210: 0->2, CH244: 1->0;
DELTRAN: CH131: 0->2;
ACCTRAN: CH4: 1->0, CH24: 0->1, CH35: 0->1, CH73: 0->1, CH190: 0->1, CH255: 0->1.

Sinemys gamera:
Unambiguous: CH2: 0->1;
DELTRAN: CH24: 0->1, CH35: 0->1, CH73: 0->1, CH190: 0->1.

Sinemys lens:
Unambiguous: CH107: 2->1;
DELTRAN: CH219: 0->1, CH227: 0->1, CH255: 0->1.

Xinjiangchelyidae:
Unambiguous: CH38: 0->1, CH91: 1->0, CH125: 0->1, CH203: 0->1, CH257: 0->1, CH270: 0->1;
DELTRAN: CH179: 0->1, CH235: 0->1;
ACCTRAN: CH34: 1->2, CH107: 2->1, CH152: 1->0, CH226: 0->1, CH294: 1->0, CH340: 1->0.

Annemys levensis:
Unambiguous: CH136: 0->1, CH208: 0->1, CH225: 1->0;
DELTRAN: CH4: 0->1, CH34: 1->2, CH107: 2->1, CH226: 0->1;
ACCTRAN: CH175: 1->0.

(*Annemys latiens* ++ *Xinjiangchelys*):
Unambiguous: CH7: 0->1, CH145: 1->0;
ACCTRAN: CH4: 1->0, CH116: 0->2.

Annemys latiens:
Unambiguous: CH88: 1->0, CH121: 0->1;
DELTRAN: CH226: 0->1.

(*Annemys* sp. ++ *Xinjiangchelys*):
Unambiguous: CH2: 0->1;
DELTRAN: CH116: 0->2;
ACCTRAN: CH226: 1->0.

Annemys sp. IVPP V18106:
Unambiguous: CH81: 0->1, CH96: 1->0, CH131: 0->1, CH143: 1->0, CH155: 0->1;
DELTRAN: CH34: 1->2, CH40: 0->1, CH107: 2->1, CH152: 1->0.

(*Xinjiangchelys wusu* + *Xinjiangchelys radiplactoides*):
Unambiguous: CH75: 0->1, CH76: 2->1;
ACCTRAN: CH34: 2->1, CH62: 0->1, CH107: 1->2, CH123: 1->0, CH139: 1->2.

Xinjiangchelys wusu:
Unambiguous: CH257: 1->0;
ACCTRAN: CH152: 0->1.

Xinjiangchelys radiplicatoides:
Unambiguous: CH91: 0->1; CH109: 1->0, CH185: 0->1;
DELTRAN: CH62: 0->1, CH123: 1->0, CH139: 1->2, CH152: 1->0, CH175: 0->1;
Unambiguous: CH94: 1->2.

Paracryptodira:
Unambiguous: CH7: 0->1, CH43: 0->1, CH145: 1->2;
ACCTRAN: CH2: 0->1, CH24: 0->1, CH28: 0->1, CH58: 0->1, CH65: 2->0, CH72: 1->0, CH147: 1->0, CH190: 0->1, CH230: 1->0, CH246: 0->1, CH249: 1->0, CH251: 1->0, CH252: 0->1, CH277: 0->1, CH304: 0->1;
DELTRAN: CH24: 0->1.

(*Eubaena* ++ *Pleurosternon*):
Unambiguous: CH116: 0->2, CH131: 0->1, CH137: 0->1;
DELTRAN: CH28: 0->1;
ACCTRAN: CH69: 0->1, CH128: 0->1, CH133: 0->1.

Eubaena cephalica:
Unambiguous: CH7: 1->2, CH11: 1->0, CH15: 0->1, CH75: 0->1, CH87: 0->1, CH90: 1->2, CH129: 0->1, CH162: 0->1;
DELTRAN: CH69: 0->1;
ACCTRAN: CH2: 1->0, CH65: 0->2.

Pleurosternidae:
Unambiguous: CH3: 0->1, CH18: 2->0, CH76: 2->1, CH94: 1->2, CH107: 2->1, CH132: 0->1;
DELTRAN: CH2: 0->1, CH65: 2->0, CH190: 0->1, CH230: 1->0, CH248: 0->1, CH252: 0->1;
ACCTRAN: CH17: 0->1, CH80: 0->1, CH120: 2->0.

Pleurosternon bullockii:
Unambiguous: CH35: 0->1, CH58: 1->0, CH131: 1->2, CH191: 0->3, CH217: 1->0, CH219: 0->1, CH258: 0->1;
DELTRAN: CH17: 0->1, CH22: 0->1, CH80: 0->1, CH128: 0->1, CH133: 0->1.

Glyptops plicatulus:
DELTRAN: CH120: 2->0, CH246: 0->1, CH277: 0->1, CH294: 0->1, CH304: 0->1.

Arundelemys dardeni:
Unambiguous: CH105: 0->1, CH122: 1->0, CH125: 0->1;
DELTRAN: CH2: 0->1, CH65: 2->0;
ACCTRAN: CH22: 1->0.

Meiolania planiceps:
Unambiguous: CH25: 1->0, CH33: 0->1, CH36: 0->1, CH37: 0->1, CH58: 0->2, CH66: 0->1, CH75: 0->1, CH76: 2->0, CH77: 1->3, CH78: 0->1, CH90: 1->2, CH104: 1->0, CH111: 0->1, CH139: 1->0, CH142: 1->0, CH159: 1->0, CH161: 0->1, CH182: 0->1, CH221: 1->0, CH231: 0->1, CH278: 0->1, CH300: 0->1;
DELTRAN: CH72: 0->1, CH121: 0->1, CH147: 0->1, CH149: 0->1, CH155: 0->1, CH166: 0->1, CH170: 0->1, CH248: 0->1, CH249: 0->1, CH274: 0->1, CH297: 0->2, CH340: 0->1;
ACCTRAN: CH11: 1->0, CH149: 0->1, CH155: 0->1, CH166: 0->1, CH170: 0->1, CH242: 1->0, CH274: 0->1, CH296: 1->0, CH297: 1->2.

Kallokibotion bajazidi:
Unambiguous: CH60: 0->1, CH79: 1->2, CH117: 0->1, CH129: 0->1, CH144: 0->1, CH146: 0->1, CH175: 0->1, CH218: 0->1, CH253: 0->2, CH305: 0->1;
DELTRAN: CH11: 0->1, CH121: 0->1, CH242: 0->1, CH251: 0->1.

Chubutemys copelloi:
Unambiguous: CH4: 0->1, CH27: 1->0, CH29: 1->0, CH62: 0->1, CH95: 0->1, CH277: 0->1;
DELTRAN: CH58: 1->0;
ACCTRAN: CH11: 1->0.

(*Eileanchelys* + *Kayentachelys*):
Unambiguous: CH7: 0->1, CH28: 0->1, CH47: 0->1, CH109: 0->1, CH172: 0->1;
DELTRAN: CH11: 0->1, CH132: 0->1;
ACCTRAN: CH89: 1->0, CH134: 0->1, CH155: 0->1, CH206: 0->1.

Eileanchelys waldmanni:
Unambiguous: CH203: 0->1;
DELTRAN: CH20: 0->1, CH155: 0->1, CH165: 0->1, CH202: 0->1, CH239: 0->1.

Kayentachelys aprix:
Unambiguous: CH84: 0->1, CH130: 2->1, CH214: 1->0, CH217: 1->0;
DELTRAN: CH24: 0->1, CH76: 0->1, CH134: 0->1, CH140: 0->1, CH206: 0->1, CH296: 0->1;
ACCTRAN: CH20: 1->0, CH165: 1->0, CH202: 1->0, CH239: 1->0.

Australochelys africanus:
Unambiguous: CH129: 0->1;
DELTRAN: CH24: 0->1, CH74: 0->1, CH89: 0->1, CH132: 0->1, CH140: 0->1.

Proganochelys quenstedti:
DELTRAN: CH42: 0->1, CH69: 0->1, CH161: 0->1, CH208: 0->1, CH262: 0->1, CH274: 0->1;
ACCTRAN: CH42: 0->1, CH69: 0->1, CH161: 0->1, CH208: 0->1, CH262: 0->1, CH274: 0->1.

S1.6. Analysis of reduced dataset (marine characters omitted)

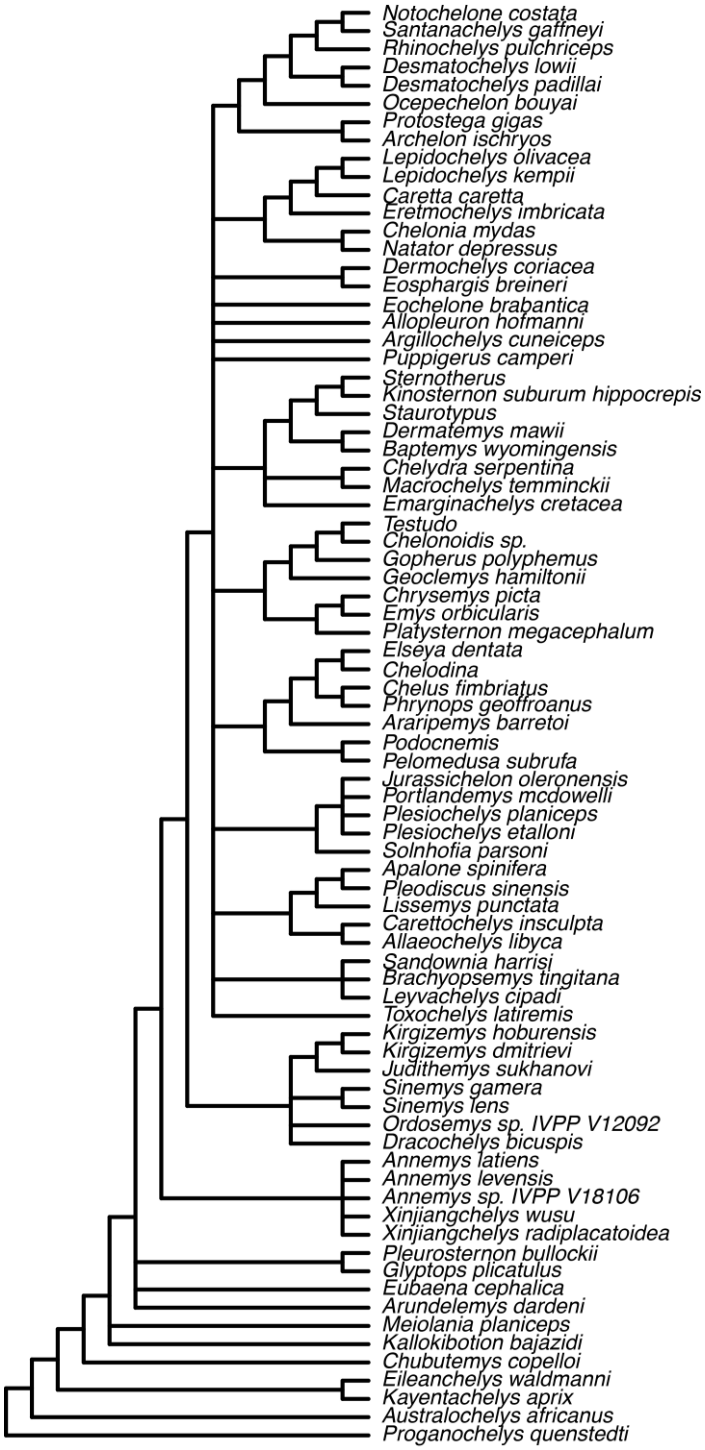


FIG S1.76. Strict consensus tree from 104 MPTs 1480 steps long resulting from analysing a dataset from which characters optimised as synapomorphies that support chelonioid relationships for protostegids and which are plausibly linked to a marine lifestyle (chs 39, 58, 68, 210, 231, 333, 337, 338, 342) have been deleted. Note that protostegids are still recovered as chelonioids.

S1.7. 'Least specialised taxa analyses'

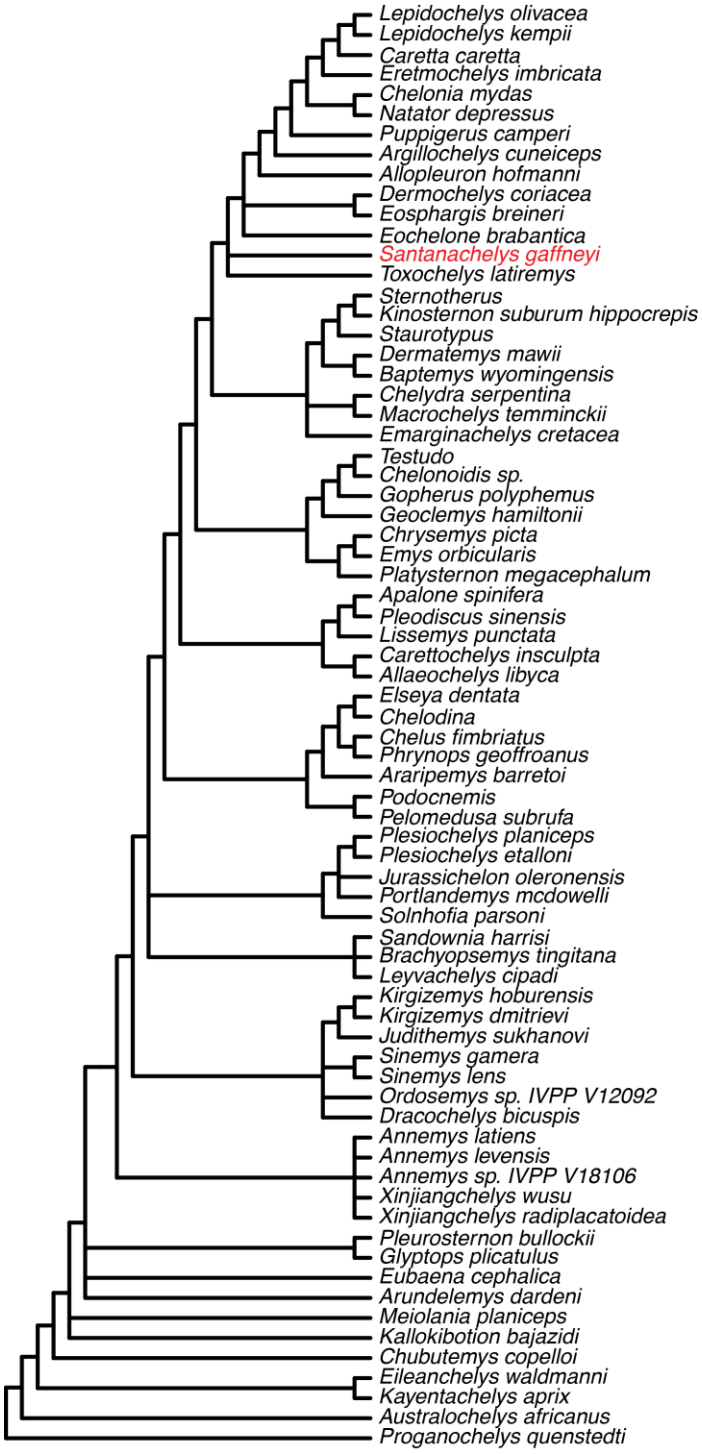


FIG S1.77. 'Least specialised taxa analysis 1'. Strict consensus tree from 120 MPTs 1443 steps long resulting from analysing a dataset from which all protostegids but *Santanachelys gaffneyi* were deleted. Note that protostegids are recovered as stem-group chelonioids.

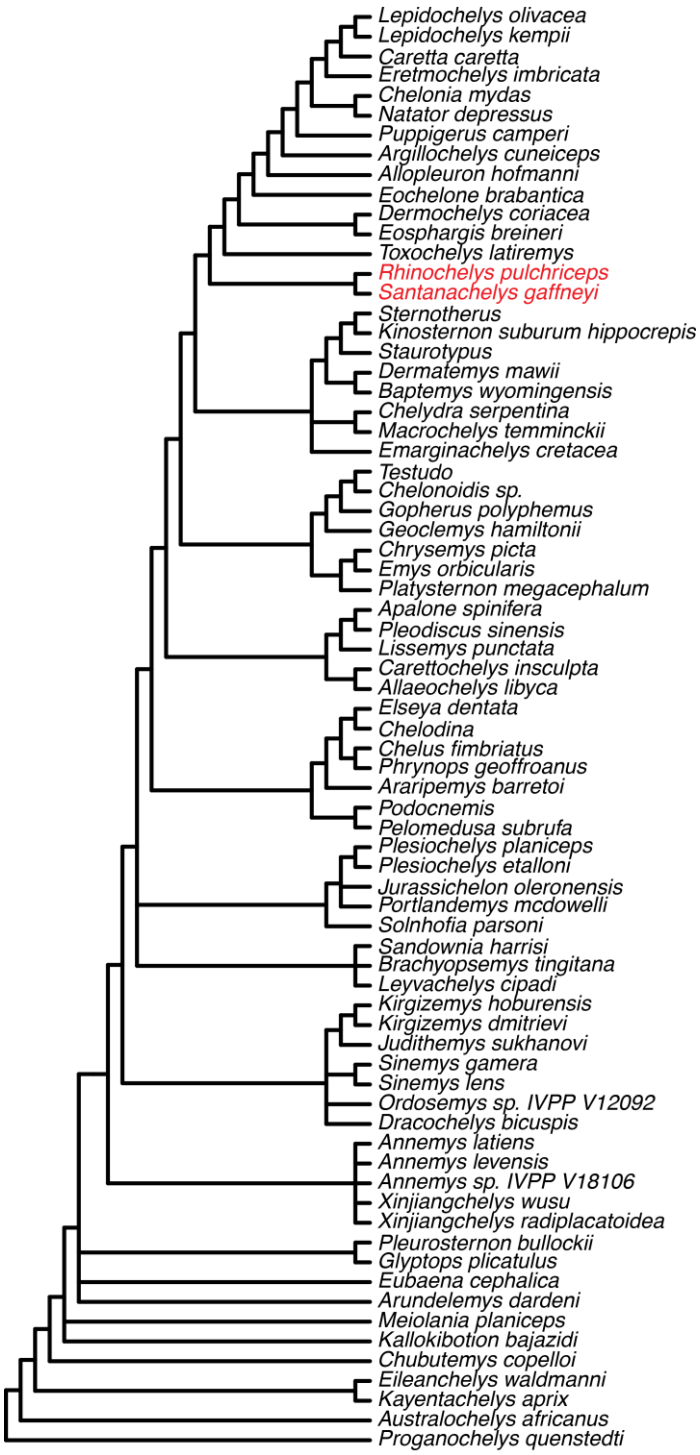


FIG S1.78. 'Least specialised taxa analysis 2'. Strict consensus tree from 42 MPTs 1453 steps long resulting from analysing a dataset from which all protostegids but *Santanachelys gaffneyi* and *Rhinochelys pulchriceps* were deleted. Note that protostegids are recovered as stem-group chelonioids.

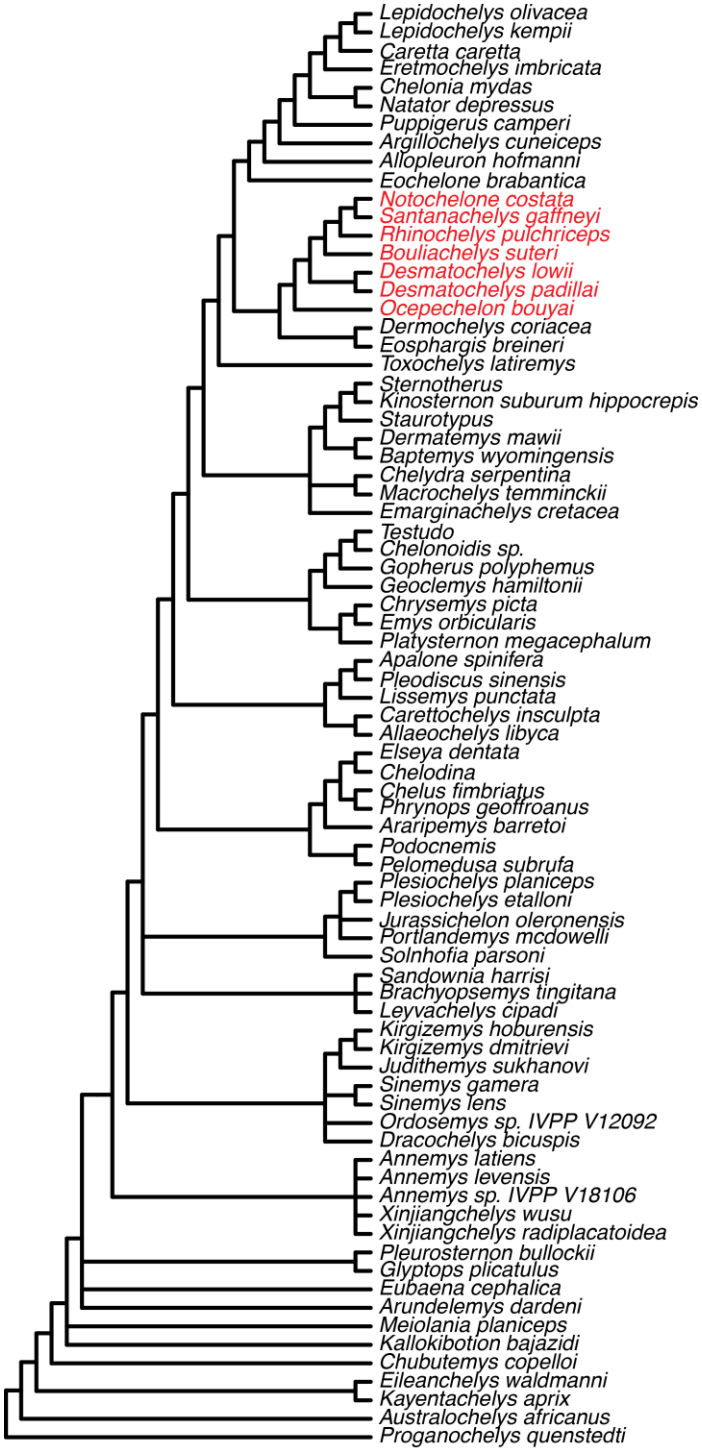


FIG S1.79. 'Least specialised taxa analysis 1'. Strict consensus tree from 12 MPTs 1510 steps long resulting from analysing a dataset from which the 'advanced' protostegids *Protostega gigas* and *Archelon ischryos* were deleted. Note that protostegids are recovered as crown-group chelonioids.

S.1.8. Topologies of constraint analyses

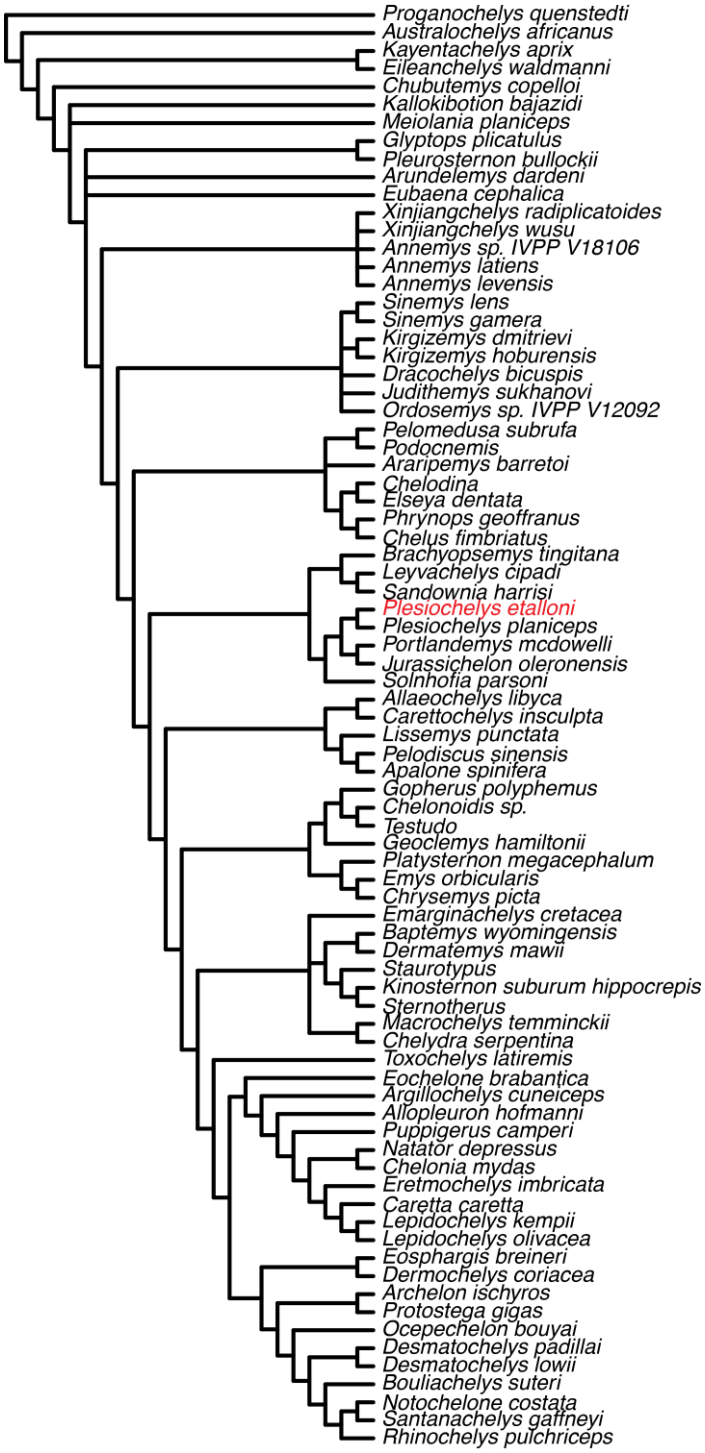


FIG S1.80. Strict consensus tree of constraint analysis 1, forcing *Plesiochelys etalloni* to be a stem-group cryptodire.

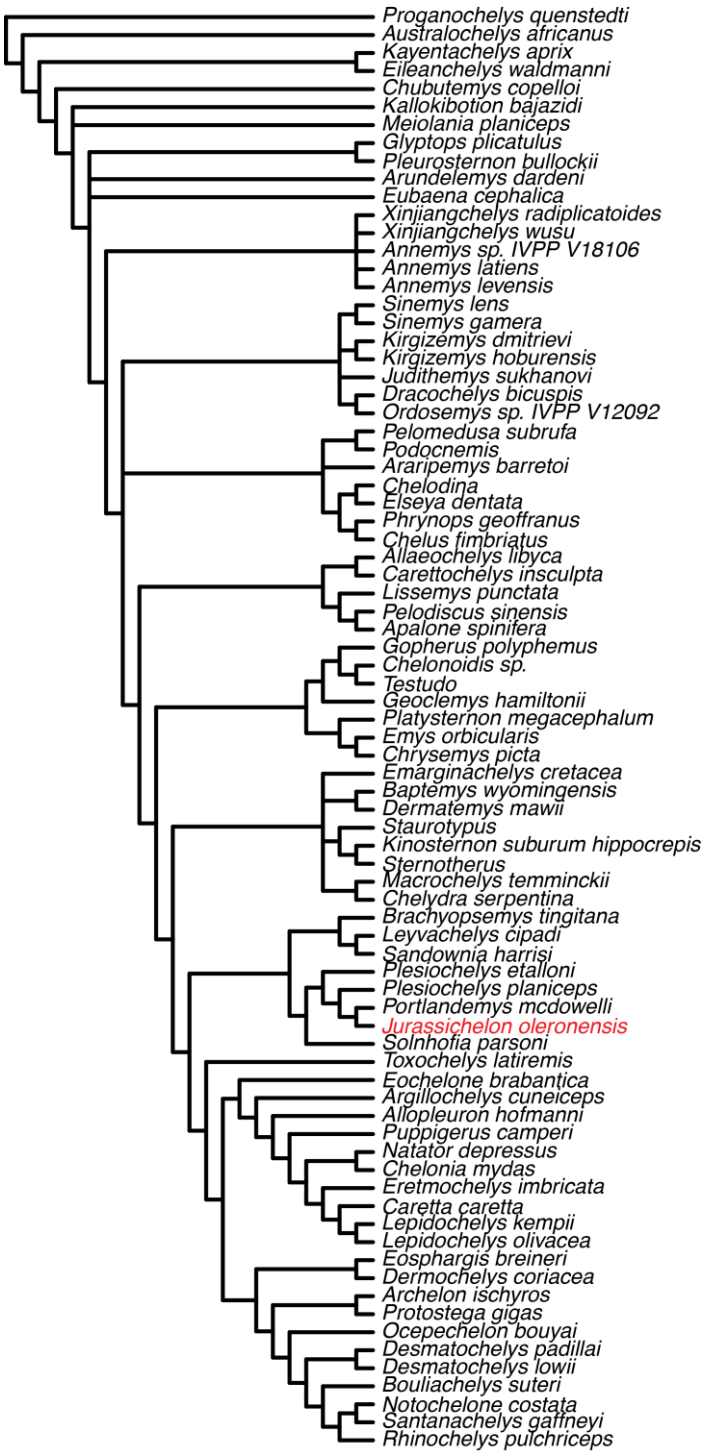


FIG S1.81. Strict consensus tree of constraint analysis 2, forcing *Jurassichelon oleronensis* to be a stem-group chelonioid.

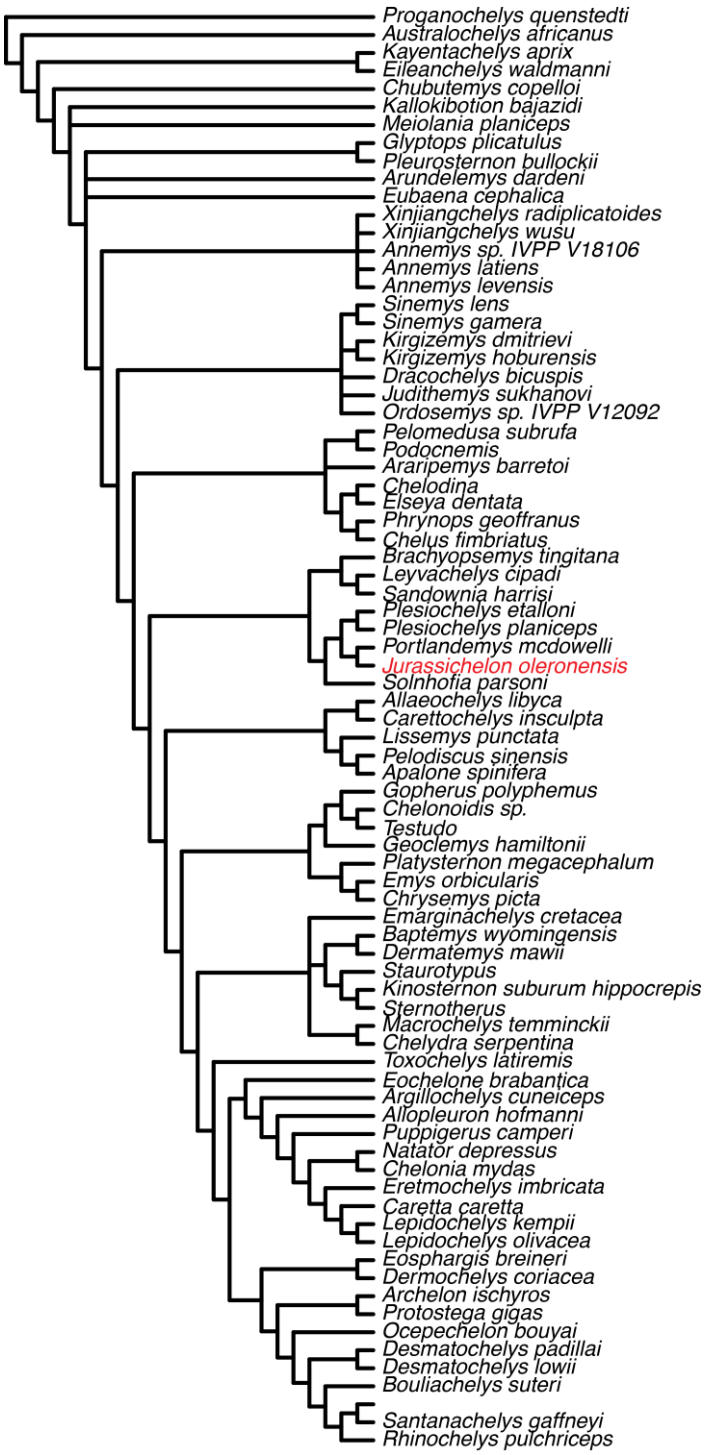


FIG S1.82. Strict consensus tree of constraint analysis 3, forcing *Jurassichelon oleronensis* to be a stem-group cryptodire.

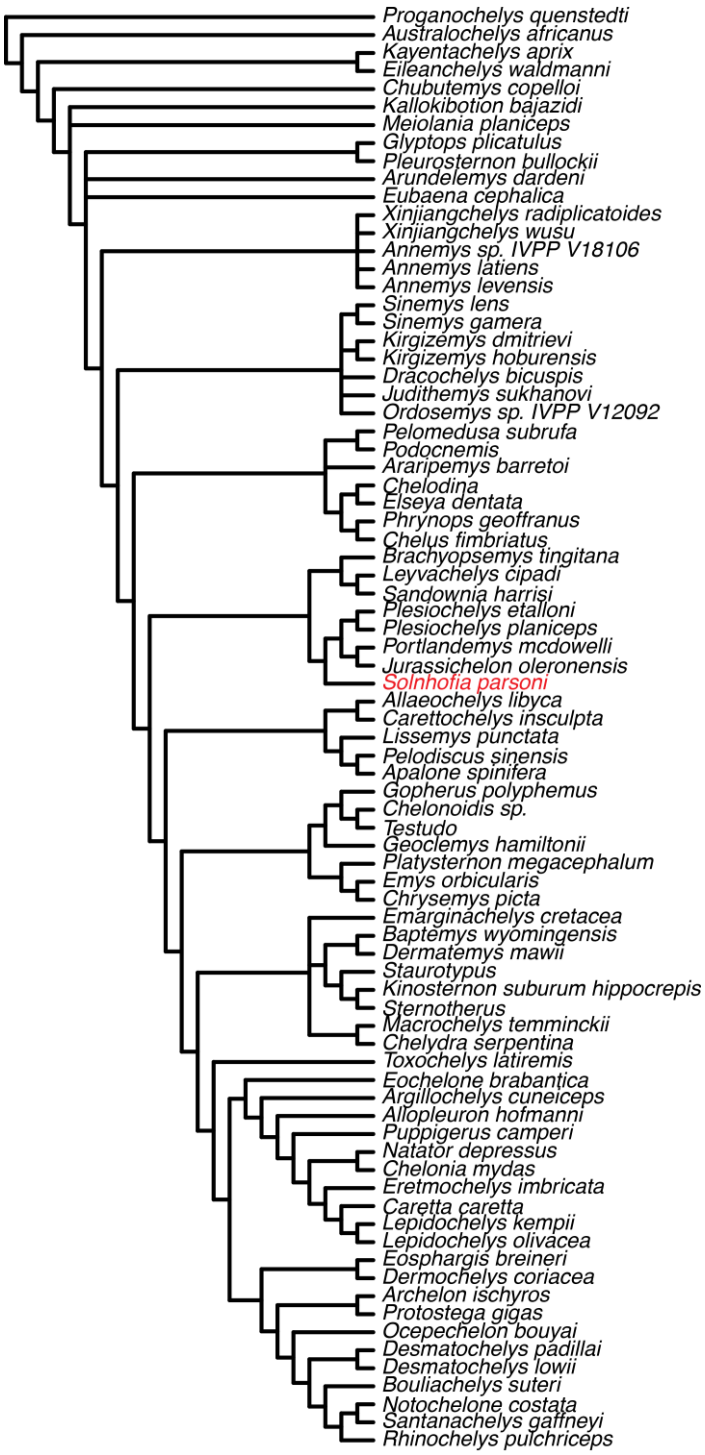


FIG S1.83. Strict consensus tree of constraint analysis 4, forcing *Solnhofia parsoni* to be a stem-group cryptodire.

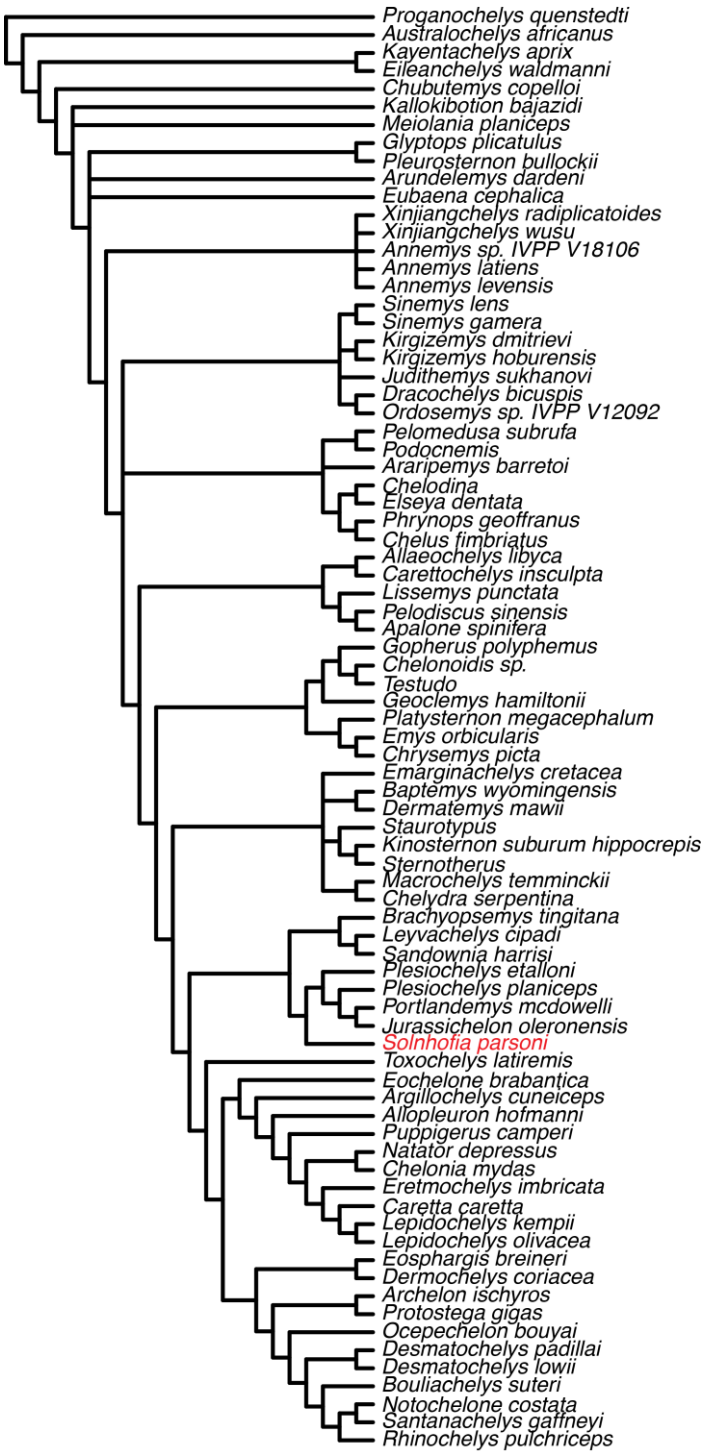


FIG S1.84. Strict consensus tree of constraint analysis 5, forcing *Solnhofia parsoni* to be a stem-group chelonioid.

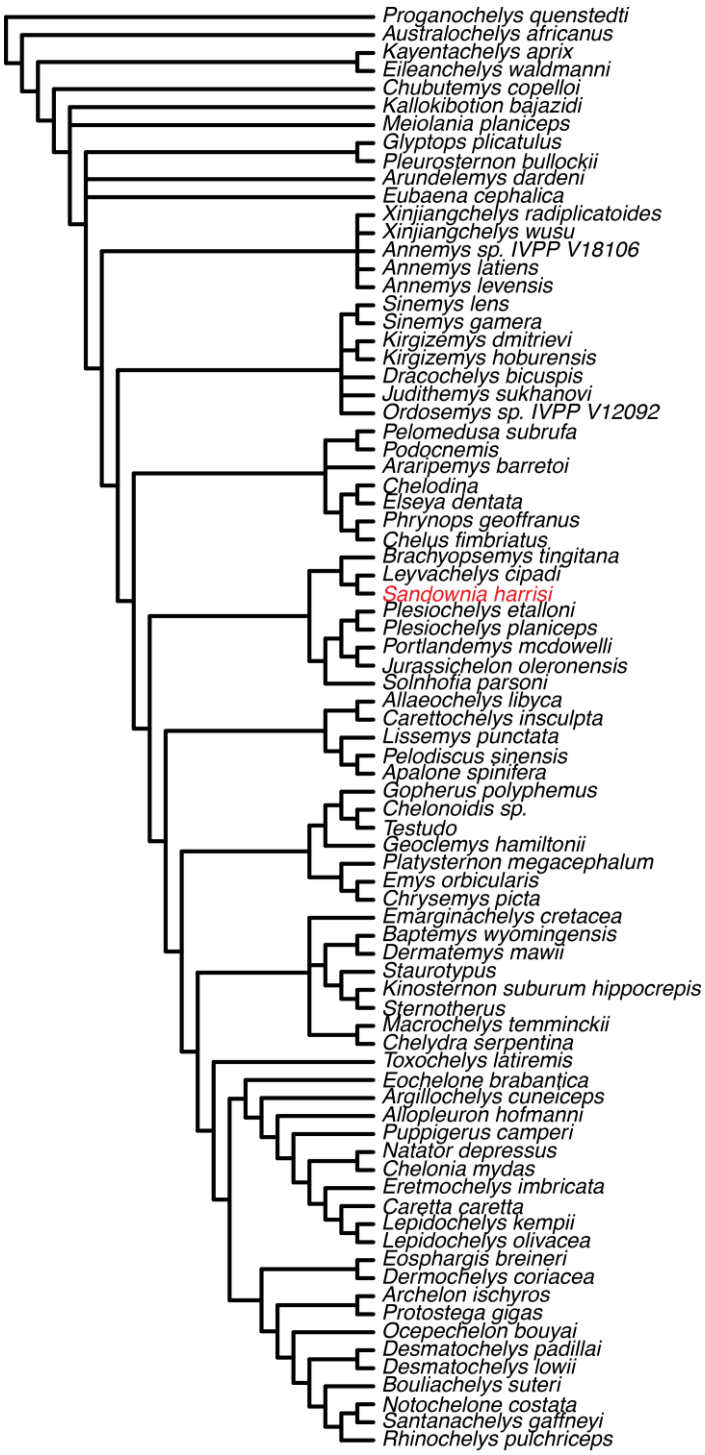


FIG S1.85. Strict consensus tree of constraint analysis 6, forcing *Sandownia harrisi* to be a stem-group cryptodire.

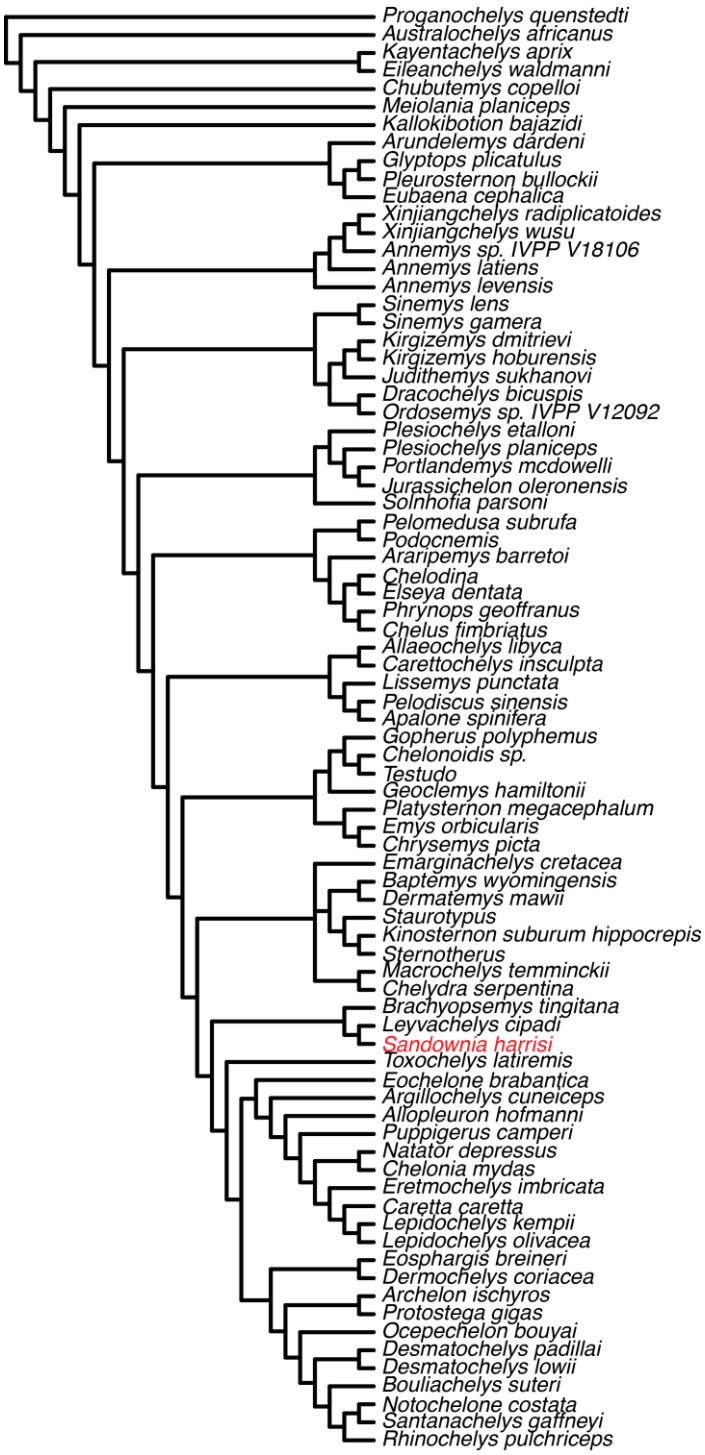


FIG S1.86. Strict consensus tree of constraint analysis 7, forcing *Sandownia harrisi* to be a stem-group chelonioid.

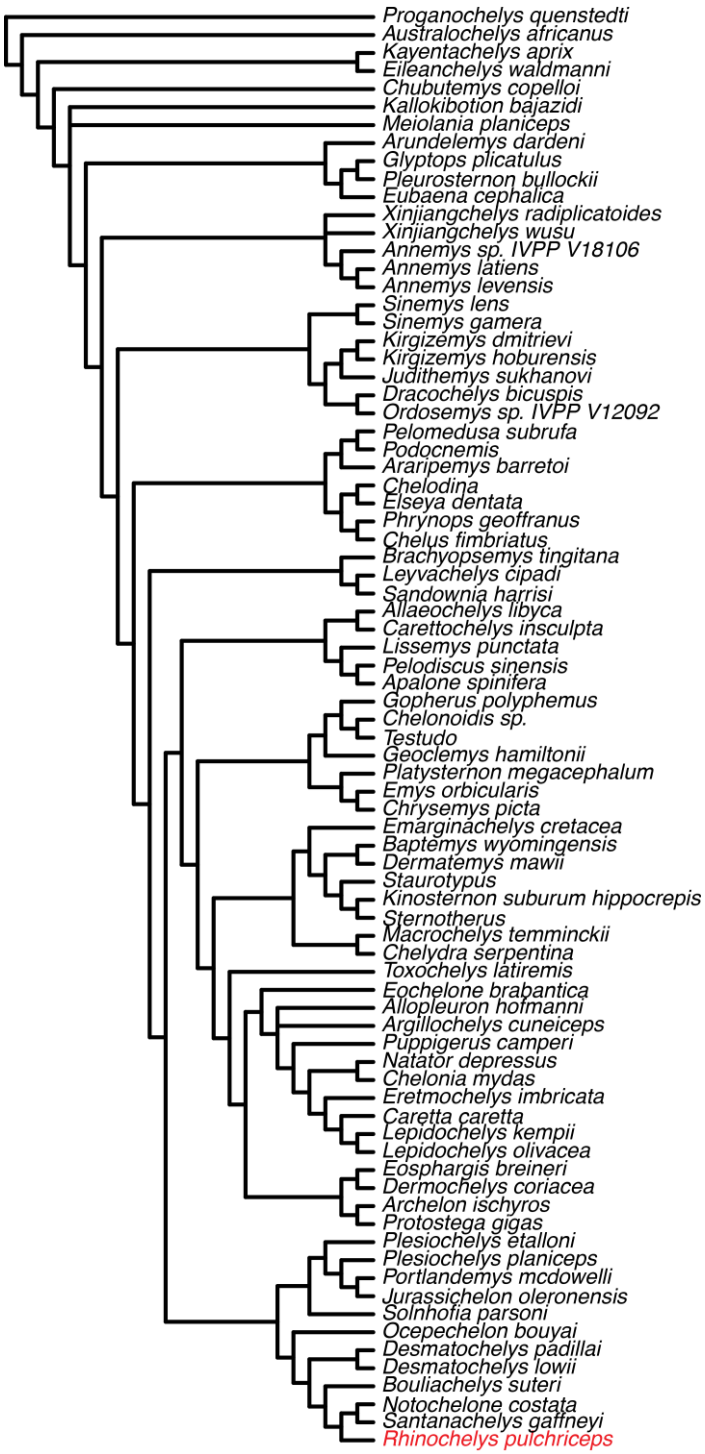


FIG S1.87. Strict consensus tree of constraint analysis 8, forcing *Rhinochelys pulchriceps* to be a stem-group cryptodire.

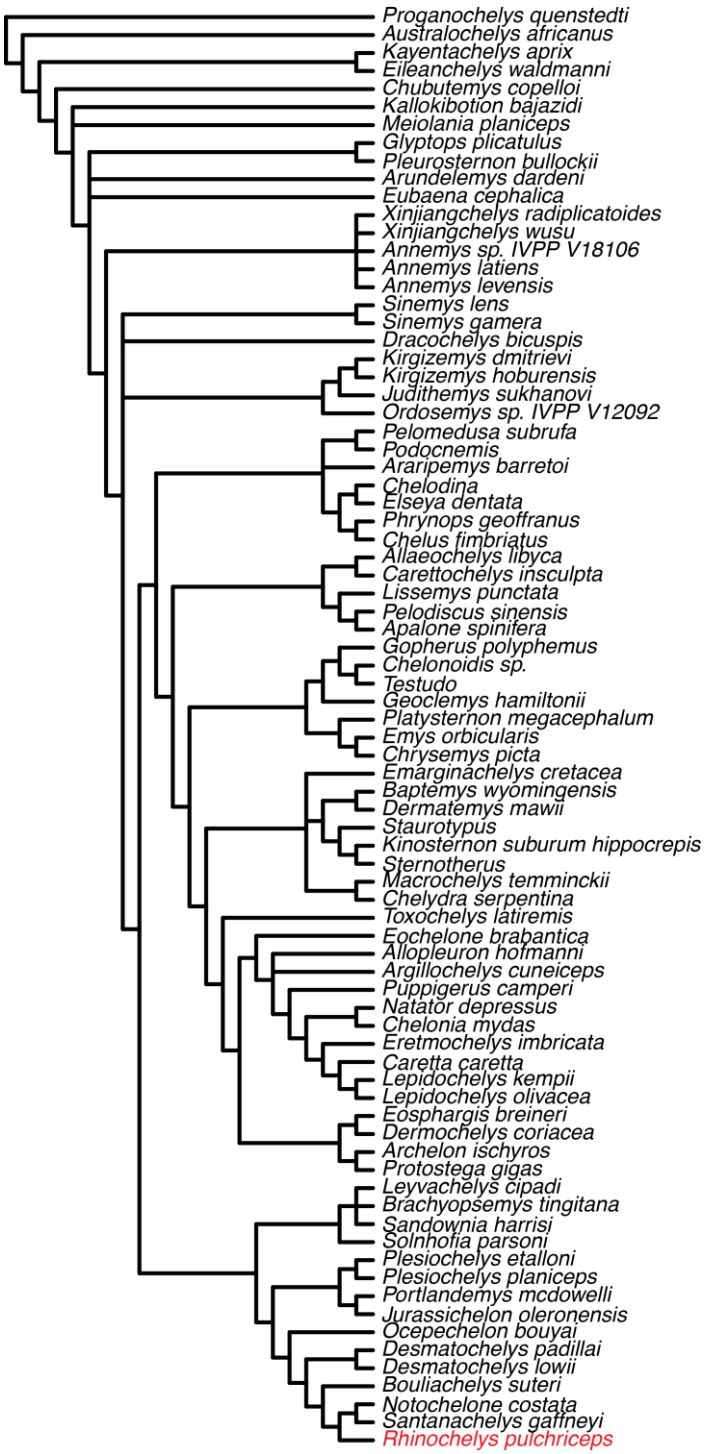


FIG S1.88. Strict consensus tree of constraint analysis 9, forcing *Rhinochelys pulchriceps* to be a stem-group turtle.

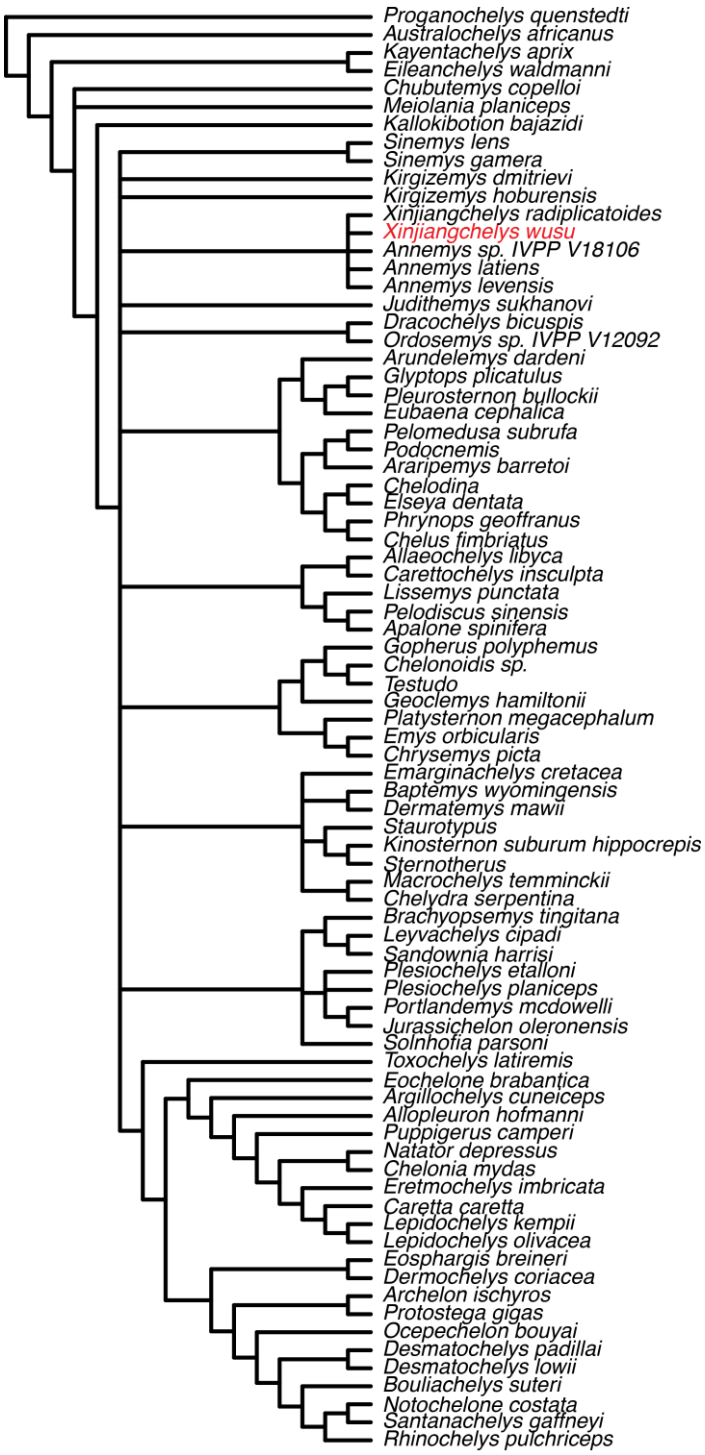


FIG S1.89. Strict consensus tree of constraint analysis 10, forcing *Xinjiangchelys wusu* to be a stem-group cryptodire.

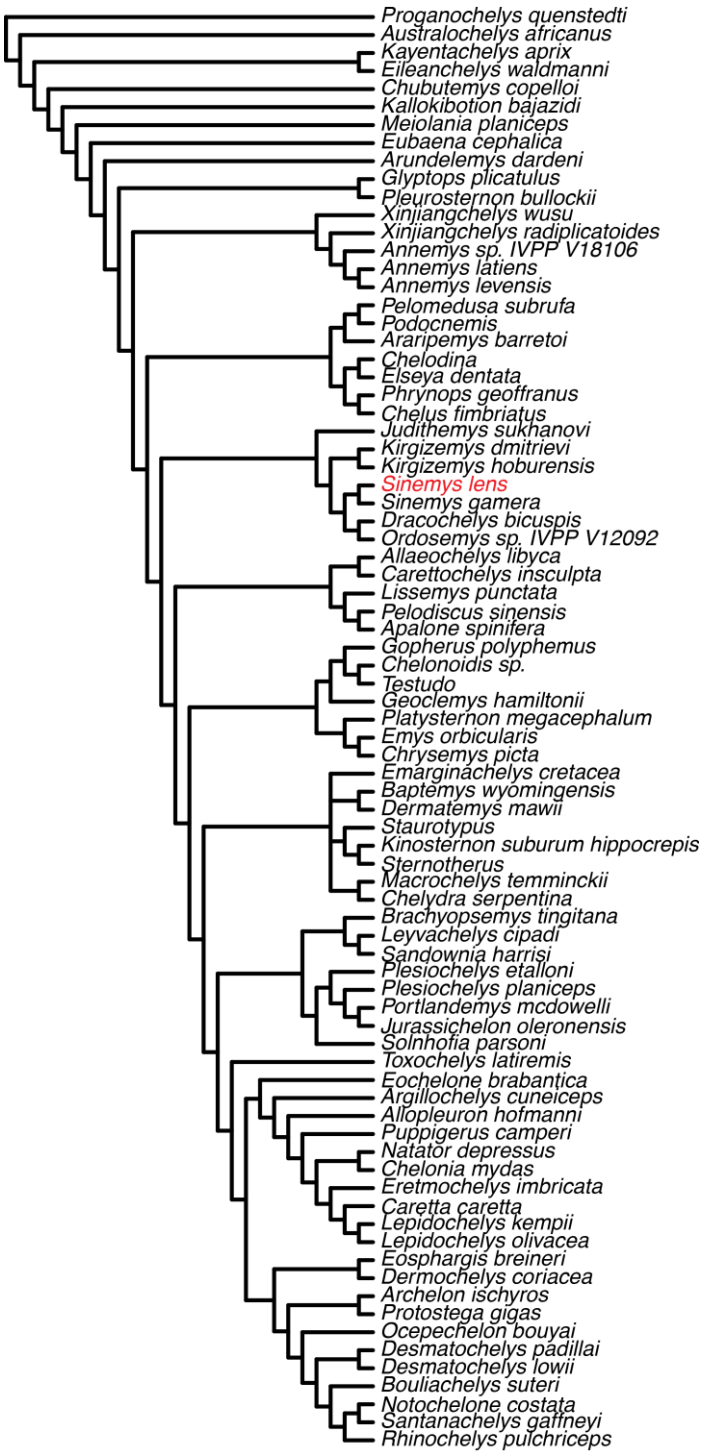


FIG S1.90. Strict consensus tree of constraint analysis 11, forcing *Sinemys lens* to be a stem-group cryptodire.

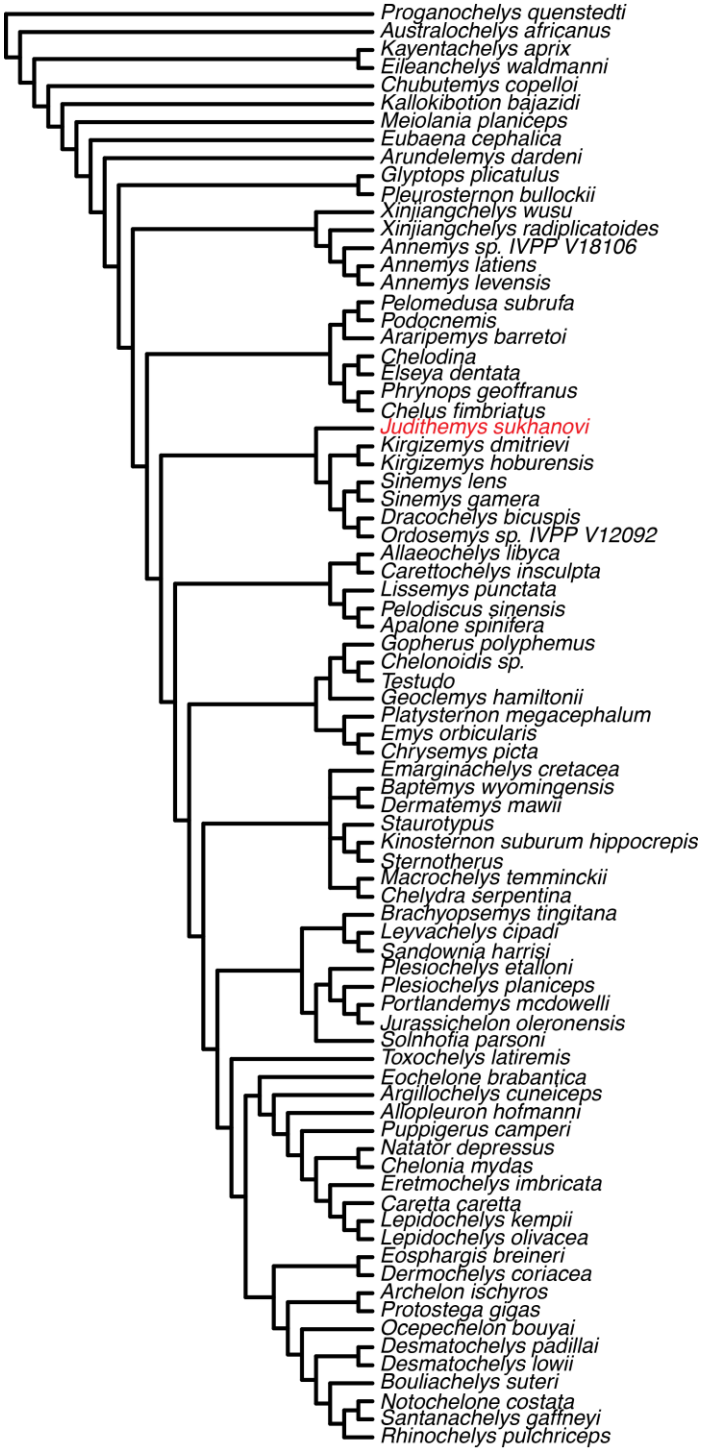


FIG S1.91. Strict consensus tree of constraint analysis 12, forcing *Judithemys sukhanovi* to be a stem-group cryptodire.

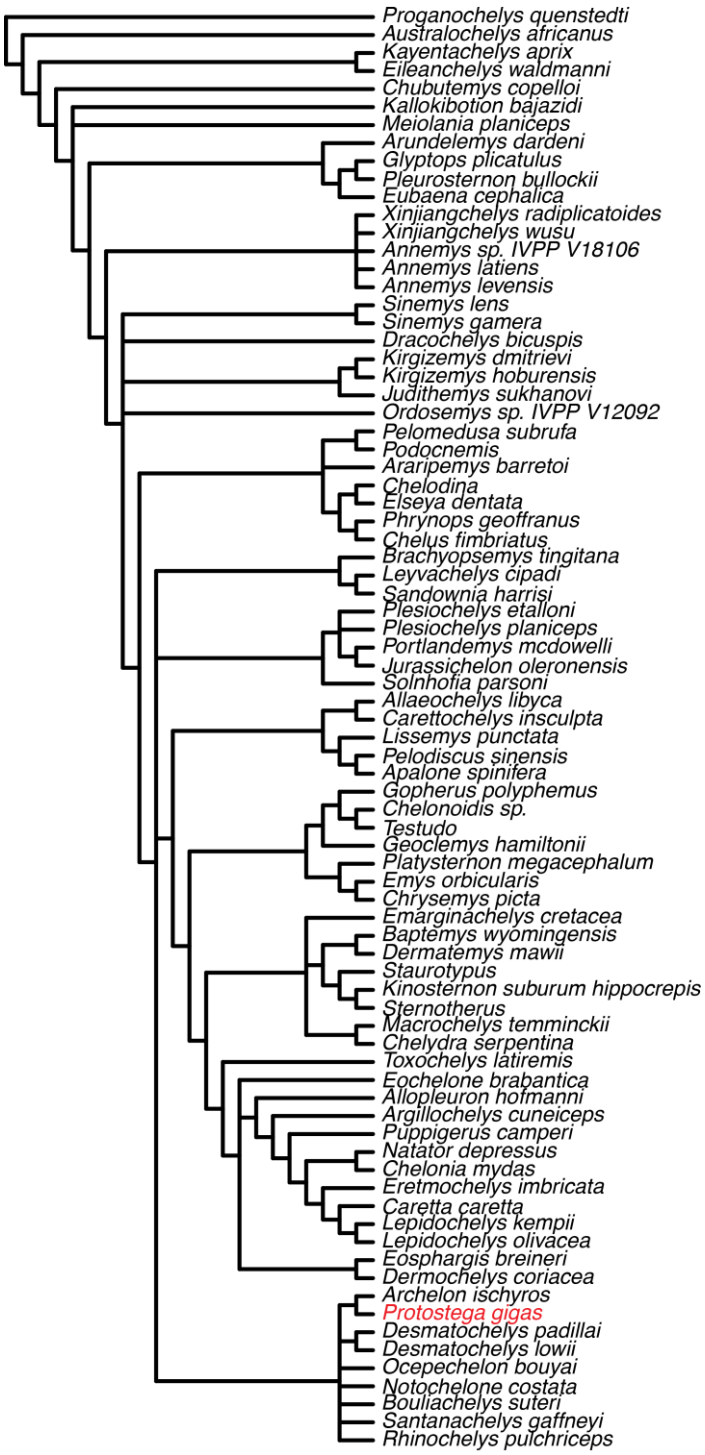


FIG S1.92. Strict consensus tree of constraint analysis 13, forcing *Protostega gigas* to be a stem-group cryptodire.

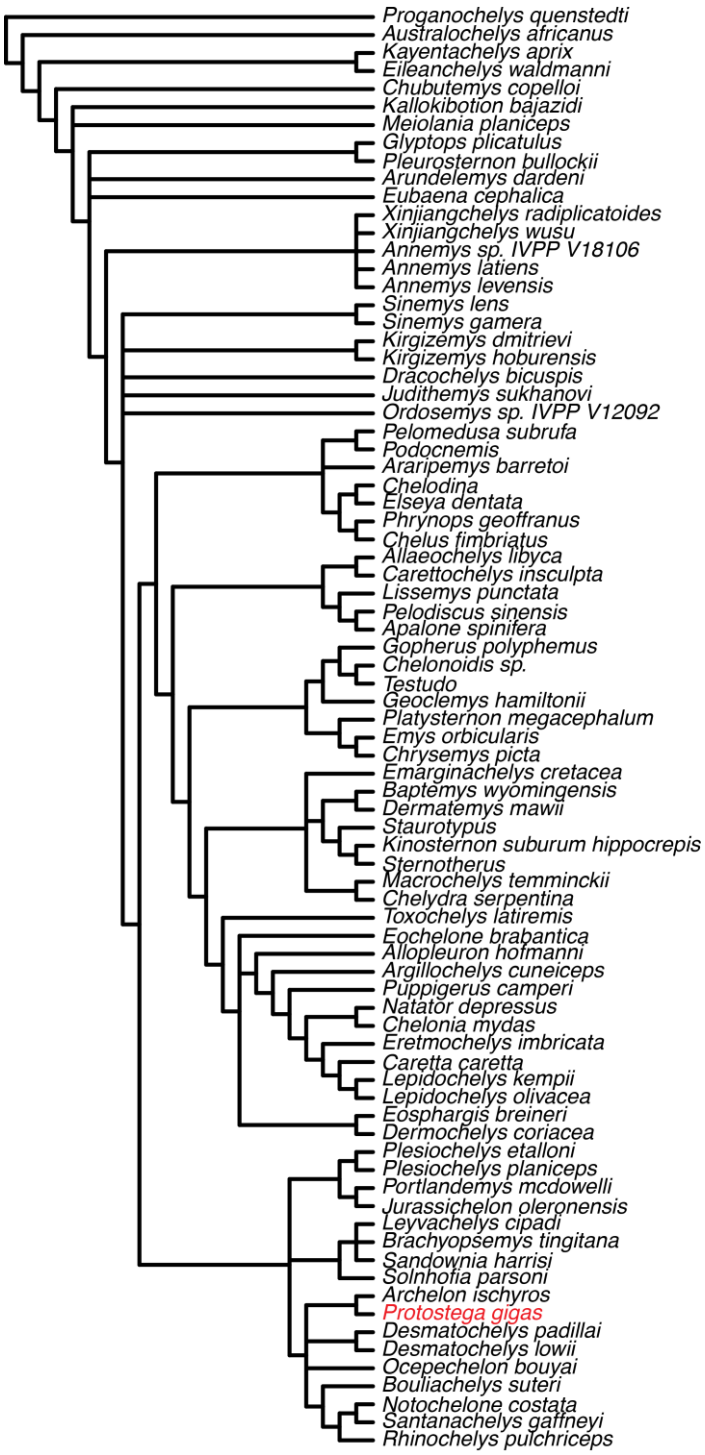


FIG S1.93. Strict consensus tree of constraint analysis 14, forcing *Protostega gigas* to be a stem-group turtle.

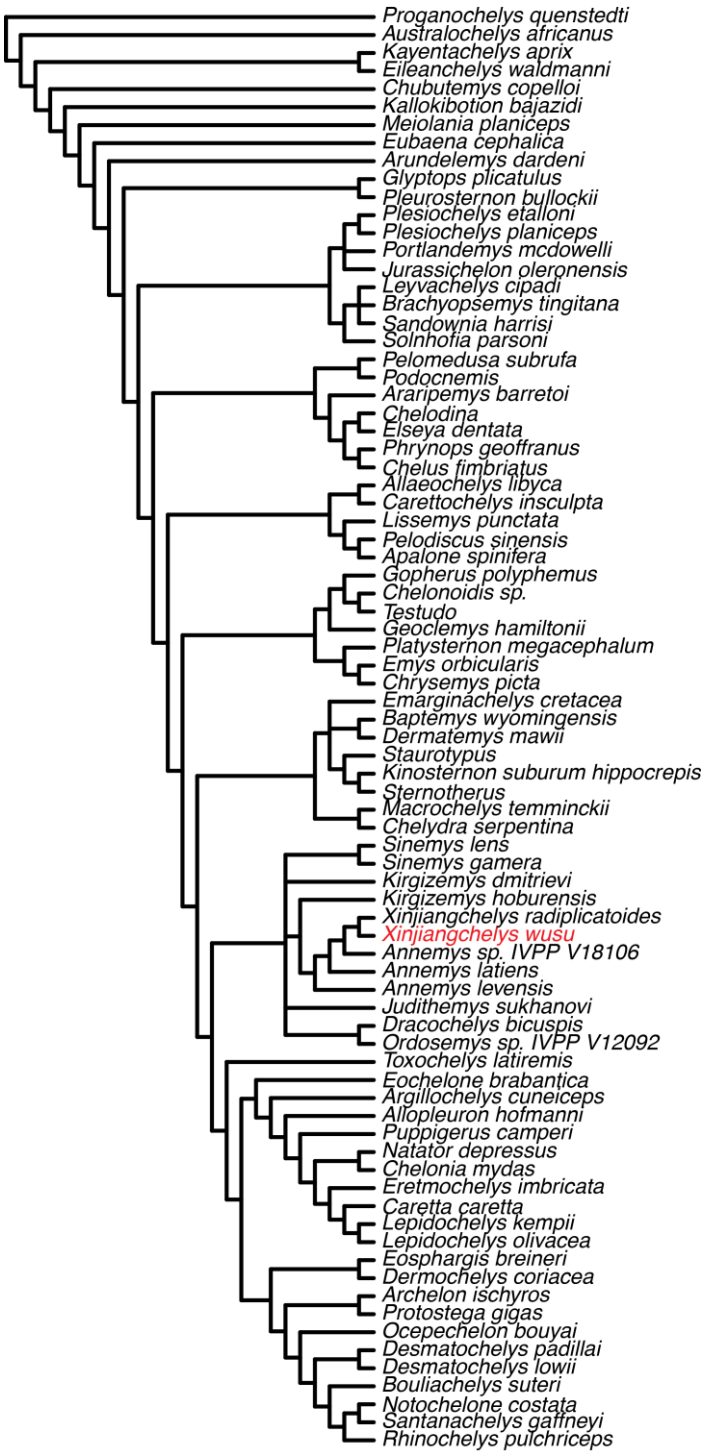


FIG S1.94. Strict consensus tree of constraint analysis 15, forcing *Xinjiangchelys wusu* to be a stem-group chelonioid.

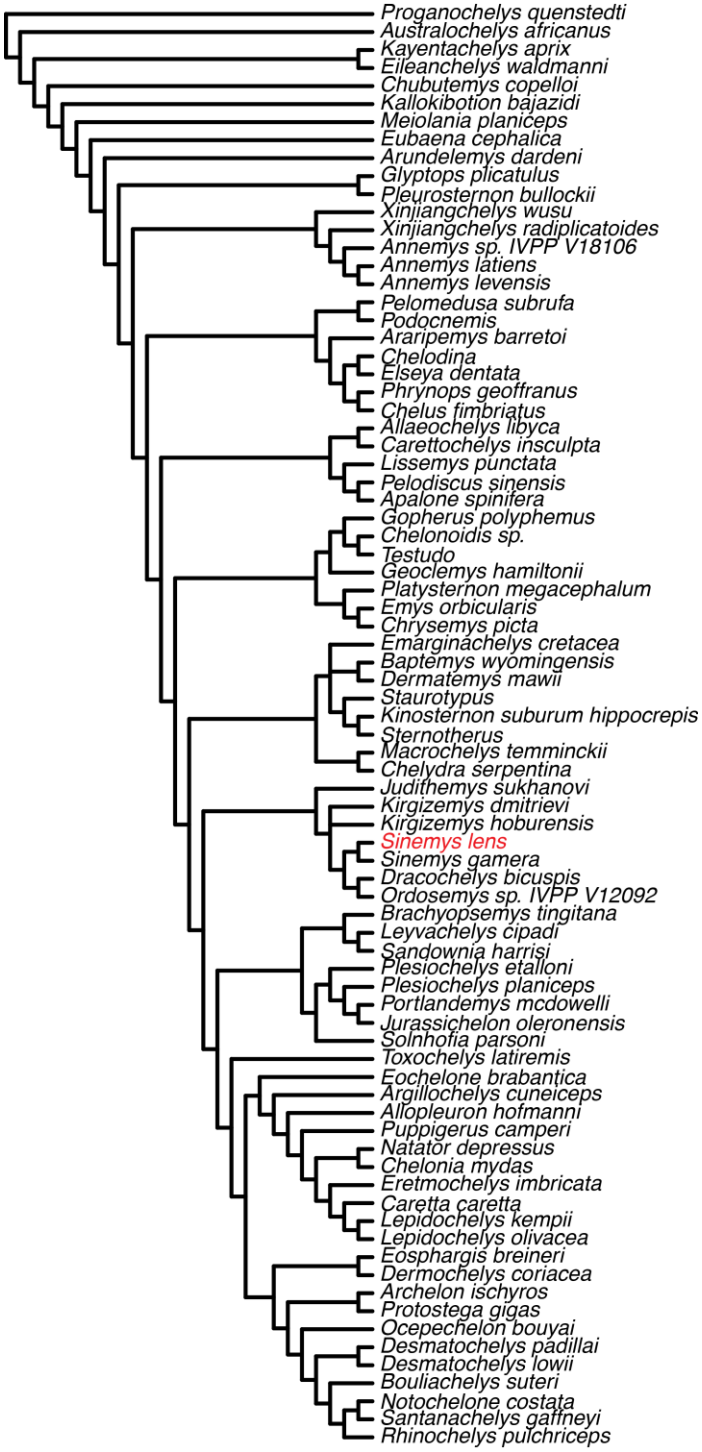


FIG S1.95. Strict consensus tree of constraint analysis 16, forcing *Sinemys lens* to be a stem-group chelonioid.

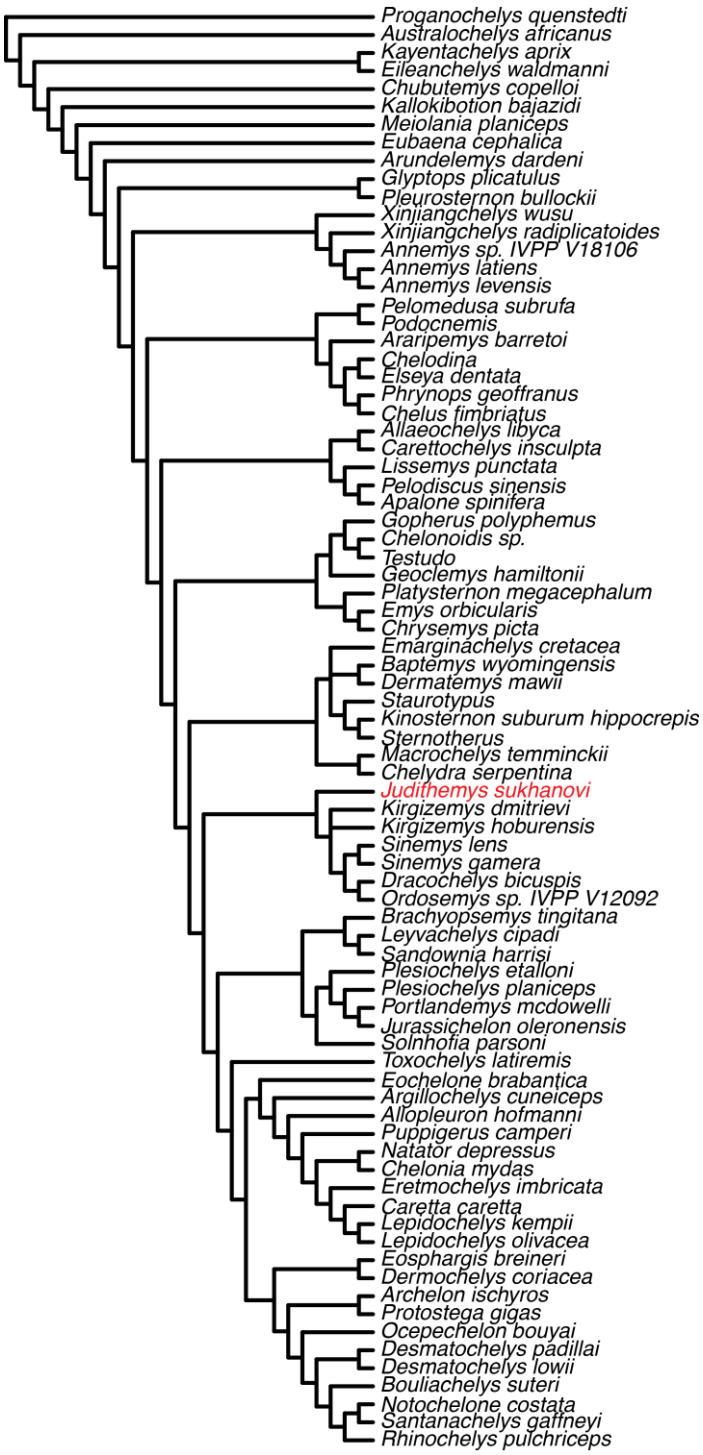


FIG S1.96. Strict consensus tree of constraint analysis 17, forcing *Judithemys sukhanovi* to be a stem-group chelonioid.

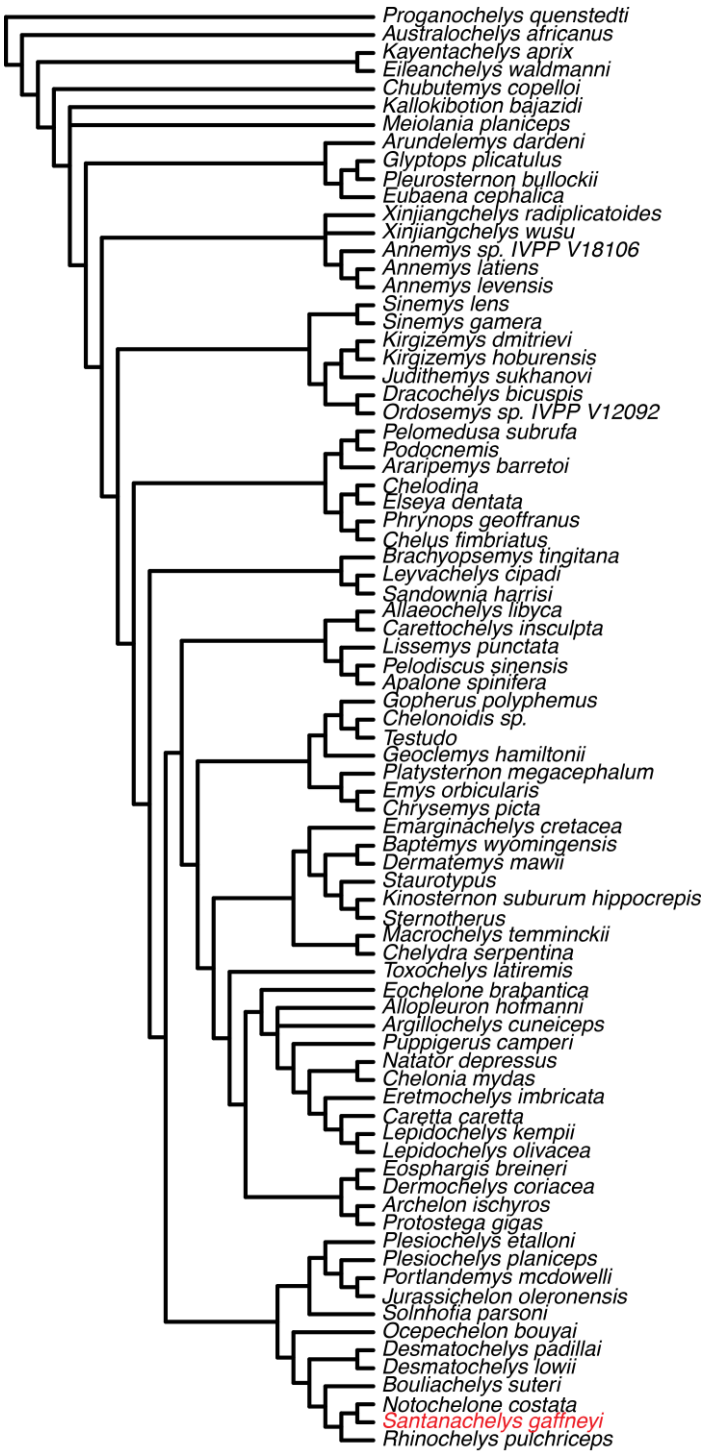


FIG S1.97. Strict consensus tree of constraint analysis 18, forcing *Santanachelys gaffneyi* to be a stem-group cryptodire.

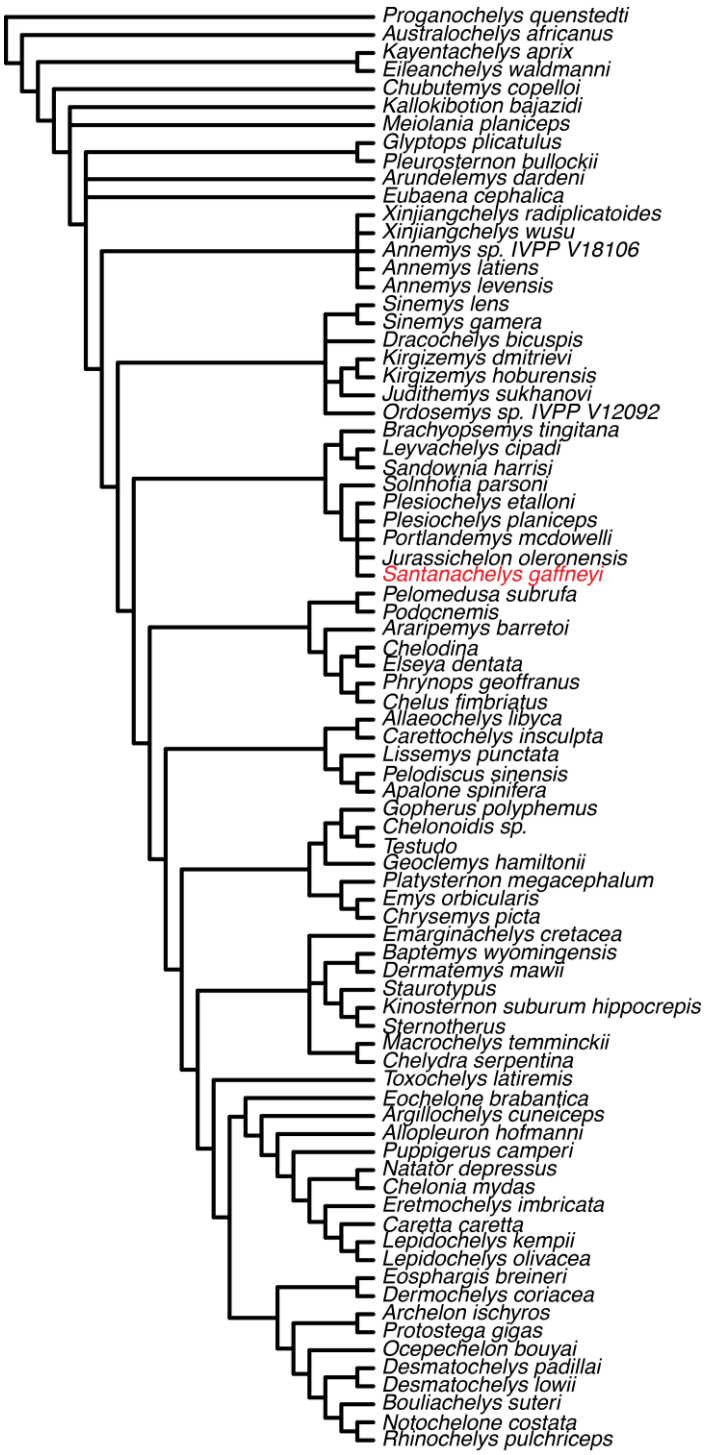


FIG S1.98. Strict consensus tree of constraint analysis 19, forcing *Santanachelys gaffneyi* to be a stem-group turtle.

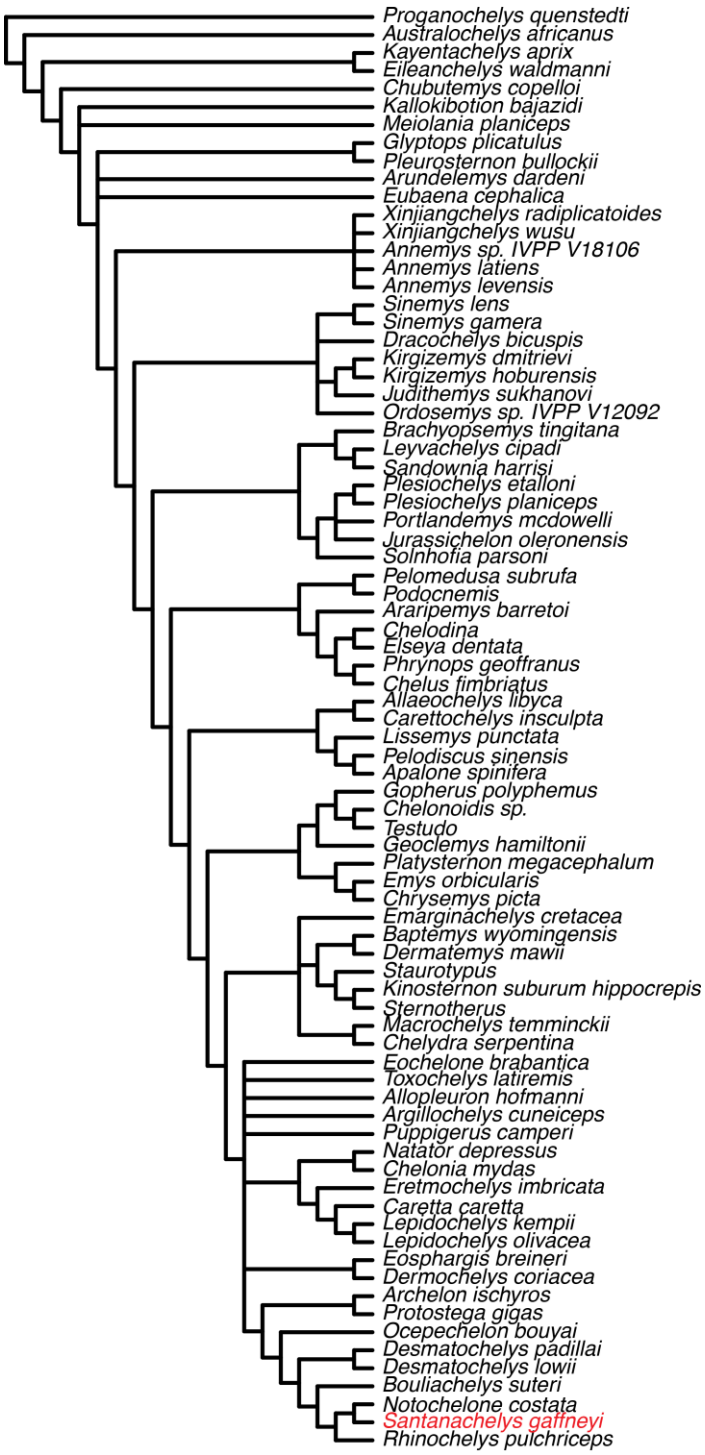


FIG S1.99. Strict consensus tree of constraint analysis 20, forcing *Santanachelys gaffneyi* to be a stem-group chelonioid.

S1.9 Character taxon-matrix

The following character-taxon matrix (ntax=80; nchar=345) was used for the phylogeny presented in section 2.2 of this thesis.

```
Rhinochelys_pulchriceps 0010000011100210000110-0100--
000000000110000111000000000001-0111010100001020[1 2]10201000011-
12101101001100111200?000002010000000001020200000220021O-
121000011000011001-1?????00110[0
1]1?000000?????????????????????????????????????????????????????????????
????????????????????????????????????????????????????????????????????
????????????????????
Santanachelys_gaffneyi  0010000?11100?10?00110-?100--
000000000??00001110?00000000?-01110101O?001021?1020?0?0011-
12101000001100110120010O?0???10?????0????2???0000???????-
1200?0011?????????1??????00???0????????00000?0??0-000101001?00-20-0100--
??01-0000?01100-0110111211?0011--
0?00?0?????????????????11??????????0?????0?1?1????111021????0??--
0???1?1??2?0---?010110102?1???
Bouliachelys_suteri     0011000?010001?0000110-0100--
000?00?0?1?0?0011100000000001-011101010000102001O201010011-
12101011001100111120010000020100010000010202100002210210-
121000111000011101-
1??????00110111O0?001?????????????????????????????????????????????????
????????????????????????????????????????????????????????????????????
????????????????????????????????????
Notochelone ????000?111002??0?0110-0?00--00?000???1?00001110O0?0000001-
?11101000100l0???102000?0?11-
12101000001100111200???1???0??000001001020000O?02210210-
121000011000011001-
1??????0011?????????????????????????????????????????????????????????
????????????????????????????????????????????????0????????????????????
????????????????????????????????????
Ocepechelon_bouyai      0000?01011101?0?00011???100--
000000001?10000111100000?0000-011101000?00?0202102O?0?00101121020-
100110010-1200000?0120100???????002??00000221?1??-1210?0111?000????1-
1?????????????????????????????????????????????????????????????????????
????????????????????????????????????????????????????????????????????
????????????????????????????????????
Desmatochelys_lowii     001000101110011[0 1]001111?0100--
000000000100000111010000000001-011101010?001020110201000011-
12100011001100l??1200100O???0???0?001?00021200000221021?-
121000111000011101-1??????0001?0???????100000-0100-0101010??001120-
010???01?1-?100001110-0110111211101-1--0-
0000?????????????????10110111202?00100002O1?????111021111-0?1--
00111011120011010111111102?1?1?
Desmatochelys_padillai  0010??1?11100?10011????100--
000000000?100001110??000?000??01110???0?001020110202?0?001??1210100100200
111120010O?01201000???????02?2?0000???????-1210?0011?00011101-
1??????00???0???0?00?00000-0100-0001010??00??2??0?0???01?1-
```

```
???0001?????????????????????????????????????????????10110111200000100002?10?
????1110211?????????????????1120011012?11?1102?1???

Protostega_gigas  1--0??0011000??0?00?????100--
000000?0???00001110?001000001-011100000???102?21?21?0?0?1??1?102?-102-
1011??1?0?100?0?0?1000???????02???000????????-
1200?0011?000??????1??????000100??00?0001-010-0100-000101001000-20-00000-
1-11----0--1110-0110111312101-1--0-021----------------
111?011120????10000201011110111021111-001--00111011120011011111111020101?

Archelon_ischyros 1--0??0011000?00?001????100--
00000?000100001111O?001000001-011100000????021210???0?0?101121020-102-
?011??1200100?0?0?10?0???????02???000????????-
??????????000??????1??????0001?0???????11-010-0100-00011-001000-20-00000-
1-11----0--1110-0110111312101-1--0-021----------------
101?011??????????0??201?11110111021111-001--00111011120011011111111020101?

Dermochelys_coriacea    1--1010011000001-00100-0000--
00000000010010011101000100010-0101010000011021210100000011-121021-002--
0000-1200000[0 1]00001030-01-001020200000021011l-1211?0111000011101-1----
--0001011--0-2011--0-?0110--00-1--1-00-------0---1--1-------111-?0011----
-1101-1--0-021----------------11110111200011000012O-011110111021111-011--
0011-011130100110100111O2?1?10

Eosphargis_breineri     1--1??0?11000??1?00????100--
0000000?????0001110?0001?0011-010101010????02??10???000?1??120020-002-
?1000-1200000?00?0111?????????0????0110???????-1211?011?????????1-
1?????????????????????????????????????????????????????????????????????????
??????????????????????????????????????????????0??????????????????????
??????????????????????????????????

Lepidochelys_olivacea   1--1010111000101000110-
0101100000000001000011110000000011l0-0101000211011021210201000011-121020-
100201100-1201100[0 1]0000110000010010201001002210210-121010111000011001-
1??????0111111100100100010-0110-00011-00?000-2110100110111-1100?11110-
0000111211101-1--0-020001---00[0
1]000000011110111200011100012011111110111020111-001--
0011101112010001111011101010 20

Caretta_caretta   1--1010111000101000110-
0101100000000001000011110000000011l0-1101100210011021210201000[0 1]011-
121020-101-11100-12011100000011-000011010202001002210211-
121010111000011101-1??????000111110010010001O-0110-000101000000-
3110100100111-1100011110-0000111211101-1--0-020001---[0 1]0[0
1]000000011110111200011100012011111110111020111-001--
0011101112010001111011101010 20

Chelonia_mydas    1--1010?11100101000110-
0101110000000001000011110000000011120010100021000102121010100001[0
1]1121020-102-00000-120110010100111000111010200001002O-0111-
121010111000011001-1??????0011110100000100010-0110-0[0 1]011-001000-
3100100110111-1100001110-0000111211101-1--0-020001---10[0
1]000000011110111200011100[0 1]120111111010111021111-001--
0011101112010001111011101010 1?10

Eretmochelys_imbricata  1--1010111100101000110-
0101100000000001000011110000000011120010100021101102121020100001l-121020-
100211100-120110000010111000010010200001002210111-121010111000011001-
1??????000011110000010000O-0110-0[0 1]011-001000-2110100110101-
1100001110-0000111211101-1--0-020001---10[0
1]000000011110111200011100012011111110111021111-001--
0011101112010001111011101010 20
```

```
Lepidochelys_kempii     1--1010111100101000110-
0101110000000001000011110000100111 2-0101000211011021210201000011-121020-
100211000-1201100[0 1]0000110000011010202001002210110-121010111000011001-
1??????001110110000010000-0110-00011-00?000-2110100110111-1100011110-
0000111211101-1--0-020001---00[0
1]000000011110111200011100012011111110111020111-001--
0011101112010001111011101010 20

Natator_depressus 1--1010011100101000110-
0101110000000001000011110000000111200101000211011020210101000011-121020-
100211100-1201100100001100000100102020010022102 11-121010111000011001-
1??????001011010010010000 0-0110-000101001000-2110100110101-1100001110-
0000111211101-1--0-020001---10[0
1]000000011110111200011100012011111110111021111-001--
0011101112010001?1101110101011

Puppigerus_camperi      1--1010011100100000110-
0101110000000001000011110000000011 10-0101010210011021210 21?000011-121020-
100211100-1201100100001100000010102020010012001 10-121100111000011001-
1??????011110110 0?00100000-0100-000101001000-2100100110111-1100001110-
0000111211101-1--0-
02000??????????000??111101112000111000120 1?????111021111-
0???????????1120000010110?1101?1?11

Argillochelys_cuneiceps 1--1000011100101000110-
0101110000000001000011110000000011 11-0101000210001021210201000010112 1020-
1002?1100-1201100101001100000100102020010022102 10111-121100110000011001-
1??????001110110 0?001??????????????????????????????????????????????????
????????????????????????????????????1111011120001110001?010?????????????
?????????????????????????????????

Allopleuron_hoffmanni   1--1000011100 1?1000110-
00011?000000000100100111010000011 10-
0101000 21?00102111011100101011210001100 2?1100-
1201???100001100000100002120010022101 11-
121000111000011000 11?????0000???10000001-010-0100-000101001000-20-
0100111-01-1100001110-0100111211101-1--0-021----------------
1111011120001110001201011110111021111-001--0011101112000001011011101010 1?

Toxochelys_latiremis
      0011000?1110111001011???101010000000011?00001110100000[0 1]011-
01010001[0
1]000102121020000001011210000100010001112001000000010 00?000?0?02020010002
00111-121000111000011001-1??????1001[0 1]11100100100000-0110-
010101001000-20-0100110111-11000011[0 1]0-0000111211101-1--0-
0200???1??0???1011011?10111200??0????1?0101??001110?00???00?--
0???111??100---?01101010??1?00

Eochelone   1--1000011100100000110-0101110000000001000011111000000000001-
0101000110001021210100000010112 1020-100210000-
1201100001001120000110102000010012 00011-
1210001110000110010 1??????00011?11000001?????????????????????????????????
????????????????????????????????????????????????????????????????????0??
????????????????????????????????????????????

Solnhofia_parsoni
      0011000?111011??100111101010100001?00?000?0011100000000100-
1111100200001020210201011010112 10001001-000110110 0???100201110[0
1]000011020000000010011 0-121000111000011001-1??????011100111110100000 0-
0????0?0101001?01121-01002?01?1-0100?01100-0000???111?0001--
```

```
000000?????000?000??110?00--------???????1?1????111020????0??--
??0?1?1??000---1?0?0100?0000?

Jurassichelon_oleronensis     0010001?1110110001011110100--
00001000010000011101000000001-
01110000000010212102000110101111011010011001101201000l0?00100010001100212
000000200110-111000011100011001-1??????????????????0000??0100-
0001010???0??????10???????????0???1?0-000????1?1?1001--
????00??????0?0?00???11??00--------
0?0??1?????????????????????????????1?????????????????????????

Portlandemys_mcdowelli  0010001?111011??00011110?00--
???0??000100?0011101000000001-
0101000000001O2?2102010110101111000010001O0?101201?0010100100010001[0
1]00212000000200110-121000011000011001-
1??????000000?1001010?????????????????????????????????????????????????
????????????????????????????????????????????????????????????????????
??????????????????????????????????

Plesiochelys_planiceps  ???0000?111011?00?011110100--
0?0?2?00?100?0?11?0100?000001-
01110000000010Z?2102010110101121010000011001101101100101201000000001110202
000000210110-121000011100011001-
1??????000000110110l0?????????????????????????????????????????????????
????????????????????????????????????????????????????????????????????
??????????????????????????????????

Plesiochelys_etalloni   0011000?111011?00?011110100--
00001000010000111101000000001-
0101000000001020210201011010112?0100000110010-
1200?????????00000011102020000002l0100-
12100001110001100l?1??????000000010110100000?0100-000101001?01121-
0100100001-0100000[0 1]00-0000111101?1??1--
10000000010000001001O?????????????????0010?????1110??????0?1--
0?????1??000---10?001000??????

Sandownia_harrisi
      0111001?111011?000012110101010000000?0?000011100000011110-
0101000210001020220200011010111100011O1--00110121100000010-
0?010001010201000-00000010-111000111000011001-
1??????01010??1111011?????????????????????????????????????????????????
????????????????????????????????????????????????????????????????????
??????????????????????????????????

Brachyopsemys_tingitana
      0111000?1110110100011??0101010000000000?000011110000000110-
0101100210011O2?2102000110l??1?10000101-
1001111211100001001O?0?0?????0201?---0?2??0?0-
121000111?0001110011??????010100?1111011?????????????????????????????
????????????????????????????????????????????????????????????????????
??????????????????????????????????????????????????

Leyvachelys_cipadi      0001??1?1110110100012???100--
00000000001000011101000000110-0111000?1?0?10202202O?0110101l?10000?01-
?001111211100?00?0-010???????0??1?---00001l?0-1210?0111?000?????-
1??????01???0?????0?1?????00??0-?0????001?0??00-
0????????1??1?????0?????????????????????1?????????????????????111?01???????
?1?0??201??????????2?0???0??--0?0????100000?01?0???000??????

Chelydra_serpentina     1--
1000001000110020111011010100000000001000011101001000001-
0101010001001021220201000010112100011000100010120010[0
```

```
1]10100100001011010200000000101010-
12110011000001100011?????00110110000000100000-01012000001001000-20-
01002?0101-1100001100-?000111211101-1--0-010001-1-
0010?01100111101112001011101020111120011102001l-001--00011?110000---
1?00010001?????

Macrochelys_temmincki  1--
10000110001100201110010111000000000000000011101001000000-
01010000010010212202010010101121000110001000101200l0[0
1]10110100000011010200000000-0110-
12100011100001100011??????00110110000001000000-01011000001001000-00-01000-
010001100001100-1000111211101-1--01000001-1-
00?000110011110111200101110102011122001110200l1-001--000011110000---
1?000100011O?0?

Sternotherus      1--1000011000110120120-11[0
1]11100100100001000011101000010000-
01010102110010212202000000101121001l001-
10001012001000000010200100100021000001010001O-12110011000101100011------
000000?0100111001101010110001010021111OO-01000-0111-110000000111001---?-
110021--01000001-1-11-1-1-00111110111100101110102l-111110111020011-011--
111010110010---1?000100010000?

Staurotypus 1--100001100[0 1]110120120-0111110010010010[0
1]010011100000010000-
01010102110010212202010000101121001110020000111200100001201020110010102l?
0000000-0010-12110011000101100011------
000100?0100101001101010110001010021O[0 1]?00-01000-0111-
11?000000111000111111110021--01010001-1-00-1-1-00111110111100101110102l-
111?10111020011-001--111010110010---1?00010001???0?

Kinosternon_suburum_hippocrepis    1--1000011000110120120-
11111100100100001010011101001010000-
01010101010010212102000000101121001110020000101200000011201000010110102l0
000000101010-12110011000100100011------
000100?00101110011010101100001010020110O0-01000-0111-110000000111001---?-
110021--01000001-1-11-1-1-00111110111102??11101021-111110111020011-011--
111110110010---1?000100100?0?

Dermatemys_mawii  1--1000011[0 1]00110020120-
01011100001100001000011101000010002O[0
1]10111010100102121010000001011210011000210000-
120010000020100011000010 2[0 1]00000000-0010-12110011001------011------
000010?010010100000-01011000101001101000-01000-0111-1100000000-
1000111101?1011--00100001-1-100100000011110110-
00101110102011l??10111020011-011--00101?110010---1?0001000?0000?

Baptemys_wyomingensis  1--1000?1110?110020120-
01011100001100000000001110100001000210101010100?00102121010000?00101121001[0
1]0002?000101200100001201120???????020000000010?1?0-12100011l?1------??1-
-----100010?000001100110-01011000101001?00-00-010???0111-1100000000-
100011110111011--1?000001-1-
00110000001l?1?111?????????????2111??1?111020?11-011--
1???1?1??????????0??10001?????

Emarginachelys_cretacea 1--
1000?11100110020l????10110000001000?000001110100000?00?21010101?10????021?
102010?001??1210011?00210001011011O?0????1?00?0?????020??000001??0?0-
12110011O?0001100???------?????????????0011??01011??0???001?00-00-
?10??????1-1100001000-10001111?1?0??1--0?000001-1-
00???010??11???111?????????????1?????11102?????0?1--
01????1??????????0??1000??????
```

```
Chrysemys_picta   1--100001110[0 1]110020110-
0101110000110010100001110100000000200101020011001021210200000010112100110
00210000-120010010020101111000010200000000100010-12110011000001100011----
--000010111000010000-0100-100101001000-00-01000-0101-1100000000-
100011110111011--10100001-1-
000010000111110111211101110102011111110111020011-011--000111110010---
1?000100010000?

Emys_orbicularis  1--
100001100011002011110101010000110000100001110100000000-
0101000001000021210100000010112000011000210000-
120010000120100101001010200000000101011-12110011O?0001100011------
0000?0???????100000-0100-100101001000-00-01000-0101-
110000100101000101101100 11-?01000001-1-
00100000??111101112101011101020111111?111020011-011--00?11?110010---
1?000100010000?

Geoclemys_hamiltonii    1--
100001100011012011110111110000010000101001110100000000-
0101021111000021210200000010112100110002100010120010000020103101001010200
000000100010-12110011111000110001 1------000010?010000100110-0100-
100101001100-00-0100100111-1100000000-100011110101011--11100001-1-
001010000111110111210101110102011111110111020011-011--000111110010---
1?000100010000?

Testudo     1--1000011100110120111101 00--
000011000010100111010000000020010102000100002012010000001011210011000200 0
00-120010010100100101001010200000000101010-12110011010001100011------
000000000010100000-0100-100001001000-00-1100100111-1100000000-
100011110101001--00100001-1-
000010000111110111210101110102011111110111020011-011--000111110010---
1?000000011000?

Gopherus_polyphemus     1--1000011100110020120-0100--0000110000[0
1]000011101000010002001010210010100211201000000101121001000021010 0-
1200100001001000-1100010220000000 0-1010-12110011010001100011------
000010001000010000 0-0100-100001001000-00-1100100111-1100000000-
100011110101001--10100001-1-
000010000111110111210101110102011111110111020011-011--000111100010---
1?000000011000?

Chelonoidis_sp.   1--1000011101[1 2]1012011110100--
000011000000000111010000000020010102100100002012010000001011210010000021 00
011120010000100100 0-1001010220[0 1]00000101010-12110011010001110011------
000000000000010000 0-0100-000001001100-00-0100100101-1100001000-
1000111101101-1--02100001-1-
000000000011010111210101110002011112001110200 11-001--000111100000---
1?000100010 0?0?

Platysternon_megacephalum     1--1000011000[1
2]110001110010111001000000000010111010010000 01-
010101000100102022010000001011210001000201001012011000002010000 1111010200
0000020-0110-12110011100000 1001-1------0000001[0 1]01001100000-0100-
000001001100-00-0100100101-1100001000-1000111101101-1--02100001-1-
000000000011010111210101110002011112001110200 11-001--000111100000---
1?00010001 00?0?

Apalone_spinifera 1--1010011101110120120-
111111100001001000100111101100 10001-
111112000101102122021000001011210020101-10-10-
120010110110100000011010201000000100010-120000111000011001-1------
```

```
000100011100111-00120100-000101-1-001000-0101--1--1-------11[0 1]0-
1000111411101-1--0-001----1-----------11010120-0010111000201-
11110111020011-001--001110111010---1?0001001100l0?

Pelodiscus_sinensis     1--10100111011101201 20-
11111110000100100010011110110010000-
11111200010110212202100000101121002l101-10-10-
12001011011010001001101020100000010001 0-12000011100001100[0 1]11------
000100011100111-00120100-000101-1-001000-0101--1--1-------1110-
10001114111-1-1----001----------------110?0120-00?011100020--
1??10??????????????????????????0??????????????00l0?

Lissemys_punctata 1--10100111011101201 20-
11111010000100100010011110110010000-
11111200000110212202100000101121002l101-00-20-
12001011011010000001101020100000010001 0-12000011100001100001------
000?00???0?0011-00120100-000101-1-001000-0101--1--1-------1110-
1000111411101-1--0-0-1----1-----------11010120-0010111000201-1--
10111020011-001--011110111010---1?0??1001?001??

Carettochelys_insculpta 1--10100111001101201 20-
11011100100100101000011110000010001-
01111010010110210202000?011011210021101-10-11[0
1]12001011012011300011101020100001010001 0-12100011100001100011------
000010111100110100120000-000101000001000-01000-1-11-------1000-
100011110110021--01001----1---------??11010110-
00101110002011111110111020011-001--011110100000---1?0001002200l0?

Allaeochelys_libyca     1--
1??0?1110?1101201???11????00?0?10????1????1????????????????????????????0211
20200000110112l0???10???0?11[0 1]1201??1101201130001?0010201?0001?10?010-
12100011100001100011?????????????????????????????????????????????????????
??????????????????????????????????????????????????????????????????????0??
????????????????????????????????????????????????

Chelus_fimbriatus 1--010101110110[0 1]-20110-01011101--21000011-
0011111000000000-01010000001-00202300--000011-120101000---0000-200-
000011321010120012002010000001000l0-120001110-0010100011------
1001?0???????000111[0 3]0100-100001001100-00-01000-0101-1100000000-
100011110111011--31100010211001000001-
10111111310000101002010111110111120011-10111000110110000---1?0001000100l0?

Phrynops_geoffranus     011011101110110[0 1]-20111011011101--21000011-
0011101000000000-01010000001-00202300--000011-120101000---0010-200-
000011321010120012102010000001010l0-121001100-0011100011------
1001?0?10?100000000-0100-100101101101000-01000-0111-1100000000-
100011110111011--10100010010000000001-
10001111310000100002010111110111120011-10111000110110000---1?0001000100l0?

Elseya_dentata    0110111011101101-00111111011101--21000011-
0011101000000002011010000001-00202300--000011-120101000---0000-200-
1000012010001200121020100000010001 0-1[1 2]1001110-00111001-1------
0010000100110000002?0100-100-1-001?11100-010???1-11-1-00000000-
1000111101?1001--1010001001?00?000001-
10?01111310000l0?0020101??10111120011-1?11100??101??0?0---??00010001???0?

Chelodina   0110111011111110-20111001011101--21000011-0011101000000000-
01010000001-00202300--100011-120101000---0010-200-
000011221000120012002010000001000l0-121001100-00111001-1------
1001000000000000000130100-100-1-001111100-01000-0111-1-00000000-
100011110111011--01100010110000000001-
10001111310000101002010111110111120011-10111000110111000---1?0001000100l0?
```

```
Araripemys_barretoi     1--1111011101110-
20111001011100001100101100011101000000000-??11??000?1-01202100--000011-
120102100---0-00-200-???000001010120012102010000000100010-121001100-
00111001-1------1001000000000010011140100-100101001001020-01000-1-11-
1101001110-000011111111011--01100011---000000101-
100?1111000000101002??01111011?20011-1???????????11?000---1?0??100010000?

Podocnemis  1--1110011101110-
00121111011110001100001110011101000011002002110000001-11202300--100011-
120101101---0000-200-1000002010001000121020100000010010-120000101-
0001100011------000000011000010000[0 1]30100-100101001101000-01000-1-11-
1100000000-000011110111010111010001001[0 1]001000001-
1000111100000010000201011110111120011-10111000110111000---1?000100010000?

Pelomedusa_subrufa      1--1110011101110-20120-
010111000011001011000111010000010002002110-0---1-11202300--100011-
120101000---0010-200-1000010010001210121020100000010100 0-121001110-
0011100011------0000?0?110000100000-0100-100101001101000-01000-1-11-
1100000000-000011110111010111010001001 0000000001-
1000111100000010000201011110111020011-10111000110110000---1?000100010000?

Ordosemys_sp._IVPP_V12092     0010000-
111011?0010111?0?0101000?1?001?0?00011101000000000-
010102000?00102021011101[0
1]010111?00101002?00?101201?00100201?00??0011002?0?1000???1???-1110-
0011?000????1-
1?????????????????????????????????????????????????????????????????????????
??????????????????????????????????????????????0?????????????????????
??????????????????????????????

Judithemys_sukhanovi
      ???1??0?11?01??0?101????101???0001?001000?00111??0?00?000??01010200
0?0??021210???0?001??121001010001000101200100?0100100????????0????1000010
101?-1110-0111?000????1-1??????000100??????0?00000?0100-000101001?00-00-
01001001?1-1100001000-1000111211?0001--00000001-1?0000000[0
1]00?111011120[0 1]0001[0 1]0102?101121011102 00?1-0?1--00??1?100000---
1?0??1000?00?0?

Annemys_levensis  00110000111011?00201110?101?10000200010[0
1]000011101000000000-
010102000?0??020210100000010111000 10?0001000??1101100001001000??01???0200
00010???????1?110-0?11?00011001-1011?0?000000?100000000000-0100-
000101101101000-0100100111-1010101000-100011110110001--
000001000100000000100?????????????????????0?00?????111020010 10?1--
?0?????00000---1?0????????????

Annemys_latiens
      0010??1?11101??00201110?10???0?0???0???????01?1??0???0????????????
?????????101000?0010011?0?1??0???0??????0??0????????0?1????????2???00?0???
????0[0 1]110-0?11?0001100?????????????????????????00000-0100-000101101?0[0
1]?00-0100100111-1[0 1]10101000-100011110110001--
000001000100000000100?????????????????????????????????????0??--
???????00000---1?0????????????

Annemys_sp._IVPP_V18106
      0110001?1110110002011??0101010000200010100 0?11101000000000-
0101020000001020210101 00?0101110001000001000101101100?0?201000?10111?0210
?00000101100-1110-0011100011001-
1?????????????????????????????????????????????????????????????????????????
??????????????????????????????????????????????????????????????????????????
??????????????????????????????
```

```
Xinjiangchelys_wusu
      0110?01011101?00020?????101??000010001O?0000111O?0000??????01?1?2?0
0????021110100O?001??110001010001OO???1201100?0?201000??????0200?0000???
????0[0 1]110-0111?00011001-1011???00???0?1????0000000-0?0??000101101l0[0
1]?00-0100100111-1100101000-10001?110110001--
0000000001000000001000O???0?-------
1?0??????????????????????????????????0?000---1?0??1000000000?

Xinjiangchelys_radiplicatoides
      0110??1?111011?00?011????0???0?????0??????00111??00??0???????11????
?????0211101O?0?0?1011110?2??0???0-
?1012?0?000012010O0?001???020000000020111O-1110-0011000011001-
1????????0?1?????????100000-0100-000???101?00-00-0100100111-1100???000-
10001?110110001--
000001000100000000100?????????????????????0????????111?200101?????????????00
000---1?????????????

Dracochelys_bicuspis
      ???1000?11101??0??01????10101000O1?0?????000111010001?0001-
010100000?00?020?10101000010111100101000100010120l?0??0?2010??????????02??
?0000???????10110-0?11?0001100??1??????000?00?0?0?0010000??1100-
000101001?00-10-0110101-0??1101?01100-1000???211?0001--
00000?????????????????0111?110-
000001000?0010????01110200???0???????????0?000---1?0???000??????

Kirgizemys_hoburensis
      0011000?11101100010111101010l?002000101O?0011101000000000-
010102000?001020?10100000010111100l0?000100010110010010100100001001??02?0
?10000101O?0-1111-0110?0001100011?????0001?0????????00000-0100-
000101101?00-00-010???0111-1100001000-100011121110001--0?000001-
1?0000000[0 1]10?111?11120000011O??2?10??????????2???1-0?1?????????0?000--
-1?????????????

Kirgizemys_dmitrievi
      ???1000?111001?001?111??10101000020001000000111O?0000?0001-
000101000?00102021020?00001011?100100000?000????00100?0??01000??00???02?0
?1000?1110??-1111-0?1??00011101-
???????000100?000000?????????????????????????????????????????????????????
????????????????????????????????????????????????????????????????????????
??????????????????????????????????

Sinemys_gamera
      01100?1?11101110020l1??1101010??02100?000?0011???0??0?0??0-
0?????????????1202201000000101110O0?000010001012011001O?001000??00??00220
?1000???????-1110-0111?00011001-
1?????????????????????00001?0???????1?????100-2??010??????1-
?10???1????100??????01?00???00??0????1??????00?????????????????????????
????????????????????????????0000????1?????????????

Sinemys_lens
      0010??1?11101?100201????101??0??02?0000???00111??0000??0??????????0?
??????2022010O0?0?1??1?000100000?000101101l0??????10?0???????022??1000???
????-1110-0111?0001100??1??????00?????????????0000??0100-000101001100-20-
0100101--1-1101001[0 1]00-100011121010001--
000100???1??0?0000?10?1?0?????0?????????0???1?????????????0?????????????
???????????1000?000??

Meiolania_planiceps     00000000110001010001l0-
000101000100110000000110010000000020010102100000102103110000[0
1]0101121001[0 1]100000000-12001100000[0 1]11211100110020?0000000-
101010111-0111100001101-11111110000000000100000000-?100-00????001000-00-
```

```
?1????0101-0?00101100-00001010012?0011--
00000000010002????????0100011120000000000002?0022011110000101011--
00001??00000---0?0000000100002

Chubutemys_copelloi
      ???1000?11000?01?0011???10000000?000??00000011???0??000000-
011102000????0202101?000001??1100011000000001?01001000?00110???????0020?
?0000???????100-------?????????1-
1?????????????????????00????0??????????0???0???????0??????????0??????????
??????????????????????????????????????1?1?????????0?????0?????1110?0????
????????????????????????????????

Eubaena_cephalica
      0000002?110001100201l???10111000010000000010111010000000001-
0101020001000021210100000011-
12100101000?000101201100000201020??00???1210?0001010?110200-------
?00011011-
1??????0000?0???????0?????????????????????????????????????????????????????
??????????????????????????????????????????????????????????????????????????
????????????????????????????????

Arundelemys_dardeni     0100001?111001??020110-
1?01?1??0???0????0?10?1101000000001-
0101000000?0?02??10100000010111100101000100011120l?000000010200l011100020?
000000101110200-------0000????1-
1??????????????????????????????????????????????????????????????????????????
??????????????????????????????????????????????????????????????????????????
????????????????????????????????

Pleurosternon_bullockii
      0110001?111001001001?1?1101110000110000000101110100000?0000-
01??00000????020110110000010111?0020?00010-
0101101?00?0??????011001110221100010101111[0 1]200---
????00001100??1?????????????????????0000130??0-0?0101001?00-00-01000-1-11-
0100100000-00001??101??0101010000010010000000000000???0--------
??0?000?????????????????0?1--00????????????????????????????

Glyptops_plicatulus
      01100?1?111001?0?0011???101?100?0100000?0010111???0?0?00?1-
0101000?0????0201101?000001011110020?00010-
0101101??0?002?100?1100???0211?000101011?0200---
????0000??????1??????00?0??0????0?00000100100-000101001?00-00-0100100111-
0100100000-000011110111010101000000001000000000000?00010--------
??0?000101???0111120010102?1--00??1?100000---1?0????????????

Kallokibotion_bajazidi
      0000??0?1110010100011???10???000000000000??00110010000?00??110102??
0????020210200?00101111?0??00???0001?1200?00?00-
11121110001012000000000101111-10-------000011001-
1??????00?1???????00?00000-0000-000101???000-00-010011??1??00?000?000-
00001?1101??00011?2000000010000?0000000?00000--------0?0???????--
001110100101011--0000???00000---0?????????????

Eileanchelys_waldmanni  00000?1?1110??0?-
001????1011?0000?00??0?00???11010000??0???01?100000????020?100-
000001????0????00???0?0??01010?00000[0
1]1000010?01002010?000?????????????????100011001-
1??????10???????????00??0-0????000001101?00-00-01001001?1-0000???00-
00001??00?????????0?0?00???00?0????00?????????????????????????????????????
????????????????????????????????????
```

```
Kayentachelys_aprix     0000001011100101-00000-
1101110000000000000000?110?000000001-0101000??????0201100--
0010100010001000000000-0101000?0?001000?-0???001-101000-11111[0 1]000---
----?0001100--0??????1000?0?000000000000-0000-00000000?100-00-00000-0111-
0000001000-0000001000?0000100000000001000000000000?0?00--------
??000000010000101O?00101011--00001?10?000---??????000????0?

Australochelys_africanus      ????10??00??0101-00000-
1?0????0000??000?0000?10??00?000001-0?01?01000???01?00-0--
000?1??11000?0000000000-00000?01??0?0??0?-??0?010-1-00?0-211?10000-------
????????--
0??????????????????????????????????????????????????????????????????????
??????????????????????????????????????????????????????????????????????
??????????????????????????????????

Proganochelys_quenstedti      0000100?00000101-00000-0001010000000000-
0100010000000000001-000000100100000--0-0--00000??0000010000000000-000-
0001000000-0?-0-0?000-0-0000-200100000-------?0001010--
0??????000000000000000000[0 1]00000-?0?000000001000-??0???010000-
00?00000-0000000000?0??0100?000000001000000000??010000--------
000000000000000000000000010--00000?000000---0?000000000000?
```

S1.10 Molecular backbone constraint

Molecular backbone constraint was enforced in TNT using the following commands:

```
force/(Proganochelys(((Pelomedusa_subrufa Podocnemis)((Chelus_fimbriatus
Phrynops_geoffranus)(Chelodina Elseya_dentata)))((Carettochelys_insculpta
(Lissemys_punctata (Pelodiscus_sinensis
Apalone_spinifera)))(((Platysternon_megacephalum(Emys_orbicularis
Chrysemys_picta))(Geoclemys_hamiltonii (Gopherus_polyphemus (Testudo
Chelonoidis_sp.))))(((Macrochelys_temmincki
Chelydra_serpentina)(Dermatemys_mawii (Staurotypus
(Kinosternon_suburum_hippocrepis Sternotherus))))(Dermochelys_coriacea
((Chelonia_mydas  Natator_depressus) (Eretmochelys_imbricata
(Caretta_caretta (Lepidochelys_olivacea  Lepidochelys_kempii)))))))))
;constrain=;
```

S1.13 R code for similarity matrix

The following code was used to produce the similarity matrices shown in section 2 (see 2.2.5 for methods, and 2.3.1 for results). The following text follows R syntax, with '#' indicating comments.

```
## CODE FOR SIMILARITY MATRIX
```

```
# The object "Similarity_matrix.txt" is the same matrix as shown in
# section S1.9. However, polymorphisms have been removed and replaced by
# "?" in "Similarity_matrix.txt", and taxa have been re-arranged
# to mirror the phylogenetic results of the unordered analysis to
# facilitate an easier reading of the similarity matrices produced. The
# respective file is available in the Dryad depository (see Evers &
# Benson 2018c).

# Load character-taxon matrix

data.matrix<-read.table("Similarity_matrix.txt", header=T,
na.strings=c("-","?"))

# Transpose matrix

data.matrix<-t(data.matrix)

# Make a matrix of same dimensions is which the entries are numerical

data2<-matrix(nrow=dim(data.matrix)[1],ncol=dim(data.matrix)[2])
for(i in 1:ncol(data.matrix)) data2[,i]<-as.numeric(data.matrix[,i])
colnames(data2)<-colnames(data.matrix)

# Create a dissimilarity matrix based on 'data2' with taxa in numeric
columns

sim.data<-matrix(nrow=ncol(data2),ncol=ncol(data2))
rownames(sim.data)<-colnames(data2)
colnames(sim.data)<-colnames(data2)

# Calculate dissmilarity values

for(i in 1:ncol(data2)) {for(j in 1:ncol(data2)) {sim.data[j,i]<-
length(grep(TRUE,data2[,j]==data2[,i]))/length(grep(TRUE,complete.cases(d
ata2[,j]==data2[,i])))}}

# PLOTTING THE DISTANCE MATRIX AS A HEATMAP

# Load required packages for coloring matrices

install.packages("gclus")
require(gclus)

# Load packages for additional colors

library(RColorBrewer)
display.brewer.all(type="seq")

# Assign colours to the similarity matrix (because the colour scheme
# works better in the inverse order, the data is transformed to a
# dissimilarity matrix)

hm.cols<-dmat.color(1-sim.data, byrank=FALSE, colors=brewer.pal(9,
"PuRd"))

# Plot and export matrix as PDF

dev.new()
pdf("Heatmap.Sim.Matrix.pdf", useDingbats=FALSE)
plotcolors(hm.cols,rlabels=rownames(sim.data),clabels=colnames(sim.data))
dev.off()
```

```
### HEATMAPS CRANIAL DATA

# Subsetting data to only cranial characters

cranial.data<-data.matrix[1:185,]

# Calculate percentages of missing data

perc.NA<-as.matrix(apply(cranial.data, 2,
function(col)sum(is.na(col)/length(col))))

# No taxon with 10% or more missing data present for cranial data, so
# nothing else done but see below for other cases

# Make a matrix of same dimensions is which the entries are numerical

data3<-matrix(nrow=dim(cranial.data)[1],ncol=dim(cranial.data)[2])
for(i in 1:ncol(cranial.data)) data3[,i]<-as.numeric(cranial.data[,i])
colnames(data3)<-colnames(cranial.data)

# Create a similarity matrix based on 'data3' with taxa in numeric
# columns

sim.data.cranial<-matrix(nrow=ncol(data3),ncol=ncol(data3))
rownames(sim.data.cranial)<-colnames(data3)
colnames(sim.data.cranial)<-colnames(data3)

# Calculate smilarity values

for(i in 1:ncol(data3)) {for(j in 1:ncol(data3)) {sim.data.cranial[j,i]<-
length(grep(TRUE,data3[,j]==data3[,i]))/length(grep(TRUE,complete.cases(d
ata3[,j]==data3[,i])))}}

# Plot cranial similarity data as heatmap

hm.cols2<-dmat.color(1-sim.data.cranial, byrank=FALSE,
colors=brewer.pal(9, "PuRd"))
dev.new()
pdf("Heatmap.Sim.Matrix.Cranial.pdf", useDingbats=FALSE)
plotcolors(hm.cols2,rlabels=rownames(sim.data.cranial),clabels=colnames(s
im.data.cranial))
dev.off()

### HEATMAPS SHELL DATA

# Subsetting data to only shell characters

shell.data<-data.matrix[186:272,]

# Calculate percentages of missing data

perc.NA<-as.matrix(apply(shell.data, 2,
function(col)sum(is.na(col)/length(col))))
perc.NA>=0.9

# Create object with names of taxa with more than 90% missing data

drop.taxa<-which(perc.NA %% 2 >= 0.9, arr.ind=TRUE, useNames=TRUE)
drop.taxa<-attributes(drop.taxa)$dimnames[[1]]

# Create object with numbers of columns to be dropped from dataset
```

```
drop.cols<-which(match(colnames(shell.data), drop.taxa) != "NA")

# Create reduced dataset that only contains taxa with more than 90%
# scored characters

shell.data.red <- shell.data[,-drop.cols]

# Make a matrix of same dimensions is which the entries are numerical

data4<-matrix(nrow=dim(shell.data.red)[1],ncol=dim(shell.data.red)[2])
for(i in 1:ncol(shell.data.red)) data4[,i]<-
as.numeric(shell.data.red[,i])
colnames(data4)<-colnames(shell.data.red)

# Create a similarity matrix based on 'data4' with taxa in numeric
columns

sim.data.shell.red<-matrix(nrow=ncol(data4),ncol=ncol(data4))
rownames(sim.data.shell.red)<-colnames(data4)
colnames(sim.data.shell.red)<-colnames(data4)

# Calculate smilarity values

for(i in 1:ncol(data4)) {for(j in 1:ncol(data4))
{sim.data.shell.red[j,i]<-
length(grep(TRUE,data4[,j]==data4[,i]))/length(grep(TRUE,complete.cases(d
ata4[,j]==data4[,i])))}}

# Plot shell similarity data as heatmap

hm.cols3<-dmat.color(1-sim.data.shell.red, byrank=FALSE,
colors=brewer.pal(9, "PuRd"))
dev.new()
pdf("Heatmap.Sim.Matrix.Shell.Reduced.pdf", useDingbats=FALSE)
plotcolors(hm.cols3,rlabels=rownames(sim.data.shell.red),clabels=colnames
(sim.data.shell.red))
dev.off()

### HEATMAPS AXIAL-GIRDLE DATA

# Subsetting my data to only axial-girdle characters, herein
# 'postcranial' for shorter syntax

postcranial.data<-data.matrix[273:322,]

# Calculate percentages of missing data

perc.NA<-as.matrix(apply(postcranial.data, 2,
function(col)sum(is.na(col)/length(col))))
perc.NA>=0.9

# Create object with names of taxa with more than 90% missing data

drop.taxa<-which(perc.NA %% 2 >= 0.9, arr.ind=TRUE, useNames=TRUE)
drop.taxa<-attributes(drop.taxa)$dimnames[[1]]

# Create object with numbers of columns to be dropped from dataset

drop.cols<-which(match(colnames(postcranial.data), drop.taxa) != "NA")

# Create reduced dataset that only contains taxa with more than 90%
# scored characters
```

```
postcranial.data.red <- postcranial.data[,-drop.cols]

# Make a matrix of same dimensions is which the entries are numerical

data5<-
matrix(nrow=dim(postcranial.data.red)[1],ncol=dim(postcranial.data.red)[2
])
for(i in 1:ncol(postcranial.data.red)) data5[,i]<-
as.numeric(postcranial.data.red[,i])
colnames(data5)<-colnames(postcranial.data.red)

# Create a similarity matrix based on 'data5' with taxa in numeric
# columns

sim.data.postcranial.red<-matrix(nrow=ncol(data5),ncol=ncol(data5))
rownames(sim.data.postcranial.red)<-colnames(data5)
colnames(sim.data.postcranial.red)<-colnames(data5)

# Calculate smilarity values

for(i in 1:ncol(data5)) {for(j in 1:ncol(data5))
{sim.data.postcranial.red[j,i]<-
length(grep(TRUE,data5[,j]==data5[,i]))/length(grep(TRUE,complete.cases(d
ata5[,j]==data5[,i])))}}

# Plot postcranial similarity data as heatmap

hm.cols4<-dmat.color(1-sim.data.postcranial.red, byrank=FALSE,
colors=brewer.pal(9, "PuRd"))
dev.new()
pdf("Heatmap.Sim.Matrix.Axial+Girdle.Reduced.pdf", useDingbats=FALSE)
plotcolors(hm.cols4,rlabels=rownames(sim.data.postcranial.red),clabels=co
lnames(sim.data.postcranial.red), na.color="Lightblue")
dev.off()

### HEATMAPS LIMB DATA

# Subsetting data to only limb characters

limb.data<-data.matrix[323:345,]

# Calculate percentages of missing data

perc.NA<-as.matrix(apply(limb.data, 2,
function(col)sum(is.na(col)/length(col))))
perc.NA>=0.9

# Create object with names of taxa with more than 90% missing data

drop.taxa<-which(perc.NA %% 2 >= 0.9, arr.ind=TRUE, useNames=TRUE)
drop.taxa<-attributes(drop.taxa)$dimnames[[1]]

# Create object with numbers of columns to be dropped from dataset
drop.cols<-which(match(colnames(limb.data), drop.taxa) != "NA")

# Create reduced dataset that only contains taxa with more than 90%
scored characters
limb.data.red <- limb.data[,-drop.cols]

# Make a matrix of same dimensions is which the entries are numerical
```

```
data6<-matrix(nrow=dim(limb.data.red)[1],ncol=dim(limb.data.red)[2])
for(i in 1:ncol(limb.data.red)) data6[,i]<-as.numeric(limb.data.red[,i])
colnames(data6)<-colnames(limb.data.red)

# Create a similarity matrix based on 'data6' with taxa in numeric
# columns

sim.data.limb.red<-matrix(nrow=ncol(data6),ncol=ncol(data6))
rownames(sim.data.limb.red)<-colnames(data6)
colnames(sim.data.limb.red)<-colnames(data6)

# Calculate smilarity values

for(i in 1:ncol(data6)) {for(j in 1:ncol(data6))
{sim.data.limb.red[j,i]<-
length(grep(TRUE,data6[,j]==data6[,i]))/length(grep(TRUE,complete.cases(d
ata6[,j]==data6[,i])))}}

# Plot limb diss data as heatmap

hm.cols5<-dmat.color(1-sim.data.limb.red, byrank=FALSE,
colors=brewer.pal(9, "PuRd"))
dev.new()
pdf("Heatmap.Sim.Matrix.Limb.Reduced.pdf", useDingbats=FALSE)
plotcolors(hm.cols5,rlabels=rownames(sim.data.limb.red),clabels=colnames(
sim.data.limb.red), na.color="Lightblue")
dev.off()
```

S1.12 R code for timescaled trees

The following code was used to time calibrate the trees shown in section 2 of this thesis (note that the trees were further modified with figure editing programmes). The "Turtle_Ages.txt" file used in the code below is the same data as shown in Table 2 of section 2. Note that some clades have been collapsed in this code. The following text follows R syntax, with '#' indicating comments.

```
# Load required packages

require(ape)
require(paleotree)
require(devtools)
require(msm)
require(rgl)
require(strap)
require(Claddis)

# Read tree

tree<-
read.tree(file=NA,text="(Proganochelys_quenstedti,(Australochelys_african
us,((Kayentachelys_aprix,Eileanchelys_waldmanni),(Chubutemys_copelloi,(Ka
```

```
llokibotion_bajazidi,Meiolania_planiceps,(Arundelemys_dardeni,Eubaena_cep
halica,(Glyptops_plicatulus,Pleurosternon_bullockii),((Xinjiangchelys_rad
iplicatoides,Xinjiangchelys_wusu,Annemys_sp,Annemys_latiens,Annemys_leven
sis),((Dracochelys_biscuspis,Ordosemys,(Sinemys_lens,Sinemys_gamera),(Jud
ithemys_sukhanovi,(Kirgizemys_dmitrievi,Kirgizemys_hoburensis))),(((Leyva
chelys_cipadi,Brachyopsemys_tingitana,Sandownia_harrisi),(Solnhofia_parso
ni,(Portlandemys_mcdowelli,Jurassichelon_oleronensis,(Plesiochelys_planic
eps,Plesiochelys_etalloni)))),((PELOMEDUSOIDES,(Araripemys_barretoi,CHELI
DAE)),(TRIONYCHIA,(TESTUDINOIDEA,((Emarginachelys_cretacea,CHELYDRIDAE,((
Baptemys_wyomingensis,Dermatemys_mawii),KINOSTERNIDAE)),(Toxochelys_latir
emis,((Eochelone,(Allopleuron_hofmanni,Argillochelys_cuneiceps,Puppigerus
_camperi,CROWN-GROUP_CHELONIIDAE)),((Eosphargis_breineri,
Dermochelys_coriacea),((Archelon_ischyros,
Protostega_gigas),(Ocepechelon_bouyai,(Desmatochelys_padillai,
Desmatochelys_lowii, Notochelone, Bouliachelys_suteri,
Santanachelys_gaffneyi, Rhinochelys_pulchriceps)))))))))))))))));")

ctree<-collapse.singles(tree, root.edge = FALSE)

# Load and organise age data

turtle.ages <- read.table("Turtle_Ages.txt" , header = T)

# Load and organise tip ages

ages <- cbind(turtle.ages $Age_Max , turtle.ages $Age_Min )
rownames( ages) <- turtle.ages $Name_on_Tree
colnames (ages) <- c("FAD", "LAD")

# Define time constraints as min.ages for certain nodes

node.mins<-rep(NA, ctree$Nnode)

      node.mins[mrca(ctree)[" PELOMEDUSOIDES ", " CHELIDAE "] - length(
ctree$tip.label )] <- 157.3 #Pleurodira minimum
      node.mins[mrca(ctree)[" TRIONYCHIA ", " TESTUDINOIDEA "] - length(
ctree$tip.label )] <- 145.0 #Cryptodira minimum
      node.mins[mrca(ctree)[" Emarginachelys_cretacea ", " KINOSTERNIDAE
"] - length( ctree$tip.label )] <- 72.1 #Chelydroidea minimum

# Calibrate tree

scaled.tree.reduced <- timePaleoPhy(tree=ctree, timeData=ages,
type="mbl", vartime=1, node.mins=node.mins)

# Plot tree

dev.new(width=12, height=10)
pdf("Scaled_tree_reduced.pdf", width=12, height=10)
geoscalePhylo(ladderize(scaled.tree.reduced, right=T), ages, cex.ts=1.5,
cex.tip=0.8,cex.age=0.5, label.offset=0.3, x.lim= c(0,225),
boxes="Epoch")
dev.off()
```

S1.13 Code for Templeton's test in PAUP* and R

As explained in section the main text of the thesis, I calculated symmetric distance matrices in PAUP*. For this procedure, I created nexus files for every Templeton's test comparison that includes (i) the character-taxon matrix, (ii) all MPTs from the original analysis (copied from a .tre file), (iii) all MPTs from the constraint (suboptimal) analyses. The respective files are archived online in the Dryad repository (Evers & Benson 2018*c*).

The set of commands used in PAUP* for each of these files is (italics indicate comments):

```
open PAUP*
set maxtrees=35000 increase=AUTO;
execute first file
treedist file=treedist_constraint_insertnumber.txt;
quit
repeat for all files
```

The respective treedist_constraint.txt files were further processed in R to select tree-pairs for the Templeton's test. The following code was used:

```
# Read distance matrix as matrix in which top triangle of symmetric
# matrix is filled with NAs, and "0"'s from
# diagonal are changed to NAs

dist.matrix    <-    data.matrix(read.table("treedist_constraint20.txt",
sep="\t", header=T, fill=T, na.strings="0"))
dist.matrix <- dist.matrix[,-c(1)]
rownames(dist.matrix) <- c(1:nrow(dist.matrix))
head(dist.matrix)

# Reduce the matrix so it contains only columns of the original MPTs
# (column argument is equal to # of original MPTs+1),
# and only the rows of the constraint MPTs (row argument is 1:# of MPTs
# in original analysis)

dist.matrix <- dist.matrix[-c(1:12),-c(13:ncol(dist.matrix))]
head(dist.matrix)

# Rename row names sequentially from 1

row.names(dist.matrix) <- c(1:nrow(dist.matrix))
head(dist.matrix)

# Find maximum distance value

max(dist.matrix, na.rm=TRUE)

# Define object that stores all matrix entries for which the maximum
# distance value is realised.
```

```
# The row number specifies the tree that should be selected from the
# constraint MPTs, the column number
# specifies the tree that should be selected from the original MPTs

max.dist<- data.matrix(which(dist.matrix == max(dist.matrix, na.rm=TRUE),
arr.ind = TRUE))

# Sample one row (i.e constraint MPT) - column (i.e. original MPT) at
# random for the Templeton's test

max.dist[sample(nrow(max.dist),1),]

# Same for minimum distance

min(dist.matrix, na.rm=TRUE)
min.dist<- data.matrix(which(dist.matrix == min(dist.matrix, na.rm=TRUE),
arr.ind = TRUE))
min.dist[sample(nrow(min.dist),1),]
```

In a next step, nexus files were created for every Templeton's test (i.e. each minimum and maximum distance comparison for each constraint analysis), each including (i) the character taxon matrix, (ii) MPT from original analysis; (iii) one MPT from constraint analysis. MPTs are selected according to previous step. The respective nexus files are archived online in the Dryad repository (Evers & Benson 2018*c*).

The Templeton's test were then performed in PAUP*, using the following commands (italics indicating comments):

```
open PAUP*
execute first file;
outgroup Proganochelys_quenstedti;
set root=outgroup;
pscores all / nonparamTest = yes testdetails = yes;
quit
Repeat for all MPT-constraint comparisons
```

S1.14 Supplementary references

ALBRECHT, P. W. 2012. The cranial arteries of turtles and their evolutionary significance. *Journal of Morphology*, **149**, 159–182.

ANQUETIN, J. 2012. Reassessment of the phylogenetic interrelationships of basal turtles (Testudinata). *Journal of Systematic Palaeontology*, **10**, 3–45.

———, PÜNTENER, C. and BILLON-BRUYAT, J.-P. 2015. Portlandemys gracilis n. sp., a New Coastal Marine Turtle from the Late Jurassic of Porrentruy (Switzerland) and a Reconsideration of Plesiochelyid Cranial Anatomy. *PLOS ONE*, **10**, e0129193.

BARDET, N., JALIL, N. E., DE LAPPARENT DE BROIN, F., GERMAIN, D., LAMBERT, O. and AMAGHZAZ, M. 2013. A giant chelonioid turtle from the Late Cretaceous of Morocco with a suction feeding apparatus unique among tetrapods. *PLoS ONE*, **8**, 1–10.

BHULLAR, B.-A. S. and BEVERS, G. S. 2009. An archosaur-like laterosphenoid in early turtles (Reptilia: Pantestudines). *Breviora*, **518**, 1–11.

BRINKMAN, D. B. and PENG, J.-H. 1993*a*. New material of *Sinemys* (Testudines, Sinemydidae) from the Early Cretaceous of China. *Canadian Journal of Earth Sciences*, **30**, 2139–2152.

BRINKMAN, D. B. and PENG, J.-H. 1993*b*. *Ordosemys leios*, n.gen., n.sp., a new turtle from the Early Cretaceous of the Ordos Basin, Inner Mongolia. *Canadian Journal of Earth Sciences*, **30**, 2128–2138.

——— and WU, X.-C. 1999. The skull of *Ordosemys*, an early Cretaceous turtle from Inner Mongolia, People's Republic of China, and the interrelationships of Eucryptodira (Chelonia, Cryptodira). *Paludicola*, **2**, 134–147.

———, EBERTH, D. A., XU, X., CLARK, J. M. and WU, X.-C. 2013. Turtles from the Jurassic Shishugou Formation of the Junggar Basin, People's Republic of China, with comments on the basicranial region of basal eucryptodires. *In* BRINKMAN, D. B., HOLROYD, P. A. and GARDNER, J. D. (eds.) *Morphology and Evolution of Turtles*, Springer, Dordrecht, 147–172 pp.

CADENA, E. 2015. The first South American sandownid turtle from the Lower Cretaceous of Colombia. *PeerJ*, **3**, e1431.

——— and PARHAM, J. F. 2015. Oldest known marine turtle? A new protostegid from the Lower Cretaceous of Colombia. *PaleoBios*, **32**, 1–421.

COLLINS, J. I. 1970. The chelonian *Rhinochelys* Seeley from the Upper Cretaceous of England and France. *Palaeontology*, **13**, 355–378.

CRAWFORD, N. G., PARHAM, J. F., SELLAS, A. B., FAIRCLOTH, B. C., GLENN, T. C., PAPENFUSS,

T. J., HENDERSON, J. B., HANSEN, M. H. and SIMISON, W. B. 2015. A phylogenomic analysis of turtles. *Molecular Phylogenetics and Evolution*, **83**, 250–257.

DANILOV, I. G., AVERIANOV, A. O., SKUTCHAS, P. P. and REZVYI, A. S. 2006. *Kirgizemys* (Testudines, 'Macrobaenidae'): New material from the Lower Cretaceous of Buryatia (Russia) and taxonomic revision. *In* DANILOV, I. G. and PARHAM, J. F. (eds.) *Fossil Turtle Research. Proceedings of the Symposium on Turtle Origins, Evolution and Systematics*, St. Petersburg.

GAFFNEY, E. S. 1972. An illustrated glossary of turtle skull nomenclature. *American Museum Novitates*, **2486**, 1–33.

——— 1979. Comparative cranial morphology of recent and fossil turtles. *Bulletin of the American Museum of Natural History*, **164**, 65–376.

——— 1983. The cranial morphology of the extinct horned turtle, *Meiolania platyceps*, from the Pleistocene of Lord Howe Island, Australia. *Bulletin of the American Museum of Natural History*, **175**, 361–480.

——— 1990. The comparative osteology of the Triassic turtle *Proganochelys*. *Bulletin of the American Museum of Natural History*, **194**, 1–176.

——— and JENKINS JR, F. A. 2010. The cranial morphology of *Kayentachelys* , an Early Jurassic cryptodire, and the early history of turtles. *Acta Zoologica*, **91**, 335–368.

——— and KITCHING, J. W. 1994. The most ancient African turtle. *Nature*, **369**, 55–58.

——— and KITCHING, J. W. 1995. The morphology and relationships of *Australochelys*, an early Jurassic turtle from South Africa. *American Museum Novitates*, **3130**, 1–29.

——— and YE, X. 1992. *Dracochelys*: a new cryptodiran turtle from the early Cretaceous of China. *American Museum Novitates,* **3048**, pages.

———, RICH, T. H., VICKERS-RICH, P., CONSTANTINE, A., VACCA, R. and KOOL, L. 2007. *Chubutemys*, a new eucryptodiran turtle from the Early Cretaceous of Argentina, and the relationships of the Meiolaniidae. *American Museum Novitates*, **3599**, 1–35.

HAVLIK, P. E., JOYCE, W. G. and BÖHME, M. 2014. *Allaeochelys libyca* , a new carettochelyine turtle from the Middle Miocene (Langhian) of Libya. *Bulletin of the Peabody Museum of*

Natural History, **55**, 201–214.

HIRAYAMA, R. 1994. Phylogenetic systematics of chelonioid sea turtles. *Island Arc*, **3**, 270–284.

——— 1998. Oldest known sea turtle. *Nature*, **392**, 705–708.

Holliday, C. M. and WITMER, L. M. 2007. Archosaur adductor chamber evolution: Integration of musculoskeletal and topological criteria in jaw muscle homology. *Journal of Morphology*, **268**, 457–484.

JOYCE, W. G. 2007. Phylogenetic relationships of Mesozoic turtles. *Bulletin of the Peabody Museum of Natural History*, **48**, 3–102.

JOYCE, W. G. and Lyson, T. R. 2015. A review of the fossil record of turtles of the clade Baenidae. *Bulletin of the Peabody Museum of Natural History*, **56** (2), 147–183.

KEAR, B. P. and LEE, M. S. Y. 2006. A primitive protostegid from Australia and early sea turtle evolution. *Biology letters*, **2**, 116–119.

KNAUSS, G. E. 2014. A morphological description of *Baptemys wyomingensis* and an analysis of its phylogenetic relationship within Kinosternoidea. Unpublished M.Sc. thesis, University of Iowa, Iowa City, 181 pp.

LIPKA, T. R., THERRIEN, F., WEISHAMPEL, D. B., JAMNICZKY, H. a., JOYCE, W. G., COLBERT, M. W. and BRINKMAN, D. B. 2006. A new turtle from the Arundel Clay facies (Potomac Formation, Early Cretaceous) of Maryland, U.S.A. *Journal of Vertebrate Paleontology*, **26**, 300–307.

MEYLAN, P. A. and GAFFNEY, E. S. 1989. The skeletal morphology of the Cretaceous cryptodiran turtle, *Adocus*, and the relationships of the Trionychoidea. *American Museum Novitates*, **2941**, 1–60.

MÜLLER, J., Sterli, J. and ANQUETIN, J. 2011. Carotid circulation in amniotes and its implications for turtle relationships. *Neues Jahrbuch für Geologie und Paläontologie*, **261** (3), 289–297.

PARHAM, J. F. and HUTCHISON, J. H. 2003. A new eucryptodiran turtle from the Late Cretaceous of North America (Dinosaur Provincial Park, Alberta, Canada). *Journal of*

Vertebrate Paleontology, **23**, 783–798.

——— and PYENSON, N. D. 2010. New sea turtle from the Miocene of Peru and the iterative evolution of feeding ecomorphologies since the Cretaceous. *Journal of Paleontology*, **84**, 231–247.

RABI, M., ZHOU, C.-F., WINGS, O., GE, S. and JOYCE, W. G. 2013. A new xinjiangchelyid turtle from the Middle Jurassic of Xinjiang, China and the evolution of the basipterygoid process in Mesozoic turtles. *BMC Evolutionary Biology*, **13**, 203.

———, SUKHANOV, V. B., EGOROVA, V. N., DANILOV, I. G. and JOYCE, W. G. 2014. Osteology, relationships, and ecology of *Annemys* (Testudines, Eucryptodira) from the Late Jurassic of Shar Teg, Mongolia, and phylogenetic definitions for Xinjiangchelyidae, Sinemydidae, and Macrobaenidae. *Journal of Vertebrate Paleontology*, **34**, 327–352.

RIEPPEL, O. 1993. Patterns and diversity in the reptilian skull. *In* Hanken, J. and HALL, B. K. (eds). The skull, volume 2. The University of Chicago Press, Chicago, 580 pp.

ROLLOT, Y., LYSON, T. R. and JOYVE, W. G. *in press*. A description of Eubaena cephalica (Hay, 1904) and new insights into the cranial circulation and innervation of baenid turtles. *Journal of Vertebrate Paleontology*.

SIEBENROCK, F. 1897. Das Kopfskelett der Schildkröten. *Sitzungsberichte der Kaiserliche Akademie der Wissenschaften (Wien), Mathematik-Naturwissenschaften,* **106***,* 245–328.

SOLIMAN, M. A. 1964. Die Kopfnerven der Schildkröten. *Zeitschrift für Wissenschaftliche Zoologie,* **169***,* 216–312.

STERLI, J. 2008. A new, nearly complete stem turtle from the Jurassic of South America with implications for turtle evolution. *Biology Letters*, **4**, 286–289.

——— and DE LA FUENTE, M. S. 2010. Anatomy of *Condorchelys antiqua* Sterli, 2008, and the origin of trhe modern jaw closure mechanism in turtles. *Journal of* Vertebrate *Paleontology,* **30** (2), 351–366.

——— and DE LA FUENTE, M. S. 2011. A new turtle from the La Colonia Formation (Campanian-Maastrichtian), Patagonia, Argentina, with remarks on the evolution of the vertebral column in turtles. *Palaeontology,* **54**, 63–78.

———— and DE LA FUENTE, M. S. 2013. New evidence from the Palaeocene of Patagonia (Argentina) on the evolution and palaeo-biogeography of Meiolaniformes (Testudinata, new taxon name). *Journal of Systematic Palaeontology*, **11**, 835–852.

————, DE LA FUENTE, M. S. and ROUGIER, G. W. 2007. Anatomy and relationships of *Palaeochersis talampayensis*, a Late Triassic turtle from Argentina. *Palaeontographica Abteilung A*, 281, 1–61.

————, DE LA FUENTE, M. S. and UMAZANO, A. M. 2015. New remains and new insights on the Gondwanan meiolaniform turtle *Chubutemys copelloi* from the Lower Cretaceous of Patagonia, Argentina. *Gondwana Research*, **27**, 978–994.

SUKHANOV, V. B. 2000. Mesozoic turtles of middle and central Asia. *The age of dinosaurs in Russia and Mongolia*, **17**, 309–367.

TONG, H. and MEYLAN, P. 2013. Morphology and Relationships of *Brachyopsemys tingitana* gen. et sp. nov. from the Early Paleocene of Morocco and Recognition of the New Eucryptodiran Turtle Family: Sandownidae. 187–212. *In* BRINKMAN, D. B., HOLROYD, P. A. and GARDNER, J. D. (eds.). *Morphology and Evolution of Turtles*. Springer, Dordrecht, 577 pp.

VINEYARD, D. 2009. A new eucryptodiran turtle from the Lower Cretaceous Glen Rose Formation of Texas. Unpublished M.Sc. thesis, Southern Methodist University, Dallas, 123pp.

WEVER, E. G. 1978. The reptile ear: its structure and function. Princeton University Press, Princeton, New Jersey, 1024 pp.

ZANGERL, R. 1953. The vertebrate fauna of the Selma Formation of Alabama. Part IV. The turtles of the family Toxochelyidae. *Fieldiana. Geology Memoirs*, **3**, 1–176.

————. 1980. Patterns of phylogenetic differentiation in the toxochelyid and cheloniid sea turtles. *Integrative and Comparative Biology*, **20**, 585–596.

ZHOU, C.-F. and RABI, M. 2015. A sinemydid turtle from the Jehol Biota provides insights into the basal divergence of crown turtles. *Scientific Reports*, **5**, 16299.

————, and RABI, M.and JOYCE, W. G. 2014. A new specimen of *Manchurochelys*

manchoukuoensis from the Early Cretaceous Jehol Biota of Chifeng, Inner Mongolia, China and the phylogeny of Cretaceous basal eucryptodiran turtles. *BMC Evolutionary Biology*, **14**, 77.

APPENDIX S2

S2.1 Additional anatomical illustrations

The following illustrations are provided as additional guides for the description provided in the main text of section 3.4 of this thesis.

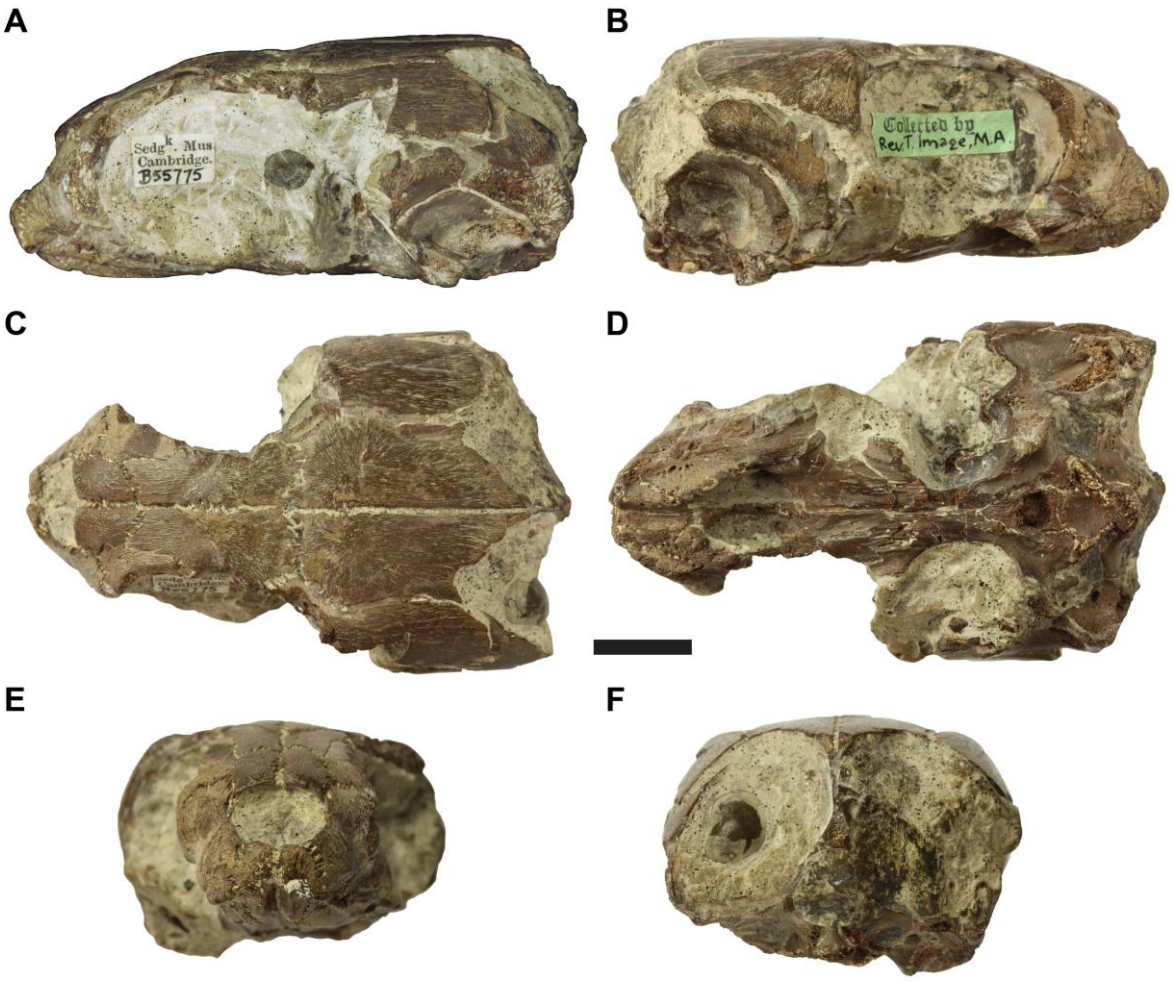


FIG. S2.1. Photographs of CAMSM B55775, the holotype of *R. pulchriceps*. **A**, left lateral view; **B**, right lateral view; **C**, dorsal view; **D**, ventral view; **E**, anterior view; **F**, posterior view. Scale bar equals 10 mm.

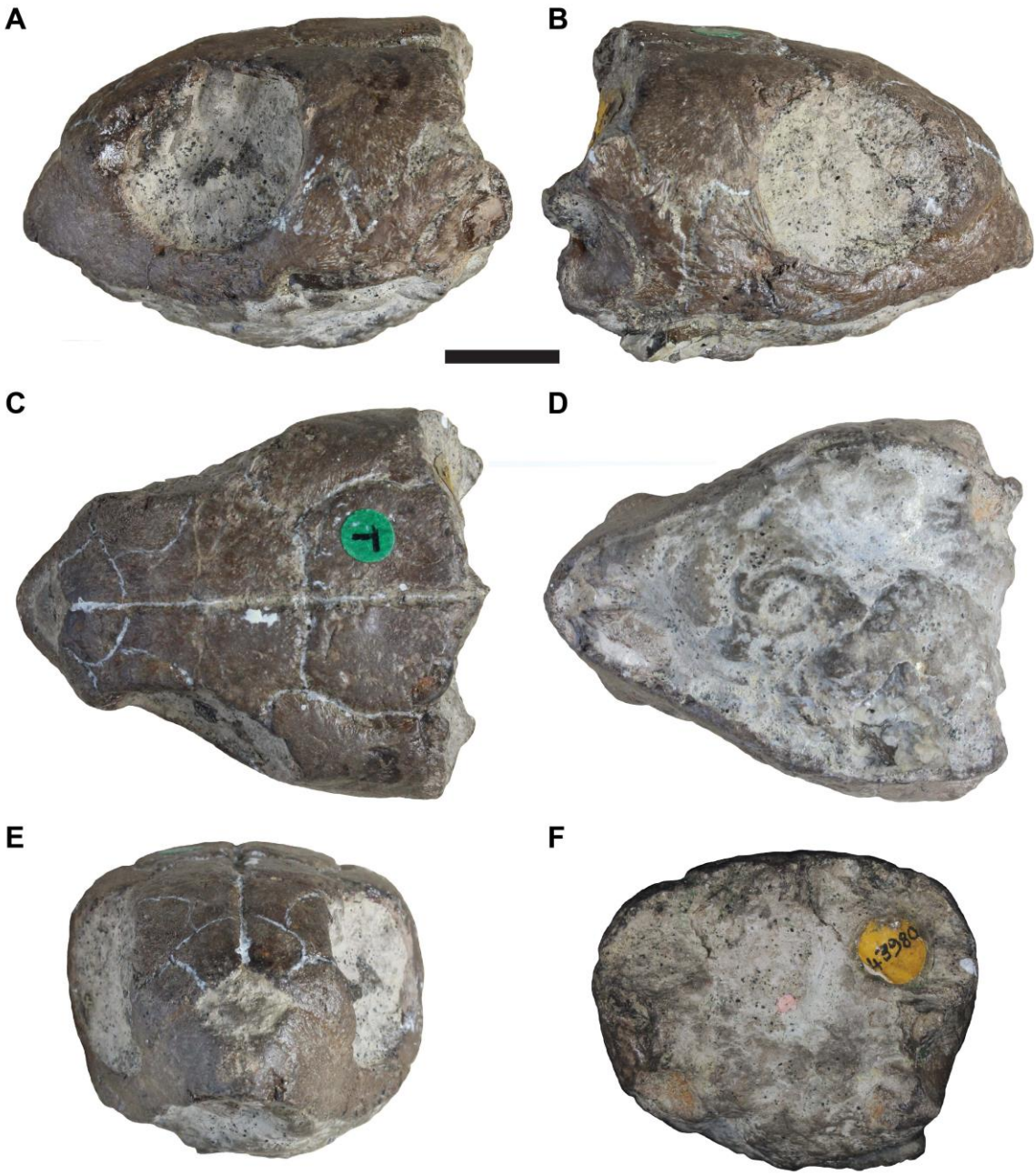


FIG. S2.2. Photographs of NHMUK 43980, the holotype of *R. cantabrigiensis*. **A**, left lateral view; **B**, right lateral view; **C**, dorsal view; **D**, ventral view; **E**, anterior view; **F**, posterior view. Scale bar equals 10 mm.

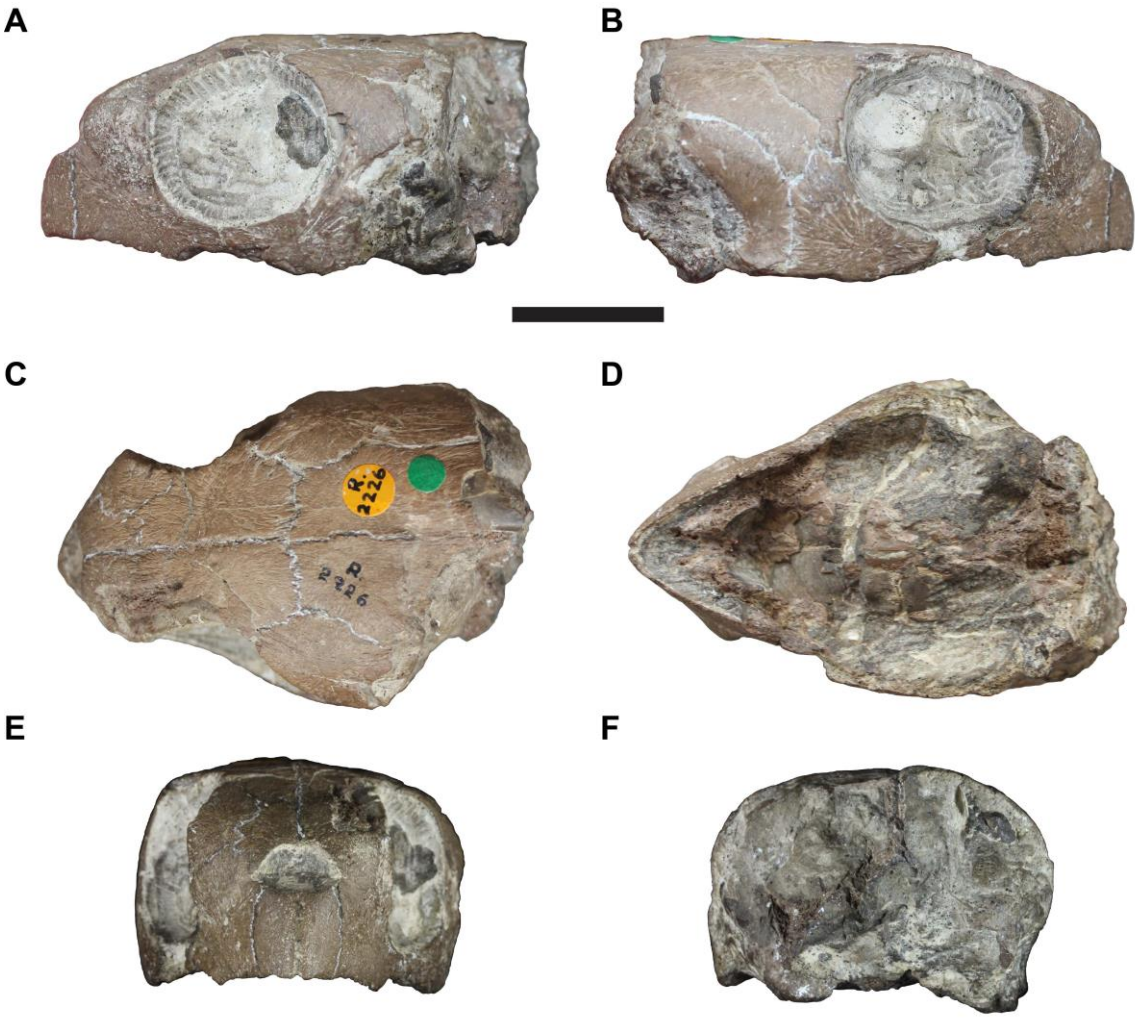


FIG. S2.3. Photographs of NHMUK 2226, the holotype of *R. elegans*. **A**, left lateral view; **B**, right lateral view; **C**, dorsal view; **D**, ventral view; **E**, anterior view; **F**, posterior view. Scale bar equals 20 mm.

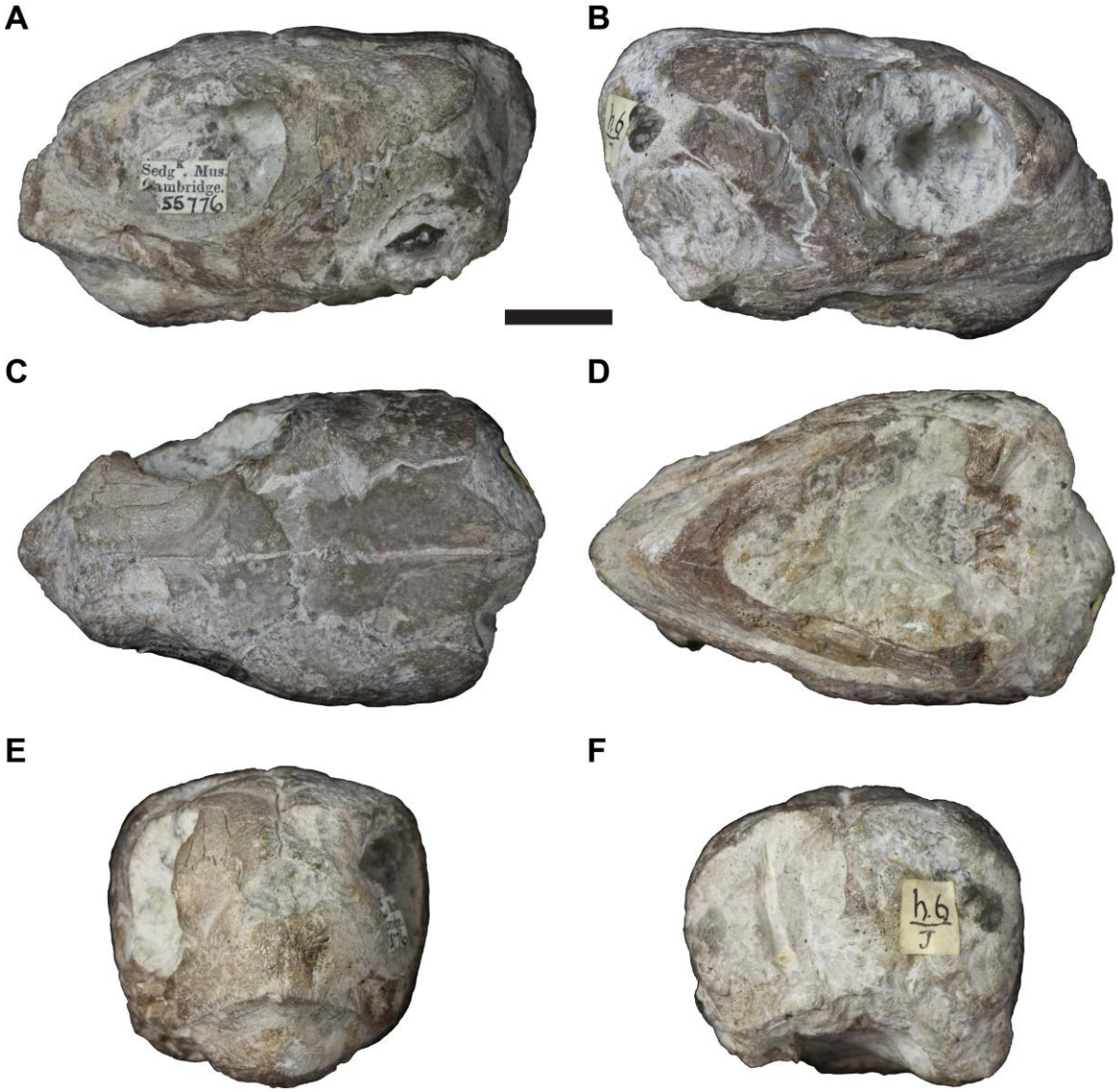


FIG. S2.4. Photographs of CAMSM B55776. **A**, left lateral view; **B**, right lateral view; **C**, dorsal view; **D**, ventral view; **E**, anterior view; **F**, posterior view. Scale bar equals 10 mm.

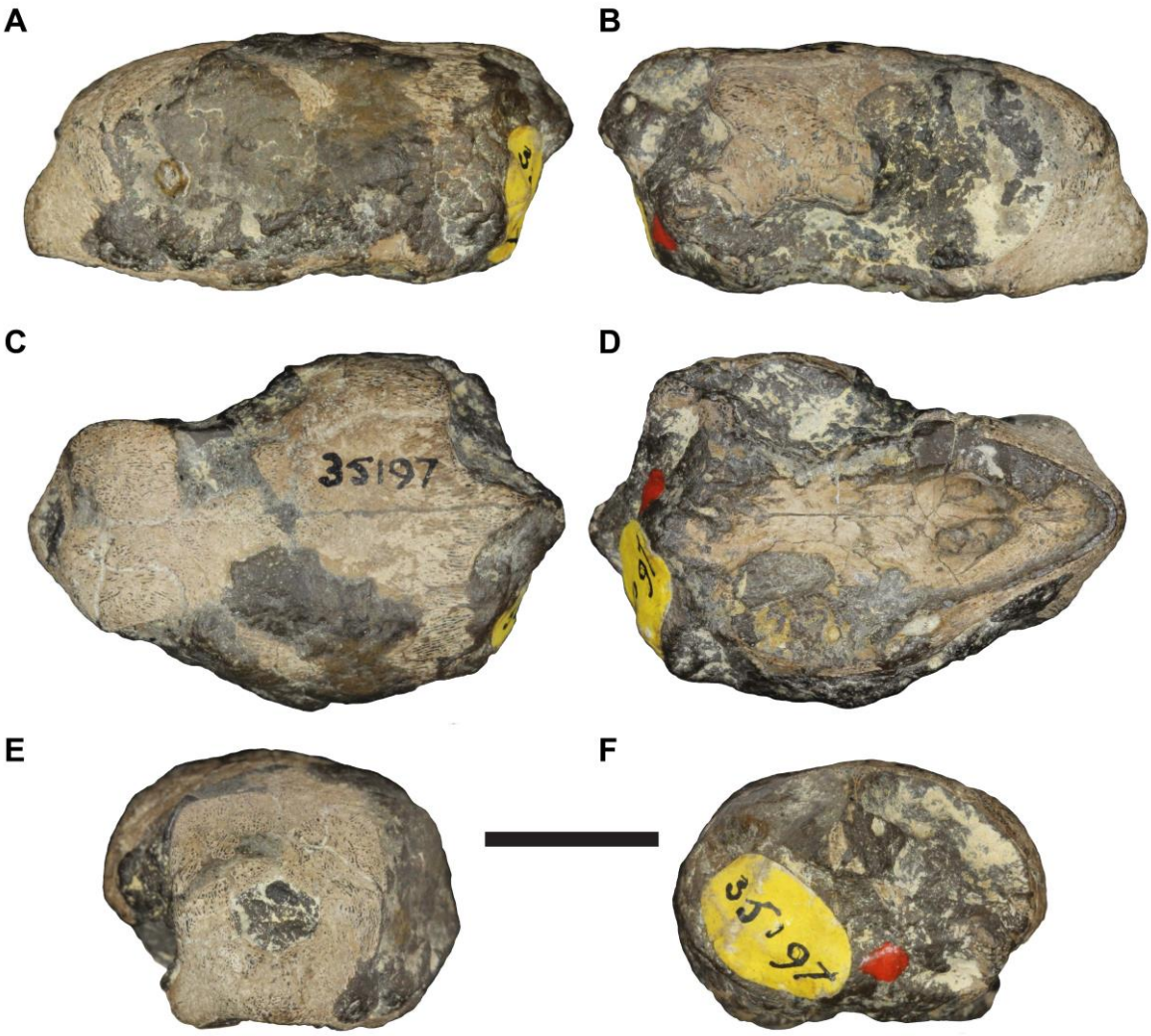


FIG. S2.5. Photographs of NHMUK 35197. **A**, left lateral view; **B**, right lateral view; **C**, dorsal view; **D**, ventral view; **E**, anterior view; **F**, posterior view. Scale bar equals 10 mm.

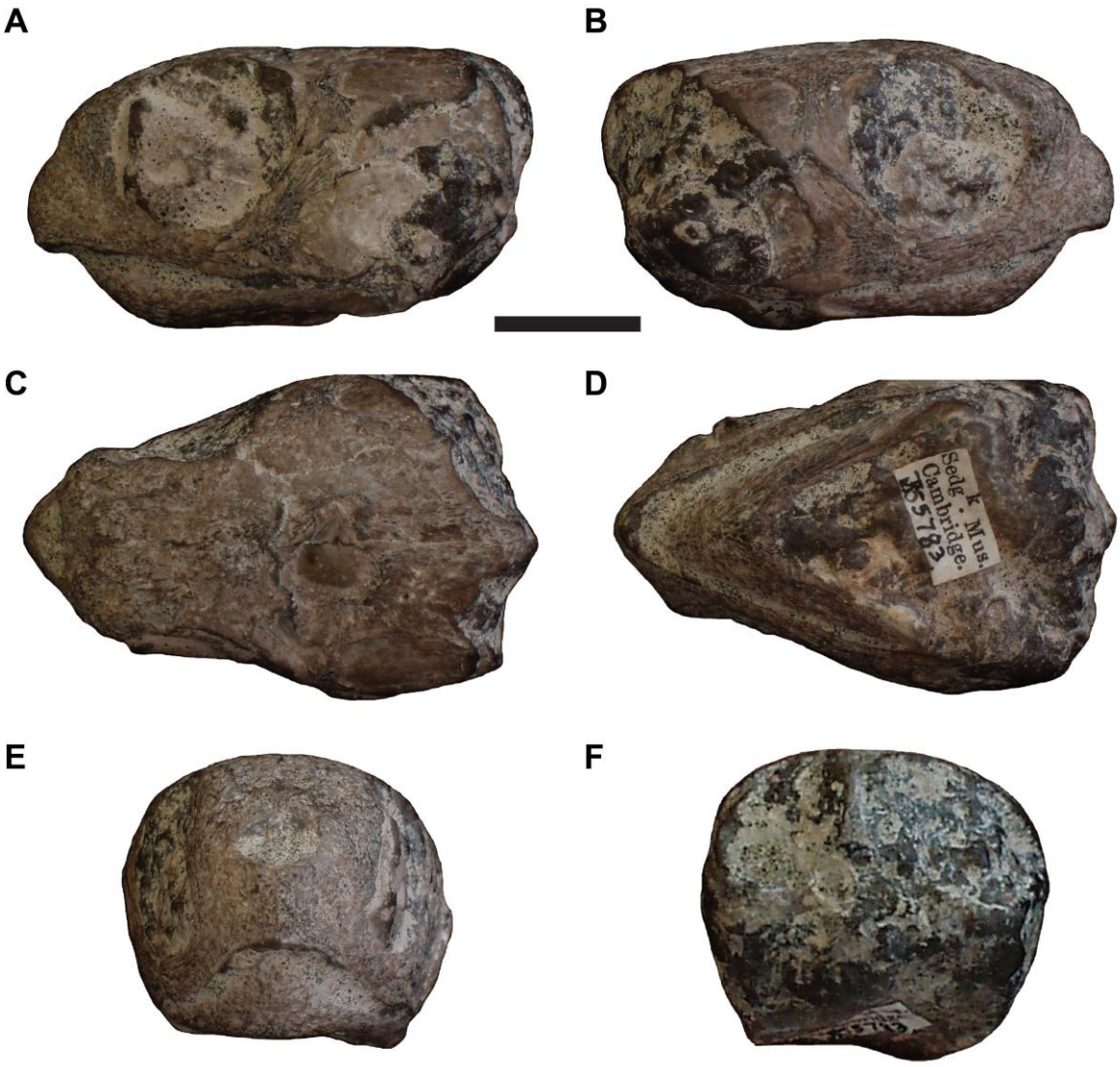


FIG. S2.6. Photographs of CAMSM B55783. **A**, left lateral view; **B**, right lateral view; **C**, dorsal view; **D**, ventral view; **E**, anterior view; **F**, posterior view. Scale bar equals 10 mm.

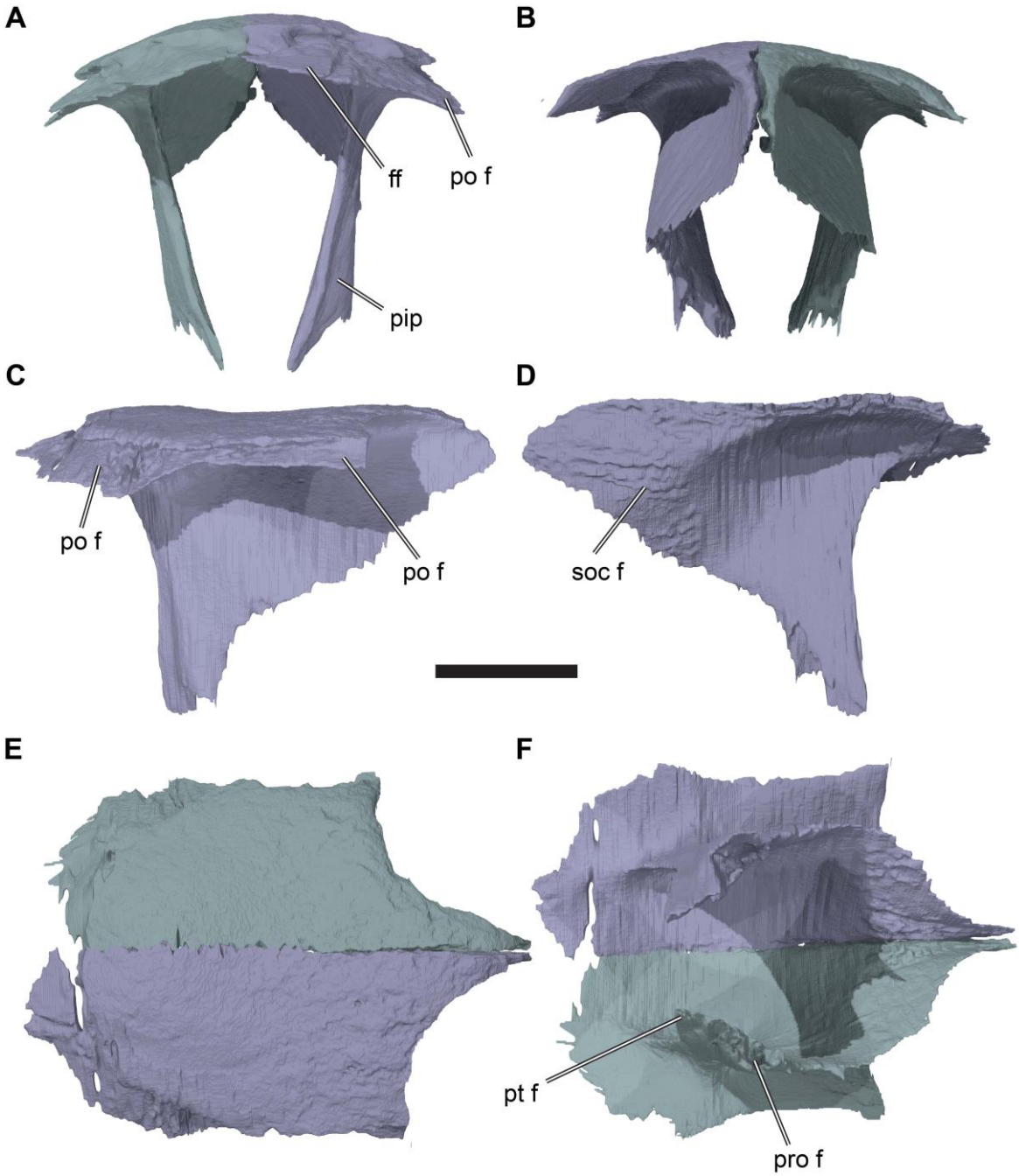


FIG. S2.7. 3D rendering of the left and right parietals of NHMUK R35197. Scale bar equals 5 mm. Abbreviations: *ff*, facet for frontal, *pip*, processus inferior parietalis, po f, facet for postorbital, *pro f*, facet for prootic, *pt f*, facet for pterygoid, *soc f*, facet for supraoccipital.

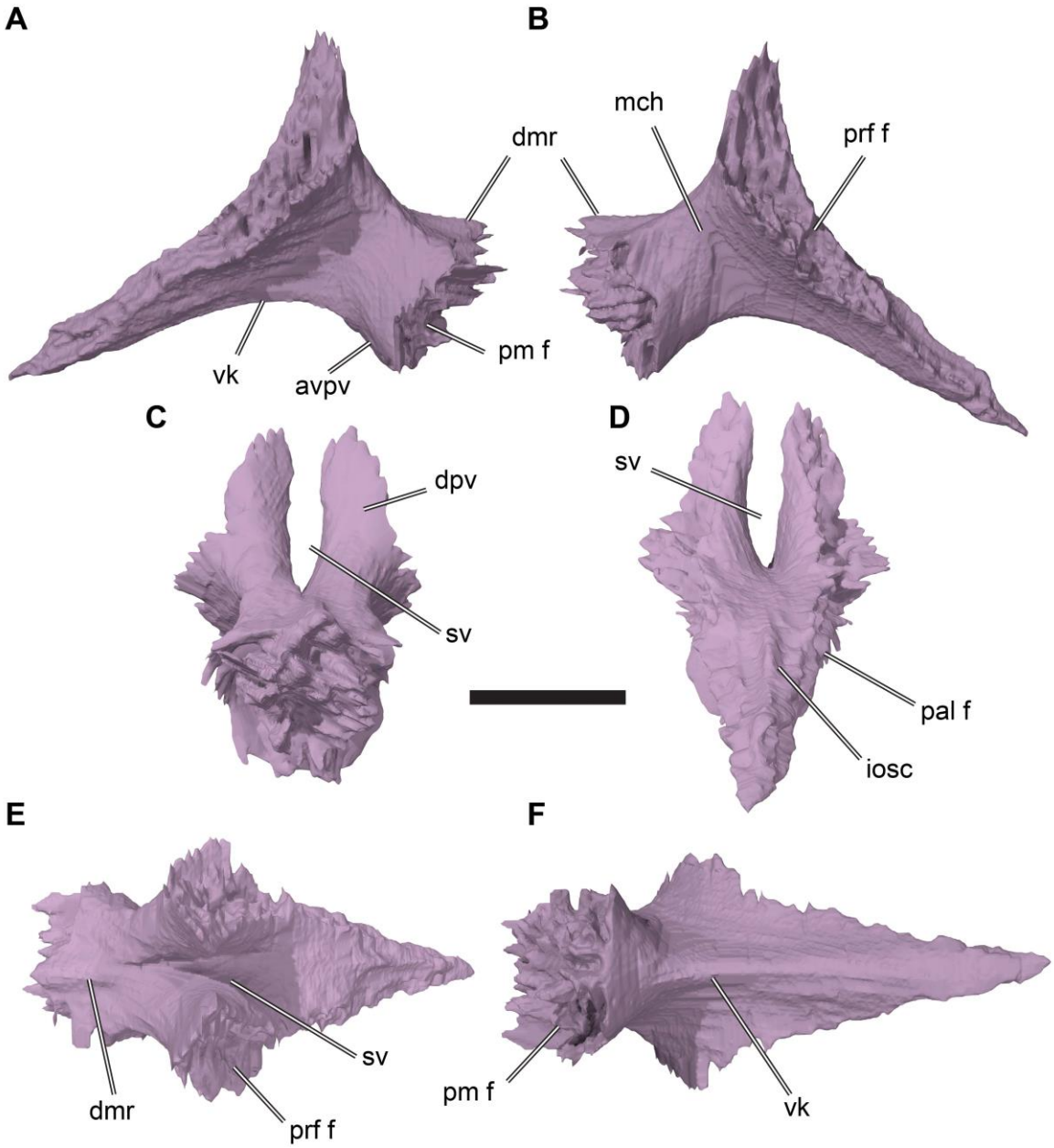


FIG. S2.8. 3D rendering of vomer of CAMSM B5583. **A**, right lateral view; **B**, left lateral view; **C**, anterior view; **D**, posterior view; **E**, dorsal view; **F**, ventral view. Scale bar equals 3 mm. Abbreviations: *avpv*, anteroventral process of vomer; *dmr*, dorsal medial ridge of vomer; *dvp*, dorsal process of vomer; *iosc*, interorbital septum crest; *mch*, meatus choanae; *pm f*, facet for premaxilla; *prf f*, facet for prefrontal; *sv*, sulcus vomeri; *vk*, vomer keel;

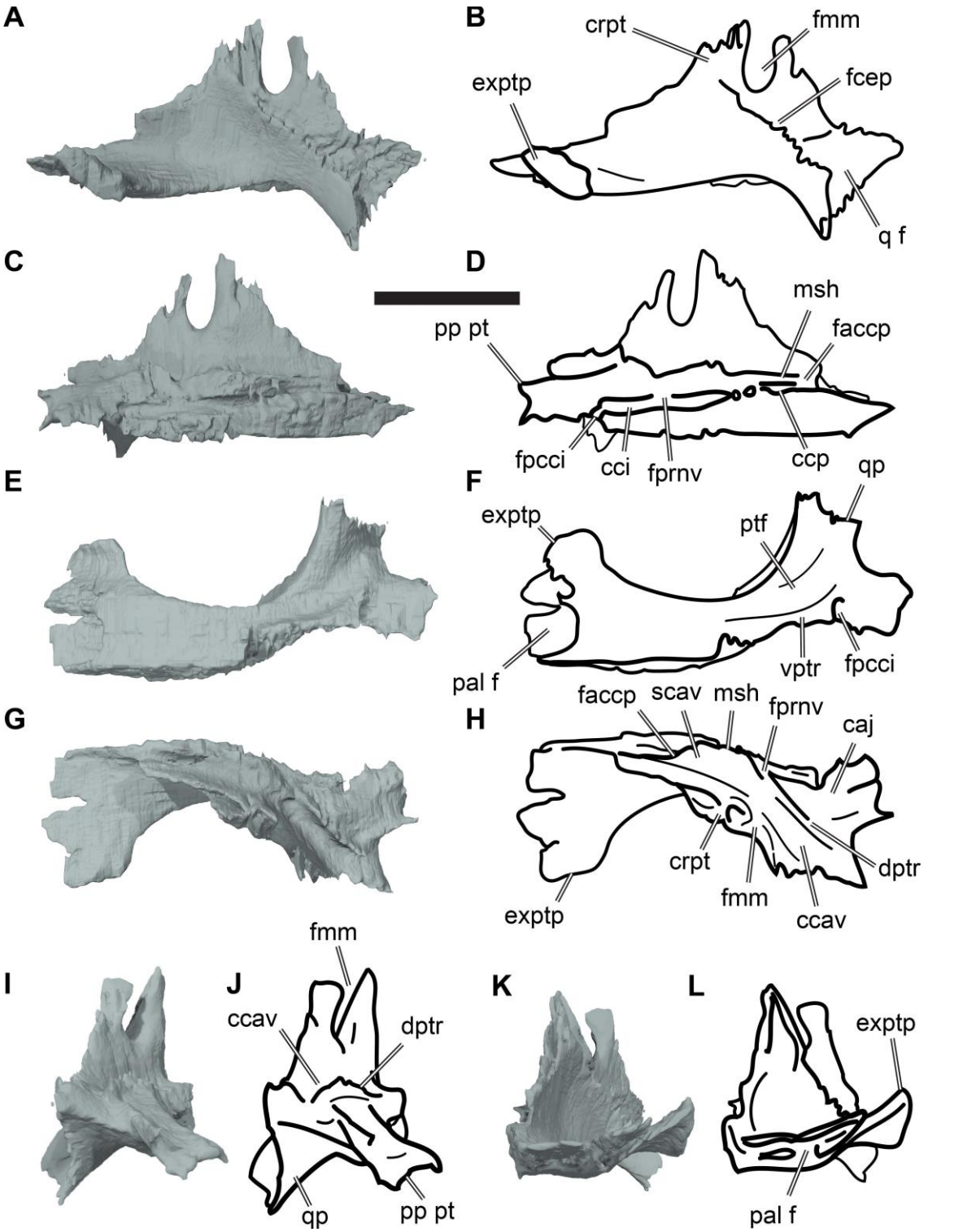


FIG. S2.9. Left pterygoid of CAMSM B5583. **A**, 3D rendering in lateral view; **B**, interpretative line drawing of A; **C**, 3D rendering in medial view; **D**, interpretative line drawing of B; **E**, 3D rendering in ventral view; **F**, interpretative line drawing of E; **G**, 3D rendering in dorsal view; **H**, interpretative line drawing of H; **I**, 3D rendering in posterior view; **J**, interpretative line drawing of I; **K**, 3D rendering in anterior view; **L**, interpretative line drawing of K. Scale bar equals 5 mm. Abbreviations: *caj*, cavum acustico-jugulare; *ccav*, canalis cavernosus; *cci*, canalis caroticus internus; *ccp*, canalis caroticus palatinus; *crpt*, crista pterygoidei; *dptr*, dorsal pterygoid ridge; *exptp*, external pterygoid process; *faccp*, foramen anterius canalis carotici palatinum; *fcep*, fossa cartilaginis expipterygoidei; *fmm*, maxillo-mandibular foramen; *fpcci*, foramen posterius canalis carotici interni; *fprnv*, foramen pro ramo nervi vidani; *msh*, medial shelf; *pal f*, facet for palatine; *pp pt*, posterior process of pterygoid; *ptf*, pterygoid fossa; *q f*, facet for quadrate; *qp*, quadrate process of pterygoid; *scav*, sulcus cavernosus; *vptr*, ventral pterygoid ridge.

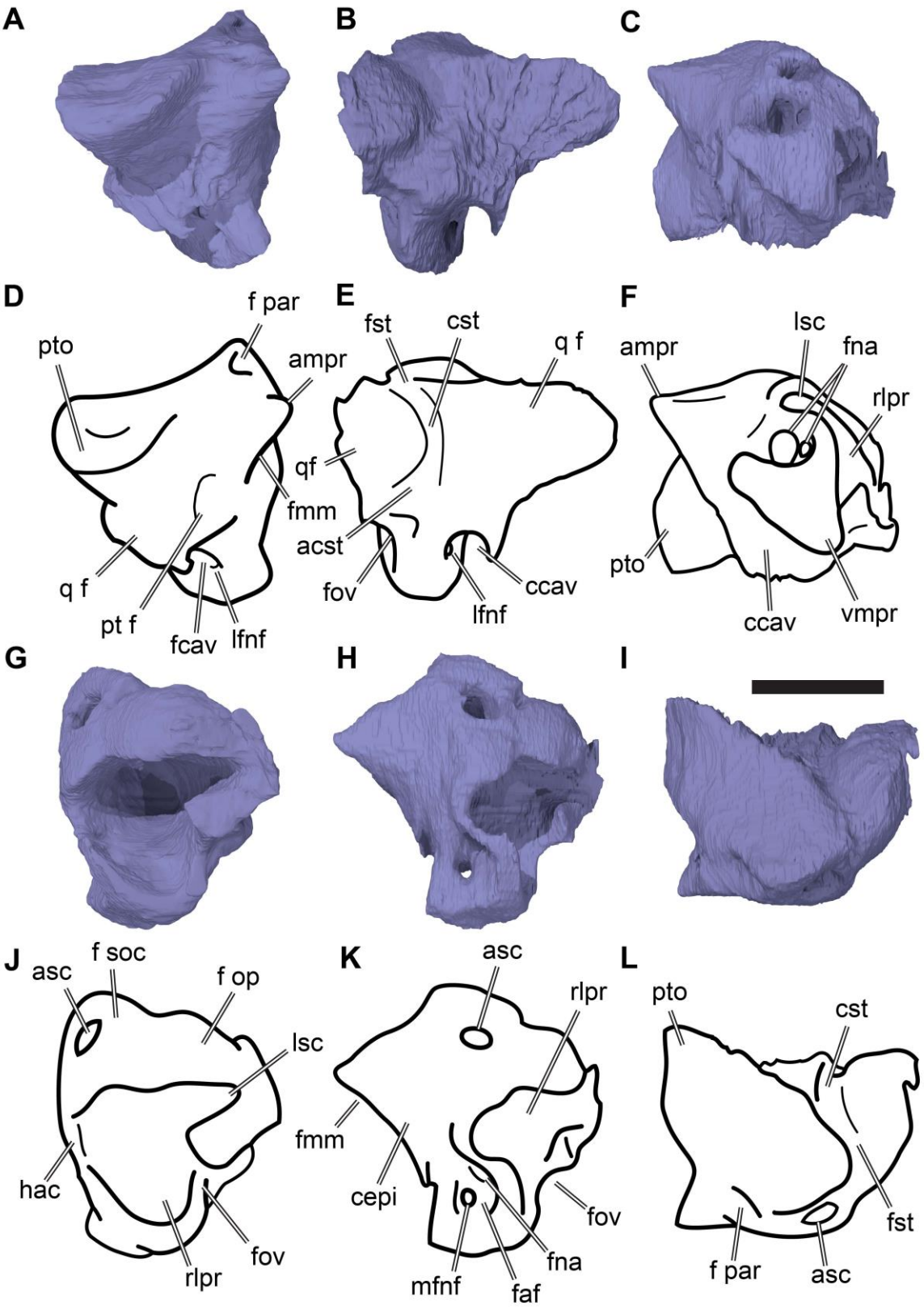


FIG. S2.10. Right prootic of CAMSM B55775. **A**, 3D rendering in anterior view; **B**, 3D rendering in medial view; **C**, 3D rendering in ventral view; **D**, interpretative line drawing of A; **E**, interpretative line drawing of B; **F**, interpretative line drawing of C; **G**, 3D rendering in posterior view; **H**, 3D rendering in medial view; **I** 3D rendering in dorsal view; **J**, interpretative line drawing of G; **K**, interpretative line drawing of H; **L**, interpretative line drawing of I. Scale bar equals 5 mm. Abbreviations: *acst*, aditus canalis stapedio-temporalis; *asc*, anterior semicircular canal; *ampr*, anteromedial process of prootic; *ccav*, canalis cavernosus; *cepi*, cavum epiptericum; *cst*, canalis stapedio-temporalis; *faf*, fossa acustico-facialis; *fcav*, foramen cavernosum; *fmm*, maxillo-

mandibular foramen; *fna*, foramina nervi acustici; *f par*, facet for parietal; *f op*, facet for opisthotic; *fov*, fenestra ovalis; *fst*, foramen stapedio-temporale; *f soc*, facet for supraoccipital; *hac*, hiatus acusticus; *lfnf*, lateral foramen nervi facialis; *mfnf*, medial foramen nervi facialis; *lsc*, lateral semicircular canal; *pt f*, facet for pterygoid; *pto*, processus trochlearis oticum; *q f*, facet for quadrate; *rlpr*, recessus labyrinthicus prooticus; *vmpr*, ventromedial process of prootic.

(continued from previous page)

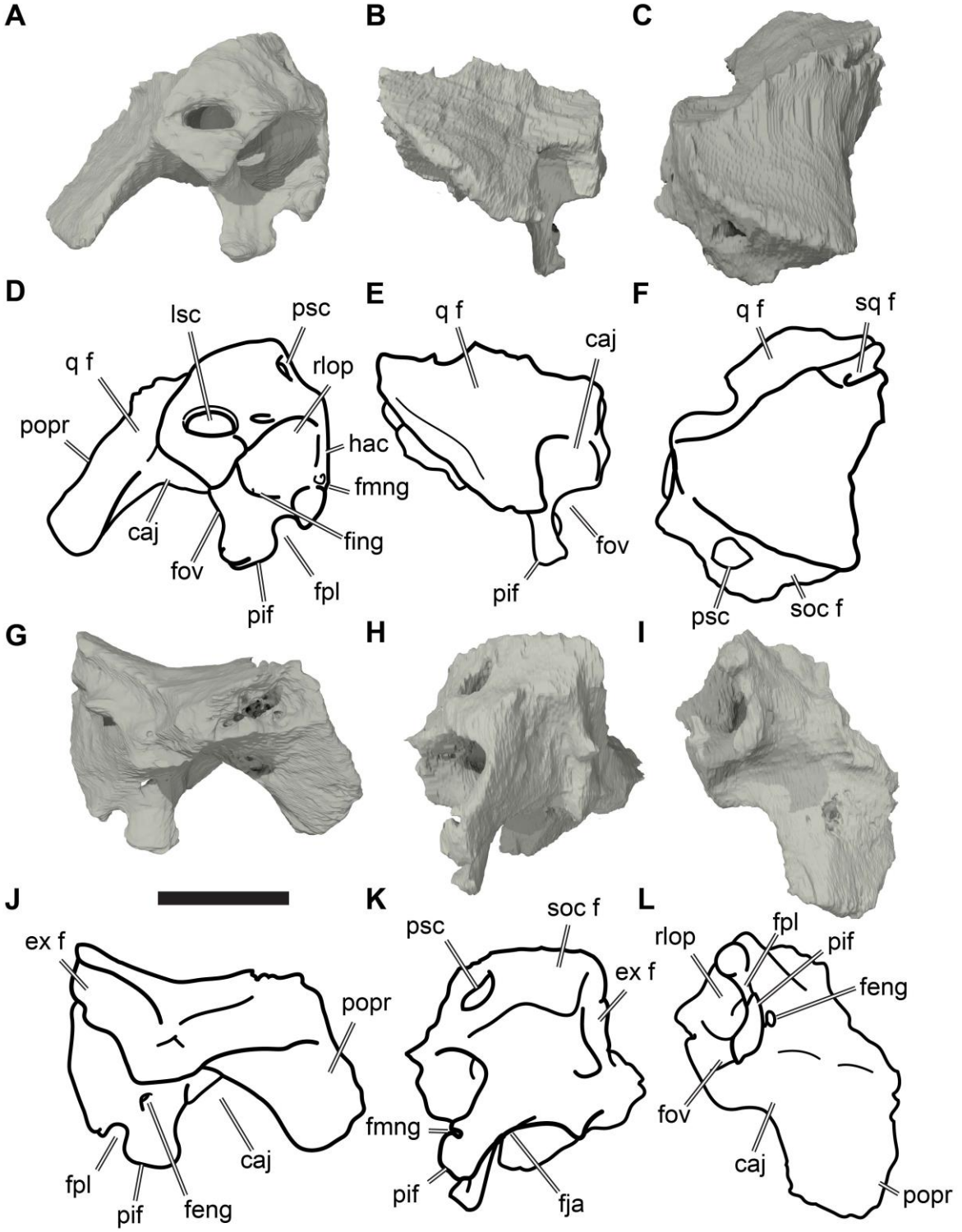


FIG. S2.11. Right opisthotic of CAMSM B55775. **A**, 3D rendering in anterior view; **B**, 3D rendering in lateral view; **C**, 3D rendering in dorsal view; **D**, interpretative line drawing of A; **E**, interpretative line drawing of B; **F**, interpretative line drawing of C; **G**, 3D rendering in posterior view; **H**, 3D rendering in medial view; **I**, 3D rendering in ventral view; **J**, interpretative line drawing of G; **K**, interpretative line drawing of H; **L**, interpretative line drawing of I. Scale bar

equals 5 mm. Abbreviations: *caj*, cavum acustico-jugulare; *feng*, foramen externum nervi glosspharyngei; *fing*, foramen internum nervi glossopharyngei; *fja*, foramen jugulare anterius; *fmng*, foramen medialis nervi glosspharyngei; *fov*, fenestra ovalis; *fpl*, fenestra perilymphatica; *ex f*, facet for exoccipital; *hac*, hiatus acusticus; *lsc*, lateral semicircular canal; *pif*, processus interfenestralis; *popr*, parociipital process of opisthotic; *psc*, posterior semicircular canal; *q f*, facet for quadrate; *rlop*, recessus labyrinthicus opisthoticus; *soc f*, facet for supraoccipital; *sq f*, facet for squamosal. *(continued from previous page)*

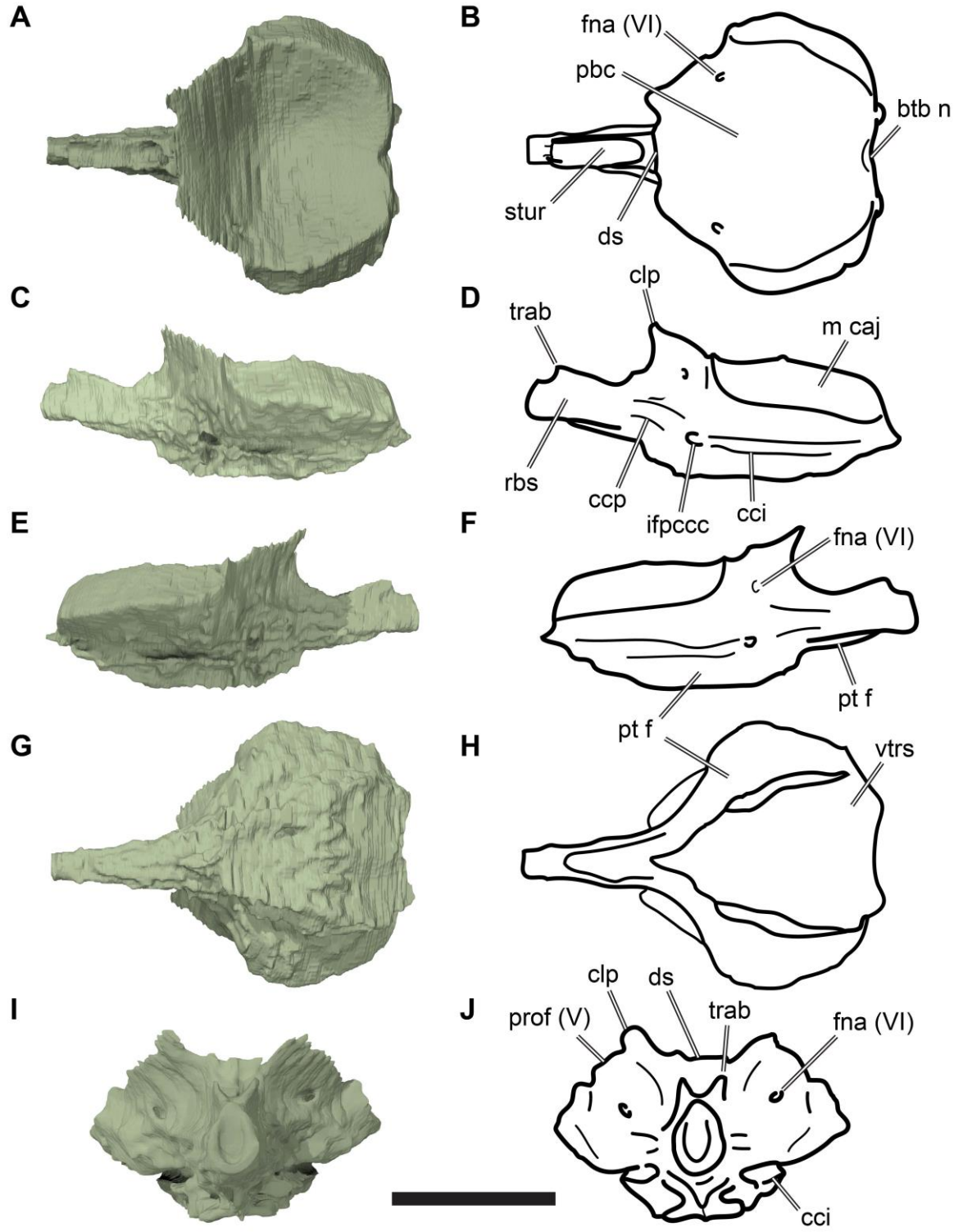


FIG. S2.12. **A**, 3D rendering in dorsal view; **B**, interpretative line drawing of B; **C**, 3D rendering in left lateral view; **D**, interpretative line drawing of C; **E**, 3D rendering in right lateral view; **F**, interpretative line drawing of E; **G**, 3D rendering in ventral view; **H**,

interpretative line drawing of H; **I**, 3D rendering in anterior view; **J**, interpretative line drawing of I. Scale bar equals 3 mm. Abbreviations: *btb n*, basis tuberculi basalis notch; *cci*, canalis caroticus internus; *ccp*, canalis caroticus palatinum; *clp*, clinoid process; *ds*, dorsum sellae; *fna (VI)*, foramen nervi abducentis; *ifpccc*, internal foramen posterius canalis carotici cerebralis; *m caj*, margin of parabasisphenoid facing cavum acustico-jugulare; *pbc*, parabasisphenoid cup; *prof (V)*, prootic foramen; *pt f*, facet for pterygoid; *rbs*, rostrum basisphenoidale; *stur*, sella turcica; *trab*, trabeculae; *vtrs*, ventral triangular surface.

(continued from previous page)

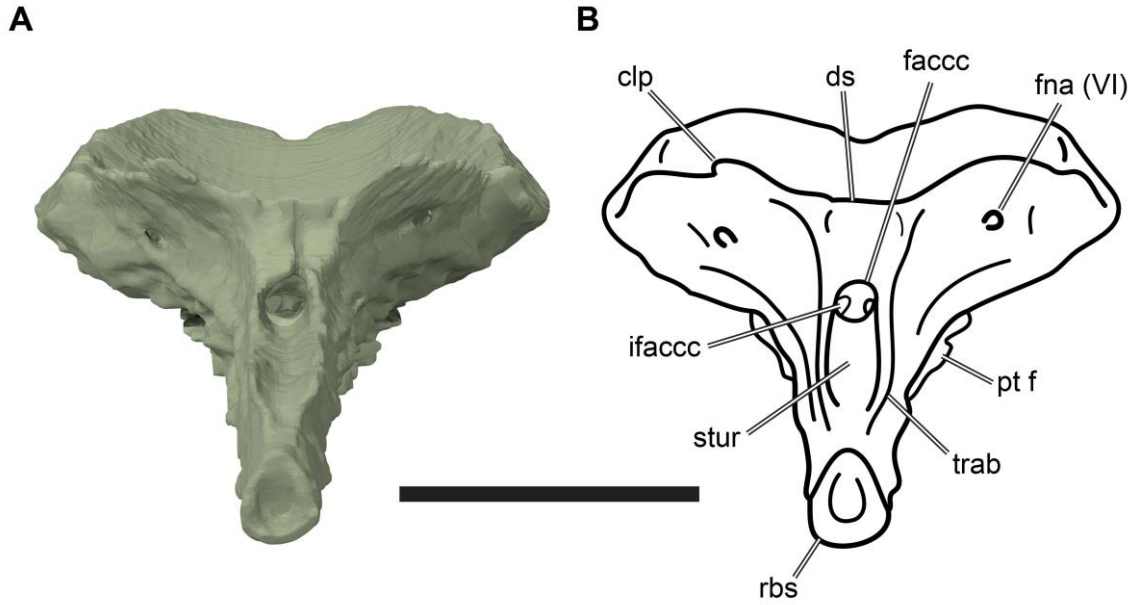


FIG. S2.13. Anterodorsal view of parabasisphenoid of NHMUK 35197. **A**, 3D rendering; **B**, interpretative line drawing. Scale bar equals 3 mm. Abbreviations: *clp*, clinoid process; *ds*, dorsum sellae; *faccc*, foramen anterius canalis carotici cerebralis; *fna (VI)*, foramen nervi abducentis; *ifaccc*, internal foramen anterius canalis carotici cerebralis; *pt f*, pterygoid facet; *rbs*, rostrum basisphenoidale; *stur*, sella turcica; *trab*, trabecular.

S2.2 PCA Supplementary information

S2.2.1 R code

The procedure for the PCA shown in section 2 of this thesis is described in the main thesis text. The below text is the R code used to compute the PCA including all measurements. Note that the dataset "Rhinochelys_measurements_full.txt" is a text file containing all Rhinochelys specimens for which all measurements could be taken (see Table 3.2 of main thesis text).

```
# Load dataset
# Data contains measurements of different units
```

```
measurements <-read.table("Rhinochelys_measurements_full.txt", header=T)
measurements[,apply(is.na(measurements),2,sum)==0]

# Define data for PCA input

input<-measurements[,apply(is.na(measurements),2,sum)==0]
      rownames(input) <- input[,1]
            input<-input[,-1]

# Compute PCA with prcomp()

# scale = TRUE for correlation matrix, i.e. when different units
# are used. It does a z-transformation to the data, scaling it to
# equal variance and equal means. This is equivalent to using a
# correlation matrix.

options(digits=3)
PCA.result <- prcomp(input, scale=TRUE)
PrincipalComponents <- summary(PCA.result)
Eigenvalues <- PCA.result$sdev^2

# Compare/Compute proportion of variance explained and rescaled
# proportion when PC1 is excluded

proportion.of.variance <- Eigenvalues/sum(Eigenvalues)
rescaled.proportion.of.variance <- Eigenvalues[2:7]/sum(Eigenvalues[2:7])

# Values for specimens that will be plotted

str(PCA.result)
PCA.result$x

# print results for table

PrincipalComponents
PCA.result
Eigenvalues
proportion.of.variance
rescaled.proportion.of.variance

# Define species according to Collins

pulchriceps <- c("CAMSM_B55775", "NHMUK_R2224")
cantabrigiensis <- c("CAMSM_B55774", "CAMSM_B55782", "CAMSM_B55783",
"CAMSM_B55785", "CAMSM_B55786", "CAMSM_B55787", "CAMSM_B55791",
"CAMSM_B56574", "NHMUK_R2227", "NHMUK_R2233", "NHMUK_R2234",
"NHMUK_R43980")
elegans <- c("CAMSM_B55776", "CAMSM_B55784", "NHMUK_R2226",
"NHMUK_R35197", "NHMUK_R46371a")
ambareti <- c("R_ambaretti")
notassigned <- c("CAMSM_B55794", "CAMSM_B56570", "CAMSM_B56571",
"CAMSM_B56575", "CAMSM_B56583", "NHMUK_R11521", "NHMUK_R8339")

# Define colours for species

species <- rep("black", length(measurements[,1]))
      species[measurements$Specimen %in% pulchriceps] <- "red"
      species[measurements$Specimen %in% cantabrigiensis] <- "lightblue"
      species[measurements$Specimen %in% elegans] <- "purple"
      species[measurements$Specimen %in% ambareti] <- "orange"
      species[measurements$Specimen %in% notassigned] <- "darkgrey"
      species
```

```
# Define holotypes

holotype.specimens <- c("CAMSM_B55775", "R_ambaretti", "NHMUK_R43980",
"NHMUK_R2226")
      holotypes <- rep(21, length(measurements[,1]))
            holotypes[measurements$Specimen %in% holotype.specimens] <-
23
      holotypes

# Define cex for sepecimens

symbol.size <- rep(1.3, length(measurements[,1]))
      symbol.size[measurements$Specimen %in% holotype.specimens] <- 1.6
      symbol.size

# Plot PCA

dev.new( width = 11 , height = 6)
pdf("PCA_all_measurements.pdf", width = 11 , height = 6,
useDingbats=FALSE)
#close.screen(all.screens=T)
split.screen(c(1,2))
      screen(1)
      plot(PCA.result$x[,2],PCA.result$x[,3], bty="o", bg=species,
cex=symbol.size, pch=holotypes, xlab="PC2 [56.3 %]", ylab="PC3 [24.7 %]")
      legend("topright", ncol=2, cex=0.7, legend=c("R. pulchriceps", "R.
cantabrigiensis", "R. elegans", "R. ambareti", "not assigned",
"holotypes"), bty="o", pch= c(21, 21, 21, 21, 21, 23), pt.bg = c("red",
"lightblue", "purple", "orange", "darkgrey", "black"))
      screen(2)
      plot(PCA.result$x[,2],PCA.result$x[,4], bty="o", bg=species,
cex=symbol.size, pch=holotypes, xlab="PC2 [56.3%]", ylab="PC4 [8.0 %]")
      legend("bottomleft", ncol=2, cex=0.7, legend=c("R. pulchriceps",
"R. cantabrigiensis", "R. elegans", "R. ambareti", "not assigned",
"holotypes"), bty="o", pch= c(21, 21, 21, 21, 21, 23), pt.bg = c("red",
"lightblue", "purple", "orange", "darkgrey", "black"))
dev.off()
```

S2.2.2 Additional analysis: PCA using measurements of Collins (1970)

As described in the main text section on PCA in section 3.5 of the present thesis, I carried out a PCA analysis using the four measurements reported by Collins (1970) to be of taxonomic importance. These were the skull width, the skull height, the pre-parietal skull length and the 'jaw angle'. 31 specimens were well enough preserved the retrieve all four measurements. The PCA analysis was conducted in R (R Core Team 2016), using the *prcomp* command. The data was transformed to have unit variance with the 'Scale = TRUE' argument, which was necessary as one of our measurements (the 'jaw angle') is in different units that the other measurements. As in the second analysis, the first Principal Component (PC1) described size

and allometric shape changes (see Results S2.2.4), I excluded it for constructing bivarite morphospace plots and re-scaled the absolute variance explained by the remaining PCs to represent the proportion of non-size (i.e. shape) variation.

S2.2.3 R Code Analysis Collins (1970)

The following block represents the R code used to compute the PCA and figure below. Note that the dataset "Rhinochelys_measurements_reduced" is a text file containing all Rhinochelys specimens for which all measurements of Collins (1970) could be taken (see Table 3.2 of main thesis text).

```
## Analysis only with Collin's (1970) measurements

# Load dataset with additional specimens (more specimens
# could be used for this analysis condidering fewer
# measurements)

# Data contains measurements of different units

measurements <-read.table("Rhinochelys_measurements_reduced.txt",
header=T)

# Define data for PCA input

Collins.input<-measurements
      rownames(Collins.input) <- Collins.input[,1]
            Collins.input<-Collins.input[,-1]

# Compute PCA

options(digits=3)
PCA.result.Collins<-prcomp(Collins.input, scale=TRUE)
PrincipalComponents_Collins <- summary(PCA.result.Collins)
Eigenvalues.Collins <- PCA.result.Collins$sdev^2
proportion.of.variance_Collins <-
Eigenvalues.Collins/sum(Eigenvalues.Collins)
rescaled.proportion.of.variance_Collins <-
Eigenvalues.Collins[2:4]/sum(Eigenvalues.Collins[2:4])

# Display results

PCA.result.Collins
PrincipalComponents_Collins
Eigenvalues.Collins
proportion.of.variance_Collins
rescaled.proportion.of.variance_Collins

# Plot PCA
```

```
dev.new( width = 11 , height = 6)
pdf("PCA_Collins_measurements.pdf", width = 11 , height = 6,
useDingbats=FALSE)
#close.screen(all.screens=T)
split.screen(c(1,2))
      screen(1)
      plot(PCA.result.Collins$x[,2],PCA.result.Collins$x[,3], bty="o",
bg=species, cex=symbol.size, pch=holotypes, xlab="PC2 [68.4 %]",
ylab="PC3 [21.1%]")
      legend("bottomleft", ncol=2, cex=0.7, legend=c("R. pulchriceps",
"R. cantabrigiensis", "R. elegans", "R. ambareti", "not assigned",
"holotypes"), bty="o", pch= c(21, 21, 21, 21, 21, 23), pt.bg = c("red",
"lightblue", "purple", "orange", "darkgrey", "black"))
      screen(2)
      plot(PCA.result.Collins$x[,2],PCA.result.Collins$x[,4], bty="o",
bg=species, cex=symbol.size, pch=holotypes, xlab="PC2 [68.4 %]",
ylab="PC4 [10.5 %]")
      legend("bottomright", ncol=2, cex=0.7, legend=c("R. pulchriceps",
"R. cantabrigiensis", "R. elegans", "R. ambareti", "not assigned",
"holotypes"), bty="o", pch= c(21, 21, 21, 21, 21, 23), pt.bg = c("red",
"lightblue", "purple", "orange", "darkgrey", "black"))
dev.off()
```

S2.2.4 Results

The PCA results are shown in Table S2.1. PC1 explains 72.1% of the variance in the data. As the eigenvector coefficients have the same sign, indicating relative increases/decreases in all measurements, PC1 represents size and allometric changes. We re-scaled the remaining PC axes to exclude size and allometric changes. PC2 explains 68.4% of shape variance in the data, and describes relative increases in skull size with relative decreases in the 'jaw angle'. PC3 explains 21.1% of the shape variance, and largely accounts for relative increases in skull length and height with relative decreases in skull width. PC3 explains 10.5% of the shape variance, and is associated with relative increases in skull length and decreases in skull height.

Table S2.1. PCA results from an analysis using four cranial measurements (n=31).

	PC1	PC2	PC3	PC4
Eigenvalues	2.884	0.736	0.236	0.117
Proportion of total variance explained	0.721	0.191	0.059	0.029
Proportion of shape variance explained	-	0.684	0.211	0.105
Eigenvector coefficients				
Jaw angle	0.357	-0.904	0.123	-0.199
Width	0.519	0.313	0.796	0.008
Pre-parietal length	0.539	0.292	-0.459	-0.643
Heigth	0.539	0.007	-0.375	0.739

As is the case for the PCA including all measurements (see main text, section 3.5.2), the data only using the measurements of Collins (1970) does not show clusters of specimens that have been reported to belong to the same species, and also no previously unrecognized clusters (Fig. S2.14). Instead, the data is seemingly randomly distributed, and the holotype specimens are relatively closely clustered.

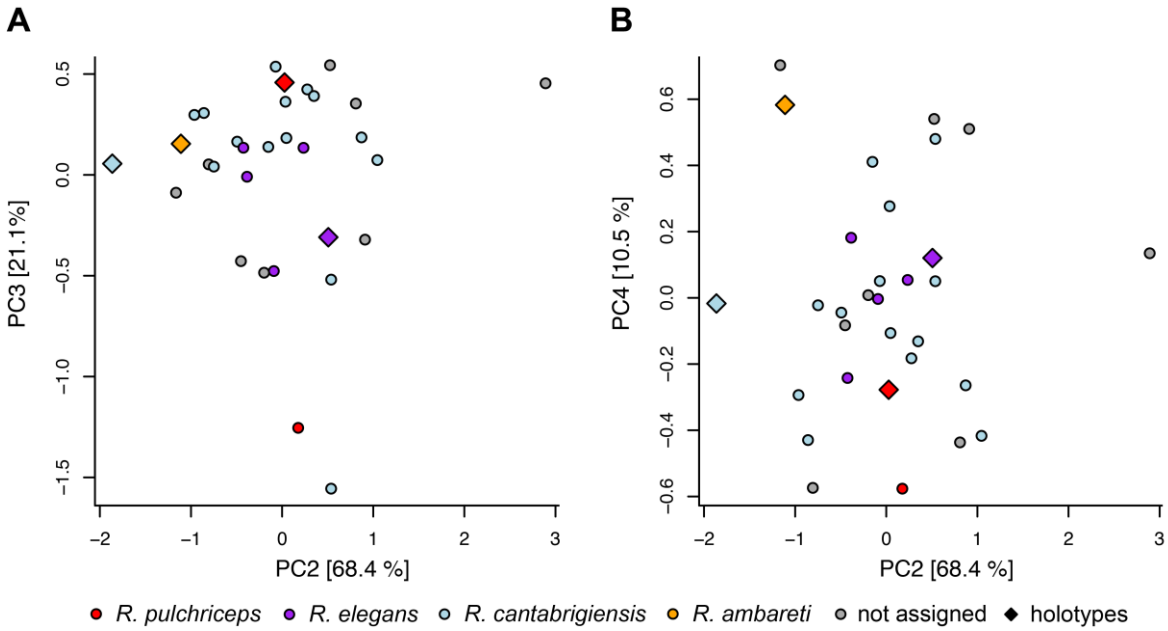


FIG. S2.14 <Collins_PCA>. Distribution of specimens of *Rhinochelys* (n = 31) in cranial geometry morphospaces recovered by Principal Component Analysis of four cranial measurements. **A**, PC1 vs. PC2; **B**, PC1 vs. PC3.

S2.3 Supplementary References

COLLINS, J. I. 1970. The chelonian *Rhinochelys* Seeley from the Upper Cretaceous of England and France. *Palaeontology*, **13**, 355–378.

R CORE TEAM. 2016. *R: a language and environment for statistical computing*. Version 3.3.1. R Foundation for Statistical Computing. http://www.R-project.org

SWOFFORD, D. L. 2002. PAUP*. Phylogenetic Analysis Using Parsimony (*and other methods). Version. 4.0. Sinauer Associates, Sunderland, MA.

APPENDIX S3

S3.1 Character optimization

S3.1.1 Methods

Because character optimization should be carried out on a fully bifurcated tree, a single MPT was selected from all MPTs. To select an MPT for optimisation, I computed a 50% majority rule consensus tree from the MPTs gained from the original analysis (Fig. S3.1). The topology of this majority rule consensus tree was used as a constraint in PAUP* for Macintosh (Swofford 2002) to find all MPTs compatible with the majority consensus rule topology. One of these MPTs was chosen at random for the optimisation. The topology of this tree is shown in Fig. S3.2.

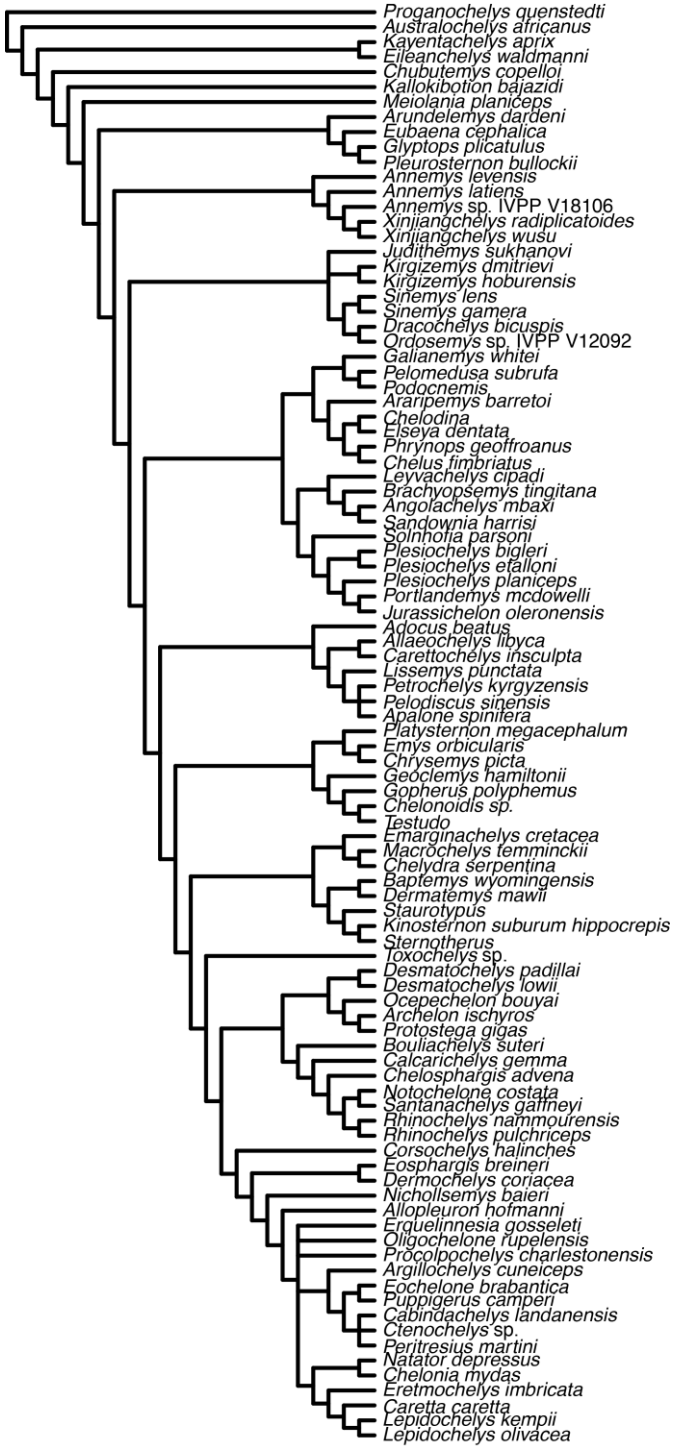


FIG. S3.1. 50%-Majority rule consensus tree. For clarity, only nodes that have been recovered in less than 100% of the MPTs have node labels indicating the proportion (in %) with which the respective nodes have been found. Unresolved nodes are those for which no resolved bifurcation was found in at least 50% of the MPTs.

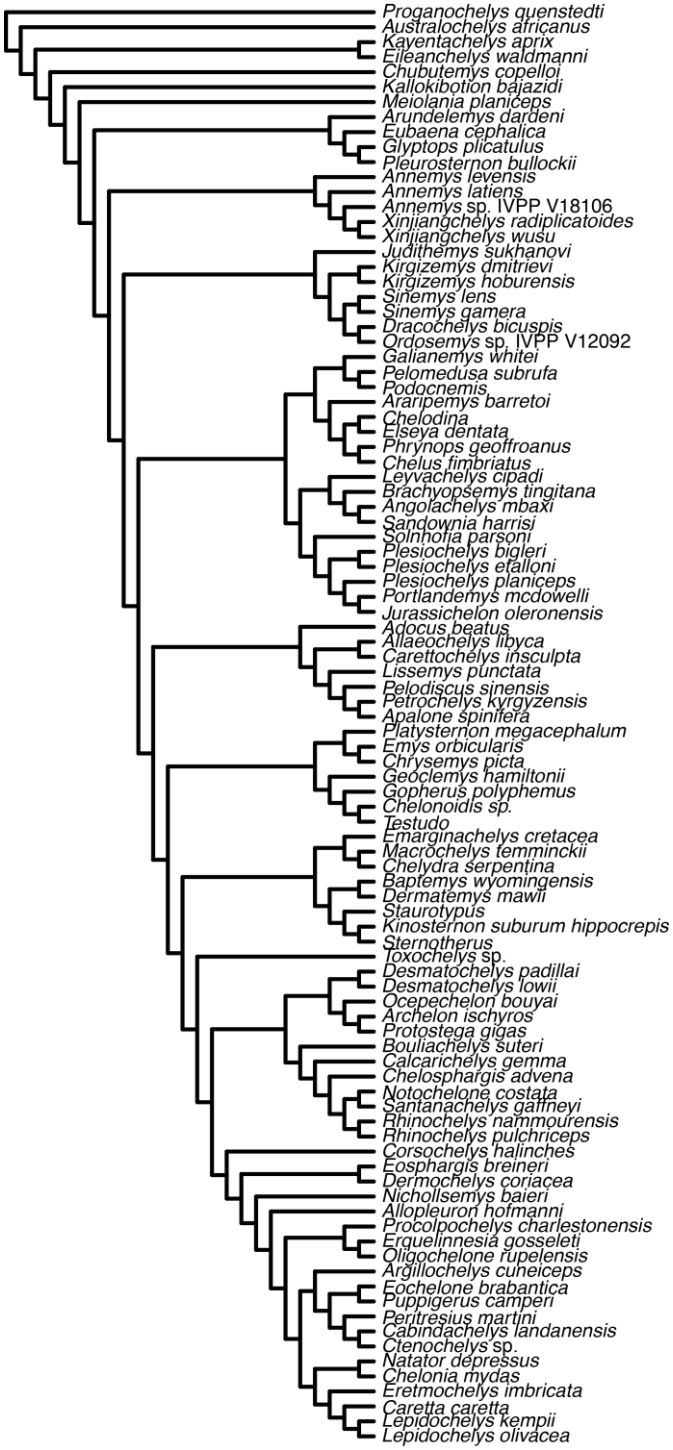


FIG. S3.2. MPT used for optimization of characters.

S3.1.2 Results

The optimizations are listed here for all nodes of the MPT (Fig. S3.2). 'Unambiguous' synapomorphies are those found both under ACCTRAN and DELTRAN optimization. For unnamed nodes in our tree, I use a code to describe clades. The notation 'Taxon+++' indicates

the clade comprising the named taxon as well as all taxa that a re more crownwardly positioned and member of the clade. '(Taxon A + Taxon B)' denotes the most inclusive clade including taxa A and B.

Australochelys+++:
DELTRAN:
CH64: 0->1, CH87: 0->1, CH91: 0->1, CH143: 0->1, CH145: 0->1;
ACCTRAN:
CH12: 0->1, CH25: 0->1, CH26: 0->1, CH46: 0->1, CH50: 0->1, CH62: 0->1, CH64: 0->1, CH73: 0->1, CH75: 0->1, CH87: 0->1, CH90: 0->1, CH91: 0->1, CH134: 0->1, CH142: 0->1, CH143: 0->1, CH145: 0->1, CH162: 0->1, CH204: 0->1, CH207: 0->1, CH226: 0->1, CH227: 0->1, CH235: 0->1, CH244: 0->1, CH245: 0->1, CH268: 0->1, CH303: 0->1, CH308: 0->1, CH310: 0->1, CH315: 0->1, CH317: 0->1, CH320: 0->1, CH327: 0->1, CH329: 0->1, CH344: 0->1.

(*Kayentachelys* + *Eileanchelys*)+++:
Unambiguous:
CH5: 1->0, CH9: 0->1, CH11: 0->1, CH67: 1->0, CH78: 0->1, CH109: 0->1, CH115: 1->0, CH120: 0->1, CH132: 0->2, CH141: 2->1;
DELTRAN:
CH26: 0->1, CH50: 0->1, CH62: 0->1, CH75: 0->2, CH162: 0->1, CH207: 0->1, CH226: 0->1, CH227: 0->1, CH235: 0->1, CH245: 0->1, CH268: 0->1, CH308: 0->1, CH310: 0->1, CH315: 0->1, CH317: 0->1, CH320: 0->1, CH327: 0->1, CH329: 0->1;
ACCTRAN:
CH21: 0->1, CH75: 1->2, CH77: 0->1, CH167: 0->1.

Chubutemys+++:
Unambiguous:
CH22: 0->1, CH66: 0->2, CH80: 0->1, CH106: 0->1, CH112: 0->1, CH121: 0->1, CH147: 0->1, CH309: 0->1;
DELTRAN:
CH21: 0->1, CH46: 0->1, CH77: 0->2, CH90: 0->1, CH167: 0->1;
ACCTRAN:
CH25: 1->0, CH59: 1->0, CH77: 1->2, CH89: 0->1, CH123: 0->1, CH124: 0->1, CH134: 1->0, CH142: 1->0, CH202: 0->1, CH246: 0->1, CH256: 0->1, CH301: 0->1, CH304: 0->1, CH305: 0->2, CH354: 1->0.

Kallokibotion+++:
Unambiguous:
CH92: 0->1, CH108: 0->1, CH109: 1->2, CH122: 0->2;
DELTRAN:
CH89: 0->1, CH202: 0->1, CH204: 0->1, CH244: 0->1.

Meiolania+++:
Unambiguous:
CH98: 0->1, CH128: 0->1, CH195: 0->1, CH233: 0->1;
DELTRAN:
CH305: 0->2, CH354: 1->0;
ACCTRAN:
CH149: 0->1, CH230: 0->1, CH253: 0->1, CH254: 0->1.

Paracryptodira+++:

Unambiguous:
CH17: 1->0, CH19: 0->2, CH35: 0->1, CH48: 0->1, CH102: 0->1, CH121: 1->0, CH312: 0->2, CH335: 0->1;
DELTRAN:
CH12: 0->1, CH230: 0->1, CH246: 0->1, CH303: 0->1;
ACCTRAN:
CH23: 0->1, CH111: 0->1, CH123: 1->0, CH124: 1->0, CH181: 0->1, CH208: 0->1, CH294: 0->1, CH306: 0->1, CH319: 1->0, CH326: 0->1, CH340: 0->1, CH347: 0->1.

Xinjiangchelyidae+++:
Unambiguous:
CH3: 0->1, CH14: 0->1, CH117: 0->1, CH122: 2->0, CH148: 0->1, CH229: 0->1, CH240: 0->1;
DELTRAN:
CH23: 0->1, CH59: 1->0, CH73: 0->1, CH149: 0->1, CH254: 0->1, CH294: 0->1, CH340: 0->1, CH347: 0->1;
ACCTRAN:
CH4: 0->1, CH39: 0->1, CH41: 0->1, CH177: 0->1, CH180: 0->1, CH253: 1->0, CH282: 0->1, CH283: 0->1.

Sinemydidae/Macroabenidae+++:
Unambiguous:
CH144: 1->0, CH187: 0->1, CH233: 1->0, CH285: 0->1, CH299: 0->2, CH316: 0->1;
DELTRAN:
CH4: 0->1, CH177: 0->1, CH281: 0->1, CH301: 0->1, CH304: 0->1, CH306: 0->1;
ACCTRAN:
CH16: 0->1, CH24: 0->1, CH36: 0->1, CH91: 1->2, CH111: 1->0, CH281: 0->1.

Testudines:
Unambiguous:
CH80: 1->2, CH125: 1->0, CH130: 0->1, CH143: 1->0, CH149: 1->2, CH182: 0->1, CH280: 0->1, CH305: 2->1;
DELTRAN:
CH41: 0->1, CH91: 1->2, CH181: 0->1, CH326: 0->1, CH344: 0->1;
ACCTRAN:
CH1: 0->1, CH29: 0->1, CH39: 1->0, CH101: 0->1, CH129: 1->0, CH208: 1->0, CH210: 0->1, CH330: 0->1.

Cryptodira:
Unambiguous:
CH14: 1->0, CH70: 0->1, CH97: 0->1, CH165: 1->0, CH291: 0->1, CH293: 0->1, CH295: 0->1, CH302: 0->1;
DELTRAN:
CH1: 0->1, CH16: 0->1, CH29: 0->1, CH36: 0->1, CH101: 0->2, CH129: 1->0, CH180: 0->1, CH283: 0->1;
ACCTRAN:
CH35: 1->0, CH76: 0->1, CH101: 1->2, CH178: 0->1, CH193: 0->1, CH213: 0->1, CH258: 0->1, CH297: 0->1.

Durocryptodira:
Unambiguous:
CH253: 0->1, CH266: 0->1;
DELTRAN:
CH76: 0->1, CH282: 0->1;
ACCTRAN:
CH117: 1->0, CH151: 0->1, CH210: 1->0.

Americhelydia:
Unambiguous:
CH66: 2->1, CH68: 0->1, CH248: 0->1;
DELTRAN:
CH35: 1->0, CH330: 0->1;
ACCTRAN:
CH24: 1->0, CH178: 1->0, CH179: 0->1, CH182: 1->0, CH223: 0->1, CH252: 0->1, CH325: 0->1.

total-group Chelonioidea:
Unambiguous:
CH36: 1->0, CH40: 0->1, CH70: 1->0, CH96: 1->0, CH107: 0->1, CH134: 0->2, CH141: 1->2, CH165: 0->1, CH196: 0->1, CH212: 0->1, CH236: 0->1, CH240: 1->0, CH241: 0->1, CH246: 1->2, CH249: 0->1, CH261: 0->1, CH302: 1->0, CH332: 0->2, CH337: 0->1, CH338: 0->1, CH342: 0->1, CH350: 0->1;
DELTRAN:
CH117: 1->0, CH182: 1->0, CH213: 0->1, CH223: 0->1, CH252: 0->1;
ACCTRAN:
CH1: 1->0, CH19: 2->0, CH29: 1->0, CH58: 0->1, CH59: 0->1, CH97: 1->0, CH101: 2->0, CH128: 1->0, CH144: 0->1, CH151: 1->0, CH211: 0->1, CH237: 0->1, CH270: 0->1, CH291: 1->0, CH293: 1->0, CH295: 1->0, CH297: 1->0, CH298: 0->1, CH344: 1->2.

Protostegidae+++:
Unambiguous:
CH142: 0->1, CH163: 0->1, CH224: 0->1, CH260: 0->1, CH313: 0->1, CH314: 0->1, CH328: 1->0, CH334: 0->1, CH341: 0->1, CH345: 0->1, CH352: 0->1, CH354: 0->1;
DELTRAN:
CH19: 2->0, CH128: 1->0, CH144: 0->2, CH237: 0->1, CH291: 1->0, CH295: 1->0, CH325: 0->1, CH344: 1->2;
ACCTRAN:
CH28: 1->0, CH82: 0->1, CH88: 0->1, CH140: 0->2, CH144: 1->2, CH214: 0->1, CH242: 0->1, CH331: 0->1.

Protostegidae:
Unambiguous:
CH63: 0->1, CH76: 1->0, CH93: 0->1, CH101: 0->1, CH105: 0->1, CH118: 0->2, CH222: 1->0, CH249: 1->2, CH339: 0->1;
DELTRAN:
CH1: 1->0, CH28: 1->0, CH59: 0->1, CH82: 0->1, CH140: 0->2, CH214: 0->1, CH242: 0->1, CH293: 1->0;
ACCTRAN:
CH50: 1->0, CH58: 1->0, CH95: 0->1, CH179: 1->0, CH191: 0->1, CH298: 1->0.

(*Bouliachelys* + *Rhinochelys*):
Unambiguous:
CH23: 1->0, CH176: 0->1;
DELTRAN:
CH50: 1->0, CH88: 0->1, CH95: 0->1;
ACCTRAN:
CH17: 0->1, CH226: 1->0.

(*Calcarichelys* + *Rhinochelys*):
Unambiguous:
CH154: 1->0, CH163: 1->0;
DELTRAN:

CH191: 0->1;
ACCTRAN:
CH98: 1->0.

(*Chelosphargis* + *Rhinochelys*):
Unambiguous:
CH4: 1->0;
DELTRAN:
CH17: 0->1, CH226: 1->0.

(*Santanachelys* ++ *Rhinochelys*):
Unambiguous:
CH15: 1->2, CH260: 1->0;
DELTRAN:
CH97: 1->0;
ACCTRAN:
CH187: 1->0.

(*Rhinochelys pulchriceps* + *Rhinochelys nammourensis*):
Unambiguous:
CH10: 0->1;
ACCTRAN:
CH96: 0->1, CH98: 0->1, CH142: 1->0, CH213: 1->0, CH219: 1->0.

Rhinochelys pulchriceps:
DELTRAN:
CH96: 0->1, CH142: 1->0, CH187: 1->0.

Rhinochelys nammourensis:
Unambiguous:
CH17: 1->0;
DELTRAN:
CH213: 1->0, CH219: 1->0.

(*Santanachelys* + *Notochelone*):
DELTRAN:
CH98: 1->0;
ACCTRAN:
CH70: 0->1, CH76: 0->1, CH82: 1->0, CH115: 0->1, CH134: 2->0, CH191: 1->0, CH229: 1->0, CH230: 1->0, CH237: 1->0, CH338: 1->0, CH341: 1->0.

Santanachelys gaffneyi:
Unambiguous:
CH107: 1->0, CH150: 1->0;
DELTRAN:
CH76: 0->1, CH191: 1->0, CH229: 1->0, CH230: 1->0, CH237: 1->0, CH338: 1->0, CH341: 1->0.

Notochelone costata:
Unambiguous:
CH68: 1->0, CH127: 0->1;
DELTRAN:
CH70: 0->1, CH82: 1->0, CH115: 0->1, CH134: 2->0.

Chelosphargis advena:
Unambiguous:

CH144: 2->1.

Calcarichelys gemma:
Unambiguous:
CH1: 0->1, CH106: 1->0, CH247: 0->1;
DELTRAN:
CH98: 1->0.

Bouliachelys suteri:
Unambiguous:
CH9: 1->0, CH12: 1->0, CH77: 2->0, CH84: 0->1, CH124: 0->1, CH135: 0->1;
DELTRAN:
CH179: 0->1;
ACCTRAN:
CH97: 0->1, CH179: 0->1.

(*Desmatochelys* ++ *Protostega*):
Unambiguous:
CH4: 1->0, CH117: 0->1, CH130: 1->0, CH196: 1->0, CH241: 1->2;
DELTRAN:
CH331: 0->1;
ACCTRAN:
CH7: 0->1, CH127: 0->1, CH133: 0->1, CH281: 1->0.

(*Ocepechelon* ++ *Protostega*):
Unambiguous:
CH16: 1->0, CH68: 1->0, CH95: 1->2;
ACCTRAN:
CH3: 1->0, CH88: 1->0, CH106: 1->0, CH188: 0->1, CH215: 0->1, CH219: 1->0, CH247: 0->1, CH263: 0->1, CH332: 2->3, CH336: 0->1.

Ocepechelon bouyai:
Unambiguous:
CH14: 0->1, CH39: 0->1, CH49: 0->1, CH59: 1->0, CH93: 1->0, CH112: 1->0, CH144: 2->1;
DELTRAN:
CH3: 1->0, CH7: 0->1, CH50: 1->0, CH106: 1->0.

(*Protostega* + *Archelon*):
Unambiguous:
CH1: 0->1, CH12: 1->0, CH53: 0->1, CH66: 1->0, CH100: 0->2, CH104: 0->1, CH118: 2->0;
DELTRAN:
CH188: 0->1, CH191: 0->1, CH215: 0->1, CH219: 1->0, CH247: 0->1, CH263: 0->1, CH332: 2->3, CH336: 0->1;
ACCTRAN:
CH7: 1->0, CH41: 1->0, CH76: 0->1, CH81: 0->1, CH150: 1->0, CH154: 1->0.

Protostega gigas:
Unambiguous:
CH187: 1->0;
DELTRAN:
CH81: 0->1, CH150: 1->0, CH154: 1->0, CH319: 1->0;
ACCTRAN:
CH281: 0->1.

Archelon ischyros:

Unambiguous:
CH45: 0->1;
DELTRAN:
CH41: 1->0, CH76: 0->1, CH281: 1->0;
ACCTRAN:
CH319: 0->1.

(*Desmatochelys lowii* + *Desmatochelys padillai*):
Unambiguous:
CH20: 0->1, CH77: 2->1, CH224: 1->0;
DELTRAN:
CH7: 0->1, CH281: 1->0;
ACCTRAN:
CH50: 0->1, CH191: 1->0, CH210: 0->1.

Desmatochelys lowii:
Unambiguous:
CH41: 1->0, CH200: 0->1;
DELTRAN:
CH88: 0->1, CH127: 0->1, CH133: 0->1, CH210: 0->1, CH211: 0->1;
ACCTRAN:
CH95: 1->0, CH97: 0->1.

Desmatochelys padillai:
Unambiguous:
CH19: 0->1, CH101: 1->2, CH154: 1->0;
DELTRAN:
CH95: 0->1, CH97: 1->0.

Corsochelys+++:
Unambiguous:
CH16: 1->0, CH41: 1->0, CH106: 1->0, CH115: 0->1, CH216: 0->1;
ACCTRAN:
CH1: 0->1, CH59: 1->0, CH121: 0->1, CH188: 0->1, CH262: 0->1, CH263: 0->1, CH292: 0->1, CH293: 0->1, CH294: 1->0, CH330: 1->0, CH347: 1->0, CH348: 0->1.

crown-group Chelonioidea:
Unambiguous:
CH23: 1->0, CH146: 0->1;
DELTRAN:
CH58: 0->1, CH144: 2->1, CH214: 0->1, CH262: 0->1, CH292: 0->1, CH298: 0->1, CH330: 1->0, CH331: 0->1, CH347: 1->0, CH348: 0->1;
ACCTRAN:
CH127: 0->1, CH137: 0->1, CH144: 2->1, CH215: 0->1, CH217: 0->2.

Dermochelyidae:
Unambiguous:
CH12: 1->0, CH17: 0->1, CH54: 0->1, CH95: 0->2, CH98: 1->0, CH100: 0->2, CH112: 1->0, CH151: 0->1, CH332: 2->3, CH333: 0->1;
DELTRAN:
CH28: 1->0, CH188: 0->1, CH242: 0->1, CH263: 0->1, CH294: 1->0, CH319: 1->0;
ACCTRAN:
CH6: 0->1, CH15: 1->0, CH22: 1->0, CH72: 0->1, CH80: 2->1, CH82: 1->0, CH122: 0->1, CH126: 0->1, CH140: 2->0, CH185: 0->2, CH202: 1->0, CH243: 0->1, CH338: 1->0.

Dermochelys coriacea:
Unambiguous:
CH26: 1->0, CH43: 0->1, CH68: 1->0, CH96: 0->1, CH203: 0->1, CH206: 0->1, CH241: 1->0, CH353: 0->1;
DELTRAN:
CH6: 0->1, CH15: 1->0, CH22: 1->0, CH72: 0->1, CH80: 2->1, CH88: 0->1, CH122: 0->3, CH126: 0->1, CH179: 0->1, CH185: 0->2, CH243: 0->1, CH338: 1->0;
ACCTRAN:
CH121: 1->0, CH122: 1->3, CH137: 1->0.

Eosphargis breineri:
Unambiguous:
CH92: 1->0, CH103: 0->1, CH138: 0->1, CH191: 0->1;
DELTRAN:
CH59: 0->1, CH121: 0->1, CH122: 0->1, CH137: 0->1, CH202: 1->0, CH215: 0->1;
ACCTRAN:
CH59: 0->1.

total-group Cheloniidae:
Unambiguous:
CH66: 1->0, CH104: 0->1, CH111: 0->1, CH163: 1->0;
DELTRAN:
CH82: 0->1, CH121: 0->1, CH127: 0->1, CH137: 0->1, CH140: 0->2;
ACCTRAN:
CH28: 0->1, CH130: 1->0, CH178: 0->1, CH242: 1->0, CH294: 0->1, CH319: 0->1, CH344: 2->1, CH346: 0->1.

Allopleuron+++:
Unambiguous:
CH56: 0->1, CH57: 0->1, CH68: 1->2, CH69: 0->1, CH103: 0->1;
DELTRAN:
CH344: 2->1, CH346: 0->1;
ACCTRAN:
CH29: 0->1, CH88: 1->0, CH97: 0->1, CH101: 0->2.

(*Erquelinnesia* ++ *Lepidochelys*):
Unambiguous:
CH17: 0->1, CH45: 0->1, CH50: 1->0, CH95: 0->2, CH224: 1->0;
DELTRAN:
CH178: 0->1, CH217: 0->2;
ACCTRAN:
CH130: 0->1, CH188: 1->0, CH215: 1->0, CH263: 1->0, CH326: 1->0.

(*Puppigerus* ++ *Lepidochelys*):
Unambiguous:
CH330: 0->1;
DELTRAN:
CH319: 1->0;
ACCTRAN:
CH176: 0->1, CH319: 1->0.

crown-group Cheloniidae:
Unambiguous:
CH6: 0->1, CH152: 0->1, CH217: 2->1, CH302: 0->1, CH336: 0->1, CH353: 0->1;
DELTRAN:

CH88: 0->1, CH179: 0->1;
ACCTRAN:
CH59: 0->2, CH70: 0->1, CH72: 0->1, CH88: 0->1, CH326: 0->1.

(*Eretmochelys* ++ *Lepidochelys*):
Unambiguous:
CH8: 0->1, CH30: 1->0, CH115: 1->0;
DELTRAN:
CH72: 0->1;
ACCTRAN:
CH176: 1->0.

(*Caretta* ++ *Lepidochelys*):
Unambiguous:
CH234: 0->1, CH313: 1->0;
ACCTRAN:
CH12: 1->0, CH59: 2->0, CH128: 0->1, CH144: 1->2, CH184: 0->1, CH191: 0->1, CH207: 1->0, CH270: 1->0.

(*Lepidochelys olivacea* + *Lepidochelys kempii*):
Unambiguous:
CH146: 1->0, CH204: 1->0;
DELTRAN:
CH70: 0->1, CH176: 0->1;
ACCTRAN:
CH176: 0->1.

Lepidochelys olivacea:
Unambiguous:
CH102: 1->0, CH134: 2->1, CH175: 0->1;
DELTRAN:
CH12: 1->0, CH144: 1->2, CH184: 0->1, CH191: 0->1;
ACCTRAN:
CH128: 1->0.

Lepidochelys kempii:
Unambiguous:
CH30: 0->1, CH53: 0->1, CH104: 1->0, CH179: 1->0;
DELTRAN:
CH59: 0->2, CH128: 0->1;
ACCTRAN:
CH12: 0->1, CH59: 0->2, CH144: 2->1, CH184: 1->0, CH191: 1->0.

Caretta caretta:
Unambiguous:
CH61: 0->1, CH65: 0->1, CH100: 0->1, CH163: 0->1, CH223: 1->0;
DELTRAN:
CH12: 1->0, CH128: 0->1, CH144: 1->2, CH184: 0->1, CH191: 0->1, CH207: 1->0;
ACCTRAN:
CH70: 1->0.

Eretmochelys imbricata:
Unambiguous:
CH118: 0->1, CH122: 0->1, CH134: 2->0, CH177: 1->0, CH226: 1->0;
DELTRAN:

CH59: 0->2, CH70: 0->1, CH270: 0->1.

(*Chelonia* + *Natator*):
Unambiguous:
CH80: 2->1, CH180: 1->0;
DELTRAN:
CH59: 0->2, CH176: 0->1, CH270: 0->1.

Chelonia mydas:
Unambiguous:
CH100: 0->2, CH102: 1->0, CH103: 1->0, CH104: 1->0, CH117: 0->1, CH122: 0->1, CH126: 0->1, CH128: 0->1, CH134: 2->0, CH141: 2->0, CH191: 0->1, CH217: 1->0;
ACCTRAN:
CH70: 1->0, CH72: 1->0.

Natator depressus:
Unambiguous:
CH76: 1->0, CH144: 1->2, CH177: 1->0, CH184: 0->1, CH226: 1->0, CH355: 0->1;
DELTRAN:
CH70: 0->1, CH72: 0->1.

(*Argillochelys* ++ *Puppigerus*):
Unambiguous:
CH117: 0->1;
DELTRAN:
CH176: 0->1;
ACCTRAN:
CH179: 1->0, CH262: 1->0, CH328: 0->1, CH355: 0->1.

(*Puppigerus* ++ *Ctenochelys*):
Unambiguous:
CH25: 0->1;
DELTRAN:
CH262: 1->0, CH328: 0->1, CH355: 0->1;
ACCTRAN:
CH104: 1->0, CH142: 1->0.

(*Puppigerus* + *Eochelone*):
Unambiguous:
CH115: 1->0, CH237: 1->0, CH241: 1->0;
DELTRAN:
CH142: 1->0;
ACCTRAN:
CH122: 0->1, CH294: 1->0.

Puppigerus camperi:
Unambiguous:
CH92: 1->0, CH102: 1->0, CH146: 1->0, CH151: 0->1, CH175: 0->1, CH212: 1->0, CH223: 1->0, CH260: 1->0;
DELTRAN:
CH88: 0->1, CH122: 0->1, CH294: 1->0, CH326: 1->0;
ACCTRAN:
CH88: 0->1, CH104: 0->1.

Eochelone brabantica:

Unambiguous:
CH56: 1->0, CH57: 1->0, CH58: 1->0, CH66: 0->1, CH68: 2->1, CH134: 2->0, CH140: 2->1, CH176: 1->0, CH330: 1->0;
DELTRAN:
CH104: 1->0, CH122: 0->2;
ACCTRAN:
CH122: 1->2.

(*Ctenochelys* ++ *Peritresius*):
Unambiguous:
CH190: 0->1, CH191: 0->1, CH195: 1->0, CH200: 0->1, CH226: 1->0;
ACCTRAN:
CH14: 0->1, CH16: 0->1, CH45: 1->0, CH95: 2->0, CH101: 2->0, CH103: 1->0, CH127: 1->0, CH179: 0->1, CH286: 1->0, CH316: 1->0, CH332: 2->0.

Peritresius martini:
Unambiguous:
CH230: 1->0, CH279: 0->1, CH297: 0->1, CH319: 0->1.

(*Ctenochelys* + *Cabindachelys*):
DELTRAN:
CH14: 0->1, CH45: 1->0, CH95: 2->0, CH101: 2->0, CH103: 1->0, CH104: 1->0, CH127: 1->0;
ACCTRAN:
CH217: 2->0.

Ctenochelys sp.:
Unambiguous:
CH6: 0->1, CH17: 1->0, CH59: 0->1, CH66: 0->1, CH67: 0->1, CH68: 2->1, CH106: 0->1, CH140: 2->1, CH163: 0->1, CH164: 0->1;
DELTRAN:
CH16: 0->1, CH179: 0->1, CH217: 2->0, CH286: 1->0, CH316: 1->0, CH332: 2->0;
ACCTRAN:
CH142: 0->1.

Cabindachelys landanensis:
Unambiguous:
CH22: 1->2;
DELTRAN:
CH88: 0->1, CH97: 1->0, CH142: 1->0;
ACCTRAN:
CH88: 0->1, CH97: 1->0.

Argillochelys cuneiceps:
Unambiguous:
CH59: 0->1, CH151: 0->1, CH156: 1->0.

(*Procolpochelys* ++ *Erquelinnesia*):
Unambiguous:
CH175: 0->1;
ACCTRAN:
CH30: 1->0, CH100: 0->1, CH102: 1->0.

Procolpochelys charlestonensis:
Unambiguous:
CH204: 1->0, CH213: 1->0, CH222: 1->0, CHs 199: 0->1.

DELTRAN:
CH30: 1->0, CH100: 0->1, CH102: 1->0, CH179: 0->1.

(*Oligochelone* + *Erquelinnesia*):
DELTRAN:
CH326: 1->0;
ACCTRAN:
CH14: 0->1, CH49: 0->1, CH179: 1->0.

Erquelinnesia gosseleti:
Unambiguous:
CH214: 1->0, CH230: 1->0, CH334: 1->0;
DELTRAN:
CH14: 0->1, CH49: 0->1.

Allopleuron hofmanni:
Unambiguous:
CH26: 1->0, CH43: 0->1, CH77: 2->1, CH80: 2->1, CH81: 0->1, CH85: 0->1, CH133: 0->1, CH165: 1->0, CH177: 1->0, CH187: 1->0, CH191: 0->1, CH196: 1->0, CH226: 1->0;
DELTRAN:
CH130: 1->0, CH188: 0->1, CH215: 0->1, CH263: 0->1.

Nichollsemys baieri:
Unambiguous:
CH19: 0->1, CH35: 0->1, CH63: 0->1, CH90: 1->0, CH105: 0->1, CH125: 0->1, CH128: 0->1, CH152: 0->1;
DELTRAN:
CH29: 1->0, CH88: 0->1, CH97: 1->0, CH101: 2->0, CH130: 1->0.

Corsochelys halinches:
Unambiguous:
CH14: 0->1, CH119: 0->1, CH129: 0->1, CH140: 2->1, CH157: 0->1, CH285: 1->0, CH332: 2->1;
DELTRAN:
CH294: 1->0;
ACCTRAN:
CH88: 1->0, CH214: 1->0, CH331: 1->0.

Toxochelys sp.:
Unambiguous:
CH14: 0->1, CH39: 0->1, CH66: 1->0, CH137: 0->1, CH146: 0->1, CH174: 0->1, CH184: 0->1, CH200: 0->1, CH275: 0->1, CH277: 0->1, CH278: 0->1, CH306: 1->0;
DELTRAN:
CH1: 1->0, CH19: 2->1, CH29: 1->0, CH58: 0->1, CH59: 0->1, CH97: 1->0, CH101: 2->0, CH144: 0->1, CH179: 0->1, CH293: 1->0, CH298: 0->1, CH319: 1->0;
ACCTRAN:
CH19: 0->1.

Chelydroidea:
Unambiguous:
CH156: 1->0, CH181: 1->0, CH197: 0->1, CH222: 1->0;
DELTRAN:
CH151: 0->1, CH297: 0->1;
ACCTRAN:

CH60: 0->1, CH117: 0->1, CH190: 0->1, CH191: 0->1, CH213: 1->0, CH239: 0->1, CH272: 0->1, CH326: 1->0.

total-group Chelydridae:
Unambiguous:
CH82: 0->1, CH249: 0->2, CH276: 0->1;
ACCTRAN:
CH41: 1->0, CH127: 0->1, CH176: 0->1, CH202: 1->0, CH226: 1->0, CH305: 1->2, CH306: 1->0, CH325: 1->0, CH349: 0->1.

crown-group Chelydridae:
Unambiguous:
CH12: 1->0, CH36: 1->0, CH53: 0->1, CH68: 1->0, CH78: 1->2, CH96: 1->0, CH101: 2->0, CH115: 0->1, CH212: 0->1, CH236: 0->1, CH246: 1->2, CH260: 0->1, CH261: 0->1, CH277: 0->1;
DELTRAN:
CH127: 0->1, CH176: 0->1, CH179: 0->1, CH182: 1->0, CH202: 1->0, CH226: 1->0, CH252: 0->1, CH305: 1->2, CH306: 1->0, CH319: 1->0;
ACCTRAN:
CH190: 1->0, CH191: 1->0.

Chelydra serpentina:
Unambiguous:
CH9: 1->0, CH25: 0->1, CH29: 1->0, CH59: 0->1, CH125: 0->1, CH143: 0->1, CH198: 1->2, CH222: 0->2;
DELTRAN:
CH272: 0->1;
ACCTRAN:
CH41: 0->1, CH326: 0->1.

Macrochelys temminckii:
Unambiguous:
CH66: 1->0, CH85: 0->1, CH118: 0->1, CH141: 1->0, CH144: 0->1, CH151: 1->0, CH156: 0->1, CH227: 1->0, CH304: 1->2;
DELTRAN:
CH41: 1->0, CH258: 0->1, CH326: 1->0, CH349: 0->1.

Emarginachelys cretacea:
Unambiguous:
CH30: 1->0, CH59: 0->2, CH109: 2->1, CH111: 0->1, CH324: 0->1, CH345: 0->1;
DELTRAN:
CH41: 1->0, CH60: 0->1, CH190: 0->1, CH191: 0->1.

Kinosternoidea:
Unambiguous:
CH22: 1->2, CH23: 1->0, CH55: 0->1, CH118: 0->2, CH125: 0->1, CH208: 0->1, CH235: 1->0, CH273: 0->1;
DELTRAN:
CH325: 0->1, CH326: 1->0;
ACCTRAN:
CH122: 0->2, CH124: 0->1, CH159: 0->1, CH179: 1->0, CH182: 0->1, CH185: 0->1, CH210: 0->1, CH252: 1->0, CH288: 2->1, CH319: 0->1, CH323: 0->1, CH328: 1->0.

Kinosternidae:
Unambiguous:

CH12: 1->0, CH18: 0->1, CH27: 0->1, CH33: 0->1, CH133: 0->1, CH207: 1->2, CH238: 0->1, CH253: 1->2, CH275: 0->1, CH279: 0->1, CH300: 0->1, CH324: 0->1;
DELTRAN:
CH159: 0->1, CH185: 0->1, CH190: 0->1, CH191: 0->1, CH193: 0->1, CH239: 0->1, CH258: 0->1, CH288: 2->1, CH323: 0->1, CH328: 1->0;
ACCTRAN:
CH43: 0->1, CH68: 1->2, CH69: 0->1, CH78: 1->2, CH102: 1->0, CH345: 0->1.

Kinosterninae:
Unambiguous:
CH25: 0->1, CH186: 0->1, CH209: 0->1, CH243: 0->1, CH270: 0->1, CH271: 0->1;
DELTRAN:
CH210: 0->1;
ACCTRAN:
CH124: 1->0.

Sternotherus:
Unambiguous:
CH98: 1->0, CH100: 0->1, CH117: 1->0, CH118: 2->0, CH130: 1->0, CH139: 0->1, CH177: 1->0, CH211: 0->1;
DELTRAN:
CH68: 1->2, CH69: 0->1, CH78: 1->2, CH122: 0->2, CH345: 0->1;
ACCTRAN:
CH43: 1->0, CH102: 0->1.

Kinosternon suburum hippocrepis:
Unambiguous:
CH112: 1->0, CH116: 0->1, CH127: 0->1, CH143: 0->1, CH161: 1->0, CH183: 0->1, CH208: 1->0, CH326: 0->1, CHis 53: 0->1.
DELTRAN:
CH43: 0->1, CH102: 1->0, CH182: 1->0.
ACCTRAN:
CH68: 2->1, CH69: 1->0, CH78: 2->1, CH122: 2->0, CH182: 1->0.

Staurotypus:
Unambiguous:
CH39: 0->1, CH50: 1->0, CH82: 0->1, CH107: 0->1, CH141: 1->0;
DELTRAN:
CH43: 0->1, CH68: 1->2, CH69: 0->1, CH78: 1->2, CH102: 1->0, CH122: 0->2, CH124: 0->1, CH319: 1->0;
ACCTRAN:
CH319: 1->0.

total-group Dermatemydidae:
Unambiguous:
CH35: 0->1, CH59: 0->2, CH80: 2->1, CH98: 1->0, CH158: 0->1, CH177: 1->0, CH178: 0->1, CH248: 1->0, CH251: 0->1;
ACCTRAN:
CH128: 1->0, CH258: 1->0.

Dermatemys mawii:
Unambiguous:
CH65: 0->1, CH106: 1->0, CH117: 1->0, CH141: 1->0, CH259: 0->1, CH270: 0->1, CH287: 1->0;
DELTRAN:

CH124: 0->1, CH128: 1->0, CH185: 0->1, CH210: 0->1;
ACCTRAN:
CH60: 1->0, CH122: 2->0, CH190: 1->0, CH191: 1->0, CH272: 1->0, CH323: 1->0.

Baptemys wyomingensis:
Unambiguous:
CH41: 1->0, CH121: 0->1, CH144: 0->1, CH151: 1->0, CH156: 0->1, CH174: 0->1, CH186: 0->1, CH257: 0->1;
DELTRAN:
CH60: 0->1, CH122: 0->2, CH182: 1->0, CH190: 0->1, CH191: 0->1, CH272: 0->1, CH323: 0->1;
ACCTRAN:
CH182: 1->0, CH185: 1->0, CH210: 1->0.

Testudinoidea:
Unambiguous:
CH98: 1->0, CH125: 0->1, CH177: 1->0, CH259: 0->1, CH289: 0->1;
DELTRAN:
CH151: 0->1;
ACCTRAN:
CH12: 1->0, CH80: 2->1, CH118: 0->2, CH199: 0->1, CH279: 0->1, CH319: 0->1.

Emysternia:
Unambiguous:
CH226: 1->0, CH345: 0->1;
DELTRAN:
CH118: 0->2.

Emydidae:
Unambiguous:
CH106: 1->0, CH123: 0->1, CH156: 1->0, CH222: 1->0;
DELTRAN:
CH199: 0->1, CH297: 0->1, CH330: 0->1;
ACCTRAN:
CH35: 0->1, CH347: 1->0.

Chrysemys picta:
Unambiguous:
CH23: 1->0, CH39: 0->1, CH59: 0->2, CH69: 0->1, CH115: 0->1, CH122: 0->1, CH124: 0->1, CH128: 1->0, CH235: 1->0, CH251: 0->1, CH257: 0->1, CH274: 0->1, CH290: 0->1;
DELTRAN:
CH117: 1->0, CH178: 0->1, CH279: 0->1;
ACCTRAN:
CH12: 0->1, CH80: 1->2, CH258: 1->0.

Emys orbicularis:
Unambiguous:
CH29: 1->0, CH66: 2->0, CH73: 1->0, CH92: 1->0, CH143: 0->1, CH146: 0->1, CH238: 0->1, CH259: 1->0, CH272: 0->1;
DELTRAN:
CH12: 1->0, CH24: 0->1, CH80: 2->1, CH258: 0->1, CH347: 1->0;
ACCTRAN:
CH117: 0->1.

Platysternon megacephalum:

Unambiguous:
CH17: 0->1, CH19: 2->0, CH33: 0->1, CH36: 1->0, CH41: 1->0, CH44: 0->1, CH53: 0->1, CH59: 0->1, CH66: 2->1, CH76: 1->0, CH78: 1->2, CH96: 1->0, CH102: 1->0, CH103: 0->1, CH111: 0->1, CH126: 0->1, CH127: 0->1, CH140: 0->2, CH141: 1->0, CH144: 0->1, CH161: 1->0, CH165: 0->1, CH182: 1->0, CH183: 0->1, CH186: 0->1, CH202: 1->0, CH208: 0->1, CH252: 0->1, CH258: 1->2, CH282: 1->0, CH305: 1->2, CH306: 1->0;
DELTRAN:
CH12: 1->0, CH35: 1->0, CH80: 2->1, CH117: 1->0, CH319: 1->0;
ACCTRAN:
CH24: 1->0, CH178: 1->0, CH199: 1->0, CH279: 1->0, CH297: 1->0, CH319: 1->0, CH330: 1->0.

Testuguria:
Unambiguous:
CH67: 0->1, CH73: 1->0, CH157: 0->1, CH181: 1->0, CH235: 1->0, CH250: 1->0, CH251: 0->1, CH274: 0->1;
DELTRAN:
CH24: 0->1, CH199: 0->1, CH279: 0->1, CH297: 0->1;
ACCTRAN:
CH18: 0->1, CH180: 1->0, CH257: 0->1, CH354: 0->1.

Geoclemys hamiltonii:
Unambiguous:
CH27: 0->1, CH43: 0->1, CH68: 0->1, CH69: 0->1, CH122: 0->3, CH123: 0->1, CH190: 0->1, CH191: 0->1, CH208: 0->1, CH272: 0->1, CH334: 0->1;
DELTRAN:
CH12: 1->0, CH18: 0->1, CH35: 1->0, CH117: 1->0, CH118: 0->2, CH178: 0->1, CH257: 0->1, CH258: 0->1, CH330: 0->1, CH354: 0->1;
ACCTRAN:
CH80: 1->2.

Testudinidae:
Unambiguous:
CH28: 1->0, CH59: 0->2, CH77: 2->1, CH78: 1->2, CH143: 0->1, CH156: 1->0, CH202: 1->0, CH253: 1->0;
DELTRAN:
CH80: 2->1, CH180: 1->0;
ACCTRAN:
CH12: 0->1, CH35: 0->1, CH97: 1->0, CH106: 1->0, CH107: 0->1, CH117: 0->1, CH118: 2->0, CH133: 0->2, CH218: 0->1, CH258: 1->0, CH330: 1->0, CH340: 1->0, CH349: 0->1.

(*Testudo* + *Chelonoidis*):
Unambiguous:
CH76: 1->0, CH182: 1->0;
DELTRAN:
CH18: 0->1;
ACCTRAN:
CH178: 1->0, CH257: 1->0.

Testudo:
Unambiguous:
CH43: 0->1, CH67: 1->0, CH102: 1->0, CH115: 0->1, CH123: 0->1, CH185: 0->1;
DELTRAN:
CH106: 1->0, CH218: 0->1, CH330: 0->1, CH340: 1->0, CH349: 0->1;
ACCTRAN:
CH97: 0->1, CH133: 2->0, CH330: 0->1.

Chelonoidis sp.:
Unambiguous:
CH14: 0->1, CH41: 1->0, CH163: 0->1, CH199: 1->0, CH208: 0->1, CH226: 1->0, CH235: 0->1, CH250: 0->1, CH251: 1->0, CH252: 0->1, CH258: 0->2, CH274: 1->0, CH279: 1->0, CH282: 1->0, CH297: 1->0, CH305: 1->2, CH306: 1->0, CH319: 1->0;
DELTRAN:
CH97: 1->0, CH107: 0->1, CH133: 0->2;
ACCTRAN:
CH106: 0->1, CH218: 1->0, CH340: 0->1, CH349: 1->0.

Gopherus polyphemus:
Unambiguous:
CH22: 1->2, CH23: 1->0, CH55: 0->1, CH72: 0->1, CH104: 0->1, CH126: 0->1, CH128: 1->0, CH141: 1->0;
DELTRAN:
CH97: 1->0, CH106: 1->0, CH133: 0->2, CH178: 0->1, CH218: 0->1, CH257: 0->1, CH340: 1->0, CH349: 0->1;
ACCTRAN:
CH18: 1->0.

total-group Trionychia:
Unambiguous:
CH18: 0->1, CH22: 1->2, CH23: 1->0, CH55: 0->1, CH118: 0->1, CH186: 0->1, CH287: 1->0, CH324: 0->1;
DELTRAN:
CH39: 0->1;
ACCTRAN:
CH25: 0->1, CH39: 0->1, CH60: 0->1, CH121: 0->1, CH127: 0->1, CH193: 1->2, CH222: 1->0, CH233: 0->1, CH264: 0->1, CH272: 0->1, CH274: 0->1, CH278: 0->1, CH330: 1->0.

crown-group Trionychia:
Unambiguous:
CH6: 0->1, CH49: 0->1, CH50: 1->0, CH63: 0->1, CH65: 0->1, CH72: 0->1, CH78: 1->2, CH96: 1->2, CH100: 0->1, CH105: 0->1, CH114: 0->1, CH115: 0->1, CH134: 0->1, CH192: 0->1, CH224: 0->1, CH263: 0->1, CH325: 0->1, CH328: 1->0, CH334: 0->1, CH345: 0->1;
DELTRAN:
CH25: 0->1, CH35: 1->0, CH76: 0->1, CH127: 0->1, CH193: 0->2, CH210: 0->1, CH319: 1->0;
ACCTRAN:
CH183: 0->1, CH189: 0->1, CH207: 1->0, CH253: 0->2, CH282: 1->0, CH297: 1->0, CH343: 0->1.

Trionychidae:
Unambiguous:
CH14: 0->1, CH27: 0->1, CH31: 0->1, CH41: 1->0, CH43: 0->1, CH51: 0->1, CH52: 0->1, CH61: 0->1, CH81: 0->1, CH106: 1->0, CH150: 1->0, CH188: 0->1, CH206: 0->1, CH221: 0->1, CH236: 0->1, CH237: 0->1, CH246: 1->3, CH248: 0->1, CH249: 0->3, CH252: 0->1, CH286: 1->2, CH331: 0->1, CH351: 0->1;
DELTRAN:
CH330: 0->1, CH343: 0->1;
ACCTRAN:
CH121: 1->0, CH178: 1->0, CH180: 1->0, CH330: 0->1.

Trionychinae:
Unambiguous:

CH212: 0->1;
DELTRAN:
CH180: 1->0, CH183: 0->1, CH213: 0->1;
ACCTRAN:
CH165: 0->1, CH324: 1->0.

(*Apalone* + *Petrochelys*):
DELTRAN:
CH165: 0->1;
ACCTRAN:
CH59: 0->1, CH97: 1->0, CH347: 1->0.

Apalone spinifera:
DELTRAN:
CH59: 0->1, CH97: 1->0, CH324: 1->0, CH347: 1->0.

Pelodiscus sinensis:
Unambiguous:
CH124: 0->1.

Lissemys punctata:
Unambiguous:
CH30: 1->0, CH70: 1->0, CH102: 1->0, CH105: 1->2, CH166: 1->0, CH186: 1->0;
ACCTRAN:
CH183: 1->0.

total-group Carettochelyidae:
Unambiguous:
CH86: 0->1, CH118: 1->2, CH122: 0->3, CH126: 0->1, CH139: 0->1;
DELTRAN:
CH121: 0->1;
ACCTRAN:
CH33: 0->1, CH59: 0->1, CH66: 2->0, CH67: 0->1, CH77: 2->0, CH177: 1->0, CH195: 1->0, CH343: 1->2, CH344: 1->2, CH346: 0->1, CH347: 1->0.

Carettochelys insculpta:
DELTRAN:
CH33: 0->1, CH59: 0->1, CH66: 2->0, CH67: 0->1, CH77: 2->0, CH177: 1->0, CH178: 0->1, CH183: 0->1, CH189: 0->1, CH195: 1->0, CH207: 1->0, CH222: 1->0, CH253: 0->2, CH258: 0->1, CH343: 0->2, CH344: 1->2, CH346: 0->1, CH347: 1->0.

Allaeochelys libyca:
Unambiguous:
CH111: 0->1, CH128: 1->0;
DELTRAN:
CH77: 2->1;
ACCTRAN:
CH77: 0->1.

Adocus beatus:
Unambiguous:
CH59: 0->2, CH82: 0->1, CH111: 0->1, CH144: 0->1, CH149: 2->1, CH199: 0->1, CH201: 0->1, CH235: 1->0, CH286: 1->0;
DELTRAN:

CH60: 0->1, CH121: 0->1, CH178: 0->1, CH233: 0->1, CH264: 0->1, CH272: 0->1, CH274: 0->1, CH278: 0->1, CH282: 0->1, CH297: 0->1;
ACCTRAN:
CH35: 0->1, CH76: 1->0, CH258: 1->0, CH319: 0->1.

total-group Pleurodira:
Unambiguous:
CH63: 0->1, CH66: 2->0, CH235: 1->0, CH251: 0->1, CH257: 0->1, CH265: 0->1, CH311: 0->1;
DELTRAN:
CH330: 0->1;
ACCTRAN:
CH98: 1->0, CH100: 0->1, CH105: 0->1, CH122: 0->1, CH124: 0->1, CH134: 0->1, CH282: 1->0, CH283: 1->0, CH288: 2->0, CH334: 0->1.

Angolachelonia:
Unambiguous:
CH19: 2->0, CH84: 0->1, CH85: 0->1, CH96: 1->0, CH117: 1->0, CH183: 0->1, CH184: 0->1, CH186: 0->1;
DELTRAN:
CH24: 0->1, CH105: 0->1;
ACCTRAN:
CH1: 1->0, CH16: 1->0, CH29: 1->0, CH36: 1->0, CH57: 0->1, CH68: 0->2, CH144: 0->1, CH175: 0->1, CH236: 0->1, CH354: 0->1.

Thalassochelydia:
Unambiguous:
CH41: 1->0, CH82: 0->1, CH115: 0->1, CH187: 1->0, CH216: 0->1, CH229: 1->0, CH285: 1->0, CH294: 1->0;
DELTRAN:
CH98: 1->0, CH144: 0->1, CH236: 0->1, CH334: 0->1, CH354: 0->1;
ACCTRAN:
CH109: 2->1, CH118: 0->2, CH124: 1->0, CH129: 0->1, CH134: 1->0, CH299: 2->1.

Solnhofia parsoni:
Unambiguous:
CH18: 0->1, CH50: 1->0, CH61: 0->1, CH65: 0->1, CH97: 0->1, CH102: 1->0, CH121: 0->1, CH128: 1->0, CH176: 0->1, CH212: 0->1, CH222: 1->2, CH235: 0->1;
DELTRAN:
CH57: 0->1, CH68: 0->2, CH100: 0->1, CH109: 2->1, CH118: 0->2, CH122: 0->1, CH175: 0->1, CH180: 0->1;
ACCTRAN:
CH210: 1->0.

Plesiochelyidae:
Unambiguous:
CH28: 1->0, CH40: 0->1, CH59: 0->1, CH95: 0->1, CH141: 1->2, CH154: 1->0, CH157: 0->1, CH177: 1->0, CH182: 1->0;
DELTRAN:
CH101: 0->1, CH134: 0->2;
ACCTRAN:
CH57: 1->0, CH68: 2->0, CH100: 1->0, CH122: 1->0, CH134: 0->2, CH175: 1->0, CH225: 1->0, CH325: 0->1.

(*Plesiochelys planiceps* ++ *Jurassichelon*):
Unambiguous:

CH4: 1->0, CH111: 0->1, CH117: 0->1;
ACCTRAN:
CH76: 0->1.

(*Jurassichelon* + *Portlandemys*):
Unambiguous:
CH7: 0->1, CH91: 2->1, CH98: 0->1, CH130: 1->0, CH133: 0->1;
DELTRAN:
CH124: 0->1;
ACCTRAN:
CH109: 1->2, CH112: 1->0, CH118: 2->0, CH124: 0->1, CH183: 1->0.

Jurassichelon oleronensis:
Unambiguous:
CH19: 0->1, CH82: 1->0, CH96: 0->1, CH149: 2->1;
DELTRAN:
CH76: 0->1, CH112: 1->0, CH299: 2->1.

Portlandemys mcdowelli:
Unambiguous:
CH63: 1->0, CH95: 1->0, CH101: 1->0, CH157: 1->0;
DELTRAN:
CH183: 1->0.

Plesiochelys planiceps:
Unambiguous:
CH35: 1->2, CH142: 0->1;
DELTRAN:
CH109: 2->1, CH118: 0->2, CH180: 0->1.

(*Plesiochelys etalloni* + *Plesiochelys bigleri*):
Unambiguous:
CH63: 1->0, CH219: 1->0;
DELTRAN:
CH210: 0->1, CH225: 1->0;
ACCTRAN:
CH45: 0->1, CH180: 1->0.

Plesiochelys etalloni:
Unambiguous:
CH106: 1->0, CH142: 0->1, CH145: 1->0;
DELTRAN:
CH45: 0->1;
ACCTRAN:
CH109: 1->2.

Plesiochelys bigleri:
Unambiguous:
CH144: 1->0, CH149: 2->1;
DELTRAN:
CH109: 2->1, CH325: 0->1.

Sandownidae:
Unambiguous:
CH17: 0->1, CH35: 1->0, CH58: 0->1, CH69: 0->1, CH110: 0->1, CH111: 0->1, CH141: 1->0;

DELTRAN:
CH57: 0->1, CH100: 0->1, CH134: 0->1, CH175: 0->1;
ACCTRAN:
CH22: 1->2, CH78: 1->2, CH91: 2->1, CH98: 0->1, CH107: 0->1, CH282: 0->1.

(*Brachyopsemys* ++ *Sandownia*):
Unambiguous:
CH2: 0->1, CH50: 1->0, CH63: 1->0;
DELTRAN:
CH68: 0->2;
ACCTRAN:
CH49: 0->1, CH144: 1->0.

(*Sandownia* + *Angolachelys*):
Unambiguous:
CH56: 0->1, CH112: 1->0, CH118: 0->1;
DELTRAN:
CH22: 1->2, CH78: 1->2;
ACCTRAN:
CH39: 0->1, CH55: 0->1, CH97: 0->1, CH107: 1->0.

Sandownia harrisi:
Unambiguous:
CH7: 0->1, CH17: 1->0, CH149: 2->1;
DELTRAN:
CH55: 0->1, CH91: 2->1, CH97: 0->1, CH124: 0->1, CH129: 1->0;
ACCTRAN:
CH49: 1->0.

Angolachelys mbaxi:
Unambiguous:
CH29: 0->1, CH48: 1->0, CH95: 0->2, CH106: 1->0, CH111: 1->0, CH134: 1->2;
DELTRAN:
CH39: 0->1, CH49: 0->1.

Brachyopsemys tingitana:
Unambiguous:
CH65: 0->1, CH72: 0->1, CH117: 0->1, CH141: 0->2, CH163: 0->1, CH165: 1->0;
DELTRAN:
CH49: 0->1, CH107: 0->1;
ACCTRAN:
CH22: 2->1, CH78: 2->1.

Leyvachelys cipadi:
Unambiguous:
CH3: 1->0, CH7: 0->1, CH28: 1->0, CH143: 0->1;
DELTRAN:
CH22: 1->2, CH78: 1->2, CH107: 0->1, CH122: 0->1, CH144: 0->1, CH282: 0->1.

crown-group Pleurodira:
Unambiguous:
CH5: 0->1, CH6: 0->1, CH42: 0->1, CH71: 0->1, CH80: 2->0, CH88: 0->1, CH92: 1->0, CH94: 0->1, CH106: 1->0, CH108: 1->2, CH109: 2->0, CH160: 0->1, CH193: 0->3, CH199: 0->1, CH222: 1->0, CH253: 0->1, CH259: 0->1, CH278: 0->1, CH281: 1->0, CH284: 0->1, CH318: 0->1, CH328: 1->0;

DELTRAN:
CH29: 0->1, CH36: 0->1, CH98: 1->0, CH124: 0->1, CH134: 0->1, CH210: 0->1, CH288: 2->0, CH319: 1->0;
ACCTRAN:
CH2: 0->1, CH24: 1->0, CH78: 1->3, CH112: 1->0, CH129: 0->2, CH180: 1->0, CH208: 0->1, CH224: 0->1, CH240: 1->0.

total-group Chelidae:
Unambiguous:
CH7: 0->1, CH73: 1->0, CH125: 0->2, CH153: 0->1, CH156: 1->0, CH174: 0->1, CH182: 1->0, CH192: 0->1, CH296: 0->1;
DELTRAN:
CH129: 1->2;
ACCTRAN:
CH105: 1->0, CH155: 1->0, CH258: 0->1, CH334: 1->0.

crown-group Chelidae:
Unambiguous:
CH4: 1->0, CH32: 0->1, CH35: 1->2, CH63: 1->0, CH187: 1->0, CH288: 0->3, CH289: 0->1;
DELTRAN:
CH2: 0->1, CH78: 1->3, CH208: 0->1;
ACCTRAN:
CH1: 1->0, CH16: 1->0, CH116: 0->1, CH118: 0->2, CH119: 0->2, CH184: 0->1, CH224: 1->0, CH240: 0->1, CH345: 0->1.

Chelinae:
Unambiguous:
CH165: 1->0;
DELTRAN:
CH112: 1->0, CH116: 0->1, CH118: 0->3, CH119: 0->2, CH122: 0->1;
ACCTRAN:
CH118: 2->3.

Chelus fimbriatus:
Unambiguous:
CH6: 1->0, CH23: 1->0, CH49: 0->1, CH130: 1->0, CH150: 1->0, CH161: 1->0, CH190: 0->1, CH191: 0->1, CH202: 1->0, CH210: 1->0, CH226: 1->0, CH257: 1->3, CH267: 0->2, CH269: 0->1, CH272: 0->1, CH282: 0->1, CH283: 0->1;
DELTRAN:
CH1: 0->1, CH258: 0->1, CH345: 0->1;
ACCTRAN:
CH1: 0->1, CH155: 0->1.

Phrynops geoffroanus:
Unambiguous:
CH25: 0->1, CH143: 0->1, CH192: 1->0, CH205: 0->1, CH296: 1->0;
DELTRAN:
CH105: 0->1, CH155: 1->0, CH184: 0->1;
ACCTRAN:
CH105: 0->1, CH258: 1->0, CH345: 1->0.

Chelodininae:
Unambiguous:
CH209: 0->1, CH211: 0->1, CH347: 1->0;
DELTRAN:

CH118: 0->2, CH345: 0->1;
ACCTRAN:
CH122: 1->0, CH331: 0->1.

Elseya dentata:
Unambiguous:
CH17: 0->1, CH19: 2->0, CH24: 0->1, CH25: 0->1, CH59: 0->2, CH61: 0->1, CH174: 1->0, CH176: 0->1, CH177: 1->0, CH185: 0->1, CH253: 1->0, CH346: 0->1;
DELTRAN:
CH184: 0->1, CH224: 0->1, CH334: 0->1;
ACCTRAN:
CH112: 0->1, CH116: 1->0, CH119: 2->0, CH155: 0->1, CH224: 0->1, CH258: 1->0, CH334: 0->1.

Chelodina:
Unambiguous:
CH13: 0->1, CH83: 0->1, CH130: 1->0, CH181: 1->0, CH257: 1->0, CH267: 0->1;
DELTRAN:
CH16: 0->1, CH105: 0->1, CH112: 1->0, CH116: 0->1, CH119: 0->2, CH155: 1->0, CH258: 0->1, CH331: 0->1;
ACCTRAN:
CH16: 0->1, CH105: 0->1, CH184: 1->0.

Araripemys barretoi:
Unambiguous:
CH39: 0->1, CH74: 0->1, CH96: 1->2, CH97: 0->1, CH117: 1->0, CH181: 1->0, CH190: 0->1, CH191: 0->1, CH193: 3->4, CH212: 0->1, CH232: 0->1, CH235: 0->1, CH236: 0->1, CH237: 0->1, CH248: 0->1, CH249: 0->1, CH257: 1->0, CH266: 0->1, CH276: 0->1, CH346: 0->1;
DELTRAN:
CH1: 0->1, CH16: 0->1, CH122: 0->1, CH155: 1->0, CH224: 0->1, CH240: 1->0, CH258: 0->1;
ACCTRAN:
CH78: 3->1, CH208: 1->0.

total-group Pelomedusoides:
Unambiguous:
CH22: 1->2, CH55: 0->1, CH83: 0->1;
DELTRAN:
CH1: 0->1, CH16: 0->1;
ACCTRAN:
CH25: 0->1, CH99: 0->1, CH122: 1->0, CH150: 1->0, CH177: 1->0, CH254: 1->0, CH347: 1->0.

crown-group Pelomedusoides:
Unambiguous:
CH59: 0->2, CH62: 1->2, CH74: 0->1, CH165: 1->0;
DELTRAN:
CH78: 1->3, CH129: 1->2, CH177: 1->0, CH208: 0->1, CH224: 0->1, CH240: 1->0, CH254: 1->0, CH256: 0->1, CH334: 0->1, CH347: 1->0;
ACCTRAN:
CH24: 0->1, CH112: 0->1.

Podocnemis:
Unambiguous:
CH19: 2->0, CH31: 0->1, CH43: 0->1, CH56: 0->1, CH97: 0->1, CH117: 1->0, CH118: 0->2, CH155: 1->0, CH160: 1->0, CH272: 0->1, CH331: 0->1, CH345: 0->1, CH346: 0->1;
DELTRAN:

CH24: 0->1, CH25: 0->1, CH99: 0->1, CH150: 1->0;
ACCTRAN:
CH105: 1->0.

Pelomedusa subrufa:
Unambiguous:
CH23: 1->0, CH39: 0->1, CH125: 0->2, CH126: 0->1, CH143: 0->1, CH145: 1->0, CH153: 0->1, CH156: 1->0, CH311: 1->0;
DELTRAN:
CH105: 0->1;
ACCTRAN:
CH25: 1->0, CH99: 1->0, CH150: 0->1.

Galianemys whitei:
Unambiguous:
CH33: 0->1, CH35: 1->0, CH44: 0->1, CH85: 0->1, CH115: 0->1, CH133: 0->1, CH140: 0->2, CH154: 1->0;
DELTRAN:
CH25: 0->1, CH78: 1->2, CH99: 0->1, CH105: 0->1, CH112: 1->0, CH150: 1->0;
ACCTRAN:
CH78: 3->2, CH129: 2->1.

(*Judithemys* ++ *Sinemys*):
Unambiguous:
CH19: 2->1, CH136: 0->1, CH246: 1->2, CH248: 0->1, CH266: 0->1;
DELTRAN:
CH39: 0->1, CH282: 0->1, CH283: 0->1;
ACCTRAN:
CH41: 1->0, CH115: 0->1, CH133: 0->2, CH181: 1->0, CH249: 0->1.

(*Sinemys* ++ *Kirgizemys*):
Unambiguous:
CH278: 0->1;
DELTRAN:
CH115: 0->1;
ACCTRAN:
CH35: 1->2, CH91: 2->1, CH98: 1->0.

Sinemydidae:
Unambiguous:
CH111: 0->1, CH212: 0->1, CH224: 0->1, CH232: 0->1, CH299: 2->0;
ACCTRAN:
CH4: 1->0, CH117: 1->0, CH192: 0->1, CH226: 1->0, CH236: 0->1, CH249: 1->0, CH261: 0->1, CH287: 1->0.

(*Ordosemys* + *Dracochelys*):
Unambiguous:
CH82: 0->1, CH118: 0->2;
ACCTRAN:
CH35: 2->1, CH98: 0->1, CH154: 1->0, CH194: 0->1, CH220: 0->1.

Ordosemys sp. IVPP V12092:
Unambiguous:
CH81: 0->1, CH84: 0->1, CH101: 0->2;
DELTRAN:

CH4: 1->0, CH117: 1->0, CH154: 1->0, CH261: 0->1.

Dracochelys bicuspis:
Unambiguous:
CH54: 0->1, CH59: 0->1, CH66: 2->0, CH136: 1->0, CH148: 1->0;
DELTRAN:
CH194: 0->1, CH220: 0->1, CH226: 1->0, CH236: 0->1, CH287: 1->0;
ACCTRAN:
CH4: 0->1, CH261: 1->0.

(*Sinemys gamera* + *Sinemys lens*):
Unambiguous:
CH7: 0->1, CH19: 1->2, CH78: 1->2, CH92: 1->0;
DELTRAN:
CH4: 1->0, CH16: 0->1, CH35: 1->2, CH98: 1->0, CH133: 0->2, CH208: 0->1;
ACCTRAN:
CH25: 0->1, CH39: 1->0, CH74: 0->1, CH283: 1->0, CH332: 0->1.

Sinemys gamera:
Unambiguous:
CH2: 0->1;
DELTRAN:
CH25: 0->1, CH36: 0->1, CH74: 0->1, CH192: 0->1, CH332: 0->1.

Sinemys lens:
Unambiguous:
CH109: 2->1;
DELTRAN:
CH39: 1->0, CH261: 0->1, CH283: 1->0.

(*Kirgizemys hoburensis* + *Kirgizemys dmitrievi*):
Unambiguous:
CH151: 0->1;
DELTRAN:
CH35: 1->2, CH249: 0->1;
ACCTRAN:
CH16: 1->0, CH36: 1->0, CH109: 2->1, CH156: 1->0, CH205: 0->1, CH295: 0->1.

Kirgizemys hoburensis:
Unambiguous:
CH41: 0->1, CH165: 1->0;
DELTRAN:
CH24: 0->1, CH109: 2->1, CH156: 1->0, CH205: 0->1, CH295: 0->1.

Kirgizemys dmitrievi:
Unambiguous:
CH14: 1->0, CH59: 0->1, CH62: 1->0, CH66: 2->1, CH80: 1->2, CH142: 0->1, CH163: 0->1;
DELTRAN:
CH98: 1->0.

Judithemys sukhanovi:
Unambiguous:
CH76: 0->1, CH297: 0->1;
DELTRAN:
CH91: 1->2, CH249: 0->1.

Xinjiangchelyidae:
Unambiguous:
CH92: 1->0, CH127: 0->1, CH205: 0->1, CH264: 0->1, CH277: 0->1;
DELTRAN:
CH39: 0->1, CH111: 0->1, CH181: 0->1, CH208: 0->1;
ACCTRAN:
CH35: 1->2, CH109: 2->1, CH154: 1->0, CH231: 0->1, CH301: 1->0, CH344: 1->0, CH345: 0->1.

Annemys levensis:
Unambiguous:
CH138: 0->1, CH210: 0->1, CH230: 1->0;
DELTRAN:
CH4: 0->1, CH35: 1->2, CH109: 2->1, CH231: 0->1;
ACCTRAN:
CH177: 1->0.

(*Annemys latiens* ++ *Xinjiangchelys*):
Unambiguous:
CH7: 0->1, CH147: 1->0;
ACCTRAN:
CH4: 1->0, CH118: 0->2.

Annemys latiens:
Unambiguous:
CH89: 1->0, CH123: 0->1;
DELTRAN:
CH231: 0->1.

(*Annemys* sp. IVPP V18106 ++ *Xinjiangchelys*):
Unambiguous:
CH2: 0->1;
DELTRAN:
CH118: 0->2;
ACCTRAN:
CH231: 1->0.

Annemys sp. IVPP V18106:
Unambiguous:
CH82: 0->1, CH98: 1->0, CH133: 0->1, CH145: 1->0, CH157: 0->1;
DELTRAN:
CH35: 1->2, CH41: 0->1, CH109: 2->1, CH154: 1->0.

(*Xinjiangchelys wusu* + *Xinjiangchelys radiplicatoides*):
Unambiguous:
CH76: 0->1, CH77: 2->1;
ACCTRAN:
CH35: 2->1, CH63: 0->1, CH109: 1->2, CH125: 1->0, CH141: 1->2.

Xinjiangchelys wusu:
Unambiguous:
CH264: 1->0;
DELTRAN:
CH345: 0->1;
ACCTRAN:

CH154: 0->1.

*Xinjiangchelys radiplicatoide*s:
Unambiguous:
CH96: 1->2, CH111: 1->0, CH187: 0->1, CHs 92: 0->1.

Xinjiangchelys radiplicatoides:
DELTRAN:
CH63: 0->1, CH125: 1->0, CH141: 1->2, CH154: 1->0, CH177: 0->1.

Paracryptodira:
Unambiguous:
CH7: 0->1, CH44: 0->1, CH147: 1->2;
DELTRAN:
CH25: 0->1, CH111: 0->1;
ACCTRAN:
CH2: 0->1, CH25: 0->1, CH29: 0->1, CH59: 0->1, CH66: 2->0, CH73: 1->0, CH149: 1->0, CH192: 0->1, CH235: 1->0, CH251: 0->1, CH254: 1->0, CH256: 1->0, CH257: 0->1, CH284: 0->1, CH311: 0->1.

(*Eubaena* + *Pleurosternidae*):
Unambiguous:
CH118: 0->2, CH133: 0->1, CH139: 0->1;
DELTRAN:
CH29: 0->1;
ACCTRAN:
CH70: 0->1, CH124: 0->1, CH130: 0->1, CH135: 0->1.

Eubaena cephalica:
Unambiguous:
CH7: 1->2, CH12: 1->0, CH16: 0->1, CH76: 0->1, CH88: 0->1, CH91: 1->2, CH131: 0->1, CH164: 0->1;
DELTRAN:
CH70: 0->1;
ACCTRAN:
CH2: 1->0, CH66: 0->2.

Pleurosternidae:
Unambiguous:
CH3: 0->1, CH19: 2->0, CH77: 2->1, CH96: 1->2, CH109: 2->1, CH134: 0->1;
DELTRAN:
CH2: 0->1, CH66: 2->0, CH124: 0->1, CH192: 0->1, CH235: 1->0, CH253: 0->1, CH257: 0->1;
ACCTRAN:
CH18: 0->1, CH81: 0->1, CH122: 2->0.

Pleurosternon bullockii:
Unambiguous:
CH36: 0->1, CH59: 1->0, CH133: 1->2, CH193: 0->3, CH222: 1->0, CH224: 0->1, CH265: 0->1;
DELTRAN:
CH18: 0->1, CH23: 0->1, CH81: 0->1, CH130: 0->1, CH135: 0->1.

Glyptops plicatulus:
DELTRAN:
CH122: 2->0, CH251: 0->1, CH284: 0->1, CH301: 0->1, CH311: 0->1.

Arundelemys dardeni:
Unambiguous:
CH107: 0->1, CH127: 0->1;
DELTRAN:
CH2: 0->1, CH66: 2->0;
ACCTRAN:
CH23: 1->0.

Meiolania planiceps:
Unambiguous:
CH26: 1->0, CH34: 0->1, CH37: 0->1, CH38: 0->1, CH59: 0->2, CH67: 0->1, CH76: 0->1, CH77: 2->0, CH78: 1->3, CH79: 0->1, CH91: 1->2, CH106: 1->0, CH113: 0->1, CH141: 1->0, CH144: 1->0, CH161: 1->0, CH163: 0->1, CH184: 0->1, CH226: 1->0, CH236: 0->1, CH285: 0->1, CH307: 0->1;
DELTRAN:
CH73: 0->1, CH123: 0->1, CH124: 0->1, CH149: 0->1, CH151: 0->1, CH157: 0->1, CH168: 0->1, CH172: 0->1, CH253: 0->1, CH254: 0->1, CH281: 0->1, CH304: 0->2, CH344: 0->1;
ACCTRAN:
CH12: 1->0, CH151: 0->1, CH157: 0->1, CH168: 0->1, CH172: 0->1, CH246: 1->0, CH281: 0->1, CH303: 1->0, CH304: 1->2.

Kallokibotion bajazidi:
Unambiguous:
CH61: 0->1, CH80: 1->2, CH119: 0->1, CH131: 0->1, CH146: 0->1, CH148: 0->1, CH177: 0->1, CH223: 0->1, CH258: 0->2, CH312: 0->1;
DELTRAN:
CH12: 0->1, CH123: 0->1, CH124: 0->1, CH246: 0->1, CH256: 0->1.

Chubutemys copelloi:
Unambiguous:
CH4: 0->1, CH28: 1->0, CH30: 1->0, CH63: 0->1, CH97: 0->1, CH284: 0->1;
DELTRAN:
CH59: 1->0;
ACCTRAN:
CH12: 1->0.

(*Kayentachelys* + *Eileanchelys*):
Unambiguous:
CH7: 0->1, CH29: 0->1, CH48: 0->1, CH111: 0->1, CH174: 0->1;
DELTRAN:
CH12: 0->1, CH134: 0->1;
ACCTRAN:
CH90: 1->0, CH136: 0->1, CH157: 0->1, CH208: 0->1.

Eileanchelys waldmanni:
Unambiguous:
CH205: 0->1;
DELTRAN:
CH21: 0->1, CH157: 0->1, CH167: 0->1, CH204: 0->1, CH244: 0->1.

Kayentachelys aprix:
Unambiguous:
CH85: 0->1, CH132: 2->1, CH219: 1->0, CH222: 1->0;
DELTRAN:
CH25: 0->1, CH77: 0->1, CH136: 0->1, CH142: 0->1, CH208: 0->1, CH303: 0->1;

ACCTRAN:
CH21: 1->0, CH167: 1->0, CH204: 1->0, CH244: 1->0.

Australochelys africanus:
Unambiguous:
CH131: 0->1;
DELTRAN:
CH25: 0->1, CH75: 0->1, CH90: 0->1, CH134: 0->1, CH142: 0->1.

Proganochelys quenstedti:
DELTRAN:
CH43: 0->1, CH70: 0->1, CH163: 0->1, CH210: 0->1, CH269: 0->1, CH281: 0->1;
ACCTRAN:
CH43: 0->1, CH70: 0->1, CH163: 0->1, CH210: 0->1, CH269: 0->1, CH281: 0->1.

S3.2 Time-calibrated phylogeny

For the time-calibrated phylogeny shown in section 4 of this thesis, I used the age data shown in Table S3.1.

Table S3.1. Age data used for time calibration.

Taxon	Age Maximum	Age Minimum	Source
Adocus beatus	70.6	66.043	PalaeoDB
Allaeochelys libyca	15.97	13.82	Havlik *et al.* 2014
Allopleuron hofmanni	72.1	66	Janssen *et al.* 2013
Angolachelys mbaxi	94.3	89.3	PalaeoDB
Annemys latiens	163.5	145.500	Rabi *et al.* 2010
Annemys levensis	157.3	145.500	Rabi *et al.* 2010
Annemys sp. IVPP V18106	167.700	145	PalaeoDB
Araripemys barretoi	112.600	109.000	PalaeoDB
Archelon ischyros	83.6	72.1	Hirayama 1997
Argillochelys cuneiceps	56	47.8	Weems & Brown2017
Arundelemys dardeni	122.460	112.600	PalaeoDB
Australochelys africanus	201.600	189.600	PalaeoDB
Baptemys wyomingensis	55.800	40.400	PalaeoDB
Bouliachelys suteri	105.300	99.700	PalaeoDB
Brachyopsemys tingitana	66.043	61.700	PalaeoDB
Cabindachelys landanensis	66	61.6	Myers *et al.* 2018
Calcarichelys gemma	84.9	70.6	PalaeoDB
Chelosphargis advena	85.8	84.9	PalaeoDB
Chubutemys copelloi	125.450	112.600	PalaeoDB
Corsochelys halinches	84.9	70.6	PalaeoDB
Ctenochelys	88.8	79.5	Gentry *et al.* 2018
Desmatochelys lowii	93.9	89.8	Hirayama 1997

Taxon	Age Maximum	Age Minimum	Source
Desmatochelys padillai	125.000	120	Cadena & Parham 2015
Dracochelys bicuspis	125	100.5	Rabi *et al.* 2010
Eileanchelys waldmanni	168.3	166.1	Joyce *et al.* 2016
Emarginachelys cretacea	70.600	66.043	PalaeoDB
Eochelone brabantica	47.8	41.2	Weems & Brown 2017
Eosphargis breineri	56	47.8	Fur Formation (Ypresian)
Eubaena cephalica	70.6	66.043	PalaeoDB
Erquelinnesia gossleti	56	47.8	Weems & Brown 2018
Galianemys whitei	99.7	94.3	PalaeoDB
Glyptops plicatulus	150.8	145.5	PalaeoDB
Judithemys sukhanovi	84.900	70.600	PalaeoDB
Jurassichelon oleronensis	152.1	145	Rieppel 1980; Anquetin *et al.* 2017*a*
Kallokibotion bajazidi	72.1	66	Joyce *et al.* 2016
Kayentachelys aprix	199.3	182.700	Joyce *et al.* 2016
Kirgizemys dmitrievi	130.000	112.600	PalaeoDB
Kirgizemys_hoburensis	125	100.5	Rabi *et al.* 2010
Leyvachelys cipadi	130.000	109.000	PalaeoDB
Meiolania planiceps	0	0	'Extant'
Nichollsemys baieri	84.9	70.6	PalaeoDB
Notochelone costata	109.000	99.700	PalaeoDB
Ocepechelon bouyai	70.600	66.043	PalaeoDB
Oligochelone rupelensis	33.9	28. Apr	PalaeoDB
Ordosemys sp. IVPP V12092	129.4	113	Rabi *et al.* 2010
Petrochelys kyrgyzensis	99.7	94.3	PalaeoDB
Peritresius martini	72	68.5	Gentry *et al.* 2018
Plesiochelys bigleri	155.7	150.8	PalaeoDB
Plesiochelys etalloni	157.300	150	Anquetin *et al.* 2017*a*
Plesiochelys planiceps	152.100	145.000	Anquetin *et al.* 2017*a*
Pleurosternon bullockii	145.2	140.2	PalaeoDB
Portlandemys mcdowelli	152.100	145.000	Anquetin *et al.* 2017*a*
Procolpochelys charlestonensis	28.4	23.3	Weems & Brown2018
Proganochelys quenstedti	208.5	201.300	Joyce *et al.* 2016
Protostega gigas	85.800	70.600	Hirayama 1997
Puppigerus camperi	56	41.2	Weems & Brown 2017
Rhinochelys nammourensis	99.7	94.3	PalaeoDB
Rhinochelys pulchriceps	105.300	102	FAD: PalaeoDB; LAD: Collins 1970
Sandownia harrisi	125.450	122.460	PalaeoDB
Santanachelys gaffneyi	112.600	109.000	PalaeoDB
Sinemys gamera	129.4	100.5	Rabi *et al.* 2010
Sinemys lens	163.5	145	Rabi *et al.* 2010
Solnhofia parsoni	155.700	145.500	Joyce 2000
Toxochelys sp.	85.800	70.600	Weems & Brown 2017
Xinjiangchelys radiplicatoides	168.3	152.1	Rabi *et al.* 2010
Xinjiangchelys wusu	163.5	152.1	PalaeoDB
Chelus fimbriatus	0	0	Extant

Taxon	Age Maximum	Age Minimum	Source
Phrynops geoffroanus	0	0	Extant
Elseya dentata	0	0	Extant
Chelodina	0	0	Extant
Podocnemis	0	0	Extant
Pelomedusa subrufa	0	0	Extant
Apalone spinifera	0	0	Extant
Pelodiscus sinensis	0	0	Extant
Lissemys punctata	0	0	Extant
Carettochelys insculpta	0	0	Extant
Chrysemys picta	0	0	Extant
Emys orbicularis	0	0	Extant
Geoclemys hamiltonii	0	0	Extant
Testudo	0	0	Extant
Gopherus polyphemus	0	0	Extant
Chelonoidis sp.	0	0	Extant
Platysternon megacephalum	0	0	Extant
Chelydra serpentina	0	0	Extant
Macrochelys temminckii	0	0	Extant
Dermatemys mawii	0	0	Extant
Staurotypus	0	0	Extant
Kinosternon suburum	0	0	Extant
Sternotherus	0	0	Extant
Dermochelys coriacea	0	0	Extant
Lepidochelys olivacea	0	0	Extant
Caretta caretta	0	0	Extant
Chelonia mydas	0	0	Extant
Eretmochelys imbricata	0	0	Extant
Lepidochelys kempii	0	0	Extant
Natator depressus	0	0	Extant

S3.2.1 R code for timescaled trees

The following code was used to time calibrate the tree shown in section 4 of this thesis (note that the trees were further modified with figure editing programmes). The "Turtle_Ages.txt" file used in the code below is the same data as shown in Table S3.1, except for that ages for nodes that have been collapsed in the phylogeny have been summarized by taking the FAD of the earliest taxon and the LAD of the latest taxon of the respective node. The following text follows R syntax, with '#' indicating comments.

```
# Load required packages

require(ape)
require(paleotree)
require(devtools)
require(msm)
require(rgl)
require(strap)
require(Claddis)

# Read tree

tree<-
read.tree(file=NA,text="(Proganochelys_quenstedti,(Australochelys_african
us,((Eileanchelys_waldmanni,Kayentachelys_aprix),(Chubutemys_copelloi,(Me
iolania_planiceps,Kallokibotion_bajazidi,(PARACRYPTODIRA,(XINJIANGCHELYID
AE,(SINEMYDIDAE-MACROBAENIDAE,((((Galianemys_whitei,CROWN-
PELOMEDUSOIDES),(Araripemys_barretoi,CROWN-
CHELIDAE)),(SANDOWNIDAE,THALASSOCHELYDIA)),((Adocus_beatus,((Lissemys_pun
ctata,Petrochelys_kyrgyzensis),(Allaeochelys_libyca,Carettochelys_insculp
ta))),(TESTUDINOIDEA,(((Emarginachelys_cretacea,(Chelydra_serpentina,Macr
ochelys_temminckii)),((Dermatemys_mawii,Baptemys_wyomingensis),(Staurotyp
us,(Kinosternon_suburum_hippocrepis,Sternotherus)))),(Toxochelys_sp,((Cor
sochelys_halinches,(Dermochelys_coriacea,Eosphargis_breineri),(Nichollsem
ys_baieri,(Allopleuron_hofmanni,((Procolpochelys_charlestonensis,(Cabinda
chelys_landanensis,Peritresius_martini,Ctenochelys),(Puppigerus_camperi,E
ochelone_brabantica),Argillochelys_cuneiceps),CROWN-
CHELONIIDAE)))),(Calcarichelys_gemma,Bouliachelys_suteri,(Chelosphargis_a
dvena,(Notochelone_costata,Santanachelys_gaffneyi,(Rhinochelys_pulchricep
s,Rhinochelys_nammourensis))),((Desmatochelys_lowii,Desmatochelys_padilla
i),(Ocepechelon_bouyai,(Protostega_gigas,Archelon_ischyros)))))))))))))))
));")

ctree<-collapse.singles(tree, root.edge = FALSE)

#Load and organise age data

data.reduced <- read.table("Turtle_Ages.txt" , header = T)
data.reduced

#Load and organise tip ages

ages.reduced <- cbind( data.reduced$Age_Max , data.reduced$Age_Min )
rownames( ages.reduced ) <- data.reduced$Name_on_Tree
colnames (ages.reduced) <- c("FAD", "LAD")

# Use additional time constraints as min.ages for certain nodes

node.mins<-rep(NA, scaled.tree.reduced$Nnode)
node.mins[mrca(scaled.tree.reduced)["CROWN-PELOMEDUSOIDES", "CROWN-
CHELIDAE"] - length( scaled.tree.reduced$tip.label )] <- 157.3
#Pleurodira minimum
node.mins[mrca(scaled.tree.reduced)["Lissemys_punctata", "TESTUDINOIDEA"]
- length( scaled.tree.reduced$tip.label )] <- 145.0 #Cryptodira minimum

# Calibration of tree with additional min-node ages

scaled.tree.reduced <- timePaleoPhy(ctree , ages.reduced , type = "mbl"
,vartime = 1, node.mins=node.mins )

# Plot tree
```

```
dev.new(width=12, height=10)
pdf("Scaled_tree_reduced.pdf", width=12, height=10)
geoscalePhylo(ladderize(scaled.tree.reduced, right=T), ages.reduced,
cex.ts=1.5, cex.tip=0.8,cex.age=0.5, label.offset=0.3, x.lim= c(0,225),
boxes="Epoch")
dev.off()
```

S3.3 Character list

S3.3.1. General notes on my character list

My character list aims to capture all variation documented so far for non-pleurodiran turtles. This includes 32 characters that, with respect to my taxon sampling, are parsimony uninformative because they are only scored for one taxon differently from all other taxa or invariant. I keep these characters in the list, because other people might chose to test the phylogenetic positions of additional taxa using our matrix in future.

The sources for characters listed as 'Evers & Benson (2018)' in most instances, because I used the character list of that paper as a baseline for further modifications. However, most characters are ultimately from older analyses. The original sources are summarized in Evers & Benson (2018), and also in Cadena & Parham (2015).

Each character is followed by a section called "character optimization", which lists the characters state changes of that character for each node in our phylogeny. "Unambiguous" synapomorphies are those found under both ACCTRAN and DELTRAN optimization. Because some nodes of the phylogeny represent unnamed clades, I use a code to denote the content of these clades. Hereby, the notation "Taxon+++" indicates the clade comprising the named taxon and all more crownwardly positioned taxa. The notation "(Taxon A ++ Taxon B)" indicates the most inclusive clade including Taxon A and Taxon B.

S3.3.2. Character list with documentation of modified characters

CRANIUM

Character 1 (Evers & Benson [2018]: character 1). Nasals: 0 = present; 1 = absent.

Character optimisation: Unambiguous: *Calcarichelys gemma* (0->1), (*Protostega* + *Archelon*) (0->1); DELTRAN: Cryptodira (0->1), Protostegidae (1->0), *Toxochelys* sp. (1->0), *Chelus fimbriatus* (0->1), *Araripemys barretoi* (0->1), total-group Pelomedusoides (0->1); ACCTRAN: Testudines (0->1), total-group Chelonioidea (1->0), *Corsochelys*+++ (0->1), Angolachelonia (1->0), crown-group Chelidae (1->0), *Chelus fimbriatus* (0->1).

Character 2 (Evers & Benson [2018]: character 2). Nasal, medial contact of nasals: 0 = nasals contact one another medially along their entire length; 1 = medial contact of nasals partially or fully hindered by long an- terior frontal process.

Character optimisation: Unambiguous: (*Brachyopsemys* ++ *Sandownia*) (0->1), *Sinemys gamera* (0->1), (*Annemys* sp. IVPP V18106 ++ *Xinjiangchelys*) (0->1); DELTRAN: crown-group Chelidae (0->1), Pleurosternidae (0->1), *Arundelemys dardeni* (0->1); ACCTRAN: crown-group Pleurodira (0->1), Paracryptodira (0->1), *Eubaena cephalica* (1->0).

Character 3 (Evers & Benson [2018]: character 3).

Character optimisation: Unambiguous: Xinjiangchelyidae+++ (0->1), *Leyvachelys cipadi* (1->0), Pleurosternidae (0->1); DELTRAN: *Ocepechelon bouyai* (1->0); ACCTRAN: (*Ocepechelon* ++ *Protostega*) (1->0).

Character 4 (Evers & Benson [2018]: character 4). Prefrontals, medial contact of prefrontals on the dorsal skull surface: 0 = absent; 1 = present, absence of contact between the nasal or apertura narium externa and the frontal.

Character optimisation: Unambiguous: (*Chelosphargis* + *Rhinochelys*) (1->0), (*Desmatochelys* ++ *Protostega*) (1->0), (*Plesiochelys planiceps* ++ *Jurassichelon*) (1->0), crown-group Chelidae (1->0), *Chubutemys copelloi* (0->1); DELTRAN: Sinemydidae/Macroabenidae+++ (0->1), *Ordosemys* sp. IVPP V12092 (1->0), (*Sinemys gamera* + *Sinemys lens*) (1->0), *Annemys levensis* (0->1); ACCTRAN: Xinjiangchelyidae+++ (0->1), Sinemydidae (1->0), *Dracochelys bicuspis* (0->1), (*Annemys latiens* ++ *Xinjiangchelys*) (1->0).

Character 5 (Evers & Benson [2018]: character 5). Prefrontal, prefrontal-vomer contact: 0 = present; 1 = absent.

Character optimisation: Unambiguous: (*Kayentachelys*+*Eileanchelys*)+++ (1->0), crown-group Pleurodira (0->1).

Character 6 (Evers & Benson [2018]: character 6). Prefrontal, prefrontal-palatine contact: 0 = present; 1 = absent.

Character optimisation: Unambiguous: crown-group Cheloniidae (0->1), *Ctenochelys* (0->1), crown-group Trionychia (0->1), crown-group Pleurodira (0->1), *Chelus fimbriatus* (1->0); DELTRAN: *Dermochelys coriacea* (0->1); ACCTRAN: Dermochelyidae (0->1).

Character 7 (Evers & Benson [2018]: character 7). Prefrontal, dorsal prefrontal exposure: 0 = present, large; 1 = reduced; 2 = absent or near absent.

Character optimisation: Unambiguous: (*Jurassichelon* + *Portlandemys*) (0->1), *Sandownia harrisi* (0->1), *Leyvachelys cipadi* (0->1), total-group Chelidae (0->1), (*Sinemys gamera* + *Sinemys lens*) (0->1), (*Annemys latiens* ++ *Xinjiangchelys*) (0->1), Paracryptodira (0->1), *Eubaena cephalica* (1->2), (*Kayentachelys* + *Eileanchelys*) (0->1); DELTRAN: *Ocepechelon bouyai* (0->1), (*Desmatochelys lowii* + *Desmatochelys padillai*) (0->1); ACCTRAN: (*Desmatochelys* ++ *Protostega*) (0->1), (*Protostega* + *Archelon*) (1->0).

Character 8 (Evers & Benson [2018]: character 8). Prefrontal, cranial scutes on the prefrontal: 0 = one pair; 1= two pairs or more.

Character optimisation: Unambiguous: (*Eretmochelys* ++ *Lepidochelys*) (0->1).

Character 9 (Evers & Benson [2018]: character 9). Prefrontal, sculpturing: 0 = heavily sculptured; 1 = sculpturing absent.

Character optimisation: Unambiguous: (*Kayentachelys*+*Eileanchelys*)+++ (0->1), *Bouliachelys suteri* (1->0), *Chelydra serpentina* (1->0).

Character 10 (new character): Prefrontal, preorbital bulge formed between the prefrontal and premaxilla: 0 = absent; 1 = present.

Character optimisation: Unambiguous: (*Rhinochelys pulchriceps* + *Rhinochelys nammourensis*) (0->1).

Character 11 (Evers & Benson [2018]: character 10). Lacrimal: 0 = present; 1 = absent. JY1 & Sterli & de la Fuente (2013: ch 9, Lacrimal A).

Character optimisation: Unambiguous: (*Kayentachelys*+*Eileanchelys*)+++ (0->1).

Character 12 (Evers & Benson [2018]: character 11). Frontal, frontal contribution to orbit: 0 = absent, contact between prefrontal and postorbital; 1 = present.

Character optimisation: Unambiguous: *Bouliachelys suteri* (1->0), (*Protostega* + *Archelon*) (1->0), Dermochelyidae (1->0), crown-group Chelydridae (1->0), Kinosternidae (1->0), *Eubaena cephalica* (1->0); DELTRAN: Paracryptodira+++ (0->1), *Lepidochelys olivacea* (1->0), *Caretta Caretta* (1->0), *Emys orbicularis* (1->0), *Platysternon megacephalum* (1->0), *Geoclemys hamiltonii* (1->0), *Kallokibotion bajazidi* (0->1), (*Kayentachelys* + *Eileanchelys*) (0->1); ACCTRAN: *Australochelys*+++ (0->1), (*Caretta* ++ *Lepidochelys*) (1->0), *Lepidochelys kempii* (0->1), Testudinoidea (1->0), *Chrysemys picta* (0->1), Testudinidae (0->1), *Meiolania planiceps* (1->0), *Chubutemys copelloi* (1->0).

Character 13 (Evers & Benson [2018]: character 12). Frontals, both frontals medially fused: 0 = absent; 1 = present.

Character optimisation: Unambiguous: *Chelodina* (0->1).

Character 14 (Evers & Benson [2018]: character 13). Frontal, direction of the orbits in dorsal view of the skull: 0 = laterally facing, with a very narrow to almost complete absent dorsal exposure of the maxilla and jugal; 1 = dorsolateral facing, with portions of the maxilla and jugal dorsally exposed.

Character optimisation: Unambiguous: Xinjiangchelyidae+++ (0->1), Cryptodira (1->0), *Ocepechelon bouyai* (0->1), *Corsochelys halinches* (0->1), *Toxochelys* sp. (0->1), *Chelonoidis* sp. (0->1), Trionychidae (0->1), *Kirgizemys dmitrievi* (1->0); DELTRAN: (*Ctenochelys* + *Cabindachelys*) (0->1), *Erquelinnesia gosseleti* (0->1); ACCTRAN: (*Ctenochelys* ++ *Peritresius*) (0->1), (*Oligochelone* + *Erquelinnesia*) (0->1).

Character 15 (Evers & Benson [2018]: character 14). Frontals, development of crista cranii: 0 = crista cranii on ventral surface of frontals very shallow, sulcus olfactorius developed is a low trough; 1 = crista cranii developed as moderately deep parasagittal ridges on the ventral surface of each frontal, forming a ventrally open, median trough (the sulcus olfactorius) that extends from the anterior margin of the cavum cranii posteriorly to the fissura ethmoidalis anteriorly; 2 = crista cranii very deep anteriorly, forming extended processes that meet along the midline of the cranium and are sutured to one another, forming an ossified olfactory canal.

Character optimisation: Unambiguous: (*Santanachelys* ++ *Rhinochelys*) (1->2); DELTRAN: *Dermochelys coriacea* (1->0); ACCTRAN: Dermochelyidae (1->0).

Character 16 (Evers & Benson [2018]: character 15). Parietal, parietal-squamosal contact: 0 = present, upper temporal emargination absent or poorly developed; 1 = absent, upper temporal emargination well developed.

Character optimisation: Unambiguous: (*Ocepechelon* ++ *Protostega*) (1->0), *Corsochelys*+++ (1->0), *Eubaena cephalica* (0->1); DELTRAN: Cryptodira (0->1), *Ctenochelys* (0->1), *Chelodina* (0->1), *Araripemys barretoi* (0->1), total-group Pelomedusoides (0->1), (*Sinemys gamera* + *Sinemys lens*) (0->1); ACCTRAN: Sinemydidae/Macroabenidae+++ (0->1), (*Ctenochelys* ++ *Peritresius*) (0->1), Angolachelonia (1->0), crown-group Chelidae (1->0), *Chelodina* (0->1), (*Kirgizemys hoburensis* + *Kirgizemys dmitrievi*) (1->0).

Character 17 (Evers & Benson [2018]: character 16). Parietal, posterodorsal margin of the temporal fossa roofed by an overhanging process of the skull roof: 0 = absent; 1 = present.

Character optimisation: Unambiguous: Paracryptodira+++ (1->0), *Rhinochelys nammourensis* (1->0), Dermochelyidae (0->1), (*Erquelinnesia* ++ *Lepidochelys*) (0->1), *Ctenochelys* (1->0), *Platysternon megacephalum* (0->1), Sandownidae (0->1), *Sandownia harrisi* (1->0), *Elseya dentata* (0->1); DELTRAN: (*Chelosphargis* + *Rhinochelys*) (0->1); ACCTRAN: (*Bouliachelys* + *Rhinochelys*) (0->1).

Character 18 (Evers & Benson [2018]: character 17). Parietal, contribution to the processus trochlearis oticum: 0 = absent; 1 = present.

Character optimisation: Unambiguous: Kinosternidae (0->1), total-group Trionychia (0->1), *Solnhofia parsoni* (0->1); DELTRAN: *Geoclemys hamiltonii* (0->1), (*Testudo* + *Chelonoidis*) (0->1), *Pleurosternon bullockii* (0->1); ACCTRAN: Testuguria (0->1), *Gopherus polyphemus* (1->0), Pleurosternidae (0->1).

Character 19 (Evers & Benson [2018]: character 18). Parietals, foramen stapedio-temporalis: 0 = absent or weak, foramen stapedio- temporale concealed in dorsal view; 1 = moderate foramen stapedio-temporale, partial exposition of the processes trochlearis in dorsal view; 2 = strong, entire exposition of the processus trochlearis in dorsal view.

Character optimisation: Unambiguous: Paracryptodira+++ (0->2), *Desmatochelys padillai* (0->1), *Nichollsemys baieri* (0->1), *Platysternon megacephalum* (2->0), Angolachelonia (2->0), *Jurassichelon oleronensis* (0->1), *Elseya dentata* (2->0), *Podocnemis* (2->0), (*Judithemys* ++ *Sinemys*) (2->1), (*Sinemys gamera* + *Sinemys lens*) (1->2), Pleurosternidae (2->0); DELTRAN: Protostegidae+++ (2->0), *Toxochelys* sp. (2->1); ACCTRAN: total-group Chelonioidea (2->0), *Toxochelys* sp. (0->1).

Character 20 (Evers & Benson [2018]: character 19). Parietal, pineal foramen located medially between parietals: 0 = absent; 1 = present.

Character optimisation: Unambiguous: (*Desmatochelys lowii* + *Desmatochelys padillai*) (0->1).

Character 21 (Evers & Benson [2018]: character 20). Parietal, processus inferior parietalis: 0 = weak or absent, parietal does not contact the pterygoid, epipterygoid, and/or

palatine; 1 = present and well developed, the parietal contacts the pterygoid, epipterygoid, and/or palatine.

Character optimisation: DELTRAN: *Chubutemys*+++ (0->1), *Eileanchelys waldmanni* (0->1); ACCTRAN: (*Kayentachelys*+*Eileanchelys*)+++ (0->1), *Kayentachelys aprix* (1->0).

Character 22 (Evers & Benson [2018]: character 21). Parietal, closure of foramen nervi trigemini and the length of the anterior extension of the lateral braincase wall: 0 = foramen nervi trigemini anteriorly open, anterior extension of lateral braincase wall absent; 1 = foramen nervi trigemini anteriorly closed, processus inferior parietalis only produces a narrow strut anterior to the foramen nervi trigemini, usually absence of contact with palatine; 2 = foramen nerivi trigemini anteriorly closed, processus inferior parietalis produces an ex- tended process anterior to the foramen nervi trigemini, contact with palatine commonly present.

Character optimisation: Unambiguous: *Chubutemys*+++ (0->1), *Cabindachelys landanensis* (1->2), Kinosternoidea (1->2), *Gopherus polyphemus* (1->2), total-group Trionychia (1->2), total-group Pelomedusoides (1->2); DELTRAN: *Dermochelys coriacea* (1->0), (*Sandownia* + *Angolachelys*) (1->2), *Leyvachelys cipadi* (1->2); ACCTRAN: Dermochelyidae (1->0), Sandownidae (1->2), *Brachyopsemys tingitana* (2->1).

Character 23 (Evers & Benson [2018]: character 22). Parietal, posterior ramus of processus inferior parietalis forming the posterior margin of the trigeminal foramen: 0 = absent; 1 = present.

Character optimisation: Unambiguous: (*Bouliachelys* + *Rhinochelys*) (1->0), crown-group Chelonioidea (1->0), Kinosternoidea (1->0), *Chrysemys picta* (1->0), *Gopherus polyphemus* (1->0), total-group Trionychia (1->0), *Chelus fimbriatus* (1->0), *Pelomedusa subrufa* (1->0); DELTRAN: Xinjiangchelyidae+++ (0->1), *Pleurosternon bullockii* (0->1); ACCTRAN: Paracryptodira+++ (0->1), *Arundelemys dardeni* (1->0).

Character 24 (Evers & Benson [2018]: character 23). Posterior ramus of processus inferior parietalis of the parietal: 0 = short; 1 = long, excludes the prootic from the trigeminal foramen. This character is scored inapplicable for taxa that lack the process altogether.

Character optimisation: Unambiguous: *Elseya dentata* (0->1); DELTRAN: *Emys orbicularis* (0->1), Testuguria (0->1), Angolachelonia (0->1), *Podocnemis* (0->1), *Kirgizemys hoburensis* (0->1); ACCTRAN: Sinemydidae/Macroabenidae+++ (0->1), Americhelydia (1->0), *Platysternon megacephalum* (1->0), crown-group Pleurodira (1->0), crown-group Pelomedusoides (0->1).

Character 25 (Evers & Benson [2018]: character 24). Parietal, ridge on lateral surface of processus inferior parietalis: 0 = absent; 1 = present, a ridge between the ventral surface of the parietal and the lateral surface of the descending process marks the border between the temporal and orbital fossae.

Character optimisation: Unambiguous: (*Puppigerus* ++ *Ctenochelys*) (0->1), *Chelydra serpentina* (0->1), Kinosterninae (0->1), *Phrynops geoffroanus* (0->1), *Elseya dentata* (0->1); DELTRAN: crown-group Trionychia (0->1), *Podocnemis* (0->1), *Galianemys whitei* (0->1), *Sinemys gamera* (0->1), Paracryptodira (0->1), *Kayentachelys aprix* (0->1), *Australochelys africanus* (0->1); ACCTRAN: *Australochelys*+++ (0->1), *Chubutemys*+++ (1->0), total-group Trionychia (0->1), total-group Pelomedusoides (0->1), *Pelomedusa subrufa* (1->0), (*Sinemys gamera* + *Sinemys lens*) (0->1), Paracryptodira (0->1).

Character 26 (Evers & Benson [2018]: character 25). Jugal, jugal-squamosal contact: 0 = present; 1 = absent.

Character optimisation: Unambiguous: *Dermochelys coriacea* (1->0), *Allopleuron hoffmanni* (1->0), *Meiolania planiceps* (1->0); DELTRAN: (*Kayentachelys*+*Eileanchelys*)+++ (0->1); ACCTRAN: *Australochelys*+++ (0->1).

Character 27 (Evers & Benson [2018]: character 26). Jugal, jugal participation in the margin of the upper temporal emargination: 0 = absent; 1 = present, upper temporal emargination extensive.

Character optimisation: Unambiguous: Kinosternidae (0->1), *Geoclemys hamiltonii* (0->1), Trionychidae (0->1).

Character 28 (Evers & Benson [2018]: character 27). Jugal, medial process of jugal ventral to orbit: 0 = weakly developed or absent, jugal contacts only the maxilla; 1 = present and well developed, jugal contacts the maxilla as well as the palatine and/or pterygoid.

Character optimisation: Unambiguous: Testudinidae (1->0), Plesiochelyidae (1->0), *Leyvachelys cipadi* (1->0), *Chubutemys copelloi* (1->0); DELTRAN: Protostegidae (1->0), Dermochelyidae (1->0); ACCTRAN: Protostegidae+++ (1->0), total-group Cheloniidae (0->1).

Character 29 (Evers & Benson [2018]: character 28). Jugal, contact with the palatine: 0 = absent; 1 = present. This character is scored as inapplicable when the jugal lacks a medial process (ch 27.0).

Character optimisation: Unambiguous: *Chelydra serpentina* (1->0), *Emys orbicularis* (1->0), *Angolachelys mbaxi* (0->1), (*Kayentachelys* + *Eileanchelys*) (0->1); DELTRAN: Cryptodira (0->1), *Nichollsemys baieri* (1->0), *Toxochelys* sp. (1->0), crown-group Pleurodira (0->1), (*Eubaena* + Pleurosternidae) (0->1); ACCTRAN: Testudines (0->1), total-group Chelonioidea (1->0), *Allopleuron*+++ (0->1), Angolachelonia (1->0), Paracryptodira (0->1).

Character 30 (Evers & Benson [2018]: character 29). Jugal, contact with the pterygoid: 0 = absent; 1 = present. This character is scored as inapplicable when the jugal lacks a medial process (ch 27.0).

Character optimisation: Unambiguous: (*Eretmochelys* ++ *Lepidochelys*) (1->0), *Lepidochelys kempii* (0->1), *Emarginachelys cretacea* (1->0), *Lissemys punctata* (1->0), *Chubutemys copelloi* (1->0); DELTRAN: *Procolpochelys charlestonensis* (1->0); ACCTRAN: (*Procolpochelys* ++ *Erquelinnesia*) (1->0).

Character 31 (Evers & Benson [2018]: character 30). Jugal, jugal-parietal contact: 0 = absent; 1 = present.

Character optimisation: Unambiguous: Trionychidae (0->1), *Podocnemis* (0->1).

Character 32 (Evers & Benson [2018]: character 31). Quadratojugal: 0 = present; 1 = absent.

Character optimisation: Unambiguous: crown-group Chelidae (0->1).

Character 33 (Evers & Benson [2018]: character 32). Quadratojugal, quadratojugal-maxilla contact: 0 = absent; 1 = present, jugal does not contribute to lower temporal emargination.

Character optimisation: Unambiguous: Kinosternidae (0->1), *Platysternon megacephalum* (0->1), *Galianemys whitei* (0->1); DELTRAN: *Carettochelys insculpta* (0->1); ACCTRAN: total-group Carettochelyidae (0->1).

Character 34 (Evers & Benson [2018]: character 33). Quadratojugal, quadratojugal-squamosal contact below the cavum tympani: 0 = absent; 1 = present.

Character optimisation: Unambiguous: *Meiolania planiceps* (0->1).

Character 35 (Evers & Benson [2018]: character 34). Quadratojugal, lower temporal emargination: 0 = weak to no emargination, the margin of the lower temporal emargination is formed by the quadratojugal or quadratojugal and jugal; 1 = moderate emargination, the margin of the lower temporal emargination is principally formed by the quadratojugal and jugal, but the maxilla is included in the anterior section of the margin and/or the quadrate is included in the posterior section of the margin; 2 = large emargination, the postorbital and/or squamosal and parietal are included in the margin of the lower temporal emargination.

Character optimisation: Unambiguous: Paracryptodira+++ (0->1), *Nichollsemys baieri* (0->1), total-group Dermatemydidae (0->1), *Plesiochelys planiceps* (1->2), Sandownidae (1->0), crown-group Chelidae (1->2), *Galianemys whitei* (1->0); DELTRAN: Americhelydia (1->0),

Platysternon megacephalum (1->0), *Geoclemys hamiltonii* (1->0), crown-group Trionychia (1->0), (*Sinemys gamera* + *Sinemys lens*) (1->2), (*Kirgizemys hoburensis* + *Kirgizemys dmitrievi*) (1->2), *Annemys levensis* (1->2), *Annemys* sp. IVPP V18106 (1->2); ACCTRAN: Cryptodira (1->0), Emydidae (0->1), Testudinidae (0->1), *Adocus beatus* (0->1), (*Sinemys* ++ *Kirgizemys*) (1->2), (*Ordosemys* + *Dracochelys*) (2->1), Xinjiangchelyidae (1->2), (*Xinjiangchelys wusu* + *Xinjiangchelys radiplicatoides*) (2->1).

Character 36 (Evers & Benson [2018]: character 35). Squamosal, squamosal-postorbital contact: 0 = present; 1 = absent.

Character optimisation: Unambiguous: total-group Chelonioidea (1->0), crown-group Chelydridae (1->0), *Platysternon megacephalum* (1->0), *Pleurosternon bullockii* (0->1); DELTRAN: Cryptodira (0->1), crown-group Pleurodira (0->1), *Sinemys gamera* (0->1); ACCTRAN: Sinemydidae/Macroabenidae+++ (0->1), Angolachelonia (1->0), (*Kirgizemys hoburensis* + *Kirgizemys dmitrievi*) (1->0).

Character 37 (Evers & Benson [2018]: character 36). Squamosal, squamosal-supraoccipital contact: 0 = absent; 1 = present.

Character optimisation: Unambiguous: *Meiolania planiceps* (0->1).

Character 38 (Evers & Benson [2018]: character 37). Squamosal, posterolateral protuberances developing horns: 0 = absent; 1 = present.

Character optimisation: Unambiguous: *Meiolania planiceps* (0->1).

Character 39 (Evers & Benson [2018]: character 38). Squamosal, very long posterior process, formed exclusively by the squamosal and protruding beyond condyles occipitalis: 0 = absent; 1 = present.

Character optimisation: Unambiguous: *Ocepechelon bouyai* (0->1), *Toxochelys* sp. (0->1), *Staurotypus* (0->1), *Chrysemys picta* (0->1), *Araripemys barretoi* (0->1), *Pelomedusa subrufa* (0->1); DELTRAN: total-group Trionychia (0->1), *Angolachelys mbaxi* (0->1), (*Judithemys* ++ *Sinemys*) (0->1), *Sinemys lens* (1->0), Xinjiangchelyidae (0->1); ACCTRAN:

Xinjiangchelyidae+++ (0->1), Testudines (1->0), total-group Trionychia (0->1), (*Sandownia* + *Angolachelys*) (0->1), (*Sinemys gamera* + *Sinemys lens*) (1->0).

Character 40 (Evers & Benson [2018]: character 39). Squamosal, squamosal-quadrate contact: 0 = tightly sutured; 1 = wide open.

Character optimisation: Unambiguous: total-group Chelonioidea (0->1), Plesiochelyidae (0->1).

Character 41 (Evers & Benson [2018]: character 40). Squamosal, posterodorsal margin of cavum tympanum: 0 = the squamosal forms the posterodorsal margin of the cavum tympanum; 1 = the squamosal is excluded from the posterodorsal margin of the cavum tympanum.

Character optimisation: Unambiguous: *Desmatochelys lowii* (1->0), *Corsochelys*+++ (1->0), *Baptemys wyomingensis* (1->0), *Platysternon megacephalum* (1->0), *Chelonoidis* sp. (1->0), Trionychidae (1->0), Thalassochelydia (1->0), *Kirgizemys hoburensis* (0->1); DELTRAN: Testudines (0->1), *Archelon ischyros* (1->0), *Macrochelys temminckii* (1->0), *Emarginachelys cretacea* (1->0), *Annemys* sp. IVPP V18106 (0->1); ACCTRAN: Xinjiangchelyidae+++ (0->1), (*Protostega* + *Archelon*) (1->0), total-group Chelydridae (1->0), *Chelydra serpentina* (0->1), (*Judithemys* ++ *Sinemys*) (1->0).

Character 42 (Evers & Benson [2018]: character 41). Postorbital, postorbital-palatine contact: 0 = absent; 1 = present, foramen palatinum posterius situated posterior to the orbital wall.

Character optimisation: Unambiguous: crown-group Pleurodira (0->1).

Character 43 (Evers & Benson [2018]: character 42). Postorbital, contact with the quadratojugal: 0 = present; 1 = absent.

Character optimisation: Unambiguous: *Dermochelys coriacea* (0->1), *Allopleuron hoffmanni* (0->1), *Geoclemys hamiltonii* (0->1), *Testudo* (0->1), Trionychidae (0->1), *Podocnemis* (0->1);

DELTRAN: *Kinosternon suburum hippocrepisis* (0->1), *Staurotypus* (0->1), *Proganochelys quenstedti* (0->1); ACCTRAN: Kinosternidae (0->1), *Sternotherus* (1->0), *Proganochelys quenstedti* (0->1).

Character 44 (Evers & Benson [2018]: character 43). Postorbital, postorbital-maxilla contact preventing the jugal from entering the orbital margin: 0 = absent; 1 = present.

Character optimisation: Unambiguous: *Platysternon megacephalum* (0->1), *Galianemys whitei* (0->1), Paracryptodira (0->1).

Character 45 (Evers & Benson [2018]: character 44). Postorbital, dorsal margin of orbit: 0 = continuously and concavely curved margin between frontals and jugal; 1 = frontal margin relatively narrow, with lateral bulge of postorbital.

Character optimisation: Unambiguous: *Archelon ischyros* (0->1), (*Erquelinnesia* ++ *Lepidochelys*) (0->1); DELTRAN: (*Ctenochelys* + *Cabindachelys*) (1->0), *Plesiochelys etalloni* (0->1); ACCTRAN: (*Ctenochelys* ++ *Peritresius*) (1->0), (*Plesiochelys etalloni* + *Plesiochelys bigleri*) (0->1).

Character 46 (Evers & Benson [2018]: character 45). Supratemporal: 0 = present; 1 = absent.

Character optimisation: DELTRAN: *Chubutemys*+++ (0->1); ACCTRAN: *Australochelys*+++ (0->1).

Character 47 (Evers & Benson [2018]: character 46). Teeth in premaxilla, maxilla, and dentary: 0 = present; 1 = absent.

Character optimisation: -.

Character 48 (Evers & Benson [2018]: character 47). Premaxilla, subdivision of the apertura narium externa by an internarial process of the premaxilla: 0 = present; 1 = absent.

Character optimisation: Unambiguous: Paracryptodira+++ (0->1), *Angolachelys mbaxi* (1->0), (*Kayentachelys* + *Eileanchelys*) (0->1).

Character 49 (Evers & Benson [2018]: character 48). Premaxilla, fusion of premaxillae: 0 = absent; 1 = present.

Character optimisation: Unambiguous: *Ocepechelon bouyai* (0->1), crown-group Trionychia (0->1), *Chelus fimbriatus* (0->1); DELTRAN: *Erquelinnesia gosseleti* (0->1), *Angolachelys mbaxi* (0->1), *Brachyopsemys tingitana* (0->1); ACCTRAN: (*Oligochelone* + *Erquelinnesia*) (0->1), (*Brachyopsemys* ++ *Sandownia*) (0->1), *Sandownia harrisi* (1->0).

Character 50 (Evers & Benson [2018]: character 49). Premaxilla, foramen praepalatinum: 0 = absent; 1 = present.

Character optimisation: Unambiguous: (*Erquelinnesia* ++ *Lepidochelys*) (1->0), *Staurotypus* (1->0), crown-group Trionychia (1->0), *Solnhofia parsoni* (1->0), (*Brachyopsemys* ++ *Sandownia*) (1->0); DELTRAN: (*Kayentachelys*+*Eileanchelys*)+++ (0->1), (*Bouliachelys* + *Rhinochelys*) (1->0), *Ocepechelon bouyai* (1->0); ACCTRAN: *Australochelys*+++ (0->1), Protostegidae (1->0), (*Desmatochelys lowii* + *Desmatochelys padillai*) (0->1).

Character 51 (Evers & Benson [2018]: character 50). Premaxilla, foramen intermaxillaris: 0 = absent; 1 = present.

Character optimisation: Unambiguous: Trionychidae (0->1).

Character 52 (Evers & Benson [2018]: character 51). Premaxilla, exclusion of the premaxillae from the apertura narium externa: 0 = absent; 1 = present.

Character optimisation: Unambiguous: Trionychidae (0->1).

Character 53 (Evers & Benson [2018]: character 52). Premaxilla, distinct, median premaxillary hook along the labial margin of the premaxillae: 0 = absent; 1 = present.

Character optimisation: Unambiguous: *Kinosternon suburum hippocrepis* (0->1), (*Protostega* + *Archelon*) (0->1), *Lepidochelys kempii* (0->1), crown-group Chelydridae (0->1), *Platysternon megacephalum* (0->1).

Character 54 (Evers & Benson [2018]: character 53) Premaxilla, cusps developed on the labial ridge in conjunction with maxilla: 0 = absent; 1 = present.

Character optimisation: Unambiguous: Dermochelyidae (0->1), *Dracochelys bicuspis* (0->1).

Character 55 (Evers & Benson [2018]: character 54). Palatine, contribution to the anterior extension of the lateral braincase wall: 0 = absent; 1 = present.

Character optimisation: Unambiguous: Kinosternoidea (0->1), *Gopherus polyphemus* (0->1), total-group Trionychia (0->1), total-group Pelomedusoides (0->1); DELTRAN: *Sandownia harrisi* (0->1); ACCTRAN: (*Sandownia* + *Angolachelys*) (0->1).

Character 56 (Evers & Benson [2018]: character 55). Palatine, contribution to the upper triturating surface: 0 = absent or less than 30% of the total width of the triturating surface; 1 = present, at least 30% or more of the total width of the triturating surface.

Character optimisation: Unambiguous: *Allopleuron*+++ (0->1), *Eochelone brabantica* (1->0), (*Sandownia* + *Angolachelys*) (0->1), *Podocnemis* (0->1).

Character 57 (Evers & Benson [2018]: character 56). Palatine, secondary palate: 0 = absent; 1 = present, complete separation of the narial cavity from the oral cavity.

Character optimisation: Unambiguous: *Allopleuron*+++ (0->1), *Eochelone brabantica* (1->0); DELTRAN: *Solnhofia parsoni* (0->1), Sandownidae (0->1); ACCTRAN: Angolachelonia (0->1), Plesiochelyidae (1->0).

Character 58 (Evers & Benson [2018]: character 57). Palatine, vomer-palatine contact anterior to internal naris (apertura narium interna): 0 = absent; 1 = present.

Character optimisation: Unambiguous: *Eochelone brabantica* (1->0), Sandownidae (0->1); DELTRAN: crown-group Chelonioidea (0->1), *Toxochelys* sp. (0->1); ACCTRAN: total-group Chelonioidea (0->1), Protostegidae (1->0).

Character 59 (Evers & Benson [2018]: character 58). Maxilla, triturating surface definition: 0 = triturating surface with labial ridge only; 1 = triturating surface with labial and lingual ridge; 2 = triturating surface with labial, lingual, and accessory ridge(s).

Character optimisation: Unambiguous: *Ocepechelon bouyai* (1->0), *Ctenochelys* (0->1), *Argillochelys cuneiceps* (0->1), *Chelydra serpentina* (0->1), *Emarginachelys cretacea* (0->2), total-group Dermatemydidae (0->2), *Chrysemys picta* (0->2), *Platysternon megacephalum* (0->1), Testudinidae (0->2), *Adocus beatus* (0->2), Plesiochelyidae (0->1), *Elseya dentata* (0->2), crown-group Pelomedusoides (0->2), *Dracochelys bicuspis* (0->1), *Kirgizemys dmitrievi* (0->1), *Pleurosternon bullockii* (1->0), *Meiolania planiceps* (0->2); DELTRAN: Xinjiangchelyidae+++ (1->0), Protostegidae (0->1), *Eosphargis breineri* (0->1), *Lepidochelys kempii* (0->2), *Eretmochelys imbricata* (0->2), (*Chelonia* + *Natator*) (0->2), *Toxochelys* sp. (0->1), *Apalone spinifera* (0->1), *Carettochelys insculpta* (0->1), *Chubutemys copelloi* (1->0); ACCTRAN: *Chubutemys*+++ (1->0), total-group Chelonioidea (0->1), *Corsochelys*+++ (1->0), *Eosphargis breineri* (0->1), crown-group Cheloniidae (0->2), (*Caretta* ++ *Lepidochelys*) (2->0), *Lepidochelys kempii* (0->2), (*Apalone* + *Petrochelys*) (0->1), total-group Carettochelyidae (0->1), Paracryptodira (0->1).

Character 60 (Evers & Benson [2018]: character 59). Maxilla, accessory ridge(s): 0 = accessory ridge(s) on maxilla present along the triturating surface; 1 = accessory ridge(s) only in some sectors of the triturating surface. Thic character is scored as inapplicable when no accessory ridges are present (ch 58.0 or ch 58.1).

Character optimisation: DELTRAN: *Emarginachelys cretacea* (0->1), *Baptemys wyomingensis* (0->1), *Adocus beatus* (0->1); ACCTRAN: Chelydroidea (0->1), *Dermatemys mawii* (1->0), total-group Trionychia (0->1).

Character 61 (Evers & Benson [2018]: character 60). Maxilla, median contact between right and left maxilla on the palate: 0 = absent; 1 = present.

Character optimisation: Unambiguous: *Caretta Caretta* (0->1), Trionychidae (0->1), *Solnhofia parsoni* (0->1), *Elseya dentata* (0->1), *Kallokibotion bajazidi* (0->1).

Character 62 (Evers & Benson [2018]: character 61). Vomer, number of vomer(s): 0 = paired; 1 = single, but large; 2 = single and greatly reduced or absent.

Character optimisation: Unambiguous: crown-group Pelomedusoides (1->2), *Kirgizemys dmitrievi* (1->0); DELTRAN: (*Kayentachelys*+*Eileanchelys*)+++ (0->1); ACCTRAN: *Australochelys*+++ (0->1).

Character 63 (Evers & Benson [2018]: character 62). Vomer, vomer-pterygoid contact in palatal view: 0 = present; 1 = absent, medial contact of palatines present.

Character optimisation: Unambiguous: Protostegidae (0->1), *Nichollsemys baieri* (0->1), crown-group Trionychia (0->1), total-group Pleurodira (0->1), *Portlandemys mcdowelli* (1->0), (*Plesiochelys etalloni* + *Plesiochelys bigleri*) (1->0), (*Brachyopsemys* ++ *Sandownia*) (1->0), crown-group Chelidae (1->0), *Chubutemys copelloi* (0->1); DELTRAN: *Xinjiangchelys radiplicatoides* (0->1); ACCTRAN: (*Xinjiangchelys wusu* + *Xinjiangchelys radiplicatoides*) (0->1).

Character 64 (Evers & Benson [2018]: character 63). Vomer, vomerine and palatine teeth: 0 = present; 1 = absent.

Character optimisation: DELTRAN: *Australochelys*+++ (0->1); ACCTRAN: *Australochelys*+++ (0->1).

Character 65 (Evers & Benson [2018]: character 64). Vomer, vomer-premaxilla contact in ventral view: 0 = present; 1 = absent.

Character optimisation: Unambiguous: *Caretta Caretta* (0->1), *Dermatemys mawii* (0->1), crown-group Trionychia (0->1), *Solnhofia parsoni* (0->1), *Brachyopsemys tingitana* (0->1).

Character 66 (Evers & Benson [2018]: character 65). Vomer, ventral median crest: 0 = absent, ventral surface of vomer is smooth; 1 = present, shallow ridge extends along the

ventral surface posterior to ventral process of the vomer, ridge becomes shallower posteriorly; 2 = narrow and tall ventral crest present all along the vomer.

Character optimisation: Unambiguous: *Chubutemys*+++ (0->2), Americhelydia (2->1), (*Protostega* + *Archelon*) (1->0), total-group Cheloniidae (1->0), *Eochelone brabantica* (0->1), *Ctenochelys* (0->1), *Toxochelys* sp. (1->0), *Macrochelys temminckii* (1->0), *Emys orbicularis* (2->0), *Platysternon megacephalum* (2->1), total-group Pleurodira (2->0), *Dracochelys bicuspis* (2->0), *Kirgizemys dmitrievi* (2->1); DELTRAN: *Carettochelys insculpta* (2->0), Pleurosternidae (2->0), *Arundelemys dardeni* (2->0); ACCTRAN: total-group Carettochelyidae (2->0), Paracryptodira (2->0), *Eubaena cephalica* (0->2).

Character 67 (Evers & Benson [2018]: character 66). Vomer, shape of the palate roof: 0 = flat; 1 = domed.

Character optimisation: Unambiguous: (*Kayentachelys*+*Eileanchelys*)+++ (1->0), *Ctenochelys* (0->1), Testuguria (0->1), *Testudo* (1->0), *Meiolania planiceps* (0->1); DELTRAN: *Carettochelys insculpta* (0->1); ACCTRAN: total-group Carettochelyidae (0->1).

Character 68 (Evers & Benson [2018]: character 67). Vomer, shape of anterior end contacting the maxillae and praemaxillae: 0 = flat, near horizontal contact with maxillae; 1 = the anterior end of the vomer is anteroventrally directed and laterally expanded; 2 = the anterior end of the vomer is ventrally expanded to form a horizontal footplate with a flat ventral surface.

Character optimisation: Unambiguous: Americhelydia (0->1), *Notochelone* (1->0), (*Ocepechelon* ++ *Protostega*) (1->0), *Dermochelys coriacea* (1->0), *Allopleuron*+++ (1->2), *Eochelone brabantica* (2->1), *Ctenochelys* (2->1), crown-group Chelydridae (1->0), *Geoclemys hamiltonii* (0->1); DELTRAN: *Sternotherus* (1->2), *Staurotypus* (1->2), *Solnhofia parsoni* (0->2), (*Brachyopsemys* ++ *Sandownia*) (0->2); ACCTRAN: Kinosternidae (1->2), *Kinosternon suburum hippocrepis* (2->1), Angolachelonia (0->2), Plesiochelyidae (2->0).

Character 69 (Evers & Benson [2018]: character 68). Vomer, contribution to the upper triturating surface: 0 = absent, triturating surface narrow to absent; 1 = present.

Character optimisation: Unambiguous: *Allopleuron*+++ (0->1), *Chrysemys picta* (0->1), *Geoclemys hamiltonii* (0->1), Sandownidae (0->1); DELTRAN: *Sternotherus* (0->1), *Staurotypus* (0->1); ACCTRAN: Kinosternidae (0->1), *Kinosternon suburum hippocrepis* (1->0).

Character 70 (Evers & Benson [2018]: character 69). Vomer, median trough on dorsal surface posterior to sulcus vomeri: 0 = absent, dorsal surface of vomer flat or transversely convex; 1 = present, dorsal surface bears a median trough that extends posteriorly from the sulcus vomeri.

Character optimisation: Unambiguous: Cryptodira (0->1), total-group Chelonioidea (1->0), *Lissemys punctata* (1->0); DELTRAN: *Notochelone* (0->1), (*Lepidochelys olivacea* + *Lepidochelys kempii*) (0->1), *Eretmochelys imbricata* (0->1), *Natator depressus* (0->1), *Eubaena cephalica* (0->1), *Proganochelys quenstedti* (0->1); ACCTRAN: (*Santanachelys* + *Notochelone*) (0->1), crown-group Cheloniidae (0->1), *Caretta Caretta* (1->0), *Chelonia mydas* (1->0), (*Eubaena* + Pleurosternidae) (0->1), *Proganochelys quenstedti* (0->1).

Character 71 (Evers & Benson [2018]: character 70). Foramen orbito-nasale: 0 = formed as true foramen that is surrounded by bone from all sides; 1 = foramen orbito-nasale is not completely surrounded by bone and coalescent with the passage between the fossa orbitalis and the fossa nasalis.

Character optimisation: Unambiguous: crown-group Pleurodira (0->1).

Character 72 (Evers & Benson [2018]: character 71). Foramen orbito-nasale, contribution of vomer: 0 = absent; 1 = present.

Character optimisation: Unambiguous: *Gopherus polyphemus* (0->1), crown-group Trionychia (0->1), *Brachyopsemys tingitana* (0->1); DELTRAN: *Dermochelys coriacea* (0->1), (*Eretmochelys* ++ *Lepidochelys*) (0->1), *Natator depressus* (0->1); ACCTRAN: Dermochelyidae (0->1), crown-group Cheloniidae (0->1), *Chelonia mydas* (1->0).

Character 73 (Evers & Benson [2018]: character 72). Foramen orbito-nasale, contribution of the maxilla: 0 = absent; 1 = present.

Character optimisation: Unambiguous: *Emys orbicularis* (1->0), Testuguria (1->0), total-group Chelidae (1->0); DELTRAN: Xinjiangchelyidae+++ (0->1), *Meiolania planiceps* (0->1); ACCTRAN: *Australochelys*+++ (0->1), Paracryptodira (1->0).

Character 74 (Evers & Benson [2018]: character 73). Quadrate, precolumellar fossa: 0 = absent; 1 = present.

Character optimisation: Unambiguous: *Araripemys barretoi* (0->1), crown-group Pelomedusoides (0->1); DELTRAN: *Sinemys gamera* (0->1); ACCTRAN: (*Sinemys gamera* + *Sinemys lens*) (0->1).

Character 75 (Evers & Benson [2018]: character 74). Quadrate, development of the cavum tympani: 0 = shallow, but not developed anteroposteriorly; 1 = shallow, but anteroposteriorly developed; 2 = deep and anteroposteriorly developed.

Character optimisation: DELTRAN: (*Kayentachelys*+*Eileanchelys*)+++ (0->2), *Australochelys africanus* (0->1); ACCTRAN: *Australochelys*+++ (0->1), (*Kayentachelys*+*Eileanchelys*)+++ (1->2).

Character 76 (Evers & Benson [2018]: character 75). Quadrate, anterior margin of the cavum tympanum: 0 = formed entirely by the quadrate; 1 = formed by the quadratojugal, which overlaps the lateral surface of the quadrate, reaching the anterior margin of the cavum tympanum.

Character optimisation: Unambiguous: Protostegidae (1->0), *Natator depressus* (1->0), *Platysternon megacephalum* (1->0), (*Testudo* + *Chelonoidis*) (1->0), *Judithemys sukhanovi* (0->1), (*Xinjiangchelys wusu* + *Xinjiangchelys radiplicatoides*) (0->1), *Eubaena cephalica* (0->1), *Meiolania planiceps* (0->1); DELTRAN: Durocryptodira (0->1), *Santanachelys gaffneyi* (0->1), *Archelon ischyros* (0->1), crown-group Trionychia (0->1), *Jurassichelon oleronensis* (0->1);

ACCTRAN: Cryptodira (0->1), (*Santanachelys* + *Notochelone*) (0->1), (*Protostega* + *Archelon*) (0->1), *Adocus beatus* (1->0), (*Plesiochelys planiceps* ++ *Jurassichelon*) (0->1).

Character 77 (Evers & Benson [2018]: character 76). Quadrate, antrum postoticum: 0 = absent; 1 = incipient, the antrum postoticum is completely formed within quadrate (irrespective of the elements involved in forming the margin of the cavum tympanum); 2 = antrum postoticum fully developed, and extending posterodorsally into the squamosal (i.e. there is a large posterodorsal fenestra in the quadrate that leads to a pocket within the squamosal). This character is scored as inapplicable for turtles without a cavum tympanum.

Character optimisation: Unambiguous: *Bouliachelys suteri* (2->0), (*Desmatochelys lowii* + *Desmatochelys padillai*) (2->1), *Allopleuron hoffmanni* (2->1), Testudinidae (2->1), (*Xinjiangchelys wusu* + *Xinjiangchelys radiplicatoides*) (2->1), Pleurosternidae (2->1), *Meiolania planiceps* (2->0); DELTRAN: *Chubutemys*+++ (0->2), *Carettochelys insculpta* (2->0), *Allaeochelys libyca* (2->1), *Kayentachelys aprix* (0->1); ACCTRAN: (*Kayentachelys*+*Eileanchelys*)+++ (0->1), *Chubutemys*+++ (1->2), total-group Carettochelyidae (2->0), *Allaeochelys libyca* (0->1).

Character 78 (Evers & Benson [2018]: character 77). Quadrate, incisura columellae auris: 0 = absent, stapes extends posteroventrall to quadrate body; 1 = present, but open posteroventrally; 2 = present and closed, but only enclosing the stapes; 3 = present and closed, enclosing stapes and the Eustachian tube.

Character optimisation: Unambiguous: (*Kayentachelys*+*Eileanchelys*)+++ (0->1), crown-group Chelydridae (1->2), *Platysternon megacephalum* (1->2), Testudinidae (1->2), crown-group Trionychia (1->2), (*Sinemys gamera* + *Sinemys lens*) (1->2), *Meiolania planiceps* (1->3); DELTRAN: *Sternotherus* (1->2), *Staurotypus* (1->2), (*Sandownia* + *Angolachelys*) (1->2), *Leyvachelys cipadi* (1->2), crown-group Chelidae (1->3), crown-group Pelomedusoides (1->3), *Galianemys whitei* (1->2); ACCTRAN: Kinosternidae (1->2), *Kinosternon suburum hippocrepis* (2->1), Sandownidae (1->2), *Brachyopsemys tingitana* (2->1), crown-group Pleurodira (1->3), *Araripemys barretoi* (3->1), *Galianemys whitei* (3->2).

Character 79 (Evers & Benson [2018]: character 78). Quadrate, formation of incisura columella auris: 0 = formed exclusively by quadrate; 1 = formed by quadrate and squamosal and/or quadratojugal.

Character optimisation: Unambiguous: *Meiolania planiceps* (0->1)

Character 80 (Evers & Benson [2018]: character 79). Quadrate, processus trochlearis oticum: 0 = absent; 1 = present, very reduced; 2 = present, large forming a well defined musculatory facet.

Character optimisation: Unambiguous: *Chubutemys*+++ (0->1), Testudines (1->2), (*Chelonia* + *Natator*) (2->1), *Allopleuron hoffmanni* (2->1), total-group Dermatemydidae (2->1), crown-group Pleurodira (2->0), *Kirgizemys dmitrievi* (1->2), *Kallokibotion bajazidi* (1->2); DELTRAN: *Dermochelys coriacea* (2->1), *Emys orbicularis* (2->1), *Platysternon megacephalum* (2->1), Testudinidae (2->1); ACCTRAN: Dermochelyidae (2->1), Testudinoidea (2->1), *Chrysemys picta* (1->2), *Geoclemys hamiltonii* (1->2).

Character 81 (Evers & Benson [2018]: character 80). Quadrate, contribution to the musculatory facet of the processus trochlearis oticum: 0 = extensive contribution; 1 = small contribution, facet formed principally by the protic and/or parietal. This character is scored as inapplicable when a processus trochlearis oticum is absent (ch 79.0).

Character optimisation: Unambiguous: *Allopleuron hoffmanni* (0->1), Trionychidae (0->1), *Ordosemys* sp. IVPP V12092 (0->1); DELTRAN: *Protostega gigas* (0->1), *Pleurosternon bullockii* (0->1); ACCTRAN: (*Protostega* + *Archelon*) (0->1), Pleurosternidae (0->1).

Character 82 (Evers & Benson [2018]: character 81). Quadrate, width of processus trochlearis oticum: 0 = the otic process spans all the mediolateral space between the braincase wall and the lateral surface of the skull; 1 = the otic process is limited to the medial part of the otic chamber, and there is a deep recess laterally. This character is scored as inapplicable when a processus trochlearis oticum is absent (ch 79.0).

Character optimisation: Unambiguous: total-group Chelydridae (0->1), *Staurotypus* (0->1), *Adocus beatus* (0->1), Thalassochelydia (0->1), *Jurassichelon oleronensis* (1->0), (*Ordosemys* + *Dracochelys*) (0->1), *Annemys* sp. IVPP V18106 (0->1); DELTRAN: Protostegidae (0->1), *Notochelone* (1->0), total-group Cheloniidae (0->1); ACCTRAN: Protostegidae+++ (0->1), (*Santanachelys* + *Notochelone*) (1->0), Dermochelyidae (1->0).

Character 83 (Evers & Benson [2018]: character 82). Quadrate, quadrate-basisphenoid contact: 0 = absent; 1 = present.

Character optimisation: Unambiguous: *Chelodina* (0->1), total-group Pelomedusoides (0->1).

Character 84 (Evers & Benson [2018]: character 83). Quadrate, infolding ridge on the posterior surface of the quadrate ventral to the incisura columella auris: 0 = absent; 1 = present.

Character optimisation: Unambiguous: *Bouliachelys suteri* (0->1), Angolachelonia (0->1), *Ordosemys* sp. IVPP V12092 (0->1).

Character 85 (Evers & Benson [2018]: character 84). Quadrate, direction of cranial articular process: 0 = ventrolaterally directed; 1 = with strong posterior inclination.

Character optimisation: Unambiguous: *Allopleuron hoffmanni* (0->1), *Macrochelys temminckii* (0->1), Angolachelonia (0->1), *Galianemys whitei* (0->1), *Kayentachelys aprix* (0->1).

Character 86 (Evers & Benson [2018]: character 85). Posterior quadrate fossa: 0 = absent; 1 = present.

Character optimisation: Unambiguous: total-group Carettochelyidae (0->1).

Character 87 (Evers & Benson [2018]: character 86). Stapes, lateral articulation: 0 = stapes articulates with medial surface of the quadrate, quadrate has stapedial pit; 1 = stapes articulates with tympanic membrane, pit on medial surface of quadrate is absent.

Character optimisation: DELTRAN: *Australochelys*+++ (0->1); ACCTRAN: *Australochelys*+++ (0->1).

Character 88 (Evers & Benson [2018]: character 87). Epipterygoid: 0 = present; 1 = absent.

Character optimisation: Unambiguous: crown-group Pleurodira (0->1), *Eubaena cephalica* (0->1); DELTRAN: (*Bouliachelys* + *Rhinochelys*) (0->1), *Desmatochelys lowii* (0->1), *Dermochelys coriacea* (0->1), crown-group Cheloniidae (0->1), *Puppigerus camperi* (0->1), *Cabindachelys landanensis* (0->1), *Nichollsemys baieri* (0->1); ACCTRAN: Protostegidae+++ (0->1), (*Ocepechelon* ++ *Protostega*) (1->0), *Allopleuron*+++ (1->0), crown-group Cheloniidae (0->1), *Puppigerus camperi* (0->1), *Cabindachelys landanensis* (0->1), *Corsochelys halinches* (1->0).

Character 89 (Evers & Benson [2018]: character 88). Epipterygoid, shape: 0 = rod-like element; 1 = laminar element. This character is scored as inapplicable if an epipterygoid is absent (ch 87.1).

Character optimisation: Unambiguous: *Annemys latiens* (1->0); DELTRAN: *Kallokibotion*+++ (0->1); ACCTRAN: *Chubutemys*+++ (0->1).

Character 90 (Evers & Benson [2018]: character 89). Pterygoid, pterygoid teeth: 0 = present; 1 = absent.

Character optimisation: Unambiguous: *Nichollsemys baieri* (1->0); DELTRAN: *Chubutemys*+++ (0->1), *Australochelys africanus* (0->1); ACCTRAN: *Australochelys*+++ (0->1), (*Kayentachelys* + *Eileanchelys*) (1->0).

Character 91 (Evers & Benson [2018]: character 90). Pterygoid, basipterygoid process and basipterygoid articulation: 0 = basipterygoid process present with a movable basiptergoid articulation; 1 = basipterygoid process present with a sutured basipterygoid articulation; 2 = basipterygoid process absent and sutured basipterygoid articulation.

Character optimisation: Unambiguous: (*Jurassichelon* + *Portlandemys*) (2->1), *Eubaena cephalica* (1->2), *Meiolania planiceps* (1->2); DELTRAN: *Australochelys*+++ (0->1), Testudines (1->2), *Sandownia harrisi* (2->1), *Judithemys sukhanovi* (1->2); ACCTRAN: *Australochelys*+++ (0->1), Sinemydidae/Macroabenidae+++ (1->2), Sandownidae (2->1), (*Sinemys* ++ *Kirgizemys*) (2->1).

Character 92 (Evers & Benson [2018]: character 91). Pterygoid, pterygoid-basioccipital contact: 0 = absent; 1 = present.

Character optimisation: Unambiguous: *Kallokibotion*+++ (0->1), *Eosphargis breineri* (1->0), *Puppigerus camperi* (1->0), *Emys orbicularis* (1->0), crown-group Pleurodira (1->0), (*Sinemys gamera* + *Sinemys lens*) (1->0), Xinjiangchelyidae (1->0), *Xinjiangchelys radiplicatoides* (0->1).

Character 93 (newly added from Hooks [1998]: character 10): Basioccipital, anterolateral edge of basioccipital with knob-like processes fitting into sockets on the posterior processes of the pterygoids: 0 = absent; 1 = present.

Character optimisation: Unambiguous: Protostegidae (0->1), *Ocepechelon bouyai* (1->0).

Character 94 (Evers & Benson [2018]: character 92). Pterygoid, processus trochelaris pterygoideus: 0 = absent; 1 = present.

Character optimisation: Unambiguous: crown-group Pleurodira (0->1).

Character 95 (Evers & Benson [2018]: character 93). Pterygoid, foramen palatinum posterius: 0 = present; 1 = present, but open laterally; 2 = absent.

Character optimisation: Unambiguous: (*Ocepechelon* ++ *Protostega*) (1->2), Dermochelyidae (0->2), (*Erquelinnesia* ++ *Lepidochelys*) (0->2), Plesiochelyidae (0->1), *Portlandemys mcdowelli* (1->0), *Angolachelys mbaxi* (0->2); DELTRAN: (*Bouliachelys* + *Rhinochelys*) (0->1), *Desmatochelys padillai* (0->1), (*Ctenochelys* + *Cabindachelys*) (2->0); ACCTRAN: Protostegidae (0->1), *Desmatochelys lowii* (1->0), (*Ctenochelys* ++ *Peritresius*) (2->0).

Character 96 (Evers & Benson [2018]: character 94). Pterygoid, medial contact of pterygoid: 0 = present, pterygoids in a very long medial contact with one another, longer than the basisphenoid total length in midline; 1 = present, pterygoids in medial contact with one another, contact length equal or shorter than the basisphenoid total length in midline; 2 = absent, contact of the basisphenoid with the vomer and/or palatines present.

Character optimisation: Unambiguous: total-group Chelonioidea (1->0), *Dermochelys coriacea* (0->1), crown-group Chelydridae (1->0), *Platysternon megacephalum* (1->0), crown-group Trionychia (1->2), Angolachelonia (1->0), *Jurassichelon oleronensis* (0->1), *Araripemys barretoi* (1->2), *Xinjiangchelys radiplicatoides* (1->2), Pleurosternidae (1->2); DELTRAN: *Rhinochelys pulchriceps* (0->1); ACCTRAN: (*Rhinochelys pulchriceps* + *Rhinochelys nammourensis*) (0->1).

Character 97 (Evers & Benson [2018]: character 95). Pterygoid, pterygoid contribution to foramen palatinum posterius: 0 = present; 1 = absent. This character is scored inapplicable when the foramen palatinum posterius is absent (ch. 66.0).

Character optimisation: Unambiguous: Cryptodira (0->1), *Solnhofia parsoni* (0->1), *Araripemys barretoi* (0->1), *Podocnemis* (0->1), *Chubutemys copelloi* (0->1); DELTRAN: (*Santanachelys* ++ *Rhinochelys*) (1->0), *Desmatochelys padillai* (1->0), *Cabindachelys landanensis* (1->0), *Nichollsemys baieri* (1->0), *Toxochelys* sp. (1->0), *Chelonoidis* sp. (1->0), *Gopherus polyphemus* (1->0), *Apalone spinifera* (1->0), *Sandownia harrisi* (0->1); ACCTRAN: total-group Chelonioidea (1->0), *Bouliachelys suteri* (0->1), *Desmatochelys lowii* (0->1), *Allopleuron*+++ (0->1), *Cabindachelys landanensis* (1->0), Testudinidae (1->0), *Testudo* (0->1), (*Apalone* + *Petrochelys*) (1->0), (*Sandownia* + *Angolachelys*) (0->1).

Character 98 (Evers & Benson [2018]: character 96). Pterygoid, contact with the exoccipital: 0 = absent; 1 = present.

Character optimisation: Unambiguous: *Meiolania*+++ (0->1), Dermochelyidae (1->0), *Sternotherus* (1->0), total-group Dermatemydidae (1->0), Testudinoidea (1->0), (*Jurassichelon* + *Portlandemys*) (0->1), *Annemys* sp. IVPP V18106 (1->0); DELTRAN: (*Santanachelys* + *Notochelone*) (1->0), *Calcarichelys gemma* (1->0), Thalassochelydia (1->0), crown-group Pleurodira (1->0), (*Sinemys gamera* + *Sinemys lens*) (1->0), *Kirgizemys dmitrievi*

(1->0); ACCTRAN: (*Calcarichelys* + *Rhinochelys*) (1->0), (*Rhinochelys pulchriceps* + *Rhinochelys nammourensis*) (0->1), total-group Pleurodira (1->0), Sandownidae (0->1), (*Sinemys* ++ *Kirgizemys*) (1->0), (*Ordosemys* + *Dracochelys*) (0->1).

Character 99 (Evers & Benson [2018]: character 97). Pterygoid, fossa podocnemidoidea or cavum pterygoidei: 0 = absent; 1 = present.

Character optimisation: DELTRAN: *Podocnemis* (0->1), *Galianemys whitei* (0->1); ACCTRAN: total-group Pelomedusoides (0->1), *Pelomedusa subrufa* (1->0).

Character 100 (Evers & Benson [2018]: character 98). Pterygoid, lateral margin: 0 = a processus pterygoideus externus is developed as a process that projects into the subtemporal fenestra; 1 = the lateral margin of the pterygoid is gently expanded laterally and/or expanded dorsoventrally; 2 = absent, i.e. the lateral margin of the pterygoid forms a straight or concave outline that forms the medial margin of the subtemporal fenestra. Scored inapplicable for pleurodires.

Character optimisation: Unambiguous: (*Protostega* + *Archelon*) (0->2), Dermochelyidae (0->2), *Caretta Caretta* (0->1), *Chelonia mydas* (0->2), *Sternotherus* (0->1), crown-group Trionychia (0->1); DELTRAN: *Procolpochelys charlestonensis* (0->1), *Solnhofia parsoni* (0->1), Sandownidae (0->1); ACCTRAN: (*Procolpochelys* ++ *Erquelinnesia*) (0->1), total-group Pleurodira (0->1), Plesiochelyidae (1->0).

Character 101 (Evers & Benson [2018]: character 99). Pterygoid, processus pterygoideus externus: 0 = forming an extensive process that contacts the maxilla anterolaterally at the posteromedial end of the triturating surface, is anteriorly sutured to the anterior palate, and has a posterior projection into the subtemporal fenestra; 1 = forming a large lateral wing that projects as a free process into the subtemporal fenestra; 2 = forming a pointed triangular process that projects laterally into the subtemporal fenestra. Scored inapplicable for taxa that lack a processus pterygoideus externus (i.e. ch 98.1 or 98.2)

Character optimisation: Unambiguous: Protostegidae (0->1), *Desmatochelys padillai* (1->2), crown-group Chelydridae (2->0), *Portlandemys mcdowelli* (1->0), *Ordosemys* sp. IVPP V12092 (0->2); DELTRAN: Cryptodira (0->2), (*Ctenochelys* + *Cabindachelys*) (2->0), *Nichollsemys baieri* (2->0), *Toxochelys* sp. (2->0), Plesiochelyidae (0->1); ACCTRAN: Testudines (0->1), Cryptodira (1->2), total-group Chelonioidea (2->0), *Allopleuron*+++ (0->2), (*Ctenochelys* ++ *Peritresius*) (2->0).

Character 102 (Evers & Benson [2018]: character 100). Pterygoid, vertical flange on anterolateral margin of the pterygoid: 0 = absent; 1 = present. Zhou *et al.* (2014) & Joyce (2007: ch 67) (Pterygoid I).

Character optimisation: Unambiguous: Paracryptodira+++ (0->1), *Lepidochelys olivacea* (1->0), *Chelonia mydas* (1->0), *Puppigerus camperi* (1->0), *Platysternon megacephalum* (1->0), *Testudo* (1->0), *Lissemys punctata* (1->0), *Solnhofia parsoni* (1->0); DELTRAN: *Procolpochelys charlestonensis* (1->0), *Kinosternon suburum hippocrepisis* (1->0), *Staurotypus* (1->0); ACCTRAN: (*Procolpochelys* ++ *Erquelinnesia*) (1->0), Kinosternidae (1->0), *Sternotherus* (0->1).

Character 103 (Evers & Benson [2018]: character 101). Pterygoid, level of the position of the pterygoid respect to basisphenoid: 0 = both bones are at the same level on ventral surface; 1 = two different levels, creating a step between the two bones.

Character optimisation: Unambiguous: *Eosphargis breineri* (0->1), *Allopleuron*+++ (0->1), *Chelonia mydas* (1->0), *Platysternon megacephalum* (0->1); DELTRAN: (*Ctenochelys* + *Cabindachelys*) (1->0); ACCTRAN: (*Ctenochelys* ++ *Peritresius*) (1->0).

Character 104 (Evers & Benson [2018]: character 102). Pterygoid, ventral median ridge: 0 = incipient to absent; 1 = present, ridge spans nearly the full length of the pterygoids, sometimes reaching the most posterior portion of the vomer. This character is scored as inapplicable for taxa in which the pterygoids lack a midline contact.

Character optimisation: Unambiguous: (*Protostega* + *Archelon*) (0->1), total-group Cheloniidae (0->1), *Lepidochelys kempii* (1->0), *Chelonia mydas* (1->0), *Gopherus polyphemus*

(0->1); DELTRAN: *Eochelone brabantica* (1->0), (*Ctenochelys* + *Cabindachelys*) (1->0); ACCTRAN: (*Puppigerus* ++ *Ctenochelys*) (1->0), *Puppigerus camperi* (0->1).

Character 105 (Evers & Benson [2018]: character 103). Pterygoid, extending laterally almost reaching the mandibular condyle facet: 0 = absent; 1 = present, the pterygoid contacts the medial edge of the mandibular condyle when is seem in ventral view; 2 = present, the pterygoids extends not only laterally to reach the outline of the mandibular condyle facet, but also posteriorly far from the level of the condyles.

Character optimisation: Unambiguous: Protostegidae (0->1), *Nichollsemys baieri* (0->1), crown-group Trionychia (0->1), *Lissemys punctata* (1->2); DELTRAN: Angolachelonia (0->1), *Phrynops geoffroanus* (0->1), *Chelodina* (0->1), *Pelomedusa subrufa* (0->1), *Galianemys whitei* (0->1); ACCTRAN: total-group Pleurodira (0->1), total-group Chelidae (1->0), *Phrynops geoffroanus* (0->1), *Chelodina* (0->1), *Podocnemis* (1->0).

Character 106 (Evers & Benson [2018]: character 104). Pterygoid, ventral ridge on the palatal surface lateral to skull midline. 0 = absent; 1 = present, each pterygoid has a parasagittal ridge on its ventral surface.

Character optimisation: Unambiguous: *Chubutemys*+++ (0->1), *Calcarichelys gemma* (1->0), *Corsochelys*+++ (1->0), *Ctenochelys* (0->1), *Dermatemys mawii* (1->0), Emydidae (1->0), Trionychidae (1->0), *Plesiochelys etalloni* (1->0), *Angolachelys mbaxi* (1->0), crown-group Pleurodira (1->0), *Meiolania planiceps* (1->0); DELTRAN: *Ocepechelon bouyai* (1->0), *Testudo* (1->0), *Gopherus polyphemus* (1->0); ACCTRAN: (*Ocepechelon* ++ *Protostega*) (1->0), Testudinidae (1->0), *Chelonoidis* sp. (0->1).

Character 107 (Evers & Benson [2018]: character 105). Pterygoid, extent of ventral ridge on the palatal surface lateral to skull midline: 0 = each ridge extends along most of the ventral surface of the pterygoid, from the anteromedial margin of the pterygoid fossa to the processus pterygoideus externus; 1 = each ridge extends only along the posterior part of the pterygoid, along the level of the parabasisphenoid. This character is scored inapplicable in turtles in which ventral pterygoid ridges are absent (ch 104.0).

Character optimisation: Unambiguous: total-group Chelonioidea (0->1), *Santanachelys gaffneyi* (1->0), *Staurotypus* (0->1), *Arundelemys dardeni* (0->1); DELTRAN: *Chelonoidis* sp. (0->1), *Brachyopsemys tingitana* (0->1), *Leyvachelys cipadi* (0->1); ACCTRAN: Testudinidae (0->1), Sandownidae (0->1), (*Sandownia* + *Angolachelys*) (1->0).

Character 108 (Evers & Benson [2018]: character 106). Pterygoid/Quadrate, flooring of cavum acustico-jugulare and recessus scalae typmani: 0 = absent; 1 = present, formed primarily by the posterior part of the pterygoid; 2 = present, produced by the ventral process of the quadrate or prootic or a posterolateral expansion of the parabasisphenoid.

Character optimisation: Unambiguous: *Kallokibotion*+++ (0->1), crown-group Pleurodira (1->2).

Character 109 (Evers & Benson [2018]: character 107). Pterygoid, posterior process: 0 = posterior process of pterygoid is absent, the cranioquadrate space or posterior foramen for the canalis cavernosus is not covered by the pterygoid; 1 = posterior process of pterygoid present but very short, process extends posteriorly to cover the posterior foramen for the canalis cavernosus (i.e. the modified cranioquadrate space), but the cavum-acustico jugulare remains largely exposed ventrally; 2 = posterior process of the pterygoid present and developed as an extensive sheet that projects posteriorly and covers large parts of the cavum acustico-jugulare.

Character optimisation: Unambiguous: (*Kayentachelys*+*Eileanchelys*)+++ (0->1), *Kallokibotion*+++ (1->2), *Emarginachelys cretacea* (2->1), crown-group Pleurodira (2->0), *Sinemys lens* (2->1), Pleurosternidae (2->1); DELTRAN: *Solnhofia parsoni* (2->1), *Plesiochelys planiceps* (2->1), *Plesiochelys bigleri* (2->1), *Kirgizemys hoburensis* (2->1), *Annemys levensis* (2->1), *Annemys* sp. IVPP V18106 (2->1); ACCTRAN: Thalassochelydia (2->1), (*Jurassichelon* + *Portlandemys*) (1->2), *Plesiochelys etalloni* (1->2), (*Kirgizemys hoburensis* + *Kirgizemys dmitrievi*) (2->1), Xinjiangchelyidae (2->1), (*Xinjiangchelys wusu* + *Xinjiangchelys radiplicatoides*) (1->2).

Character 110 (Evers & Benson [2018]: character 108). Pterygoid, development of a posteromedial wing covering partially to completely the basisphenoid and sometime the basioccipital too, seen in ventral view of the skull: 0 = absent; 1 = present.

Character optimisation: Unambiguous: Sandownidae (0->1).

Character 111 (Evers & Benson [2018]: character 109). Pterygoid, pterygoid fossa: 0 = weakly developed; 1 = developed as a deep concavity between the articular process of the quadrate and the basicranium.

Character optimisation: Unambiguous: total-group Cheloniidae (0->1), *Emarginachelys cretacea* (0->1), *Platysternon megacephalum* (0->1), *Allaeochelys libyca* (0->1), *Adocus beatus* (0->1), (*Plesiochelys planiceps* ++ *Jurassichelon*) (0->1), Sandownidae (0->1), *Angolachelys mbaxi* (1->0), Sinemydidae (0->1), *Xinjiangchelys radiplicatoides* (1->0), (*Kayentachelys* + *Eileanchelys*) (0->1); DELTRAN: Xinjiangchelyidae (0->1), Paracryptodira (0->1); ACCTRAN: Paracryptodira+++ (0->1), Sinemydidae/Macroabenidae+++ (1->0).

Character 112 (Evers & Benson [2018]: character 110). Supraoccipital, crista supraoccipitalis: 0 = poorly developed; 1 = protruding significantly posterior to the foramen magnum.

Character optimisation: Unambiguous: *Chubutemys*+++ (0->1), *Ocepechelon bouyai* (1->0), Dermochelyidae (1->0), *Kinosternon suburum hippocrepis* (1->0), (*Sandownia* + *Angolachelys*) (1->0); DELTRAN: *Jurassichelon oleronensis* (1->0), Chelinae (1->0), *Chelodina* (1->0), *Galianemys whitei* (1->0); ACCTRAN: (*Jurassichelon* + *Portlandemys*) (1->0), crown-group Pleurodira (1->0), *Elseya dentata* (0->1), crown-group Pelomedusoides (0->1).

Character 113 (Evers & Benson [2018]: character 111). Supraoccipital, large supraoccipital exposure on dorsal skull roof: 0 = absent; 1 = present.

Character optimisation: Unambiguous: *Meiolania planiceps* (0->1).

Character 114 (Evers & Benson [2018]: character 112). Supraoccipital, horizontal crest in the crista supraoccipitalis: 0 = absent or poorly developed anteriorly; 1 = present, along the entire crista supraoccipitalis.

Character optimisation: Unambiguous: crown-group Trionychia (0->1).

Character 115 (Evers & Benson [2018]: character 113). Supraoccipital, fossa on the posterodorsal surface of the floor of the supratemporal fossa: 0 = absent; 1 = present, fossa is formed on the lateral surface of the suparoccipital, dorsal to the contact area between exoccipital, opisthotic, and supraoccipital.

Character optimisation: Unambiguous: (*Kayentachelys*+*Eileanchelys*)+++ (1->0), *Corsochelys*+++ (0->1), (*Eretmochelys* ++ *Lepidochelys*) (1->0), (*Puppigerus* + *Eochelone*) (1->0), crown-group Chelydridae (0->1), *Chrysemys picta* (0->1), *Testudo* (0->1), crown-group Trionychia (0->1), Thalassochelydia (0->1), *Galianemys whitei* (0->1); DELTRAN: *Notochelone* (0->1), (*Sinemys* ++ *Kirgizemys*) (0->1); ACCTRAN: (*Santanachelys* + *Notochelone*) (0->1), (*Judithemys* ++ *Sinemys*) (0->1).

Character 116 (Evers & Benson [2018]: character 114). Exoccipital, medial contact of exoccipitals dorsal to foramen magnum: 0 = absent; 1 = present.

Character optimisation: Unambiguous: *Kinosternon suburum hippocrepis* (0->1); DELTRAN: Chelinae (0->1), *Chelodina* (0->1); ACCTRAN: crown-group Chelidae (0->1), *Elseya dentata* (1->0).

Character 117 (Evers & Benson [2018]: character 115). Exoccipital, median contact of exoccipitals in the floor of the foramen magnum, excluding the basioccipital from the latter: 0 = absent; 1 = present.

Character optimisation: Unambiguous: Xinjiangchelyidae+++ (0->1), (*Desmatochelys* ++ *Protostega*) (0->1), *Chelonia mydas* (0->1), (*Argillochelys* ++ *Puppigerus*) (0->1), *Sternotherus* (1->0), *Dermatemys mawii* (1->0), Angolachelonia (1->0), (*Plesiochelys planiceps* ++ *Jurassichelon*) (0->1), *Brachyopsemys tingitana* (0->1), *Araripemys barretoi* (1->0),

Podocnemis (1->0); DELTRAN: total-group Chelonioidea (1->0), *Chrysemys picta* (1->0), *Platysternon megacephalum* (1->0), *Geoclemys hamiltonii* (1->0), *Ordosemys* sp. IVPP V12092 (1->0); ACCTRAN: Durocryptodira (1->0), Chelydroidea (0->1), *Emys orbicularis* (0->1), Testudinidae (0->1), Sinemydidae (1->0).

Character 118 (Evers & Benson [2018]: character 116). Foramen nervi hypoglossi (XII), ventral covering: 0 = exposed in ventral view; 1 = covered in ventral view by an extension of the pterygoid and the basioccipital; 2 = covered in ventral view an extension of the basioccipital; 3 = covered in ventral view by an expansion of the exoccipital and basioccipital.

Character optimisation: Unambiguous: Protostegidae (0->2), (*Protostega* + *Archelon*) (2->0), *Eretmochelys imbricata* (0->1), *Macrochelys temminckii* (0->1), Kinosternoidea (0->2), *Sternotherus* (2->0), total-group Trionychia (0->1), total-group Carettochelyidae (1->2), (*Sandownia* + *Angolachelys*) (0->1), *Podocnemis* (0->2), (*Ordosemys* + *Dracochelys*) (0->2), (*Eubaena* + Pleurosternidae) (0->2); DELTRAN: Emysternia (0->2), *Geoclemys hamiltonii* (0->2), *Solnhofia parsoni* (0->2), *Plesiochelys planiceps* (0->2), Chelinae (0->3), Chelodininae (0->2), (*Annemys* sp. IVPP V18106 ++ *Xinjiangchelys*) (0->2); ACCTRAN: Testudinoidea (0->2), Testudinidae (2->0), Thalassochelydia (0->2), (*Jurassichelon* + *Portlandemys*) (2->0), crown-group Chelidae (0->2), Chelinae (2->3), (*Annemys latiens* ++ *Xinjiangchelys*) (0->2).

Character 119 (Evers & Benson [2018]: character 117). Exoccipital, foramina nervi hypoglossi: 0 = the foramina nervi hypoglossi exit the exoccipital on the occipital surface posteriorly to the margin of the fenestra postotica; 1 = at least one foramen nervi hypoglossi opens within the recessus scalae tympani anterior to margin of the fenestra postotica, and the others exit the exoccipital on the occipital surface; 2 = all foramina nervi hypoglossi open within the recessus scalae tympani anterior to the margin of the fenestra postotica.

Character optimisation: Unambiguous: *Corsochelys halinches* (0->1), *Kallokibotion bajazidi* (0->1); DELTRAN: Chelinae (0->2), *Chelodina* (0->2); ACCTRAN: crown-group Chelidae (0->2), *Elseya dentata* (2->0).

Character 120 (Evers & Benson [2018]: character 118). Basioccipital, morphology of the anteriormost part of the basioccipital: 0 = with two or one ventral tubercle; 1 = tubercle absent.

Character optimisation: Unambiguous: (*Kayentachelys*+*Eileanchelys*)+++ (0->1).

Character 121 (Evers & Benson [2018]: character 119). Basioccipital, deep C-shaped concavity between basioccipital tubera: 0 = absent; 1 = present.

Character optimisation: Unambiguous: *Chubutemys*+++ (0->1), Paracryptodira+++ (1->0), *Baptemys wyomingensis* (0->1), *Solnhofia parsoni* (0->1); DELTRAN: *Eosphargis breineri* (0->1), total-group Cheloniidae (0->1), total-group Carettochelyidae (0->1), *Adocus beatus* (0->1); ACCTRAN: *Corsochelys*+++ (0->1), *Dermochelys coriacea* (1->0), total-group Trionychia (0->1), Trionychidae (1->0).

Character 122 (Evers & Benson [2018]: character 120). Basioccipital, basal tubera: 0 = the basal tubera are completely formed by the basioccipital; 1 = the exoccipitals and the basioccipital form the basal tubera; 2 = the pterygoids and the basioccipital form the basal tubera; 3 = the basal tubera are formed by the exoccipitals, basioccipital and pterygoids.

Character optimisation: Unambiguous: *Kallokibotion*+++ (0->2), Xinjiangchelyidae+++ (2->0), *Eretmochelys imbricata* (0->1), *Chelonia mydas* (0->1), *Chrysemys picta* (0->1), *Geoclemys hamiltonii* (0->3), total-group Carettochelyidae (0->3); DELTRAN: *Dermochelys coriacea* (0->3), *Eosphargis breineri* (0->1), *Puppigerus camperi* (0->1), *Eochelone brabantica* (0->2), *Sternotherus* (0->2), *Staurotypus* (0->2), *Baptemys wyomingensis* (0->2), *Solnhofia parsoni* (0->1), *Leyvachelys cipadi* (0->1), Chelinae (0->1), *Araripemys barretoi* (0->1), *Glyptops plicatulus* (2->0); ACCTRAN: Dermochelyidae (0->1), *Dermochelys coriacea* (1->3), (*Puppigerus* + *Eochelone*) (0->1), *Eochelone brabantica* (1->2), Kinosternoidea (0->2), *Kinosternon suburum hippocrepis* (2->0), *Dermatemys mawii* (2->0), total-group Pleurodira (0->1), Plesiochelyidae (1->0), Chelodininae (1->0), total-group Pelomedusoides (1->0), Pleurosternidae (2->0).

Character 123 (Evers & Benson [2018]: character 121). Prootic, dorsal exposure: 0 = large; 1 = very reduced or absent.

Character optimisation: Unambiguous: Emydidae (0->1), *Geoclemys hamiltonii* (0->1), *Testudo* (0->1), *Annemys latiens* (0->1); DELTRAN: *Meiolania planiceps* (0->1), *Kallokibotion bajazidi* (0->1); ACCTRAN: *Chubutemys*+++ (0->1), Paracryptodira+++ (1->0).

Character 124 (Evers & Benson [2018]: character 122). Prootic, lateral semicircular canal enclosure by bone: 0 = canal only formed by bone of the opisthotic, the prootic portion of the canal is not ossified and is instead medially confluent with the recessus labyrinthicus prooticus; 1 = prootic and opisthotic both contribute to the formation of the lateral semicircular canal.

Character optimisation: Unambiguous: *Bouliachelys suteri* (0->1), *Chrysemys picta* (0->1), *Pelodiscus sinensis* (0->1); DELTRAN: *Staurotypus* (0->1), *Dermatemys mawii* (0->1), (*Jurassichelon* + *Portlandemys*) (0->1), *Sandownia harrisi* (0->1), crown-group Pleurodira (0->1), Pleurosternidae (0->1), *Meiolania planiceps* (0->1), *Kallokibotion bajazidi* (0->1); ACCTRAN: *Chubutemys*+++ (0->1), Paracryptodira+++ (1->0), Kinosternoidea (0->1), Kinosterninae (1->0), total-group Pleurodira (0->1), Thalassochelydia (1->0), (*Jurassichelon* + *Portlandemys*) (0->1), (*Eubaena* + Pleurosternidae) (0->1).

Character 125 (Evers & Benson [2018]: character 123). Prootic, ventral process: 0 = ventral process is short and without extensive posterior contact with the pterygoid; 1 = ventral process is large, with a broad contact with the pterygoid along a posteriorly expanded footplate, forming parts of the floor of the inner ear cavity; 2 = ventral process is extensive, and forms parts of the floor of the basicranium so that it is visible on the ventral surface of the skull. This character is scored as inapplicable for taxa that lack an anatomically modern middle ear chamber.

Character optimisation: Unambiguous: Testudines (1->0), *Nichollsemys baieri* (0->1), *Chelydra serpentina* (0->1), Kinosternoidea (0->1), Testudinoidea (0->1), total-group Chelidae (0->2),

Pelomedusa subrufa (0->2); DELTRAN: *Xinjiangchelys radiplicatoides* (1->0); ACCTRAN: (*Xinjiangchelys wusu* + *Xinjiangchelys radiplicatoides*) (1->0).

Character 126 (Evers & Benson [2018]: character 124). Prootic, unnamed foramen exiting into the subtemporal fossa from the canalis cavernosus: 0 = absent; 1 = present.

Character optimisation: Unambiguous: *Chelonia mydas* (0->1), *Platysternon megacephalum* (0->1), *Gopherus polyphemus* (0->1), total-group Carettochelyidae (0->1), *Pelomedusa subrufa* (0->1); DELTRAN: *Dermochelys coriacea* (0->1); ACCTRAN: Dermochelyidae (0->1).

Character 127 (Evers & Benson [2018]: character 125). Prootic/pterygoid, posteroventral elongation of the trigeminal foramen: 0 = absent, the trigeminal foramen is approximately circular or oval, but the ventral margin of the foramen is positioned above the level of the canalis/sulcus cavernosus; 1 = the trigeminal foramen is oval, anterodorsally-posteroventrally elongate and anteroventrally-posterodorsaly narrow, and the ventral margin is level with the canalis/sulcus cavernosus. This character is scored inapplicable for turtles without a trigeminal foramen (i.e. without a neomorphic secondary lateral wall of the braincase formed by the parietal and pterygoid).

Character optimisation: Unambiguous: *Notochelone* (0->1), *Kinosternon suburum hippocrepis* (0->1), *Platysternon megacephalum* (0->1), Xinjiangchelyidae (0->1), *Arundelemys dardeni* (0->1); DELTRAN: *Desmatochelys lowii* (0->1), total-group Cheloniidae (0->1), (*Ctenochelys* + *Cabindachelys*) (1->0), crown-group Chelydridae (0->1), crown-group Trionychia (0->1); ACCTRAN: (*Desmatochelys* ++ *Protostega*) (0->1), crown-group Chelonioidea (0->1), (*Ctenochelys* ++ *Peritresius*) (1->0), total-group Chelydridae (0->1), total-group Trionychia (0->1).

Character 128 (Evers & Benson [2018]: character 126). Prootic, recess on posterior surface of the element anterodorsolaterally to the fenestra ovalis: 0 = absent; 1 = present.

Character optimisation: Unambiguous: *Meiolania*+++ (0->1), *Chelonia mydas* (0->1), *Nichollsemys baieri* (0->1), *Chrysemys picta* (1->0), *Gopherus polyphemus* (1->0), *Allaeochelys libyca* (1->0), *Solnhofia parsoni* (1->0); DELTRAN: Protostegidae+++ (1->0), *Lepidochelys*

kempii (0->1), *Caretta Caretta* (0->1), *Dermatemys mawii* (1->0); ACCTRAN: total-group Chelonioidea (1->0), (*Caretta* ++ *Lepidochelys*) (0->1), *Lepidochelys olivacea* (1->0), total-group Dermatemydidae (1->0).

Character 129 (Evers & Benson [2018]: character 127). Prootic, position of the geniculate ganglion and the split of the facial nerve into the hyomandibular and palatine branches: 0 = the geniculate ganglion is positioned with the canalis cavernosus; 1 = the geniculate ganglion is positioned within the facial nerve canal; 2 = the geniculate ganglion is positioned in the canalis carotici interni.

Character optimisation: Unambiguous: *Corsochelys halinches* (0->1); DELTRAN: Cryptodira (1->0), *Sandownia harrisi* (1->0), total-group Chelidae (1->2), crown-group Pelomedusoides (1->2); ACCTRAN: Testudines (1->0), Thalassochelydia (0->1), crown-group Pleurodira (0->2), *Galianemys whitei* (2->1).

Character 130 (Evers & Benson [2018]: character 128). Prootic/opisthotic, enclosure of fenestra ovalis: 0 = the fenestra ovalis is ventrally enclosed by the prootic and opisthotic; 1 = the prootic and opisthotic do not have a contact ventrally to the fenestra ovalis.

Character optimisation: Unambiguous: Testudines (0->1), (*Desmatochelys* ++ *Protostega*) (1->0), *Sternotherus* (1->0), (*Jurassichelon* + *Portlandemys*) (1->0), *Chelus fimbriatus* (1->0), *Chelodina* (1->0); DELTRAN: *Allopleuron hoffmanni* (1->0), *Nichollsemys baieri* (1->0), *Pleurosternon bullockii* (0->1); ACCTRAN: total-group Cheloniidae (1->0), (*Erquelinnesia* ++ *Lepidochelys*) (0->1), (*Eubaena* + Pleurosternidae) (0->1).

Character 131 (Evers & Benson [2018]: character 129). Opisthotic, wide transverse occipital plane with depression for the nuchal musculature: 0 = absent; 1 = present.

Character optimisation: Unambiguous: *Eubaena cephalica* (0->1), *Kallokibotion bajazidi* (0->1), *Australochelys africanus* (0->1).

Character 132 (Evers & Benson [2018]: character 130). Opisthotic, processus interfenestralis: 0 = developed as a robust ridge that does not form a ventrally projecting

process and does not reach closely to the floor of the basicranium; 1 = incipient, developed as a ventrally low and mediolaterally broad, robust structure that separates the cavum labyrinthicum anteriorly from an incipient recessus scalae tympani posteriorly; 2 = present, developed as a ventrally directed process that separates the cavum labyrinthicum anteriorly from the recessus scalae tympani posteriorly.

Character optimisation: Unambiguous: (*Kayentachelys*+*Eileanchelys*)+++ (0->2), *Kayentachelys aprix* (2->1).

Character 133 (Evers & Benson [2018]: character 131). Opisthotic, development of the processus interfenestralis: 0 = developed as a ventrally directed process that separates the cavum labyrinthicum anteriorly from the recessus scalae tympani posteriorly, the process is not expanded at its ventral end, and almost or just about reaches the floor of the basicranium, but a small gap (hiatus postlagenum) usually remains; 1 = developed as a ventrally directed process that separates the cavum labyrinthicum anteriorly from the recessus scalae tympani posteriorly, but the process has a horizontally expanded footplate at its ventral end that is sutured to elements of the basicranium; 2 = developed as a ventrally directed process that separates the cavum labyrinthicum anteriorly from the recessus scalae tympani posteriorly, and the ventral surface of the process is integrated into the basicranium to form parts of the ventral surface of the cranium. This character is scored as inapplicable if an anatomically modern processus interfenestralis is absent (i.e. ch 131.0 or 131.1).

Character optimisation: Unambiguous: *Allopleuron hoffmanni* (0->1), Kinosternidae (0->1), (*Jurassichelon* + *Portlandemys*) (0->1), *Galianemys whitei* (0->1), *Annemys* sp. IVPP V18106 (0->1), (*Eubaena* + Pleurosternidae) (0->1), *Pleurosternon bullockii* (1->2); DELTRAN: *Desmatochelys lowii* (0->1), *Chelonoidis* sp. (0->2), *Gopherus polyphemus* (0->2), (*Sinemys gamera* + *Sinemys lens*) (0->2); ACCTRAN: (*Desmatochelys* ++ *Protostega*) (0->1), Testudinidae (0->2), *Testudo* (2->0), (*Judithemys* ++ *Sinemys*) (0->2).

Character 134 (Evers & Benson [2018]: character 132). Opisthotic, posterior surface of paroccipital process: 0 = the occipital side of the paroccipital process is developed as a

posteriorly exposed, broad, planar or gently concave surface; 1 = the occipital side of the paroccipital process is dorsoventrally flattened and forms a posterior ridge that traverses the paroccipital process mediolaterally; 2 = the paroccipital process has a dorsoventrally convex surface.

Character optimisation: Unambiguous: total-group Chelonioidea (0->2), *Lepidochelys olivacea* (2->1), *Eretmochelys imbricata* (2->0), *Chelonia mydas* (2->0), *Eochelone brabantica* (2->0), crown-group Trionychia (0->1), *Angolachelys mbaxi* (1->2), Pleurosternidae (0->1); DELTRAN: *Notochelone* (2->0), Plesiochelyidae (0->2), Sandownidae (0->1), crown-group Pleurodira (0->1), (*Kayentachelys* + *Eileanchelys*) (0->1), *Australochelys africanus* (0->1); ACCTRAN: *Australochelys*+++ (0->1), *Chubutemys*+++ (1->0), (*Santanachelys* + *Notochelone*) (2->0), total-group Pleurodira (0->1), Thalassochelydia (1->0), Plesiochelyidae (0->2).

Character 135 (Evers & Benson [2018]: character 133). Fenestra perilymphatica: 0 = large; 1 = reduced in size to that of a small foramen.

Character optimisation: Unambiguous: *Bouliachelys suteri* (0->1); DELTRAN: *Pleurosternon bullockii* (0->1); ACCTRAN: (*Eubaena* + Pleurosternidae) (0->1).

Character 136 (Evers & Benson [2018]: character 134). Parabasisphenoid, paired pits on ventral surface of basisphenoid: 0 = absent; 1 = present.

Character optimisation: Unambiguous: (*Judithemys* ++ *Sinemys*) (0->1), *Dracochelys bicuspis* (1->0); DELTRAN: *Kayentachelys aprix* (0->1); ACCTRAN: (*Kayentachelys* + *Eileanchelys*) (0->1).

Character 137 (Evers & Benson [2018]: character 135). Parabasiphenoid, ventral surface: 0= flat to slightly convex, with posterior margin straight or slightly concave; 1= V-shaped crest, with posterior margin forming the basipterygoid process projected posterolaterally.

Character optimisation: Unambiguous: *Toxochelys* sp. (0->1); DELTRAN: *Eosphargis breineri* (0->1), total-group Cheloniidae (0->1); ACCTRAN: crown-group Chelonioidea (0->1), *Dermochelys coriacea* (1->0).

Character 138 (Evers & Benson [2018]: character 136). Parabasiphenoid, rough surface between basisphenoid and basioccipital: 0 = absent; 1 = present.

Character optimisation: Unambiguous: *Eosphargis breineri* (0->1), *Annemys levensis* (0->1).

Character 139 (Evers & Benson [2018]: character 137). Parabasisphenoid, posterolateral processes lapping onto the ventral surface of the basioccipital: 0 = absent; 1 = present.

Character optimisation: Unambiguous: *Sternotherus* (0->1), total-group Carettochelyidae (0->1), (*Eubaena* + Pleurosternidae) (0->1).

Character 140 (Evers & Benson [2018]: character 138). Parabasisphenoid, rostrum basisphenoidale: 0 = flat; 1 = flat base, but with trabeculae contact one another medially forming a short rod at the anterior end of the parabasisphenoid; 2 = singular median, rod-like, thick and rounded process.

Character optimisation: Unambiguous: *Eochelone brabantica* (2->1), *Ctenochelys* (2->1), *Corsochelys halinches* (2->1), *Platysternon megacephalum* (0->2), *Galianemys whitei* (0->2); DELTRAN: Protostegidae (0->2), total-group Cheloniidae (0->2); ACCTRAN: Protostegidae+++ (0->2), Dermochelyidae (2->0).

Character 141 (Evers & Benson [2018]: character 139). Parabasisphenoid, dorsum sellae: 0 = deep, i.e. the dorsal surface of parabasisphenoid between the clinoid processes is a transversely concave floor forming a trough between the posterior part of the dorsal surface of the parabasisphenoid, which is usually cup-like, and the anterior portion of the parabasisphenoid forming the rostrum basisphenoidale and sella turcica; 1 = low, i.e. the dorsum sellae is formed as a transverse ridge between the clinoid processes that projects anteriorly at a low angle from posterodorsal surface of the parabasisphenoid; 2 = high, i.e. a transverse ridge or wall of bone between the clinoid processes is present that projects

dorsally at a high angle from the posteriorly positioned cup, separating the cup very clearly from of the anteriorly positioned rostrum basisphenoidale and sella turcica.

Character optimisation: Unambiguous: (*Kayentachelys*+*Eileanchelys*)+++ (2->1), total-group Chelonioidea (1->2), *Chelonia mydas* (2->0), *Macrochelys temminckii* (1->0), *Staurotypus* (1->0), *Dermatemys mawii* (1->0), *Platysternon megacephalum* (1->0), *Gopherus polyphemus* (1->0), Plesiochelyidae (1->2), Sandownidae (1->0), *Brachyopsemys tingitana* (0->2), *Meiolania planiceps* (1->0); DELTRAN: *Xinjiangchelys radiplicatoides* (1->2); ACCTRAN: (*Xinjiangchelys wusu* + *Xinjiangchelys radiplicatoides*) (1->2).

Character 142 (Evers & Benson [2018]: character 140). Parabasisphenoid, anterior surface of dorsum sellae: 0 = anterior surface of the dorsum sellae is flat and smooth; 1 = vertical median ridge on anterior surface of dorsum sellae between the clinoid processes is present, ridge may have a small anterodorsal projection.

Character optimisation: Unambiguous: Protostegidae+++ (0->1), *Plesiochelys planiceps* (0->1), *Plesiochelys etalloni* (0->1), *Kirgizemys dmitrievi* (0->1); DELTRAN: *Rhinochelys pulchriceps* (1->0), (*Puppigerus* + *Eochelone*) (1->0), *Cabindachelys landanensis* (1->0), *Kayentachelys aprix* (0->1), *Australochelys africanus* (0->1); ACCTRAN: *Australochelys*+++ (0->1), *Chubutemys*+++ (1->0), (*Rhinochelys pulchriceps* + *Rhinochelys nammourensis*) (1->0), (*Puppigerus* ++ *Ctenochelys*) (1->0), *Ctenochelys* (0->1).

Character 143 (Evers & Benson [2018]: character 141). Parabasisphenoid, retractor bulbi pits on anterolateral surface: 0 = absent; 1 = present.

Character optimisation: Unambiguous: Testudines (1->0), *Chelydra serpentina* (0->1), *Kinosternon suburum hippocrepis* (0->1), *Emys orbicularis* (0->1), Testudinidae (0->1), *Leyvachelys cipadi* (0->1), *Phrynops geoffroanus* (0->1), *Pelomedusa subrufa* (0->1); DELTRAN: *Australochelys*+++ (0->1); ACCTRAN: *Australochelys*+++ (0->1).

Character 144 (Evers & Benson [2018]: character 142). Parabasisphenoid, foramina anterius canalis carotici cerebralis: 0 = widely separated; 1 = close together; 2 = right and left

cerebral arteries converge within the parabasisphenoid and run within a short joint canal, and exit anteriorly into the cavum cranii via a single foramen within the sella turcica.

Character optimisation: Unambiguous: Sinemydidae/Macroabenidae+++ (1->0), *Chelosphargis* advena (2->1), *Ocepechelon bouyai* (2->1), *Natator depressus* (1->2), *Macrochelys temminckii* (0->1), *Baptemys wyomingensis* (0->1), *Platysternon megacephalum* (0->1), *Adocus beatus* (0->1), *Plesiochelys bigleri* (1->0), *Meiolania planiceps* (1->0); DELTRAN: Protostegidae+++ (0->2), crown-group Chelonioidea (2->1), *Lepidochelys olivacea* (1->2), *Caretta Caretta* (1->2), *Toxochelys* sp. (0->1), Thalassochelydia (0->1), *Leyvachelys cipadi* (0->1); ACCTRAN: total-group Chelonioidea (0->1), Protostegidae+++ (1->2), crown-group Chelonioidea (2->1), (*Caretta* ++ *Lepidochelys*) (1->2), *Lepidochelys kempii* (2->1), Angolachelonia (0->1), (*Brachyopsemys* ++ *Sandownia*) (1->0).

Character 145 (Evers & Benson [2018]: character 143). Parabasisphenoid, prootic foramen in primary lateral wall of the braincase: 0 = present, the clinoid process of the parabasisphenoid and parts of the prootic, an ossified pila antotica, the laterosphenoid, and/or parts of the parietal form a foramen medially to the cavum epiptericum; 1 = the prootic foramen is reduced, and the clinoid processes are free structures.

Character optimisation: Unambiguous: *Plesiochelys etalloni* (1->0), *Pelomedusa subrufa* (1->0), *Annemys* sp. IVPP V18106 (1->0); DELTRAN: *Australochelys*+++ (0->1); ACCTRAN: *Australochelys*+++ (0->1).

Character 146 (Evers & Benson [2018]: character 144). Parabasisphenoid, crista tuberculi basalis developed on posterior part of dorsal surface: 0 = absent, parabasisphenoid dorsal surface is relatively flat or gently concavely excavated; 1 = present as median, dorsally high projecting tubercle or ridge.

Character optimisation: Unambiguous: crown-group Chelonioidea (0->1), (*Lepidochelys olivacea* + *Lepidochelys kempii*) (1->0), *Puppigerus camperi* (1->0), *Toxochelys* sp. (0->1), *Emys orbicularis* (0->1), *Kallokibotion bajazidi* (0->1).

Character 147 (Evers & Benson [2018]: character 145). Carotid artery/Pterygoid, interpterygoid vacuity: 0 = large opening, triangular in shape; 1 = reduced to an interpterygoid slit; 2 = entirely closed, no foramina posterius canalis carotici palatinum present. Scored inapplicable for taxa with a bony canal for the palatine artery (ch 146.1)

Character optimisation: Unambiguous: *Chubutemys*+++ (0->1), (*Annemys latiens* ++ *Xinjiangchelys*) (1->0), Paracryptodira (1->2).

Character 148 (Evers & Benson [2018]: character 146). Embedding of the palatine division of carotid artery: 0 = the palatine artery is not encased in a bony canal (artery enters the skull through the interpterygoid cavuity, interpterygoid slit, or possibly other skull openings); 1 = the palatine artery is encased in a bony canal (irrespective of the exposure or embedding of the internal carotid artery split).

Character optimisation: Unambiguous: Xinjiangchelyidae+++ (0->1), *Dracochelys bicuspis* (1->0), *Kallokibotion bajazidi* (0->1).

Character 149 (Evers & Benson [2018]: character 147). Embedding of internal carotid artery and its bifurcation: 0 = Internal carotid arterial system is not embedded by bone, a foramen posterius canalis carotici is absent, and the split into palatine and cerebral artery occurs extracranially; 1 = internal carotid arterial system is partially embedded, a foramen posterius canalis carotici interni is present, and the split into palatine and cerebral artery happens at the fenestra caroticus and is thus ventrally exposed; 2 = internal carotid arterial system is ventrally fully embedded by bone, a foramen posterius canalis carotici interni is present and the split into palatine and cerebral artery is ventrally covered by bone.

Character optimisation: Unambiguous: Testudines (1->2), *Adocus beatus* (2->1), *Jurassichelon oleronensis* (2->1), *Plesiochelys bigleri* (2->1), *Sandownia harrisi* (2->1); DELTRAN: Xinjiangchelyidae+++ (0->1), *Meiolania planiceps* (0->1); ACCTRAN: *Meiolania*+++ (0->1), Paracryptodira (1->0).

Character 150 (Evers & Benson [2018]: character 148). Position of the foramen posterius canalis carotici interni (fpcci): 0 = the fpcci is located at the ventral surface of the skull in a position far anterior to the margin of the fenestra postotica; 1 = the fpcci is located at the posterior end of the skull, either on the ventral surface of the skull close to the margin of the fenestra postotica, or on the posterior surface of the skull at the ventral margin of the fenestra postotica. This character is scored inapplicable for taxa that lack a foramen posterius canalis carotici interni.

Character optimisation: Unambiguous: *Santanachelys gaffneyi* (1->0), Trionychidae (1->0), *Chelus fimbriatus* (1->0); DELTRAN: *Protostega gigas* (1->0), *Podocnemis* (1->0), *Galianemys whitei* (1->0); ACCTRAN: (*Protostega* + *Archelon*) (1->0), total-group Pelomedusoides (1->0), *Pelomedusa subrufa* (0->1).

Character 151 (Evers & Benson [2018]: character 149). Entry of the internal carotid artery into skull relative to cavum acustico-jugulare: 0 = internal carotid enters the skull ventrally to the level of the cavum acustico-jugulare; 1 = internal carotid artery enters the skull within the cavum acustico-jugulare, artery lies in dorsally open trough on dorsal surface of pterygoid and only becomes dorsally covered within the cavum acustico-jugulare.

Character optimisation: Unambiguous: Dermochelyidae (0->1), *Puppigerus camperi* (0->1), *Argillochelys cuneiceps* (0->1), *Macrochelys temminckii* (1->0), *Baptemys wyomingensis* (1->0), (*Kirgizemys hoburensis* + *Kirgizemys dmitrievi*) (0->1); DELTRAN: Chelydroidea (0->1), Testudinoidea (0->1), *Meiolania planiceps* (0->1); ACCTRAN: Durocryptodira (0->1), total-group Chelonioidea (1->0), *Meiolania planiceps* (0->1).

Character 152 (Evers & Benson [2018]: character 150). Dorsal exposure of the palatine artery and/or anterior parts of the internal carotid artery: 0 = absent, the split of the internal carotid artery is dorsally covered by bone, and the palatine artery exits the basicranium into the cavum cranii via the foramen anterius canalis carotici palatinum; 1 = the internal carotid artery exits the braincase anterodorsally into the sulcus cavernosus where it continues on the floor of the sulcus cavernosus (= sulcus caroticus of Gaffney 1979), and the split into cerebral

and palatine arteries occurs within the sulcus cavernosus. The cerebral artery enters the parabasisphenoid medially, whereas the palatine artery continues in the sulcus cavernosus anteriorly without ever being embedded in a canal. This character is scored as inapplicable when the carotid split is ventrally exposed (i.e. ch 148.0 or 148.1).

Character optimisation: Unambiguous: crown-group Cheloniidae (0->1), *Nichollsemys baieri* (0->1).

Character 153 (Evers & Benson [2018]: character 151). Formation of the foramen posterius canalis carotici interni, pterygoid involvement: 0 = present; 1 = absent.

Character optimisation: Unambiguous: total-group Chelidae (0->1), *Pelomedusa subrufa* (0->1).

Character 154 (Evers & Benson [2018]: character 152). Formation of the foramen posterius canalis carotici interni, parabasisphenoid involvement: 0 = present; 1 = absent.

Character optimisation: Unambiguous: (*Calcarichelys* + *Rhinochelys*) (1->0), *Desmatochelys padillai* (1->0), Plesiochelyidae (1->0), *Galianemys whitei* (1->0); DELTRAN: *Protostega gigas* (1->0), *Ordosemys* sp. IVPP V12092 (1->0), *Annemys* sp. IVPP V18106 (1->0), *Xinjiangchelys radiplicatoides* (1->0); ACCTRAN: (*Protostega* + *Archelon*) (1->0), (*Ordosemys* + *Dracochelys*) (1->0), Xinjiangchelyidae (1->0), *Xinjiangchelys wusu* (0->1).

Character 155 (Evers & Benson [2018]: character 153). Formation of the foramen posterius canalis carotici interni, quadrate involvement: 0 = present; 1 = absent.

Character optimisation: Unambiguous: *Podocnemis* (1->0); DELTRAN: *Phrynops geoffroanus* (1->0), *Chelodina* (1->0), *Araripemys barretoi* (1->0); ACCTRAN: total-group Chelidae (1->0), *Chelus fimbriatus* (0->1), *Elseya dentata* (0->1).

Character 156 (Evers & Benson [2018]: character 154). Formation of the foramen posterius canalis carotici interni, prootic involvement: 0 = present; 1 = absent.

Character optimisation: Unambiguous: *Argillochelys cuneiceps* (1->0), Chelydroidea (1->0), *Macrochelys temminckii* (0->1), *Baptemys wyomingensis* (0->1), Emydidae (1->0), Testudinidae (1->0), total-group Chelidae (1->0), *Pelomedusa subrufa* (1->0); DELTRAN: *Kirgizemys hoburensis* (1->0); ACCTRAN: (*Kirgizemys hoburensis* + *Kirgizemys dmitrievi*) (1->0).

Character 157 (Evers & Benson [2018]: character 155). Hyomandibular branch of the facial nerve: 0 = contained within the canalis cavernosus; 1 = contained in a sulcus or separate canal paralleling the canalis cavernosus.

Character optimisation: Unambiguous: *Corsochelys halinches* (0->1), Testuguria (0->1), Plesiochelyidae (0->1), *Portlandemys mcdowelli* (1->0), *Annemys* sp. IVPP V18106 (0->1); DELTRAN: *Meiolania planiceps* (0->1), *Eileanchelys waldmanni* (0->1); ACCTRAN: *Meiolania planiceps* (0->1), (*Kayentachelys* + *Eileanchelys*) (0->1).

Character 158 (Evers & Benson [2018]: character 156). Stapedial artery, foramen stapedio-temporale: 0 = present; 1 = absent.

Character optimisation: Unambiguous: total-group Dermatemydidae (0->1).

Character 159 (Evers & Benson [2018]: character 157). Stapedial artery, size of foramen stapedio-temporale: 0 = relatively large (the size of a large blood foramina, ≥5 mm diameter); 1 = significantly reduced in size (the size of a nerve foramina, ≤3 mm diameter. This character is scored as inapplicable for taxa without a foramen stepedio-temporale (i.e. ch 156.1).

Character optimisation: DELTRAN: Kinosternidae (0->1); ACCTRAN: Kinosternoidea (0->1).

Character 160 (Evers & Benson [2018]: character 158). Stapedial artery, foramen stapedio-temporale location in the otic chamber: 0 = on dorsal part and pointing dorsally; 1 = on the anterior wall of the otic region, pointing anteriorly. This character is scored as inapplicable for taxa without a foramen stepedio-temporale (i.e. ch 156.1).

Character optimisation: Unambiguous: crown-group Pleurodira (0->1), *Podocnemis* (1->0).

Character 161 (Evers & Benson [2018]: character 159). Stapedial artery, formation of the foramen stapedio-temporale, contribution of the quadrate: 0 = absent; 1 = present. Scored inapplicable for taxa without a foramen stapedio-temporale. This character is scored as inapplicable for taxa without a foramen stepedio-temporale (i.e. ch 156.1).

Character optimisation: Unambiguous: *Kinosternon suburum hippocrepis* (1->0), *Platysternon megacephalum* (1->0), *Chelus fimbriatus* (1->0), *Meiolania planiceps* (1->0).

Character 162 (Evers & Benson [2018]: character 160). Stapedial artery, formation of the foramen stapedio-temporale, contribution of the prootic: 0 = absent; 1 = present. Scored inapplicable for taxa without a foramen stapedio-temporale. This character is scored as inapplicable for taxa without a foramen stepedio-temporale (i.e. ch 156.1).

Character optimisation: DELTRAN: (*Kayentachelys*+*Eileanchelys*)+++ (0->1); ACCTRAN: *Australochelys*+++ (0->1).

Character 163 (Evers & Benson [2018]: character 161). Stapedial artery, formation of the foramen stapedio-temporale, contribution of the opisthotic: 0 = absent; 1 = present. Scored inapplicable for taxa without a foramen stapedio-temporale. This character is scored as inapplicable for taxa without a foramen stepedio-temporale (i.e. ch 156.1).

Character optimisation: Unambiguous: Protostegidae+++ (0->1), (*Calcarichelys* + *Rhinochelys*) (1->0), total-group Cheloniidae (1->0), *Caretta Caretta* (0->1), *Ctenochelys* (0->1), *Chelonoidis* sp. (0->1), *Brachyopsemys tingitana* (0->1), *Kirgizemys dmitrievi* (0->1), *Meiolania planiceps* (0->1); DELTRAN: *Proganochelys quenstedti* (0->1); ACCTRAN: *Proganochelys quenstedti* (0->1).

Character 164 (Evers & Benson [2018]: character 162). Stapedial artery, formation of the foramen stapedio-temporale, contribution of the supraoccipital: 0 = absent; 1 = present.

Scored inapplicable for taxa without a foramen stapedio-temporale. This character is scored as inapplicable for taxa without a foramen stepedio-temporale (i.e. ch 156.1).

Character optimisation: Unambiguous: *Ctenochelys* (0->1), *Eubaena cephalica* (0->1).

Character 165 (Evers & Benson [2018]: character 163). Foramen jugulare posterius, relationship with the fenestra postotica: 0 = separate from fenestra postotica; 1 = coalescent with fenestra postotica.

Character optimisation: Unambiguous: Cryptodira (1->0), total-group Chelonioidea (0->1), *Allopleuron hoffmanni* (1->0), *Platysternon megacephalum* (0->1), *Brachyopsemys tingitana* (1->0), Chelinae (1->0), crown-group Pelomedusoides (1->0), *Kirgizemys hoburensis* (1->0); DELTRAN: (*Apalone* + *Petrochelys*) (0->1); ACCTRAN: Trionychinae (0->1).

Character 166 (Evers & Benson [2018]: character 164). Foramen jugulare posterius, formation of lateral bar separating foramen from fenestra postotica: 0 = formed by pterygoid; 1 = formed by opisthotic and/or exoccipital. The character is scored inapplicable for taxa in which the foramen jugulare posterius is coalescent with the fenestra postotica (ch. 163.1).

Character optimisation: Unambiguous: *Lissemys punctata* (1->0).

Character 167 (Evers & Benson [2018]: character 165). Recessus scalae tympani: 0 = almost nonexistent, not surrounded by bone; 1 = well developed.

Character optimisation: DELTRAN: *Chubutemys*+++ (0->1), *Eileanchelys waldmanni* (0->1); ACCTRAN: (*Kayentachelys*+*Eileanchelys*)+++ (0->1), *Kayentachelys aprix* (1->0

Character 168 (Evers & Benson [2018]: character 166). Cranial scutes, scute D meeting in midline: 0 = absent; 1 = present.

Character optimisation: DELTRAN: *Meiolania planiceps* (0->1); ACCTRAN: *Meiolania planiceps* (0->1).

Character 169 (Evers & Benson [2018]: character 167). Cranial scutes, scute X much smaller than scute D: 0 = absent; 1 = present.

Character optimisation: -.

Character 170 (Evers & Benson [2018]: character 168). Cranial scutes, scute X partially separates scutes G: 0 = absent; 1 = present.

Character optimisation: -.

Character 171 (Evers & Benson [2018]: character 169). Cranial scutes, scutes A, B, and C forming a continuous posterolateral shelf: 0 = absent; 1 = present.

Character optimisation: -.

Character 172 (Evers & Benson [2018]: character 170). Cranial scutes, scute F: 0 = formed by several scutes; 1 = formed by a single scute.

Character optimisation: DELTRAN: *Meiolania planiceps* (0->1); ACCTRAN: *Meiolania planiceps* (0->1).

Character 173 (Evers & Benson [2018]: character 171). Cranial scutes, scute J: 0 = formed by several scutes; 1 = formed by a single scute.

Character optimisation: -.

Character 174 (Evers & Benson [2018]: character 172). Dentary, medial contact of dentaries: 0 = fused; 1 = open suture.

Character optimisation: Unambiguous: *Toxochelys* sp. (0->1), *Baptemys wyomingensis* (0->1), total-group Chelidae (0->1), *Elseya dentata* (1->0), (*Kayentachelys* + *Eileanchelys*) (0->1).

Character 175 (Evers & Benson [2018]: character 173). Dentary, width triturating surface vs. jaw length: 0 = narrow triturating surface, symphysis less than 1/3 of jaw length; 1 = broad triturating surface, symphysis ≥1/3 jaw length.

Character optimisation: Unambiguous: *Lepidochelys olivacea* (0->1), *Puppigerus camperi* (0->1), (*Procolpochelys* ++ *Erquelinnesia*) (0->1); DELTRAN: *Solnhofia parsoni* (0->1), Sandownidae (0->1); ACCTRAN: Angolachelonia (0->1), Plesiochelyidae (1->0).

Character 176 (Evers & Benson [2018]: character 174). Dentary, symphyseal ridge: 0 = absent; 1 = present.

Character optimisation: Unambiguous: (*Bouliachelys* + *Rhinochelys*) (0->1), *Eochelone brabantica* (1->0), *Solnhofia parsoni* (0->1), *Elseya dentata* (0->1); DELTRAN: (*Lepidochelys olivacea* + *Lepidochelys kempii*) (0->1), (*Chelonia* + *Natator*) (0->1), (*Argillochelys* ++ *Puppigerus*) (0->1), crown-group Chelydridae (0->1); ACCTRAN: (*Puppigerus* ++ *Lepidochelys*) (0->1), (*Eretmochelys* ++ *Lepidochelys*) (1->0), (*Lepidochelys olivacea* + *Lepidochelys kempii*) (0->1), total-group Chelydridae (0->1).

Character 177 (Evers & Benson [2018]: character 175). Dentary, lingual (tomial) ridge: 0 = prominent; 1 = weak or absent.

Character optimisation: Unambiguous: *Eretmochelys imbricata* (1->0), *Natator depressus* (1->0), *Allopleuron hoffmanni* (1->0), *Sternotherus* (1->0), total-group Dermatemydidae (1->0), Testudinoidea (1->0), Plesiochelyidae (1->0), *Elseya dentata* (1->0), *Kallokibotion bajazidi* (0->1); DELTRAN: Sinemydidae/Macroabenidae+++ (0->1), *Carettochelys insculpta* (1->0), crown-group Pelomedusoides (1->0), *Xinjiangchelys radiplicatoides* (0->1); ACCTRAN: Xinjiangchelyidae+++ (0->1), total-group Carettochelyidae (1->0), total-group Pelomedusoides (1->0), *Annemys levensis* (1->0).

Character 178 (Evers & Benson [2018]: character 176). Dentary, size of foramen dentofaciale majus: 0 = small, size of a small vessel; 1 = enlarged, foramen is several mm in diameter.

Character optimisation: Unambiguous: total-group Dermatemydidae (0->1); DELTRAN: (*Erquelinnesia* ++ *Lepidochelys*) (0->1), *Chrysemys picta* (0->1), *Geoclemys hamiltonii* (0->1), *Gopherus polyphemus* (0->1), *Carettochelys insculpta* (0->1), *Adocus beatus* (0->1); ACCTRAN: Cryptodira (0->1), Americhelydia (1->0), total-group Cheloniidae (0->1), *Platysternon megacephalum* (1->0), (*Testudo* + *Chelonoidis*) (1->0), Trionychidae (1->0).

Character 179 (Evers & Benson [2018]: character 177). Dentary-Surangular arrangement: 0 = lack of a posterior expansion of dentary and anterior projection of surangular; 1 = posterior expansion of dentary present almost reaching the articular surface, covering the dorsal half of the surangular in lateral view, surangular with anterior projection.

Character optimisation: Unambiguous: *Lepidochelys kempii* (1->0); DELTRAN: *Bouliachelys suteri* (0->1), *Dermochelys coriacea* (0->1), crown-group Cheloniidae (0->1), *Ctenochelys* (0->1), *Procolpochelys charlestonensis* (0->1), *Toxochelys* sp. (0->1), crown-group Chelydridae (0->1); ACCTRAN: Americhelydia (0->1), Protostegidae (1->0), *Bouliachelys suteri* (0->1), (*Argillochelys* ++ *Puppigerus*) (1->0), (*Ctenochelys* ++ *Peritresius*) (0->1), (*Oligochelone* + *Erquelinnesia*) (1->0), Kinosternoidea (1->0).

Character 180 (Evers & Benson [2018]: character 178). Surangular, with anteromedial process forming a vertical lamina that projects anteriorly into the fossa meckelii: 0 = absent; 1 = present.

Character optimisation: Unambiguous: (*Chelonia* + *Natator*) (1->0); DELTRAN: Cryptodira (0->1), Testudinidae (1->0), Trionychinae (1->0), *Solnhofia parsoni* (0->1), *Plesiochelys planiceps* (0->1); ACCTRAN: Xinjiangchelyidae+++ (0->1), Testuguria (1->0), Trionychidae (1->0), (*Plesiochelys etalloni* + *Plesiochelys bigleri*) (1->0), crown-group Pleurodira (1->0).

Character 181 (Evers & Benson [2018]: character 179). Coronoid, anteromedial process: 0 = absent; 1 = present.

Character optimisation: Unambiguous: Chelydroidea (1->0), Testuguria (1->0), *Chelodina* (1->0), *Araripemys barretoi* (1->0); DELTRAN: Testudines (0->1), Xinjiangchelyidae (0->1); ACCTRAN: Paracryptodira+++ (0->1), (*Judithemys* ++ *Sinemys*) (1->0).

Character 182 (Evers & Benson [2018]: character 180). Coronoid, contribution to triturating surface: 0 = absent; 1 = present.

Character optimisation: Unambiguous: Testudines (0->1), *Platysternon megacephalum* (1->0), (*Testudo* + *Chelonoidis*) (1->0), Plesiochelyidae (1->0), total-group Chelidae (1->0); DELTRAN: total-group Chelonioidea (1->0), crown-group Chelydridae (1->0), *Kinosternon suburum hippocrepisis* (1->0), *Baptemys wyomingensis* (1->0); ACCTRAN: Americhelydia (1->0), Kinosternoidea (0->1), *Kinosternon suburum hippocrepis* (1->0), *Baptemys wyomingensis* (1->0)

Character 183 (Evers & Benson [2018]: character 181). Coronoid, notch on posterior margin of coronoid: 0 = absent; 1 = present.

Character optimisation: Unambiguous: *Kinosternon suburum hippocrepis* (0->1), *Platysternon megacephalum* (0->1), Angolachelonia (0->1); DELTRAN: Trionychinae (0->1), *Carettochelys insculpta* (0->1), *Portlandemys mcdowelli* (1->0); ACCTRAN: crown-group Trionychia (0->1), *Lissemys punctata* (1->0), (*Jurassichelon* + *Portlandemys*) (1->0).

Character 184 (Evers & Benson [2018]: character 182). Coronoid, foramen at anterior end, leading from fossa meckelii into space between mandibular rami: 0 = absent; 1 = present.

Character optimisation: Unambiguous: *Natator depressus* (0->1), *Toxochelys* sp. (0->1), Angolachelonia (0->1), *Meiolania planiceps* (0->1); DELTRAN: *Lepidochelys olivacea* (0->1), *Caretta Caretta* (0->1), *Phrynops geoffroanus* (0->1), *Elseya dentata* (0->1); ACCTRAN: (*Caretta* ++ *Lepidochelys*) (0->1), *Lepidochelys kempii* (1->0), crown-group Chelidae (0->1), *Chelodina* (1->0).

Character 185 (Evers & Benson [2018]: character 183). Coronoid process, principally formed by: 0 = coronoid; 1 = dentary; 2 = surangular.

Character optimisation: Unambiguous: *Testudo* (0->1), *Elseya dentata* (0->1); DELTRAN: *Dermochelys coriacea* (0->2), Kinosternidae (0->1), *Dermatemys mawii* (0->1); ACCTRAN: Dermochelyidae (0->2), Kinosternoidea (0->1), *Baptemys wyomingensis* (1->0).

Character 186 (Evers & Benson [2018]: character 184). Coronoid process: 0 = relatively low, dorsally well rounded; 1 = relatively high, process is dorsally or posterodorsally pointed.

Character optimisation: Unambiguous: Kinosterninae (0->1), *Baptemys wyomingensis* (0->1), *Platysternon megacephalum* (0->1), total-group Trionychia (0->1), *Lissemys punctata* (1->0), Angolachelonia (0->1).

Character 187 (Evers & Benson [2018]: character 185). Splenial: 0 = present; 1 = absent.

Character optimisation: Unambiguous: Sinemydidae/Macroabenidae+++ (0->1), *Protostega gigas* (1->0), *Allopleuron hoffmanni* (1->0), Thalassochelydia (1->0), crown-group Chelidae (1->0), *Xinjiangchelys radiplicatoides* (0->1); DELTRAN: *Rhinochelys pulchriceps* (1->0); ACCTRAN: (*Santanachelys* ++ *Rhinochelys*) (1->0).

POSTCRANIUM

Character 188 (Evers & Benson [2018]: character 186). Carapace, carapacial scutes: 0 = present; 1 = absent.

Character optimisation: Unambiguous: Trionychidae (0->1); DELTRAN: (*Protostega* + *Archelon*) (0->1), Dermochelyidae (0->1), *Allopleuron hoffmanni* (0->1); ACCTRAN: (*Ocepechelon* ++ *Protostega*) (0->1), *Corsochelys*+++ (0->1), (*Erquelinnesia* ++ *Lepidochelys*) (1->0).

Character 189 (Evers & Benson [2018]: character 187). Carapace, carapacial scutes: 0 = present, ful9y covering the carapace; 1 = reduced not fully covering the carapace.

Character optimisation: DELTRAN: *Carettochelys insculpta* (0->1); ACCTRAN: crown-group Trionychia (0->1).

Character 190 (Evers & Benson [2018]: character 188). Carapace, continuous keel on costals: 0 = absent; 1 = present.

Character optimisation: Unambiguous: (*Ctenochelys* ++ *Peritresius*) (0->1), *Geoclemys hamiltonii* (0->1), *Chelus fimbriatus* (0->1), *Araripemys barretoi* (0->1); DELTRAN: *Emarginachelys cretacea* (0->1), Kinosternidae (0->1), *Baptemys wyomingensis* (0->1); ACCTRAN: Chelydroidea (0->1), crown-group Chelydridae (1->0), *Dermatemys mawii* (1->0).

Character 191 (Evers & Benson [2018]: character 189). Carapace, continuous keel on neurals: 0 = absent; 1 = present.

Character optimisation: Unambiguous: *Eosphargis breineri* (0->1), *Chelonia mydas* (0->1), (*Ctenochelys* ++ *Peritresius*) (0->1), *Allopleuron hoffmanni* (0->1), *Geoclemys hamiltonii* (0->1), *Chelus fimbriatus* (0->1), *Araripemys barretoi* (0->1); DELTRAN: (*Calcarichelys* + *Rhinochelys*) (0->1), *Santanachelys gaffneyi* (1->0), (*Protostega* + *Archelon*) (0->1), *Lepidochelys olivacea* (0->1), *Caretta Caretta* (0->1), *Emarginachelys cretacea* (0->1), Kinosternidae (0->1), *Baptemys wyomingensis* (0->1); ACCTRAN: Protostegidae (0->1), (*Santanachelys* + *Notochelone*) (1->0), (*Desmatochelys lowii* + *Desmatochelys padillai*) (1->0), (*Caretta* ++ *Lepidochelys*) (0->1), *Lepidochelys kempii* (1->0), Chelydroidea (0->1), crown-group Chelydridae (1->0), *Dermatemys mawii* (1->0).

Character 192 (Evers & Benson [2018]: character 190). Shell, sculpturing of dorsal surface (carapace) and ventral surface (plastron): 0 = absent, smooth to slightly rugose; 1 = present, development of striations, vermiculations, striations, or pitting.

Character optimisation: Unambiguous: crown-group Trionychia (0->1), total-group Chelidae (0->1), *Phrynops geoffroanus* (1->0); DELTRAN: *Sinemys gamera* (0->1), Pleurosternidae (0->1); ACCTRAN: Sinemydidae (0->1), Paracryptodira (0->1).

Character 193 (Evers & Benson [2018]: character 191). Shell, pattern of sculpturing of the dorsal surface (carapace) and ventral surface (plastron): 0 = parallel to radial striations; 1 =

vermiculation; 2 = highly dense pattern of pitting combined with striations; 3 = dichotomic striations; 4 = spread pitting without marked striation pattern; 5 = granules (positive relief).

Character optimisation: Unambiguous: crown-group Pleurodira (0->3), *Araripemys barretoi* (3->4), *Pleurosternon bullockii* (0->3); DELTRAN: Kinosternidae (0->1), crown-group Trionychia (0->2); ACCTRAN: Cryptodira (0->1), total-group Trionychia (1->2).

Character 194 (Evers & Benson [2018]: character 192). Carapacial Sutures: 0 = carapacial elements finely sutured or the contact is smooth; 1 = carapacial sutures strongly serrated in adult stage.

Character optimisation: DELTRAN: *Dracochelys bicuspis* (0->1); ACCTRAN: (*Ordosemys* + *Dracochelys*) (0->1).

Character 195 (Evers & Benson [2018]: character 193). Nuchal, articulation of nuchal with neural spine of eighth cervical vertebra: 0 = articulation via a blunt facet is present; 1 = articulation along a blunt facet absent.

Character optimisation: Unambiguous: *Meiolania*+++ (0->1), (*Ctenochelys* ++ *Peritresius*) (1->0); DELTRAN: *Carettochelys insculpta* (1->0); ACCTRAN: total-group Carettochelyidae (1->0).

Character 196 (Evers & Benson [2018]: character 194). Raised pedestal on the visceral surface of the nuchal for the articulation with the neural spine of the eighth cervical vertebra: 0 = absent; 1 = present.

Character optimisation: Unambiguous: total-group Chelonioidea (0->1), (*Desmatochelys* ++ *Protostega*) (1->0), *Allopleuron hoffmanni* (1->0).

Character 197 (Evers & Benson [2018]: character 195). Nuchal, elongate costiform process: 0 = absent; 1 = present.

Character optimisation: Unambiguous: Chelydroidea (0->1).

Character 198 (Evers & Benson [2018]: character 196). Nuchal, length of costiform process: 0 = crosses peripheral 1; 1 = reaches peripherals 2 or 3. This character is scored inapplicable for taxa without a costiform process on the nuchal (ch. 195.0).

Character optimisation: Unambiguous: *Chelydra serpentina* (1->2).

Character 199 (Evers & Benson [2018]: character 197). Nuchal, length versus width: 0 = wider than long; 1 = longer than wide or as long as wide.

Character optimisation: Unambiguous: *Chelonoidis* sp. (1->0), *Adocus beatus* (0->1), crown-group Pleurodira (0->1), *Procolpochelys charlestonensi*s (0->1); DELTRAN: Emydidae (0->1), Testuguria (0->1); ACCTRAN: Testudinoidea (0->1), *Platysternon megacephalum* (1->0).

Character 200 (Evers & Benson [2018]: character 198). Nuchal, posteriomedial fontanelles: 0 = absent; 1 = present.

Character optimisation: Unambiguous: *Desmatochelys lowii* (0->1), (*Ctenochelys* ++ *Peritresius*) (0->1), *Toxochelys* sp. (0->1).

Character 201 (Evers & Benson [2018]: character 199). Neurals, neural formula 6>4<6<6<6<6: 0 = absent; 1 = present.

Character optimisation: Unambiguous: *Adocus beatus* (0->1).

Character 202 (Evers & Benson [2018]: character 200). Neurals, shape of neurals: 0 = very irregular in shape, wider than long or squared; 1 = regular, often perfectly hexagonal or pentagonal, longer than wide.

Character optimisation: Unambiguous: *Platysternon megacephalum* (1->0), Testudinidae (1->0), *Chelus fimbriatus* (1->0); DELTRAN: *Kallokibotion*+++ (0->1), *Eosphargis breineri* (1->0),

crown-group Chelydridae (1->0); ACCTRAN: *Chubutemys*+++ (0->1), Dermochelyidae (1->0), total-group Chelydridae (1->0).

Character 203 (Evers & Benson [2018]: character 201). Neurals: 0 = present; 1 = absent.

Character optimisation: Unambiguous: *Dermochelys coriacea* (0->1).

Character 204 (Evers & Benson [2018]: character 202). Neurals, number of neurals: 0 = ten or more; 1 = nine or less.

Character optimisation: Unambiguous: (*Lepidochelys olivacea* + *Lepidochelys kempii*) (1->0), *Procolpochelys charlestonensis* (1->0); DELTRAN: *Kallokibotion*+++ (0->1), *Eileanchelys waldmanni* (0->1); ACCTRAN: *Australochelys*+++ (0->1), *Kayentachelys aprix* (1->0).

Character 205 (Evers & Benson [2018]: character 203). Peripheral Gutter: 0 = peripheral gutter absent of only anteriorly developed; 1 = peripheral gutter extensively developed along anterior and bridge peripherals.

Character optimisation: Unambiguous: *Phrynops geoffroanus* (0->1), Xinjiangchelyidae (0->1), *Eileanchelys waldmanni* (0->1); DELTRAN: *Kirgizemys hoburensis* (0->1); ACCTRAN: (*Kirgizemys hoburensis* + *Kirgizemys dmitrievi*) (0->1).

Character 206 (Evers & Benson [2018]: character 204). Peripherals,: 0 = present; 1 = absent.

Character optimisation: Unambiguous: *Dermochelys coriacea* (0->1), Trionychidae (0->1).

Character 207 (Evers & Benson [2018]: character 205). Peripherals, number of peripherals: 0 = more than 11 pairs of peripherals present; 1 = 11 pairs of peripherals present; 2 = 10 pairs of peripherals present. This character is scored as inapplicable when peripherals are absent (ch. 204.1).

Character optimisation: Unambiguous: Kinosternidae (1->2); DELTRAN: (*Kayentachelys*+*Eileanchelys*)+++ (0->1), *Caretta Caretta* (1->0), *Carettochelys insculpta* (1->0); ACCTRAN: *Australochelys*+++ (0->1), (*Caretta* ++ *Lepidochelys*) (1->0), crown-group Trionychia (1->0).

Character 208 (Evers & Benson [2018]: character 206). Peripherals, anterior peripherals incised by musk ducts: 0 = absent; 1 = present.

Character optimisation: Unambiguous: Kinosternoidea (0->1), *Kinosternon suburum hippocrepis* (1->0), *Platysternon megacephalum* (0->1), *Geoclemys hamiltonii* (0->1), *Chelonoidis* sp. (0->1); DELTRAN: crown-group Chelidae (0->1), crown-group Pelomedusoides (0->1), (*Sinemys gamera* + *Sinemys lens*) (0->1), Xinjiangchelyidae (0->1), *Kayentachelys aprix* (0->1); ACCTRAN: Paracryptodira+++ (0->1), Testudines (1->0), crown-group Pleurodira (0->1), *Araripemys barretoi* (1->0), (*Kayentachelys* + *Eileanchelys*) (0->1).

Character 209 (Evers & Benson [2018]: character 207). Costals, medial contact of the first pair of costals: 0 = absent; 1 = present.

Character optimisation: Unambiguous: Kinosterninae (0->1), Chelodininae (0->1).

Character 210 (Evers & Benson [2018]: character 208). Costals, medial contact of posterior costals: 0 = absent; 1 = present.

Character optimisation: Unambiguous: *Chelus fimbriatus* (1->0), *Annemys levensis* (0->1); DELTRAN: *Desmatochelys lowii* (0->1), Kinosterninae (0->1), *Dermatemys mawii* (0->1), crown-group Trionychia (0->1), (*Plesiochelys etalloni* + *Plesiochelys bigleri*) (0->1), crown-group Pleurodira (0->1), *Proganochelys quenstedti* (0->1); ACCTRAN: Testudines (0->1), Durocryptodira (1->0), (*Desmatochelys lowii* + *Desmatochelys padillai*) (0->1), Kinosternoidea (0->1), *Baptemys wyomingensis* (1->0), *Solnhofia parsoni* (1->0), *Proganochelys quenstedti* (0->1).

Character 211 (Evers & Benson [2018]: character 209). Costals, number of costals involved in medial contact: 0 = medial contact of up to three posterior costals; 1 = medial

contact of all costals. This character is scored as inapplicable for turtles without a medial contact of posterior costals.

Character optimisation: Unambiguous: *Sternotherus* (0->1), Chelodininae (0->1); DELTRAN: *Desmatochelys lowii* (0->1); ACCTRAN: total-group Chelonioidea (0->1).

Character 212 (modified from Evers & Benson [2018]: character 210): Costals, lateral ossification: 0 = all costals fully ossified laterally with strong sutural contact with peripherals, lack of dorsal exposure of distal end of costal ribs and absence of costo-peripheral fontanelles; 1 = lateral sutural contact contact between costals and peripherals absent in at least parts of the costo-peripherial series, resulting in the presence of costo-peripheral fontanelles and/or the exposure of the distal rib ends.

Character optimisation: Unambiguous: total-group Chelonioidea (0->1), *Puppigerus camperi* (1->0), crown-group Chelydridae (0->1), Trionychinae (0->1), *Solnhofia parsoni* (0->1), *Araripemys barretoi* (0->1), Sinemydidae (0->1).

Character 213 (modified from Evers & Benson [2018]: character 210): Costals, position of costo-peripheral fontanelles and exposure of dorsal rib ends: 0 = limited to parts of the carapace; 1 = fontanelles and exposed rib ends present and retained in adults between all costals and along the anterior margin of the first costal. Scored as inapplicable for taxa that lack costo-peripheral fontanelles (character 212.0).

Character optimisation: Unambiguous: *Procolpochelys charlestonensis* (1->0); DELTRAN: total-group Chelonioidea (0->1), *Rhinochelys nammourensis* (1->0), Trionychinae (0->1); ACCTRAN: Cryptodira (0->1), (*Rhinochelys pulchriceps* + *Rhinochelys nammourensis*) (1->0), Chelydroidea (1->0).

Character 214 (new character): Costal, fontanelle along anterior margin of costal 1: 0 = anterior margin of first costal positioned very close to nuchal and/or anteriormost peripherals, reducing the fontanelle to an anteroposteriorly narrow, slot-like opening; 1 =

extensive fontanelle between first costal and anterior margin of carapace. Scored inapplicable for taxa without costo-peripheral fontanelles (character 212.0) or when costo-peripheral fontanelles are absent along the first costal.

Character optimisation: Unambiguous: *Erquelinnesia gosseleti* (1->0); DELTRAN: Protostegidae (0->1), crown-group Chelonioidea (0->1); ACCTRAN: Protostegidae+++ (0->1), *Corsochelys halinches* (1->0).

Character 215 (new character): Posterior costals, shape: 0 = rectangular, much wider mediolaterally than long anteroposteriorly; 1 = square or hexagonal, as wide as long.

Character optimisation: DELTRAN: (*Protostega* + *Archelon*) (0->1), *Eosphargis breineri* (0->1), *Allopleuron hoffmanni* (0->1); ACCTRAN: (*Ocepechelon* ++ *Protostega*) (0->1), crown-group Chelonioidea (0->1), (*Erquelinnesia* ++ *Lepidochelys*) (1->0).

Character 216 (Evers & Benson [2018]: character 211). Rib free peripherals: 0 = absent; 1 = present.

Character optimisation: Unambiguous: *Corsochelys*+++ (0->1), Thalassochelydia (0->1).

Character 217 (Evers & Benson [2018]: character 212). Position of rib free peripherals: 0 = only present anterior and posterior to ribs; 1 = present between sixth and seventh ribs. This character is scored as inapplicable for taxa that lack rib free peripherals (ch. 211.0).

Character optimisation: Unambiguous: crown-group Cheloniidae (2->1), *Chelonia mydas* (1->0); DELTRAN: (*Erquelinnesia* ++ *Lepidochelys*) (0->2), *Ctenochelys* (2->0); ACCTRAN: crown-group Chelonioidea (0->2), (*Ctenochelys* + *Cabindachelys*) (2->0).

Character 218 (Evers & Benson [2018]: character 213). Costals, alternative short and long ends in the lateral part of costals: 0 = absent; 1 = present.

Character optimisation: DELTRAN: *Testudo* (0->1), *Gopherus polyphemus* (0->1); ACCTRAN: Testudinidae (0->1), *Chelonoidis* sp. (1->0).

Character 219 (Evers & Benson [2018]: character 214). Costals, costal 9: 0 = present; 1 = absent.

Character optimisation: Unambiguous: (*Plesiochelys etalloni* + *Plesiochelys bigleri*) (1->0), *Kayentachelys aprix* (1->0); DELTRAN: *Rhinochelys nammourensis* (1->0), (*Protostega* + *Archelon*) (1->0); ACCTRAN: (*Rhinochelys pulchriceps* + *Rhinochelys nammourensis*) (1->0), (*Ocepechelon* ++ *Protostega*) (1->0).

Character 220 (Evers & Benson [2018]: character 215). Costals, shape of Costal 3: 0 = tapering towards the lateral side of the shell or with parallel anterior and posterior borders; 1 = broadens towards the lateral side of the shell.

Character optimisation: DELTRAN: *Dracochelys bicuspis* (0->1); ACCTRAN: (*Ordosemys* + *Dracochelys*) (0->1).

Character 221 (Evers & Benson [2018]: character 216). Suprapygals: 0 = present; 1 = absent.

Character optimisation: Unambiguous: Trionychidae (0->1).

Character 222 (Evers & Benson [2018]: character 217). Suprapygals, number of suprapygals: 0 = one; 1 = two; 2 = more than two.

Character optimisation: Unambiguous: Protostegidae (1->0), *Procolpochelys charlestonensis* (1->0), Chelydroidea (1->0), *Chelydra serpentina* (0->2), Emydidae (1->0), *Solnhofia parsoni* (1->2), crown-group Pleurodira (1->0), *Pleurosternon bullockii* (1->0), *Kayentachelys aprix* (1->0); DELTRAN: *Carettochelys insculpta* (1->0); ACCTRAN: total-group Trionychia (1->0).

Character 223 (Evers & Benson [2018]: character 218). Suprapygals, size between suprapygal 1 and 2: 0 = suprapygal 1 smaller than suprapygal 2; 1 = suprapygal 1 larger. Reworded from KL (ch 88). Turtles with only one suprapygal or suprapygals absent are coding as inapplicable.

Character optimisation: Unambiguous: *Caretta Caretta* (1->0), *Puppigerus camperi* (1->0), *Kallokibotion bajazidi* (0->1); DELTRAN: total-group Chelonioidea (0->1); ACCTRAN: Americhelydia (0->1).

Character 224 (Evers & Benson [2018]: character 219). Cervical scutes: 0 = present; 1 = cervical scutes absent.

Character optimisation: Unambiguous: Protostegidae+++ (0->1), (*Desmatochelys lowii* + *Desmatochelys padillai*) (1->0), (*Erquelinnesia* ++ *Lepidochelys*) (1->0), crown-group Trionychia (0->1), Sinemydidae (0->1), *Pleurosternon bullockii* (0->1); DELTRAN: *Elseya dentata* (0->1), *Araripemys barretoi* (0->1), crown-group Pelomedusoides (0->1); ACCTRAN: crown-group Pleurodira (0->1), crown-group Chelidae (1->0), *Elseya dentata* (0->1).

Character 225 (Evers & Benson [2018]: character 220). Number of cervical scutes: 0 = more than one cervical scute present; 1 = one cervical scute present. This character is scored as inapplicable when cervical scutes are absent (ch. 219.1)

Character optimisation: DELTRAN: (*Plesiochelys etalloni* + *Plesiochelys bigleri*) (1->0); ACCTRAN: Plesiochelyidae (1->0).

Character 226 (Evers & Benson [2018]: character 221). Pygal, posterior notch: 0 = present; 1 = absent.

Character optimisation: Unambiguous: *Eretmochelys imbricata* (1->0), *Natator depressus* (1->0), (*Ctenochelys* ++ *Peritresius*) (1->0), *Allopleuron hoffmanni* (1->0), Emysternia (1->0), *Chelonoidis* sp. (1->0), *Chelus fimbriatus* (1->0), *Meiolania planiceps* (1->0); DELTRAN: (*Kayentachelys*+*Eileanchelys*)+++ (0->1), (*Chelosphargis* + *Rhinochelys*) (1->0), crown-group Chelydridae (1->0), *Dracochelys bicuspis* (1->0); ACCTRAN: *Australochelys*+++ (0->1), (*Bouliachelys* + *Rhinochelys*) (1->0), total-group Chelydridae (1->0), Sinemydidae (1->0).

Character 227 (Evers & Benson [2018]: character 222). Supramarginals: 0 = present; 1 = absent.

Character optimisation: Unambiguous: *Macrochelys temminckii* (1->0); DELTRAN: (*Kayentachelys*+*Eileanchelys*)+++ (0->1); ACCTRAN: *Australochelys*+++ (0->1).

Character 228 (Evers & Benson [2018]: character 223). Supramarginals, separating marginal and pleurals: 0 = complete row present, fully separating marginals from pleurals; 1 = partial row present, incompletely separating marginals from pleurals. This character is scored as inapplicable for turtles in which supramarginals are absent.

Character optimisation: -.

Character 229 (Evers & Benson [2018]: character 224). Vertebrals, shape of the verterbrals: 0 = vertebrals 2 to 4 signicantly broader than pleurals; 1 = vertebrals 2 to 4 as narrow as, or narrower than, pleurals.

Character optimisation: Unambiguous: Xinjiangchelyidae+++ (0->1), Thalassochelydia (1->0); DELTRAN: *Santanachelys gaffneyi* (1->0); ACCTRAN: (*Santanachelys* + *Notochelone*) (1->0).

Character 230 (Evers & Benson [2018]: character 225). Vertebrals, position of vertebral 3-4 sulcus in taxa with five vertebrals: 0 = sulcus positioned on neural 6; 1 = sulcus positioned on neural 5.

Character optimisation: Unambiguous: *Peritresius martini* (1->0), *Erquelinnesia gosseleti* (1->0), *Annemys levensis* (1->0); DELTRAN: Paracryptodira+++ (0->1), *Santanachelys gaffneyi* (1->0); ACCTRAN: *Meiolania*+++ (0->1), (*Santanachelys* + *Notochelone*) (1->0).

Character 231 (Evers & Benson [2018]: character 226). Vertebrals, vertebral 3-4 sulcus with a wide posteriorly oriented medial embayment: 0 = absent; 1 = present.

Character optimisation: DELTRAN: *Annemys levensis* (0->1), *Annemys latiens* (0->1); ACCTRAN: Xinjiangchelyidae (0->1), (*Annemys* sp. IVPP V18106 ++ *Xinjiangchelys*) (1->0).

Character 232 (Evers & Benson [2018]: character 227). Vertebrals, verebral 1: 0 = vertebral 1 does not enter anterior margin of carapace; 1 = enters anterior margin.

Character optimisation: Unambiguous: *Araripemys barretoi* (0->1), Sinemydidae (0->1).

Character 233 (Evers & Benson [2018]: character 228). Marginals, marginal scutes overlap onto costals: 0 = absent, marginals restricted to peripherals; 1 = present.

Character optimisation: Unambiguous: *Meiolania*+++ (0->1), Sinemydidae/Macroabenidae+++ (1->0); DELTRAN: *Adocus beatus* (0->1); ACCTRAN: total-group Trionychia (0->1).

Character 234 (Evers & Benson [2018]: character 229). Pleurals, at least one pair of additional pleural scutes located laterally of vertebral scute 1, with anterior contact with cervical scute: 0 = absent; 1 = present.

Character optimisation: Unambiguous: (*Caretta* ++ *Lepidochelys*) (0->1).

Character 235 (Evers & Benson [2018]: character 230). Plastron, connection between carapace and plastron: 0 = osseous; 1 = ligamentous.

Character optimisation: Unambiguous: Kinosternoidea (1->0), *Chrysemys picta* (1->0), Testuguria (1->0), *Chelonoidis* sp. (0->1), *Adocus beatus* (1->0), total-group Pleurodira (1->0), *Solnhofia parsoni* (0->1), *Araripemys barretoi* (0->1); DELTRAN: (*Kayentachelys*+*Eileanchelys*)+++ (0->1), Pleurosternidae (1->0); ACCTRAN: *Australochelys*+++ (0->1), Paracryptodira (1->0).

Character 236 (Evers & Benson [2018]: character 231). Plastron, central plastral fontanelle: 0 = absent; 1 = present.

Character optimisation: Unambiguous: total-group Chelonioidea (0->1), crown-group Chelydridae (0->1), Trionychidae (0->1), *Araripemys barretoi* (0->1), *Meiolania planiceps* (0-

>1); DELTRAN: Thalassochelydia (0->1), *Dracochelys bicuspis* (0->1); ACCTRAN: Angolachelonia (0->1), Sinemydidae (0->1).

Character 237 (Evers & Benson [2018]: character 232). Plastron, posterior plastral fontanelle, posterior plastral fontanelle between the xiphiplastra and/or the hypoplastra: 0 = absent in adult stage; 1 = retained in adult stage.

Character optimisation: Unambiguous: (*Puppigerus* + *Eochelone*) (1->0), Trionychidae (0->1), *Araripemys barretoi* (0->1); DELTRAN: Protostegidae+++ (0->1), *Santanachelys gaffneyi* (1->0); ACCTRAN: total-group Chelonioidea (0->1), (*Santanachelys* + *Notochelone*) (1->0).

Character 238 (Evers & Benson [2018]: character 233). Plastron, plastral kinesis: 0 = absent, scutes sulci and bony sutures do not overlap; 1 = present, scutes sulci coincide with epiplastral-hyoplastral contact.

Character optimisation: Unambiguous: Kinosternidae (0->1), *Emys orbicularis* (0->1).

Character 239 (Evers & Benson [2018]: character 234). Plastron, plastral kinesis: 0 = between hyoplastron and hypoplastron; 1 = between hyoplastron and epiplastron-entoplastron.

Character optimisation: DELTRAN: Kinosternidae (0->1); ACCTRAN: Chelydroidea (0->1).

Character 240 (Evers & Benson [2018]: character 235). Plastron, hyo-hypoplastra contact: 0 = contact between hyo-hyoplastra absent or reduced; 1 = extensive contact between hyo-hyoplastra (even for those taxa with plastral kinesis).

Character optimisation: Unambiguous: Xinjiangchelyidae+++ (0->1), total-group Chelonioidea (1->0); DELTRAN: *Araripemys barretoi* (1->0), crown-group Pelomedusoides (1->0); ACCTRAN: crown-group Pleurodira (1->0), crown-group Chelidae (0->1).

Character 241 (modified from Evers & Benson [2018]: character 236): Plastron, hyo-hypoplastra serrations: 0 = serrations on the lateral and medial margins absent or weakly developed; 1 = strong serrations present along the surfaces that face other bones, but serrations are absent along the margin of the central fontanelle and the lateral contact area of hyo- and hypoplastro; 2 = strong serrations along all margins but the anterolateral margin of the hyoplastra and the posterlateral margin of the hypoplastra present, giving these elements a 'star-shaped' appearance.

Character optimisation: Unambiguous: total-group Chelonioidea (0->1), (*Desmatochelys* ++ *Protostega*) (1->2), *Dermochelys coriacea* (1->0), (*Puppigerus* + *Eochelone*) (1->0).

Character 242 (Evers & Benson [2018]: character 237). Axillar and inguinal notches: 0 = deep U or V-shaped axillar and inguinal notches; 1 = very shallow axillar and inguinal notches, and long lateral edges.

Character optimisation: DELTRAN: Protostegidae (0->1), Dermochelyidae (0->1); ACCTRAN: Protostegidae+++ (0->1), total-group Cheloniidae (1->0).

Character 243 (Evers & Benson [2018]: character 238). Entoplastron: 0 = present; 1 = absent.

Character optimisation: Unambiguous: Kinosterninae (0->1); DELTRAN: *Dermochelys coriacea* (0->1); ACCTRAN: Dermochelyidae (0->1).

Character 244 (Evers & Benson [2018]: character 239). Entoplastron, anterior entoplastral process: 0= present, medial contact of epiplastra absent; 1 = absent, medial contact of epiplastra present.

Character optimisation: DELTRAN: *Kallokibotion*+++ (0->1), *Eileanchelys waldmanni* (0->1); ACCTRAN: *Australochelys*+++ (0->1), *Kayentachelys aprix* (1->0).

Character 245 (Evers & Benson [2018]: character 241). Entoplastron, distinct posterolateral process: 0 = present; 1 = absent.

Character optimisation: DELTRAN: (*Kayentachelys*+*Eileanchelys*)+++ (0->1); ACCTRAN: *Australochelys*+++ (0->1).

Character 246 (modified from Evers & Benson [2018]: characters 240 & 242): Entoplastron, shape of the entoplastron: 0 = 'dagger-shaped', with dorsoventrally thick anterior end and long posterior process that extends along the dorsal surface of the plastron and sometimes reaches the mesoplastra; 1 = plate like and diamond-shaped or hexagonal in ventral view, with all margins of subequal length; 2 = T-shaped or triangular, i.e. entoplastron has a mediolaterally expanded anterior end and a progressively narrowing posterior process; 3 = strap like and V-shaped, with posterolateral processes diverging from the midline of the plastron.

Character optimisation: Unambiguous: total-group Chelonioidea (1->2), crown-group Chelydridae (1->2), Trionychidae (1->3), (*Judithemys* ++ *Sinemys*) (1->2); DELTRAN: Paracryptodira+++ (0->1), *Kallokibotion bajazidi* (0->1); ACCTRAN: *Chubutemys*+++ (0->1), *Meiolania planiceps* (1->0).

Character 247 (new character): Entepiplastron: 0 = absent, entoplastron and epiplastra are separate elements; 1 = present, entoplastron is fused with epiplastra, resulting in a laterally extremely expanded entepiplastron wings.

Character optimisation: Unambiguous: *Calcarichelys gemma* (0->1); DELTRAN: (*Protostega* + *Archelon*) (0->1); ACCTRAN: (*Ocepechelon* ++ *Protostega*) (0->1).

Character 248 (Evers & Benson [2018]: character 243). Entoplastron, suture with hyoplastra: 0 = tightly sutured; 1 = lightly sutured to almost absent contact between both.

Character optimisation: Unambiguous: Americhelydia (0->1), total-group Dermatemydidae (1->0), Trionychidae (0->1), *Araripemys barretoi* (0->1), (*Judithemys* ++ *Sinemys*) (0->1).

Character 249 (modified from Evers & Benson [2018]: character 244): Epiplastra, shape: 0 = epiplastra squarish in shape and forming parts of the anterior plastral lobe; 1 = epiplastra elongate, become narrower posteriorly along the anterolateral margin of the hyoplastron, and with gently convex lateral margin; 2 = epiplastra are laterally strongy expanded to a wing-like shape; 3 = epiplastra rod-like and anteriorly as narrow as posteriorly, with concave lateral margin.

Character optimisation: Unambiguous: total-group Chelonioidea (0->1), Protostegidae (1->2), total-group Chelydridae (0->2), Trionychidae (0->3), *Araripemys barretoi* (0->1); DELTRAN: (*Kirgizemys hoburensis* + *Kirgizemys dmitrievi*) (0->1), *Judithemys sukhanovi* (0->1); ACCTRAN: (*Judithemys* ++ *Sinemys*) (0->1), Sinemydidae (1->0).

Character 250 (Evers & Benson [2018]: character 245). Epiplastra, very thick anterior lip in dorsal view: 0 = present; 1 = absent.

Character optimisation: Unambiguous: Testuguria (1->0), *Chelonoidis* sp. (0->1).

Character 251 (Evers & Benson [2018]: character 246). Hyoplastra, contacts of axillary buttresses: 0 = absent to slightly contacting peripherals only; 1 = peripherals and costal 1.

Character optimisation: Unambiguous: total-group Dermatemydidae (0->1), *Chrysemys picta* (0->1), Testuguria (0->1), *Chelonoidis* sp. (1->0), total-group Pleurodira (0->1); DELTRAN: *Glyptops plicatulus* (0->1); ACCTRAN: Paracryptodira (0->1).

Character 252 (Evers & Benson [2018]: character 247). Hyoplastra, axillary buttresses: 0 = present; 1 = ossified axillary buttresses absent.

Character optimisation: Unambiguous: *Platysternon megacephalum* (0->1), *Chelonoidis* sp. (0->1), Trionychidae (0->1); DELTRAN: total-group Chelonioidea (0->1), crown-group Chelydridae (0->1); ACCTRAN: Americhelydia (0->1), Kinosternoidea (1->0).

Character 253 (Evers & Benson [2018]: character 248). Hyoplastra, termination of axillary buttresses: 0 = terminates on peripheral 1 or 2; 1 = terminates on peripheral 3; 2 = terminates on peripheral 4 or 5 level. This character is scored as inapplicable for turtles without axillary buttresses (ch. 247.1).

Character optimisation: Unambiguous: Durocryptodira (0->1), Kinosternidae (1->2), Testudinidae (1->0), crown-group Pleurodira (0->1), *Elseya dentata* (1->0); DELTRAN: *Carettochelys insculpta* (0->2), Pleurosternidae (0->1), *Meiolania planiceps* (0->1); ACCTRAN: *Meiolania*+++ (0->1), Xinjiangchelyidae+++ (1->0), crown-group Trionychia (0->2).

Character 254 (Evers & Benson [2018]: character 249). Mesoplastron: 0 = present; 1 = absent.

Character optimisation: DELTRAN: Xinjiangchelyidae+++ (0->1), crown-group Pelomedusoides (1->0), *Meiolania planiceps* (0->1); ACCTRAN: *Meiolania*+++ (0->1), total-group Pelomedusoides (1->0), Paracryptodira (1->0).

Character 255 (Evers & Benson [2018]: character 250). Number of mesoplastra: 0 = two; 1 = one. This character is scored as inapplicable when mesoplastra are absent (ch. 249.1).

Character optimisation: -.

Character 256 (Evers & Benson [2018]: character 251). Mesoplastron, medial contact of mesoplastra: 0=present, or virtually present when a central plastral fonta- nelle is present, absence of contact between hyoplastron and hypoplastron; 1 = absent, partial contact between hyoplastron and hypoplastron present.

Character optimisation: DELTRAN: crown-group Pelomedusoides (0->1), *Kallokibotion bajazidi* (0->1); ACCTRAN: *Chubutemys*+++ (0->1), Paracryptodira (1->0).

Character 257 (Evers & Benson [2018]: character 252). Hypoplastra, contacts of inguinal buttresses: 0 = absent to slightly contacting peripherals; 1 = peripheral and costal 5; 2 = peripheral, costals 5 and 6; 3 = peripherals and costal 4.

Character optimisation: Unambiguous: *Baptemys wyomingensis* (0->1), *Chrysemys picta* (0->1), total-group Pleurodira (0->1), *Chelus fimbriatus* (1->3), *Chelodina* (1->0), *Araripemys barretoi* (1->0); DELTRAN: *Geoclemys hamiltonii* (0->1), *Gopherus polyphemus* (0->1), Pleurosternidae (0->1); ACCTRAN: Testuguria (0->1), (*Testudo* + *Chelonoidis*) (1->0), Paracryptodira (0->1).

Character 258 (Evers & Benson [2018]: character 253). Hypoplastra, termination of inguinal buttresses: 0 = peripheral 8; 1 = peripheral 7; 2 = peripheral 6.

Character optimisation: Unambiguous: *Platysternon megacephalum* (1->2), *Chelonoidis* sp. (0->2), *Kallokibotion bajazidi* (0->2); DELTRAN: *Macrochelys temminckii* (0->1), Kinosternidae (0->1), *Emys orbicularis* (0->1), *Geoclemys hamiltonii* (0->1), *Carettochelys insculpta* (0->1), *Chelus fimbriatus* (0->1), *Chelodina* (0->1), *Araripemys barretoi* (0->1); ACCTRAN: Cryptodira (0->1), total-group Dermatemydidae (1->0), *Chrysemys picta* (1->0), Testudinidae (1->0), *Adocus beatus* (1->0), total-group Chelidae (0->1), *Phrynops geoffroanus* (1->0), *Elseya dentata* (1->0).

Character 259 (Evers & Benson [2018]: character 254). Xiphiplastra, distinct anal notch: 0 = absent; 1 = present.

Character optimisation: Unambiguous: *Dermatemys mawii* (0->1), Testudinoidea (0->1), *Emys orbicularis* (1->0), crown-group Pleurodira (0->1).

Character 260 (modified from Evers & Benson [2018]: character 255): Xiphiplastra, shape of xiphiplastra: 0 = triangular, trapezoidal, or rectangular plate-like element; 1 = anteroposterior elongate rods.

Character optimisation: Unambiguous: Protostegidae+++ (0->1), (*Santanachelys* ++ *Rhinochelys*) (1->0), *Puppigerus camperi* (1->0), crown-group Chelydridae (0->1).

Character 261 (modified from Evers & Benson [2018]: character 255): Xiphiplastra, articulation with hypoplastron: 0 = the xiphiplastra articulate with the hypoplastra along an anteriorly facing margin, forming a mediolaterally broad suture; 1 = the xiphiplastra have an elongate anterolateral process articulating along the posterolateral margin of the hypoplastron, resulting in an oblique suture, and the hypoplastra extend posteriorly along the anteromedial margin of the xiphiplastra.

Character optimisation: Unambiguous: total-group Chelonioidea (0->1), crown-group Chelydridae (0->1); DELTRAN: *Ordosemys* sp. IVPP V12092 (0->1), *Sinemys lens* (0->1); ACCTRAN: Sinemydidae (0->1), *Dracochelys bicuspis* (1->0).

Character 262 (modified from Evers & Benson [2018]: character 255): Xiphiplastra, posteriorly in contact with one another, often sutured along the midline and forming a plastral lobe: 0 = present; 1 = absent.

Character optimisation: DELTRAN: crown-group Chelonioidea (0->1), (*Puppigerus* ++ *Ctenochelys*) (1->0); ACCTRAN: *Corsochelys*+++ (0->1), (*Argillochelys* ++ *Puppigerus*) (1->0).

Character 263 (Evers & Benson [2018]: character 256). Plastral scutes: 0 = present; 1 = absent.

Character optimisation: Unambiguous: crown-group Trionychia (0->1); DELTRAN: (*Protostega* + *Archelon*) (0->1), Dermochelyidae (0->1), *Allopleuron hoffmanni* (0->1); ACCTRAN: (*Ocepechelon* ++ *Protostega*) (0->1), *Corsochelys*+++ (0->1), (*Erquelinnesia* ++ *Lepidochelys*) (1->0).

Character 264 (Evers & Benson [2018]: character 257). Plastral scutes, midline sulcus: 0 = straight; 1 = distinctly sinuous, at least for part of its length.

Character optimisation: Unambiguous: Xinjiangchelyidae (0->1), *Xinjiangchelys wusu* (1->0); DELTRAN: *Adocus beatus* (0->1); ACCTRAN: total-group Trionychia (0->1).

Character 265 (Evers & Benson [2018]: character 258). Gular, number of gulars: 0 = one pair of scutes; 1 = only one scute.

Character optimisation: Unambiguous: total-group Pleurodira (0->1), *Pleurosternon bullockii* (0->1).

Character 266 (Evers & Benson [2018]: character 259). Extragulars: 0 = present; 1 = absent.

Character optimisation: Unambiguous: Durocryptodira (0->1), *Araripemys barretoi* (0->1), (*Judithemys* ++ *Sinemys*) (0->1).

Character 267 (Evers & Benson [2018]: character 260). Extagulars, medial contact: 0 = absent; 1 = present, contacting one another anterior to gular(s); 2 = present, contacting one another posterior to gular(s).

Character optimisation: Unambiguous: *Chelus fimbriatus* (0->2), *Chelodina* (0->1).

Character 268 (Evers & Benson [2018]: character 261). Extragulars, anterior plastral tuberosities: 0 = present; 1 = absent.

Character optimisation: DELTRAN: (*Kayentachelys*+*Eileanchelys*)+++ (0->1); ACCTRAN: *Australochelys*+++ (0->1).

Character 269 (Evers & Benson [2018]: character 262). Extragulars, restricted to epiplastra: 0 = present; 1 = absent, extragulars reach the entoplastron.

Character optimisation: Unambiguous: *Chelus fimbriatus* (0->1); DELTRAN: *Proganochelys quenstedti* (0->1); ACCTRAN: *Proganochelys quenstedti* (0->1).

Character 270 (Evers & Benson [2018]: character 263). Intergulars: 0 = absent; 1 = present.

Character optimisation: Unambiguous: Kinosterninae (0->1), *Dermatemys mawii* (0->1); DELTRAN: *Eretmochelys imbricata* (0->1), (*Chelonia* + *Natator*) (0->1); ACCTRAN: total-group Chelonioidea (0->1), (*Caretta* ++ *Lepidochelys*) (1->0).

Character 271 (Evers & Benson [2018]: character 264). Humerals, number of pairs: 0 = one pair present; 1 = two pairs present, subdivided by a plastral hinge.

Character optimisation: Unambiguous: Kinosterninae (0->1).

Character 272 (Evers & Benson [2018]: character 265). Humerals, humero-pectoral sulcus: 0 = restricted to hyoplastra; 1 = crossing the posterior portion of ento- plastron.

Character optimisation: Unambiguous: *Emys orbicularis* (0->1), *Geoclemys hamiltonii* (0->1), *Chelus fimbriatus* (0->1), *Podocnemis* (0->1); DELTRAN: *Chelydra serpentina* (0->1), *Baptemys wyomingensis* (0->1), *Adocus beatus* (0->1); ACCTRAN: Chelydroidea (0->1), *Dermatemys mawii* (1->0), total-group Trionychia (0->1).

Character 273 (Evers & Benson [2018]: character 266). Pectorals: 0 = present; 1 = absent.

Character optimisation: Unambiguous: Kinosternoidea (0->1).

Character 274 (Evers & Benson [2018]: character 267). Pectorals, antero-posteriorly developed: 0 = present; 1 = absent, very short antero-posterior development.

Character optimisation: Unambiguous: *Chrysemys picta* (0->1), Testuguria (0->1), *Chelonoidis* sp. (1->0); DELTRAN: *Adocus beatus* (0->1); ACCTRAN: total-group Trionychia (0->1).

Character 275 (Evers & Benson [2018]: character 268). Abdominals: 0 = present; 1 = absent.

Character optimisation: Unambiguous: *Toxochelys* sp. (0->1), Kinosternidae (0->1).

Character 276 (Evers & Benson [2018]: character 269). Abdominals, medial contact to one another: 0 = present; 1 = absent. This character is scored as inapplicable for turtles that lack abdominals.

Character optimisation: Unambiguous: total-group Chelydridae (0->1), *Araripemys barretoi* (0->1).

Character 277 (Evers & Benson [2018]: character 270). Anals: 0 = only cover parts of the xiphiplastra; 1 = overlap anteromedially onto the hypoplastra.

Character optimisation: Unambiguous: *Toxochelys* sp. (0->1), crown-group Chelydridae (0->1), Xinjiangchelyidae (0->1).

Character 278 (Evers & Benson [2018]: character 271). Inframarginals: 0 = present; 1 = absent.

Character optimisation: Unambiguous: *Toxochelys* sp. (0->1), crown-group Pleurodira (0->1), (*Sinemys* ++ *Kirgizemys*) (0->1); DELTRAN: *Adocus beatus* (0->1); ACCTRAN: total-group Trionychia (0->1).

Character 279 (Evers & Benson [2018]: character 272). Number of inframarginals: 0 = more than two pair present, plastral scales do not contact marginals; 1 = two pair present (axillaries and inguinals), limited contact between plastral scales and marginals present. This character is scored as inapplicable when inframarginals are absent (ch. 271.1).

Character optimisation: Unambiguous: *Peritresius martini* (0->1), Kinosternidae (0->1), *Chelonoidis* sp. (1->0); DELTRAN: *Chrysemys picta* (0->1), Testuguria (0->1); ACCTRAN: Testudinoidea (0->1), *Platysternon megacephalum* (1->0).

Character 280 (Evers & Benson [2018]: character 273). Cervical ribs: 0 = large cervical ribs present; 1 = cervical ribs reduced or absent.

Character optimisation: Unambiguous: Testudines (0->1).

Character 281 (Evers & Benson [2018]: character 274). Cervicals, position of the transverse processes: 0 = middle of the centrum; 1 = anterior end of the centrum.

Character optimisation: Unambiguous: crown-group Pleurodira (1->0); DELTRAN: Sinemydidae/Macroabenidae+++ (0->1), *Archelon ischyros* (1->0), (*Desmatochelys lowii* + *Desmatochelys padillai*) (1->0), *Meiolania planiceps* (0->1), *Proganochelys quenstedti* (0->1); ACCTRAN: Sinemydidae/Macroabenidae+++ (0->1), (*Desmatochelys* ++ *Protostega*) (1->0), *Protostega gigas* (0->1), *Meiolania planiceps* (0->1), *Proganochelys quenstedti* (0->1).

Character 282 (Evers & Benson [2018]: character 275). Cervicals, posterior cervicals with strongly developed ventral keels: 0 = absent or slightly developed in all vertebrae; 1 = present, more developed on posterior vertebrae.

Character optimisation: Unambiguous: *Platysternon megacephalum* (1->0), *Chelonoidis* sp. (1->0), *Chelus fimbriatus* (0->1); DELTRAN: Durocryptodira (0->1), *Adocus beatus* (0->1), *Leyvachelys cipadi* (0->1), (*Judithemys* ++ *Sinemys*) (0->1); ACCTRAN: Xinjiangchelyidae+++ (0->1), crown-group Trionychia (1->0), total-group Pleurodira (1->0), Sandownidae (0->1).

Character 283 (Evers & Benson [2018]: character 276). Cervicals, cervical 8 centrum significantly shorter than cervical 7: 0 = absent; 1 = present.

Character optimisation: Unambiguous: *Chelus fimbriatus* (0->1); DELTRAN: Cryptodira (0->1), (*Judithemys* ++ *Sinemys*) (0->1), *Sinemys lens* (1->0); ACCTRAN: Xinjiangchelyidae+++ (0->1), total-group Pleurodira (1->0), (*Sinemys gamera* + *Sinemys lens*) (1->0).

Character 284 (Evers & Benson [2018]: character 277). Cervicals, triangular diapophyses: 0 = absent; 1 = present.

Character optimisation: Unambiguous: crown-group Pleurodira (0->1), *Chubutemys copelloi* (0->1); DELTRAN: *Glyptops plicatulus* (0->1); ACCTRAN: Paracryptodira (0->1).

Character 285 (Evers & Benson [2018]: character 278). Cervicals, central articulations of cervical vertebrae: 0 = articulations not formed, cervical vertebrae am- phicoelous or platycoelous; 1 = articulations formed, cervical vertebrae procoelous or opisthocoelous.

Character optimisation: Unambiguous: Sinemydidae/Macroabenidae+++ (0->1), *Corsochelys halinches* (1->0), Thalassochelydia (1->0), *Meiolania planiceps* (0->1).

Character 286 (Evers & Benson [2018]: character 279). Cervicals, articulation between cervical 8 and dorsal vertebrae 1: 0 = 8 (dorsal 1; 1 = 8) dorsal 1; 2 = vertebrae articulate along zygapophyses only.

Character optimisation: Unambiguous: Trionychidae (1->2), *Adocus beatus* (1->0); DELTRAN: *Ctenochelys* (1->0); ACCTRAN: (*Ctenochelys* ++ *Peritresius*) (1->0).

Character 287 (Evers & Benson [2018]: character 280). Cervicals, biconvex cervical vertebrae in the middle of the neck: 0 = absent; 1 = present.

Character optimisation: Unambiguous: *Dermatemys mawii* (1->0), total-group Trionychia (1->0); DELTRAN: *Dracochelys bicuspis* (1->0); ACCTRAN: Sinemydidae (1->0).

Character 288 (Evers & Benson [2018]: character 281). Cervicals, biconvex cervical vertebra in the middle of the neck: 0 = cervical 2; 1 = cervical 3; 2 = cervical 4; 3 = cervical 5.

Character optimisation: Unambiguous: crown-group Chelidae (0->3); DELTRAN: Kinosternidae (2->1), crown-group Pleurodira (2->0); ACCTRAN: Kinosternoidea (2->1), total-group Pleurodira (2->0).

Character 289 (Evers & Benson [2018]: character 282). Cervicals, biconcave cervical vertebrae: 0 = absent; 1 = present.

Character optimisation: Unambiguous: Testudinoidea (0->1), crown-group Chelidae (0->1).

Character 290 (Evers & Benson [2018]: character 283). Cervicals, double articulation between cervical 5 and 6: 0 = absent; 1 = present.

Character optimisation: Unambiguous: *Chrysemys picta* (0->1).

Character 291 (Evers & Benson [2018]: character 284). Cervicals, double articulation between cervical 6 and 7: 0 = absent; 1 = present.

Character optimisation: Unambiguous: Cryptodira (0->1); DELTRAN: Protostegidae+++ (1->0); ACCTRAN: total-group Chelonioidea (1->0).

Character 292 (Evers & Benson [2018]: character 285). Cervicals, central articulation between cervical 6 and 7: 0 = cervical 6 concave (cervical 7 convex; 1 = platycoelous, cervical 6 II cervical 7.

Character optimisation: DELTRAN: crown-group Chelonioidea (0->1); ACCTRAN: *Corsochelys*+++ (0->1).

Character 293 (Evers & Benson [2018]: character 286). Cervicals, double articulation between cervical 7 and 8: 0 = absent; 1 = present.

Character optimisation: Unambiguous: Cryptodira (0->1); DELTRAN: Protostegidae (1->0), *Toxochelys* sp. (1->0); ACCTRAN: total-group Chelonioidea (1->0), *Corsochelys*+++ (0->1).

Character 294 (Evers & Benson [2018]: character 287). Cervicals, height versus length of centra and neural arch: 0 = total height of centra and neural arch longer than the anteroposterior length of the cervical centra; 1 = total height of centra and neural arch much shorter than the anteroposterior length of the cervical centra.

Character optimisation: Unambiguous: Thalassochelydia (1->0); DELTRAN: Xinjiangchelyidae+++ (0->1), Dermochelyidae (1->0), *Puppigerus camperi* (1->0), *Corsochelys*

halinches (1->0); ACCTRAN: Paracryptodira+++ (0->1), *Corsochelys*+++ (1->0), total-group Cheloniidae (0->1), (*Puppigerus* + *Eochelone*) (1->0).

Character 295 (Evers & Benson [2018]: character 288). Cervicals, modification of neural arch on cervical 8: 0 = neural arch without modificiation of postzygapophyses; 1 = neural arch with postzygapophyses pointing anteroventrally.

Character optimisation: Unambiguous: Cryptodira (0->1); DELTRAN: Protostegidae+++ (1->0), *Kirgizemys hoburensis* (0->1); ACCTRAN: total-group Chelonioidea (1->0), (*Kirgizemys hoburensis* + *Kirgizemys dmitrievi*) (0->1).

Character 296 (Evers & Benson [2018]: character 289). Cervicals, postzygapophyses united in midline: 0 = absent; 1 = present.

Character optimisation: Unambiguous: total-group Chelidae (0->1), *Phrynops geoffroanus* (1->0).

Character 297 (Evers & Benson [2018]: character 290). Cervicals, ventral process on cervical 8: 0 = absent; 1 = present, well developed (as tall or taller than the height of the centrum).

Character optimisation: Unambiguous: *Peritresius martini* (0->1), *Chelonoidis* sp. (1->0), *Judithemys sukhanovi* (0->1); DELTRAN: Chelydroidea (0->1), Emydidae (0->1), Testuguria (0->1), *Adocus beatus* (0->1); ACCTRAN: Cryptodira (0->1), total-group Chelonioidea (1->0), *Platysternon megacephalum* (1->0), crown-group Trionychia (1->0).

Character 298 (Evers & Benson [2018]: character 291). Cervicals, shape of central articulation of cervicals 7 and 8: 0 = as high as wide; 1 = much wider than high.

Character optimisation: DELTRAN: crown-group Chelonioidea (0->1), *Toxochelys* sp. (0->1); ACCTRAN: total-group Chelonioidea (0->1), Protostegidae (1->0).

Character 299 (Evers & Benson [2018]: character 292). Ribs, length of first dorsal rib: 0 = long, extends full length of first costal and may even contact peripherals distally; 1 = intermediate, in contact with well-developed anterior bridge buttresses; 2 = intermediate to short, extends less than halfway across first costal.

Character optimisation: Unambiguous: Sinemydidae/Macroabenidae+++ (0->2), Sinemydidae (2->0); DELTRAN: *Jurassichelon oleronensis* (2->1); ACCTRAN: Thalassochelydia (2->1).

Character 300 (Evers & Benson [2018]: character 293). Ribs, contact of dorsal ribs 9 and 10 with costals: 0 = present; 1 = absent.

Character optimisation: Unambiguous: Kinosternidae (0->1).

Character 301 (Evers & Benson [2018]: character 294). Dorsal rib 10: 0 = long, spanning full length of costals and contacting peripherals distally; 1 = short, not span- ning father distally than pelvis.

Character optimisation: DELTRAN: Sinemydidae/Macroabenidae+++ (0->1), *Glyptops plicatulus* (0->1); ACCTRAN: *Chubutemys*+++ (0->1), Xinjiangchelyidae (1->0).

Character 302 (Evers & Benson [2018]: character 295). Dorsals, anterior articulation of the first dorsal centrum: 0 = faces at most slightly anteroventrally; 1 = faces strongly anteroventrally.

Character optimisation: Unambiguous: Cryptodira (0->1), total-group Chelonioidea (1->0), crown-group Cheloniidae (0->1).

Character 303 (Evers & Benson [2018]: character 296). Caudals, tail club: 0 = present; 1 = absent.

Character optimisation: DELTRAN: Paracryptodira+++ (0->1), *Kayentachelys aprix* (0->1); ACCTRAN: *Australochelys*+++ (0->1), *Meiolania planiceps* (1->0).

Character 304 (Evers & Benson [2018]: character 297). Caudals, anterior caudal centra: 0 = amphicoelous; 1 = procoelous or platycoelous; 2 = opisthocoelous.

Character optimisation: Unambiguous: *Macrochelys temminckii* (1->2); DELTRAN: Sinemydidae/Macroabenidae+++ (0->1), *Meiolania planiceps* (0->2); ACCTRAN: *Chubutemys*+++ (0->1), *Meiolania planiceps* (1->2).

Character 305 (Evers & Benson [2018]: character 298). Caudals, posterior caudal centra: 0 = amphicoelous; 1 = procoelous or platycoelous: 2 = opisthocoelous.

Character optimisation: Unambiguous: Testudines (2->1), *Platysternon megacephalum* (1->2), *Chelonoidis* sp. (1->2); DELTRAN: *Meiolania*+++ (0->2), crown-group Chelydridae (1->2); ACCTRAN: *Chubutemys*+++ (0->2), total-group Chelydridae (1->2).

Character 306 (Evers & Benson [2018]: character 299). Caudals, chevrons: 0 = present on nearly all caudal vertebrae: 1 = absent, or only poorly developed, along the posterior caudal vertebrae.

Character optimisation: Unambiguous: *Toxochelys* sp. (1->0), *Platysternon megacephalum* (1->0), *Chelonoidis* sp. (1->0); DELTRAN: Sinemydidae/Macroabenidae+++ (0->1), crown-group Chelydridae (1->0); ACCTRAN: Paracryptodira+++ (0->1), total-group Chelydridae (1->0).

Character 307 (Evers & Benson [2018]: character 300). Caudals, tail ring: 0 = absent; 1 = present.

Character optimisation: Unambiguous: *Meiolania planiceps* (0->1).

Character 308 (Evers & Benson [2018]: character 301). Scapula, anterodorsal ridge of acromion: 0 = present; 1 = absent.

Character optimisation: DELTRAN: (*Kayentachelys*+*Eileanchelys*)+++ (0->1); ACCTRAN: *Australochelys*+++ (0->1).

Character 309 (Evers & Benson [2018]: character 302). Scapula, ventral ridge of acromion: 0 = present; 1 = absent developed proximally near glenoid.

Character optimisation: Unambiguous: *Chubutemys*+++ (0->1).

Character 310 (Evers & Benson [2018]: character 303). Scapula, horizontal ridge of acromion: 0 = well-developed, coracoid foramen present; 1 = reduced, only developed along distal portion of acromion.

Character optimisation: DELTRAN: (*Kayentachelys*+*Eileanchelys*)+++ (0->1); ACCTRAN: *Australochelys*+++ (0->1).

Character 311 (Evers & Benson [2018]: character 304). Scapula, glenoid neck on scapula: 0 = absent; 1 = present.

Character optimisation: Unambiguous: total-group Pleurodira (0->1), *Pelomedusa subrufa* (1->0); DELTRAN: *Glyptops plicatulus* (0->1); ACCTRAN: Paracryptodira (0->1).

Character 312 (Evers & Benson [2018]: character 305). Scapula, lamina between the dorsal process of the scapula and the acromion: 0 = well developed; 1 = reduced; 2 = absent.

Character optimisation: Unambiguous: Paracryptodira+++ (0->2), *Kallokibotion bajazidi* (0->1).

Character 313 (Evers & Benson [2018]: character 306). Scapula, internal angle between acromion process and scapular process ≥110°: 0 = absent; 1 = present.

Character optimisation: Unambiguous: Protostegidae+++ (0->1), (*Caretta* ++ *Lepidochelys*) (1->0).

Character 314 (Evers & Benson [2018]: character 307). Coracoid, coracoid vs humerus length: 0 = shorter than humerus; 1 = at least as long as humerus.

Character optimisation: Unambiguous: Protostegidae+++ (0->1).

Character 315 (Evers & Benson [2018]: character 308). Coracoid, foramen: 0 = present; 1 = absent.

Character optimisation: DELTRAN: (*Kayentachelys*+*Eileanchelys*)+++ (0->1); ACCTRAN: *Australochelys*+++ (0->1).

Character 316 (Evers & Benson [2018]: character 309). Cleithrum: 0 = present; 1 = absent.

Character optimisation: Unambiguous: Sinemydidae/Macroabenidae+++ (0->1); DELTRAN: *Ctenochelys* (1->0); ACCTRAN: (*Ctenochelys* ++ *Peritresius*) (1->0).

Character 317 (Evers & Benson [2018]: character 310). Cleithrum, contact with carapace: 0 = present; 1 = osseous contact with carapace absent.

Character optimisation: DELTRAN: (*Kayentachelys*+*Eileanchelys*)+++ (0->1); ACCTRAN: *Australochelys*+++ (0->1).

Character 318 (Evers & Benson [2018]: character 311). Pelvis, pelvis-shell attachment: 0 = pelvis-shell attachment by ligaments; 1 = pelvis attached by strong sutural contact of the ischium and pubis with the plastron, and illium with the carapace.

Character optimisation: Unambiguous: crown-group Pleurodira (0->1).

Character 319 (Evers & Benson [2018]: character 312). Pelvis, thyroid fenestra: 0 = coalescent; 1 = two separated fenestra completely or partially separated.

Character optimisation: Unambiguous: *Peritresius martini* (0->1), *Chelonoidis* sp. (1->0); DELTRAN: *Protostega gigas* (1->0), Dermochelyidae (1->0), (*Puppigerus* ++ *Lepidochelys*) (1->0), *Toxochelys* sp. (1->0), crown-group Chelydridae (1->0), *Staurotypus* (1->0), *Platysternon*

megacephalum (1->0), crown-group Trionychia (1->0), crown-group Pleurodira (1->0); ACCTRAN: Paracryptodira+++ (1->0), *Archelon ischyros* (0->1), total-group Cheloniidae (0->1), (*Puppigerus* ++ *Lepidochelys*) (1->0), Kinosternoidea (0->1), *Staurotypus* (1->0), Testudinoidea (0->1), *Platysternon megacephalum* (1->0), *Adocus beatus* (0->1).

Character 320 (Evers & Benson [2018]: character 313). Ilium, elongated iliac neck: 0 = absent; 1 = present.

Character optimisation: DELTRAN: (*Kayentachelys*+*Eileanchelys*)+++ (0->1); ACCTRAN: *Australochelys*+++ (0->1).

Character 321 (Evers & Benson [2018]: character 314). Ilium, iliac scar: 0 = extends from costals onto the peripherals and pygal; 1 = positioned on costals only.

Character optimisation: -.

Character 322 (Evers & Benson [2018]: character 315). Ilium, shape of the ilium articular site on the visceral surface of the carapace: 0 = narrow and pointed poste- riorly; 1 = oval.

Character optimisation: -.

Character 323 (Evers & Benson [2018]: character 316). Ilium, posterior notch in acetabulum: 0 = absent; 1 = present.

Character optimisation: DELTRAN: Kinosternidae (0->1), *Baptemys wyomingensis* (0->1); ACCTRAN: Kinosternoidea (0->1), *Dermatemys mawii* (1->0).

Character 324 (Evers & Benson [2018]: character 317). Ilium, thelial process: 0 = absent; 1 = present.

Character optimisation: Unambiguous: *Emarginachelys cretacea* (0->1), Kinosternidae (0->1), total-group Trionychia (0->1); DELTRAN: *Apalone spinifera* (1->0); ACCTRAN: Trionychinae (1->0).

Character 325 (Evers & Benson [2018]: character 318). Pubis, lateral process: 0 = small, poorly developed, columnar; 1 = well developed and flat.

Character optimisation: Unambiguous: crown-group Trionychia (0->1); DELTRAN: Protostegidae+++ (0->1), Kinosternoidea (0->1), *Plesiochelys bigleri* (0->1); ACCTRAN: Americhelydia (0->1), total-group Chelydridae (1->0), Plesiochelyidae (0->1).

Character 326 (Evers & Benson [2018]: character 319). Pubis, epipubis process: 0 = osseus or calcified; 1 = cartilaginous or absent.

Character optimisation: Unambiguous: *Kinosternon suburum hippocrepis* (0->1); DELTRAN: Testudines (0->1), *Puppigerus camperi* (1->0), (*Oligochelone* + *Erquelinnesia*) (1->0), *Macrochelys temminckii* (1->0), Kinosternoidea (1->0); ACCTRAN: Paracryptodira+++ (0->1), (*Erquelinnesia* ++ *Lepidochelys*) (1->0), crown-group Cheloniidae (0->1), Chelydroidea (1->0), *Chelydra serpentina* (0->1).

Character 327 (Evers & Benson [2018]: character 320). Ischium, ischial contacts with plastron: 0 = contact via a large central tubercle; 1 = contact via two separate ischial processes.

Character optimisation: DELTRAN: (*Kayentachelys*+*Eileanchelys*)+++ (0->1); ACCTRAN: *Australochelys*+++ (0->1).

Character 328 (Evers & Benson [2018]: character 321). Ischium, lateral process of ischium or metischial process: 0 = absent; 1 = present.

Character optimisation: Unambiguous: Protostegidae+++ (1->0), crown-group Trionychia (1->0), crown-group Pleurodira (1->0); DELTRAN: (*Puppigerus* ++ *Ctenochelys*) (0->1), Kinosternidae (1->0); ACCTRAN: (*Argillochelys* ++ *Puppigerus*) (0->1), Kinosternoidea (1->0).

Character 329 (Evers & Benson [2018]: character 322). Hypoischium: 0 = present; 1 = absent.

Character optimisation: DELTRAN: (*Kayentachelys*+*Eileanchelys*)+++ (0->1); ACCTRAN: *Australochelys*+++ (0->1).

Character 330 (Evers & Benson [2018]: character 323). Humerus, ectepicondylar foramen: 0 = in a channel; 1 = only a groove.

Character optimisation: Unambiguous: (*Puppigerus* ++ *Lepidochelys*) (0->1), *Eochelone brabantica* (1->0); DELTRAN: Americhelydia (0->1), crown-group Chelonioidea (1->0), Emydidae (0->1), *Geoclemys hamiltonii* (0->1), *Testudo* (0->1), Trionychidae (0->1), total-group Pleurodira (0->1); ACCTRAN: Testudines (0->1), *Corsochelys*+++ (1->0), *Platysternon megacephalum* (1->0), Testudinidae (1->0), *Testudo* (0->1), total-group Trionychia (1->0), Trionychidae (0->1).

Character 331 (Evers & Benson [2018]: character 324). Humerus, proximal articular surface of humerus: 0 = with shoulder on preaxial side, upturned; 1 = without shoulder, not upturned.

Character optimisation: Unambiguous: Trionychidae (0->1), *Podocnemis* (0->1); DELTRAN: (*Desmatochelys* ++ *Protostega*) (0->1), crown-group Chelonioidea (0->1), *Chelodina* (0->1); ACCTRAN: Protostegidae+++ (0->1), *Corsochelys halinches* (1->0), Chelodininae (0->1).

Character 332 (Evers & Benson [2018]: character 325). Humerus, lateral process of humerus: 0 = abuts caput humeri; 1 = slightly separated from caput humeri; 2 = located distal to caput humeri but along proximal end of shaft; 3 = located at middle of humeral shaft.

Character optimisation: Unambiguous: total-group Chelonioidea (0->2), Dermochelyidae (2->3), *Corsochelys halinches* (2->1); DELTRAN: (*Protostega* + *Archelon*) (2->3), *Ctenochelys* (2->0), *Sinemys gamera* (0->1); ACCTRAN: (*Ocepechelon* ++ *Protostega*) (2->3), (*Ctenochelys* ++ *Peritresius*) (2->0), (*Sinemys gamera* + *Sinemys lens*) (0->1).

Character 333 (Evers & Benson [2018]: character 330). Humerus, prominent anterior projection of lateral process: 0 = absent; 1 = present.

Character optimisation: Unambiguous: Dermochelyidae (0->1).

Character 334 (new character): Humerus, distal articulation: 0 = articular surface forms distinct trochlea; 1 = rounded epiphyseal surface without clearly defined articulation facets.

Character optimisation: Unambiguous: Protostegidae+++ (0->1), *Erquelinnesia gosseleti* (1->0), *Geoclemys hamiltonii* (0->1), crown-group Trionychia (0->1); DELTRAN: Thalassochelydia (0->1), *Elseya dentata* (0->1), crown-group Pelomedusoides (0->1); ACCTRAN: total-group Pleurodira (0->1), total-group Chelidae (1->0), *Elseya dentata* (0->1).

Character 335 (Evers & Benson [2018]: character 331). Humerus, length of the humerus versus the width of the proximal end: 0 = two times or less the width of the proximal end: 1 = more than two times the width of the proximal end.

Character optimisation: Unambiguous: Paracryptodira+++ (0->1).

Character 336 (Evers & Benson [2018]: character 332). Humerus, scar for Muscle latissimus dorsi and Muscle teres major: 0 = located anterior to humeral shaft; 1 = located at middle of shaft.

Character optimisation: Unambiguous: crown-group Cheloniidae (0->1); DELTRAN: (*Protostega* + *Archelon*) (0->1); ACCTRAN: (*Ocepechelon* ++ *Protostega*) (0->1).

Character 337 (Evers & Benson [2018]: character 333). Humerus, humerus length vs femur length: 0 = shorter than femur; 1 = longer than femur.

Character optimisation: Unambiguous: total-group Chelonioidea (0->1).

Character 338 (Evers & Benson [2018]: character 334). Ulna, contact with radius through rugosity and ridge: 0 = absent; 1 = present.

Character optimisation: Unambiguous: total-group Chelonioidea (0->1); DELTRAN: *Santanachelys gaffneyi* (1->0), *Dermochelys coriacea* (1->0); ACCTRAN: (*Santanachelys* + *Notochelone*) (1->0), Dermochelyidae (1->0).

Character 339 (Evers & Benson [2018]: character 335). Radius, curves towards anterior: 0 = absent; 1 = present.

Character optimisation: Unambiguous: Protostegidae (0->1).

Character 340 (Evers & Benson [2018]: character 336). Manus, phalangeal formula of the manus: 0 = most digits with two shortenened phalanges: 1 = most digits with three elongated phalanges.

Character optimisation: DELTRAN: Xinjiangchelyidae+++ (0->1), *Testudo* (1->0), *Gopherus polyphemus* (1->0); ACCTRAN: Paracryptodira+++ (0->1), Testudinidae (1->0), *Chelonoidis* sp. (0->1).

Character 341 (Evers & Benson [2018]: character 337). Manus, rigid articulations in 1st and 2nd digit: 0 = absent; 1 = present.

Character optimisation: Unambiguous: Protostegidae+++ (0->1); DELTRAN: *Santanachelys gaffneyi* (1->0); ACCTRAN: (*Santanachelys* + *Notochelone*) (1->0).

Character 342 (Evers & Benson [2018]: character 338). Manus, rigid articulations in 3rd to 5th digit: 0 = absent; 1 = present.

Character optimisation: Unambiguous: total-group Chelonioidea (0->1).

Character 343 (Evers & Benson [2018]: character 339). Manus, flippers: 0 = absent; 1 = short flippers present; 2 = elongate flippers present. Joyce (2007: ch 134, Manus C).

Character optimisation: DELTRAN: Trionychidae (0->1), *Carettochelys insculpta* (0->2); ACCTRAN: crown-group Trionychia (0->1), total-group Carettochelyidae (1->2).

Character 344 (Evers & Benson [2018]: character 340). Ulnare, size of the ulnare vs the intermedium: 0 = smaller than intermedium: 1 = nearly as large as intermedium; 2 = much larger than intermedium.

Character optimisation: DELTRAN: Testudines (0->1), Protostegidae+++ (1->2), *Allopleuron*+++ (2->1), *Carettochelys insculpta* (1->2), *Meiolania planiceps* (0->1); ACCTRAN: *Australochelys*+++ (0->1), total-group Chelonioidea (1->2), total-group Cheloniidae (2->1), total-group Carettochelyidae (1->2), Xinjiangchelyidae (1->0).

Character 345 (new character): Size of proximal carpals vs. distal carpals: 0 = proximal carpals are of similar size with respect to distal carpals; 1 = proximal carpals are much larger than distal carpals.

Character optimisation: Unambiguous: Protostegidae+++ (0->1), *Emarginachelys cretacea* (0->1), Emysternia (0->1), crown-group Trionychia (0->1), *Podocnemis* (0->1); DELTRAN: *Sternotherus* (0->1), *Chelus fimbriatus* (0->1), Chelodininae (0->1), *Xinjiangchelys wusu* (0->1); ACCTRAN: Kinosternidae (0->1), crown-group Chelidae (0->1), *Phrynops geoffroanus* (1->0), Xinjiangchelyidae (0->1).

Character 346 (new character): Relative lengths of manual phalanges on the 3rd and 4th digit: 0 = the 1st phalanx is longer than or equally long as the 2nd phalanx; 1 = the 2nd phalanx is longer than the 1st phalanx. This character is scored as inapplicable when the manus digits only have two phalanges (i.e. the second phalanx is an ungual).

Character optimisation: Unambiguous: *Elseya dentata* (0->1), *Araripemys barretoi* (0->1), *Podocnemis* (0->1); DELTRAN: *Allopleuron*+++ (0->1), *Carettochelys insculpta* (0->1); ACCTRAN: total-group Cheloniidae (0->1), total-group Carettochelyidae (0->1).

Character 347 (new character): 3rd phalanx on 5th manual digit: 0 = absent; 1 = present.

Character optimisation: Unambiguous: Chelodininae (1->0); DELTRAN: Xinjiangchelyidae+++ (0->1), crown-group Chelonioidea (1->0), *Emys orbicularis* (1->0), *Apalone spinifera* (1->0),

Carettochelys insculpta (1->0), crown-group Pelomedusoides (1->0); ACCTRAN: Paracryptodira+++ (0->1), *Corsochelys*+++ (1->0), Emydidae (1->0), (*Apalone* + *Petrochelys*) (1->0), total-group Carettochelyidae (1->0), total-group Pelomedusoides (1->0).

Character 348 (new character): Longest digit in the manus: 0 = 4th digit; 1 = 3rd digit. This character is scored as inapplicable when the 3rd and 4th digits are equally long.

Character optimisation: DELTRAN: crown-group Chelonioidea (0->1); ACCTRAN: *Corsochelys*+++ (0->1).

Character 349 (Evers & Benson [2018]: character 341). Pes, number of digits: 0 = five; 1 = four.

Character optimisation: DELTRAN: *Macrochelys temminckii* (0->1), *Testudo* (0->1), *Gopherus polyphemus* (0->1); ACCTRAN: total-group Chelydridae (0->1), Testudinidae (0->1), *Chelonoidis* sp. (1->0).

Character 350 (Evers & Benson [2018]: character 342). Manus and Pes, flattening of carpals and tarsal elements: 0 = absent; 1 = present.

Character optimisation: Unambiguous: total-group Chelonioidea (0->1).

Character 351 (Evers & Benson [2018]: character 343). Manus and Pes, hyperphalangy manus digits 4 and 5, pes digit 4: 0 = absent; 1 = present.

Character optimisation: Unambiguous: Trionychidae (0->1).

Character 352 (modified from Evers & Bensons [2018]: character 344): Femur, femoral trochanters: 0 = distinct, and separated from one another; 1 = connected by a ridge.

Character optimisation: Unambiguous: Protostegidae+++ (0->1).

Character 353 (modified from Evers & Bensons [2018]: character 344): Femur, intertrochanteric ridge: 0 = ridge is low and concave, creating a notch between the major and minor trachenter; 1 = ridge is high and obliterates intertrochanteric notch, and the proximal surface of the trochanters and their connecting ridge forms a continuous surface. This character is scored as inapplicable when an intertrochanteric ridge is absent (character 352.0)

Character optimisation: Unambiguous: *Dermochelys coriacea* (0->1), crown-group Cheloniidae (0->1).

Character 354 (new character): Femur, connection between femoral head surface and the major trochanter: 0 = the femoral head and major trochanter have distinct proximal surfaces separated by a deep notch; 1 = the femoral head surface slopes toward the major trochanter and forms a continuous proximal surface with it.

Character optimisation: Unambiguous: Protostegidae+++ (0->1); DELTRAN: *Meiolania*+++ (1->0), *Geoclemys hamiltonii* (0->1), Thalassochelydia (0->1); ACCTRAN: *Chubutemys*+++ (1->0), Testuguria (0->1), Angolachelonia (0->1).

Character 355 (Evers & Benson [2018]: character 345). Tibia, tibial pit for pubotibialis and flexor tibialis internus muscles: 0 = absent; 1 = present.

Character optimisation: Unambiguous: *Natator depressus* (0->1); DELTRAN: (*Puppigerus* ++ *Ctenochelys*) (0->1); ACCTRAN: (*Argillochelys* ++ *Puppigerus*) (0->1).

S3.4 Character-taxon matrix

The following character-taxon matrix was used for the phylogeny presented in section 4 of this thesis. Because this matrix is the latest version developed during my PhD, I post this matrix below in nexus format, which can be directly used for analysis in PAUP* or TNT when copied into a text file.

```
#NEXUS

BEGIN TAXA;
      TITLE Taxa;
      DIMENSIONS NTAX=96;
      TAXLABELS

      Rhinochelys_pulchriceps Santanachelys_gaffneyi Bouliachelys_suteri
Notochelone_costata Ocepechelon_bouyai Desmatochelys_lowii
Desmatochelys_padillai Rhinochelys_nammourensis Chelosphargis_advena
Calcarichelys_gemma Protostega_gigas Archelon_ischyros
Dermochelys_coriacea Eosphargis_breineri Lepidochelys_olivacea
Caretta_caretta Chelonia_mydas Eretmochelys_imbricata Lepidochelys_kempii
Natator_depressus Puppigerus_camperi Argillochelys_cuneiceps
Allopleuron_hofmanni Nichollsemys_baieri Eochelone_brabantica
Corsochelys_halinches Procolpochelys_charlestonensis Peritresius_martini
Ctenochelys_sp Cabindachelys_landanensis Oligochelone_rupelensis
Erquelinnesia_gosseleti Toxochelys_sp Solnhofia_parsoni
Jurassichelon_oleronensis Portlandemys_mcdowelli Plesiochelys_planiceps
Plesiochelys_etalloni Plesiochelys_bigleri Sandownia_harrisi
Brachyopsemys_tingitana Leyvachelys_cipadi Angolachelys_mbaxi
Chelydra_serpentina Macrochelys_temminckii Sternotherus Staurotypus
Kinosternon_suburum_hippocrepis Dermatemys_mawii Baptemys_wyomingensis
Emarginachelys_cretacea Chrysemys_picta Emys_orbicularis
Geoclemys_hamiltonii Testudo Gopherus_polyphemus Chelonoidis_sp.
Platysternon_megacephalum Apalone_spinifera Pelodiscus_sinensis
Lissemys_punctata Carettochelys_insculpta Allaeochelys_libyca
Chelus_fimbriatus Phrynops_geoffroanus Elseya_dentata Chelodina
Araripemys_barretoi Podocnemis Pelomedusa_subrufa
Ordosemys_sp._IVPP_V12092 Judithemys_sukhanovi Annemys_levensis
Annemys_latiens Annemys_sp._IVPP_V18106 Xinjiangchelys_wusu
Xinjiangchelys_radiplicatoides Dracochelys_bicuspis Kirgizemys_hoburensis
Kirgizemys_dmitrievi Sinemys_gamera Sinemys_lens Meiolania_planiceps
Chubutemys_copelloi Eubaena_cephalica Arundelemys_dardeni
Pleurosternon_bullockii Glyptops_plicatulus Kallokibotion_bajazidi
Eileanchelys_waldmanni Kayentachelys_aprix Australochelys_africanus
Proganochelys_quenstedti Adocus_beatus Petrochelys_kyrgyzensis
Galianemys_whitei
      ;
END;


BEGIN CHARACTERS;
      TITLE  Character_Matrix;
      DIMENSIONS  NCHAR=355;
      FORMAT DATATYPE = STANDARD GAP = - MISSING = ? SYMBOLS = "  0 1 2 3
4 5";
      MATRIX

Rhinochelys_pulchriceps 0010000011110021100011 0-0100--
0000000001100001110000000000 1-0111010100001020(1 2)10201000011-
12110110100110011111200?0000020100000000010202000002200210-
12100001100001100 1-1??????00110(0
1)1?000000??????????????????????????????????????????????????????????????
????????????????????????????????????????????????????????????????????????
????????????????????????????????

Santanachelys_gaffneyi  0010000?101100?11?00110-?100--
000000000??00001110?00000000?-01110101 0?001021?1020?0?0011-
121?0100000110011012001 00?0???10?????0????2???0000???????-
1200?0011??????????1??????00???0????????00000?0??0-000101001?00-11100-
01000-??01-0000?01100-0110112012?01-1--
```

```
0?0010?0??????????????????11?????????????0????????1?1????111021????0??--
0???1?1??2-??0101101021010?1?1???

Bouliachelys_suteri     0011000?0010001??000110-0100--
000?00?0?1?0?0011100000000001-011101010000102001020101001 1-
121101011001100111120010000020100010000010202100002210210-
121000111000011101-
1??????0011011100?001?????????????????????????????????????????????????????
????????????????????????????????????????????????????????????????????????
??????????????????????????????????????????

Notochelone_costata     ????000?101100 2??0?0110-0?00--
00?000???1?0000111000?0000001-?1110100010010???102000?0?11-
121?0100000110011112 00???1???0??0000010010200000?02210210-
121000011000011001-
1??????0011?????????????????????????????????????????????????????????????
????????????????????????????????????????????????????????0?????????????????
??????????????????????????????????????

Ocepechelon_bouyai      0000?010101101?0000011???100--
000000001?10000111100000?0000-011101000?00?0202102 0?0?001011210020-
100110010-1200000?0120100???????002??00000221?1??-1210?0111?000????1-
1?????????????????????????????????????????????????????????????????????????
????????????????????????????????????????????????????????????????????????
??????????????????????????????????????

Desmatochelys_lowii     0010001010110011000 1111?0100--
000000000100000111010000000001-01110101 0?001020110201000011-
121?000110011001??12001000???0???0?001?00021200000221021?-
121000111000011101-1?????0001?0???????100000-0100-0101010??001111100-
010???01?1-?100001110-021011201?101-1--0-
011000?????????????????10110111 20??0010000201?????111021111-0?1--
001110111201101111110 2?????1?101?

Desmatochelys_padillai  0010??1?101100?10011?????100--
000000000?100001110??000?000??01110???0?001020110 2??0?001??1211010010 02?0
011112001 00?01201000???????02?2?0000???????-1210?0011?00011101-
1??????00???0???0?00?00000-0100-0001010??00??1110??0?0???01?1-
???0001?????????????????????????????????????????????1011011120000010000 2?1
0?????111021 1?????????????????12011??11?11021????1?????

Rhinochelys_nammourensis      0010??00111100?10?00?????100--
000000000???0001110??0?0?????????????????????????????????1??????0?????????
????????1000?????????????????????????????????????????????????????????????
???????????00010-0??0-000101001?00-10-00-00000-?????1100?01110-
0110112012101-1--0-
0010?????????????????????????????????01?????????????????0???????????1?
2??1?11111102 1010?1?????

Chelosphargis_advena    0010??0?10110011 10?01???0100--
00000000???00?01110?0000??0?1-
01???????????0?0?10????0?01??1??1?????????????120??0???020?????????????
??????????1?0-1210?0011????????1-???????0011?????0??010?010-???0-
0001???01000-11100-01?00-??01-110?0?11?000110112012101-1--0-
0110?????????????????????????????????????????????????????0?????????????
????????????????????????

Calcarichelys_gemma     1--
1??0?101?00???0?011???????????00?000?????0?1110?00000???1-(0
1)1??0??????????02?2102010000 1??12110?0?00???0010-
1200100?00201000?0?????020??0000022??210-
1210?0011?0001100??1?????0011?????????0?010-?110-000101?01000-11100-
```

```
01?00-1-?1-110?0011?0-0110112112101-1--0-011?0001---
?0?0000?????????????????????????201?????????????????0????????1?????????????????
????????????

Protostega_gigas  1--0??00101000??0?00?????100--
000000?0???00001110?001000001-011100000???102?21?21?0?0?1??1?1102?-102-
1011??1?0?100?0?0?1000???????02???000?????2??-
1200?0011?000??????1??????000100??00?0001-010-0100-000101001000-11110-
00000-1-11----0--1110-0210112112101-1--0-01101----------------
111?011120????10000201011110111021111-001--
00111011130111111111021010010101?

Archelon_ischyros 1--0??00101000?00?001????100--
00000?000100001111O?001000001-011100000????021210???0?0?1011211020-102-
?011??1200100?0?0?10?0????????02???000????????-
??????????000??????1??????0001?0???????11-010-0100-000101001000-11110-
00000-1-11----0--1110-0210112112101-1--0-01101----------------
101?011?????????0??201?11110111021111-011--
00111011130111111111021010010101?

Dermochelys_coriacea    1--10100101000001-00100-0000--
00000000010010011101000100010-0101010000011021210100000011-1210021-002--
0000-1200000(0 1)00001030-01-001020200000021011l-1211?0111000011101-1----
--0001011--0-2011--0-?0110--00-1--1-00----------0---1--1-------111-?0011-
----1101-1--0-01111----------------1111011120001100001200-0111101110211l1-
001--0011-0101311101001110210O1?1?1110

Eosphargis_breineri     1--1??0?101000??1?00?????100--
0000000?????0001110?0001?0011-010101010????02??10???000?1??1200020-002-
?1000-1200000?00?0111????????0????0110???????-1211?011?????????1-
1?????????????????????1-
01??0???????00??0?????11111?????????????????????11??011?????????????????111
1----------------
?11?01????????0?0?????????????????1????01????11?0101311l?1???110?1????1?1
01?

Lepidochelys_olivacea   1--10101101000101000110-
0101100000000001000011110000000l110-0101000211011021210201000011-1210020-
100201100-1201100(0 1)0000110000010010201001002210210-121010111000011001-
1??????011111110010010001O-0110-00010000?000-1110110100110111-1100?11110-
0100112011101-1--0-01110001---00(0
1)0000000111101112000111000120111111101110201l1-001--
00111011120111110111010111010101110

Caretta_caretta   1--10101101000101000110-
0101100000000001000011110000000l110-1101100210011021210201000(0 1)011-
1210020-101-11100-12011000000011-0000110102020010022102l1-
121010111000011101-1??????000111110010010001O-0110-000101000000-
1110110100100111-1100011110-0100112011101-1--0-01110001---(0 1)0(0
1)0000000111101112000111000120111111101110201l1-001--
00111011120111110111010111010101110

Chelonia_mydas    1--1010?101100101000110-
0101110000000001000011110000000011120010100021000102121010100001(0
1)11210020-102-00000-12011001010011100011101020000l0020-0111-
121010111000011001-1??????00111101000001000l0-0110-0(0 1)0101001000-
1110100100110111-1100001110-0100112011101-1--0-01110001---10(0
1)000000011110111200011100(0 1)12011111101110211l1-001--
00111011120111110111011101O1?1110

Eretmochelys_imbricata  1--10101101100101000110-
0101100000000001000011110000000l1120010100021101102121020l000011-1210020-
```

```
100211100-120110000010111000010010200001002210111-121010111000011001-
1??????000011110000010000-0110-0(0 1)0101001000-1110110100110101-
1100001110-0100112011101-1--0-01110001---10(0
1)000000011110111200011100012011111110111021111-001--
001110111201111101110111010101110

Lepidochelys_kempii     1--10101101100101000110-
010111000000000100001111100001001112-010100021101102121020100011-1210020-
100211000-1201100(0 1)000011000001101020200100221011O-121010111000011001-
1??????001110110000010000-0110-00010000?000-1110110100110111-1100011110-
0100112011101-1--0-01110001---00(0
1)000000011110111200011100012011111110111020111-001--
001110111201111101110111010101110

Natator_depressus 1--10100101100101000110-
010111000000000100001111000000011120010100021101102021010100011-1210020-
100211100-120110010000110000010010202001002210211-121010111000011001-
1??????001011010010010000-0110-000101001000-1110110100110101-1100001110-
0100112011101-1--0-01110001---10(0
1)000000011110111200011100012011111110111021111-001--
001110111201?110111011010101111

Puppigerus_camperi      1--10000101100101000110-
110111000000000100001111000000001110-010100021000102121020100001-1200020-
100201100-120110000100111000?0102020010022001l0-121100111000011001-
1??????011110110000010000-0??0-000101001000-0--0120100100111-1100001100-
0000112011101-1--0-
0010000??????????000??111101112000l?0000120???????111021111-
001??0010?111120110l?0?1101?????1?1??1

Argillochelys_cuneiceps 1--10000101100101000110-
010111000000000100001111000000001111-010100021000102121020100001011210020-
1002?1100-120110010100110000010010202001002210111-121100110000011001-
1??????001110110O?001??????????????????????????????????????????????????????
???????0????????????????????????????????1111011120001110001?010??????????
??????????????????????????????????????????

Allopleuron_hofmanni    1--100001011001?0000110-
00011?000000000100100111010000011l0-
010100021?00102111011100101011210000110O2?1100-
1201???10000110000010000212001002210111-
121000111000011000l1?????0000???10000001-010-0100-000101001000-
1111??0100111-01-1100001110-0100112011101-1--0-01111----------------
111101112000111000120101111011l021111-011--
00111010120110110111011101010??1?

Nichollsemys_baieri     1--1000?1011001?0010110-
010101000010000100000111O?000000010-011100010000102121020100001l-
021?0000100010110-1201100?000011000101l?00202001002210111-
121010111?00011001-
1??????0001?????0?00??????????????????????????????????????????????????????
???????????????????????????????????????????????????????????????????????????
??????????????????????????????????????????

Eochelone_brabantica    1--10000101100101000110-
110111000000000100001111000000000000-010101011000102121020100001011210020-
100211000-120110000100112000l?0102000010012001l1-121000111000011001-
1??????000110110000010000-0110-0?010?001000-1110120100110111-1100001100-
0000112011101-1--0-
0110?????????????????????11??1??????????0??20???1???111021????0?1???0?????01
201101???110?1???01?1011
```

```
Corsochelys_halinches
      ??????????101100?0111?0??????????0000?0??????????????????????????
??????????2???????0?101121???0?10???00?0-
120010010?1???0000001?02?20000121?210-12??00?11100011101-
1?????????????????????????000-0??0-00??01001??0-11001001?011????????????110-
01??1??011101-1--0-?????????????????????11?00--------
0?00?????????1110211????1??00??????01011????????2???????????

Procolpochelys_charlestonensis     1--
1000?101100101?001????10110000000000100001111000000?1110-
010100021?0?1021210???00001??12?0020-?01-01100-
1201100?????11???????????2???010022?????-121??0111????????1-
1??????0101111?00?00100000-0??0-100100001000-10-01201000-??1??11????1110-
010011201??01-1--0-
0111?????????????????????11??1?????01?????1?????1???????2111?????????????????01
20110?????????????????101?

Peritresius_martini
      ????????????????????????????????????????????????????????????????????
??????????????????????????????????????????????????????????????????????????
??????????????????????????????????????????????00110-0010-010101001000-
????120100110101-1000001110?010??????1101-1-
?0?011000?????000000?01??1??1???????1???11201?????????????????011??001??1
??????????????????????????

Ctenochelys_sp    1--
1010?10110111000011??1101110000000001000001110?000001111-
010101111?00102?2102010000101121000011000100011120110010100110??00???02?
??01001210111-121000111?00011111-1??????0011111?00?00100110-0010-
010101001000-1110100100110101-1100001110-0100112011101-1--0-01100001---
?000000?00111??10120001110001201015?????11?21110-001--
001??1?1100110110?1101?????1????1

Cabindachelys_landanensis     1--
1000?1011011?100012??1101110000000?????000011100000001110-
01010002100?1021210201000011-121?0000100010000-
1201100?0?001100?000?0??????01002200111-
12100011100001100??1?????????????????????00110-
0????????1????????????????????????????????????????????????????????????????
??????????????????????????????????????????????????????????????????????????
??????????????????

Oligochelone_rupelensis
      ????????????????????????????????????????????????????????????????????
??????????????????????????????????????????????????????????????????????????
??????????????????????????????????????????????00000-0??0-000101001000-
11101?0100110111-1100001110-0100112011101-1--0-
0111?????????????????1???1??????11??0?1?0???????111021?11-
0?1??0010???0120110?????????????????

Erquelinnesia_gosseleti 1--
10?0?1011011???001???0?0???00?0??????00?0?1111?0000?1110-
01?1000210???021?1020??0001??1???0?????????0?????????????????????????
??????????????????????????????????????????0101101100000100000-0??0-0(0
1)0101001000-1100120100011??11-1000001l?0-010????????01-1--0-
011?????????????????????1?1?11???0011???01?0??????????????????011??0010???01
2001?1?????????????1?1010

Toxochelys_sp
      0011000?10110111001011???10101000000001l?000011101000000011-
01010001(0
1)000102121020000001011210000010001000111200100000001000?000?0?0202001000
```

```
200111-12100011000011001-1??????1001(0 1)11100100100000-0110-
010101001000-11000-0100110111-11000011(0 1)0-0100112011101-1--0-
001000???1??0???1011011?1011120??0????1?0101??001110?00???00?--
0???11110200?01101010?0010?1?0-00

Solnhofia_parsoni
      0011000?1011011??1001111010101000001?00?000?0011100000000100-
1111100200001020210201011010112100001001-00011011100???100201110(0
1)0000110200000000100110-121000111000011001-1??????011100111111010000000-
0????0?0101001?00010-01-01002?01?1-0100?01100-100????????1001--
10000000?????2000?000??110?00--------0?0????1?1????111120????0??--
??0?1?1?00011?0?01000?0???0000-1?

Jurassichelon_oleronensis     0010001?10110110001011110100--
000010000100000111010000000001-
011100000000102121020001101011110011010011001101201000102001000100011002120
2000000200110-111000011100011001-1?????????????????????0000??0100-
0001010???0?????????10???????????0????1?0-100???10???1001--
??????00??????0?0?00???11??00--------
0?0??1?????????????????????????????1?????????????????????????0-1?

Portlandemys_mcdowelli  0010001?1011011??00011110?00--
???0??000100?0011101000000001-
0101000000000102?2102010110101111000001000100?101201?0010100100010001(0
1)00212000000200110-121000011000011001-
1??????000000?1001010?????????????????????????????????????????????????????
????????????????????????????????????????????????????????????????????????????
??????????????????????????????????????????

Plesiochelys_planiceps  ???0000?1011011?00?011110100--
0?0?2?00?100?0?11?0100?000001-
011100000000102?2102010110101121001000001100110110110010120100000000111020
2000000210110-121000011100011001-
1??????000000110110101?????????????????????????????????????????????????????
????????????????????????????????????????????????????????????????????????????
??????????????????????????????????????????

Plesiochelys_etalloni   0011000?1011011?00?011110100--
000010000100001111010000000001-
010100000000102021020101101011 2?00100000110010-
1200?????????????000000111020200000210100-
121000011100011001?1?????0000000101101000000?0100-000101001?0100--01-
0000100011-0100000(0 1)00-1000111000?10?1--
1000000010010000000000??????????????????????010?????1111??????0?1--
0?????1??00110?001000???????????

Plesiochelys_bigleri    ??????????????????0?011110100--
0000???0010000?1???????000?1-
?101?????????020210201011010112100100?001100110110 0?00100?010000000111020
2000000200010-111000011100011001-1??????????????????????00000-0??0-
00010100100100--0??0000100011-01000?0(0 1)00-100011100011 0?1--
1?000000100100000000000??????????????????????????????1111?0??????1??0?1??1?
?000??0??0?????????????0-10

Sandownia_harrisi
      0111001?1011011?000012110101010000000?0?000011100000011110-
010100021000102022020001101011 11?0001101--00110121100000010-
0?010001010201000-00000010-111000111000011001-
1??????01010??1111011?????????????????????????????????????????????????????
????????????????????????????????????????????????????????????????????????????
??????????????????????????????????????????
```

```
Brachyopsemys_tingitana
      0111000?10110110100011??0101010000000000?000011110000000110-
0101100210011O2?2102000110l??1?1?0000101-
1001111211100001001O?0?0?????0201?---0?2??0?0-
12100011l?0001110011??????010100?1111011?????????????????????????????????
????????????????????????????????????????????????????????????????????????
????????????????????????????????????????????????????????

Leyvachelys_cipadi      0001??1?10110110100012???100--
000000000010000111010000000110-0111000?1?0?10202202O?01101011?1?0000?01-
?00111121110O?00?0-010????????0??1?---000011?0-1210?0111?000?????-
1??????01???0?????0?1?????00??0-?0????001?0??0--00-
0????????1??1?????0??????????????????????1?????????????????????111?01?????
???1?0??201???????????2?0???0??--0?0????1000?1?0???000???????????
Angolachelys_mbaxi
      ???1000?101101?0100012???10111000000010?00001101?0000?1110-
?101?0021????02?22020?011010?1?10020-?01-1-0?0-
1210000?0?1010??????????02?2??000???????-1210?0111?00011001-
1??????0101?????????????????????????????????????????????????????????????
????????????????????????????????????????????????????????????????????????
??????????????????????????????????????????
Chelydra_serpentina     1--
10000001000110020111011010100000000001000011101001000001-
0101010001001021220201000010112l?000110001000l0120010(0
1)10100100001011010200000000101010-
12110011000001100011??????001101100000010000O-01012000001001000-10-00-
01002?0101-1100001100-?000112012101-1--0-01100001-1-
0010?011001111011120010111010201111200111020011-001--
00011?1100001?00010001001-???????
Macrochelys_temminckii  1--
10000101000110020111001011100000000000000011101001000000-
0101000001001021220201001010112l?000110001000l0120010(0
1)10110100000011010200000000-0110-
12100011100001100011??????001101100000010000O-01011000001001000-10-00-
01000-010001100001100-1000112012101-1--0101100001-1-
00?000110011110111200101110102011122001110200l1-001--
000011111000?1?00010001001-10?????
Sternotherus      1--1000010100011012012O-11(0
1)11100100100001000011101000010000-
0101010211001021220200000010112l?0011001-
1000101200100000001020010010002100000101000l0-12110011000101100011------
000000?0100111001101010110000101002111l0--00-01000-0111-110000000111001--
??-010021--0100000001-1-11-1-1-00111110111100l011101021-111110111020011-
011--11101011000?1?00010001101-000????
Staurotypus 1--1000010100(0 1)110120120-0111110010010010(0
1)010011100000010000-
0101010211001021220201000010112l?00111002000011120010000120102011001010l1
?0000000-0010-12110011000101100011------
000100?0100101001101010110001010021O(0 1)?0--00-01000-0111-
11?000000111000111010100l1--0100000001-1-00-1-1-00111110111100l011101021-
111?10111020011-001--11101011000012000100012????????????
Kinosternon_suburum_hippocrepis     1--10000101000110120120-
11111100100100001010011101001010000-
0101010101001021210200000010112l?00111002000010120000001120100001011010210
0000000101010-12110011000100100011------
000100?00101110011010101100010100201100--00-01000-0111-110000000111001--
```

```
??-010021--0100000001-1-11-1-1-00111110111110???11101021-111110111020011-
011--11111011000?1?00010001????00?0-0?

Dermatemys_mawii  1--10000101(0 1)00110020120-
0101110000110000100001110100001000 20(0
1)10111010100102121010000001011 21?0011000210000-
120010000020100011000010 2(0 1)00000000-0010-12110011001------011------
000010?010010100000-010110001010011010 0--00-01000-0111-1100000000-
1000111000?1011--0010000001-1-100100000011110110-
0010111010201 11??10111020011-011--00101?11000?1?0001000?001-0000-0?

Baptemys_wyomingensis   1--1000?10110?110020120-
0101110000110000000000111010000100021010101010?00102121010000?00101121?001(
0 1)0002?000101200100001201120??????020000000010?1?0-121000111?1------
??1------1000 10?000001100110-0101100010100 1?00-0--00-010???0111-
1100000000-100011100011011--1?00000001-1-
0011000000 11?1?111???????????2?111??1?111020?11-011--
1???1?1????0??0??10001???????0-0?

Emarginachelys_cretacea 1--
1000?10110011002 01????10110000001000?0000011101000 0?00?2101010 1?10????021
?102010?001??121?0011?00210001011011 0?0????1?00?0?????020??000001??0?0-
121100110?0001100???------?????????????0011??01011??0???001?00-0--00-
?10??????1-1100001000-10001110?2?0??1--0?00000001-1-
00???010??11???111?????????????1?????11102?????0?1--
01????1???????0??1000?101-???0-0?

Chrysemys_picta   1--1000010110(0 1)110020110-
0101110000110010100001110100000000200101020011001021210200000010 1121?0011
000210000-120010010020101111000010200000000100010-121100110000011100011---
---0000101110000100000-0100-100101001000-0--00-01000-0101-1100000000-
100011100011011--1010000001-1-
0000100001111110111211101110102011111110111020011-011--
000111111000?1?00010001????000????

Emys_orbicularis  1--
1000010100011002011110101010000110000100001110100000000 0-
0101000001000021210100000010112 0?0011000210000-
120010000120100101001010200000000101011-121100110?0001100011------
0000?0???????100000-0100-100101001000-0--00-01000-0101-
1100001001010001110001001 1-?0100000001-1-
00100000??111101112101011101020111111?111020011-011--
00?11?1100001?00010001100-0000-0?

Geoclemys_hamiltonii    1--
1000010100011012011110111111000001000010100111010000000000-
0101021111000021210200000010112 1?0011000210001012001000002010310100101020
0000000100010-121100111100011000 11------000010?010000100110-0100-
100101001100-0--00-0100100111-1100000000-100011100001011--1110000001-1-
0010100001111110111210101110102011111110111020011-011--
000111110001 1?00010001????0000-1?

Testudo     1--1000010110011012011110100--
0000110000101001110100000000200101020001000020120100000010112 1?0011000200
000-120010010100100101001010200000000101010-121100110100011100011------
0000000000010100000-0100-100001001000-0--00-1100100111-1100000000-
100011100001001--0010000001-1-
0000100001111110111210101110102011111110111020011-011--
000111111000 01?00000001????100????

Gopherus_polyphemus     1--1000010110011002012 0-0100--0000110000(0
1)0000111010000100020010102100101002112010000010112 1?0010000210100-
```

```
1200100001001000-1100010220000000-1010-12110011010001100011------
0000100010000100000-0100-100001001000-0--00-1100100111-1100000000-
100011100001001--1010000001-1-
0000100001111101112101011101020111111010111020011-011--
0001111000001?00000001001-100????

Chelonoidis_sp.   1--10000101101(1 2)1012011110100--
0000110000000001110100000000200101021001000020120100000010112 1?0010000210
0011120010000100100 0-1001010220(0 1)00000101010-12110011010001110011-----
-0000000000000100000-0100-000001001100-0--00-0100100101-1100001000-
1000111000101-1--0210000001-1-
0000000000110101112101011100020111120011102 0011-001--
0001111000001?00010001001-00?????

Platysternon_megacephalum     1--10000101000(1
2)1100011100101110010000000001011101001000001-
0101010001001020220100000010112 1?0001000201001012011000002010000111101020
00000020-0110-12110011100000100 1-1------0000001(0 1)01001100000-0100-
000001001100-0--00-0100100101-1100001000-1000111000101-1--0210000001-1-
0000000000110101112101011100020111120011102 0011-001--
0001111000001?00010001101-00?0-0?

Apalone_spinifera 1--10100101101110120120-
1111111000010010001001111011001 0001-
1111120001011021220210000010112 1?0020101-10-10-
1200101101101000000110102010000001000 10-12000011100001100 1-1------
000100011100111-00120100-000101-1-001011000-0101--1--1-------11(0 1)0-
1000113013101-1--0-00001----1-----------11010120-0010111000201-
11110111020011-001--0011101110011?00010011100-0010-0?

Pelodiscus_sinensis     1--10100101101110120120-
1111111000010010001001111011001 0000-
1111120001011021220210000010112 1?0021101-10-10-
1200101101101000100110102010000001000 10-12000011100001100(0 1)11------
000100011100111-00120100-000101-1-001011000-0101--1--1-------1110-
10001130131-1-1----00001----------------110?0120-00?011100020--
1??10??????????????????????????0???????????101-0010-0?

Lissemys_punctata 1--10100101101110120120-
1111101000010010001001111011001 0000-
1111120000011021220210000010112 1?0021101-00-20-
1200101101101000000110102010000001000 10-12000011100001100001------
000?00???0?0011-00120100-000101-1-00100--00-0101--1--1-------1110-
1000113013101-1--0-00001----1-----------11010120-0010111000201-1--
10111020011-001--0111101110011?0??1001?101-001????

Carettochelys_insculpta 1--10100101100110120120-
1101110010010010100001111100000 10001-
0111101001011021020200 0?0110112 1?0021101-10-11(0
1)1200101101201130001110102010000101000 10-12100011100001100011------
000010111100110100120000-00010100000100--00-01000-1-11-------1000-
100011100010021--0100001----1---------??11010110-
0010111000201111110111020011-001--0111101000011?0001002211000000-0?

Allaeochelys_libyca     1--
1??0?1?110?1101201???11????00?0?10???1????1?????????????????????????????021
1202000001101121?0???10???0?11(0
1)1201??1101201130001?0010201?0001?10?010-
1210001110000110001 1?????????????????????????????????????????????????
????????????????????????????????????????????????????????????????????
??0????????????????????????????????????????????????
```

Chelus_fimbriatus 1--0101010110110(0 1)-20110-01011101--21000011-
0011111000000000-01010000001-00202300--000011-120?101000---0000-200-
000011321010120012002010000000100010-120001110-0010100011------
1001?0???????000111(0 3)0100-100001001100-0--00-01000-0101-1100000000-
100011100011011--3110000010211001000001-
1011111131000010100201011110111120011-1011100011011000001?00010001101-
0000-0?

Phrynops_geoffroanus 0110111010110110(0 1)-20111011011101--21000011-
0011101000000000-01010000001-00202300--000011-120?101000---0010-200-
000011321010120012102010000000101010-121001100-0011100011------
1001?0?10?100000000-0100-10010110110100--00-01000-0111-1100000000-
100011100011011--1010000010010000000001-
1000111131000010000201011110111120011-
1011100011011000001?00010001100??0000-0?

Elseya_dentata 01101110101101101-00111111011101--21000011-
0011101000000002011010000001-00202300--000011-120?101000---0000-200-
1000012010001200121020100000010010-1(1 2)1001110-00111001-1------
0010000100110000000??0100-100-01001?1110--00-010???1-11-1-00000000-
1000111000?1001--1010000010001?00?000001-
10?0111131000010?0020101??10111120011-1?11100??101??001??00010001110-
???0-0?

Chelodina 01101110101111110-20111001011101--21000011-0011101000000000-
01010000001-00202300--100011-120?101000---0010-200-
000011221000120012002010000000100010-121001100-00111001-1------
1001000000000000000130100-100-0100111110--00-01000-0111-1-00000000-
100011100011011--0110000010110000000001-
1000111131000010100201011110111120011-1011100011011110001?00010001100-
0000-0?

Araripemys_barretoi 1--11110101101110-
2011100101110000110010110001110100000000-??11??000?1-01202100--000011-
120?102100---0-00-200-???000001010120012102010000000100010-121001100-
00111001-1------1001000000000010011140100-100101001001010-00-01000-1-11-
1101001110-000011101111011--0110000011---000000101-
100?1111000000101002??01111011?20011-
1??????????11?00?1?0??1000101100000-0?

Podocnemis 1--11100101101110-
0012111101111000110000111001110100001100200211000000 1-11202300--100011-
120?101101---0000-200-1000002010001000121020100000010001 0-120000101-
0001100011------000000011000010000(0 1)30100-100101001101 00--00-01000-1-
11-1100000000-0000111000110101111010000010 01(0 1)001000001-
1000111100000010000201011110111120011-1011100011011100 11?00010001110-
0000-0?

Pelomedusa_subrufa 1--111001011011 10-20120-
0101110000110010110001110100001000200211 0-0---1-11202300--100011-
120?101000---0010-200-1000010010001210121020100000010100 0-121001110-
0011100011------0000?0?110000100000-0100-10010100110100--00-01000-1-11-
1100000000-0000111000110101111010000010010000000001-
1000111100000010000201011110111020011-1011100011011000 11?00010001000-
0000-0?

Ordosemys_sp._IVPP_V12092 0010000-
1011011?0010111?0?0101000?1?001?0?00011101000000000-
010102000?00102021011101(0
1)010111??00101002?00?101201?00100201?00??0011002?0?1000???1???-1110-
0011?000????1-
1???

```
????????????????????010?????????????????????????????????0??????????????????
??????????????????????????????????0??????????

Judithemys_sukhanovi
      ???1??0?101?01??0?101????101???0001?001000?00111??0?00?000??0101020
00?0??021210???0?001??121?00101000100010120010?0100100????????0????10000
10101?-1110-0111?000????1-1??????000100??????0?00000?0100-000101001?00-0-
-00-01001001?1-1100001000-1000112011?0001--0000000001-1?0000000(0
1)00?111011120(0 1)0001(0 1)0102?1011210111020?1-0?1--
00??1?1000001?0??1000?????00?0-??

Annemys_levensis  00110000101101l?00201110?101?10000200010(0
1)000011101000000000-
010102000?0??020210100000010111?0010?0001000??1101100001001000??01???020
000010???????1?110-0?11?00011001-1011?0?000000?100000000000-0100-
00010110110100--00-0100100111-1010101000-100011100010001--
000000010001000000000100?????????????????????0?00?????1110200101O?1--
?0?????000001?0?????????????0-0?

Annemys_latiens
      0010??1?101101??00201110?10????0?0???0????????01?1??0???0????????????
??????????101000?0010011??0?1??0???0??????0??0????????0?1????????2???00?0?
??????0(0 1)110-0?11?0001100?????????????????????????00000-0100-
00010110l?0(0 1)?0--00-0100100111-1(0 1)10101000-100011100010001--
000000010001000000000100?????????????????????????????????????0??--
???????000001?0?????????????????

Annemys_sp._IVPP_V18106
      0110001?10110110002011??0101010000200010100?11101000000000-
010102000000102021010100?0101110?00100000100010111011O0?0?201000?10111?021
0?00000101100-1110-0011100011001-
1?????????????????????????????????????????????????????????????????????????
????????????????????????????????????????????????????????????????????????
??????????????????????????????????????????

Xinjiangchelys_wusu
      0110?01010l101?00020?????101??000010001O?0000111O?0000??????01?1?2?
00????02111010002001??110?00101000100???1201100?0?201000???????0200?0000?
??????0(0 1)110-0111?00011001-1011???00????0?1????0000000-
0?0??00010110110(0 1)?0--00-0100100111-1100101000-100011100010001--
000000000001000000010000???0?-------
1?0?????????????????????????????????0?0001?0??1000010100000-0?

Xinjiangchelys_radiplicatoides
      0110??1?1011011?00?011????0???0?????0??????00111??00??0???????11???
??????02111010?0?0?101111?0?2??0???0-
?1012?0?00001201000?001???020000000201110-1110-0011000011001-
1????????0?1?????????100000-0100-000???101?00-0--00-0100100111-1100???000-
100011100010001--
000000010001000000001O0????????????????????0????????111?200101???????????
000001?????????????????0-0?

Dracochelys_bicuspis
      ???1000?101101??0??01????10101000O1?0?????000111010001?0001-
010100000?00?020?10101000010111?00101000100010120l?0??0?2010?????????02?
??0000??????710110-0?11?0001100??1??????000?00?0?0?0010000??1100-
000101001?00-10-00-0110101-0??1101?01100-1000????1??0001--
0000000?????????????????0111?110-
000001000?0010????01110200???0??????????0?0001?0???000????????????

Kirgizemys_hoburensis
      0011000?10110110001011111010101O?002000101O?0011101000000000-
```

```
01010200?001020?10100000010111?0010?000100010110010010100100001001??02?
0?10000101O?0-1111-0110?0001100011?????0001?0????????00000-0100-
000101101?00-0--00-010???0111-1100001000-100011201110001--0?00000001-
1?0000000(0 1)10?111?11120000011O??2?10??????????2???1-
0?1?????????0?0001?????????????????
```

```
Kirgizemys_dmitrievi
      ???1000?1011001?001?111??10101000020001000000111O?0000?0001-
000101000?00102021020?00001011?1?00100000?000????00100?0??01000??00???02?
0?1000?1110??-1111-0?1??00011101-
??????000100?000000?????????????????????????-
0??????????????????????????????20?1????????????????????????????????????
????????????????????????????????????????????????????????????????????
```

```
Sinemys_gamera
      01100?1?10110111002011??1101010??02100?000?0011???0??0?0??0-
0???????????1202201000000101110?00?000001000101201100l0?001000??00??0022
0?1000???????-1110-0111?00011001-
1?????????????????????00001?0???????1????100-10-0??010??????1-
?10???1????100???????1?00???00????0????1??????00?????????????????????
????????????????????????????001001?????????????????
```

```
Sinemys_lens
      0010??1?101101?100201????101??0??02?0000???00111??0000??0?????????0
???????20220100?0?1??1?0?00100000?00010110110??????10?0???????022??1000?
??????-1110-0111?0001100??1??????00?????????????0000??0100-000101001100-
10-00-0100101--1-1101001(0 1)00-1000112?1010001--
00001000???1??0?0000?10?1?0?????0??????????0???1?????????????0???????????
?????????1000????000????
```

```
Meiolania_planiceps     0000000010100010100011O-
000101000100110000000110010000000020010102100000102103110000(0
1)0101121?001(0 1)100000000-12001100000(0 1)11211100110020?0000000-
101010111-0111100001101-11111110000000000100000000-?100-00????001000-0--
00-?1????0101-0?00101100-00001100O?0011--
000000000001000????????0100011120000000000000?002201111000010101l--
00001??000000?000000010-0-0000-0?
```

```
Chubutemys_copelloi
      ???1000?101000?01?0011???10000000?000??00000011???0??000000-
011102000????0202101?000001??110?00110000000l?0100100O0?00110???????0020
??0000???????100-------????????1-
1?????????????????????00????0??????????0???0??????????0???????????0???????
?????????????????????????????????????????1?1?????????0?????0?????1110?
0??????????????????????????????????????
```

```
Eubaena_cephalica
      0000002?10100011002011???101110000100000000101110100000000l-
0101020001000021210100000011-
121?00101000?000101201100000201020??00???1210?0001010?110200-------
?00011011-
1??????0000?0???????0?????????????????????????????????????????????????
????????????????????????????????????????????????????????????????????
????????????????????????????????????????
```

```
Arundelemys_dardeni     0100001?1011001??020110-
1?01?1??0???0????0?10?1101000000001-
0101000000?0?02??10100000010111?00101000100011120l?0000000102001011100l0
?000000101110200-------0000????1-
1?????????????????????????????????????????????????????????????????????
????????????????????????????????????????????????????????????????????
????????????????????????????????????????
```

```
Pleurosternon_bullockii
      0110001?10110010010O1?1?1101110000110000000101110100O0?0000-
01??00000????020110110000010111??0020?00010-
0101101?00?0??????011001110221100010101l1(0 1)200---
????000011100??1????????????????????????0000130??0-0?0101001?00-0--00-01000-1-
11-0100100000-00001?1000??0101010000000100100000000000000???0--------
??0?000?????????????????????0?1--00?????????????????????????????????

Glyptops_plicatulus
      01100?1?1011001?0?0011???101?100?0100000?0010111???0?0?00?1-
0101000?0????0201101?000001011l1?0020?00010-
0101101??0?002?100?1100???0211?000101011?0200---
????0000??????1??????00?0??0????0?00000100100-00010100l?00-0--00-
0100100111-0100100000-000011100011010101000000000010000000000?00010-----
---??0?000101???01111200101O?1--00??1?10000?1?0???????????????????

Kallokibotion_bajazidi
      0000??0?10110010100011???10???000000000000??00110010000O?00??110102?
?0????020210200?00101111??0??00???0001?1200?00?00-
11121110001012000000000101111-10-------000011001-
1??????00?1???????00?00000-0000-000101???000-0--00-010011??1??00?000?000-
0000111000??00011?2000000000l000?0000000?00000--------0?0???????--
001110100101011--0000???000000?????????????????????

Eileanchelys_waldmanni  00000?1?10110??0?-
001????1011?0000?00??0?00???11010000??0???01?100000????020?100-
000001????0??????00???0?0??01010?00000(0
1)1000010?01002010?000?????????????????100011001-
1??????10????????????00??0-0????000001101?00-0--00-0100100l?1-0000???00-
00001?0000?????????0???0?00???00?0????00?????????????????????????????????
??????????????????????????????????????????

Kayentachelys_aprix     00000010101100101-00000-
1101110000000000000000?110?000000001-010100000????0201100--
0010100010?0010000000000-0101000?0?001000?-0???001-101000-11111(0 1)000--
-----?0001100--0??????1000?0?000000000000-0000-00000000?100-0--00-00000-
0111-0000001000-0000010000?0000100000000000010000000000000?0?00--------
??000000010000101O?00101011--00001?10?000?????000?????????0-1?

Australochelys_africanus      ????10??000??0101-00000-
1?0????0000??000?0000?10??00?000001-0?01?01000???01?00-0--
000?1??110?00?0000000000-00000?01??0?0??0?-??0?010-1-00?0-211?10000------
-????????--
0??????????????????????????????????????????????????????????????????????
??????????????????????????????????????????????????????????????????????
????????????????????????????????????????

Proganochelys_quenstedti      0000100?000000101-00000-0001010000000000-
0100010000000000001-000000100100000--0-0--00000??000?0010000000000-000-
0001000000-0?-0-0?000-0-0000-200100000-------?0001010--
0??????000000000000000000(0 1)00000-?0?00000000100--00-??0???010000-
00?00000-0000000000?0??0100?000000000010000000??010000--------
000000000000000000000000010--00000?0000000?000000000-0-0000-1?

Adocus_beatus     1--1000?101100110120120-
?10111000011001010000111010000100021010102000?00102021020l0?00101121?0011
1002100010120110000?1011?0???????020000000010?1?0-11100011l?00011000-
1??????000?101110001100000-0100-10110100l?0(0 1)?0--00-010???0111-
1100100000-100011100010001--000000010001000101000101111?100-
0010111010Z?111????111020011-011--0101111000001?0??10001001-???????
```

```
Petrochelys_kyrgyzensis
      ??????????0?????101201?????????????????0????????1???????????????????1????
??????02?22021?00001???21????2?101-?0-?0-
120010?101101000000??0?020100000??????0-1200?0111?00011001-1------
????????????????????????????????????????????????????????????????????????????
????????????????????????????????????????????????????????????????????????????
????????????????????????????????????

Galianemys_whitei 1--11100101101110-
20121011011100100100001101011101000001(0 1)000-011100000?1-10202200--
101011-120?101001---0010-200-000101001000100?11021100000210?010-
120000011-00111001-1------
????????????????????????????????????????????????????????????????????????????
????????????????????????????????????????????????????????????????????????????
????????????????????????????????????
;
END;
```

S3.5 Supplementary References

ANQUETIN, J., PÜNTENER, C. and JOYCE, W. G. 2017*a*. A Review of the Fossil Record of Turtles of the Clade Thalassochelydia. *Bulletin of the Peabody Museum of Natural History*, **58**, 317–369.

CADENA, E. and PARHAM, J. F. 2015. Oldest known marine turtle? A new protostegid from the Lower Cretaceous of Colombia. *PaleoBios*, **32**, 1–421.

COLLINS, J. I. 1970. The chelonian *Rhinochelys* Seeley from the Upper Cretaceous of England and France. *Palaeontology*, **13**, 355–378.

GENTRY, A. D., PARHAM, J. F., EHRET, D. J., and EVERSOLE J. A. 2018. A new species of *Peritresius* Leidy, 1856 (Testudines: Pan-Cheloniidae) from the Late Cretaceous (Campanian) of Alabama, USA, and the occurrence of the genus within the Mississippi Embayment of North America. *PLoS ONE*, **13** (4), e0195651.

EVERS, S. W. and BENSON, R. B. J. 2018. A new phylogenetic hypothesis of turtles with implications for the number of evolutionary transitions to marine lifestyles supports an Early Cretaceous origin and rapid diversification of Chelonioidea. *Palaeontology*, 1–42.

HAVLIK, P. E., JOYCE, W. G. and BÖHME, M. 2014. *Allaeochelys libyca* , a new carettochelyine turtle from the Middle Miocene (Langhian) of Libya. *Bulletin of the Peabody Museum of Natural History*, **55**, 201–214.

HIRAYAMA, R. 1997. Distribution and Diversity of Cretaceous Chelonioids. *In Ancient Marine Reptiles*, Elsevier, 225–241 pp.

HOOKS, G. E. 1998. Systematic revision of the Protostegidae, with a redescription of *Calcarichelys gemma* Zangerl, 1953. *Journal of Vertebrate Paleontology*, **18**, 85–98.

JANSSEN, R., VAN BAAL, R. R. and SCHULP, A. S. 2011. On the taphonomy of the late Maastrichtian (Late Cretaceous) marine turtle *Allopleuron hofmanni*. *Geologie en Mijnbouw/Netherlands Journal of Geosciences*, **90**, 187–196.

JOYCE, W. G. 2000. The first complete skeleton of *Solnhofia parsonsi* (Cryptodira, Eurysternidae) from the Upper Jurassic of Germany and its taxonomic implications. *Journal of Paleontology*, **74**, 684–700.

MYERS, T. S., POLCYN, M. J., MATEUS, O., VINEYARD, D. P., GONÇALVES, A. O. and JACOBS, L. L. 2018. A nre durophagous stem cheloniid turtle from the Lower Paleocene of Cabinda, Angola. *Papers in Palaeontology*, **4** (2), 161–176.

R CORE TEAM. 2016. *R: a language and environment for statistical computing*. Version 3.3.1. R Foundation for Statistical Computing. http://www.R-project.org

RABI, M., JOYCE, W. G. and WINGS, O. 2010. A review of the Mesozoic turtles of the Junggar Basin (Xinjiang, Northwest China) and the paleobiogeography of Jurassic to Early Cretaceous Asian testudinates. *Palaeobiodiversity and Palaeoenvironments*, **90**, 259–273.

RIEPPEL, O. 1980. The skull of the Upper Jurassic cryptodire turtle *Thalassemys*, with a reconsideration of the chelonian braincase. *Palaeontographica Abteilung A*, 105–140.

SWOFFORD, D. L. 2002. PAUP*. Phylogenetic Analysis Using Parsimony (*and other methods). Version. 4.0. Sinauer Associates, Sunderland, MA.

WEEMS, R. E. and BROWN, K. M. 2017. More-complete remains of *Procolpochelys charlestonensis* (Oligocene, South Carolina), an occurrence of *Euclastes* (upper Eocene, South Carolina), and their bearing on Cenozoic pancheloniid sea turtle distribution and phylogeny. *Journal of Paleontology*, **91**, 1228–1243.

APPENDIX S4

S4.1 MrBayes code

The following code was appended to the nexus file shown in Appendix S3.4 and executed in MrMayes 3.2.6 to produce the analysis explained in section 5.3 of this thesis.

```
begin mrbayes;

log start filename=turtles-log_2018.09.24.txt;

lset rates=gamma coding=variable;

outgroup Proganochelys_quenstedti;
constraint root = 1-. ;

constraint lepidochelys partial = Lepidochelys_olivacea
    Lepidochelys_kempii : Pelomedusa_subrufa Podocnemis Chelus_fimbriatus
    Phrynops_geoffroanus Chelodina Elseya_dentata Carettochelys_insculpta
    Lissemys_punctata Pelodiscus_sinensis  Apalone_spinifera
    Platysternon_megacephalum Emys_orbicularis Chrysemys_picta
    Geoclemys_hamiltonii Gopherus_polyphemus Testudo Chelonoidis_sp.
    Macrochelys_temminckii Chelydra_serpentina Dermatemys_mawii
    Staurotypus Kinosternon_suburum_hippocrepis Sternotherus
    Dermochelys_coriacea Chelonia_mydas Natator_depressus
    Eretmochelys_imbricata Caretta_caretta Proganochelys_quenstedti;

constraint lepido-caretta partial = Caretta_caretta Lepidochelys_olivacea
    Lepidochelys_kempii : Pelomedusa_subrufa Podocnemis Chelus_fimbriatus
    Phrynops_geoffroanus Chelodina Elseya_dentata Carettochelys_insculpta
    Lissemys_punctata Pelodiscus_sinensis  Apalone_spinifera
    Platysternon_megacephalum Emys_orbicularis Chrysemys_picta
    Geoclemys_hamiltonii Gopherus_polyphemus Testudo Chelonoidis_sp.
    Macrochelys_temminckii Chelydra_serpentina Dermatemys_mawii
    Staurotypus Kinosternon_suburum_hippocrepis Sternotherus
    Dermochelys_coriacea Chelonia_mydas Natator_depressus
    Eretmochelys_imbricata Proganochelys_quenstedti;

constraint lepido-eretmo partial = Eretmochelys_imbricata Caretta_caretta
    Lepidochelys_olivacea Lepidochelys_kempii : Pelomedusa_subrufa
    Podocnemis Chelus_fimbriatus Phrynops_geoffroanus Chelodina
    Elseya_dentata Carettochelys_insculpta Lissemys_punctata
    Pelodiscus_sinensis  Apalone_spinifera Platysternon_megacephalum
    Emys_orbicularis Chrysemys_picta Geoclemys_hamiltonii
    Gopherus_polyphemus Testudo Chelonoidis_sp. Macrochelys_temminckii
    Chelydra_serpentina Dermatemys_mawii Staurotypus
    Kinosternon_suburum_hippocrepis Sternotherus Dermochelys_coriacea
    Chelonia_mydas Natator_depressus Proganochelys_quenstedti;

constraint chelonia-natator partial = Chelonia_mydas Natator_depressus :
```

```
    Eretmochelys_imbricata Caretta_caretta Lepidochelys_olivacea
    Lepidochelys_kempii Pelomedusa_subrufa Podocnemis Chelus_fimbriatus
    Phrynops_geoffroanus Chelodina Elseya_dentata Carettochelys_insculpta
    Lissemys_punctata Pelodiscus_sinensis  Apalone_spinifera
    Platysternon_megacephalum Emys_orbicularis Chrysemys_picta
    Geoclemys_hamiltonii Gopherus_polyphemus Testudo Chelonoidis_sp.
    Macrochelys_temminckii Chelydra_serpentina Dermatemys_mawii
    Staurotypus Kinosternon_suburum_hippocrepis Sternotherus
    Dermochelys_coriacea Proganochelys_quenstedti;

constraint cheloniidae partial = Chelonia_mydas Natator_depressus
    Eretmochelys_imbricata Caretta_caretta Lepidochelys_olivacea
    Lepidochelys_kempii : Pelomedusa_subrufa Podocnemis Chelus_fimbriatus
    Phrynops_geoffroanus Chelodina Elseya_dentata Carettochelys_insculpta
    Lissemys_punctata Pelodiscus_sinensis  Apalone_spinifera
    Platysternon_megacephalum Emys_orbicularis Chrysemys_picta
    Geoclemys_hamiltonii Gopherus_polyphemus Testudo Chelonoidis_sp.
    Macrochelys_temminckii Chelydra_serpentina Dermatemys_mawii
    Staurotypus Kinosternon_suburum_hippocrepis Sternotherus
    Dermochelys_coriacea Proganochelys_quenstedti;

constraint chelonioidea partial = Dermochelys_coriacea Chelonia_mydas
    Natator_depressus Eretmochelys_imbricata Caretta_caretta
    Lepidochelys_olivacea Lepidochelys_kempii : Pelomedusa_subrufa
    Podocnemis Chelus_fimbriatus Phrynops_geoffroanus Chelodina
    Elseya_dentata Carettochelys_insculpta Lissemys_punctata
    Pelodiscus_sinensis  Apalone_spinifera Platysternon_megacephalum
    Emys_orbicularis Chrysemys_picta Geoclemys_hamiltonii
    Gopherus_polyphemus Testudo Chelonoidis_sp. Macrochelys_temminckii
    Chelydra_serpentina Dermatemys_mawii Staurotypus
    Kinosternon_suburum_hippocrepis Sternotherus
    Proganochelys_quenstedti;

constraint kinosterninae partial = Kinosternon_suburum_hippocrepis
    Sternotherus : Pelomedusa_subrufa Podocnemis Chelus_fimbriatus
    Phrynops_geoffroanus Chelodina Elseya_dentata Carettochelys_insculpta
    Lissemys_punctata Pelodiscus_sinensis  Apalone_spinifera
    Platysternon_megacephalum Emys_orbicularis Chrysemys_picta
    Geoclemys_hamiltonii Gopherus_polyphemus Testudo Chelonoidis_sp.
    Macrochelys_temminckii Chelydra_serpentina Dermatemys_mawii
    Staurotypus Dermochelys_coriacea Chelonia_mydas Natator_depressus
    Eretmochelys_imbricata Caretta_caretta Lepidochelys_olivacea
    Lepidochelys_kempii Proganochelys_quenstedti;

constraint kinosternidae partial = Staurotypus
    Kinosternon_suburum_hippocrepis Sternotherus : Pelomedusa_subrufa
    Podocnemis Chelus_fimbriatus Phrynops_geoffroanus Chelodina
    Elseya_dentata Carettochelys_insculpta Lissemys_punctata
    Pelodiscus_sinensis  Apalone_spinifera Platysternon_megacephalum
    Emys_orbicularis Chrysemys_picta Geoclemys_hamiltonii
    Gopherus_polyphemus Testudo Chelonoidis_sp. Macrochelys_temminckii
    Chelydra_serpentina Dermatemys_mawii Dermochelys_coriacea
    Chelonia_mydas Natator_depressus Eretmochelys_imbricata
    Caretta_caretta Lepidochelys_olivacea Lepidochelys_kempii
    Proganochelys_quenstedti;

constraint kinosternoidea partial = Dermatemys_mawii Staurotypus
    Kinosternon_suburum_hippocrepis Sternotherus : Pelomedusa_subrufa
    Podocnemis Chelus_fimbriatus Phrynops_geoffroanus Chelodina
    Elseya_dentata Carettochelys_insculpta Lissemys_punctata
    Pelodiscus_sinensis  Apalone_spinifera Platysternon_megacephalum
    Emys_orbicularis Chrysemys_picta Geoclemys_hamiltonii
```

```
    Gopherus_polyphemus Testudo Chelonoidis_sp. Macrochelys_temminckii
    Chelydra_serpentina Dermochelys_coriacea Chelonia_mydas
    Natator_depressus Eretmochelys_imbricata Caretta_caretta
    Lepidochelys_olivacea Lepidochelys_kempii Proganochelys_quenstedti;

constraint chelydridae partial = Macrochelys_temminckii
    Chelydra_serpentina : Pelomedusa_subrufa Podocnemis Chelus_fimbriatus
    Phrynops_geoffroanus Chelodina Elseya_dentata Carettochelys_insculpta
    Lissemys_punctata Pelodiscus_sinensis  Apalone_spinifera
    Platysternon_megacephalum Emys_orbicularis Chrysemys_picta
    Geoclemys_hamiltonii Gopherus_polyphemus Testudo Chelonoidis_sp.
    Dermatemys_mawii Staurotypus Kinosternon_suburum_hippocrepis
    Sternotherus Dermochelys_coriacea Chelonia_mydas Natator_depressus
    Eretmochelys_imbricata Caretta_caretta Lepidochelys_olivacea
    Lepidochelys_kempii Proganochelys_quenstedti;

constraint chelydroidea partial = Macrochelys_temminckii
    Chelydra_serpentina Dermatemys_mawii Staurotypus
    Kinosternon_suburum_hippocrepis Sternotherus : Pelomedusa_subrufa
    Podocnemis Chelus_fimbriatus Phrynops_geoffroanus Chelodina
    Elseya_dentata Carettochelys_insculpta Lissemys_punctata
    Pelodiscus_sinensis  Apalone_spinifera Platysternon_megacephalum
    Emys_orbicularis Chrysemys_picta Geoclemys_hamiltonii
    Gopherus_polyphemus Testudo Chelonoidis_sp. Dermochelys_coriacea
    Chelonia_mydas Natator_depressus Eretmochelys_imbricata
    Caretta_caretta Lepidochelys_olivacea Lepidochelys_kempii
    Proganochelys_quenstedti;

constraint americhelydia partial = Macrochelys_temminckii
    Chelydra_serpentina Dermatemys_mawii Staurotypus
    Kinosternon_suburum_hippocrepis Sternotherus Dermochelys_coriacea
    Chelonia_mydas Natator_depressus Eretmochelys_imbricata
    Caretta_caretta Lepidochelys_olivacea Lepidochelys_kempii :
    Pelomedusa_subrufa Podocnemis Chelus_fimbriatus Phrynops_geoffroanus
    Chelodina Elseya_dentata Carettochelys_insculpta Lissemys_punctata
    Pelodiscus_sinensis  Apalone_spinifera Platysternon_megacephalum
    Emys_orbicularis Chrysemys_picta Geoclemys_hamiltonii
    Gopherus_polyphemus Testudo Chelonoidis_sp. Proganochelys_quenstedti;

constraint emydidae partial = Emys_orbicularis Chrysemys_picta :
    Pelomedusa_subrufa Podocnemis Chelus_fimbriatus Phrynops_geoffroanus
    Chelodina Elseya_dentata Carettochelys_insculpta Lissemys_punctata
    Pelodiscus_sinensis  Apalone_spinifera Platysternon_megacephalum
    Geoclemys_hamiltonii Gopherus_polyphemus Testudo Chelonoidis_sp.
    Macrochelys_temminckii Chelydra_serpentina Dermatemys_mawii
    Staurotypus Kinosternon_suburum_hippocrepis Sternotherus
    Dermochelys_coriacea Chelonia_mydas Natator_depressus
    Eretmochelys_imbricata Caretta_caretta Lepidochelys_olivacea
    Lepidochelys_kempii Proganochelys_quenstedti;

constraint emysternidae partial = Platysternon_megacephalum
    Emys_orbicularis Chrysemys_picta : Pelomedusa_subrufa Podocnemis
    Chelus_fimbriatus Phrynops_geoffroanus Chelodina Elseya_dentata
    Carettochelys_insculpta Lissemys_punctata Pelodiscus_sinensis
    Apalone_spinifera Geoclemys_hamiltonii Gopherus_polyphemus Testudo
    Chelonoidis_sp. Macrochelys_temminckii Chelydra_serpentina
    Dermatemys_mawii Staurotypus Kinosternon_suburum_hippocrepis
    Sternotherus Dermochelys_coriacea Chelonia_mydas Natator_depressus
    Eretmochelys_imbricata Caretta_caretta Lepidochelys_olivacea
    Lepidochelys_kempii Proganochelys_quenstedti;

constraint testudininae partial = Gopherus_polyphemus Testudo :
```

```
    Pelomedusa_subrufa Podocnemis Chelus_fimbriatus Phrynops_geoffroanus
    Chelodina Elseya_dentata Carettochelys_insculpta Lissemys_punctata
    Pelodiscus_sinensis  Apalone_spinifera Platysternon_megacephalum
    Emys_orbicularis Chrysemys_picta Geoclemys_hamiltonii Chelonoidis_sp.
    Macrochelys_temminckii Chelydra_serpentina Dermatemys_mawii
    Staurotypus Kinosternon_suburum_hippocrepis Sternotherus
    Dermochelys_coriacea Chelonia_mydas Natator_depressus
    Eretmochelys_imbricata Caretta_caretta Lepidochelys_olivacea
    Lepidochelys_kempii Proganochelys_quenstedti;

constraint testudindidae partial = Gopherus_polyphemus Testudo
    Chelonoidis_sp. : Pelomedusa_subrufa Podocnemis Chelus_fimbriatus
    Phrynops_geoffroanus Chelodina Elseya_dentata Carettochelys_insculpta
    Lissemys_punctata Pelodiscus_sinensis  Apalone_spinifera
    Platysternon_megacephalum Emys_orbicularis Chrysemys_picta
    Geoclemys_hamiltonii Macrochelys_temminckii Chelydra_serpentina
    Dermatemys_mawii Staurotypus Kinosternon_suburum_hippocrepis
    Sternotherus Dermochelys_coriacea Chelonia_mydas Natator_depressus
    Eretmochelys_imbricata Caretta_caretta Lepidochelys_olivacea
    Lepidochelys_kempii Proganochelys_quenstedti;

constraint testuguria partial = Geoclemys_hamiltonii Gopherus_polyphemus
    Testudo Chelonoidis_sp. : Pelomedusa_subrufa Podocnemis
    Chelus_fimbriatus Phrynops_geoffroanus Chelodina Elseya_dentata
    Carettochelys_insculpta Lissemys_punctata Pelodiscus_sinensis
    Apalone_spinifera Platysternon_megacephalum Emys_orbicularis
    Chrysemys_picta Macrochelys_temminckii Chelydra_serpentina
    Dermatemys_mawii Staurotypus Kinosternon_suburum_hippocrepis
    Sternotherus Dermochelys_coriacea Chelonia_mydas Natator_depressus
    Eretmochelys_imbricata Caretta_caretta Lepidochelys_olivacea
    Lepidochelys_kempii Proganochelys_quenstedti;

constraint testudinoidea partial = Platysternon_megacephalum
    Emys_orbicularis Chrysemys_picta Geoclemys_hamiltonii
    Gopherus_polyphemus Testudo Chelonoidis_sp. : Pelomedusa_subrufa
    Podocnemis Chelus_fimbriatus Phrynops_geoffroanus Chelodina
    Elseya_dentata Carettochelys_insculpta Lissemys_punctata
    Pelodiscus_sinensis  Apalone_spinifera  Macrochelys_temminckii
    Chelydra_serpentina Dermatemys_mawii Staurotypus
    Kinosternon_suburum_hippocrepis Sternotherus Dermochelys_coriacea
    Chelonia_mydas Natator_depressus Eretmochelys_imbricata
    Caretta_caretta Lepidochelys_olivacea Lepidochelys_kempii
    Proganochelys_quenstedti;

constraint durocryptodira partial = Platysternon_megacephalum
    Emys_orbicularis Chrysemys_picta Geoclemys_hamiltonii
    Gopherus_polyphemus Testudo Chelonoidis_sp. Macrochelys_temminckii
    Chelydra_serpentina Dermatemys_mawii Staurotypus
    Kinosternon_suburum_hippocrepis Sternotherus Dermochelys_coriacea
    Chelonia_mydas Natator_depressus Eretmochelys_imbricata
    Caretta_caretta Lepidochelys_olivacea Lepidochelys_kempii :
    Pelomedusa_subrufa Podocnemis Chelus_fimbriatus Phrynops_geoffroanus
    Chelodina Elseya_dentata Carettochelys_insculpta Lissemys_punctata
    Pelodiscus_sinensis  Apalone_spinifera Proganochelys_quenstedti;

constraint trionychinae partial = Pelodiscus_sinensis  Apalone_spinifera
    : Pelomedusa_subrufa Podocnemis Chelus_fimbriatus
    Phrynops_geoffroanus Chelodina Elseya_dentata Carettochelys_insculpta
    Lissemys_punctata Platysternon_megacephalum Emys_orbicularis
    Chrysemys_picta Geoclemys_hamiltonii Gopherus_polyphemus Testudo
    Chelonoidis_sp. Macrochelys_temminckii Chelydra_serpentina
    Dermatemys_mawii Staurotypus Kinosternon_suburum_hippocrepis
```

```
    Sternotherus Dermochelys_coriacea Chelonia_mydas Natator_depressus
    Eretmochelys_imbricata Caretta_caretta Lepidochelys_olivacea
    Lepidochelys_kempii Proganochelys_quenstedti;

constraint trionychidae partial = Lissemys_punctata Pelodiscus_sinensis
    Apalone_spinifera : Pelomedusa_subrufa Podocnemis Chelus_fimbriatus
    Phrynops_geoffroanus Chelodina Elseya_dentata Carettochelys_insculpta
    Platysternon_megacephalum Emys_orbicularis Chrysemys_picta
    Geoclemys_hamiltonii Gopherus_polyphemus Testudo Chelonoidis_sp.
    Macrochelys_temminckii Chelydra_serpentina Dermatemys_mawii
    Staurotypus Kinosternon_suburum_hippocrepis Sternotherus
    Dermochelys_coriacea Chelonia_mydas Natator_depressus
    Eretmochelys_imbricata Caretta_caretta Lepidochelys_olivacea
    Lepidochelys_kempii Proganochelys_quenstedti;

constraint trionychia partial = Carettochelys_insculpta Lissemys_punctata
    Pelodiscus_sinensis  Apalone_spinifera : Pelomedusa_subrufa
    Podocnemis Chelus_fimbriatus Phrynops_geoffroanus Chelodina
    Elseya_dentata Platysternon_megacephalum Emys_orbicularis
    Chrysemys_picta Geoclemys_hamiltonii Gopherus_polyphemus Testudo
    Chelonoidis_sp. Macrochelys_temminckii Chelydra_serpentina
    Dermatemys_mawii Staurotypus Kinosternon_suburum_hippocrepis
    Sternotherus Dermochelys_coriacea Chelonia_mydas Natator_depressus
    Eretmochelys_imbricata Caretta_caretta Lepidochelys_olivacea
    Lepidochelys_kempii Proganochelys_quenstedti;

constraint cryptodira partial = Carettochelys_insculpta Lissemys_punctata
    Pelodiscus_sinensis  Apalone_spinifera Platysternon_megacephalum
    Emys_orbicularis Chrysemys_picta Geoclemys_hamiltonii
    Gopherus_polyphemus Testudo Chelonoidis_sp. Macrochelys_temminckii
    Chelydra_serpentina Dermatemys_mawii Staurotypus
    Kinosternon_suburum_hippocrepis Sternotherus Dermochelys_coriacea
    Chelonia_mydas Natator_depressus Eretmochelys_imbricata
    Caretta_caretta Lepidochelys_olivacea Lepidochelys_kempii :
    Pelomedusa_subrufa Podocnemis Chelus_fimbriatus Phrynops_geoffroanus
    Chelodina Elseya_dentata Proganochelys_quenstedti;

constraint chelodininae partial = Chelodina Elseya_dentata :
    Pelomedusa_subrufa Podocnemis Chelus_fimbriatus Phrynops_geoffroanus
    Carettochelys_insculpta Lissemys_punctata Pelodiscus_sinensis
    Apalone_spinifera Platysternon_megacephalum Emys_orbicularis
    Chrysemys_picta Geoclemys_hamiltonii Gopherus_polyphemus Testudo
    Chelonoidis_sp. Macrochelys_temminckii Chelydra_serpentina
    Dermatemys_mawii Staurotypus Kinosternon_suburum_hippocrepis
    Sternotherus Dermochelys_coriacea Chelonia_mydas Natator_depressus
    Eretmochelys_imbricata Caretta_caretta Lepidochelys_olivacea
    Lepidochelys_kempii Proganochelys_quenstedti;

constraint chelodinidae partial = Chelus_fimbriatus Phrynops_geoffroanus
    : Pelomedusa_subrufa Podocnemis Chelodina Elseya_dentata
    Carettochelys_insculpta Lissemys_punctata Pelodiscus_sinensis
    Apalone_spinifera Platysternon_megacephalum Emys_orbicularis
    Chrysemys_picta Geoclemys_hamiltonii Gopherus_polyphemus Testudo
    Chelonoidis_sp. Macrochelys_temminckii Chelydra_serpentina
    Dermatemys_mawii Staurotypus Kinosternon_suburum_hippocrepis
    Sternotherus Dermochelys_coriacea Chelonia_mydas Natator_depressus
    Eretmochelys_imbricata Caretta_caretta Lepidochelys_olivacea
    Lepidochelys_kempii Proganochelys_quenstedti;

constraint chelidae partial = Chelus_fimbriatus Phrynops_geoffroanus
    Chelodina Elseya_dentata : Pelomedusa_subrufa Podocnemis
    Carettochelys_insculpta Lissemys_punctata Pelodiscus_sinensis
```

```
    Apalone_spinifera Platysternon_megacephalum Emys_orbicularis
    Chrysemys_picta Geoclemys_hamiltonii Gopherus_polyphemus Testudo
    Chelonoidis_sp. Macrochelys_temminckii Chelydra_serpentina
    Dermatemys_mawii Staurotypus Kinosternon_suburum_hippocrepis
    Sternotherus Dermochelys_coriacea Chelonia_mydas Natator_depressus
    Eretmochelys_imbricata Caretta_caretta Lepidochelys_olivacea
    Lepidochelys_kempii Proganochelys_quenstedti;

constraint pelomedusoides partial = Pelomedusa_subrufa Podocnemis :
    Chelus_fimbriatus Phrynops_geoffroanus Chelodina Elseya_dentata
    Carettochelys_insculpta Lissemys_punctata Pelodiscus_sinensis
    Apalone_spinifera Platysternon_megacephalum Emys_orbicularis
    Chrysemys_picta Geoclemys_hamiltonii Gopherus_polyphemus Testudo
    Chelonoidis_sp. Macrochelys_temminckii Chelydra_serpentina
    Dermatemys_mawii Staurotypus Kinosternon_suburum_hippocrepis
    Sternotherus Dermochelys_coriacea Chelonia_mydas Natator_depressus
    Eretmochelys_imbricata Caretta_caretta Lepidochelys_olivacea
    Lepidochelys_kempii Proganochelys_quenstedti;

constraint pleurodira partial = Pelomedusa_subrufa Podocnemis
    Chelus_fimbriatus Phrynops_geoffroanus Chelodina Elseya_dentata :
    Carettochelys_insculpta Lissemys_punctata Pelodiscus_sinensis
    Apalone_spinifera Platysternon_megacephalum Emys_orbicularis
    Chrysemys_picta Geoclemys_hamiltonii Gopherus_polyphemus Testudo
    Chelonoidis_sp. Macrochelys_temminckii Chelydra_serpentina
    Dermatemys_mawii Staurotypus Kinosternon_suburum_hippocrepis
    Sternotherus Dermochelys_coriacea Chelonia_mydas Natator_depressus
    Eretmochelys_imbricata Caretta_caretta Lepidochelys_olivacea
    Lepidochelys_kempii Proganochelys_quenstedti;

constraint testudines partial = Pelomedusa_subrufa Podocnemis
    Chelus_fimbriatus Phrynops_geoffroanus Chelodina Elseya_dentata
    Carettochelys_insculpta Lissemys_punctata Pelodiscus_sinensis
    Apalone_spinifera Platysternon_megacephalum Emys_orbicularis
    Chrysemys_picta Geoclemys_hamiltonii Gopherus_polyphemus Testudo
    Chelonoidis_sp. Macrochelys_temminckii Chelydra_serpentina
    Dermatemys_mawii Staurotypus Kinosternon_suburum_hippocrepis
    Sternotherus Dermochelys_coriacea Chelonia_mydas Natator_depressus
    Eretmochelys_imbricata Caretta_caretta Lepidochelys_olivacea
    Lepidochelys_kempii : Proganochelys_quenstedti;

constraint ingroup = 2-96;

prset topologypr = constraints (lepidochelys, lepido-caretta, lepido-
    eretmo, chelonia-natator, cheloniidae, chelonioidea, kinosterninae,
    kinosternidae, kinosternoidea, chelydridae, chelydroidea,
    americhelydia, emydidae, emysternidae, testudininae, testudindidae,
    testuguria, testudinoidea, durocryptodira, trionychinae,
    trionychidae, trionychia, cryptodira, chelodininae, chelodinidae,
    chelidae, pelomedusoides, pleurodira, testudines, ingroup);

CALIBRATE   Apalone_spinifera                = fixed (0);
CALIBRATE   Caretta_caretta                  = fixed (0);
CALIBRATE   Carettochelys_insculpta          = fixed (0);
CALIBRATE   Chelodina                        = fixed (0);
CALIBRATE   Chelonia_mydas                   = fixed (0);
CALIBRATE   Chelonoidis_sp.                  = fixed (0);
CALIBRATE   Chelus_fimbriatus                = fixed (0);
CALIBRATE   Chelydra_serpentina              = fixed (0);
CALIBRATE   Chrysemys_picta                  = fixed (0);
CALIBRATE   Dermatemys_mawii                 = fixed (0);
CALIBRATE   Dermochelys_coriacea             = fixed (0);
```

```
CALIBRATE   Elseya_dentata                      = fixed (0);
CALIBRATE   Emys_orbicularis                    = fixed (0);
CALIBRATE   Eretmochelys_imbricata              = fixed (0);
CALIBRATE   Geoclemys_hamiltonii                = fixed (0);
CALIBRATE   Gopherus_polyphemus                 = fixed (0);
CALIBRATE   Kinosternon_suburum_hippocrepis     = fixed (0);
CALIBRATE   Lepidochelys_kempii                 = fixed (0);
CALIBRATE   Lepidochelys_olivacea               = fixed (0);
CALIBRATE   Lissemys_punctata                   = fixed (0);
CALIBRATE   Macrochelys_temminckii              = fixed (0);
CALIBRATE   Natator_depressus                   = fixed (0);
CALIBRATE   Pelodiscus_sinensis                 = fixed (0);
CALIBRATE   Pelomedusa_subrufa                  = fixed (0);
CALIBRATE   Phrynops_geoffroanus                = fixed (0);
CALIBRATE   Platysternon_megacephalum           = fixed (0);
CALIBRATE   Podocnemis                          = fixed (0);
CALIBRATE   Staurotypus                         = fixed (0);
CALIBRATE   Sternotherus                        = fixed (0);
CALIBRATE   Testudo                             = fixed (0);

[Use uniform priors for fossils]

CALIBRATE   Adocus_beatus                 = uniform (66.043,70.6);
CALIBRATE   Allaeochelys_libyca           = uniform (15.97,18.82);
CALIBRATE   Allopleuron_hofmanni          = uniform (66.0,72.1);
CALIBRATE   Angolachelys_mbaxi            = uniform (89.3,94.3);
CALIBRATE   Annemys_latiens               = uniform (145.500,163.5);
CALIBRATE   Annemys_levensis              = uniform (145.500,157.3);
CALIBRATE   Annemys_sp._IVPP_V18106       = uniform (145.00,167.700);
CALIBRATE   Araripemys_barretoi           = uniform (109.000,112.600);
CALIBRATE   Archelon_ischyros             = uniform (72.1,83.6);
CALIBRATE   Argillochelys_cuneiceps       = uniform (47.8,56.00);
CALIBRATE   Arundelemys_dardeni           = uniform (112.600,122.460);
CALIBRATE   Australochelys_africanus      = uniform (189.600,201.600);
CALIBRATE   Baptemys_wyomingensis         = uniform (40.400,55.800);
CALIBRATE   Bouliachelys_suteri           = uniform (99.700,105.300);
CALIBRATE   Brachyopsemys_tingitana       = uniform (61.700,66.043);
CALIBRATE   Cabindachelys_landanensis     = uniform (61.6,66.0);
CALIBRATE   Calcarichelys_gemma           = uniform (70.6,84.9);
CALIBRATE   Chelosphargis_advena          = uniform (84.9,85.8);
CALIBRATE   Chubutemys_copelloi           = uniform (112.600,125.450);
CALIBRATE   Corsochelys_halinches         = uniform (70.6,84.9);
CALIBRATE   Ctenochelys                   = uniform (79.5,88.8);
CALIBRATE   Desmatochelys_lowii           = uniform (89.8,93.9);
CALIBRATE   Desmatochelys_padillai        = uniform (120.0,125.000);
CALIBRATE   Dracochelys_bicuspis          = uniform (100.5,125.0);
CALIBRATE   Eileanchelys_waldmanni        = uniform (166.1,168.3);
CALIBRATE   Emarginachelys_cretacea       = uniform (66.043,70.600);
CALIBRATE   Eochelone_brabantica          = uniform (41.2,47.8);
CALIBRATE   Eosphargis_breineri           = uniform (47.8,56.00);
CALIBRATE   Erquelinnesia_gosseleti       = uniform (47.8,56.0);
CALIBRATE   Eubaena_cephalica             = uniform (66.043,70.6);
CALIBRATE   Galianemys_whitei             = uniform (94.3,99.7);
CALIBRATE   Glyptops_plicatulus           = uniform (145.5,150.8);
CALIBRATE   Judithemys_sukhanovi          = uniform (70.600,84.900);
CALIBRATE   Jurassichelon_oleronensis     = uniform (145.0,152.1);
CALIBRATE   Kallokibotion_bajazidi        = uniform (66.0,72.1);
CALIBRATE   Kayentachelys_aprix           = uniform (182.700,199.3);
CALIBRATE   Kirgizemys_dmitrievi          = uniform (112.600,130.000);
CALIBRATE   Kirgizemys_hoburensis         = uniform (100.5,125.0);
CALIBRATE   Leyvachelys_cipadi            = uniform (109.000,130.000);
CALIBRATE   Meiolania_planiceps           = uniform (0.012,0.781);
```

```
CALIBRATE   Nichollsemys_baieri          = uniform (70.6,84.9);
CALIBRATE   Notochelone_costata          = uniform (99.700,109.000);
CALIBRATE   Ocepechelon_bouyai           = uniform (66.043,70.600);
CALIBRATE   Oligochelone_rupelensis      = uniform (27.82,33.9);
CALIBRATE   Ordosemys_sp._IVPP_V12092    = uniform (113.0,129.4);
CALIBRATE   Peritresius_martini          = uniform (68.5,72.0);
CALIBRATE   Petrochelys_kyrgyzensis      = uniform (94.3,99.7);
CALIBRATE   Plesiochelys_bigleri         = uniform (150.8,155.7);
CALIBRATE   Plesiochelys_etalloni        = uniform (150.0,157.300);
CALIBRATE   Plesiochelys_planiceps       = uniform (145.000,152.100);
CALIBRATE   Pleurosternon_bullockii      = uniform (140.2,145.2);
CALIBRATE   Portlandemys_mcdowelli       = uniform (145.000,152.100);
CALIBRATE   Procolpochelys_charlestonensis     = uniform (23.03,28.4);
CALIBRATE   Proganochelys_quenstedti     = uniform (201.300,208.5);
CALIBRATE   Protostega_gigas             = uniform (70.600,85.800);
CALIBRATE   Puppigerus_camperi           = uniform (41.2,56.0);
CALIBRATE   Rhinochelys_nammourensis     = uniform (94.3,99.7);
CALIBRATE   Rhinochelys_pulchriceps      = uniform (102.0,105.300);
CALIBRATE   Sandownia_harrisi            = uniform (122.460,125.450);
CALIBRATE   Santanachelys_gaffneyi       = uniform (109.000,112.600);
CALIBRATE   Sinemys_gamera               = uniform (100.5,129.4);
CALIBRATE   Sinemys_lens                 = uniform (145.0,163.5);
CALIBRATE   Solnhofia_parsoni            = uniform (145.500,155.700);
CALIBRATE   Toxochelys_sp                = uniform (70.600,85.800);
CALIBRATE   Xinjiangchelys_radiplicatoides     = uniform (152.1,168.3);
CALIBRATE   Xinjiangchelys_wusu          = uniform (152.1,163.5);

PRSET nodeagepr = calibrated;
    prset clockvarpr=igr;
    prset igrvarpr=exp(10);
    prset clockratepr = normal(0.001,0.01);

PRSET brlenspr = clock:fossilization; [
PRSET sampleprob = 0.09254;
PRSET samplestrat = diversity;

PRSET speciationpr = exponential(10);
PRSET extinctionpr = beta(1,1);
PRSET fossilizationpr = beta(1,1) ;

PRSET treeagepr = offsetexponential(208.5, 220);

mcmcp nrun = 2 nchain = 6 temp=0.05 ngen=10000000 samplefreq=500
    printfreq=500 diagnfr = 5000  savebrlens=yes relburnin=yes
    burninfrac=0.25;
mcmc;

sumt contype = allcompat conformat = Figtree relburnin=yes
    burninfrac=0.25;
sump relburnin=yes burninfrac=0.25;

end;
```